Marine Compounds and Cancer

Edited by

Sergey A. Dyshlovoy and

Friedemann Honecker

Printed Edition of the Special Issue Published in *Marine Drugs*

www.mdpi.com/journal/marinedrugs

Sergey A. Dyshlovoy and Friedemann Honecker (Eds.)

Marine Compounds and Cancer

MDPI

This book is a reprint of the Special Issue that appeared in the online, open access journal, *Marine Drugs* (ISSN 1660-3397) from 2013–2015 (available at: http://www.mdpi.com/journal/marinedrugs/special_issues/marine-compounds-cancer).

Guest Editors
Friedemann Honecker
Tumor and Breast Center ZeTuP St. Gallen
Switzerland

Sergey A. Dyshlovoy
Laboratory of Marine Natural Products Chemistry
G.B. Elyakov Pacific Institute of Bioorganic Chemistry FEB RAS
Russia

Laboratory of Experimental Oncology
Department of Internal Medicine II and Clinic (Oncology Center)
University Medical Center Hamburg-Eppendorf
Germany

Editorial Office
MDPI AG
Klybeckstrasse 64
Basel, Switzerland

Publisher
Shu-Kun Lin

Managing Editor
Tina Yan

1. Edition 2015

MDPI • Basel • Beijing • Wuhan

ISBN 978-3-03842-131-3 (PDF)
ISBN 978-3-03842-132-0 (Hbk)

Table of Contents

List of Contributors

Catherine A. Abbott: School of Biological Sciences, Flinders University, GPO Box 2100, Adelaide, SA 5001, Australia; Flinders Centre for Innovation in Cancer, Flinders University, GPO Box 2100, Adelaide 5001, Australia.

Philip Adams Adams: Marine Immunology Program, Mote Marine Laboratory, 1600 Ken Thompson Parkway, Sarasota, FL 34236, USA; Marine Biomedical Program, Mote Marine Laboratory, 1600 Ken Thompson Parkway, Sarasota, FL 34236, USA.

Mohamed R. Akl: Department of Basic Pharmaceutical Sciences, School of Pharmacy, University of Louisiana at Monroe, 1800 Bienville Drive, Monroe, LA 71201, USA.

Paola Allavena: Department Immunology and Inflammation, IRCCS Clinical and Research Institute Humanitas, Rozzano, Milan 20089, Italy.

Dmitry L. Aminin: G.B. Elyakov Pacific Institute of Bioorganic Chemistry, Far-Eastern Branch of the Russian Academy of Science, Prospect 100 letya Vladivostoka, 159, Vladivostok 690022, Russia.

Paula B. Andrade: REQUIMTE/Laboratory of Pharmacognosy, Department of Chemistry, Faculty of Pharmacy, University of Porto, Rua de Jorge Viterbo Ferreira, nº 228, Porto 4050-313, Portugal.

Sergey A. Avilov: G.B. Elyakov Pacific Institute of Bioorganic Chemistry, Far-Eastern Branch of the Russian Academy of Science, Prospect 100 letya Vladivostoka, 159, Vladivostok 690022, Russia.

Nehad M. Ayoub: Department of Clinical Pharmacy, Faculty of Pharmacy, Jordan University of Science and Technology, Irbid 22110, Jordan.

Hoon Bae: College of Pharmacy, Seoul National University, Seoul 151-742, Korea.

Bakran-Petricioli: Department of Biology, Faculty of Science, University of Zagreb, Zagreb 10000, Croatia.

Robert Belužić: Division of Molecular Medicine, Ruđer Bošković Institute, Zagreb 10000, Croatia.

Kirsten Benkendorff: Marine Ecology Research Centre, School of Environment, Science and Engineering, Southern Cross University, GPO Box 157, Lismore, NSW 2480, Australia.

Courtney Bennett: Marine Immunology Program, Mote Marine Laboratory, 1600 Ken Thompson Parkway, Sarasota, FL 34236, USA; Marine Biomedical Program, Mote Marine Laboratory, 1600 Ken Thompson Parkway, Sarasota, FL 34236, USA.

Ashby B. Bodine: Department of Animal and Veterinary Sciences, Clemson University, Clemson, SC 29634, USA.

Armando Burgos-Hernández: Department of Research and Food Science Graduate Program, University of Sonora, Apartado Postal 1658, Hermosillo, Sonora 83000, Mexico.

Librada Cañedo: Biomar Microbial Technologies, Parque Tecnológico de León, Parcela M-10.4, Armunia (León) 24009, Spain.

Theresa Cantu: Marine Immunology Program, Mote Marine Laboratory, 1600 Ken Thompson Parkway, Sarasota, FL 34236, USA; Marine Biomedical Program, Mote Marine Laboratory, 1600 Ken Thompson Parkway, Sarasota, FL 34236, USA.

Helena Ćetković: Division of Molecular Biology, Ruđer Bošković Institute, Zagreb 10000, Croatia.

Hsueh-Wei Chang: Cancer Center, Kaohsiung Medical University Hospital, Kaohsiung Medical University, Kaohsiung 80708, Taiwan; Department of Biomedical Science and Environmental Biology, Kaohsiung Medical University, Kaohsiung 80708, Taiwan; Institute of Medical Science and Technology, National Sun Yat-sen University, Kaohsiung 80424, Taiwan; Research Center of Environmental Medicine, Kaohsiung Medical University, Kaohsiung 80708, Taiwan.

Wen-Been Chang: National Museum of Marine Biology & Aquarium, Pingtung 944, Taiwan.

Wen-Liang Chen: Department of Physiology, Faculty of Medicine, University of Toronto, Toronto, ON M5S 1A8, Canada; Department of Surgery, Faculty of Medicine, University of Toronto, Toronto, ON M5S 1A8, Canada; Department of Pharmacology, Faculty of Medicine, University of Toronto, Toronto, ON M5S 1A8, Canada.

Yangmin Chen: Ernest Mario School of Pharmacy, Rutgers, the State University of New Jersey, New Brunswick, NJ 08901, USA.

Yu-Cheng Chen: National Museum of Marine Biology & Aquarium, Pingtung 944, Taiwan.

Yu-Kuei Chen: Department of Food Science and Nutrition, Meiho University, Pingtung 91202, Taiwan.

Zhe-Sheng Chen: Department of Pharmaceutical Sciences, College of Pharmacy and Health Sciences, St. John's University, Queens, NY 11439, USA.

Zhi-Yong Chen: Department of Neurosurgery and Pituitary Tumour Center, The First Affiliated Hospital of Sun Yat-sen University, No.74, Zhongshan Road 2, Guangzhou 510080, China.

Michael Y. Chiang: Department of Chemistry, National Sun Yat-sen University, Kaohsiung 804, Taiwan.

Chien-Chih Chiu: Department of Biotechnology, Kaohsiung Medical University, Kaohsiung 80761, Taiwan.

Cheol-Hee Choi: Research Center for Resistant Cells and Department of Pharmacology, College of Medicine, Chosun University, Seosuk-dong, Dong-gu, Gwangju 501-759, Korea.

Eun-Ju Choi: Division of Sport Science, Konkuk University, Chungju, 380-701, Korea.

Young Kug Choo: Department of Biological Science, College of Natural Science, Wonkwang University, Iksan, Jeonbuk 570-749, Korea; Institute for Glycoscience, Wonkwang University, Iksan, Jeonbuk 570-749, Korea.

Yalan Chou: Institute of Marine Biology, National Sun Yat-sen University, Kaohsiung, Taiwan.

Marissa Ciesla: Marine Immunology Program, Mote Marine Laboratory, 1600 Ken Thompson Parkway, Sarasota, FL 34236, USA; Marine Biomedical Program, Mote Marine Laboratory, 1600 Ken Thompson Parkway, Sarasota, FL 34236, USA.

Veena Coothankandaswamy: Department of BioMolecular Sciences and Research Institute of Pharmaceutical Sciences, School of Pharmacy, University of Mississippi, University, MS 38677, USA.

Georgina Correia-da-Silva: Laboratory of Biochemistry, Department of Biological Sciences, Faculty of Pharmacy, University of Porto, Rua de Jorge Viterbo Ferreira, nº 228, Porto 4050-313, Portugal; IBMC—Instituto for Molecular and Cell Biology, University of Porto, Porto 4150-180, Portugal.

Gordon M. Cragg: Natural Products Branch, Developmental Therapeutics Program, Division of Cancer Treatment and Diagnosis, Frederick National Laboratory, P.O. Box B, Frederick, MD 21702, USA.

Pradeep Dewapriya: Department of Chemistry, Pukyong National University, Busan 608-737, Korea.

Maurizio D'Incalci: Department of Oncology, IRCCS-Istituto di Ricerche Farmacologiche Mario Negri, Milan 20156, Italy.

Sylvatrie-Danne Dinzouna-Boutamba: Department of Parasitology and Tropical Medicine, Kyungpook National University, Daegu 700-422, Korea.

Ying-Chi Du: Graduate Institute of Natural Products, College of Pharmacy, Kaohsiung Medical University, Kaohsiung 807, Taiwan.

Sergey A. Dyshlovoy: Department of Oncology, Hematology and Bone Marrow Transplantation with Section Pneumology, Hubertus Wald-Tumorzentrum, University Medical Center Hamburg-Eppendorf, 20246 Hamburg, Germany; Laboratory of Marine Natural Products Chemistry, G.B. Elyakov Pacific Institute of Bioorganic Chemistry, Far-East Branch, Russian Academy of Sciences, 690022 Vladivostok, Russian Federation; School of Natural Sciences, Far East Federal University, 690022 Vladivostok, Russian Federation.

Hassan Y. Ebrahim: Department of Basic Pharmaceutical Sciences, School of Pharmacy, University of Louisiana at Monroe, 1800 Bienville Drive, Monroe, LA 71201, USA.

Mohamed El-Shazly: Graduate Institute of Natural Products, College of Pharmacy, Kaohsiung Medical University, Kaohsiung 807, Taiwan; Department of Pharmacognosy and Natural Products Chemistry, Faculty of Pharmacy, Ain-Shams University, Organization of African Unity Street, Abassia, Cairo 11566, Egypt.

Svetlana P. Ermakova: G.B. Elyakov Pacific Institute of Bioorganic Chemistry, Far-Eastern Branch of the Russian Academy of Science, Prospect 100 let Vladivostoku, 159, Vladivostok 690022, Russia.

Babak Esmaeelian: School of Biological Sciences, Flinders University, GPO Box 2100, Adelaide, SA 5001, Australia.

Ammad Ahmad Farooqi: Laboratory for Translational Oncology and Personalized Medicine, Rashid Latif Medical College, Lahore 54000, Pakistan.

Sundas Fayyaz: Laboratory for Translational Oncology and Personalized Medicine, Rashid Latif Medical College, Lahore 54000, Pakistan.

Sergey N. Fedorov: G.B. Elyakov Pacific Institute of Bioorganic Chemistry, Far-Eastern Branch of the Russian Academy of Science, Prospect 100 let Vladivostoku, 159, Vladivostok 690022, Russia; Elyakov Pacific Institute of Bioorganic Chemistry, Far-Eastern Branch of the Russian Academy of Science, Prospect 100 let Vladivostoku, 159, Vladivostok 690950, Russia.
Zhong-Ping Feng: Department of Physiology, Faculty of Medicine, University of Toronto, Toronto, ON M5S 1A8, Canada.
Antonio Fernández-Medarde: Biomar Microbial Technologies, Parque Tecnológico de León, Parcela M-10.4, Armunia (León) 24009, Spain.
Metka Filipič: Department of Genetic Toxicology and Cancer Biology, National Institute of Biology, 1000 Ljubljana, Slovenia.
Ahmed I. Foudah: Department of Basic Pharmaceutical Sciences, School of Pharmacy, University of Louisiana at Monroe, 1800 Bienville Drive, Monroe, LA 71201, USA.
Changqing Fu: Qingdao Medical University Affiliated Hospital, Qingdao 266070, China.
Haruhiko Fuwa: Graduate School of Life Sciences, Tohoku University, 2-1-1 Katahira, Aoba-ku, Sendai 980-8577, Japan.
Carlos M. Galmarini: Cell Biology Department, PharmaMar, Avda de los Reyes 1, Pol. Ind. La Mina, Colmenar Viejo, Madrid 28770, Spain; Cell Biology and Pharmacogenomics Department, PharmaMar, Madrid 28770, Spain.
Shu-Shan Gao: Key Laboratory of Experimental Marine Biology, Institute of Oceanology, Chinese Academy of Sciences, Nanhai Road 7, Qingdao 266071, China.
Melissa García-Caballero: Department of Molecular Biology and Biochemistry, Faculty of Sciences, University of Málaga, Campus de Teatinos, Málaga 29071, Spain; Unidad 741 de CIBER "de Enfermedades Raras", University of Málaga, Málaga E-29071, Spain; International Campus of Excellence Andalucía Tech, Málaga 29071, Spain.
William H. Gerwick: Center for Marine Biotechnology and Biomedicine, Scripps Institution of Oceanography and Skaggs School of Pharmacy and Pharmaceutical Sciences, University of California San Diego, La Jolla, CA 920933, USA.
Ivana Grbeša: The Mina and Everard Goodman Faculty of Life Sciences, Bar-Ilan University, Ramaty-Gan 5290002, Israel.
Yong-Yuan Guan: Department of Pharmacology, Zhongshan School of Medicine, Sun Yat-sen University, Guangzhou 510080, China.
Marijana Popović Hadžija: Division of Molecular Medicine, Ruđer Bošković Institute, Zagreb 10000, Croatia.
Tímea Hajdu: Department of Biophysics and Cell Biology, University of Debrecen, Nagyerdei krt. 98, Debrecen 4032, Hungary.
Gerhard Hamilton: Ludwig Boltzmann Cluster of Translational Oncology, A-1090, Vienna, Austria; Department of Surgery, Medical University of Vienna, A-1090 Vienna, Austria.
Geun-Hee Han: College of Pharmacy, Seoul National University, Seoul 151-742, Korea.
S.W.A. Himaya: Marine Bioprocess Research Center, Pukyong National University, Busan 608-737, Korea.

Peter Hohenberger: University of Heidelberg, Mannheim University Medical Center, Interdisciplinary Tumor Center Mannheim, Sarcoma Unit, Theodor-Kutzer-Ufer 1-3, D-68167 Mannheim, Germany.

Friedemann Honecker: Department of Oncology, Hematology and Bone Marrow Transplantation with Section Pneumology, Hubertus Wald-Tumorzentrum, University Medical Center Hamburg-Eppendorf, 20246 Hamburg, Germany; Tumor and Breast Center ZeTuP St. Gallen, 9006 St. Gallen, Switzerland.

Masashi Hosokawa: Faculty of Fisheries Sciences, Hokkaido University, 3-1-1, Minato Cho, Hakodate, Hokkaido 041-8611, Japan.

Lin Hou: College of Life Science, Liaoning Normal University, Dalian 116081, China.

Ming-Feng Hou: Cancer Center, Kaohsiung Medical University Hospital, Kaohsiung Medical University, Kaohsiung 80708, Taiwan; Institute of Clinical Medicine, Kaohsiung Medical University, Kaohsiung 80708, Taiwan; Kaohsiung Municipal Ta-Tung Hospital, Kaohsiung 80145, Taiwan.

Bin Hu: Department of Neurosurgery and Pituitary Tumour Center, The First Affiliated Hospital of Sun Yat-sen University, No.74, Zhongshan Road 2, Guangzhou 510080, China.

Hongbo Huang: CAS Key Laboratory of Tropical Marine Bio-resources and Ecology, Guangdong Key Laboratory of Marine Materia Medica, RNAM Center for Marine Microbiology, South China Sea Institute of Oceanology, Chinese Academy of Sciences, 164 West Xingang Road, Guangzhou 510301, China.

Sammen Huang: Department of Physiology, Faculty of Medicine, University of Toronto, Toronto, ON M5S 1A8, Canada.

Jin-Woo Hwang: Korea Nokyong Research Center, Konkuk University, Chungju 380-701, Korea; Department of Biotechnology, Konkuk University, Chungju 380-701, Korea.

Wen-Ing Hwang: Department of Food Science and Nutrition, Meiho University, Pingtung 91202, Taiwan.

Jin-Won Hyun: Department of Medicine, School of Medicine, Institute of Medical Sciences, Jeju National University, 102 Jejudaehakno, Jeju 690-756, Korea.

Mirna Imešek: Division of Molecular Biology, Ruđer Bošković Institute, Zagreb 10000, Croatia.

Chie Ishikawa: Department of Microbiology and Oncology, Graduate School of Medicine, University of the Ryukyus, 207 Uehara, Nishihara, Okinawa 903-0215, Japan; Transdisciplinary Research Organization for Subtropics and Island Studies, University of the Ryukyus, 1 Senbaru, Nishihara, Okinawa 903-0213, Japan.

Sandeep Jain: Department of Basic Pharmaceutical Sciences, School of Pharmacy, University of Louisiana at Monroe, 1800 Bienville Drive, Monroe, LA 71201, USA.

Jekabsons: Department of Biology, University of Mississippi, University, MS 38677, USA.

Chan-Hee Jeon: Department of Medicine, School of Medicine, Institute of Medical Sciences, Jeju National University, 102 Jejudaehakno, Jeju 690-756, Korea.

You-Jin Jeon: Department of Marine Life Science, Jeju National University, Jeju 690-756, Korea.

Bo Jiang: Institute of Oceanology, Chinese Academy of Sciences, Qingdao 266071, China.

Martin R. Johnston: Flinders Centre for Nanoscale Science and Technology, School of Chemical and Physical Sciences, Flinders University, GPO Box 2100, Adelaide, SA 5001, Australia.

Robin L. Jones: Fred Hutchinson Cancer Research Center, University of Washington, 825 Eastlake Avenue East, G-3630, Seattle, WA 98109-1023, USA.

Jianhua Ju: CAS Key Laboratory of Tropical Marine Bio-resources and Ecology, Guangdong Key Laboratory of Marine Materia Medica, RNAM Center for Marine Microbiology, South China Sea Institute of Oceanology, Chinese Academy of Sciences, 164 West Xingang Road, Guangzhou 510301, China.

Vladimir I. Kalinin: G.B. Elyakov Pacific Institute of Bioorganic Chemistry, Far-Eastern Branch of the Russian Academy of Science, Prospect 100 letya Vladivostoka, 159, Vladivostok 690022, Russia.

Hee-Kyoung Kang: Department of Medicine, School of Medicine, Institute of Medical Sciences, Jeju National University, 102 Jejudaehakno, Jeju 690-756, Korea.

Jung-Il Kang: Department of Medicine, School of Medicine, Institute of Medical Sciences, Jeju National University, 102 Jejudaehakno, Jeju 690-756, Korea.

Bernd Kasper: University of Heidelberg, Mannheim University Medical Center, Interdisciplinary Tumor Center Mannheim, Sarcoma Unit, Theodor-Kutzer-Ufer 1-3, D-68167 Mannheim, Germany.

Harutaka Katano: Department of Pathology, National Institute of Infectious Diseases, 1-23-1 Toyama, Shinjuku, Tokyo 162-8640, Japan.

William R. Kem: Department of Pharmacology and Therapeutics, College of Medicine, University of Florida, Gainesville, FL 32610, USA.

Eun-Ji Kim: Department of Medicine, School of Medicine, Institute of Medical Sciences, Jeju National University, 102 Jejudaehakno, Jeju 690-756, Korea.

Eun-Kyung Kim: Division of Food Bio Science, College of Biomedical and Health Sciences, Konkuk University, Chungju 380-701, Korea; Korea Nokyong Research Center, Konkuk University, Chungju 380-701, Korea.

Ji-Sun Kim: Department of Physiology, Faculty of Medicine, University of Toronto, Toronto, ON M5S 1A8, Canada.

Sanghee Kim: College of Pharmacy, Seoul National University, Seoul 151-742, Korea.

Se-Kwon Kim: Marine Bioprocess Research Center, Pukyong National University, Busan 608-737, Korea; Department of Chemistry, Pukyong National University, Busan 608-737, Korea.

Woo-Jung Kim: College of Pharmacy, Seoul National University, Seoul 151-742, Korea.

Yon-Suk Kim: Korea Nokyong Research Center, Konkuk University, Chungju 380-701, Korea; Department of Biotechnology, Konkuk University, Chungju 380-701, Korea.

Young-Ho Kim: College of Pharmacy, Chungnam National University, Daejeon 305-764, Korea.

Ryuichiro Kimura: Department of Microbiology and Oncology, Graduate School of Medicine, University of the Ryukyus, 207 Uehara, Nishihara, Okinawa 903-0215, Japan; Transdisciplinary Research Organization for Subtropics and Island Studies, University of the Ryukyus, 1 Senbaru, Nishihara, Okinawa 903-0213, Japan.

Anna Király: Department of Biophysics and Cell Biology, University of Debrecen, Nagyerdei krt. 98, Debrecen 4032, Hungary.

Kisung Ko: Department of Medicine, College of Medicine, Chung-Ang University, Seoul 156-756, Korea.

Young-Sang Koh: Department of Medicine, School of Medicine, Institute of Medical Sciences, Jeju National University, 102 Jejudaehakno, Jeju 690-756, Korea.

Katja Kološa: Department of Genetic Toxicology and Cancer Biology, National Institute of Biology, 1000 Ljubljana, Slovenia.

Marina Korolija: Forensic Science Centre "Ivan Vučetić", Zagreb 10000, Croatia.

Sangeetha Ravi Kumar: Faculty of Fisheries Sciences, Hokkaido University, 3-1-1, Minato Cho, Hakodate, Hokkaido 041-8611, Japan.

Dong Hoon Kwak: Department of Biological Science, College of Natural Science, Wonkwang University, Iksan, Jeonbuk 570-749, Korea； Institute for Glycoscience, Wonkwang University, Iksan, Jeonbuk 570-749, Korea.

Jeon-Won Kwak: Department of Medicine, School of Medicine, Institute of Medical Sciences, Jeju National University, 102 Jejudaehakno, Jeju 690-756, Korea.

Jong-Young Kwak: Department of Biochemistry, School of Medicine and Immune-Network Pioneer Research Center, Dong-A University, 32, Daesingongwon-ro, Seo-gu, Busan 602-714, Korea.

Yongseok Kwon: College of Pharmacy, Seoul National University, Seoul 151-742, Korea.

Richard K. Le Leu: Flinders Centre for Innovation in Cancer, Flinders University, GPO Box 2100, Adelaide 5001, Australia; Preventative Health National Research Flagship, CSIRO, PO Box 10041, Adelaide BC 5000, Australia.

Dae Hoon Lee: Department of Biological Science, College of Natural Science, Wonkwang University, Iksan, Jeonbuk 570-749, Korea.

Ji-Hyeok Lee: Department of Marine Life Science, Jeju National University, Jeju 690-756, Korea.

Joo-Youn Lee: College of Pharmacy, Seoul National University, Seoul 151-742, Korea.

Sang Kook Lee: College of Pharmacy, Seoul National University, Seoul 151-742, Korea.

Seung-Hong Lee: Division of Food Bio Science, College of Biomedical and Health Sciences, Konkuk University, Chungju 380-701, Korea; Korea Nokyong Research Center, Konkuk University, Chungju 380-701, Korea.

Stephanie R. Leggett: Marine Immunology Program, Mote Marine Laboratory, 1600 Ken Thompson Parkway, Sarasota, FL 34236, USA; Marine Biomedical Program, Mote Marine Laboratory, 1600 Ken Thompson Parkway, Sarasota, FL 34236, USA.

Ni Lei: Department of Histology and Embryology, Medical school of Sun Yat-sen University, No.74, Zhongshan Road 2, Guangzhou 510080, China; Key Laboratory of Functional Molecules from Marine Microorganisms, Department of Education of Guangdong Province, Sun Yat-sen University, No.74, Zhongshan Road 2, Guangzhou 510080, China.
Brittany Leigh: Marine Immunology Program, Mote Marine Laboratory, 1600 Ken Thompson Parkway, Sarasota, FL 34236, USA; Marine Biomedical Program, Mote Marine Laboratory, 1600 Ken Thompson Parkway, Sarasota, FL 34236, USA.
Rolf Lewensohn: Department of Oncology and Pathology, Karolinska Biomics Center, Karolinska Institutet, 17176 Stockholm, Sweden.
Chun-Shun Li: Key Laboratory of Experimental Marine Biology, Institute of Oceanology, Chinese Academy of Sciences, Nanhai Road 7, Qingdao 266071, China.
Hsing-Hui Li: National Museum of Marine Biology and Aquarium, Pingtung 94450, Taiwan.
Jen-Jie Lin: Graduate Institute of Veterinary Medicine, National Pingtung University of Science and Technology, Pingtung 91202, Taiwan.
Jessalyn Li: Department of Pharmaceutical Sciences, College of Pharmacy and Health Sciences, St. John's University, Queens, NY 11439, USA; Current Address: William A. Shine Great Neck South High School, 341 Lakeville Road, Great Neck, NY 11020, USA.
Jian Li: Qingdao Medical University Affiliated Hospital, Qingdao 266070, China.
Jie Li: CAS Key Laboratory of Tropical Marine Bio-resources and Ecology, Guangdong Key Laboratory of Marine Materia Medica, RNAM Center for Marine Microbiology, South China Sea Institute of Oceanology, Chinese Academy of Sciences, 164 West Xingang Road, Guangzhou 510301, China.
Kun-Tzu Li: Department of Biomedical Science and Environmental Biology, Kaohsiung Medical University, Kaohsiung 80708, Taiwan.
Qiaomei Li: Department of Biotechnology, Dalian Medical University, Dalian 116044, China.
Xiao-Ming Li: Key Laboratory of Experimental Marine Biology, Institute of Oceanology, Chinese Academy of Sciences, Nanhai Road 7, Qingdao 266071, China.
Yong-Xin Li: Marine Bioprocess Research Center, Pukyong National University, Busan 608-737, Korea.
Guangfu Liu: Department of Clinical Biochemistry, Institute of Clinical Laboratory Medicine, Guangdong Provincial Key Laboratory of Medical Molecular Diagnostics, Guangdong Medical College, No. 1 Xincheng Road, Dongguan 523808, China.
Li-Lian Liu: Institute of Marine Biology, National Sun Yat-sen University, Kaohsiung, Taiwan.
Yang Liu: Department of BioMolecular Sciences and Research Institute of Pharmaceutical Sciences, School of Pharmacy, University of Mississippi, University, MS 38677, USA.
Zhichao Liu: Department of Biotechnology, Dalian Medical University, Dalian 116044, China.
Yu-Hsuan Lo: Excellence Biotech Co., Kaohsiung 80655, Taiwan.
Elizabeth T. Loggers: Fred Hutchinson Cancer Research Center, University of Washington, 825 Eastlake Avenue East, G-3630, Seattle, WA 98109-1023, USA.

Carmen-María López-Saiz: Department of Research and Food Science Graduate Program, University of Sonora, Apartado Postal 1658, Hermosillo, Sonora 83000, Mexico.

Mei-Chin Lu: National Museum of Marine Biology & Aquarium, Pingtung 944, Taiwan; Graduate Institute of Marine Biotechnology, National Dong Hwa University, Pingtung 944, Taiwan.

Yan-Hua Lu: State Key Laboratory of Bioreactor Engineering, East China University of Science & Technology, Shanghai 200237, China.

Carl A. Luer: Marine Biomedical Program, Mote Marine Laboratory, 1600 Ken Thompson Parkway, Sarasota, FL 34236, USA.

Jiao Luo: Institute of Oceanology, Chinese Academy of Sciences, Qingdao 266071, China.

Fakhri Mahdi: Department of BioMolecular Sciences and Research Institute of Pharmaceutical Sciences, School of Pharmacy, University of Mississippi, University, MS 38677, USA.

Zhi-Gang Mao: Department of Neurosurgery and Pituitary Tumour Center, The First Affiliated Hospital of Sun Yat-sen University, No.74, Zhongshan Road 2, Guangzhou 510080, China.

Cyr Abel Ogandaga Maranguy: Department of Biological Science, College of Natural Science, Wonkwang University, Iksan, Jeonbuk 570-749, Korea.

Melanija Posavec Marjanović: Division of Molecular Biology, Ruđer Bošković Institute, Zagreb 10000, Croatia.

Monika Mathew: University of Heidelberg, Mannheim University Medical Center, Interdisciplinary Tumor Center Mannheim, Sarcoma Unit, Theodor-Kutzer-Ufer 1-3, D-68167 Mannheim, Germany.

Miguel Ángel Medina: Department of Molecular Biology and Biochemistry, Faculty of Sciences, University of Málaga, Campus de Teatinos, Málaga 29071, Spain; Unidad 741 de CIBER "de Enfermedades Raras", University of Málaga, Málaga E-29071, Spain.

Ekaterina S. Menchinskaya: G.B. Elyakov Pacific Institute of Bioorganic Chemistry, Far-Eastern Branch of the Russian Academy of Science, Prospect 100 letya Vladivostoka, 159, Vladivostok 690022, Russia.

Jodi Miedema: Marine Immunology Program, Mote Marine Laboratory, 1600 Ken Thompson Parkway, Sarasota, FL 34236, USA; Marine Biomedical Program, Mote Marine Laboratory, 1600 Ken Thompson Parkway, Sarasota, FL 34236, USA.

Andreja Mikoč: Division of Molecular Biology, Ruđer Bošković Institute, Zagreb 10000, Croatia.

Kazuo Miyashita: Faculty of Fisheries Sciences, Hokkaido University, 3-1-1, Minato Cho, Hakodate, Hokkaido 041-8611, Japan.

Mohamed M. Mohyeldin: Department of Basic Pharmaceutical Sciences, School of Pharmacy, University of Louisiana at Monroe, 1800 Bienville Drive, Monroe, LA 71201, USA.

J. Brian Morgan: Department of BioMolecular Sciences and Research Institute of Pharmaceutical Sciences, School of Pharmacy, University of Mississippi, University, MS 38677, USA.

Naoki Mori: Department of Microbiology and Oncology, Graduate School of Medicine, University of the Ryukyus, 207 Uehara, Nishihara, Okinawa 903-0215, Japan.
Christine Morrow: Queen's University Belfast, Marine Laboratory, Portaferry BT22 1PF, Northern Ireland, UK.
Ghislain Moussavou: Department of Biological Science, College of Natural Science, Wonkwang University, Iksan, Jeonbuk 570-749, Korea.
Dale G. Nagle: Department of BioMolecular Sciences and Research Institute of Pharmaceutical Sciences, School of Pharmacy, University of Mississippi, University, MS 38677, USA.
Peter Nagy: Department of Biophysics and Cell Biology, University of Debrecen, Nagyerdei krt. 98, Debrecen 4032, Hungary.
David J. Newman: Natural Products Branch, Developmental Therapeutics Program, Division of Cancer Treatment and Diagnosis, Frederick National Laboratory, P.O. Box B, Frederick, MD 21702, USA.
Brice Wilfried Obiang-Obonou: Department of Food Science and Nutrition, Keimyung University, Daegu 704-701, Korea.
Khaled Y. Orabi: Department of Pharmaceutical Chemistry, Faculty of Pharmacy, Health Sciences Center, Kuwait University, Safat 13110, Kuwait.
Laura Paleari: Epidemiology, Biostatistics and Clinical Trials, IRCCS A.O.U. S. Martino-IST, National Institute for Cancer Research, 16132 Genoa, Italy.
Pyo-Jam Park: Korea Nokyong Research Center, Konkuk University, Chungju 380-701, Korea; Department of Biotechnology, Konkuk University, Chungju 380-701, Korea.
David M. Pereira: REQUIMTE/Laboratory of Pharmacognosy, Department of Chemistry, Faculty of Pharmacy, University of Porto, Rua de Jorge Viterbo Ferreira, nº 228, Porto 4050-313, Portugal.
Dragutin Perina: Division of Molecular Biology, Ruđer Bošković Institute, Zagreb 10000, Croatia.
Bradley J. Petek: University of Washington, 1959 NE Pacific St, Seattle, WA 98195, USA.
Daniel Pink: HELIOS Klinikum Bad Saarow, Pieskower Straße 33, D-15526 Bad Saarow, Germany.
Evgeny A. Pisliagin: G.B. Elyakov Pacific Institute of Bioorganic Chemistry, Far-Eastern Branch of the Russian Academy of Science, Prospect 100 letya Vladivostoka, 159, Vladivostok 690022, Russia.
Ordelia Gwenaelle Manvoudou Pissibanganga: Department of Civil and Environmental Engineering, Kookmin University, Seoul 136-702, Korea.
Maribel Plascencia-Jatomea: Department of Research and Food Science Graduate Program, University of Sonora, Apartado Postal 1658, Hermosillo, Sonora 83000, Mexico.
Seth M. Pollack: Fred Hutchinson Cancer Research Center, University of Washington, 825 Eastlake Avenue East, G-3630, Seattle, WA 98109-1023, USA.
Ana R. Quesada: Department of Molecular Biology and Biochemistry, Faculty of Sciences, University of Málaga, Campus de Teatinos, Málaga 29071, Spain; Unidad 741 de CIBER "de Enfermedades Raras", University of Málaga, Málaga E-29071, Spain.

Geraldine Rauch: University of Heidelberg, Institute of Medical Biometry and Informatics, Im Neuenheimer Feld 305, D-69120 Heidelberg, Germany.

Peter Reichardt: HELIOS Klinikum Berlin-Buch, Sarcoma Center Berlin-Brandenburg, Schwanebecker Chaussee 50, D-13125 Berlin, Germany.

Takayoshi Rokkaku: Department of Microbiology and Oncology, Graduate School of Medicine, University of the Ryukyus, 207 Uehara, Nishihara, Okinawa 903-0215, Japan; Department of Orthopedic Surgery, Graduate School of Medicine, University of the Ryukyus, 207 Uehara, Nishihara, Okinawa 903-0215, Japan.

Ralph Rühl: Department of Biochemistry and Molecular Biology, University of Debrecen, Nagyerdei krt. 98, Debrecen 4032, Hungary.

James T. Rutka: Department of Surgery, Faculty of Medicine, University of Toronto, Toronto, ON M5S 1A8, Canada.

Makoto Sasaki: Graduate School of Life Sciences, Tohoku University, 2-1-1 Katahira, Aoba-ku, Sendai 980-8577, Japan.

Mizuho Sato: Graduate School of Life Sciences, Tohoku University, 2-1-1 Katahira, Aoba-ku, Sendai 980-8577, Japan.

Khalid A. El Sayed: Department of Basic Pharmaceutical Sciences, School of Pharmacy, University of Louisiana at Monroe, 1800 Bienville Drive, Monroe, LA 71201, USA.

Masachika Senba: Department of Pathology, Institute of Tropical Medicine, Nagasaki University, 1-12-4 Sakamoto, Nagasaki 852-8523, Japan.

Jae In Seo: College of Pharmacy, Yonsei University, Veritas D, Yonsei International Campus, Songdo-dong, Yeonsu-gu, Incheon 406-840, Korea.

Zhi-Gang She: Department of Histology and Embryology, Medical school of Sun Yat-sen University, No.74, Zhongshan Road 2, Guangzhou 510080, China; Key Laboratory of Functional Molecules from Marine Microorganisms, Department of Education of Guangdong Province, Sun Yat-sen University, No.74, Zhongshan Road 2, Guangzhou 510080, China.

Dayong Shi: Institute of Oceanology, Chinese Academy of Sciences, Qingdao 266071, China.

Silchenko: G.B. Elyakov Pacific Institute of Bioorganic Chemistry, Far-Eastern Branch of the Russian Academy of Science, Prospect 100 letya Vladivostoka, 159, Vladivostok 690022, Russia.

Michaela Sommer: University of Heidelberg, Mannheim University Medical Center, Interdisciplinary Tumor Center Mannheim, Sarcoma Unit, Theodor-Kutzer-Ufer 1-3, D-68167 Mannheim, Germany.

Jayoung Song: College of Pharmacy, Seoul National University, Seoul 151-742, Korea.

Yongxiang Song: CAS Key Laboratory of Tropical Marine Bio-resources and Ecology, Guangdong Key Laboratory of Marine Materia Medica, RNAM Center for Marine Microbiology, South China Sea Institute of Oceanology, Chinese Academy of Sciences, 164 West Xingang Road, Guangzhou 510301, China.

Valentin A. Stonik: G.B. Elyakov Pacific Institute of Bioorganic Chemistry, Far-Eastern Branch of the Russian Academy of Science, Prospect 100 let Vladivostoku, 159, Vladivostok 690022, Russia; Elyakov Pacific Institute of Bioorganic Chemistry, Far-Eastern Branch of the Russian Academy of Science, Prospect 100 let Vladivostoku, 159, Vladivostok 690950, Russia; School of Natural Sciences, Far East Federal University, Vladivostok 690950, Russia.
Chiang-Wen Su: National Museum of Marine Biology & Aquarium, Pingtung 944, Taiwan; Graduate Institute of Marine Biotechnology, National Dong Hwa University, Pingtung 944, Taiwan; Graduate Institute of Marine Biotechnology, National Dong Hwa University, Pingtung 944, Taiwan.
Jui-Hsin Su: National Museum of Marine Biology and Aquarium, Pingtung 94450, Taiwan.
Yin-Di Su: National Museum of Marine Biology & Aquarium, Pingtung 944, Taiwan; Department of Marine Biotechnology and Resources and Asia-Pacific Ocean Research Center, National Sun Yat-sen University, Kaohsiung 804, Taiwan.
Guadalupe-Miroslava Suárez-Jiménez: Department of Research and Food Science Graduate Program, University of Sonora, Apartado Postal 1658, Hermosillo, Sonora 83000, Mexico.
Christopher L. F. Sun: Faculty of Applied Science & Engineering, University of Toronto, Toronto, ON M5S 1A4, Canada.
Hong-Shuo Sun: Department of Physiology, Faculty of Medicine, University of Toronto, Toronto, ON M5S 1A8, Canada; Department of Surgery, Faculty of Medicine, University of Toronto, Toronto, ON M5S 1A8, Canada; Department of Pharmacology, Faculty of Medicine, University of Toronto, Toronto, ON M5S 1A8, Canada; Institute of Medical Science, Faculty of Medicine, University of Toronto, Toronto, ON M5S 1A8, Canada.
János Szöllősi: Department of Biophysics and Cell Biology, University of Debrecen, Nagyerdei krt. 98, Debrecen 4032, Hungary; MTA-DE Cell Biology and Signaling Research Group, University of Debrecen, Nagyerdei krt. 98, Debrecen 4032, Hungary.
Shinji Takeda: Kanehide Bio Co., Ltd., 5-2-2 Nishizaki-cho, Itoman, Okinawa 901-0305, Japan.
Ting Tan: Department of Histology and Embryology, Medical school of Sun Yat-sen University, No.74, Zhongshan Road 2, Guangzhou 510080, China; Key Laboratory of Functional Molecules from Marine Microorganisms, Department of Education of Guangdong Province, Sun Yat-sen University, No.74, Zhongshan Road 2, Guangzhou 510080, China.
Junichi Tanaka: Department of Chemistry, Biology and Marine Science, University of the Ryukyus, 1 Senbaru, Nishihara, Okinawa 903-0213, Japan.
Jen-Yang Tang: Department of Radiation Oncology, Kaohsiung Municipal Ta-Tung Hospital, Kaohsiung 80145, Taiwan; Department of Radiation Oncology, Faculty of Medicine, College of Medicine, Kaohsiung Medical University, Kaohsiung 80708, Taiwan; Department of Radiation Oncology, Kaohsiung Medical University Hospital, Kaohsiung 80708, Taiwan.

Yujiao Tang: Division of Food Bio Science, College of Biomedical and Health Sciences, Konkuk University, Chungju 380-701, Korea； Korea Nokyong Research Center, Konkuk University, Chungju 380-701, Korea.
Natércia Teixeira: Laboratory of Biochemistry, Department of Biological Sciences, Faculty of Pharmacy, University of Porto, Rua de Jorge Viterbo Ferreira, nº 228, Porto 4050-313, Portugal; IBMC—Instituto for Molecular and Cell Biology, University of Porto, Porto 4150-180, Portugal.
Hongming Teng: Department of Biotechnology, Dalian Medical University, Dalian 116044, China.
Chia-Wei Tsao: National Museum of Marine Biology & Aquarium, Pingtung 944, Taiwan.
Nguyen-Huu Tung: College of Pharmacy, Chungnam National University, Daejeon 305-764, Korea.
Tom Turk: Department of Biology, Biotechnical Faculty, University of Ljubljana, 1000 Ljubljana, Slovenia.
Ekaterina Turlova: Department of Physiology, Faculty of Medicine, University of Toronto, Toronto, ON M5S 1A8, Canada.
Patrícia Valentão: REQUIMTE/Laboratory of Pharmacognosy, Department of Chemistry, Faculty of Pharmacy, University of Porto, Rua de Jorge Viterbo Ferreira, nº 228, Porto 4050-313, Portugal.
Frederick A. Valeriote: Department of Internal Medicine, Division of Hematology and Oncology, Henry Ford Hospital, Detroit, MI 48202, USA.
Tímea Váradi: Department of Biophysics and Cell Biology, University of Debrecen, Nagyerdei krt. 98, Debrecen 4032, Hungary.
Kristina Viktorsson: Department of Oncology and Pathology, Karolinska Biomics Center, Karolinska Institutet, 17176 Stockholm, Sweden.
Saurabh G. Vispute: Department of Pharmaceutical Sciences, College of Pharmacy and Health Sciences, St. John's University, Queens, NY 11439, USA.
Catherine J. Walsh: Marine Immunology Program, Mote Marine Laboratory, 1600 Ken Thompson Parkway, Sarasota, FL 34236, USA.
Bin-Gui Wang: Key Laboratory of Experimental Marine Biology, Institute of Oceanology, Chinese Academy of Sciences, Nanhai Road 7, Qingdao 266071, China.
Changhui Wang: Qingdao Medical University Affiliated Hospital, Qingdao 266070, China.
Guan-Lei Wang: Department of Pharmacology, Zhongshan School of Medicine, Sun Yat-sen University, Guangzhou 510080, China; Key Laboratory of Functional Molecules from Oceanic Microorganisms, Department of Education of Guangdong Province, Sun Yat-sen University, Guangzhou 510080, China.
Hai-Jun Wang: Department of Neurosurgery and Pituitary Tumour Center, The First Affiliated Hospital of Sun Yat-sen University, No.74, Zhongshan Road 2, Guangzhou 510080, China.
Huaxin Wang: Department of Biotechnology, Dalian Medical University, Dalian 116044, China.

Lijun Wang: Institute of Oceanology, Chinese Academy of Sciences, Qingdao 266071, China.
Peisheng Wang: Department of Biotechnology, Dalian Medical University, Dalian 116044, China.
Shuaiyu Wang: Institute of Oceanology, Chinese Academy of Sciences, Qingdao 266071, China.
Xin Wang: Department of Histology and Embryology, Medical school of Sun Yat-sen University, No.74, Zhongshan Road 2, Guangzhou 510080, China; Department of Neurosurgery and Pituitary Tumour Center, The First Affiliated Hospital of Sun Yat-sen University, No.74, Zhongshan Road 2, Guangzhou 510080, China; Key Laboratory of Functional Molecules from Marine Microorganisms, Department of Education of Guangdong Province, Sun Yat-sen University, No.74, Zhongshan Road 2, Guangzhou 510080, China.
Yi-Jun Wang: Department of Pharmaceutical Sciences, College of Pharmacy and Health Sciences, St. John's University, Queens, NY 11439, USA.
Zong-Ming Wang: Department of Neurosurgery and Pituitary Tumour Center, The First Affiliated Hospital of Sun Yat-sen University, No.74, Zhongshan Road 2, Guangzhou 510080, China.
Ning Wu: Institute of Oceanology, Chinese Academy of Sciences, Qingdao 266071, China.
Yu-Jen Wu: Department of Biotechnology, Kaohsiung Medical University, Kaohsiung 80761, Taiwan.
Hong Xing: Department of Pharmacology and Therapeutics, College of Medicine, University of Florida, Gainesville, FL 32610, USA.
Lili Yang: Department of Biotechnology, Dalian Medical University, Dalian 116044, China.
Wenbo Yang: Department of Biotechnology, Dalian Medical University, Dalian 116044, China.
Zih-Yan Yang: Graduate Institute of Food Science, National Pingtung University of Science and Technology, Pingtung 91202, Taiwan.
Yao-Tsung Yeh: Department of Medical Laboratory Sciences and Biotechnology, Fooyin University, Kaohsiung 831, Taiwan.
Eun-Sook Yoo: Department of Medicine, School of Medicine, Institute of Medical Sciences, Jeju National University, 102 Jejudaehakno, Jeju 690-756, Korea.
Jennifer E. Yordy: Marine Immunology Program, Mote Marine Laboratory, 1600 Ken Thompson Parkway, Sarasota, FL 34236, USA; Marine Biomedical Program, Mote Marine Laboratory, 1600 Ken Thompson Parkway, Sarasota, FL 34236, USA.
Diaa T. A. Youssef: Department of Natural Products, Faculty of Pharmacy, King Abdulaziz University, 21589 Jeddah, Saudi Arabia.
Chen Zhang: Shanghai Tenth People's Hospital, Tongji University School of Medicine, Shanghai 200072, China.
Hua Zhang: Department of Clinical Biochemistry, Institute of Clinical Laboratory Medicine, Guangdong Provincial Key Laboratory of Medical Molecular Diagnostics, Guangdong Medical College, No. 1 Xincheng Road, Dongguan 523808, China.

Xing Zhang: CAS Key Laboratory of Tropical Marine Bio-resources and Ecology, Guangdong Key Laboratory of Marine Materia Medica, RNAM Center for Marine Microbiology, South China Sea Institute of Oceanology, Chinese Academy of Sciences, 164 West Xingang Road, Guangzhou 510301, China.

Yongchao Zhang: Department of General Surgery, The Affiliated Cancer Hospital of Zhengzhou University/Henan Cancer Hospital, Zhengzhou 450003, Henan, China.

Yun-Kai Zhang: Department of Pharmaceutical Sciences, College of Pharmacy and Health Sciences, St. John's University, Queens, NY 11439, USA.

Xiao Zhong: Department of Physiology, Faculty of Medicine, University of Toronto, Toronto, ON M5S 1A8, Canada; Department of Surgery, Faculty of Medicine, University of Toronto, Toronto, ON M5S 1A8, Canada.

Yu-Dong Zhou: Department of BioMolecular Sciences and Research Institute of Pharmaceutical Sciences, School of Pharmacy, University of Mississippi, MS 38677, USA.

Yong-Hong Zhu: Department of Histology and Embryology, Medical school of Sun Yat-sen University, No.74, Zhongshan Road 2, Guangzhou 510080, China; Key Laboratory of Functional Molecules from Marine Microorganisms, Department of Education of Guangdong Province, Sun Yat-sen University, No.74, Zhongshan Road 2, Guangzhou 510080, China.

Xiangyang Zou: Department of Biotechnology, Dalian Medical University, Dalian 116044, China.

Ana Zovko: Department of Biology, Biotechnical Faculty, University of Ljubljana, 1000 Ljubljana, Slovenia; Department of Oncology and Pathology, Karolinska Biomics Center, Karolinska Institutet, 17176 Stockholm, Sweden.

Tatyana N. Zvyagintseva: G.B. Elyakov Pacific Institute of Bioorganic Chemistry, Far-Eastern Branch of the Russian Academy of Science, Prospect 100 let Vladivostoku, 159, Vladivostok 690022, Russia.

About the Guest Editors

Sergey A. Dyshlovoy, PhD, trained in chemistry and biochemistry in the Russian Federation and in Germany. He started his scientific career in 2006. From 2009 to 2012, he did his PhD in chemistry; specifically, he researched the mechanisms of anticancer action of novel, small-molecule marine bioactive compounds at the G.B. Elyakov Pacific Institute of Bioorganic Chemistry (Vladivostok, Russian Federation). Since 2012, he has been a researcher at this institute and a senior researcher at the Far Eastern Federal University (Vladivostok). Since 2013, he has been a post-doctoral researcher at the University Medical Center Hamburg-Eppendorf. Since 2014, he has been a member of the Commission of Experts of the Russian Scientific Foundation. His main research interest is the investigation of mechanisms of anticancer action of novel marine compounds. He has published over 30 original articles.

Friedemann Honecker, MD, PhD, trained in medicine in Germany and in the UK. In 1999, he started his medical and scientific career in oncology and hematology at the University Medical Center in Tübingen, Germany. From 2002 to 2004, he did his PhD in experimental pathology at Rotterdam Erasmus MC in Rotterdam, NL. From 2005 to 2013, he worked in oncology and hematology at Hamburg University Hospital. Since 2013, he has been working as an oncologist and researcher at the Tumor and Breast Center ZeTuP in St. Gallen, Switzerland. His main research interests are genitourinary cancers, the development of new anti-cancer substances, and the treatment of elderly cancer patients. He has published over 75 original Pub-Med listed articles and reviews, and is the author of numerous book chapters.

Preface

Marine Compounds and Cancer: Where Do We Stand?

In Western countries, cancer is among the most frequent causes of death. Despite striking advances in cancer therapy, there is still an urgent need for new drugs in oncology. Current development favors so called "targeted agents" or drugs that target the immune system, *i.e.*, therapeutic antibodies that enhance or facilitate an immune response against tumor cells (also referred to as "checkpoint inhibitors"). However, until recently, roughly 60% of drugs used in hematology and oncology were originally derived from natural sources, and one third of the top-selling agents are either natural agents or derivatives [1]. There is justified hope for the discovery and development of new anticancer agents from the marine environment. Historically, this habitat has proven to be a rich source of potent natural compounds such as alkaloids, steroids, terpenes, macrolides, peptides, and polyketides, among others. Interestingly, marine agents and cancer treatment have had a special relationship from the beginning. One of the first marine-derived compounds, discovered in 1945 that was later developed into a clinically used drug, was spongothymidine [2–4], which was the lead compound for the discovery of cytarabine [5]. Until today, cytarabine remains one of the most widely used agents in the treatment of acute myeloid leukemia and relapsed aggressive lymphomas.

To date, four marine cytotoxic substances, namely cytarabine, trabectidin, eribulin, and monomethylauristatin E (vedotin, derived from dolastatin 10, as part of an antibody–drug conjugate together with brentuximab), have made their way into clinical routine. Many more are in different phases of testing within clinical trials, and a plethora of substances has already been tested for their *in vitro* and *in vivo* activity.

More and more precise research tools allow the dissection of the molecular mode of action of these cytotoxic substances, thereby uncovering the specific drug targets in cancer cells. This development will potentially blur the edges between "targeted" and "untargeted" therapy in the future, and will hopefully lead to a more targeted use of cancer medicine in general, based on a substance's molecular mode of action and increasing knowledge regarding specific tumor characteristics on an individual level, *i.e.*, by next generation sequencing.

The Special Issue "Marine Compounds and Cancer" (http://www.mdpi.com/journal/marinedrugs/special_issues/marine-compounds-cancer) of the open access journal, *Marine Drugs* (ISSN 1660-3397) was running for two years (2013–2015). It comprises 39 articles in total, a quarter of which are reviews, summarizing the current state of the art in different topics. It covers the full scope from agents with cancer-preventive activity, to novel and previously characterized compounds with anti-cancer activity, both *in vitro* and *in vivo*, and the latest status of clinical development of marine agents used in clinical trials.

The Issue covers a representative selection of different classes of natural or synthetically-derived biomolecules, such as polysaccharides, peptides, lipids, and small-molecule secondary metabolites, isolated from different marine organisms—sponges, ascidia, holothurians, algae,

marine fungi, bacteria, and others. Of note, several research articles and reviews submitted to our Special Issue independently from each other, chose the topic of the anticancer properties of the polysaccharide **fucoidan**, indicating that this compound has become one of the most promising and "hot" topics in the field of marine drugs. Likewise, several articles describe different aspects of **trabectedin**. In contrast to fucoidan, trabectedin may be considered to "have made it already"—it is one of first marine-derived anticancer drugs which has been approved for clinical use.

In the following sections, we want to provide a short overview of what the reader will find (and hopefully will also find interesting!) in this Special Issue.

Review Articles

This Special Issue contains 11 reviews on different topics related to anticancer properties of marine natural compounds. López-Saiz and colleagues from Mexico review the cancer-preventive **lipid compounds from shrimps**, based on their structures and mechanisms of action [6]. Fedorov and colleagues from the Russian Federation discuss structural diversity, biological activity, and the molecular mechanisms of action of **polysaccharides** from different classes of marine organisms, such as macro- and micro-algae, as well as marine fungi, bacteria, and marine animals [7]. Another related review by Kwak from Korea specifically focuses on the polysaccharide **fucoidan**, derived from brown algae. This review provides information on its promising cancer-preventive and anti-cancer activity and mechanism of action both *in vitro* and *in vivo,* and, in addition, summarizes the current status of its preclinical development [8]. A review on the anticancer activity of **small-molecular and polymer compounds isolated from seaweeds** is provided by another Korean group, represented by Moussavou and colleagues [9]. The activity of different compounds, with special emphasis on the polysaccharide fucoidan against colon and breast cancer is reviewed. Kumar and colleagues from Japan contribute a review of the anti-cancer effect of the carotenoid, **fucoxanthin**, including its multiple mechanisms of action *in vitro* and *in vivo* [10]. Newman and Cragg from the USA discuss marine-derived anti-cancer compounds which were under investigation within late pre-clinical development, up to clinical trials in Phases I–III by the end of 2013. Besides cytotoxic (in particular, antibody-drug-conjugates) agents, they also focus on agents that show promising activity against cancer-related pain [11]. Galmarini and colleagues from Italy discuss the mechanisms of action of the marine-derived anti-cancer agents, **trabectedin** and **plitidepsin**. Interestingly, besides direct effects against cancer cells, these substances also exhibit action against the so called tumor microenvironment [12]. Another review on **trabectedin** is provided by Petek and colleagues from the USA. The authors discuss the mechanism of action of the drug, and its activity and development in the treatment of soft tissue sarcomas [13]. Stonik and Fedorov from the Russian Federation provide an up-date on marine cancer preventive **small-molecule compounds**. The literature published between 2003 and 2013 is analyzed, and mechanisms of action are described [14]. Farooqi and colleagues from Pakistan and Taiwan discuss the **ROS modulating effects** of marine-derived compounds, mainly their connection to the regulation

of apoptosis and especially autophagy. The effect of both marine- and non-marine derived autophagy modulators (both inducers and inhibitors) in cancer therapy is discussed [15]. Aminin and colleagues from the Russian Federation summarize recent findings on anticancer activity of **triterpene glycosides** derived from sea cucumbers, and their molecular mechanisms of action [16].

Research Articles

Recent findings in chemistry and biology of anticancer compounds isolated from marine animals can be found in this Special Issue in 28 original research articles. Yang and colleagues from China report the apoptosis-inducing activity of the polysaccharide **fucoidan**, isolated from *Undaria pinnatifida,* in human hepatocellular carcinoma cells *in vitro*. A ROS-mediated mitochondrial pathway is suggested to be critical for this process [17]. Another comparative study analyzing cytotoxic (apoptosis-inducing) effects of native **fucoidan** and **fucoidan lipid nanoparticles** on osteosarcoma cells *in vitro* and *in vivo* is provided by Kimura and colleagues from Japan [18]. Zovco and colleagues from Slovenia, Sweden, USA, and Italy show that **APS8** (a synthetic analog of 3-alkylpyridinium polymer from the marine sponge *Reniera sarai*) inhibits the growth and induces apoptosis in non-small cell lung cancer cells, while normal lung fibroblasts are not affected. APS8 also reduces anti-apoptotic and pro-proliferative effects of nicotine [19]. Li and colleagues from China apply a global proteome screening approach to identify the molecular targets of **sinulariolide** (a compound from the cultured soft coral *Sinularia flexibilis*) in melanoma cells. The results suggest that sinulariolide-induced apoptosis might be related to activation of caspase cascades and mitochondria dysfunction pathways [20]. Li and colleagues from China isolated five new anthranilic acid derivatives, **penipacids A–E**, from the marine sediment-derived fungus *Penicillium paneum* SD-44. Penipacids A and E are cytotoxic to human colon cancer RKO cells [21]. Walsh and colleagues from the USA describe caspase-dependent and mitochondrial pathway-related apoptosis in leukemia cells in response to treatment with **epigonal conditioned medium** from the bonnethead shark, *Sphyrna tiburo* [22]. Su and colleagues from Taiwan and Egypt investigate the mechanism underlying the cytotoxic action of **(1′*R*,5′*S*,6′*S*)-2-(3′,5′-dibromo-1′,6′-dihydroxy-4′-oxocyclohex-2′-enyl) acetonitrile**, previously isolated from the sponge *Pseudoceratina* sp., in leukemia cells. The effect is associated with mitochondrial dysfunction-dependent apoptosis, and the process is mediated by oxidative stress, induced through inhibition of IKK/NFkB and activation of PI3K/Akt pathways [23]. Ishikawa and colleagues from Japan examined anticancer activity and the mode of action of **hippuristanol** isolated from the Okinawan coral, *Isis hippuris,* on primary effusion lymphoma cells. The authors show that this compound induces cell cycle arrest and apoptosis and suppresses several pro-survival pathways *in vitro,* and growth and invasiveness *in vivo* [24]. Esmaeelian and colleagues from Australia report the bioassay guided isolation of semi-pure **tyrindoleninone** and **6-bromoisatin** from an egg mass extract of the marine gastropod, *Dicathais orbita*. The compounds induce apoptosis and G2/M cell cycle arrest in colorectal cancer cells [25]. In a subsequent manuscript, *in vivo* activity of the synthetic 6-

bromoisatin in a mouse model of colorectal cancer cells was reported from the same group [26]. Király and colleagues from Hungary and Spain investigated the effect of hypoxia on the efficiency of the substance **elisidepsin** (**Irvalec®**). The authors show that hypoxia significantly inhibits the anti-tumor effect of elisidepsin, and they show that this is mediated by reduced levels of 2-hydroxy lipids in the cancer cell membranes [27]. Li and colleagues from Korea and China investigated the *in vitro* anti-cancer activity of the alkaloid **fumigaclavine C**, isolated from the marine-derived fungus *Aspergillus fumigatus*, using a breast cancer model. They show regulation of several apoptosis- and proliferation/migration-related proteins, as well as inhibition of the NFkB pathway [28]. Pereira and colleagues from Portugal investigated the effect of an extract of the sea star *Marthasterias glacialis* L. on human breast cancer and neuroblastoma cells. **Palmitic acid** and **ergosta-7,22-dien-3-ol** are the main components of the extract responsible for the anti-cancer activity [29]. García-Caballero and colleagues from Spain report *in vitro* and *in vivo* anti-angiogenetic activity of the **pyrrolidinedione AD0157**, isolated from the marine fungus *Paraconiothyrium* sp. They attribute the activity to an inhibition of the Akt signaling pathway, which could place the substance in the group of targeted agents in the future [30]. Hamilton from Austria investigated the cytotoxic effect of the marine spongean alkaloid **fascaplysin** in small cell lung cancer cells. The mechanism of action appears to be multi-factorial, and can be related to alteration of topoisomerase I activity, impaired integrity of DNA, and ROS generation [31]. Fuwa and colleagues from Japan report the induction of both apoptotic and non-apoptotic cell death by **(−)-8,9-dehydroneopeltolide**—a synthetic analog of the marine macrolide (+)-neopeltolide—under cellular stress conditions. The induction of non-apoptotic cell death was explained by an intracellular ATP depletion induced by the compound [32]. Akl and colleagues from USA, Jordan and Kuwait describe the ability of **araguspongine C** (a macrocyclic oxaquinolizidine alkaloid isolated from the marine sponge *Xestospongia* sp.) to act as a tyrosine kinases receptor inhibitor, providing even more evidence that naturally occurring substances might act like targeted agents. Interestingly, this inhibitory effect induces autophagic cell death in breast cancer cells [33]. Kasper and colleagues from Germany report the results of a Phase I study of gemcitabine in combination with **trabectedin** in advanced soft tissue sarcomas. The study had to be stopped due to excessive toxicity, which adds important clinical information for further development of combination therapies in patients with advanced and/or metastatic leiomyosarcoma or liposarcoma [34]. Kwon and colleagues from Korea present data on the synthesis and *in vitro* anti-cancer activity of derivatives of **pachastrissamine**—a marine sphingolipid initially isolated from the marine sponge *Pachastrissa* sp. An enyne/diene-ene metathesis reaction was used as the key step of the synthesis. One of the derivatives synthesized exhibits more potent sphingosine kinases inhibitory activity in comparison with the mother, pachastrissamine [35]. Wu and colleagues from China describe the anticancer activity of the synthetical **bis-(2,3-Dibromo-4,5-dihydroxy-phenyl)-methane**, initially isolated from marine algae *Rhodomelaceae confervoides*. The compound inhibits proliferation, migration, and invasion of hepatocellular carcinoma cells, which is explained by modulation of the β1-integrin/FAK signaling pathway [36]. Kim and colleagues from Korea investigated the anticancer effect of

(1*S*,2*S*,3*E*,7*E*,11*E*)-3,7,11,15-cembratetraen-17,2-olide, isolated from the marine soft coral *Lobophytum* sp., in fluorouracil-resistant human colon cancer cells. They suggest that the mechanism of action is related to the activation of TGF-β signaling [37]. Song and colleagues from China report the isolation of two new and three previously known C-glycoside **angucyclines** from an extract of the deep-sea sediment bacteria *Streptomyces* sp. Several of these compounds exhibit strong cytotoxic activity in human cancer cells, comparable to cisplatin [38]. Morgan and colleagues from the USA studied bioactivity of the lipopeptide **kalkitoxin**, which was previously isolated from the marine cyanobacteria, *Moorea producens* (*Lyngbya majuscula*). The compound inhibits angiogenesis, disrupts cellular hypoxic signaling, and blocks mitochondrial electron transport in human cancer cells [39]. Wang and colleagues from China describe the ability of the marine anthraquinone derivative **SZ-685C** (isolated from the fungus *Halorosellinia* sp.) to induce apoptosis of primary human nonfunctioning pituitary adenoma cells. The effect is explained by the ability to inhibit the Akt pathway [40]. Kim and colleagues from Korea studied the ability of **dieckol** (or **2,7″-phloroglucinol-6,6′-bieckol**) isolated from brown algae *Ecklonia cava* to inhibit the migration of human breast cancer cells. Expression of several metastasis-related genes is regulated in cancer cells treated with the compound [41]. Zhang and colleagues from China, Saudi Arabia, and the USA report the ability of esters of the **sipholenol A**—a sipholane triterpenoid from the marine sponge *Siphonochalina siphonella*—to specifically reverse P-glycoprotein-mediated multidrug resistance, and *in vitro* and *in silico* analyses are presented [42]. Chen and colleagues from Canada and China describe the suppressive effect of **xyloketal B**, isolated from the mangrove fungus *Xylaria* sp., on glioblastoma cell proliferation and migration. Another "targeted" action via inhibition of TRPM7-regulated PI3K/Akt and MEK/ERK signaling is suggested as the underlying mechanism [43]. Finally, Perina and colleagues from Croatia, Israel, and the United Kingdom studied the role of the highly conservative ***FAU* gene** from the sponge *Suberites domuncula*. The authors describe a pro-apoptotic activity of both spongean and human FAU proteins. These findings provide an opportunity to use pre-bilaterian animals as a simpler model for studying complex interactions in human cancerogenesis [44].

In summary, this Issue covers a broad spectrum of excellent work recently done in the field of marine compounds and cancer. It will serve as a valuable source for current state-of-the-art knowledge in the field, comprising both exciting new research and up-to-date reviews. The guest editors are thankful to all scientists currently working in diverse research institutes, universities, and commercial companies all over the world, namely in Australia, Austria, Canada, China, Croatia, Egypt, Germany, Hungary, Israel, Italy, Japan, Jordan, Korea, Kuwait, Mexico, Pakistan, Portugal, the Russian Federation, Saudi Arabia, Slovenia, Spain, Sweden, Taiwan, the United Kingdom and the USA, who contributed to the success of our Special Issue "Marine Compounds and Cancer". We are all looking forward to new exciting discoveries!

Dr. Sergey A. Dyshlovoy and Dr. Friedemann Honecker
Guest Editors

References

1. Singh, R.; Sharma, M.; Joshi, P.; Rawat, D.S. Clinical status of anti-cancer agents derived from marine sources. *Anticancer Agents Med. Chem.* **2008**, *8*, 603–617.
2. Bergmann, W.; Burke, D.C. Contributions to the Study of Marine Products. XL. The Nucleosides of Sponges.1 IV. Spongosine 2. *J. Org. Chem.* **1956**, *21*, 226–228.
3. Bergmann, W.; Feeney, R.J. Contributions to the study of marine products. XXXII. The nucleosides of spongies. I. *J. Org. Chem.* **1951**, *16*, 981–987.
4. Bergmann, W.; Stempien, M.F. Contributions to the Study of Marine Products. XLIII. The Nucleosides of Sponges. V. The Synthesis of Spongosine 1. *J. Org. Chem.* **1957**, *22*, 1575–1577.
5. Stonik, V. Marine natural products: A way to new drugs. *Acta Naturae* **2009**, *2*, 15–25.
6. López-Saiz, C.-M.; Suárez-Jiménez, G.-M.; Plascencia-Jatomea, M.; Burgos-Hernández, A. Shrimp Lipids: A Source of Cancer Chemopreventive Compounds. *Mar. Drugs* **2013**, *11*, 3926–3950.
7. Fedorov, S.; Ermakova, S.; Zvyagintseva, T.; Stonik, V. Anticancer and Cancer Preventive Properties of Marine Polysaccharides: Some Results and Prospects. *Mar. Drugs* **2013**, *11*, 4876–4901.
8. Kwak, J.-Y. Fucoidan as a Marine Anticancer Agent in Preclinical Development. *Mar. Drugs* **2014**, *12*, 851–870.
9. Moussavou, G.; Kwak, D.; Obiang-Obonou, B.; Maranguy, C.; Dinzouna-Boutamba, S.-D.; Lee, D.; Pissibanganga, O.; Ko, K.; Seo, J.; Choo, Y. Anticancer Effects of Different Seaweeds on Human Colon and Breast Cancers. *Mar. Drugs* **2014**, *12*, 4898–4911.
10. Kumar, S.; Hosokawa, M.; Miyashita, K. Fucoxanthin: A Marine Carotenoid Exerting Anti-Cancer Effects by Affecting Multiple Mechanisms. *Mar. Drugs* **2013**, *11*, 5130–5147.
11. Newman, D.; Cragg, G. Marine-Sourced Anti-Cancer and Cancer Pain Control Agents in Clinical and Late Preclinical Development. *Mar. Drugs* **2014**, *12*, 255–278.
12. Galmarini, C.; Incalci, M.; Allavena, P. Trabectedin and Plitidepsin: Drugs from the Sea that Strike the Tumor Microenvironment. *Mar. Drugs* **2014**, *12*, 719–733.
13. Petek, B.; Loggers, E.; Pollack, S.; Jones, R. Trabectedin in Soft Tissue Sarcomas. *Mar. Drugs* **2015**, *13*, 974–983.
14. Stonik, V.; Fedorov, S. Marine Low Molecular Weight Natural Products as Potential Cancer Preventive Compounds. *Mar. Drugs* **2014**, *12*, 636–671.
15. Farooqi, A.; Fayyaz, S.; Hou, M.-F.; Li, K.-T.; Tang, J.-Y.; Chang, H.-W. Reactive Oxygen Species and Autophagy Modulation in Non-Marine Drugs and Marine Drugs. *Mar. Drugs* **2014**, *12*, 5408–5424.
16. Aminin, D.; Menchinskaya, E.; Pisliagin, E.; Silchenko, A.; Avilov, S.; Kalinin, V. Anticancer Activity of Sea Cucumber Triterpene Glycosides. *Mar. Drugs* **2015**, *13*, 1202–1223.

17. Yang, L.; Wang, P.; Wang, H.; Li, Q.; Teng, H.; Liu, Z.; Yang, W.; Hou, L.; Zou, X. Fucoidan Derived from Undaria pinnatifida Induces Apoptosis in Human Hepatocellular Carcinoma SMMC-7721 Cells via the ROS-Mediated Mitochondrial Pathway. *Mar. Drugs* **2013**, *11*, 1961–1976.
18. Kimura, R.; Rokkaku, T.; Takeda, S.; Senba, M.; Mori, N. Cytotoxic Effects of Fucoidan Nanoparticles against Osteosarcoma. *Mar. Drugs* **2013**, *11*, 4267–4278.
19. Zovko, A.; Viktorsson, K.; Lewensohn, R.; Kološa, K.; Filipič, M.; Xing, H.; Kem, W.; Paleari, L.; Turk, T. APS8, a Polymeric Alkylpyridinium Salt Blocks α7 nAChR and Induces Apoptosis in Non-Small Cell Lung Carcinoma. *Mar. Drugs* **2013**, *11*, 2574–2594.
20. Li, H.-H.; Su, J.-H.; Chiu, C.-C.; Lin, J.-J.; Yang, Z.-Y.; Hwang, W.-I.; Chen, Y.-K.; Lo, Y.-H.; Wu, Y.-J. Proteomic Investigation of the Sinulariolide-Treated Melanoma Cells A375: Effects on the Cell Apoptosis through Mitochondrial-Related Pathway and Activation of Caspase Cascade. *Mar. Drugs* **2013**, *11*, 2625–2642.
21. Li, C.-S.; Li, X.-M.; Gao, S.-S.; Lu, Y.-H.; Wang, B.-G. Cytotoxic Anthranilic Acid Derivatives from Deep Sea Sediment-Derived Fungus *Penicillium paneum* SD-44. *Mar. Drugs* **2013**, *11*, 3068–3076.
22. Walsh, C.; Luer, C.; Yordy, J.; Cantu, T.; Miedema, J.; Leggett, S.; Leigh, B.; Adams, P.; Ciesla, M.; Bennett, C.; Bodine, A. Epigonal Conditioned Media from Bonnethead Shark, *Sphyrna tiburo*, Induces Apoptosis in a T-Cell Leukemia Cell Line, Jurkat E6-1. *Mar. Drugs* **2013**, *11*, 3224–3257.
23. Su, J.-H.; Chen, Y.-C.; El-Shazly, M.; Du, Y.-C.; Su, C.-W.; Tsao, C.-W.; Liu, L.-L.; Chou, Y.; Chang, W.-B.; Su, Y.-D.; *et al*. Towards the Small and the Beautiful: A Small Dibromotyrosine Derivative from *Pseudoceratina* sp. Sponge Exhibits Potent Apoptotic Effect through Targeting IKK/NFκB Signaling Pathway. *Mar. Drugs* **2013**, *11*, 3168–3185.
24. Ishikawa, C.; Tanaka, J.; Katano, H.; Senba, M.; Mori, N. Hippuristanol Reduces the Viability of Primary Effusion Lymphoma Cells both *in Vitro* and *in Vivo*. *Mar. Drugs* **2013**, *11*, 3410–3424.
25. Esmaeelian, B.; Benkendorff, K.; Johnston, M.; Abbott, C. Purified Brominated Indole Derivatives from Dicathais orbita Induce Apoptosis and Cell Cycle Arrest in Colorectal Cancer Cell Lines. *Mar. Drugs* **2013**, *11*, 3802–3822.
26. Esmaeelian, B.; Abbott, C.; Le Leu, R.; Benkendorff, K. 6-Bromoisatin Found in Muricid Mollusc Extracts Inhibits Colon Cancer Cell Proliferation and Induces Apoptosis, Preventing Early Stage Tumor Formation in a Colorectal Cancer Rodent Model. *Mar. Drugs* **2013**, *12*, 17–35.
27. Király, A.; Váradi, T.; Hajdu, T.; Rühl, R.; Galmarini, C.; Szöllősi, J.; Nagy, P. Hypoxia Reduces the Efficiency of Elisidepsin by Inhibiting Hydroxylation and Altering the Structure of Lipid Rafts. *Mar. Drugs* **2013**, *11*, 4858–4875.
28. Li, Y.-X.; Himaya, S. W. A.; Dewapriya, P.; Zhang, C.; Kim, S.-K. Fumigaclavine C from a Marine-Derived Fungus Aspergillus Fumigatus Induces Apoptosis in MCF-7 Breast Cancer Cells. *Mar. Drugs* **2013**, *11*, 5063–5086.

29. Pereira, D.; Correia-da-Silva, G.; Valentão, P.; Teixeira, N.; Andrade, P. Palmitic Acid and Ergosta-7,22-dien-3-ol Contribute to the Apoptotic Effect and Cell Cycle Arrest of an Extract from *Marthasterias glacialis* L. in Neuroblastoma Cells. *Mar. Drugs* **2013**, *12*, 54–68.
30. García-Caballero, M.; Cañedo, L.; Fernández-Medarde, A.; Medina, M.; Quesada, A. The Marine Fungal Metabolite, AD0157, Inhibits Angiogenesis by Targeting the Akt Signaling Pathway. *Mar. Drugs* **2014**, *12*, 279–299.
31. Hamilton, G. Cytotoxic Effects of Fascaplysin against Small Cell Lung Cancer Cell Lines. *Mar. Drugs* **2014**, *12*, 1377–1389.
32. Fuwa, H.; Sato, M.; Sasaki, M. Programmed Cell Death Induced by (−)-8,9-Dehydroneopeltolide in Human Promyelocytic Leukemia HL-60 Cells under Energy Stress Conditions. *Mar. Drugs* **2014**, *12*, 5576–5589.
33. Akl, M.; Ayoub, N.; Ebrahim, H.; Mohyeldin, M.; Orabi, K.; Foudah, A.; Sayed, K. Araguspongine C Induces Autophagic Death in Breast Cancer Cells through Suppression of c-Met and HER2 Receptor Tyrosine Kinase Signaling. *Mar. Drugs* **2015**, *13*, 288–311.
34. Kasper, B.; Reichardt, P.; Pink, D.; Sommer, M.; Mathew, M.; Rauch, G.; Hohenberger, P. Combination of Trabectedin and Gemcitabine for Advanced Soft Tissue Sarcomas: Results of a Phase I Dose Escalating Trial of the German Interdisciplinary Sarcoma Group (GISG). *Mar. Drugs* **2015**, *13*, 379–388.
35. Kwon, Y.; Song, J.; Bae, H.; Kim, W.-J.; Lee, J.-Y.; Han, G.-H.; Lee, S.; Kim, S. Synthesis and Biological Evaluation of Carbocyclic Analogues of Pachastrissamine. *Mar. Drugs* **2015**, *13*, 824–837.
36. Wu, N.; Luo, J.; Jiang, B.; Wang, L.; Wang, S.; Wang, C.; Fu, C.; Li, J.; Shi, D. Marine Bromophenol Bis(2,3-Dibromo-4,5-dihydroxy-phenyl)-methane Inhibits the Proliferation, Migration, and Invasion of Hepatocellular Carcinoma Cells via Modulating β1-Integrin/FAK Signaling. *Mar. Drugs* **2015**, *13*, 1010–1025.
37. Kim, E.-J.; Kang, J.-I.; Kwak, J.-W.; Jeon, C.-H.; Tung, N.-H.; Kim, Y.-H.; Choi, C.-H.; Hyun, J.-W.; Koh, Y.-S.; Yoo, E.-S.; *et al*. The Anticancer Effect of (1*S*,2*S*,3*E*,7*E*,11*E*)-3,7,11,15-Cembratetraen-17,2-olide(LS-1) through the Activation of TGF-β Signaling in SNU-C5/5-FU, Fluorouracil-Resistant Human Colon Cancer Cells. *Mar. Drugs* **2015**, *13*, 1340–1359.
38. Song, Y.; Liu, G.; Li, J.; Huang, H.; Zhang, X.; Zhang, H.; Ju, J. Cytotoxic and Antibacterial Angucycline- and Prodigiosin-Analogues from the Deep-Sea Derived *Streptomyces* sp. SCSIO 11594. *Mar. Drugs* **2015**, *13*, 1304–1316.
39. Morgan, J.; Liu, Y.; Coothankandaswamy, V.; Mahdi, F.; Jekabsons, M.; Gerwick, W.; Valeriote, F.; Zhou, Y.-D.; Nagle, D. Kalkitoxin Inhibits Angiogenesis, Disrupts Cellular Hypoxic Signaling, and Blocks Mitochondrial Electron Transport in Tumor Cells. *Mar. Drugs* **2015**, *13*, 1552–1568.
40. Wang, X.; Tan, T.; Mao, Z.-G.; Lei, N.; Wang, Z.-M.; Hu, B.; Chen, Z.-Y.; She, Z.-G.; Zhu, Y.-H.; Wang, H.-J. The Marine Metabolite SZ-685C Induces Apoptosis in Primary Human Nonfunctioning Pituitary Adenoma Cells by Inhibition of the Akt Pathway *in Vitro*. *Mar. Drugs* **2015**, *13*, 1569–1580.

41. Kim, E.-K.; Tang, Y.; Kim, Y.-S.; Hwang, J.-W.; Choi, E.-J.; Lee, J.-H.; Lee, S.-H.; Jeon, Y.-J.; Park, P.-J. First Evidence that *Ecklonia cava*-Derived Dieckol Attenuates MCF-7 Human Breast Carcinoma Cell Migration. *Mar. Drugs* **2015**, 13, 1785–1797.
42. Zhang, Y.; Zhang, Y.-K.; Wang, Y.-J.; Vispute, S.; Jain, S.; Chen, Y.; Li, J.; Youssef, D.; Sayed, K.; Chen, Z.-S. Esters of the Marine-Derived Triterpene Sipholenol A Reverse P-GP-Mediated Drug Resistance. *Mar. Drugs* **2015**, *13*, 2267–2286.
43. Chen, W.-L.; Turlova, E.; Sun, C.; Kim, J.-S.; Huang, S.; Zhong, X.; Guan, Y.-Y.; Wang, G.-L.; Rutka, J.; Feng, Z.-P.; *et al*. Xyloketal B Suppresses Glioblastoma Cell Proliferation and Migration *in Vitro* through Inhibiting TRPM7-Regulated PI3K/Akt and MEK/ERK Signaling Pathways. *Mar. Drugs* **2015**, *13*, 2505–2525.
44. Perina, D.; Korolija, M.; Hadžija, M.; Grbeša, I.; Belužić, R.; Imešek, M.; Morrow, C.; Marjanović, M.; Bakran-Petricioli, T.; Mikoč, A.; *et al*. Functional and Structural Characterization of FAU Gene/Protein from Marine Sponge *Suberites domuncula*. *Mar. Drugs* **2015**, *13*, 4179–4196.

Shrimp Lipids: A Source of Cancer Chemopreventive Compounds

Carmen-María López-Saiz, Guadalupe-Miroslava Suárez-Jiménez, Maribel Plascencia-Jatomea and Armando Burgos-Hernández

Abstract: Shrimp is one of the most popular seafoods worldwide, and its lipids have been studied for biological activity in both, muscle and exoskeleton. Free fatty acids, triglycerides, carotenoids, and other lipids integrate this fraction, and some of these compounds have been reported with cancer chemopreventive activities. Carotenoids and polyunsaturated fatty acids have been extensively studied for chemopreventive properties, in both *in vivo* and *in vitro* studies. Their mechanisms of action depend on the lipid chemical structure and include antioxidant, anti-proliferative, anti-mutagenic, and anti-inflammatory activities, among others. The purpose of this review is to lay groundwork for future research about the properties of the lipid fraction of shrimp.

Reprinted from *Mar. Drugs*. Cite as: López-Saiz, C.-M.; Suárez-Jiménez, G.-M.; Plascencia-Jatomea, M.; Burgos-Hernández, A. Shrimp Lipids: A Source of Cancer Chemopreventive Compounds. *Mar. Drugs* **2013**, *11*, 3926-3950.

1. Introduction

Shrimp is one of the most popular seafoods of traditional diets [1] worldwide, and the top ten shrimp-producing nations include some of the richest and poorest nations in the world [2]. World shrimp production has increased in the last few years, from 2.85 up to 3.12 million tons (2002 and 2008, respectively) [3]. Shrimp muscle is rich in high quality proteins and minerals, and is low in fat content [1,4]; in addition, its lipids exhibit chemopreventive and chemoprotective activities, which are important biological properties in thin product.

Several biological activities have been reported for methanolic and lipidic extracts from shrimp muscle [5,6] and waste [7]. These activities, which are capable of modifying biological processes [8], have been related to cancer prevention throughout mechanisms grouped in a term called chemoprevention, a term that is used to describe the use of natural or synthetic substances to prevent cancer development [9]. Cancer, the leading cause of death in economically developed countries and second in developing countries [10], affects approximately one of three individuals in Europe and in the United States of America, appearing as one of one hundred different kinds of this disease, with a mortality rate of approximately 20% [11]. By the year 2020, world population is expected to increase up to 7.5 billion, and approximately 17 million new cancer cases will be diagnosed [12].

In addition to socioeconomic status [13,14], geographic variability [13,15], age [16], and physical activity [13,17], nutrition is one of the factors that may influence the development of cancer and other human diseases. Nowadays, changes in the life style that include the consumption of chemopreventive compounds, such as those found in a great variety of foods, are highly

recommended. In this review, the mechanisms of action of compounds that are found in a very popular seafood such as shrimp, especially in its lipidic fraction, will be discussed.

2. Chemoprevention

2.1. Definition of Chemoprevention

Epidemiological studies have provided convincing evidence that naturally occurring bioactive extracts or isolated compounds may benefit human health through the inhibition of carcinogenic processes and cell death mechanisms [18,19]. New technologies and genetic engineering have accounted for unlimited possibilities in scientific discoveries, which have raised a potential for a number of health beneficial products such as chemopreventive compounds [20]; this constitutes an area of research in disease prevention [21]. Chemoprevention was originally defined by Sporn (1976) as the use of natural, synthetic, or biologic chemical agents, in order to reverse, suppress, or prevent cancer progression [9]. Chemoprevention strategies address four goals: inhibition of carcinogens, logical intervention in persons at genetic risk, treatment of pre-malignant lesions, and translation of leads from dietary epidemiology to intervention strategies. Agents that may be useful to achieve at least one of these goals are broadly classified into three categories: blocking agents, suppressing agents, and those that reduce tissue vulnerability to carcinogenesis [22,23].

2.2. Types of Chemopreventive Activities

Chemopreventive compounds can be subdivided according to the benefit they offer to human health; among those are antioxidant, antimutagenic, antiproliferative, antiinflamatory, and antiangiogenic.

Antioxidant chemopreventive compounds prevent or delay oxidation at low concentrations, offering protection against oxidation mainly due to free radicals [24], molecules that are characterized by high reactivity due to non-paired electrons of external orbitals in some of their atoms. Free radicals have mechanisms of action that harm cells and body tissues, damage proteins, DNA, and lipids [25]. Antioxidants prevent cellular damage by reacting with oxidizing free radicals and promoting their elimination from the organism; these free radicals may be present in the cell at an oxidative stress event or during an event induced by an external source such as chemical compounds or ionizing radiation (including singlet oxygen, hydroxyl radical, peroxyl radicals, superoxide anion, hydrogen peroxide, nitric oxide, among others). Antioxidants can be found in foods as micro and macronutrients and may be able to promote the regression of premalignant lesions and inhibit their development into a cancer [26].

Antimutagenic chemopreventive compounds offer protection against cell DNA mutation caused by mutagenic agents (that alters the DNA) and slow cancer initiation [27], while antiproliferative compounds interfere in the cell cycle preventing and/or slowing down uncontrolled cancer cell division.

Inflammation promotes cell proliferation and is linked to carcinogenesis. Although proliferation alone does not cause cancer, a sustained proliferation in an environment rich in inflammatory cells, growth factor, activated stroma, and DNA-damage-promoting agents, potentiates and/or increases neoplastic risk [28]. Anti-inflammatory compounds might help to prevent the development of suitable environments for tumors [21]. Finally, antiangiogenic compounds prevent proliferation of

cancerous cells by reducing the amount of blood nutrients in the tumor environment. Angiogenesis, described as the formation of new blood vessels that allow sustained tumor growth [29], is the result of loss balance between pro- and anti-angiogenic factors.

Molecules with these activities are directed to one or more cancer stages, including anti-initiation, anti-promotional, and anti-progression strategies (Figure 1). Nature is a vast source of novel therapeutic compounds with diverse origins in plants, animals, and marine species, as well as from microorganisms that have been also reported as chemopreventive. Most chemopreventive compounds have been found in fruits and vegetables [30,31]; however, the marine environment, due to its extensive biodiversity, is a rich source of biological active compounds, such as lipids, sterols, proteins, polysaccharides, among others [32–34] yet to be discovered and studied.

Figure 1. Stages during cancer development where chemopreventive compounds exert their activity.

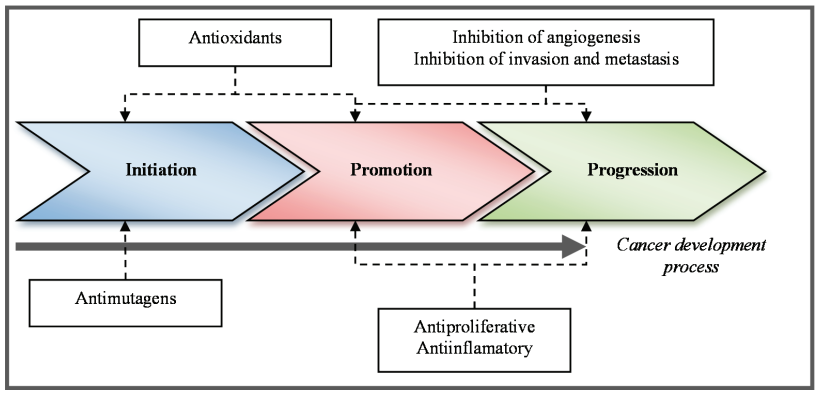

3. Chemopreventive Compounds in the Lipidic Fraction of Shrimp

More than 15,000 natural compounds and extracts have been obtained from marine organisms [35] and have been tested for biological activities. These include compounds such as peptides and depsipeptides, extracted from tunicates, sponges, and mollusks [36]; shark's cartilage [37], and squalamine [38], obtained from the squalidae family; lipidic extracts, isolated from yellowtail fish [39], shrimp [5], and octopus [40]; marine pigments, among others. Some of these, such as carotenoids, appear to fit the criteria for the development of functional food ingredients [34]. Contribution of the marine environment to therapeutic approaches for cancer and other chronic-degenerative diseases are expected to increase in the future [41]. Shrimp is a marine organism in which chemopreventive molecules have been detected, such as lipids and lipophylic compounds. Wilson-Sanchez *et al*. (2010) [5] demonstrated that several compounds in the lipidic fraction of shrimp muscle have antimutagenic and antiproliferative activities. Also, Sindhu and Sherief (2011) [42] proved antioxidant and antiinflamatory activities in carotenoids and lipids obtained from shrimp shell. Different compounds integrate the lipidic fraction of shrimp and their mechanisms of action are diverse, which mainly depend on their chemical structures; these issues will be discussed in the subsequent sections.

3.1. Lipidic Content of Shrimp Muscle

The lipid fraction represents the 1%–2% [43] of shrimp muscle weight (dry basis) and it is integrated by carotenoids, phospholipids, neutral lipids (including cholesterol, triglycerides, free fatty acids, diglycerides, and monoglycerides) and glycolipids. Carotenoids have been studied for chemopreventive properties and they constitute the main group of pigments found in aquatic animals [44] producing colors from yellow to dark red [45]. The main chain of their chemical structure is 40 carbon long, highly unsaturated, inflexible, and easily oxidizable [46], most of them symmetrical around the central carbon atom. These pigments are lipophylic and those with polar hydroxyl and keto functionalities have increased affinities for lipid/water interfaces [47,48]. To date, more than 750 carotenoids have been identified in nature and over 250 of those are from marine origin [49]; nevertheless only 24 have been identified in human tissues.

Fatty acids, known as any aliphatic monocarboxylic acid that may be released by hydrolysis of natural fat [50], have a carboxyl group at the head end and a methyl group at the tail end [51], and constitute the starting point in many lipid structures [52]. Fatty acids can be classified as saturated, monounsaturated, and polyunsaturated, according to the number of double bounds in their structure. The polyunsaturated compounds are characteristic in marine animals. Their mechanisms of action involved in cancer chemoprevention are discussed in the next section.

3.2. Carotenoids

Carotenoids are synthesized by members of the plant kingdom and they are transferred to animals through the food chain [48]. The industrial use of these compounds for animal feed supplementation has been suggested in order to enhance the pigmentation of fish skin and flesh, and also as a human nutraceutical [53]. Since various natural carotenoids (such as zeaxanthin, lycopene, β-cryptoxanthin, fucoxanthin, astaxanthin, capsanthin, crocetin, and phytoene), have proven to have anticarcinogenic activity, they have been proposed for cancer treatment and bio-chemoprevention [54] at concentrations obtained from food supply. Higher concentrations have been related to adverse effects on cellular function, and even augment cancer risk [55].

β-Carotene and cantaxanthin have proved chemopreventive activity in induced skin cancer in female Swiss albino mice [56]; these carotenoids have a protective effect against indirectly-induced skin and breast cancer, and also against directly-induced gastric carcinogenesis [57]. Thus, many studies have been focused on proving that dietary carotenoids are in fact chemopreventive agents, highly valued information that could be used for the benefit of general population.

Shrimp is a source of different carotenoids; the main one found in the Penaeidae family is astaxanthin, a keto-oxycarotenoid that contains oxygen functional groups on the lateral rings, which classifies it among the xanthophylls. This carotenoid is found in high amounts in the exoskeleton of crustaceans, in the flesh of salmon and trout, and in other marine organisms as well [58]. Astaxhantin esters [59,60], β-criptoxanthin, α-carotene, β-carotene [61], meso-zeaxanthin [62], canthaxanthin, lutein, zeaxanthin, and crustacyanin [63] can also be found in this organisms at lower concentrations (Figure 2).

Figure 2. Chemical structure of the main carotenoids found in shrimp.

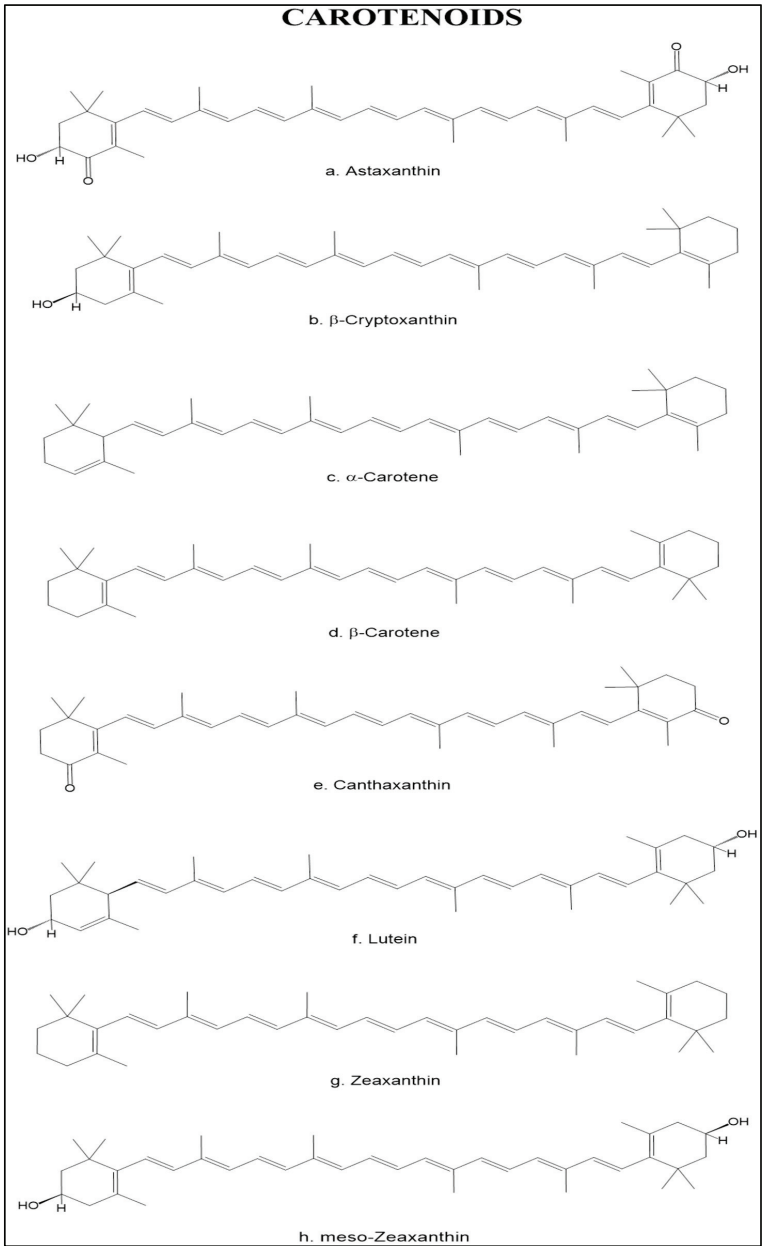

Carotenoids have been associated to cancer prevention, which may undergo by five mechanisms of action: (1) membrane antioxidant [64]; (2) involvement in the control of cell differentiation and proliferation [65]; (3) antimutagenic effect; (4) as anti-inflammatory agents; and (5) their ability to produce an immune response in cancer (Figure 3).

Figure 3. Mechanism of action for chemopreventive/chemoprotective activity of shrimp's carotenoids.

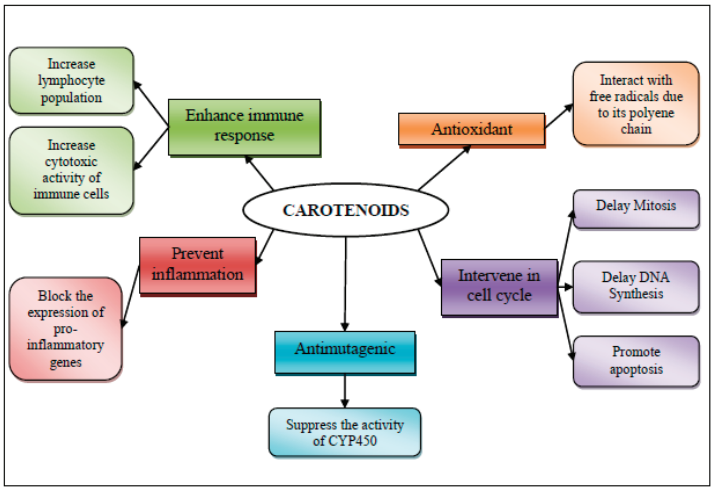

3.2.1. Antioxidant Mechanism

A number of studies have shown that carotenoids act as antioxidants by quenching singlet oxygen and free radicals [66]; this antioxidant activity directly emerges from the molecular structure of carotenoids [64], specifically due to the vibration of the polyene C=C and C–C bonds, where the energy of the singlet state oxygen is transferred to the carotenoid by direct contact [67,68].

The quenching activity of the different carotenoids mainly depends on the number of conjugated double bonds of their molecule and is influenced to a lesser extent by the functional end groups or by the nature of substituent in carotenoids containing cyclic groups [69]. In fact, carotenoids containing nine or more conjugated double bounds in their structure are potent singlet oxygen quenchers, a biological function which is independent of the provitamin A activity [70].

Astaxanthin and its esters, the main carotenoids present in the lipidic fraction of shrimp, have reported strong antioxidant activity in *in vitro* assays, as well as in membrane model system using phospholipid liposomes [7]. This carotenoid has a higher antioxidant activity than α-tocopherol, α-carotene, lutein, β-carotene, lycopene [71], and even higher than trolox [72], a synthetic antioxidant with a known high antioxidant activity. Martínez *et al.* (2008) [73] proposed the creation of a donor-acceptor map by measuring the electro-donating and the electron-accepting power; using this method, astaxanthin had the most effective antiradical effect in terms of its electro-acceptor capacity compared to other dietary carotenoids. This efficient antioxidant capacity is attributed to the unique structure of the terminal ring moiety. Due to these characteristics, astaxanthin may inhibit the production of lipid peroxides [74], as well as maintain the mitochondria in a reduced state even under oxidative challenge [75]. Liang *et al*. (2009) [48] suggested that astaxanthin scavenges radicals in the water/lipid interface and transfers an electron from a non-polar and more reducing carotenoid in the membrane. In cell cultures, astaxanthin has been able to act as an antioxidant even

at high concentrations, when cells are exposed to oxidative stress [76]; however, other studies have reported pro-oxidant behavior in the same concentrations [77–79] this effect is reported when the experimental conditions include a low α-tocopherol diet, this compound usually helps carotenes to be regenerated; if there is an absence it can induce the formation of peroxyl radicals and or augment the rate of carotenoid auto-oxidation.

In *in vivo* studies, astaxanthin attenuates the promotion of hepatic metastasis induced by restraint stress in mice, throughout inhibition of the stress-induced lipid peroxidation [80]. In another study, when rats were exposed to mercuric chloride (a nephrotoxic compound that increases reactive oxygen species by decreasing glutathione levels due to its affinity to SH groups) and astaxanthin, the xantophyl was able prevent the increase of lipid and protein oxidation and attenuated histopathological changes [81].

Although these studies have proved the antioxidant activity of carotenoids, these compounds may shift into a pro-oxidant effect, depending on different factors such as oxygen tension or concentration. Mixtures of carotenoids alone or in association with others antioxidants may increase their activity against lipid peroxidation [69].

3.2.2. Intervention in Cell Cycle

The cell cycle, a sequence of events by which a growing cell duplicates and divides into two identical daughter cells [82], involves numerous regulatory proteins that drive the cell throughout a sequence of specific events called cycle phases: G_1, S, G_2, and M [83]. Cells in G_1 phase can, before commitment to DNA replication, enter into a resisting state called G_0, the state where most non-growing and non-proliferating cells are in human body [84]. G_1 and G_2 phases are the "gaps" in the cell cycle that occur between the two landmarks, DNA synthesis (S) and mitosis (M); during G_1 and G_2 phases, the cell is preparing for DNA synthesis, and for mitosis, respectively [83].

Each of the cell cycle phases involves a number of proteins that regulate cell's progression such as cyclin-dependent kinases (CDKs) and cyclin proteins [83,85]. Cancer cells are frequently associated with genetic or epigenetic alteration and these proteins help cells to sustain proliferation independent of external mitogenic or anti-mitogenic signals [84]; therefore, the regulation of the cell cycle may constitute a strategy to inhibit proliferation of cancer cells. It has been proposed that carotenoids affect differentiation and proliferation of cancerous cells. Different carotenoids (such as α-tocopherol, β-carotene, lycopene, and lutein) show different abilities to control cell cycle [86].

β-Carotene has been associated to both, cell apoptosis and inhibition of cell cycle throughout different mechanisms of action. In the cell cycle of normal human fibroblasts, β-carotene has a delaying effect on the G_1 phase [87] which is related to the expression of $p21^{waf1/cip1}$ protein (an inhibitor of CDK) [88]; in colon cancer, the presence of β-carotene has been associated to a reduced expression of cyclin A (regulator of G_2/M progression) [89]; in leukemia cells, the inhibition of cell cycle progression is attributed to the up-regulation of PPARγ signaling pathway and the expression of Nrf2, an important transcription factor in Keap 1-Nnf2/EpRE/ARE signaling pathway [90]; therefore, the *in vitro* effect of β-carotene on the cell cycle depends on the studied cell line. On the other hand, β-carotene influences and enhances cellular apoptosis by modulating the expression of regulatory genes in cancer cell lines such as colon [89], leukemia [91], melanoma [92], and

breast [93]. The mechanism of action is the suppression of apoptosis blocking proteins (specifically the protiens Bcl-2 and Bcl-xL) [91–93].

Astaxanthin has also been related to both, the inhibition of cell growth and apoptosis, in *in vitro* [94] and *in vivo* [95] studies. The apoptosis mechanism in hepatoma cell cancer has been attributed to depletion of GSH levels [94], and in leukemia cells to down-regulation of Bcl-2 protein [96]. The inhibition of cell cycle progression and apoptosis mechanisms are attributed to the up-regulation of PPARγ signaling pathway and the expression of Nrf2, an important transcription factor in Keap 1-Nnf2/EpRE/ARE signaling pathway [90].

Lycopene has been related to the insulin-like growth factor I (IGF-I); a factor that, at high blood levels, is related to breast and prostate cancer. This carotenoid changes the amount or affinity of IGF-I receptor signaling and cell cycle progression; therefore, lycopene has been related to the inhibition of cell progression at the G_1 phase throughout the reduction of cyclin-dependent kinase (cdk4 and cdk2) [97] as well as the decrease in cyclin D1 and D3 [98]. In other *in vivo* studies including α-tocopherol, β-carotene, lycopene, and mixed carotenoids, in which they were used to treat cancer-induced hamsters, these carotenoids acted as suppressors of the cell cycle inhibiting the expressions of proliferating cell nuclear antigen (PCNA) and cyclin D_1 [86].

3.2.3. Antimutagenic Activity

Individual carotenoids such as astaxanthin and its esters, meso-zeaxanthin, β-carotene, zeaxanthin, α-carotene, among others, as well as their mixture, have been tested in the Ames test [99]. Researchers have found that these structures are able to produce an antimutagenic activity [99,100]. The inhibition of mutagenicity depends on both, the structure of the carotenoid and the mutagenic agent used.

Using sodium azide, ethidium bromide, and hydroxyl amine as control mutagens, astaxanthin and its esters, have shown high antimutagenic activity followed by lutein, β-carotene, violaxanthin, zeaxanthin, and α-carotene; however, a mixture of different carotenoids has shown higher inhibition of induced mutation in *Salmonella typhimurium* tester strains [99]. These results are supported by the study by González de Mejía *et al*. (1998) [100]; they assert that carotenoids have synergistic effect when the tester strains are exposed to 1-6-dinitropyrene (1,6-DNP) and 1,8-dinitropyrene (1,8-DNP) as control mutagens. However, not only those carotenoids have antimutagenic activity, meso-zeaxanthin has also proved biological activity when tested with sodium azide, 4-nitro-*O*-phenylenediane, and *N*-methyl-*N*′-nitro-*N*-nitrosoguanidine, as control mutagens. Meso-zeaxanthin showed 41 to 93% of mutagenesis inhibition in all *Salmonella* tester strains used [62]. β-Carotene also showed positive results when tested against 1-methyl-3-nitro-1-nitrosoguanidine and benzo[a]pyrene as control mutagens in *Salmonella typhimurium* TA100 tester strain [101].

Canthaxanthin and commercial carotene have been able to inhibit neoplastic transformation in cell culture exposed to the carcinogen 3-methylcloranthrene; this inhibition stopped after the removal of the carotenoid treatment [102].

In *in vivo* studies, the antimutagenic activity can be described as the ability of a compound to inhibit the mutagenic effect of a known mutagen in an animal model. In this sense, the mechanism

of action for meso-zeaxanthin is the inhibition of CYP450 enzymes, which was demonstrated in a rat model, where even low concentrations of meso-zeaxanthin showed inhibitory effect towards various isoforms of CYP450 [63]. β-carotene has also proved *in vivo* activity in a Haffkine Swiss mouse tumor model [101], as well as in a Fisher 344 rats model [103] in which cancer was induced with *N*-ethyl-*N*-nitrosourea; the authors attributed the effect the unmetabolized β-carotene molecule, they concluded that this compound is absorbed, stored, and exerted antimutagenic effects against the chemical carcinogen without being transformed in the gastrointestinal tract.

3.2.4. Anti-Inflammatory Mechanism and Tumor Immunity

The mechanism by which carotenoids enhance the immune system is still unclear. Studies have revealed that astaxanthin can prevent inflammatory processes by blocking the expression of pro-inflammatory genes, as a consequence of suppressing the nuclear factor kappaB (NF-κB) activation; moreover, carotenoids inhibits the production of nitric oxide and prostaglandin E2, and the pro-inflammatory cytokines tumor necrosis factor-alpha (TNF-R), as well as the interleukin-1 beta (IL-1β) [104]; this cytokines are molecules that mediate cell-to-cell interactions [105].

The immuno-regulatory action of carotenoids have been demonstrated through their role in tumor immunity [105]. These carotenoids enhance lymphocyte blastogenesis, increase the population of specific lymphocyte subsets, increase lymphocyte cytotoxic activity, and stimulate the production of various cytokines [106].

Wang *et al*. (1989) [107] demonstrated the inhibitory effect of carotenoids (beta-carotene, lycopene, and crocetin) on the growth and development of the C-6 glioma cells inoculated in rats, cells whose growth was inhibited in 57%–67% after 7 weeks without any observable hepatotoxic effect.

Lutein decreases H_2O_2 accumulation by scavenging superoxide and H_2O_2, and the NF-κB regulates inflammatory genes, iNOS, TNF-α, IL-1β, and cyclooxygenase-2, in lipopolysaccharide (LPS)-stimulated macrophages [108].

In other *in vivo* studies, dietary astaxanthin heightened immune response in domestic cats, which was attributed to the enhanced delayed-type of hypersensitivity response, peripheral blood mononuclear cell proliferation, natural killer cell cytotoxic activity, and increased T cell population [109]. In a similar way, dietary astaxanthin in dogs enhances lymphocyte proliferation, and natural killer (NK) cell cytotoxic activity; it also increases concentrations of immunoglobulin G and M (IgG and IgM), and B cell population. Therefore, dietary astaxanthin heightened cell-mediated and humoral immune response, and reduced DNA damage and inflammation in dogs [58,71]. In rats, astaxanthin was able to modulate the expression of NFkB, COX-2, MMPs-2/9, and ERK-2; therefore, it had an anti-inflammatory effect [95].

3.3. Polyunsaturated Fatty Acids

Polyunsaturated fatty acids (PUFAs) in shrimp account for about 40% of the total fatty acid content [110] with about 15% occurring in the form of ω-3 and ω-6 fatty acids such as eicosapentaenoic acid (EPA) and docosahexaenoic acid (DHA) (Figure 4). Therefore, the quality of

the fatty acid profile is similar to that of most of the marine fish species in terms of EPA and DHA content [1]. Both, fat and unsaturated fatty acids contents in shrimp muscle vary with diet [44], species [1], and maturity stage [111]. PUFAs are a subclass of bioactive components divided into two groups ω-6 and ω-3 fatty acids, both studied for cancer chemoprevention [112].

Figure 4. Chemical structure of polyunsaturated acids eicosapentaenoic acid (EPA) and docosahexaenoic acid (DHA).

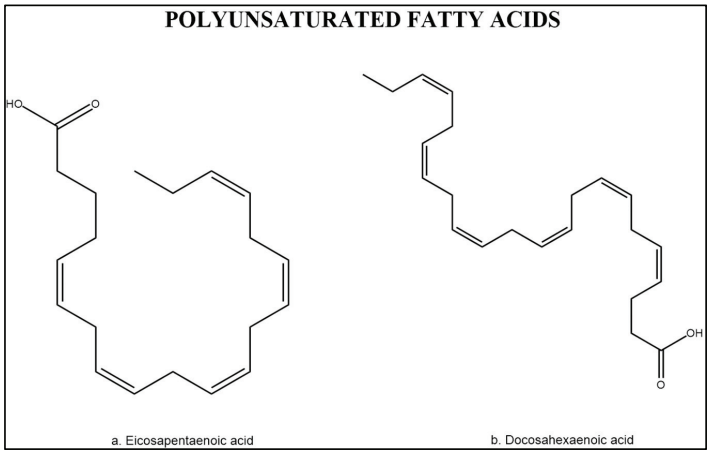

The polyunsaturated fatty acids have been identified to have a role in ameliorating various human diseases [113]. The pioneering epidemiological work on Greenland Inuit [114,115] suggested a possible link between the low incidence of heart diseases and the high consumption of seafood. Recently, the Women's Intervention Nutrition Study (WINS) provided evidence that dietary lipids may influence local or distant recurrences, and in turn influence survivorship of woman in breast cancer treatment [116]. PUFAs uptake has also been inversely related to prostate [117], breast [118], and colorectal [119,120] cancer. Nevertheless, the association between fatty acid consumption and the reduction of cancer is still controversial. Some studies have related it with no effect [121,122] or even an increase in the risk for cancer [123], whereas clinical trials on the effect of polyunsaturated fatty acids are currently being conducted [124]. The inconsistent association observed in epidemiologic studies has been attributed mainly to three reasons [125,126], (1) the intake of the long-chain fatty acids used in the studies was too low to produce a protective effect; (2) in observational research, there has been weakness in estimating PUFAs consumption, mainly due to the difference in oil content between the different species of fish; and (3) the inclusion of low variability within-population in the intake of fish or ω-3 fatty acid.

Zhang *et al*. (2010) [127] proved three different oils diets containing ω-3, ω-6, and ω-9, suggesting that diets rich in ω-3 fatty acid oil attenuates the neoplastic effect of acrylamide-induced neoplasia in mice, while diets rich in ω-6 and ω-9 oils seemed to promote this activity.

The mechanisms of action for the chemopreventive properties of ω-3 fatty acids are presumably five [125]: (1) suppression of arachidonic acid-derived eicosanoid biosynthesis[128]; (2) influence on transcription factor activity [129]; (3) increased or decreased production of free radicals and radical

oxygen species; (4) mechanisms involving insulin sensitivity and membrane fluidity; and (5) antiangiogenic potential (Figure 5).

Figure 5. Mechanisms of action for the chemopreventive/chemoprotective activity of polyunsaturated fatty acids (PUFAs).

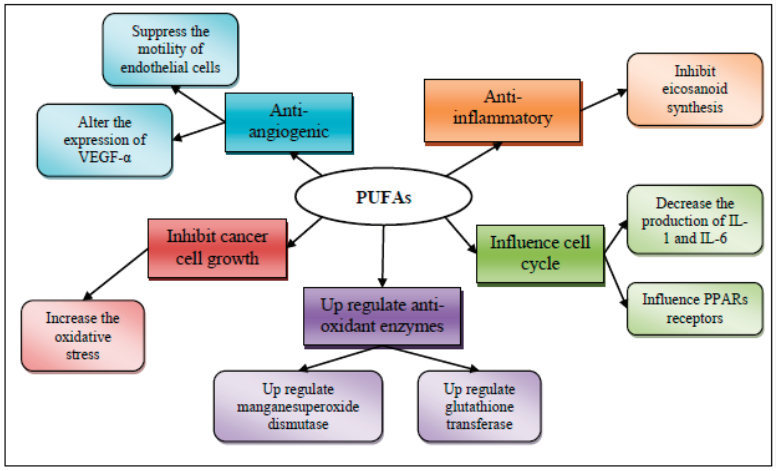

3.3.1. Anti-Inflammatory Effect of Polyunsaturated Fatty Acids

As mentioned above, PUFAs have been associated to cancer chemoprevention through the inhibition of the arachidonic acid-derived eicosanoids formation. These compounds, characterized by 20 carbon long lipophilic molecules derived from arachidonic acid, are powerful regulators of cell function.

The generation process of eicosanoid compounds consists in a series of steps beginning with the mobilization of arachidonic acid from the cellular membrane glycerolipid pools by phospholipase A_2 (PLA_2). Then, arachidonic acid can be oxidized by three different enzymes: (1) the cyclooxigenases (COX-1 and COX-2) to form prostanglandins, protacyclin or tromboxanes; (2) lypoxigenase (LOX) to form 5(S)-, 8(S)-, 12(S)-, and 15(S)-hydroxyeicosatetraenic acid (HETE) leukotrienes, lipoxins, and hepoxilins; and (3) P450 epoxygenase (EOX) to form HETEs and epoxyeicosatrienoic acid (EET) [130].

The overexpression of eicosanoid-forming enzymes [COX, LOX, and prostaglandin E synthase (PGE)] has been related to cancer development in a wide variety of human and animal tumors [131]. These enzymes promote tumor proliferation and angiogenesis, and inhibit apoptosis [132]; for example, COX2 is normally absent in most cells, however, is highly induced in early stages of tumor progression [133].

Some studies have proved that PUFAs enhance the anti-inflammatory response in people with other conditions such as rheumatoid arthritis [134,135], and it has even been concluded that fatty acids can even be used as non-steroidal anti-inflammatory drug (NSAID) in patients with this

pathology [136]. This type of drugs has been reported to be beneficial, since they reduce the risk of developing solid tumors in breast, colon, lung, and prostate cancers [137,138].

Gogos (1998) [139] carried out a randomized prospective study with patients with solid tumors who received fish oil supplementation; patients treated with ω-3 PUFA had an increased immunomodulating effect and prolonged survival.

The anti-inflammatory effect of PUFAs may also be attributed to their action on macrophages [140]; they decrease the production of IL-1, IL-6, and the tumor necrosis factor-α (TNF-α) when feeding ω-3 PUFA containing oil to rats [141].

3.3.2. Influence in Transcription Factor Activity

According to Larsson *et al*. (2004) [125], one of the chemopreventive mechanisms of PUFAs is the modification of gene expression and signal transduction involved in the cell cycle. One of the transcription factor regulated by fatty acids is the peroxisome proliferator-activated receptors (PPARs), which are members of the nuclear hormone receptor family, the largest family of transcription factors [142]. Three PPAR have been identified including PPARα, PPARβ/δ, and PPARγ [143], all of them can be activated by naturally occurring fatty acids or fatty acid derivatives [144]. Their functions underlie a multitude of cellular and physiological processes by directly modulating target gene expression and indirectly modulating other transcription factors [142,143].

The effect of activating PPARβ/δ in cancer models and cancer cell lines depends on the cell line. Colon cancer is the most studied type of cancer and one of the proposed mechanisms of regulation is throughout the up-regulation of the adenomatous polyposis coli (APC)/β-CATENIN/transcription factor 4 (TCF4), pathway in which PPARβ/δ is activated by COX2-derived ligands (such as prostacyclins), leading to the expression of target genes that increase cell proliferation and promote tumor growth. Another proposed mechanism is the ligand activation of PPARβ/δ, which mediates terminal differentiation of colonocytes and inhibits cell proliferation [145]. Most fatty acids are considered PPARs agonist; nevertheless DHA suppresses its activation. This statement was demonstrated by Lee and Hwang (2002) [146] in colon tumor cells (HCT116).

3.3.3. Increased or Decreased Production of Free Radicals and Radical Oxygen Species

Free radicals and reactive oxygen species (ROS) produced in cells seems to attack fatty acids present in the cell, in order to form a variety of by-products from lipid oxidation, including more free radicals and reactive aldehydes [50]. These metabolites potentially generate pro-mutagenic compounds, which eventually can lead to cancer development [147]. Nevertheless, highly polyunsaturated fatty acids, specifically EPA and DHA present in fish oil, have been proved to help up-regulate some antioxidant enzymes such as glutathione transferases and manganese superoxide dismutase in an *in vivo* study with mice [148].

The metabolites from the oxidation of *n*-3 PUFAs inhibit breast [149] and colon [150] cancer cells. This effect, observed in cell culture studies *in vitro*, was related to the formation of lipid peroxidation products, but the inhibitory effect is lost when they are exposed to vitamins that have

antioxidant activity (specifically vitamin C and E [149]). Nevertheless, clinical trials have demonstrated that the DNA damage decreases with the intake of vitamin E when a high intake of PUFAs is taken [151].

3.3.4. Antiangiogenic Potential

A high rate in neovascularization in solid tumors has been associated with a negative prognosis for cancer patients [152,153], since cancerous cells need the nutrients from the vascular system. Therefore, antiangiogenic agents may be helpful in cancer.

EPA [154] has proved *in vitro* antiangiogenic activity with a dose-dependent response for inhibition. PUFAs has also been used in an *in vivo* study, to prove an enhanced response of docetaxel (a drug used for antiangiogenic purposes in chemotherapy) with the aid of DHA [155], where both, micro and macrovascularization in the Sprague-Dawley rat model, were inhibited.

Two mechanisms have been suggested for the anti-angiogenic potential of PUFAs: the suppression of motility of endothelial cells [156], and alterations in the expression of the pro-angiogenic vascular endothelial growth factor (VEGF)-α [157].

3.4. ω-3 Fatty Acids as a Co-Treatment during Chemotherapy

In *in vitro* studies, DHA and/or EPA have been found to improve the cytotoxic effects of several anticancer drugs toward cell lines such as breast, colon, bladder, neuroblastoma, and glioblastoma [158,159]. This observation has also been made in animal models in different types of cancer such as lung, colon, mammary, and prostate [51]. The proposed mechanism of action for this beneficial effects is attributed to the change of the phospholipids in the cell membrane to more polyunsaturated fatty acids, mainly DHA and EPA; this alters the physical properties of the plasma membrane, resulting in an increase in membrane fluidity, enhancing the uptake of the chemotherapy drugs [160]. However, they can only be used at a maximum dose of 0.3 g/kg, according to a phase I clinical trial where adverse effects, mainly diarrhea and vomit, were observed [161].

Xenographic studies have been carried out to explain the benefits of a diet rich in PUFA's in chemotherapy treatment. Atkinson *et al*. (1997) [162] inoculated fibrosarcoma tumor cells into Fisher 344 rats and fed them with diets containing different proportions of safflower oil and DHA oil, and treated them with arabinosylcytosine (AraC) or saline. Authors concluded that consumption of a diet rich in DHA could slow tumor growth, prevent hyperlipidemia, and enhance bone marrow cellularity, compared to a moderate-fat diet rich in ω-6 fatty acids. In a similar work, Cha *et al*. (2002) [163] investigated the effect of dietary supplementation with DHA in combination with AraC chemotherapy and found that DHA diet (1.8 g DHA/kg/day) can be associated with a longer life span and no incidence of death due to drug toxicity; nevertheless, the overconsumption of DHA (up to 4.5 g DHA/kg/day) shorten survival time, increases circulating tumor cell burden, and reduces red blood cell concentration.

The increased permeability of the small intestine of mice caused by methotrexate has been reported. Horie *et al*. (1998) [164] proved that oral administration of DHA protects the small

intestine from the effects of methotrexate by reducing the permeability. Gomez de Segura *et al*. (2004) [165] studied the effect of DHA in male rats treated with 5-fluorouracil (5-FU), an antitumoral drug, and concluded that enriching diet with DHA protects the intestine from lesions produced by 5-FU.

In dogs with lymphoma, treated with doxorubicin chemotherapy in combination with PUFAs and arginine, Ogilvie *et al*. (2000) [166] observed that subjects with higher DHA plasma levels had better diet tolerance, and increased disease free interval and survival time.

A very specific example of the beneficial effects of ω-3 fatty acids was reported by Pardini *et al*. (2005) [167]. They reported that an old man diagnosed with malignant fibrous histiocytoma of the lungs, declined the conventional chemotherapy and elected nutritional intervention by changing his diet to a high ω-3 and low ω-6 supplementation. This study demonstrated that the size of the tumors was reduced, which was attributed to the intake of DHA, specifically to the ω-6/ω-3 ratio.

A proposed mechanism for the effect of the ω-3 fatty acids in chemotherapy is through the inhibition of the NF-κB transduction way, which suggests ω-3 PUFAs may be used during chemotherapy in cancer treatment [168].

4. Conclusions

There is an extensive research effort aimed to obtain efficient chemopreventive compounds in nature, mostly from vegetable sources. However, since the number of cancer cases is constantly increasing, the search, isolation, and study of chemopreventive compounds, has become an important area of research. Many of this research has focused on land organism; however, the great biodiversity that characterizes the marine environment, makes the search for bioactive compounds in this ecosystem a topic of great interest.

The lipidic fraction in shrimp is a source of chemopreventive compounds because its' component, mainly attributed to carotenoids and PUFAs, have proved biological activity in both, *in vivo* and *in vitro* studies, as well as in xenographic research. Carotenoids exert their chemopreventive/chemoprotective activity mainly by four mechanisms: antioxidation, antiproliferation, antimutagenisis, and anti-inflammatory action, and these activities are mainly attributed to their chemical structure. On the other hand, PUFAs exert their chemopreventive potential mainly throughout four mechanisms: antiinflamatory and antiangiogenic activities, the ability to influence the transcription factor activity and the increased or decreased production of free radicals.

PUFAs could also be used as a co-treatment in cancer patients in order to enhance chemotherapy treatment as well as a chemopreventive agent without adverse toxic effects.

Based on the above, the lipidic fraction of shrimp represents an important commodity with high potential for the search of chemopreventive agents. However, in order to select the appropriate compound to be proposed as chemotherapeutic agent, a good knowledge is required concerning the pathways that each type of compound may modulate.

Acknowledgments

The authors wish to thank Mexico's National Council of Science and Technology (CONACyT), for financing grant No. 107102, and for the graduated student scholarships granted to López-Saiz Carmen-María and Suárez-Jiménez Guadalupe-Miroslava.

Conflicts of Interest

The authors declare no conflict of interest.

References

1. Oksuz, A.; Ozylmaz, A.; Aktas, M.; Gercek, G.; Motte, J. A comparative study on proximate, mineral and fatty acid compositions of deep seawater rose shrimp (*Parapenaus longirostris*, Lucas 1846) and red shrimp (*Plesionika martia*, A. Milne-Edwards, 1883). *J. Anim. Vet. Adv.* **2009**, *8*, 183–189.
2. Gillett, R. *Global Study of Shrimp Fisheries*; FAO: Rome, Italy, 2008; Volume 475.
3. FAO. *Cultured Aquatic Species Information Programme. Penaeus Vannamei. Cultured Aquatic Species Information Programme*; FAO Fisheries and Aquaculture Department: Rome, Italy, 2006.
4. Silva, E.; Seidman, C.; Tian, J.; Hudgins, L.; Sacks, F.; Breslow, J. Effects of shrimp consumption on plasma lipoproteins. *Am. J. Clin. Nutr.* **1996**, *64*, 712–717.
5. Wilson-Sanchez, G.; Moreno-Félix, C.; Velazquez, C.; Plascencia-Jatomea, M.; Acosta, A.; Machi-Lara, L.; Aldana-Madrid, M.L.; Ezquerra-Brauer, J.M.; Robles-Zepeda, R.; Burgos-Hernandez, A. Antimutagenicity and antiproliferative studies of lipidic extracts from white shrimp (*Litopenaeus vannamei*). *Mar. Drugs* **2010**, *8*, 2795–809.
6. De Rosenzweig-Pasquel, L.J.; Babbitt, J.K. Isolation and partial characterization of a natural antioxidant from shrimp (*Pandalus jordani*). *J. Food Sci.* **1991**, *56*, 143–145.
7. Sowmya, R.; Sachindra, N.M. Evaluation of antioxidant activity of carotenoid extract from shrimp processing byproducts by *in vitro* assays and in membrane model system. *Food Chem.* **2012**, doi:10.1016/j.foodchem.2012.02.147.
8. Jackson, C.; Esnouf, M.; Winzor, D.; Duewer, D. Defining and measuring biological activity: Applying the principles of metrology. *Accredit. Qual. Assur.* **2007**, *12*, 283–294.
9. Tsao, A.S.; Kim, E.S.; Hong, W.K. Chemoprevention of cancer. *CA Cancer J. Clin.* **2004**, *54*, 150–180.
10. Jemal, A.; Bray, F.; Center, M.; Ferlay, J.; Ward, E.; Forman, D. Global cancer statistics. *CA Cancer J. Clin.* **2011**, *61*, 69–90.
11. Brenner, C.; Duggan, D. *Oncogenomics: Molecular Approaches to Cancer*; John Wiley & Sons, Inc.: Hoboken, NJ, USA, 2005.
12. Bray, F.; Møller, B. Predicting the future burden of cancer. *Nat. Rev. Cancer* **2006**, *6*, 63–74.
13. American Cancer Society. *Cancer Prevention & Early Detection Facts & Figures*; American Cancer Society: Atlanta, GA, USA, 2010.
14. Society, A.C. *Cancer Facts & Figures*; American Cancer Society: Atlanta, GA, USA, 2011.

15. Robbins, S.L.; Kumar, V.; Cotran, R.S. *Patologia Humana*; Elsevier: Madrid, Spain, 2004.
16. Carreca, I.; Balducci, L.; Extermann, M. Cancer in the older person. *Cancer Treat. Rev.* **2005**, *31*, 380–402.
17. Slattery, M.L.; Edwards, S.; Curtin, K.; Ma, K.; Edwards, R.; Holubkov, R.; Schaffer, D. Physical activity and colorectal cancer. *Am. J. Epidemiol.* **2003**, *158*, 214–224.
18. Nerurkar, P.; Ray, R.B. Bitter melon: Antagonist to cancer. *Pharm. Res.* **2010**, *27*, 1049–1053.
19. Wang, Y.K.; He, H.L.; Wang, G.F.; Wu, H.; Zhou, B.C.; Chen, X.L.; Zhang, Y.Z. Oyster (*Crassostrea gigas*) hydrolysates produced on a plant scale have antitumor activity and immunostimulating effects in BALB/c mice. *Mar. Drugs* **2010**, *8*, 255–268.
20. Pelayo-Zaldivar, C. Las frutas y hortalizas como alimentos funcionales. *Contactos* **2003**, *47*, 12–19.
21. Ramawat, K.G.; Goyal, S. Natural Products in Cancer Chemoprevention and Chemotherapy. In *Herbal Drugs: Ethnomedicine to Modern Medicine*; Ramawat, K.G., Ed.; Springer: Berlin, Germany, 2009.
22. Pezzuto, J.M.; Kosmeder, J.W., II; Park, E.-J.; Lee, S.K.; Cuendet, M.; Gills, J.; Bhat, K.; Grubjesic, S.; Hye-Sung Park; Mata-Greenwood, E.; *et al*. Characterization of Natural Product Chemopreventive Agents. In *Cancer Chemoprevention*; Kellof, G.J., Hawk, E.T., Sigman, C.C., Eds.; Humana Press: Totowa, NJ, USA, 2005; Volume 2.
23. Manoharan, S.; Singh, R.B.; Balakrishnan, S. Chemopreventive mechanisms of natural products in oral, mammary and skin carcinogenesis: An overview. *Open Nutraceuticals J.* **2009**, *2*, 52–63.
24. Chipault, J.R. Antioxidants for Use in Foods. In *Autoxidation and Antioxidants*; Lundberg, W.O., Ed.; Wiley: New York, NY, USA, 1962; Volume 2, pp. 477–542.
25. Brambilla, D.; Mancuso, C.; Scuderi, M.R.; Bosco, P.; Cantarella, G.; Lempereur, L.; di Benedetto, G.; Pezzino, S.; Bernardini, R. The role of antioxidant supplement in immune system, neoplastic, and neurodegenerative disorders: A point of view for an assessment of the risk/benefit profile. *Nutr. J.* **2008**, *7*, 29.
26. Kim, S.K.; Thomas, N.V.; Li, X. Anticancer compounds from marine macroalgae and their application as medicinal foods. *Adv. Food Nutr. Res.* **2011**, *64*, 213–224.
27. Shankel, D.M.; Pillai, S.P.; Telikepalli, H.; Menon, S.R.; Pillai, C.A.; Mitscher, L.A. Role of antimutagens/anticarcinogens in cancer prevention. *Biofactors* **2000**, *12*, 113–121.
28. Coussens, L.; Werb, Z. Inflammation and cancer. *Nature* **2002**, *420*, 860–867.
29. Rose, D.P.; Connolly, J.M. Regulation of tumor angiogenesis by dietary fatty acids and eicosanoids. *Nutr. Cancer* **2000**, *37*, 119–127.
30. De Kok, T.; van Breda, S.; Manson, M. Mechanisms of combined action of different chemopreventive dietary compounds. *Eur. J. Nutr.* **2008**, *47*, 51–59.
31. Thomson, C.A.; LeWinn, K.; Newton, T.R.; Alberts, D.S.; Martinez, M.E. Nutrition and diet in the development of gastrointestinal cancer. *Curr. Oncol. Rep.* **2003**, *5*, 192–202.
32. Stankevicins, L.; Aiub, C.; Maria, L.C.; Lobo-Hajdu, G.; Felzenszwalb, I. Genotoxic and antigenotoxic evaluation of extracts from *Arenosclera brasiliensis*, a Brazilian marine sponge. *Toxicol. In Vitro* **2008**, *22*, 1869–1877.

33. De Vries, D.J.; Beart, P.M. Fishing for drugs from the sea: Status and strategies. *Trends Pharmacol*. *Sci*. **1995**, *16*, 275–279.
34. Lordan, S.; Ross, R.P.; Stanton, C. Marine bioactives as functional food ingredients: Potential to reduce the incidence of chronic diseases. *Mar*. *Drugs* **2011**, *9*, 1056–1100.
35. Munro, M.H.G.; Blunt, J.W. *MarinLit, a Marine Literature Database*, version 13.5; Marine Chemistry Group, University of Canterbury: Christchurch, New Zealand, 2007.
36. Suarez-Jimenez, G.M.; Burgos-Hernandez, A.; Ezquerra-Brauer, J.M. Bioactive peptides and depsipeptides with anticancer potential: Sources from marine animals. *Mar*. *Drugs* **2012**, *10*, 963–986.
37. Davis, P.F.; He, Y.; Furneaux, R.H.; Johnston, P.S.; Rüger, B.M.; Slim, G.C. Inhibition of angiogenesis by oral ingestion of powdered shark cartilage in a rat model. *Microvasc*. *Res*. **1997**, *54*, 178–182.
38. Moore, K.S.; Wehrli, S.; Roder, H.; Rogers, M.; Forrest, J.N.; McCrimmon, D.; Zasloff, M. Squalamine: An aminosterol antibiotic from the shark. *Proc*. *Natl*. *Acad*. *Sci*. *USA* **1993**, *90*, 1354–1358.
39. Burgos-Hernandez, A.; Peña-Sarmiento, M.; Moreno-Ochoa, F. Mutagencity and antimutagencity studies of lipidic extracts from yellowtail fish (*Seriola lalandi*), lisa fish (*Mugil cephalus*) and cazón fish (*Mustelus lunulatus*). *Food Chem*. *Toxicol*. **2002**, *40*, 1469–1474.
40. Moreno-Felix, C.; Wilson-Sanchez, G.; Cruz-Ramirez, S.G.; Velazquez-Contreras, C.; Plascencia-Jatomea, M.; Acosta, A.; Machi-Lara, L.; Aldana-Madrid, M.L.; Ezquerra-Brauer, J.M.; Rocha-Alonzo, F.; *et al.* Bioactive lipidic extracts from octopus (*Paraoctopus limaculatus*): Antimutagenicity and antiproliferative studies. *Evid*. *Based Complement*. *Altern*. *Med*. **2013**, *2013*, doi:10.1155/2013/273582.
41. Jimeno, J.; Faircloth, G.; Sousa-Faro, J.M.; Scheuer, P.; Rinehart, K. New marine derived anticancer therapeutics—A journey from the sea to clinical trials. *Mar*. *Drugs* **2004**, *2*, 14–29.
42. Sindhu, S.; Sherief, P.M. Extraction, characterization, antioxidant and anti-inflammatory properties of carotenoids from the shell waste of arabian red shrimp *Aristeus alcocki*, ramadan 1938. *Open Conf*. *Proc*. *J*. **2011**, *2*, 95–103.
43. Ezquerra-Brauer, J.M.; Brignas-Alvarado, L.; Burgos-Hernández, A.; Rouzaud-Sández, O. Control de la Composición Química y Atributos de Calidad de Camarones Cultivados. In *Avances en Nutrición Acuícola VII*, Proceedings of the Memorias del VII Simposium Internacional de Nutrición Acuícola, Hermosillo, Sonora, México, 16–19 November 2004; Suárez, L.E., Ricque Marie, D., Nieto López, M.G., Villarreal, D., Scholz, U., González, M., Eds.; Universidad Autónoma de Nuevo León: Monterrey, México, 2004.
44. Meyers, S.P. Papel del Carotenoide Astaxantina en Nutrición de Especies Acuáticas. In *Avances en Nutrición Acuícola IV*, Proceedings of the Memorias del IV Simposium Internacional de Nutrición Acuícola, La Paz, Baja California Sur, México, 2000; Civera-Cerecedo, R., Pérez-Estrada, C.J., Ricque-Marie, D., Cruz-Suárez, L.E., Eds.; Universidad Autónoma de Nuevo León: Monterrey, México, 2004; pp. 473–491.

45. Latscha, T. The Role of Astaxanthin in Shrimp Pigmentation. In *Advances in Tropical Aquaculture*; Aquacop IFREMER Actes de Collegue: Tahiti, French Polynesia, 1989; Volume 9, pp. 319–325.
46. Olson, J. Absorption, transport, and metabolism of carotenoids in humans. *Pure Appl. Chem.* **1994**, *66*, 1011–1016.
47. Latscha, T. The role of astaxanthin in shrimp pigmentation. *Adv. Trop. Aquac.* **1989**, *9*, 319–325.
48. Liang, J.; Tian, Y.-X.; Yang, F.; Zhang, J.-P.; Skibsted, L.H. Antioxidant synergism between carotenoids in membranes. Astaxanthin as a radical transfer bridge. *Food Chem.* **2009**, *115*, 1437–1442.
49. Maoka, T. Carotenoids in marine animals. *Mar. Drugs* **2011**, *9*, 278–293.
50. Nawar, W.W. Lipids. In *Food Chemistry*, 3rd ed.; Fennema, O.R., Ed.; Marcel Dekker: New York, NY, USA, 1996; pp. 225–320.
51. Hardman, W.E. (*n*-3) Fatty acids and cancer therapy. *J. Nutr.* **2004**, *134*, 3427S–3430S.
52. Akoh, C.C.; Min, D.B. *Food Lipids: Chemistry*, *Nutrition*, *and Biotechnology*, 2nd ed.; Marcel Dekker, Inc.: New York, NY, USA, 2002; p. 464.
53. Cahú, T.B.; Santos, S.D.; Mendes, A.; Córdula, C.R.; Chavante, S.F.; Carvalho, L.B., Jr.; Nader, H.B.; Bezerra, R.S. Recovery of protein, chitin, carotenoids and glycosaminoglycans from Pacific white shrimp (*Litopenaeus vannamei*) processing waste. *Process Biochem.* **2012**, *47*, 570–577.
54. Nishino, H.; Murakosh, M.; Ii, T.; Takemura, M.; Kuchide, M.; Kanazawa, M.; Mou, X.Y.; Wada, S.; Masuda, M.; Ohsaka, Y.; *et al.* Carotenoids in cancer chemoprevention. *Cancer Metastasis Rev.* **2002**, *21*, 257–264.
55. Rock, C.L. Carotenoids and Cancer. In *Carotenoids*; Britton, G., Pfander, H., Liaaen-Jensen, S., Eds.; Birkhäuser Verlag: Berlin, Germany, 2009; Volume 5, pp. 269–286.
56. Santamaria, L.; Bianchi, A.; Arnaboldi, A.; Andreoni, L. Prevention of the benzo(a)pyrene photocarcinogenic effect by beta-carotene and canthaxanthine. Preliminary study. *Boll. Chim. Farm.* **1980**, *119*, 745–748.
57. Santamaria, L.; Bianchi, A. Cancer chemoprevention by supplemental carotenoids in animals and humans. *Prev. Med.* **1989**, *18*, 603–623.
58. Chew, B.P.; Mathison, B.D.; Hayek, M.G.; Massimino, S.; Reinhart, G.A.; Park, J.S. Dietary astaxanthin enhances immune response in dogs. *Vet. Immunol. Immunopathol.* **2011**, *140*, 199–206.
59. Arredondo-Figueroa, J.L.; Pedroza-Islas, R.; Ponce-Palafox, J.T.; Vernon-Carter, E.J. Pigmentation of Pacific white shrimp (*Litopenaeus vannamei*, Boone 1931) with esterified and saponified carotenoids from red chili (*Capsicum annuum*) in comparison to astaxanthin. *Rev. Mex. Ing. Quim.* **2003**, *2*, 101–108.
60. Sánchez-Camargo, A.P.; Almeida Meireles, M.Â.; Lopes, B.L.F.; Cabral, F.A. Proximate composition and extraction of carotenoids and lipids from Brazilian redspotted shrimp waste (*Farfantepenaeus paulensis*). *J. Food Eng.* **2011**, *102*, 87–93.

61. Mezzomo, N.; Maestri, B.; dos Santos, R.L.; Maraschin, M.; Ferreira, S.R.S. Pink shrimp (*P. brasiliensis* and *P. paulensis*) residue: Influence of extraction method on carotenoid concentration. *Talanta* **2011**, *85*, 1383–1391.
62. Firdous, A.; Sindhu, E.; Ramnath, V.; Kuttan, R. Anti-mutagenic and anti-carcinogenic potential of the carotenoid meso-zeaxanthin. *Asian Pac. J. Cancer Prev.* **2010**, *11*, 1795–1800.
63. Babu, C.M.; Chakrabarti, R.; Surya Sambasivarao, K.R. Enzymatic isolation of carotenoid-protein complex from shrimp head waste and its use as a source of carotenoids. *LWT Food Sci. Technol.* **2008**, *41*, 227–235.
64. Vílchez, C.; Forján, E.; Cuaresma, M.; Bédmar, F.; Garbayo, I.; Vega, J.M. Marine carotenoids: Biological functions and commercial applications. *Mar. Drugs* **2011**, *9*, 319–333.
65. Linnewiel, K.; Ernst, H.; Caris-Veyrat, C.; Ben-Dor, A.; Kampf, A.; Salman, H.; Danilenko, M.; Levy, J.; Sharoni, Y. Structure activity relationship of carotenoid derivatives in activation of the electrophile/antioxidant response element transcription system. *Free Radic. Biol. Med.* **2009**, *47*, 659–667.
66. Tsuchiya, M.; Scita, G.; Freisleben, H.-J.; Kagan, V.E.; Packer, L. Antioxidant radical-scavenging activity of carotenoids and retinoids compared to α-tocopherol. *Methods Enzymol.* **1992**, *213*, 460–472.
67. Miki, W. Biological functions and activities of animal carotenoids. *Pure Appl. Chem.* **1991**, *63*, 141–146.
68. Burton, G.W. Antioxidant action of carotenoids. *J. Nutr.* **1989**, *119*, 109–111.
69. Paiva, S.A.; Russell, R.M. Beta-carotene and other carotenoids as antioxidants. *J. Am. Coll. Nutr.* **1999**, *18*, 426–433.
70. Bendich, A.; Canfield, L.; Krinsky, N.; Olson, J. Biological functions of dietary carotenoids. *Ann. N. Y. Acad. Sci.* **1993**, *691*, 61–67.
71. Naguib, Y.M.A. Antioxidant activities of astaxanthin and related carotenoids. *J. Agric. Food Chem.* **2000**, *48*, 1150–1154.
72. Nishida, Y.; Yamashita, E.; Miki, W. Quenching activities of common hydrophilic and lipophilic antioxidants against singlet oxygen using chemiluminescence detection system. *Carotenoid Sci.* **2007**, *11*, 16–20.
73. Martínez, A.; Rodríguez-Gironés, M.A.; Barbosa, A.S.; Costas, M. Donator acceptor map for carotenoids, melatonin and vitamins. *J. Phys. Chem. A* **2008**, *112*, 9037–9042.
74. Goto, S.; Kogure, K.; Abe, K.; Kimata, Y.; Kitahama, K.; Yamashita, E.; Terada, H. Efficient radical trapping at the surface and inside the phospholipid membrane is responsible for highly potent antiperoxidative activity of the carotenoid astaxanthin. *Biochim. Biophys. Acta* **2001**, *1512*, 251–258.
75. Wolf, A.M.; Asoh, S.; Hiranuma, H.; Ohsawa, I.; Iio, K.; Satou, A.; Ishikura, M.; Ohta, S. Astaxanthin protects mitochondrial redox state and functional integrity against oxidative stress. *J. Nutr. Biochem.* **2010**, *21*, 381–389.
76. Jaswir, I.; Kobayashi, M.; Koyama, T.; Kotake-Nara, E.; Nagao, A. Antioxidant behaviour of carotenoids highly accumulated in HepG2 cells. *Food Chem.* **2012**, *132*, 865–872.

77. Palozza, P. Prooxidant actions of carotenoids in biologic systems. *Nutr. Rev*. **1998**, *56*, 257–265.
78. Young, A.J.; Lowe, G.M. Antioxidant and prooxidant properties of carotenoids. *Arch. Biochem. Biophys*. **2001**, *385*, 20–27.
79. Zhang, P.; Omaye, S.T. Antioxidant and prooxidant roles for β-carotene, α-tocopherol and ascorbic acid in human lung cells. *Toxicol. In Vitro* **2001**, *15*, 13–24.
80. Kurihara, H.; Koda, H.; Asami, S.; Kiso, Y.; Tanaka, T. Contribution of the antioxidative property of astaxanthin to its protective effect on the promotion of cancer metastasis in mice treated with restraint stress. *Life Sci*. **2002**, *70*, 2509–2520.
81. Augusti, P.R.; Conterato, G.M.M.; Somacal, S.; Sobieski, R.; Spohr, P.R.; Torres, J.V.; Charão, M.F.; Moro, A.M.; Rocha, M.P.; Garcia, S.C.; *et al*. Effect of astaxanthin on kidney function impairment and oxidative stress induced by mercuric chloride in rats. *Food Chem. Toxicol*. **2008**, *46*, 212–219.
82. Tyson, J.; Novák, B. Cell Cycle Controls. In *Computational Cell Biology*; Fall, C.P., Marland, E.S., Wagner, J.M., Tyson, J.J., Marsden, J.E., Sirovich, L., Wiggins, S., Eds.; Springer: New York, NY, USA, 2002; Volume 20, pp. 261–284.
83. Schafer, K.A. The cell cycle: A review. *Vet. Pathol*. **1998**, *35*, 461–478.
84. Vermeulen, K.; van Bockstaele, D.R.; Berneman, Z.N. The cell cycle: A review of regulation, deregulation and therapeutic targets in cancer. *Cell. Prolif*. **2003**, *36*, 131–149.
85. Clurman, B.E.; Roberts, J.M. Cell cycle and cancer. *J. Natl. Cancer Inst*. **1995**, *87*, 1499–1501.
86. Cheng, H.-C.; Chien, H.; Liao, C.-H.; Yang, Y.-Y.; Huang, S.-Y. Carotenoids suppress proliferating cell nuclear antigen and cyclin D1 expression in oral carcinogenic models. *J. Nutr. Biochem*. **2007**, *18*, 667–675.
87. Stivala, L.A.; Savio, M.; Cazzalini, O.; Pizzala, R.; Rehak, L.; Bianchi, L.; Vannini, V.; Prosperi, E. Effect of beta-carotene on cell cycle progression of human fibroblasts. *Carcinogenesis* **1996**, *17*, 2395–2401.
88. Stivala, L.A.; Savio, M.; Quarta, S.; Scotti, C.; Cazzalini, O.; Rossi, L.; Scovassi, I.A.; Pizzala, R.; Melli, R.; Bianchi, L.; *et al*. The antiproliferative effect of beta-carotene requires p21waf1/cip1 in normal human fibroblasts. *Eur. J. Biochem*. **2000**, *267*, 2290–2296.
89. Palozza, P.; Serini, S.; Maggiano, N.; Angelini, M.; Boninsegna, A.; Di Nicuolo, F.; Ranelletti, F.O.; Calviello, G. Induction of cell cycle arrest and apoptosis in human colon adenocarcinoma cell lines by beta-carotene through down-regulation of cyclin A and Bcl-2 family proteins. *Carcinogenesis* **2002**, *23*, 11–18.
90. Zhang, X.; Zhao, W.-E.; Hu, L.; Zhao, L.; Huang, J. Carotenoids inhibit proliferation and regulate expression of peroxisome proliferators-activated receptor gamma (PPARγ) in K562 cancer cells. *Arch. Biochem. Biophys*. **2011**, *512*, 96–106.
91. Sacha, T.; Zawada, M.; Hartwich, J.; Lach, Z.; Polus, A.; Szostek, M.; Zdzitowska, E.; Libura, M.; Bodzioch, M.; Dembińska-Kieć, A.; *et al.* The effect of β-carotene and its derivatives on cytotoxicity, differentiation, proliferative potential and apoptosis on the three human acute leukemia cell lines: U-937, HL-60 and TF-1. *Biochim. Biophys. Acta* **2005**, *1740*, 206–214.

92. Guruvayoorappan, C.; Kuttan, G. β-Carotene down-regulates inducible nitric oxide synthase gene expression and induces apoptosis by suppressing bcl-2 expression and activating caspase-3 and p53 genes in B16F-10 melanoma cells. *Nutr. Res.* **2007**, *27*, 336–342.
93. Cui, Y.; Lu, Z.; Bai, L.; Shi, Z.; Zhao, W.-E.; Zhao, B. β-Carotene induces apoptosis and up-regulates peroxisome proliferator-activated receptor γ expression and reactive oxygen species production in MCF-7 cancer cells. *Eur. J. Cancer* **2007**, *43*, 2590–2601.
94. Nagaraj, S.; Rajaram, M.G.; Arulmurugan, P.; Baskaraboopathy, A.; Karuppasamy, K.; Jayappriyan, K.R.; Sundararaj, R.; Rengasamy, R. Antiproliferative potential of astaxanthin-rich alga Haematococcus pluvialis Flotow on human hepatic cancer (HepG2) cell line. *Biomed. Prev. Nutr.* **2012**, doi:10.1016/j.bionut.2012.03.009.
95. Nagendraprabhu, P.; Sudhandiran, G. Astaxanthin inhibits tumor invasion by decreasing extracellular matrix production and induces apoptosis in experimental rat colon carcinogenesis by modulating the expressions of ERK-2, NFkB and COX-2. *Investig. New Drugs* **2011**, *29*, 207–224.
96. Song, X.D.; Zhang, J.J.; Wang, M.R.; Liu, W.B.; Gu, X.B.; Lv, C.J. Astaxanthin induces mitochondria-mediated apoptosis in rat hepatocellular carcinoma CBRH-7919 cells. *Biol. Pharm. Bull.* **2011**, *34*, 839–844.
97. Karas, M.; Amir, H.; Fishman, D.; Danilenko, M.; Segal, S.; Nahum, A.; Koifmann, A.; Giat, Y.; Levy, J.; Sharoni, Y. Lycopene interferes with cell cycle progression and insulin-like growth factor I signaling in mammary cancer cells. *Nutr. Cancer* **2000**, *36*, 101–111.
98. Nahum, A.; Hirsch, K.; Danilenko, M.; Watts, C.K.; Prall, O.W.; Levy, J.; Sharoni, Y. Lycopene inhibition of cell cycle progression in breast and endometrial cancer cells is associated with reduction in cyclin D levels and retention of p27(Kip1) in the cyclin E-cdk2 complexes. *Oncogene* **2001**, *20*, 3428–3436.
99. Bhagavathy, S.; Sumathi, P.; Madhushree, M. Antimutagenic assay of carotenoids from green algae Chlorococcum humicola using Salmonella typhimurium TA98, TA100 and TA102. *Asian Pac. J. Trop. Dis.* **2011**, *1*, 308–316.
100. González de Mejía, E.; Quintanar-Hernández, J.A.; Loarca-Piña, G. Antimutagenic activity of carotenoids in green peppers against some nitroarenes. *Mutat. Res.* **1998**, *416*, 11–19.
101. Azuine, M.A.; Goswami, U.C.; Kayal, J.J.; Bhide, S.V. Antimutagenic and anticarcinogenic effects of carotenoids and dietary palm oil. *Nutr. Cancer* **1992**, *17*, 287–295.
102. Merriman, R.L.; Bertram, J.S. Reversible inhibition by retinoids of 3-methylcholanthrene-induced neoplastic transformation in C3H/10T1/2 clone 8 cells. *Cancer Res.* **1979**, *39*, 1661–1666.
103. Aidoo, A.; Lyncook, L.; Lensing, S.; Bishop, M.; Wamer, W. *In-vivo* antimutagenic activity of beta-carotene in rat spleen lymphocytes. *Carcinogenesis* **1995**, *16*, 2237–2241.
104. Hussein, G.; Sankawa, U.; Goto, H.; Matsumoto, K.; Watanabe, H. Astaxanthin, a carotenoid with potential in human health and nutrition. *J. Nat. Prod.* **2006**, *69*, 443–449.
105. Chew, B.P.; Park, J.S. Carotenoid action on the immune response. *J. Nutr.* **2004**, *134*, 257S–261S.
106. Chew, B.P. Role of Carotenoids in the Immune Response. *J. Dairy Sci.* **1993**, *76*, 2804–2811.

107. Wang, C.J.; Chou, M.Y.; Lin, J.K. Inhibition of growth and development of the transplantable C-6 glioma cells inoculated in rats by retinoids and carotenoids. *Cancer Lett*. **1989**, *48*, 135–142.
108. Kim, J.H.; Na, H.J.; Kim, C.K.; Kim, J.Y.; Ha, K.S.; Lee, H.; Chung, H.T.; Kwon, H.J.; Kwon, Y.G.; Kim, Y.M. The non-provitamin A carotenoid, lutein, inhibits NF-kappaB-dependent gene expression through redox-based regulation of the phosphatidylinositol 3-kinase/PTEN/Akt and NF-kappaB-inducing kinase pathways: Role of H(2)O(2) in NF-kappaB activation. *Free Radic*. *Biol*. *Med*. **2008**, *45*, 885–896.
109. Park, J.S.; Mathison, B.D.; Hayek, M.G.; Massimino, S.; Reinhart, G.A.; Chew, B.P. Astaxanthin stimulates cell-mediated and humoral immune responses in cats. *Vet*. *Immunol*. *Immunopathol*. **2011**, *144*, 455–461.
110. De Moura, A.; Torres, R.; Mancini, J.; Tenuta, A. Characterization of the lipid portion of pink shrimp commercial samples. *Arch*. *Latinoam Nutr*. **2002**, *52*, 207–211.
111. Kher-un-Nisa; Sultana, R. Variation in the proximate composition of shrimp, *Fenneropenaeus penicillatus* at different stages of maturity. *Pak*. *J*. *Biochem*. *Mol*. *Biol*. **2010**, *43*, 135–139.
112. Bougnoux, P.; Hajjaji, N.; Maheo, K.; Couet, C.; Chevalier, S. Fatty acids and breast cancer: Sensitization to treatments and prevention of metastatic re-growth. *Prog*. *Lipid Res*. **2010**, *49*, 76–86.
113. Sahena, F.; Zaidul, I.; Jinap, S.; Saari, N.; Jahurul, H.; Abbas, K.; Norulaini, N. PUFAs in fish: Extraction, fractionation, importance in health. *Compr*. *Rev*. *Food Sci*. *Food Safety* **2009**, *8*, 59–74.
114. Dyerberg, J.; Bang, H.O. Haemostatic function and platelet polyunsaturated fatty acids in Eskimos. *Lancet* **1979**, *2*, 433–435.
115. Dyerberg, J. Linolenate-derived polyunsaturated fatty acids and prevention of atherosclerosis. *Nutr*. *Rev*. **1986**, *44*, 125–134.
116. Chlebowski, R.T.; Blackburn, G.L.; Thomson, C.A.; Nixon, D.W.; Shapiro, A.; Hoy, M.K.; Goodman, M.T.; Giuliano, A.E.; Karanja, N.; McAndrew, P.; *et al*. Dietary fat reduction and breast cancer outcome: Interim efficacy results from the Women's Intervention Nutrition Study. *J*. *Natl*. *Cancer Inst*. **2006**, *98*, 1767–1776.
117. Augustsson, K.; Michaud, D.S.; Rimm, E.B.; Leitzmann, M.F.; Stampfer, M.J.; Willett, W.C.; Giovannucci, E. A prospective study of intake of fish and marine fatty acids and prostate cancer. *Cancer Epidemiol*. *Biomark*. *Prev*.**2003**, *12*, 64–67.
118. Shannon, J.; King, I.B.; Moshofsky, R.; Lampe, J.W.; Gao, D.L.; Ray, R.M.; Thomas, D.B. Erythrocyte fatty acids and breast cancer risk: A case-control study in Shanghai, China. *Am*. *J*. *Clin*. *Nutr*. **2007**, *85*, 1090–1097.
119. Caygill, C.P.; Hill, M.J. Fish, *n*-3 fatty acids and human colorectal and breast cancer mortality. *Eur*. *J*. *Cancer Prev*. **1995**, *4*, 329–332.
120. De Deckere, E.A. Possible beneficial effect of fish and fish *n*-3 polyunsaturated fatty acids in breast and colorectal cancer. *Eur*. *J*. *Cancer Prev*. **1999**, *8*, 213–221.

121. Virtanen, J.K.; Mozaffarian, D.; Chiuve, S.E.; Rimm, E.B. Fish consumption and risk of major chronic disease in men. *Am. J. Clin. Nutr.* **2008**, *88*, 1618–1625.
122. Simon, J.A.; Fong, J.; Bernert, J.T.; Browner, W.S. Serum fatty acids and the risk of fatal cancer. MRFIT research group. Multiple risk factor intervention trial. *Am. J. Epidemiol.* **1998**, *148*, 854–858.
123. Williams, C.D.; Whitley, B.M.; Hoyo, C.; Grant, D.J.; Iraggi, J.D.; Newman, K.A.; Gerber, L.; Taylor, L.A.; McKeever, M.G.; Freedland, S.J. A high ratio of dietary *n*-6/*n*-3 polyunsaturated fatty acids is associated with increased risk of prostate cancer. *Nutr. Res.* **2011**, *31*, 1–8.
124. Manson, J.E.; Bassuk, S.S.; Lee, I.M.; Cook, N.R.; Albert, M.A.; Gordon, D.; Zaharris, E.; Macfadyen, J.G.; Danielson, E.; Lin, J.; *et al.* The VITamin D and OmegA-3 TriaL (VITAL): Rationale and design of a large randomized controlled trial of vitamin D and marine omega-3 fatty acid supplements for the primary prevention of cancer and cardiovascular disease. *Contemp. Clin. Trials* **2012**, *33*, 159–171.
125. Larsson, S.C.; Kumlin, M.; Ingelman-Sundberg, M.; Wolk, A. Dietary long-chain *n*-3 fatty acids for the prevention of cancer: A review of potential mechanisms. *Am. J. Clin. Nutr.* **2004**, *79*, 935–945.
126. Hull, M.A. Omega-3 polyunsaturated fatty acids. *Best Pract. Res. Clin. Gastroenterol.* **2011**, *25*, 547–554.
127. Zhang, X.; Zhao, C.; Jie, B. Various dietary polyunsaturated fatty acids modulate acrylamide-induced preneoplatic urothelial proliferation and apoptosis in mice. *Exp. Toxicol. Pathol.* **2010**, *62*, 9–16.
128. Nicosia, S.; Patrono, C. Eicosanoid biosynthesis and action: Novel opportunities for pharmacological intervention. *FASEB J.* **1989**, *3*, 1941–1948.
129. Bordoni, A.; Di Nunzio, M.; Danesi, F.; Biagi, P.L. Polyunsaturated fatty acids: From diet to binding to ppars and other nuclear receptors. *Genes Nutr.* **2006**, *1*, 95–106.
130. Nie, D.; Che, M.; Grignon, D.; Tang, K.; Honn, K.V. Role of Eicosanoids in Prostate Cancer Progression. In *Prostate Cancer: New Horizons in Research and Treatment*; Cher, M.L., Raz, A., Honn, K.V., Eds.; Kluwer Academic Publishers: New York, NY, USA, 2002.
131. Marks, F.; Müller-Decker, K.; Fürstenberger, G. A causal relationship between unscheduled eicosanoid signaling and tumor development: Cancer chemoprevention by inhibitors of arachidonic acid metabolism. *Toxicology* **2000**, *153*, 11–26.
132. Bunn, P.A., Jr.; Keith, R.L. The future of cyclooxygenase-2 inhibitors and other inhibitors of the eicosanoid signal pathway in the prevention and therapy of lung cancer. *Clin. Lung Cancer* **2002**, *3*, 271–277.
133. Dubois, R.N.; Abramson, S.B.; Crofford, L.; Gupta, R.A.; Simon, L.S.; van de Putte, L.B.; Lipsky, P.E. Cyclooxygenase in biology and disease. *FASEB J.* **1998**, *12*, 1063–1073.
134. Kremer, J.M. Clinical studies of omega-3 fatty acid supplementation in patients who have rheumatoid arthritis. *Rheum. Dis. Clin. N. Am.* **1991**, *17*, 391–402.

135. Nielsen, G.L.; Faarvang, K.L.; Thomsen, B.S.; Teglbjaerg, K.L.; Jensen, L.T.; Hansen, T.M.; Lervang, H.H.; Schmidt, E.B.; Dyerberg, J.; Ernst, E. The effects of dietary supplementation with *n*-3 polyunsaturated fatty acids in patients with rheumatoid arthritis: A randomized, double blind trial. *Eur*. *J*. *Clin*. *Investig*. **1992**, *22*, 687–691.
136. Galarraga, B.; Ho, M.; Youssef, H.M.; Hill, A.; McMahon, H.; Hall, C.; Ogston, S.; Nuki, G.; Belch, J.J. Cod liver oil (*n*-3 fatty acids) as an non-steroidal anti-inflammatory drug sparing agent in rheumatoid arthritis. *Rheumatology* **2008**, *47*, 665–669.
137. Pidgeon, G.P.; Lysaght, J.; Krishnamoorthy, S.; Reynolds, J.V.; O'Byrne, K.; Nie, D.; Honn, K.V. Lipoxygenase metabolism: Roles in tumor progression and survival. *Cancer Metastasis Rev*. **2007**, *26*, 503–524.
138. Greene, E.R.; Huang, S.; Serhan, C.N.; Panigrahy, D. Regulation of inflammation in cancer by eicosanoids. *Prostaglandins Other Lipid Mediat.* **2011**, *96*, 27–36.
139. Gogos, C.A.; Ginopoulos, P.; Salsa, B.; Apostolidou, E.; Zoumbos, N.C.; Kalfarentzos, F. Dietary omega-3 polyunsaturated fatty acids plus vitamin E restore immunodeficiency and prolong survival for severely ill patients with generalized malignancy: A randomized control trial. *Cancer* **1998**, *82*, 395–402.
140. Kim, W.; Khan, N.A.; McMurray, D.N.; Prior, I.A.; Wang, N.; Chapkin, R.S. Regulatory activity of polyunsaturated fatty acids in T-cell signaling. *Progr*. *Lipid Res*. **2010**, *49*, 250–261.
141. Yaqoob, P.; Calder, P. Effects of dietary lipid manipulation upon inflammatory mediator production by murine macrophages. *Cell*. *Immunol*. **1995**, *163*, 120–128.
142. Mangelsdorf, D.J.; Thummel, C.; Beato, M.; Herrlich, P.; Schütz, G.; Umesono, K.; Blumberg, B.; Kastner, P.; Mark, M.; Chambon, P.; *et al*. The nuclear receptor superfamily: The second decade. *Cell* **1995**, *83*, 835–839.
143. Peters, J.M.; Gonzalez, F.J. Regulation of Squamous Cell Carcinoma Carcinogenesis by Peroxisome Proliferator-Activated Receptors. In *Signaling Pathways in Squamous Cancer*; Glick, A.B., van Maes, C., Eds.; Springer: New York, NY, USA, 2011; pp. 223–240.
144. Fajas, L.; Debril, M.B.; Auwerx, J. Peroxisome proliferator-activated receptor-gamma: From adipogenesis to carcinogenesis. *J*. *Mol*. *Endocrinol*. **2001**, *27*, 1–9.
145. Peters, J.M.; Gonzalez, F.J. Sorting out the functional role(s) of peroxisome proliferator-activated receptor-β/δ (PPARβ/δ) in cell proliferation and cancer. *Biochim*. *Biophys*. *Acta* **2009**, *1796*, 230–241.
146. Lee, J.Y.; Hwang, D.H. Docosahexaenoic acid suppresses the activity of peroxisome proliferator-activated receptors in a colon tumor cell line. *Biochem*. *Biophy*. *Res*. *Commun*. **2002**, *298*, 667–674.
147. Nair, J.; Vaca, C.E.; Velic, I.; Mutanen, M.; Valsta, L.M.; Bartsch, H. High dietary omega-6 polyunsaturated fatty acids drastically increase the formation of etheno-DNA base adducts in white blood cells of female subjects. *Cancer Epidemiol*. *Biomark*. *Prev*. **1997**, *6*, 597–601.
148. Takahashi, M.; Tsuboyama-Kasaoka, N.; Nakatani, T.; Ishii, M.; Tsutsumi, S.; Aburatani, H.; Ezaki, O. Fish oil feeding alters liver gene expressions to defend against PPARalpha activation and ROS production. *Am*. *J*. *Physiol*. *Gastrointest Liver Physiol*. **2002**, *282*, G338–G348.

149. Chajès, V.; Sattler, W.; Stranzl, A.; Kostner, G.M. Influence of *n*-3 fatty acids on the growth of human breast cancer cells *in vitro*: Relationship to peroxides and vitamin-E. *Breast Cancer Res*. *Treat*. **1995**, *34*, 199–212.
150. Sato, S.; Sato, S.; Kawamoto, J.; Kurihara, T. Differential roles of internal and terminal double bonds in docosahexaenoic acid: Comparative study of cytotoxicity of polyunsaturated fatty acids to HT-29 human colorectal tumor cell line. *Prostaglandins Leukot. Essent. Fat*. *Acids* **2011**, *84*, 31–37.
151. Jenkinson, A.M.; Collins, A.R.; Duthie, S.J.; Wahle, K.W.; Duthie, G.G. The effect of increased intakes of polyunsaturated fatty acids and vitamin E on DNA damage in human lymphocytes. *FASEB J*. **1999**, *13*, 2138–2142.
152. Srivastava, A.; Laidler, P.; Davies, R.P.; Horgan, K.; Hughes, L.E. The prognostic significance of tumor vascularity in intermediate-thickness (0.76–4.0 mm thick) skin melanoma. A quantitative histologic study. *Am*. *J*. *Pathol*. **1988**, *133*, 419–423.
153. Heimann, R.; Ferguson, D.; Powers, C.; Recant, W.M.; Weichselbaum, R.R.; Hellman, S. Angiogenesis as a predictor of long-term survival for patients with node-negative breast cancer. *J*. *Natl*. *Cancer Inst*. **1996**, *88*, 1764–1769.
154. Kanayasu, T.; Morita, I.; Nakao-Hayashi, J.; Asuwa, N.; Fujisawa, C.; Ishii, T.; Ito, H.; Murota, S. Eicosapentaenoic acid inhibits tube formation of vascular endothelial cells *in vitro*. *Lipids* **1991**, *26*, 271–276.
155. Vibet, S.; Mahéo, K.; Goré, J.; Hardy, T.; Bougnoux, P.; Tranquart, F.; Goupille, C. Potentiation of antitumoral and antiangiogenic actions of docetaxel by docosahexaenoic acid (DHA): Impact on micro- and macro-vascularization. *EJC Suppl*. **2008**, *6*, 124.
156. Jiang, W.G.; Bryce, R.P.; Mansel, R.E. Gamma linolenic acid regulates gap junction communication in endothelial cells and their interaction with tumour cells. *Prostaglandins Leukot. Essent. Fat*. *Acids* **1997**, *56*, 307–316.
157. Tevar, R.; Jho, D.H.; Babcock, T.; Helton, W.S.; Espat, N.J. Omega-3 fatty acid supplementation reduces tumor growth and vascular endothelial growth factor expression in a model of progressive non-metastasizing malignancy. *J*. *Parenter*. *Enter*. *Nutr*. **2002**, *26*, 285–289.
158. Biondo, P.D.; Brindley, D.N.; Sawyer, M.B.; Field, C.J. The potential for treatment with dietary long-chain polyunsaturated *n*-3 fatty acids during chemotherapy. *J*. *Nutr*. *Biochem*. **2008**, *19*, 787–796.
159. Pardini, R.S. Nutritional intervention with omega-3 fatty acids enhances tumor response to anti-neoplastic agents. *Chem*. *Biol*. *Interact*. **2006**, *162*, 89–105.
160. Burns, C.P.; Spector, A.A. Membrane fatty acid modification in tumor cells: A potential therapeutic adjunct. *Lipids* **1987**, *22*, 178–184.
161. Burns, C.P.; Halabi, S.; Clamon, G.H.; Hars, V.; Wagner, B.A.; Hohl, R.J.; Lester, E.; Kirshner, J.J.; Vinciguerra, V.; Paskett, E. Phase I clinical study of fish oil fatty acid capsules for patients with cancer cachexia: Cancer and leukemia group B study 9473. *Clin*. *Cancer Res*. **1999**, *5*, 3942–3947.

162. Atkinson, T.G.; Murray, L.; Berry, D.M.; Ruthig, D.J.; Meckling-Gill, K.A. DHA feeding provides host protection and prevents fibrosarcoma-induced hyperlipidemia while maintaining the tumor response to araC in Fischer 344 rats. *Nutr. Cancer* **1997**, *28*, 225–235.
163. Cha, M.C.; Meckling, K.A.; Stewart, C. Dietary docosahexaenoic acid levels influence the outcome of arabinosylcytosine chemotherapy in L1210 leukemic mice. *Nutr. Cancer* **2002**, *44*, 176–181.
164. Horie, T.; Nakamaru, M.; Masubuchi, Y. Docosahexaenoic acid exhibits a potent protection of small intestine from methotrexate-induced damage in mice. *Life Sci.* **1998**, *62*, 1333–1338.
165. Gómez de Segura, I.A.; Valderrábano, S.; Vázquez, I.; Vallejo-Cremades, M.T.; Gómez-García, L.; Sánchez, M.; de Miguel, E. Protective effects of dietary enrichment with docosahexaenoic acid plus protein in 5-fluorouracil-induced intestinal injury in the rat. *Eur. J. Gastroenterol. Hepatol.* **2004**, *16*, 479–485.
166. Ogilvie, G.K.; Fettman, M.J.; Mallinckrodt, C.H.; Walton, J.A.; Hansen, R.A.; Davenport, D.J.; Gross, K.L.; Richardson, K.L.; Rogers, Q.; Hand, M.S. Effect of fish oil, arginine, and doxorubicin chemotherapy on remission and survival time for dogs with lymphoma: A double-blind, randomized placebo-controlled study. *Cancer* **2000**, *88*, 1916–1928.
167. Pardini, R.S.; Wilson, D.; Schiff, S.; Bajo, S.A.; Pierce, R. Nutritional intervention with omega-3 fatty acids in a case of malignant fibrous histiocytoma of the lungs. *Nutr. Cancer* **2005**, *52*, 121–129.
168. Xin-Xin, L.; Jian-Chun, Y.; Wei-Ming, K.; Quan, W.; Zhi-Qiang, M.; Hai-Liang, F.; Bei, G.; Yu-Qin, L. ω-3 Polyunsaturated fatty acid enhance chemotherapy sensitivity by inhibiting NF-κB pathway. *ESPEN J.* **2011**, *6*, e36–e40.

Anticancer and Cancer Preventive Properties of Marine Polysaccharides: Some Results and Prospects

Sergey N. Fedorov, Svetlana P. Ermakova, Tatyana N. Zvyagintseva and Valentin A. Stonik

Abstract: Many marine-derived polysaccharides and their analogues have been reported as showing anticancer and cancer preventive properties. These compounds demonstrate interesting activities and special modes of action, differing from each other in both structure and toxicity profile. Herein, literature data concerning anticancer and cancer preventive marine polysaccharides are reviewed. The structural diversity, the biological activities, and the molecular mechanisms of their action are discussed.

Reprinted from *Mar. Drugs*. Cite as: Fedorov, S.N.; Ermakova, S.P.; Zvyagintseva, T.N.; Stonik, V.A. Anticancer and Cancer Preventive Properties of Marine Polysaccharides: Some Results and Prospects. *Mar. Drugs* **2013**, *11*, 4876-4901.

1. Introduction

Polysaccharides are characteristic metabolites of many marine organisms, particularly of algae. Macrophytes such as brown, red, and green algae are known as traditional food ingredients for people populating seaboard geographic areas. In many countries, brown algae belonging to *Laminaria*, *Saccharina*, *Fucus*, *Alaria*, *Sargassum*, *Undaria*, *Pelvetia* genera, green algae such as *Ulva* spp., *Caulerpa lentilifera* as well as red algae such as *Gracilaria* spp., *Porphyra* spp. and others represent an important part of diet, while the purified gelling and thickening ingredients are predominant as food products of algal origin in European countries and the USA. Nowadays, algae have been marketed worldwide as constituents of dietary supplements due to their antimutagenic, anticoagulant, and antitumor properties as well as the high content of so-called dietary fiber.

High content of polysaccharides not only in algae, but also in many other marine organisms, their unusual structures and useful properties make these compounds promising natural products for medicinal and dietary applications, and are utilized in various biotechnologies [1]. Polysaccharides are used in drug compositions, burn dressings, as materials for encapsulation, in various drinks, *etc.* The therapeutic potential of marine polysaccharides enables their utilization for cell therapy and tissue engineering [2].

Many polysaccharides and/or their derivatives such as degraded and semi-synthetic products, obtained by chemical modifications, demonstrate anticancer and cancer preventive properties. They can possess either a direct inhibitory action on cancer cells and tumors or influence different stages of carcinogenesis and tumor development, recover the broken balance between proliferation and programmed cell death (apoptosis) and are useful for cancer prophylactics. Some of these marine natural products have advantages due to their availability, low toxicity, suitability for oral application as well as having a great variety of mechanisms of action [3]. The methods of extraction, fractionation, and purification of polysaccharides from various sources are well known and have been published in many articles [4–8].

Herein, we review some of the literature data concerning anticancer and cancer preventive activity of marine polysaccharides with particular attention to results of the last 10 years.

2. Polysaccharides from Brown Algae

2.1. Fucoidans

Polysaccharides from brown algae (Phaeophyceae) are well known for their anticancer and cancer preventive properties [9]. These compounds have various important biological functions including a protective role against heavy metal toxicity [10].

Fucoidans can be roughly divided into structural types as follows: α-L-fucans, galactofucans, fucomannouronans and other intermediate structures [11]. Fucoidans isolated from many edible brown algae contain mainly sulfated L-fucose residues attached to each other by α-1,3- or interchangeable α-1,3- and α-1,4-bonds. The regular structures may be masked by random acetylation and sulfation. Some fucoidans have branched structures. As a rule, fucoidans from different algal species differ from each other and vary not only in positions and level of sulfation and molecular mass, but sometimes in the structures of the main carbohydrate chains [12,13]. For example, the fucoidan from the brown alga *Saccharina* (=*Laminaria*) *cichorioides* is 2,4-disulfated 1,3-α-L-fucan (Figure 1), while the fucoidan from *Fucus evanescens* (Figure 2) contains blocks of α-1,3-fucooligosaccharides and α-1,4-fucooligosaccharides sulfated at the position 2 in fucose residues [14–17].

Figure 1. Fucoidan from *Laminaria cichorioides*.

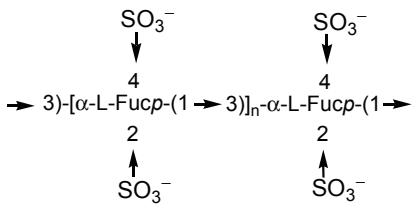

Figure 2. Fucoidan from *F. evanescens*.

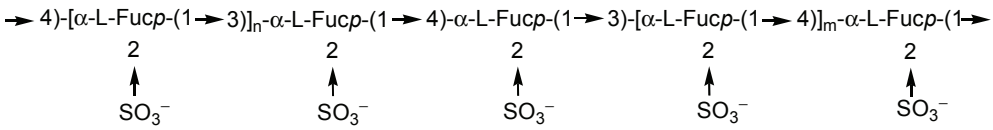

Galactofucans in contradistinction from α-L-fucans demonstrate considerable structural diversity [18,19]. Sulfated and often acetylated galactofucans are also widespread in brown algae, including edible ones, such as *Undaria pinnatifida* and *Laminaria japonica*. The main chain of galactofucan can be constructed of blocks or of alternating residues of fucose and galactose. The type of bonds between the monosaccharide residues in galactofucans, the structure of branchings,

the position of sulfates or acetates, as well as the molecular weight can be very multifarious [13,20]. For example the structural fragment of galactofucan from *L. japonica* [21] is provided in Figure 3.

Figure 3. Galactofucan from *L. japonica*.

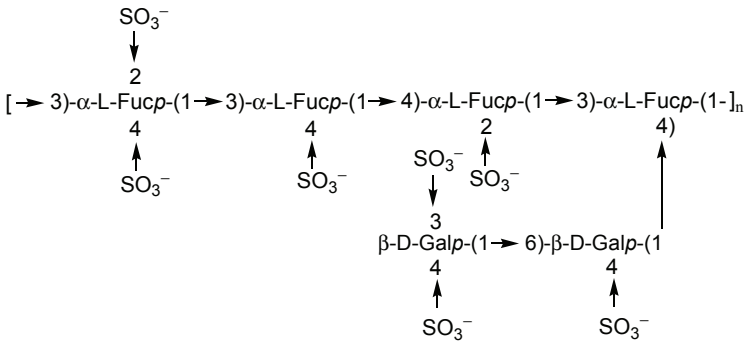

Some brown algae species contain other fucose-embracing heteropolysaccharides such as rhamnofucanes, uronofucanes, *etc.* For example, the main structure of the fucoglucuronomannan from *Kjellmaniella crassifolia* is [-4-D-Glc*p*UAβ1-2(L-Fuc*p*(3-*O*-sulfate)α1-3)D-Man*p*α1-]$_n$ [22]. Uronofucanes are often named as U-fucoidans.

The structural diversity of fucoidans has not yet been sufficiently studied. The structural complexity of fucoidans, the existence of many sub-classes of these glycans in their biological sources as well as a lack of automatic sequencing methods for these polysaccharides have stimulated structure-function studies on the so-called fucanomes in the corresponding marine organisms [23,24]. This research is necessary for the solution of problems of standardization of preparations on the basis of fucoidans, which have attracted attention as practically nontoxic natural products [25–27] with antitumor, immunomodulatory, and other useful properties [24,28–30].

The anticancer properties of fucoidans have been established many times by *in vitro* and *in vivo* experiments [9,12,13,31–33]. It was reported that *Cladosiphon* fucoidan prevented the attachment of *Helicobacter pylori* to the mucin of the gastric tract and, therefore, reduced the risk of associated gastric cancer [34]. While using AGS human gastric adenocarcinoma cells and fucoidan from *Fucus vesiculosus*, it was established that treatment with fucoidan resulted not only in apoptosis of these cells, but also in autophagy with the formation of autophagosomes in fucoidan-treated cells, the conversion of microtubule-associated protein light chain 3 to light chain 3-II and the increase of beclin-1 level [35]. Several reports have also suggested cancer preventive effects of fucoidans on different cellular models. Galactofucan from *U. pinnatifida* inhibited proliferation of prostate cancer PC-3, cervical cancer HeLa, alveolar carcinoma A549, and hepatocellular carcinoma HepG2 cells in a similar pattern to the commercial fucoidan from *F. vesiculosus* [20]. Fucose-containing sulfated polysaccharides from brown algae *Sargassum henslowianum* and *F. vesiculosus* decreased the proliferation of melanoma B16 cells in a dose-response manner. Flow cytometric analysis by Annexin V staining established that both preparations influenced the translocation of membrane phospholipids and activated caspase-3 followed by apoptosis of tumor cells in *in vitro*

experiments [36]. Fucoidan from *Ascophyllum nodosum* induced the activation of caspases-9 and -3 and the cleavage of PARP led to apoptotic morphological changes and altered the mitochondrial membrane permeability [37]. Sulfated polysaccharide isolated from the enzymatic digest of *Ecklonia cava* had an effect on caspases-7 and -8 and controlled the cellular membrane molecules Bax and Bcl-xL [38]. The fucoidan from *Sargassum filipendula* showed antiproliferative activity on HeLa cells [39] and induced apoptosis by mitochondrial release of apoptosis inducing factor (AIF) into cytosol, but was not able to activate caspases [40]. The caspase-independent apoptotic pathway was demonstrated for fucoidan from *Cladosiphon novae-caledoniae* [41]. The differences in the mechanisms of apoptosis probably depend upon the structural characteristics of fucoidans and the type of cell lines. Fucoidans were shown to induce apoptosis of some other cancer cells, for example HT-29, HCT116, and HCT-15 human colon cancer cells [42,43] as well as MCF-7 (breast adenocarcinoma) [44], melanoma SK-Mel-28, breast cancer T-47D [45], and human promyeloid leukemic cell lines [46]. MAPK pathways are involved in cellular proliferation, differentiation, and apoptosis induced by fucoidans. The fucoidan from *F. vesiculosus* clearly decreased the phosphorylation of ERKs but not p38 [47]. Another group reported that the pro-apoptotic effect of fucoidan from *F. vesiculosus* was mediated by the activation of ERKs, p38 and by the blocking of PI3K/Akt signaling pathway in HCT-15 cells [42].

Angiogenesis is a multistep process whereby the new blood vessels develop from the pre-existing vasculature. It involves migration, proliferation and differentiation of mature endothelial cells, and is regulated by interactions of endothelial cells with angiogenesis-inducing factors and extracellular matrix components [48]. Fucoidans may suppress tumor growth by inhibiting tumor-induced angiogenesis. Natural and oversulfated fucoidans suppressed the $VEGF_{165}$ induced proliferation and the migration of human umbilical vein endothelial cells (HUVEC) by preventing the binding of $VEGF_{165}$ to its cell surface receptor and inhibiting the VEGF-mediated signaling transduction [49]. In addition, the growth of two types of murine tumor cells inoculated into the footpads of mice was suppressed by administration of natural and oversulfated fucoidans. The relationship between sulfate content in fucoidan from *U. pinnatifida* and the proliferation of human stomach cancer cell line AGS was published [50]. These data showed that antiangiogenic and antitumor activity of fucoidans can be potentiated by increasing the sulfate groups in the molecule [51]. The relationship between the sulfate content of fucoidan and its inhibitory effect on the proliferation of U937 cells was also reported [52]. These results indicated that oversulfated fucoidan induced apoptosis through caspase-3 and -7 activation. The effect of the molecular weight of fucoidan from *U. pinnatifida* on the inhibition of cancer cell growth has been investigated. The anticancer activity of fucoidans could be increased by lowering their molecular weight whereby they are depolymerized by mild hydrolysis without a considerable amount of desulfation [53]. The mechanism by which fucoidans inhibited the invasion/angiogenesis of tumor cells has not been clearly elucidated. VEGF is a known angiogenic factor. Fucoidan from *C. novae-caledonia kylin* digested with the abalone glycosidase was responsible for the reduction of MMP-2/9 activities and the decrease in VEGF expression with subsequent inhibition of invasion and suppression of tubules formation in tumor cells [54].

Fucoidans are able to inhibit metastasis of cancer cells. Cell surface receptors belonging to the integrin family have been demonstrated to be involved in the invasion and the metastasis of tumors. The fucoidan from *A. nodosum* inhibited adhesion of MDA-MB-231 (breast adenocarcinoma) cells to fibronectin by binding it and modulating the reorganization of the integrin 5 subunit and down-regulating the expression of vinculin [55].

Cancer preventive properties of fucoidans have been shown in many experiments. For example, decrease of clonogenic growth of tumor cells was demonstrated after treatment with fucoidans [30,45,56]. The inhibition of cell transformation provided evidence on the anti-tumorigenic potential of fucoidans from *A. nodosum* [57], *S. japonica*, *U. pinnatifida*, *Alaria* sp., and *F. evanescens* [29,45,58].

Fucoidans may enhance the anticancer action of some low molecular weight compounds. For example, the fucoidan from the Far-eastern brown seaweed *F. evanescens* at a concentration of 500 μg/mL was not cytotoxic in human malignant lymphoid MT-4 or Namalwa cells. Pretreatment of MT-4, but not Namalwa cells with fucoidan followed by the exposure to DNA topoisomerase II inhibitor etoposide led to about a two-fold increase in the relative apoptotic index as compared with etoposide itself [56]. The fucoidan from *S. cichorioides* enhanced the antiproliferative activity of resveratrol at nontoxic doses and facilitated the resveratrol-induced apoptosis in the HCT116 cell line. Furthermore, the cells were sensitized by the fucoidan to the action of resveratrol and the inhibition of HCT116 clonogenic capacity was indicated [59].

Some fucoidans showed cytoprotective properties. It is important that fucoidan may be useful for the recovery of 5-fluorouracil (5-FU)-treated antigen-presenting dendritic cells, because this clinical anticancer agent induces immunosuppression in cancer patients as a side effect [60].

In the majority of cases, molecular mechanisms of anticancer and cancer preventive actions of fucoidans were established by *in vitro* studies. Many fucoidans induced apoptosis of tumor cells through activation of the caspases and by enhancing mitochondrial membrane permeability. Sometimes this mechanism involved the reactive oxygen species (ROS)-dependent JNK activation as was shown for partly digested fucoidan from commercially available seaweed *C. novae-caledoniae* using MCF-7 and MDA-MB-10A tumor cells [41].

Fucoidans modulate the immune system and may induce functional maturation of human monocyte-derived dendritic cells (DC) [61]. Ligand scavenger receptor class A (SR-A) indirectly participates in maturation of human blood dendritic cells via production of tumor necrosis factor followed by stimulation of T-cells. Thereby, fucoidan acts as a scavenger receptor agonist and maturation is eliminated by pretreatment with TNF-neutralizing antibodies [62]. At a later date, it was confirmed that SR-A plays a crucial role in affecting the DC-mediated presentation of cancer antigens to T cells in human cancer cells, and it was also established that fucoidan promoted the DCs maturation. The fucoidan-treated DCs stimulated the $CD8^+$ T limphocytes to release more interferon-γ than non-fucoidan-treated cells. It was found that fucoidan enhanced the cross-presentation of NY-ESO-1 cancer testis antigen to T cells and it led to the increase of T-cell cytotoxicity against NY-ESO-1 human cancer cells [63]. Cytotoxic activities of natural killer cells were also activated *in vivo* after administration of fucoidans from *Sargassum* sp. and *F. vesiculosus* to mice [36].

Fucoidan from *F. vesiculosus* inhibited the migration and the invasion of human lung cancer cells decreasing the cytosolic and nuclear levels of kappa-B nuclear factor [64]. Treatment of mouse breast cancer cells with fucoidan showed that the enhanced antitumor activity was associated with decreased angiogenesis via the down-regulation of vascular endothelial growth factor and increased induction of apoptosis [65].

It has been suggested that the anticarcinogenic action of fucoidan from *S. cichorioides* is connected with its ability to interact directly with epidermal growth factor (EGF) and prevents its binding to EGF receptor (EGFR). Actually, in experiments with neoplastic transformation of JB6 mouse epidermal cells induced by EGF or 12-*O*-tetradecanoylphorbol-13 acetate, a Russian-Korean group of scientists reported that inhibition of EGFR phosphorylation was followed by inhibition of the activities of some extracellular signal regulated kinases that resulted in the inhibition of AP-1 nuclear factor transactivation [66,67].

Ultraviolet irradiation is known to induce skin aging and cause skin cancer. UVB stimulates the activation of cellular signaling transduction followed by the production of metalloproteinases (MMPs). Fucoidans suppressed the UVB induced MMP-1 expression and inhibited ERKs activity in human skin fibroblasts in a dose-dependent manner. They inhibited significantly MMP-1 promoter activity and increased type I procollagen mRNA and protein expression. It was concluded that *Costaria costata* fucoidan may be considered as a potential agent for the prevention and treatment of skin photoaging [68–70]. The fucoidan from *F. vesiculosus* post-translationally regulated MMP-9 secretion from human monocyte cell line U937 [71].

Thus, the molecular mechanisms of anticancer and cancer preventive actions of fucoidans are rather complicated and may include inhibitory effects against cancer cell proliferation and induction of tumor cells apoptosis. In addition, these polysaccharides stimulate immunity and inhibit angiogenesis. The cancer preventive action of fucoidans includes such useful properties as anti-inflammatory, anti-adhesive [72], antioxidant and antiviral effects [73–76] as well as their capability to bind heavy metals. Moreover, these compounds may delay and decrease the action of such factors of carcinogenesis as some tumor promoters (EGF, phorbol esters), defend against UV radiation and inhibit the tumor invasion by modulation of metalloproteinases. Possibly, these effects depend on the differences in the structures of fucoidans isolated from various biological sources and on their physico-chemical characteristics such as molecular weight.

Daily consumption of fucoidan-containing algae was proposed as a factor in the lowering of postmenopausal breast cancer incidence and mortality. Urinary human urokinase-type plasminogen activator receptor concentration is higher among postmenopausal women breast cancer patients. It was shown that this concentration was decreased by about 50% after seaweed supplementation [77]. In addition, fucoidans reduced the toxicity of chemotherapy for patients with unresectable advanced or recurrent colorectal cancer. Fucoidan may enable the continuous administration of such drugs as oxaliplatin plus 5FU/leucovorin and, as a result, may prolong the survival of patients [78]. In some countries food supplements and drinks containing fucoidans are used to treat patients having different cancers. In many countries fucoidan-containing extracts are used as a remedy in traditional medicine.

In our opinion, the perspectives of studies on fucoidans are connected with further search for new structural variants of these types of polysaccharides and the relationships established between the structures and the biological activities. The great diversity of fucoidans, presenting in brown algae and covering a much broader range than only those having a fucan backbone, provides potential for the future discovery of numerous new polysaccharides of this class and their derivatives. Fucoidan bioactivities depend on the extraction and the purification methods used, because fucoidans obtained from the same biological source using different methods differ from each other in the content of sulfate groups and in the impurities [79]. Furthermore it is known that the content and structure of fucoidans depends on the seaweed species, the parts of the plant, the harvest season and mainly on the stage of development of the algae [58,80,81].

The recent rapid progress in studies on fucoidans has been achieved by application of modern methods of structural investigation such as 2D NMR, MALDI-TOF and tandem ESI mass-spectrometry [82,83] as well as new techniques of molecular biology and pharmacology such as fluorescent staining, flow cytometry, *mi*-RNA, Western blot, *etc.*

2.2. Laminarans

Important results have been obtained in the studies on other algal polysaccharides from brown algae laminarans, as potential cancer preventive agents. Laminarans are low molecular weight polysaccharides (MW about 3–6 kDa) consisting mainly of 1,3-linked β-D-glucopyranose residues with a small number of 1,6-bonded β-D-glucopyranose units in the main and the branching chains. Their carbohydrate chains are terminated with D-mannitol residues (so-called M-chains) or contain glucopyranose residues only (so-called G-chains) (Figure 4). Sometimes terminal residues of M-chains may be additionally glycosylated or M-chains may be completely absent [84]. Branching at positions 2 and 6 was found in the laminaran from *Saccharina longicrucis* [85].

Figure 4. The structures of G- and M-chains of laminarans.

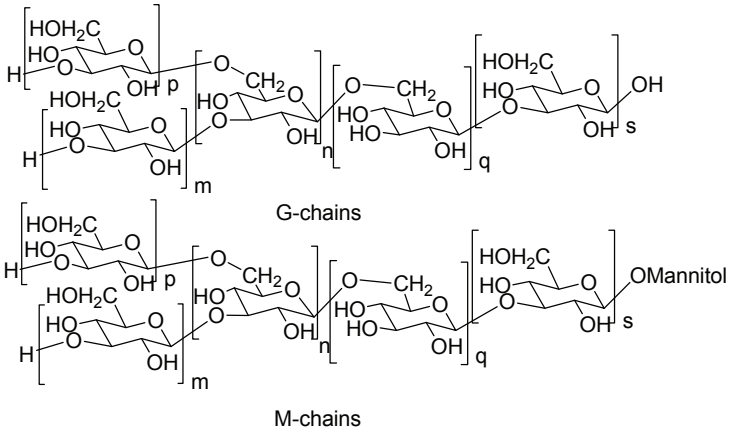

High molecular weight laminaran (19–27 kDa) was recently isolated from the brown seaweed *Eisenia bicyclis.* It was shown that this 1,3;1,6-β-D-glucan contained 1,6-linked glucose residues in

both branches and the main chain, basically in the non-reduced ends of the molecules. This laminaran and its products of enzymatic degradation inhibited the colony formation of SK-Mel-28 and colon cancer DLD cells. The increase of the content of 1,6-linked glucose residues and the decrease of the molecular weight improved the anticancer effect in this series of substances [85]. It is known that algal glucans suppress angiogenesis in tumor growth. Recent findings show that they enhanced the tumor response to photodynamic therapy in C57BL/6 mice, administered subcutaneously with Lewis lung carcinoma cells. Ten days after implantation, the mice were treated with sodium porfimer, 24 h prior to laser irradiation with or without oral administration of β-D-glucans. When algal β-D-glucan was used, significantly reduced tumor growth was indicated [86].

Laminarans noticeably inhibited the formation of putrefactive and harmful compounds, such as indoles, p-cresol, ammonia, phenol, and sulfide, produced by the fecal microflora. These putrefactive compounds in rats fed low molecular alginate also tended to be lower. In both experiments (with laminaran and with alginic acid) the intestinal bacterial flora of rats was changed. Polysaccharides were fermented into propionic and butyric acids by intestinal microbiota, similar to the effects of prebiotics. These results suggest that the fermentation of laminaran by intestinal bacteria could suppress the risk of colorectal cancer [87,88]. It is of special interest that not only laminarans, but also other β-D-glucans, isolated from yeast, fungi and cereals demonstrated anti-cytotoxic, anti-mutagenic, and anti-tumorigenic properties, making this class of polysaccharides a promising promoter of health [89].

Tumor metastasis is connected with expression of heparanase, an endo-β-D-glucuronidase that degrades the main polysaccharide constituent of the extracellular matrix and the basement membrane. In fact, expression of the heparanase gene is associated with the invasive potential of tumors. Laminaran sulfate inhibited heparanase enzymatic activity and reduced the incidence of metastasis in experimental animals [90].

2.3. Alginic Acids

Alginic acids are widely distributed in the cell walls of brown seaweeds. These anionic polysaccharides were proved to be linear polymers containing blocks of 1,4-linked β-D-polymannouronate and α-L-polyguluronate (so-called M- and G-blocks) (Figure 5). Molecular masses of alginic acids ranged between 10 kDa and 600 kDa. These polysaccharides are used in the pharmaceutical industry and in biotechnology, particularly for cell immobilization and encapsulation.

Figure 5. Structure of alginic acid.

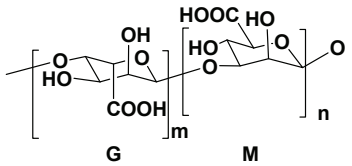

Alginic acid-coated chitosan nanoparticles have been constructed as an oral delivery carrier for the legumain-based DNA vaccine. It was shown that this vaccine could effectively improve autoimmune response and protect against breast cancer in mice [91].

Biopreparations containing alginic acids probably have some cancer preventive properties because of the ability of polysaccharides to bind toxins and heavy metals in the intestines and transform these dangerous compounds into less harmful forms.

3. Polysaccharides from Red Algae

Red algae (Rhodophyta) contain several classes of well known polysaccharides, having wide application in microbiology, biotechnology and other fields, mainly due to the ability of their aqueous solutions to form strong gels. Sulfated galactans such as agar, agarose and carrageenans usually contain repeating disaccharides of β-(1→3)-linked and α-(1→4)-linked galactopyranosyl (Galp) residues. Several red algae species contain other polysaccharides, for example mannans and xylans [92].

All carrageenans consist of either galactose or galactose and 3,6-anhydrogalactose monosaccharide units and differ from each other in monosaccharide composition, level of sulfation, positions of sulfate groups and molecular weights. Three groups of carrageenans, so-called kappa-, iota- and lambda-carrageenans, are of commercial significance (Figure 6). Hybrid forms of carrageenans are also known.

Figure 6. Structures of repeating units of some carrageenans.

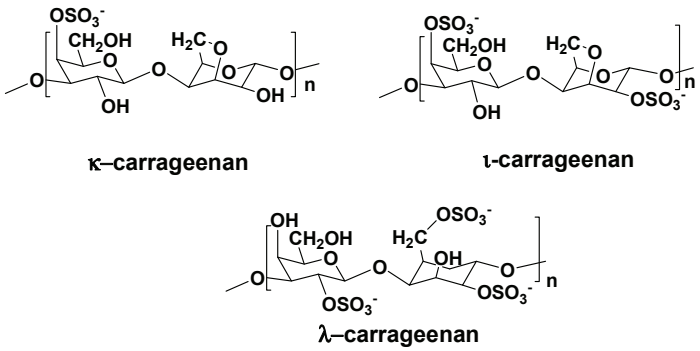

Some representatives of this polysaccharide class demonstrate properties connected with cancer prevention, mainly due to antiviral, antioxidant properties, and stimulation of antitumor immunity. As is known, certain sexually transmitted human papillomavirus types are associated with the development of cervical cancer. Recently, it was established that carrageenan in nanomolar concentrations inhibits papillomavirus. However, clinical trials are needed to determine, whether carrageenans are effective as antiviral drugs against genital human papilloma viral infection or not [93].

κ-Carrageenans degraded by an oxidative method involving hydrogen peroxide (H_2O_2) treatment were evaluated as scavengers of superoxide anions and hydroxyl radicals by application of flow

injection chemiluminescence technology. The values of IC_{50} of degraded κ-carrageenans labeled A, B, C, and D against the superoxide anion showed a positive correlation with molecular weight. As for hydroxyl radical scavenging, the EC_{50} values of degraded κ-carrageenans A, B, C, and D showed the same correlation. Therefore, these results indicated that κ-carrageenans with lower molecular weights have better antioxidant properties and may be promising for cancer prevention [94]. Carrageenan oligosaccharides from the red alga *Kappaphycus striatum* were perorally administrated during 14 days into mice inoculated with S180 tumor cell suspension. This resulted in growth inhibition of transplantable sarcoma cells, increased macrophage phagocytosis, enhanced antibody production, increased lymphocyte proliferation, stronger NK cell activity, and elevated levels of IL-2 and TNF-α. These results suggested that the studied oligosaccharides exert their antitumor effects by promoting the immune system [95]. *In vivo* antitumor activities for κ-carrageenan oligosachharides and low molecular λ-carrageenan from *Chondrus ocellatus* have been established. The latter also potentiated the antitumor effect of 5-FU [96,97]. Similar data were obtained in studies of sulfated polysaccharide from the red alga *Champia feldmannii* [98]. Thus, low molecular carrageenans and carrageenan oligosaccharides seem to be more promising cancer preventive agents than high molecular natural products belonging to this class of polysaccharides.

However, harmful gastrointestinal effects of both native and degraded carrageenans followed by the induction of neoplasms in animal experiments were reported [99]. Later, it was confirmed that degraded carrageenan induces colitis in rats *in vivo* and induces inflammation. However, in experiments *in vitro*, the preparation inhibited proliferation of THP-1 cells and arrested the cells in the G1 phase [100]. In another review concerning the toxicological effects of carrageenan on the gastrointestinal tract, it was demonstrated that systematically perorally administrated carrageenan was not carcinogenic. It was noted that previous toxicological studies involved administration of doses that exceeded those to which humans are exposed by several magnitudes [101]. Similar conclusion about the safety of peroral application of κ-carrageenan was made as a result of a 90-day dietary study in rats [102].

Thus, further investigations are needed to determine the applicability of partly degraded carrageenans as cancer preventive agents.

4. Polysaccharides from Green Algae

Among marine macrophytes, marine green algae have been less studied in comparison to brown and red algae as sources of polysaccharides with anticancer and cancer preventive properties. However, their antitumor properties have been sometimes reported, mainly for the polysaccharides belonging to the so-called ulvans. Ulvans, water soluble sulfated polysaccharides from the cell walls of green algae are characteristic of the plants, belonging to the genera *Ulva*, *Enteromorpha*, *Monostroma*, *Caulerpa*, *Codium*, and some others. They are composed of repeating disaccharide moieties, containing sulfated rhamnose and uronic acid (glucuronic or iduronic). The structure of the disaccharide moieties of ulvans resembles that of glycosaminoglycans, which occur in the extracellular matrix of connective tissues of animals. Some ulvans include also xylose residues (Figure 7) [103].

Figure 7. Structure of the main repeating disaccharide in *Ulva rigida*.

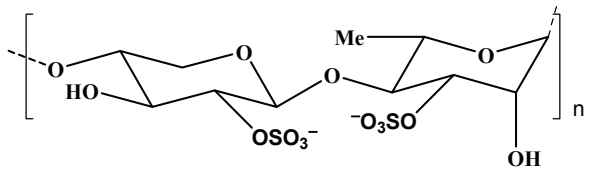

[→ 4)-β-D-Xyl 2S(1→ 4)-α-L-Rha3S(1→]

The highly pyruvated 1,3-β-D-galactan sulfate from the Pacific *Codium yezoense* and the similar polysaccharide from *Codium isthmocladium* represent another type of polysaccharides found in green algae [104,105]. Sulfated β-D-mannans like that isolated from *Codium vermilara* [106] have also been found.

Promising antioxidant and antiproliferative activities were recently found in the sulfated polysaccharides isolated from several tropical species of green algae. HeLa cell proliferation was inhibited between 36.3% and 58.4% after 72 h incubation with the polysaccharide isolated from *Caulerpa prolifera* [107]. Two polysaccharide fractions obtained from the green alga *Caulerpa racemosa* showed antitumor activities, and their inhibition rates of H22 tumor transplanted in mice were 59.5%–83.8% (48 h) and 53.9% (14 days) at a dose of 100 mg/kg/day, respectively [108].

In vivo and *in vitro* stimulation of immunity was indicated as the action of water-soluble sulfated polysaccharide fractions from *Enteromorpha prolifera*. These polysaccharides significantly increased ConA-induced splenocyte proliferation and induced the production of various cytokines via up-regulated m-RNA expression [109]. The ulvan from *Ulva rigida* induced more than a two times increase in the expression of some cytokines, stimulated the secretion and activity of murine macophages as well as inducing an increase in COX-2 and NOS-2 expression [110]. Ulvans from *Ulva pertusa* had little cytotoxicity against tumor cells, but significantly stimulated immunity, inducing considerable amounts of nitric oxide and cytokine production [111]. There are several reports concerning the antioxidant activities of ulvans in experimental D-galactosamine-induced hepatitis in rats [112,113].

The strong immuno-modulatory potencies as well as the antioxidant properties of polysaccharides from green algae suggest their potential cancer preventive activity and their future utilization as experimental immuno-stimulants.

5. Polysaccharides from Microalgae

There is little information concerning cancer preventive and anticarcinogenic properties of polysaccharides from marine microalgae, although these organisms have been used for a long time as food for humans, particularly *Arthrospira* (the former name *Spirulina)* and *Porphyridium*. Similar marine organisms belong to the classes Bacillariophyceae (diatoms), Cyanophyceae (blue-green algae), Porphyridiophyceae and partly to Chlorophyceae and Rhodophyceae. However, after the nuclear accident of Fukushima and the resulting radioactive pollution, the ability of marine algae to bio-accumulate radionuclides, has become a major concern. For example, the

newly discovered green microalga, *Parachlorella* sp. *binos* (Binos) exhibited highly efficient incorporation of radioactive isotopes of iodine, strontium and cesium. The authors also showed the ability of microalgae to accumulate radioactive nuclides from water and soil samples collected from the heavily contaminated area in Fukushima [114]. Determination of the potential radioactive contamination of seaweeds is therefore crucial before further search for bioactive compounds. Polysaccharides isolated from various microalgae ranging from diatoms to green-blue algae demonstrated different activities, although direct anticancer properties were rarely reported [91]. Apoptogenic properties of red microalgal polysaccharides in two human tumor cell lines MCF-7 and HeLa were established [115]. Some microalgal polysaccharides were found to show antiviral activities against retroviruses. These viruses, containing reverse transcriptase are implicated in various types of leukemias and other tumors. Polysaccharides from the fresh water red microalga *Porphyridium* sp. were more active than those from *Porphyridium aerogineum* and *Rhodella reticulata* against murine leukemia virus (MULV) and murine sarcoma virus (MuSV-124) in cell culture [116]. Marine red microalgae polysaccharides and polysaccharides from other microalgae were also studied in this respect. For example, sulfated polysaccharides from the marine microalga *Cochlodinium polykrikoides* showed a significant *in vitro* antiviral activity against human immunodeficiency virus and absence of a cytotoxic effect directed against the host cells [117]. Antiviral properties were found in several other polysaccharides, isolated from different microalgae [118,119].

In addition, blue green algal polysaccharides were immuno-active and showed antioxidant and free radical scavenging properties [115]. High molecular weight polysaccharides from the fresh water *Spirulina platensis* and related species [120] were between one hundred and one thousand times more immuno-active than polysaccharide preparations from other biological sources that are used clinically for cancer immunotherapy. Actually, related compounds with similar properties should be found in the corresponding marine species. Antioxidant activity was also reported for polysaccharides from *Porphiridium cruentum* [121].

All these activities are usually associated with anticancer and cancer preventive properties. For example, it is known that oxidative stress can lead to cancer and some antioxidant marine products proved to be chemopreventive antitumor agents [122]. Cancer preventive action of the oligosaccharide derived from the microalga *P. cruentum* was reported [123]. Another example concerns the extract from the deep-sea water *Spirulina maxima*, which effectively suppressed the expression of Bcl2 in A549 cells and inhibited viability of other human cancer cells [124]. *Spirulina platensis* preparations showed the chemopreventive effect against carcinogenesis induced by dibutyl nitrosamine with the decrease of the incidence of liver tumors from 80% to 20%. However, it is unknown, whether polysaccharide contribution is significant in this case or not [125].

6. Polysaccharides from Marine Bacteria and Fungi

A great diversity of polysaccharides from marine bacteria and fungi also attract attention because of their structures, anticancer and cancer preventive properties. Polysaccharide B1 from the marine *Pseudomonas* sp. has repeating units as -2)-β-D-Gal*p*(4-sulfate)(1,4)[β-D-Glc*p*(1,6)]-β-

D-Gal*p*(3-sulfate)(1- and demonstrated cytotoxicity against tumor cells, being more active to the central nervous system and lung cancer cell lines. It induced apoptosis in U937 cells [126].

The marine filamentous fungus *Keissleriella* sp. YS 4108 polysaccharide with a mean molecular weight of 130,000 Da showed radical eliminating and antioxidant actions in various *in vitro* systems. In addition to scavenging activities, the polysaccharide effectively blocked the non site-specific DNA strand-break induced by the Fenton reaction at concentrations of 0.1 and 1 mg/mL. These results suggested that this preparation could be of preventive and therapeutic significance to some life-threatening health problems such as cancer [127].

7. Polysaccharides from Marine Animals

Polysaccharides can be found in various marine animals such as sea cucumbers, sea urchins, sponges, starfish, ascidians, *etc.* They contain a great variety of polysaccharide compounds, including glycosaminoglycans, fucans, and galactans [23,128–130]. These compounds demonstrate diverse biological properties, including anticoagulant and antitrombotic [131–133], antioxidative [134], neuroprotective [135,136], and antiviral activity as well [8,137]. However, anticancer and cancer preventive activities of the polysaccharides from marine animals have been studied insufficiently. Polysaccharide SEP isolated from the eggs of the sea urchin *Strongylocentrotus nudus* effectively inhibited the growth of S180 tumor and the hepatocellular carcinoma *in vivo* via the activation of lymphocytes and macrophages, amplification of B and T cell proliferation, and increased secretion of such cytokines as IL-2, TNF-α and IFN-γ [138–141]. The sulfated polysaccharide conjugate from viscera of abalone *Heliotis discus hannai*, administered at doses of 1–40 mg/kg to mice inhibited tumor growth and increased lymphocyte proliferation, as well as natural killer cell activity and antibody production. A significant increase of immune function was observed in cyclophosphamide-induced immunosuppressive mice on administration of 40 mg/kg dose [142].

Cancer chemoprevention implies the use of natural or synthetic compounds for prevention, suppression or reversal of the process of carcinogenesis [143]. Cancer preventive compounds may stimulate anticancer immunity, inhibit inflammation, angiogenesis and tumor invasion, or protect from UV-radiation damage [144–147]. Preincubation with mytilan, a polysaccharide isolated from the mussel *Crenomytilus grayanus*, was followed by a normalization of the activity indicators of human peripheral blood lymphocytes and by a reduction of the number of morphological defects of the marine invertebrates larvae after UV-irradiation [148]. Sulfated polysaccharide obtained from the sea cucumber *Cucumaria frondosa* affected the maturation of monocyte-derived dendritic cells and their activation of allogeneic CD4(+) T cells *in vitro* by down regulation of the secretion of IL-10 and IL-12p40 at 100 μg/mL [149]. Some polysaccharides from the marine animals inhibited the binding of pro-inflammatory molecules, P- and L-selectins, to immobilized carbohydrate determinant sialyl Lewis^x which is a component of cell surface glycoproteins presented in leukocytes and overexpressed in several tumor cells. As a consequence of their antiselectin activity, these polysaccharides attenuated metastasis and inflammation [150–152]. Oral administration (100 mg/kg body weight) for five days of sea cucumber fucoidan (SC-FUC) extracted from *Acaudina molpadioides* can significantly prevent the formation of gastric ulcer in rats. Moreover, SC-FUC pretreatment could alleviate ethanol-induced histological damage, reverse changes in tissue

oxidation and antioxidase activities, and regulate the signaling pathways of mitogen-activated protein kinases and matrix metalloproteinases [153]. Chondroitin sulfate isolated from ascidian *Styela clava* inhibited phorbol ester- and TNF-α-induced expression of inflammatory factors VCAM-1, COX-2 and iNOS by blocking Akt/NF-κB activation in mouse skin [154,155]. Anti-inflammatory activity of heparin analogues from ascidians and marine shrimps was also reported [156,157]. The heparin isolated from white leg shrimp demonstrated anti-angiogenic activity [158].

8. Conclusion

To date, numerous polysaccharides have been isolated from different marine organisms ranging from marine bacteria to marine animals and several dozen of them have attracted attention as promising anticancer and cancer preventive substances. Some of these compounds are already used in clinical practice. Polysaccharide anticancer and cancer preventive substances demonstrate a wide variety of useful properties and mechanisms of action, including inhibition of tumor cell proliferation, induction of apoptosis, inhibition of angiogenesis, *etc.* These biopolymers and their derivatives frequently show radical scavenging, antiviral, and immuno-stimulatory properties. Polysaccharides obtained from marine invertebrates possess unique physico-chemical and biological properties, which justify intensive research efforts in the future. The increasing exploration of marine biological sources will help to identify the most promising of these compounds.

Acknowledgments

The study was supported by the Program of the Presidium of RAS “Molecular and Cell Biology” (grant 12-IP6-11), Grant No. 13-03-00986 from the RFBR, and Grant of President of Russia No. 546.2012.4 supporting leading Russian scientific schools.

Conflicts of Interest

The authors declare no conflict of interest.

References

1. Laurienzo, P. Marine polysaccharides in pharmaceutical application: An overview. *Mar. Drugs* **2010**, *8*, 2435–2465.
2. Senni, K.; Pereira, J.; Gueniche, F.; Delbarre-Ladrat, C.; Sinquin, C.; Ratiskol, J.; Godeau, G.; Fischer, A.M.; Helley, D.; Colliec-Jouault, S. Marine polysaccharides: A source of bioactive molecules for cell therapy and tissue engineering. *Mar. Drugs* **2011**, *9*, 1664–1681.
3. Stonik, V.A.; Fedorov, S.N. Cancer preventive marine natural product. In *Cellular and Genetic Practices for Translational Medicine*; Kwak, H., Ed.; Research Signpost: Karalla, India, 2011; pp. 1–36.

4. Beress, A.; Wassermann, O.; Bruhn, T.; Beress, L.; Kraiselburd, E.N.; Gonzalez, L.V.; de Motta, G.E.; Chavez, P.I. A new procedure for the isolation of anti-HIV compounds (polysaccharides and polyphenols) from the marine alga *Fucus vesiculosus*. *J. Nat. Prod.* **1993**, *56*, 478–488.
5. Ponce, N.M.A.; Pujol, C.A.; Damonte, E.B.; Flores, M.L.; Stortz, C.A. Fucoidans from the brown seaweed *Adenocystis utricularis*: Extraction methods, antiviral activity and structural studies. *Carbohydr. Res*. **2003**, *338*, 153–165.
6. Ray, B. Polysaccharides from *Enteromorpha compressa*: Isolation, purification and structural features. *Carbohydr. Polym*. **2006**, *66*, 408–416.
7. Ye, H.; Wang, K.; Zhou, C.; Liu, J.; Zeng, X. Purification, antitumor and antioxidant activities *in vitro* of polysaccharides from the brown seaweed *Sargassum pallidum*. *Food Chem*. **2008**, *111*, 428–432.
8. Esteves, A.I.S.; Nicolai, M.; Humanes, M.; Gonsalves, J. Sulfated polysaccharides in marine sponges: Extraction methods and anti-HIV activity. *Mar. Drugs* **2011**, *9*, 139–153.
9. Smit, A.J. Medicinal and pharmaceutical uses of seaweed natural products: A review. *J. Appl. Phycol.* **2004**, *16*, 245–262.
10. Andrade, L.R.; Leal, R.N.; Noseda, M.; Duarte, M.E.; Pereira, M.S.; Mourao, P.A.; Farina, M.; Amado Filho, G.M. Brown algae overproduce cell wall polysaccharides as a protection mechanism against the heavy metal toxicity. *Mar. Pollut. Bull.* **2010**, *60*, 1482–1488.
11. Berteau, O.; Mulloy, B. Sulfated fucans, fresh perspectives: Structures, functions, and biological properties of sulfated fucans and an overview of enzymes active toward this class of polysaccharide. *Glycobiology* **2003**, *13*, 29R–40R.
12. Jiao, G.; Yu, G.; Zhang, J.; Ewart, H.S. Chemical structures and bioactivities of sulfated polysaccharides from marine algae. *Mar. Drugs* **2011**, *9*, 196–223.
13. Li, B.; Lu, F.; Wei, X.; Zhao, R. Fucoidan: Structure and bioactivity. *Molecules* **2008**, *13*, 1671–1695.
14. Bilan, M.I.; Grachev, A.A.; Ustuzhanina, N.E.; Shashkov, A.S.; Nifantiev, N.E.; Usov, A.I. Structure of a fucoidan from the brown seaweed *Fucus evanescens* C.Ag. *Carbohydr. Res.* **2002**, *337*, 719–730.
15. Chizhov, A.O.; Dell, A.; Morris, H.R.; Haslam, S.M.; McDowell, R.A.; Shashkov, A.S.; Nifant'ev, N.E.; Khatuntseva, E.A.; Usov, A.I. A study of fucoidan from the brown seaweed *Chorda filum*. *Carbohydr. Res.* **1999**, *320*, 108–119.
16. Li, B.; Wei, X.J.; Sun, J.L.; Xu, S.Y. Structural investigation of a fucoidan containing a fucose-free core from the brown seaweed *Hizikia fusiforme*. *Carbohydr. Res.* **2006**, *341*, 1135–1146.
17. Usov, A.I.; Smirnova, G.P.; Bilan, M.I.; Shashkov, A.S. Polysaccharides of algae. 53. Brown alga *Laminaria cicchorioides*. *Bioorg. Khim.* **1998**, *24*, 382–389.
18. Shevchenko, N.M.; Anastiuk, S.D.; Gerasimenko, N.I.; Dmitrenok, P.S.; Isakov, V.V.; Zvyagintseva, T.N. Polysaccharide and lipid composition of the brown seaweed *Laminaria gurjanovae*. *Rus. J. Bioorg. Chem.* **2007**, *33*, 88–98.

19. Thinh, P.D.; Menshova, R.V.; Ermakova, S.P.; Anastyuk, S.D.; Ly, B.M.; Zvyagintseva, T.N. Structural characteristics and anticancer activity of fucoidan from the brown alga *Sargassum mcclurei*. *Mar. Drugs* **2013**, *11*, 1456–1476.
20. Synytsya, A.; Kim, W.J.; Kim, S.M.; Pohl, R.; Synytsya, A.; Kvasnicka, F.; Copikova, J.; Park, Y.I. Structure and antitumour activity of fucoidan isolated from sporophyll of Korean brown seaweed *Undaria pinnatifida*. *Carbohydr. Polym.* **2010**, *81*, 41–48.
21. Wang, J.; Zhang, Q.; Zhang, Z.; Zhang, H.; Niu, X. Structural studies on a novel fucogalactan sulfate extracted from the brown seaweed *Laminaria japonica*. *Int. J. Biol. Macromol.* **2010**, *47*, 126–131.
22. Sakai, T.; Kimura, H.; Kojima, K.; Shimanaka, K.; Ikai, K.; Kato, I. Marine bacterial sulfated fucoglucuronomannan (SFGM) lyase digests brown algal SFGM into trisaccharides. *Mar. Biotechnol.* **2003**, *5*, 70–78.
23. Pomin, V.H. Fucanomics and galactanomics: Marine distribution, medicinal impact, conceptions, and challenges. *Mar. Drugs* **2012**, *10*, 793–811.
24. Pomin, V.H.; Mourao, P.A. Structure, biology, evolution, and medical importance of sulfated fucans and galactans. *Glycobiology* **2008**, *18*, 1016–1027.
25. Chung, H.J.; Jeun, J.; Houng, S.J.; Jun, H.J.; Kweon, D.K.; Lee, S.J. Toxicological evaluation of fucoidan from *Undaria pinnatifida in vitro* and *in vivo*. *Phytother. Res.* **2010**, *24*, 1078–1083.
26. Kim, K.J.; Lee, O.H.; Lee, B.Y. Genotoxicity studies on fucoidan from Sporophyll of *Undaria pinnatifida*. *Food Chem. Toxicol.* **2010**, *48*, 1101–1104.
27. Kim, K.J.; Lee, O.H.; Lee, H.H.; Lee, B.Y. A 4-week repeated oral dose toxicity study of fucoidan from the sporophyll of *Undaria pinnatifida* in Sprague-Dawley rats. *Toxicology* **2010**, *267*, 154–158.
28. Mizuno, T.; Kinoshita, T.; Zhuang, C.; Ito, H.; Mayuzumi, Y. Antitumor-active heteroglycans from niohshimeji mushroom, *Tricholoma giganteum*. *Biosci. Biotechnol. Biochem.* **1995**, *59*, 568–571.
29. Vishchuk, O.S.; Ermakova, S.P.; Zvyagintseva, T.N. The fucoidans from brown algae of Far-Eastern seas: Anti-tumor activity and structure-function relationship. *Food Chem.* **2013**, *141*, 1211–1217.
30. Wijesekara, I.; Pangestuti, R.; Kim, S. Biological activities and potential health benefits of sulfated polysaccharides derived from marine algae. *Carbohydr. Polym.* **2011**, *84*, 14–21.
31. Alekseyenko, T.V.; Zhanayeva, S.Y.; Venediktova, S.Y.; Zvyagintseva, T.N.; Kuznetsova, T.A.; Besednova, N.N.; Korolenko, T.A. Antitumor and antimetastatic activity of fucoidan, a sulfated polysaccharide from the Okhotsk sea *Fucus evanescens* brown alga. *Bull. Exp. Biol. Med.* **2007**, *143*, 730–732.
32. Itoh, H.; Noda, H.; Amano, H.; Zhuaug, C.; Mizuno, T.; Ito, H. Antitumor activity and immunological properties of marine algal polysaccharides, especially fucoidan, prepared from *Sargassum thunbergii* of Phaeophyceae. *Anticancer Res.* **1993**, *13*, 2045–2052.
33. Kusaykin, M.; Bakunina, I.; Sova, V.; Ermakova, S.; Kuznetsova, T.; Besednova, N.; Zaporozhets, T.; Zvyagintseva, T. Structure, biological activity, and enzymatic transformation of fucoidans from the brown seaweeds. *Biotechnol. J.* **2008**, *3*, 904–915.

34. Shibata, H.; Iimuro, M.; Uchiya, N.; Kawamori, T.; Nagaoka, M.; Ueyama, S.; Hashimoto, S.; Yokokura, T.; Sugimura, T.; Wakabayashi, K. Preventive effects of *Cladosiphon* fucoidan against *Helicobacter pylori* infection in Mongolian gerbils. *Helicobacter* **2003**, *8*, 59–65.
35. Park, H.S.; Kim, G.Y.; Nam, T.J.; Deuk Kim, N.; Hyun Choi, Y. Antiproliferative activity of fucoidan was associated with the induction of apoptosis and autophagy in AGS human gastric cancer cells. *J. Food Sci.* **2011**, *76*, T77–T83.
36. Ale, M.T.; Maruyama, H.; Tamauchi, H.; Mikkelsen, J.D.; Meyer, A.S. Fucoidan from *Sargassum* sp. and *Fucus vesiculosus* reduces cell viability of lung carcinoma and melanoma cells *in vitro* and activates natural killer cells in mice *in vivo*. *Int. J. Biol. Macromol.* **2011**, *49*, 331–336.
37. Foley, S.A.; Szegezdi, E.; Mulloy, B.; Samali, A.; Tuohy, M.G. An unfractionated fucoidan from *Ascophyllum nodosum*: Extraction, characterization, and apoptotic effects *in vitro*. *J. Nat. Prod.* **2011**, *74*, 1851–1861.
38. Athukorala, Y.; Ahn, G.N.; Jee, Y.H.; Kim, G.Y.; Kim, S.H.; Ha, J.H.; Kang, J.S.; Lee, K.W.; Jeon, Y.J. Antiproliferative activity of sulfated polysaccharide isolated from an enzymatic digest of *Ecklonia cava* on the U-937 cell line. *J. Appl. Phycol.* **2009**, *21*, 307–314.
39. Costa, L.S.; Fidelis, G.P.; Telles, C.B.; Dantas-Santos, N.; Camara, R.B.; Cordeiro, S.L.; Costa, M.S.; Almeida-Lima, J.; Melo-Silveira, R.F.; Oliveira, R.M.; Albuquerque, I.R.L; Andrade, G.P.V.; Rocha, H.A.O. Antioxidant and antiproliferative activities of heterofucans from the seaweed *Sargassum filipendula*. *Mar. Drugs* **2011**, *9*, 952–966.
40. Costa, L.S.; Telles, C.B.; Oliveira, R.M.; Nobre, L.T.; Dantas-Santos, N.; Camara, R.B.; Costa, M.S.; Almeida-Lima, J.; Melo-Silveira, R.F.; Albuquerque, I.R.; *et al.* Heterofucan from *Sargassum filipendula* induces apoptosis in HeLa cells. *Mar. Drugs* **2011**, *9*, 603–614.
41. Zhang, Z.; Teruya, K.; Eto, H.; Shirahata, S. Fucoidan extract induces apoptosis in MCF-7 cells via a mechanism involving the ROS-dependent JNK activation and mitochondria-mediated pathways. *PLoS One* **2011**, *6*, e27441.
42. Hyun, J.H.; Kim, S.C.; Kang, J.I.; Kim, M.K.; Boo, H.J.; Kwon, J.M.; Koh, Y.S.; Hyun, J.W.; Park, D.B.; Yoo, E.S.; *et al*. Apoptosis inducing activity of fucoidan in HCT-15 colon carcinoma cells. *Biol. Pharm. Bull.* **2009**, *32*, 1760–1764.
43. Kim, E.J.; Park, S.Y.; Lee, J.Y.; Park, J.H. Fucoidan present in brown algae induces apoptosis of human colon cancer cells. *BMC Gastroenterol.* **2010**, *10*, 96.
44. Yamasaki-Miyamoto, Y.; Yamasaki, M.; Tachibana, H.; Yamada, K. Fucoidan induces apoptosis through activation of caspase-8 on human breast cancer MCF-7 cells. *J. Agric. Food Chem.* **2009**, *57*, 8677–8682.
45. Vishchuk, O.S.; Ermakova, S.P.; Zvyagintseva, T.N. Sulfated polysaccharides from brown seaweeds *Saccharina japonica* and *Undaria pinnatifida*: isolation, structural characteristics, and antitumor activity. *Carbohydr. Res.* **2011**, *346*, 2769–2776.
46. Jin, J.O.; Song, M.G.; Kim, Y.N.; Park, J.I.; Kwak, J.Y. The mechanism of fucoidan-induced apoptosis in leukemic cells: Involvement of ERK1/2, JNK, glutathione, and nitric oxide. *Mol. Carcinog.* **2010**, *49*, 771–782.

47. Aisa, Y.; Miyakawa, Y.; Nakazato, T.; Shibata, H.; Saito, K.; Ikeda, Y.; Kizaki, M. Fucoidan induces apoptosis of human HS-sultan cells accompanied by activation of caspase-3 and down-regulation of ERK pathways. *Am. J. Hematol.* **2005**, *78*, 7–14.
48. Carmeliet, P. Angiogenesis in health and disease. *Nat. Med.* **2003**, *9*, 653–660.
49. Narazaki, M.; Segarra, M.; Tosato, G. Sulfated polysaccharides identified as inducers of neuropilin-1 internalization and functional inhibition of VEGF165 and semaphorin3A. *Blood* **2008**, *111*, 4126–4136.
50. Cho, M.L.; Lee, B.Y.; You, S.G. Relationship between oversulfation and conformation of low and high molecular weight fucoidans and evaluation of their *in vitro* anticancer activity. *Molecules* **2011**, *16*, 291–297.
51. Koyanagi, S.; Tanigawa, N.; Nakagawa, H.; Soeda, S.; Shimeno, H. Oversulfation of fucoidan enhances its anti-angiogenic and antitumor activities. *Biochem. Pharmacol.* **2003**, *65*, 173–179.
52. Teruya, T.; Konishi, T.; Uechi, S.; Tamaki, H.; Tako, M. Anti-proliferative activity of oversulfated fucoidan from commercially cultured *Cladosiphon okamuranus* TOKIDA in U937 cells. *Int. J. Biol. Macromol.* **2007**, *41*, 221–226.
53. Yang, C.; Chung, D.; Shin, I.S.; Lee, H.; Kim, J.; Lee, Y.; You, S. Effects of molecular weight and hydrolysis conditions on anticancer activity of fucoidans from sporophyll of *Undaria pinnatifida*. *Int. J. Biol. Macromol.* **2008**, *43*, 433–437.
54. Ye, J.; Li, Y.; Teruya, K.; Katakura, Y.; Ichikawa, A.; Eto, H.; Hosoi, M.; Hosoi, M.; Nishimoto, S.; Shirahata, S. Enzyme-digested fucoidan extracts derived from seaweed Mozuku of *Cladosiphon novae-caledoniae* kylin inhibit invasion and angiogenesis of tumor cells. *Cytotechnology* **2005**, *47*, 117–126.
55. Liu, J.M.; Bignon, J.; Haroun-Bouhedja, F.; Bittoun, P.; Vassy, J.; Fermandjian, S.; Wdzieczak-Bakala, J.; Boisson-Vidal, C. Inhibitory effect of fucoidan on the adhesion of adenocarcinoma cells to fibronectin. *Anticancer Res.* **2005**, *25*, 2129–2133.
56. Philchenkov, A.; Zavelevich, M.; Imbs, T.; Zaporozhets, T.; Zvyagintseva, T. Sensitization of human malignant lymphoid cells to etoposide by fucoidan, a brown seaweed polysaccharide. *Exp. Oncol.* **2007**, *29*, 181–185.
57. Jiang, Z.; Okimura, T.; Yokose, T.; Yamasaki, Y.; Yamaguchi, K.; Oda, T. Effects of sulfated fucan, ascophyllan, from the brown alga *Ascophyllum nodosum* on various cell lines: A comparative study on ascophyllan and fucoidan. *J. Biosci. Bioeng.* **2010**, *110*, 113–117.
58. Vishchuk, O.S.; Tarbeeva, D.V.; Ermakova, S.P.; Zvyagintseva, T.N. The structural characteristics and biological activity of fucoidans from the brown algae *Alaria* sp. and *Saccharina japonica* of different reproductive status. *Chem. Biodivers.* **2012**, *9*, 817–828.
59. Vishchuk, O.S.; Ermakova, S.P.; Zvyagintseva, T.N. The effect of sulfated (1→3)-alpha-L-fucan from the brown alga *Saccharina cichorioides* Miyabe on resveratrol-induced apoptosis in colon carcinoma cells. *Mar. Drugs* **2013**, *11*, 194–212.
60. Jeong, B.E.; Ko, E.J.; Joo, H.G. Cytoprotective effects of fucoidan, an algae-derived polysaccharide on 5-fluorouracil-treated dendritic cells. *Food Chem. Toxicol.* **2012**, *50*, 1480–1484.

61. Yang, M.; Ma, C.; Sun, J.; Shao, Q.; Gao, W.; Zhang, Y.; Li, Z.; Xie, Q.; Dong, Z.; Qu, X. Fucoidan stimulation induces a functional maturation of human monocyte-derived dendritic cells. *Int. Immunopharmacol.* **2008**, *8*, 1754–1760.
62. Jin, J.O.; Park, H.Y.; Xu, Q.; Park, J.I.; Zvyagintseva, T.; Stonik, V.A.; Kwak, J.Y. Ligand of scavenger receptor class A indirectly induces maturation of human blood dendritic cells via production of tumor necrosis factor-alpha. *Blood* **2009**, *113*, 5839–5847.
63. Hu, Y.; Cheng, S.C.; Chan, K.T.; Ke, Y.; Xue, B.; Sin, F.W.; Zeng, C.; Xie, Y. Fucoidin enhances dendritic cell-mediated T-cell cytotoxicity against NY-ESO-1 expressing human cancer cells. *Biochem. Biophys. Res. Commun.* **2010**, *392*, 329–334.
64. Lee, H.; Kim, J.S.; Kim, E. Fucoidan from seaweed *Fucus vesiculosus* inhibits migration and invasion of human lung cancer cell via PI3K-Akt-mTOR pathways. *PLoS One* **2012**, *7*, e50624.
65. Xue, M.; Ge, Y.; Zhang, J.; Wang, Q.; Hou, L.; Liu, Y.; Sun, L.; Li, Q. Anticancer properties and mechanisms of fucoidan on mouse breast cancer *in vitro* and *in vivo*. *PLoS One* **2012**, *7*, e43483.
66. Lee, N.Y.; Ermakova, S.P.; Choi, H.K.; Kusaykin, M.I.; Shevchenko, N.M.; Zvyagintseva, T.N.; Choi, H.S. Fucoidan from *Laminaria cichorioides* inhibits AP-1 transactivation and cell transformation in the mouse epidermal JB6 cells. *Mol. Carcinog.* **2008**, *47*, 629–637.
67. Lee, N.Y.; Ermakova, S.P.; Zvyagintseva, T.N.; Kang, K.W.; Dong, Z.; Choi, H.S. Inhibitory effects of fucoidan on activation of epidermal growth factor receptor and cell transformation in JB6 Cl41 cells. *Food Chem. Toxicol.* **2008**, *46*, 1793–1800.
68. Moon, H.J.; Lee, S.H.; Ku, M.J.; Yu, B.C.; Jeon, M.J.; Jeong, S.H.; Stonik, V.A.; Zvyagintseva, T.N.; Ermakova, S.P.; Lee, Y.H. Fucoidan inhibits UVB-induced MMP-1 promoter expression and down regulation of type I procollagen synthesis in human skin fibroblasts. *Eur. J. Dermatol.* **2009**, *19*, 129–134.
69. Moon, H.J.; Lee, S.R.; Shim, S.N.; Jeong, S.H.; Stonik, V.A.; Rasskazov, V.A.; Zvyagintseva, T.; Lee, Y.H. Fucoidan inhibits UVB-induced MMP-1 expression in human skin fibroblasts. *Biol. Pharm. Bull.* **2008**, *31*, 284–289.
70. Moon, H.J.; Park, K.S.; Ku, M.J.; Lee, M.S.; Jeong, S.H.; Imbs, T.I.; Zvyagintseva, T.N.; Ermakova, S.P.; Lee, Y.H. Effect of *Costaria costata* fucoidan on expression of matrix metalloproteinase-1 promoter, mRNA, and protein. *J. Nat. Prod.* **2009**, *72*, 1731–1734.
71. Jintang, S.; Alei, F.; Yun, Z.; Weixu, H.; Meixiang, Y.; Fengcai, W.; Xun, Q. Fucoidan increases TNF-alpha-induced MMP-9 secretion in monocytic cell line U937. *Inflamm. Res.* **2010**, *59*, 271–276.
72. Cumashi, A.; Ushakova, N.A.; Preobrazhenskaya, M.E.; D'Incecco, A.; Piccoli, A.; Totani, L.; Tinari, N.; Morozevich, G.E.; Berman, A.E.; Bilan, M.I.; *et al*. A comparative study of the anti-inflammatory, anticoagulant, antiangiogenic, and antiadhesive activities of nine different fucoidans from brown seaweeds. *Glycobiology* **2007**, *17*, 541–552.
73. Hemmingson, J.A.; Falshaw, R.; Furneaux, R.H.; Thompson, K. Structure and antiviral activity of the galactofucans from *Undaria pinnatifida*. *J. Appl. Phycol.* **2006**, *18*, 185–193.

74. Makarenkova, I.D.; Deriabin, P.G.; L'vov, D.K.; Zvyagintseva, T.N.; Besednova, N.N. Antiviral activity of sulfated polysaccharide from the brown alga *Laminaria japonica* against avian influenza A (H5N1) virus infection in the cultured cells. *Vopr. Virusol.* **2010**, *55*, 41–45.
75. Wang, J.; Zhang, Q.; Zhang, Z.; Song, H.; Li, P. Potential antioxidant and anticoagulant capacity of low molecular weight fucoidan fractions extracted from *Laminaria japonica*. *Int. J. Biol. Macromol.* **2010**, *46*, 6–12.
76. Zhu, W.; Ooi, V.E.; Chan, P.K.; Ang, P.O., Jr. Isolation and characterization of a sulfated polysaccharide from the brown alga *Sargassum patens* and determination of its anti-herpes activity. *Biochem. Cell. Biol.* **2003**, *81*, 25–33.
77. Teas, J.; Vena, S.; Cone, D.L.; Irhimeh, M. The consumption of seaweed as a protective factor in the etiology of breast cancer: proof of principle. *J. Appl. Phycol.* **2013**, *25*, 771–779.
78. Ikeguchi, M.; Yamamoto, M.; Arai, Y.; Maeta, Y.; Ashida, K.; Katano, K.; Miki, Y.; Kimura, T. Fucoidan reduces the toxicities of chemotherapy for patients with unresectable advanced or recurrent colorectal cancer. *Oncol. Lett.* **2011**, *2*, 319–322.
79. Ale, M.T.; Mikkelsen, J.D.; Meyer, A.S. Important determinants for fucoidan bioactivity: A critical review of structure-function relations and extraction methods for fucose-containing sulfated polysaccharides from brown seaweeds. *Mar. Drugs* **2011**, *9*, 2106–2130.
80. Imbs, T.I.; Shevchenko, N.M.; Semenova, T.L.; Sukhoverkhov, S.V.; Zvyagintseva, T.N. Compositional heterogeneity of sulfated polysaccharides synthesized by the brown alga *Costaria costata*. *Chem. Nat. Comp*. **2011**, *47*, 96–97.
81. Skriptsova, A.V.; Shevchenko, N.M.; Tarbeeva, D.V.; Zvyagintseva, T.N. Comparative study of polysaccharides from reproductive and sterile tissues of five brown seaweeds. *Mar. Biotechnol.* **2012**, *14*, 304–311.
82. Anastyuk, S.D.; Shevchenko, N.M.; Nazarenko, E.L.; Dmitrenok, P.S.; Zvyagintseva, T.N. Structural analysis of a fucoidan from the brown alga *Fucus evanescens* by MALDI-TOF and tandem ESI mass spectrometry. *Carbohydr. Res.* **2009**, *344*, 779–787.
83. Bilan, M.I.; Usov, A.I. Structural analysis of fucoidans. *Nat. Prod. Commun.* **2008**, *3*, 1639–1648.
84. Usov, A.I.; Chizhov, A.O. New data on the structure of laminaran from *Chorda filum* (L.) Lam. and reserve glycans from other brown algae. *Russ. Chem. Bull.* **1993**, *42*, 1597–1601.
85. Rioux, L.E.; Turgeon, S.L.; Beaulieu, M. Structural characterization of laminaran and galactofucan extracted from the brown seaweed *Saccharina longicruris. Phytochemistry* **2010**, *71*, 1586–1595.
86. Menshova, R.V.; Ermakova, S.P.; Anastyuk, S.D.; Isakov, V.V.; Dubrovskaya, Y.V.; Kusaikin, M.I.; Um, B.H.; Zvyagintseva, T.N. Structure, enzymatic transformation and anticancer activity of branched high molecular weight laminaran from brown alga *Eisenia bicyclis*. *Carbohydr. Polym.* **2014**, *99*, 101–109.

87. Akramiene, D.; Aleksandraviciene, C.; Grazeliene, G.; Zalinkevicius, R.; Suziedelis, K.; Didziapetriene, J.; Simonsen, U.; Stankevicius, E.; Kevelaitis, E. Potentiating effect of beta-glucans on photodynamic therapy of implanted cancer cells in mice. *Tohoku J. Exp. Med.* **2010**, *220*, 299–306.
88. Kuda, T.; Yano, T.; Matsuda, N.; Nishizawa, M. Inhibitory effects of laminaran and low molecular alginate against the putrefactive compounds produced by intestinal microflora *in vitro* and in rats. *Food Chem.* **2005**, *91*, 745–749.
89. Mantovani, M.S.; Bellini, M.F.; Angeli, J.P.; Oliveira, R.J.; Silva, A.F.; Ribeiro, L.R. beta-Glucans in promoting health: prevention against mutation and cancer. *Mutat. Res.* **2008**, *658*, 154–161.
90. Miao, H.Q.; Elkin, M.; Aingorn, E.; Ishai-Michaeli, R.; Stein, C.A.; Vlodavsky, I. Inhibition of heparanase activity and tumor metastasis by laminarin sulfate and synthetic phosphorothioate oligodeoxynucleotides. *Int. J. Cancer* **1999**, *83*, 424–431.
91. Liu, Z.; Lv, D.; Liu, S.; Gong, J.; Wang, D.; Xiong, M.; Chen, X.; Xiang, R.; Tan, X. Alginic acid-coated chitosan nanoparticles loaded with legumain DNA vaccine: effect against breast cancer in mice. *PLoS One* **2013**, *8*, e60190.
92. Usov, A.I. Polysaccharides of the red algae. *Adv. Carbohydr. Chem. Biochem.* **2011**, *65*, 115–217.
93. Buck, C.B.; Thompson, C.D.; Roberts, J.N.; Muller, M.; Lowy, D.R.; Schiller, J.T. Carrageenan is a potent inhibitor of papillomavirus infection. *PLoS Pathog.* **2006**, *2*, e69.
94. Sun, T.; Tao, H.; Xie, J.; Zhang, S.; Xu, X. Degradation and antioxidant activity of κ-Carrageenans. *J. Appl. Polym. Sci.* **2010**, *117*, 194–199.
95. Hu, X.; Jiang, X.; Aubree, E.; Boulenguer, P.; Critchley, A.T. Preparation and *in vivo* antitumor activity of kappa-carrageenan oligosaccharides. *Pharm. Biol.* **2006**, *44*, 646–650.
96. Zhou, G.; Xin, H.; Sheng, W.; Li, Z.; Xu, Z. *In vivo* growth-inhibition of S180 tumor by mixture of 5-Fu and low molecular lambda-carrageenan from *Chondrus ocellatus*. *Pharmacol. Res.* **2005**, *51*, 153–157.
97. Yuan, H.; Song, J.; Li, X.; Li, N.; Dai, J. Immunomodulation and antitumor activity of kappa-carrageenan oligosaccharides. *Cancer Lett.* **2006**, *243*, 228–234.
98. Lins, K.O.; Bezerra, D.P.; Alves, A.P.; Alencar, N.M.; Lima, M.W.; Torres, V.M.; Farias, W.R.; Pessoa, C.; de Moraes, M.O.; Costa-Lotufo, L.V. Antitumor properties of a sulfated polysaccharide from the red seaweed *Champia feldmannii* (Diaz-Pifferer). *J. Appl. Toxicol.* **2009**, *29*, 20–26.
99. Tobacman, J.K. Review of harmful gastrointestinal effects of carrageenan in animal experiments. *Environ. Health Perspect.* **2001**, *109*, 983–994.
100. Benard, C.; Cultrone, A.; Michel, C.; Rosales, C.; Segain, J.P.; Lahaye, M.; Galmiche, J.P.; Cherbut, C.; Blottiere, H.M. Degraded carrageenan causing colitis in rats induces TNF secretion and ICAM-1 upregulation in monocytes through NF-kappaB activation. *PLoS One* **2010**, *5*, e8666.

101. Cohen, S.M.; Ito, N. A critical review of the toxicological effects of carrageenan and processed eucheuma seaweed on the gastrointestinal tract. *Crit. Rev. Toxicol.* **2002**, *32*, 413–444.
102. Weiner, M.L.; Nuber, D.; Blakemore, W.R.; Harriman, J.F.; Cohen, S.M. A 90-day dietary study on kappa carrageenan with emphasis on the gastrointestinal tract. *Food Chem. Toxicol.* **2007**, *45*, 98–106.
103. Lahaye, M.; Robic, A. Structure and functional properties of ulvan, a polysaccharide from green seaweeds. *Biomacromolecules* **2007**, *8*, 1765–1774.
104. Bilan, M.I.; Vinogradova, E.V.; Shashkov, A.S.; Usov, A.I. Structure of a highly pyruvylated galactan sulfate from the Pacific green alga *Codium yezoense* (Bryopsidales, Chlorophyta). *Carbohydr. Res.* **2007**, *342*, 586–596.
105. Farias, E.H.; Pomin, V.H.; Valente, A.P.; Nader, H.B.; Rocha, H.A.; Mourao, P.A. A preponderantly 4-sulfated, 3-linked galactan from the green alga *Codium isthmocladum*. *Glycobiology* **2008**, *18*, 250–259.
106. Fernandez, P.V.; Estevez, J.M.; Cerezo, A.S.; Ciancia, M. Sulfated β-D-mannan from green seaweed *Codium vermilara*. *Cabohydr. Polym.* **2012**, *87*, 916–919.
107. Costa, L.S.; Fidelis, G.P.; Cordeiro, S.L.; Oliveira, R.M.; Sabry, D.A.; Camara, R.B.; Nobre, L.T.; Costa, M.S.; Almeida-Lima, J.; Farias, E.H.; *et al.* Biological activities of sulfated polysaccharides from tropical seaweeds. *Biomed. Pharmacother.* **2010**, *64*, 21–28.
108. Ji, H.; Shao, H.; Zhang, C.; Hong, P.; Xiong, H. Separation of the polysaccharides in *Caulerpa racemosa* and their chemical composition and antitumor activity. *J. Appl. Polym. Sci.* **2008**, *110*, 1435–1440.
109. Kim, J.K.; Cho, M.L.; Karnjanapratum, S.; Shin, I.S.; You, S.G. *In vitro* and *in vivo* immunomodulatory activity of sulfated polysaccharides from *Enteromorpha prolifera*. *Int. J. Biol. Macromol.* **2011**, *49*, 1051–1058.
110. Leiro, J.M.; Castro, R.; Arranz, J.A.; Lamas, J. Immunomodulating activities of acidic sulphated polysaccharides obtained from the seaweed *Ulva rigida* C. Agardh. *Int. Immunopharmacol.* **2007**, *7*, 879–888.
111. Tabarsa, M.; Han, J.H.; Kim, C.Y.; You, S.G. Molecular characteristics and immunomodulatory activities of water-soluble sulfated polysaccharides from *Ulva pertusa*. *J. Med. Food* **2012**, *15*, 135–144.
112. Devaki, T.; Sathivel, A.; BalajiRaghavendran, H.R. Stabilization of mitochondrial and microsomal function by polysaccharide of *Ulva lactuca* on D-galactosamine induced hepatitis in rats. *Chem. Biol. Interact.* **2009**, *177*, 83–88.
113. Sathivel, A.; Raghavendran, H.R.; Srinivasan, P.; Devaki, T. Anti-peroxidative and anti-hyperlipidemic nature of *Ulva lactuca* crude polysaccharide on D-galactosamine induced hepatitis in rats. *Food Chem. Toxicol.* **2008**, *46*, 3262–3267.
114. Shimura, H.; Itoh, K.; Sugiyama, A.; Ichijo, S.; Ichijo, M.; Furuya, F.; Nakamura, Y.; Kitahara, K.; Kobayashi, K.; Yukawa, Y.; *et al*. Absorption of radionuclides from the Fukushima nuclear accident by a novel algal strain. *PLoS One* **2012**, *7*, e44200.

115. de Jesus Raposo, M.F.; de Morais, R.M.; de Morais, A.M. Bioactivity and applications of sulphated polysaccharides from marine microalgae. *Mar. Drugs* **2013**, *11*, 233–252.
116. Talyshinsky, M.M.; Souprun, Y.Y.; Huleihel, M.M. Anti-viral activity of red microalgal polysaccharides against retroviruses. *Cancer Cell Int.* **2002**, *2*, 8–14.
117. Hasui, M.; Matsuda, M.; Okutani, K.; Shigeta, S. *In vitro* antiviral activities of sulfated polysaccharides from a marine microalga (*Cochlodinium polykrikoides*) against human immunodeficiency virus and other enveloped viruses. *Int. J. Biol. Macromol.* **1995**, *17*, 293–297.
118. Fabregas, J.; Carcia, D.; Fernandez-Alonso, M.; Rocha, A.I.; Gomez-Puertas, P.; Escribano, J.M.; Otero, A.; Coll, J.M. *In vitro* inhibition of the replication of haemorrhagic septicaemia virus (VHSV) and African swine fever virus (ASFV) by extracts from marine microalgae. *Antiviral Res.* **1999**, *44*, 67–73.
119. Huleihel, M.; Ishanu, V.; Tal, J.; Arad, S.M. Antiviral effects of red microalgal polysaccharides on *Herpes simplex* and *Varicella zoster* viruses. *J. Appl. Phycol.* **2001**, *13*, 127–134.
120. Pugh, N.; Ross, S.A.; ElSohly, H.N.; ElSohly, M.A.; Pasco, D.S. Isolation of three high molecular weight polysaccharide preparations with potent immunostimulatory activity from *Spirulina platensis*, aphanizomenon flos-aquae and *Chlorella pyrenoidosa*. *Planta Med.* **2001**, *67*, 737–742.
121. Sun, L.; Wang, C.; Shi, Q.; Ma, C. Preparation of different molecular weight polysaccharides from *Porphyridium cruentum* and their antioxidant activities. *Int. J. Biol. Macromol.* **2009**, *45*, 42–47.
122. Park, E.J.; Pezzuto, J.M. Antioxidant marine products in cancer chemoprevention. *Antioxid. Redox Signal.* **2013**, *19*, 115–138.
123. Gardeva, E.; Toshkova, R.; Minkova, K.; Gigova, L. Cancer protective action of polysaccharide derived from microalga *Porphyridium cruentum*—biological background. *Biotechnol. Biotechnol. Equip.* **2009**, *23*, 783–787.
124. Choi, W.Y.; Kang D.H.; Lee, H.Y. Enhancement of immune activation activities of *Spirulina maxima* grown in deep-sea water. *Int. J. Mol. Sci.* **2013**, *14*, 12205–12221.
125. Ismail, M.F.; Ali, D.A.; Fernando, A.; Abdraboh, M.E.; Gaur, R.L.; Ibrahim, W.M.; Raj, M.H.; Ouhtit, A. Chemoprevention of rat liver toxicity and carcinogenesis by *Spirulina*. *Int. J. Biol. Sci.* **2009**, *5*, 377–387.
126. Matsuda, M.; Yamori, T.; Naitoh, M.; Okutani, K. Structural revision of sulfated polysaccharide B-1 isolated from a marine Pseudomonas species and its cytotoxic activity against human cancer cell lines. *Mar. Biotechnol.* **2003**, *5*, 13–19.
127. Sun, C.; Wang, J.W.; Fang, L.; Gao, X.D.; Tan, R.X. Free radical scavenging and antioxidant activities of EPS2, an exopolysaccharide produced by a marine filamentous fungus *Keissleriella* sp. YS 4108. *Life Sci.* **2004**, *75*, 1063–1073.
128. Heath-Heckman, E.A.C.; McFall-Ngai, M.J. The occurrence of chitin in the hemocytes of invertebrates. *Zoology* **2011**, *114*, 191–198.

129. Kozlowski, E.O.; Gomes, A.M.; Silva, C.S.; Pereira, M.S.; de Vilela Silva, A.C.; Pavao, M.S.G. Structure and biological activities of glycosaminoglycan analogs from marine invertebrates: New therapeutic agents? In *Glycans in Diseases and Therapeutics*; Pavao, M.S.G., Ed.; Springer-Verlag: Heidelberg, Berlin, Germany, 2011; pp. 159–184.
130. Yin, H.; Du, Y.; Zhang, J. Low molecular weight and oligomeric chitosans and their bioactivities. *Curr. Top. Med. Chem.* **2009**, *9*, 1546–1559.
131. Pomin, V.H.; de Souza Mourao, P.A. Structure *versus* anticoagulant and antithrombotic actions of marine sulfated polysaccharides. *Braz. J. Pharmacogn.* **2012**, *22*, 921–928.
132. Luo, L.; Wu, M.; Xu, L.; Lian, W.; Xiang, J.; Lu, F.; Gao, N.; Xiao, C.; Wang, S.; Zhao, J. Comparison of physicochemical characteristics and anticoagulant activities of polysaccharides from three sea cucumbers. *Mar. Drugs* **2013**, *11*, 399–417.
133. Chen, S.; Li, G.; Wu, N.; Guo, X.; Liao, N.; Ye, X.; Liu, D.; Xue, C.; Chai, W. Sulfation pattern of the fucose branch is important for the anticoagulant and antithrombotic activities of fucosylated chondroitin sulfates. *Biochim. Biophys. Acta* **2013**, *1830*, 3054–3066.
134. Zhang, W.; Wang, J.; Jin, W.; Zhang, Q. The antioxidant activities and neuroprotective effects of polysaccharides from the starfish *Asterias rollestoni*. *Carbohydr. Polym*. **2013**, *95*, 9–15.
135. Zhang, Y.; Song, S.; Liang, H.; Wang, Y.; Wang, W.; Ji, A. Enchancing effect of a sea cucumber *Stichopus japonicus* sulfated polysaccharide on neurosphere formation *in vitro*. *J. Biosci. Bioeng*. **2010**, *110*, 479–486.
136. Sheng, X.; Zhang, N.; Song, S.; Li, M.; Liang, H.; Zhang, Y.; Wang, Y.; Ji, A. Morphological transformation and proliferation of rat astrocytes as induced by sulfated polysaccharides from the sea cucumber *Stichopus japonicus*. *Neurosci. Lett.* **2011**, *503*, 37–42.
137. Lian, W.; Wu, M.; Huang, N.; Gao, N.; Li, Z.; Zhang, Z.; Zheng, Y.; Peng, W.; Zhao, J. Anti-HIV-1 activity and structure-activity-relationship study of a fucosylated glycosaminoglycan from an echinoderm by targeting the conserved CD4 induced epitope. *Biochim. Biophys. Acta* **2013**, *1830*, 4681–4691.
138. Liu, C.H.; Lin, Q.X.; Gao, Y.; Ye, L.; Xing, Y.Y.; Xi, T. Characterization and antitumor activity of a polysaccharide from *Strongylocentrotus nudus* eggs. *Carbohydr. Polym*. **2007**, *67*, 313–318.
139. Liu, C.; Xi, T.; Lin, Q.; Xing, Y.; Ye, L.; Luo, X.; Wang, F. Immunomodulatory activity of polysaccharides isolated from *Strongylocentrotus nudus* eggs. *Int. Immunopharmacol.* **2008**, *8*, 1835–1841.
140. Wang, M.; Wang, H.; Tang, Y.; Kang, D.; Gao, Y.; Ke, M.; Dou, J.; Xi, T.; Zhou, C. Effective inhibition of a *Strongylocentrotus nudus* eggs polysaccharide against hepatocellular carcinoma is mediated via immunoregulation *in vivo*. *Immunol. Lett*. **2011**, *141*, 74–82.
141. Wang, H.; Wang, M.; Chen, J.; Tang, Y.; Dou, J.; Yu, J.; Xi, T.; Zhou, C. A polysaccharide from *Strongylocentrotus nudus* eggs protect against myelosuppression and immunosuppression in cyclophosphamide-treated mice. *Int. Immunopharmacol.* **2011**, *11*, 1946–1953.

142. Suna L.; Zhua, B.; Lia, D.; Wanga, L.; Donga, X.; Muratab, Y.; Xingc, R.; Dongd, Y. Purification and bioactivity of a sulfated polysaccharide conjugate from viscera of abalone *Haliotis discus hannai* Ino. *Food Agric. Immunol.* **2010**, *21*, 15–26.
143. Azmi, A.S.; Ahmad, A.; Banerjee, S.; Rangnekar, V.M.; Mohammad, R.M.; Sarkar, F.H. Chemoprevention of pancreatic cancer: Characterization of Par-4 and its modulation by 3,3′-diindolylmethane (DIM). *Pharm. Res*. **2008**, *25*, 2117–2124.
144. Surh, Y.-J. Molecular mechanisms of chemopreventive effects of selected dietary and medicinal phenolic compounds. *Mutat. Res*. **1999**, *428*, 305–327.
145. Pan, M.-H.; Ho, C.-T. Chemopreventive effects of natural dietary compounds on cancer development. *Chem. Soc. Rev*. **2008**, *37*, 2558–2574.
146. Cerella, C.; Sobolewski, C.; Dicato, M.; Diederich, M. Targeting COX-2 expression by natural compounds: A promising alternative strategy to synthetic COX-2 inhibitors for cancer chemoprevention and therapy. *Biochem. Pharmacol*. **2010**, *80*, 1801–1815.
147. Schumacher, M.; Kelkel, M.; Dicato, M.; Diederich, M. Gold from the sea: Marine compounds as inhibitors of the hallmarks of cancer. *Biotechnol. Adv*. **2011**, *29*, 531–547.
148. Kiprushina, Yu.O.; Lukyanov, P.A.; Odintsova, N.A. Effect of mytilan on the UV-radiation resistance of marine invertebrate larvae and human lymphocytes. *Russ. J. Mar. Biol*. **2010**, *36*, 305–310.
149. Kale, V.; Freysdottir, J.; Paulsen, B.S.; Fridjonsson, O.H.; Hreggvidsson, G.O.; Omarsdottir, S. Sulfated polysaccharide from the sea cucumber *Cucumaria frondosa* affect maturation of human dendritic cells and their activation of allogeneic CD4(+) T cells *in vitro*. *Bioact. Carbohydr. Diet. Fibre* **2013**, *2*, 108–117.
150. Borsig, L.; Wang, L.; Cavalcante, M.C.M.; Cardilo-Reis, L.; Ferreira, P.L.; Mourao, P.A.S.; Esko, J.D.; Pavao, M.S.G. Selectin bloking activity of a fucosylated chondroitin sulfate glycosaminoglycan from sea cucumber. Effect on tumor metastasis and neutrophil recruitment. *J. Biol. Chem*. **2007**, *282*, 14984–14991.
151. Kawashima, H.; Atarashi, K.; Hirose, M.; Hirose, J.; Yamada, S.; Sugahara, K.; Miyasaka, M. Oversulfated chondroitin/dermatan sulfates containing glcabeta1/iodaalpha1-3galnac (4,6-*o*-disulfate) interact with L- and P-selectin and chemokines. *J. Biol. Chem*. **2002**, *277*, 12921–12930.
152. Wang, L.; Brown, J.R.; Vaki, A.; Esko, J.D. Heparin's anti-inflammatory effects require glucosamine 6-*o*-sulfation and are mediated by blockade of L- and P-selectins. *J. Clin. Invest*. **2002**, *110*, 127–136.
153. Wang, Y.; Su, W.; Zhang, C.; Xue, C.; Chang, Y.; Wu, X.; Tang, Q.; Wang, J. Protective effect of sea cucumber (*Acaudina molpadioides*) fucoidan against ethanol-induced gastric damage. *Food Chem*. **2012**, *133*, 1414–1419.
154. Xu, C.X.; Jin, H.; Chung, Y.S.; Shin, J.Y.; Lee, K.H.; Beck, G.R., Jr.; Palmos, G.N.; Choi, B.D.; Cho, M.H. Chondroitin sulfate extracted from ascidian tunic inhibits phorbol ester-induced expression of inflammatory factors VCAM-1 and COX-2 by blocking NF-κB activation in mouse skin. *J. Agric. Food Chem*. **2008**, *56*, 9667–9675.

155. Xu, C.X.; Jin, H.; Chung, Y.S.; Shin, J.Y.; Woo, M.A.; Lee, K.H.; Palmos, G.N.; Choi, B.D.; Cho, M.H. Chondroitin sulfate extracted from the *Styela clava* tunic suppresses TNF-α-induced expression of inflammatory factors, VCAM-1 and iNOS by blocking Akt/NF-κB signal in JB6 cells. *Cancer Lett.* **2008**, *264*, 93–100.
156. Brito, A.S.; Arimateia, D.S.; Souza, L.R.; Lima, M.A.; Santos, V.O.; Medeiros, V.P.; Ferreira, P.A.; Silva, R.A.; Ferreira, C.V.; Justo, G.Z.; *et al.* Ant-inflammatory properties of a geparin-like glycosaminoglycan with reduced anti-coagulant activity isolated from a marine shrimp. *Bioorg. Med. Chem.* **2008**, *16*, 9588–9595.
157. Belmiro, C.L.; Castelo-Branco, M.T.; Melim, L.M.; Schanaider, A.; Elia, C.; Madi, K.; Pavao, M.S.; de Souza, H.S. Unfractionated heparin and new heparin analogues from ascidians (chordate-tunicate) ameliorate colitis in rats. *J. Biol. Chem*. **2009**, *284*, 11267–11278.
158. Dreyfuss, J.L.; Regatieri, C.V.; Lima, M.A.; Paredes-Gamero, E.J.; Brito, A.S.; Chavante, S.F.; Belfort, R.; Farah, M.E.; Nader, H.B. A heparin mimetic isolated from a marine shrimp suppresses neovascularization. *J. Thromb. Haemost.* **2010**, *8*, 1828–1837.

Fucoidan as a Marine Anticancer Agent in Preclinical Development

Jong-Young Kwak

Abstract: Fucoidan is a fucose-containing sulfated polysaccharide derived from brown seaweeds, crude extracts of which are commercially available as nutritional supplements. Recent studies have demonstrated antiproliferative, antiangiogenic, and anticancer properties of fucoidan *in vitro*. Accordingly, the anticancer effects of fucoidan have been shown to vary depending on its structure, while it can target multiple receptors or signaling molecules in various cell types, including tumor cells and immune cells. Low toxicity and the *in vitro* effects of fucoidan mentioned above make it a suitable agent for cancer prevention or treatment. However, preclinical development of natural marine products requires *in vivo* examination of purified compounds in animal tumor models. This review discusses the effects of systemic and local administration of fucoidan on tumor growth, angiogenesis, and immune reaction and whether *in vivo* and *in vitro* results are likely applicable to the development of fucoidan as a marine anticancer drug.

Reprinted from *Mar. Drugs*. Cite as: Kwak, J.-Y. Fucoidan as a Marine Anticancer Agent in Preclinical Development. *Mar. Drugs* **2014**, *12*, 851-870.

1. Introduction

Fucoidan is a polysaccharide that consists of sulfated fucose residues. The richest sources of fucoidan are marine organisms, including brown algae species such as *Laminaria* and *Fucus* [1]. Fucoidan-rich brown algae have been marketed as a dietary supplement or nutraceutical. Fucoidan has advantages of low toxicity, oral bioavailability, and multiple mechanisms of action. Pharmacologically, fucoidan affects many pathophysiological processes, including inflammation, vascular physiology, carcinogenesis, and oxidative stress [2,3]. Furthermore, fucoidan can easily be extracted using either hot water or acidic solutions [4]. Thus, fucoidan-containing food supplements or drinks have been traditionally administered to cancer patients in Korea, Japan, China, and other countries. Although the underlying anticancer effects of fucoidan are largely unknown, it can directly induce cytotoxicity and apoptosis in cancer cells [5]. Fucoidan can also affect cancer cells indirectly e.g., as an antiangiogenic agent. Furthermore, fucoidan has immune-stimulating effects on dendritic cells (DCs) [6–9] and natural killer (NK) cells [10,11]. Thus, fucoidan can enhance anticancer immunity through immune cell activation and influx and stimulation of the production of anticancer cytokines.

Fucoidan has been reported to be effective *in vivo* upon oral, intraperitoneal, or intravenous administration (Table 1). Australian groups have reported clinical trials using fucoidan [12–15]. Recently, Fitton reviewed the potential therapeutic use of fucoidan in various diseases, including infection, chronic inflammation and fibrosis, liver diseases, arthritis, and radiation injury [2]. Biological activities of fucoidan, including anticancer activity, may vary depending on the source of seaweed, compositional and structural traits, charge density, distribution, bonding of the sulfate substitutions, and purity of the fucoidan preparation [4,16].

The structure and function relationships of fucoidan and other sulfated polysaccharides have been reviewed previously [1,3,16]. This review discusses the preclinical development and use of fucoidan as a marine anticancer agent, based on *in vivo* findings in animal models of cancers or other diseases.

2. Cancer Cell Apoptosis *in Vitro*

Although the mechanisms underlying the antitumor activity of fucoidan are diverse, it has antitumor activity by inducing apoptosis in cancer cells. Fucoidan-mediated apoptosis of cancer cells likely involves up-regulation or down-regulation of multiple signaling pathways. However, signaling pathways leading to the apoptosis of cancer cells by fucoidan have not been fully characterized [5]. Recently, *in vitro* studies have shown the molecular mechanisms of fucoidan in the induction of apoptosis in various human cancer cells, including HL-60, NB4, THP-1, and U937 leukemic cells [17,18], MCF-7 breast cancer cells [19], AGS human gastric adenocarcinoma cells [20], A549 lung carcinoma cells [21], PC-3 prostatic cancer cells [22], and SMMC-7721 hepatocellular carcinoma cells [23]. Xue *et al.* demonstrated that intraperitoneally injected crude extracts of *Fucus vesiculosus* induced apoptosis of 4T1 breast cancer cells in tumor-bearing mice, but fucoidan alone did not cause apoptosis of some other cancer cells *in vitro* [24]. Thinh *et al.* demonstrated that highly purified fucoidan derived from the brown algae *Sargassum mcclurei* was less cytotoxic, but inhibited colony formation in DLD-1 colon cancer cells when used at up to 200 μg/mL for 48 h [25]. We showed previously that fucoidan derived from *Fucus vesiculosus* failed to induce apoptosis in K562 erythroleukemic [17] and mouse CT26 colon cancer cells [26], while it inhibited cell proliferation. These results suggest that apoptotic activity of fucoidan on cancer cells may be cell type specific.

Table 1. *In vivo* effect of fucoidan on tumor growth in tumor-bearing mice.

Fucoidan	Route/Dose	Tumor Type	Action Mechanism	References
Cladosiphon okamuranus	p.o. 5 g/kg	26 colon cancer cells	Natural killer (NK)cell-mediated	[11]
Fucus vesiculosus (Sigma, St. Louis, MO, USA)	i.p. 5 mg/kg	4T1 breast cancer cells	Inhibition of angiogenesis and induction of apoptosis	[24,25]
Fucus evanescence	10 mg/kg	Lewis lung carcinoma cells	Unknown	[27]
From Ze Lang Nanjing Med. Tech Co.	i.p. 200 mg/kg	Bel-7402 hepatocellular carcinoma in nude mice	Inhibition of proliferation	[28]
Fucus vesiculosus (Sigma, St. Louis, MO, USA)	Foot-pad injection 0.25 mg/mice	4T1-xenograft mice	Prevention of metastasis	[29]
Sargassum plagiophyllum	p.o. 75 mg/kg	Diethylnitrosamine-induced hepatocellular carcinoma	Inhibition of carcinogen metabolism	[30]
Cladosiphon okamuranus Tokida	p.o. 100 mg/kg	Sarcoma 180 (S-180)-xenograft	Delayed tumor growth by nitric oxide produced by macrophages	[31]
Undaria pinnatifida	Diet containing 1% Mekabu (34 mg/day)	A20 leukemia cells	Cytolytic activity by NK cell activation	[32]
Fucus vesiculosus (Sigma, St. Louis, MO, USA)	i.v. 5 mg/kg	Lewis lung carcinoma cells B16 melanoma cells	Antiangiogenic effect	[33]
Ascophyllum nodosum	1 mg/mice	MOPC-315 plasma cell tumor	Prevention of angiogenesis in tumor tissues	[34]

3. *In Vivo* Anticancer Effects

Tumor-bearing animal models are commonly utilized to study the effects of therapeutic interventions. Recently, fucoidan was shown to inhibit the growth of tumor cells in several animal models (Table 1). Importantly, fucoidan treatment is relatively safe in animals. For example, tumor-bearing mice tolerated repeated injections of a moderate dose of fucoidan (10 mg/kg) [27]. However, fucoidan at 25 mg/kg caused toxicity in the same mouse model [27]. When fucoidan derived from *Laminaria japonica* was administered to rats orally at 300 mg/kg per day, there were no significant toxic effects [35]. Other groups also demonstrated that there was no difference in body weight between controls and animals treated with 200 mg/kg of fucoidan administered intraperitoneally [28]. Importantly, in a recent phase-two clinical trial in humans conducted by Myers *et al.*, a seaweed-derived nutrient supplement, containing 75 mg fucoidan plus vitamin B6, zinc, and manganese, was found to be safe when taken orally over four weeks [15]. These results suggest that fucoidan generally has low toxicity and is well tolerated.

A substantial number of animal studies have been conducted for the treatment of cancer using fucoidan. Alekseyenko *et al.* showed that while a single injection of fucoidan at 25 mg/kg failed to inhibit tumor growth in mice with transplanted Lewis lung adenocarcinoma, repeated injections of fucoidan at 10 mg/kg resulted in pronounced antitumor and antimetastatic effects [27]. In a hepatocellular carcinoma xenograft mouse model established by implanting Bel-7402 cells in nu/nu mice, administering fucoidan at 200 mg/kg intraperitoneally caused an anticancer effect partly by inhibiting the proliferation of cancer cells *in vivo*, but not by apoptosis [28]. Xue *et al.* investigated the effects of fucoidan on the metastasis of cancer cells. They demonstrated that crude extracts of fucoidan suppressed lung metastasis of 4T1 breast cancer cells as well as tumor growth [24,36]. Fucoidan markedly reduced the growth rate of 4T1 cells and significantly diminished the number of metastatic tumor nodules present in the lungs of 4T1-xenografted mice [29]. Collectively, these results suggest that fucoidan treatment suppresses tumorigenesis and metastasis, supporting the potential development of fucoidan as an anticancer drug.

Molecular mechanisms underlying the mode of action of fucoidan were studied *in vivo*. Fucoidan was found to prevent diethylnitrosamine-induced hepatocarcinogenesis by inhibiting metabolic activation of the carcinogen [30]. Takeda *et al.* found that oral administration of fucoidan effectively inhibited growth of implanted Sarcoma-180 cells in xenograft mouse models [31]. Fucoidan likely mediated nitric oxide (NO) release by stimulated macrophages in the tumor microenvironment, thus causing apoptosis. Furthermore, supernatants from fucoidan-stimulated macrophages were found to cause apoptosis of Sarcoma-180 cells. This effect was negated by the addition of a NO synthase inhibitor, N^G-nitro-L-arginine methyl ester (L-NAME) [31]. Xue *et al.* demonstrated that β-catenin expression in tumor lesions was decreased significantly by fucoidan treatment of tumor-bearing mice [36]. In addition, fucoidan treatment lowered expression of cyclin D1 and c-myc *in vivo*. Similar to the *in vivo* results, *in vitro* experimental results also demonstrated that fucoidan modulated the Wnt/β-catenin signaling pathway. These results suggest that fucoidan exerts anticancer activity at least partly by down-regulating β-catenin signaling both *in vitro* and *in vivo*.

It has been suggested that differing *in vivo* effects of fucoidans may depend on electrical charge density, extent of sulfonation, and the molecular weight of different preparations [37]. The requirement for continuous administration may limit the use of high-molecular-weight (HMW) fucoidan in pharmaceutical and clinical applications [38]. The *in vitro* anticancer activity of fucoidans derived from the sporophyll of *Undaria pinnatifida* was significantly higher for low-molecular-weight fucoidan (490 kDa) than for native fucoidan of 5100 kDa [39]. Azuma *et al.* further investigated molecular-weight dependent effects of fucoidan on tumor growth and survival time in tumor-bearing mouse models [11]. They showed that oral administration of fucoidan extracted from *Cladosiphon okamuranus* in tumor-bearing mice suppressed colon tumor growth, but the tumor weight was lowered in mice treated with either LMW (6.4–40 kDa) or HMW fucoidan (300–330 kDa) preparations. Therefore, studying the anticancer efficacy of LMW and HMW fucoidan preparations in animal models should be an area of future research efforts.

4. *In Vivo* Anticancer Immune Responses

Maruyama *et al.* studied mice that were fed a diet containing Mekabu fucoidan, derived from the sporophyll of *Undaria pinnatifida* [32]. Mice were on the diet for 10 days before subcutaneous inoculation with lymphoma cells. Thereafter, the mice were fed the same diet for 40 days. Cell growth was significantly inhibited in these mice. However, tumor growth was not inhibited in mice fed with fucoidan diet only 40 days after inoculation of lymphoma cells [32]. The authors suggested that this anticancer activity may have been due to activation of an immune response initiated even before inoculation of cancerous cells rather than a direct cytotoxic effect by fucoidan on lymphoma cells. Further *in vivo* studies have elucidated potential mechanisms underlying the fucoidan-mediated anticancer immune responses. For example, fucoidan can affect immune cell activity and cytokine production. The killer activities of T cell-mediated NK cells were enhanced in mice fed with fucoidan compared to control mice [10,32]. NK cell activation was associated with increased production of interferon (IFN)-γ and interleukin (IL)-12 by splenic T cells in fucoidan-fed mice [32,40]. Furthermore, oral administration of fucoidan increased the number of splenic NK cells in tumor-bearing mice [11].

It has been suggested that immunostimulation and immunosuppression occur simultaneously in cancer patients, and deactivation of certain cytokines could offer an unexploited and novel anticancer treatment approach [41]. Cancer-induced immune suppression is related to a defective IL-12–IFN-γ−HLA-DR axis [41]. Proinflammatory cytokines such as IL-12 are essential for inducing the Th1 response [42]. *In vitro* experiments in our laboratory have shown that the secretion of IL-12p70 and IFN-γ is enhanced by co-culturing T cells with fucoidan-activated human peripheral blood DCs, whereas fucoidan-activated DCs alone failed to produce IL-12p70 [8]. On the other hand, Hu *et al.* demonstrated that fucoidan could enhance the maturation of DCs and the cross-presentation of cancer testis antigen, NY-ESO-1 to $CD8^+$ T cells, thus augmenting the cytotoxicity of T cells against NY-ESO-1-expressing cancer cells [9]. Interestingly, fucoidan was found to increase NY-SEO-1 binding to human DCs [9]. Cancer immunotherapy using DCs generated *in vitro* has been proven to be safe in clinical trials in combination with a DC activator [43]. Accordingly, we observed that the co-administration of DCs and fucoidan in tumor-bearing mice

significantly decreased tumor growth when compared to the administration of DCs or fucoidan alone (in preparation). Therefore, fucoidan could modulate anticancer immune responses against different cancer cell types.

5. Antiangiogenic Effects of Fucoidan *in Vivo*

Targeting tumor angiogenesis or new vasculature formation has advanced cancer therapy [44]. Limiting new blood vessel formation by antiangiogenic agents reduces intratumoral blood flow, hence limiting growth and metastatic potential. There have been contradictory reports of the effects of fucoidan on angiogenesis. Oversulfated fucoidan was found to inhibit tumor-induced angiogenesis [33,45], whereas fucoidan has been associated with neovascularization in other diseases [46].

Oversulfated fucoidan was found to inhibit the basic fibroblast growth factor (bFGF)-induced tube formation by human umbilical vein endothelial cells [45], while other sulfated polysaccharides inhibited the proliferation and migration of vascular endothelial cells by altering FGF binding to cell surface FGF receptors [47]. In contrast, fucoidan promoted FGF-2 effects *in vivo* [37] and LMW fucoidan (MW. *ca*. 4 kDa) prepared by radical degradation promoted bFGF-induced tube formation of endothelial cells [48,49]. On the other hand, in *ex vivo* angiogenesis assays, where rat aortic tissue was placed on Matrigel™ and capillary tube formation was measured, fucoidan derived from *Undaria pinnatifida* suppressed angiogenesis in the aortic rings when used at 100 μg/mL [50]. However, LMW fucoidan reduced intimal hyperplasia in a rat aortic allograft model of transplant atherosclerosis, while stimulating formation of an endothelial lining in the vascular allograft [51]. Wang and Miao reviewed the currently used marine-derived angiogenesis inhibitors, suggesting that different fucoidan preparations affect angiogenesis differently, depending on molecular weight and extent of sulfation: (1) LMW fucoidans (4–9 kDa) stimulated angiogenesis in different assays; (2) mid-molecular-weight fucoidans (15–20 kDa) enhanced HUVEC migration, but have not been shown to inhibit HUVEC tube formation; and (3) natural fucoidans of HMW (30 kDa) showed antiangiogenic properties by inhibiting proliferation, migration, and tube formation of endothelial cells and inhibiting vascular network formation [52].

Koyanagi *et al.* demonstrated that fucoidan prevented phosphorylation of the receptor for vascular endothelial growth factor (VEGF) upon VEGF binding [33]. Furthermore, the authors observed that repetitive intravenous administration of fucoidan at 5 mg/kg in mice suppressed neovascularization from surrounding blood vessels in the region adjacent to implanted Sarcoma 180 cells. Similarly, intraperitoneal administration of fucoidan (1 mg/mouse) in mice implanted with the murine plasma cell tumor line, MOPC-315, which expresses VEGF, reduced VEGF-induced angiogenesis, tumor neovascularization, and tumor growth [34]. In 2012, Xue *et al.* demonstrated that fucoidan caused a significant reduction in intratumoral VEGF expression in mice implanted with 4T1 breast cancer cells compared to untreated control animals [24]. These promising results indicate that fucoidan could play an important role as an antiangiogenic factor in cancer. Further investigations of angiogenesis using various *in vivo* cancer models treated with fucoidan are warranted.

6. Mobilization of Hematopoietic Progenitor Cells

Reportedly, fucoidan can inhibit selectin function *in vitro* and *in vivo* [53]. Fucoidan blocks leukocyte rolling and interferes with various inflammatory responses in animal models [54–58]. In addition, it can reduce platelet aggregation by inhibiting P-selectin [59]. However, significant mobilization of progenitor cells and leukocytosis could be elicited in selectin-deficient mice similar to that of wild-type controls, suggesting that the mode of action of fucoidan is not through selectins [60,61]. The *in vivo* effects of fucoidan on leukocytes in other disease models are summarized in Table 2.

Table 2. *In vivo* effects of fucoidan on leukocytes in various disease models.

Test	Route	Dose	Possible *in vivo* effects	References
Human	p.o.	330 mg	Mobilization of leukocytes	[12]
Human	p.o.	100 mg	Immune modulation	[15]
Rabbit	i.v.	10 mg/kg	Decreased influx of leukocytes into cerebrospinal fluid in meningitis	[58]
Mice	i.v. i.p.	50 mg/kg 50 mg/kg	Mobilization of hematopoietic progenitor stem cells (HPCs)	[61–63]
Rat	i.p.	25 mg/kg	Inhibition of extravasation of macrophages and $CD4^+$ T cells to myocardium	[64]
Mice	p.o.	200 mg/kg	Th1 switch in *Leishmania* infection	[65]
Mice	i.p.	50 mg/kg	Improvement of pulmonary inflammation	[66]
Rat	i.p.	50 mg/kg	Inhibition of leukocyte infiltration in ischemic lesion	[67]
Mice	i.v.	10 mg/kg	Inhibition of infiltration of γδ T cells in pleural cavity	[68]
Mice	p.o.	0.05% (w/w) in mouse chow	Improvement of chronic colitis	[69]
Mice	i.v.	25 mg/kg	Inhibition of leukocyte rolling	[70]
Rat	p.o.	100 mg/kg	Decreased infiltration of neutrophils in myocardial infarct size	[71]
Cat	i.v.	25 mg/kg	Inhibition of leukocyte rolling	[72]

Interaction between stromal-derived factor-1 (SDF-1, CXCL12) and SDF-1α-binding chemokine (C-X-C motif) receptor 4 (CXCR4) is involved in the mobilization of hematopoietic progenitor stem cells (HPC), which are used after high-dose chemotherapy to support bone marrow regeneration [73]. In addition, CXCR4 is expressed on various cancer cell types [41,74], and the CXCL12–CXCR4 axis is involved in tumor progression, angiogenesis, metastasis, and survival [74–76]. Therefore, modulation of the CXCL12–CXCR4 axis by fucoidan seems an interesting target for cancer therapy. Fucoidan binds CXCL12, which is normally retained by heparan sulfate proteoglycans on the membrane of stromal cells or the extracellular matrix in bone marrow, thereby releasing CXCL12 into the circulation [60,77–79]. Negatively charged fucoidan seems to interact with basic residues of CXCL12 [80]. When mice were injected intravenously or

intraperitoneally with 50 or 100 mg/kg of fucoidan, HPCs were mobilized from bone marrow [60–62], and plasma concentration of CXCL12 increased rapidly and dramatically [37,61,63]. In clinical trials, Irhimeh *et al.* demonstrated that oral fucoidan increased surface expression of CXCR4 on human $CD34^+$ cells and the release of $CD34^+$ cells from bone marrow to peripheral blood [12]. Therefore, future studies are warranted to determine whether fucoidan can affect the CXCL12–CXCR4 axis in tumor growth *in vivo*.

7. Role of Scavenger Receptor Type A in the Action of Fucoidan

Fucoidan is known to bind to various types of scavenger receptors (SR), including class A-, B-, and F-SRs [81–83]. Fucoidan has been used as an effective competitor for oxidized low-density lipoproteins in SR-A binding assays [84]. SR-A is mainly expressed in macrophages and DCs [85] and is implicated in changing the immune microenvironment in cancer. However, the reports on the role of SR-A in anticancer immunity have been contradictory. Wang *et al.* demonstrated that anticancer responses in SR-$A^{-/-}$ mice were improved and correlated with an increased antigen-specific T cell response [86]. The authors showed that SR-$A^{-/-}$ mice were highly responsive to inflammatory stimuli, such as lipopolysaccharide. Thus, the immunosuppressive role of SR-A in cancer might be due to its inhibition of proinflammatory responses by ligation of the toll-like receptor 4 (TLR4) rather than a direct inhibition of tumor immunity [87]. Indeed, it was shown that fucoidan, as a common SR-A ligand, also activated TLR4 signaling, and combined signaling through two distinct receptors resulting in a functional outcome not achieved by either receptor alone [88].

SR-A expression was lower in cancerous than in normal tissues and SR-A depletion was found to boost growth and angiogenesis of implanted Lewis lung carcinoma in mice [89]. Tumor cells caused SR-A up-regulation on macrophages [90], and elimination of SR-A-positive tumor-infiltrating leukocytes from the peritoneum of tumor-bearing mice relieved the T cell suppression and inhibited tumor growth [91,92]. Moreover, SR-$A^{-/-}$ mice showed delayed growth of injected EL4 tumors and expression of inducible NO synthase, while showing significantly increased IFN-γ mRNA expression, suggesting that tumor-associated macrophages are highly active in SR-A-depleted conditions [93]. Recently, *in vitro* experimental results revealed that fucoidan can inhibit macrophage-induced tumor cell invasion [94]. Results obtained using an experimental autoimmune myocarditis model also showed that fucoidan administration attenuated progression of myocarditis by decreasing myocardial macrophage infiltration [64]. Therefore, we can speculate that macrophages are associated with immune suppression in tumor tissues and macrophage depletion in cancerous tissues by fucoidan may inhibit tumor progression.

In vitro testing indicated that LMW fucoidan is internalized via endocytosis [38]. Recently, Zhu *et al.* demonstrated that fucoidan-SR-A internalization occurred through clathrin- and caveolae-dependent pathways [95]. They also revealed the mechanism involving the production of tumor necrosis factor (TNF)-α following SR-A binding by fucoidan. Fucoidan treatment of macrophages could promote recruitment of the major vault protein to lipid rafts to form an SR-A-major vault protein complex, leading to TNF-α production [96]. NO production by macrophages was significantly decreased in SR-$A^{-/-}$ compared with the wild-type mice when

macrophages were treated with fucoidan [97]. In addition, fucoidan abrogated SR-A-mediated chaperone uptake into macrophages [98] and DCs [83]. Our previous results also demonstrated that fucoidan decreased the binding of the anti-SR-A antibody to human blood DCs and failed to activate SR-A-depleted DCs [8]. These results suggest that the binding of SR-A by fucoidan leads to DC activation. Herber *et al.* demonstrated that DCs with high lipid content had low antigen-processing capacity and the frequencies of these cells were significantly increased in tumor-bearing mice and cancer patients [99]. Accumulation of lipids by DCs *in vitro* and *in vivo* was induced by tumor-derived factors that up-regulated SR-A expression on DCs. It was shown that SR-A overexpressing DCs could internalize modified lipoproteins from serum and fucoidan inhibited DC lipid uptake. Therefore, fucoidan might be effective in decreasing the frequency of lipid-laden and poorly antigen-presenting DCs in cancer patients by blocking SR-A, thus leading to an enhanced immune response. Consequently, further studies to reveal the possible effects of fucoidan on tumor growth in SR-A$^{-/-}$ mice may help to unravel the immunological roles of fucoidan in cancer.

8. *In Vivo* Cytokine Production by Fucoidan in Other Diseases

In contrast to effects on cytokine expression in tumor-bearing mice, serum analysis of cytokines after fucoidan treatment has shown discrepant effects in several other disease models (Table 3). For example, splenic cytokine analysis in *Leishmania*-infected mice showed that fucoidan treatment at 200 mg/kg (p.o.) significantly increased levels of IFN-γ, IL-12, and TNF-α [65]. In an aspirin-induced stomach ulceration model, IFN-γ was increased, and levels of IFN-γ were further increased in rats treated with both aspirin and fucoidan at 400 mg/kg [100]. On the other hand, Maruyama *et al.* demonstrated that Mekabu-derived fucoidan suppressed production of Th2 cytokines in the bronchoalveolar lavage fluid after ovalbumin aerosol challenge [66]. Under normal conditions, intravenous treatment of mice and nonhuman primates with fucoidan was shown to increase levels of IL-8, monocyte chemoattractant protein 1, and matrix metalloproteinase 9 [60,63].

Other studies have shown that fucoidan suppresses cytokine levels in several disease models. Kang *et al.* demonstrated that treatment of rats with fucoidan at 50 mg/kg (i.p.) significantly decreased the number of the TNF-α-immunoreactive cells in the cerebral cortex and striatum, induced by lipopolysaccharide [67]. Concanavalin A-induced liver injury and a concomitant increase of plasma TNF-α and IFN-γ levels were prevented, but plasma IL-10 levels were increased by fucoidan treatment at 30 mg/kg (i.v.) [101]. Interestingly, the above mentioned inhibitory effects of fucoidan were reversed by pretreatment with an anti-mouse IL-10 antibody. Intravenous administration of fucoidan inhibited ovalbumin-induced γδ T cell accumulation in pleural cavities and lymph nodes in a murine model of ovalbumin-induced allergic pleurisy [68]. Moreover, pleural γδ T lymphocytes from fucoidan-treated mice showed reduced ovalbumin-induced IL-5 production, leading to decreased ovalbumin-induced eosinophil influx [68]. These results indicate that cytokine production profiles of fucoidan-stimulated immune cells in cancer patients may differ from those in patients with inflammatory or immune diseases.

9. *In Vivo* Antioxidant and Prooxidant Effects of Fucoidan

Prooxidant cytotoxic effects are important in clearing transformed cells from the body and limiting tumor growth. In contrast, oxidative stress is also associated with membrane lipid peroxidation, DNA damage, and mutagenesis, leading to tumor formation [102]. Fucoidan may have both antioxidant and prooxidant effects in cancer cells. We previously showed that fucoidan-induced apoptosis in leukemic cells was inhibited by glutathione and/or NAME addition [17]. Furthermore, fucoidan treatment of leukemic cells decreased intracellular glutathione concentrations and stimulated NO production. Zhang *et al.* demonstrated that fucoidan enhanced the apoptosis of cancer cells that responded to cisplatin, tamoxifen, or paclitaxel treatment via reduced glutathione levels, and enhanced production of intracellular reactive oxygen species in breast cancer cells [103]. According to Yang *et al.*, fucoidan isolated from *Undaria pinnatifida* induces the death of hepatocellular carcinoma cells by causing intracellular accumulation of high levels of reactive oxygen species, accompanied by damage to the mitochondrial ultrastructure, depolarization of the mitochondrial membrane potential, and caspase activation [23]. These results suggest that induction of oxidative stress may be an important event in fucoidan-induced cancer cell death.

In general, fucoidan preparations show antioxidant effects in other disease models *in vivo* [107–109] (summarized in Table 4). Pre-treating rats with fucoidan preparations caused suppression of lactate dehydrogenase and malondialdehyde levels, but caused normalization of superoxide dismutase, catalase, and glutathione peroxidase levels, decreasing necrosis and cirrhosis incidences in the liver of CCL_4-treated rats [107]. Similarly, fibrosis and acetaminophen-induced liver injury were significantly suppressed by oral fucoidan intake [110,111]. Luo *et al.* investigated the effects of fucoidan on 1-methyl-4-phenyl-1,2,3,6-tetrahydropyridine (MPTP)-induced animal models of parkinsonism in C57/BL mice. The authors demonstrated that the administration of fucoidan at 25 mg/kg (i.p.) inhibited MPTP-induced lipid peroxidation and reduced the activities of antioxidant enzymes [108]. This fucoidan-induced alteration in antioxidant activity might lead to increased levels of striatal dopamine and its metabolite, increased expression of tyrosine hydroxylase, and reduced behavioral deficits. Suresh *et al.* demonstrated that fucoidan prevented increase of drug-metabolizing hepatic enzyme levels, which result from oxidative stress by diethylnitrosamine, a carcinogen in rats [30]. In contrast, splenocytes of fucoidan-treated mice infected with *Leishmania donovani* generated significantly high levels of superoxide and NO [65].

Similar to fucoidan, green tea has shown both antioxidant and prooxidant effects in cancer cells [113]. Prooxidant effects of green tea apparently cause tumor cell apoptosis and also induce endogenous antioxidant mechanisms that protect against carcinogenic insults in normal tissues [113]. Fucoidan has antioxidative and prooxidative potential in animal models of renal ischemia-reperfusion injury, however, fucoidan alone did not affect malondialdehyde and superoxide dismutase levels in the sham-operated group [112]. Recently, it was shown that intracellular and secreted H_2O_2 from HT1080 human fibrosarcoma cells were both greatly repressed upon tumor cell treatment with enzyme-digested fucoidan preparations extracted from seaweed Mozuku of *Cladosiphon novae-caledoniae kylin* [114]. However, Ye *et al.* suggested that H_2O_2 release by cancer cells is

one of the triggering factors to promote angiogenesis rather than apoptosis [114]. Therefore, more careful *in vivo* studies using highly purified fucoidan preparations are essential to determine whether fucoidan has an antioxidant or prooxidant role in cancer prevention and treatment.

Table 3. Changes of cytokine and growth factor levels by *in vivo* administration of fucoidan in cancer and other disease models.

Cytokines	*In Vivo* Changes	References
CXCL12	Increase in plasma	[37,51,61,63,80]
	Increase in myocardial ischemic tissue	[46]
IFN-γ	Increase in splenic T cells/A20 lymphoma	[32]
	Increase in splenic T cells/P-388	[40]
	Increase of secretion in plasma by aspirin	[100]
	Inhibition of increase in gastric ulcer lesion	[104]
TNF-α	Inhibition of increase in acute bacterial meningitis	[58]
	Inhibition of expression in ischemic lesion	[67]
	Inhibition of increase in ischemia-reperfusion injury	[71]
	Inhibition of increase in gastric ulcer lesion	[104]
	Inhibition of lipopolysaccharide-induced increase in brain	[105]
IL-1	Inhibition of increase in acute bacterial meningitis	[58]
IL-4	Decrease in bronchoalveolar lavage fluid	[66]
	Decrease in ovalbumin-sensitized spleen cells	[106]
IL-5	Inhibition of increase in pleural cavity of allergic pleurisy	[68]
IL-6	Decrease in plasma	[15]
	Inhibition of increase in colonic lamina propria of colitis	[69]
	Inhibition of increase in ischemia-reperfusion injury	[71]
IL-8	Increase in plasma	[63]
	Inhibition of lipopolysaccharide-induced increase in brain	[67,105]
IL-10	Increase in plasma level in liver injury	[101]
	Inhibition of decrease in ischemia-reperfusion injury	[71]
IL-12	Increase in splenic T cells/A20 lymphoma	[32]
	Increase in *Leishmania* infection	[65]
	Inhibition of increase in gastric ulcer lesion	[104]
MCP-1	Increase in plasma	[63]
VEGF	Reduction of mRNA expression in tumor tissues	[24]
	Increase in myocardial ischemic tissue	[46]
FGF-2	Potentiation of activity	[37]

Table 4. *In vivo* effects of fucoidan on other diseases related to the oxidant production.

Test	Route	Dose	Possible *in vivo* effects	References
Mice	i.p.	25 mg/kg	Prevention of MPTP-induced neurotoxicity	[108]
		15 mg/kg	Prevention of lipopolysaccharide-induced neurotoxicity	[105]
Mice	i.p.	25 mg/kg	Neuroprotection via antioxidant activity	[108]
Mice	i.p.	100 mg/kg	Prevention of ischemia-reperfusion injury	[112]
Rat	p.o. i.p.	100 mg/kg	Suppression of liver fibrogenesis and drug-induced liver injury	[110,111]

10. Conclusions

Fucoidan shows promising characteristics that warrant further development of the substance as a future marine drug. Recent *in vivo* studies suggest fucoidan to be a potential preventive or therapeutic agent for controlling cancers. However, the *in vitro* and *in vivo* mechanisms underlying the observed anticancer effects of fucoidan have not been fully investigated. The anticancer effects of fucoidan *in vivo* may be due to the inhibition of tumorigenesis and metastasis. More importantly, fucoidan may act by promoting immune responses or antiangiogenesis in tumor tissues. The mobilization of hematopoietic progenitor cells by fucoidan is yet another interesting characteristic of the substance that harbors therapeutic potential. These findings need to be corroborated by further preclinical studies. Orally delivered fucoidan appears promising as a marine drug in several diseases [2], but fucoidan administration via other routes is also possible. However, fucoidan preparations isolated from different sources have shown differential anticancer effects *in vivo* because of correspondingly different structural properties. Therefore, as a next step, the determination of the structural characteristics responsible for the *in vivo* anticancer activities of fucoidan will be essential for its potential use as a marine drug.

Acknowledgments

This work was supported by the Pioneer Research Center Program through the National Research Foundation of Korea funded by the Ministry of Science, ICT & Future Planning (2012-0009583 and 2012-0009664).

Conflicts of Interest

The authors declare no conflict of interest.

References

1. Pomin, V.H.; Mourão, P.A. Structure, biology, evolution, and medical importance of sulfated fucans and galactans. *Glycobiology* **2008**, *18*, 1016–1027.
2. Fitton, J.H. Therapies from fucoidan; multifunctional marine polymers. *Mar. Drugs* **2011**, *9*, 1731–1760.
3. Pomin, V.H. Fucanomics and galactanomics: Current status in drug discovery, mechanisms of action and role of the well-defined structures. *Biochim. Biophys. Acta* **2012**, *1820*, 1971–1979.
4. Berteau, O.; Mulloy, B. Sulfated fucans, fresh perspectives: Structures, functions, and biological properties of sulfated fucans and an overview of enzymes active towards this class of polysaccharide. *Glycobiology* **2003**, *13*, 29–40.
5. Senthilkumar, K.; Manivasagan, P.; Venkatesan, J.; Kim, S.K. Brown seaweed fucoidan: Biological activity and apoptosis, growth signaling mechanism in cancer. *Int. J. Biol. Macromol.* **2013**, *60*, 366–374.
6. Kim, M.H.; Joo, H.G. Immunostimulatory effects of fucoidan on bone marrow-derived dendritic cells. *Immunol. Lett.* **2008**, *115*, 138–143.

7. Yang, M.; Ma, C.; Sun, J.; Shao, Q.; Gao, W.; Zhang, Y.; Li, Z.; Xie, Q.; Dong, Z.; Qu, X. Fucoidan stimulation induces a functional maturation of human monocyte-derived dendritic cells. *Int. Immunopharmacol.* **2008**, *8*, 1754–1760.
8. Jin, J.O.; Park, H.Y.; Xu, Q.; Park, J.I.; Zvyagintseva, T.; Stonik, V.A.; Kwak, J.Y. Ligand of scavenger receptor class A indirectly induces maturation of human blood dendritic cells via production of tumor necrosis factor-α. *Blood* **2009**, *113*, 5839–5847.
9. Hu, Y.; Cheng, S.C.; Chan, K.T.; Ke, Y.; Xue, B.; Sin, F.W.; Zeng, C.; Xie, Y. Fucoidin enhances dendritic cell-mediated T-cell cytotoxicity against NY-ESO-1 expressing human cancer cells. *Biochem. Biophys. Res. Commun.* **2010**, *392*, 329–334.
10. Ale, M.T.; Maruyama, H.; Tamauchi, H.; Mikkelsen, J.D.; Meyer, A.S. Fucoidan from *Sargassum* sp. and *Fucus vesiculosus* reduces cell viability of lung carcinoma and melanoma cells *in vitro* and activates natural killer cells in mice *in vivo*. *Int. J. Biol. Macromol.* **2011**, *49*, 331–336.
11. Azuma, K.; Ishihara, T.; Nakamoto, H.; Amaha, T.; Osaki, T.; Tsuka, T.; Imagawa, T.; Minami, S.; Takashima, O.; Ifuku, S.; Morimoto, M.; *et al*. Effects of oral administration of fucoidan extracted from *Cladosiphon okamuranus* on tumor growth and survival time in a tumor-bearing mouse model. *Mar. Drugs* **2012**, *10*, 2337–2348.
12. Irhimeh, M.R.; Fitton, J.H.; Lowenthal, R.M. Fucoidan ingestion increases the expression of CXCR4 on human $CD34^+$ cells. *Exp. Hematol.* **2007**, *35*, 989–994.
13. Irhimeh, M.R.; Fitton, J.H.; Lowenthal, R.M. Pilot clinical study to evaluate the anticoagulant activity of fucoidan. *Blood Coagul. Fibrinolysis* **2009**, *20*, 607–610.
14. Myers, S.P.; O'Connor, J.; Fitton, J.H.; Brooks, L.; Rolfe, M.; Connellan, P.; Wohlmuth, H.; Cheras, P.A.; Morris, C. A combined phase I and II open label study on the effects of a seaweed extract nutrient complex on osteoarthritis. *Biologics* **2010**, *4*, 33–44.
15. Myers, S.P.; O'Connor, J.; Fitton, J.H.; Brooks, L.; Rolfe, M.; Connellan, P.; Wohlmuth, H.; Cheras, P.A.; Morris, C. A combined Phase I and II open-label study on the immunomodulatory effects of seaweed extract nutrient complex. *Biologics* **2011**, *5*, 45–60.
16. Kusaykin, M.; Bakunina, I.; Sova, V.; Ermakova, S.; Kuznetsova, T.; Besednova, N.; Zaporozhets, T.; Zvyagintseva, T. Structure, biological activity, and enzymatic transformation of fucoidans from the brown seaweeds. *Biotechnol. J.* **2008**, *3*, 904–915.
17. Jin, J.O.; Song, M.G.; Kim, Y.N.; Park, J.I.; Kwak, J.Y. The mechanism of fucoidan-induced apoptosis in leukemic cells: Involvement of ERK1/2, JNK, glutathione, and nitric oxide. *Mol. Carcinog.* **2010**, *49*, 771–782.
18. Park, H.S.; Hwang, H.J.; Kim, G.Y.; Cha, H.J.; Kim, W.J.; Kim, N.D.; Yoo, Y.H.; Choi, Y.H. Induction of apoptosis by fucoidan in human leukemia U937 cells through activation of p38 MAPK and modulation of Bcl-2 family. *Mar. Drugs* **2013**, *11*, 2347–2364.
19. Zhang, Z.; Teruya, K.; Eto, H.; Shirahata, S. Fucoidan extract induces apoptosis in MCF-7 cells via a mechanism involving the ROS-dependent JNK activation and mitochondria-mediated pathways. *PLoS One* **2011**, *6*, e27441.

20. Park, H.S.; Kim, G.Y.; Nam, T.J.; Kim, N.D.; Choi, Y.H. Antiproliferative activity of fucoidan was associated with the induction of apoptosis and autophagy in AGS human gastric cancer cells. *J. Food Sci.* **2011**, *76*, T77–T83.
21. Boo, H.J.; Hyun, J.H.; Kim, S.C.; Kang, J.I.; Kim, M.K.; Kim, S.Y.; Cho, H.; Yoo, E.S.; Kang, H.K. Fucoidan from *Undaria pinnatifida* induces apoptosis in A549 human lung carcinoma cells. *Phytother. Res.* **2011**, *25*, 1082–1086.
22. Boo, H.J.; Hong, J.Y.; Kim, S.C.; Kang, J.I.; Kim, M.K.; Kim, E.J.; Hyun, J.W.; Koh, Y.S.; Yoo, E.S.; Kwon, J.M.; *et al*. The anticancer effect of fucoidan in PC-3 prostate cancer cells. *Mar. Drugs* **2013**, *11*, 2982–2999.
23. Yang, L.; Wang, P.; Wang, H.; Li, Q.; Teng, H.; Liu, Z.; Yang, W.; Hou, L.; Zou, X. Fucoidan derived from *Undaria pinnatifida* induces apoptosis in human hepatocellular carcinoma SMMC-7721 cells via the ROS-mediated mitochondrial pathway. *Mar. Drugs* **2013**, *11*, 1961–1976.
24. Xue, M.; Ge, Y.; Zhang, J.; Wang, Q.; Hou, L.; Liu, Y.; Sun, L.; Li, Q. Anticancer properties and mechanisms of fucoidan on mouse breast cancer *in vitro* and *in vivo*. *PLoS One* **2012**, *7*, e43483.
25. Thinh, P.D.; Menshova, R.V.; Ermakova, S.P.; Anastyuk, S.D.; Ly, B.M.; Zvyagintseva, T.N. Structural characteristics and anticancer activity of fucoidan from the brown alga *Sargassum mcclurei*. *Mar. Drugs* **2013**, *11*, 1456–1476.
26. Kim, C.H.; Kim, C.G.; Kwak, J.Y. Role of scavenger receptor type A in the migration of dendritic cells and immunogenic antitumor effects by fucoidan. Dong-A University, Busan, Korea. 2014, unpublished work.
27. Alekseyenko, T.V.; Zhanayeva, S.Y.; Venediktova, A.A.; Zvyagintseva, T.N.; Kuznetsova, T.A.; Besednova, N.N.; Korolenko, T.A. Antitumor and antimetastatic activity of fucoidan, a sulfated polysaccharide isolated from the Okhotsk Sea *Fucus evanescens* brown alga. *Bull. Exp. Biol. Med.* **2007**, *143*, 730–732.
28. Zhu, C.; Cao, R.; Zhang, S.X.; Man, Y.N.; Wu, X.Z. Fucoidan inhibits the growth of hepatocellular carcinoma independent of angiogenesis. *Evid. Based Complement. Alternat. Med.* **2013**, *2013*, doi:10.1155/2013/692549.
29. Hsu, H.Y.; Lin, T.Y.; Hwang, P.A.; Tseng, L.M.; Chen, R.H.; Tsao, S.M.; Hsu, J. Fucoidan induces changes in the epithelial to mesenchymal transition and decreases metastasis by enhancing ubiquitin-dependent TGFβ receptor degradation in breast cancer. *Carcinogenesis* **2013**, *34*, 874–884.
30. Suresh, V.; Anbazhagan, C.; Thangam, R.; Senthilkumar, D.; Senthilkumar, N.; Kannan, S.; Rengasamy, R.; Palani, P. Stabilization of mitochondrial and microsomal function of fucoidan from *Sargassum plagiophyllum* in diethylnitrosamine induced hepatocarcinogenesis. *Carbohydr. Polym.* **2013**, *92*, 1377–1385.
31. Takeda, K.; Tomimori, K.; Kimura, R.; Ishikawa, C.; Nowling, T.K.; Mori, N. Anti-tumor activity of fucoidan is mediated by nitric oxide released from macrophages. *Int. J. Oncol.* **2012**, *40*, 251–260.

32. Maruyama, H.; Tamauchi, H.; Iizuka, M.; Nakano, T. The role of NK cells in antitumor activity of dietary fucoidan from *Undaria pinnatifida* sporophylls (Mekabu). *Planta Med.* **2006**, *72*, 1415–1417.
33. Koyanagi, S.; Tanigawa, N.; Nakagawa, H.; Soeda, S.; Shimeno, H. Oversulfation of fucoidan enhances its anti-angiogenic and antitumor activities. *Biochem. Pharmacol.* **2003**, *65*, 173–179.
34. Narazaki, M.; Segarra, M.; Tosato, G. Sulfated polysaccharides identified as inducers of neuropilin-1 internalization and functional inhibition of VEGF165 and semaphorin3A. *Blood* **2008**, *111*, 4126–4136.
35. Li, N.; Zhang, Q.; Song, J. Toxicological evaluation of fucoidan extracted from *Laminaria japonica* in Wistar rats. *Food Chem. Toxicol.* **2005**, *43*, 421–426.
36. Xue, M.; Ge, Y.; Zhang, J.; Liu, Y.; Wang, Q.; Hou, L.; Zheng, Z. Fucoidan inhibited 4T1 mouse breast cancer cell growth *in vivo* and *in vitro* via downregulation of Wnt/β-catenin signaling. *Nutr. Cancer* **2013**, *65*, 460–468.
37. Luyt, C.E.; Meddahi-Pellé, A.; Ho-Tin-Noe, B.; Colliec-Jouault, S.; Guezennec, J.; Louedec, L.; Prats, H.; Jacob, M.P.; Osborne-Pellegrin, M.; Letourneur, D.; *et al*. Low-molecular-weight fucoidan promotes therapeutic revascularization in a rat model of critical hindlimb ischemia. *J. Pharmacol. Exp. Ther.* **2003**, *305*, 24–30.
38. Deux, J.F.; Meddahi-Pellé, A.; le Blanche, A.F.; Feldman, L.J.; Colliec-Jouault, S.; Brée, F.; Boudghène, F.; Michel, J.B.; Letourneur, D. Low molecular weight fucoidan prevents neointimal hyperplasia in rabbit iliac artery in-stent restenosis model. *Arterioscler. Thromb. Vasc. Biol.* **2002**, *22*, 1604–1609.
39. Yang, C.; Chung, D.; Shin, I.S.; Lee, H.; Kim, J.; Lee, Y.; You, S. Effects of molecular weight and hydrolysis conditions on anticancer activity of fucoidans from sporophyll of *Undaria pinnatifida*. *Int. J. Biol. Macromol.* **2008**, *43*, 433–437.
40. Maruyama, H.; Tamauchi, H.; Hashimoto, M.; Nakano, T. Antitumor activity and immune response of Mekabu fucoidan extracted from Sporophyll of *Undaria pinnatifida*. *In Vivo* **2003**, *17*, 245–249.
41. Lippitz, B.E. Cytokine patterns in patients with cancer: A systematic review. *Lancet Oncol.* **2013**, *14*, e218–e228.
42. Menges, M.; Rössner, S.; Voigtländer, C.; Schindler, H.; Kukutsch, N.A.; Bogdan, C.; Erb, K.; Schuler, G.; Lutz, M.B. Repetitive injections of dendritic cells matured with tumor necrosis factor α induce antigen-specific protection of mice from autoimmunity. *J. Exp. Med.* **2002**, *195*, 15–21.
43. Palucka, K.; Banchereau, J. Cancer immunotherapy via dendritic cells. *Nat. Rev. Cancer* **2012**, *12*, 265–277.
44. Tejpar, S.; Prenen, H.; Mazzone, M. Overcoming resistance to antiangiogenic therapies. *Oncologist* **2012**, *17*, 1039–1050.
45. Soeda, S.; Kozako, T.; Iwata, K.; Shimeno, H. Oversulfated fucoidan inhibits the basic fibroblast growth factor-induced tube formation by human umbilical vein endothelial cells: Its possible mechanism of action. *Biochim. Biophys. Acta* **2000**, *1497*, 127–134.

46. Manzo-Silberman, S.; Louedec, L.; Meilhac, O.; Letourneur, D.; Michel, J.B.; Elmadbouh, I. Therapeutic potential of fucoidan in myocardial ischemia. *J. Cardiovasc. Pharmacol.* **2011**, *58*, 626–632.
47. Foxall, C.; Wei, Z.; Schaefer, M.E.; Casabonne, M.; Fugedi, P.; Peto, C.; Castellot, J.J., Jr.; Brandley, B.K. Sulfated malto-oligosaccharides bind to basic FGF, inhibit endothelial cell proliferation, and disrupt endothelial cell tube formation. *J. Cell. Physiol.* **1996**, *168*, 657–667.
48. Chabut, D.; Fischer, A.-M.; Colliec-Jouault, S.; Laurendeau, I.; Matou, S.; Le Bonniec, B.; Helley, D. Low molecular weight fucoidan and heparin enhance the basic fibroblast growth factor-induced tube formation of endothelial cells through heparin sulfate-dependent α6 overexpression. *Mol. Pharmcol.* **2003**, *64*, 696–702.
49. Chabut, D.; Fischer, A.M.; Helley, D.; Colliec, S. Low molecular weight fucoidan promotes FGF-2-induced vascular tube formation by human endothelial cells, with decreased PAI-1 release and ICAM-1 downregulation. *Thrombosis Res.* **2004**, *113*, 93–95.
50. Liu, F.; Wang, J.; Chang, A.K.; Liu, B.; Yang, L.; Li, Q.; Wang, P.; Zou, X. Fucoidan extract derived from *Undaria pinnatifida* inhibits angiogenesis by human umbilical vein endothelial cells. *Phytomedicine* **2012**, *19*, 797–803.
51. Fréguin-Bouilland, C.; Alkhatib, B.; David, N.; Lallemand, F.; Henry, J.P.; Godin, M.; Thuillez, C.; Plissonnier, D. Low molecular weight fucoidan prevents neointimal hyperplasia after aortic allografting. *Transplantation* **2007**, *83*, 1234–1241.
52. Wang, Y.Q.; Miao, Z.H. Marine-derived angiogenesis inhibitors for cancer therapy. *Mar. Drugs* **2013**, *11*, 903–933.
53. Arfors, K.E.; Ley, K. Sulfated polysaccharides in inflammation. *J. Lab. Clin. Med.* **1993**, *121*, 201–202.
54. Lindbom, L.; Xie, X.; Raud, J.; Hedqvist, P. Chemoattractant-induced firm adhesion of leukocytes to vascular endothelium *in vivo* is critically dependent on initial leukocyte rolling. *Acta Physiol. Scand.* **1992**, *146*, 415–421.
55. Ley, K.; Linnemann, G.; Meinen, M.; Stoolman, L.M.; Gaehtgens, P. Fucoidin, but not yeast polyphosphomannan PPME, inhibits leukocyte rolling in venules of the rat mesentery. *Blood* **1993**, *81*, 177–185.
56. Shimaoka, M.; Ikeda, M.; Iida, T.; Taenaka, N.; Yoshiya, I.; Honda, T. Fucoidin, a potent inhibitor of leukocyte rolling, prevents neutrophil influx into phorbol-ester-induced inflammatory sites in rabbit lungs. *Am. J. Respir. Crit. Care Med.* **1996**, *153*, 307–311.
57. Hickey, M.J.; Reinhardt, P.H.; Ostrovsky, L.; Jones, W.M.; Jutila, M.A.; Payne, D.; Elliott, J.; Kubes, P. Tumor necrosis factor-α induces leukocyte recruitment by different mechanisms *in vivo* and *in vitro*. *J. Immunol.* **1997**, *158*, 3391–3400.
58. Granert, C.; Raud, J.; Waage, A.; Lindquist, L. Effects of polysaccharide fucoidin on cerebrospinal fluid interleukin-1 and tumor necrosis factor a in pneumococcal meningitis in the rabbit. *Infect. Immun.* **1999**, *67*, 2071–2074.

59. Bachelet, L.; Bertholon, I.; Lavigne, D.; Vassy, R.; Jandrot-Perrus, M.; Chaubet, F.; Letourneur, D. Affinity of low molecular weight fucoidan for P-selectin triggers its binding to activated human platelets. *Biochim. Biophys. Acta* **2009**, *1790*, 141–146.
60. Sweeney, E.A.; Priestley, G.V.; Nakamoto, B.; Collins, R.G.; Beaudet, A.L.; Papayannopoulou, T. Mobilization of stem/progenitor cells by sulfated polysaccharides does not require selectin presence. *Proc. Natl. Acad. Sci. USA* **2000**, *97*, 6544–6549.
61. Hidalgo, A.; Peired, A.J.; Weiss, L.A.; Katayama, Y.; Frenette, P.S. The integrin αMβ2 anchors hematopoietic progenitors in the bone marrow during enforced mobilization. *Blood* **2004**, *104*, 993–1001.
62. Frenette, P.S.; Weiss, L. Sulfated glycans induce rapid hematopoietic progenitor cell mobilization: Evidence for selectin-dependent and independent mechanisms. *Blood* **2000**, *96*, 2460–2468.
63. Sweeney, E.A.; Lortat-Jacob, H.; Priestley, G.V.; Nakamoto, B.; Papayannopoulou, T. Sulfated polysaccharides increase plasma levels of SDF-1 in monkeys and mice: Involvement in mobilization of stem/progenitor cells. *Blood* **2002**, *99*, 44–51.
64. Tanaka, K.; Ito, M.; Kodama, M.; Tomita, M.; Kimura, S.; Hoyano, M.; Mitsuma, W.; Hirono, S.; Hanawa, H.; Aizawa, Y. Sulfated polysaccharide fucoidan ameliorates experimental autoimmune myocarditis in rats. *J. Cardiovasc. Pharmacol. Ther.* **2011**, *16*, 79–86.
65. Kar, S.; Sharma, G.; Das, P.K. Fucoidan cures infection with both antimony-susceptible and -resistant strains of *Leishmania donovani* through Th1 response and macrophage-derived oxidants. *Antimicrob. Chemother.* **2011**, *66*, 618–625.
66. Maruyama, H.; Tamauchi, H.; Hashimoto, M.; Nakano, T. Suppression of Th2 immune responses by mekabu fucoidan from *Undaria pinnatifida* sporophylls. *Int. Arch. Allergy Immunol.* **2005**, *137*, 289–294.
67. Kang, G.H.; Yan, B.C.; Cho, G.S.; Kim, W.K.; Lee, C.H.; Cho, J.H.; Kim, M.; Kang, I.J.; Won, M.H.; Lee, J.C. Neuroprotective effect of fucoidin on lipopolysaccharide accelerated cerebral ischemic injury through inhibition of cytokine expression and neutrophil infiltration. *J. Neurol. Sci.* **2012**, *318*, 25–30.
68. Costa, M.F.; Nihei, J.; Mengel, J.; Henriques, M.G.; Penido, C. Requirement of L-selectin for γδ T lymphocyte activation and migration during allergic pleurisy: Co-relation with eosinophil accumulation. *Int. Immunopharmacol.* **2009**, *9*, 303–312.
69. Matsumoto, S.; Nagaoka, M.; Hara, T.; Kimura-Takagi, I.; Mistuyama, K.; Ueyama, S. Fucoidan derived from *Cladosiphon okamuranus* Tokida ameliorates murine chronic colitis through the down-regulation of interleukin-6 production on colonic epithelial cells. *Clin. Exp. Immunol.* **2004**, *136*, 432–439.
70. Zhang, X.W.; Liu, Q.; Thorlacius, H. Inhibition of selectin function and leukocyte rolling protects against dextran sodium sulfate-induced murine colitis. *Scand. J. Gastroenterol*. **2001**, *36*, 270–275.
71. Li, C.; Gao, Y.; Xing, Y.; Zhu, H.; Shen, J.; Tian, J. Fucoidan, a sulfated polysaccharide from brown algae, against myocardial ischemia-reperfusion injury in rats via regulating the inflammation response. *Food Chem. Toxicol.* **2011**, *49*, 2090–2095.

72. Granert, C.; Raud, J.; Xie, X.; Lindquist, L.; Lindbom, L. Inhibition of leukocyte rolling with polysaccharide fucoidin prevents pleocytosis in experimental meningitis in the rabbit. *J. Clin. Investig.* **1994**, *93*, 929–936.
73. Nervi, B.; Link, D.C.; DiPersio, J.F. Cytokines and hematopoietic stem cell mobilization. *J. Cell. Biochem.* **2006**, *99*, 690–705.
74. Zlotnik, A. New insights on the role of CXCR4 in cancer metastasis. *J. Pathol.* **2008**, *215*, 211–213.
75. Furusato, B.; Mohamed, A.; Uhlén, M.; Rhim, J.S. CXCR4 and cancer. *Pathol. Int.* **2010**, *60*, 497–505.
76. Teicher, B.A.; Fricker, S.P. CXCL12 (SDF-1)/CXCR4 pathway in cancer. *Clin. Cancer Res.* **2010**, *16*, 2927–2931.
77. Amara, A.; Lorthioir, O.; Valenzuela, A.; Magerus, A.; Thelen, M.; Montes, M.; Virelizier, J.L.; Delepierre, M.; Baleux, F.; Lortat-Jacob, H.; *et al*. Stromal cell-derived factor-1α associates with heparan sulfates through the first β-strand of the chemokine. *J. Biol. Chem.* **1999**, *274*, 23916–23925.
78. Sadir, R.; Baleux, F.; Grosdidier, A.; Imberty, A.; Lortat-Jacob, H. Characterization of the stromal cell-derived factor-1α-heparin complex. *J. Biol. Chem.* **2001**, *276*, 8288–8296.
79. Lortat-Jacob, H.; Grosdidier, A.; Imberty, A. Structural diversity of heparan sulfate binding domains in chemokines. *Proc. Natl. Acad. Sci. USA* **2002**, *99*, 1229–1234.
80. Sweeney, E.A.; Papayannopoulou, T. Increase in circulating SDF-1 after treatment with sulphated glycans, the role of SDF-1 in mobilization. *Ann. N. Y. Acad. Sci.* **2001**, *938*, 48–52.
81. Peiser, L.S.; Gordon, S. The function of scavenger receptors expressed by macrophages and their role in the regulation of inflammation. *Microbes Infect.* **2001**, *3*, 149–159.
82. Tamura, Y.; Adachi, H.; Osuga, J.; Ohashi, K.; Yahagi, N.; Sekiya, M.; Okazaki, H.; Tomita, S.; Iizuka, Y.; Shimano, H.; *et al*. FEEL-1 and FEEL-2 are endocytic receptors for advanced glycation end products. *J. Biol. Chem.* **2003**, *278*, 12613–12617.
83. Berwin, B.; Delneste, Y.; Lovingood, R.V.; Post, S.R.; Pizzo, S.V. SREC-I, a type F scavenger receptor, is an endocytic receptor for calreticulin. *J. Biol. Chem.* **2004**, *279*, 51250–51257.
84. Brown, M.S.; Goldstein, J.L. Lipoprotein metabolism in the macrophage: Implications for cholesterol deposition in atherosclerosis. *Annu. Rev. Biochem.* **1983**, *52*, 223–261.
85. Platt, N.; Gordon, S. Is the class A macrophage scavenger receptor (SR-A) multifunctional?—The mouse's tale. *J. Clin. Investig.* **2001**, *108*, 649–654.
86. Wang, X.Y.; Facciponte, J.; Chen, X.; Subjeck, J.R.; Repasky, E.A. Scavenger receptor—A negatively regulates antitumor immunity. *Cancer Res.* **2007**, *67*, 4996–5002.
87. Becker, M.; Cotena, A.; Gordon, S.; Platt, N. Expression of the class A macrophage scavenger receptor on specific subpopulations of murine dendritic cells limits their endotoxin response. *Eur. J. Immunol.* **2006**, *36*, 950–960.
88. Seimon, T.A.; Obstfeld, A.; Moore, K.J.; Golenbock, D.T.; Tabas, I. Combinatorial pattern recognition receptor signaling alters the balance of life and death in macrophages. *Proc. Natl. Acad. Sci. USA* **2006**, *103*, 19794–19799.

89. Ben, J.; Jin, G.; Zhang, Y.; Ma, B.; Bai, H.; Chen, J.; Zhang, H.; Gong, Q.; Zhou, X.; Zhang, H.; *et al*. Class A scavenger receptor deficiency exacerbates lung tumorigenesis by cultivating a procarcinogenic microenvironment in humans and mice. *Am. J. Respir. Crit. Care Med.* **2012**, *186*, 763–772.
90. Hagemann, T.; Wilson, J.; Burke, F.; Kulbe, H.; Li, N.F.; Plüddemann, A.; Charles, K.; Gordon, S.; Balkwill, F.R. Ovarian cancer cells polarize macrophages toward a tumor-associated phenotype. *J. Immunol.* **2006**, *176*, 5023–5032.
91. Bak, S.P.; Walters, J.J.; Takeya, M.; Conejo-Garcia, J.R.; Berwin, B.L. Scavenger receptor-A-targeted leukocyte depletion inhibits peritoneal ovarian tumor progression. *Cancer Res.* **2007**, *67*, 4783–4789.
92. Peter, S.; Bak, G.; Hart, K.; Berwin, B. Ovarian tumor-induced T cell suppression is alleviated by vascular leukocyte depletion. *Transl. Oncol.* **2009**, *2*, 291–299.
93. Komohara, Y.; Takemura, K.; Lei, X.F.; Sakashita, N.; Harada, M.; Suzuki, H.; Kodama, T.; Takeya, M. Delayed growth of EL4 lymphoma in SR-A-deficient mice is due to upregulation of nitric oxide and interferon-γ production by tumor-associated macrophages. *Cancer Sci.* **2009**, *100*, 2160–2166.
94. Neyen, C.; Plüddemann, A.; Mukhopadhyay, S.; Maniati, E.; Bossard, M.; Gordon, S.; Hagemann, T. Macrophage scavenger receptor a promotes tumor progression in murine models of ovarian and pancreatic cancer. *J. Immunol.* **2013**, *190*, 3798–3805.
95. Zhu, X.D.; Zhuang, Y.; Ben, J.J.; Qian, L.L.; Huang, H.P.; Bai, H.; Sha, J.H.; He, Z.G.; Chen, Q. Caveolae-Dependent endocytosis is required for class A macrophage scavenger receptor-mediated apoptosis in macrophages. *J. Biol. Chem.* **2011**, *286*, 8231–8239.
96. Ben, J.; Zhang, Y.; Zhou, R.; Zhang, H.; Zhu, X.; Li, X.; Zhang, H.; Li, N.; Zhou, X.; Bai, H.; *et al*. Major vault protein regulates class A scavenger receptor-mediated tumor necrosis factor-α synthesis and apoptosis in macrophages. *J. Biol. Chem.* **2013**, *288*, 20076–20084.
97. Nakamura, T.; Suzuki, H.; Wada, Y.; Kodama, T.; Doi, T. Fucoidan induces nitric oxide production via p38 mitogen-activated protein kinase and NF-κB-dependent signaling pathways through macrophage scavenger receptors. *Biochem. Biophys. Res. Commun.* **2006**, *343*, 286–294.
98. Berwin, B.; Hart, J.P.; Rice, S.; Gass, C.; Pizzo, S.V.; Post, S.R.; Nicchitta, C.V. Scavenger receptor-A mediates gp96/GRP94 and calreticulin internalization by antigen-presenting cells. *EMBO J.* **2003**, *22*, 6127–6136.
99. Herber, D.L.; Cao, W.; Nefedova, Y.; Novitskiy, S.V.; Nagaraj, S.; Tyurin, V.A.; Corzo, A.; Cho, H.I.; Celis, E.; Lennox, B.; *et al*. Lipid accumulation and dendritic cell dysfunction in cancer. *Nat. Med.* **2010**, *16*, 880–886.
100. Choi, J.I.; Raghavendran, H.R.; Sung, N.Y.; Kim, J.H.; Chun, B.S.; Ahn, D.H.; Choi, H.S.; Kang, K.W.; Lee, J.W. Effect of fucoidan on aspirin-induced stomach ulceration in rats. *Chem. Biol. Interact.* **2010**, *183*, 249–254.
101. Saito, A.; Yoneda, M.; Yokohama, S.; Okada, M.; Haneda, M.; Nakamura, K. Fucoidan prevents concanavalin A-induced liver injury through induction of endogenous IL-10 in mice. *Hepatol. Res.* **2006**, *35*, 190–198.

102. Cleveland, J.L.; Kastan, M.B. Cancer. A radical approach to treatment. *Nature* **2000**, *407*, 309–311.
103. Zhang, Z.; Teruya, K.; Yoshida, T.; Eto, H.; Shirahata, S. Fucoidan extract enhances the anti-cancer activity of chemotherapeutic agents in MDA-MB-231 and MCF-7 breast cancer cells. *Mar. Drugs* **2013**, *11*, 81–98.
104. Raghavendran, H.R.; Srinivasan, P.; Rekha, S. Immunomodulatory activity of fucoidan against aspirin-induced gastric mucosal damage in rats. *Int. Immunopharmacol.* **2011**, *11*, 157–163.
105. Cui, Y.Q.; Jia, Y.J.; Zhang, T.; Zhang, Q.B.; Wang, X.M. Fucoidan protects against lipopolysaccharide-induced rat neuronal damage and inhibits the production of proinflammatory mediators in primary microglia. *CNS Neurosci. Ther.* **2012**, *18*, 827–833.
106. Yanase, Y.; Hiragun, T.; Uchida, K.; Ishii, K.; Oomizu, S.; Suzuki, H.; Mihara, S.; Iwamoto, K.; Matsuo, H.; Onishi, N.; *et al*. Peritoneal injection of fucoidan suppresses the increase of plasma IgE induced by OVA-sensitization. *Biochem. Biophys. Res. Commun.* **2009**, *387*, 435–439.
107. Kang, K.S.; Kim, I.D.; Kwon, R.H.; Lee, J.Y.; Kang, J.S.; Ha, B.J. The effects of fucoidan extracts on CCl_4-induced liver injury. *Arch. Pharm. Res.* **2008**, *31*, 622–627.
108. Luo, D.; Zhang, Q.; Wang, H.; Cui, Y.; Sun, Z.; Yang, J.; Zheng, Y.; Jia, J.; Yu, F.; Wang, X.; *et al*. Fucoidan protects against dopaminergic neuron death *in vivo* and *in vitro*. *Eur. J. Pharmacol.* **2009**, *617*, 33–40.
109. Balboa, E.M.; Conde, E.; Moure, A.; Falqué, E.; Domínguez, H. *In vitro* antioxidant properties of crude extracts and compounds from brown algae. *Food Chem.* **2013**, *138*, 1764–1785.
110. Hong, S.W.; Jung, K.H.; Lee, H.S.; Zheng, H.M; Choi, M.J.; Lee, C.; Hong, S.S. Suppression by fucoidan of liver fibrogenesis via the TGF-β/Smad pathway in protecting against oxidative stress. *Biosci. Biotechnol. Biochem.* **2011**, *75*, 833–840.
111. Hong, S.W.; Lee, H.S.; Jung, K.H.; Lee, H.; Hong, S.S. Protective effect of fucoidan against acetaminophen-induced liver injury. *Arch. Pharm. Res.* **2012**, *35*, 1099–1105.
112. Chen, J.; Wang, W.; Zhang, Q.; Li, F.; Lei, T.; Luo, D.; Zhou, H.; Yang, B. Low molecular weight fucoidan against renal ischemia-reperfusion injury via inhibition of the MAPK signaling pathway. *PLoS One* **2013**, *8*, e56224.
113. Lambert, J.D.; Elias, R.J. The antioxidant and pro-oxidant activities of green tea polyphenols: A role in cancer prevention. *Arch. Biochem. Biophys.* **2010**, *501*, 65–72.
114. Ye, J.; Li, Y.; Teruya, K.; Katakura, Y.; Ichikawa, A.; Eto, H.; Hosoi, M.; Hosoi, M.; Nishimoto, S.; Shirahata, S. Enzyme-Digested fucoidan extracts derived from seaweed Mozuku of *Cladosiphon novae-caledoniae kylin* inhibit invasion and angiogenesis of tumor cells. *Cytotechnology* **2005**, *47*, 117–126.

Anticancer Effects of Different Seaweeds on Human Colon and Breast Cancers

Ghislain Moussavou, Dong Hoon Kwak, Brice Wilfried Obiang-Obonou, Cyr Abel Ogandaga Maranguy, Sylvatrie-Danne Dinzouna-Boutamba, Dae Hoon Lee, Ordelia Gwenaelle Manvoudou Pissibanganga, Kisung Ko, Jae In Seo and Young Kug Choo

Abstract: Seafoods and seaweeds represent some of the most important reservoirs of new therapeutic compounds for humans. Seaweed has been shown to have several biological activities, including anticancer activity. This review focuses on colorectal and breast cancers, which are major causes of cancer-related mortality in men and women. It also describes various compounds extracted from a range of seaweeds that have been shown to eradicate or slow the progression of cancer. Fucoidan extracted from the brown algae *Fucus* spp. has shown activity against both colorectal and breast cancers. Furthermore, we review the mechanisms through which these compounds can induce apoptosis *in vitro* and *in vivo*. By considering the ability of compounds present in seaweeds to act against colorectal and breast cancers, this review highlights the potential use of seaweeds as anticancer agents.

Reprinted from *Mar. Drugs*. Cite as: Moussavou, G.; Kwak, D.H.; Obiang-Obonou, B.W.; Maranguy, C.A.O.; Dinzouna-Boutamba, S.-D.; Lee, D.H.; Pissibanganga, O.G.M.; Ko, K.; Seo, J.I.; Choo, Y.K. Anticancer Effects of Different Seaweeds on Human Colon and Breast Cancers. *Mar. Drugs* **2014**, *12*, 4898-4911.

1. Introduction

Cancers are a group of diseases characterized by uncontrolled cell growth and spread [1]. Colorectal cancer is the third most common cancer in the world, with nearly 1.4 million new cases diagnosed in 2012 [1]. Moreover, the incidence of this disease has increased steadily in recent years [2]. Despite advances in therapeutic interventions over the past few decades, the mortality rate of patients diagnosed with colorectal cancer remains approximately 40%, mainly due to metastasis to the liver [3].

Breast cancer is the leading cause of death among women in many countries [4]. This is the second most common cancer overall, with nearly 1.7 million new cases diagnosed worldwide in 2012 [1]. As breast cancer progresses, survival factors that inhibit apoptotic cell death are expressed by the cancer cells [5,6].

Due to the increasing incidence of cancer in both developing and developed countries, the use of new chemotherapeutic molecules is needed [7]. Employing natural or synthetic agents to prevent or suppress the progression of invasive cancers has recently been recognized as an approach with enormous potential [8].

Seaweeds (marine algae) are extensively used as functional foods and medicinal herbs, and have a long history of use in Asian countries [9]. Since certain seaweeds have long been used for the treatment of cancer, many crude or partially purified polysaccharides from various brown, green, and red algae have been tested for their antitumor activities [10] (Table 1). These studies have indicated that marine algae constitute a promising source of novel compounds with potential as human therapeutic agents. In particular, algae have been considered as a potential source of new bioactive compounds [7].

Several studies have reported that compounds extracted from seaweed may be effective anticancer agents. This review summarizes the various effects of seaweed-derived compounds on colorectal and breast cancers via promotion of cancer cell apoptosis.

2. Seaweed and Colorectal Cancer

Colorectal cancer is one of the most common cancers in men and women and it is particularly prevalent in developed countries. The worldwide incidence of this cancer has increased steadily in recent years, and this has been attributed to rapid changes in dietary patterns and preferences. Dietary habits can influence the risk for colorectal cancer [25], and the identification of food components that can prevent the tumorigenic process may contribute to the development of effective anti-colorectal cancer agents [2]. Many investigations have aimed to find effective ways to combat colorectal cancer. Some studies have reported that colorectal cancer can be successfully treated with marine natural products, which contain an abundance of biologically active substances with novel chemical structures and favorable pharmacological activities [11].

The inhibition of apoptosis in colorectal cancer cells enhances tumor growth, promotes neoplastic progression, and confers resistance to cytotoxic anticancer agents [26]. Thus, bioactive compounds that induce apoptosis in cancer cells can be used as agents for cancer chemoprevention and/or chemotherapy [2]. Accumulating evidence suggests that bioactive compounds extracted from algae produce anticancer effects through multiple mechanisms of action, including inhibition of cancer cell growth, invasion, and metastasis, and through the induction of apoptosis in cancer cells [27]. Apoptosis may be initiated either by an intrinsic (mitochondrial-mediated) pathway or by an extrinsic (death receptor-mediated) pathway [28–30]. Each of these pathways involves the activation of caspases and ultimately leads to apoptosis [12].

Table 1. The effects of seaweeds and their compounds on colorectal, breast and other cancers.

Seaweed	Nature	Colorectal Cancer	Breast Cancer	Other Cancers	Therapeutic Element	IC_{50}	Reference
Fucus sp.	Brown algae	+	+	-	Fucoidan	5–20 μg/mL	Kim *et al.* 2010 [2]
Stypopodium sp.	Brown algae	+	-	+	Meroditerpenoids	12.2 μM and 14 μM	Pereira *et al.* 2011 [7]
Sargassum muticum	Brown algae	-	+	-	Polyphenol	0.2 μg/mL	Namvar *et al.* 2013 [9]
Ulva fasciata	Green algae	-	-	+	Flavoids	200 μg/mL	Ruy *et al.* 2013 [11]
Laminaria sp.	Brown algae	+	-	-	Laminarin		Park *et al.* 2012; 2013 [12,13]
Laurencia sp.	Red algae	+	-	-	Dactylone	45.4 μmol/L	Federov *et al.* 2007 [14]
Ishige okamurae *Phoma herbarum*	Red algae	-	-	+	Ethanol extracts		Kim *et al.* 2009 [15]
Lithothamnion sp.	Red algae	+	-	-	Cellfood *		Aslam et *al.* 2009 [16]
Porphyra dentata	Red algae	-	+	-	Sterol fraction	48.3 μg/mL	Kazlowska *et al.* 2013 [17]
Cymopolia barbata	Green algae	-	+	-	CYP1 inhibitors	19.82 μM and 55.65 μM	Badal *et al.* 2013 [18]
Lophocladia sp.	Red algae	-	+	-	Lophocladines	3.1 μM and 64.6 μM	Gross 2006 [19]
Ascophyllum nodosum	Brown algae	-	+	-	Fucoidan		Pavia *et al.* 1996 [20]
Gracilaria termistipitata	Red algae	-	-	+	Methanol extracts		Ji *et al.* 2012 [21]
Enteromorpha intestinalis *Rhizoclonium riparium*	Green algae	-	-	+	Methanol extracts	309.05 μg/mL and 506.08 μg/m	Paul *et al.* 2013 [22]
Aspergillus sp.	Brown algae	-	-	+	Gliotoxin		Nguyen *et al.* 2014 [23]
Undaria pinnatifida	Brown algae				Fucoidan		Yang *et al.* 2013 [24]

+: effects reported; -: no effects reported; IC_{50} = the half-maximal inhibitory concentration; Seaweeds with two IC_{50} values had two different therapeutic compounds tested; * Cellfood designates all of the mineral salts and trace elements extracted from seaweeds.

Table 2. Seaweed-derived compounds and their effects on apoptosis.

Therapeutic Compounds (Seaweed)	Action Site						References
	Cell Cycle Arrest	Mitochondrial Membrane	Caspases or Cyclins	GFR	P53	Pro- or Anti-Apoptotic Proteins	
Fucoidan (*Fucus* sp.)	+	+	+	+		+	Kim *et al*. 2010 [2]/ Xue *et al*. 2012 [31]
Laminarin (*Laminaria* sp.)	+	+	+	+		+	Park *et al*. 2012; 2013 [12,13]
Dactylone (*Laurencia* sp.)	+	-	+	-	+		Fedorov *et al*. 2007 [14]
Steorol fraction (*Porphyra dentata*)	+	-	-	-	-	-	Kazlowska *et al*. 2013 [17]
Methanol extracts (*Sargassum muticum*)	+	-	-	-	-	-	Paul *et al*. 2013 [22]

+: effects reported; -: no effects reported.

Consumption of various types of seafood, including seaweed, has been suggested to be responsible for the low incidence of cancer in Japan and in other countries whose inhabitants traditionally consume high levels of marine organisms [14]. Numerous studies have examined the effects of seaweeds on apoptotic pathways (Table 2). The effects of laminarin, a storage glycan composed of β-glycan (β-1,3-β-1,6-glycan) found in brown algae, on colorectal cancer cells were investigated as well as the mechanisms through which laminarin induced apoptosis in these cells. Treatment with laminarin from *Laminaria* spp. (brown algae) inhibited the proliferation of colon cancer cells via Fas and IGF-IR signaling through the intrinsic apoptotic and ErbB pathways, respectively (Table 3) [12,13]. According to previous studies, Fas and Fas receptors induced the activation of members of the caspase family, leading to cleavage of apoptosis markers such as poly (ADP-ribose) polymerase (PARP) [32]. Other studies showed that laminarin regulated Fas and FADD protein levels, suggesting that it induced Fas-mediated apoptosis. Laminarin also increased the expression of Fas and FADD, which also increased the activation of caspases [33,34].

ErbB receptors control key pathways that govern cellular processes such as proliferation, cell migration, metabolism, and survival [35,36]. Dysregulation of the ErbB receptor signal transduction pathway is observed in several types of cancer, including colon cancer. Abnormal activation of the ErbB receptor is thought to be one of the potential causes of cancer [37]. Laminarin decreased Bcl-2 family protein expression and inhibited cell cycle progression by regulating the ErbB signaling pathway [13]. These studies also showed that treatment of HT-29 cells with laminarin inhibited phosphorylation and ErbB2 expression, as well as the phosphorylation of Akt.

Table 3. Properties of seaweeds in fight against colorectal cancer.

Colorectal Cancer		References
Seaweeds	**Therapeutic compounds and their properties**	
Laminaria digitata	Laminarin from *Laminaria digitata* induced apoptosis in HT-29 colon cancer cells; affected insulin-like growth factor (IGF-IR); decreased mitogen-activated protein kinase (MAPK) and ERK phosphorylation; decreased IGF-IR-dependent proliferation	Park *et al.* 2012; 2013 [12,13]
Lithothamnion calcareum (Pallas), also known as *Phymatolithon calcareum* (Pallas)	Multi-mineral extract from *Lithothamnion calcareum* can protect mice on a high-fat diet against adenomatous polyp formation in the colon	Aslam *et al.* 2009 [16]
Cymopolia barbata	Prenylated bromohydroquinones (PBQs) isolated from *Cymopolia barbata* show selectivity and potency against HT-29 cells and inhibit CYP1 enzyme activity, which may be a lead in chemoprevention	Badal *et al.* 2012 [18]
Undaria pinnatifida	Fucoxanthin from *Undaria pinnatifida* attenuated rifampin-induced CYP3A4, MDR1 mRNA and CYP3A4 protein expression	Yang *et al.* 2013 [24]

Fucoidan, a sulfated polysaccharide often found in brown algae, has shown a number of biological effects including anticancer activities [2]. A range of fucoidan structures and compositions exist in diverse brown seaweed species; however, in general the compound consists primarily of L-fucose and sulfate, along with small quantities of D-galactose, D-mannose, D-xylose, and uronic acid [38–40]. Recently, the diverse biological activities of fucoidan have been studied intensively, including its anticancer activities [31]. Many studies assessed whether fucoidan could inhibit the growth of colon cancer cells and studied the molecular pathways involved. Several studies showed that fucoidan exerted anticancer effects, including the suppression of growth [41–46]; it also decreased metastasis [43,47,48] and inhibited angiogenesis [48] in a variety of cancer cells. Fucoidan has been reported to inhibit the growth of a wide range of tumor cells [43,46]. It has also been shown to induce apoptosis in colon cancer HT-29 and HCT116 cells in a dose-dependent manner [15,49]. Kim *et al*. revealed that low concentrations of fucoidan (5–20 μg/mL) induced apoptosis of HT-29 and HCT-116 cells in a dose- and time-dependent manner. However, fucoidan showed a smaller effect on HTC116 cells than on HT-29 cells. According to Hyun *et al*. [50], fucoidan was able to induce apoptosis in HCT-15 human colon cancer cells at a concentration of 100 μg/mL. These results showed that the efficacy of fucoidan varied with the type of colon cancer cell studied. It was reported that fucoidan activated caspases, resulting in the induction of apoptosis through both death receptor-mediated and mitochondria-mediated apoptotic pathways [2].

Dactylone is representative of a new group of natural cancer-preventive agents [14]. Its chemical structure is closely related to that of sesquiterpenoids extracted from red algae *Laurencia* spp. The effects of dactylone have been studied in many cancer cell lines, including human colon cancer HCT116 cells, and the molecular mechanism underlying these effects was assessed [14]. Dactylone was able to suppress the phenotype expression of various human cancer cell lines and was shown to induce G1-S cell cycle arrest and apoptosis in tumor cells; it decreased Rb protein phosphorylation at Ser^{795}, Ser^{780}, and $Ser^{807/811}$ sites, and also inhibited the expression of cyclin D3 and cyclin-dependent

kinase (Cdk)4 [14]. Other studies revealed that inositol hexaphosphate, a dietary constituent found in rice, seems to act in a similar manner as dactylone. Indeed, inositol hexaphosphate has also been reported to decrease Cdk4 and cyclin D1 protein expression levels in addition to the inhibition of Rb phosphorylation at Ser^{780}, Ser^{807}, and Ser^{811}, causing G_1 arrest and apoptotic death of human cancers [14].

Meroditerpenoids such as plastoquinones, chromanols, and chromenes are a class of natural products consisting of a polyprenyl chain attached to a hydroquinone ring moiety, and are commonly present in brown algae (Phaeophyceae) [7]. Pereira *et al*. tested six meroditerpenoids (epitaondiol, epitaondiol diacetate, epitaondiol monoacetate, stypotriol triacetate, 14-ketostypodiol diacetate, and stypodiol) isolated from the brown algae *Stypopodium flabelliforme.* These meroditerpenoids inhibited cell proliferation in five cell lines: human neuroblastoma (SH-SY5Y), rat basophilic leukemia (RBL-2H3), murine macrophages (Raw267), Chinese hamster fibroblasts (V79), and human colon adenocarcinoma (Caco-2) cells. Overall, the compounds' activities against all cell lines were efficient. Stypotriol triacetate showed the most inhibition of the colon adenocarcinoma cell line, Caco-2, followed by epitaondiol monoacetate and epitaondiol.

Over their lifetime, marine algae accumulate high levels of minerals from seawater [16]. The proliferation and differentiation of human colon carcinoma cell lines were assessed in the presence of a mineral-rich extract from the red marine alga, *Lithothamnion calcareum* [16]. This algal extract was as effective as inorganic calcium in both inhibition of colon carcinoma cell growth and induction of its differentiation. Both epidemiological studies [51–55] and interventional studies [56,57] in humans have demonstrated that calcium has the capacity to reduce polyp formation in the colon. Other studies have found that different minerals obtained from marine algae could also contribute to the reduction of polyp formation (Table 3). In another study, Aslam *et al.* [16] reported that a multi-mineral product obtained from marine algae was able to reduce colon polyp formation in C57BL/6 mice receiving either a high-fat diet or a low-fat diet [16]. Based on these results, they suggested that the effects of calcium alone could not explain the protective effects of the multi-mineral supplement and that a multi-mineral approach to colon polyp chemoprevention may prove to be more efficacious than an approach based on the use of calcium alone.

Ulva fasciata extract (UFE) from *Ulva fasciata* Delile (sea lettuce), which grows abundantly along costal seashores, was used to assess the mechanisms underlying the cytotoxicity of green algae [11]. The anti-proliferative effects of UFE against colon cancer cells involved induction of apoptosis. Reactive oxygen species (ROS) have been reported to regulate apoptotic signal transduction and induce depolarization of the mitochondrial membrane, leading to increases levels of pro-apoptotic molecules in the cytosol [58,59]. Rye *et al*. [11] demonstrated that UFE significantly increased ROS generation in HCT116 cells and that antioxidant-mediated scavenging of UFE-induced ROS reduced the UFE-mediated cell death. UFE was able to inhibit the growth of HCT116 human colon cancer cells by 50% at a concentration of 200 μg/mL. It induced apoptosis through alteration in Bcl-2 family protein expression, increasing mitochondrial membrane permeability, and activation of caspase 9 and caspase 3 [11].

3. Seaweed and Breast Cancer

Breast cancer is the leading cause of death among women in many countries [4]. Although male breast cancer is less common, a few studies have revealed that the incidence has increased over the past 25 years [60]. Scientists have aimed to treat breast cancer without harming the patient by exploiting the differences between cancerous and normal cells. Nutritional strategies have been applied to study populations with a low incidence of breast cancer. In Asia, seaweeds have been eaten for at least 5000 years [61]. These populations have a low incidence of breast cancer. Certain brown and red algae are known for their anticancer properties [10,62]. In cells treated with seaweed, apoptosis was observed [63], and the authors speculated that seaweed could be a breast cancer-preventing food.

Some studies recently evaluated the effect of a brown seaweed (*Sargassum muticum*) methanol extract (SMME) on the proliferation of MCF-7 and MDA-MB-231 breast cancer cell lines [9] by conducting morphological assessments of apoptosis, caspase assays, and chick chorioallantoic membrane (CAM) assays. These methods were used to determine the morphological alterations induced by SMME to evaluate its time-dependent effects on caspases 8, 9, and 3 by using caspase assays, and also to evaluate the anti-angiogenic effects of SMME using the CAM assay. They observed that treatment with SMME significantly decreased angiogenesis, leading them to speculate that SMME could decrease cancer cell proliferation and increase apoptosis of human breast cancer cells in a time- and dose-dependent manner (Table 4).

Fucoidan was reported to enhance the activity of natural killer (NK) cells, which have anticancer activity [64]. The effects of crude fucoidan extracted from *Fucus vesiculosus* on the growth of breast cancer have been determined *in vitro* and *in vivo* [31]. Crude fucoidan significantly reduced the number of viable 4T1 cells (a mouse tumor cell line used as a model of highly metastatic breast cancer), enhanced apoptosis, and down-regulated the expression of vascular endothelial growth factor (VEGF). The mechanisms thought to be responsible for these fucoidan-mediated effects are inhibition of the expression of Bcl-2 (Bcl-2 preserves the mitochondria integrity), survivin, extracellular signal-regulated kinases (ERKs), and VEGF, and an increase in caspase-3 activation.

A sterol fraction extract of *Porphyra dentata*, an edible red alga used as a folk medicine in Asia, was evaluated for its effects on myeloid derived suppressor cells (MDSCs) in 4T1 cancer cells (Table 4) [17]. Previous findings indicated that phytosterols such as β-sitosterol, either alone or in combination with campesterol, may offer protection from various tumors [65–67]. MDSCs play an important role in tumorigenesis [18–20,68,69]. The authors associated the anticancer activity of *Porphyra dentata* with the presence of β-sitosterol and campesterol, which reduced the suppressive activity of MDSCs and consequently decreased tumor size. These two mechanisms might affect phytosterol-related downregulation of the suppressive activity of MDSCs, which is related to their ROS accumulation and arginase activity.

Table 4. Properties of seaweeds in fight against breast cancer.

Seaweed	Therapeutic Compounds and Their Properties	References
Sargassum muticum	*Sargassum muticum* methanol extract (SMME) Induced apoptosis of MCF-7 cells; showed anti-angiogenic activity in the chorioallantoic membrane (CAM) assay; antioxidant effects	Namvar *et al*. 2013 [9]
Fucus vesiculosus	Fucoidan (sulfated polysaccharide derived from brown algae) Decreased the viable number of 4T1 cells; induced apoptosis; down-regulated VEGF expression In colon cancer reduced in viable cell numbers and induced apoptosis of human lung carcinoma A549 cells as well as colon cancer HT-29 and HCT116 cells	Xue *et al*. 2012 [31]/ Kim *et al*. 2010 [2]
Porphyra dentata	Sterol fraction (containing cholesterol, β-sitosterol, and campesterol) from *Porphyra dentata* Significantly inhibited cell growth *in vitro* and induced apoptosis in 4T1 cancer cells; decreased the reactive oxygen species (ROS) and arginase activity of MDSCs in tumor-bearing mice	Kaslowska *et al*. 2013 [17]
Lophocladia sp.	Lophocladines A and B are 2,7-naphthyridine alkaloids from *Lophocladia sp.* Lophocladine A has affinity for NMDA receptors and is a δ-opioid receptor antagonist; Lophocladine B was cytotoxic to NCI-H460 human lung tumor cells and MDAMB-435 breast cancer cells	Gross *et al*. 2006 [19]

4. Conclusions

Many studies have explored the use of seaweed in the fight against several diseases, including colorectal and breast cancers. Various therapeutic compounds from seaweed are able to induce apoptosis through different pathways and molecular mechanisms. Several studies indicated that fucoidan was able to induce apoptosis, inhibit angiogenesis, and suppress lung metastasis of breast cancer *in vitro* and *in vivo* [21–24,31,70]. Furthermore, fucoidan inhibited growth and induced apoptosis of HT-29 colon cancer cells [2]. Laminarin induced apoptosis through the Fas and IGF-IR signaling pathways and through the intrinsic apoptotic and ErbB pathways [29]. This review highlights the importance of seaweed in the fight against colorectal and breast cancer.

Acknowledgements

This research was supported by the KRIBB Research Initiative Program (KGM4251415), and the Cooperative Research Program for Agriculture Science and Technology Development (Project No. PJ00999901), Rural Development Administration and Republic of Korea.

Author Contributions

Ghislain Moussavou, Dong Hoon Kwak, and Young-Kug Choo planned the initial version of the review, provided oversight of all work, and wrote the Abstract, Introduction, Seaweed and colorectal cancer, and Conclusion sections, and prepared a table 1. Brice Wilfried Obiang Obonou and Sylvatrie Danne Dinzouna Boutamba wrote the Seaweed and breast cancer section. Cyr Abel Ogandaga Maranguy, Ordelia Gwenaelle Manvoudou Pissibanganga and Dae Hoon Lee prepared the last three tables. Kisung Ko and Jae In Seo edited and reviewed the manuscript.

Conflicts of Interest

The authors declare no conflict of interest.

References

1. Ferlay, J.; Soerjomataram, I.; Ervik, M.; Dikshit, R.; Eser, S.; Mathers, C.; Rebelo, M.; Parkin, D.M.; Forman, D.; Bray, F. Cancer incidence and mortality worldwide: GLOBOCAN 2012 v1.0, IARC Cancer Base No. 11. International Agency for Research on Cancer: Lyon, France, 2013. Available online: http://globocan.iarc.fr (accessed on 13 December 2013).
2. Kim, E.J.; Park, S.Y.; Lee, J.Y.; Park, J.H. Fucoidan present in brown algae induces apoptosis of human colon cancer cells. *BMC Gastroenterol.* **2010**, *10*, 96.
3. Siegel, R.; Naishadham, D.; Jemal, A. Cancer statistics. *CA Cancer J. Clin.* **2012**, *62*, 10–29.
4. Giacinti, L.; Claudio, P.P.; Lopez, M.; Giordano, A. Epigenetic information and estrogen receptor alpha expression in breast cancer. *Oncologist.* **2006**, *11*, 1–8.
5. Luo, T.; Wang, J.; Yin, Y.; Hua, H.; Jing, J.; Sun, X.; Li, M.; Zhang, Y.; Jiang, Y. Epigallocatechin gallate sensitizes breast cancer cells to paclitaxel in a murine model of breast carcinoma. *Breast Cancer Res.* **2010**, *12*, R8.
6. Pulaski, B.A.; Ostrand-Rosenberg, S. Mouse 4T1 breast tumor model. In *Current Protocols in Immunology*; Wiley Online Library: Baltimore, MD, USA, 2001; Chapter 20, unit 20.22.
7. Pereira, D.M.; Cheel, J.; Arche, C.; San-Martin, A.; Rovirosa, J.; Silva, L.R.; Valentao, P.; Andrade, P.B. Anti-proliferative activity of meroditerpenoids isolated from the brown alga *Stypopodium flabelliforme* against several cancer cell lines. *Mar. Drugs* **2011**, *9*, 852–862.
8. Mann, J.R.; Backlund, M.G.; DuBois, R.N. Mechanisms of disease: Inflammatory mediators and cancer prevention. *Nat. Clin. Pract. Oncol.* **2005**, *2*, 202–210.
9. Namvar, F.; Mahamad, R.; Baharara, J.; Balnejah, S.Z.; Fargahi, F.; Rahman, H.S. Antioxidant, antiproliferative, and antiangiogenesis effects of polyphenol-rich seaweed (*Sargassum muticum*). *Biomed Res. Int.* **2013**, *2013*, 604787.

10. Ramberg, J.E.; Nelson, E.D.; Sinnott, R.A. Immunomodulatory dietary polysaccharides: A systematic review of the literature. *Nut. J.* **2010**, *9*, 54.
11. Ryu, M.J.; Kim, A.D.; Kang, K.A.; Chung, H.S.; Kim, H.S.; Suh, I.S.; Chang, W.Y.; Hyun, J.W. The green algae *Ulva fasciata* Delile extract induces apoptotic cell death in human colon cancer cells. *In Vitro Cell. Dev. Biol. Anim.* **2013**, *49*, 74–81.
12. Park, H.K.; Kim, I.H.; Kim, J.; Nam, T.J. Induction of apoptosis by laminarin, regulating the insulin-like growth factor-IR signaling pathways in HT-29 human colon cells. *Int. J. Mol. Med.* **2012**, *30*, 734–738.
13. Park, H.K.; Kim, J.; Nam, T.J. Induction of apoptosis and regulation of ErbB signaling by laminarin in HT-29 human colon cancer cells. *Int. J. Mol. Med.* **2013**, *32*, 291–295.
14. Fedorov, S.N.; Shubina, L.K.; Bode, A.M.; Stonik, V.A.; Dong, Z. Dactylone inhibits epidermal growth factor-induced transformation and phenotype expression of human cancer cells and induces G1-S arrest and apoptosis. *Cancer Res.* **2007**, *67*, 5914–5920.
15. Kim, M.M.; Rajapakse, N.; Kim, S.K. Anti-inflammatory effect of *Ishighe okamurae* ethanolic extract via inhibition of NF-kappaB transcription factor RAW264.7 cells. *Phytother. Res.* **2009**, *23*, 628–634.
16. Aslam, M.N.; Bhagavathula, N.; Paruchuri, T.; Hu, X.; Chakrabarty, S.; Varani, J. Growth-inhibitory of mineralized extract from red marine algae, *Lithothamnion calcareum*, on Ca^{2+}-sensitive and Ca^{2+}-resistant human colon carcinoma cells. *Cancer Lett.* **2009**, *283*, 186–192.
17. Kazlowska, K.; Victor Lin, H.T.; Chang, S.H.; Tsai, G.J. *In vitro* and *in vivo* anticancer effects of sterol fraction from red algae Porphyra dentata. *Evid. Based Complement. Alternat. Med.* **2013**, *2013*, 493869.
18. Badal, S.; Gallimore, W.; Huang, G.; Tseng, T.R.J.; Delgoda, R. Cytotoxic and potent CYP1 inhibitors from the marine algae *Cymopolia barbata*. *Org. Med. Chem. Lett.* **2012**, *2*, 21.
19. Gross, H.; Goeger, D.E.; Hills, P.; Mooberry, S.L.; Bellatine, D.L.; Murray, T.F.; Valeriote, F.A.; Gerwick, W.H. Lopohocladines, bioactive alkaloids from the red alga *Lophocladia sp. J. Nat. Prod*. **2006**, *69*, 640–644.
20. Pavia, H.; Aberg, P. Spatial variation in polyphenolic content of *Ascophyllum nodosum* (Fucales, Phaeophyta). *Hydrobiologia* **1996**, *327*, 199–203.
21. Ji, Y.; Yeh, C.C.; Lee, J.C.; Yi, S.C.; Huang, H.W.; Tseng, C.N.; Chang, H.W. Aqueous extracts of edible *Gracilaria tenuistipitata* are protective against HO induced DNA damage, growth inhibition, and cell cycle arrest. *Molecules* **2012**, *17*, 7241–7254.
22. Paul, S.; Kundu, R. Antiproliferative activity of methanolic extracts from two green algae, Enteromorpha intestinalis and Rhizoclonium riparium, on HeLa cells. *Daru* **2013**, *21*, 72.
23. Nguyen, V.T.; Lee, J.S.; Qian, Z.J.; Li, Y.X.; Kim, K.N.; Heo, S.J.; Jeon, Y.J.; Park, W.S.; Choi, I.W.; Je, J.Y.; *et al*. Gliotoxin isolated from marine fungus *Aspergillus* sp. induces apoptosis of human cervical cancer and chondrosarcoma cells. *Mar. Drugs* **2013**, *12*, 69–87.
24. Yang, L.; Wang, P.; Wang, H.; Li, Q.; Teng, H.; Liu, Z.; Yang, W.; Hou, L.; Zou, X. Fucoidan derived from *Undaria pinnatifada* induces apoptosis in human hepatocellular carcinoma SMMC 7721 cells via the ROS mediated mitochondrial pathway. *Mar. Drugs* **2013**, *11*, 1961–1976.
25. *WCRF/AICR: Food, Nutrition, Physical Activity and Prevention of Cancer: A Global Perspective*; American Institute for Cancer Research: Washington, DC, USA, 2009.

26. Bedi, A.; Pasricha, P.J.; Akhtar, A.J.; Barber, J.P.; Bedi, G.C.; Giardiello, F.M.; Zehnbauer, B.A.; Hamilton, S.R.; Jones, J.R. Inhibition of apoptosis during development of colorectal cancer. *Cancer Res.* **1995**, *55*, 1811–1816.
27. Farooqi, A.A.; Butt, G.; Razzaq, Z. Algae extracts and methyl jasmonate anti-cancer activities in prostate cancer: Choreographers of "the dance macabre". *Cancer Cell Int.* **2012**, *12*, 50.
28. Brenner, D.; Mak, T.W. Mitochondrial cell death effectors. *Curr. Opin. Cell Biol.* **2009**, *21*, 871–877.
29. Jeong, S.Y.; Seol, D.W. The role of mitochondria in apoptosis. *BMB Rep.* **2008**, *41*, 11–22.
30. Mellier, G.; Huang, G.; Shenoy, K.; Pervaiz, S. TRAILing death in cancer. *Mol. Aspects Med.* **2010**, *31*, 93–112.
31. Xue, M.; GE, Y.; Zhang, J.; Wanq, Q.; Hou, L.; Liu, Y.; Sun, L.; Li, Q. Anticancer properties and mechanisms of fucoidan on mouse breast cancer *in vitro* and *in vivo*. *PLoS One* **2012**, *7*, e43483.
32. Enari, M.; Talanian, R.V.; Wong, W.W.; Nagata, S. Sequential activation of ICE-like and CPP32-like proteases during Fas-mediated apoptosis. *Nature* **1996**, *380*, 723–726.
33. Kischkel, F.C.; Hellbardt, S.; Behrmann, I.; Germer, M.; Pawlita, M.; Krammer, P.H.; Peter, M.E. Cytotoxicity-dependent APO-1 (Fas/CD95)-associated proteins form a death-inducing signaling complex (DISC) with the receptor. *EMBO J.* **1995**, *14*, 5579–5588.
34. Salvesen, G.S.; Dixit, V.M. Caspases: Intracellular signaling by proteolysis. *Cell* **1997**, *91*, 443–446.
35. Hynes, N.E.; Lane, H.A. ERBB receptors and cancer: The complexity of targeted inhibitors. *Nat. Rev. Cancer* **2005**, *5*, 341–354.
36. Citri, A.; Yarden, Y. EGF-ERBB signalling: Towards the systems level. *Nat. Rev. Mol. Cell Biol.* **2006**, *7*, 505–516.
37. Salomon, D.S.; Brandt, R.; Ciardiello, F.; Normanno, N. Epidermal growth factor-related peptides and their receptors in human malignancies. *Crit. Rev. Oncol. Hematol.* **1995**, *19*, 183–232.
38. Li, B.; Lu, F.; Wein, X.; Zhao, R. Fucoidan: Structure and bioactivity. *Molecules* **2008**, *13*, 1671–1695.
39. Bilan, M.I.; Grachev, A.A.; Ustuzhanina, N.E.; Shashkov, A.S.; Nifantiev, N.E.; Usov, A.I. Structure of fucoidan from the brown seaweed Fucus evanescences C.Ag. *Carbohydr. Res.* **2002**, *337*, 719–730.
40. Bilan, M.I.; Grachev, A.A.; Shashkov, A.S.; Nifantiev, N.E.; Usov, A.I. Structure of a fucoidan from the brown seaweed Fucus serratus L. *Carbohydr. Res.* **2006**, *341*, 238–245.
41. Itoh, H.; Noda, H.; Amano, H.; Zhuaug, C.; Mizuno, T.; Ito, H. Antitumor activity and immunological properties of marine algal polysaccharides, especially fucoidan, prepared from *Sargassum thunbergii* of Phaeophyceae. *Anticancer Res.* **1993**, *13*, 2045–2052.
42. Zhuang, C.; Itoh, H.; Mizuno, T.; Ito, H. Antitumor active fucoidan from the brown seaweed umitoranoo (*Sargassum thubergii*). *Biosci. Biotechnol. Biochem.* **1995**, *59*, 563–567.
43. Alekseyenko, T.V.; Zhanayeva, S.Y.; Venediktova, A.A.; Zvyagintseva, T.N.; Kuznetsova, T.A.; Besednova, N.N.; Korolenko, T.A. Antitumor and antimetastatic activity of fucoidan, a sulfated polysaccharide isolate from the Okhotsk Sea *Fucus evanescens* brown alga. *Bull. Exp. Biol. Med.* **2007**, *143*, 730–732.

44. Riou, D.; Colliec-Jouault, S.; Pinczon du Sel, D.; Bosch, S.; Siavoshian, S.; le Bert, V.; Tomasoni, C.; Sinquin, C.; Durand, P.; Roussakis, C. Antitumor and antiproliferative effects of a fucan extracted from ascophyllum nodosum against a non-small-cell bronchopulmonary carcinoma line. *Anticancer Res.* **1996**, *16*, 1213–1218.
45. Aisa, Y.; Miyakawa, Y.; Nakazato, T.; Shibata, H.; Saito, K.; Ikeda, Y.; Kizaki, M. Fucoidan induces apoptosis of human HS-sultan cells accompanied by activation of caspase-3 and down-regulation of ERK pathways. *Am. J. Hematol.* **2005**, *78*, 7–14.
46. Teruya, T.; Konishi, T.; Uechi, S.; Tamaki, H.; Tako, M. Anti-proliferative activity of oversulfated fucoidan from commercially cultured *Cladosiphon okamuranus* TOKIDA in U937 cells. *Int. J. Biol. Macromol.* **2007**, *41*, 221–226.
47. Coombe, D.R.; Parish, C.R.; Ramshaw, I.A.; Snowden, J.M. Analysis of the inhibition of tumor metastasis by sulphated polysaccharides. *Int. J. Cancer* **1987**, *39*, 82–88.
48. Ye, J.; Li, Y.; Teruya, K.; Katakura, Y.; Ichikawa, A.; Eto, H.; Hosoi, M.; Nishimoto, S.; Shirahata, S. Enzyme-digested fucoidan extracts derived from seaweed mozuku of Cladosiphon novae-caledoniae kylin inhibit invasion and angiogenesis of tumor cells. *Cytotechnology* **2005**, *47*, 117–126.
49. Boo, H.J.; Hyun, J.H.; Kim, S.C.; Kang, J.I.; Kim, M.K.; Kim, S.Y.; Cho, H.; Yoo, E.S.; Kang, H.K. Fucoidan from *Undaria pinnatifida* induces apoptosis in A549 human lung carcinoma cells. *Phytother. Res.* **2011**, *25*, 1082–1086.
50. Hyun, J.H.; Kim, S.C.; Kang, J.I.; Kim, M.K.; Boo, H.J.; Kwon, J.M.; Koh, Y.S.; Hyun, J.W.; Park, D.B.; Yoo, E.S.; *et al*. Apoptosis inducing activity of fucoidan in HCT 15 colon carcinoma cells. *Biol. Pharm. Bull.* **2009**, *32*, 1760–1764.
51. McCullough, M.L.; Robertson, A.S.; Rodriguez, C.; Jacobs, E.J.; Chao, A.; Carolyn, J.; Calle, E.E.; Willett, W.C.; Thun, M.J. Calcium, vitamin D, dairy products, and risk of colorectal cancer in the Cancer Prevention Study II Nutrition Cohort (United States). *Cancer Causes Control* **2003**, *14*, 1–12.
52. Flood, A.; Peters, U.; Chatterjee, N.; Lacey, J.V., Jr.; Schairer, C.; Schatzkin, A. Calcium from diet and supplements is associated with reduced risk of colorectal cancer in a prospective cohort of women. *Cancer Epidemiol. Biomark. Prev*. **2005**, *14*, 126–132.
53. Bostick, R.M.; Potter, J.D.; Sellers, T.A.; McKenzie, D.R.; Kushi, L.H.; Folsom, A.R. Relation of calcium, vitamin D and dairy food intake to incidence of colon cancer among older women. The Iowa Women's Health Study. *Am. J. Epidemiol.* **1993**, *137*, 1302–1317.
54. Kampman, E.; Giovannucci, E.; Veer, P.V.; Rimm, E.; Stampfer, M.J.; Colditz, G.A.; Kok, F.J.; Willett, W.C. Calcium, vitamin D, dairy foods, and the occurrence of colorectal adenomas among men and women in two prospective studies. *Am. J. Epidemiol.* **1994**, *139*, 16–29.
55. Kampman, E.; Slattery, M.L.; Caan, B.; Potter, J.D. Calcium, vitamin D, sunshine exposure, dairy products and colon cancer risk (United States). *Cancer Causes Control* **2000**, *11*, 459–466.
56. Baron, J.A.; Beach, M.; Mandel, J.S.; van Stolk, R.U.; Haile, R.W.; Sandler, R.S.; Rothstein, R.; Summers, R.W.; Snover, D.C.; Beck, G.J.; *et al*. Calcium supplements for the prevention of colorectal adenomas. Calcium Polyp Prevention Study Group. *N. Engl. J. Med.* **1999**, *340*, 101–107.

57. Grau, M.V.; Baron, J.A.; Sandler, R.S.; Haile, R.W.; Beach, M.L.; Church, T.R.; Heber, D. Vitamin D, calcium supplementation, and colorectal adenomas: Results of a randomized trial. *J. Natl. Cancer Inst.* **2003**, *95*, 1765–1771.
58. Green, D.R.; Reed, J.C. Mitochondria and apoptosis. *Science* **1998**, *281*, 1309–1312.
59. Li, J.; Huang, C.Y.; Zheng, R.L.; Cui, K.R.; Li, J.F. Hydrogen peroxide induces apoptosis in human hepatoma cells and alters cell redox status. *Cell Biol. Int.* **2000**, *24*, 9–23.
60. Sanguinetti, A.; Polisterna, A.; D'Ermo, G.; Lucchini, R.; Triola, R.; Conti, C.; Avenia, S.; Cavallaro, G.; de Toma, G.; Avenia, N. Male breast cancer in the twenty-first century*:* What's new? *Ann. Ital. Chir.* **2014**, *85*, pii:S0003469X14022143.
61. Liu, L.; Heinrich, M.; Myers, S.; Dworjanyn, S.A. Towards a better understanding of medicinal uses of the brown seaweed Sargassum in Traditional Chinese Medicine: A phytochemical and pharmacological review. *J. Ethnopharmacol.* **2012**, *142*, 591–619.
62. Khan, M.N.; Choi, J.S.; Lee, M.C.; Kim, E.; Nam, T.J.; Fujii, H.; Hong, Y.K. Anti-inflammatory activities of methanol extracts from various seaweed species*. J. Environ. Biol*. **2008**, *29*, 465–469.
63. Funahashi, H.; Imai, T.; Mase, T.; Sekiya, M.; Yokoi, K.; Hayashi, H.; Shibata, A.; Hayashi, T.; Nishikawa, M.; Suda, M.; *et al*. Seaweed prevents breast cancer? *Jpn. J. Cancer Res.* **2001**, *92*, 483–487.
64. Maruyama, H.; Taumachi, H.; Lizuka, M.; Nakano, T. The role of NK cells in antitumor activity of dietary fucoidan from *Undaria pinnatifida* sporophylls (Mekabu)*. Planta Medica* **2006**, *72*, 1415–1417.
65. Awad, A.B.; Fink, C.S. Phytosterols as anticancer dietary components: Evidence and mechanism of action. *J. Nutr.* **2000**, *130*, 2127–2130.
66. Awad, A.B.; Fink, C.S.; Williams, H.; Kim, U. *In vitro* and *in vivo* (SCID mice) effects of phytosterols on the growth and dissemination of human prostate cancer PC-3 cells*. Eur. J. Cancer Prev.* **2001**, *10*, 507–513.
67. Von Holtz, R.L.; Fink, C.S.; Awad, A.B. beta-Sitosterol activates the sphingomyelin cycle and induces apoptosis in LNCaP human prostate cancer cells*. Nutr. Cancer* **1998**, *32*, 8–12.
68. Ochoa, A.C.; Zea, A.H.; Hernandez, C.; Rodrigue, P.C. Arginase, prostaglandins, and myeloid-derived suppressor cells in renal cell carcinoma. *Clin. Cancer Res*. **2007**, *13*, 721s–726s.
69. Zea, A.H.; Rodriguez, P.C.; Atkins, M.B.; Hernandez, C.; Signoretti, S.; Zabaleta, J.; McDermott, D.; Quiceno, D.; Youmans, A.; O'Neill, A.; *et al*. Arginase-producing myeloid suppressor cells in renal cell carcinoma patients: A mechanism of tumor evasion*. Cancer Res*. **2005**, *65*, 3044–3048.
70. Moghadamtousi, S.Z.; Karimian, H.; Khanabdali, R.; Razavi, M.; Firoozinia, M.; Zandi, K.; Abdul Kadir, H. Anticancer and Antitumor Potential of Fucoidan and Fucoxanthin, Two Main Metabolites Isolated from Brown Algae. *Sci. World J.* **2014**, *2014*, 768323:1–768323:10.

Fucoxanthin: A Marine Carotenoid Exerting Anti-Cancer Effects by Affecting Multiple Mechanisms

Sangeetha Ravi Kumar, Masashi Hosokawa and Kazuo Miyashita

Abstract: Fucoxanthin is a marine carotenoid exhibiting several health benefits. The anti-cancer effect of fucoxanthin and its deacetylated metabolite, fucoxanthinol, is well documented. In view of its potent anti-carcinogenic activity, the need to understand the underlying mechanisms has gained prominence. Towards achieving this goal, several researchers have carried out studies in various cell lines and *in vivo* and have deciphered that fucoxanthin exerts its anti-proliferative and cancer preventing influence via different molecules and pathways including the Bcl-2 proteins, MAPK, NFκB, Caspases, GADD45, and several other molecules that are involved in either cell cycle arrest, apoptosis, or metastasis. Thus, in addition to decreasing the frequency of occurrence and growth of tumours, fucoxanthin has a cytotoxic effect on cancer cells. Some studies show that this effect is selective, *i.e.*, fucoxanthin has the capability to target cancer cells only, leaving normal physiological cells unaffected/less affected. Hence, fucoxanthin and its metabolites show great promise as chemotherapeutic agents in cancer.

Reprinted from *Mar. Drugs*. Cite as: Kumar, S.R.; Hosokawa, M.; Miyashita, K. Fucoxanthin: A Marine Carotenoid Exerting Anti-Cancer Effects by Affecting Multiple Mechanisms. *Mar. Drugs* **2013**, *11*, 5130-5147.

1. Introduction

Fucoxanthin is a marine carotenoid found in numerous classes of microalgae (e.g., bacillariophytes, bolidophytes, chrysophytes, silicoflagellates, pinguiophytes) and brown macroalgae (phaeophytes) [1,2]. The chemical structure of fucoxanthin includes an allenic bond and oxygenic functional groups, such as hydroxyl, epoxy, carbonyl, and carboxyl groups in addition to its polyene chain (Figure 1). It is speculated that one of the reasons for the longevity of certain populations is the regular consumption of seaweeds including brown algae [3], which are known to be the major sources of fucoxanthin. Studies on brown seaweeds rich in fucoxanthin have revealed their anti-cancer effects [4–8]. Hence, the effect of fucoxanthin on cancer is of interest and has been studied by several researchers. The unanimous result of the studies on fucoxanthin in cancer has established that fucoxanthin performs a protective role and exhibits anti-proliferative behavior in various types of cancer. Recently, Gagez *et al*. [1] have reviewed the biological activities of epoxycarotenoids including fucoxanthin in cancer cells grown *in vitro* and described the various cellular targets of fucoxanthin. With the establishment of the anti-carcinogenic property of fucoxanthin, it was important to understand the mechanism by which it exerted its effect in cells. With this goal in mind, several researchers have been trying to elucidate the molecules and pathways that can be modulated and regulated by fucoxanthin. Mechanistic studies by various researchers have shown that fucoxanthin can affect many cellular processes, and so far have failed to establish a single primary mechanism of action. The objective of this review is to summarize the

effect of fucoxanthin in cancer and the underlying mechanisms that have been elucidated in reported studies. The various mechanisms discussed further in this review are shown in Figure 2.

Figure 1. Chemical structure of fucoxanthin (**a**) and its deacetylated metabolite, fucoxanthinol (**b**).

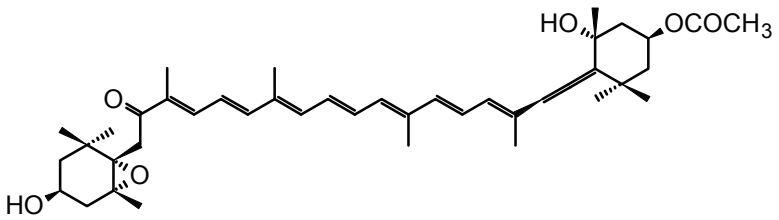

(**a**)

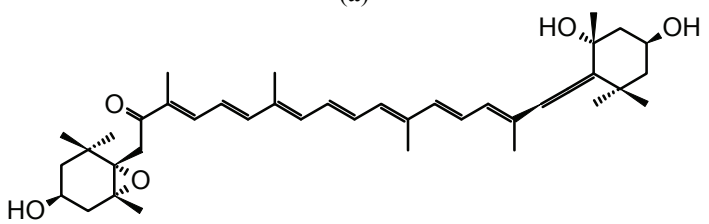

(**b**)

2. Anti-Carcinogenic Effects of Fucoxanthin

2.1. Decreased Incidence of Tumors

Nishino [9] has reported suppression of skin tumor formation as well as *N*-ethyl-*N*′-nitro-*N*-nitrosoguanidine (ENNG)-induced mouse duodenal carcinogenesis. In addition to the decrease in the percentage of tumor bearing mice, the mean number of tumors per mouse was also significantly lower in fucoxanthin fed mice. A decrease in the percentage of tumor-bearing mice as well as a decrease in the number of tumors induced per mouse by ENNG in the fucoxanthin group was also observed by Okuzumi and co-workers [10,11]. Administration of fucoxanthin resulted in significant decrease of sarcoma weight in mice [12]. Das *et al*. [4] and Kim *et al*. [13] have observed that aberrant crypt foci (ACF) formation in rats was decreased by fucoxanthin. The *in vivo* study by Ishikawa *et al*. [14] revealed unchanged tumor incidence but delayed tumor growth and decreased tumor volume with the deacetylated metabolite of fucoxanthin, namely fucoxanthinol. In addition, in contrast to the untreated tumors, abundant apoptotic cells were observed in tumors from the fucoxanthinol treated group. Fucoxanthin also suppressed the growth of B16F10 melanoma in Balb/c mice [15].

Figure 2. Factors (molecules and mechanisms) regulated by fucoxanthin, resulting in its anti-carcinogenic effects. Dashed lines indicate inter-relation/inter-effects between the factors; up and down arrows indicate up- and down-regulation (by fucoxanthin/fucoxanthinol), respectively.

2.2. Antioxidant Effect of Fucoxanthin

Several reports on the potent antioxidant property of fucoxanthin and its metabolites are available [16–20]. While its antioxidant property was initially thought to be the main reason behind its anti-carcinogenic effect, it is now established that the realm of fucoxanthin's effect is wider and involves several other biological processes as well. Moreover, some studies have reported the pro-oxidant effect of fucoxanthin on cancer cells with the production of free radicals and have proposed this to be one of the mechanisms by which it protects against cancer cells. Kotake-Nara *et al.* [21] have hypothesized that the prooxidant actions of fucoxanthin and other carotenoids used in their study may be the reason for the induction of apoptosis in cancer cells. However, in their subsequent study [22], they have found similar apoptotic activity of fucoxanthin in promyelocytic leukemia cell lines but from their results in H_2O_2 resistant cell lines, they have

concluded that reactive oxygen species (ROS) is not the mainstream pathway for apoptosis caused. Contradictory to this, Kim *et al*. [23] have observed the growth inhibition in leukemia cell lines by fucoxanthin and have attributed it to radical oxygen species (ROS) generation by fucoxanthin that leads to apoptosis. They observed increased production of H_2O_2 and O_2^- as a result of treatment with fucoxanthin along with accumulation of cells containing sub G1 DNA content (indicating cell cycle arrest in G1 stage). On co-treatment with a commercial antioxidant (NAC), the number of apoptotic bodies and DNA fragmentation of cells was decreased, attributing the apoptotic effect of fucoxanthin to ROS generated. Thus, they have concluded that cytotoxic effect of fucoxanthin is by ROS generation that triggers apoptosis in HL-60 cells, which is contrary to the results of Kotake-Nara *et al*. [22]. Shimoda *et al*. [24] have reported the anti-pigmentation effect of fucoxanthin and suppression of melanogenesis in melanoma and tyrosinase activity in UV-irradiated guinea pigs. Heo and Jeon [25] have reported the protective effect of fucoxanthin on exposure of human fibroblasts to UVB exposure and attributed the protective effects to the antioxidant activity of fucoxanthin.

2.3. Cell Viability/Anti-Proliferation of Cells

The effect of fucoxanthin on cell viability in cancer cells such as GOTO, HL-60, Caco-2, HepG-2, Neuro2a, DU145, PEL, PC-3, HeLa, H1299, HT-29, DLD-1 cells, and *in vivo* has been explored by many researchers [10,14,21,22,26–34]. Liu *et al*. [29] have reported the anti-proliferative effect of fucoxanthin against SK-Hep-1 (human hepatoma) cells and BNL CL.2 (murine embryonic liver) cells. They have reported a strong correlation between fucoxanthin concentration and anti-proliferative effect on SK-Hep-1 cells at 24 h. However, the suppressive effect was similar for concentrations >1 μM after 48 h. Fucoxanthin, however, was found to facilitate the growth of BNL CL.2 cells until 24 h after which there was a slight decrease in proliferation at 48 h indicating that fucoxanthin was selectively more effective against the SK-Hep-1 cells. In a separate study, Hosokawa *et al*. [27] compared the effects of fucoxanthin and other carotenoids such as β-carotene and astaxanthin on colon cancer cell lines (Caco-2, HT-29, and DLD-1). Cell viability was found to be significantly decreased with fucoxanthin as compared to the other carotenoids and the Caco-2 cell line was found to be most sensitive to the action of fucoxanthin.

Yamamoto *et al*. [31] have concluded that the effect of fucoxanthinol (deacetylated metabolite of fucoxanthin) was more potent than fucoxanthin and PEL cells were more susceptible to the effects of fucoxanthin and fucoxanthinol than HeLa cells. Kotake-Nara *et al*. [21] have reported a dose dependent reduction in cell viability in prostate cancer cell lines exposed to fucoxanthin along with morphological changes such as rounding up, detachment and reduction in cell volume and apoptotic bodies. The DNA fragmentation observed in cells treated with fucoxanthin suggested that apoptosis was the cause of suppression of cell viability. In a separate study on the effect of neoxanthin and fucoxanthin on PC-3 prostate cancer cells, Kotake-Nara *et al*. [35] have reported decreased cell viability, rounding up, reduced cell volume, chromatin condensation, nuclei fragmentation, formation of apoptotic bodies in addition to the apoptotic DNA ladder indicating apoptosis in the cells. In a recent study by Ganesan *et al*. [26] on 11 carotenoids, two marine carotenoids, siphonaxanthin and fucoxanthin were found to possess potent growth inhibitory and

apoptosis inducing effect in HL-60 leukemia cells. Cell viability was reduced with fucoxanthin treatment and apoptosis was characterized by DNA fragmentation and chromatin condensation. Jaswir *et al*. [28] have reported the dose dependent growth inhibition of H1299 (lung cancer) cells and morphological changes, such as decrease in cell size and nuclear condensation.

Thus, fucoxanthin was found to have a significant effect on cell viability and anti-proliferative effect and in several studies the potency was different for different cell types/lines. In addition, in several studies, the normal cells were unaffected/less affected than cancer cells indicating differential effect of fucoxanthin and focused targeting of cancer cells [29,31,34,36–38]. However, it is important to note that due to different growth rates of cancer and normal cells, attention to experimental detail is a very important factor while drawing conclusions. Therefore, very rigorous methods are essential to prove cancer selectivity over normal cells in experimental studies. Another interesting finding in a few of the studies was the greater potency of the deacetylated metabolite of fucoxanthin (fucoxanthinol). Fucoxanthinol is known to be the major fucoxanthin metabolite [39–41]. Dietary fucoxanthin is hydrolyzed to fucoxanthinol in the gastrointestinal tract by digestive enzymes such as lipase and cholesterol esterase. Fucoxanthinol was detectable at 0.8 nM in human plasma after a daily intake (6 g dry weight containing 6.1 mg (9.26 mmol) of fucoxanthin) of cooked edible brown seaweed, *Undaria pinnatifida* (Wakame), for one week [41]. In another study, Hashimoto *et al*. [42] have reported 7.6 nM of fucoxanthinol after 24 h, on administration of kombu extract containing 31 mg of fucoxanthin in human subjects.

2.4. Cell Cycle Arrest

The arrest of the cell cycle in the G_0/G_1 stage by fucoxanthin has been observed in many studies involving different cell lines [10,14,15,31,32,43–46] while Yu *et al*. [47] have observed cell cycle arrest in G_2/M phase. Muthuirullappan and Francis [48] have attempted to review some of these studies recently and explored the possibility of a nano-suspension formulation for fucoxanthin. Liu *et al*. [29] have reported the anti-proliferative effect of fucoxanthin with enhanced gap junction intracellular communication (GJIC) and increased intracellular calcium ions. They have suggested that the enhanced expression of connexin genes and GJIC may increase intracellular calcium levels resulting in cell cycle arrest and apoptosis. Accumulation of cells in the G_0-G_1 phase with a significant decrease in cells in the S phase, indicating a block in the progression of the cells to S phase from the G_0-G_1 phase, resulting in inhibition of proliferation of the cells has been reported in GOTO cell line [10]. Fucoxanthin arrested cell growth in the G_1 stage and this was accompanied by alteration in the expression of more than 50 genes in HEPG2 cells [32]. In addition to the GADD45 gene expression, the expression of other growth related genes such as PIM 1, IFRDI, p21, and p27 was also increased. Ishikawa *et al*. [14] have found decreased expression of cyclin D1, cyclin D2, CDK4, CDK6, and cIAP2 on fucoxanthin treatment in leukemia. Kim *et al*. [15] have observed inhibited cell growth, morphological changes and apoptosis in melanoma cells (B16F10) on exposure to fucoxanthin. This was accompanied by a sub G_1 peak along with concentration of cells in G_0/G_1 phase and their decrease in the S and G_2/M phases. In addition, pRb, cyclin D1, cyclin D2, and CDK4 levels were decreased along with increased $p^{15INK4B}$, p^{27KIP1} levels. Murakami *et al*. [49]

have reported the inhibition of DNA polymerases, especially pol α activity at lower concentrations (79 μM) and pol β as well at higher concentrations (100 μM) by fucoxanthin, *in vitro*.

Das *et al*. [45] have observed continuous cell cycle arrest at G_0/G_1 phase at lower concentrations of fucoxanthin (25 μM), followed by apoptosis at high concentrations (>50 μM) with increased cells in sub G_1 phase (index of apoptotic DNA fragmentation) and fragmentation of nuclei. Low and high concentrations of fucoxanthin up regulated the protein and mRNA levels of $p21^{WAF1/Cip1}$ followed by increased levels of pRb (retinoblastoma protein), while high levels up regulated $p27^{Kip1}$ as well (cdk inhibitory proteins) leading to the conclusion that fucoxanthin-induced G_0/G_1 cell arrest is mediated by the up regulation of $p21^{WAF1/Cip1}$. They have speculated that the apoptosis observed at higher concentration may be due to partial conversion of fucoxanthin to its metabolites such as fucoxanthinol. From their results they have concluded that $p21^{WAF1/Cip1}$ is important for the cell cycle arrest while $p27^{Kip1}$ regulation may be a means for pro-apoptotic effect of fucoxanthin. Reduction in the phosphorylation of pRb protein, which is a regulator of cell cycle progression and down-regulation of other cell cycle regulatory proteins like cyclin D2, CDK4, CDK6, and c-Myc was reported by Yamomoto *et al*. [28]. A decrease was observed in the pRb levels while the total Rb protein concentration remained constant and the activity of cyclin D/cdk4 was decreased by fucoxanthin in the study of Das *et al*. [46]. Fucoxanthin treatment resulted in decreased protein and mRNA levels of cyclins D1 and D3 while protein level of cdk4 was unaffected at 12 h. The protein levels of $p27^{Kip1}$ $p21^{Waf/Cip1}$, p57, and p16 were unchanged over this period indicating that inhibition of cyclin D/cdk4 activity by fucoxanthin was brought about by suppressing the levels of proteolysis and transcription of cyclin D. An increase in proteosomal activity was observed after 12 h of fucoxanthin treatment. Thus, they have suggested that fucoxanthin induced cell cycle arrest by suppression of cyclin D by proteosomal degradation and transcriptional repression. They have speculated that the decreased cyclin D expression may be due to change in the GADD45A expression.

2.5. Apoptosis: Cytotoxic Effect

Apoptosis of cancer cells is a promising method to control and treat cancer. In this regard, the apoptotic effect of fucoxanthin is of interest and has been studied by several researchers. Hosokawa *et al*. [33] have reported DNA fragmentation and the DNA ladder characteristic of apoptosis in HL-60 cells treated with fucoxanthin. In a separate study, fucoxanthin was found to induce cellular DNA fragmentation/internucleosomal DNA degradation by activation of endogenous nucleases in a dose dependent manner unlike β-carotene and astaxanthin. The authors have hypothesized that since fucoxanthin is converted to fucoxanthinol prior to uptake and also fucoxanthinol shows greater inhibition of growth, the superior anti-proliferative effect of fucoxanthin may be due to its metabolites [27]. DNA fragmentation typical of apoptotic cells was observed in NSCLC-N6 (human non-small cell bronchopulmonary carcinoma) cells treated with fucoxanthin along with typical morphological changes such as rounding up, reduction in cell volume, chromatin condensation, nuclei fragmentation, and formation of apoptotic bodies [36]. However, in the same study, no apoptosis was observed in SRA (human lens epithelial cells) indicating the specific action of fucoxanthin against carcinogenic cells.

The results obtained by Konishi *et al*. [50] show the dose and time dependent anti-proliferative effect of fucoxanthinol and fucoxanthin in HL-60, MCF-7 (breast cancer), and Caco-2 cells. In their studies, they found the anti-proliferative effects of fucoxanthinol to be greater than fucoxanthin. Their experiments involved studying the effect of metabolites like fucoxanthinol and halocynthiaxanthin and comparing it with fucoxanthin. They have concluded that both the metabolites showed superior anti-proliferative activity and have speculated that one of the factors that may contribute to this may be the presence of hydroxyl functional group in place of the acetyl group of fucoxanthin, a feature common to both metabolites, in addition to unique structures such as 5,6-epoxide, acetylenic and allenic bonds. Zhang *et al*. [51] have reported the anti-proliferative effect of fucoxanthin on EJ-1 (urinary bladder cancer) cells. Apoptosis characterized by condensed chromatin, nuclear fragmentation, and apoptotic bodies in addition to the DNA ladder was observed.

Expression of v-FLIP and v-cyclin was inhibited and may be responsible for growth inhibition and apoptosis observed with fucoxanthin treatment [34]. The authors have suggested that the effective concentration for the induction of apoptosis is different in different cell lines and fucoxanthinol exhibits more potent activity as compared to fucoxanthin. GADD153 known to be associated with apoptosis was also induced by fucoxanthin in a study [35].

2.6. Metastasis

Metastasis is the stage of cancer at which tumor cells acquire the advantageous characteristics that allows them to escape from the primary tumor and migrate to surrounding and distant organs and tissues. Metastasis involves the interaction of the tumor cells with numerous factors and cell components including matrix metalloproteinases (MMPs). MMPs are thought to assist tumor cells in metastasis and their enhanced levels have been associated with extra-cellular matrix degradation and cancer cell invasion [52]. Chung *et al*. [53] have studied the effect of fucoxanthin in B16-F10 cells (metastatic murine melanoma) MMP-2 and MMP-9. These MMPs are expressed in cancer cells and degrade type IV collagen during cancer invasion. Fucoxanthin treatment resulted in decreased expression and secretion levels of MMP-9. Moreover; the numbers of invaded B16-F10 cells were also decreased. In addition to MMPs; they have also studied CD44 and CXR4; a cell surface glycoprotein and CXC chemokine receptor respectively; that are also known to be up-regulated in cancer metastasis. Fucoxanthin was found to reduce the mRNA expression of CD44 and CXCR4 in a dose dependent manner. Fucoxanthin was also shown to decrease cell motility of melanoma cells which was ascertained by reduction in stress fiber and lamellipodia formation that are important in cell migration. Hence; by suppressing cancer cell motility and invasion factors; fucoxanthin may be valuable in preventing cancer cell metastasis.

3. Molecules and Mechanisms Related to Apoptosis

3.1. Bcl-2 Proteins

The family of Bcl-2 proteins has anti-apoptotic and pro-apoptotic members. Anti-apoptotic Bcl-2 family proteins include Bcl-2, Bcl-x_L, A1, Bcl-w, and Boo, while the pro-apoptotic members include Bax and Bak, Bok, Bcl-xs, Bim, Bad, Bid, Bik, Bmf, Puma, Noxa, and Hrk [54,55].

Several researchers who have tried to elucidate the mechanism underlying the anti-proliferative effect of fucoxanthin have studied the Bcl-2 family of proteins. Many studies have reported the down regulation of Bcl-2 expression in HL-60, Caco-2 cells [12,27,50]. Nakazawa *et al*. [56] observed down-regulation of Bcl-2 proteins, which was associated with the apoptosis in their study, which compared the effects of cis and trans forms of fucoxanthin. Their results have suggested that while the uptake of trans form was higher in the cells (HL-60 human leukemia, Caco-2 colon cancer, PC-3 and LNCap prostate), the apoptosis effect of the cis forms was higher. They have attributed this difference to the stearic hindrances arising from their different chemical structures. As the ratio of pro and anti-apoptotic Bcl-2 members is an important determinant of cell viability and apoptosis, Liu *et al*. [57] studied these factors and reported an increase in Bax/Bcl-2 mRNA expression when a combination of cisplatin and fucoxanthin were administered. Down-regulation of Bcl-x_L and XIAP by fucoxanthin was observed by Yamamoto *et al*. [31] and Kim *et al*. [15], while Ishikawa *et al*. [14] reported decreased expression of Bcl-2 and XIAP, and Kim *et al*. [23] observed decreased expression of Bcl-x_L, Kotake-Nara *et al*. [35] on the other hand have speculated that as Bax (pro-apoptotic) and Bcl-2 (anti-apoptotic) were down-regulated by fucoxanthin while Bcl-x_L was unaltered, unlike other apoptosis-inducing agents that modulate the ratios of the pro- and anti-apoptotic proteins, fucoxanthin may operate through a different pathway.

3.2. The Caspase Pathway

The caspases are cysteine proteases that control apoptosis. The extrinsic pathway involves the tumor necrosis factor and activates the caspases 8 and 10 while the intrinsic pathway involves the mitochondria and release of cytochrome c from damaged mitochondria, activating Caspase-9, which is an initiator and in turn can cleave and activate the effector Caspases such as Caspases-3, -6, and -7. These two Caspase pathways, intrinsic and extrinsic, can result in apoptosis. The intrinsic pathway involving the mitochondria and caspases-3, -6, -7, and -9 are controlled by the Bcl-2 protein family [55]. The activation of one or more members of the caspase pathways by fucoxanthin has been reported by several researchers. Wang *et al*. [12], Ganesan *et al*. [26], Zhang *et al*. [51] have observed the increased expression of caspase-3 on exposure to fucoxanthin. Fucoxanthin and fucoxanthinol treatments resulted in production of cleaved products and thus activation of PARP, caspase-3, -8, and -9 demonstrating that caspase activation plays a role in the apoptosis observed [31]. Fucoxanthinol activated caspase pathways with cleavage of caspase-3, -8, -9, and PARP [14]. Expression of caspase-3 and -9 was increased by fucoxanthin. PARP, a substrate of caspases was detected in its intact and cleaved form, indicating apoptosis [15]. Fucoxanthin was found to activate the caspase pathway with the cleavage of caspase-3 and PARP and increased activities of caspase -8 and -9 as well [22]. The results suggested that fucoxanthin accumulates in the mitochondrial membranes causing a reduction in the membrane potential and release of cytochrome c from mitochondria to the cytosol, followed by caspase-9 and caspase-3 activation, leading to the apoptotic effects of fucoxanthin in the leukemia cell lines. In a separate study where the authors compared the effect of fucoxanthin and neoxanthin in PC-3 prostate cells, the down regulation of procaspase-3 and PARP and the increased active fragment of caspase-3 and cleaved PARP indicated caspase-3 dependent apoptosis by fucoxanthin [35].

3.3. MAPK and GADD45

The MAPK family or the mitogen activated protein kinase includes four well characterized sub-groups: (1) ERK1 and ERK2 that are extracellular signal kinases; (2) JNK1, JNK2, and JNK3 with the c-Jun NH_2 terminal kinases, also called as stress-activated protein kinases (SAPK); (3) p38 enzymes including p38α, p38β, p38γ, p38δ, and the recently identified; (4) ERK5. ERK1 and ERK2 regulate cell processes like mitosis, meiosis, post mitotic functions, and are responsible for proliferation, cell division, differentiation, development and survival. STAT (signal transducers and activators of transcription) proteins such as Stat3 are substrates that are phosphorylated by ERK and are activators of transcription. The JNK/SAPKs are activated by conditions such as oxidative stress and result in programmed cell death or apoptosis, growth and cell cycle arrest as well as inflammation and tumorigenesis and cell survival under certain conditions. C-Jun is a component of the AP-1 complex that is an important regulator of gene function and is activated by environmental stress, radiation and growth factors. The p38 MAPKs control the expression of several cytokines and are involved in the immune response mechanism in addition to cell motility, apoptosis, chromatin remodeling, and osmoregulation [58,59]. Gadd45 proteins include the subtypes GADD45A, GADD45B, GADD45G, and are involved in cell cycle arrest at the G2/M and G1 stages (depending on the interactions), DNA repair, cell survival and apoptosis and are known to interact with the members of the MAPK family. In addition, GADD45A and GADD45G are repressed by the activated members of the NFκB family in various types of cancer [60,61].

Fucoxanthin was found to attenuate cisplatin induced phosphorylation of ERK, p38, and P13K/AKT (phosphatidylinositol 3 kinase family) in the studies carried out by Liu *et al*. [57]. Their experiments with specific inhibitors also revealed that fucoxanthin may inhibit ERCC1 mRNA expression via the ERK and P13K/AKT pathway while thymidine phosphorylase mRNA expression may be inhibited through the p38 pathway. Ishikawa *et al*. [14] have observed decreased AP-1 DNA binding activity and JunD expression indicating the inactivation of AP-1 by depletion of JunD. Their results indicated that up-regulation of the GADD45α observed was independent of p53.

In a separate study, Satomi and Nishino [43] found that fucoxanthin activated the p38 and ERK1/2 MAPKs in HepG2 cells and SAPK/JNK pathways were activated in DU145 cells, indicating that SAPK/JNK are upstream activators of GADD45 expression. Thus, each MAPK and each GADD45 subtype (a and b) play different roles in cell cycle progression. They have concluded that fucoxanthin induces cell arrest by a GADD45A dependent pathway and the GADD45A expression and G1 arrest are negatively regulated by p38 MAPK in HepG2 cells and positively regulated by the SAPK/JNK pathway in DU145 cells. In another study, CYP1A1 gene expression and other cell cycle and growth related genes such as GADD45A, GADD45B, PIM1 and IFRDI were induced by fucoxanthin as well as the expression of other cell cycle related genes such as p21, p27 and c-myc [32]. Further, Satomi [44] has reported the role of fucoxanthin on the MAPKs (extracellular signal-regulated kinases ERK1/2, ERK5, p38 MAPK kinases, c-Jun *N*-terminal kinases (SAPK/JNK)) and its association with the GADD45 activation for cell growth arrest in LNCap cells (prostate cancer). GADD45A may be implicated in the G1 arrest observed in the study. While the GADD45A gene was enhanced, GADD45B gene expression was unaffected

after fucoxanthin treatment. With respect to the MAPK family, SAPK/JNK was increased, phosphorylation of ERK 1/2 was reduced and phosphorylation of p38 was unaffected. While it is suggested that MAPKs including SAPK/JNK induce GADD45A in a p53 dependent or independent manner, the author has suggested a p53 independent mechanism in the present study. In addition, inhibition of the SAPK/JNK pathway reduced GADD45A induction while inhibition of ERK 1/2 and p38 pathways stimulated GADD45A induction. The author has suggested that each MAPK plays a different role in GADD45A induction and G1 arrest by fucoxanthin based on the negative regulation of p38 MAPK resulting in increased GADD45A expression along with other observations in prostate cancer cells. Contrasting results obtained for ERK 1/2 MAPK in LNCap cells and in DU145 cells earlier indicate that GADD45A may not be the only factor responsible for the G1 cell arrest observed in that study. Thus the growth inhibitory effect exhibited by fucoxanthin may in part be due to a GADD45A-dependent pathway and the enhanced GADD45A expression and G1 arrest are positive regulated by SAPK/JNK in prostate cancer cells.

Yu *et al*. [47] have observed the down-regulation of STAT3 at mRNA and protein levels, which indicated the inhibition of the JAK/STAT pathway by fucoxanthin as the JAK are known to activate the STAT members. Further, Wang *et al*. [12] reported that the STAT3 and p-STAT3 (phosphorylated STAT3) was down regulated by fucoxanthin. EGFR (epidermal growth factor receptor) expression, which is often dysregulated in many human cancers, was decreased with fucoxanthin. They have concluded that down regulation of STAT3/EGFR was involved in the anti tumor and apoptosis inducing effects of fucoxanthin.

3.4. NFκB

The nuclear factor kappa B (NF-κB) is a family of closely related transcription factors that are held in the cytoplasm in the inactive form by their interaction with the inhibitor of κB (IκB). IκBs include IκBα, IκBβ, IκBε, and BCL-3. The phosphorylation of IκB results in activation of NFκB and its translocation to the nucleus, followed by induction of target genes and the resulting effects. NF-κB may be activated by many cytokines, growth factors and their receptors, tyrosine kinases, tumor necrosis factor receptor families, other signaling pathways, such as Ras/MAPK and PI3K/Akt. NF-κB promotes resistance to apoptosis and may also exhibit pro-apoptotic properties. NF-κB inhibits p53-induced apoptosis by up-regulating anti-apoptotic genes, and decreasing p53 levels. As NF-kB is associated with several tumor/cancer related processes, such as its activation by pro-inflammatory cytokines and its ability to induce cell proliferation and anti-apoptotic gene expression, as well as induction of angiogenesis, it is often considered as a hallmark of cancer [62,63].

Cisplatin has the potential to bind to the DNA molecules, forming platinum-DNA adducts which interfere with transcription and replication of the DNA, resulting in cell death [64,65]. Several mechanisms responsible for resistance to cisplatin are known. Elevated mRNA levels of excision repair cross-complementation group 1 (ERCC1) are reported in clinical resistance to platinum-based chemotherapy for various cancers. NFκB induces cell proliferation, metastasis, suppression of apoptosis, oncogenesis, and cancer therapy resistance. NFκB induces anti-apoptotic proteins and suppresses pro-apoptotic genes and thus inhibits apoptosis. Cisplatin and several other cancer drugs are shown to induce NFκB translocation and activation, resulting in drug resistance.

In addition, thymidine phosphorylase (TP) expression is higher in tumors, and results in their enhanced resistance to apoptosis. Mise and Yasumoto [30] found that that the antioxidative potential of fucoxanthin did not decrease the cytotoxicity of the platinum anti-cancer drug, cisplatin. In another study, Liu *et al*. [57] have also reported the similar effectiveness of fucoxanthin with cisplatin, in HepG2 cells. The results of their study clearly indicated an enhanced anti-proliferative effect of cisplatin when used in combination with fucoxanthin. NFκB binding was decreased and restoration of IκB by inhibition of phosphorylation was increased. Their results involving an NFκB inhibitor suggests an inhibition of the NFκB pathway when the combination is administered as compared to cisplatin alone. While cisplatin resulted in increased expression of ERCC1 and TP, combined treatment with fucoxanthin resulted in their inhibition. In another study, fucoxanthin and fucoxanthinol reduced the phosphorylation of IKKβ and IκBα and levels of IKKα, IKKβ, and IKKγ (indicating Hsp90 chaperone inhibition) [31]. Different genes showed different susceptibility to the fucoxanthin treatment and were associated with the down regulation of DNA-binding activities of NFκB, pIκBα, and increased IκBα [14].

3.5. CYP3A4 Enzyme

Due to their wide range of substrate selectivity CYP3A enzymes play a major role in metabolism and are of special relevance in the metabolism of clinically used drugs [66]. The cytochrome P 450 3A4 (CYP3A4) is the most abundant of the P450 isoforms and is found in the liver and intestines of humans. Activation of pregnane X Receptor (PXR) results in the induction of CYP3A4. Cytochrome P450 enzymes are regulated by both the PXR and CAR (constitutive androstane receptor) pathways [67]. PXR is known to act as a xenobiotic sensor and can prevent intracellular accumulation of drugs by activation of cytochrome P450 and multiple drug resistance 1 (MDR 1). PXR activation has an anti-apoptotic role and PXR antagonists can decrease cell proliferation and interfere with cancer drug resistance [68,69]. Liu *et al*. [70] have examined the possible role of fucoxanthin as an adjuvant to prevent or overcome rifampin induced drug resistance in HepG2 and LS174T cells. In their study, decreased basal CYP3A4 enzyme activity, CYP3A4 mRNA expression, CYP3A4 protein expression, CYP3A4 promoter activity through CAR and decreased PXR and SRC-1(co-activator of PXR) interaction in fucoxanthin treated group and with co-incubation of fucoxanthin with rifampin was observed. Their results indicate that fucoxanthin may play an important role as not only a chemotherapeutic agent, but also in assisting other cancer drugs by attenuating the prevailing drug resistance. Satomi and Nishino [32] have observed induction of the CYP1A1 gene expression as a result of fucoxanthin treatment in prostate cancer cell lines.

3.6. Gap Junctional Intracellular Communication/Connexin Genes

Gap junctional intracellular communication (GJIC) is a mechanism for intercellular cell communication and operates at sites of cell adhesion where plasma membranes of cells can be connected by buried paired channels. Thus, GJIC regulates the communication between cells of tissues of an organ, allowing for direct communication between the cytoplasm of cells without

transit through the extracellular space, making it possible for the cells to achieve a common and integrated target/metabolic activity [71]. Gap junctions in vertebrates are composed of the connexin family of proteins, which are about 20 in number in humans [72]. Loss and impairment of GJIC has been associated with pathologies such as cancer, heart and skin diseases, cataracts, hereditary deafness, and some forms of neuropathy [73]. The enhancement of GJIC in cancer on treatment with several carotenoids such as β-carotene, canthaxanthin, lutein, α-carotene, lycopene astaxanthin, has been reported [74–76]. Liu *et al*. [29] have attempted to elucidate the mechanism of the anti-proliferative action of fucoxanthin by studying the GJIC, expression of connexin genes and DNA damage. The GJIC and expression of connexin genes (Cx 32 and Cx 43) was improved at both protein and mRNA levels in the SK-Hep-1 cells in a concentration dependent manner by fucoxanthin while the BNL CL.2 cells were unaffected. Their results indicated that fucoxanthin can regulate pathways, such as MAPK and PI3 kinase/Akt cascades, which are known to have a negative effect on GJIC. They have concluded that fucoxanthin exhibits anti-proliferative activity in SK-Hep-1 cells along with enhanced expression of connexin genes and GJIC. Satomi and Nishino [32] have also observed an increase in expression of connexin 43 and AP-1.

3.7. Expression of N-Myc Oncogene, Survivin, and Angiogenic Activity

N-Myc oncogene, known to be over expressed in neuroblastoma, was reduced by fucoxanthin treatment in GOTO neuroblastoma cell line and this effect was found to be reversible when fucoxanthin was removed from the media [10]. Survivin is known to be prominently expressed in many common human cancers. Yu *et al*. [47] studied the role of JAK/STAT pathway and have speculated that other pathways may inhibit the expression of survivin. Further, the expression of survivin and VEGF (vascular endothelial growth factor; induced by STAT3) positive cells was down regulated by fucoxanthin in the study of Wang *et al*. [12]. Yamamoto *et al*. [31] and Ishikawa *et al*. [14] also observed the down-regulation of survivin.

Sugawara *et al*. [77] have reported the anti-angiogenic activity of fucoxanthin and postulated that this may be another protective effect of fucoxanthin in pathologies such as cancer. They have observed the reduced tube length of HUVEC (human umbilical vein endothelial cells) cells and the inhibition of their proliferation by fucoxanthin but have observed no effect on their migration. Fucoxanthin and fucoxanthinol were found to suppress development of blood vessel like structures in embryonic stem cell derived embyoid bodies and outgrowth of micro-vessels. In addition they have hypothesized that antioxidant activity of fucoxanthin may be involved in its anti-angiogenic effect as ROS are known to stimulate angiogenesis.

4. Conclusions

Fucoxanthin influences a multitude of molecular and cellular processes. It exerts strong effects on cancer cells and shows synergistic activity in combination with established cytotoxic drugs. This raises the possibility that it could become an interesting anti-cancer compound in various types of cancer.

Acknowledgments

Sangeetha RK is grateful to JSPS (Japan Society for the Promotion of Science) for the award of a Post-Doctoral Fellowship.

Conflicts of Interest

The authors declare no conflict of interest.

References

1. Gagez, A.-L.;Thiery, V.; Pasquet, V.; Cadoret, J.-P.; Picot, L. Epoxycarotenoids and cancer. Review. *Curr. Bioact. Compd.* **2012**, *8*, 109–141.
2. Peng, J.; Yuan, J.-P.; Wu, C.-F.; Wang, J.-H. Fucoxanthin, a marine carotenoid present in brown seaweeds and diatoms: Metabolism and bioactivities relevant to human health. *Mar. Drugs* **2011**, *9*, 1806–1828.
3. Sho, H. History and characteristics of Okinawan longevity food. *Asia Pac. J. Clin. Nutr.* **2001**, *10*, 159–164.
4. Das, S.K.; Hashimoto, T.; Baba, M.; Nishino, H.; Komoto, A.; Kanazawa, K. Japanese kelp (kombu) extract suppressed the formation of aberrant crypt foci in azoxymethane challenged mouse colon. *J. Clin. Biochem. Nutr.* **2006**, *38*, 119–125.
5. Funahashi, H.; Imai, T.; Mase, T.; Sekiya, M.; Yokoi, K.; Hayashi, H.; Shibata, A; Hayashi, T.; Nishikawa, M.; Suda, N.; *et al*. Seaweed prevents breast cancer? *Jpn. J. Cancer Res.* **2001**, *92*, 483–487.
6. Funahashi, H.; Imai, T.; Tanaka, Y.; Tsukamura, K.; Hayakawa, Y.; Kikumori, T.; Mase, T.; Itoh, T.; Nishikawa, M.; Hayashi, H.; *et al*. Wakame seaweed suppresses the proliferation of 7,12-dimethylbenz(a)-anthracene-induced mammary tumors in rats. *Jpn. J. Cancer Res.* **1999**, *90*, 922–927.
7. Okai, Y.; Higashi-okai, K.; Nakamura, S. Identification of heterogenous antimutagenic activities in the extract of edible brown seaweeds, *Laminaria japonica* (Makonbu) and *Undaria pinnatifida* (Wakame) by the *umu* gene expression system in *Salmonella typhimurium* (TA1535/pSKlO02). *Mutat. Res.* **1993**, *303*, 63–70.
8. Teas, J.; Vena, S.; Cone, D.L.; Irhimeh, M. The consumption of seaweed as a protective factor in the etiology of breast cancer: Proof of principle. *J. Appl. Phycol.* **2013**, *25*, 771–779.
9. Nishino, H. Cancer chemoprevention by natural carotenoids and their related compounds. *J. Cell. Biochem. Suppl.* **1995**, *22*, 231–235.
10. Okuzumi, J.; Nishino, H.; Murakoshi, M.; Iwashima, A; Tanaka, Y.; Yamane, T.; Fujita, Y.; Takahashi, T. Inhibitory effects of fucoxanthin, a natural carotenoid, on N-myc expression and cell cycle progression in human malignant tumor cells. *Cancer Lett.* **1990**, *55*, 75–81.
11. Okuzumi, J.; Takahashi, T.; Yamanea, T.; Kitao, Y.; Inagake, M.; Ohya, K.; Nishino, H.; Tanaka, Y. Inhibitory effects of fucoxanthin , a natural carotenoid, on *N*-ethyl-*N*′-nitro-*N*-nitrosoguanidine-induced mouse duodenal carcinogenesis. *Cancer Lett.* **1993**, *68*, 159–168.

12. Wang, J.; Chen, S.; Xu, S.; Yu, X.; Ma, D.; Hu, X.; Cao, X. *In vivo* induction of apoptosis by fucoxanthin, a marine carotenoid, associated with down-regulating STAT3/EGFR signaling in sarcoma 180 (S180) xenografts-bearing mice. *Mar. Drugs* **2012**, *10*, 2055–2068.
13. Kim, J.M.; Araki, S.; Kim, D.J.; Park, C.B.; Takasuka, N.; Baba-Toriyama, H.; Ota, T.; Nir, Z.; Khachik, F.; Shimidzu, N.; *et al*. Chemopreventive effects of carotenoids and curcumins on mouse colon carcinogenesis after 1,2-dimethylhydrazine initiation. *Carcinogenesis* **1998**, *19*, 81–85.
14. Ishikawa, C.; Tafuku, S.; Kadekaru, T.; Sawada, S.; Tomita, M.; Okudaira, T.; Nakazato, T.; Toda, T.; Uchihara, J.-N.; Taira, N.; *et al*. Antiadult T-cell leukemia effects of brown algae fucoxanthin and its deacetylated product, fucoxanthinol. *Int. J. Cancer* **2008**, *123*, 2702–2712.
15. Kim, K.-N.; Ahn, G.; Heo, S.-J.; Kang, S.-M.; Kang, M.-C.; Yang, H.-M.; Kim, D.; Roh, S.W.; Kim, S.-K.; Jeon, B.-T.; *et al*. Inhibition of tumor growth *in vitro* and *in vivo* by fucoxanthin against melanoma B16F10 cells. *Environ. Toxicol. Pharmacol.* **2013**, *35*, 39–46.
16. Nomura, T.; Kikuchi, M.; Kubodera, A.; Kawakami, Y. Proton-donative antioxidant activity of fucoxanthin with 1,1-diphenyl-2-picrylhydrazyl (DPPH). *Biochem. Mol. Biol. Int.* **1997**, *42*, 361–370.
17. Sangeetha, R.K.; Bhaskar, N.; Baskaran, V. Comparative effects of β-carotene and fucoxanthin on retinol deficiency induced oxidative stress in rats. *Mol. Cell. Biochem.* **2009**, *331*, 59–67.
18. Sachindra, N.M.; Sato, E.; Maeda, H.; Hosokawa, M.; Niwano, Y.; Kohno, M.; Miyashita, K. Radical scavenging and singlet oxygen quenching activity of marine carotenoid fucoxanthin and its metabolites. *J. Agric. Food Chem.* **2007**, *55*, 8516–8522.
19. Sangeetha R.K.; Bhaskar, N.; Baskaran, V. Fucoxanthin restrains oxidative stress induced by retinol deficiency through modulation of Na^+K^+-ATPase and antioxidant enzyme activities in rats. *Eur. J. Nutr.* **2008**, *47*, 432–441.
20. Chandini, S.K.; Ganesan, P.; Bhaskar, N. *In vitro* antioxidant activities of three selected brown seaweeds of India. *Food Chem.* **2008**, *107*, 707–713.
21. Kotake-Nara, E.; Kushiro, M.; Zhang, H.; Sugawara, T.; Miyashita, K.; Nagao, A. Carotenoids affect proliferation of human prostate cancer cells. *J. Nutr.* **2001**, *131*, 3303–3306.
22. Kotake-Nara, E.; Terasaki, M.; Nagao, A. Characterization of apoptosis induced by fucoxanthin in human promyelocytic leukemia cells. *Biosci. Biotechnol. Biochem.* **2005**, *69*, 224–227.
23. Kim, K.-N.; Heo, S.-J.; Kang, S.-M.; Ahn, G.; Jeon, Y.-J. Fucoxanthin induces apoptosis in human leukemia HL-60 cells through a ROS-mediated Bcl-xL pathway. *Toxicol. In Vitro* **2010**, *24*, 1648–1654.
24. Shimoda, H.; Tanaka, J.; Shan, S.-J.; Maoka, T. Anti-pigmentary activity of fucoxanthin and its influence on skin mRNA expression of melanogenic molecules. *J. Pharm. Pharmacol.* **2010**, *62*, 1137–1145.
25. Heo, S.-J.; Jeon, Y.-J. Protective effect of fucoxanthin isolated from *Sargassumsiliquastrum* on UV-B induced cell damage. *J. Photochem. Photobiol. B: Biol.* **2009**, *95*, 101–107.

26. Ganesan, P.; Noda, K.; Manabe, Y.; Ohkubo, T.; Tanaka, Y.; Maoka, T.; Sugawara, T.; Hirata, T. Siphonaxanthin, a marine carotenoid from green algae, effectively induces apoptosis in human leukemia (HL-60) cells. *Biochim. Biophys. Acta* **2011**, *1810*, 497–503.
27. Hosokawa, M.; Kudo, M.; Maeda, H.; Kohno, H.; Tanaka, T.; Miyashita, K. Fucoxanthin induces apoptosis and enhances the antiproliferative effect of the PPARγ ligand, troglitazone, on colon cancer cells. *Biochim. Biophys. Acta* **2004**, *1675*, 113–119.
28. Jaswir, I.; Noviendri, D.; Salleh, H.M.; Taher, M.; Miyashita, K. Isolation of fucoxanthin and fatty acids analysis of Padina australis and cytotoxic effect of fucoxanthin on human lung cancer (H1299) cell lines. *Afr. J. Biotechnol.* **2011**, *10*, 18855–18862.
29. Liu, C.-L.; Huang, Y.-S.; Hosokawa, M.; Miyashita, K.; Hu, M.-L. Inhibition of proliferation of a hepatoma cell line by fucoxanthin in relation to cell cycle arrest and enhanced gap junctional intercellular communication. *Chem.-Biol. Interact.* **2009**, *182*, 165–172.
30. Mise, T.; Yasumoto, T. Simultaneous treatment of cancer cells lines with the anticancer drug cisplatin and the antioxidant fucoxanthin. *Br. J. Pharmacol. Toxicol.* **2011**, *2*, 127–131.
31. Yamamoto, K.; Ishikawa, C.; Katano, H.; Yasumoto, T.; Mori, N. Fucoxanthin and its deacetylated product, fucoxanthinol, induce apoptosis of primary effusion lymphomas. *Cancer Lett.* **2011**, *300*, 225–234.
32. Satomi, Y.; Nishino, H. Fucoxanthin, a natural carotenoid, induces G1 arrest and GADD45 gene expression in human cancer cells. *In Vivo* **2007**, *21*, 305–310.
33. Hosokawa, M.; Wanezaki, S.; Miyauchi, K.; Kurihara, H.; Kohno, H.; Kawabata, J.; Odashima, S.; Takahashi, K. Apoptosis-inducing effect of fucoxanthin on human leukemia cell HL-60. *Food Sci. Technol. Res.* **1999**, *5*, 243–246.
34. Kotake-Nara, E.; Sugawara, T.; Nagao, A. Antiproliferative effect of neoxanthin and fucoxanthin on cultured cells. *Fish. Sci.* **2005**, *75*, 459–461.
35. Kotake-Nara, E.; Asai, A.; Nagao, A. Neoxanthin and fucoxanthin induce apoptosis in PC-3 human prostate cancer cells. *Cancer Lett.* **2005**, *220*, 75–84.
36. Moreau, D.; Tomasoni, C.; Jacquot, C.; Kaas, R.; Le Guedes, R.; Cadoret, J.-P.; Muller-Feuga, A.; Kontiza, I.; Vagias, C.; Roussis, V.; *et al*. Cultivated microalgae and the carotenoid fucoxanthin from *Odontella aurita* as potent anti-proliferative agents in bronchopulmonary and epithelial cell lines. *Environ. Toxicol. Pharmacol.* **2006**, *22*, 97–103.
37. Matsumoto, M.; Hosokawa, M.; Matsukawa, N.; Hagio, M.; Shinoki, A.; Nishimukai, M.; Miyashita, K.; Yajima, T.; Hara, H. Suppressive effects of the marine carotenoids, fucoxanthin and fucoxanthinol on triglyceride absorption in lymph duct-cannulated rats. *Eur. J. Nutr.* **2010**, *49*, 243–249.
38. Sugawara, T.; Baskaran, V.; Tsuzuki, W.; Nagao, A. Brown algae fucoxanthin is hydrolyzed to fucoxanthinol during absorption by Caco-2 human intestinal cells and mice. *J. Nutr.* **2002**, *132*, 946–951.
39. De la Mare, J.-A.; Sterrenberg, J.N.; Sukhthankar, M.G.; Chiwakata, M.T.; Beukes, D.R.; Blatch, G.L.; Edkins, A.L. Assessment of potential anti-cancer stem cell activity of marine algal compounds using and *in vitro* mammosphere assay. *Cancer Cell Int.* **2013**, *13*, doi:10.1186/1475-2867-13-39.

40. Asai, A.; Sugawara, T.; Ono, H.; Nagao, A. Biotransformation of fucoxanthinol into amarouciaxanthin A in mice and HepG2 cells: Formation and cytotoxicity of fucoxanthin metabolites. *Drug Metab. Dispos.* **2004**, *32*, 205–211.
41. Asai, A.; Yonekura, L.; Nagao, A. Low bioavailability of dietary epoxyxanthophylls in humans. *Br. J. Nutr.* **2008**, *100*, 273–277.
42. Hashimoto, T.; Ozaki, Y.; Mizuno, M.; Yoshida, M.; Nishitani, Y.; Azuma, T.; Komoto, A.; Maoka, T.; Tanini, Y.; Kanazawa, K. Pharmacokinetics of fucoxanthinol in human plasma after the oral administration of kombu extract. *Br. J. Nutr.* **2012**, *107*, 1566–1569.
43. Satomi, Y.; Nishino, H. Implication of mitogen-activated protein kinase in the induction of G1 cell cycle arrest and *gadd45* expression by the carotenoid fucoxanthin in human cancer cells. *Biochim. Biophys. Acta* **2009**, *1790*, 260–266.
44. Satomi, Y. Fucoxanthin Induces *GADD45A* Expression and G 1 Arrest with SAPK/JNK Activation in LNCap Human Prostate Cancer Cells. *Anticancer Res.* **2012**, *32*, 807–814.
45. Das, S.K.; Hashimoto, T.; Shimizu, K.; Yoshida, T.; Sakai, T.; Sowa, Y.; Komoto, A.; Kanazawa, K. Fucoxanthin induces cell cycle arrest at G_0/G_1 phase in human colon carcinoma cells through up-regulation of $p21^{WAF1/Cip1}$. *Biochim. Biophys. Acta* **2005**, *1726*, 328–335.
46. Das, S.K.; Hashimoto, T.; Kanazawa, K. Growth inhibition of human hepatic carcinoma HepG2 cells by fucoxanthin is associated with down-regulation of cyclin D. *Biochim. Biophys. Acta* **2008**, *1780*, 743–749.
47. Yu, R.; Hu, X.; Xu, S.; Jiang, Z.; Yang, W. Effects of fucoxanthin on proliferation and apoptosis in human gastric adenocarcinoma MGC-803 cells via JAK/STAT signal pathway. *Eur. J. Pharmacol.* **2011**, *657*, 10–19.
48. Muthuirulappan, S.; Francis, S.P. Anti-cancer mechanism and possibility of nano-suspension formulation for a marine algae product fucoxanthin. *Asian Pac. J. Cancer Prev.* **2013**, *14*, 2213–2216.
49. Murakami, C.; Takemura, M.; Sugiyama, Y.; Kamisuki, S.; Asahara, H.; Kawasaki, M.; Ishidoh, T.; Linn, S.; Yoshida, S.; Sugawara, F.; *et al*. Vitamin A-related compounds, all-*trans* retinal and retinoic acids, selectively inhibit activities of mammalian replicative DNA polymerases. *Biochim. Biophys. Acta* **2002**, *1574*, 85–92.
50. Konishi, I.; Hosokawa, M.; Sashima, T.; Kobayashi, H.; Miyashita, K. Halocynthiaxanthin and fucoxanthinol isolated from *Halocynthia roretzi* induce apoptosis in human leukemia, breast and colon cancer cells. *Comp. Biochem. Physiol. Part C* **2006**, *142*, 53–59.
51. Zhang, Z.; Zhang, P.; Hamada, M.; Takahashi, S.; Xing, G.; Liu, J.; Sugiura, N. Potential chemoprevention effect of dietary fucoxanthin on urinary bladder cancer EJ-1 cell line. *Oncol. Rep.* **2008**, *20*, 1099–1103.
52. Deryugina, E.I.; Quigley, J.P. Matrix metalloproteinases and tumor metastasis. *Cancer Metastasis Rev.* **2006**, *25*, 9–34.
53. Chung, T.W.; Choi, H.-J.; Lee, J.-Y.; Jeong, H.-S.; Kim, C.-H.; Joo, M.; Choi, J.-Y.; Han, C.-W.; Kim, S.-Y.; Choi, J.-S.; *et al*. Marine algal fucoxanthin inhibits the metastatic potential of cancer cells. *Biochem. Biophys. Res. Commun.* **2013**, *439*, 580–585.

54. Ola, M.S.; Nawaz, M.; Ahsan, H. Role of Bcl-2 family proteins and caspases in the regulation of apoptosis. *Mol. Cell. Biochem.* **2011**, *351*, 41–58.
55. Adams, J.M.; Cory, S. Bcl-2-regulated apoptosis: Mechanism and therapeutic potential. *Curr. Opin. Immunol.* **2007**, *19*, 488–496.
56. Nakazawa, Y.; Sashima, T.; Hosokawa, M.; Miyashita, K. Comparative evaluation of growth inhibitory effect of stereoisomers of fucoxanthin in human cancer cell lines. *J. Funct. Foods* **2009**, *1*, 88–97.
57. Liu, C.-L.; Lim, Y.-P.; Hu, M.-L. Fucoxanthin enhances cisplatin-induced cytotoxicity via NFκB-mediated pathway and downregulates DNA repair gene expression in human hepatoma HepG2 cells. *Mar. Drugs* **2013**, *11*, 50–66.
58. Johnson, G.L.; Lapadat, R. Mitogen-activated protein kinase pathways mediated by ERK, JNK, and p38 Protein Kinases. *Science* **2013**, *298*, 1911–1912.
59. Cowan, K.J.; Storey, K.B. Mitogen-activated protein kinases: New signaling pathways functioning in cellular responses to environmental stress. *J. Exp. Biol.* **2003**, *206*, 1107–1115.
60. Zerbini, L.F.; Wang, Y.; Czibere, A.; Correa, R.G.; Cho, J.-Y.; Ijiri, K.; Wei, W.; Joseph, M.; Gu, X.; Grall, F.; *et al*. NF-κB-mediated repression of growth arrest- and DNA-damage-inducible proteins 45α and γ is essential for cancer cell survival. *Proc. Natl. Acad. Sci. USA* **2004**, *101*, 13618–13623.
61. Liebermann, D.; Tront, J.S.; Sha, X.; Mukherjee, K.; Mohamed-Hadley, A.; Hoffman, B. Gadd45 stress sensors in malignancy and leukemia. *Crit. Rev. Oncog.* **2011**, *16*, 129–140.
62. Dolcet, X.; Llobet, D.; Pallares, J.; Matias-Guiu, X. NF-κB in development and progression of human cancer. *Virchows Arch.* **2005**, *446*, 475–482.
63. Viatour, P.; Merville, M.-P.; Bours, V.; Chariot, A. Phosphorylation of NF-κB and IκB proteins: Implications in cancer and inflammation. *Trends Biochem. Sci.* **2005**, *30*, 43–52.
64. Zorbas, H.; Keppler, B.K. Cisplatin damage: Are DNA repair proteins saviors or traitors to the cell? *ChemBioChem* **2005**, *6*, 1157–1566.
65. Cepeda, V.; Fuertes, M.A.; Castilla, J.; Alonso, C.; Quevedo, C.; Pérez, J.M. Biochemical mechanisms of cisplatin cytotoxicity. *Anti-Cancer Agents Med. Chem.* **2007**, *7*, 3–18.
66. Klein, K.; Zanger, U.M. Pharmacogenomics of cytochrome P450 3A4: Recent progress toward the "missing heritability" problem. *Front. Genet.* **2013**, *4*, 1–15.
67. Fahmi, O.A.; Kish, M.; Boldt, S.; Obach, R.S. Cytochrome P450 3A4 mRNA is a more reliable marker than CYP3A4 activity for detecting pregnane X receptor-activated induction of drug-metabolizing enzymes. *Drug Metab. Dispos.* **2010**, *38*, 1605–1611.
68. Chen, Y.; Nie, D. Pregnane X receptor and its potential role in drug resistance in cancer treatment. *Recent Pat. Anti-Cancer Drug Discov.* **2009**, *4*, 19–27.
69. Miki, Y.; Suzuki, T.; Kitada, K.; Yabuki, N.; Shibuya, R.; Moriya, T.; Ishida, T.; Ohuchi, N.; Blumberg, B.; Sasano, H. Expression of the steroid and xenobiotic receptor and its possible target gene, organic anion transporting polypeptide-A, in human breast carcinoma. *Cancer Res.* **2006**, *66*, 535–542.

70. Liu, C.-L.; Lim, Y.-P.; Hu, M.-L. Fucoxanthin attenuates rifampin-induced cytochrome P450 3A4 (*CYP3A4*) and multiple drug resistance 1 (*MDR1*) gene expression through pregnane X receptor (PXR)-mediated pathways in human hepatoma HepG2 and colon adenocarcinoma LS174T cells. *Mar. Drugs* **2012**, *10*, 242–257.
71. Evans, W.H.; Martin, P.E.M. Gap junctions: Structure and function (Review). *Mol. Membr. Biol.* **2002**, *19*, 121–136.
72. Lampe, P.D.; Lau, A.F. The effects of connexin phosphorylation on gap junctional communication. *Int. J. Biochem. Cell Biol.* **2004**, *36*, 1171–1186.
73. Willecke, K.; Eiberger, J.; Degen, J.; Eckardt, D.; Romualdi, A.; Güldenagel, M.; Deutsch, U.; Söhl, G. Structural and functional diversity of connexin genes in the mouse and human genome. *Biol. Chem.* **2002**, *383*, 725–737.
74. Zhang, L.-X.; Cooney, R.V.; Bertram, J.S. Carotenoids enhance gap junctional communication and inhibit lipid peroxidation in C3H/10T1/2 cells: Relationship to their cancer chemopreventive action. *Carcinogenesis* **1991**, *12*, 2109–2114.
75. Hix, L.M.; Lockwood, S.F.; Bertram, J.S. Upregulation of connexin 43 protein expression and increased gap junctional communication by water soluble disodium disuccinate astaxanthin derivatives. *Cancer Lett.* **2004**, *211*, 25–37.
76. Aust, O.; Ale-Agha, N.; Zhang, L.; Wollersen, H.; Sies, H.; Stahl, W. Lycopene oxidation product enhances gap junctional communication. *Food Chem. Toxicol.* **2003**, *41*, 1399–1407.
77. Sugawara, T.; Matsubara, K.; Akagi, R.; Mori, M.; Hirata, T. Antiangiogenic activity of brown algae fucoxanthin and its deacetylated product, fucoxanthinol. *J. Agric. Food Chem.* **2006**, *54*, 9805–9810.

Marine-Sourced Anti-Cancer and Cancer Pain Control Agents in Clinical and Late Preclinical Development

David J. Newman and Gordon M. Cragg

Abstract: The marine habitat has produced a significant number of very potent marine-derived agents that have the potential to inhibit the growth of human tumor cells *in vitro* and, in a number of cases, in both *in vivo* murine models and in humans. Although many agents have entered clinical trials in cancer, to date, only Cytarabine, Yondelis® (ET743), Eribulin (a synthetic derivative based on the structure of halichondrin B), and the dolastatin 10 derivative, monomethylauristatin E (MMAE or vedotin) as a warhead, have been approved for use in humans (Adcetris®). In this review, we show the compounds derived from marine sources that are currently in clinical trials against cancer. We have included brief discussions of the approved agents, where they are in trials to extend their initial approved activity (a common practice once an agent is approved), and have also included an extensive discussion of the use of auristatin derivatives as warheads, plus an area that has rarely been covered, the use of marine-derived agents to ameliorate the pain from cancers in humans, and to act as an adjuvant in immunological therapies.

Reprinted from *Mar. Drugs*. Cite as: Newman, D.J.; Cragg, G.M. Marine-Sourced Anti-Cancer and Cancer Pain Control Agents in Clinical and Late Preclinical Development. *Mar. Drugs* **2014**, *12*, 255-278.

1. Introduction

Rather than discuss the agents that are currently in use from marine sourced organisms, which will be covered in another review in this journal, we will discuss agents that are from marine or marine-derived sources that are either in clinical trials, or are in advanced preclinical status. Obviously we will not be covering all such agents, as some are known only by a code number without any other information being available, whilst others are in "preclinical status" according to the authors of a paper or communication, but in truth, most of these are simply reports of some *in vitro* activity against cell lines or have some preliminary data on *in vivo* activity in rodents.

We will also avoid using the source organism as the method of classification as it is now becoming quite evident that the majority of compounds reported from the marine environment are in fact produced by, or in concert with, single-celled organisms ranging from protists (frequently dinoflagellates) to bacteria, including a very significant number of as yet uncultured organisms.

We will mention some of the materials that have been approved for use in one or more countries that are in fact in clinical trials in others, or are now being used in conjunction with other drug moieties as these are very common occurrences with antitumor agents once they are approved. For example, although not a marine-derived agent, taxol® is still in clinical trials, usually as part of a multi-drug regimen more than 20 years after it was approved for use by the US Food and Drug Administration (FDA) for treatment of refractory ovarian cancer.

We have organized this review in a manner that is the reverse to what most authors would do, in that we will commence with agents that have been approved but are still in clinical trials, followed by agents in stages of clinical development (nominally Phase I to III), rather than start with preclinical agents and work forwards.

Since a number of the agents that are in clinical trials are very close relatives to approved materials, we have elected to group these agents after the "approved parent", so that the similarities and differences can be more easily seen, thus giving the full "chemical lineage" in certain cases below. In addition, we have elected to commence with compounds from marine sources that could be considered as "adjuvant therapies" though, with one exception, not in the immunological sense.

2. Treatment of Pain Associated with Cancer

*2.1. Tetrodotoxin (Tectin ®, Phase III; Figure 1, **1**)*

One of the most unusual agents at this stage is a very well known "marine toxin", the highly substituted guanidine-derivative, tetrodotoxin (**1**) [1–3]. Although this is not a formal anti-tumor agent, it is in fact in Phase III trials as an agent (Tectin®) against inadequately controlled pain related to cancer by WEX Pharmaceuticals in the USA, together with a Phase II trial under the same company, again in the USA, against the neuropathic pain resulting from chemotherapy-induced peripheral neuropathy. Although there was debate in years gone by over the actual source of this agent, there is now little doubt that it is produced by a commensal microbe, though which one(s) is still open for debate [4]. The synthesis of the compound and other derivatives has been published from a variety of chemists with an excellent recent review by Nishikawa and Isobe giving the highlights of their methodologies and covering some of the early history of this class of toxins [5].

Figure 1. Pain control agents.

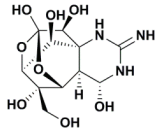

1. Tetrodotoxin (Tectin(R))

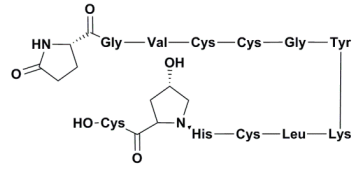

2. XEN-2174

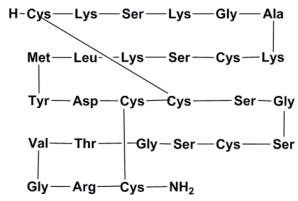

3. Leconotide

2.2. XEN-2174 (Phase II; Figure 1, ***2****)*

This compound, a very slight modification of the naturally occurring χ-conotoxin MrIA, was originally isolated from *C. marmoreus* and then optimized by medicinal chemistry [6]. Unlike the other conotoxins either approved or in various levels of testing, this particular agent is a modified 13-residue peptide and is a noncompetitive inhibitor of the neuronal norepinephrine transporter (NET) [7].

2.3. Leconotide (AM-336, ω-Conotoxin CVID; Phase I; Figure 1, ***3****)*

This molecule, a 27 residue peptide with three internal CYS-CYS bonds, is similar to the well-known pain treatment ziconotide, and is currently in Phase I trials sponsored by Relevare Pharmaceuticals (previous name was CNSBio) for treatment of pain related to cancer. It is a calcium channel blocker and was originally identified by researchers at the University of Queensland. Although initial experiments used the intrathecal route (as with ziconotide) [8], the current protocol uses systemic administration [9].

2.4. Immunological Use of Keyhole Limpet Hemocyanin (KLH; Phase I–III)

KLH has been used for many years as a classical immunoadjuvant, and had been approved in countries from Austria to South Korea, mainly for treatment of bladder cancer [10]. Two recent publications gave results from Phase III trials, the first being in metastatic breast cancer where it did not demonstrate any increase in median life span [11], but in the other Phase III trial in bladder cancer, using mitomycin as a comparative agent, there were indications that KLH had a positive effect on disease progression [12]. Currently, the ClinicalTrials.gov web site [13] lists Phase III (NCT01480479) and Phase II (NCT01498328) trials using KLH in its adjuvant status against relapsed glioblastoma, and Phase I trials in conjunction with KLH as part of a vaccine against high risk neuroblastoma (NCT00911560) and fallopian tube, epithelial ovarian and peritoneal cancers in patients following a first remission (NCT01248273).

3. Approved Marine-Derived Antitumor Agents Still in Clinical Trials (and Close Chemical Relatives)

3.1. Cytarabine (Phases I to IV; Figure 2, ***4****)*

As mentioned in a news interview in the early 1990s and then formally in a review by the authors in 2000 [14] this agent, though not found in a marine environment as “Ara-C” can trace its chemical lineage back to the discovery of bioactive nucleosides that contained arabinose rather than ribose or deoxyribose. Though we were not the first to recognize the importance of such substitutions, as Suckling [15] in a review in 1991 reported on the chemistry involved in the syntheses of these and other such arabinose-linked nucleosides with common or uncommon bases, we were perhaps the first to formally link the discoveries of the marine-sourced natural arabinoses by the Bergmann group to the “design” of this agent [16–18]. So Ara-C can be legitimately

considered to be a marine-derived agent, since without the arabinose, it would simply have been a normal component of nucleic acids.

Even today, there are 840 trials listed in the NIH (National Institutes of Health, Bethesda, MD, USA) clinical trials database (ClinicalTrials.gov), with 240 of them being open studies that are recruiting, covering a large number of cancers and ranging from Phase IV down to Phase I. In the corresponding European database, 43 clinical trials covering the same phases, but with some overlap, are listed. As with other well-known approved drugs, it is still in use, more than 40 years after its initial approval, with an interesting recent paper questioning the use of high dose cytarabine therapy during remission in adults of acute myeloid leukemia [19].

3.2. ET743 (Trabectedin; Yondelis®; Phases I to III; Figure 2, ***5****)*

This compound may well be considered the "poster child" for marine-derived antitumor agents, as it is currently the only molecule in use as an antitumor agent that is identical to one of the compounds originally isolated from *E. turbinata*. The stories around the discovery and development of this compound using materials from in-sea and on land aquaculture, followed by the semi-synthesis from a precursor molecule from a marine microorganism, cyanosafracin B, have been told by many authors over the years. These ranged from the initial reports of bioactivity in this organism in 1970 by Sigel *et al.* [20], the initial identification of the series by Holt in his PhD thesis in 1986 [21], to the simultaneous publications from the laboratories of Rinehart at the University of Illinois (Urbana Champaign, IL, USA) [22], and Wright at Harbor Branch Oceanographic Institution (Fort Pierce, FL, USA) [23] in 1990 of the structure of ET743. This work was followed with the thorough discussion given by the investigators at PharmaMar (Madrid, Spain) in 2009 [24], demonstrating the power of both semi-synthesis and optimization of processes to obtain active drug principles. The molecule was approved in the EU (European Union) in 2007 for treatment of advanced soft tissue sarcoma and in some of the EU countries for treatment of recurrent platinum-sensitive ovarian cancer when coupled to liposomal doxorubicin in 2009, but the corresponding U.S. FDA (Food and Drug Administration) application was withdrawn.

The commonalities and differences in the pharmacological response of trabectedin and its close relatives, Zalypsis® and lurbinectedin (*vide infra*) have been discussed recently with respect to their experimental effect upon the Fanconi anemia pathway. Martinez *et al.* [25] demonstrated that these three agents inhibited the Fanconi anemia pathway in the cell lines tested, increasing their sensitivity to mitomycin C, in contrast to mitomycin C which always activated that pathway in the same cell lines. The authors suggested that as a result of these findings these three agents might be useful clinically in "Fanconizing" cancer cells in order to gain sensitivity against other anti-tumor drugs. In another paper the same year, Romano *et al.* [26] reported that in *in vitro* and *in vivo* models, no relationship was found between the *in vitro* cytotoxic potency and *in vivo* antitumor activity in syngeneic mouse models, suggesting that there might well be a host response in these models. In addition, the pharmacokinetics differ, even between the quite similar trabectedin and lurbinectedin in humans, and as expected due to the differences in structure, Zalypsis® has been shown to differ in pharmacokinetics in humans [27].

Figure 2. Approved marine-derived drugs and close analogues in clinical trials.

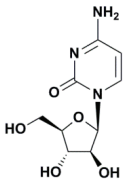

4. Cytarabine (Cytosar$^{(R)}$)

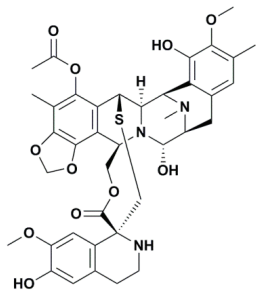

5. Trabectedin (Yondelis$^{(R)}$)

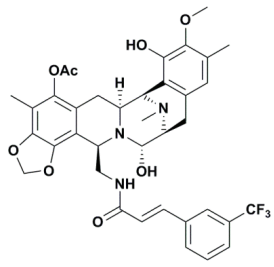

6. PM-10450 (Zalypsis$^{(R)}$)

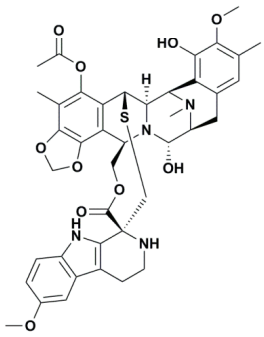

7. PM-01183 (Lurbinectedin)

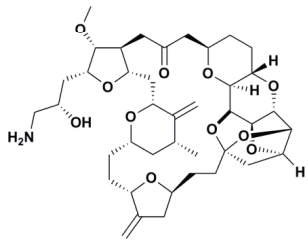

8. Eribulin (Halaven$^{(R)}$)

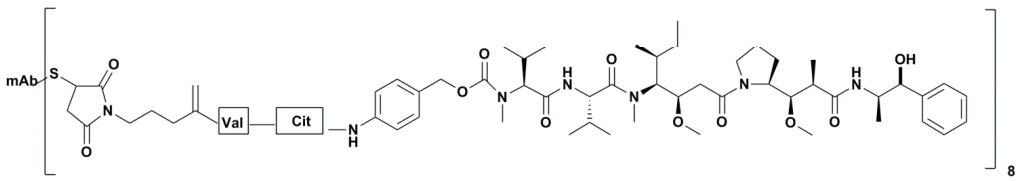

9. Brentuximab vedotin (Adcetris$^{(R)}$)

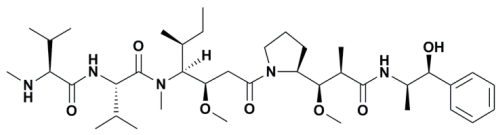

10. Monomethylauristatin E (Vedotin)

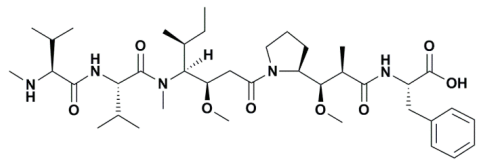

11. Monomethylauristatin F

As of the end of October 2013, there were 15 studies found for ET743 in the NIH clinical trials database, 12 at Phase II and three at Phase I, all being listed as completed, with cancer types covering breast, prostate, soft tissue sarcoma and osteosarcoma, plus general carcinomas. Searching the corresponding EU Clinical Trials Register, 19 trials were listed ranging from 2005 to 2013 with three being Phase III trials not found on the NIH site. These were two trials against refractory ovarian cancer with liposomal doxorubicin, and the third was for patients with translocation-related sarcomas. Again these listings demonstrates that once a compound has been approved for treatment of one type of cancer, it will be placed in clinical trials for many others, either individually or as part of a new drug regimen.

A discussion of the probabilities of ET743 and its congeners being produced by as yet uncultured microbes associated with the source tunicate was recently published by Giddings and Newman [28] which should be consulted for further details.

3.2.1. PM-10450 (Zalypsis®; Phases I–II; Figure 2, **6**)

This compound, another variation on the basic structure of the dimeric isoquinoline alkaloids, was derived from the structure of jorumycin, a compound isolated from the skin and mucin of the nudibranch *Joruna funebris* [29], and renieramycin J from a species of the marine sponge, *Netropsia*. Zalypsis® was synthesized by workers at PharmaMar (Madrid, Spain) using methodologies related to the ET743 synthesis from safracin B [30]. The initial report of the molecular pharmacology of this agent was described by Leal *et al.* in 2009 [31] and even though it has a close resemblance to ET743, it does not activate the DNA damage checkpoint response.

Currently both the NIH and EU clinical trials sites show three clinical trials at Phase II/I levels with one in Spain showing as still continuing. There are eleven reports to date in the literature with recent results from Phase I studies being reported in 2012 from work in the UK [27]. These were then followed by further reports in 2013, where objective responses, mainly stable disease, were seen in a small number of patients [32,33]. In contrast, also in 2013, a report was published demonstrating a lack of response and termination of the Phase II trial of this compound in a heavily pretreated population with advanced and/or metastatic endometrial or cervical cancers [34].

3.2.2. Lurbinectedin (PM-01183; Phases I–II; Figure 2, **7**)

This compound is another variation on the basic structure of the dimeric isoquinoline alkaloids, but has a tetrahydro-β-carboline moiety instead of the tetrahydroisoquinoline present in ring C, and binds in the DNA minor groove [35]. The compound was shown to have different pharmacokinetics in patients and also like trabectedin, to attenuate nuclear excision repair (NER). It also demonstrated synergy with platinum-based agents *in vitro* thus suggesting a possible treatment regimen since it also demonstrated activity against platinum-resistant cell lines [36]. Two Phase II clinical trials with lurbinectedin are shown on the NIH clinical trials site, one recruiting and one approved but not yet recruiting, with two Phase I trials recruiting and one approved but not yet recruiting. On the European clinical trials site, one Phase II trial corresponding to the" not yet

recruiting trial" listed on the NIH site in the USA, is on-going in Spain, and the other is a two year old trial against metastatic pancreatic cancer in Spain and the UK.

3.3. Eribulin (Halaven®; Phases I–IV; Figure 2, ***8****)*

The story of the discovery of this compound (a totally synthetic variation on halichondrin B has been given in a variety of formats over the years, from the chapter by the Eisai scientists in Woburn, MA that showed the progression from the synthesis of halichondrin B to the initial synthesis of eribulin [37], to two recent papers on the industrial methodologies that enabled the production of this molecule, certainly the most complex synthetic drug to date [38,39].

As with the other approved compounds mentioned earlier, Halaven® is currently shown as being in 28 trials that are recruiting patients with 27 being Phase I or II or I/II. The one Phase III trial is a physician's choice model with Halaven® being one of the three drugs to choose from. In addition, of the other 43 trials shown, 21 are active but not recruiting with the majority being at Phase I or II, though two are at Phase III and one (Phase IV) is a post market surveillance. One trial in the list was terminated with no reason given. In addition, a new liposomal formulation of eribulin mesilate is currently in a Phase I clinical trial (NCT01945710) in the United Kingdom under the auspices of Eisai.

The geographic areas of these trials effectively cover the world, but the majority are either in the USA or Europe. Summation of the figures on the map in the Clinicaltrials web site always gives a higher figure as a significant number of trials cross geographic boundaries within the one trial.

3.4. Brentuximab Vedotin (Adcetris®; Phases 0 to IV; Figure 2, ***9****)*

This immunoconjugate with a "warhead" derived from dolastatin 10, monomethylauristatin E (vedotin; Figure 2, **10**), a secondary metabolite from a *Symploca* species of cyanophyte, was approved in the USA in 2011 for treatment of CD30 positive lymphoproliferative disorders such as Hodgkin's lymphoma. This combination was the second immunoglobulin-warhead combination to be approved for leukemias following the initial approval of Mylotarg® by the FDA in 2000.

Subsequently Mylotarg® was withdrawn in the USA in 2010 due to concerns about the product's safety that were raised by a confirmatory study conducted after approval, as patients on the preparation and also receiving chemotherapy had a higher death rate and no objective increase in life when compared to a group using just chemotherapy. This combination is still in use in other countries. A relationship to marine sources for the "warhead endiyne molecule" was established when investigators at the Scripps Oceanographic Institution (La Jolla, CA, USA) showed the presence of endiyne cryptic clusters in marine bacteria of the genus *Salinospora* [40].

Adcetris® is the product of extensive work by Seattle Genetics (Seattle, WA, USA), first in optimizing the vedotin warhead (**10**) and then developing the linkers that couple the antibody to the compound [41]. Some of these, discussed later, are designed to release the warhead (vedotin) by simple hydrolysis of a linker bond, whereas others require the enzymatic digestion of the antibody, releasing the warhead plus appendages. It was approved by the FDA in 2011 and subsequently approval was given in the EU late in 2012 and launched in the UK in early 2013, all for CD30

positive leukemias. Full explanations of the methodologies used and the utility of this agent against a variety of lymphomas have been published in the last three years and should be consulted by the interested reader [42–45]. In addition, a recent report from Takeda (Osaka, Japan) shows the strategy that this company is adopting, including the further development of this agent [46].

Currently, this agent is in 37 trials mainly in the USA from Phase 0 to Phase IV where the latter trial is listed as recruiting on the NIH clinical trials site. Six more are listed in the EU clinical trials site covering Phase II to Phase IV.

3.4.1. Glembatumumab Vedotin (Phase II)

This is monomethylauristatin E (MMAE) linked to a fully human monoclonal antibody CR011 (an anti-CG56972) via a stable valine-citrulline dipeptide linker. It was targeted against patients with unresectable melanomas at stage III or IV who have failed one cytotoxic chemotherapy regimen and has expanded to include metastatic breast cancer as well. The combination has a variety of names during its early days including CDX-011, CR-011 and CR011-vcMMAE, so searching for data can be a trifle challenging.

The initial report of the use of this combination was given by investigators from CuraGen in 2006 [47], followed by a report of xenograft activity in 2007 from the same group [48]. The value of the monoclonal's target in triple negative breast cancer was described in 2010 by Rose *et al.* [49], with the corresponding details in melanoma described in 2012 by a group from the People's Republic of China [50]. Currently three completed studies at the Phase I/II levels are reported in the NIH clinical trials database with one preliminary report of clinical activity in breast cancer patients [51].

3.4.2. ABT-414 (Phase I–II)

This is an antibody-drug conjugate (ADC) linking the anti-Epidermal Growth Factor Receptor (EGFR) antibody ABT-806 to another variation on auristatin; in this case, monomethylaurisatin F (Figure 2, **11**) is used in place of the "E" variant. The ADC was designed to bind to a unique epitope of EGFR that is usually not accessible when EGFR is expressed at physiological levels. However, the ADC binds when tumors express EGFRde2-7 (EGFRvIII) and in other tumors with amplified EGFR or excessive EGFR activation under "normal wild-type conditions" [52].

Abbvie (North Chicago, IL, USA), which is the renamed Abbott Pharmaceutical Division, recently instituted two human clinical trials as trials in mice using human wild-type EGFR-overexpressing tumors gave complete regressions and "cures" [52]. Phase I studies where patients must have a solid tumor type likely to over-express (EGFR), are underway evaluating the safety, pharmacokinetics and efficacy of ABT-414, with a Phase IIa expansion (NCT 01741727) at the maximum tolerated dose (MTD) where patients, accepted by invitation only, must have squamous cell Non-Small Cell Lung Cancer (NSCLC). The other trial at the Phase I level (NCT01800695) is a study evaluating the safety and pharmacokinetics of ABT-414 in subjects with glioblastoma multiforme in combination with radiation plus temozolomide or temozolomide alone; the study is currently recruiting patients with this particular disease.

3.4.3. PSMA-ADC (Phase II)

This ADC is a fully human monoclonal antibody against prostate specific antigen that is coupled via the valine-citrulline dipeptide linker to mono-methylauristatin E (MMAE) and was designed to undergo release via proteolysis by human cathepsin B. The initial report demonstrating activity in prostate cancer cells and in xenografts was published in 2006 [53]. This was followed in 2011 by a report showing expanded activity against androgen sensitive and insensitive cell lines in xenografts [54].

Since there are now reports of the PSMA antigen being present in glioblastoma multiforme, this ADC is in a Phase II trial currently recruiting patients with this specific cancer, in addition to the Phase I and II trials against prostate cancer. All three trials are listed as current in the NIH clinical trials database, but no trials are shown in the EU database at this time.

3.4.4. DCDT-2980S (Phase II)

This ADC from Genentech (Roche, San Francisco, CA, USA) is a humanized IgG1 antibody directed against the CD22 epitope linked to sulfhydryl groups on the antibody via a maleimide derivative. This derivative is the same as that used in Adcetris®, releasing monomethylauristatin E on protease cleavage. Since the CD22 epitope is not expressed in rodents, trials for safety were performed in cynomolgus monkeys and demonstrated adequate safety in primates plus efficacy in xenografts [55]. Currently there is one Phase II trial recruiting and one active trial in the NIH clinical database and no records in the EU equivalent. These trials are in leukemias, not solid tumors.

3.4.5. DCDS-4501A (Phase II)

This is also from Genentech/Roche, and is an ADC with monomethylauristatin E linked to an anti-CD79b monoclonal. It is currently in the same Phase II trial as DCDT-2980S as an alternative treatment against follicular B cell lymphoma, and is also in an ongoing Phase I trial against various lymphomas in a dose escalation study. As with the earlier Roche agent (Section 3.4.4), no trials are listed in the EU database.

3.4.6. Enfortumab vedotin (Phase I)

This combination, a fully human IgG1k antibody linked to monomethyl auristatin E via a cleavable valine-citrulline linker is also known under the code names AGS-22MSE and AGS-22ME and is currently undergoing Phase I evaluation under the aegis of Agensys (Ashburn, VA, USA), Seattle Genetics and Astellas Pharma (Tokyo, Japan). It should be pointed out that Agensys is a subsidiary of Astellas Pharma and the philosophy behind the approach from their standpoint was reported by Yanagita and Takenaka in 2012 [56]. The only record at the moment of the initial development of this agent is in an abstract of the 2011 AACR Meeting in Orlando, Florida [57].

3.4.7. Vorsetuzumab Mafdotin (SGN-75; Phase I)

This ADC, from Seattle Genetics, has monomethylauristatin F linked to the humanized anti-CD70 monoclonal antibody 1F6 through a maleimidocaproyl linker that is non-cleavable, so the release has to rely upon invagination and then proteolytic digestion [58]. This ADC is currently being evaluated in Phase I trials against relapsed and refractory non-Hodgkin's lymphoma and also metastatic renal cancer where the cancers express the CD70 epitope. Currently the NIH database shows one completed Phase I trial and one recruiting for renal cell carcinoma, but no trials in the EU database. There are reports in the conference literature on some of the findings, but as yet, no peer-reviewed reports.

3.4.8. SGN-19A (SGN-CD19A; Phase I)

This is another Seattle Genetics ADC where a humanized anti-CD19 antibody is linked to monomethylauristatin F through a maleimidocaproyl-valine-citrulline linker. Currently there are two Phase I trials in the NIH database at the Phase I level that are actively recruiting for trials in lymphomas including Burkitt's lymphoma. One presentation at the 2013 AACR meeting is the only published report of progress at the moment [59].

3.4.9. BAY 79-4620 (3ee9/MMAE; Phase I)

This ADC is monomethylauristatin E linked to an antibody against the human carbonic anhydrase IX, and was made using the Seattle Genetics techniques as described for the anti-CD30 ADC (now known as Adcetris®) by Francisco *et al.* in 2003 [60]. Two Phase I trials are listed in the NIH database with one showing completed (determination of MTD in patients with advanced solid tumors) but the other, again an MTD-based study, was terminated for safety reasons. The differences between the two trials from the database descriptions appeared to be the frequency of treatment, three weeks in the completed trial *versus* two weeks in the terminated one. No data in the EU database.

3.4.10. AGS-16C3F (AGS-16M8F; Phase I)

This ADC is a fully human IgG2k monoclonal antibody directed against the AGS-16 antigen and conjugated to monomethylauristatin F (MMAF) via a noncleavable maleimido-caproyl linker. This particular ADC is directed against renal and liver carcinomas as a result of the AGS-16 antigen. Details of the initial discovery and results of cell line and xenograft testing were presented at the 2010 Genitourinary Cancers Symposium by Gudas *et al.* [61]. Currently there is one Phase I trial against renal cancer recruiting according to the NIH database, and one completed Phase I looking at the safety of dose escalation.

3.4.11. DMUC-5754A (RG-7458; Phase I)

This ADC is a monoclonal antibody against the epitope MUC16 linked to monomethylauristatin E and it is targeted against ovarian carcinomas, but no further details other than a report in an

abstract at the 2013 AACR meeting [62], are available at the present time. Currently the NIH web site shows that Genentech is recruiting patients for a Phase I trial against both ovarian and pancreatic cancer.

3.4.12. DNIB-0600A (RG-7599; Phase I)

This ADC is a humanized IgG1 monoclonal antibody directed against the NaPi2b epitope linked to monomethylauristatin E. No information as to the method of linkage is available and the only report is in an abstract at the 2013 ASCO meeting [63]. Phase I trials against non-small cell lung cancer and platinum resistant ovarian cancer are actively recruiting patients according to the NIH database.

3.4.13. A1-mcMMAF (PF-06263507; Phase I)

This ADC is monomethylauristatin F linked via a maleimidocaproyl linker to a humanized monoclonal antibody directed against the 5T4 tumor antigen. The ADC was prepared using the basic techniques described by Doronina *et al.* [41], and demonstrated potent antitumor activity in *in vivo* xenograft models and exhibited no overt toxicities when delivered to cynomolgus monkeys [64]. Currently Pfizer is recruiting patients for a Phase I trial against advanced solid tumors according to the NIH database.

3.4.14. DMOT-4039A (Phase I)

This ADC is a monoclonal antibody identified as MMOT-0530A that was raised against an un-named antigen that is overexpressed in pancreatic and ovarian cancer, conjugated to monomethylauristatin E. Currently the ADC is in two Phase I clinical trials with one in the USA and The Netherlands recruiting patients with unresectable pancreatic or platinum-resistant cancers (NCT01469793), whilst the other one (NCT01832116), also directed against the same cancers and actively recruiting patients in The Netherlands, is designed to use PET imaging using ^{89}Zr-linked to the MMOT antibody as the imaging agent, followed by use of the ADC thus permitting an assessment of the imaging and the subsequent response to therapy.

3.4.15. RG-7600 (Phase I)

This ADC, which from the comments on the Genentech web site [65], is in Phase I studies against ovarian cancers, does not have any other information in the literature. However, since the web site states that it is in collaboration with Seattle Genetics, the warhead may be an auristatin derivative. No details as to current trials can be found in the NIH database.

3.4.16. DEDN-6526A (RG-7636; Phase I)

As with RG-7600, the only information is from the Genentech web site where this ADC is listed as being in Phase I against unresectable melanoma. Since Seattle Genetics is also involved, the

warhead may be an auristatin derivative, and the antibody may well be directed against endothelin ETB receptors. One trial that is recruiting patients is shown in the NIH database (NCT01522664).

3.4.17. DSTP-3086S (RG-7450; thio-antiSTEAP1-MC-vc-PAB-MMAE; Phase I)

This is another of Genentech (Roche) ADCs using, in this case, an antibody against a humanized anti-STEAP1 IgG1 antibody modified via determination/modification of reactive thiols according to the patent application by Bhakta and Junutula [66], and coupled to monomethylauristatin E. The antibody is directed against the six-transmembrane epithelial antigen of prostate 1, hence the STEAP1 acronym, and was evaluated as both the basic ADC with monomethylauristatin E and the thio-modified antibody, with the decision being to go with the thio modified version from the PK determinations [67,68]. Currently there is one Phase I study recruiting patients with metastatic castration-resistant prostate cancer (NCT01283373) with a preliminary report showing some clinical responses given at the 2013 ASCO Meeting [69].

3.4.18. MLN-0264 (Phase I)

This is an ADC composed of a fully human monoclonal IgG antibody (5F9) directed against guanylyl cyclase C (GCC) and is conjugated to monomethylauristatin E via a cleavable linker (licenced from Seattle Genetics). The antibody is directed against gastrointestinal tumors that express GCC. This is a first in class drug candidate with the initial report of the rationale being given in November 2012 at the 14th EORTC-NCI-AACR meeting in Dublin, Ireland [70]. A report at the next conference in the series was given in 2013, demonstrating activity both alone and in conjunction with gemcitabine in xenograft models of pancreatic cancer [71]. The compound is in a Phase I trial (NCT01577758) and is currently recruiting patients with GI cancers expressing the required antigen.

3.4.19. RG-7598 (Phase I)

As with RG-7600 (Section 3.4.15), the only information is from the Genentech web site where this ADC is listed as being in Phase I against multiple myeloma. Since Seattle Genetics is also involved, the warhead is probably an auristatin derivative. No trials can be found in the NIH database as of early November 2013.

3.4.20. SGN-LIV1A (Phase I)

This ADC is being developed by Seattle Genetics and is an anti-LIV-1 humanized monoclonal antibody linked to monomethylauristatin E. The LIV-1 epitope is also known as SLC39A6 or ZIP6, and is a member of the zinc transporter family. It was first identified as an estrogen-inducible gene in breast cancer derived cell lines. It is a downstream target of STAT3, and promotes the epithelial to mesenchymal transition important in the malignant progression of breast cancer to the metastatic form. It is expressed in subtypes of metastatic breast cancers (ER+/HER2−; HER2+ and triple negative). However, in healthy human tissues, its expression is limited to four hormonally-regulated

organs. Both *in vitro* and *in vivo* models demonstrated significant delay of tumor growth on treatment with the ADC [72]. This ADC is in a Phase I study that is currently recruiting patients (NCT01969643) with metastatic breast cancer to determine safety and any antitumor activity during the trial.

3.4.21. AGS-15E (AGS-15ME; Phase I)

This is an ADC with the fully human IgG2 monoclonal antibody (AGS15) whose target is SLITRK6, conjugated to monomethylauristatin E (MMAE) through the maleimidocaproyl-valine-citrulline linker from Seattle Genetics. The target of this antibody, SLITRK6, is a member of the SLITRK family of neuronal transmembrane proteins, and was discovered by Agensys using suppressive subtractive hybridization on biopsies from bladder cancer patients [73].

Immunohistochemical (IHC) analysis of SLITRK6 expression was evaluated in various human cancers including bladder, using a SLITRK6-specific antibody M15-68(2)22. This mouse monoclonal antibody demonstrated that 90% of 452 human bladder transitional cell carcinomas from *in situ*, advanced primary and metastatic tumors express this epitope. In addition, the same expression was seen in some lung, breast and glioblastomas as well. In normal tissues, expression is significantly restricted [73]. Currently a Phase I trial (NCT01963052) is actively recruiting patients with metastatic urothelial cancer.

3.5. Preclinical Auristatin-Linked ADCs

The following ADCs are currently in advanced preclinical trials but the current information that is available is minimal.

3.5.1. CDX-014 (CR-014-vcMMAE)

From the code name, this is a valine-citrulline-linked monomethylauristatin E linked to a fully human anti-TIM1 monoclonal antibody CR-014. This antibody was developed to selectively target TIM 1 (Kd = 2.7 nM), a type I transmembrane protein expressed on the surface of ovarian and renal carcinoma cells with poor expression in normal tissues.

3.5.2. HuMax-CD74

This auristatin-linked ADC in preclinical development uses HuMax-CD74, an antibody that targets HLA class II histocompatibility antigen gamma chain (CD74). This epitope is expressed in a wide range of hematological malignancies and solid tumors, and is being developed by a collaboration between Genmab (city, state, country) and Seattle Genetics [74].

3.5.3. HuMab-TF-011-vcMMAE (HuMax-TF-ADC; TF-011-MMAE IND Filed)

TF-011-vcMMAE is an ADC under development for the treatment of solid tumors. It is composed of a human tissue factor (TF) specific antibody (TF-011), linked to a protease cleavable

valine-citrulline (vc) linker and monomethylauristatin E (MMAE). TF is aberrantly expressed in many solid tumors, and its expression has been associated with poor prognosis [75].

4. Other Marine-Derived Compounds in Clinical Trials against Cancer (Phases I–III)

4.1. Aplidine (Ptilidepsin, Aplidin®; Phase II–III; Figure 3, **12***)*

This compound is currently the only non-approved marine-derived agent in Phase III clinical trials for cancer. Its history is quite convoluted as it was originally identified from an extract of the Mediterranean tunicate *Aplidium albicans.* It was first reported in a patent from the Rinehart laboratory at the University of Illinois in Champaign-Urbana during the time that that laboratory was working on the synthesis of didemnin B (the first direct from the sea compound to go into human clinical trials against cancer) [76]. Subsequently, with the withdrawal of didemnin B due to toxicity and immunosuppressive effects which may have been exacerbated by the then current drug regimens (a bolus at the MTD), PharmaMar began developing aplidine.

Figure 3. Other marine-derived compounds in phase I–III trials.

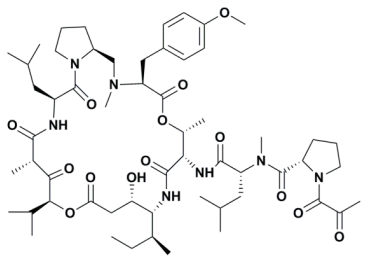

12. Plitidepsin (Aplidin(R))

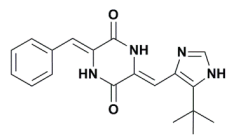

14. NPI-2358 (Plinabulin)

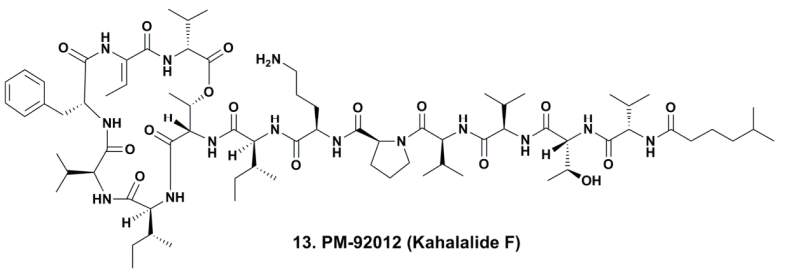

13. PM-92012 (Kahalalide F)

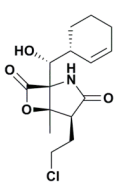

15. Salinosporamide A (Marizomib(R))

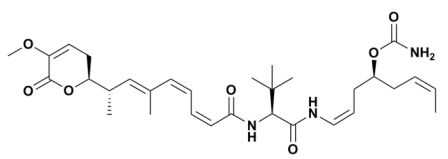

16. PM-060184

This time the agent was made by total synthesis using data from the Rinehart patents [77,78], and then further developed by Jou *et al.* [79]. The compound could also be made by modification of didemnin A with a patent covering this process being published in 1995 [80]. Further information as to synthetic methodologies of aplidine and other related compounds can be found in the excellent publication from the Joullie group published in 2012 [81].

The mechanism of action of this agent is still not fully identified but involves multiple regulatory pathways as can be seen in the discussion in the review by the PharmaMar group in 2012 [82], but the compound does demonstrate activity in a variety of cancers. These include a recent report of activity in pediatric medulloblastomas, with demonstrable partial responses and disease stabilization but the small patient number did not allow an efficacy determination [83].

Currently, this agent is shown as being in one Phase III trial in the NIH clinical trials database and in five Phase II trials covering a variety of leukemias and liposarcomas. What is also of interest is the recent report that didemnin B has been produced by fermentation of a free-living marine-sourced microbe, with the complete genomic cluster identified and production of didemnin B confirmed by "MALDI-TOF interrogation" of the metabolites in real time [84]. To date, no report of aplidine from this source has been published but it is highly likely that a microbe is the producer of either aplidine or that there is a simple oxidation of didemnin B to produce aplidine, since the only difference is the presence of a carbonyl in the side chain of aplidine instead of a C–OH in the same position in didemnin B.

4.2. Kahalalide F (PM-92102, Phase II; Figure 3, **13***)*

This compound, a depsipeptide originally isolated from the sacoglossan mollusk *Elysia rufescens* and then subsequently isolated from the alga *Bryopsis pennata* upon which it feeds, was also found in an Indian Ocean *Elysia* but from a different species [85]. There is a possibility that the material is actually produced by a commensal microbe on the alga but this has not yet been definitively proven. The compound was licensed to PharmaMar by the University of Hawaii at Manoa (Honolulu, HI, USA) and then PharmaMar developed synthetic methods to produce the compound in bulk using peptide chemistry techniques.

It entered clinical trials against prostate cancer, malignant melanoma and non-small cell lung cancer, with a mechanism of action that involved oncosis (ischemic cell death) [86]. At this moment in time, it appears that PharmaMar does not have any current clinical trials underway from inspection of the NIH database, but in the EU Clinical Trials Register, a Phase II trial on non-small cell lung cancer is still ongoing in Spain under the EudraCT number 2004-001253-39. The compound was "out-licensed" for the treatment of psoriasis (a proliferative disease) to Medimetriks Pharmaceuticals (Fairfield, NJ, USA) in 2009 for other than oncology and neurology indications.

The original discoverer of this group of compounds published an interesting paper on selected kahalalide F analogs with antitumor and antifungal activities in 2011 [87], and recently in the middle of 2012, PharmaMar stopped development of the kahalalide derivative 1-[*N*-[(4*S*)-4-methyl-1-oxohexyl]-D-valine]-kahalalide F which they were developing as an antitumor agent under the generic name elisidepsin and trade name of Irvalec® [82], even though it

had activity in gastroesophageal tumors. This appeared to be a business decision due to the very low numbers of potential patients.

4.3. Plinabulin (NPI-2358, Phase II; Figure 3, **14***)*

This compound, a simple modification of the terrestrial and also marine fungal metabolite halimide [88], entered Phase II clinical trials under Nereus Pharmaceuticals (San Diego, CA, USA). Two completed trials under that sponsor are shown in the NIH database, one at Phase I and the other at Phase I/II. However, no work/reports have appeared recently and with reports that Nereus Pharmaceuticals is no longer operative the fate of this compound is uncertain [89].

4.4. Marizomib® (Salinosporamide A; NPI-0052; Phase I, Figure 3, **15***)*

The story of this compound from its discovery from the marine actinomycete, *Salinispora tropica* and its identification as a proteasome inhibitor has been covered extensively in the scientific literature. The reports include work-up to give cGMP product from the first marine-medium based large-scale fermentation, through synthesis by a variety of chemists both in academia and companies, and identification of the biosynthetic cluster in the producing organism(s) [90–94].

Currently one clinical trial is shown in the NIH database as recruiting patients for a study in multiple myeloma (NCT00461045). What is of note is that the site now lists the sponsor as Triphase Research and Development Corporation, a CRO rather than Nereus Pharmaceuticals, and the other three completed Phase I trials in the NIH database no longer show Nereus but TriPhase. This may well confirm information about the current status of Nereus Pharmaceuticals [89].

4.5. PM-060184 (Phase I; Figure 3, **16***)*

Recently, workers at PharmaMar reported the isolation and then total synthesis of two novel polyketides from the Madagascan sponge *Lithoplocamia lithistoides* [95]. These two novel agents PM050489 and PM060184 demonstrated sub-nanomolar *in vitro* activity in human cancer cell lines, also potent antimitotic activity, and specifically, demonstrated a new biochemical mechanism when interacting with tubulin [96]. The compounds also demonstrated potent *in vivo* activity in different animal models and one of the two, PM-060184 is currently in Phase I clinical trials (NCT01299636). Thus, even today, more than 25 years after the identification of the MOA of Taxol® novel tubulin interaction mechanisms are still being discovered.

5. Conclusions

In an entirely different aspect of marine pharmacology, the work described in the first section of this review, with “toxins” controlling cancer-related pain, is a beautiful example of where agents considered to be deadly poisons to humans, tetrodotoxin and the *Conus* peptides, are now leading to potential drugs for use in humans.

In a considerable number of papers covering the topic of natural product-based antitumor drugs (irrespective of the natural source), compounds are quoted as being in clinical trials, even though no new trial has been reported in the previous four-plus years, and earlier trials are listed as completed. From this perspective, there are two papers, one in this journal in 2010 [97], and a very recent and truly comprehensive compilation of clinical trials of a large number of marine-related drugs and drug candidates [98], that could be considered to have partially covered the topic from a marine source perspective. In these two papers, however, a significant number of the agents discussed are no longer in clinical trials.

In contrast to this approach, we have checked for current or recent antitumor trials in all of the compounds above (except for the three listed as preclinical) and have demonstrated that, although the number of marine-derived agents in active clinical studies en route to approval is small compared to earlier years, all listed have current or recent clinical trials shown in either the NIH or the corresponding EU clinical trials databases.

We used the qualifier "small" above even though there are 24 ADCs (5 ADCs at Phase II, 16 ADCs at Phase I and 3 ADCs in advanced preclinical status) that are using either auristatin E or auristatin F as their warheads. If one is being conservative, then these are composed of only two different basal structures with the other differences being in the monoclonal antibody and the method of linkage. We would also be remiss in not pointing out that none of these ADCs would have been made except for the discovery of the dolastatins and subsequent syntheses in the middle to late 1970s [99].

With the number of marine-sourced compounds in the literature now over 25,000, there are many other agents just "waiting in the wings" for their chance of stardom; it is our task as marine natural product chemists to find them and, ultimately, to develop them as either drugs or leads thereto. We would be remiss in not mentioning that nowadays it is recognized that the probable source of most of the agents that we have described are single celled organisms, ranging from eubacteria through to eukaryotes such as fungi and protists. As yet, we are not aware of any published compounds from the archaea that have antitumor activity, but they may well occur in due course.

Conflicts of Interest

The authors declare no conflicts of interest.

References

1. Turabi, A.; Plunkett, A.R. The application of genomic and molecular data in the treatment of chronic cancer pain. *J. Surg. Oncol.* **2012**, *105*, 494–501.
2. Nieto, F.R.; Cobos, E.J.; Tejada, M.Á.; Sánchez-Fernández, C.; González-Cano, R.; Cendán, C.M. Tetrodotoxin (TTX) as a therapeutic agent for pain. *Mar. Drugs* **2012**, *10*, 281–305.
3. Moczydlowski, E.G. The molecular mystique of tetrodotoxin. *Toxicon* **2013**, *63*, 165–183.

4. Chau, R.; Kalaitzis, J.A.; Neilan, B.A. On the origins and biosynthesis of tetrodotoxin. *Aquat. Toxicol.* **2011**, *104*, 61–72.
5. Nishikawa, T.; Isobe, M. Synthesis of tetrodotoxin, a classic but still fascinating natural product. *Chem. Rec.* **2013**, *13*, 286–302.
6. Brust, A.; Palant, E.; Croker, D.E.; Colless, B.; Drinkwater, R.; Patterson, B.; Schroeder, C.I.; Wilson, D.; Nielsen, C.K.; Smith, M.T.; *et al*. χ-Conopeptide pharmacophore development: Toward a novel class of norepinephrine transporter inhibitor (Xen2174) for pain. *J. Med. Chem.* **2009**, *52*, 6991–7002.
7. Sharpe, I.A.; Palant, E.; Schroeder, C.I.; Kaye, D.M.; Adams, D.J.; Alewood, P.F.; Lewis, R.J. Inhibition of the norepinephrine transporter by the venom peptide chi-MrIA. Site of Action, Na^+ dependence, and structure-activity relationship. *J. Biol. Chem.* **2003**, *278*, 40317–40322.
8. Jayamanne, A.; Jeong, H.J.; Schroeder, C.J.; Lewis, R.J.; Christie, M.J.; Vaughan, C.W. Spinal actions of omega-conotoxins, CVID, MVIIA and related peptides in a rat neuropathic pain model. *Br. J. Pharmacol.* **2013**, *170*, 245–254.
9. Daly, N.L.; Craik, D.J. Conopeptides as novel options for pain management. *Drugs Future* **2011**, *36*, 25–32.
10. Jurincic, C.D.; Engelmann, U.; Gasch, J.; Klippel, K.F. Immunotherapy in bladder cancer with keyhole limpet hemocyanin: A randomized study. *J. Urol.* **1988**, *139*, 723–726.
11. Miles, D.; Roche, H.; Martin, M.; Perren, T.J.; Cameron, D.A.; Glaspy, J.; Dodwell, D.; Parker, J.; Mayordomo, J.; Tres, A.; *et al*. Phase III multicenter clinical trial of the Sialyl-TN (STn)-Keyhole limpet hemocyanin (KLH) vaccine for metastatic breast cancer. *Oncologist* **2011**, *16*, 1092–1100.
12. Lammers, R.J.; Witjes, W.P.; Janzing-Pastors, M.H.; Caris, C.T.; Witjes, J.A. Intracutaneous and intravesical immunotherapy with keyhole limpet hemocyanin compared with intravesical mitomycin in patients with non-muscle-invasive bladder cancer: Results from a prospective randomized phase III trial. *J. Clin. Oncol.* **2012**, *30*, 2273–2279.
13. ClinicalTrials.gov. Available online: http://clinicaltrials.gov/ (accessed on 15 October 2013).
14. Newman, D.J.; Cragg, G.M.; Snader, K.M. The influence of natural products upon drug discovery. *Nat. Prod. Rep.* **2000**, *17*, 215–234.
15. Suckling, C.J. Chemical approaches to the discovery of new drugs. *Sci. Prog.* **1991**, *75*, 323–359.
16. Bergmann, W.; Feeney, R.J. Isolation of a new thymine pentoside from sponges. *J. Am. Chem. Soc.* **1950**, *72*, 2809–2810.
17. Bergmann, W.; Feeney, R.J. Marine products. XXXII. The nucleosides of sponges. I. *J. Org. Chem.* **1951**, *16*, 981–987.
18. Bergmann, W.; Burke, D.C. Marine products. XXXIX. The nucleosides of sponges. III. Spongothymidine and spongouridine. *J. Org. Chem.* **1955**, *20*, 1501–1507.
19. Löwenberg, B. Sense and nonsense of high-dose cytarabine for acute myeloid leukemia. *Blood* **2013**, *121*, 26–28.

20. Sigel, M.M.; Wellham, L.L.; Lichter, W.; Dudeck, L.E.; Gargus, J.L.; Lucas, L.H. *Food-Drugs from the Sea: Proceedings 1969*; Marine Technology Society: Washington, DC, USA, 1970.
21. Holt, T.G. The Isolation and Structural Characterization of the Ecteinascidins. Ph.D Thesis, Department of Chemistry, University of Illinois at Urbana-Champaign, Champaign, IL, USA, 1986.
22. Rinehart, K.; Holt, T.G.; Fregeau, N.L.; Stroh, J.G.; Kiefer, P.A.; Sun, F.; Li, L.H.; Martin, D.G. Ecteinascidins 729, 743, 745, 759A, 759B and 770: Potent antitumor agents from the Caribbean tunicate *Ecteinascidia turbinata*. *J. Org. Chem.* **1990**, *55*, 4512–4515.
23. Wright, A.E.; Forleo, D.A.; Gunawardana, G.P.; Gunasekera, S.P.; Koehn, F.E.; McConnell, O.J. Antitumor tetrahydroisoquinoline alkaloids from the colonial ascidian *Ecteinascidia turbinata*. *J. Org. Chem.* **1990**, *55*, 4508–4512.
24. Cuevas, C.; Francesch, A.; Reports, N.P. Development of Yondelis® (trabectedin, ET-743). A semisynthetic process solves the supply problem. *Nat. Prod. Rep.* **2009**, *26* 322–337.
25. Martínez, S.; Pérez, L.; Galmarini, C.M.; Aracil, M.; Tercero, J.C.; Gago, F.; Albella, B.; Bueren, J.A. Inhibitory effects of marine-derived DNA-binding anti-tumour tetrahydroisoquinolines on the Fanconi anaemia pathway. *Br. J. Pharmacol.* **2013**, *170*, 871–882.
26. Romano, M.; Frapolli, R.; Zangarini, M.; Bello, E.; Porcu, L.; Galmarini, C.M.; Garcia-Fernandez, L.F.; Cuevas, C.; Allavena, P.; Erba, E.; D'Incalci, M. Comparison of *in vitro* and *in vivo* biological effects of trabectedin, lurbinectedin (PM01183) and Zalypsis® (PM00104). *Int. J. Cancer* **2013**, *133*, 2024–2033.
27. Yap, T.A.; Cortes-Funes, H.; Shaw, H.; Rodriguez, R.; Olmo, S.D.; Lal, R.; Fong, P.C.; Tan, D.S.; Harris, D.; Capdevila, J.; *et al*. First-in-man phase I trial of two schedules of the novel synthetic tetrahydroisoquinoline alkaloid PM00104 (Zalypsis) in patients with advanced solid tumours. *Br. J. Cancer* **2012**, *106*, 1379–1385.
28. Giddings, L.-A.; Newman, D.J. Microbial natural products: Molecular blueprints for antitumor drugs. *J. Ind. Microbiol. Biotechnol.* **2013**, *40*, 1181–1210.
29. Fontana, A.; Cavaliere, P.; Wahidullah, S.; Naik, C.G.; Cimino, G. A new antitumor isoquinoline alkaloid from teh marine numdibranch *Jorunna funebris*. *Tetrahedron* **2000**, *56*, 7305–7308.
30. Perez, M.; Fernandez, C.; Chicharro, J.L.; Zarzuelo, M.; de la Calle, F.; Cuevas, C.; Francesch, A.; Gallego, P.; Manzanares, I. Hemisynthetic Methods and New Compounds. *WO 20000069862*, 23 November 2000.
31. Leal, J.F.M.; Garcia-Hernandez, V.; Moneo, V.; Domingo, A.; Bueren-Calabuig, J.A.; Negri, A.; Gago, F.; Gulillen-Navarro, M.J.; Aviles, P.; Cuevas, C.; *et al*. Molecular pharmacology and antitumor activity of Zalypsis® in several human cell lines. *Biochem. Pharmacol.* **2009**, *78*, 162–170.

32. Massard, C.; Margetts, J.; Amellal, N.; Drew, Y.; Bahleda, R.; Stevens, P.; Armand, J.P.; Calvert, H.; Soria, J.C.; Coronado, C.; *et al*. Phase I study of PM00104 (Zalypsis®) administered as a 1-hour weekly infusion resting every fourth week in patients with advanced solid tumors. *Invest. New Drugs* **2013**, *31*, 623–630.
33. Capdevila, J.; Clive, S.; Casado, E.; Michie, C.; Piera, A.; Sicart, E.; Carreras, M.J.; Coronado, C.; Kahatt, C.; Soto Matos-Pita, A.; *et al*. A phase I pharmacokinetic study of PM00104 (Zalypsis) administered as a 24-h intravenous infusion every 3 weeks in patients with advanced solid tumors. *Cancer Chemother. Pharmacol.* **2013**, *71*, 1247–1254.
34. Martin, L.P.; Krasner, C.; Rutledge, T.; Luque Ibanes, M.; Fernandez-Garcıa, E.M.; Kahatt, C.; Siguero Gomez, M.; McMeekin, S. Phase II study of weekly PM00104 (ZALYPSIS®) in patients with pretreated advanced/metastatic endometrial or cervical cancer. *Med. Oncol.* **2013**, *30*, 627–631.
35. Leal, J.F.; Martínez-Díez, M.; García-Hernández, V.; Moneo, V.; Domingo, A.; Bueren-Calabuig, J.A.; Negri, A.; Gago, F.; Guillén-Navarro, M.J.; Avilés, P.; *et al*. PM01183, a new DNA minor groove covalent binder with potent *in vitro* and *in vivo* anti-tumour activity. *Br. J. Pharmacol.* **2010**, *161*, 1099–1110.
36. Soares, D.G.; Machado, M.S.; Rocca, C.J.; Poindessous, V.; Ouaret, D.; Sarasin, A.; Galmarini, C.M.; Henriques, J.A.; Escargueil, A.E.; Larsen, A.K. Trabectedin and its C subunit modified analogue PM01183 attenuate nucleotide excision repair and show activity toward platinum-resistant cells. *Mol. Cancer Ther.* **2011**, *10*, 1481–1489.
37. Yu, M.J.; Kishi, Y.; Littlefield, B.A. Discovery of E7389, a Fully Synthetic Macrocyclic Ketone Analog of Halichondrin B. In *Anticancer Agents from Natural Products*, 2nd ed.; Cragg, G.M., Kingston, D.G.I., Newman, D.J., Eds.; Taylor and Francis: Boca Raton, FL, USA, 2012; pp. 317–345.
38. Yu, M.J.; Zheng, W.; Seletsky, B.M. From micrograms to grams: Scale-up synthesis of eribulin mesylate. *Nat. Prod. Rep.* **2013**, *30*, 1158–1164.
39. Austad, B.C.; Calkins, T.L.; Chase, C.E.; Fang, F.G.; Horstmann, T.E.; Hua, Y.; Lewis, B.M.; Niu, X.; Noland, T.A.; Orr, J.D.; *et al*. Commercial manufacture of Halaven®: Chemoselective transformations en route to structurally complex macrocyclic ketones. *Synlett* **2013**, *24*, 333–337.
40. Udwary, D.W.; Zeigler, L.; Asolkar, R.N.; Singan, V.; Lapidus, A.; Fenical, W.; Jensen, P.R.; Moore, B.S. Genome sequencing reveals complex secondary metabolome in the marine actinomycete *Salinispora tropica*. *Proc. Natl. Acad. Sci. USA* **2007**, *104*, 10376–10381.
41. Doronina, S.O.; Mendelsohn, B.A.; Bovee, T.D.; Cerveny, C.G.; Alley, S.C.; Meyer, D.L.; Oflazoglu, E.; Toki, B.E.; Sanderson, R.J.; Zabinski, R.F.; *et al*. Enhanced activity of monomethylauristatin F through monoclonal antibody delivery: Effects of linker technology on efficacy and toxicity. *Bioconjug. Chem.* **2006**, *17*, 114–124.
42. Copeland, A.; Younes, A. Brentuximab vedotin; Anti-CD30 antibody-drug conjugate oncolytic. *Drugs Future* **2010**, *35*, 797–801.
43. Ansell, S.M. Brentuximab vedotin: Delivering an antimitotic drug to activated lymphoma cells. *Expert Opin. Investig. Drugs.* **2011**, *20*, 99–105.

44. Haddley, K. Brentuximab vedotin: Its role in the treatment of anaplastic large cell and Hodgkin's lymphoma. *Drugs Today* **2012**, *48*, 259–270.
45. Newland, A.M.; Li, J.X.; Wasco, L.E.; Aziz, M.T.; Lowe, D.K. Brentuximab vedotin: A CD30-directed antibody-cytotoxic drug conjugate. *Pharmacother* **2013**, *33*, 93–104.
46. DeSchuytner, B.; Kuvalanka, K.; Hibner, B.; Bolen, J. Takeda's oncology discovery strategy. *Jpn. J. Clin. Oncol.* **2013**, *43*, 357–361.
47. Tse, K.F.; Jeffers, M.; Pollack, V.A.; McCabe, D.A.; Shadish, M.L.; Khramtsov, N.V.; Hackett, C.S.; Shenoy, S.G.; Kuang, B.; Boldog, F.L.; *et al*. CR011, a fully human monoclonal antibody-auristatin E conjugate, for the treatment of melanoma. *Clin. Cancer Res.* **2006**, *12*, 1373–1382.
48. Pollack, V.A.; Alvarez, E.; Tse, K.F.; Torgov, M.Y.; Xie, S.; Shenoy, S.G.; MacDougall, J.R.; Arrol, S.; Zhong, H.; Gerwien, R.W.; *et al*. Treatment parameters modulating regression of human melanoma xenografts by an antibody-drug conjugate (CR011-vcMMAE) targeting GPNMB. *Cancer Chemother. Pharmacol.* **2007**, *60*, 423–435.
49. Rose, A.A.; Grosset, A.A.; Dong, Z.; Russo, C.; Macdonald, P.A.; Bertos, N.R.; St-Pierre, Y.; Simantov, R.; Hallett, M.; Park, M.; *et al*. Glycoprotein nonmetastatic B is an independent prognostic indicator of recurrence and a novel therapeutic target in breast cancer. *Clin. Cancer Res.* **2010**, *16*, 2147–2156.
50. Zhou, L.T.; Liu, F.Y.; Li, Y.; Peng, Y.M.; Liu, Y.H.; Li, J. Gpnmb/osteoactivin, an attractive target in cancer immunotherapy. *Neoplasma* **2012**, *59*, 1–5.
51. Yardley, D.A.; Weaver, R.; Melisko, M.E.; Saleh, M.N.; Arena, F.P.; Forero, A.; Cigler, T.; Stopeck, A.; Citron, D.; Oliff, I.; *et al*. A Randomized Phase 2 Study of the Antibody-Drug Conjugate CDX-011 in Advanced GPNMB-Overexpressing Breast Cancer: The EMERGE Study. In Proceedings of the CTRC-AACR San Antonio Breast Cancer Symposium, San Antonio, TX, USA, 4–8 December 2012.
52. Phillips, A.C.; Boghaert, E.R.; Vaidya, K.S.; Ansell, P.J.; Shalinsky, D.R.; Zhang, Y.; Voorbach, M.J.; Mudd, S.; Holen, K.D.; Humerickhouse, R.A.; *et al*. ABT-414: An Anti-EGFR Antibody-Drug Conjugate as a Potential Therapeutic for the Treatment of Patients with Squamous Cell Tumors. In Proceedings of the 25th EORTC-NCI-AACR Symposium on Molecular Targets Cancer Therapeutics, Boston, MA, USA, 19–23 October 2013.
53. Ma, D.; Hopf, C.E.; Malewicz, A.D.; Donovan, G.P.; Senter, P.D.; Goeckeler, W.F.; Maddon, P.J.; Olson, W.C. Potent antitumor activity of an auristatin-conjugated, fully human monoclonal antibody to prostate-specific membrane antigen. *Clin. Cancer Res.* **2006**, *12*, 2591–2596.
54. Wang, X.; Ma, D.; Olson, W.C.; Heston, W.D. *In vitro* and *in vivo* responses of advanced prostate tumors to PSMA ADC, an auristatin-conjugated antibody to prostate-specific membrane antigen. *Mol. Cancer Ther.* **2011**, *10*, 1728–1739.
55. Li, D.; Poon, K.A.; Yu, S.F.; Dere, R.; Go, M.; Lau, J.; Zheng, B.; Elkins, K.; Danilenko, D.; Kozak, K.R.; *et al*. DCDT2980S, an anti-CD22-monomethyl auristatin E antibody-drug conjugate, is a potential treatment for non-Hodgkin lymphoma, *Mol. Cancer Ther.* **2013**, *12*, 1255–1265.

56. Yanagita, Y.; Takenaka, T. Astellas' drug discovery strategy: Focus on oncology. *Jpn. J. Clin. Oncol.* **2012**, *42*, 241–246.
57. Satpayev, D.; Torgov, M.; Yang, P.; Morrison, K.; Shostak, Y.; Raitano, A.; Liu, W.; Lortie, D.; An, Z.; Capo, L.; *et al*. Development of AGS-22M6E, a Novel Antibody Drug Conjugate (ADC) Targeting Nectin-4 for the Treatment of Solid Tumors. In Proceedings of the 102nd Annual Meeting American Association Cancer Research (AACR), Orlando, FL, 2–6 April 2011; Abstract 2832.
58. Iyer, U.; Kadambi, V.J. Antibody drug conjugates—Trojan horses in the war on cancer. *J. Pharmacol. Toxicol. Methods* **2011**, *64*, 207–212.
59. Albertson, T.M.; Sandalic, L.; Law, C.-L.; Broglio, K.; Berry, S. Phase 1, Open Label, Dose-Escalation Studies of SGN-CD19A in Patients with Relapsed or Refractory B-Lineage Acute Leukemia and Non-Hodgkin Lymphoma. In Proceedings of the 104th Annual Meeting American Association Cancer Research (AACR), Washington, DC, USA, 6–10 April 2013; Abstract 2412.
60. Francisco, J.A.; Cerveny, C.G.; Meyer, D.L.; Mixan, B.J.; Klussman, K.; Chace, D.F.; Rejniak, S.X.; Gordon, K.A.; DeBlanc, R.; Toki, B.E.; *et al*. cAC10-vcMMAE, an anti-CD30-monomethyl auristatin E conjugate with potent and selective antitumor activity. *Blood* **2003**, *102*, 1458–1465.
61. Gudas, J.M.; Torgov, M.; An, Z.; Jia, X.C.; Morrison, K.J.; Morrison, R.K.; Kanner, S.B.; Raitano, A.B.; Jakobovits, A. AGS-16M8F: A Novel Antibody Drug Conjugate (ADC) for Treating Renal and Liver Cancers. In Proceedings of the Genitourinary Cancers Symposium, San Francisco, CA, USA, 5–7 March 2010; Abstract 328.
62. Liu, J.; Moore, K.; Birrer, M.; Berlin, S.; Matulonis, U.; Infante, J.; Xi, J.; Kahn, R.; Wang, Y.; Wood, K.; *et al*. Targeting MUC16 with the Antibody-Drug Conjugate (ADC) DMUC5754A in Patients with Platinum-Resistant Ovarian Cancer: A Phase I Study of Safety and Pharmacokinetics. In Proceedings of the 104th Annual Meeting American Association Cancer Research (AACR), Washington, DC, USA, 6–10 April 2013; Abstract LB-290.
63. Gordon, M.S.; Gerber, D.E.; Infante, J.R.; Xu, J.; Shames, D.S.; Choi, Y.; Kahn, R.S. A Phase I Study of the Safety and Pharmacokinetics of DNIB0600A, an Anti-NaPi2b Antibody-Drug-Conjugate (ADC), in Patients (pts) with Non-Small Cell Lung Cancer (NSCLC) and Platinum-Resistant Ovarian Cancer (OC). In proceedings of the 2013 ASCO Annual Meeting, Chicago, IL, USA, 31 May–4 June 2013; Abstract 2507.
64. Sapra, P.; Damelin, M.; Dijoseph, J.; Marquette, K.; Geles, K.G.; Golas, J.; Dougher, M.; Narayanan, B.; Giannakou, A.; Khandke, K.; *et al*. Long-term tumor regression induced by an antibody-drug conjugate that targets 5T4, an oncofetal antigen expressed on tumor-initiating cells. *Mol. Cancer Ther.* **2013**, *12*, 38–47.
65. Product Development Portfolio. Available online: http://www.roche.com/research_and_development/who_we_are_how_we_work/pipeline.htm (accessed on 12 November 2013).
66. Bhakta, S.; Junutula, J.R. Cysteine Engineered Antibodies and Conjugates. *US 2011/0301334 A1*, 7 June 2011.

67. Boswell, C.A.; Mundo, E.E.; Zhang, C.; Bumbaca, D.; Valle, N.R.; Kozak, K.R.; Fourie, A.; Chuh, J.; Koppada, N.; Saad, O.; *et al*. Impact of drug conjugation on pharmacokinetics and tissue distribution of anti-STEAP1 antibody-drug conjugates in rats. *Bioconjug. Chem.* **2011**, *22*, 1994–2004.
68. Lin, K.; Tibbitts, J. Pharmacokinetic considerations for antibody drug conjugates. *Pharm. Res.* **2012**, *29*, 2354–2366.
69. Danila, D.C.; Szmulewitz, R.Z.; Higano, C.S.; Gilbert, H.; Kahn, R.S.; Wood, K.; Agarwal, P.; Lin, K.; Kabbarah, O.; Fine, B.M.; *et al*. A Phase I Study of the Safety and Pharmacokinetics of DSTP3086S, an Anti-STEAP1 Antibody-Drug Conjugate (ADC), in Patients (pts) with Metastatic Castration-Resistant Prostate Cancer (CRPC). In proceedings of the 2013 ASCO Annual Meeting, Chicago, IL, USA, 31 May–4 June 2013; Abstract 5020.
70. Veiby, P.; Zhang, J.; Yang, J.; McDonald, A.; Fasanmade, A.; Wyant, T.; Almhanna, K.; Kalebic, T. The Investigational Drug MLN0264 First-in-Human, First in Class ADC Targeting GCC: Phase I Dose-Escalation Study and Supportive Scientific Rationale. In Proceedings of the 24th EORTC-NCI-AACR Symposium Molecular Targets Cancer Therapeutics, Dublin, Ireland, 6–9 November 2012; Abstract 329.
71. Zhang, J.; Gallery, M.; Wyant, T.; Stringer, B.; Manfredi, M.; DAnaee, H.; Veiby, P. MLN0264, an Investigational, First-in-Class Antibody-Drug Conjugate (ADC) Targeting Guanylyl Cyclase C (GCC), Demonstrates Antitumor Activity Alone and in Combination with Gemcitabine in Human Pancreatic Cancer Xenograft Models Expressing GCC. In Proceedings of the 25th EORTC-NCI-AACR Symposium Molecular Targets Cancer Therapeutics, Boston, MA, USA, 19–23 October 2013; Abstract B194.
72. Sussman, D.; Smith, L.M.; Anderson, M.E.; Duniho, S.; Hunter, J.H.; Kostner, H.; Miyamoto, J.B.; Nesterova, A.; Westendorf, L.; van Epps, H.A.; *et al*. SGN-LIV1A: A Development Stage Antibody Drug-Conjugate Targeting LIV-1 for the Treatment of Metastatic Breast Cancer. In Proceedings of the 104th Annual Meeting American Association Cancer Research (AACR), Washington, DC, USA, 6–10 April 2013; Abstract 3962.
73. Yang, P.; Coleman, J.; Li, Y.; Zhang, Y.; Junge, C.; Morrison, K.; Donate, F.; Stover, D.; Morrison, K. SLITRK6, the Target of a Novel Antibody Drug Conjugate AGS15E, is Expressed in Bladder and Other Cancers. In Proceedings of the 104th Annual Meeting American Association Cancer Research (AACR), Washington, DC, USA, 6–10 April 2013; Abstract 1274.
74. Verploegen, S.; Overdijk, M.; van Dijkhuizen, R.; Bleeker, W.K.; van Berkel, P.; Parren, P.; Lisby, S. Human Antibodies and Antibody-Drug Conjugates Against CD74. *WO 2012/104344A1*, 9 August 2012.
75. Breij, E.C.W.; Satijn, D.; Verploegen, S.; de Goeij, B.E.; Schuurhuis, D.H.; Bleeker, W.K.; Houtkamp, M.; Parren, P.W. Use of an Antibody-Drug Conjugate Targeting Tissue Factor to Induce Complete Tumor Regression in Xenograft Models with Heterogeneous Target Expression. In Proceedings of the 2013 ASCO Annual Meeting, Chicago, IL, USA, 31 May–4 June 2013.

76. Rinehart, K.L., Jr.; Lithgow-Bertelloni, A.M. Novel Antiviral and Cytotoxic Agent. *WO 9104985 A1*, 19 April 1991.
77. Rinehart, K.L., Jr.; Katauskas, A.J. Semi-synthetic studies toward didemnin analogues. *WO 98/17275*, 24 October 1997.
78. Rinehart, K.L., Jr.; Lithgow-Bertelloni, A.M. Dehydrodidemnin B. *US5834586*, 10 November 1998.
79. Jou, G.; González, I.; Albericio, F.; Lloyd-Williams, P.; Giralt, E. Total synthesis of dehydrodidemnin B. Use of uronium and phosphonium salt coupling reagents in peptide synthesis in solution. *J. Org. Chem.* **1997**, *62*, 354–366.
80. Giralt, E.; Albericio, F.; Lloyd-Williams, P.; González-Valcarcel, I.; Jou, G.; Gómez, A.; Manzanares, I. Procedimiento de Preparación de Didemnina A. *ES 2102322*, 16 July 1997 (in Spanish).
81. Lee, J.; Currano, J.N.; Carroll, P.J.; Joullie, M.M. Didemnins, tamandarins and related natural products. *Nat. Prod. Rep.* **2012**, *29*, 404–424.
82. Cuevas, C.; Francesch, A.; Galmarini, C.M.; Aviles, P.; Munt, S. Ecteinascidin-743 (Yondelis®). Aplidin® and Irvalec®. In *Anticancer Agents from Natural Products*, 2nd ed.; Cragg, G.M., Kingston, D.G.I., Newman, D.J., Eds.; Taylor and Francis: Boca Raton, FL, USA, 2012; pp. 291–316.
83. Geoerger, B.; Estlin, E.J.; Aerts, I.; Kearns, P.; Gibson, B.; Corradini, N.; Doz, F.; Lardelli, P.; Miguel, B.D.; Soto, A.; *et al*. A phase I and pharmacokinetic study of plitidepsin in children with advanced solid tumours: An innovative therapies for children with cancer (ITCC) study. *Eur. J. Cancer* **2012**, *48*, 289–296.
84. Xu, Y.; Kersten, R.D.; Nam, S.-J.; Lu, L.; Al-Suwailem, A.M.; Zheng, H.; Fenical, W.; Dorrestein, P.C.; Moore, B.S.; Qian, P.-Y. Bacterial biosynthesis and maturation of the didemnin anti-cancer agents. *J. Am. Chem. Soc.* **2012**, *134*, 8625–8632.
85. Ashour, M.; Edrada, R.; Ebel, R.; Wray, V.; Wätjen, W.; Padmakumar, K.; Müller, W.E.; Lin, W.H.; Proksch, P. Kahalalide derivatives from the Indian sacoglossan mollusk *Elysia grandifolia*. *J. Nat. Prod.* **2006**, *69*, 1547–1553.
86. Von Schwarzenberg, K.; Vollmar, A.M. Targeting apoptosis pathways by natural compounds in cancer: Marine compounds as lead structures and chemical tools for cancer therapy. *Cancer Lett.* **2013**, *332*, 295–303.
87. Shilabin, A.G.; Hamann, M.T. *In vitro* and in *vivo* evaluation of select kahalalide F analogs with antitumor and antifungal activities. *Bioorg. Med. Chem.* **2011**, *19*, 6628–6632.
88. Hayashi, Y.; Yamazaki-Nakamura, Y.; Yakushiji, F. Medicinal chemistry and chemical biology of diketopiperazine-type antimicrotubule and vascular-disrupting agents. *Chem. Pharm. Bull.* **2013**, *61*, 889–901.
89. Fenical, W. Scripps Institution of Oceanography, La Jolla, CA, USA. Personal Communication, 2013.
90. Nett, M.; Gulder, T.A.; Kale, A.J.; Hughes, C.C.; Moore, B.S. Function-oriented biosynthesis of beta-lactone proteasome inhibitors in *Salinispora tropica*. *J. Med. Chem.* **2009**, *52*, 6163–6167.

91. Fenical, W.; Jensen, P.R.; Palladino, M.A.; Lam, K.S.; Lloyd, G.K.; Potts, B.C. Discovery and development of the anticancer agent salinosporamide A (NPI-0052). *Bioorg. Med. Chem.* **2009**, *17*, 2175–2180.
92. Nguyen, H.; Ma, G.; Gladysheva, T.; Fremgen, T.; Romo, D. Bioinspired total synthesis and human proteasome inhibitory activity of (−)-salinosporamide A, (−)-homosalinosporamide A, and derivatives obtained via organonucleophile promoted bis-cyclizations. *J. Org. Chem.* **2011**, *76*, 2–12.
93. Lechner, A.; Eustáquio, A.S.; Gulder, T.A.; Hafner, M.; Moore, B.S. Selective overproduction of the proteasome inhibitor salinosporamide A via precursor pathway regulation. *Chem. Biol.* **2011**, *18*, 1527–1536.
94. Eustáquio, A.S.; Nam, S.J.; Penn, K.; Lechner, A.; Wilson, M.C.; Fenical, W.; Jensen, P.R.; Moore, B.S. The discovery of salinosporamide K from the marine bacterium "Salinispora pacifica" by genome mining gives insight into pathway evolution. *Chembiochem* **2011**, *12*, 61–64.
95. Martin, M.J.; Coello, L.; Fernandez, R.; Reyes, F.; Rodriguez, A.; Murcia, C.; Garranzo, M.; Mateo, C.; Sanchez-Sancho, F.; Bueno, S.; *et al*. Isolation and first total synthesis of PM050489 and PM060184, two new marine anticancer compounds. *J. Am. Chem. Soc.* **2013**, *135*, 10164–10171.
96. Pera, B.; Barasoain, I.; Canales, A.; Matesanz, R.; Rodríguez-Salarichs, J.; García-Fernández, L.F.; Moneo, V.; Jiménez-Barbero, J.; Galmarini, C.M.; Cuevas, C.; *et al*. New interfacial microtubule inhibitors of marine origin with potent antitumor activity and a distinct mechanism. *ACS Chem. Biol.* **2013**, *8*, 2084–2094.
97. Bhatnagar, I.; Kim, S.K. Marine antitumor drugs: Status, shortfalls and strategies. *Mar. Drugs* **2010**, *8*, 2702–2720.
98. Petit, K.; Biard, J.-F. Marine natural products and related compounds as anticancer agents: An overview of their clinical status. *Anticaner Agents Med. Chem.* **2013**, *13*, 603–631.
99. Flahive, E.; Srirangam, J. The dolastatins: Novel Antitumor Agents from *Dolabella auricularia*. In *Anticancer Agents from Natural Products*, 2nd ed.; Cragg, G.M., Kingston, D.G.I., Newman, D.J., Eds.; Taylor and Francis: Boca Raton, FL, USA, 2012; pp. 263–289.

Trabectedin and Plitidepsin: Drugs from the Sea that Strike the Tumor Microenvironment

Carlos M. Galmarini, Maurizio D'Incalci and Paola Allavena

Abstract: The prevailing paradigm states that cancer cells acquire multiple genetic mutations in oncogenes or tumor suppressor genes whose respective activation/up-regulation or loss of function serve to impart aberrant properties, such as hyperproliferation or inhibition of cell death. However, a tumor is now considered as an organ-like structure, a complex system composed of multiple cell types (e.g., tumor cells, inflammatory cells, endothelial cells, fibroblasts, *etc.*) all embedded in an inflammatory stroma. All these components influence each other in a complex and dynamic cross-talk, leading to tumor cell survival and progression. As the microenvironment has such a crucial role in tumor pathophysiology, it represents an attractive target for cancer therapy. In this review, we describe the mechanism of action of trabectedin and plitidepsin as an example of how these specific drugs of marine origin elicit their antitumor activity not only by targeting tumor cells but also the tumor microenvironment.

Reprinted from *Mar. Drugs*. Cite as: Galmarini, C.M.; D'Incalci, M.; Allavena, P. Trabectedin and Plitidepsin: Drugs from the Sea that Strike the Tumor Microenvironment. *Mar. Drugs* **2014**, *12*, 719-733.

1. Introduction

According to the prevailing paradigm of carcinogenesis, normal cells become cancer cells by acquiring multiple genetic mutations in oncogenes or tumor suppressor genes in which respective activation/up-regulation or loss of function served to impart aberrant properties, such as hyperproliferation, blockade of differentiation or inhibition of cell death [1–3]. However, a tumor is now considered as an organ-like structure, a complex system composed of multiple cell types (e.g., tumor cells, inflammatory cells, endothelial cells, fibroblasts, *etc.*) all embedded in an inflammatory stroma. All these components influence each other in a complex and dynamic cross-talk, leading to tumor survival and progression [4]. For example, growth factors and cytokines released by non-tumor cells support malignant cell progression and contribute to suppress the immune system inside tumors. Therefore, the microenvironment of a tumor is an integral part of its anatomy and physiology, and functionally, one cannot dissociate this microenvironment from what have traditionally been called "cancer cells" [5,6].

As the microenvironment has such a crucial role in tumor pathophysiology, it represents an attractive target for cancer therapy. There is already a wealth of information about specific cells and molecules in the tumor microenvironment that can be used as targets for cancer therapy at present [7,8]. For this reason, new molecules with antitumor features are looked at with new eyes. Anti-angiogenic therapies, for example, have been shown to improve clinical outcome in patients with different tumor types; similarly, signaling by the extracellular matrix (ECM) and its receptors are also becoming attractive targets of therapy, especially, as it is clear that ECM receptors and

growth factor receptors cooperate to maintain tissue specificity. In this review, we describe the mechanism of action of trabectedin and plitidepsin as an example of how drugs of marine origin elicit their antitumor activity by targeting tumor cells but also the tumor microenvironment.

2. The Tumor Microenvironment

Organs are composed of parenchymal cells that perform the main organ function and the stroma that gives the supportive framework. In normal tissues, the parenchyma is formed by cells inter-connected by cell-cell junctions that define cell morphology, proliferation, migration, adhesion, differentiation, and cell death [9]. On the other hand, the stroma includes the ECM, fibroblasts, migratory immune cells, and neural elements supported by a vascular network, all within a milieu of cytokines and growth factors. The interstitial matrix is an intricate and highly dynamic network of fibers composed of glycosaminoglycan (GAG)-containing glycoproteins. Different types of fibrous collagen together with fibronectin, hyaluronan, and proteoglycans confer mechanical strength, elasticity and a precise spatial organization to tissues. Organ architecture and function are maintained by dynamic interactions between parenchymal cells and their microenvironment [10]. Both components, cells and stroma, communicate via complex autocrine, juxtacrine, and paracrine mechanisms consisting of soluble molecules, including growth factors, cytokines, hormones, and proteases, insoluble factors, such as ECM components, and direct cell-cell interactions. For example, the ECM contains a wide range of growth factors that are bound in an inactive form to matricellular proteins, but can be rapidly released and activated in case of need, for example during tissue repair.

As any organ, tumors are also composed of cells and stroma. However, both these components are altered. Tumor cells are characterized by the presence of mutations that alter their normal functioning but also their relationship with the surrounding microenvironment. For example, as cancer cells begin to expand, they produce factors that activate myofibroblasts and recruit tumor-associated fibroblasts. These mesenchymal cells, as well as adipocytes, are responsible for many of the tumor-associated changes in the extracellular matrix that promote and foster tumor progression [11]. Normal cells are also active participants that shape the features of tumors. Inflammatory cells, including neutrophils, and macrophages, are frequently the first immune cells recruited to the tumor, and may be either tumor-promoting or tumor-inhibiting depending on their degree of activation and polarization [5,12]. Another inflammatory cell type, the mast cell, is also recruited early and promotes tumor progression by releasing proteases that activate angiogenesis [13]. Myeloid-derived suppressor cells inhibit T-cell activation and promote angiogenesis, cancer cell invasion, and metastasis [14]. Natural killer cells and different types of T cells may have either pro- or antitumor functions, depending on their mode of activation. Immunoglobulins released by B cells promote tumor growth by initiating the inflammatory response. Finally, cytokines and chemokines produced by tumor cells, leukocytes and other cell types are key orchestrators of the cancer-related inflammation and have long been associated with the recruitment of leukocytes in tumors and therefore with the sustained presence of inflammatory cells [15–17]. These molecules are involved in important biological processes that govern proliferation and migration of different

cells, regulation of innate and adaptive immune responses, and angiogenic and repair programs of the tissues.

On the other hand, the nature of the ECM in the tumor is different from that of the host tissue. The tumor stroma is characterized by a remarkable subversion of the tissue architecture and by a different composition of some ECM components. For instance, whereas the host organ may have been relatively soft and pliable, tumors are often tough and fibrotic. It has recently been shown that these alterations in the mechanical properties of the tissue contribute to the malignant phenotype [18–20]. Ultrastructural and immunohistochemical analyses also revealed the up-regulation of several proteins, such as tenascin, decorin, byglican, α-smooth muscle actin, osteopontin, fibulin-1, fibronectin, and the appearance of spliced protein isoforms that are not normally expressed [21,22]. This changed architecture may promote cell invasion by enabling cells to migrate along the collagen fibers or by enhancing integrin signaling [19,23]. Moreover, these matricellular proteins are degraded by specific proteases, such as matrix metalloproteases (MMPs), cathepsins, hyaluronidases, heparanase, elastase, urokinase-type plasminogen activator (uPA), plasmin and others in which activity is generally increased in tumors [24,25]. Finally, tumor blood vessels are also different from those of the normal vasculature as they are irregular and dilated. Furthermore, perivascular cells in tumors are loosely associated with endothelial cells [26,27]. These changes result in abnormal blood flow and leaky blood vessels with extravasation of excess fluid and proteins from the capillaries. The increase in the interstitial fluid pressure generates areas of hypoxia and acidosis inside tumors.

In summary, both normal (fibroblasts, endothelial cells, lymphocytes, macrophages, mast cells, and other cell types) and cancer cells inhabit a complex cellular and matrix ecosystem all of which may interact via juxtacrine and paracrine mechanisms. The constant disruption of homeostasis by proliferating tumor cells produces a chronic inflammatory reaction [28]. However, the classic players in acute inflammation (granulocytes, macrophages, endothelial cells, and fibroblasts) that ordinarily lead to the resolution of a wound through an orderly series of events, instead react paradoxically to the presence of dysfunctional epithelial cells by promoting their survival and replication [28]. This process also includes inflammatory angiogenesis and tissue remodeling. Thus, from this perspective, the microenvironment becomes an integral, essential part of a tumor [29,30].

3. Trabectedin Targets Tumor-Associated Macrophages (TAMs)

Trabectedin is an anticancer drug that was originally isolated from the marine Caribbean tunicate *Ecteinascidia turbinata* and now is produced synthetically (Figure 1) [31]. Trabectedin is used for the treatment of soft tissue sarcoma patients and, in combination with pegylated liposomal doxorubicin, for relapsed platinum-sensitive ovarian cancer patients [32,33]. It is a well-tolerated drug; the most common adverse effects observed after administration are reversible neutropenia and reversible AST/ALT elevation. The mechanism of action of trabectedin on tumor cells has been reviewed elsewhere [31]. Of note, the drug shows unique and high-specific inhibition of the transcription process. Transcription inhibition, that affects both the transcribing and the non-transcribing strands, occurs by different mechanisms such as the displacement of specific transcription factors from their promoters, the stabilization of the DNA duplex structure, a direct

interaction with RNA Pol II or the induction of the massive degradation of transcribing Pol II [34–37]. For example, through transcription inhibition, trabectedin modulates the expression of downstream targets, alters tumor biology, and induces the resumption of natural cellular differentiation in sarcomas resulting from the dysregulation of transcription factors, such as EWS-Fli1 fusion protein and FUS-CHOP [31,38–40].

Figure 1. Trabectedin targets tumor-associated macrophages (TAMs). (**A**) Chemical structure. (**B**) Trabectedin acts on the tumor microenvironment by directly affecting monocytes and TAMs or indirectly by inhibiting the secretion of inflammatory mediators involved in different pathophysiological processes, such as inflammatory cell recruitment or tumor angiogenesis.

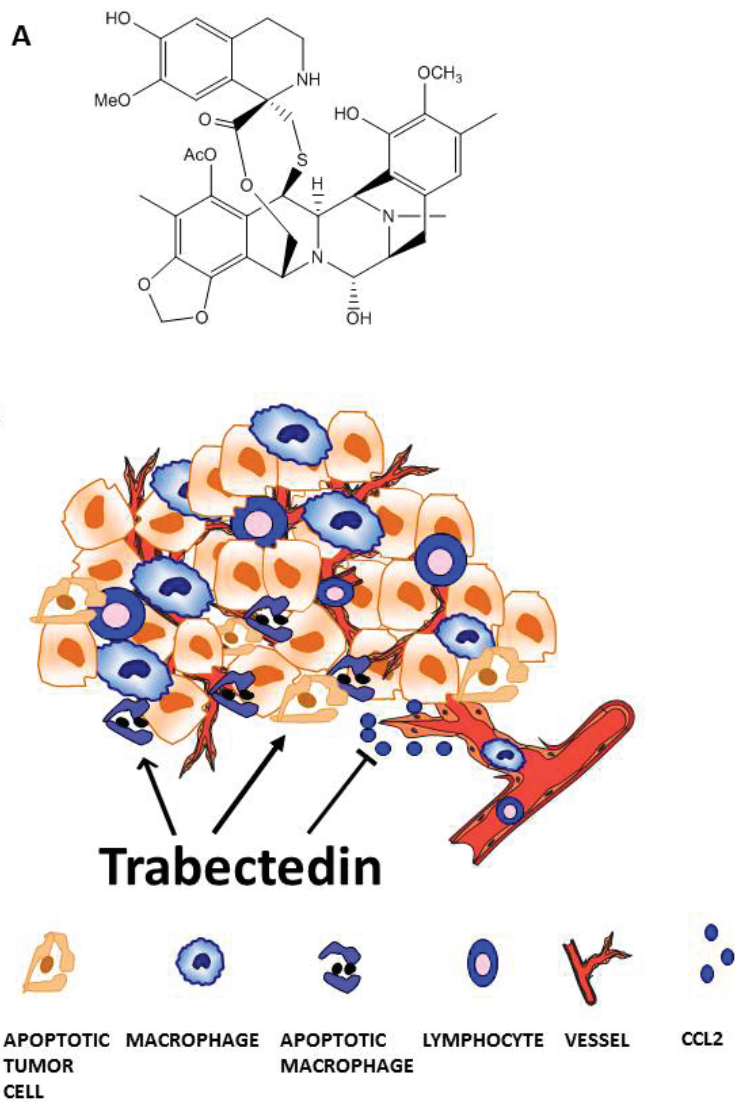

In addition to its activity on tumor cells, trabectedin also targets key processes in the biology of tumors, indicating that the drug is more versatile than currently available chemotherapeutic agents. First evidence came from the finding that, among all leukocytes, blood human monocytes and macrophages were hypersensitive to the drug [41]. This finding prompted a series of experiments to understand the exquisite selectivity of trabectedin for mononuclear phagocytes. It was demonstrated that the drug rapidly triggered the activation of caspase 8, downstream of membrane TRAIL receptors (TRAIL-R) [42]. Leukocyte subsets have different sets of TRAIL-R. Monocytes and macrophages mainly express the signaling TRAIL-Rs and are sensitive to trabectedin. In contrast, neutrophils and T lymphocytes preferentially express the non-signaling TRAIL-R (which prevents caspase 8 activation) and are therefore non-susceptible to trabectedin. On the other hand, low, non-cytotoxic concentrations of trabectedin not only inhibit monocyte differentiation into TAMs, but also the production of specific inflammatory mediators, such as CCL2, IL-6, VEGF, and CXC chemokine ligand-8 (CXCL8). This effect was observed particularly in monocytes, TAMs, myxoid liposarcoma cells and ovarian cancer cells [12,31,41]. Other chemokines involved in monocyte recruitment are also transcriptionally affected by trabectedin treatment (e.g., CCL7, CCL3, and CCL14). Importantly, all these effects are not reported for chemotherapeutic agents other than trabectedin (e.g., cisplatin, doxorubicin) [31,41]. Trabectedin also affected the expression of ECM-related genes produced by TAMs and fibroblast, such as fibronectin, osteopontin and matrix-metallo protease-2 (MMP2) or collagen type 1 [43,44]. These results indicate that trabectedin may reduce the high turnover of the tumor stroma.

As described previously, macrophages are a major cellular component of human tumors, where they are commonly termed tumor-associated macrophages (TAMs). These TAMs are derived from monocytes recruited into tumors by chemokines secreted by both malignant and stromal cells [45]. As macrophages, TAMs are versatile cells that are capable of displaying different functional activities. Based on their plasticity, macrophages can be classified in two extreme types: “classical” (or M1) and “alternative” (or M2) [46,47]. After stimulation with interferon gamma (IFN-γ), granulocyte-monocyte-colony stimulating factor (GM-CSF) and tumor necrotic factor-α (TNF-α), M1 macrophages secrete high levels of pro-inflammatory cytokines, such as interleukin-12 (IL-12), interleukin-1 (IL-1), and interleukin-6 (IL-6) and have potent antitumor efficacy [48]. Alternatively, monocytes exposed to interleukin-4 (IL-4) and interleukin-13 (IL-13) become polarized toward the M2-type. This is characterized by higher production of the anti-inflammatory cytokine interleukin-10 (IL-10) and low expression of pro-inflammatory cytokines and amplification of metabolic pathways that can suppress adaptive immune responses [47,49,50]. M2-related activities favor disease progression [51–53]. For instance, M2-type TAMs promote tumor angiogenesis by releasing several angiogenic factors, such as vascular endothelial growth factor (VEGF) or platelet-derived growth factor (PDGF) [54]. TAMs also release chemokines (e.g., CCL17, CCL18, CCL22), which increase intratumoral recruitment of lymphoid cells without cytotoxic activity (T-helper 2 lymphocytes; Th2) or with suppressive activity (regulatory T cells; T_{reg}) [55]. The impressive array of tumor-promoting functions is consistent with clinical studies showing high macrophage density in many human cancer types to be associated with increased

tumor angiogenesis and metastasis, and/or a poor prognosis [56–64]. Thus, TAMs are key players of the tumor microenvironment that promote disease progression [12,53,65,66].

The above-mentioned inhibitory activity of trabectedin on TAMs is not only observed *in vitro* but also in various animal tumor models [42,67]. In those models, trabectedin significantly decreased the number of blood monocytes and of tumor-associated macrophages but not of other leukocyte subsets (e.g., neutrophils or lymphocytes) [42]. To prove that the cytotoxic activity on mononuclear phagocytes is an important mechanism of its anti-tumor efficacy, tumor cells resistant to trabectedin *in vitro* were injected into mice [42]. Interestingly, in the *in vivo* setting, trabectedin still showed anti-tumor activity, in spite of the confirmed tumor cell resistance to the drug when exposed *in vitro*. Tumor growth was significantly restored after administration of myeloid cells from tumor-bearing untreated mice after each drug treatment cycle. Therefore, macrophage targeting *in vivo* appear to be a key component of the anti-tumor activity of trabectedin. Effects other than macrophage depletion also account for its antitumor efficacy. Using human liposarcoma xenografts grown in nude mice, Trabectedin induces a significant decrease in the expression of relevant tumor mediators such as the chemokines CCL2 and CXCL8, IL-6 or the angiogenic factor VEGF, and an overall effect on the angiogenic network [42,67]. Thus, in addition to direct activity on mononuclear phagocytes, trabectedin reduces the secretion of inflammatory mediators affecting main tumor pathophysiological processes such as the recruitment of circulating monocytes into tumors or angiogenesis [41,42].

The key evidence that trabectedin presents selective activity against monocytes and TAMs finally came from experiments conducted on human samples from patients receiving the drug as part of their therapy. Firstly, a decrease in monocytes was observed within few days after injection of trabectedin in most patients with soft tissue sarcoma [42]. Furthermore, by comparing tumor sections collected before and after neo-adjuvant therapy, a dramatic decrease of macrophage infiltration and vessel network was evidenced, reinforcing the concept that this compound strikes both the neoplastic compartment and the tumor micro-environment. Similarly, monocytes and TAMs from ovarian cancer biopsies were sensitive to trabectedin at low nM concentrations and were much more sensitive than lymphocytes. Moreover, at those concentrations, trabectedin significantly inhibited chemokine (CCL2), inflammatory cytokine (IL-6), and angiogenic factor (e.g., angiopoietin-2, VEGF) production by monocytes, macrophages, and TAMs [31,41].

4. Plitidepsin Targets Monocytes and Nurse-Like Cells (NLCs)

Plitidepsin (Aplidin) is a synthetic depsipeptide originally isolated from the tunicate *Aplidium albicans* and now obtained by total synthesis (Figure 2). The compound is currently being evaluated in a Phase III trial for the treatment of refractory/relapsed multiple myeloma patients (clinicaltrial.gov code: NCT01102426). Plitidepsin is a well-tolerated drug. The most common plitidepsin-related adverse events are nausea, fatigue, and myalgia. The mechanism of action of plitidepsin on tumor cells was reviewed elsewhere [68]. Briefly, after interacting with a moderately high-affinity binding site in the cell membrane, plitidepsin led to the rapid activation of Rac1 and the sustained activation of JNK and p38/MAPK that will finally provoke the appearance of a caspase-dependent apoptosis [68–71]. Results of several studies associated the activation of JNK

by plitidepsin with an increased oxidative stress characterized by a rise in the levels of reactive oxygen species (ROS) and a fall in reduced glutathion GSH [71,72]. The oxidative stress induced by Plitidepsin also provokes an endoplasmic reticulum (ER) stress associated to cell death [73]. After cell treatment, plitidepsin triggers the activation of several key molecular components of the classical ER stress-induced unfolded protein response (UPR). These include the proteolytic processing of ATF6 and the alternative splicing of XBP1, as well as the phosphorylation of eIF2α and JNK. Plitidepsin also induces the decrease of CHOP protein levels, due to its rapid degradation by the ubiquitin/proteasome machinery.

Figure 2. Plitidepsin (Aplidin) targets tumor-associated Nurse-Like cells (NLCs). (**A**) Chemical structure. (**B**) Besides inducing apoptosis of Chronic Lymphocytic Leukemia (CLL) cells, Plitidepsin also acts on monocytes and NLCs. NLCs promote survival of CLL cells by releasing pro-survival factors such as CXCL12.

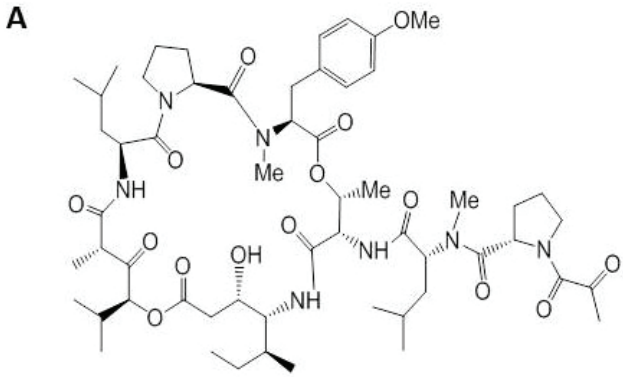

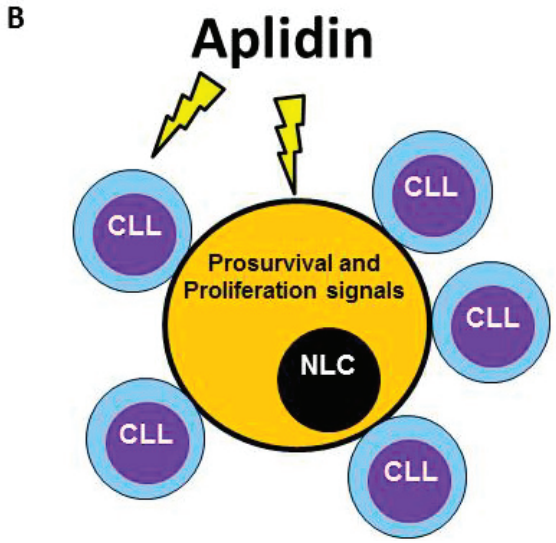

In addition to the previously mentioned effects, plitidepsin is also acting on the tumor microenvironment. This is clearly observed on chronic lymphocytic leukemia models (CLL). It was recently published that besides its direct effects on CLL cells, plitidepsin exhibits a potent activity against monocytes and NLCs, a subset of cells derived from peripheral monocytes of CLL patients [74]. The high sensitivity of monocyte and monocytic-derived cells to plitidepsin indirectly affects leukemic cell survival by impairing the delivery of pro-survival signals from these cell populations. As with TAMs in solid tumors, NLCs promote survival of CLL cells and play a crucial role for CLL cell progression. Among other pro-survival factors, NLCs secrete CXCL12, a chemokine that not only induces the migration of CLL cells to lymphoid tissues but also protects them from spontaneous and drug-induced apoptosis in a contact-dependent fashion [75,76]. NLCs can be found in the spleen and secondary lymphoid tissue of patients with CLL [77]. In line with the protective function of NLCs on CLL cells, it was also observed that the previous treatment of isolated NLCs with Plitidepsin impairs the survival of CLL cells. Plitidepsin induced monocyte and NLCs death by triggering apoptosis, as evidenced by early exposure of phosphatidylserine in the outer leaflet of plasma membrane, the activation of caspase-3 and subsequent cleavage of PARP [74]. The production of ROS induced by plitidepsin plays a central role in monocyte death, as drug-induced apoptosis was blocked when preincubating monocytes with ebselen, a compound that increases intracellular GSH levels. It is currently known that ROS and reactive nitrogen species (RNS) regulate the molecular and biochemical pathways responsible for human monocyte survival and that any disbalance in this strict regulation (e.g., induction of oxidative stress), can be detrimental for these cells [78]. In this regard, it was reported that monocytes are more susceptible than lymphocytes to cell death triggered by oxidative stress [79]. These data indicate that, besides its direct antitumor activity on CLL cells, plitidepsin also affects other main drivers of CLL biology, such as monocytic-derived cells.

5. Conclusions

In the last decades the concept that the tumor microenvironment is simply a supporting structure for the preservation of tissue architecture has dramatically changed. Indeed, microenvironmental components provide signals affecting cell adhesion, migration, proliferation, differentiation, and death. Monocytic-derived cells are key players of the cancer-related inflammation present at tumor sites. Such a reactive milieu eventually supports tumor cell proliferation and the full-blown development of neo-angiogenesis. There is increasing evidence that successful anti-cancer therapies are not only dependent on the cancer phenotype but also on the normalization of the tumor stroma. In this view, the findings showing that trabectedin and plitidepsin have wider mechanisms of action acting not only on tumor cells but also modifying the whole microenvironment is of great interest and may contribute to the development of new drugs from marine origin as anticancer therapies.

The opportunity to combine direct antiproliferative activity on tumor cells with the capacity to counteract the pro-tumoral properties of the tumor microenvironment is emerging as an especially appealing therapeutic effect of some drugs of marine origin. As reviewed above, the antitumor activity of trabectedin and plitidepsin is not only related to their effects on tumor cells, but also on

their ability to affect the tumor microenvironment, in particular monocytic-derived cell (TAMs and NLCs, respectively) and their pro-tumoral functions. Of note, the effects of trabectedin on tumor microenvironment are in line with response patterns evident in several patients, such as tumor shrinkage or delayed response and prolonged stabilization even in the absence of evident tumor shrinkage [80]. Trabectedin can therefore be considered a particularly important antitumor agent with mechanisms of action that make it especially appropriate for targeting key processes in the biology of cancer. Similar considerations can be taken into account for plitidepsin.

To our knowledge, there are no other reports showing this specific activity with other marine-derived drugs. Therefore, whether this is a common feature of marine natural products or a specific mechanism for trabectedin and plitidepsin remains to be elucidated.

6. Future Directions

Several questions need to be further addressed concerning the activity of drugs of marine origin on tumor microenvironment. We first need to understand if the activities observed for trabectedin or plitidepsin on the tumor microenvironment can be observed for other marine-derived drugs. A second question is whether these drugs are also affecting other stromal components besides the myeloid-derived compartment. We also need to understand whether the depletion of monocytic-derived cells is similar in all treated patients or if individual variability may result in different therapeutic efficacy. Another important question is whether, by affecting myeloid cells, marine-derived drugs independently influence main pathophysiological pathways of a given tumor. For example, it would be of interest to know if the anti-angiogenic activity of trabectedin is due to a direct effect on the vessel network or is mediated via the reduction of pro-angiogenic cytokines released by TAMs. While it is clear that marine-derived drugs have favorable mechanisms on tumor cells and the tumor microenvironment, additional research into the following actions would be beneficial. All these questions need to be addressed in order to improve the drug discovery and developmental process that would translate into more effective treatments with drugs of marine origin.

Conflicts of Interest

The authors declare no conflict of interest.

References

1. Farber, E. The multistep nature of cancer development. *Cancer Res.* **1984**, *44*, 4217–4223.
2. Weinberg, R.A. Oncogenes, antioncogenes, and the molecular bases of multistep carcinogenesis. *Cancer Res.* **1989**, *49*, 3713–3721.
3. Hanahan, D.; Weinberg, R.A. The hallmarks of cancer. *Cell* **2000**, *100*, 57–70.
4. Hanahan, D.; Weinberg, R.A. Hallmarks of cancer: The next generation. *Cell* **2011**, *144*, 646–674.
5. Albini, A.; Sporn, M.B. The tumour microenvironment as a target for chemoprevention. *Nat. Rev. Cancer* **2007**, *7*, 139–147.

6. Egeblad, M.; Nakasone, E.S.; Werb, Z. Tumors as organs: Complex tissues that interface with the entire organism. *Dev. Cell* **2010**, *18*, 884–901.
7. Mueller, M.M.; Fusenig, N.E. Friends or foes—bipolar effects of the tumour stroma in cancer. *Nat. Rev. Cancer* **2004**, *4*, 839–849.
8. Joyce, J.A. Therapeutic targeting of the tumor microenvironment. *Cancer Cell* **2005**, *7*, 513–520.
9. O'Brien, L.E.; Zegers, M.M.; Mostov, K.E. Opinion: Building epithelial architecture: Insights from three-dimensional culture models. *Nat. Rev. Mol. Cell Biol.* **2002**, *3*, 531–537.
10. Bissell, M.J.; Weaver, V.M.; Lelievre, S.A.; Wang, F.; Petersen, O.W.; Schmeichel, K.L. Tissue structure, nuclear organization, and gene expression in normal and malignant breast. *Cancer Res.* **1999**, *59*, 1757s–1763s.
11. Kalluri, R.; Zeisberg, M. Fibroblasts in cancer. *Nat. Rev. Cancer* **2006**, *6*, 392–401.
12. Allavena, P.; Mantovani, A. Immunology in the clinic review series; focus on cancer: Tumour-associated macrophages: Undisputed stars of the inflammatory tumour microenvironment. *Clin. Exp. Immunol.* **2012**, *167*, 195–205.
13. Coussens, L.M.; Raymond, W.W.; Bergers, G.; Laig-Webster, M.; Behrendtsen, O.; Werb, Z.; Caughey, G.H.; Hanahan, D. Inflammatory mast cells up-regulate angiogenesis during squamous epithelial carcinogenesis. *Genes Dev.* **1999**, *13*, 1382–1397.
14. Gabrilovich, D.I.; Nagaraj, S. Myeloid-derived suppressor cells as regulators of the immune system. *Nat. Rev. Immunol.* **2009**, *9*, 162–174.
15. Allavena, P.; Germano, G.; Marchesi, F.; Mantovani, A. Chemokines in cancer related inflammation. *Exp. Cell Res.* **2011**, *317*, 664–673.
16. Mantovani, A. Molecular pathways linking inflammation and cancer. *Curr. Mol. Med.* **2010**, *10*, 369–373.
17. Germano, G.; Mantovani, A.; Allavena, P. Targeting of the innate immunity/inflammation as complementary anti-tumor therapies. *Ann. Med.* **2011**, *43*, 581–593.
18. Paszek, M.J.; Zahir, N.; Johnson, K.R.; Lakins, J.N.; Rozenberg, G.I.; Gefen, A.; Reinhart-King, C.A.; Margulies, S.S.; Dembo, M.; Boettiger, D.; *et al.* Tensional homeostasis and the malignant phenotype. *Cancer Cell* **2005**, *8*, 241–254.
19. Levental, K.R.; Yu, H.; Kass, L.; Lakins, J.N.; Egeblad, M.; Erler, J.T.; Fong, S.F.; Csiszar, K.; Giaccia, A.; Weninger, W.; *et al.* Matrix crosslinking forces tumor progression by enhancing integrin signaling. *Cell* **2009**, *139*, 891–906.
20. Provenzano, P.P.; Eliceiri, K.W.; Campbell, J.M.; Inman, D.R.; White, J.G.; Keely, P.J. Collagen reorganization at the tumor-stromal interface facilitates local invasion. *BMC Med.* **2006**, *4*, 38:1–38:16.
21. Hynes, R.O. The extracellular matrix: Not just pretty fibrils. *Science* **2009**, *326*, 1216–1219.
22. Allen, M.; Louise Jones, J. Jekyll and Hyde: the role of the microenvironment on the progression of cancer. *J. Pathol.* **2011**, *223*, 162–176.
23. Condeelis, J.; Pollard, J.W. Macrophages: Obligate partners for tumor cell migration, invasion, and metastasis. *Cell* **2006**, *124*, 263–266.

24. Roycik, M.D.; Fang, X.; Sang, Q.X. A fresh prospect of extracellular matrix hydrolytic enzymes and their substrates. *Curr. Pharm. Des.* **2009**, *15*, 1295–1308.
25. Giraudo, E.; Inoue, M.; Hanahan, D. An amino-bisphosphonate targets MMP-9-expressing macrophages and angiogenesis to impair cervical carcinogenesis. *J. Clin. Invest.* **2004**, *114*, 623–633.
26. Bergers, G.; Benjamin, L.E. Tumorigenesis and the angiogenic switch. *Nat. Rev. Cancer* **2003**, *3*, 401–410.
27. Tredan, O.; Galmarini, C.M.; Patel, K.; Tannock, I.F. Drug resistance and the solid tumor microenvironment. *J. Natl. Cancer Inst.* **2007**, *99*, 1441–1454.
28. Albini, A.; Tosetti, F.; Benelli, R.; Noonan, D.M. Tumor inflammatory angiogenesis and its chemoprevention. *Cancer Res.* **2005**, *65*, 10637–10641.
29. Bissell, M.J.; Labarge, M.A. Context, tissue plasticity, and cancer: Are tumor stem cells also regulated by the microenvironment? *Cancer Cell* **2005**, *7*, 17–23.
30. Bhowmick, N.A.; Neilson, E.G.; Moses, H.L. Stromal fibroblasts in cancer initiation and progression. *Nature* **2004**, *432*, 332–337.
31. D'Incalci, M.; Galmarini, C.M. A review of trabectedin (ET-743): a unique mechanism of action. *Mol. Cancer Ther.* **2010**, *9*, 2157–2163.
32. Demetri, G.D.; Chawla, S.P.; von Mehren, M.; Ritch, P.; Baker, L.H.; Blay, J.Y.; Hande, K.R.; Keohan, M.L.; Samuels, B.L.; Schuetze, S.; *et al.* Efficacy and safety of trabectedin in patients with advanced or metastatic liposarcoma or leiomyosarcoma after failure of prior anthracyclines and ifosfamide: results of a randomized phase II study of two different schedules. *J. Clin. Oncol.* **2009**, *27*, 4188–4196.
33. Monk, B.J.; Herzog, T.J.; Kaye, S.B.; Krasner, C.N.; Vermorken, J.B.; Muggia, F.M.; Pujade-Lauraine, E.; Lisyanskaya, A.S.; Makhson, A.N.; Rolski, J.; *et al.* Trabectedin plus pegylated liposomal Doxorubicin in recurrent ovarian cancer. *J. Clin. Oncol.* **2010**, *28*, 3107–3114.
34. Aune, G.J.; Takagi, K.; Sordet, O.; Guirouilh-Barbat, J.; Antony, S.; Bohr, V.A.; Pommier, Y. Von Hippel-Lindau-coupled and transcription-coupled nucleotide excision repair-dependent degradation of RNA polymerase II in response to trabectedin. *Clin. Cancer Res.* **2008**, *14*, 6449–6455.
35. Bueren-Calabuig, J.A.; Giraudon, C.; Galmarini, C.M.; Egly, J.M.; Gago, F. Temperature-induced melting of double-stranded DNA in the absence and presence of covalently bonded antitumour drugs: insight from molecular dynamics simulations. *Nucleic Acids Res.* **2011**, *39*, 8248–8257.
36. Feuerhahn, S.; Giraudon, C.; Martinez-Diez, M.; Bueren-Calabuig, J.A.; Galmarini, C.M.; Gago, F.; Egly, J.M. XPF-dependent DNA breaks and RNA polymerase II arrest induced by antitumor DNA interstrand crosslinking-mimetic alkaloids. *Chem. Biol.* **2011**, *18*, 988–999.
37. Friedman, D.; Hu, Z.; Kolb, E.A.; Gorfajn, B.; Scotto, K.W. Ecteinascidin-743 inhibits activated but not constitutive transcription. *Cancer Res.* **2002**, *62*, 3377–3381.

38. Charytonowicz, E.; Terry, M.; Coakley, K.; Telis, L.; Remotti, F.; Cordon-Cardo, C.; Taub, R.N.; Matushansky, I. PPARgamma agonists enhance ET-743-induced adipogenic differentiation in a transgenic mouse model of myxoid round cell liposarcoma. *J. Clin. Invest.* **2012**, *122*, 886–898.
39. Grohar, P.J.; Griffin, L.B.; Yeung, C.; Chen, Q.R.; Pommier, Y.; Khanna, C.; Khan, J.; Helman, L.J. Ecteinascidin 743 interferes with the activity of EWS-FLI1 in Ewing sarcoma cells. *Neoplasia* **2011**, *13*, 145–153.
40. Di Giandomenico, S.; Frapolli, R.; Bello, E.; Uboldi, S.; Licandro, S.A.; Marchini, S.; Beltrame, L.; Brich, S.; Mauro, V.; Tamborini, E.; *et al.* Mode of action of trabectedin in myxoid liposarcomas. *Oncogene* **2013**, in press.
41. Allavena, P.; Signorelli, M.; Chieppa, M.; Erba, E.; Bianchi, G.; Marchesi, F.; Olimpio, C.O.; Bonardi, C.; Garbi, A.; Lissoni, A.; *et al.* Anti-inflammatory properties of the novel antitumor agent yondelis (trabectedin): Inhibition of macrophage differentiation and cytokine production. *Cancer Res.* **2005**, *65*, 2964–2971.
42. Germano, G.; Frapolli, R.; Belgiovine, C.; Anselmo, A.; Pesce, S.; Liguori, M.; Erba, E.; Uboldi, S.; Zucchetti, M.; Pasqualini, F.; *et al.* Role of macrophage targeting in the antitumor activity of trabectedin. *Cancer Cell* **2013**, *23*, 249–262.
43. Louneva, N.; Saitta, B.; Herrick, D.J.; Jimenez, S.A. Transcriptional inhibition of type I collagen gene expression in scleroderma fibroblasts by the antineoplastic drug ecteinascidin 743. *J. Biol. Chem.* **2003**, *278*, 40400–40407.
44. Liguori, M.; Solinas, G.; Germano, G.; Mantovani, A.; Allavena, P. Tumor-associated macrophages as incessant builders and destroyers of the cancer stroma. *Cancers* **2011**, *3*, 3740–3761.
45. Murdoch, C.; Muthana, M.; Coffelt, S.B.; Lewis, C.E. The role of myeloid cells in the promotion of tumour angiogenesis. *Nat. Rev. Cancer* **2008**, *8*, 618–631.
46. Biswas, S.K.; Mantovani, A. Macrophage plasticity and interaction with lymphocyte subsets: Cancer as a paradigm. *Nat. Immunol.* **2010**, *11*, 889–896.
47. Mantovani, A.; Sozzani, S.; Locati, M.; Allavena, P.; Sica, A. Macrophage polarization: Tumor-associated macrophages as a paradigm for polarized M2 mononuclear phagocytes. *Trends Immunol.* **2002**, *23*, 549–555.
48. Mosser, D.M.; Edwards, J.P. Exploring the full spectrum of macrophage activation. *Nat. Rev. Immunol.* **2008**, *8*, 958–969.
49. Gordon, S.; Martinez, F.O. Alternative activation of macrophages: Mechanism and functions. *Immunity* **2010**, *32*, 593–604.
50. Qian, B.Z.; Pollard, J.W. Macrophage diversity enhances tumor progression and metastasis. *Cell* **2010**, *141*, 39–51.
51. Mantovani, A.; Allavena, P.; Sica, A.; Balkwill, F. Cancer-related inflammation. *Nature* **2008**, *454*, 436–444.
52. DeNardo, D.G.; Johansson, M.; Coussens, L.M. Immune cells as mediators of solid tumor metastasis. *Cancer Metastas. Rev.* **2008**, *27*, 11–18.

53. Movahedi, K.; Laoui, D.; Gysemans, C.; Baeten, M.; Stange, G.; Van den Bossche, J.; Mack, M.; Pipeleers, D.; In't Veld, P.; De Baetselier, P.; *et al.* Different tumor microenvironments contain functionally distinct subsets of macrophages derived from Ly6C(high) monocytes. *Cancer Res.* **2010**, *70*, 5728–5739.
54. Pollard, J.W. Macrophages define the invasive microenvironment in breast cancer. *J. Leukoc. Biol.* **2008**, *84*, 623–630.
55. Mantovani, A.; Romero, P.; Palucka, A.K.; Marincola, F.M. Tumour immunity: effector response to tumour and role of the microenvironment. *Lancet* **2008**, *371*, 771–783.
56. Bingle, L.; Brown, N.J.; Lewis, C.E. The role of tumour-associated macrophages in tumour progression: Implications for new anticancer therapies. *J. Pathol.* **2002**, *196*, 254–265.
57. Clear, A.J.; Lee, A.M.; Calaminici, M.; Ramsay, A.G.; Morris, K.J.; Hallam, S.; Kelly, G.; Macdougall, F.; Lister, T.A.; Gribben, J.G. Increased angiogenic sprouting in poor prognosis FL is associated with elevated numbers of CD163+ macrophages within the immediate sprouting microenvironment. *Blood* **2010**, *115*, 5053–5056.
58. Heusinkveld, M.; van der Burg, S.H. Identification and manipulation of tumor associated macrophages in human cancers. *J. Transl. Med.* **2011**, *9*, 216:1–216:13.
59. Leek, R.D.; Lewis, C.E.; Whitehouse, R.; Greenall, M.; Clarke, J.; Harris, A.L. Association of macrophage infiltration with angiogenesis and prognosis in invasive breast carcinoma. *Cancer Res.* **1996**, *56*, 4625–4629.
60. Hagemann, T.; Wilson, J.; Burke, F.; Kulbe, H.; Li, N.F.; Pluddemann, A.; Charles, K.; Gordon, S.; Balkwill, F.R. Ovarian cancer cells polarize macrophages toward a tumor-associated phenotype. *J. Immunol.* **2006**, *176*, 5023–5032.
61. Lee, C.H.; Espinosa, I.; Vrijaldenhoven, S.; Subramanian, S.; Montgomery, K.D.; Zhu, S.; Marinelli, R.J.; Peterse, J.L.; Poulin, N.; Nielsen, T.O.; *et al.* Prognostic significance of macrophage infiltration in leiomyosarcomas. *Clin. Cancer Res.* **2008**, *14*, 1423–1430.
62. Lissbrant, I.F.; Stattin, P.; Wikstrom, P.; Damber, J.E.; Egevad, L.; Bergh, A. Tumor associated macrophages in human prostate cancer: relation to clinicopathological variables and survival. *Int. J. Oncol.* **2000**, *17*, 445–451.
63. Jensen, T.O.; Schmidt, H.; Moller, H.J.; Hoyer, M.; Maniecki, M.B.; Sjoegren, P.; Christensen, I.J.; Steiniche, T. Macrophage markers in serum and tumor have prognostic impact in American Joint Committee on Cancer stage I/II melanoma. *J. Clin. Oncol.* **2009**, *27*, 3330–3337.
64. van Dongen, M.; Savage, N.D.; Jordanova, E.S.; Briaire-de Bruijn, I.H.; Walburg, K.V.; Ottenhoff, T.H.; Hogendoorn, P.C.; van der Burg, S.H.; Gelderblom, H.; van Hall, T. Anti-inflammatory M2 type macrophages characterize metastasized and tyrosine kinase inhibitor-treated gastrointestinal stromal tumors. *Int. J. Cancer* **2010**, *127*, 899–909.
65. Coussens, L.M.; Werb, Z. Inflammation and cancer. *Nature* **2002**, *420*, 860–867.
66. Nagai, T.; Tanaka, M.; Tsuneyoshi, Y.; Xu, B.; Michie, S.A.; Hasui, K.; Hirano, H.; Arita, K.; Matsuyama, T. Targeting tumor-associated macrophages in an experimental glioma model with a recombinant immunotoxin to folate receptor beta. *Cancer Immunol. Immunother.* **2009**, *58*, 1577–1586.

67. Germano, G.; Frapolli, R.; Simone, M.; Tavecchio, M.; Erba, E.; Pesce, S.; Pasqualini, F.; Grosso, F.; Sanfilippo, R.; Casali, P.G.; *et al.* Antitumor and anti-inflammatory effects of trabectedin on human myxoid liposarcoma cells. *Cancer Res.* **2010**, *70*, 2235–2244.
68. Munoz-Alonso, M.J.; Gonzalez-Santiago, L.; Martinez, T.; Losada, A.; Galmarini, C.M.; Munoz, A. The mechanism of action of plitidepsin. *Curr. Opin. Investig. Drugs* **2009**, *10*, 536–542.
69. Suarez, Y.; Gonzalez-Santiago, L.; Zarich, N.; Davalos, A.; Aranda, J.F.; Alonso, M.A.; Lasuncion, M.A.; Rojas, J.M.; Munoz, A. Plitidepsin cellular binding and Rac1/JNK pathway activation depend on membrane cholesterol content. *Mol. Pharmacol.* **2006**, *70*, 1654–1663.
70. Garcia-Fernandez, L.F.; Losada, A.; Alcaide, V.; Alvarez, A.M.; Cuadrado, A.; Gonzalez, L.; Nakayama, K.; Nakayama, K.I.; Fernandez-Sousa, J.M.; Munoz, A.; *et al.* Aplidin induces the mitochondrial apoptotic pathway via oxidative stress-mediated JNK and p38 activation and protein kinase C delta. *Oncogene* **2002**, *21*, 7533–7544.
71. Gonzalez-Santiago, L.; Suarez, Y.; Zarich, N.; Munoz-Alonso, M.J.; Cuadrado, A.; Martinez, T.; Goya, L.; Iradi, A.; Saez-Tormo, G.; Maier, J.V.; *et al.* Aplidin induces JNK-dependent apoptosis in human breast cancer cells via alteration of glutathione homeostasis, Rac1 GTPase activation, and MKP-1 phosphatase downregulation. *Cell Death Differ.* **2006**, *13*, 1968–1981.
72. Cuadrado, A.; Garcia-Fernandez, L.F.; Gonzalez, L.; Suarez, Y.; Losada, A.; Alcaide, V.; Martinez, T.; Fernandez-Sousa, J.M.; Sanchez-Puelles, J.M.; Munoz, A. Aplidin induces apoptosis in human cancer cells via glutathione depletion and sustained activation of the epidermal growth factor receptor, Src, JNK, and p38 MAPK. *J. Biol. Chem.* **2003**, *278*, 241–250.
73. Losada, A.; Martínez-Leal, J.F.; Bejarano, A.; Cuevas, C.; García-Fernández, L.F.; Galmarini, C.M. Aplidin triggers the activation of molecular components of the UPR as part of its pro-apoptotic program in tumor cells. In Proceedings of the AACR 104th Annual Meeting of the American Association for Cancer Research Washington, Washington, DC, USA, 6–10 April 2013; doi:10.1158/1538-7445.AM2013-2129.
74. Morande, P.E.; Zanetti, S.R.; Borge, M.; Nannini, P.; Jancic, C.; Bezares, R.F.; Bitsmans, A.; Gonzalez, M.; Rodriguez, A.L.; Galmarini, C.M.; *et al.* The cytotoxic activity of Aplidin in chronic lymphocytic leukemia (CLL) is mediated by a direct effect on leukemic cells and an indirect effect on monocyte-derived cells. *Invest. New Drugs* **2012**, *30*, 1830–1840.
75. Burger, J.A.; Tsukada, N. leukemia B cells from spontaneous apoptosis through stromal cell-derived factor-1. *Blood* **2000**, *96*, 2655–2663.
76. Nishio, M.; Endo, T.; Tsukada, N.; Ohata, J.; Kitada, S.; Reed, J.C.; Zvaifler, N.J.; Kipps, T.J. Nurselike cells express BAFF and APRIL, which can promote survival of chronic lymphocytic leukemia cells via a paracrine pathway distinct from that of SDF-1alpha. *Blood* **2005**, *106*, 1012–1020.
77. Tsukada, N.; Burger, J.A.; Zvaifler, N.J.; Kipps, T.J. Distinctive features of “nurselike” cells that differentiate in the context of chronic lymphocytic leukemia. *Blood* **2002**, *99*, 1030–1037.
78. Baran, C.P.; Zeigler, M.M.; Tridandapani, S.; Marsh, C.B. The role of ROS and RNS in regulating life and death of blood monocytes. *Curr. Pharm. Des.* **2004**, *10*, 855–866.

79. Zurgil, N.; Solodeev, I.; Gilburd, B.; Shafran, Y.; Afrimzon, E.; Avtalion, R.; Shoenfeld, Y.; Deutsch, M. Monitoring the apoptotic process induced by oxidized low-density lipoprotein in Jurkat T-lymphoblast and U937 monocytic human cell lines. *Cell Biochem. Biophys.* **2004**, *40*, 97–113.
80. Sanfilippo, R.; Casali, P.G. The intriguing patterns of tumor response to trabectedin. *Expert Rev. Anticancer Ther.* **2013**, *13*, 21–24.

Trabectedin in Soft Tissue Sarcomas

Bradley J. Petek, Elizabeth T. Loggers, Seth M. Pollack and Robin L. Jones

Abstract: Soft tissue sarcomas are a group of rare tumors derived from mesenchymal tissue, accounting for about 1% of adult cancers. There are over 60 different histological subtypes, each with their own unique biological behavior and response to systemic therapy. The outcome for patients with metastatic soft tissue sarcoma is poor with few available systemic treatment options. For decades, the mainstay of management has consisted of doxorubicin with or without ifosfamide. Trabectedin is a synthetic agent derived from the Caribbean tunicate, *Ecteinascidia turbinata*. This drug has a number of potential mechanisms of action, including binding the DNA minor groove, interfering with DNA repair pathways and the cell cycle, as well as interacting with transcription factors. Several phase II trials have shown that trabectedin has activity in anthracycline and alkylating agent-resistant soft tissue sarcoma and suggest use in the second- and third-line setting. More recently, trabectedin has shown similar progression-free survival to doxorubicin in the first-line setting and significant activity in liposarcoma and leiomyosarcoma subtypes. Trabectedin has shown a favorable toxicity profile and has been approved in over 70 countries for the treatment of metastatic soft tissue sarcoma. This manuscript will review the development of trabectedin in soft tissue sarcomas.

Reprinted from *Mar. Drugs*. Cite as: Petek, B.J.; Loggers, E.T.; Pollack, S.M.; Jones, R.L. Trabectedin in Soft Tissue Sarcomas. *Mar. Drugs* **2015**, *13*, 974-983.

1. Introduction

Soft tissue sarcomas are a group of rare solid tumors of mesenchymal origin. Surgical resection with or without radiation is the mainstay of management for localized disease. However, approximately 50% of patients with high-grade tumors will develop recurrent disease. Systemic therapy may additionally be considered in the localized setting, but its role in management remains controversial. The outcome of patients with metastatic soft tissue sarcoma is poor with a median overall survival (OS) of about 12 months. Systemic therapy is at the core of management for patients with metastatic disease; however, there are few effective agents available. Doxorubicin and ifosfamide have shown consistent activity, and recently, the anti-angiogenic agent, pazopanib, has been approved based on the results of a randomized, placebo-controlled phase III trial showing a significant, but modest, benefit in progression-free survival (PFS) for patients treated with pazopanib [1].

Trabectedin is a synthetic, marine-derived alkylating agent derived from the Caribbean tunicate, *Ecteinascidia turbinata* [2]. The success of trabectedin in preliminary clinical trials for soft tissue sarcomas has led to the approval of the drug in many countries and a large, randomized phase III trial. With limited systemic therapy options available for sarcomas as a whole, trabectedin has the opportunity to be significantly beneficial for patients with metastatic disease.

2. Mechanism of Action

Trabectedin is a natural alkaloid composed of three tetrahydroisoquinolone rings (Figure 1). The unique structure of trabectedin allows it to bind to the N2 amino group of guanine residues in the minor groove of the DNA double helix and can lead to double-strand breaks [3,4]. Studies have suggested that the nucleotide excision repair mechanism may be essential for the antitumor activity of trabectedin and that the resulting double-strand breaks are more persistent if there is loss of homologous repair [5,6]. Evidence shows that disruption of DNA by trabectedin ultimately causes apoptosis and sensitization of cancer cells to Fas-mediated cell death [7]. Multiple studies, including specific experiments in soft tissue sarcomas, have also validated that trabectedin works at the tumor microenvironment with selective activity against monocytes and tumor-associated macrophages [8,9]. The inhibition of these immune factors allows for the prevention of angiogenesis and further disease progression [10,11]. Deprivation of inflammatory-mediated support in the tumor microenvironment may be one of the most important aspects of trabectedin's mechanism of action, making the drug efficacious as a cancer treatment. Other mechanisms for the chemotherapeutic actions of trabectedin may include modulation of the cell cycle and interaction with transcription factors [12,13].

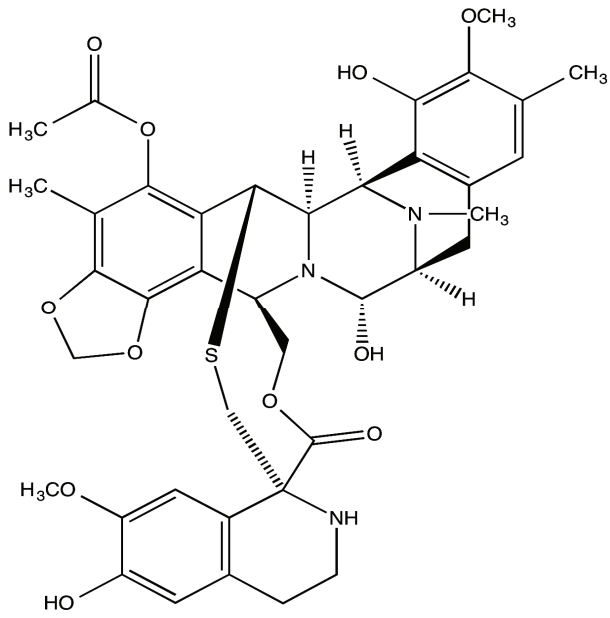

Figure 1. Chemical structure of trabectedin.

Recent studies have also proposed specific mechanisms of action for trabectedin in myxoid/round cell liposarcoma. The most common translocation in the disease is t(12;16)(q13;p11), creating a *FUS-CHOP* fusion gene, and rarely, a t(12;22)(q13;q12) translocation takes place resulting in a *EWS-CHOP* fusion gene. These fusion-encoded proteins are believed to function as abnormal transcription factors [14]. Notably, an *in vivo* study showed that mesenchymal

stem cells expressing the FUS-CHOP protein were committed to adipocytic differentiation, but were unable to terminally differentiate [15]. Trabectedin administration in this experiment downregulated *FUS:CHOP* expression, which promoted terminal adipocytic differentiation. Others have hypothesized that trabectedin prevents the binding of the FUS-CHOP oncogenic chimera protein to its target promoters, which may modulate the transcription of genes that are essential for adipocytic differentiation [14,16]. Recent studies have also characterized regulatory networks leading to trabectedin resistance, as well as have uncovered the antiangiogenic activity of trabectedin in myxoid/round cell liposarcoma [17,18].

3. Phase I Trials

A number of phase I trials have assessed differential dosing and infusion schedules for the administration of trabectedin [19–25]. Results from these studies have established the optimal regimen of administration to be a 1.5-mg/m^2 infusion over 24 h every three weeks [26]. Notably, Taamma and colleagues performed a phase I trial of trabectedin in 52 patients with treatment refractory tumors that recommended the current optimal dosing schedule of 1.5 mg/m^2 for a 24-h continuous infusion [22]. The most prevalent dose limiting toxicities in the study were hematological in nature. At the recommended dose, severe neutropenia was reported in 33% of cycles, severe thrombocytopenia in 10% of cycles and reversible, but severe, elevations in transaminase levels in 38% of cycles. The investigators also observed that patients with baseline hepatobiliary function abnormalities had a higher likelihood of severe hematological toxicity, indicating the need for dose reduction in such patients.

Combination therapies of trabectedin with other chemotherapeutic agents, including gemcitabine, doxorubicin, Doxil and cisplatin, have also been assessed in phase I trials [27–32]. The most promising results from these studies in sarcoma patients have been from the trials administering trabectedin in combination with doxorubicin. One of the trials showed a response rate (RR) of 18% and stable disease in 56% of soft tissue sarcoma patients (n = 29) [31]. Another study assessing combination therapy with doxorubicin reported a RR of 12% with median PFS of 9.2 months for 41 patients with solid tumors [27]. Of the 41 patients, 20 had liposarcoma and 11 had leiomyosarcoma. With success in phase I trials, the efficacy of combination therapy with doxorubicin and trabectedin is currently under investigation in larger studies.

4. Phase II Trials

Two phase II trials in 2004 provided the initial analysis of trabectedin in soft tissue sarcomas. The first of these studies was run on 54 pretreated soft tissue sarcoma patients and reported a low response rate of 4%, but a high disease control rate at six months of 24% [33]. Trabectedin was administered at a dose of 1.5 mg/m^2, over 24 h every three weeks. Approximately half of the patients in the study eventually developed grade 3/4 aspartate aminotransferase (AST) and alanine aminotransferase (ALT) levels. Another common adverse event was neutropenia, being grade 3/4 in 61% of patients. In this trial, four patients (7.4%) discontinued trabectedin due to adverse events.

In addition, there were two treatment-related deaths, and both were patients who developed acute renal failure.

The second phase II trial, published in 2004, again reported a low response rate of 8% and a one-year overall survival rate of 53% in 36 previously treated sarcoma patients [34]. This study also utilized the same dosing schedule of trabectedin (1.5 mg/m^2, over 24 h every three weeks). The toxicity profile of the drug was similar to previous trials with patients experiencing elevations in transaminases, fatigue and hematological toxicity. Growth factors, such as, granulocyte-colony stimulating factor (G-CSF), can be administered to help prevent hematological toxicity; however, a recent retrospective study showed that G-CSF administration has only been used in about 10% of phase II trials on trabectedin in solid tumors [35].

Early promising results in these phase II studies led the European Organization for the Research and Treatment of Cancer (EORTC) to initiate a phase II trial of trabectedin in 104 patients treated in the second- and third-line setting [36]. This trial also reported a low response rate of 8%. The six-month PFS was 29%, and the median overall survival (OS) was reported as 9.2 months. Subsequently, a further phase II trial in 36 patients was run to evaluate the activity of trabectedin in the first-line setting. The overall response rate was reported as 17%, and the one-year PFS and OS rates were 21% and 72%, respectively [37]. This study also importantly concluded that trabectedin has similar ranges of objective responses and overall survival rates in the first-line setting to the two most active drugs in soft tissue sarcomas: doxorubicin and ifosfamide.

Demetri and colleagues performed a phase II trial randomizing 270 patients with leiomyosarcoma and liposarcoma to receive either 1.5 mg/m^2 of trabectedin over 24 h every three weeks, or 0.58 mg/m^2 over 3 h every week for three out of four weeks [38]. Patients were required to have experienced documented disease progression while on doxorubicin and ifosfamide prior to trial entry. The 24-h infusion schedule showed a significantly longer median time to progression (TTP) (3.7 *vs.* 2.3 months) and PFS (3.3 *vs.* 2.3 months), as compared to the 3-h infusion schedule. No significant difference in overall survival was observed between the two arms of the trial; however, there was a strong trend favoring the 24-h infusion schedule (13.9 months *vs.* 11.8 months). Trabectedin was generally well tolerated in this study, with the most frequently reported grade 3/4 adverse events being neutropenia and elevated transaminases. Febrile neutropenia occurred in 1% of patients, and the majority of adverse events were mild to moderate. There was also no documentation of cumulative toxicities. Another phase II trial recommended the use of trabectedin as a neoadjuvant therapy for patients with advanced myxoid liposarcoma [39].

The results of these phase II trials led to licensing approval of trabectedin by the European Union for advanced soft tissue sarcoma in 2007, and the drug is now approved in over 70 countries.

5. Phase III Trials

Trabectedin has yet to be approved by the FDA in the United States, and consequently a phase III trial has been performed randomizing over 500 patients with leiomyosarcoma and liposarcoma to receive either trabectedin or dacarbazine (2:1 ratio). The primary end point of the trial is overall survival. This trial has closed to enrollment, and the results are eagerly awaited (NCT01343277).

In addition, there is an ongoing worldwide, expanded access program (NCT00210665). A recent analysis from this study reported that of the 1,895 soft tissue sarcoma patients entered into the program, patients with leiomyosarcoma and liposarcoma had significantly longer OS compared to all other histological subtypes (16.2 *vs.* 8.4 months, respectively), as well as a higher objective response rate (6.9% *vs.* 4%, respectively) [40].

Another phase III trial randomized 121 patients with translocation-related sarcomas to receive trabectedin or doxorubicin in the first-line setting with progression-free survival as the primary end point [41]. There was no significant difference in PFS between the two arms of the trial. At the time of analysis, 63.9% and 58.3% of patients were alive in the trabectedin and doxorubicin arms, respectively (with no statistically significant difference in overall survival). The response rate according to RECIST 1.0 was significantly higher in the doxorubicin (27%) compared to the trabectedin (5.9%) arm of the trial. In contrast, the response according to Choi criteria showed fewer differences between the doxorubicin (45.9%) and trabectedin (37.3%) arms, in terms of response rate.

6. Retrospective Studies

Trabectedin has shown particular activity in myxoid/round cell liposarcoma. In a retrospective analysis of 51 patients treated at five referral centers, a median overall response rate of 51% was reported, and the median PFS was 14 months [42]. Progression-free survival at six months was also reported as 88%. In another retrospective study assessing the efficacy of trabectedin in specific translocation-related sarcomas, the rate of PFS at six months was documented as 64% in myxoid/round cell liposarcoma (n = 27) and 22% in synovial sarcoma (n = 45) [43]. These results suggest that trabectedin may have significant activity in these two histological subtypes and should be further analyzed in larger randomized clinical trials.

Other retrospective studies have shown that trabectedin may also be effective in uterine leiomyosarcoma. In a study assessing 66 patients with metastatic uterine leiomyosarcoma, PFS for the entire cohort was 3.3 months with 16% of patients achieving a partial response and 35% showing stable disease [44]. Furthermore, a prospective phase II trial of trabectedin in uterine leiomyosarcoma reported a median PFS of 5.8 months and OS of 26.1 months [45]. Two patients in the study also had a partial response to trabectedin administration (10%).

Retrospective analysis was also used to assess the effect of age on the efficacy and safety of trabectedin administration in the treatment of soft tissue sarcomas [46]. Patients under the age of 60 were part of the younger cohort, and patients 60 or older were a part of the older cohort. The analysis pooled five prior phase II trials and showed similar response rates (younger 10.1% *vs.* older 9.6%), no significant difference in median progression-free survival (younger 2.5 *vs.* older 3.7 months) and similar overall survival rates between cohorts (younger 13.0 *vs.* older 14.0 months). However, older patients did show a higher incidence of grade 3/4 neutropenia (43.6% *vs.* 60.2%) and fatigue (6.3% *vs.* 14.4%). A small subset of patients 70 or older were also included in the analysis and showed no significant differences in efficacy or safety outcomes. This study therefore indicates that trabectedin can have meaningful benefits and an acceptable safety profile in young and elderly patients.

7. Conclusions

Trabectedin has shown consistent activity in patients with previously treated soft tissue sarcoma. The results of a number of phase II trials have led to the drug being approved in over 70 countries worldwide. The results of a phase III trial randomizing leiomyosarcoma and liposarcoma patients to receive trabectedin or dacarbazine are awaited and could lead to the drug being approved by the FDA.

Further evaluation is required for combination strategies of trabectedin, particularly with doxorubicin [27,31]. Investigation of this agent in the neoadjuvant and adjuvant setting may also be warranted in certain histological subtypes.

Acknowledgments

SMP, ETL and RLJ are supported by the Bob and Eileen Gilman Family Sarcoma Research Fund.

Author Contributions

All authors provided significant contributions in writing and editing the manuscript.

Conflicts of Interest

Jones has been an investigator on clinical trials sponsored by Pharmamar and Johnson and Johnson.

References

1. Van der Graaf, W.T.A.; Blay, J.-Y.; Chawla, S.P.; Kim, D.-W.; Bui-Nguyen, B.; Casali, P.G.; Schöffski, P.; Aglietta, M.; Staddon, A.P.; Beppu, Y.; *et al.* Pazopanib for metastatic soft-tissue sarcoma (palette): A randomised, double-blind, placebo-controlled phase 3 trial. *Lancet* **2012**, *379*, 1879–1886.
2. Cuevas, C.; Francesch, A. Development of yondelis[registered sign] (trabectedin, et-743). A semisynthetic process solves the supply problem. *Nat. Prod. Rep.* **2009**, *26*, 322–337.
3. D'Incalci, M.; Galmarini, C.M. A review of trabectedin (et-743): A unique mechanism of action. *Mol. Cancer Ther.* **2010**, *9*, 2157–2163.
4. Guirouilh-Barbat, J.; Redon, C.; Pommier, Y. Transcription-coupled DNA double-strand breaks are mediated via the nucleotide excision repair and the mre11-rad50-nbs1 complex. *Mol. Biol. Cell* **2008**, *19*, 3969–3981.
5. Soares, D.G.; Escargueil, A.E.; Poindessous, V.; Sarasin, A.; de Gramont, A.; Bonatto, D.; Henriques, J.A.P.; Larsen, A.K. Replication and homologous recombination repair regulate DNA double-strand break formation by the antitumor alkylator ecteinascidin 743. *Proc. Natl. Acad. Sci. USA* **2007**, *104*, 13062–13067.
6. Tavecchio, M.; Simone, M.; Erba, E.; Chiolo, I.; Liberi, G.; Foiani, M.; D'Incalci, M.; Damia, G. Role of homologous recombination in trabectedin-induced DNA damage. *Eur. J. Cancer* **2008**, *44*, 609–618.

7. Martínez-Serra, J.; Maffiotte, E.; Martín, J.; Bex, T.; Navarro-Palou, M.; Ros, T.; Plazas, J.M.; Vögler, O.; Gutiérrez, A.; Amat, J.C.; *et al.* Yondelis® (et-743, trabectedin) sensitizes cancer cell lines to cd95-mediated cell death: New molecular insight into the mechanism of action. *Eur. J. Pharmacol.* **2011**, *658*, 57–64.
8. Allavena, P.; Signorelli, M.; Chieppa, M.; Erba, E.; Bianchi, G.; Marchesi, F.; Olimpio, C.O.; Bonardi, C.; Garbi, A.; Lissoni, A.; *et al.* Anti-inflammatory properties of the novel antitumor agent yondelis (trabectedin): Inhibition of macrophage differentiation and cytokine production. *Cancer Res.* **2005**, *65*, 2964–2971.
9. Germano, G.; Frapolli, R.; Belgiovine, C.; Anselmo, A.; Pesce, S.; Liguori, M.; Erba, E.; Uboldi, S.; Zucchetti, M.; Pasqualini, F.; *et al.* Role of macrophage targeting in the antitumor activity of trabectedin. *Cancer Cell* **2013**, *23*, 249–262.
10. Galmarini, C.M.; Incalci, M.; Allavena, P. Trabectedin and plitidepsin: Drugs from the sea that strike the tumor microenvironment. *Mar. Drugs* **2014**, *12*, 719–733.
11. D'Incalci, M.; Badri, N.; Galmarini, C.M.; Allavena, P. Trabectedin, a drug acting on both cancer cells and the tumour microenvironment. *Br. J. Cancer* **2014**, *111*, 646–650.
12. Bonfanti, M.; la Valle, E.; Fernandez Sousa Faro, J.M.; Faircloth, G.; Caretti, G.; Mantovani, R.; D'Incalci, M. Effect of ecteinascidin-743 on the interaction between DNA binding proteins and DNA. *Anti-Cancer Drug Des.* **1999**, *14*, 179–186.
13. Erba, E.; Bergamaschi, D.; Bassano, L.; Damia, G.; Ronzoni, S.; Faircloth, G.T.; D'Incalci, M. Ecteinascidin-743 (et-743), a natural marine compound, with a unique mechanism of action. *Eur. J. Cancer* **2001**, *37*, 97–105.
14. Di Giandomenico, S.; Frapolli, R.; Bello, E.; Uboldi, S.; Licandro, S.A.; Marchini, S.; Beltrame, L.; Brich, S.; Mauro, V.; Tamborini, E.; *et al.* Mode of action of trabectedin in myxoid liposarcomas. *Oncogene* **2014**, *33*, 5201–5210.
15. Charytonowicz, E.; Terry, M.; Coakley, K.; Telis, L.; Remotti, F.; Cordon-Cardo, C.; Taub, R.N.; Matushansky, I. Pparγ agonists enhance et-743-induced adipogenic differentiation in a transgenic mouse model of myxoid round cell liposarcoma. *J. Clin. Investig.* **2012**, *122*, 886–898.
16. Forni, C.; Minuzzo, M.; Virdis, E.; Tamborini, E.; Simone, M.; Tavecchio, M.; Erba, E.; Grosso, F.; Gronchi, A.; Aman, P.; *et al.* Trabectedin (et-743) promotes differentiation in myxoid liposarcoma tumors. *Mol. Cancer Ther.* **2009**, *8*, 449–457.
17. Dossi, R.; Frapolli, R.; Di Giandomenico, S.; Paracchini, L.; Bozzi, F.; Brich, S.; Castiglioni, V.; Borsotti, P.; Belotti, D.; Uboldi, S.; *et al.* Antiangiogenic activity of trabectedin in myxoid liposarcoma: Involvement of host timp-1 and timp-2 and tumor thrombospondin-1. *Int. J. Cancer* **2015**, *136*, 721–729.
18. Uboldi, S.; Calura, E.; Beltrame, L.; Fuso Nerini, I.; Marchini, S.; Cavalieri, D.; Erba, E.; Chiorino, G.; Ostano, P.; D'Angelo, D.; *et al.* A systems biology approach to characterize the regulatory networks leading to trabectedin resistance in an *in vitro* model of myxoid liposarcoma. *PLoS One* **2012**, *7*, e35423.

19. Forouzesh, B.; Hidalgo, M.; Chu, Q.; Mita, A.; Mita, M.; Schwartz, G.; Jimeno, J.; Gómez, J.; Alfaro, V.; Lebedinsky, C.; *et al.* Phase I and pharmacokinetic study of trabectedin as a 1- or 3-h infusion weekly in patients with advanced solid malignancies. *Clin. Cancer Res.* **2009**, *15*, 3591–3599.
20. Puchalski, T.; Ryan, D.; Garcia-Carbonero, R.; Demetri, G.; Butkiewicz, L.; Harmon, D.; Seiden, M.; Maki, R.; Lopez-Lazaro, L.; Jimeno, J.; *et al.* Pharmacokinetics of ecteinascidin 743 administered as a 24-h continuous intravenous infusion to adult patients with soft tissue sarcomas: Associations with clinical characteristics, pathophysiological variables and toxicity. *Cancer Chemother. Pharmacol.* **2002**, *50*, 309–319.
21. Ryan, D.P.; Supko, J.G.; Eder, J.P.; Seiden, M.V.; Demetri, G.; Lynch, T.J.; Fischman, A.J.; Davis, J.; Jimeno, J.; Clark, J.W. Phase I and pharmacokinetic study of ecteinascidin 743 administered as a 72-h continuous intravenous infusion in patients with solid malignancies. *Clin. Cancer Res.* **2001**, *7*, 231–242.
22. Taamma, A.; Misset, J.L.; Riofrio, M.; Guzman, C.; Brain, E.; Lopez Lazaro, L.; Rosing, H.; Jimeno, J.M.; Cvitkovic, E. Phase I and pharmacokinetic study of ecteinascidin-743, a new marine compound, administered as a 24-h continuous infusion in patients with solid tumors. *J. Clin. Oncol.* **2001**, *19*, 1256–1265.
23. Twelves, C.; Hoekman, K.; Bowman, A.; Vermorken, J.B.; Anthoney, A.; Smyth, J.; van Kesteren, C.; Beijnen, J.H.; Uiters, J.; Wanders, J.; *et al.* Phase I and pharmacokinetic study of yondelis™ (ecteinascidin-743; et-743) administered as an infusion over 1 h or 3 h every 21 days in patients with solid tumours. *Eur. J. Cancer* **2003**, *39*, 1842–1851.
24. Van Kesteren, C.; Cvitkovic, E.; Taamma, A.; López-Lázaro, L.; Jimeno, J.M.; Guzman, C.; Mathôt, R.A.A.; Schellens, J.H.M.; Misset, J.-L.; Brain, E.; *et al.* Pharmacokinetics and pharmacodynamics of the novel marine-derived anticancer agent ecteinascidin 743 in a phase I dose-finding study. *Clin. Cancer Res.* **2000**, *6*, 4725–4732.
25. Villalona-Calero, M.A.; Eckhardt, S.G.; Weiss, G.; Hidalgo, M.; Beijnen, J.H.; van Kesteren, C.; Rosing, H.; Campbell, E.; Kraynak, M.; Lopez-Lazaro, L.; *et al.* A phase I and pharmacokinetic study of ecteinascidin-743 on a daily × 5 schedule in patients with solid malignancies. *Clin. Cancer Res.* **2002**, *8*, 75–85.
26. Schöffski, P.; Dumez, H.; Wolter, P.; Stefan, C.; Wozniak, A.; Jimeno, J.; van Oosterom, A.T. Clinical impact of trabectedin (ecteinascidin-743) in advanced/metastatic soft tissue sarcoma. *Expert Opin. Pharmacother.* **2008**, *9*, 1609–1618.
27. Blay, J.-Y.; von Mehren, M.; Samuels, B.L.; Fanucchi, M.P.; Ray-Coquard, I.; Buckley, B.; Gilles, L.; Lebedinsky, C.; Elsayed, Y.A.; le Cesne, A. Phase I combination study of trabectedin and doxorubicin in patients with soft-tissue sarcoma. *Clin. Cancer Res.* **2008**, *14*, 6656–6662.
28. Messersmith, W.; Jimeno, A.; Ettinger, D.; Laheru, D.; Brahmer, J.; Lansey, D.; Khan, Y.; Donehower, R.; Elsayed, Y.; Zannikos, P.; *et al.* Phase I trial of weekly trabectedin (et-743) and gemcitabine in patients with advanced solid tumors. *Cancer Chemother. Pharmacol.* **2008**, *63*, 181–188.

29. Sessa, C.; Cresta, S.; Noberasco, C.; Capri, G.; Gallerani, E.; Braud, F.D.; Zucchetti, M.; D'Incalci, M.; Locatelli, A.; Marsoni, S.; *et al.* Phase I clinical and pharmacokinetic study of trabectedin and cisplatin in solid tumours. *Eur. J. Cancer* **2009**, *45*, 2116–2122.
30. Sessa, C.; del Conte, G.; Christinat, A.; Cresta, S.; Perotti, A.; Gallerani, E.; Lardelli, P.; Kahatt, C.; Alfaro, V.; Iglesias, J.; *et al.* Phase I clinical and pharmacokinetic study of trabectedin and cisplatin given every three weeks in patients with advanced solid tumors. *Investig. New Drugs* **2013**, *31*, 1236–1243.
31. Sessa, C.; Perotti, A.; Noberasco, C.; De Braud, F.; Gallerani, E.; Cresta, S.; Zucchetti, M.; Viganò, L.; Locatelli, A.; Jimeno, J.; *et al.* Phase I clinical and pharmacokinetic study of trabectedin and doxorubicin in advanced soft tissue sarcoma and breast cancer. *Eur. J. Cancer* **2009**, *45*, 1153–1161.
32. Von Mehren, M.; Schilder, R.J.; Cheng, J.D.; Temmer, E.; Cardoso, T.M.; Renshaw, F.G.; Bayever, E.; Zannikos, P.; Yuan, Z.; Cohen, R.B. A phase I study of the safety and pharmacokinetics of trabectedin in combination with pegylated liposomal doxorubicin in patients with advanced malignancies. *Ann. Oncol.* **2008**, *19*, 1802–1809.
33. Yovine, A.; Riofrio, M.; Blay, J.Y.; Brain, E.; Alexandre, J.; Kahatt, C.; Taamma, A.; Jimeno, J.; Martin, C.; Salhi, Y.; *et al.* Phase II study of ecteinascidin-743 in advanced pretreated soft tissue sarcoma patients. *J. Clin. Oncol.* **2004**, *22*, 890–899.
34. Garcia-Carbonero, R.; Supko, J.G.; Manola, J.; Seiden, M.V.; Harmon, D.; Ryan, D.P.; Quigley, M.T.; Merriam, P.; Canniff, J.; Goss, G.; *et al.* Phase II and pharmacokinetic study of ecteinascidin 743 in patients with progressive sarcomas of soft tissues refractory to chemotherapy. *J. Clin. Oncol.* **2004**, *22*, 1480–1490.
35. Le Cesne, A.; Yovine, A.; Blay, J.-Y.; Delaloge, S.; Maki, R.; Misset, J.-L.; Frontelo, P.; Nieto, A.; Jiao, J.; Demetri, G. A retrospective pooled analysis of trabectedin safety in 1132 patients with solid tumors treated in phase ii clinical trials. *Investig. New Drugs* **2012**, *30*, 1193–1202.
36. Le Cesne, A.; Blay, J.Y.; Judson, I.; Van Oosterom, A.; Verweij, J.; Radford, J.; Lorigan, P.; Rodenhuis, S.; Ray-Coquard, I.; Bonvalot, S.; *et al.* Phase ii study of et-743 in advanced soft tissue sarcomas: A european organisation for the research and treatment of cancer (eortc) soft tissue and bone sarcoma group trial. *J. Clin. Oncol.* **2005**, *23*, 576–584.
37. Garcia-Carbonero, R.; Supko, J.G.; Maki, R.G.; Manola, J.; Ryan, D.P.; Harmon, D.; Puchalski, T.A.; Goss, G.; Seiden, M.V.; Waxman, A.; *et al.* Ecteinascidin-743 (et-743) for chemotherapy-naive patients with advanced soft tissue sarcomas: Multicenter phase II and pharmacokinetic study. *J. Clin. Oncol.* **2005**, *23*, 5484–5492.
38. Demetri, G.D.; Chawla, S.P.; von Mehren, M.; Ritch, P.; Baker, L.H.; Blay, J.Y.; Hande, K.R.; Keohan, M.L.; Samuels, B.L.; Schuetze, S.; *et al.* Efficacy and safety of trabectedin in patients with advanced or metastatic liposarcoma or leiomyosarcoma after failure of prior anthracyclines and ifosfamide: Results of a randomized phase ii study of two different schedules. *J. Clin. Oncol.* **2009**, *27*, 4188–4196.

39. Gronchi, A.; Bui, B.N.; Bonvalot, S.; Pilotti, S.; Ferrari, S.; Hohenberger, P.; Hohl, R.J.; Demetri, G.D.; le Cesne, A.; Lardelli, P.; *et al.* Phase II clinical trial of neoadjuvant trabectedin in patients with advanced localized myxoid liposarcoma. *Ann. Oncol.* **2012**, *23*, 771–776.
40. Samuels, B.L.; Chawla, S.; Patel, S.; von Mehren, M.; Hamm, J.; Kaiser, P.E.; Schuetze, S.; Li, J.; Aymes, A.; Demetri, G.D. Clinical outcomes and safety with trabectedin therapy in patients with advanced soft tissue sarcomas following failure of prior chemotherapy: Results of a worldwide expanded access program study. *Ann. Oncol.* **2013**, *24*, 1703–1709.
41. Blay, J.-Y.; Leahy, M.G.; Nguyen, B.B.; Patel, S.R.; Hohenberger, P.; Santoro, A.; Staddon, A.P.; Penel, N.; Piperno-Neumann, S.; Hendifar, A.; *et al.* Randomised phase III trial of trabectedin *versus* doxorubicin-based chemotherapy as first-line therapy in translocation-related sarcomas. *Eur. J. Cancer* **2014**, *50*, 1137–1147.
42. Grosso, F.; Jones, R.L.; Demetri, G.D.; Judson, I.R.; Blay, J.-Y.; le Cesne, A.; Sanfilippo, R.; Casieri, P.; Collini, P.; Dileo, P.; *et al.* Efficacy of trabectedin (ecteinascidin-743) in advanced pretreated myxoid liposarcomas: A retrospective study. *Lancet Oncol.* **2007**, *8*, 595–602.
43. Cesne, A.L.; Cresta, S.; Maki, R.G.; Blay, J.Y.; Verweij, J.; Poveda, A.; Casali, P.G.; Balaña, C.; Schöffski, P.; Grosso, F.; *et al.* A retrospective analysis of antitumour activity with trabectedin in translocation-related sarcomas. *Eur. J. Cancer* **2012**, *48*, 3036–3044.
44. Sanfilippo, R.; Grosso, F.; Jones, R.L.; Banerjee, S.; Pilotti, S.; D'Incalci, M.; Tos, A.P.D.; Raspagliesi, F.; Judson, I.; Casali, P.G. Trabectedin in advanced uterine leiomyosarcomas: A retrospective case series analysis from two reference centers. *Gynecol. Oncol.* **2011**, *123*, 553–556.
45. Monk, B.J.; Blessing, J.A.; Street, D.G.; Muller, C.Y.; Burke, J.J.; Hensley, M.L. A phase II evaluation of trabectedin in the treatment of advanced, persistent, or recurrent uterine leiomyosarcoma: A gynecologic oncology group study. *Gynecol. Oncol.* **2012**, *124*, 48–52.
46. Cesne, A.L.; Judson, I.; Maki, R.; Grosso, F.; Schuetze, S.; Mehren, M.V.; Chawla, S.P.; Demetri, G.D.; Nieto, A.; Tanovic, A.; *et al.* Trabectedin is a feasible treatment for soft tissue sarcoma patients regardless of patient age: A retrospective pooled analysis of five phase ii trials. *Br. J. Cancer* **2013**, *109*, 1717–1724.

Marine Low Molecular Weight Natural Products as Potential Cancer Preventive Compounds

Valentin A. Stonik and Sergey N. Fedorov

Abstract: Due to taxonomic positions and special living environments, marine organisms produce secondary metabolites that possess unique structures and biological activities. This review is devoted to recently isolated and/or earlier described marine compounds with potential or established cancer preventive activities, their biological sources, molecular mechanisms of their action, and their associations with human health and nutrition. The review covers literature published in 2003–2013 years and focuses on findings of the last 2 years.

Reprinted from *Mar. Drugs*. Cite as: Stonik, V.A.; Fedorov, S.N. Marine Low Molecular Weight Natural Products as Potential Cancer Preventive Compounds. *Mar. Drugs* **2014**, *12*, 636-671.

1. Introduction

The outstanding biological/biochemical diversity of marine environment serves as a source of inspiration and attracts great interest of chemists and pharmacologists. Some new secondary metabolites of marine origin, produced by diverse marine organisms are important leads for the development of anti-cancer pharmaceuticals. Recent research has also included previously known physiologically active marine natural products, which themselves or their synthetic derivatives are applicable in cancer therapy or cancer prevention [1–8].

The latter involves the employment of natural or synthetic compounds for prevention, suppression or reversion of the process of carcinogenesis [9]. This area is a fast growing scientific field, because cancer prevention is suggested to be a promising way to decrease the number of human cancer cases. Increasing attention is also being paid to the possibility of application of natural products with cancer preventive properties for individuals at the high risk of neoplastic development [10].

The carcinogenic process consists of three phases: initiation, promotion, and progression [11,12]. Initiation and progression are relatively fulminant and irreversible, so promotion is the most appropriate phase for chemoprevention [13,14]. Anti-promotional agents selectively inhibit the process of preneoplastic changes. It often requires the continuous presence of chemopreventive agents [15]. Showing, as a rule, low cytotoxic activities against tumor cells, cancer preventive compounds inhibit the malignant transformation of normal cells into tumor cells, or influence other stages of carcinogenesis [15–18]. Some of them are known antagonists of cancer promoters and oncogenes, others stimulate anticancer immunity, induce apoptosis, or arrest the cell cycle, inhibit tumor invasion, angiogenesis, or inflammation [19–22].

Recent progress in the research of marine anticancer compounds resulted in identification of various molecular targets for chemopreventive drugs, such as indoleamine 2,3-dioxygenase, histone deacetylases and methyl-transferases, matrix metalloproteinases (MMPs), hypoxia-inducible factor-1 (HIF-1), retinoic acid receptor, peroxisome proliferator-activated receptor (PPAR) isoforms,

ubiquitin-proteasome pathway, oncogenic nuclear factors activator protein-1 (AP-1) and nuclear factor-κB (NF-κB), tumor suppressor protein p53-mouse double minute 2 protein (Mdm2) interaction, different tumor-related kinases, *etc.* [23–32].

Natural products are particularly useful as cancer preventive or anticarcinogenic agents if they show good availability, low toxicity, suitability for oral application, and a vast variety of mechanisms of their action. It is believed more and more that cancer may be prevented or at least delayed and inhibited through the use of natural compounds [20]. In fact, there are clear links between human cancer and diet, and seafood is considered to be exclusively useful with respect to cancer prevention.

Herein, we review the studies, mainly published in recent years, on several groups of the marine naturally occurring compounds, which are potentially useful for cancer prevention as can be judged from *in vitro* and/or *in vivo* results. Mostly, these compounds are noncytotoxic, or at least show their anticancer properties at nontoxic concentrations. Our review highlights biological sources, structures and mechanisms of action of the marine lipids, carotenoids, glycosides, terpenoids, alkaloids, and other marine natural products that are currently undergoing evaluation as cancer preventive agents either in laboratories or in clinical trials.

2. Marine Lipids

Many marine edible organisms contain lipids enriched by polyunsaturated fatty acids (PUFAs). Marine ω-3 fatty acids, mainly consisting of eicosapentaenoic (EPA) (**1**, Figure 1) and docosahexaenoic acids (DHA) (**2**, Figure 1), compete in various enzymatic processes with ω-6 polyunsaturated acids such as arachidonic acid. The role played by ω-3 (DHA and EPA) and the ratio of ω-3/ω-6 PUFAs needed to optimally suppress the development of most cancers, including breast, colon, prostate, liver, and pancreatic tumors, were established in many experimental studies [33–35]. The mechanisms by which ω-3 PUFAs are thought to possess antineoplastic activity, as well as preclinical and current clinical trials, investigating the potential therapeutic roles of ω-3 PUFAs at different stages of colorectal carcinogenesis, have been reported [36].

Figure 1. Structures of the compounds **1** and **2**.

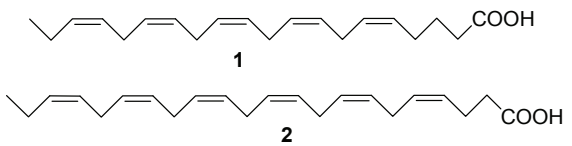

Recently, in a large colonoscopy-based case-control study that involved 5307 Western individuals, the association of dietary PUFA intake and the risk of colorectal polyps were evaluated. It was found that the dietary intake of the marine-derived ω-3 PUFAs was associated with a decreased risk of adenomatous polyps in women, but not in men. For women, higher intake of the marine-derived ω-3 PUFAs was associated with lower levels of prostaglandin E2, which may suggest that the alteration of eicosanoid production is an important mechanism that underlies the chemopreventive effects of the marine- derived ω-3 PUFAs [37].

Another recent study showed that marine ω-3 PUFA ameliorated inflammation, fibrosis, and vascular abnormalities in fat tissue through a decrease in adipose tissue macrophages, an increase in adipose capillaries, and a decrease in macrophage chemoattractant protein 1 (MCP-1) levels [38].

Numerous experiments on animals confirmed the cancer preventive properties of fish oils and ω-3 fatty acids from the marine sources. The chemopreventive effect of ω3 PUFA was evaluated in rats with colorectal cancer, induced via the carcinogen 1,2-dimethylhydrazine (DMH). Lower levels of aberrant crypt foci were found in rats fed with ω3 PUFA. In addition, this group of carcinogen-treated rats showed greater expression of transforming growth factor β and lower interleukin-8 expression, resulting in a protective effect on the colonic precancerous mucosa and a beneficial effect on inflammatory modulation [39]. Using the Fat-1 mice, a genetic model that synthesizes long-chain ω-3 PUFAs *de novo*, it was shown that ω-3 PUFAs can modulate the colonic mucosal microenvironment to suppress Th17 cell accumulation and inflammatory damage following the induction of chronic colitis [40]. The anti-inflammatory properties of ω-6 docosapentaenoic acid derivatives *in vitro* and *in vivo* were demonstrated using murine macrophage RAW 264.7 cells and mice with dextran sodium sulfate (DSS)-induced colitis. Intake of the compounds modulated macrophage function and alleviated the experimental colitis [41]. The regulation of the cellular anti-apoptotic glucose related protein of 78 kDa (GRP78) expression and location have been demonstrated to be a possible route through which DHA can exert pro-apoptotic and antitumoral effects in colon cancer cells [42].

Some other marine lipids also showed potential cancer preventive properties. Monogalactosyldiacylglycerols (MGDGs) **3** and **4** (Figure 2) isolated from the marine microalgae *Tetraselmis chui* were tested for their nitric oxide (NO) inhibitory activity on lipopolysaccharide-induced NO production in RAW264.7 macrophage cells. The compounds showed strong NO inhibitory activity compared to NG-methyl-L-arginine acetate salt, a well known NO inhibitor used as a positive control. Isolated MGDGs suppressed NO production through down-regulation of inducible NO synthase protein [43].

Figure 2. Structures of the compounds **3** and **4**.

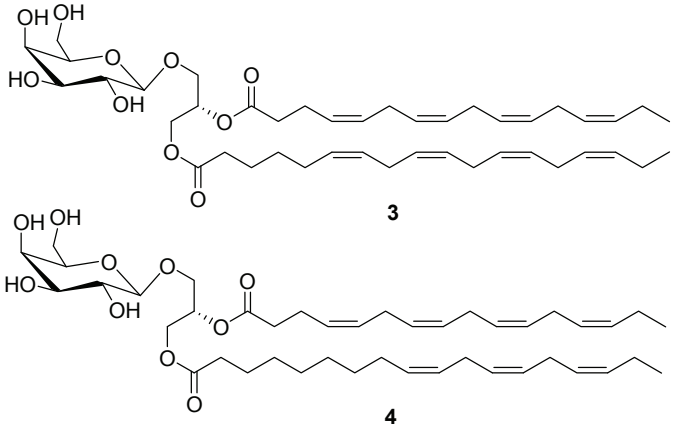

Leucettamol A (**5**, Figure 3), a bipolar lipid that inhibits the formation of the complex composed of the ubiquitin-conjugated E2 enzyme (Ubc13) and ubiquitin-conjugated enzyme variant 1A (Uev1A), was isolated from the marine sponge *Leucetta* aff. *microrhaphis*. Its inhibition of Ubc13-Uev1A interaction was tested by the enzyme-linked immunosorbent assay (ELISA), revealing IC_{50} value of 50 μg/mL. Such inhibitors are presumed to be leads for anti-cancer agents that upregulate activity of the tumor suppressor p53 protein [44]. They may therefore be interesting as the cancer preventive agents.

Figure 3. Structure of the compound **5**.

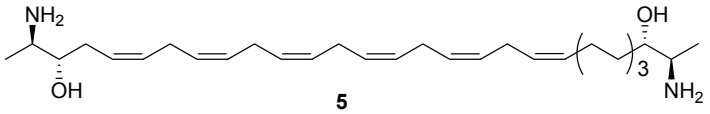

5

Chemical investigation of polar lipids from the marine eustigmatophyte microalga *Nannochloropsis granulata* led to the isolation of six betaine lipid diacylglyceryltrimethylhomoserines (**6**–**11**, Figure 4). The isolated betaine lipids showed dose-dependent nitric oxide (NO) inhibitory activity against lipopolysaccharide-induced nitric oxide production in RAW264.7 macrophage cells. Further study suggested that this activity is exerted by the compounds through downregulation of inducible nitric oxide synthase expression, indicating a possible value as anti-inflammatory agents [45].

Figure 4. Structures of the compounds **6**–**11**.

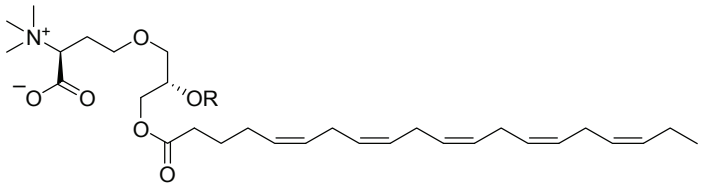

6: R = eicosapentaenoyl
7: R = arachidonoyl
8: R = myristoyl
9: R = palmitoyl
10: R = palmitoleoyl
11: R = linoleoyl

3. Marine Carotenoids

Marine carotenoids are fat-soluble pigments that provide bright coloration to animals and seaweeds. The most common marine carotenoids are: Astaxanthin (**12**, Figure 5), fucoxanthin (**13**, Figure 5), canthaxanthin and related carotenoids (xanthophylls) from salmon, shrimp, mollusks, β-carotene from microalgae and some other marine organisms. All these carotenoids showed anticarcinogenic activities *in vitro* and *in vivo* by interrupting several stages of carcinogenesis including initiation, promotion, progression, and metastasis [46–53]. Astaxanthin demonstrated strong antioxidant properties in the variety of *in vitro* and *in vivo* studies and has a great potential for reducing the burden of human diseases related to oxidative damage. Being the effective radical quencher [54], astaxanthin forms radical cations, which are converted into the stable compound very easily *via* electron transfer from vitamin E [55]. Peroxynitrite ($ONOO^-$), the reactive nitrogen species, was found to induce various forms of cell oxidative damage such as low-density

lipoprotein oxidation, lipid peroxidation, deoxyribonucleic acid (DNA) strand breakage, and nitration of protein tyrosine residues that may lead to tumor-promotion [56]. It was reported that astaxanthin and lutein, a major carotenoid in green algae, could take up peroxynitrite through the formation of 15-nitroastaxanthin and 15-nitrolutein, respectively, thus inhibiting oxidative damage to cells, eventually leading to carcinogenesis [57]. The antioxidant activities of fucoxanthin and its two metabolites, fucoxanthinol and halocynthiaxanthin, were assessed *in vitro* with respect to radical scavenging and singlet oxygen quenching abilities. The 1,1-diphenyl-2-picrylhydrazyl radical scavenging activity of fucoxanthin and fucoxanthinol was higher than that of halocynthiaxanthin, with the effective concentration for 50% scavenging (EC_{50}) being 164, 153, and 826 μM, respectively. Hydroxyl radical scavenging activity as measured by the chemiluminescence technique showed that the scavenging activity of fucoxanthin was 7.9 times higher than that of fucoxanthinol and 16.3 times higher than that of halocynthiaxanthin [58]. Fucoxanthin protection against oxidative stress induced by ultraviolet B (UVB) radiation in human fibroblasts might be applicable in the cosmetic industry [59]. The role of the both major marine carotenoids as dietary antioxidants has been suggested to be one of the main mechanisms underlying their preventive effect against cancer and inflammatory diseases. In addition, it has been demonstrated that fucoxanthin improves insulin resistance and decreases blood glucose level, at least in part, through the downregulation of tumor necrosis factor-α (TNF-α) in white adipose tissue (WAT) of animals [60].

Figure 5. Structures of the compounds **12** and **13**.

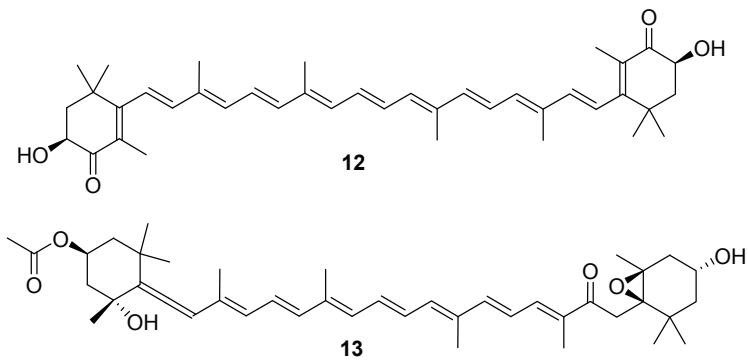

All xanthophylls studied so far are active as inhibitors of cancer cell proliferation *in vitro* and *in vivo*. The inhibitory effect of astaxanthin against inflammation-related mouse colon carcinogenesis and dextran sulfate sodium (DSS)-induced colitis in male imprinting control region (ICR) mice was investigated. Dietary astaxanthin suppressed colitis and colitis-related colon carcinogenesis, partly through inhibition of NF-κB, and downregulation of the messenger ribonucleic acid (mRNA) expression of inflammatory cytokines, including interleukin-1β (IL-1β), interleukin-6 (IL)-6, and cyclooxygenase (COX)-2 [61]. Astaxanthin from the alga *Haematococcus pluvialis* inhibited growth of HCT-116 and HT-29 human colon cancer cells in a dose- and time-dependent manner by arresting cell cycle progression and promoting apoptosis [62].

Fucoxanthin induced apoptosis and cell cycle arrest in human leukemia HL-60, gastric adenocarcinoma MGC-803, LNCap prostate cancer cells, and primary effusion lymphomas [63–66]. Another marine carotenoid, siphonaxanthin from the green algae *Codium fragile* potently induced apoptosis in HL-60 cells. The effective apoptotic activity of siphonaxanthin was observed by increased numbers of terminal deoxynucleotidyl transferase dUTP nick end labeling (TUNEL)-positive cells, and by increased chromatin condensation. This induction of apoptosis was associated with a decreased expression of B-cell lymphoma-2 (Bcl-2) protein and a subsequently increased activation of cysteine-aspartic acid protease-3 (caspase-3) [67].

All the properties of astaxanthin and the related marine carotenoids confirm the potential role for these dietary constituents in cancer prevention or inhibition of carcinogenesis and make astaxanthin and fucoxanthin candidates for further investigation as anticancer agents in humans.

4. Glycosides

Various marine invertebrates such as echinoderms, octocorals and sponges contain steroid and triterpene glycosides. These compounds demonstrate a wide spectrum of biological activities including antitumor and cancer preventive effects both *in vitro* and *in vivo* [68–70]. All the studied sea cucumbers, including edible species, contain physiologically active triterpene glycosides. These substances are ingested as a part of traditional seafood diet all over the world, especially in Asian countries. Although triterpene glycosides are cytotoxic *in vitro*, uptake via the peroral application reduces their toxicity and induces a rather stimulatory action, mainly on the immune system. Immunostimulatory effects of these natural products are observed when very small noncytotoxic doses of the glycosides are used in *in vitro* and *in vivo* experiments. That is why these compounds are considered to be both anticancer and cancer preventive agents, depending on both the dose and the route of administration. Glycosides from distinctive biological sources differ from each other in their structures and activities, although some similarity in their action has also been indicated [69–71].

The patented pharmaceutical lead, named cumaside, was created on the basis of monosulfated cucumariosides from the edible sea cucumber *Cucumaria japonica*. This preparation demonstrates potent immunostimulatory properties and activates the cellular immunity, in particular lysosomal, phagocytic and bactericide activities of macrophages. Being less toxic than glycosides themselves, it retains immunostimulatory activity and showed inhibition of Ehrlich carcinoma cells *in vivo* [72,73]. When cumaside was injected intraperitoneally in mice at a dose of 200 ng/mouse (days—4 and —1 before tumor inoculation), about 40% of animals were without tumor on day 15 after inoculation. Prophylactic treatment with cumaside (using peroral administration) and subsequent application of 5-fluorouracil suppressed tumor growth by 43% [74]. Recently, it was shown that cucumarioside A_2-2 (**14**, Figure 6), one of the main components of cumaside, exhibited a cytostatic effect against Ehrlich carcinoma cells at a subcytotoxic range of concentrations by blocking cell proliferation and DNA biosynthesis in the S phase. It also induced apoptosis in tumor cells in a caspase-dependent way, by-passing the activation of the p53-dependent pathway [75].

Figure 6. Structures of the compounds **14** and **15**.

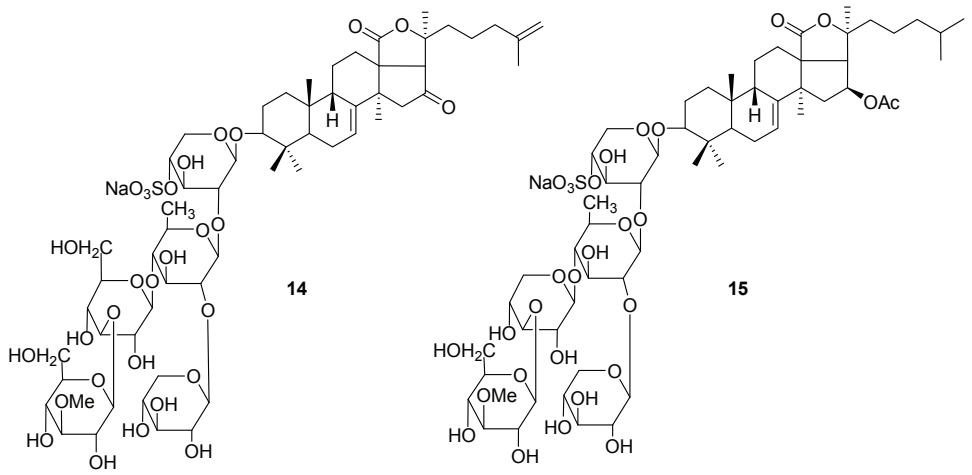

Cucumariosides I2, B2, and A5 isolated from the sea cucumber *Eupentacta fraudatrix* (Djakonov et Baranova) stimulated an increase of the lysosomal activity of mouse peritoneal macrophages of 15%–16% at doses of 1–5 μg/mL. It was demonstrated that this immunostimulatory activity depended on structures of both the aglycone and carbohydrate chains and was not directly correlated to cytotoxic activities of the glycosides [76]. The structures, antitumor and cytotoxic activities against mouse Ehrlich carcinoma cells and mouse splenic lymphocytes, along with hemolytic activities against mouse erythrocytes, and antifungal activities of twenty eight new triterpene glycosides from three species of holothurians, namely *Eupentacta fraudatrix*, *Cladolabes schmeltzii*, and *Actinocucumis typica1*, were recently investigated. The structure-activity relationships of these compounds were also studied [77–82].

As it was recently demonstrated, frondoside A (**15**, Figure 6) from the sea cucumber *Cucumaria okhotensis* and cucumarioside A_2-2 from *C. japonica*, as well as their complexes with cholesterol can be considered as potential inhibitors of multidrug resistance of tumor cells. These substances in non-cytotoxic concentrations blocked the activity of the transmembrane transporter P-glycoprotein of mouse Ehrlich carcinoma cells and prevented an efflux of the fluorescent probe Calcein from the cells [83].

Stichoposide C (STC) isolated from *Thelenota anax* induced apoptosis in human leukemia and colorectal cancer cells in a dose-dependent manner and led to the activation of Fas and caspase-8, cleavage of BH3 interacting-domain death agonist (Bid), mitochondrial damage, and activation of caspase-3. Furthermore, STC activated acid sphingomyelinase (SMase) and neutral SMase, that resulted in the generation of ceramide. Specific inhibition of acidic SMase or neutral SMase and siRNA knockdown experiments partially blocked STC-induced apoptosis. Moreover, STC markedly reduced tumor growth of HL-60 xenograft and mouse colon adenocarcinoma CT-26 subcutaneous tumors and increased ceramide generation *in vivo*. It was therefore concluded that STC may have therapeutic relevance for human leukemia and colorectal cancer [84].

5. Terpenoids

Cembrane diterpenoids and their semisynthetic derivatives attracted attention as the potential anticarcinogenic agents. The most intensively investigated cembrane diterpenoid sarcophytol A (Sarc A) (**16**, Figure 7) with the 14-membered ring from the soft coral *Sarcophyton glaucum* inhibited tumor promotion induced by okadaic acid [85], teleocidin [86], and 12-*O*-tetradecanoylphorbol-13-acetate (TPA) [87]. Sarc A inhibited TPA-induced invasion of neutrophils, their levels of myeloperoxidase, and DNA oxidation in the epidermis of sensitive to carcinogenesis (SENCAR) mice exposed to TPA [88]. Inhibition of oxidative stress induced by TPA in human cervix adenocarcinoma HeLa cells led to a 50% decrease in H_2O_2 levels when Sarc A was used at a concentration of 75 μM [89]. Nude mice with transplanted human pancreatic cancer cells were fed with a diet containing 0.01% Sarc A. On day 29 after transplantation, tumor volume was significantly smaller in the Sarc A group than in the control group [90]. Sarc A also inhibited methylnitrosourea-induced large bowel-cancer in rats and the development of spontaneous hepatomas in mice [91,92].

Recently, a chemical investigation of an ethyl acetate extract of the Red Sea soft coral *Sarcophyton glaucum* has led to the isolation of five cembranoids **17**–**21** (Figure 7). These compounds were found to be the inhibitors of cytochrome P450 1A activity as well as the inducers of glutathione *S*-transferases (GST), quinone reductase (QR), and epoxide hydrolase (mEH), establishing potential modes of action with regards to cancerpreventive activity of these agents [93].

Figure 7. Structures of the compounds **16**–**21**.

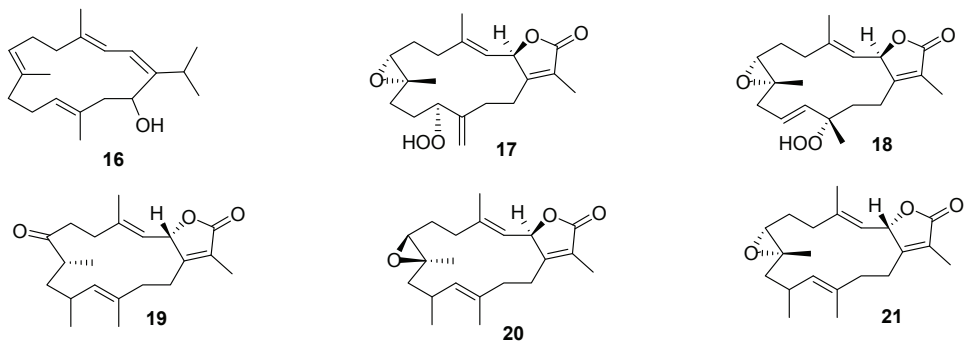

Sesterterpenoid luffariellolide (**22**, Figure 8) isolated earlier from the marine sponge *Luffariella* sp. [94], was uncovered as a novel agonist for retinoic acid receptors by inducing co-activator binding to these receptors *in vitro*, further inhibiting cell growth and regulating RAR target genes in various cancer cells [95]. Triterpenoid stellettin A (**23**, Figure 8), obtained from the marine sponge *Geodia japonica*, inhibited the growth of B16 murine melanoma cells by the induction of endoplasmic reticulum stress, abnormal protein glycosylation and autophagy [96]. Cadinane-type sesquiterpene **24** (Figure 8), isolated from the marine-derived fungus *Hypocreales* sp. strain HLS-104, associated with the sponge *Gelliodes carnosa*, showed moderate anti-inflammatory

activity in lipopolysaccharide (LPS)-treated RAW264.7 cells with an average maximum inhibition (E_{max}) value of 10.22% at the concentration of 1 μM [97].

Figure 8. Structures of the compounds **22**–**24**.

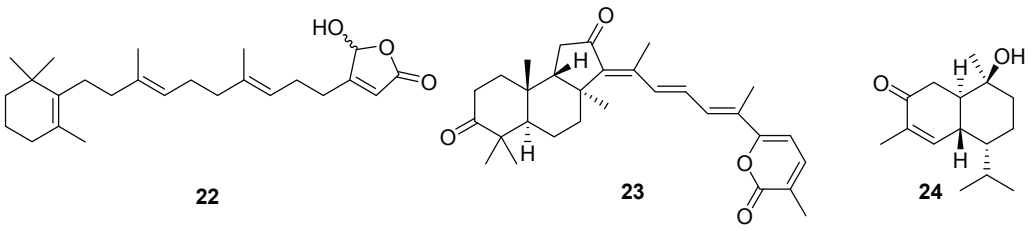

A chemical study on the alga *Cystoseira usneoides* has led to the isolation of twelve meroterpenoids. In antioxidant assays, meroterpenes **25**–**32** (Figure 9) exhibited radical-scavenging activity. In anti-inflammatory assays, usneoidone *Z* (**31**) and its 6*E* isomer (**32**) showed significant activities as inhibitors of the production of the proinflammatory cytokine tumor necrosis factor-α (TNF-α) in LPS-stimulated THP-1 human macrophages [98].

Figure 9. Structures of the compounds **25**–**34**.

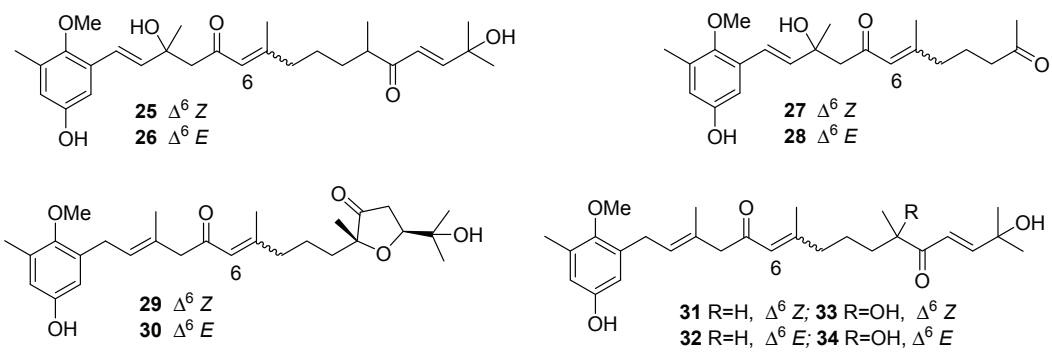

Ansellone B (**35**) and phorbasone A acetate (**36**) (Figure 10), isolated from the Korean marine sponge *Phorbas* sp., exhibited potent inhibitory activity on nitric oxide production in RAW 264.7 LPS-activated mouse macrophage cells with IC_{50} values of 4.5 and 2.8 μM, respectively. In particular, ansellone B showed a favorable selectivity index (SI) of 3.8, which is indicative of its inducible isoform nitric oxide synthase (iNOS) inhibitory activity without significant cytotoxicity [99].

Metachromins are a series of sesquiterpenoid quinones with an amino acid residue isolated from Okinawan marine sponges. Metachromins L–Q (**37**–**42**, Figure 11) showed inhibitory activities against receptor tyrosine kinases HER2 with an IC_{50} in the range from 18 to 190 μg/mL [100].

Figure 10. Structures of the compounds **35** and **36**.

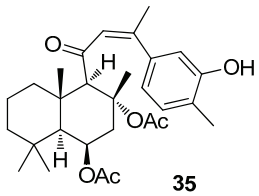

35

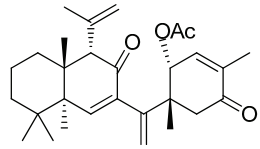

36

Figure 11. Structures of the compounds **37**–**42**.

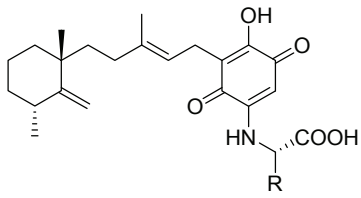

37 R = H; **38** R =  ; **39** R = 

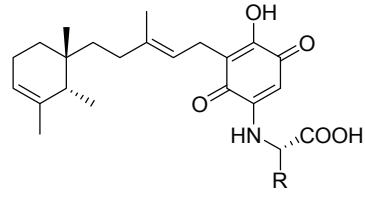

40 R = H; **41** R =  ; **42** R = 

Nine unusual isomalabaricane-type triterpenoids with new skeletons in respect to the unprecedented side chains, namely globostelletins J–R (**43**–**51**, Figure 12) were isolated from the marine sponge *Rhabdastrella globostellata*. All compounds were tested for their inhibitory activities against a profile of human tumor-related protein kinases and showed moderate inhibition against the protein kinases ALK (anaplastic lymphoma kinase), FAK (focal adhesion kinase), Aurora-B (serine/threonine kinase), IGF-1R (insulin-like growth factor receptor-1), SRC (proto-oncogene tyrosine-protein kinase), and VEGF-R2 (vascular endothelial growth factor receptor 2) [101].

6. Alkaloids

The known marine alkaloid aaptamine (**52**, Figure 13) and related compounds **53**–**60** (Figure 13) from the sponge *Aaptos* sp. were shown to inhibit epidermal growth factor (EGF)-induced malignant transformation of mouse epidermal JB6 $P^{+}Cl41$ cells, to possess potent antioxidant properties, and to induce apoptosis in human cancer cells. It was therefore suggested that these agents possess cancer preventive properties [102–104]. Recently, the mechanisms of anticancer action of the aaptamine derivatives have become somewhat clearer. Dyshlovoy *et al.* analyzed the effects of aaptamine and its derivatives on the proliferation and protein expression of the pluripotent human embryonal carcinoma cell line NT2. Effects on cell cycle and induction of apoptosis were also analyzed. At lower concentrations, including the IC_{50} of 50 μM, aaptamine treatment resulted in a G2/M arrest, whereas at higher concentrations, induction of apoptosis was observed. Proteomic screening revealed that aaptamine treatment of NT2 cells at the IC_{50} for 48 h resulted in an alteration of 10 proteins. Interestingly, these studies identified the posttranslational hypusine modification of the eukaryotic translation initiation factor 5A-1 (eIF5A) as a prominent

target of aaptamine action [105]. It was also shown that aaptamine and its derivatives 9-demethyl(oxy)aaptamine (**56**, Figure 13) and isoaaptamine (**53**, Figure 13) were equally effective as anti-cancer agents in cisplatin-sensitive and -resistant germ cell tumour cells [106]. Again, proteomic profiling was performed, and identified several altered proteins when cisplatin-resistant embryonal carcinoma cells NT2-R were treated with compounds **52**, **53**, and **56** at the corresponding IC_{50}.

Figure 12. Structures of the compounds **43**–**51**.

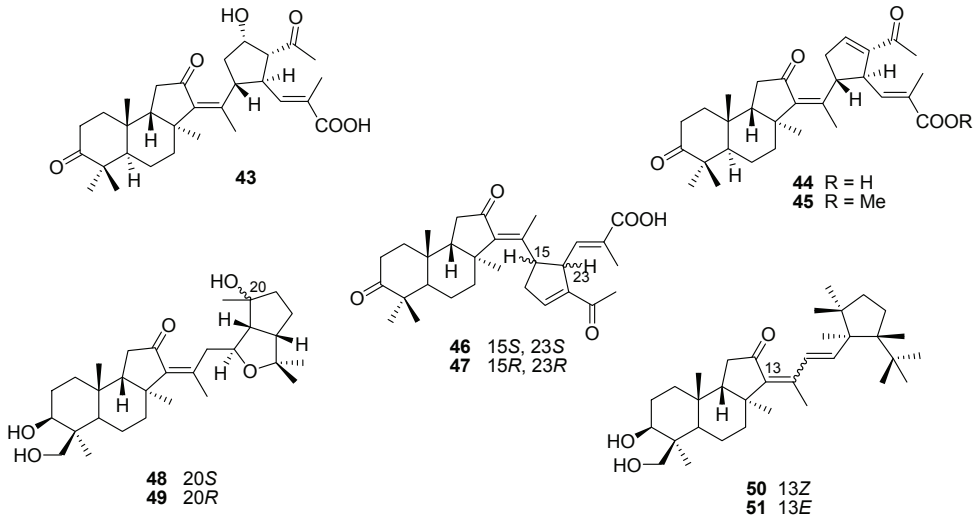

Figure 13. Structures of the compounds **52**–**60**.

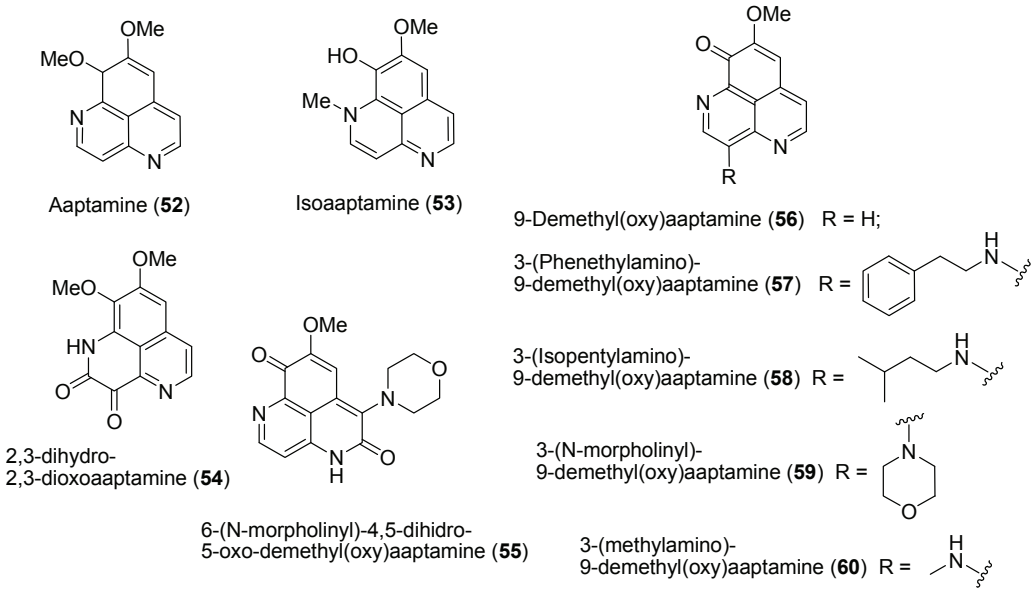

Treatment of lymphoma U937 cells with pentacyclic alkaloids, papuamine and haliclonadiamine (**61** and **62**, Figure 14), isolated from an Indonesian marine sponge *Haliclona* sp., resulted in accumulation of cells in the sub-G1 phase, and induced a condensation of chromatin and fragmentation of nucleus [107]. Streptocarbazole A (**63**, Figure 14), isolated from the marine-derived actinomycete strain *Streptomyces* sp., arrested the cell cycle of HeLa cells in the G2/M phase at the noncytotoxic concentration of 10 μM [108].

Figure 14. Structures of the compounds **61**–**63**.

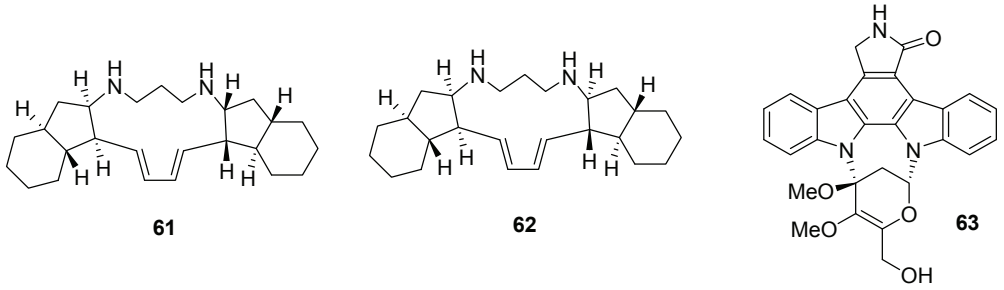

Bengamides **64**–**69** (Figure 15), isolated from two disparate sources, *Myxococcus virescens* (bacterium) and *Jaspis coriacea* (sponge) was shown to be a new class of immune modulators exerting their activity through the inhibition of NF-κB without exerting cytotoxicity in RAW264.7 macrophage immune cells. Western blot and qPCR analysis indicated that bengamides A and B reduce the phosphorylation of nuclear factor of κ light polypeptide gene enhancer in B-cells inhibitor α (IκBα) and the LPS-induced expression of the proinflammatory cytokines/chemokines TNFα, IL-6 and monocyte chemoattractant protein-1 (MCP-1), but do not affect NO production or the expression of iNOS [109].

Figure 15. Structures of bengamides **64**–**69** and their effects on the NF-κB activity.

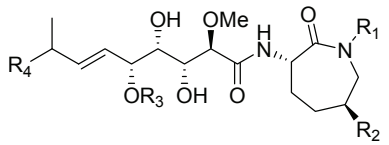

Compound	R_1	R_2	R_3	R_4	NF-κB Inhibition (IC_{50}, μM)
Bengamide A (**64**)	H	$OC(CH_2)_{12}CH_3$	H	Me	0.075
Bengamide B (**65**)	Me	$OC(CH_2)_{12}CH_3$	H	Me	0.085
Bengamide E (**66**)	H	H	H	Me	7.5
Bengamide F (**67**)	Me	H	H	Me	0.7
Bengamide E′ (**68**)	H	H	H	CH_2CH_3	2.0
Bengamide F′ (**69**)	Me	H	H	CH_2CH_3	2.0

New macrocyclic pyrrole alkaloids densanins A and B (**70** and **71**, Figure 16) were isolated from the sponge *Haliclona densaspicula*. The compounds showed relatively potent inhibitory effects on lipopolysaccharide-induced nitric oxide production in BV2 microglial cells, with IC_{50}

values of 1.05 and 2.14 μM, respectively [110]. β-Carboline alkaloid, variabine B (**72**, Figure 16), was isolated from the Indonesian marine sponge *Luffariella variabilis*. The compound inhibited chymotrypsin-like activity of the proteasome and Ubc13 (E2)–Uev1A interaction with IC_{50} values of 4 and 5 μg/mL, respectively [111].

The components of the ubiquitin–proteasome system like ubiquitin-specific-processing protease 7 (USP7) have become attractive structures for the development of anticancer agents. USP7, a deubiquitylating enzyme hydrolyzing the isopeptide bond at the *C*-terminus of ubiquitin, is an emerging cancer target. USP7 inhibitors stabilize p53 in cells through degradation of Hdm2 (also known as MDM2), which subsequently results in the suppression of cancer. Spongiacidin C (**73**, Figure 16) isolated from the marine sponge *Stylissa massa* is the first USP7 inhibitor obtained from a natural source. This compound inhibited USP7 with an IC_{50} of 3.8 μM [112].

Figure 16. Structures of the compounds **70**–**73**.

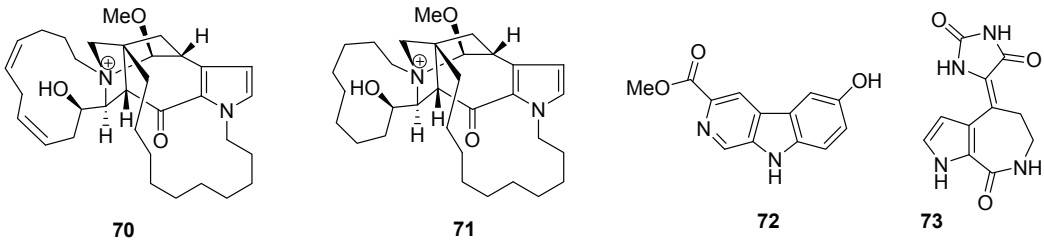

7. Other Low Molecular Weight Marine Natural Compounds

Some other marine natural products, isolated from invertebrates, algae and microorganisms showed cancer preventive activities, mainly *in vitro*. For example, C_{11} cyclopentenone, 5-hydroxy-7-prop-2-en-(*E*)-ylidene-7,7*a*-dihydro-2*H*-cyclopenta[*b*]-pyran-6-one (**74**, Figure 17), isolated from a sponge and ascidians, inhibited EGF-induced neoplastic JB6 Cl41 P^+ cell transformation in soft agar, and induced apoptosis of HL-60 and THP-1 human leukemia cells [113].

Figure 17. Structures of the compounds **74**–**76**.

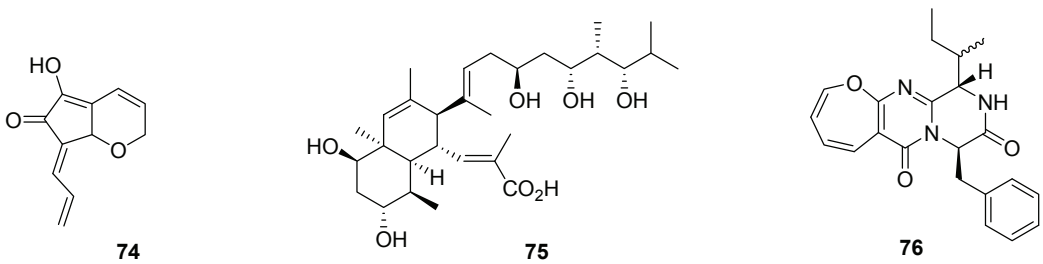

The highly hydroxylated polyketide nahuoic acid A (**75**, Figure 17), produced in culture by a *Streptomyces* sp. obtained from a marine sediment, is a selective S-adenosylmethionine (SAM) competitive inhibitor of the histone methyltransferase SETD8 *in vitro* [114]. SETD8 is

overexpressed in various types of cancer, and aberrant monomethylation by SETD8 may lead to human carcinogenesis [115]. A new oxepin-containing diketopiperazine-type compound protuboxepin A (**76**, Figure 17), binds to α, β-tubulin heterodimers, and accelerates tubulin polymerization *in vitro*, resulting in chromosome misalignment and metaphase arrest which leads to apoptosis in tumor cells [116].

Mycalamide A (**77**, Figure 18), isolated from sponges and known as a protein synthesis inhibitor at nanomolar concentrations, inhibits EGF-induced neoplastic transformation and induces caspase-3-dependent apoptosis of mouse JB6 Cl41 P^+ cells. The compound also inhibits transcriptional activity of oncogenic AP-1 and NF-κB nuclear factors [117].

Figure 18. Structures of the compounds **77**–**80**.

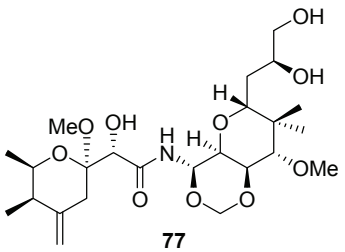

77

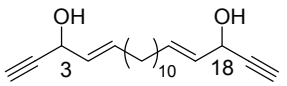

78 (-)-3R,18R
79 (+)-3S,18S

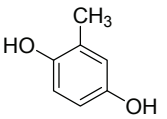

80

Two enantiomeric C-20 bisacetylenic alcohols **78**; **79** (Figure 18) were isolated from a marine sponge *Callyspongia* sp. as a result of screening of antilymphangiogenic agents from marine invertebrates. Both compounds showed inhibition of the capillary-like tube formation of temperature-sensitive rat lymphatic endothelial from thoracic duct (TR-LE) cells [118].

Toluquinol (**80**, Figure 18), a methylhydroquinone produced by a marine fungus, was selected in the course of an unselected screening for new potential inhibitors of angiogenesis. The compound demonstrated antiangiogenic effects both *in vitro* and *in vivo* that were exerted partly by suppression of the VEGF and FGF-induced cytosolic protein kinase Akt activation of endothelial cells [119].

The tricyclic peptides neopetrosiamides A and B, isolated from the marine sponge *Neopetrosia* sp., differ in the stereochemistry of the methionine sulfoxide. They are potential antimetastatic agents that prevent tumour cell invasion by inhibition of both amoeboid and mesenchymal migration pathways [120].

Pterocidin (**81**, Figure 19), a linear polyketide with a δ-lactone terminus, was rediscovered from a *Streptomyces* strain of a marine sediment-origin and was found to exhibit potent anti-invasive activity at non-cytotoxic concentrations. The invasion of murine colon 26-L5 carcinoma cells across a matrigel-fibronectin membrane was inhibited by pterocidin at an IC_{50} value of 0.25 μM, whereas the cytotoxicity was not apparent upon treatment with concentrations up to 7 μM [121].

Sungsanpin (**82**, Figure 19) from a *Streptomyces* species, isolated from deep-sea sediment, displayed inhibitory activity in a cell invasion assay using the human lung cancer cell line A549 [122]. Agelasine B (**83**, Figure 19), a compound purified from the marine sponge *Agelas clathrodes*, induced fragmentation of DNA, reduced the expression of Bcl-2, and was able to activate caspase 8

in MCF-7 human breast cancer cells [123]. Alterporriol L (**84**, Figure 19), a new bianthraquinone derivative, was isolated from the marine fungus *Alternaria* sp. The reactive oxygen species, mitochondrial membrane potential, and cytosolic free calcium level in MCF-7 breast cancer cells were changed after treatment with alterporriol L, suggesting that alterporriol L plays a vital role in cancer cells through destroying the mitochondrial potential and inducing apoptosis [124].

Figure 19. Structures of the compounds **81**–**84**.

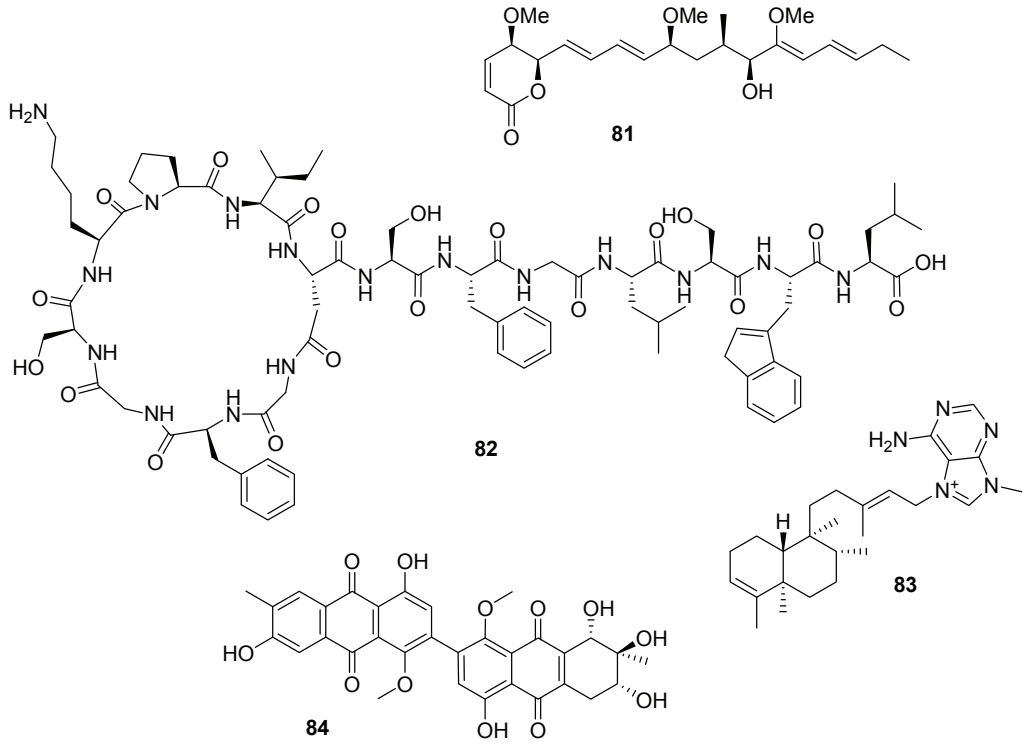

Marine macrolides aplyronine A and mycalolide B (**85** and **86**, Figure 20) were shown to induce apoptosis in human leukemia HL60 cells and human epithelial carcinoma HeLa S3 cells [125].

Figure 20. Structures of the compounds **85** and **86**.

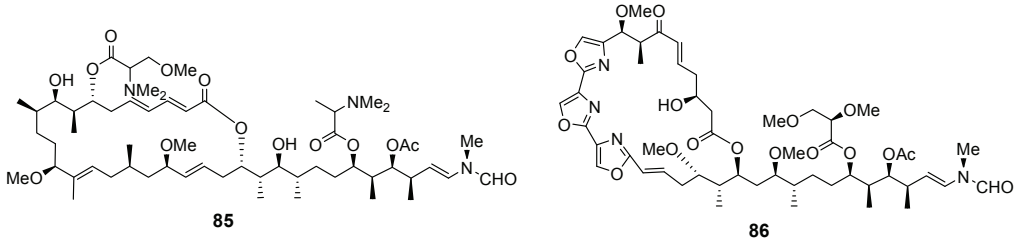

Biselyngbyaside (**87**), biselyngbyolide A (**88**), and biselyngbyaside B (**89**) (Figure 21), isolated from the marine cyanobacterium *Lyngbya* sp., induced apoptosis and increased cytosolic Ca^{2+} concentration in human cancer HeLa S_3 and HL60 cells [126].

Dieckol (**90**, Figure 21), a nutrient polyphenol compound from the brown alga *Ecklonia cava,* inhibited migration and invasion of human fibrosarcoma HT1080 cells by scavenging intracellular reactive oxygen species (ROS). Dieckol treatment also decreases complex formation of focal adhesion kinase (FAK)-proto-oncogene tyrosine-protein kinase Src-p130 Crk-associated substrate (p130Cas) and expression of MMP2, 9, and 13 [127].

Figure 21. Structures of the compounds **87**–**90**.

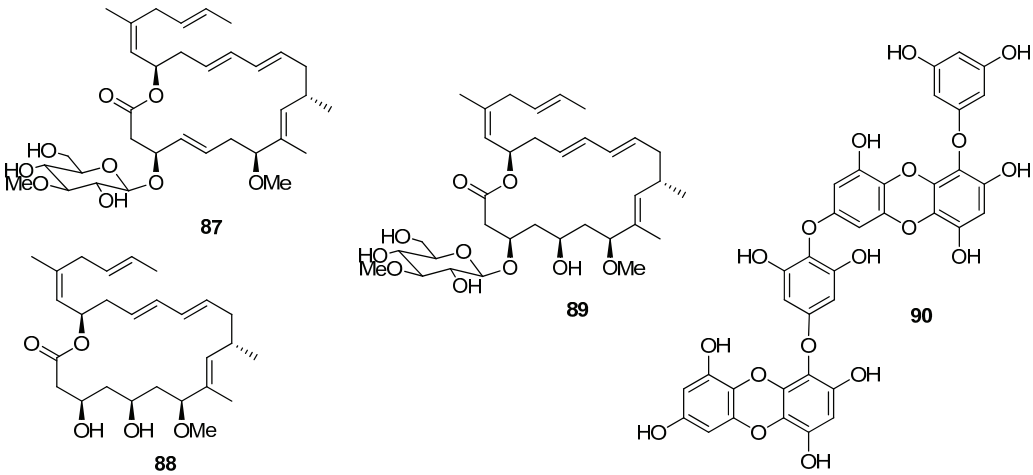

Palmadorin M (**91**, Figure 22), isolated from the Antarctic nudibranch *Austrodoris kerguelenensis,* inhibited Janus kinase 2 (Jak2), signal transducer and activator of transcription 5 (STAT5), and extracellular signal-regulated kinase 1/2 (Erk1/2) activation in human erythroleukemia HEL cells and caused apoptosis at a concentration of 5 μM [128].

Thienodolin (**92**, Figure 22), isolated from a *Streptomyces* sp. derived from Chilean marine sediment, inhibited nitric oxide production in LPS-stimulated RAW 264.7 cells (IC_{50} = 17.2 ± 1.2 μM). At both the mRNA and protein levels, inducible nitric oxide synthase (iNOS) was suppressed in a dose dependent manner. The compound blocked the degradation of IκBα, resulting in an inhibition of NF-κB p65 nuclear translocation, and inhibited the phosphorylation of the signal transducer and activator of transcription (STAT1) at Tyr701 [129].

Two new merohexaprenoids, halicloic acids A and B (**93** and **94**, Figure 22), have been isolated from the marine sponge *Haliclona (Halichoclona)* sp., collected in the Philippine waters. The compounds showed inhibition of indoleamine 2,3-dioxygenase (IDO) at 10 and 11 μM, respectively [130].

Figure 22. Structures of the compounds **91**–**94**.

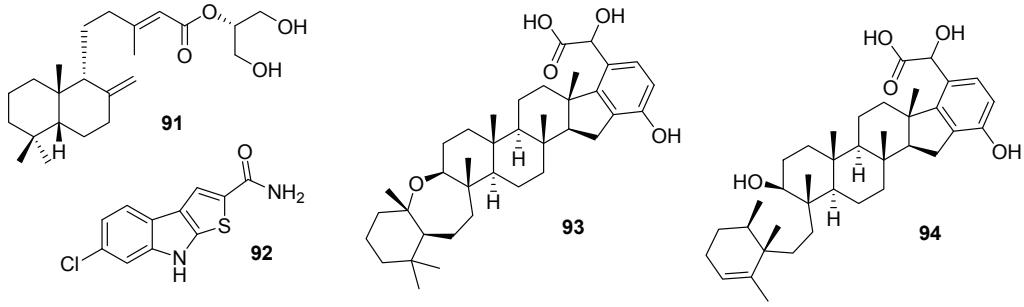

Polyketides coibacins **95**–**98** (Figure 23), isolated from a Panamanian marine cyanobacterium cf. *Oscillatoria* sp., were tested for anti-inflammatory activity in a cell-based nitric oxide (NO) inhibition assay. In this assay, coibacin B (**96**) was determined to be the most active of these natural compounds. Coibacin A (**95**) significantly reduced gene transcription of four cytokines (TNF-R, IL-6, IL-1β, and iNOS), with especially notable effects on IL-1β and iNOS, at a concentration of 10 μg/mL. Using ELISA, changes in protein expression for some of these inflammatory cytokines were measured in murine RAW264.7 cells stimulated with lipopolysaccharide (LPS) in the absence or presence of the coibacins. Coibacin A (**95**) at 10 μg/mL was found to significantly reduce TNF-R and IL-6 secretion. Coibacins B-D (**96**–**98**) also affected protein expression of TNF-R and IL-6, albeit to a lesser extend [131].

Figure 23. Structures of the compounds **95**–**98**.

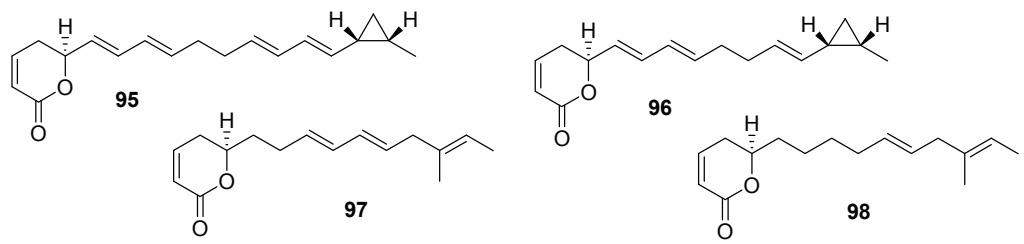

Five new cyclopeptides, perthamides G-K (**99**–**103**, Figure 24), were isolated from the polar extract of the marine sponge *Theonella swinhoei*. Pharmacological analysis demonstrated that these natural cyclopeptides are endowed with anti-inflammatory potential, as assessed by their ability to reduce carrageenan-induced mouse paw oedema [132].

Figure 24. Structures of the compounds **99**–**103**.

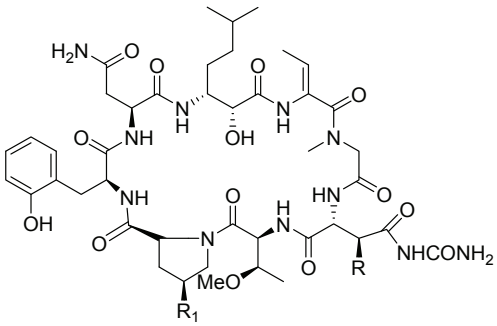

99 R = OSO_3Na R_1 = H
100 R = OH R_1 = CH_3

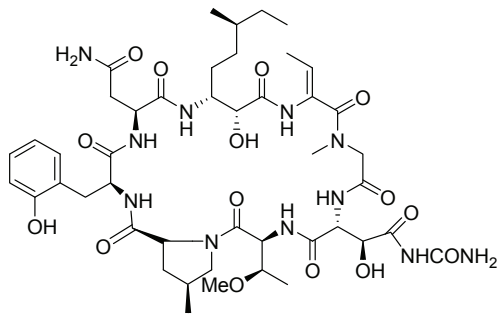

101

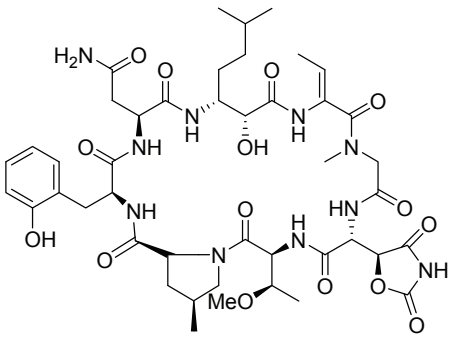

102

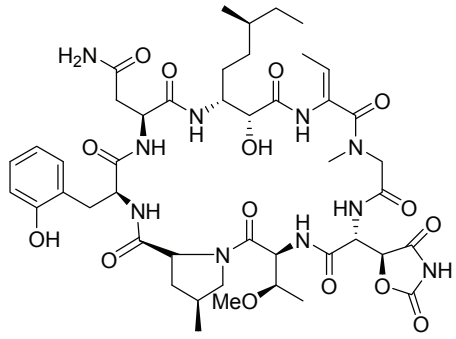

103

New elastase inhibitors symplostatins 5–9 (**104**–**109**, Figure 25) were isolated from red cyanobacterium collected from Cetti Bay, Guam. Symplostatin 5 (**104)** was shown to attenuate the downstream cellular effects of elastase in an epithelial lung airway model system, alleviating clinical hallmarks of chronic pulmonary diseases such as cell death, cell detachment, and inflammation. This compound attenuated the effects of elastase on receptor activation, proteolytic processing of the inter-cellular adhesion molecule-1 (ICAM-1), NF-κB activation, and transcriptomic changes, including the expression of pro-inflammatory cytokines IL1A, IL1B, and IL8 [133].

Figure 25. Structures of the compounds **104**–**109**.

	R_1	R_2	R_3	R_4
Symplostatin 5 (**104**)	Et	H	Me	SO3Na
Symplostatin 6 (**105**)	Me	H	Me	SO3Na
Symplostatin 7 (**106**)	Et	H	Et	SO3Na
Symplostatin 8 (**107**)	Et	OH	Me	SO3Na
Symplostatin 9 (**108**)	Me	OH	Me	SO3Na
Symplostatin 10 (**109**)	Et	OH	Et	SO3Na

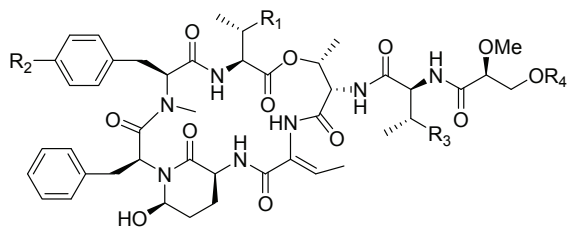

Flexibilisquinone (**110**, Figure 26), isolated from the cultured soft coral *Sinularia flexibilis*, originally distributed in the waters of Taiwan, was found to inhibit the accumulation of the pro-inflammatory iNOS and cyclooxygenase-2 (COX-2) proteins of LPS-stimulated RAW264.7 macrophage cells [134]. Compound **111** (Figure 26), isolated from the marine-derived fungus *Hypocreales* sp. strain HLS-104, isolated from a sponge *Gelliodes carnosa*, was effective against the nitric oxide (NO) production in lipopolysaccharide (LPS)-treated RAW264.7 cells and showed moderate inhibition with E_{max} values of 26.5% at a concentration of 1 μM [97].

Mycoepoxydiene (MED) (**112**, Figure 26) is a polyketide isolated from the marine fungal strain *Diaporthe* sp. HLY-1. MED induced DNA damage through the production of reactive oxygen species (ROS), which resulted in the phosphorylation of H2A histone family memeber X (H2AX) and the activation of the Ataxia telangiectasia mutated kinase (ATM) and p53 signaling pathways. In addition, MED increased the accumulation of IkBα and enhanced the association between IκB kinase γ (IKKγ) and heat shock protein 27 (Hsp27) via the activation of Hsp27, which eventually resulted in the inhibition of TNF-α-induced NF-κB transactivation [135].

Figure 26. Structures of the compounds **110**–**113**.

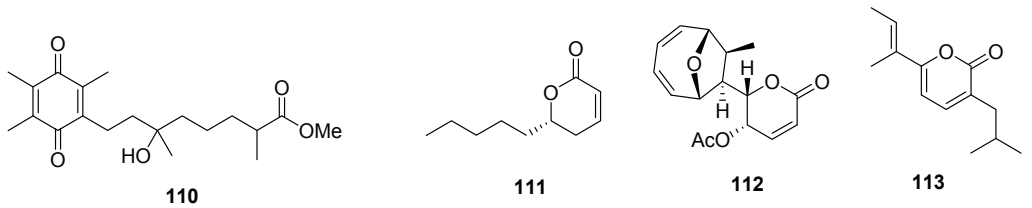

Nocapyrone H (**113**, Figure 26) isolated from the marine actinomycete *Nocardiopsis* sp. KMF-001 reduced the pro-inflammatory factors such as nitric oxide (NO), prostaglandin E-2 (PGE(2)) and interleukin-1 β (IL-1 β). Moreover, nocapyrone H showed a 5.8% stronger inhibitory effect on NO production than chrysin at a concentration of 10 μM in lipopolysaccharide (LPS)-stimulated BV-2 microglial cells [136].

Bis-*N*-norgliovictin (**114**, Figure 27), a small molecule, isolated during the screening of natural products against inflammation from the culture broth of a marine derived fungus named S3-1-c, significantly inhibited LPS (ligand of toll-like receptor 4 (TLR4))-induced TNF-α production in RAW264.7 cells. In this cell line and in mouse peritoneal macrophages, bis-*N*-norgliovictin inhibited LPS-induced production of TNF-α, IL-6, interferon-β (IFN-β) and monocyte chemoattractant protein (MCP-1) in a dose-dependent manner, without suppressing cell viability. The anti-inflammatory effect was attributed to the down-regulation of the TLR4-triggered myeloid differentiation primary response protein 88 (MyD88) and TIR-containing adapter inducing interferon-β (TRIF) signaling pathways, including p38 and c-Jun *N*-terminal kinase (JNK) of mitogen-activated protein kinases (MAPKs), NF-κB, and interferon regulatory factor 3 (IRF3) cascades. Importantly, bis-*N*-norgliovictin also protected mice against LPS-induced endotoxic shock [137].

Biochemical characterization of a library of 13 oxygenated polyketides isolated from the marine sponge *Plakinastrella mamillaris* led to the discovery of gracilioethers B and C, and plakilactone C (**115**, **116**, and **117**, Figure 27) as selective PPARγ ligands in transactivation assays [138]. PPAR ligands activated PPAR signaling and exerted cancer-preventive and cytotoxic effects *in vitro* and/or *in vivo* [31].

Figure 27. Structures of the compounds **114**–**117**.

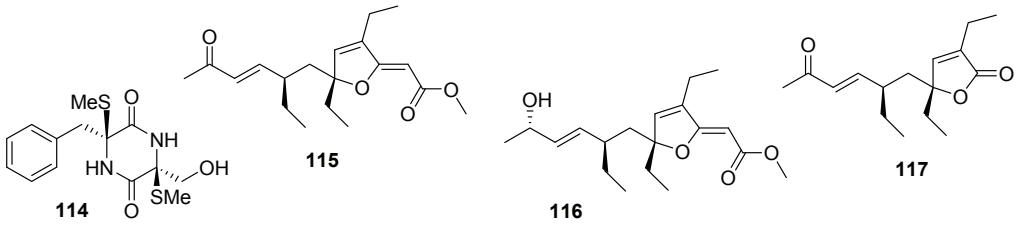

Isoindole pseudoalkaloid conioimide (**118**, Figure 28) and the polyketide cereoanhydride (**119**, Figure 28) were isolated from the fungus *Coniothyrium cereale* isolated from the Baltic Sea alga *Enteromorpha* sp. Conioimide has prominent and selective inhibitory activity towards the protease human leukocyte elastase (HLE), an enzyme involved in many inflammatory diseases, with an IC_{50} value of 0.2 μg/mL, whereas cereoanhydride showed weaker inhibition (IC_{50} = 16 μg/mL) [139].

Figure 28. Structures of the compounds **118**–**121**.

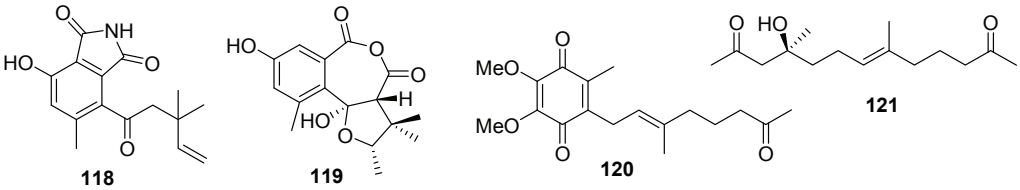

A ubiquinone derivative, pseudoalteromone A (**120**, Figure 28), possessing a 9C nor-monoterpenoid moiety, and a 15C compound, pseudoalteromone B (**121**, Figure 28), were obtained from the marine bacterium *Pseudoalteromonas* sp. CGH2XX, originally isolated from a cultured-type octocoral *Lobophytum crassum*. Pseudoalteromones A and B exhibited anti-inflammatory activity through inhibitory effects (inhibition rates 45.1% and 20.7%, correspondingly) on the release of elastase by human neutrophils at a concentration of 10 μg/mL [140,141].

Two dimeric sterols, manadosterols A and B (**122** and **123**, Figure 29), were isolated from the marine sponge *Lissodendryx fibrosa* collected in Indonesia. The compounds inhibited the Ubc13-Uev1A interaction with IC_{50} values of 0.09 and 0.13 μM, respectively [142] They are the second and third natural compounds showing inhibitory activities against the Ubc13–Uev1A interaction and are more potent than leucettamol A (IC_{50}, 106 μM), the first such inhibitor, isolated from another marine sponge [44].

Figure 29. Structures of the compounds **122** and **123**.

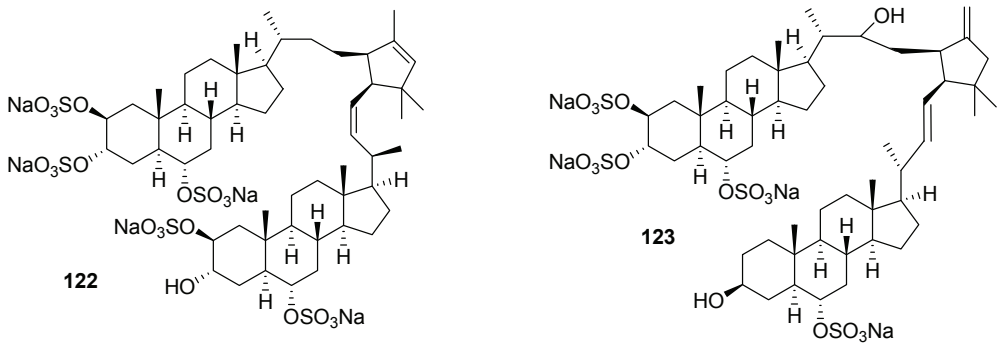

The symmetrical disulfide psammaplin A (**124**, Figure 30) was isolated from the marine sponge *Pseudoceratina* sp. and could be interesting for treatment approaches targeting epigenetic alterations, since it showed potent inhibition of histone deacetylases (HDAC, IC_{50} 4.2 ± 2.4 nM) [143]. The psammaplin-derived thiol (**125**, Figure 30) exhibited potent activity against histone deacetylases in a low nanomolar range, but showed low cytotoxicity [144]. Five HDAC1 inhibitors, trichostatin A (**126**, Figure 30) and its analogues trichostatic acid, JBIR-109, JBIR-110, and JBIR-111 (**127**–**130**, Figure 30) were isolated from the culture of the marine sponge-derived *Streptomyces* sp. strain RM72. The IC_{50} values against HDAC1 of **126**–**130** were 0.012, 73, 48, 74, and 57 μM, respectively [145].

Figure 30. Structures of the compounds **124**–**130**.

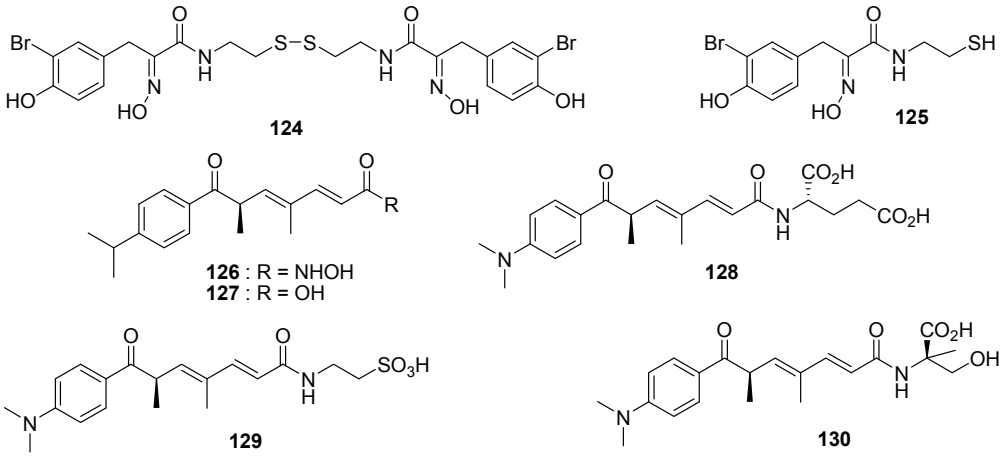

Ten extracts from various marine sponges were identified as containing inhibitors of the transcription factor HIF-2α which has been shown to play a distinct role in tumorigenesis. Chemical exploration of these sponge extracts led to isolation of seven specific HIF inhibitors, compounds **131**–**136** (Figure 31) and haliclonadiamine (**62**) [146].

Figure 31. Structures of the compounds **131**–**136**.

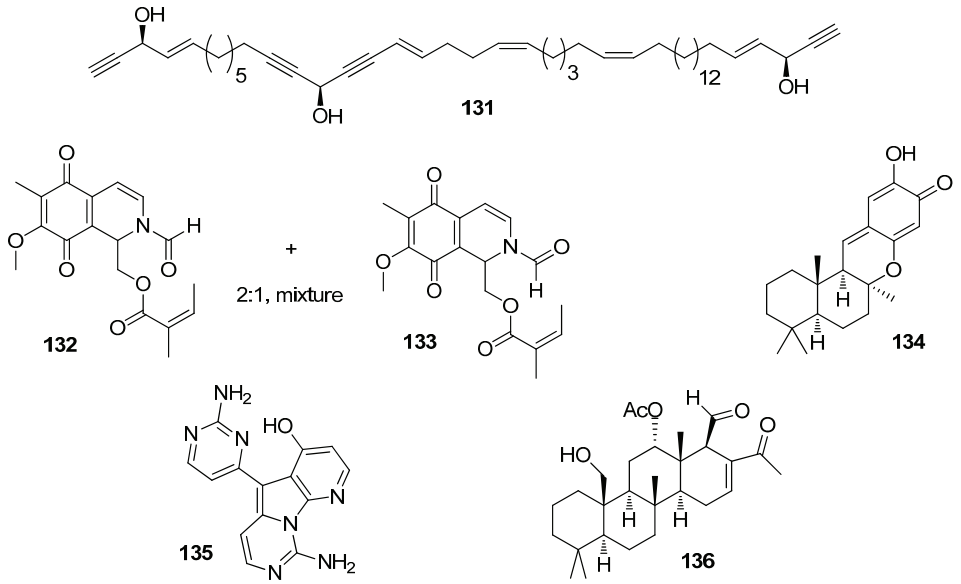

The organic extract of a marine sponge, *Petrosia alfiani*, selectively inhibited iron chelator-induced hypoxia-inducible factor-1 (HIF-1) activation in a human breast tumor T47D cell-based reporter assay. Bioassay-guided fractionation yielded seven xestoquinones **137**–**143** (Figure 32). Among them, compounds **141** and **142**, which possess a 3,4-dihydro-2*H*-1,4-thiazine-1,1-dioxide moiety, potently and selectively inhibited HIF-1 activation in T47D cells, each with an IC_{50} value of 0.2 μM, whereas other compounds showed IC_{50} in the range of 1.2 to 30 μM [147].

Figure 32. Structures of the compounds **137**–**143**.

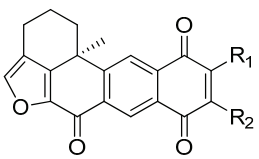

137 R_1 = H; R_2 = CH_2OH
138 R_1 = CH_2OH; R_2 = H
139 R_1 = H; R_2 = H

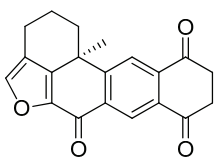

140

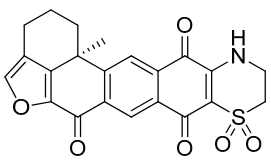

141

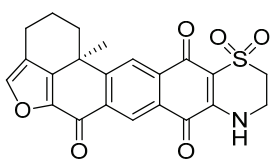

142

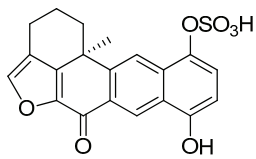

143

Gliotoxin-related compounds **144**–**147** (Figure 33), containing a disulfide or tetrasulfide bond, were isolated from the fungus *Penicillium* sp. strain JMF034, obtained from deep sea sediments of Suruga Bay, Japan. They showed inhibitory activity against histone methyltransferase (HMT) G9a [148].

Figure 33. Structures of the compounds **144**–**147**.

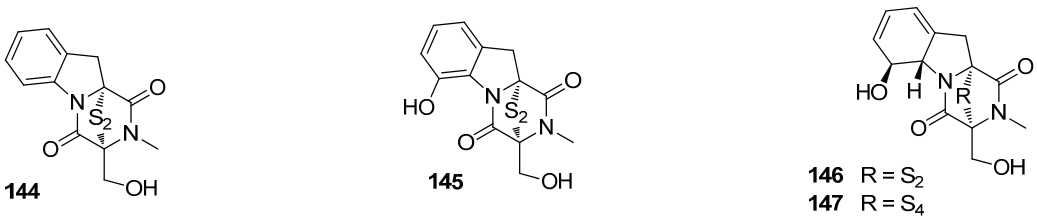

A new proline-rich cyclic octapeptide named stylissamide X **148** (Figure 34) was isolated from an Indonesian marine sponge *Stylissa* sp. as an inhibitor of cell migration using a wound-healing assay. Compound **148** showed inhibitory activity against migration of HeLa cells in the concentration range of 0.1–10 μM in both a wound-healing assay and a chemotaxicell chamber assay, while cell viability was maintained at more than 75% at even the highest concentration of 10 μM [149].

The oligopeptide **149** (Figure 34) was isolated from the digests of abalone *Haliotis discus hannai* intestine. This marine gastropod is an important fishery and food industrial resource that is massively maricultured in Asia, Africa, Australia, and America. The purified abalone oligopeptide **149** (AOP) exhibited a specific inhibitory effect against MMP-2/-9 activity and attenuated protein expression of p50 and p65 in human fibrosarcoma (HT1080) cells via the nuclear factor-κB (NF-κB) pathway. This data suggest that AOP may possess therapeutic and preventive potential for the treatment of MMPs-related disorders such as angiogenesis and metastasis formation [150].

Figure 34. Structures of the compounds **148** and **149**.

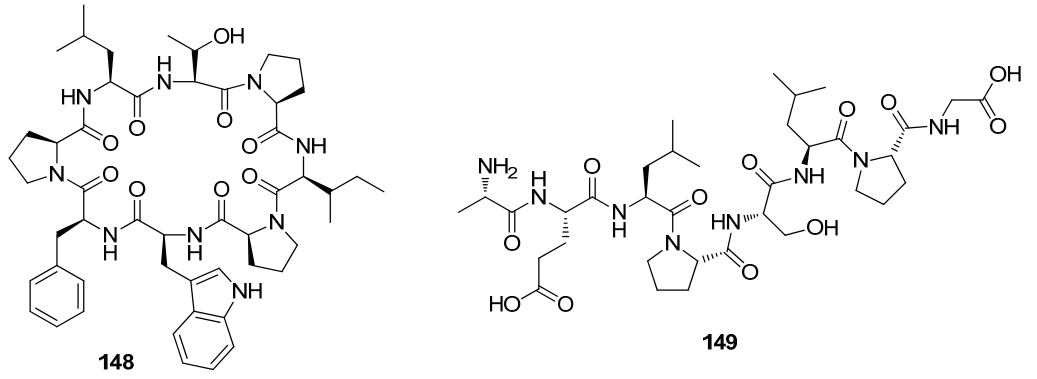

Targeting Mdm2/Hdm2 is a promising way to reactivate p53, inducing apoptosis in transformed human cells. New sulfonated serinol derivatives, siladenoserinols A–L (**150**–**161**, Figure 35) were isolated from a tunicate of the family Didemnidae as inhibitors of p53-Hdm2 interaction. The compounds inhibited p53-Hdm2 interaction with IC_{50} values ranging from 2.0 to 55 μM. Among them, siladenoserinol A and B (**150**, **151**) exhibited the strongest inhibition with an IC_{50} value of 2.0 μM [151]. Reactivation of p53 via this approach is also considered a potential way to cancer-prevention, although this needs further study.

Figure 35. Structures of the compounds **150**–**162**.

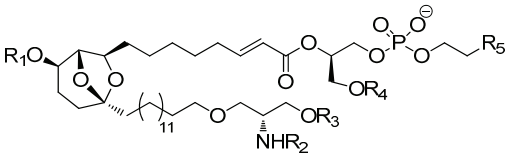

	R_1	R_2	R_3	R_4	R_5
150	Ac	SO_3H	H	Ac⊕	NMe_3
151	Ac	SO_3H	H	Ac⊕	NH_3
152	H	H	SO_3H	Ac⊕	NH_3
153	Ac	SO_3H	H	H⊕	NMe_3
154	H	H	SO_3H	Ac⊕	NMe_3
155	H	SO_3H	H	Ac⊕	NMe_3
156	Ac	H	SO_3H	Ac	NMe_3

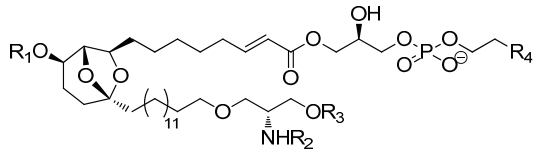

	R_1	R_2	R_3	R_4
157	Ac	SO_3H	H⊕	NMe_3
158	Ac	H	SO_3H⊕	NMe_3
159	H	H	SO_3H⊕	NH_3
160	H	SO_3H	H⊕	NMe_3
161	H	H	SO_3H	NMe_3

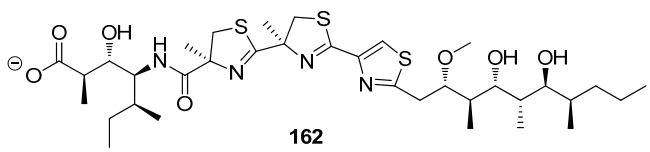

162

Bioassay-guided fractionation of two cyanobacterial extracts from Papua New Guinea has yielded hoiamide D (**162**, Figure 35), a polyketide synthase (PKS)/non-ribosomal peptide synthetase (NRPS)-derived natural product that features two consecutive thiazolines and a thiazole, as well as a modified isoleucine residue. Hoiamide D (**162**) displayed inhibitory activity against p53/Mdm2 interaction (EC_{50} = 4.5 μM) [152].

Two rare bromoditerpenes, parguerenes I and II (**163**, **164**, Figure 36), were isolated as P-gp inhibitors from a southern Australian collection of the red alga *Laurencia filiformis*. It was determined that the parguerenes were non-cytotoxic, dose-dependent inhibitors of P-gp mediated drug efflux, by modifying the extracellular antibody binding epitope of P-gp in a manner that differs markedly from that of the other known P-gp inhibitors verapamil and cyclosporine A [153]. Their cancer preventive activities, however, have not been studied yet.

Figure 36. Structures of the compounds **163–170**.

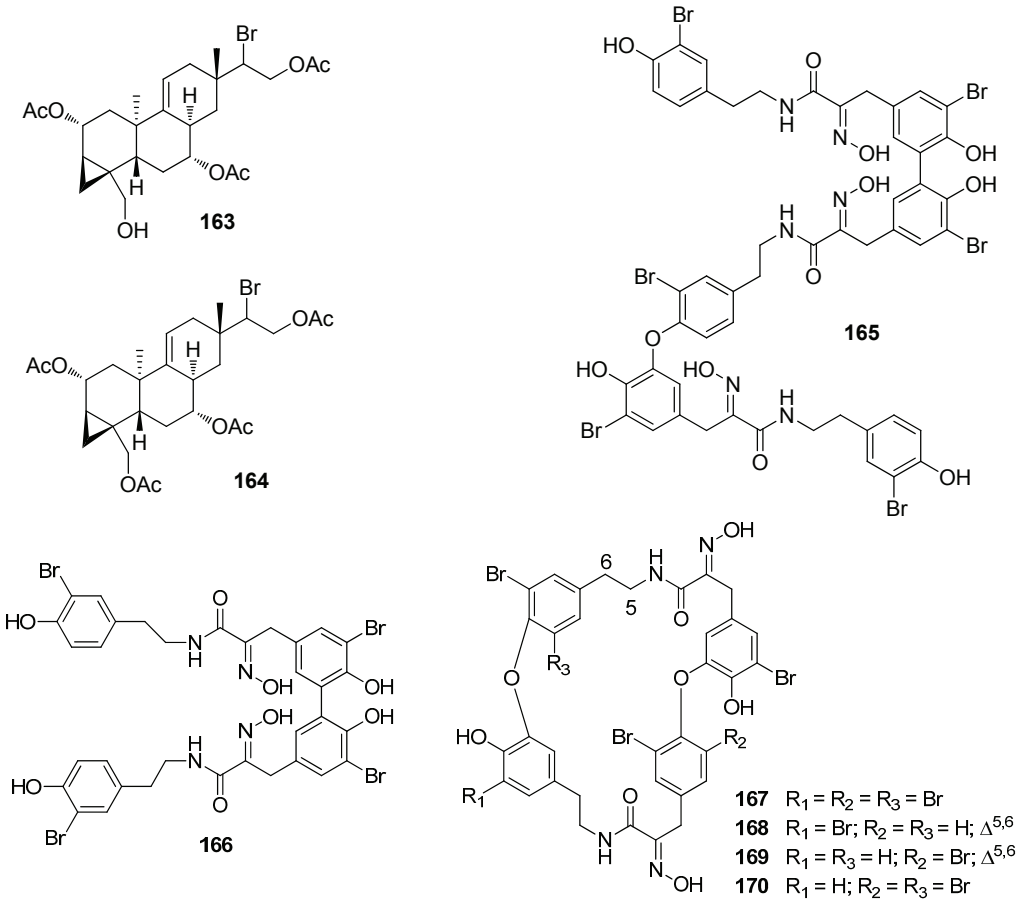

Naturally occurring trimeric hemibastadin congeners, sesquibastadin 1 (**165**, Figure 36), and bastadins 3, 6, 7, 11, and 16 (**166–170**, Figure 36) were isolated from the marine sponge *Ianthella basta*, collected in Indonesia. The compounds showed inhibition of several protein kinases with IC_{50} values between 0.1 and 10.2 μM [154]. They may well be interesting for their potential anticancer and chemo-preventive properties.

8. Conclusions

Many secondary metabolites, isolated from marine organisms in recent years, were shown to be potential anticarcinogenic and chemo-preventive agents using mainly *in vitro* and sometimes *in vivo* experiments. Among these agents are compounds with such different activities as inhibition of transformation of normal cells into cancer cells, abrogation of tumor cell growth and formation of microtumors, and induction of apoptosis. Some compounds showing mainly antioxidative, immunostimulatory, and anti-inflammatory activity also may be promising agents for cancer prevention. Notably, the availability of ever more precise research tools allows the dissection of the

molecular mode of action of many natural compounds, which will lead to a more differentiated therapeutic use of these agents in the era of "targeted therapy". Numerous reports cited in this review clearly indicate that marine organisms are an irreplaceable source of bioactive and often low toxic compounds, which may play an important role in prevention and inhibition of cancer development in humans in the near future. Particularly, natural products isolated from edible species seem an attractive source of cancer-preventive agents. Interdisciplinary studies on marine natural products and close cooperation of bioorganic chemists with the molecular biologists, pharmacologists, and clinicians should help to find new and effective ways of cancer prevention.

Acknowledgments

The study was supported by the Program of the Presidium of RAS "Molecular and Cell Biology" (grant 12-IP6-11), Grant No. 13-03-00986 from the RFBR, and Grant of President of Russia No. 148.2014.4 supporting leading Russian scientific schools.

Conflicts of Interest

The authors declare no conflict of interest.

References

1. Fujiki, H.; Suganuma, M.; Yatsunami, J.; Komori, A.; Okabe, S.; Nishiwaki-Matsushima, R.; Ohta, T. Significant marine natural products in cancer research. *Gazz. Chim. Ital.* **1993**, *123*, 309–316.
2. Simmons, T.L.; Andrianasolo, E.; McPhail, K.; Flatt, P.; Gerwick, W.H. Marine natural products as anticancer drugs. *Mol. Cancer Ther*. **2005**, *4*, 333–342.
3. Bhatnagar, I.; Kim, S.-K. Marine antitumor drugs: Status, shortfalls and strategies. *Mar. Drugs* **2010**, *8*, 2702–2720.
4. Schumacher, M.; Kelkel, M.; Dicato, M.; Diederich, M. Gold from the sea: Marine compounds as inhibitors of the hallmarks of cancer. *Biotechnol. Adv*. **2011**, *29*, 531–547.
5. Stonik, V.A.; Fedorov, S.N. Cancer preventive marine natural product. In *Cellular and Genetic Practices for Translational Medicine*; Kwak, J.-Y., Han, J.-Y., Eds.; Research Signpost: Karalla, India, 2011; pp. 1–36.
6. Gerwick, W.H.; Moore, B.S. Lessons from the past and charting the future of marine natural products drug discovery and chemical biology. *Chem. Biol*. **2012**, *19*, 85–98.
7. Vinothkumar, S.; Parameswaran, P.S. Recent advances in marine drug research. *Biotechnol. Adv.* **2013**, *31*, 1826–1845.
8. Sawadogo, W.R.; Schumacher, M.; Teiten, M.-H.; Cerella, C.; Dicato, M.; Diederich, M. A survey of marine natural compounds and their derivatives with anti-cancer activity reported in 2011. *Molecules* **2013**, *18*, 3641–3673.
9. Azmi, A.S.; Ahmad, A.; Banerjee, S.; Rangnekar, V.M.; Mohammad, R.M.; Sarkar, F.H. Chemoprevention of pancreatic cancer: characterization of Par-4 and its modulation by 3,3′-diindolylmethane (DIM). *Pharm. Res*. **2008**, *25*, 2117–2124.

10. Tsuda, H.; Ohshima, Y.; Nomoto, H.; Fujita, K.; Matsuda, E.; Iigo, M.; Takasuka, N.; Moore, M.A. Cancer prevention by natural compounds. *Drug Metab. Pharmacokin.* **2004**, *19*, 245–263.
11. Berenblum, I.; Armuth, V. Two independent aspects of tumor promotion. *Biochim. Biophys. Acta* **1981**, *651*, 51–63.
12. Heidelberger, C.; Freeman, A.E.; Pienta, R.J.; Sivak, A.; Bertram, J.S.; Casto, B.C.; Dunkel, V.C.; Francis, M.W.; Kakunaga, T.; Little, J.B.; *et al.* Cell transformation by chemical agents—a review and analysis of the literature. A report of the U.S. Environmental Protection Agency Gene-Tox Program. *Mutat. Res*. **1983**, *114*, 283–385.
13. Sporn, M.B. Approaches to prevention of epithelial cancer during the preneoplastic period. *Cancer Res*. **1976**, *36*, 2699–2702.
14. Umar, A.; Viner, J.L.; Hawk, E.T. The future of colon cancer prevention. *Ann. N. Y. Acad. Sci*. **2001**, *952*, 88–108.
15. Mehta, R.G.; Pezzuto, J.M. Discovery of cancer preventive agents from natural products: From plants to prevention. *Curr. Oncol. Rep*. **2002**, *4*, 478–486.
16. Hong, W.K.; Sporn, M.B. Recent advances in chemoprevention of cancer. *Science* **1997**, *278*, 1073–1077.
17. Hanahan, D.; Weinberg, R.A. The hallmarks of cancer. *Cell* **2000**, *100*, 57–70.
18. Nobili, S.; Lippi, D.; Witort, E.; Donnini, M.; Bausi, L.; Mini, E.; Capaccioli, S. Natural compounds for cancer treatment and prevention. *Pharm. Res*. **2009**, *59*, 365–378.
19. Surh, Y.-J. Molecular mechanisms of chemopreventive effects of selected dietary and medicinal phenolic compounds. *Mutat. Res*. **1999**, *428*, 305–327.
20. Pan, M.-H.; Ho, C.-T. Chemopreventive effects of natural dietary compounds on cancer development. *Chem. Soc. Rev*. **2008**, *37*, 2558–2574.
21. Cerella, C.; Sobolewski, C.; Dicato, M.; Diederich, M. Targeting COX-2 expression by natural compounds: A promising alternative strategy to synthetic COX-2 inhibitors for cancer chemoprevention and therapy. *Biochem. Pharmacol*. **2010**, *80*, 1801–1815.
22. Von Schwarzenberg, K.; Vollmar, A.M. Targeting apoptosis pathways by natural compounds in cancer: Marine compounds as lead structures and chemical tools for cancer therapy. *Cancer Lett*. **2013**, *332*, 295–303.
23. Gupta, S.C.; Sundaram, C.; Reuter, S.; Aggarwal, B.B. Inhibiting NF-κB activation by small molecules as a therapeutic strategy. *Biochim. Biophys. Acta* **2010**, *1799*, 775–787.
24. Bharate, S.B.; Sawant, S.D.; Pal Singh, P.; Vishwakarma, R.A. Kinase inhibitors of marine origin. *Chem. Rev*. **2013**, *113*, 6761–6815.
25. Muller, A.J.; DuHadaway, J.B.; Chang, M.Y.; Ramalingam, A.; Sutanto-Ward, E.; Boulden, J.; Soler, A.P.; Mandik-Nayak, L.; Gilmour, S.K.; Prendergast, G.C. Nonhematopoietic expression of IDO is integrally required for inflammatory tumor promotion. *Cancer Immunol. Immunother*. **2010**, *59*, 1655–1663.
26. Marks, P.A.; Richon, V.M.; Rifkind, R.A. Histone deacetylase inhibitors: Inducers of differentiation or apoptosis of transformed cells. *J. Natl. Cancer Inst*. **2000**, *92*, 1210–1216.

27. Simeone, A.-M.; Tari, A.M. How retinoids regulate breast cancer cell proliferation and apoptosis. *Cell. Mol. Life Sci.* **2004**, *61*, 1475–1484.
28. Xia, Y.; Choi, H.-K.; Lee, K. Recent advances in hypoxia-inducible factor (HIF)-1 inhibitors. *Eur. J. Med. Chem*. **2012**, *49*, 24–40.
29. Nencioni, A.; Grunebach, F.; Patrone, F.; Ballestrero, A.; Brossart, P. Proteasome inhibitors: Antitumor effects and beyond. *Leukemia* **2007**, *21*, 30–36.
30. Zhang, C.; Kim, S.K. Matrix metalloproteinase inhibitors (MMPs) from marine natural products: The current situation and future prospects. *Mar. Drugs* **2009**, *7*, 71–84.
31. Yasui, Y.; Kim, M.; Tanaka, T. PPAR ligands for cancer chemoprevention. *PPAR Res*. **2008**, *2008*, doi:10.1155/2008/548919.
32. Fedorov, S.N.; Krasokhin, V.B.; Shubina, L.K.; Dyshlovoy, S.A.; Nam, N.H.; Minh, C.V. The extracts of some marine invertebrates and algae collected off the coast of Vietnam induce the inhibitory effects on the Activator Protein-1 transcriptional activity in JB6 Cl41 cells. *J. Chem*. **2013**, *2013*, doi:10.1155/2013/896709.
33. Candela, C.G.; Lopez, L.; Kohen, V. Importance of a balanced omega 6/omega 3 ratio for the maintenance of health. Nutritional recommendations. *Nutr. Hosp.* **2011**, *26*, 323–329.
34. Wendel, M.; Heller, A.R. Anticancer actions of omega-3 fatty acids—Current state and future perspectives. *Anticancer Agents Med. Chem*. **2009**, *9*, 457–470.
35. Hall, M.N.; Chavarro, J.E.; Lee, I.-M.; Willett, W.C.; Ma, J. A 22-year prospective study of fish, *n*-3 fatty acid intake, and colorectal cancer risk in men. *Cancer Epidemiol. Biomarkers Prev*. **2008**, *17*, 1136–1143.
36. Cockbain, A.J.; Toogood, G.J.; Hull, M.A. Omega-3 polyunsaturated fatty acids for the treatment and prevention of colorectal cancer. *Gut* **2012**, *61*, 135–149.
37. Murff, H.J.; Shrubsole, M.J.; Cai, Q.; Smalley, W.E.; Dai, Q.; Milne, G.L.; Ness, R.M.; Zheng, W. Dietary intake of PUFAs and colorectal polyp risk. *Am. J. Clin. Nutr.* **2012**, *95*, 703–712.
38. Spencer, M.; Finlin, B.S.; Unal, R.; Zhu, B.; Morris, A.J.; Shipp, L.R.; Lee, J.; Walton, R.G.; Adu, A.; Erfani, R.; *et al.* Omega-3 fatty acids reduce adipose tissue macrophages in human subjects with insulin resistance. *Diabetes* **2013**, *62*, 1709–1717.
39. Rosa, D.D.; Lourenco, F.C.; da Fonseca, A.C.M.; de Sales, R.L.; Ribeiro, S.M.R.; Neves, C.A.; Peluzio, M.C.G. Fish oil improves the lipid profile and reduces inflammatory cytokines in Wistar rats with precancerous colon lesions. *Nutr. Cancer* **2012**, *64*, 569–579.
40. Monk, J.M.; Jia, Q.; Callaway, E.; Weeks, B.; Alaniz, R.C.; McMurray, D.N.; Chapkin, R.S. Th17 cell accumulation is decreased during chronic experimental colitis by (*n*-3) PUFA in Fat-1 mice. *J. Nutr*. **2012**, *142*, 117–124.
41. Chiu, C.-Y.; Gomolka, B.; Dierkes, C.; Huang, N.R.; Schroeder, M.; Purschke, M.; Manstein, D.; Dangi, B.; Weylandt, K.H. Omega-6 docosapentaenoic acid-derived resolvins and 17-hydroxydocosahexaenoic acid modulate macrophage function and alleviate experimental colitis. *Inflamm. Res*. **2012**, *61*, 967–976.

42. Fasano, E.; Serini, S.; Piccioni, E.; Toesca, A.; Monego, G.; Cittadini, A.R.; Ranelletti, F.O.; Calviello, G. DHA induces apoptosis by altering the expression and cellular location of GRP78 in colon cancer cell lines. *Biochim. Biophys. Acta* **2012**, *1822*, 1762–1772.
43. Banskota, A.H.; Gallant, P.; Stefanova, R.; Melanson, R.; O'Leary, S.J.B. Monogalactosyldiacylglycerols, potent nitric oxide inhibitors from the marine microalga *Tetraselmis chui*. *Nat. Prod. Res*. **2013**, *27*, 1084–1090.
44. Tsukamoto, S.; Takeuchi, T.; Rotinsulu, H.; Mangindaan, R.E.P.; van Soest, R.W.M.; Ukai, K.; Kobayashi, H.; Namikoshi, M.; Ohta, T.; Yokosawa, H. Leucettamol A: A new inhibitor of Ubc13-Uev1A interaction isolated from a marine sponge, *Leucetta* aff. *Microrhaphis*. *Bioorg. Med. Chem. Lett.* **2008**, *18*, 6319–6320.
45. Banskota, A.H.; Stefanova, R.; Sperker, S.; McGinn, P.J. New diacylglyceryltrimethyl-homoserines from the marine microalga *Nannochloropsis granulata* and their nitric oxide inhibitory activity. *J. Appl. Phycol*. **2013**, *25*, 1513–1521.
46. Tang, F.-Y. The silver bullet for cancer prevention: Chemopreventive effects of carotenoids. *Bio. Med*. **2012**, *2*, 117–121.
47. Tanaka, T.; Shnimizu, M.; Moriwaki, H. Cancer chemoprevention by carotenoids. *Molecules* **2012**, *17*, 3202–3242.
48. Nishino, H.; Tokuda, H.; Satomi, Y.; Masuda, M.; Bu, P.; Onozuka, M.; Yamaguchi, S.; Okuda, Y.; Takayasu, J.; Tsuruta, J.; *et al.* Cancer prevention by carotenoids. *Pure Appl. Chem*. **1999**, *71*, 2273–2278.
49. Nishino, H.; Murakoshi, M.; Ii, T.; Takemura, M.; Kuchide, M.; Kanazawa, M.; Mou, X.Y.; Wada, S.; Masuda, M.; Ohsaka, Y.; *et al.* Carotenoids in cancer chemoprevention. *Cancer Metastasis Rev*. **2002**, *21*, 257–264.
50. Amaro, H.M.; Barros, R.; Guedes, A.C.; Sousa-Pinto, I.; Malcata, F.X. Microalgal compounds modulate carcinogenesis in the gastrointestinal tract. *Trends Biotechnol*. **2013**, *31*, 92–98.
51. Mikami, K.; Hosokawa, M. Biosynthetic pathway and health benefits of fucoxanthin, an algae-specific xanthophyll in brown seaweeds. *Int. J. Mol. Sci.* **2013**, *14*, 13763–13781.
52. Abd El Baky, H.H.; El-Baroty, G.S. Healthy Benefit of Microalgal Bioactive Substances. *J. Aquat. Sci.* **2013**, *1*, 11–23.
53. D'Orazio, N.; Gemello, E.; Gammone, M.A.; de Girolamo, M.; Ficoneri, C.; Riccioni, G. Fucoxantin: A treasure from the sea. *Mar. Drugs* **2012**, *10*, 604–616.
54. Cantrell, A.; McGarvey, D.J.; Truscott, T.G., Rancan, F.; Böhm, F. Singlet oxygen quenching by dietary carotenoids in a model membrane environment. *Arch. Biochem. Biophys*. **2003**, *412*, 47–54.
55. Edge, R.; Land, E.J.; McGarvey, D.; Mulroy, L.; Truscott, T.G. Relative one-electron reduction potentials of carotenoid radical cations and the interactions of carotenoids with the vitamin E radical cation. *J. Am. Chem. Soc.* **1998**, *120*, 4087–4090.
56. Halliwell, B. Free radicals, antioxidants, and human disease: Curiosity, cause or consequence? *Lancet* **1994**, *344*, 721–724.

57. Maoka, T.; Tokuda, H.; Suzuki, N.; Kato, H.; Etoh, H. Anti-oxidative, anti-tumor-promoting, and anti-carcinogensis activities of nitroastaxanthin and nitrolutein, the reaction products of astaxanthin and lutein with peroxynitrite. *Mar. Drugs* **2012**, *10*, 1391–1399.
58. Sachindra, N.M.; Sato, E.; Maeda, H.; Hosokawa, M.; Niwano, Y.; Kohno, M.; Miyashita, K. Radical scavenging and singlet oxygen quenching activity of marine carotenoid fucoxanthin and its metabolites. *J. Agric. Food Chem*. **2007**, *55*, 8516–8522.
59. Heo, S.-J.; Jeon, Y.-J. Protective effect of fucoxanthin isolated from *Sargassum siliquastrum* on UV-B induced cell damage. *J. Photochem. Photobiol. B* **2009**, *95*, 101–107.
60. Miyashita, K. Function of marine carotenoids. *Forum Nutr.* **2009**, *61*, 136–146.
61. Yasui, Y.; Hosokawa, M.; Mikami, N.; Miyashita, K.; Tanaka, T. Dietary astaxanthin inhibits colitis and colitis-associated colon carcinogenesis in mice via modulation of the inflammatory cytokines. *Chem. Biol. Interact*. **2011**, *193*, 79–87.
62. Palozza, P.; Torelli, C.; Boninsegna, A.; Simone, R.; Catalano, A.; Mele, M.C.; Picci, N. Growth-inhibitory effects of the astaxanthin-rich alga *Haematococcus pluvialis* in human colon cancer cells. *Cancer Lett.* **2009**, *283*, 108–117.
63. Kim, K.N.; Heo, S.J.; Kang, S.M.; Ahn, G.; Jeon, Y.J. Fucoxanthin induces apoptosis in human leukemia HL-60 cells through a ROS-mediated Bcl-xL pathway. *Toxicol. in Vitro* **2010**, *24*, 1648–1654.
64. Yu, R.X.; Hu, X.M.; Xu, S.Q.; Jiang, Z.J.; Yang, W. Effects of fucoxanthin on proliferation and apoptosis in human gastric adenocarcinoma MGC-803 cells via JAK/STAT signal pathway. *Eur. J. Pharmacol.* **2011**, *657*, 10–19.
65. Satomi, Y. Fucoxanthin induces GADD45A expression and G1 arrest with SAPK/JNK activation in LNCap human prostate cancer cells. *Anticancer Res*. **2012**, *32*, 807–813.
66. Yamamoto, K.; Ishikawa, C.; Katano, H.; Yasumoto, T.; Mori, N. Fucoxanthin and its deacetylated product, fucoxanthinol, induce apoptosis of primary effusion lymphomas. *Cancer Lett.* **2011**, *300*, 225–234.
67. Ganesan, P.; Noda, K.; Manabe, Y.; Ohkubo, T.; Tanaka, Y.; Maoka, T.; Sugawara, T.; Hirata, T. Siphonaxanthin, a marine carotenoid from green algae, effectively induces apoptosis in human leukemia (HL-60) cells. *Biochim. Biophys. Acta* **2011**, *1810*, 497–503.
68. Ivanchina, N.V.; Kicha, A.A.; Stonik V.A. Steroid glycosides from marine organisms. *Steroids* **2011**, *76*, 425–454.
69. Stonik, V.A.; Kalinin, V.I.; Avilov, S.A. Toxins from sea cucumbers (holothuroids): Chemical structures, properties, taxonomic distribution, biosynthesis, and evolution. *J. Nat. Toxins* **1999**, *8*, 235–248.
70. Kalinin, V.I.; Aminin, D.L.; Avilov, S.A.; Silchenko, A.S.; Stonik, V.A. Triterpene glycosides from sea cucumbers (Holothurioidea, Echinodermata), biological activities and functions. In *Studies in Natural Product Chemistry*; ur Rahman, A., Ed.; Elsevier: Amsterdam, The Netherlands, 2008; pp. 135–196.

71. Aminin, D.L.; Pislyagin, E.A.; Menchinskaya, E.S.; Silchenko, A.S.; Avilov, S.A.; Kalinin, V.I. Immunomodulatory and Anticancer Activity of Sea Cucumber Triterpene Glycosides. In *Studies in Natural Products Chemistry*; ur Rahman, A., Ed.; Elsevier: Amsterdam, The Netherlands, 2014; pp. 73–91.
72. Aminin, D.L.; Agafonova, I.G.; Berdyshev, E.V.; Isachenko, E.G.; Avilov, S.A.; Stonik, V.A. Immunomodulatory properties of cucumariosides from the edible Far-Eastern holothurian *Cucumaria japonica*. *J. Med. Food* **2001**, *4*, 127–135.
73. Aminin, D.L.; Pinegin, B.V.; Pichugina, L.V.; Zaporozhets, T.S.; Agafonova, I.G.; Boguslavski, V.M.; Silchenko, A.S.; Avilov, S.A.; Stonik, V.A. Immunomodulatory properties of cumaside. *Int. Immunopharm*. **2006**, *6*, 1070–1082.
74. Aminin, D.L.; Chaikina, E.L.; Agafonova, I.G.; Avilov, S.A.; Kalinin, V.I.; Stonik, V.A. Antitumor activity of the immunomodulatory lead cumaside. *Int. Immunopharm*. **2010**, *10*, 648–654.
75. Menchinskaya, E.S.; Pislyagin, E.A.; Kovalchyk, S.N.; Davydova, V.N.; Silchenko, A.S.; Avilov, S.A.; Kalinin, V.I.; Aminin, D.L. Antitumor Activity of Cucumarioside A_2-2. *Chemotherapy* **2013**, *59*, 181–191.
76. Silchenko, A.S.; Kalinovsky, A.I.; Avilov, S.A.; Andryjaschenko, P.V.; Dmitrenok, P.S.; Menchinskaya, E.S.; Aminin, D.L.; Kalinin, V.I. Structure of cucumarioside I2 from the sea cucumber *Eupentacta fraudatrix* (Djakonov et Baranova) and cytotoxic and immunostimulatory activities of this saponin and relative compounds. *Nat. Prod. Res*. **2013**, *27*, 1776–1783.
77. Silchenko, A.S.; Kalinovsky, A.I.; Avilov, S.A.; Andryjaschenko, P.V.; Dmitrenok, P.S.; Martyyas, E.A.; Kalinin, V.I. Triterpene glycosides from the sea cucumber *Eupentacta fraudatrix*. Structure and biological action of cucumariosides A1, A3, A4, A5, A6, A12 and A15, seven new minor non-sulfated tetraosides and unprecedented 25-keto, 27-norholostane aglycone. *Nat. Prod. Commun.* **2012**, *7*, 517–525.
78. Silchenko, A.S.; Kalinovsky, A.I.; Avilov, S.A.; Andryjaschenko, P.V.; Dmitrenok, P.S.; Martyyas, E.A.; Kalinin, V.I. Triterpene glycosides from the sea cucumber *Eupentacta fraudatrix*. Structure and cytotoxic action of cucumariosides A2, A7, A9, A10, A11, A13 and A14, seven new minor non-sulfated tetraosides and an aglycone with an uncommon 18-hydroxy group. *Nat. Prod. Commun.* **2012**, *7*, 845–852.
79. Silchenko, A.S.; Kalinovsky, A.I.; Avilov, S.A.; Andryjaschenko, P.V.; Dmitrenok, P.S.; Martyyas, E.A.; Kalinin, V.I. Triterpene glycosides from the sea cucumber *Eupentacta fraudatrix*. Structure and biological activity of cucumariosides B1 and B2, two new minor non-sulfated unprecedented triosides. *Nat. Prod. Commun.* **2012**, *7*, 1157–1162.
80. Silchenko, A.S.; Kalinovsky, A.I.; Avilov, S.A.; Andryjaschenko, P.V.; Dmitrenok, P.S.; Martyyas, E.A.; Kalinin, V.I.; Jayasandhya, P.; Rajan, G.C.; Padmakumar, K.P. Structures and biological activities of typicosides A1, A2, B1, C1 and C2, triterpene glycosides from the sea cucumber *Actinocucumis typica1*. *Nat. Prod. Commun.* **2013**, *8*, 301–310.

81. Silchenko, A.S.; Kalinovsky, A.I.; Avilov, S.A.; Andryjaschenko, P.V.; Dmitrenok, P.S.; Martyyas, E.A.; Kalinin, V.I. Triterpene glycosides from the sea cucumber *Eupentacta fraudatrix*. Structure and biological action of cucumariosides I1, I3, I4, three new minor disulfated pentaosides. *Nat. Prod. Commun.* **2013**, *8*, 1053–1058.
82. Silchenko, A.S.; Kalinovsky, A.I.; Avilov, S.A.; Andryjaschenko, P.V.; Dmitrenok, P.S.; Yurchenko, E.A.; Dolmatov, I.Yu.; Kalinin, V.I.; Stonik, V.A. Structure and biological action of cladolosides B1, B2, C, C1, C2 and D, six new triterpene glycosides from the sea cucumber *Cladolabes schmeltzii*. *Nat. Prod. Commun.* **2013**, *8*, 1527–1534.
83. Menchinskaya, E.S.; Aminin, D.L.; Avilov, S.A.; Silchenko, A.S.; Andryjashchenko, P.V.; Kalinin, V.I.; Stonik, V.A. Inhibition of tumor cells multidrug resistance by cucumarioside A_2-2, frondoside A and their complexes with cholesterol. *Nat. Prod. Commun.* **2013**, *8*, 1377–1380.
84. Yun, S.-H.; Park, E.-S.; Shin, S.-W.; Na, Y.-W.; Han, J.-Y.; Jeong, J.-S.; Shastina, V.V.; Stonik, V.A.; Park, J.-I.; Kwak, J.-Y. Stichoposide C induces apoptosis through the generation of ceramide in leukemia and colorectal cancer cells and shows *in vivo* antitumor activity. *Clin. Cancer Res.* **2012**, *18*, 5934–5948.
85. Fujiki, H.; Cope, F.O.; Issinger, O.G. Sarcophytol-A, a potent tumor promoter inhibitor, prevents phosphorylation of a proteolytic fragment of C23 induced by the non-TPA type tumor promoter, okadaic acid. *Proc. Am. Assoc. Cancer Res.* **1988**, *29*, 155–155.
86. Fujiki, H.; Suganuma, M.; Suguri, H.; Yoshizawa, S.; Takagi, K.; Kobayashi, M. Sarcophytol-A and sarcophytol-B inhibit tumor promotion by teleocidin in 2-stage carcinogenesis in mouse skin. *J. Cancer Res. Clin. Oncol.* **1989**, *115*, 25–28.
87. Wei, H.; Frenkel, K. Suppression of tumor promoter-induced oxidative events and DNA damage *in vivo* by sarcophytol A: A possible mechanism of antipromotion. *Cancer Res*. **1992**, *52*, 2298–2303.
88. Fujiki, H.; Suganuma, M.; Komori, A.; Yatsunami, J.; Okabe, S.; Ohta, T.; Sueoka, E. A new tumor promotion pathway and its inhibitors. *Cancer Det. Prev.* **1994**, *18*, 1–7.
89. Bhimani, R.S.; Troll, W.; Grunberger, D.; Frenkel, K. Inhibition of oxidative stress in HeLa cells by chermopreventive agents. *Cancer Res*. **1993**, *53*, 4528–4533.
90. Yokomatsu, H.; Satake, K.; Hiura, A.; Tsutsumi, M.; Suganuma, M. Sarcophytol-A—a new chemotherapeutic and chemopreventive agent for pancreatic-cancer. *Pancreas* **1994**, *9*, 526–530.
91. Narisawa, T.; Takahashi, M.; Niwa, M.; Fukaura, Y.; Fujiki, H. Inhibition of methylnitrosourea-induced large bowel-cancer development in rats by sarcophytol A, a product from a marine soft coral *Sarcophyton glaucum*. *Cancer Res.* **1989**, *49*, 3287–3289.
92. Yamauchi, O.; Omori, M.; Ninomiya, M.; Okuno, M.; Moriwaki, H.; Suganuma, M.; Fujiki, H.; Muto, Y. Inhibitory effect of sarcophytol-A on development of spontaneous hepatomas in mice. *Jpn. J. Cancer Res*. **1992**, *82*, 1234–1238.
93. Hegazy, M.-E.F.; Gamal Eldeen, A.M.; Shahat, A.A.; Abdel-Latif, F.F.; Mohamed, T.A.; Whittlesey, B.R.; Paré, P.W. Bioactive hydroperoxyl cembranoids from the Red Sea soft coral *Sarcophyton glaucum*. *Mar. Drugs* **2012**, *10*, 209–222.

94. Albizat, K.F.; Holman, T.; Faulkner, D.J.; Glaser, K.B.; Jacobs, R.S. Luffariellolide, an anti-inflammatory sesterterpene from the marine sponge *Luffariella* sp. *Experientia* **1987**, *45*, 388–390.
95. Wang, S.; Wang, Z.; Lin, S.; Zheng, W.; Wang, R.; Jin, S.; Chen, J.; Jin, L.; Li, Y. Revealing a natural marine product as a novel agonist for retinoic acid receptors with a unique binding mode and inhibitory effects on cancer cells. *Biochem. J.* **2012**, *446*, 79–87.
96. Liu, W.K.; Ling, Y.H.; Cheung, F.W.K.; Che, C.-T. Stellettin A induces endoplasmic reticulum stress in murine B16 melanoma cells. *J. Nat. Prod*. **2012**, *75*, 586–590.
97. Zhu, H.; Hua, X.; Gong, T.; Pang, J.; Hou, Q.; Zhu, P. Hypocreaterpenes A and B, cadinane-type sesquiterpenes from a marine-derived fungus, *Hypocreales* sp. *Phytochem. Lett*. **2013**, *6*, 392–396.
98. De los Reyes, C.; Zbakh, H.; Motilva, V.; Zubía, E. Antioxidant and anti-inflammatory meroterpenoids from the brown alga *Cystoseira usneoides*. *J. Nat. Prod.* **2013**, *76*, 621–629.
99. Wang, W.; Lee, Y.; Lee, T.G.; Mun, B.; Giri, A.G.; Lee, J.; Kim, H.; Hahn, D.; Yang, I.; Chin, J.; *et al.* Phorone A and isophorbasone A, sesterterpenoids isolated from the marine sponge *Phorbas* sp. *Org. Lett*. **2012**, *14*, 4486–4489.
100. Takahashi, Y.; Kubota, T.; Yamamoto, S.; Kobayashi, J. Inhibitory effects of metachromins L–Q and its related analogs against receptor tyrosine kinases EGFR and HER2. *Bioorg. Med. Chem. Lett.* **2013**, *23*, 117–118.
101. Li, J.; Zhu, H.; Ren, J.; Deng, Z.; de Voogd, N.J.; Proksch, P.; Lin, W. Globostelletins J–S, isomalabaricanes with unusual cyclopentane sidechains from the marine sponge *Rhabdastrella globostellata*. *Tetrahedron* **2012**, *68*, 559–565.
102. Shubina, L.K.; Kalinovsky, A.I.; Fedorov, S.N.; Radchenko, O.S.; Denisenko, V.A.; Dmitrenok, P.S.; Dyshlovoy, S.A.; Krasokhin, V.B.; Stonik, V.A. Aaptamine alkaloids from the Vietnamese sponge *Aaptos* sp. *Nat. Prod. Commun*. **2009**, *4*, 1085–1088.
103. Shubina, L.K.; Makarieva, T.N.; Dyshlovoy, S.A.; Fedorov, S.N.; Dmitenok, P.S.; Stonik, V.A. Three new aaptamines from the marine sponge *Aaptos* sp. and their proapoptotic properties. *Nat. Prod. Commun*. **2010**, *5*, 1881–1884.
104. Utkina, N.K. Antioxidant activity of aromatic alkaloids from the marine sponges *Aaptos aaptos* and *Hyrtios* sp. *Chem. Nat. Comp*. **2009**, *45*, 849–853.
105. Dyshlovoy, S.A.; Naeth, I.; Venz, S.; Preukschas, M.; Sievert, H.; Jacobsen, C.; Shubina, L.K.; Salazar, M.G.; Scharf, C.; Walther, R.; *et al.* Proteomic profiling of germ cell cancer cells treated with aaptamine, a marine alkaloid with antiproliferative activity. *J. Proteome Res.* **2012**, *11*, 2316–2330.
106. Dyshlovoy, S.A.; Venz, S.; Shubina, L.K.; Fedorov, S.N.; Walther, R.; Jacobsen, C.; Stonik, V.A.; Bokemeyer, C.; Balabanov, S.; Honecker, F. Activity of aaptamine and two derivatives, demethyloxyaaptamine and isoaaptamine, in cisplatin-resistant germ cell cancer. *J. Proteomics* **2014**, *96*, 223–239.

107. Yamazaki, H.; Wewengkang, D.S.; Kanno, S.; Ishikawa, M.; Rotinsulu, H.; Mangindaan, R.E.P.; Namikoshi, M. Papuamine and haliclonadiamine, obtained from an Indonesian sponge *Haliclona* sp., inhibited cell proliferation of human cancer cell lines. *Nat. Prod. Res*. **2013**, *27*, 1012–1015.
108. Fu, P.; Yang, C.; Wang, Y.; Liu, P.; Ma, Y.; Xu, L.; Su, M.; Hong, K.; Zhu, W. Streptocarbazoles A and B, two novel indolocarbazoles from the marine-derived actinomycete strain *Streptomyces* sp. FMA. *Org. Lett*. **2012**, *14*, 2422–2425.
109. Johnson, T.A.; Sohn, J.; Vaske, Y.M.; White, K.N.; Cohen, T.L.; Vervoort, H.C.; Tenney, K.; Valeriote, F.A.; Bjeldanes, L.F.; Crews, P. Myxobacteria *versus* sponge-derived alkaloids: The bengamide family identified as potent immune modulating agents by scrutiny of LC–MS/ELSD libraries. *Bioorg. Med. Chem.* **2012**, *20*, 4348–4355.
110. Hwang, B.S.; Oh, J.S.; Jeong, E.J.; Sim, C.J.; Rho, J.-R. Densanins A and B, new macrocyclic pyrrole alkaloids isolated from the marine sponge *Haliclona densaspicula*. *Org. Lett*. **2012**, *14*, 6154–6157.
111. Sakai, E.; Kato, H.; Rotinsulu, H.; Losung, F.; Mangindaan, R.E.P.; de Voogd, N.J.; Yokosawa, H.; Tsukamoto, S. Variabines A and B: New β-carboline alkaloids from the marine sponge *Luffariella variabilis*. *J. Nat. Med*. **2014**, *68*, 215–219.
112. Yamaguchi, M.; Miyazaki, M.; Kodrasov, M.P.; Rotinsulu, H.; Losung, F.; Mangindaan, R.E.P.; de Voogd, N.J.; Yokosawa, H.; Nicholson, B.; Tsukamoto, S. Spongiacidin C, a pyrrole alkaloid from the marine sponge *Stylissa massa*, functions as a USP7 inhibitor. *Bioorg. Med. Chem. Lett*. **2013**, *23*, 3884–3886.
113. Fedorov, S.N.; Dyshlovoy, S.A.; Shubina, L.K.; Guzii, A.G.; Kuzmich, A.S.; Makarieva, T.N. C11 cyclopentenone from the ascidian *Diplosoma* sp. prevents epidermal growth factor-induced transformation of JB6 cells. *Drugs Ther. Stud.* **2012**, *2*, e4.
114. Williams, D.E.; Dalisay, D.S.; Li, F.; Amphlett, J.; Maneerat, W.; Chavez, M.A.G.; Wang, Y.A.; Matainaho, T.; Yu, W.; Brown, P.J.; *et al.* Nahuoic acid A produced by a *Streptomyces* sp. isolated from a marine sediment is a selective SAM-competitive inhibitor of the histone metyltransferase SETD8. *Org. Lett*. **2013**, *15*, 414–417.
115. Takawa, M.; Cho, H.S.; Hayami, S.; Toyokawa, G.; Kogure, M.; Yamane, Y.; Iwai, Y.; Maejima, K.; Ueda, K.; Masuda, A.; *et al.* Histone lysine methyltransferase SETD8 promotes carcinogenesis by deregulating PCNA expression. *Cancer Res*. **2012**, *72*, 3217–3227.
116. Asami, Y.; Jang, J.-H.; Soung, N.-K.; He, L.; Moon, D.O.; Kim, J.W.; Oh, H.; Muroi, M.; Osada, H.; Kim, B.Y.; *et al.* Protuboxepin A, a marine fungal metabolite, inducing metaphase arrest and chromosomal misalignment in tumor cells. *Bioorg. Med. Chem*. **2012**, *20*, 3799–3806.
117. Dyshlovoy, S.A.; Fedorov, S.N.; Kalinovsky, A.I.; Shubina, L.K.; Bokemeyer, C.; Stonik, V.A.; Honecker, F. Mycalamide A shows cytotoxic properties and prevents EGF-induced neoplastic transformation through inhibition of nuclear factors. *Mar. Drugs* **2012**, *10*, 1212–1224.
118. Shirouzu, T.; Watari, K.; Ono, M.; Koizumi, K.; Saiki, I.; Tanaka, C.; van Soest, R.W.M.; Miyamoto, T. Structure, synthesis, and biological activity of a C-20 bisacetylenic alcohol from a marine sponge *Callyspongia* sp. *J. Nat. Prod*. **2013**, *76*, 1337–1342.

119. Garcia-Caballero, M.; Mari-Beffa, M.; Canedo, L.; Medina, M.A.; Quesada, A.R. Toluquinol, a marine fungus metabolite, is a new angiosuppresor that interferes the Akt pathway. *Biochem. Pharmacol.* **2013**, *85*, 1727–1740.
120. Towle, K.M.; Chaytor, J.L.; Liu, H.; Austin, P.; Roberge, M.; Roskelley C.D.; Vederas, J.C. Synthesis and biological studies of neopetrosiamides as inhibitors of cancer cell invasion. *Org. Biomol. Chem*. **2013**, *11*, 1476–1481.
121. Igarashi, Y.; Asano, D.; Furihata, K.; Oku, N.; Miyanaga, S.; Sakurai, H.; Saiki, I. Absolute configuration of pterocidin, a potent inhibitor of tumor cell invasion from a marine-derived *Streptomyces*. *Tetrahedron Lett*. **2012**, *53*, 654–656.
122. Um, S.; Kim, Y.-J.; Kwon, H.; Wen, H.; Kim, S.-H.; Kwon, H.C.; Park, S.; Shin, J.; Oh, D.-C. Sungsanpin, a Lasso Peptide from a Deep-Sea Streptomycete. *J. Nat. Prod*. **2013**, *76*, 873–879.
123. Pimentel, A.A.; Felibertt, P.; Sojo, F.; Colman, L.; Mayora, A.; Silva, M.L.; Rojas, H.; Dipolo, R.; Suarez, A.I.; Compagnone, R.S.; *et al.* The marine sponge toxin agelasine B increases the intracellular Ca^{2+} concentration and induces apoptosis in human breast cancer cells (MCF-7). *Cancer Chemother. Pharmacol*. **2012**, *69*, 71–83.
124. Huang, C.; Jin, H.; Song, B.; Zhu, X.; Zhao, H.; Cai, J.; Lu, Y.; Chen, B.; Lin, Y. The cytotoxicity and anticancer mechanisms of alterporriol L, a marine bianthraquinone, against MCF-7 human breast cancer cells. *Appl. Microbiol. Biotechnol*. **2012**, *93*, 777–785.
125. Ohno, O.; Morita, M.; Kitamura, K.; Teruya, T.; Yoneda, K.; Kita, M.; Kigoshi, H.; Suenaga, K. Apoptosis-inducing activity of the actin-depolymerizing agent aplyronine A and its side-chain derivatives. *Bioorg. Med. Chem. Lett*. **2013**, *23*, 1467–1471.
126. Morita, M.; Ohno, O.; Teruya, T.; Yamori, T.; Inuzuka, T.; Suenaga, K. Isolation and structures of biselyngbyasides B, C, and D from the marine cyanobacterium *Lyngbya* sp., and the biological activities of biselyngbyasides. *Tetrahedron* **2012**, *68*, 5984–5990.
127. Park, S.J.; Jeon, Y.J. Dieckol from *Ecklonia cava* suppresses the migration and invasion of HT1080 cells by inhibiting the focal adhesion kinase pathway downstream of Rac1-ROS signaling. *Mol. Cells* **2012**, *33*, 141–149.
128. Maschek, J.A.; Mevers, E.; Diyabalanage, T.; Chen, L.; Ren, Y.; McClintock, J.B.; Amsler, C.D.; Wu, J.; Baker, B.J. Palmadorin chemodiversity from the antarctic nudibranch *Austrodoris kerguelenensis* and inhibition of Jak2/STAT5-dependent HEL leukemia cells. *Tetrahedron* **2012**, *68*, 9095–9104.
129. Park, E.-J.; Pezzuto, J.M.; Jang, K.H.; Nam, S.-J.; Bucarey, S.A.; Fenical, W. Suppression of nitric oxide synthase by thienodolin in lipopolysaccharide-stimulated RAW 264.7 murine macrophage cells. *Nat. Prod. Commun*. **2012**, *7*, 789–794.
130. Williams, D.E.; Steino, A.; de Voogd, N.J.; Mauk, A.G.; Andersen, R.J. Halicloic acids A and B isolated from the marine sponge *Haliclona* sp. collected in the Philippines inhibit indoleamine 2,3-dioxygenase. *J. Nat. Prod*. **2012**, *75*, 1451–1458.
131. Balunas, M.J.; Grosso, M.F.; Villa, F.A.; Engene, N.; McPhail, K.L.; Tidgewell, K.; Pineda, L.M.; Gerwick, L.; Spadafora, C.; Kyle, D.E.; *et al.* Coibacins A–D, antileishmanial marine cyanobacterial polyketides with intriguing biosynthetic origins. *Org. Lett*. **2012**, *14*, 3878–3881.

132. Festa, C.; De Marino, S.; D'Auria, M.V.; Monti, M.C.; Bucci, M.; Vellecco, V.; Debitus, C.; Zampella, A. Anti-inflammatory cyclopeptides from the marine sponge *Theonella swinhoei*. *Tetrahedron* **2012**, *68*, 2851–2857.
133. Salvador, L.A.; Taori, K.; Biggs, J.S.; Jakoncic, J.; Ostrov, D.A.; Paul, V.J.; Luesch, H. Potent elastase inhibitors from cyanobacteria: Structural basis and mechanisms mediating cytoprotective and anti-inflammatory effects in bronchial epithelial cells. *J. Med. Chem*. **2013**, *56*, 1276–1290.
134. Lin, Y.-F.; Kuo, C.-Y.; Wen, Z.-H.; Lin, Y.-Y.; Wang, W.-H.; Su, J.-H.; Sheu, J.-H.; Sung, P.-J. Flexibilisquinone, a new anti-inflammatory quinone from the cultured soft coral *Sinularia flexibilis*. *Molecules* **2013**, *18*, 8160–8167.
135. Wang, J.; Zhao, B.; Yi, Y.; Zhang, W.; Wu, X.; Zhang, L.; Shen, Y. Mycoepoxydiene, a fungal polyketide inhibits MCF-7 cells through simultaneously targeting p53 and NF-κB pathways. *Biochem. Pharmacol*. **2012**, *84*, 891–899.
136. Kim, M.C.; Kwon, O.-W.; Park, J.-S.; Kim, S.Y.; Kwon, H.C. Nocapyrones H–J, 3,6-disubstituted α-pyrones from the marine actinomycete *Nocardiopsis* sp. KMF-001. *Chem. Pharm. Bull.* **2013**, *61*, 511–515.
137. Song, Y.; Dou, H.; Gong, W.; Liu, X.; Yu, Z.; Li, E.; Tan, R.; Hou, Y. Bis-*N*-norgliovictin, a small-molecule compound from marine fungus, inhibits LPS-induced inflammation in macrophages and improves survival in sepsis. *Eur. J. Pharm*. **2013**, *705*, 49–60.
138. Festa, C.; Lauro, G.; De Marino, S.; D'Auria, M.V.; Monti, M.C.; Casapullo, A.; D'Amore, C.; Renga, B.; Mencarelli, A.; Petek, S.; *et al.* Plakilactones from the marine sponge *Plakinastrella mamillaris*. Discovery of a new class of marine ligands of peroxisome proliferator-activated receptor γ. *J. Med. Chem.* **2012**, *55*, 8303–8317.
139. Elsebai, M.F.; Nazir, M.; Kehraus, S.; Egereva, E.; Ioset, K.N.; Marcourt, L.; Jeannerat, D.; Gütschow, M.; Wolfender, J.-L.; König, G.M. Polyketide skeletons from the marine alga-derived fungus *Coniothyrium cereale*. *Eur. J. Org. Chem.* **2012**, *2012*, 6197–6203.
140. Chen, Y.-H.; Lu, M.-C.; Chang, Y.-C.; Hwang, T.-L.; Wang, W.-H.; Weng, C.-F.; Kuo, J.; Sung, P.-J. Pseudoalteromone A: A novel bioactive ubiquinone from a marine bacterium *Pseudoalteromonas* sp. CGH2XX (Pseudoalteromonadaceae). *Tetrahedron Lett.* **2012**, *53*, 1675–1677.
141. Chen, Y.-H.; Kuo, J.; Su, J.-H.; Hwang, T.-L.; Chen, Y.-H.; Lee, C.-H.; Weng, C.-F.; Sung, P.-J. Pseudoalteromone B: A novel 15C compound from a marine bacterium *Pseudoalteromonas* sp. CGH2XX. *Mar. Drugs* **2012**, *10*, 1566–1571.
142. Ushiyama, S.; Umaoka, H.; Kato, H.; Suwa, Y.; Morioka, H.; Rotinsulu, H.; Losung, F.; Mangindaan, R.E.P.; de Voogd, N.J.; Yokosawa, H.; *et al.* Manadosterols A and B, sulfonated sterol dimers inhibiting the Ubc13–Uev1A interaction, isolated from the marine sponge *Lissodendryx fibrosa*. *J. Nat. Prod*. **2012**, *75*, 1495–1499.
143. Pina, I.C.; Gautschi, J.T.; Wang, G.-Y.-S.; Sanders, M.L.; Schmitz, F.J.; France, D.; Cornell-Kennon, S.; Sambucetti, L.C.; Remiszewski, S.W.; Perez, L.B.; *et al.* Psammaplins from the sponge *Pseudoceratina purpurea*: Inhibition of both histone deacetylase and DNA methyltransferase. *J. Org. Chem.* **2003**, *68*, 3866–3873.

144. Hentschel, F.; Sasseb, F.; Lindel, T. Fluorescent analogs of the marine natural product psammaplin A: Synthesis and biological activity. *Org. Biomol. Chem*. **2012**, *10*, 7120–7133.
145. Hosoya, T.; Hirokawa, T.; Takagi, M.; Shin-ya, K. Trichostatin analogues JBIR-109, JBIR-110, and JBIR-111 from the marine sponge-derived *Streptomyces* sp. RM72. *J. Nat. Prod.* **2012**, *75*, 285–289.
146. McKee, T.C.; Rabe, D.; Bokesch, H.R.; Grkovic, T.; Whitson, E.L.; Diyabalanage, T.; van Wyk, A.W.W.; Marcum, S.R.; Gardella, R.S.; Gustafson, K.R.; *et al.* Inhibition of Hypoxia Inducible Factor-2 transcription: Isolation of active modulators from marine sponges. *J. Nat. Prod*. **2012**, *75*, 1632–1636.
147. Du, L.; Mahdi, F.; Datta, S.; Jekabsons, M.B.; Zhou, Y.-D.; Nagle, D.G. Structures and mechanisms of antitumor agents: Xestoquinones uncouple cellular respiration and disrupt HIF signaling in human breast tumor cells. *J. Nat. Prod*. **2012**, *75*, 1553–1559.
148. Sun, Y.; Takada, K.; Takemoto, Y.; Yoshida, M.; Nogi, Y.; Okada, S.; Matsunaga, S. Gliotoxin analogues from a marine-derived fungus, *Penicillium* sp., and their cytotoxic and histone methyltransferase inhibitory activities. *J. Nat. Prod.* **2012**, *75*, 111–114.
149. Arai, M.; Yamano, Y.; Fujita, M.; Setiawan, A.; Kobayashi, M. Stylissamide X, a new proline-rich cyclic octapeptide as an inhibitor of cell migration, from an Indonesian marine sponge of *Stylissa* sp. *Bioorg. Med. Chem. Lett*. **2012**, *22*, 1818–1821.
150. Nguyen, V.-T.; Qian, Z.-J.; Ryu, B.M.; Kim, K.-N.; Kim, D.; Kim, Y.-M.; Jeon, Y.-J.; Park, W.S.; Choi, I.-W.; Kim, G.H.; *et al.* Matrix metalloproteinases (MMPs) inhibitory effects of an octameric oligopeptide isolated from abalone *Haliotis discus hannai*. *Food Chem*. **2013**, *141*, 503–509.
151. Nakamura, Y.; Kato, H.; Nishikawa, T.; Iwasaki, N.; Suwa, Y.; Rotinsulu, H.; Losung, F.; Maarisit, W.; Mangindaan, R.E.P.; Morioka, H.; *et al.* Siladenoserinols A–L: New sulfonated serinol derivatives from a tunicate as inhibitors of p53-Hdm2 interaction. *Org. Lett*. **2013**, *15*, 322–325.
152. Malloy, K.L.; Choi, H.; Fiorilla, C.; Valeriote, F.A.; Matainaho, T.; Gerwick, W.H. Hoiamide D, a marine cyanobacteria-derived inhibitor of p53/MDM2 interaction. *Bioorg. Med. Chem. Lett*. **2012**, *22*, 683–688.
153. Huang, X.; Sun, Y.-L.; Salim, A.A.; Chen, Z.-S.; Capon, R.J. Parguerenes: Marine red alga bromoditerpenes as inhibitors of P-glycoprotein (ABCB1) in multidrug resistant human cancer cells. *Biochem. Pharmacol*. **2013**, *85*, 1257–1268.
154. Niemann, H.; Lin, W.; Müller, W.E.G.; Kubbutat, M.; Lai, D.; Proksch, P. Trimeric hemibastadin congener from the marine sponge *Ianthella basta*. *J. Nat. Prod.* **2013**, *76*, 121–125.

Reactive Oxygen Species and Autophagy Modulation in Non-Marine Drugs and Marine Drugs

Ammad Ahmad Farooqi, Sundas Fayyaz, Ming-Feng Hou, Kun-Tzu Li, Jen-Yang Tang and Hsueh-Wei Chang

Abstract: It is becoming more understandable that an existing challenge for translational research is the development of pharmaceuticals that appropriately target reactive oxygen species (ROS)-mediated molecular networks in cancer cells. In line with this approach, there is an overwhelmingly increasing list of many non-marine drugs and marine drugs reported to be involved in inhibiting and suppressing cancer progression through ROS-mediated cell death. In this review, we describe the strategy of oxidative stress-based therapy and connect the ROS modulating effect to the regulation of apoptosis and autophagy. Finally, we focus on exploring the function and mechanism of cancer therapy by the autophagy modulators including inhibitors and inducers from non-marine drugs and marine drugs.

Reprinted from *Mar. Drugs*. Cite as: Farooqi, A.A.; Fayyaz, S.; Hou, M.-F.; Li, K.-T.; Tang, J.-Y.; Chang, H.-W. Reactive Oxygen Species and Autophagy Modulation in Non-Marine Drugs and Marine Drugs. *Mar. Drugs* **2014**, *12*, 5408-5424.

1. Introduction

1.1. Strategy of Oxidative Stress-Based Therapy

Reactive oxygen species (ROS) are essential to regulate normal cellular processes. When excess ROS stimulation appear, it may trigger DNA repair responses in normal cells to remove the ROS-mediated DNA damage [1]. For highly active metabolism, cancer cells commonly have higher levels of ROS than normal cells [2], leading to carcinogenesis by oxidative DNA damage [3] and DNA repair impairment [1]. This nature of high ROS level in cancer cells also provides a chance for drug therapy to generate overloading ROS level and induce oxidative stress-induced cell death [2,4]. Therefore, the modulation of oxidative stress is a potential strategy to anticancer therapies [5].

2. Connection between ROS and Apoptosis in Marine Drugs

In this section, we described the protective function of ROS scavengers and apoptosis induction of ROS generating drugs of marine sources as follows:

2.1. Protective Function of ROS Scavengers of Marine Sources

Several marine natural products have proved to have an anti-oxidative effect [6]. For example, aqueous extracts of the edible *Gracilaria tenuistipitata* have demonstrated to protect against H_2O_2-induced plasmid and cellular DNA damage and reverted the H_2O_2-induced cytotoxicity of

H1299 lung cancer cells [7]. Similarly, the brown alga *Sargassum horneri*-derived polysaccharides reportedly exert the protective effects against H_2O_2-induced injury in macrophage RAW264.7 cells. The results revealed that these biological effects were achieved by downregulating intracellular ROS, nitrogen oxide, and malonic dialdehyde (MDA) levels and by upregulating the level of antioxidant system (MnSOD and GSH-Px) in RAW264.7 cells [8]. Similarly, a lipid-soluble pigment of marine carotenoid astaxanthin can inhibit lipopolysaccaride-induced ROS generation and cytotoxicity via upregulation of superoxide dismutase (SOD) and catalase in mononuclear U937 cells [9].

2.2. Apoptosis Induction of ROS Generating Drugs of Marine Sources

In contrast, the accumulating evidence shows that several marine-derived extracts and compounds have the ROS inducible effects on different cancer cell lines. For example, 10-acetylirciformonin B (10AB), a marine sponge furanoterpenoid derived from irciformonin B [10], was reported to induce apoptosis via ROS generation in different cancer cell lines. Pretreatment of a ROS scavenger *N*-acetyl-L-cysteine to leukemia HL 60 cells drastically impaired 10AB-induced apoptosis, supporting that ROS generation was involved in irciformonin B-induced cytotoxicity of leukemia cells. Importantly, the protein expressions of Bcl-xL and Bcl-2, and caspase inhibitors (XIAP and surviving) were considerably repressed and the pro-apoptotic protein Bax was increased in 10AB treated leukemia HL 60 cells [11]. For another marine sponge derived compound Fascaplysin, it was apoptosis inducible in a chemoresistant NCI-H417 SCLC cells through ROS generation. Moreover, it was noted that fascaplysin worked synergistically with topoisomerase I-directed camptothecin and 10-hydroxy-camptothecin [12].

Dicitrinone B, a marine fungal metabolite, reportedly induced apoptosis via ROS generation in human malignant melanoma A375 cells. After pan-caspase inhibitor treatment to A375 cells, the dicitrinone B-induced ROS generation and apoptosis was abolished [13], suggesting that caspase pathway was involved in its ROS generation and apoptosis effects. A 48 kDa glycoprotein, isolated from a marine macroalga *Codium decorticatum*, was reported to induce ROS and apoptosis in breast cancer MDA-MB-231 cells through the intrinsic apoptosis pathway [14]. Surprisingly, it has been shown that lamellarin D, a marine alkaloid isolated from a marine mollusk *Lamellaria* sp. [15] and various ascidians [16], can induce ROS-mediated senescence in the absence of functional mitochondria in mouse leukemia P388 cells [17]. Marine triprenyl toluquinones and toluhydroquinones, originally purified from the Arminacean nudibranch *Leminda millecra*, have a similar ROS inducible effect to esophageal cancer WHCO1 cells [18]. Additionally, both methanolic extracts [19] and ethanolic extracts [20] of the editable red alga *Gracilaria tenuistipitata* showed the ROS generation and apoptosis induction in oral cancer cells. Ethyl acetate extracts from three marine algae (*Colpomenia sinuosa*, *Halimeda discoidae*, and *Galaxaura oblongata*) also displayed a ROS-mediated antiproliferative effect against human liver cancer and leukemia cells [21].

It had been reviewed that different natural products may induce different degrees of apoptosis and autophagy depending on their ROS modulating effect [22]. The marine drugs mentioned above have shown a ROS-mediated apoptotic effect, however, the possible roles of autophagy in these mechanisms warrant for further investigation.

3. Brief Introduction of Autophagy and Connection between ROS and Autophagy

In this section, we briefly introduce the autophagy and describe the relationship between ROS and autophagy as follows:

3.1. Brief Introduction of Autophagy

Autophagy is a "self-eating" behavior to ship cellular proteins and damaged organelles to lysosomes for recycling and it subsequently maintains the energy balance for cell survival during cell stress or starvation [23]. However, autophagy also reviewed to induce cell death in some cases [24]. There is a tremendously increasing amount of information regarding biology of autophagy. A substantial fraction of knowledge has been added into different steps of autophagy and it is now known that it is a highly regulated, multi-step molecular mechanism that initializes with induction, autophagosome nucleation, expansion and completion. Later steps of autophagy include lysosome fusion, degradation and recycling [25].

Structural studies have provided near complete resolution of protein network of mechanism of autophagy and mounting evidence suggested that initialization occurred through activation of AuTophaGy related 1 (Atg1) complex. It is multi-component machinery formed by assembly of Atg1, Atg13 and Atg17. Atg1 is a kinase that needs association of Atg13 and Atg17 for its activation. Vesicle nucleation is the subsequent process triggered by activation of the Vps34 and Beclin-1/Atg6. Autophagosome formation requires recruitment of proteins and lipids. Atg7 (E1-like) and Atg3 (E2-like) modulate vesicle elongation and completion by conjugation of phosphatidylethanolamine to microtubule-associated protein1 light chain 3 (LC3)/Atg8 which is initially processed by Atg4 [26]. Among them, the key step in autophagy is the proteolytic cleavage of LC3 to form LC3-I and subsequently modified to from LC3-II [27]. Moreover, Atg7 and Atg10 can join together to modulate the interaction between Atg12 and Atg5, and they are finally transferred to Atg16.

3.2. ROS May Lead to Autophagy

ROS are essential in maintaining normal cellular physiology, but ROS dysregulation may lead to tumor development and progression. Mitochondrial ROS generation play an important role for apoptosis and autophagy [25]. The autophagy may be induced to survival and cell death pathways in response to cellular oxidative stress [24]. Therefore, some of ROS-inducible drugs, such as 2-methoxyestradiol and arsenic trioxide, are used for cancer treatments [28]. Similarly, reduced scytonemin isolated from a terrestrial benthic cyanobacterium, *Nostoc commune*, induces ROS-based autophagy in human T-lymphoid Jurkat cells [29]. In the next sections, we will summarize many autophagy inhibitors and inducers derived from non-marine drugs and marine drugs to discuss the cancer therapy of those autophagy modulators.

4. Autophagy Inhibitors and Inducers from Non-Marine Drugs in Cancer Therapy

Accumulating evidence showed that it was inter-compensatory between autophagy and apoptosis. For example, autophagy may have a cytotoxic role [30]. When the autophagy was

induced, the cell death was promoted. For example, autophagic degradation of protein phosphatase Fap-1 was reported to enhance Fas-induced apoptosis. When cells displayed high autophagy, p62 recruited more Fap-1 for degradation and functional Fas ligands and receptors were highly maintained to activate more apoptotic signaling [31,32]. In this section, we described the function of the non-marine drugs derived autophagy inhibitors, autophagy inducers, clinical trial of autophagy inhibitor, clinical trial of autophagy inducers, and established anticancer drugs combined with autophagy inhibitors as follows:

4.1. Autophagy Inhibitors

Autophagy may have a cytoprotective role [30]. When the autophagy was inhibited, the cell death was promoted. For example, an autophagy inhibitor 3-methyladenine (3-MA) was reported to increase the apoptosis inducing potential of breast cancer MDA-MB 231 cells treated with a commercial mixture of tocotrienols and tocopherols (Tocomin®), which were isolated from palm oil/palm fruits [33,34]. It was revealed that mixture of tocotrienols and tocopherols can inhibit phosphoinositide 3-kinase (PI3K) and mammalian target of rapamycin (serine/threonine kinase) (mTOR) pathways, and induce the cytoprotective autophagic response in MDA-MB 231 cells, which could be overcome through inhibition of autophagy [34].

4.2. Autophagy Inducers

In accordance with the notion that Akt-mTOR signaling is a negative regulator of autophagy [35], gambogic acid, isolated from gamboge resin, can enhance the ROS accumulation and suppress phosphorylation of both Akt (S473) and mTOR (S2448) to induce autophagy in colorectal cancer HCT116 cells [36]. It is relevant to mention that extracellular signal-regulated kinases (ERK) pathway is also involved in initiation of autophagic response in hepatocellular carcinoma (HCC) cells as well as in mice xenografted with HCC cells [37]. A histone deacetylase inhibitor (HDACi) MGCD0103 has been shown to inhibit autophagy by functionalizing PI3K/AKT/mTOR pathway as well as caspases in B-cell chronic lymphocytic leukemia cells (CLL) [38]. Consistently, ATP-competitive mTOR kinase inhibitors (CC214-1 and CC214-2) were effective against rapamycin-resistant mTORC1 signaling to induce autophagy and prevent tumor cell death [39]. Cathepsin S, a lysosomal cysteine protease, was reported to overexpress in glioblastoma cells [40]. Inhibition of cathepsin S by its inhibitor Z-FL-COCHO (ZFL) can induce autophagy and mitochondrial-based apoptosis in glioblastoma cells. In autophagy-inhibitory glioblastoma cells by treating an autophagy inhibitor 3-MA or Beclin-1 shRNA, cathepsin S inhibition-induced apoptosis were drastically reduced. In cathepsin S-inhibitory glioblastoma cells, ROS-mediated PI3K/AKT/mTOR/p70S6K signaling pathway was inhibited and c-Jun N-terminal kinase (JNK) was activated [41].

4.3. Clinical Trial of Autophagy Inhibitors

Hydoxychloroquine (HCQ), a drug derived from quinolone, is antiproliferative to human dermal fibroblasts and induces autophagy in terms of upregulation of Beclin-1 [42,43]. Metastatic

pancreatic cancer patients previously treated with HCQ at a dosage of 400 mg or 600 mg twice daily did not show considerable autophagy inhibition or therapeutic value [44]. Recently, the combined treatments of autophagy inhibitor HCQ with some drugs are being tested in preclinical and ongoing clinical cancer studies [45]. For example, HCQ is noted to effectively inhibit cancer growth in combination with epirubicin in xenografted mice [46]. However, the dosages of HCQ applied to inhibit autophagy are inconsistently functional in clinic studies [47].

Additionally, Lys05, a water-soluble salt of the lead compound Lys01 show that Lys05 targets to impair autophagy and inhibit tumor growth without toxicity under lower doses of Lys05 in mice studies [47]. These results suggest that Lys05 is warranted for further clinical trial in future.

4.4. Established Anticancer Drugs Combined with Autophagy Inhibitors

Emerging evidence has shed light on the fact that autophagy induced resistance against chemotherapeutic drugs in cancer cells, *i.e.*, a cytoprotective role of autophagy. In the following section we will discuss accumulating *in vitro* and *in vivo* evidence to understand how autophagy inhibition can be helpful in maximizing chemotherapeutic drug induced therapeutic effects in cancer cells. For example, treating with 3-MA or Beclin-1 siRNA to inhibit autophagy in colorectal cancer HCT116 and RKO cells, the low dose (20–50 nM) of a clinical drug for topoisomerase I inhibitor camptothecin-induced senescence was turned to caspase 3-dependent apoptosis [48]. For the combined treatment of clinical drugs sorafenib and vorinostat (the multikinase and HDAC inhibitors, respectively), its growth inhibitory efficacy can be enhanced in the autophagy inhibitor 3-MA treated hepatoma cells [49]. Inhibition of autophagy by beclin1 siRNA in ovarian cancer SKOV3/DDP cells has been noted to considerably increase cisplatin-induced apoptosis [50]. By pre-treatment of chloroquine for autophagy inhibition, DNA damaging agent 5-fluorouracil-induced cell death were remarkably increased in gallbladder carcinoma SGC-996 and GBC-SD cells [51]. Similarly, inhibition of autophagy by chloroquine can restore sensitivity of resistant lung cancer H3122CR-1 cells to crizonitib (PF02341066, the inhibitor of ALK fusion oncoprotein) [52].

Similar cytoprotective role of autophagy was also reported in literature. For example, overexpressing high-mobility group nucleosome-binding domain 5 (HMGN5) in osteosarcoma U2OS and MG63 cell lines can induce resistance against chemotherapeutic drugs such as doxorubicin, cisplatin, and methotrexate via inducing autophagy [53]. Inhibition of autophagy with clomipramine or metformin can enhance apoptosis and show the cytoprotective role of autophagy. Gene silencing with AMP-dependent protein kinase (AMPK) siRNA can substantially inhibit AMPK-induced downstream autophagy signaling and induce apoptosis in clinical trial drug enzalutamide (ENZA) treated prostate cancer cells. In mice orthotopically transplanted with ENZA-resistant cells, the combined treatment of ENZA and autophagy inhibitors (clomipramine and metformin) can reduce tumor growth compared to control groups [54]. The signal transducer and activator of transcription 3 (STAT3) was activated by oxidative stress. Downregulated STAT3 in pancreatic cancer cells also reported to inhibit cell growth through repressing autophagy induced by the treatment of Nexrutine(R) (Nx), a bark extract from *Phellodendron amurense* [55].

There is an exciting piece of evidence highlighting diametrically opposed role of autophagy as a pro-survival (cytoprotective), as well as a cell death-inducing (cytotoxic) role in cancer cells. For

the example of cytotoxic role of autophagy, detailed investigation revealed that Akt activation and autophagy inhibition were responsible to the acquired resistance to sorafenib. A novel ATP-competitive pan-Akt inhibitor GDC0068 can reverse the acquired resistance to sorafenib, the first-line clinical drug for advanced HCC and autophagy was activated to be cytotoxic [56]. Similar cytotoxic role of autophagy was also reported that enforced expression of an imprinted tumor suppressor gene GTP-binding RAS-like 3 (DIRAS3 or ARHI) in DIRAS3-deficient ovarian cancer cells may induce autophagy and tumor dormancy [57]. In cells reconstituted with DIRAS3, growth factor-mediated intracellular signaling through PI3K and Ras/MAP kinase pathways were inhibited. Additionally, DIRAS3 can downregulate PI3K/AKT and Ras/ERK pathway and reduce phosphorylation of forkhead box O3 (FOXO3a) that facilitated transportation of FOXO3a to induce expression of autophagy-related genes (ATG4, MAP-LC3-I and Rab7) for maturation of autophagosomes and fusion with lysosomes [57]. Furthermore, DIRAS3 was reported to trigger assembly of autophagosome initiation complex to induce autophagy in dormant, nutrient-deprived ovarian cancer cells [58].

5. Autophagy Inhibitors and Inducers from Marine Drugs in Cancer Therapy

As shown in Table 1, in this section we described the autophagy inhibitors and inducers of marine drugs of several species of the marine sponges, algae, bacteria/fungi/cyanobacteria, and other marine-derived compounds as follows:

Table 1. A list of bioactive ingredients that act as autophagy inhibitors and inducers.

Function	Marine Source	Source	Chemical	Target	References
Autophagy inhibitors	Marine Sponge	*Petrosaspongia nigra*	Petrosaspongiolide M	Beclin-1 ↓	[59,60] *
	Marine bacterium	*Streptomyces* spp.	Bafilomycins	LC3-II ↓	[61]
Autophagy inducers	Marine Sponge	*Haliclona* sp.	Manzamine A	LC3-II ↑	[62]
				P62/SQTM1↑	[63] *
		Haliclona sp.	Papuamine	LC3-II ↑	[64,65] *
		Cliona celata	Clionamines A–D	LC3 ↑	[66]
		Geodia japonica	Stellettin A	LC3-II ↑	[67,68] *
		Rhabdastrella globostellata	Rhabdastrellic acid-A	pAkt ↓	[69,70] *
	Alga	Green algae (*Enteromorpha intestinalis*; *Rhizoclonium riparium*)	Methanolic extracts	LC3-II ↑	[71]
		Red alga (*Laurencia dendroidea*)	Sesquiterpene elatol	endoplasmic reticulum extension ↑	[72] [73] *
		Brown algae	Fucoxanthin	LC3-II ↑	[74]
				Beclin-1 ↑	[75] *
	Marine bacterium/fungus/ cyanobacterium	*Salinispora tropica;* *Salinispora arenicola*	Salinosporamide A	ATG5 ↑	[76]
				ATG7 ↑	[77] *
		Chondrostereum sp	Hirsutanol	LC3-II ↑	[78]
				ROS↑	[79] *
		Penicillium commune	SD118-xanthocillin X (1)	LC3-II ↑ mTOR, ERK ↓	[80]
		Leptolyngbya sp.	Coibamide	LC3-II ↑	[81]

* References state that autophagy-modulating drugs also have an apoptosis modulating effect.

5.1. Marine Sponge

5.1.1. Autophagy Inhibitors

5.1.1.1. *Petrosaspongia Nigra*

Petrosaspongiolide M, a γ-hydroxybutenolide terpenoid isolated from a marine sponge *Petrosaspongia nigra* [82], can exert inhibitory effects on autophagy in human macrophage U937 cells in terms of downregulation of Beclin-1 level [59].

5.1.2. Autophagy Inducers

5.1.2.1. *Haliclona* sp.

Manzamine A, a kind of alkaloids for the uncoupler of vacuolar ATPases isolated from a marine sponge *Haliclona*, was reported to be a potential autophagy inducer. Mechanistically, manzamine A exerted its effects via increasing LC3-II and p62/SQSTM1 in pancreatic cancer cells [62]. Moreover, manzamine A can resensitize TRAIL-induced apoptosis in the pancreatic cancer AsPC-1 cells [63].

Papuamine, one of the isolated compounds from *Haliclona* sp. has been noted to decrease survival of breast cancer MCF-7 cells. Papuamine treated MCF-7 cells revealed an increase in expression of LC3 after 4 h treatment. Overall it suggested that papuamine induced early autophagy in MCF-7 cells that later activated JNK [64].

5.1.2.2. *Cliona celata*

Aminosteroids clionamines A–D, isolated from South African sponge *Cliona celata*, was reported to induce autophagosome accumulation in terms of formation of cytoplasmic punctate Green Fluorescent Protein (GFP)-LC3 [66]. Clionamine B (2) was also reported to induce autophagy in human breast cancer MCF-7 cells [83].

5.1.2.3. *Geodia japonica*

Stellettin, isolated from a marine sponge *Geodia japonica*, has been shown to induce autophagy in B16F10 murine melanoma cells. Increased LC3-II and its co-localization with tyrosinase indicated removal of deglycosylated and unfolded proteins [67].

5.1.2.4. *Rhabdastrella globostellata*

Rhabdastrellic acid-A, an isomalabaricane Triterpenoid purified from a marine sponge *Rhabdastrella globostellata*, also notably induced autophagy in human lung cancer A549 cells. In Atg5 knockdown cells, rhabdastrellic acid-A mediated autophagy was impaired. pAkt was reduced in rhabdastrellic acid-A treated A549 cells and interestingly, transfecting constitutively active Akt in A549 cells can inhibit rhabdastrellic acid-A induced autophagy [69].

5.2. Alga

5.2.1. Autophagy Inducers

5.2.1.1. *Enteromorpha intestinalis* and *Rhizoclonium riparium*

Algal methanolic extracts from green alga *Enteromorpha intestinalis* and *Rhizoclonium riparium*, the saline/brackish water algae from Sundarbans, can induce autophagy in HeLa cells as evidenced by considerably enhanced expression of LC3-II [71].

5.2.2. *Laurencia dendroidea*

Sesquiterpene elatol, the major bioactive compound of red seaweed *Laurencia dendroidea*, was reported to be an antiproliferative agent against *Leishmania amazonensis* with endoplasmic reticulum extension, which is an autophagy marker [72].

5.2.3. Brown Algae

Fucoxanthin, a major carotenoid found in edible brown algae, was reported to be dose-responsively cytotoxic and G0/G1 arrest of HeLa cells without apoptosis change. Alternatively, autophagy-based cytotoxicity of fucoxanthin-treated HeLa cells was found involving the inhibition of Akt/mTOR signaling pathway [74].

5.3. Marine Bacterium/Fungus/Cyanobacterium

5.3.1. Autophagy Inhibitors

5.3.1.1. *Streptomyces* spp.

Eight bafilomycins (A1, B1, D, F, G, H, I, and J), purified from *Streptomyces* spp. of marine habitats, were proved to be potent inhibitors of autophagy in terms of automated microscopy screening assay-based punctate formation of EGFP-LC3 (autophagosome accumulation) and the Western blot-based EGFP-LC3 degradation assay [61]. Proteinase inhibitors, such as clasto-lactacystinblactone (LA) or epoxomicin (Epo) were recently reported to induce autophagy through inhibition of PI3K-Akt-mTOR pathway in human retinal pigment epithelial ARPE-19 cells [84]. Using the autophagy inhibitor bafilomycin A1, the protective effects of LA or Epo against menadione-induced oxidative injuries in ARPE-19 cells were reverted.

5.3.2. Autophagy Inducers

5.3.2.1. *Salinispora tropica* and *Salinispora arenicola*

Salinosporamide A, a potent proteasome inhibitor from marine bacteria *Salinispora tropica* and *Salinispora arenicola*, was reported to induce autophagy through a phospho-eukaryotic translation initiation factor 2α (eIF2α) pathway to reduce proteotoxic stresses in human prostate cancer cells [76].

5.3.2.2. *Chondrostereum* sp.

Hirsutanol is a sesquiterpene isolated from marine fungus *Chondrostereum* sp. in the coral *Sarcophyton tortuosum* [85]. In hirsutanol-treated breast cancer MCF-7 cells, LC3-I to LC3-II conversion and ROS induction were markedly increased as evidenced by Western blot assay and flow cytometry [78].

5.3.2.3. *Penicillium commune*

SD118-xanthocillin X, isolated from the marine fungus *Penicillium commune*, can induce autophagy in hepatocellular carcinoma HepG2 cells. There was a conversion of LC3-I to LC3-II, following lipidation as it incorporates into the nascent membrane of the autophagosome. Mechanistically it was noted that SD118-xanthocillin regulated different modulators of autophagy. It exerted its autophagy inducing effects via inhibition of phosphorylation of mTOR and ERK1/2. Additionally, Bcl-2 mediated inhibition of Beclin-1 to suppress autophagy was also attenuated via inhibition of Bcl-2 by SD118-xanthocillin [80].

5.3.2.4. *Leptolyngbya* sp.

Coibamide A, a depsipeptide derived from marine cyanobacterium *Leptolyngbya* sp., showed a cytotoxicity in the dose-responsive and time-dependent manner in human glioblastoma cells and mouse embryonic fibroblasts (MEF) [81]. In coibamide A treated human glioblastoma U87-MG cells, LC3-II expression was notably increased. Coibamide A also induced the autophagosome accumulation in glioblastoma and MEF cells. Detailed mechanistic insights indicated that accumulation of autophagosomes was independent of mTOR-mediated signaling.

5.4. Other Marine-Derived Agents

Marine-derived agents, including eicosapentaenoic acid (EPA) and docosahexaenoic acid (DHA), are also potent inducers of autophagy as indicated by formation of autophagosomes in DHA- or EPA-treated lung adenocarcinoma A549 cells [86].

The Na^+/K^+-ATPases (NKA) inhibitor cardiac glycosides, a family of natural or synthetic steroid hormones isolated from marine or terrestrial natural products [87], can exert their potent anti-cancer properties via activation of Src in the upstream of MEK1/2 and ERK1/2 pathway in human non-small cell lung cancer A549 and H460 cells [88]. Src inhibition by its inhibitor PP2 or siRNA can remarkably repress cardiac glycosides-induced MEK1/2 and ERK1/2 phosphorylation and autophagic cell death. Moreover, ROS was also noted to be accumulated and contributed to cardiac glycosides-induced Src mediated autophagic response in lung cancer cells.

6. Conclusions

In this review, we summarized how ROS-mediated molecular networks may result in autophagy. The autophagic effects of both clinical drugs and natural products-derived extracts and pure compounds were discussed. In the example of many autophagy modulators (inducers and

inhibitors) from non-marine drugs and marine drugs, ROS changes and signaling was demonstrated to be involved in autophagy. Many marine drugs with autophagy were also summarized from marine sponges, alga, and marine bacteria/fungi/ cyanobacteria. It suggests that marine drugs with ROS modulating effect have a potential to modulate the autophagy of cancer cells to improve cancer therapy.

Acknowledgments

This work was partly supported by funds of the Ministry of Science and Technology (MOST 103-2320-B-037-008), the Kaohsiung Medical University "Aim for the Top Universities Grant, grant No. KMU-TP103A33", the National Sun Yat-sen University-KMU Joint Research Project (#NSYSU-KMU 103-p014), and the Health and welfare surcharge of tobacco products, the Ministry of Health and Welfare, Taiwan, Republic of China (MOHW103-TD-B-111-05).

Author Contributions

A.-A.F., J.-Y.T., and H.-W.C. integrated different points of searched literatures, and drafted the manuscript. S.F., M.-F.H. and K.-T.L. conceived the idea, did literature search on specific points, and involved in discussion. All authors read and approved the final manuscript.

Conflicts of Interest

The authors declare no conflict of interest.

References

1. Trachootham, D.; Alexandre, J.; Huang, P. Targeting cancer cells by ROS-mediated mechanisms: A radical therapeutic approach? *Nat. Rev. Drug Discov.* **2009**, *8*, 579–591.
2. Nogueira, V.; Hay, N. Molecular pathways: Reactive oxygen species homeostasis in cancer cells and implications for cancer therapy. *Clin. Cancer Res.* **2013**, *19*, 4309–4314.
3. Montero, A.J.; Jassem, J. Cellular redox pathways as a therapeutic target in the treatment of cancer. *Drugs* **2011**, *71*, 1385–1396.
4. Ivanova, D.; Bakalova, R.; Lazarova, D.; Gadjeva, V.; Zhelev, Z. The impact of reactive oxygen species on anticancer therapeutic strategies. *Adv. Clin. Exp. Med.* **2013**, *22*, 899–908.
5. Gorrini, C.; Harris, I.S.; Mak, T.W. Modulation of oxidative stress as an anticancer strategy. *Nat Rev. Drug Discov.* **2013**, *12*, 931–947.
6. Lee, J.C.; Hou, M.F.; Huang, H.W.; Chang, F.R.; Yeh, C.C.; Tang, J.Y.; Chang, H.W. Marine algal natural products with anti-oxidative, anti-inflammatory, and anti-cancer properties. *Cancer Cell Int.* **2013**, *13*, 55.
7. Yang, J.I.; Yeh, C.C.; Lee, J.C.; Yi, S.C.; Huang, H.W.; Tseng, C.N.; Chang, H.W. Aqueous extracts of the edible *Gracilaria tenuistipitata* are protective against H_2O_2-induced DNA damage, growth inhibition, and cell cycle arrest. *Molecules* **2012**, *17*, 7241–7254.

8. Wen, Z.S.; Liu, L.J.; OuYang, X.K.; Qu, Y.L.; Chen, Y.; Ding, G.F. Protective effect of polysaccharides from *Sargassum horneri* against oxidative stress in RAW264.7 cells. *Int. J. Biol. Macromol.* **2014**, *68C*, 98–106.
9. Franceschelli, S.; Pesce, M.; Ferrone, A.; De Lutiis, M.A.; Patruno, A.; Grilli, A.; Felaco, M.; Speranza, L. Astaxanthin treatment confers protection against oxidative stress in U937 cells stimulated with lipopolysaccharide reducing O2- production. *PLoS One* **2014**, *9*, e88359.
10. Su, J.H.; Chang, W.B.; Chen, H.M.; El-Shazly, M.; Du, Y.C.; Kung, T.H.; Chen, Y.C.; Sung, P.J.; Ho, Y.S.; Kuo, F.W.; *et al.* 10-acetylirciformonin B, a sponge furanoterpenoid, induces DNA damage and apoptosis in leukemia cells. *Molecules* **2012**, *17*, 11839–11848.
11. Shih, H.C.; El-Shazly, M.; Juan, Y.S.; Chang, C.Y.; Su, J.H.; Chen, Y.C.; Shih, S.P.; Chen, H.M.; Wu, Y.C.; Lu, M.C. Cracking the cytotoxicity code: Apoptotic induction of 10-acetylirciformonin B is mediated through ROS generation and mitochondrial dysfunction. *Mar. Drugs* **2014**, *12*, 3072–3090.
12. Hamilton, G. Cytotoxic effects of fascaplysin against small cell lung cancer cell lines. *Mar. Drugs* **2014**, *12*, 1377–1389.
13. Chen, L.; Gong, M.W.; Peng, Z.F.; Zhou, T.; Ying, M.G.; Zheng, Q.H.; Liu, Q.Y.; Zhang, Q.Q. The marine fungal metabolite, dicitrinone B, induces A375 cell apoptosis through the ROS-related caspase pathway. *Mar. Drugs* **2014**, *12*, 1939–1958.
14. Thangam, R.; Senthilkumar, D.; Suresh, V.; Sathuvan, M.; Sivasubramanian, S.; Pazhanichamy, K.; Gorlagunta, P.K.; Kannan, S.; Gunasekaran, P.; Rengasamy, R.; *et al.* Induction of ROS-dependent mitochondria-mediated intrinsic apoptosis in MDA-MB-231 cells by glycoprotein from *Codium decorticatum*. *J. Agric. Food Chem.* **2014**, *62*, 3410–3421.
15. Andersen, R.J.; Faulkner, D.J.; He, C.H.; Van Duyne, G.D.; Clardy, J. Metabolites of the marine prosobranch mollusk *Lamellaria* sp. *J. Am. Chem. Soc.* **1985**, *107*, 5492–5495.
16. Davis, R.A.; Carroll, A.R.; Pierens, G.K.; Quinn, R.J. New lamellarin alkaloids from the Australian ascidian, *Didemnum chartaceum*. *J. Nat. Prod.* **1999**, *62*, 419–424.
17. Ballot, C.; Martoriati, A.; Jendoubi, M.; Buche, S.; Formstecher, P.; Mortier, L.; Kluza, J.; Marchetti, P. Another facet to the anticancer response to lamellarin D: Induction of cellular senescence through inhibition of topoisomerase I and intracellular ROS production. *Mar. Drugs* **2014**, *12*, 779–798.
18. Whibley, C.E.; McPhail, K.L.; Keyzers, R.A.; Maritz, M.F.; Leaner, V.D.; Birrer, M.J.; Davies-Coleman, M.T.; Hendricks, D.T. Reactive oxygen species mediated apoptosis of esophageal cancer cells induced by marine triprenyl toluquinones and toluhydroquinones. *Mol. Cancer Ther.* **2007**, *6*, 2535–2543.
19. Yeh, C.C.; Yang, J.I.; Lee, J.C.; Tseng, C.N.; Chan, Y.C.; Hseu, Y.C.; Tang, J.Y.; Chuang, L.Y.; Huang, H.W.; Chang, F.R.; *et al.* Anti-proliferative effect of methanolic extract of *Gracilaria tenuistipitata* on oral cancer cells involves apoptosis, DNA damage, and oxidative stress. *BMC Complement Altern. Med.* **2012**, *12*, 142.
20. Yeh, C.C.; Tseng, C.N.; Yang, J.I.; Huang, H.W.; Fang, Y.; Tang, J.Y.; Chang, F.R.; Chang, H.W. Antiproliferation and induction of apoptosis in Ca9-22 oral cancer cells by ethanolic extract of *Gracilaria tenuistipitata*. *Molecules* **2012**, *17*, 10916–10927.

21. Huang, H.L.; Wu, S.L.; Liao, H.F.; Jiang, C.M.; Huang, R.L.; Chen, Y.Y.; Yang, Y.C.; Chen, Y.J. Induction of apoptosis by three marine algae through generation of reactive oxygen species in human leukemic cell lines. *J. Agric. Food Chem.* **2005**, *53*, 1776–1781.
22. Chang, H.W. The fate of marine algal natural products-treated cells depend on it ROS modulating effects. *J. Rashid Latif Med. College* **2013**, *2*, 8–10.
23. Mizushima, N. Autophagy: Process and function. *Genes Dev.* **2007**, *21*, 2861–2873.
24. Li, L.; Ishdorj, G.; Gibson, S.B. Reactive oxygen species regulation of autophagy in cancer: Implications for cancer treatment. *Free Radic. Biol. Med.* **2012**, *53*, 1399–1410.
25. Li, Z.Y.; Yang, Y.; Ming, M.; Liu, B. Mitochondrial ROS generation for regulation of autophagic pathways in cancer. *Biochem. Biophys. Res. Commun.* **2011**, *414*, 5–8.
26. Denton, D.; Nicolson, S.; Kumar, S. Cell death by autophagy: Facts and apparent artefacts. *Cell Death Differ.* **2012**, *19*, 87–95.
27. Tanida, I.; Sou, Y.S.; Ezaki, J.; Minematsu-Ikeguchi, N.; Ueno, T.; Kominami, E. HsAtg4B/HsApg4B/autophagin-1 cleaves the carboxyl termini of three human Atg8 homologues and delipidates microtubule-associated protein light chain 3- and GABAA receptor-associated protein-phospholipid conjugates. *J. Biol. Chem.* **2004**, *279*, 36268–36276.
28. Azad, M.B.; Chen, Y.; Gibson, S.B. Regulation of autophagy by reactive oxygen species (ROS): Implications for cancer progression and treatment. *Antioxid. Redox Signal.* **2009**, *11*, 777–790.
29. Itoh, T.; Tsuzuki, R.; Tanaka, T.; Ninomiya, M.; Yamaguchi, Y.; Takenaka, H.; Ando, M.; Tsukamasa, Y.; Koketsu, M. Reduced scytonemin isolated from Nostoc commune induces autophagic cell death in human T-lymphoid cell line Jurkat cells. *Food Chem. Toxicol.* **2013**, *60*, 76–82.
30. Gewirtz, D.A. The four faces of autophagy: Implications for cancer therapy. *Cancer Res.* **2014**, *74*, 647–651.
31. Joshi, S.; Ryan, K.M. Autophagy chews Fap to promote apoptosis. *Nat. Cell Biol.* **2014**, *16*, 23–25.
32. Gump, J.M.; Staskiewicz, L.; Morgan, M.J.; Bamberg, A.; Riches, D.W.; Thorburn, A. Autophagy variation within a cell population determines cell fate through selective degradation of Fap-1. *Nat. Cell Biol.* **2014**, *16*, 47–54.
33. Yu, W.; Simmons-Menchaca, M.; Gapor, A.; Sanders, B.G.; Kline, K. Induction of apoptosis in human breast cancer cells by tocopherols and tocotrienols. *Nutr. Cancer* **1999**, *33*, 26–32.
34. Tran, A.T.; Ramalinga, M.; Kedir, H.; Clarke, R.; Kumar, D. Autophagy inhibitor 3-methyladenine potentiates apoptosis induced by dietary tocotrienols in breast cancer cells. *Eur. J. Nutr.* **2014**, in press [PMID: 24830781].
35. Liang, C. Negative regulation of autophagy. *Cell Death Differ.* **2010**, *17*, 1807–1815.
36. Zhang, H.; Lei, Y.; Yuan, P.; Li, L.; Luo, C.; Gao, R.; Tian, J.; Feng, Z.; Nice, E.C.; Sun, J. ROS-mediated autophagy induced by dysregulation of lipid metabolism plays a protective role in colorectal cancer cells treated with gambogic acid. *PLoS One* **2014**, *9*, e96418.

37. Gong, K.; Zhang, Z.; Chen, Y.; Shu, H.B.; Li, W. Extracellular signal-regulated kinase, receptor interacting protein, and reactive oxygen species regulate shikonin-induced autophagy in human hepatocellular carcinoma. *Eur. J. Pharmacol.* **2014**, *738*, 142–152.
38. El-Khoury, V.; Pierson, S.; Szwarcbart, E.; Brons, N.H.; Roland, O.; Cherrier-De Wilde, S.; Plawny, L.; van Dyck, E.; Berchem, G. Disruption of autophagy by the histone deacetylase inhibitor MGCD0103 and its therapeutic implication in B-cell chronic lymphocytic leukemia. *Leukemia* **2014**, *28*, 1636–1646.
39. Gini, B.; Zanca, C.; Guo, D.; Matsutani, T.; Masui, K.; Ikegami, S.; Yang, H.; Nathanson, D.; Villa, G.R.; Shackelford, D.; *et al.* The mTOR kinase inhibitors, CC214-1 and CC214-2, preferentially block the growth of EGFRvIII-activated glioblastomas. *Clin. Cancer Res.* **2013**, *19*, 5722–5732.
40. Flannery, T.; McQuaid, S.; McGoohan, C.; McConnell, R.S.; McGregor, G.; Mirakhur, M.; Hamilton, P.; Diamond, J.; Cran, G.; Walker, B.; *et al.* Cathepsin S expression: An independent prognostic factor in glioblastoma tumours—A pilot study. *Int. J. Cancer* **2006**, *119*, 854–860.
41. Zhang, L.; Wang, H.; Xu, J.; Zhu, J.; Ding, K. Inhibition of cathepsin S induces autophagy and apoptosis in human glioblastoma cell lines through ROS-mediated PI3K/AKT/mTOR/p70S6K and JNK signaling pathways. *Toxicol. Lett.* **2014**, *228*, 248–259.
42. Oikarinen, A. Hydroxychloroquine induces autophagic cell death of human dermal fibroblasts: Implications for treating fibrotic skin diseases. *J. Invest. Dermatol.* **2009**, *129*, 2333–2335.
43. Ramser, B.; Kokot, A.; Metze, D.; Weiss, N.; Luger, T.A.; Bohm, M. Hydroxychloroquine modulates metabolic activity and proliferation and induces autophagic cell death of human dermal fibroblasts. *J. Invest. Dermatol.* **2009**, *129*, 2419–2426.
44. Wolpin, B.M.; Rubinson, D.A.; Wang, X.; Chan, J.A.; Cleary, J.M.; Enzinger, P.C.; Fuchs, C.S.; McCleary, N.J.; Meyerhardt, J.A.; Ng, K.; *et al.* Phase II and pharmacodynamic study of autophagy inhibition using hydroxychloroquine in patients with metastatic pancreatic adenocarcinoma. *Oncologist* **2014**, *19*, 637–638.
45. Yang, Z.J.; Chee, C.E.; Huang, S.; Sinicrope, F.A. The role of autophagy in cancer: Therapeutic implications. *Mol. Cancer Ther.* **2011**, *10*, 1533–1541.
46. Chittaranjan, S.; Bortnik, S.; Dragowska, W.H.; Xu, J.; Abeysundara, N.; Leung, A.; Go, N.E.; DeVorkin, L.; Weppler, S.A.; Gelmon, K.; *et al.* Autophagy inhibition augments the anticancer effects of epirubicin treatment in anthracycline-sensitive and -resistant triple-negative breast cancer. *Clin. Cancer Res.* **2014**, *20*, 3159–3173.
47. McAfee, Q.; Zhang, Z.; Samanta, A.; Levi, S.M.; Ma, X.H.; Piao, S.; Lynch, J.P.; Uehara, T.; Sepulveda, A.R.; Davis, L.E.; *et al.* Autophagy inhibitor Lys05 has single-agent antitumor activity and reproduces the phenotype of a genetic autophagy deficiency. *Proc. Natl. Acad. Sci. USA* **2012**, *109*, 8253–8258.
48. Zhang, J.W.; Zhang, S.S.; Song, J.R.; Sun, K.; Zong, C.; Zhao, Q.D.; Liu, W.T.; Li, R.; Wu, M.C.; Wei, L.X. Autophagy inhibition switches low-dose camptothecin-induced premature senescence to apoptosis in human colorectal cancer cells. *Biochem. Pharmacol.* **2014**, *90*, 265–275.

49. Yuan, H.; Li, A.J.; Ma, S.L.; Cui, L.J.; Wu, B.; Yin, L.; Wu, M.C. Inhibition of autophagy signi fi cantly enhances combination therapy with sorafenib and HDAC inhibitors for human hepatoma cells. *World J. Gastroenterol.* **2014**, *20*, 4953–4962.
50. Sun, Y.; Liu, J.H.; Jin, L.; Sui, Y.X.; Lai, L.; Yang, Y. Inhibition of beclin 1 expression enhances cisplatin-induced apoptosis through a mitochondrial-dependent pathway in human ovarian cancer SKOV3/DDP cells. *Oncol. Res.* **2014**, *21*, 261–269.
51. Liang, X.; Tang, J.; Liang, Y.; Jin, R.; Cai, X. Suppression of autophagy by chloroquine sensitizes 5-fluorouracil-mediated cell death in gallbladder carcinoma cells. *Cell Biosci.* **2014**, *4*, 10.
52. Ji, C.; Zhang, L.; Cheng, Y.; Patel, R.; Wu, H.; Zhang, Y.; Wang, M.; Ji, S.; Belani, C.P.; Yang, J.M.; Ren, X. Induction of autophagy contributes to crizotinib resistance in ALK-positive lung cancer. *Cancer Biol. Ther.* **2014**, *15*, 570–577.
53. Yang, C.; Gao, R.; Wang, J.; Yuan, W.; Wang, C.; Zhou, X. High-mobility group nucleosome-binding domain 5 increases drug resistance in osteosarcoma through upregulating autophagy. *Tumour Biol.* **2014**, *35*, 6357–6363.
54. Nguyen, H.G.; Yang, J.C.; Kung, H.J.; Shi, X.B.; Tilki, D.; Lara, P.N., Jr.; Devere White, R.W.; Gao, A.C.; Evans, C.P. Targeting autophagy overcomes Enzalutamide resistance in castration-resistant prostate cancer cells and improves therapeutic response in a xenograft model. *Oncogene* **2014**, *33*, 4521–4530.
55. Gong, J.; Munoz, A.R.; Chan, D.; Ghosh, R.; Kumar, A.P. STAT3 down regulates LC3 to inhibit autophagy and pancreatic cancer cell growth. *Oncotarget* **2014**, *5*, 2529–2541.
56. Zhai, B.; Hu, F.; Jiang, X.; Xu, J.; Zhao, D.; Liu, B.; Pan, S.; Dong, X.; Tan, G.; Wei, Z.; *et al.* Inhibition of Akt reverses the acquired resistance to sorafenib by switching protective autophagy to autophagic cell death in hepatocellular carcinoma. *Mol. Cancer Ther.* **2014**, *13*, 1589–1598.
57. Lu, Z.; Yang, H.; Sutton, M.N.; Yang, M.; Clarke, C.H.; Liao, W.S.; Bast, R.C., Jr. ARHI (DIRAS3) induces autophagy in ovarian cancer cells by downregulating the epidermal growth factor receptor, inhibiting PI3K and Ras/MAP signaling and activating the FOXo3a-mediated induction of Rab7. *Cell Death Differ.* **2014**, *21*, 1275–1289.
58. Lu, Z.; Baquero, M.T.; Yang, H.; Yang, M.; Reger, A.S.; Kim, C.; Levine, D.A.; Clarke, C.H.; Liao, W.S.; Bast, R.C., Jr. DIRAS3 regulates the autophagosome initiation complex in dormant ovarian cancer cells. *Autophagy* **2014**, *10*, 1071–1092.
59. Monti, M.C.; Margarucci, L.; Riccio, R.; Bonfili, L.; Mozzicafreddo, M.; Eleuteri, A.M.; Casapullo, A. Mechanistic insights on petrosaspongiolide M inhibitory effects on immunoproteasome and autophagy. *Biochim. Biophys. Acta* **2014**, *1844*, 713–721.
60. Yadav, A.K.; Vashishta, V.; Joshi, N.; Taneja, P. AR-A 014418 used against GSK3beta downregulates expression of hnRNPA1 and SF2/ASF splicing factors. *J. Oncol.* **2014**, *2014*, 695325.

61. Carr, G.; Williams, D.E.; Diaz-Marrero, A.R.; Patrick, B.O.; Bottriell, H.; Balgi, A.D.; Donohue, E.; Roberge, M.; Andersen, R.J. Bafilomycins produced in culture by *Streptomyces* spp. isolated from marine habitats are potent inhibitors of autophagy. *J. Nat. Prod.* **2010**, *73*, 422–427.
62. Kallifatidis, G.; Hoepfner, D.; Jaeg, T.; Guzman, E.A.; Wright, A.E. The marine natural product manzamine A targets vacuolar ATPases and inhibits autophagy in pancreatic cancer cells. *Mar. Drugs* **2013**, *11*, 3500–3516.
63. Guzman, E.A.; Johnson, J.D.; Linley, P.A.; Gunasekera, S.E.; Wright, A.E. A novel activity from an old compound: Manzamine A reduces the metastatic potential of AsPC-1 pancreatic cancer cells and sensitizes them to TRAIL-induced apoptosis. *Invest. New Drugs* **2011**, *29*, 777–785.
64. Kanno, S.; Yomogida, S.; Tomizawa, A.; Yamazaki, H.; Ukai, K.; Mangindaan, R.E.; Namikoshi, M.; Ishikawa, M. Papuamine causes autophagy following the reduction of cell survival through mitochondrial damage and JNK activation in MCF-7 human breast cancer cells. *Int. J. Oncol.* **2013**, *43*, 1413–1419.
65. Yamazaki, H.; Wewengkang, D.S.; Kanno, S.; Ishikawa, M.; Rotinsulu, H.; Mangindaan, R.E.; Namikoshi, M. Papuamine and haliclonadiamine, obtained from an Indonesian sponge *Haliclona* sp., inhibited cell proliferation of human cancer cell lines. *Nat. Prod. Res.* **2013**, *27*, 1012–1015.
66. Keyzers, R.A.; Daoust, J.; Davies-Coleman, M.T.; van Soest, R.; Balgi, A.; Donohue, E.; Roberge, M.; Andersen, R.J. Autophagy-modulating aminosteroids isolated from the sponge *Cliona celata*. *Org. Lett.* **2008**, *10*, 2959–2962.
67. Liu, W.K.; Ling, Y.H.; Cheung, F.W.; Che, C.T. Stellettin A induces endoplasmic reticulum stress in murine B16 melanoma cells. *J. Nat. Prod.* **2012**, *75*, 586–590.
68. Liu, W.K.; Cheung, F.W.; Che, C.T. Stellettin A induces oxidative stress and apoptosis in HL-60 human leukemia and LNCaP prostate cancer cell lines. *J. Nat. Prod.* **2006**, *69*, 934–937.
69. Li, D.D.; Guo, J.F.; Huang, J.J.; Wang, L.L.; Deng, R.; Liu, J.N.; Feng, G.K.; Xiao, D.J.; Deng, S.Z.; Zhang, X.S.; Zhu, X.F. Rhabdastrellic acid-A induced autophagy-associated cell death through blocking Akt pathway in human cancer cells. *PLoS One* **2010**, *5*, e12176.
70. Guo, J.F.; Zhou, J.M.; Zhang, Y.; Deng, R.; Liu, J.N.; Feng, G.K.; Liu, Z.C.; Xiao, D.J.; Deng, S.Z.; Zhu, X.F. Rhabdastrellic acid-A inhibited PI3K/Akt pathway and induced apoptosis in human leukemia HL-60 cells. *Cell Biol. Int.* **2008**, *32*, 48–54.
71. Paul, S.; Kundu, R. Antiproliferative activity of methanolic extracts from two green algae, *Enteromorpha intestinalis* and *Rhizoclonium riparium* on HeLa cells. *Disab. Advocacy Resour. Unit* **2013**, *21*, 72.
72. Dos Santos, A.O.; Veiga-Santos, P.; Ueda-Nakamura, T.; Filho, B.P.; Sudatti, D.B.; Bianco, E.M.; Pereira, R.C.; Nakamura, C.V. Effect of elatol, isolated from red seaweed *Laurencia dendroidea*, on *Leishmania amazonensis*. *Mar. Drugs* **2010**, *8*, 2733–2743.
73. Campos, A.; Souza, C.B.; Lhullier, C.; Falkenberg, M.; Schenkel, E.P.; Ribeiro-do-Valle, R.M.; Siqueira, J.M. Anti-tumour effects of elatol, a marine derivative compound obtained from red algae *Laurencia microcladia*. *J. Pharm. Pharmacol.* **2012**, *64*, 1146–1154.

74. Hou, L.L.; Gao, C.; Chen, L.; Hu, G.Q.; Xie, S.Q. Essential role of autophagy in fucoxanthin-induced cytotoxicity to human epithelial cervical cancer HeLa cells. *Acta Pharmacol. Sin.* **2013**, *34*, 1403–1410.
75. Wang, J.; Chen, S.; Xu, S.; Yu, X.; Ma, D.; Hu, X.; Cao, X. *In vivo* induction of apoptosis by fucoxanthin, a marine carotenoid, associated with down-regulating STAT3/EGFR signaling in sarcoma 180 (S180) xenografts-bearing mice. *Mar. Drugs* **2012**, *10*, 2055–2068.
76. Zhu, K.; Dunner, K. Jr.; McConkey, D.J. Proteasome inhibitors activate autophagy as a cytoprotective response in human prostate cancer cells. *Oncogene* **2010**, *29*, 451–462.
77. Ahn, K.S.; Sethi, G.; Chao, T.H.; Neuteboom, S.T.; Chaturvedi, M.M.; Palladino, M.A.; Younes, A.; Aggarwal, B.B. Salinosporamide A (NPI-0052) potentiates apoptosis, suppresses osteoclastogenesis, and inhibits invasion through down-modulation of NF-kappaB regulated gene products. *Blood* **2007**, *110*, 2286–2295.
78. Yang, F.; Chen, W.D.; Deng, R.; Li, D.D.; Wu, K.W.; Feng, G.K.; Li, H.J.; Zhu, X.F. Hirsutanol A induces apoptosis and autophagy via reactive oxygen species accumulation in breast cancer MCF-7 cells. *J. Pharmacol. Sci.* **2012**, *119*, 214–220.
79. Yang, F.; Chen, W.D.; Deng, R.; Zhang, H.; Tang, J.; Wu, K.W.; Li, D.D.; Feng, G.K.; Lan, W.J.; Li, H.J.; *et al.* Hirsutanol A, a novel sesquiterpene compound from fungus *Chondrostereum* sp., induces apoptosis and inhibits tumor growth through mitochondrial-independent ROS production: Hirsutanol A inhibits tumor growth through ROS production. *J. Transl. Med.* **2013**, *11*, 32.
80. Zhao, Y.; Chen, H.; Shang, Z.; Jiao, B.; Yuan, B.; Sun, W.; Wang, B.; Miao, M.; Huang, C. SD118-xanthocillin X (1), a novel marine agent extracted from *Penicillium commune*, induces autophagy through the inhibition of the MEK/ERK pathway. *Mar. Drugs* **2012**, *10*, 1345–1359.
81. Hau, A.M.; Greenwood, J.A.; Lohr, C.V.; Serrill, J.D.; Proteau, P.J.; Ganley, I.G.; McPhail, K.L.; Ishmael, J.E. Coibamide A induces mTOR-independent autophagy and cell death in human glioblastoma cells. *PLoS One* **2013**, *8*, e65250.
82. Randazzo, A.; Debitus, C.; Minale, L.; Garcia Pastor, P.; Alcaraz, M.J.; Paya, M.; Gomez-Paloma, L. Petrosaspongiolides M–R: New potent and selective phospholipase A2 inhibitors from the New Caledonian marine sponge *Petrosaspongia nigra*. *J. Nat. Prod.* **1998**, *61*, 571–575.
83. Forestieri, R.; Donohue, E.; Balgi, A.; Roberge, M.; Andersen, R.J. Synthesis of clionamine B, an autophagy stimulating aminosteroid isolated from the sponge Cliona celata. *Org. Lett.* **2013**, *15*, 3918–3921.
84. Tang, B.; Cai, J.; Sun, L.; Li, Y.; Qu, J.; Snider, B.J.; Wu, S. Proteasome inhibitors activate autophagy involving inhibition of PI3K-Akt-mTOR pathway as an anti-oxidation defense in human RPE cells. *PLoS One* **2014**, *9*, e103364.
85. Wang, G.Y.S.; Abrell, L.M.; Avelar, A.; Borgeson, B.M.; Crews, P. New hirsutane based sesquiquiterpenes from salt water cultures of a marine sponge-derived fungus and the terrestrial fungus coriolus consors. *Tetrahedron* **1998**, *54*, 7335–7342.

86. Yao, Q.H.; Zhang, X.C.; Fu, T.; Gu, J.Z.; Wang, L.; Wang, Y.; Lai, Y.B.; Wang, Y.Q.; Guo, Y. omega-3 polyunsaturated fatty acids inhibit the proliferation of the lung adenocarcinoma cell line A549 *in vitro*. *Mol. Med. Rep.* **2014**, *9*, 401–406.
87. Ivanchina, N.V.; Kicha, A.A.; Stonik, V.A. Steroid glycosides from marine organisms. *Steroids* **2011**, *76*, 425–454.
88. Wang, Y.; Zhan, Y.; Xu, R.; Shao, R.; Jiang, J.; Wang, Z. Src mediates extracellular signal-regulated kinase 1/2 activation and autophagic cell death induced by cardiac glycosides in human non-small cell lung cancer cell lines. *Mol. Carcinog.* **2014**, in press [PMID: 24610665].

Anticancer Activity of Sea Cucumber Triterpene Glycosides

Dmitry L. Aminin, Ekaterina S. Menchinskaya, Evgeny A. Pisliagin, Alexandra S. Silchenko, Sergey A. Avilov and Vladimir I. Kalinin

Abstract: Triterpene glycosides are characteristic secondary metabolites of sea cucumbers (*Holothurioidea*, *Echinodermata*). They have hemolytic, cytotoxic, antifungal, and other biological activities caused by membranotropic action. These natural products suppress the proliferation of various human tumor cell lines *in vitro* and, more importantly, intraperitoneal administration in rodents of solutions of some sea cucumber triterpene glycosides significantly reduces both tumor burden and metastasis. The anticancer molecular mechanisms include the induction of tumor cell apoptosis through the activation of intracellular caspase cell death pathways, arrest of the cell cycle at S or G2/M phases, influence on nuclear factors, NF-κB, and up-down regulation of certain cellular receptors and enzymes participating in cancerogenesis, such as EGFR (epidermal growth factor receptor), Akt (protein kinase B), ERK (extracellular signal-regulated kinases), FAK (focal adhesion kinase), MMP-9 (matrix metalloproteinase-9) and others. Administration of some glycosides leads to a reduction of cancer cell adhesion, suppression of cell migration and tube formation in those cells, suppression of angiogenesis, inhibition of cell proliferation, colony formation and tumor invasion. As a result, marked growth inhibition of tumors occurs *in vitro* and *in vivo*. Some holothurian triterpene glycosides have the potential to be used as P-gp mediated MDR reversal agents in combined therapy with standard cytostatics.

Reprinted from *Mar. Drugs*. Cite as: Aminin, D.L.; Menchinskaya, E.S.; Pisliagin, E.A.; Silchenko, A.S.; Avilov, S.A.; Kalinin, V.I. Anticancer Activity of Sea Cucumber Triterpene Glycosides. *Mar. Drugs* **2015**, *13*, 1202-1223.

1. Introduction

Sea cucumbers (or holothurians), belonging to the class Holothuroidea (Echinodermata), are echinoderms phylogenetically related to sea stars, sea urchins and sea lilies. They are habitually found in the benthic areas and deep seas around the world. They have a leathery skin and an elongated body, and many of them are indeed shaped like soft-bodied cucumbers. This class has around 1100 described living species [1]. Some of them are edible and considered as a delicacy in many countries. Consequently, sea cucumbers have some commercial value and are extensively harvested. Sea cucumbers, also called trepang, bêche-de-mer, or balate, have been used as food and Asiatic folk medicine. Ancient Chinese medical manuscripts reveal that parts of holothurians can improve human immune status enforcing resistance to many diseases and even have an anticancer effect. That is probably why the popular Chinese name for sea cucumber is haishen, which means, roughly, “ginseng of the sea” because ginseng, a plant belonging to the family Araliaceae, has similar medicinal properties [2].

On the other hand, many holothurians, particularly tropical species, are toxic. Toxins are elaborated in the body wall and in the skin and may be released into the sea water continuously, or

only when the animal is molested [3–7]. Aborigines of Guam and other regions of the Indo-Pacific used some holothurians to poison small lagoons of coral reefs at low tide for killing fish [8].

The low molecular weight compounds, triterpene glycosides, have long been suggested the main poisonous substances of the sea cucumbers and to play a role in the defense of holothuroids as a toxin against predators and pathogens [9–11]. The lanostane triterpene glycosides are characteristic of sea cucumbers (Holothurioidea, Echinodermata). The majority of them have 18(20)-lactones in aglycone and belong to the holostane series. Their carbohydrate chains have from two to six monosaccharide residues including glucose, quinovose, xylose, and 3-*O*-methylglucose and sometimes 6-*O*-acetylglucose, 3-*O*-methylxylose, 3-*O*-methylglucuronic acid, and 3-*O*-methylquinovose. Carbohydrate chains may have from one to three sulfate groups [12].

These compounds have a wide range of pharmacological properties. During the last decade, several reviews on the study of the cytotoxic activity of triterpene glycosides have been published. These surveys have shown a correlation between the structure of triterpenoid saponins and its cytotoxic activity related to the molecular mechanisms of action [9–12]. Most of the glycosides have cytotoxic, hemolytic, antifungal, and similar biological activities caused by membranotropic action at milli- and micromolar concentrations. The membranotropic action of the glycosides is caused by their ability to attach to cell membranes and form nonselective ion-conducting complexes with 5(6)-unsaturated sterol, preferably with cholesterol, followed by an efflux of some ions, nucleotides, and peptides. The following breaking of ion homeostasis and osmolarity results in cell lysis and death [12]. In addition to cytotoxic properties, these glycosides block egg cleavage and development of sea urchin embryos, inhibit the growth of pathogenic fungi and proliferation of some types of human tumor cells *in vitro* such as U-87-MG, HCT-8, leukemia P-388, KB, Schabel, Mel-28, A-549, MICF-1, HT-29, IA9, CAKI-1, SK-MEL, PC-3, lymphoidal leukemia L 1210, MCF-7, MKN-28, HCT-116, U87MG, HepG2, HeLa, THP-1, KB-VIN, HCT-8, C33A, and some others [9–19].

In recent years, holothurian triterpene glycosides have attracted the attention of experimental oncologists as potential anticancer natural compounds. The current review summarizes the recent data on anticancer activity of sea cucumber triterpene glycosides and some aspects of their molecular mechanisms upon cancer cells.

2. Anticancer Activity

The first anticancer properties of the sea cucumber glycoside, holothurin, representing the glycoside fraction of Bahamian sea cucumber *Actinopyga agassizi,* were described in 1952 by Nigrelli [20]. He showed that the injection of holothurin, which is a mixture of triterpene glycosides containing as a main constituent holothurin A, in the region of Sarcoma-180, inhibited tumor growth and caused its regression in mice.

Later investigations of holothurin have shown promise in the field of cancer research. Thus, the injection of Krebs-2 ascitic tumor cells treated with holothurin into healthy mice failed to induce marked tumor growth for up to 80 days [21,22]. In addition, holothurin was shown to inhibit the growth of epidermal carcinoma (KB) tumor cells [23,24].

Later, more in-depth studies of the mechanisms of glycoside antitumor action were conducted. Thus, new triterpene glycosides, philinopsides A, B, E and F, as well as pentactasides I, II and III have been isolated from the sea cucumber *Pentacta quadrangularis*. All the glycosides revealed significant cytotoxicities *in vitro* against such tumor cell lines as U87MG, A-549, P-388, MCF-7, HCT-116, and MKN-28 with IC_{50} in the range of 0.60–3.95 μM [13,25].

In the most extensive research, philinopside A (**1**), one of the potent cytotoxic glycosides (Chart 1), was shown to have effects upon angiogenesis as well as tumor growth. These effects were assessed in a series of models *in vitro* and *in vivo*. Results showed that due to significant inhibition of three important stages of angiogenesis (endothelial cell proliferation, migration, and tube formation) induced by philinopside A, the formation and growth of new blood vessels were greatly decreased. At various doses, philinopside A induced inhibition of proliferation of human microvascular endothelial cells (HMECs) by 98.7%. At the same doses, the glycoside induced the inhibition of HMECs migration by 94.1%. Rat aorta culture assay provides a close imitation of *in vivo* angiogenic processes. In this model, 2–10 μM philinopside A suppressed the formation of new microvessels. Additionally, in the chick embryo chorioallantoic membrane assay, philinopside A, at 2–10 nmol/egg, significantly inhibited angiogenesis. Philinopside A also manifested strong anti-tumor activities both *in vitro* and *in vivo*. The glycoside reduced the volume of mouse Sarcoma-180 tumor by inducing apoptosis of tumor along with tumor-associated endothelial cells. Studies of the action of philinopside A on the angiogenesis-related receptor tyrosine kinases (RTKs) revealed that philinopside A broadly inhibited all tested RTKs, including fibroblast growth factor receptor-1 (FGFR1), platelet-derived growth factor receptor-β (PDGFβ), vascular endothelial growth factor receptor (VEGFR), along with epithelial growth factor receptor (EGFR), at IC_{50} values ranging from 2.6 to 4.9 μM. These results suggest that philinopside A, because of its inhibition of all the tested RTKs, might prove to be an effective inhibitor of RTK, while a lethal dose (LD_{50}) in mice was only 625 mg/kg orally [26].

Recently, anti-tumor and anti-angiogenesis activities of philinopside E (**2**), a sulfated saponin from sea cucumber *Pentacta quadrangularis* (Chart 1), were examined. Inhibition of angiogenesis was assessed *in vitro* using proliferation, migration, adhesion, tube-formation and apoptosis assays in philinopside E-treated human dermal microvascular endothelial cells and human umbilical vein endothelial cells. The results showed that philinopside E inhibited proliferation of dermal microvascular endothelial cells and umbilical vein endothelial cells with IC_{50} values of 2.22 ± 0.31 μM and 1.98 ± 0.32 μM, respectively. This glycoside induced the apoptosis of endothelial cells at concentrations <2 μM, dose-dependent suppression of cell migration, adhesion of cells and formation of tubes in those cells, and revealed anti-proliferative activities against a series of tumor cell lines (IC_{50} values of ~4 μM). Philinopside E (5 nM/egg) suppressed spontaneous angiogenesis in the chorioallantoic membrane assay *in vivo* and induced significant inhibition of growth in mouse Hepatoma-22 and Sarcoma-180 cell models. Specifically, philinopside E reduced the tumor volume of mouse Sarcoma-180 by triggering apoptosis of both tumor and tumor-associated endothelial cells, preferentially of endothelial cells over tumor cells. Philinopside E also suppressed the active (phosphorylated) forms of vascular endothelial growth factor receptors including: KDR/Flk-1 (which trigger downstream signaling pathways), VEGF2

ERK (which is required for the mitogenic activities of VEGF in endothelial cells), FAK (which regulates mitogenicity), paxillin (which associates with FAK and plays an important role in cell adhesion and migration and is involved in proliferation, adhesion, migration and survival of endothelial cells), and Akt (which regulates cell survival). These data indicate that philinopside E induces an anti-angiogenic activity associated with inhibition of signaling of VEGFR2, and has pronounced anti-tumor activity caused by the decrease of proliferation of tumor cells and increase of apoptosis of both tumor and endothelial cells [27]. Additionally, it was demonstrated that philinopside E specifically interacts with the extracellular domain of kinase insert domain-containing receptor (KDR) and blocks its interaction with VEGF and its downstream signaling. This specificity for the KDR extracellular domain is distinct from conventional small-molecule inhibitors that target the KDR cytoplasmic domain. It was also shown that philinopside E significantly suppresses $\alpha_v\beta_3$ integrin-driven downstream signaling caused by a disturbance of the interaction between KDR and $\alpha_v\beta_3$ integrin in HMECs, followed by a disruption of the cytoskeleton organization of actin and decreased adhesion of cells to vitronectin [28].

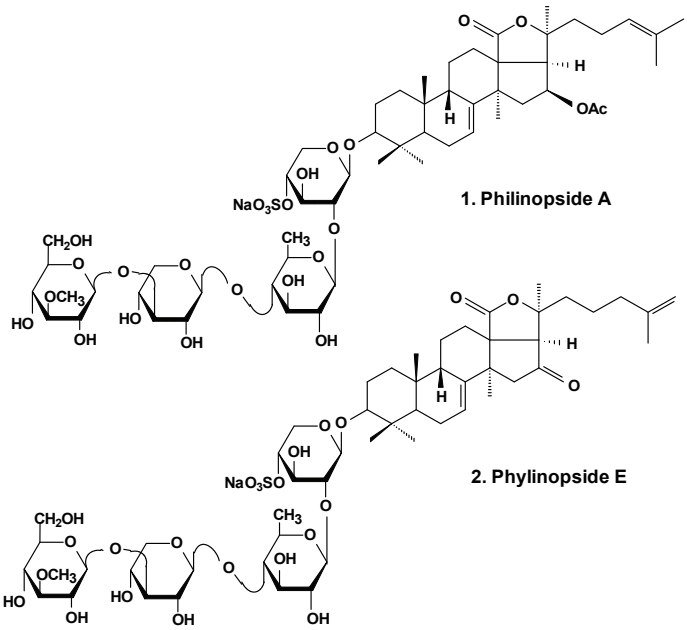

Chart 1. Structure of philinopsides.

Patagonicoside A (**3**) from *Psolus patagonicus* (Chart 2) and its desulfated analogs were studied for their cytotoxic, antiproliferative, and hemolytic activities and their influence on NF-κB activation. Both substances were able to suppress the growth of three tumor cell lines (Hep3B, MDA-MB231, and A549) and induced the activation of NF-κB, a key player linking chronic inflammation and cancer, concomitant with IK Ba degradation in the A549 tumor cell line. These compounds showed hemolytic activity with half maximal inhibitory concentration (IC_{50}) values around 80 μM. Both glycosides showed low cytotoxic activity in A549 tumor cells in comparison

with other sea cucumber triterpene glycosides containing linear tetrasaccharide chains. This probably is because of the presence of an additional sulfate at C-6 of glucose residue (third monosaccharide residue). This also could be a result of the uncommon presence of two 12α- and 17α-hydroxyl groups and a Δ^7 double bond in the aglycone moiety [29].

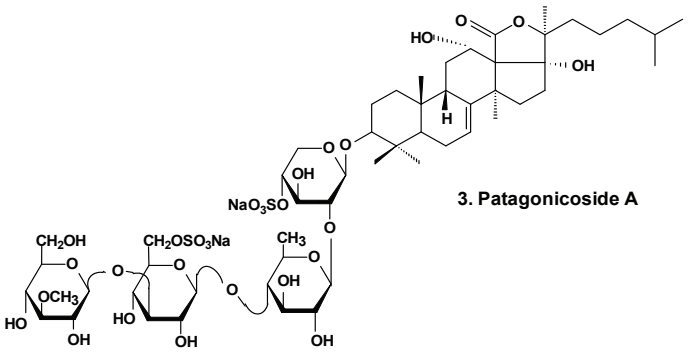

Chart 2. Structure of patagonicoside A.

In vitro and *in vivo* investigations were conducted on the effects of Ds-echinoside A (**5**), a non-sulfated triterpene glycoside isolated from the sea cucumber *Pearsonothuria graeffei* (Chart 3), on tumor cell adhesion, migration, invasion, and angiogenesis. In this study, it was found that Ds-echinoside A reduced cell viability of human hepatocellular liver carcinoma cells Hep G2, with IC_{50} of 2.65 μmol/L, and suppressed adhesion, migration, and invasion of Hep G2 cells in a concentration-dependent manner. Ds-echinoside A also decreased tube formation of human endothelial cells ECV-304 on matrigel *in vitro* and attenuated neovascularization in the chick embryo chorioallantoic membrane assay *in vivo*. Immunocytochemical analysis showed that Ds-echinoside A suppressed matrix metalloproteinase-9 (MMP-9) expression, playing an important role in breaking basement membranes associated with angiogenesis and metastasis. Ds-echinoside A also increased the expression of tissue inhibitors of metalloproteinase-1 (TIMP-1) regulating activation of MMP-9. Ds-echinoside A also reduced the expressions of vascular endothelial growth factor (VEGF) and NF-κB [30].

Both echinoside A (**6**) and Ds-echinoside A (**5**) (Chart 3) significantly arrested the cell cycle in the G_0/G_1 phase. A reverse transcriptase-polymerase chain reaction assay showed that glycosides increased the cell-cycle-related genes expression, including p16, p21, and c-myc, and decreased the expression of cyclin D_1. They decreased the expression of Bcl-2, and enhanced mitochondrial cytochrome c release, caspase-3 activation, and cleavage of adenosine diphosphate ribose polymerase. Ds-echinoside A significantly decreased Nuclear factor NF-κB expression, but echinoside A was not involved in concerning the expression. Echinoside A and Ds-echinoside A (2.5 mg/kg) induced the reduction of H22 hepatocarcinoma tumor weight by 49.8% and 55.0%, respectively [31].

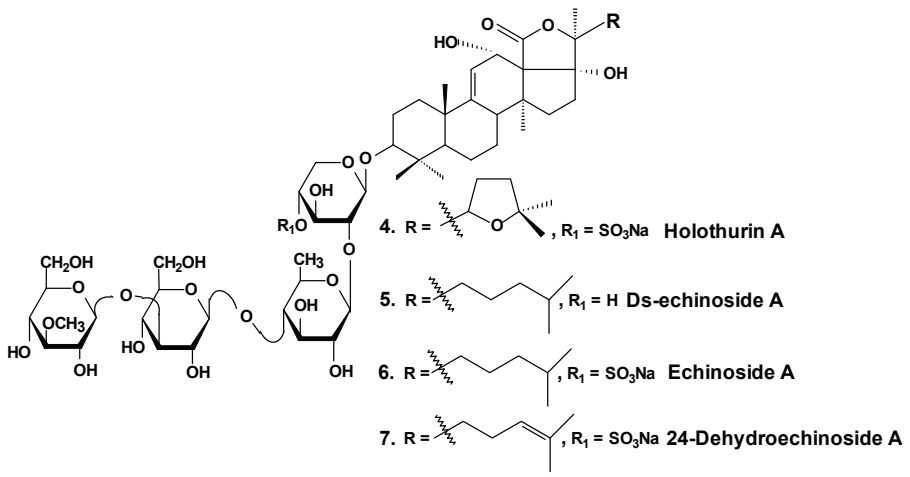

Chart 3. Structures of holothurin A and echinosides.

Moreover, it was shown that echinoside A reduced tumor growth in mouse and xenografts of human prostate carcinoma in nude mice models. Echinoside A inhibited the noncovalent binding of Top2alpha to DNA by competing with DNA for the DNA-binding domain and by interfering predominantly with the Top2alpha-mediated prestrand passage cleavage/religation equilibrium over with the poststrand passage. These characteristics distinguish echinoside A from known Top2alpha inhibitors. Hence, echinoside A induced DNA double-strand breaks in a Top2-dependent manner [32].

Similar results were obtained by the authors in an earlier study of two sulfated triterpene glycosides, namely, holothurin A (**4**) and 24-dehydroechinoside A (**7**), from the sea cucumber *Pearsonothuria graeffei* (Chart 3). Both of these glycosides exhibited significant inhibition of metastasis *in vitro* and *in vivo*. Immunocytochemical analysis revealed that both compounds significantly decreased the expression of MMP-9 and enhanced the expression level of tissue inhibitors of TIMP-1, an important regulator of MMP-9 activation. According to the results of Western blot analysis, both chemicals remarkably abolished the expression of VEGF. In contrast, the treatment of 24-dehydroechinoside had no effect on the down regulation of NF-κB expression and considerably reduced the adhesion of HepG2 to both matrigel and ECV-304 and also inhibited HepG2 cell migration and invasion in a concentration-dependent manner. 24-dehydroechinoside more effectively induced antimetastasis than holothurin A. Moreover, only holothurin A downregulated the expression of NF-κB. This suggests that antimetastatic activity of the glycosides of *P. graeffei* can be either NF-κB-dependent or -independent, depending on glycoside chemical structure [33].

It was found that the colochiroside A (**8**) from the sea cucumber *Colochirus anceps* (Chart 4) remarkably exhibited antineoplastic activities *in vitro* and *in vivo* and did not reduce the immunoregulatory function of mice. The preliminary cytotoxic assay of colochiroside A revealed significant cytotoxic activity against six types of cultured tumor cell lines of P-388, HL60, A-549, SpC-A4, MKN-28, and SGC-7901, with a mean IC_{50} of 3.61 ± 0.55 mg/L. The preliminary

anti-tumor assay of colochiroside A suggests that this glycoside exhibits strong inhibitory effects against H22 liver cancer and S180 sarcoma cells in mice. The maximal inhibition ratio to H22 liver cancer was 52.2%, while the ratio to S180 sarcoma was 70.0%. The immunoregulatory study indicated that colochiroside A has no significant effect on the developments of thymus and spleen [34].

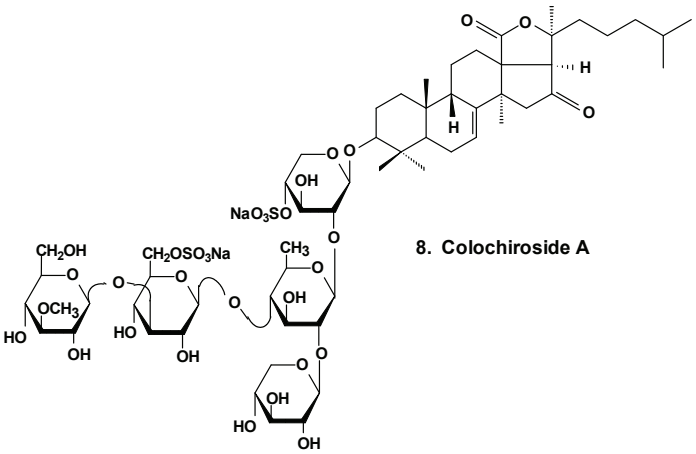

Chart 4. Structure of colohiroside A.

Intercedensides A, B, and C from *Mensamaria intercedens* exhibited cytotoxicity against human tumor cell lines. One of them, intercedenside A (**9**) (Chart 5), also revealed good antineoplastic activity against mouse Lewis lung cancer and mouse S180 sarcoma [35].

Okhotosides B_1 (**10**), B_2 (**11**) and B_3 (**12**) from *Cucumaria okhotensis* (Chart 6) were moderately toxic against cells of HeLa tumor. Frondoside A (**13**) isolated from the same holothurian revealed more potent cytotoxicity against THP-1 and against HeLa tumor cells (with IC_{50} values of 4.5 and 2.1 μg/mL, respectively). This substance decreased both the AP-1-dependent trascriptional activities induced by UVB, EGF, or TPA in JB6-LucAP-1 cells and the EGF-induced NF-κB-dependent transcriptional activity in JB6-LucNF-κB cells at doses of about 1 μg/mL. Frondoside A increased the p53-dependent transcriptional activity in nonactivated JB6-Lucp53 cells at the same doses. It also inhibited the colony formation of JB6 P (+) Cl 41 cells activated with EGF ($INCC_{50}$ = 0.8 μg/mL) [36].

The tumor suppressing and pro-apoptotic activity of the different water-soluble holothurian glycoside fractions from *Apostichopus japonicus* were examined. The 70% ethanol fraction from macroporous resin column and the pSC-2 and pSC-3 fractions from a silica gel column showed very strong tumor suppressing activity towards HeLa cells, A-549 lung cancer cells, SGC-7901 stomach cancer cells, and Bel-7402 liver cancer cells. SC-2 and SC-3 fraction purified by Sephadex LH-20 gel-filtration column chromatography, with purity above 99.6%, all had the properties of triterpenoid glycosides. Purified SC-2 fractions had remarkable tumor suppressing activity on HeLa cells in a dose- and time-dependent manner, and had prominent tumor suppressing activity on mouse S180 solid tumors in a dose-dependent manner. Additionally, the SC-2 fraction also had a

remarkable ability to elevate mouse thymus and spleen indexes. The purified SC-2 fraction induced apoptosis of HeLa cells in a dose-dependent manner and DNA fragmentation of HeLa cells occurred after 12 h treatment with 10 mg/L and 50 mg/L of SC-2 fractions [37].

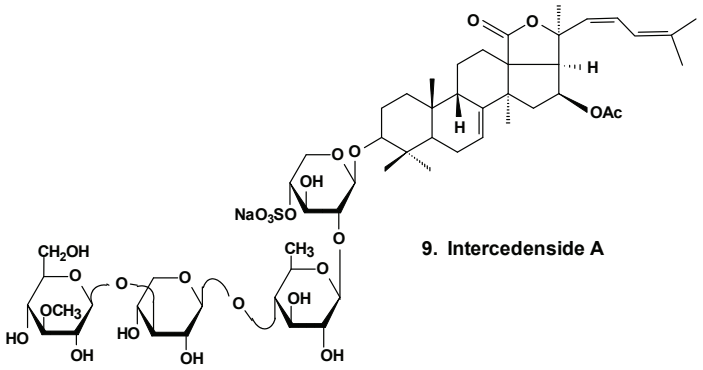

Chart 5. Structure of intercedenside A.

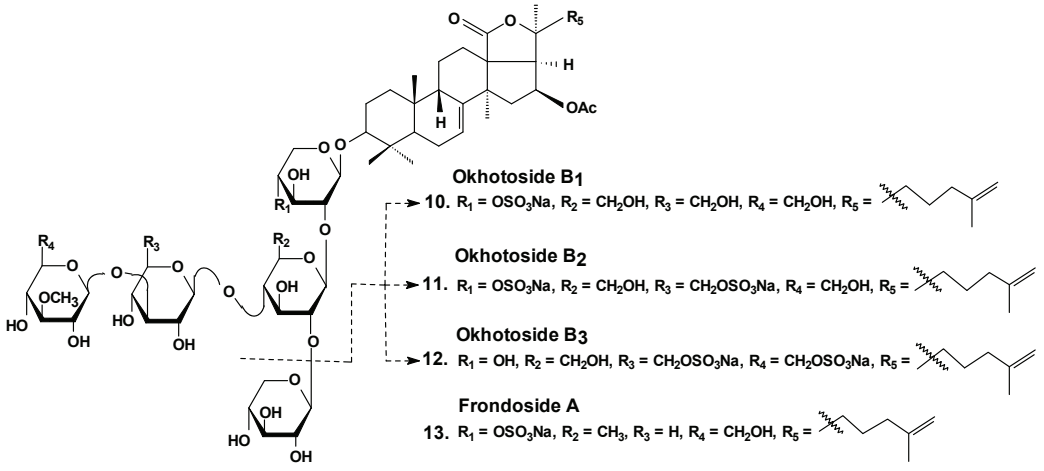

Chart 6. Structures of okhotosides and frondoside A.

Stichoposide C (**14**) from the holothurian *Thelenota anax* (Chart 7) was examined for elucidation of possible mechanisms by which it induces apoptosis of cancer cells. Stichoposide C-induced apoptosis in human leukemia and colorectal cancer cells were examined in the context of mitochondrial injury and signaling pathway disturbances. Additionally, the antitumor effects of stichoposide C in mouse CT-26 subcutaneous tumors and HL-60 leukemia xenograft models were investigated. It was found that stichoposide C induced apoptosis in these cells in a dose-dependent manner leading to the activation of Fas and caspase-8, cleavage of Bid, mitochondrial damage, and caspase-3 activation. Stichoposide C activated neutral SMase (SMase) and acid sphingomyelinase, resulting in ceramide generation. The knockdown experiments concerning specific inhibition of neutral SMase or acid SMase and siRNA partially blocked apoptosis induced by stichoposide C.

Moreover, the glycoside significantly decreased growth of HL-60 xenograft tumors and CT-26 subcutaneous tumors and increased generation of ceramide *in vivo*. The authors concluded that ceramide generation by stichoposide C because of the activation of neutral and acid SMase, may contribute to the apoptosis and the antitumor activity induced by stichoposide C [38].

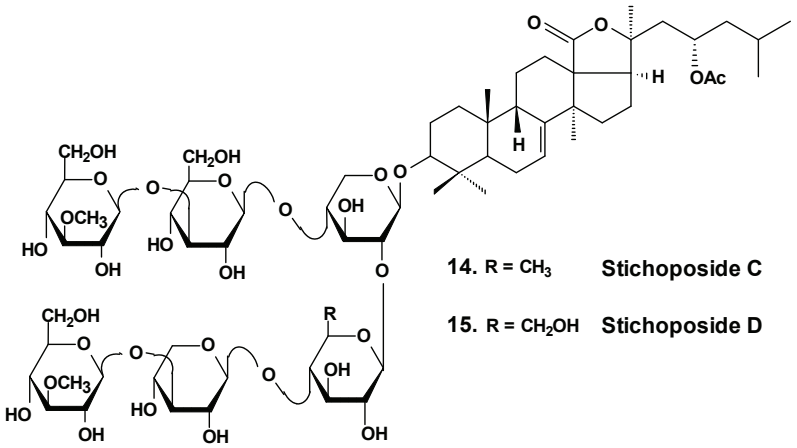

Chart 7. Structure of stichoposides.

Significant contribution to the understanding of the molecular mechanisms of antitumor actions of triterpene glycosides has been made in the study of frondoside A (**13**) (Chart 6) and its analogs isolated from the sea cucumber *Cucumaria frondosa*. Chemopreventive efficacy of Frondanol A5, a preparation from *C. frondosa* which contains several sea cucumber-derived anticancer and antiinflamatory agents including the triterpene glycoside frondoside A, was evaluated on azoxymethane-induced rat colon carcinogenesis using colonic aberrant crypt foci (ACF) as a surrogate biomarker. Rats were fed the AIN-76A diet containing 5% corn oil, and ACFs were induced by azoxymethane. Three days after azoxymethane treatment, rats were fed with diets containing Frondanol A5. It was shown that dietary administration of 150 and 450 ppm of Frondanol A5 markedly decreased total colonic ACF formation induced by azoxymethane, approximately 34% to 55%, and multicrypt aberrant foci (48%–68.5%) depending on the dosage. ACFs in rats treated with Frondanol A5 revealed marked up-regulation of p21WAF1/CIP1 and down-regulation of proliferating cell nuclear antigen. Frondanol A5 revealed inhibition of the growth at S and G2/M phases along with a decrease in Cdc25c and an increase in p21WAF1/CIP along with significant apoptosis caused by H2AX phosphorylation and the cleavage of caspase-2 in HCT116 cells. The authors concluded that Frondanol A5 exhibits potential chemopreventive properties for colon carcinogenesis [39].

A polar precipitate sub-fraction of Frondanol A5 (Frondanol A5P) was examined for anti-cancer effects in S2013 and AsPC-1 human pancreatic cancer cell lines. Frondanol-A5P inhibited cell proliferation and induced cell cycle arrest at G2/M phase in both cell lines with decreased expression of cdc25c, cyclin A, and cyclin B. Frondanol-A5P also induced phosphorylation of

Janus kinase (SAPK/JAK) and stress-activated protein kinase along with p38 mitogen-activated protein kinase (MAP) during 5 min and markedly increased expression of p21waf1 messenger RNA and protein at 3 h in both cell lines. This effect was decreased by the inhibitor of p38 kinase, SB203580. Frondanol-A5P also significantly increased annexin V binding and caspase-3 activation [40].

It was established that individual frondoside A (**13**) from *Cucumaria frondosa* inhibited cell proliferation of AsPC-1 human pancreatic cancer in a concentration- and time-dependent manner. In concert with inhibition of cell growth, frondoside A induced significant morphological changes consistent with apoptosis. Its activity led to an increase of sub-G0/G1 apoptotic cells population, a decrease in expression of Bcl-2 and Mcl-1, an increase in Bax expression, an increase in the expression of the cyclin-dependent kinase inhibitor, p21, and activation of caspases 3, 7, and 9. These data revealed that frondoside A induced apoptosis of human pancreatic cancer cells via the mitochondrial pathway and activation of the caspase cascade. Frondoside A (10 μg/kg/day) inhibited growth of AsPC-1 in xenograft mouse models [41].

The impact of frondoside A on human breast cancer cell line MDA-MB-231 was compared to the effect on a non-tumorigenic MCF10-A cell line derived from normal human mammary epithelium. The glycoside (0.01–5 μM) decreased breast cancer cell viability in a concentration- and time-dependent manner, with EC_{50} of 2.5 μM at 24 h. MCF10-A cells were more resistant to the cytotoxic action (EC_{50} superior to 5 μM at 24 h) [42].

Frondoside A significantly increased sub-G1 (apoptotic) cell fractions by the activation of p53 followed by the appearance of caspases 9 and 3/7 cell death pathways in the MDA-MB-231 cells. Moreover, frondoside A induced inhibition of MDA-MB-231 cell migration and invasion in concentration-dependent manner. Frondoside A, at the dosage of 100 μg/kg/day intraperitoneal for 24 days, effectively decreased the growth of tumor xenografts in athymic mice *in vivo* without toxic-side action. Frondoside A also increased the anti-proliferative activity of paclitaxel in such breast cancer models [42].

It was shown that frondoside A possesses potent antimetastatic activity on syngenic murine model of metastatic breast cancer. Upon intraperitoneal administration to mice with mammary gland-implanted tumors, Frondoside A inhibited spontaneous tumor metastasis in the lungs. The increase of cyclooxygenase-2 activity promotes tumor growth and metastasis by producing high levels of PGE2 that acts on the receptors of prostaglandin E, mainly EP4 and EP2. Frondoside A antagonizes the receptors EP2 and EP4 of prostaglandin E. Frondoside A inhibited $^{3}H\text{-}PGE_2$ binding to recombinant EP2 or EP4-expressing cells at a high concentration (IC_{50} of 16.5 μM and 3.7 μM, respectively) that may be caused by cytotoxic effects. Moreover, frondoside A also inhibited EP4 or EP2-linked activation of intracellular cAMP along with EP4-mediated ERK1/2 activation. Along with the antimetastatic activity found *in vivo*, frondoside A at concentrations 0.1 and 1.0 μM also inhibited migration of tumor cells *in vitro* in response to EP4 or EP2 agonists [43].

The effects of Frondoside A on the human non-small lung cancer cell LNM35 survival, migration, and invasion *in vitro*, and on tumor growth, angiogenesis, and metastasis alone, and in combination with cisplatin *in vivo* were investigated. Frondoside A induced a concentration-dependent decrease in viability of MCF-7, NCI-H460-Luc2, A549, MDA-MB-435, HepG2, and LNM35 over

24 h along with a caspase 3/7-dependent pathway of cell death. The IC_{50} concentrations of frondoside A at 24 h were 0.7–2.5 μM. Frondoside A also induced an inhibition of the migration of cells, angiogenesis, and invasion *in vitro* in time- and concentration- dependent mode. Frondoside A (0.01 and 1 mg/kg/day intraperitoneal for 25 days) strongly decreased the growth, angiogenesis, and lymph node metastasis of LNM35 tumor xenografts in athymic mice, without toxic side effects. This glycoside in concentrations between 0.1 and 0.5 μM also significantly blocked basal and bFGF induced angiogenesis in the chick embryo chorioallantoic membrane model of angiogenesis assay. Moreover, frondoside A enhanced lung tumor growth inhibition by the chemotherapeutic agent cisplatin [44].

The anti-invasive activity and anti-metastatic effects of this glycoside at non-cytotoxic concentrations against a human breast cancer cell line were investigated along with the inhibitory effect on cell invasion, clonogenicity, and migration in TPA-stimulated cells of human breast cancer. Frondoside A significantly decreased TPA-induced colony formation, migration and invasion in MBA-MB-231 human breast cancer cells. It was shown that MMP-9 induction is very important for the metastasis of different types of cancer tumor cells. It was also found that this glycoside suppresses TPA-induced enzymatic activity of MMP-9, its secretion and expression. This effect was caused by a reduction of the activation of AP-1 and NF-κB. It also correlated with an increase of TIMP-1 and TIMP-2 expression. Frondoside A inhibited the expression of TPA-induced MMP-9, probably because of the suppression of NF-κB and AP-1 signaling pathways. The glycoside decreases the activation of the PI3K/Akt, ERK1/2 and p38 MAPK signals. These data suggest that frondoside A anti-metastatic effects on human breast cancer cells may be caused by the inhibitin of TPA activation of AP-1 and NF-κB and a decrease of TPA activation of ERK1/2, PI3K/Akt and p38 MAPK signals leading to downregulation of the expression of MMP-9. Such results revealed the role of frondoside A in metastasis and its underlying molecular mechanisms. These data also suggest frondoside A may be used as a chemopreventive agent for metastatic breast cancer [45].

The estrogenic potency of holothurin A (**4**), holotoxin A_1, (**16**) (Chart 8) frondoside A (**13**), cucumarioside A_2-2 (**18**) (Chart 9) and a semi-synthesized plant glycoside, ginsenoside-Rh2, were studied using a yeast two-hybrid system including expressed genes of human estrogen receptor, hERalpha, the co-activator TIF2 and lacZ as a reporter gene. It was found that only ginsenoside-Rh2 had moderate estrogenic activity in a concentration range between 10^{-7} and 10^{-6} M. The effect was about 30% of the activity of 17beta-estradiol at half-effective concentration. Hence, ginsenosides-Rh2 is a weak phytoestrogen. Holothurin A, cucumarioside A_2-2, holotoxin A_1 and frondoside A did not interact with estrogen receptors and had no appreciable estrogenic activity. These results showed that the anticancer effect of tested holothurian glycosides upon ER-positive breast cancer cells does not involve glycoside binding to estrogen receptors. Ginsenoside-Rh2 has some similarity in chemical structure with 17beta-estradiol. It might explain the affinity of this glycoside to the hER receptors [46].

Frondoside A influenced the anti-cancer effects of gemcitabine, the standard drug in antitumor therapy, against human pancreatic cancer cell lines, AsPC-1 and S2013. The combinations of low concentrations of these preparations were used for a 72 h treatment period *in vitro*. Synergetic growth inhibition was significantly greater than their separate effects. Combinations of gemcitabine

and glycosides were tested *in vivo* on the nude mouse model. Xenografts of AsPC-1 and S2013 cells form the tumors before the dministration of the drugs alone or in combination for 30 days. Tumors grew quickly in control mice. The growth was significantly decreased in all treatment groups. Gemcitabine (4 mg/kg/dose), combined with the glycoside (100 μg/kg/day) was more effective than the use of either drug alone. It was suggested that combinations of frondoside A and gemcitabine may provide clinical benefits for patients with pancreatic cancer [47].

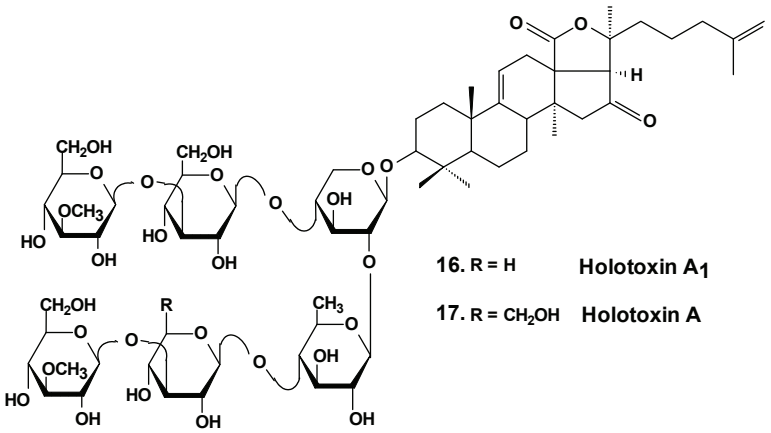

Chart 8. Structures of holotoxins.

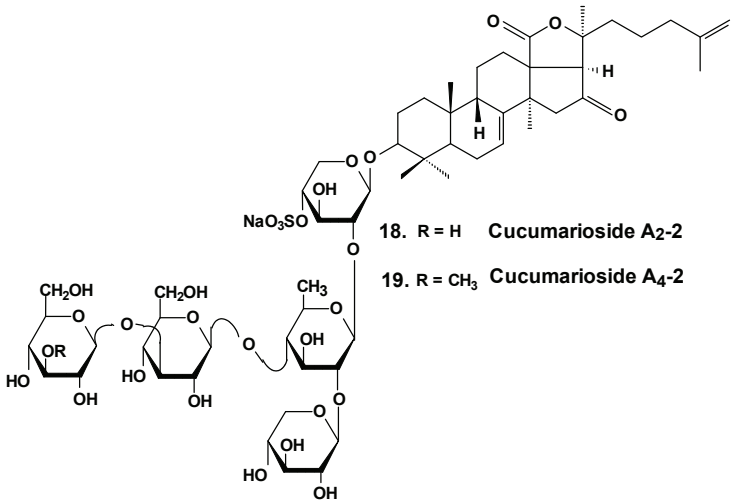

Chart 9. Structures of cucumariosides.

Sea cucumber triterpene glycosides with differing chemical structures were examined *in vitro* for effects against leukemia cell lines. Cucumariosides A_2-2 (**18**) and A_4-2 (**19**) from *Cucumaria japonica* (Chart 9) and stichoposides C (**14**) and D (**15**) from *Thelenota anax*, in cytotoxic doses, were shown to induce apoptosis in human leukemia cells HL-60, THP-1, NB-4 and K562 *in vitro*

by a caspase-dependent mechanism. Thus, sea cucumber triterpene glycosides, in spite of differing molecular structures, may nonetheless have generalized therapeutic relevance for human cancer [48].

The effects of frondoside A from *C. frondosa,* cucumarioside A_2-2, and cucumarioside A_4-2 from *C. japonica* on cell death-inducing capability were compared. These glycosides significantly induced apoptosis of leukemic cells. The apoptosis induced by frondoside A was more potent and rapid than apoptosis induced by cucumarioside A_2-2. Mitohondrial membrane permeability was not changed and accumulation of cytochrome C in the cytosolic fraction was not found in HL-60 cells treated with frondoside A, cucumarioside A_2-2 and cucumarioside A_4-2. More interestingly, the level of procaspase-3, -8, and -9 proteins in lysates from frondoside A-treated HL-60 cells were not changed, whereas frondoside A-induced apoptosis in 50%–70% of the cells. Cleavage of procaspase-3 and PARP, but not of procaspase-8, -9, and -12, were significantly increased in cucumarioside A_2-2 or cucumarioside A_4-2 treated HL-60 cells. Furthermore, the annexin-V positivity in cells treated by fronfdoside A was not inhibited by zVAD-fmk. Nevertheless, both annexin-V positivity and cleavage of caspases induced by cucumariosides were efficiently suppressed by caspase inhibitors. This suggests that holothurian triterpene glycosides may induce apoptosis of leukemic cells caspase-dependently or independently, depending on the glycoside structure [49].

In another investigation, the cytotoxicity of cucumarioside A_2-2 and its effect upon apoptosis, the cell cycle, DNA biosynthesis and p53 activity, and glycoside anticancer action against mouse Ehrlich carcinoma cells were studied. It was found that the glycoside influences viability of tumor cells at micromolar concentrations. The EC_{50} for glycoside found by non specific esterase assay and MTT assay was 2.1 and 2.7 μM, respectively. The glycoside at sub-cytotoxic range of concentrations revealed a cytostatic effect by blocking the proliferation of cells and biosynthesis of DNA in the S phase. Cucumarioside A_2-2 may induce apoptosis in cells of Ehrlich carcinoma along with caspase-dependent ways by passing activation of p53-dependent segments. It was concluded that the anticancer and pro-apoptotic properties of the glycoside may be caused by interaction of cucumarioside A_2-2 with tumor cells. The anticancer effect of cucumarioside A_2-2 *in vivo* may be caused by the ability of the substance to arrest the cell cycle in the DNA synthetic phase and induce programmed death of tumor cells [50].

Additionally, it was found that in non-cytotoxic concentrations of frondoside A and cucumarioside A_2-2, as well as their complexes with cholesterol, block the activity of membrane transport P-glycoprotein. This protein is responsible for multidrug resistance (MDR) phenomena in cells of the ascite form of mouse Ehrlich carcinoma. In this way, glycosides prevent an efflux of fluorescent probe Calcein from the cells. Cucumarioside A_2-2 was found to increase the upload and intracellular concentration of cytostatic doxorubicine, and prevent an efflux of anticancer drugs from the cancer cells. Because the interaction of the glycosides with tumor cells resulted in a decrease of MDR, these glycosides are potential inhibitors of multidrug resistance and can be used in combined therapy of cancer [51–53].

As a result of long-term investigations, a new immunomodulatory lead Cumaside with antitumor properties was invented on the base of triterpene glycosides isolated from Far Eastern sea cucumber *Cucumaria japonica*. Cumaside is a complex of monosulfated glycosides (preferably cucumarioside A_2-2) with cholesterol in molar ratio of 1:2 [54]. Recently, it was found that

Cumaside possesses less cytotoxic action against sea urchin embryos and cells of Ehrlich carcinoma than the glycosides. Furthermore, Cumaside posessed antitumor activity against experimental mouse Ehrlich carcinoma *in vivo* both alone and in combination with cytostatics. The highest result was achieved at a treatment of once per day for seven days before the tumor inoculation, followed by Cumaside treatment once per day for seven days. The treatment along with prophylactic schemes with Cumaside and subsequent therapeutic application of 5-fluorouracil inhibited tumor growth by 43% [55].

Recently, the ability of a number of cytotoxic triterpene glycosides from sea cucumbers to interact with human topoisomerase II alpha (which plays a key role in DNA replication and is a target for a variety of chemotherapeutic agents) has been investigated *in silico* using the methods of computer simulation. This study revealed possible anticancer effects of a series of triterpen glycosides including bivittoside A (**20**), holothurin A (**4**), holotoxin A (**17**), holothurinoside A (**21**) (Chart 10), and cucumarioside A_2-2 (**18**) using homology modeling of human DNA topo II α. The authors have found the possible binding site of DNA binding domain of Topo II α. These glycosides were screened for QSAR and ADME/TOX analysis as ligands. All the glycosides were able to bind with the enzyme. Binding sites have been established for all the glycosides. All the tested glycosides had a model of antitumor effects. According to this study, cucumarioside A_2-2 may be a better inhibitor of topo II α and follow most of the ADME properties [56]. The authors explain the inhibition by the interaction of "phenolic principals" of the glycosides with amino acids of the active center of the enzyme by hydrogen bonds. This seems to be an erroneous explanation because the glycosides do not contain phenolic groups. It is possible that the authors have confused pyranose forms of monosaccharide residues with phenols.

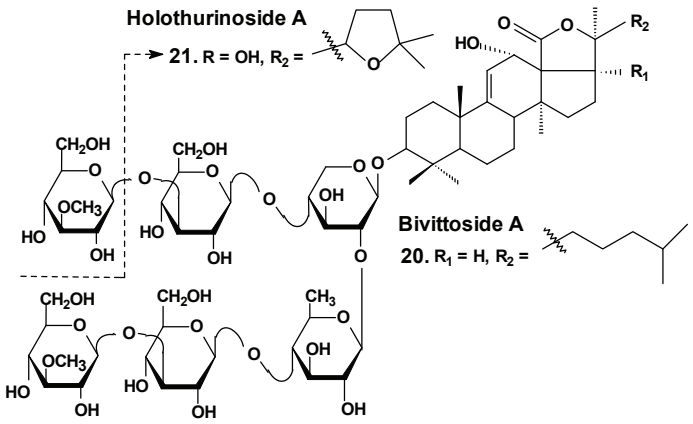

Chart 10. Structure of bivittoside A and holothurinoside A.

A brief amount of information concerning the molecular mechanisms of the biological action of certain sea cucumber triterpene glycosides was collected recently in a review [57]. This review highlights the structural characteristics and mechanisms of the action of marine triterpene glycosides, such as stichoposides, frondoside A, and cucumariosides. In particular, the membranotropic and membranolytic activities of glycosides from sea cucumbers and their ability to induce

cytotoxicity and apoptosis had been discussed, with a focus on structure-activity relationships. Membrane transporters, which are modulated by triterpene glycosides and thus can be proposed as potential therapeutic targets, were summarized. These include Na^+-K^+-ATPase and Ca^{2+}-ATPase in the sarcoplasmic/endoplasmic reticulum, L-type voltage-gated calcium channels, transient receptor potential canonical (TRPC) channels, ryanodine receptor, voltage-gated Na^+ channels (NaV1.2 and NaV1.4), K^+ channel (KV1.4), calcium-activated K^+ channel (BKCa), human Ether-à-go-go Related Gene (hERG), K^+ channels (Kv11.1), *N*-methyl-D-aspartate (NMDA) receptors and nicotinic acetylcholine receptors, as well as γ-amino butyric acid (GABA) receptors. In addition, the structural characteristics and antitumor effects of some sea cucumber glycosides have been reviewed along with underlying their molecular mechanisms.

Moreover, in recent review, the mechanisms of the anticancer effects of triterpene glycosides, frondoside A and cucumarioside A_2-2, were summarized with specific emphasis on the apoptotic activity of the glycosides and its effect on metastasis and invasion of cancer cells [58]. The authors concluded that these glycosides may be considered to be both anticancer and cancer preventive agents. Frondoside A and cucumarioside A_2-2 both posses anti-leukemic properties by inducing apoptosis.

Moreover, the anticancer effects of frondoside A and cucumarioside A_2-2 might be through inhibition of tumorigenesis and metastasis. The mechanisms are not clear and may be found in the future. Frondoside A will be useful as a caspase-independent anti-leukemic agent in order to overcome chemoresistance associated with a defect in both the extrinsic and intrinsic apoptotic pathways. As a next step, the determination of the structural characteristics responsible for the *in vivo* anticancer activities will be essential for their use as a drug. In addition, oral administration of frondoside A and cucumariosides was recommended by authors in clinical trials.

3. Conclusions

In the last few decades, scientific literature from several countries has reported that, indeed, triterpene glycosides from sea cucumbers do have a wide spectrum of biological effects including cytotoxic, hemolytic, antifungal, ichthiotoxic, and other activities. It has been shown that a majority of these activities are based on the interaction of these compounds with membrane sterols. Most triterpene glycosides of sea cucumbers have strong membranotropic action against any cellular and model membranes containing Δ^5-sterols. This interaction with biomembrane Δ^5-sterols results in pore formation, changes in membrane viscosity and ion permeability, inhibition of some membrane enzymes (such as ATPases) and others that lead finally to death of the cells.

Simultaneously, some sea cucumber triterpene glycosides exhibit pronounced anticancer effects by direct interaction with tumor cells in the sub-cytotoxic range of concentration. The summarized data of sea cucumber triterpene glycoside effects upon cancer cell viability, cell cycle/proliferation, apoptosis, migration/metastasis, angiogenesis and tumor growth *in vivo* are presented in the Table 1.

Table 1. Effects of sea cucumber triterpene glycosides upon cancer cells and tumors.

#	Glycoside	Sea Cucumber sp.	Type of Activity
1	Philinopside A	*Pentacta quadrangularis*	Reduction of cell viability [13,25], induction of apoptosis, inhibition of angiogenesis and tumor growth *in vitro* and *in vivo* [26–28]
2	Philinopside E		
3	Patagonicoside A	*Psolus patagonicus*	Suppression of cell proliferation [29]
4	Holothurin A	*Pearsonothuria graeffei*	Reduction of cell viability [30]; inhibition of cell adhesion, migration, metastasis and invasion [30,33]; induction of apoptosis [31]; cell cycle arrest, reduction of tumor growth *in vivo* [31,32]
5	Ds-echinoside A		
6	Echinoside A		
7	24-dehydro echinoside A		
8	Colochiroside A	*Colochirus anceps*	Reduction of cell viability, reduction of tumor growth *in vivo* [34]
9	Intercedenside A	*Mensamaria intercedens*	Reduction of cell viability, reduction of tumor growth *in vivo* [35]
10	Okhotoside B_1	*Cucumaria okhotensis*	Reduction of cell viability [36]
11	Okhotoside B_2		
12	Okhotoside B_3		
13	Frondoside A	*Cucumaria frondosa* *Cucumaria okhotensis*	Reduction of cell viability [36]; inhibition of colony formation [36,39,45] and cell proliferation [41,42], cell cycle arrest [39–41], induction of apoptosis [40–42,58]; inhibition of cell migration [43–45] and invasion [44,45]; inhibition of metastasis [43,44,58], angiogenesis [44]; inhibition of MDR [51–53]; reduction of tumor growth *in vivo* [41,44]; enhancement of tumor growth inhibition by cytostatics [42,44,47]
14	Stichoposide C	*Thelenota anax*	Induction of apoptosis; reduction of tumor growth *in vivo* [38]
18	Cucumariosides A_2-2	*Cucumaria japonica*	Inhibition of cell proliferation, cell cycle arrest and induction of apoptosis [48–50]; inhibition of metastasis and invasion [58]; reduction of tumor growth *in vivo* [48,49]; enhancement of tumor growth inhibition by cytostatics [55] inhibition of MDR [51–53]
19	Cucumarioside A_4-2		

Basically, the detailed mechanism(s) of the anticancer activities of these glycosides still remain largely unclear. However, the general details of this mechanism may be reduced to the following points:

(a) induction of tumor cell apoptosis was shown to be one of the primary causative factors through the activation of intracellular caspase cell death pathways (caspases 3/7 and 9);

(b) arrest of the cell cycle at S or G2/M phases and increase of the sub-G_0/G_1 cell population which leads to the block of proliferation and apoptosis;

(c) regulation (up or down) of nuclear factor NF-κB, a key player linking chronic inflammation and cancer;

(d) regulation (up or down) of certain cellular receptors and enzymes participating in cancerogenesis, such as: EGFR (epithelial growth factor receptor, mutations affecting EGFR expression or activity could result in cancer); AKt (or protein kinase B, involved in cellular survival pathways by inhibiting apoptotic processes); ERK (extracellular signal-regulated kinase controlling many cellular processes such as survival, proliferation, differentiation and motility); FAK (focal adhesion kinase, a cell growth, cell proliferation, cell survival and cell migration mediator, often dysfunctional in cells of cancer); and MMP-9 (matrix metalloproteinase-9, implicated in tumor metastasis) and some others.

Finally, administration of some sea cucumber triterpene glycosides leads to reduction in cancer cell adhesion, suppression of cell migration and tube formation in those cells, suppression of angiogenesis, inhibition of cell proliferation, colony formation and tumor invasion, and, as a result, marked growth inhibition of tumors *in vitro* and *in vivo*. Additionally, some holothurians' triterpene glycosides have the potential to be used as P-gp mediated MDR reversal agents in combined anticancer therapy with standard cytostatics.

Acknowledgments

This work was particularly supported by the Grant of RFBR No. 14-04-01822-a and the President of the Russian Federation Program for Support of the Leading Scientific Schools Grant SSh.-546.2012.4. The authors are very appreciative to John M. Lawrence, University of South Florida, Tampa, Florida, USA, for checking and correction of the manuscript.

Author Contributions

Collection and analysis of the information concerning mechanisms of antitumor action of glycosides, writting and editing: D.L.A.; collection and analysis of the information concerning antitumor action of glycosides: E.S.M. and E.S.P.; collection and analysis of the information concerning antitumor action and checking of chemical information: A.S.S. and S.A.A.; collection and analysis of the information concerning antitumor action, checking of chemical information, writing and editing: V.I.K.

Conflicts of Interest

The authors declare no conflict of interest.

References

1. Brusca, R.C.; Brusca, G.J. *Invertebrates*, 2nd ed.; Sinauer Associates, Inc.: Sunderland, MA, USA, 2003; p. 936.
2. Bordbar, S.; Anwar, F.; Saari, N. High-value components and bioactives from sea cucumbers for functional foods. A review. *Mar. Drugs* **2011**, *9*, 1761–1805.
3. Bakus, G.J. Defensive mechanisms and ecology of some tropical holothurians. *Mar. Biol.* **1968**, *2*, 23–32.
4. Rifkin, J.F. *Venomous and Poisonous Marine Animals: A Medical and Biological Handbook*; Burnett, J.W., Fenner, P.J., Eds.; UNSW Press: Kensington, NSW, Australia, 1996.
5. Flammang, P.; Ribesse, J.; Jangoux, M. Biomechanics of adhesion in sea cucumber Cuvierian tubules (Echinodermata, Holothuroidea). *Integr. Comp. Biol*. **2002**, *42*, 1107–1115.
6. Dyck, S.V.; Gerbaux, P.; Flammang, P. Qualitative and quantitative saponin contents in five sea cucumbers from the Indian Ocean. *Mar. Drugs* **2010**, *8*, 173–189.
7. Dyck, S.V.; Caulier, G.; Todesco, M.; Gerbaux, P.; Fournier, I.; Wisztorski, M.; Flammang, P. The triterpene glycosides of *Holothuria forskali*: Usefulness and efficiency as a chemical defense mechanism against predatory fish. *J. Exp. Biol.* **2011**, *214*, 1347–1356.
8. Frey, D.G. The use of sea cucumber in poisoning fishes. *Copeia* **1951**, *2*, 175–176.
9. Podolak, I.; Galanty, A.; Sobolewska, D. Saponins as cytotoxic agents: A review. *Phytochem. Rev.* **2010**, *9*, 425–474.
10. Osbourn, A.; Goss, R.J.; Field, R.A. The saponins-polar isoprenoids with important and diverse biological activities. *Nat. Prod. Rep.* **2011**, *28*, 1261–1268.
11. Kim, S.K.; Himaya, S.W. Triterpene glycosides from sea cucumbers and their biological activities. *Adv. Food. Nutr. Res.* **2012**, *65*, 297–319.
12. Kalinin, V.I.; Aminin, D.L.; Avilov, S.A.; Silchenko, A.S.; Stonik, V.A. Triterpene glycosides from sea cucumbers (Holothurioidae, Echinodermata), biological activities and functions. In *Studies in Natural Product Chemistry (Bioactive Natural Products)*; Atta-ur-Rahman, Ed.; Elsevier Science Publisher: Amsterdam, The Netherlands, 2008; Volume 35, pp. 135–196.
13. Han, H.; Xu, Q.Z.; Tang, H.F.; Yi, Y.H.; Gong, W. Cytotoxic holostane-type triterpene glycosides from the sea cucumber *Pentacta quadrangularis. Planta Med.* **2010**, *76*, 1900–1904.
14. Liu, B.S.; Yi, Y.H.; Li, L.; Sun, P.; Han, H.; Sun, G.Q.; Wang, X.H.; Wang, Z.L. Argusides D and E, two new cytotoxic triterpene glycosides from the sea cucumber *Bohadschia argus* Jaeger. *Chem. Biodivers.* **2008**, *5*, 1425–1433.
15. Avilov, S.A.; Silchenko A.S.; Antonov, A.S.; Kalinin, V.I.; Kalinovsky, A.I.; Smirnov, A.V.; Dmitrenok, P.S.; Evtushenko, E.V.; Fedorov, S.N.; Savina, A.S.; *et al*. Synaptosides A and A_1, triterpene glycosides from the sea cucumber *Synapta maculata* containing 3-*O*-methylglucuronic acid and their cytotoxic activity against tumor cells. *J. Nat. Prod.* **2008**, *71*, 525–531.

16. Althunibat, O.Y.; Ridzwan, B.H.; Taher, M.; Jamaludin, M.D.; Ikeda, M.A.; Zali, B.I. *In vitro* antioxidant and antiproliferative activities of three Malaysian sea cucumber species. *Eur. J. Sci. Res.* **2009**, *37*, 376–387.
17. Wu, J.; Yi, Y.H.; Tang, H.F.; Wu, H.M.; Zhou, Z.R. . Hillasides A and B, two new cytotoxic triterpen glycosides from the sea cucumber *Holoturia hilla*. *J. Asian. Nat. Prod. Res.* **2007**, *9*, 609–615.
18. Zhang, S.Y.; Tang, H.F.; Yi, Y.H. Cytotoxic triterpene glycosides from the sea cucumber *Pseudocolochirus violaceus*. *Fitoterapia* **2007**, *78*, 283–287.
19. Sun, P.; Liu, B.S.; Yi, Y.H.; Li, L.; Gui, M.; Tang, H.F.; Zhang, D.Z.; Zhang, S.L. New cytotoxic lanostane-type triterpene glycoside from the sea cucumber *Holothuria impatiens*. *Chem. Biodivers.* **2007**, *4*, 450–457.
20. Nigrelli, R.F. The effects of holothurin on fish and mice with sarcoma 180. *Zoologica (NY)* **1952**, *37*, 89–90.
21. Sullivan, T.D.; Ladue, K.T.; Nigrelli, R.F. The effects of holothurin, a steroid saponin of animal origin, on Krebs-2 ascites tumors in Swiss mice. *Zoologica* **1955**, *40*, 49–52.
22. Sullivan, T.D; Nigrelli, R.F. The antitumorous action of biologics of marine origin I. Survival of Swiss mice inoculated with Krebs-2 ascites tumor and treated with holothurin, a steroid saponin from the sea cucumber, *Actinopyga agassizi*. *Proc. Am. Assoc. Cancer Res.* **1956**, *2*, 151–155.
23. Friess, S.L.; Standaert, F.G.; Whitcomb, E.R.; Nigrelli, R.F.; Chanley, J.D.; Sobotka, H. Some pharmacologic properties of holothurin A, a glycosidic mixture from the sea cucumber. *Ann. N. Y. Acad. Sci*. **1960**, *90*, 893–901.
24. Nigrelli, R.F.; Stempien, M.F.J.; Ruggieri, G.D.; Liguori, V.R.; Cecil, J.T. Substances of potential biomedical importance from marine organisms. *Fed. Proc.* **1967**, *26*, 1197–1205.
25. Zhang, S.L.; Li, L.; Yi, Y.H.; Sun, P. Philinopsides E and F, two new sulfated triterpene glycosides from the sea cucumber *Pentacta quadrangularis*. *Nat Prod Res*. **2006**, *20*, 399–407.
26. Tong, Y.; Zhang, X.; Tian, F.; Yi. Y.; Xu, Q.; Li, L.; Tong, L.; Lin, L.; Ding, J. Philinopside A, a novel marine-derived compound possesing dual anti-angiogenetic and anti-tumor effects. *Int. J. Cancer* **2005**, *114*, 843–853.
27. Tian, F.; Zhang, X.; Tong, Y.; Yi, Y.; Zhang, S.; Li, L.; Sun, P.; Lin, L.; Ding, J. PE, a new sulfated saponin from sea cucumber, exhibits anti-angiogenic and anti-tumor activities *in vitro* and *in vivo*. *Cancer Biol. Ther.* **2005**, *48*, 874–882.
28. Tian, F.; Zhu, C.H.; Zhang, X.W.; Xie, X.; Xin, X.L.; Yi, Y.H.; Lin, L.P.; Geng, M.Y.; Ding, J. Philinopside E, a new sulfated saponin from sea cucumber, blocks the interaction between kinase insert domain-containing receptor (KDR) and alphavbeta3 integrin via binding to the extracellular domain of KDR. *Mol. Pharmacol.* **2007**, *72*, 545–552.
29. Careaga, V.P.; Bueno, C.; Muniain, C.; Alche, L.; Maier, M.S. Antiproliferative, cytotoxic and hemolytic activities of a triterpene glycoside from *Psolus patagonicus* and its desulfated analog. *Chemotherapy* **2009**, *55*, 60–68.

30. Zhao, Q.; Liu, Z.; Xue, Y.; Wang, J.; Li, H.; Tang, Q.; Wang, Y.; Dong, P.; Xue, C. Ds-echinoside A, a new triterpene glycoside derived from sea cucumber, exhibits antimetastatic activity via the inhibition of NF-κB-dependent MMP-9 and VEGF expressions. *J. Zhejiang Univ. Sci. B* **2011**, *12*, 534–544.
31. Zhao, Q.; Xue, Y.; Wang, J.F.; Li, H.; Long, T.T.; Li, Z.; Wang, Y.M.; Dong, P.; Xue, C. *In vitro* and *in vivo* anti-tumor activities of echinoside A and ds-echinoside A from *Pearsonothuria graeffei*. *J. Sci. Food Agric.* **2012**, *92*, 965–974.
32. Li, M.; Miao, Z.H.; Chen, Z.; Chen. Q.; Gui, M.; Lin, L.P.; Sun, P.; Yi, Y.H.; Ding, J. Echinoside A, a new marine-derived anticancer saponin, targets topoisomerase2α by unique interference with its DNA binding and catalytic cycle. *Ann. Oncol.* **2010**, *21*, 597–607.
33. Zhao, Q.; Xue, Y.; Liu, Z.; Li, H.; Wang, J.; Li, Z.; Wang, Y.; Dong, P.; Xue, C. Differential effects of sulfated triterpene glycosides, Holothurin A_1, and 24-Dehydroechinoside A, on antimetastasic activity via regulation of the MMP-9 signal pathway *J. Food Sci.* **2010**, *75*, 280–288.
34. Zhang, Y.; Yi, Y. Studies on antitumor activities of triterpene glycoside colochiroside A from sea cucumber *Colochirus anceps*. *Zhongguo Zhong Yao Za Zhi* **2011**, *36*, 504–507.
35. Zou, Z.; Yi, Y.; Wu, H.; Wu, J.; Liaw, C.; Lee, K. Intercedensides A–C, three new cytotoxic triterpene glycosides from the sea cucumber *Mensamaria intercedens* Lampert. *J. Nat. Prod.* **2003**, *66*, 1055–1060.
36. Silchenko, A.S.; Avilov, S.A.; Kalinin, V.I.; Kalinovsky, A.I.; Dmitrenok, P.S.; Fedorov, S.N.; Stepanov, V.G.; Dong, Z.; Stonik, V.A. Constituents of the Sea Cucumber Cucumaria okhotensis. Structures of okhotosides B_1–B_3 and cytotoxic activities of some glycosides from this species. *J. Nat. Prod.* **2008**, *71*, 351–356.
37. Fan, T.J.; Yuan, W.P.; Cong, R.S.; Yang, X.X.; Wang, W.W.; Jing, Z. Studies on the purification of water-soluble holothurian glycosides from *Apostichopus japonicus* and their tumor suppressing activity. *Yao Xue Xue Bao* **2009**, *44*, 25–31.
38. Yun, S.H.; Park, E.S.; Shin, S.W.; Na, Y.W.; Han, J.Y.; Jeong, J.S.; Shastina, V.V.; Stonik, V.A.; Park, J.I.; Kwak J.Y. Stichoposide C induces apoptosis through the generation of ceramide in leukemia and colorectal cancer cells and shows *in vivo* antitumor activity. *Clin. Cancer Res.* **2012**, *18*, 5934–5948.
39. Janakiram, N.B.; Mohammed, A.; Zhang, Y.; Choi, C.; Woodward, C.; Collin, P.; Steele, V.E.; Rao, C.V. Chemopreveintive effects of Frondanol A5, a *Cucumaria frondosa* extract, against rat colon carcinogenesis and inhibition of human colon cancer cell growth. *Cancer Prev. Res.* **2010**, *3*, 82–91.
40. Roginsky, A.B.; Ding, X.; Woodward, C.; Ujiki, M.B.; Singh, B.; Bell, R.H.; Collin, P.; Adrian, T.E. Woodward C. Anti-pancreatic cancer effects of a polar extract from the edible sea cucumber, *Cucumaria frondosa*. *Pancreas* **2010**, *39*, 646–652.
41. Li, X.; Roginsky, A.B.; Ding, X.; Woodward, C.; Collin, P.; Newman, R.A.; Bell, R.H.; Adrian, T.E. Review of the apoptosis pathways in pancreatic cancer and the apoptotic effects of the novel sea cucumber compound, frondoside A. *Ann. N.Y. Acad. Sci.* **2008**, *1138*, 181–198.

42. Al Marzouqi, N.; Iratni, R.; Nemmar, A.; Arafat, K.; Al Sultan, M.A.H.; Collin, P. Frondoside A inhibits human breast cancer cell survival, migration, invasion and the growth of breast tumor xenografts. *Eur. J. Pharmacol*. **2011**, *651*, 18–25.
43. Ma, X.; Kundu, N.; Collin, P.D.; Goloubeva, O.; Fulton, A.M. Frondoside A inhibits breast cancer metastasis and antagonizes prostaglandin E receptors EP4 and EP2. *Breast Cancer Res. Treat*. **2012**, *132*, 1001–1008.
44. Attoub, S.; Arafat, K.; Gelaude, A.; al Sultan, M.A.; Bracke, M.; Collin, P.; Takahashi, T.; Adrian, T.E.; de Wever, O. Frondoside A suppressive effects on lung cancer survival, tumor growth, angiogenesis, invasion, and metastasis. *PLoS One* **2013**, *8*, 1–10.
45. Park, S.Y.; Kim, Y.H.; Kim, Y.; Lee, S.J. Frondoside A has an anti-invasive effect by inhibiting TPA-induced MMP-9 activation via NF-κB and AP-1 signaling in human breast cancer cells. *Int. J. Oncol*. **2012**, *41*, 933–940.
46. Kovalchuk, S.N.; Kozhemyako, V.B.; Atopkina, L.N.; Silchenko, A.S.; Avilov, S.A.; Kalinin, V.I.; Rasskazov, V.A.; Aminin, D.L. Estrogenic activity of triterpene glycosides in yeast two-hybrid assay. *J. Steroid Biochem. Mol. Biol.* **2006**, *101*, 226–231.
47. Al Shemaili, J.; Mensah-Brown, E.; Parekh, K.; Thomas, S.A.; Attoub, S.; Hellman, B.; Nyberg, F.; Adem, A.; Collin, P.; Adrian, T.E. Frondoside A enhances the antiproliferative effects of gemcitabine in pancreatic cancer. *Eur. J. Cancer* **2014**, *50*, 1391–1398.
48. Fedorov, S.N.; Shubina, L.K.; Kapustina, I.I.; Avilov, S.A.; Kwak, J.Y.; Park, J.I.; Jin, J.O.; Kwon, J.X; Shastina, V.V.; Stonik, V.A. Agent stimulating apoptosis of human leukaemia cells. Patent of the Russian Federation 2009, 2360692, 21 December 2007.
49. Jin, J.O.; Shastina, V.V.; Shin, S.W.; Xu, Q.; Park, J.I.; Rasskazov, V.A.; Avilov, S.A.; Fedorov, S.N.; Stonik, V.A.; Kwak, J.Y. Differential effects of triterpene glycosides, frondoside A and cucumarioside A_{2-2} isolated from sea cucumbers on caspase activation and apoptosis of human leukemia cells. *FEBS Lett.* **2009**, *583*, 697–702.
50. Menchinskaya, E.S.; Pislyagin, E.A.; Kovalchyk, S.N.; Davydova, V.N.; Silchenko, A.S.; Avilov, S.A.; Kalinin, V.I.; Aminin, D.L. Antitumor activity of cucumarioside A_{2-}2. *Chemotherapy* **2013**, *59*, 181–191.
51. Aminin, D.L.; Menchinskaya, E.S.; Pislyagin, E.A.; Silchenko, A.S.; Avilov, S.A.; Kalinin, V.I.; Stonik, V.A. New anticancer compounds from sea cucumbers. Molecular mechanisms of action. *FEBS J.* **2014**, *281*, 488.
52. Menchinskaya E.S.; Aminin D.L.; Avilov S.A.; Silchenko A.S.; Andryjashchenko P.V.; Kalinin V.I.; Stonik V.A. Agent inhibiting multiple drug resistance of tumor cells. Patent of the Russian Federation 2013, 2494742, 10 August 2012.
53. Menchinskaya, E.S.; Aminin, D.L.; Avilov, S.A.; Silchenko, A.S.; Andryjashchenko, P.V.; Kalinin, V.I.; Stonik, V.A. Inhibition of tumor cells multidrug resistance by cucumarioside A_{2-}2, frondoside A and their complexes with a cholesterol. *Nat. Prod. Commun.* **2013**, *8*, 1377–1380.

54. Stonik, V.A.; Aminin, D.L.; Boguslavski, V.M.; Avilov, S.A.; Agafonova, I.G.; Silchenko, A.S.; Ponomarenko, L.P.; Prokofieva, N.G.; Chaikina E.L. Immunomodulating agent and pharmaceutical composition based on the same. Patent of the Russian Federation 2005, 2271820, 2 July 2004.
55. Aminin, D.L.; Chaykina, E.L.; Agafonova, I.G.; Avilov, S.A.; Kalinin, V.I.; Stonik, V.A. Antitumor activity of the immunomodulatory lead Cumaside. *Int. Immunopharmacol.* **2010**, *10*, 648–654.
56. Patil, T.D.; Thakare, S.V. *In silico* evaluation of selected triterpene glycosides as a human dna topoisomerase II alpha (α) inhibitor. *Int. J. Pharm. Pharm. Sci.* **2012**, *4*, 201–204.
57. Park, J.-I.; Bae, H.-R.; Kim C.G.; Stonik, V.A.; Kwak, J.-Y. Relationships between chemical structures and functions of triterpene glycosides isolated from sea cucumbers. *Front. Chem.* **2014**, *2*, 1–14.
58. Kim, C.G.; Kwak, J.-Y. Anticancer effect of triterpene glycosides, frondoside A and cucumarioside A_2-2 isolated from sea cucumbers. In *Handbook of Anticancer Drugs from Marine Origin*; Kim, S.-K., Ed.; Springer International Publishing: Cham, Switzerland, 2015; pp. 673–682.

Fucoidan Derived from *Undaria pinnatifida* Induces Apoptosis in Human Hepatocellular Carcinoma SMMC-7721 Cells via the ROS-Mediated Mitochondrial Pathway

Lili Yang, Peisheng Wang, Huaxin Wang, Qiaomei Li, Hongming Teng, Zhichao Liu, Wenbo Yang, Lin Hou and Xiangyang Zou

Abstract: Fucoidans, fucose-enriched sulfated polysaccharides isolated from brown algae and marine invertebrates, have been shown to exert anticancer activity in several types of human cancer, including leukemia and breast cancer and in lung adenocarcinoma cells. In the present study, the anticancer activity of the fucoidan extracted from the brown seaweed *Undaria pinnatifida* was investigated in human hepatocellular carcinoma SMMC-7721 cells, and the underlying mechanisms of action were investigated. SMMC-7721 cells exposed to fucoidan displayed growth inhibition and several typical features of apoptotic cells, such as chromatin condensation and marginalization, a decrease in the number of mitochondria, and in mitochondrial swelling and vacuolation. Fucoidan-induced cell death was associated with depletion of reduced glutathione (GSH), accumulation of high intracellular levels of reactive oxygen species (ROS), and accompanied by damage to the mitochondrial ultrastructure, depolarization of the mitochondrial membrane potential (MMP, $\Delta\psi$m) and caspase activation. Moreover, fucoidan led to altered expression of factors related to apoptosis, including downregulating *Livin* and *XIAP* mRNA, which are members of the inhibitor of apoptotic protein (IAP) family, and increased the Bax-to-Bcl-2 ratio. These findings suggest that fucoidan isolated from *U. pinnatifida* induced apoptosis in SMMC-7721 cells via the ROS-mediated mitochondrial pathway.

Reprinted from *Mar. Drugs*. Cite as: Yang, L.; Wang, P.; Wang, H.; Li, Q.; Teng, H.; Liu, Z.; Yang, W.; Hou, L.; Zou, X. Fucoidan Derived from *Undaria pinnatifida* Induces Apoptosis in Human Hepatocellular Carcinoma SMMC-7721 Cells via the ROS-Mediated Mitochondrial Pathway. *Mar. Drugs* **2013**, *11*, 1961-1976.

1. Introduction

Fucoidans are a class of fucose-enriched sulfated polysaccharides primarily extracted from brown seaweeds [1,2]. It has recently been reported that fucoidans possess a wide variety of biological activities, including anticoagulant, antiviral, anti-angiogenic, anticancer and immunomodulatory activities [3,4]. In particular, the anticancer activity of fucoidans has attracted considerable attention. Several investigations have demonstrated that fucoidans can effectively suppress proliferation and colony formation by cancer cells *in vitro* [5], and inhibit metastasis and angiogenesis of Lewis lung adenocarcinoma and B16 melanoma xenografts *in vivo* [6,7]. Compared to other sulfated polysaccharides, the fucoidan extracted from the sporophylls of the brown seaweed *Undaria pinnatifida* has a higher sulfate and L-fucose content, and exhibits a broader range of bioactivities [8].

Hepatocellular carcinoma (HCC) is the third leading cause of cancer-related deaths, which has high morbidity and mortality rates [9,10]. Due to the accumulation of several genetic and epigenetic

changes within the tumor cells, HCC has a relatively low therapeutic selectivity and high drug resistance, and these major issues reduce the efficacy of chemotherapy in patients with this disease [11].

Apoptosis, or programmed cell death, is an important aspect of chemotherapy-induced tumor cell death; and is the major mechanism of tumor cell death induced by many anticancer drugs and natural products [12]. Caspase-dependent apoptosis is characterized by activation of either the extrinsic pathway, initiated by activation of death receptors leading to the cleavage of caspase-8, or the intrinsic pathway, triggered by mitochondrial depolarization, release of cytochrome c and the subsequent activation of caspase-9 [13,14]. Disruptions to the factors regulating these apoptotic pathways contributes substantially to the transformation of a normal cell into a tumor cell, and the cells of some tumor types are relatively resistant to apoptosis [15,16].

Intracellular reactive oxygen species (ROS) are considered to be an apoptotic death signal [17]. However, low physiological levels of ROS also serve as a signaling messenger to mediate various biological responses, including cell proliferation, angiogenesis, innate immunity, gene expression, apoptosis and senescence [18]. It has also been established that increased levels of these short-lived reactive molecules can exert harmful effects by inducing oxidative damage to biological macromolecules and disrupting the cellular reduction-oxidation (redox) balance. Such disturbances to ROS homeostasis are generally considered to be a risk factor for the initiation and progression of diseases such as atherosclerosis, neurodegeneration and cancer [19]. ROS induce depolarization of the mitochondrial membrane potential (MMP, $\Delta\psi$m) and the release of cytochrome c from the mitochondria into the cytosol, where cytochrome c triggers activation of caspase-9 and initiates the caspase cascade, which ultimately induces the cell to undergo apoptosis [20]. Tumor cells are more sensitive to fluctuations in the levels of ROS than normal cells; therefore, ROS are also considered as an important target in anticancer drug research [21,22].

The present study was designed to evaluate the anticancer effects of the fucoidan extracted from *U. pinnatifida* sporophylls in human HCC SMMC-7721 cells, and investigate the molecular mechanisms of these effects.

2. Results and Discussion

2.1. Preparation and Properties of U. pinnatifida *Fucoidan*

The fucoidan extracted and purified from *U. pinnatifida* sporophylls was a beige, fibrous powder (purity > 90%). Infrared spectrum and ^{13}C-NMR analyses of the sample revealed strong characteristic absorption peaks for sulfated residues, fucose and galactose, respectively. The sample mainly consisted of carbohydrates (68.37%), sulfates (21%) and uronic acid (10.89%), with fucose and galactose mainly constituting the monosaccharide component; the percentage protein content was determined to be 0.85%. The molecular weight of the purified fucoidan was approximately 10.4356×10^4 Da. The optical rotation of the fucoidan (0.6 mg/mL) at 20 °C was 0.99°.

2.2. Fucoidan Induces Apoptosis in SMMC-7721 Cells

To investigate the effects of the fucoidan in human HCC cells, SMMC-7721 cells were exposed to various concentrations of the fucoidan for up to 72 h, and then subjected to 3,(4,5-dimethylthiazol-2-yl)-2,5-diphenyltetrazolium bromide (MTT) assay. The fucoidan inhibited SMMC-7721 cell viability in a concentration- and time-dependent manner (Figure 1a,b). Fucoidan-induced SMMC-7721 cell death was confirmed by Hoechst 33258 staining, and annexin V/propidium iodide (PI) staining by flow cytometry. Nuclear fragmentation and chromatin condensation, the typical morphological characteristics of apoptotic cells, were observed in fucoidan-treated cells stained with Hoechst 33258 (Figure 1c); however, these features were rarely observed in control cells. Annexin V/PI double-staining and flow cytometry revealed that fucoidan effectively induced apoptosis in SMMC-7721 cells (Figure 1d). The proportion of apoptotic cells (lower right quadrant) significantly increased from 9.8% in untreated cells to 14.5%–25.1% in fucoidan-treated cells. The proportion of necrotic cells did not significantly change after exposure to fucoidan.

2.3. Effect of Fucoidan on Cell Cycle Distribution in SMMC-7721 Cells

To determine the effects of the fucoidan on the cell cycle, the cells were treated with the fucoidan for 48 h, then the percentage of cells in each phase of cell cycle was determined by using a flow cytometry. SMMC-7721 cells treated with fucoidan (1000 μg/mL) for 48 h tended to accumulate in the S-phase; however, this increase was not significant compared to control cells (Figure 2).

Figure 1. Effects of fucoidan on cell viability and apoptosis in SMMC-7721 hepatocellular carcinoma (HCC) cells. (**a** and **b**) Viability of cells treated with various concentrations of fucoidan (65.2–1000 μg/mL) for 48 h (**a**) or with 500 μg/mL fucoidan for 6, 12, 24, 48 or 72 h (**b**) as determined by the MTT assay. Data is the mean ± SD of at least three independent experiments; * $P < 0.05$, ** $P < 0.01$ compared with control cells. (**c**) Fucoidan induces apoptosis in SMMC-7721 cells. Nuclear morphology, as indicated by Hoechst 33258 staining. (**d**) Quantification of apoptosis by the annexin V/PI double staining assay using flow cytometry. LL (low left), LR (low right), UR (upper right), and UL (upper left) denote viable (live), early apoptotic, late apoptotic and necrotic cells, respectively.

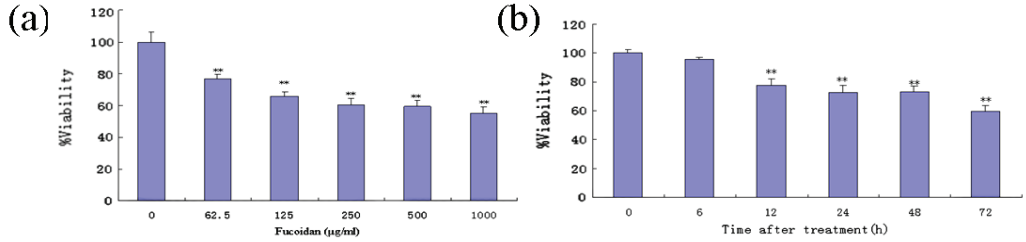

Figure 1. *Cont.*

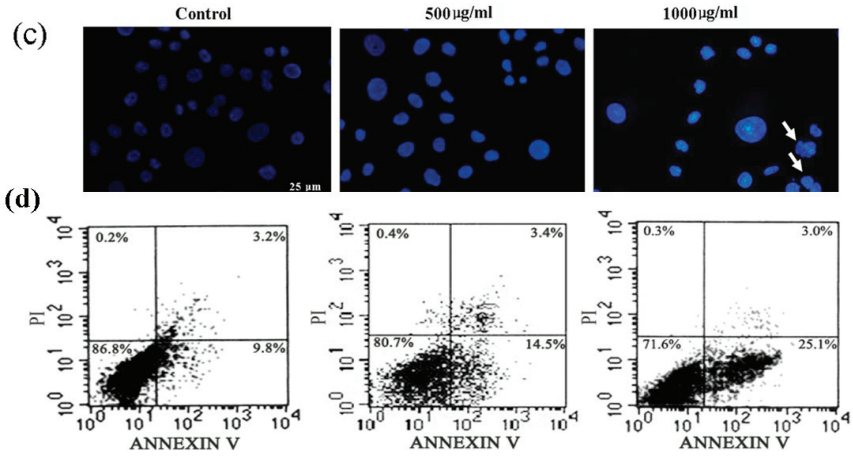

Figure 2. Changes in the cell cycle distribution in SMMC-7721 cells treated with fucoidan. The cell cycle trended towards accumulation of S phase cells in the cells treated with fucoidan (500 μg/mL or 1000 μg/mL for 24 h).

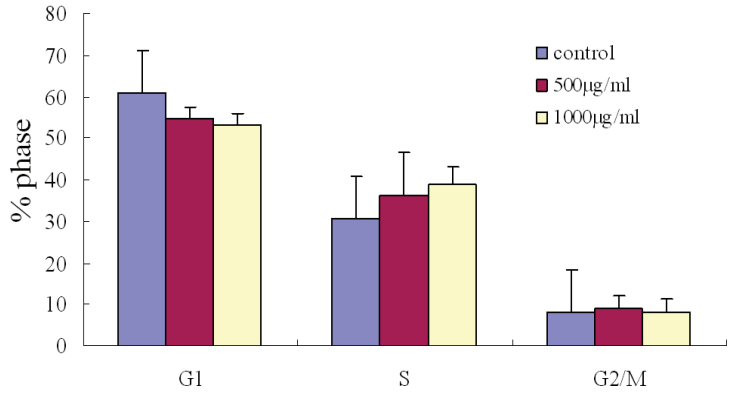

2.4. Fucoidan-Induced Apoptosis in SMMC-7721 Cells Is Dependent on Caspase Activation

To assess whether the fucoidan-induced apoptosis in SMMC-7721 cells was caspase-dependent, the enzyme activities of initiator (-8 and -9) and effector (-3) caspases were analyzed using commercial colorimetric assays. As shown in Figure 3a, 1000 μg/mL fucoidan induced activation of caspase-3 ($P < 0.01$), caspase-9 and caspase-8 ($P < 0.05$). Moreover, fucoidan lead to downregulation of *XIAP* and *Livin* mRNA expression; these proteins are endogenous inhibitors of caspase-3 and caspase-9 (Figure 3b).

Figure 3. Caspase activation and expression of inhibitor of apoptotic protein (IAP) proteins during fucoidan-induced apoptosis in SMMC-7721 cells. (**a**) Activation of caspase-3, caspase-8 and caspase-9 were examined using commercial colorimetric assays and expressed as relative activities. The relative activities of caspase-3, caspase-8 and caspase-9 in SMMC-7721 cells treated with fucoidan for 24 h were higher than that of untreated control cells. (**b**) RT-PCR analysis of *Livin* and *XIAP* mRNA expression. *GAPDH* was examined as an endogenous control.

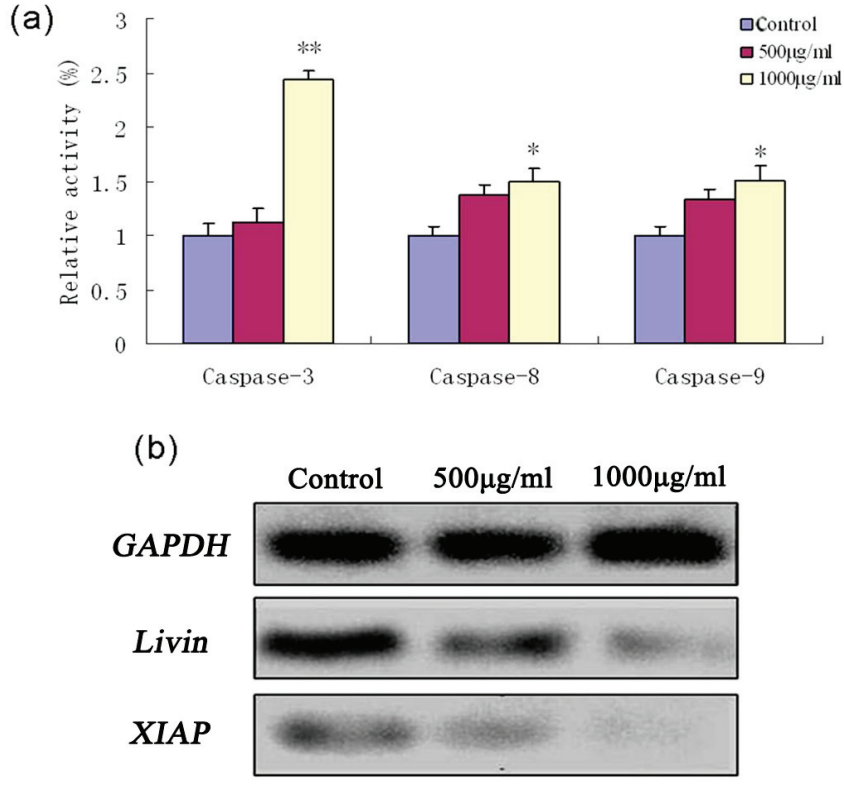

2.5. Effect of Fucoidan on Mitochondrial Morphology in SMMC-7721 Cells

The changes in mitochondrial ultrastructure were observed by transmission electron microscopy. Cells treated with fucoidan for 24 h exhibited the typical features of apoptotic cells, including swelling and vacuolation of the mitochondria (Figure 4a). The average number of mitochondria was determined in a square area of 2000 nm × 2000 nm. The average mitochondrial number in cells treated with fucoidan was significantly less than that in control cells (Figure 4b).

2.6. Fucoidan Induces Mitochondrial Dysfunction and Increases the Bax/Bcl-2 Ratio in SMMC-7721 Cells

Mitochondrial function was evaluated by measuring mitochondrial membrane potential (MMP, $\Delta\psi m$) using the fluorochrome JC-1 and flow cytometry. Fucoidan treatment of SMMC-7721 cells induced significant dissipation of the MMP (Figure 5a) in a concentration-dependent manner (Figure 5b). Immunocytochemistry and western blotting analysis revealed that fucoidan downregulated expression of the anti-apoptotic protein Bcl-2, and moderately increased expression of the pro-apoptotic protein Bax. Fucoidan induced a concentration-dependent increase in the Bax/Bcl-2 ratio in SMMC-7721 cells (Figure 5c,d).

Figure 4. Ultrastructural changes in mitochondrial morphology in SMMC-7721 cells after exposure to fucoidan. (**a**) After 24 h treatment with fucoidan, SMMC-7721 cells exhibited mitochondria swelling and vacuolation, as observed by transmission electron microscopy. Arrows indicate swollen mitochondria. (**b**) The average number of mitochondria was counted in a 2000 nm × 2000 nm square. Mitochondrial number was significantly lower in the cells treated with fucoidan (1000 μg/mL) than control cells (* $P < 0.05$).

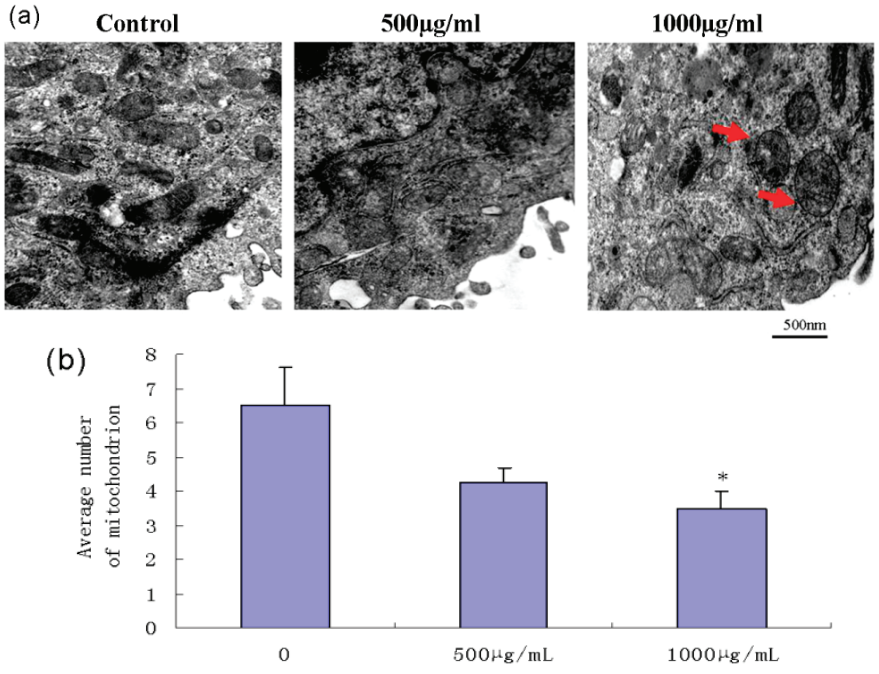

Figure 5. Fucoidan induces mitochondrial dysfunction and increases the Bax/Bcl-2 ratio in SMMC-7721 cells. (**a**) Depolarization of mitochondrial membrane potential (MMP, $\Delta\psi$m) was examined in control SMMC-7721 cells and SMMC-7721 cells exposed to fucoidan (500 μg/mL or 1000 μg/mL for 24 h); the cells were stained with JC-1 and analyzed by flow cytometry. (**b**) Percentage of cells with a low MMP ($\Delta\psi$m). Data are mean ± SD of three independent experiments; ** $P < 0.01$ compared with control cells. (**c**) Immunocytochemical localization of Bcl-2 and Bax. SMMC-7721 cells were treated with fucoidan, fixed, permeabilized with 0.2% Triton X-100 and subjected to immunofluorescent staining using anti-Bcl-2 and anti-Bax antibodies. Microphotographs were taken using a fluorescence microscope. (**d**) Western blotting analysis of Bcl-2 and Bax expression, and the Bax/Bcl-2 ratio in the cells exposed to fucoidan (500 μg/mL or 1000 μg/mL for 24 h) or unexposed. * $P < 0.05$, ** $P < 0.01$ compared to controls. Data from optical density measurements were tested using one-way ANOVA.

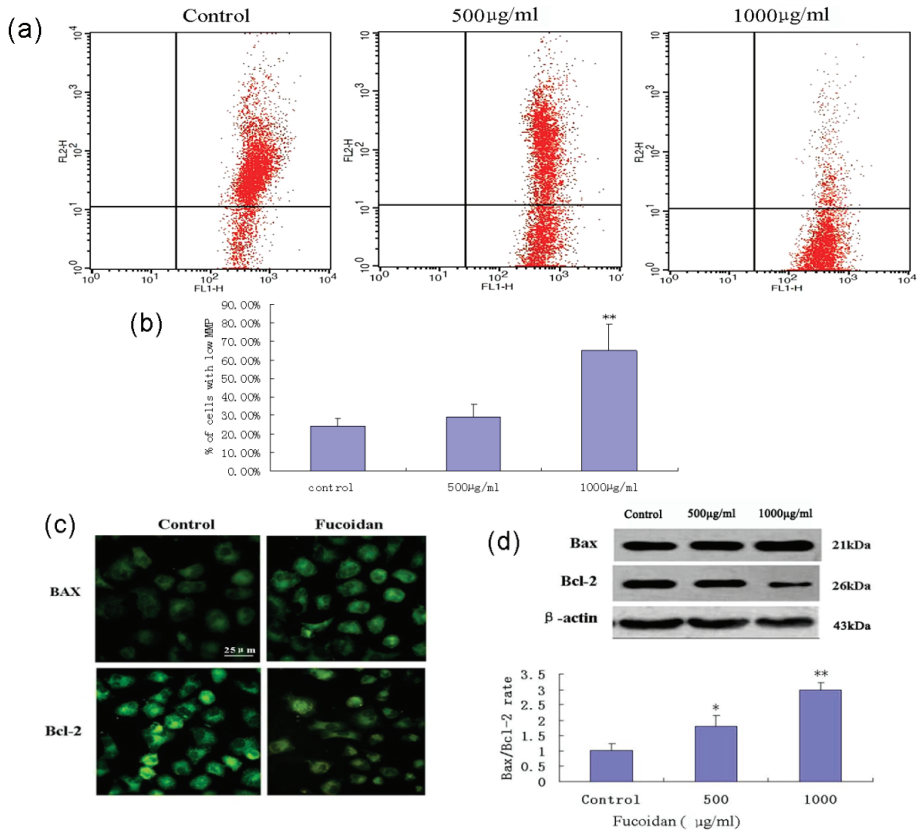

2.7. Fucoidan Induces Mitochondrial Release of Cytochrome c in SMMC-7721 Cells

Release of cytochrome c from the mitochondria to cytosol was detected using an immunofluorescent method. The results showed that treatment of SMMC-7721 cells with fucoidan induced the release of cytochrome c from the mitochondria into the cytosol (Figure 6).

Figure 6. Fucoidan induces the release of cytochrome c from the mitochondria in SMMC-7721 cells. Immunocytochemical localization of cytochrome c. SMMC-7721 cells were treated with fucoidan (1000 μg/mL) for 24 h, fixed, permeabilized with 0.2% Triton X-100 and subjected to immunofluorescent staining using a cytochrome c antibody. Microphotographs were taken using a fluorescence microscope.

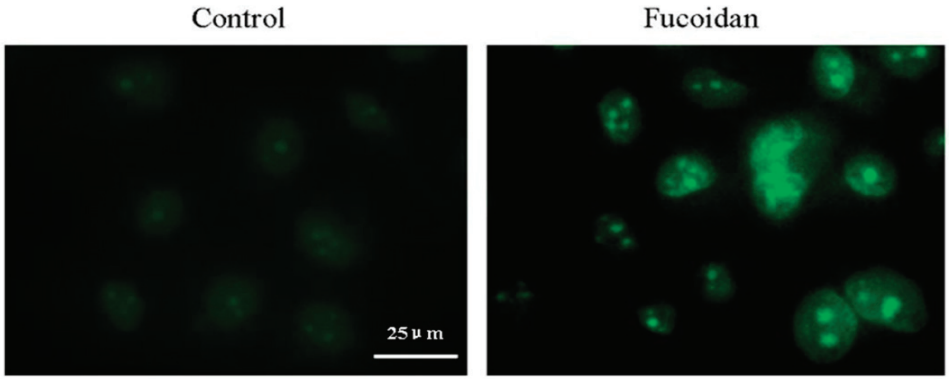

2.8. Fucoidan Induces an Intracellular ROS Burst and GSH Depletion in SMMC-7721 Cells

The generation of intracellular ROS in fucoidan-treated SMMC-7721 cells was monitored by detection of the fluorescent probe (DCFH-DA) by flow cytometry. As shown in Figure 7a,b, exposure to fucoidan triggered the production of ROS in a concentration-dependent manner. To determine whether the changes in ROS accumulation were related to GSH depletion or a decline in total anti-oxidant capability (T-AOC), we investigated the effects of fucoidan on intracellular GSH and T-AOC in SMMC-7721 cells using commercial colorimetric assays. Fucoidan partially depleted the intracellular GSH content (Figure 7c) and led to a decrease in cellular T-AOC in the cells (Figure 7d).

2.9. Discussion

Fucoidans are potent inducers of apoptosis in various cancer cell lines. The fucoidan derived from the sporophylls of *U. pinnatifida* has a higher sulfate and L-fucose content than the fucoidans extracted from other brown seaweeds. *U. pinnatifida* fucoidan has previously been shown to possess anti-cancer, anti-proliferative and anti-coagulative activities [8]. Several studies have also demonstrated that fucoidans from several brown algae can activate the extrinsic or intrinsic apoptotic pathways in a variety of cancer cell lines by altering the expression of apoptosis-associated or signaling proteins, cell cycle regulatory proteins and transcription factors [23–26]. Although these

fucoidan has been shown to induce apoptosis in SMMC-7721 HCC cells, the molecular and cellular mechanism(s) underlying these effects had not yet been determined.

Figure 7. Fucoidan induces intracellular reactive oxygen species (ROS) generation, and reduces glutathione GSH) content and total anti-oxidant capability (T-AOC) in the cells. (**a**) Levels of ROS in SMMC-7721 cells following exposure to fucoidan. Cells were treated with 500 μg/mL or 1000 μg/mL fucoidan for 24 h, then stained with detection of the fluorescent probe (DCFH-DA) commercial colorimetric kit for flow cytometric analysis. (**b**) Relative fluorescent intensity of DCFH-DA in fucoidan-treated cells, expressed as a percentage of the control group. (**c**, **d**) Generation of intracellular GSH and T-AOC were determined in cells treated with fucoidan for 24 h. ** $P < 0.01$ compared to control cells.

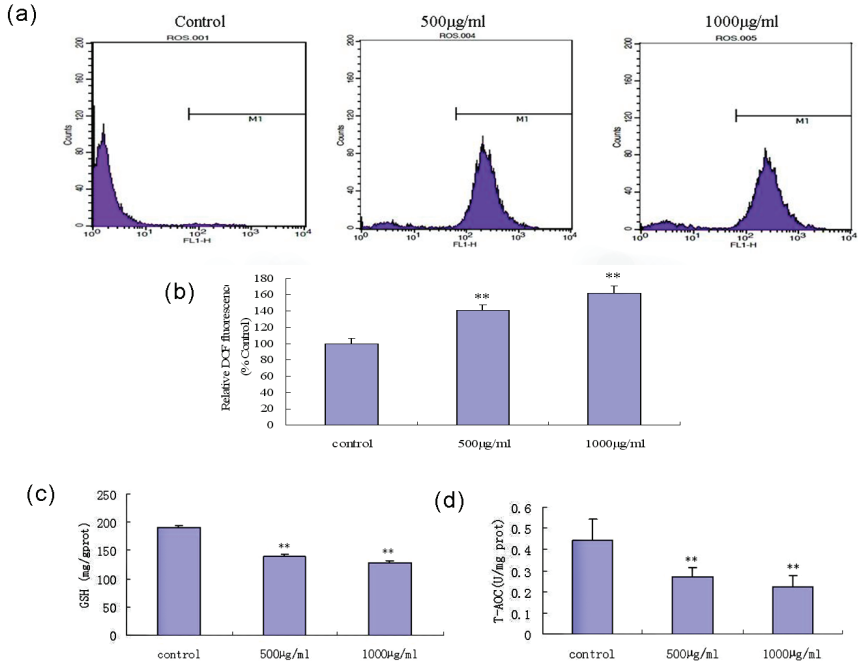

In the present study, exposure of SMMC-7721 cells to the fucoidan isolated from *U. pinnatifida* sporophylls resulted in apoptotic cell death, accompanied by nuclear fragmentation, vacuolization of the mitochondria, depolarization of the MMP, release of cytochrome c from the mitochondria and caspase activation. Furthermore, the apoptosis induced by the fucoidan in SMMC-7721 cells was related to the generation of ROS, depletion of intracellular GSH, a decrease in T-AOC, an increase in the Bax/Bcl-2 ratio, and downregulation of *XIAP* and *Livin*. These observations suggest that the fucoidan induces apoptosis in SMMC-7721 cells via the ROS-mediated mitochondrial pathway.

The ability to induce cellular apoptosis is an important property of many candidate anticancer drugs [27]. Apoptosis is a tightly regulated process, which involves at least one of the caspase-dependent signaling pathways: the cell death receptor pathway or the mitochondrial pathway [28]. In the

mitochondrial pathway, a variety of death signals trigger the release and translocation of several pro-apoptotic proteins from mitochondria to cytosol. Among the numerous factors known to modulate apoptosis in cancer cells, the proteins of the Bcl-2 family are viewed as the main regulators of apoptosis, and investigation of their function has been the focus of intensive research for more than twenty years [29]. Bcl-2 is an anti-apoptotic protein, whereas Bax is a crucial pro-apoptotic and tumor suppressor protein [30,31]. Bcl-2 also plays an important role in the regulation of mitochondrial energetics, transport of adenine nucleotides, Ca^{2+} and other metabolites, and mitochondrial membrane permeability [32]. The ratio of anti-apoptotic to pro-apoptotic molecules, such as the Bcl-2/Bax ratio, indicates the threshold sensitivity of cells to the induction of apoptosis via the intrinsic pathway [33]. In our experiment, the protein expression levels of Bcl-2 and Bax were assessed. Our results indicated that the fucoidan downregulated Bcl-2 protein expression, upregulated Bax protein expression, and increased the Bax/Bcl-2 ratio in a concentration-dependent manner in SMMC-7721 cells.

Activation of caspases is a pivotal step in the apoptotic process, and is triggered by signals from death factors, mitochondrial alterations or DNA damage due to external and/or internal insults [34]. Regardless of whether apoptosis occurs by the cell death receptor pathway or mitochondrial pathway, both pathways ultimately activate caspase-3, which in turn induces DNA fragmentation, the characteristic morphological change associated with apoptotic cells; activation of caspase-3 indicates a key and irreversible point in the induction of apoptosis [35]. Depolarization of MMP induced by apoptotic stimuli often leads to mitochondrial permeability transition pore formation, which enables the release of cytochrome c from the mitochondrial inter-membrane space into the cytosol [36], which in turn triggers the activation of caspase-9 and induces apoptosis via the caspase-dependent mitochondrial pathway [37]. In the present study, exposure to the fucoidan resulted in depolarization of the MMP, release of cytochrome c from the mitochondria, and activation of caspase-3, caspase-8 and caspase-9 in SMMC-7721 cells. Of the members of the IAP protein family, XIAP has been reported to exert the strongest anti-apoptotic function, as it inhibits caspase-3, caspase-7 and caspase-9 [38]. Livin also inhibits the activation of caspase-9 induced by cytochrome c, Apaf-1 and dATP [39]. This study demonstrated that the fucoidan downregulated the expression of *XIAP* and *Livin* mRNA, which was associated with activation of caspase-3 and caspase-9, indicating that fucoidan-induced apoptosis occurred via the mitochondrial pathway. Our results also suggest that the fucoidan-induced apoptosis also involved co-activation of the caspase-8 and caspase-9-mediated pathway.

Oxidative stress refers to an imbalance between pro-oxidant and anti-oxidant factors, which are controlled by multiple components; such imbalances may lead to cellular damage. ROS play a key role in oxidative stress, and are generated as by-products of cellular metabolism, primarily in the mitochondria [40]. Once accumulated, ROS can attack cellular proteins, DNA and lipids, which leads to a state of oxidative stress. ROS contribute to a number of human diseases including cardiovascular, inflammatory and neurodegenerative diseases, as well as cancer. Elevated levels of mitochondrial ROS have been shown to be sufficient to trigger apoptosis [41]. In this study, the apoptotic effect of the fucoidan in SMMC-7721 cells was associated with a rapid increase in the levels of intracellular ROS; after treatment with the fucoidan for 24 h, the levels of ROS significantly

increased. Additionally, the fucoidan-induced ROS generation was associated with a significant depletion of intracellular GSH, which is a major non-protein cellular antioxidant which can eliminate intracellular ROS [42]. The degree of exposure to ROS and perturbations to the GSH redox balance play a critical role in determining whether cells undergo a pro-survival or pro-death response [43]. A 10% reduction in the GSH content can induce apoptosis in a variety of cancer cells, including lung cancer, hepatoma and breast cancer cells, but has almost no effect in normal cells. Tumor cells have a significantly higher sensitivity to changes in the levels of GSH, due to the fact that tumor cells have a heightened basal level of ROS-mediated signals which contributes to their increased rate of growth, metabolism and proliferation; therefore, tumor cells may be more vulnerable to oxidative stress [22]. In this study, the total cellular antioxidant capacity (T-AOC) was remarkably decreased in fucoidan-treated SMMC-7721 cells. Fucoidan might exhausted the total cellular antioxidant capacity and increased the ROS levels beyond a "threshold", which may have contributed to the induction of apoptosis in SMMC-7721 cells. Similar findings with regards to cell cycle arrest were reported to be induced by the fucoidan from Mozuku seaweed (*Cladosiphon novae-caledoniae* Kylin) in MCF-7 breast cancer cells [44].

Taken together, our findings demonstrate that the fucoidan induces apoptosis in SMMC-7721 cells via the ROS-mediated mitochondrial pathway, by increasing ROS production, inducing mitochondrial oxidative damage, MMP depolarization and release of cytochrome c, combined with downregulation of *XIAP* and *Livin* and activation of caspase-3 and caspase-9. We suggest that the potent pro-apoptotic effects of the fucoidan be due to its high content of sulfate groups, which resulted in depletion of intracellular GSH, which in turn triggered mitochondrial oxidative damage and the activation of caspase-9 and caspase-3. This study suggests that marine fucoidans may represent candidate anti-cancer drugs. Further research is required to investigate how fucoidans enter tumor cells, and to determine whether they are absorbed directly by the tumor cells and/or accumulate in tumor tissues.

3. Experimental Section

3.1. Reagents and Antibodies

RPMI 1640 medium, antibiotics (penicillin and streptomycin), trypsin-EDTA, dimethylsulfoxide (DMSO) and fetal bovine serum (FBS) were obtained from Hyclone (Logan, UT, USA). MTT reagent and trypsin were purchased from Sigma (St. Louis, MO, USA). Mouse anti-Bcl-2, Bax and cytochrome c IgG monoclonal antibodies and rabbit anti-β-actin IgG polyclonal antibody were purchased from Santa Cruz Biotechnology (Santa Cruz, CA, USA). Horseradish peroxidase-conjugated anti-rabbit and anti-mouse IgG were purchased from Beijing Zhongshan Biotechnology Co., Ltd. (Bejing, China). FITC-conjugated rabbit anti-mouse IgG was obtained from Thermo Fisher Scientific (NY, USA). The human cytochrome c ELISA kit was obtained from Bioleaf Biotechnology Co., Ltd. (Shanghai, China). Annexin V-FITC, propidium iodide (PI) and Hoechst 33258 were supplied by KeyGen Biological Technology Co., Ltd. (Nanjing, China).

3.2. Preparation and Analysis of Fucoidan

The fucoidan was prepared from sporophylls of *U. pinnatifida* by trypsin-enzymatic hydrolysis and alcohol grade precipitation. Infrared spectra and ^{13}C-NMR spectra were recorded on Nicolet 510P spectrophotometer (Nicolet Co., USA) and Brucker AV500 NMR instrument (Brucker Co., Sweden), respectively. The total carbohydrate, sulfate radical and uronic acid contents were measured by the phenol-sulfuric acid reaction, $BaCl_2$-gelation and sulfuric acid-carbazole colorimetric methods, respectively. The molecular weight of the sample was evaluated by size exclusion chromatography using TSK-gel G 3000 PWXL (TOSOH, Tokyo, Japan). Optical rotation was measured at 589 nm using the WZZ-1 polarimeter (Yemao Co., Ltd., Shanghai, China) at 20 °C. Above tests were performed as previously reported [4].

3.3. Cell Culture

The human HCC cell line SMMC-7721 was obtained from the Cell Bank of the Chinese Academy of Sciences (Beijing, China). SMMC-7721 cells were cultured in RPMI 1640 medium containing 10% FBS, 100 μg/mL penicillin and 100 μg/mL streptomycin. The cells were incubated at 37 °C in a humidified incubator (Thermo Fisher Scientific, New York, NY, USA) in an atmosphere of 5% CO_2.

3.4. Cell Viability Assay

The effects of fucoidan on SMMC-7721 cell viability were measured using the MTT assay. Logarithmically-growing SMMC-7721 cells were seeded at a density of 2×10^4 cells/well in 96-well plates and allowed to adhere for 24 h at 37 °C. Then, the supernatant was replaced with 200 μL culture medium supplemented with different concentrations of fucoidan. The cells were incubated for 6, 12, 24, 48 or 72 h, then 20 μL MTT (5 mg/mL) was added to each well, incubated for an additional 4 h at 37 °C, the medium was removed, the formazan crystals were dissolved in 150 μL DMSO, and the absorbance values were measured at wavelength of 490 nm using a microplate reader (Thermo Fisher Scientific).

3.5. Cell Cycle Analysis

The cell cycle distribution of cells treated with fucoidan for 24 h or 48 h was assayed by measuring the DNA content of nuclei labeled with propidium iodide (PI). Briefly, the cells were harvested, fixed in 70% ethanol for 24 h, incubated with 50 μg/mL PI and 0.25 mg/mL RNase A at 37 °C for 30 min, and then analyzed using a FACSCalibur™ Flow Cytometer (BD Biosciences, San Jose, CA, USA) with excitation at 488 nm and detection at 620 nm. Data was gated to exclude cellular debris. The proportions of G1, S and G2-M phase cells were calculated from the DNA content histograms.

3.6. Apoptosis Assay

SMMC-7721 cells were seeded into 6-well plates (3×10^5 cells /well), allowed to adhere for 24 h, and treated with 500 μg/mL or 1000 μg/mL fucoidan for 24 h. The cells were collected, washed twice with chilled PBS and stained using annexin V-FITC labeling solution (annexin V-fluorescein in binding buffer containing PI (KeyGen)) according to the manufacturer's protocol. Apoptotic cells were analyzed by using a FACSCalibur flow cytometry.

3.7. Hoechst 33258 Staining

The cells treated with fucoidan were stained with Hoechst 33258 (4 μg/mL) for 30 min, fixed for 10 min in 4% *para*-formaldehyde (PFA), and then observed by DMI-4000B inverted fluorescence microscopy (Leica, Germany).

3.8. Transmission Electron Microscopy

SMMC-7721 cells were treated with fucoidan for 24 h, washed with PBS, centrifuged (1000 rpm for 10 min), and the cell pellets were fixed in 2.5% glutaraldehyde in pH 7.2 sodium cacodylate buffer overnight. The cells were post-fixed in 1% osmium tetroxide, dehydrated through an ascending alcohol series, embedded in Epon resin and sectioned using an ultramicrotome. Ultrathin sections were stained with saturated uranyl acetate and aqueous lead citrate, and examined by transmission electron microscopy using a JEM-1220 (JEOL, Japan) operating at 60 kV.

3.9. Assay of Mitochondrial Membrane Potential

Mitochondrial membrane potential ($\Delta\psi m$) was measured using the mitochondrial membrane sensor kit containing the dye JC-1 (Nanjing KeyGEN Biotech. Co., Ltd., Nanjing, China), as described by the manufacturer. The cells were treated with or without fucoidan for 24 h, and then harvested for flow cytometric analysis.

3.10. Immunofluorescence Staining

The cells were suspended in RPMI 1640 medium and transferred to 6-well plates (3×10^5 cells/well) culture dished with sterile cover slips and grown up to 60% confluency, and the cells were treated with or without fucoidan for 24 h. Cells grown on cover slips washed with cold PBS, fixed for 15 min with 4% PFA, permeabilized with 0.2% Triton X-100 in PBS for 5 min, blocked with 0.1% BSA, and then incubated with the appropriate primary antibody in 1% BSA at room temperature, detected by the appropriate fluorescence-conjugated anti-rabbit or anti-mouse IgG antibody for 15 min. After washing with PBS, the cover slips were mounted of coverslides on glass slides and analyzed under using a LSM510 fluorescence microscope (Carl Zeiss, Germany).

3.11. Caspase Activation Assays

Caspase-3, caspase-8 and caspase-9 activation was determined using Caspase Colorimetric Assay kits (KeyGen) following the manufacturer's instructions. The background absorbance value was subtracted from the absorbance results of the test wells. These experiments were performed independently three times.

3.12. Measurement of Intracellular ROS, GSH Levels and T-AOC

ROS generation was monitored by staining cells with DCFH-DA using T-AOC detection assay kit (KeyGen). Briefly, following exposure to fucoidan, the cells were incubated with 5 μM DCFH-DA at 37 °C for 30 min, trypsinized, washed with PBS and the fluorescence intensity of the cells was analyzed immediately by flow cytometry using FI-1 filters at an excitation wavelength of 488 nm. Generation of intracellular reduced glutathione (GSH), an index of cellular reducing power, and total antioxidant capability (T-AOC) were measured using the kits following the manufacturer's instructions.

3.13. Western Blot Analysis

Cells were collected, washed twice with cold PBS, lysed using lysis buffer (KeyGen) for 20 min on ice, and centrifuged at 14,000 *g* for 20 min at 4 °C. The supernatant of the protein lysates was subjected to SDS-PAGE using 12% gel, electro-transferred onto nitrocellulose membranes, incubated with the appropriate specific primary and secondary antibodies, and the bands were detected using chemiluminescence.

3.14. Semi-Quantitative RT-PCR Analysis

For RT-PCR analysis of *Livin* and *XIAP* mRNA expression, total RNA was isolated from the cells using TRIzol (Invitrogen, Carlsbad, CA, USA) and cDNA was synthesized according to the manufacturer's instructions (TaKaRa, Japan). The sequences of the forward and reverse primers were: 5′-CGTCTTGGTTCTTCCCA-3′ and 5′-GTTCCCCAGCTGTCAGTTC-3′ for *Livin*; 5′-TGTCCCTTCTGTTCTAACAG-3′ and 5′-GCAGGGTTTCTTTATACTGG for *XIAP*; and 5′-CGCGAGAAGATGACCCAGAT-3′ and 5′-GCACTGTGTTGGCGTACAGG-3′ for *GAPDH*. PCR analysis was performed under the following conditions: denaturation at 94 °C for 5 min, followed by 35 cycles of denaturation for 30 s at 94 °C, annealing for 30 s at 55 °C and extension for 60 s at 72 °C. The amplified products were analyzed by 1% agarose gel electrophoresis followed by ethidium bromide staining. *GAPDH* served as a loading control.

3.15. Statistical Analysis

Statistical analysis of the data was performed using SPSS 11.5 software. Each experiment was carried out twice with triplicate measurements for quantitative comparisons, and data are expressed as the mean ± SD values. The Student's *t*-test was used to determine the significance of the differences in multiple comparisons; * $P < 0.05$ was considered statistically significant.

4. Conclusions

Taken together, our findings demonstrate that fucoidan induces apoptosis in SMMC-7721 cells via the ROS-mediated mitochondrial pathway, by increasing ROS production, inducing mitochondrial oxidative damage, MMP depolarization and release of cytochrome c, combined with downregulation of *XIAP* and *Livin* and activation of caspase-3 and caspase-9. *U. pinnatifida* fucoidan might have potential as a candidate marine drug for human hepatocarcinoma.

Acknowledgments

This research was supported by Research Fund from Education Department of Liaoning Province of the People's Republic of China (No. 2009A199), the Science and Technology Department Program of Liaoning Province of China (2011225013).

Conflict of Interest

The authors declare no conflict of interest.

References

1. Bilan, M.I.; Grachev, A.A.; Ustuzhanina, N.E.; Shashkov, A.S.; Nifantiev, N.E.; Usov, A.I. Structure of a fucoidan from the brown seaweed *Fucus evanescens* C.Ag. *Carbohydr. Res.* **2002**, *337*, 719–730.
2. Li, B.; Wei, X.J.; Sun, J.L.; Xu, S.Y. Structural investigation of a fucoidan containing a fucose-free core from the brown seaweed, *Hizikia fusiforme*. *Carbohydr. Res.* **2006**, *341*, 1135–1146.
3. Wijesekara, I.; Pangestuti, R.; Kim, S.K. Biological activities and potential health benefits of sulfated polysaccharides derived from marine alga. *Carbohydr. Polym.* **2011**, *84*, 14–21.
4. Liu, F.; Wang, J.; Chang, A.K.; Liu, B.; Yang, L.L.; Li, Q.M.; Wang, P.S.; Zou, X.Y. Fucoidan extract derived from *Undaria pinnatifida* inhibits angiogenesis by human umbilical vein endothelial cells. *Phytomedicine* **2012**, *19*, 797–803.
5. Ermakova, S.; Sokolova, R.; Kim, S.M.; Um, B.H.; Isakov, V.; Zvyagintseva, T. Fucoidan from brown seaweeds *Sargassum hornery*, *Eclonia cava*, *Costaria costata*: Structural characteristics and anticancer activity. *Appl. Biochem. Biotechnol.* **2011**, *164*, 841–850.
6. Alekseyenko, T.V.; Zhanayeva, S.Y.; Venediktova, A.A.; Zvyagintseva, T.N.; Kuznetsova, T.A.; Besednova, N.N.; Korolenko, T.A. Antitumor and antimetastatic activity of fucoidan, a sulfated polysaccharide isolated from the Okhotsk Sea *Fucus evanescens* brown alga. *Bull. Exp. Biol. Med.* **2007**, *143*, 730–732.
7. Koyanagi, S.; Tanigawa, N.; Nakagawa, H.; Soeda, S.; Shimeno, H. Oversulfation of fucoidan enhances its anti-angiogenic and antitumor activities. *Biochem. Pharmacol.* **2003**, *65*, 173–179.
8. Kim, K.J.; Lee, O.H.; Lee, B.Y. Genotoxicity studies on fucoidan from porophyll of *Undaria pinnatifida*. *Food Chem. Toxicol.* **2010**, *48*, 1101–1104.

9. Parkin, D.M.; Bray, F.; Ferlay, J.; Pisani, P. Global cancer statistics, 2002. *CA Cancer J. Clin.* **2005**, *55*, 74–108.
10. Trevisani, F.; Cantarini, M.C.; Wands, J.R.; Bernardi, M. Recent advances in the natural history of hepatocellular carcinoma. *Carcinogenesis* **2008**, *29*, 1299–1305.
11. Chen, D.; Yao, W.J.; Zhang, X.L.; Han, X.Q.; Qu, X.Y. Effects of Gekko sulfated polysaccharide-protein complex on human hepatoma SMMC-7721 cells: Inhibition of proliferation and migration. *J. Ethnopharmacol.* **2010**, *127*, 702–708.
12. Hu, W.; Kavanagh, J.J. Anticancer therapy targeting the apoptotic pathway. *Lancet Oncol.* **2003**, *4*, 721–729.
13. Wei, M.C.; Lindsten, T.; Mootha, V.K.; Weiler, S.; Gross, A.; Ashiya, M.; Thompson, C.B.; Korsmeyer, S.J. tBID, a membrane-targeted death ligand, oligomerizes BAK to release cytochrome c. *Gene. Dev*. **2000**, *14*, 2060–2071.
14. Szegezdi, E.; Fitzgerald, U.; Samali, A. Caspase-12 and ER-stressmediated apoptosis: The story so far. *Ann. N. Y. Acad. Sci*. **2013**, *1010*, 186–194.
15. LaCasse, E.C.; Baird, S.; Korneluk, R.G.; MacKenzie, A.E. The inhibitors of apoptosis (IAPs) and their emerging role in cancer. *Oncogene* **1998**, *17*, 3247–3259.
16. Rohayem, J.; Diestelkoetter, P.; Weigle, B.; Oehmichen, A.; Schmitz, M.; Mehlhorn, J.; Conrad, K.; Rieber, E.P. Antibody response to the tumor-associated inhibitor of apoptosis protein survivin in cancer patients. *Cancer Res*. **2000**, *60*, 1815–1817.
17. Martin, K.R.; Barrett, J.C. Reactive oxygen species as double-edged swords in cellular processes: Low-dose cell signaling *versus* high-dose toxicity. *Hum. Exp. Toxicol.* **2002**, *21*, 71–75.
18. Scherz-Shouval, R.; Elazar, Z. Regulation of autophagy by ROS: Physiology and pathology. *Trends Biochem. Sci.* **2011**, *36*, 30–38.
19. Acharya, A.; Das, I.; Chandhok, D.; Saha, T. Redox regulation in cancer: A double-edged sword with therapeutic potential. *Oxid. Med. Cell. Longev.* **2010**, *3*, 23–34.
20. Simon, H.U.; Haj-Yehia, A.; Levi-Schaffer, F. Role of reactive oxygen species (ROS) in apoptosis induction. *Apoptosis* **2000**, *5*, 415–418.
21. Schumacker, P.T. Reactive oxygen species in cancer cells: Live by the sword, die by the sword. *Cancer Cell* **2006**, *10*, 175–176.
22. Pelicano, H.; Carney, D.; Huang, P. ROS stress in cancer cells and therapeutic implications. *Drug Resist. Update* **2004**, *7*, 97–110.
23. Ye, J.; Li, Y.P.; Teruya, K.; Katakura, Y.; Ichikawa, A. Enzyme-digested fucoidan extracts derived from seaweed Mozuku of *Cladosiphon novae-caledoniae* kylin inhibit invasion and angiogenesis of tumor cells. *Cytotechnology* **2005**, *47*, 117–126.
24. Aisa, Y.; Miyakawa, Y.; Nakazato, T.; Shibata, H.; Saito, K.; Ikeda, Y.; Kizaki, M. Fucoidan induces apoptosis of human HS-sultan cells accompanied by activation of caspase-3 and down-regulation of ERK pathways. *Am. J. Hematol.* **2005**, *78*, 7–14.
25. Hyun, J.H.; Kim, S.C.; Kang, J.I.; Kim, M.K.; Boo, H.J.; Kwon, J.M.; Koh, Y.S.; Hyun, J.W.; Park, D.B.; Yoo, E.S.; *et al.* Apoptosis inducing activity of fucoidan in HCT-15 colon carcinoma cells. *Biol. Pharm. Bull.* **2009**, *32*, 1760–1764.

26. Miyamoto, Y.Y.; Yamasaki, M.; Tachibana, H.; Yamada, K. Fucoidan induces apoptosis through activation of caspase-8 on human breast cancer MCF-7 cells. *J. Agric. Food Chem.* **2009**, *57*, 8677–8682.
27. Frankfurt, O.S.; Krishan, A. Apoptosis-based drug screening and detection of selective toxicity to cancer cells. *Anticancer Drugs* **2003**, *14*, 555–561.
28. Reed, J.C. Apoptosis-regulating proteins as targets for drug discovery. *Trends Mol. Med.* **2001**, *7*, 314–319.
29. Thibaud, T.R.; Oscar, T.; Bruno, A.; Laurent, M.D.; Stephen, M. Regulation of Bax mitochondrial localization by Bcl-2 and Bcl-xl: Keep your friends close but your enemies closer. *Int. J. Biochem. Cell Biol.* **2013**, *45*, 64–67.
30. Tsujimoto, Y.; Shimizu, S. Bcl-2 family: Life-or-death switch. *FEBS Lett*. **2000**, *466*, 6–10.
31. Yamaguchi, H.; Bhalla, K.; Wang, H.G. Bax plays a pivotal role in thapsigargin-induced apoptosis of human colon cancer HCT116 cells by controlling Smac/Diablo and Omi/HtrA2 release from mitochondria. *Cancer Res*. **2003**, *63*, 1483–1489.
32. Murphy, E.; Imahashi, K.I.; Steenbergen, C. Bcl-2 regulation of mitochondrial energetics. *Trends Cardiovasc. Med.* **2005**, *15*, 283–290.
33. Danial, N.N.; Korsmeyer, S.J. Cell death: Critical control points. *Cell* **2004**, *116*, 205–219.
34. Budihardjo, I.; Oliver, H.; Lutter, M.; Luo, X.; Wang, X. Biochemical pathways of caspase activation during apoptosis. *Annu. Rev. Cell Dev. Biol.* **1999**, *15*, 269–290.
35. Janicke, R.U.; Sprengart, M.L.; Wati, M.R.; Porter, A.G. Caspase-3 is required for DNA fragmentation and morphological changes associated with apoptosis. *J. Biol. Chem.* **1998**, *273*, 9357–9360.
36. Bernardi, P.; Vassanelli, S.; Veronese, P.; Colonna, R.; Szabo, I. Modulation of the mitochondrial cyclosporin A-sensitive permeability transition pore by the proton electrochemical gradient. *J. Biol. Chem.* **1998**, *267*, 8834–8839.
37. Pradelli, L.A.; Beneteau, M.; Ricci, J.E. Mitochondrial control of caspase-dependent and independent cell death. *Cell. Mol. Life Sci.* **2010**, *67*, 1589–1597.
38. Eckelman, B.P.; Salvesen, G.S.; Scott, F.L. Human inhibitor of apoptosis proteins: Why XIAP is the black sheep of the family. *EMBO Rep.* **2006**, *7*, 988.
39. Kasof, G.M.; Gomes, B.C. Livin, a novel inhibitor of apoptosis protein family member. *J. Biol. Chem.* **2001**, *276*, 3238–3246.
40. Quan, Z.W.; Gu, J.; Dong, P.; Lu, J.H.; Wu, X.S.; Wu, W.G.; Fei, X.Z.; Li, S.G.; Wang, Y.; Wang, J.W. Reactive oxygen species-mediated endoplasmic reticulum stress and mitochondrial dysfunction contribute to cirsimaritin-induced apoptosis in human gallbladder carcinoma GBC-SD cells. *Cancer Lett.* **2010**, *295*, 252–259.
41. Fleury, C.; Mignotte, B.; Vayssière, J.L. Mitochondrial reactive oxygen species in cell death signaling. *Biochimie* **2002**, *84*, 131–141.
42. Higuchi, Y. Glutathione depletion-induced chromosomal DNA fragmentation associated with apoptosis and necrosis. *J. Cell. Mol. Med.* **2004**, *8*, 455–464.

43. Yuan, L.Y.; Kaplowitz, N. Glutathione in liver diseases and hepatotoxicity. *Mol. Aspects Med.* **2009**, *30*, 29–41.
44. Zhang, Z.Y.; Teruya, K.; Eto, H.; Shirahata, S. Fucoidan extract induces apoptosis in MCF-7 cells via a mechanism involving the ROS-dependent JNK Activation and mitochondria-mediated pathways. *PLoS One* **2011**, *6*, e27441.

Cytotoxic Effects of Fucoidan Nanoparticles against Osteosarcoma

Ryuichiro Kimura, Takayoshi Rokkaku, Shinji Takeda, Masachika Senba and Naoki Mori

Abstract: In this study, we analyzed the size-dependent bioactivities of fucoidan by comparing the cytotoxic effects of native fucoidan and fucoidan lipid nanoparticles on osteosarcoma *in vitro* and *in vivo*. *In vitro* experiments indicated that nanoparticle fucoidan induced apoptosis of an osteosarcoma cell line more efficiently than native fucoidan. The more potent effects of nanoparticle fucoidan, relative to native fucoidan, were confirmed *in vivo* using a xenograft osteosarcoma model. Caco-2 cell transport studies showed that permeation of nanoparticle fucoidan was higher than native fucoidan. The higher bioactivity and superior bioavailability of nanoparticle fucoidan could potentially be utilized to develop novel therapies for osteosarcoma.

Reprinted from *Mar. Drugs*. Cite as: Kimura, R.; Rokkaku, T.; Takeda, S.; Senba, M.; Mori, N. Cytotoxic Effects of Fucoidan Nanoparticles against Osteosarcoma. *Mar. Drugs* **2013**, *11*, 4267-4278.

1. Introduction

Fucoidan, commonly found in brown seaweeds, consists mainly of fucose and sulfate with small amounts of galactose, xylose, mannose and uronic acid [1,2]. Fucoidan has steadily attracted attention in the last two decades and is currently known to have anticoagulant, antiviral, anti-inflammatory and anticancer activities [1,2]. Our laboratory has focused on the evaluation of fucoidan for the treatment of malignancies and/or viral infectious diseases [3–5]. The main mechanism of the anticancer activities of fucoidan is considered to be the regulation of molecules related to apoptosis and cell cycle [6]. One main feature of fucoidan is its high molecular weight. It cannot be degraded by human digestive enzymes [7]. Several groups have attempted to develop a method to produce a low molecular weight fucoidan (LMWF) [1]. These attempts are based on the *in vitro* finding that the anticancer activity of fucoidan in lung cancer cell line is significantly improved after lowering its molecular weight [8]. Paradoxically, high molecular weight fucoidan (HMWF) promotes a greater increase in the proportion of murine cytotoxic T cells than middle or LMWF in mice fed experimental diet [9]. Nevertheless, a recent study using a colon cancer-bearing mouse model demonstrated that oral administration of LMWF increased survival time, similar to HMWF, compared with the control [10]. Thus, there is no definite agreement on the effects of molecular weight of fucoidan on its anticancer properties.

The oral route is the conventional mean of drug administration, especially in patients requiring long-term treatment. The nanoparticle approach has been recently explored for natural products and chemotherapeutic agents [11]. Biocompatible nanoparticles have been developed, which are essentially inert systemic carriers used to deliver therapeutic compounds to target cells and tissues [11]. Based on their peculiar size, nanoparticle drugs easily penetrate the cell and cell organelles; and,

because of their large surface area and enhanced bioavailability, tend to be more active than their microstructure counterparts.

Osteosarcoma is the most common primary bone tumor. The peak incidence of this aggressive tumor coincides with the period of rapid skeletal growth, thus affecting mostly children and adolescents [12]. The recent introduction of neoadjuvant and adjuvant chemotherapy combined with surgery has increased the 5-year survival rate for localized disease by greater than 60% compared with surgery alone [13,14]. However, patients with advanced diseases with metastasis continue to have poor prognosis with 5-year survival rates below 30% [14]. Moreover, there are currently no effective therapeutic options for patients who relapse following administration of chemotherapeutic agents or those who suffer toxicities from chemotherapy. Therefore, the discovery and development of novel chemotherapeutic agents that can improve the survival rates of patients with osteosarcoma and/or lower the occurrence of the toxic side effects of currently approved agents is of utmost importance.

Although several reports have described the potent anti-neoplastic activity of fucoidan against several diverse types of malignancies, size-dependent bioactivities have attracted attention [2,8–10]. In the present study, fucoidan extracted from *Cladosiphon okamuranus* was encapsulated in nanoparticles using liposomes as nanocarriers, and its anticancer effects were assessed in a cell culture system. Furthermore, we examined the effects of oral administration of fucoidan on tumor growth and lung metastasis using an ostersarcoma tumor-bearing mouse model.

2. Results and Discussion

2.1. Cytotoxic Effects of Fucoidan on Osteosarcoma Cells

The freeze fracture electron micrography (FFEM) was undertaken to determine the structure of the obtained SLP-PC70 liposomes. Figure 1 shows a typical FFEM image of the SLP-PC70 liposomes, confirming that they are small unilamellar vesicles. The particle size of the liposomes was about 100 nm.

In the initial set of experiments, the cytotoxic effect of different concentrations of nanoparticle fucoidan on a human osteosarcoma cell line 143B was evaluated using water-soluble tetrazolium (WST)-8 assays. Nanoparticle fucoidan reduced the viability of these cells in dose- and time-dependent manners (Figure 2A). The maximum decline in cell viability of 80% after 72 h culture was achieved with nanoparticle fucoidan concentration of 2 mg/mL, beyond which the effect plateaued. Thus, in all subsequent studies, we used nanoparticle fucoidan at concentrations of 1 and 2 mg/mL.

Figure 1. Freeze fracture electron micrograph of SLP-PC70 liposomes prepared by the mechanochemical method.

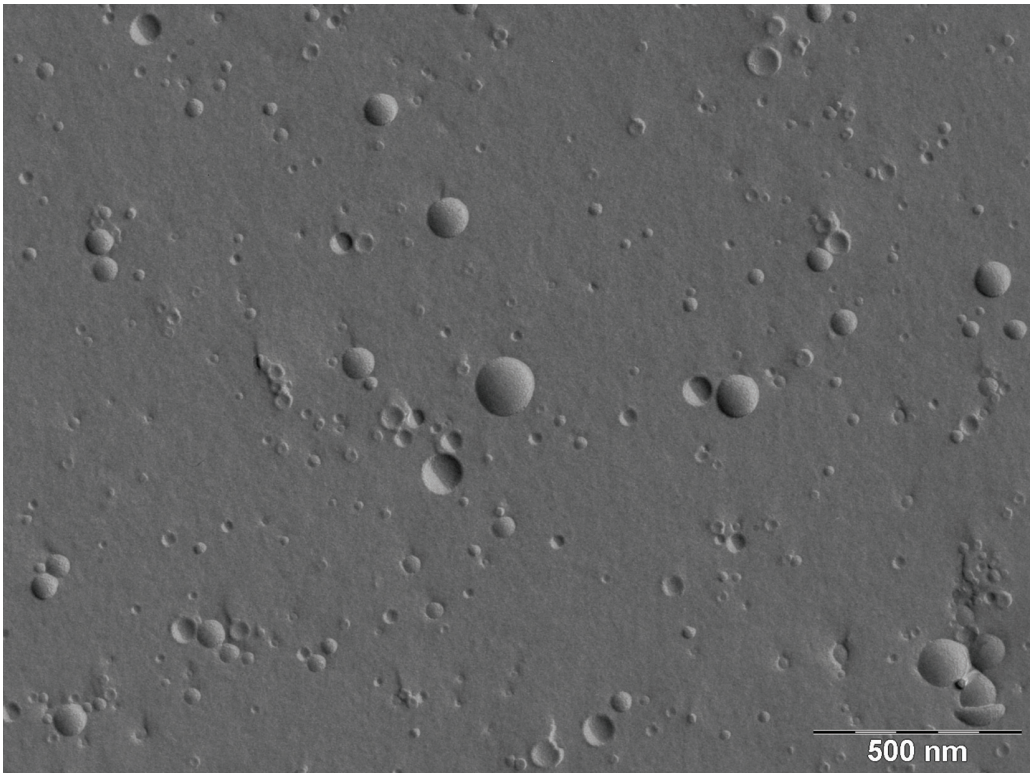

Apo2.7 specifically detects the 38 kDa mitochondrial membrane antigen 7A6 expressed on the mitochondrial outer membrane during apoptosis [15]. Nanoparticle fucoidan induced apoptosis in 143B cells, as shown by Apo2.7 staining, in dose-and time-dependent manners (Figure 2B). After incubation for 72 h, 35% and 73% of cells treated with 1 or 2 mg/mL nanoparticle fucoidan stained positively for Apo2.7, respectively, compared with only 15% of cells treated with the medium alone (Figure 2B).

Next, we investigated the effect of HMWF on the induction of apoptosis. The apoptosis-inducing activity of native fucoidan (molecular weight: 80 kDa) was lower (25%) than that of nanoparticle fucoidan (94%) when both were used at 2 mg/mL (Figure 2C). These results suggest that nanoparticle fucoidan is more active than native fucoidan in the induction of apoptosis of cultured osteosarcoma cells.

Caspases are a family of cysteine acid proteases that play an integral role in the cascade that leads to apoptosis [16]. Pre-incubation of 143B cells with the pan-caspase inhibitor Z-VAD-FMK 60 min before the addition of nanoparticle fucoidan significantly inhibited the decrease in cell viability (Figure 2D). These results indicate that nanoparticle fucoidan induces apoptosis through the activation of caspase pathway.

Figure 2. Fucoidan induces apoptosis of 143B cells, (**A**) Dose- and time-dependent reduction of cell viability in 143B cells following the addition of nanoparticle fucoidan to the cell cultures. 143B cells were treated with increasing concentrations of nanoparticle fucoidan. Twenty-four, 48 and 72 h later, cell viability was analyzed using the WST-8 assay. Data represent percentage of cell survival compared with the control and are expressed as mean ± SD (n = 3); (**B**) Flow cytometric analysis using Apo2.7 staining on nanoparticle fucoidan-treated and untreated cells. The analysis confirmed nanoparticle fucoidan-induced decline in 143B cell viability was the result of apoptosis; (**C**) Nanoparticle fucoidan is more potent than native fucoidan in inducing apoptosis. 143B cells were incubated with nanoparticle fucoidan or native fucoidan (1 and 2 mg/mL) for 72 h. Cells were stained with Apo2.7 and analyzed by flow cytometry. The data shown here are from a representative experiment repeated 3 times with similar results. Ab, antibody; Nano-Fuc, nanoparticle fucoidan; Native-Fuc, native fucoidan; (**D**) Effect of Z-VAD-FMK, a pan-caspase inhibitor, on nanoparticle fucoidan-induced apoptosis. 143B cells were pre-treated for 1 h with 20 μM of Z-VAD-FMK before the addition of nanoparticle fucoidan. Cell viability was analyzed 72 h later using the water-soluble tetrazolium (WST)-8 assay. Data represent the percentage of cell survival compared with the control and are expressed as mean ± SD (n = 3).

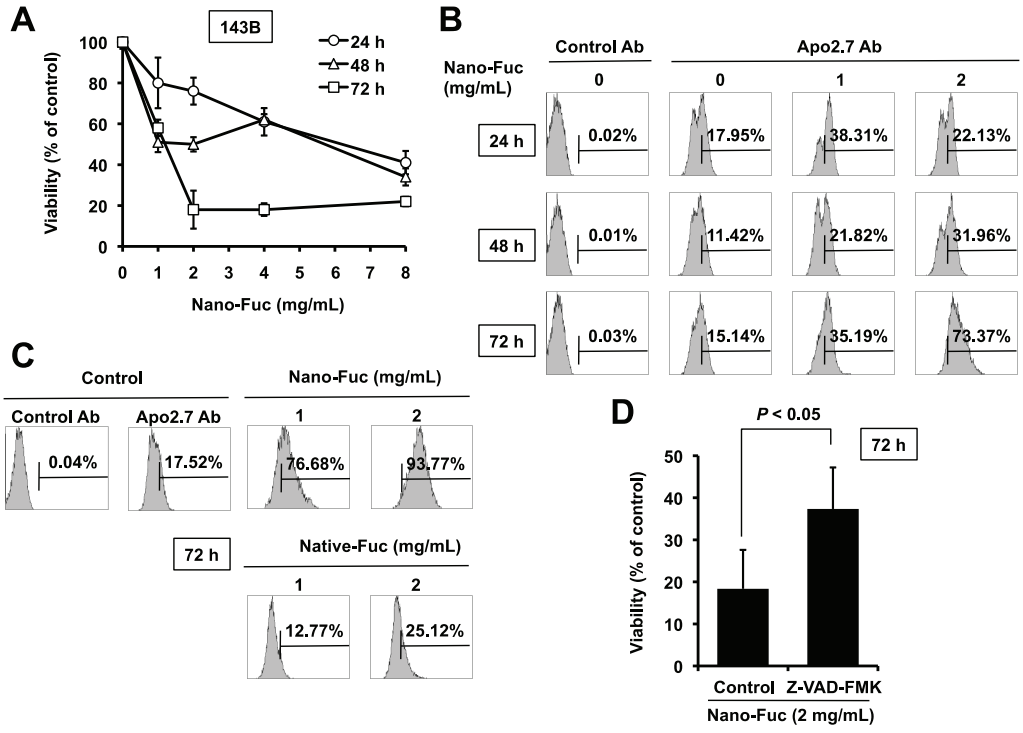

2.2. Effects of Fucoidan on Tumorigenesis of Osteosarcoma Cells in Mice

To examine the potential use of fucoidan in the treatment of osteosarcoma, we tested it's effect on tumor growth *in vivo*. After inoculation of murine osteosarcoma LM8 tumor cells in the back of C3H mice, the animals were treated with oral 100 mg/kg/day nanoparticle fucoidan or native fucoidan. Mice of the control group were treated with water (vehicle) only. Treatment with native fucoidan ($P < 0.05$) and nanoparticle fucoidan ($P < 0.01$) resulted in significant reduction in tumor volume in the LM8 xenografted mice, relative to the control (Figure 3A,D). In the next set of experiments, we demonstrated that the anti-sarcoma effect was not due to significant changes in lecithin and dextrin used for liposome preparation (Figure 3A). Relative to the control, treatment with native fucoidan and nanoparticle fucoidan resulted in reduction of tumor tissue weight, though the effect of the latter was significant ($P < 0.05$) compared with marginal significance for the former ($P = 0.065$) (Figure 3B). Importantly, both preparations did not induce significant reduction in body weight throughout the experimental period, compared with the control (Figure 3C). With regard to side effects of the drug, no gross abnormalities were noted in mice treated at the selected dose.

2.3. Fucoidan Induces Apoptosis in Osteosarcoma Xenograft Model

Hematoxylin and eosin (H&E) staining and terminal deoxynucleotidyl transferase-mediated dUTP nick end labeling (TUNEL) assay were performed to evaluate the cell death mechanism *in vivo*. Figure 4A,B shows dark blue hematoxylin-stained nuclei and pink eosin-stained cytoplasm, whereas native fucoidan- and nanoparticle fucoidan-treated tumors (Figure 4C,D, H&E) show large numbers of apoptotic cells with nuclear condensation and fragmentation. Correspondingly, the density of viable tumor cells was substantially decreased. TUNEL staining confirmed more extensive apoptosis in the native fucoidan- and nanoparticle fucoidan-treated tumors compared with the control with LM8-derived tumors (Figure 4C,D, TUNEL).

2.4. Fucoidan Inhibits Metastasis of Mouse Osteosarcoma Cells to the Lung

In this model, subcutaneous inoculation of LM8 cells in the back of C3H mice resulted in spontaneous metastasis to the lung in addition to the formation of local primary tumors. The antimetastatic activity of fucoidan was also found when spontaneous metastasis of LM8 cells to the lung was compared in tumor-bearing, fucoidan-treated mice and in water-treated control mice. A four-point scale was used for quantitative scoring of the invasion of LM8 cells into the lung, where 0 (absent or negative) indicates no invasion, and 1+, 2+ and 3+ indicate small, moderate and extensive invasion, respectively. The anatomic levels of metastatic nodules on the lung surface correlated with microscopic evaluation (Figure 4E,F). All nine control mice inoculated with LM8 cells developed spontaneous lung metastases with a mean score of 1.89 ± 0.78. In contrast, visible gross lung nodules were not found in 3/8 mice treated with native fucoidan and nanoparticle fucoidan. The mean scores of mice treated with native fucoidan and nanoparticle fucoidan were 0.88 ± 0.83 and 1.13 ± 1.13, respectively. Thus, oral administration of native fucoidan and nanoparticle fucoidan decreased the score compared with that observed in the control group, and there was a significant difference between the native fucoidan group and the control group

($P < 0.05$). Five of the six mice treated with lecithin and dextrin developed spontaneous metastasis to the lung with a mean score of 1.50 ± 1.05. Collectively, treatment with native fucoidan and nanoparticle fucoidan suppressed pulmonary metastases.

Figure 3. Effects of fucoidan on tumor growth in mice xenografted with LM8 osteosarcoma cells. Water (n = 9), lecithin and dextrin (Lec + Dex) (n = 6), native fucoidan (Native-Fuc) (n = 8) or nanoparticle fucoidan (Nano-Fuc) (n = 8) were administrated orally every day for four weeks, (**A**) Effects of fucoidan on tumor volume; (**B**) Effects of fucoidan on tumor tissue weight; (**C**) Effects of fucoidan on body weight. Data are mean ± SD (n = 3); (**D**) Photographs of nanoparticle fucoidan-treated and untreated osteosarcoma-bearing mice four weeks after subcutaneous inoculation with LM8 (top). Tumors were excised on day 28. The photographs show representative tumor of an untreated mouse (bottom left) and that of nanoparticle fucoidan-treated mouse (bottom right).

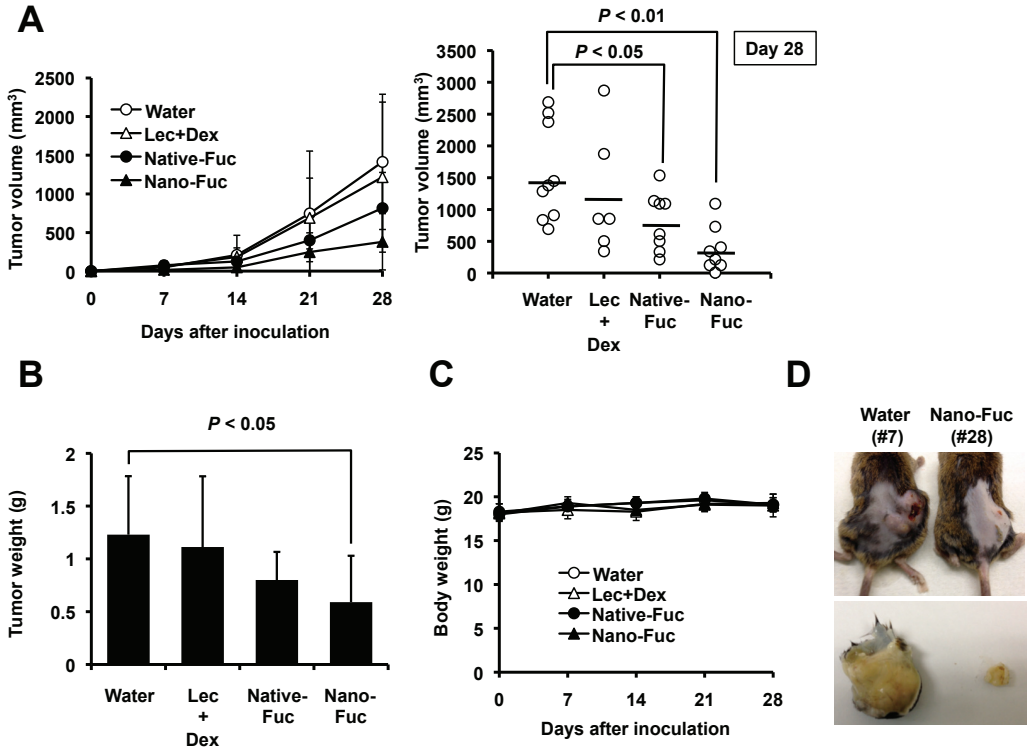

Figure 4. Fucoidan induces apoptosis in local primary tumors and inhibits lung metastases in mice, (**A**–**D**) hematoxylin and eosin (H&E) staining and *in situ* terminal deoxynucleotidyl transferase-mediated dUTP nick end labeling (TUNEL) assays of LM8-derived tumor tissues. Tumors obtained from mice treated with water (**A**), lecithin and dextrin (Lec + Dex) (**B**), native fucoidan (Native-Fuc) (**C**) or nanoparticle fucoidan (Nano-Fuc) (**D**) daily were harvested on day 28 and subjected to analysis. Magnification, ×400; (**E**) Microphotographs of the lungs in treated mice. A four-point scale was used for quantitative scoring of invasion of LM8 cells into the lung, where 0 (absent or negative) indicates no invasion, and 1+, 2+ and 3+ indicate small, moderate and extensive invasion, respectively. Magnification, ×25; (**F**) Representative pictures showing gross appearance of the lungs of mice treated (right) or untreated (left) with nanoparticle fucoidan examined on day 28.

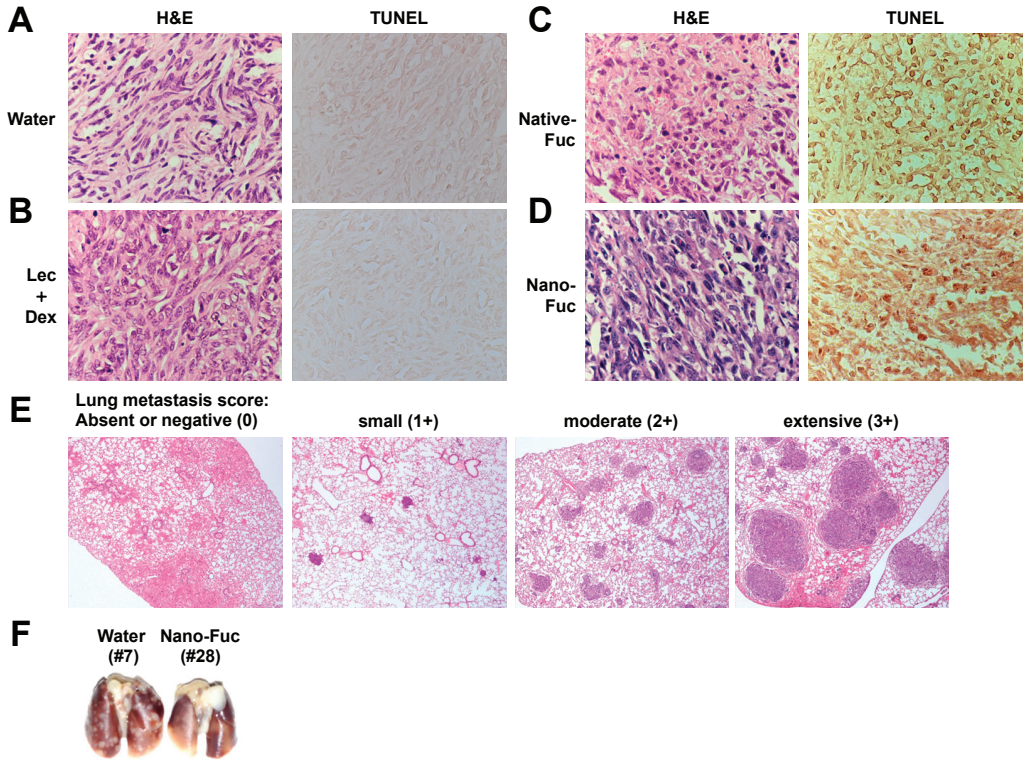

2.5. Cell Permeation of Fucoidan

Finally, Caco-2 cell transport studies were performed on native fucoidan and nanoparticle fucoidan. As shown in Table 1, the amount of permeated nanoparticle fucoidan and permeation rate of nanoparticle fucoidan were significantly higher than native fucoidan.

Table 1. Permeability of Caco-2 cell monolayers to fucoidan.

Sample	Amount of Permeated Fucoidan (μg/cm^2/h)	Permeation Rate of Fucoidan (%)
Native fucoidan	0.034 ± 0.03	0.001 ± 0.001
Nanoparticle fucoidan	5.298 ± 0.341	0.229 ± 0.015

3. Experimental Section

3.1. Cell Lines and Reagents

Human osteosarcoma cell line, 143B, and mouse osteosarcoma cell line, LM8, were maintained in RPMI 1640 and Eagle's Minimal Essential Medium supplemented with 10% heat inactivated fetal bovine serum, penicillin (50 U/mL) and streptomycin (50 μg/mL) in a humidified incubator, respectively. The human colon adenocarcinoma cell line, Caco-2, was purchased from Cell Bank, RIKEN BioResource Center (Tsukuba, Japan). For cell culture, α-Minimum Essential Medium was supplemented with 1% non-essential amino acids, 20% heat inactivated fetal bovine serum, penicillin (100 U/mL) and streptomycin (100 μg/mL). A caspase inhibitor, Z-VAD-FMK, was purchased from Promega (Madison, WI, USA).

3.2. Preparation of Native Fucoidan from Seaweed

The brown seaweed *Cladosiphon okamuranus* Tokida cultivated in Okinawa, Japan, was suspended in water, 1.13% (w/vol) citric acid was added to the solution, and then heated at 90 °C for 40 min. The suspension was neutralized with NaOH solution, then centrifuged at 3500 rpm by decantation centrifugal separator. The supernatant was collected, filtered using Cohlo filter and concentrated by ultrafiltration (molecular weight cutoff 6000). The extracts were dried by spraydrier and the molecular weight of this native fucoidan was 80 kDa. Soybean lecithin, SLP-PC70 (Tsuji Oil Mill Co., Matsusaka, Japan), and dextrin (Pinedex, Matsutani Chemical Industry Co., Itami, Japan) were added as control for nanoparticle fucoidan, and this mixture was used as native fucoidan. Native fucoidan was dissolved in RPMI 1640 before *in vitro* experiments or distilled water before *in vivo* experiments.

3.3. Preparation of Liposome Encapsulating Fucoidan

Native fucoidan was hydrolyzed to produce LMWF (molecular weight 2–10 kDa). The hydrolysis process was carried out by dissolving native fucoidan into 2.0% (w/vol) citric acid mixture at 100 °C for 24 h. After neutralization with NaOH solution, the suspension was centrifuged at 3500 rpm by decantation centrifugal separator. The supernatant was collected and filtered. The liposome fraction was prepared by the mechanochemical method [17] using the following procedure. The hydrolyzed fucoidan extract and soybean lecithin, SLP-PC70 solution, were mixed well. These solutions were dispersed by a homogenizer (TK HOMO MIXER MARK II, PRIMIX, Osaka, Japan) at a revolving rate of 8000 rpm for 10 min. The resulting solution was then treated once with the microfluidizer (M110-E/H, MIZUHO Industrial Co., Osaka, Japan). The

operation was carried out with an inlet pressure of 100 MPa. Dextrin was then added and mixed. The liposome encapsulating LMWF was dried by spraydrier for subsequent use. FFEM was used to determine the structure of lecithin (SLP-PC70) liposomes, as described previously [17].

3.4. Assessment of Cell Viability and Apoptosis

Cell viability was determined by color reaction with WST-8 (Wako Pure Chemical Industries, Osaka, Japan). Basically, mitochondrial dehydrogenase cleavage of WST-8 to formazan dye provided a measure of cell viability. Briefly, 1×10^5 cells/mL were incubated in triplicate in a 96-well microculture plate in the presence of different concentrations of fucoidan for 24–72 h. Subsequently, WST-8 was added to each well. After 4 h of additional incubation, absorption values at 450 nm were determined with an automatic microplate reader. Values were normalized to untreated control samples. Apoptotic cells were detected by staining with phycoerythrin-conjugated APO2.7 antibody (Beckman Coulter, Marseille, France), which specifically detects the 38 kDa mitochondrial membrane antigen 7A6 [15], followed by analysis by flow cytometry.

3.5. Preparation of Sarcoma Animal Model

LM8 cells (5×10^6 cells/mouse) in 0.1 mL phosphate buffered saline were injected subcutaneously into the back of five-week-old female C3H mice obtained from Japan SLC (Hamamatsu, Japan) on day 0. Treatment was initiated one day after cell injection. Groups of 6–9 mice were used to generate LM8 tumors, and each group was treated with water, lecithin and dextrin, native fucoidan or nanoparticle fucoidan. For the latter, lecithin and dextrin were used as a control. Lecithin, dextrin, native fucoidan and nanoparticle fucoidan were dissolved in distilled water, and 100 mg/kg body weight of fucoidan or vehicle only was administered by oral gavage every day for 28 days. The mice were weighed once a week and tumor diameters were measured weekly. The mice were monitored daily for evidence of morbidity including anorexia, dehydration, dyspnea, decreased activity and grooming behavior. On day 28, all mice were euthanized and autopsied to confirm metastatic lung disease. Lung infiltration by LM8 cells was evaluated by H&E staining. Primary tumors were dissected out and weighed, then processed for staining with H&E and TUNEL using a commercial kit (Roche Applied Science, Mannheim, Germany). This experiment was performed according to the guidelines for Animal Experimentation of the University of the Ryukyus and approved by the Animal Care and Use Committee of the same University.

3.6. Permeation across Caco-2 Monolayers

Caco-2 cells were seeded at a density of 30,000 cells onto 24-well Transwell plates with an insert area of 0.33 cm^2 and a pore size of the polycarbonate membrane of 0.4 μm. The culture medium was changed every 48 h for the first 10 days and every 24 h thereafter, and cell monolayers were used between 19 and 20 days post-seeding. The transepithelial electrical resistance of cultured cells on Transwell inserts was measured before and after each permeation experiment with a Millicell-Electorical Resistance System ohmmeter (Millipore, Bedford, MA,

USA). Physiologically and morphologically well-developed confluent Caco-2 monolayers (at least 19-day-old) with transepithelial electrical resistance values typically above 250 Ωcm^2 were used in the experiments. The apical side of Caco-2 cell monolayers cultured in 24-well Transwell inserts was washed twice with phosphate-buffered saline. Fucoidan was added to the apical compartment with respect to the cell monolayer which was then incubated at 37 °C for 2 h. Permeation of fucoidan across the cell monolayer was measured by sampling the solutions in both compartments after 2 h of incubation with a sample. The obtained samples were evaporated to dryness and the resulting residue was dissolved in 10 μL of distilled water. Then, 10 μL of 8 M trifluoroacetic acid solution was added to the sample solution, and the solution was incubated at 100 °C for 3 h. After cooling to room temperature, the reaction mixture was evaporated to dryness. The resulting residue was dissolved in 40 μL of 2-propanol and again evaporated to dryness. Next, 10 μL of distilled water and 40 μL of the 4-aminobenzoic acid ethyl ester reagent solution were added to the residue, and the mixture was incubated at 80 °C for 1 h. Afterwards, the mixture was cooled to room temperature, and 0.2 mL of distilled water and an equal volume of chloroform were added. After vigorous vortexing, the mixture was centrifuged and the upper aqueous layer was subjected to HPLC LC-2000Plus (JASCO, Tokyo, Japan) to determine fucose concentration in the samples.

3.7. Statistical Analysis

All values are expressed as mean ± SD. Differences between groups were analyzed for statistical significance by the unpaired Student's *t*-test. A confidence level of $P < 0.05$ was chosen as indication of statistical difference.

4. Conclusions

We have recently prepared liposome-encapsulated fucoidan for nano-formulation. In this study, we examined the anti-neoplastic activity of nanoparticle fucoidan against osteosarcoma cell lines. Our examination using viability and apoptosis assays demonstrated that nanoparticle fucoidan induced apoptosis of 143B cells and that this action was mediated through the caspase pathway. Nanoparticle fucoidan was more active than native fucoidan in inducing apoptosis *in vitro*. Furthermore, both nanoparticle fucoidan and native fucoidan demonstrated significant inhibition of tumor growth and spontaneous metastases in the lung from LM8 mice tumor xenografts. The tumor volume and weight were decreased in nanoparticle fucoidan group compared with those observed in native fucoidan group. However, the lung metastasis score was decreased in native fucoidan compared with that observed in nanoparticle fucoidan. One limitation of this study was that we did not use non-encapsulated LMWF as a control to study the effect of nanoparticles on cells and in mice. In other words, the present study did not examine the effects of molecular weight condition on anti-osteosarcoma activity of fucoidan. The sensitive sandwich ELISA method for the measurement of serum fucoidan was recently developed [18], although detection of fucoidan in the serum has been thought to be impossible. The measurement of fucoidan in blood, tissues and organs may be useful to evaluate its beneficial effects *in vivo*. The findings that fucoidan hindered osteosarcoma LM8 tumor growth, and reduced tumor mass and lung metastases *in vivo* suggest a

potential therapeutic application. Furthermore, the results demonstrate that encapsulation of fucoidan into nanoparticles enhances its anti-osteosarcoma effects, at least in part by increased permeability.

Conflict of Interest

The authors declare no conflict of interest.

References

1. Morya, V.K.; Kim, J.; Kim, E.-K. Algal fucoidan: Structural and size-dependent bioactivities and their perspectives. *Appl. Microbiol. Biotechnol.* **2012**, *93*, 71–82.
2. Fitton, J.H. Therapies from fucoidan; Multifunctional marine polymers. *Mar. Drugs* **2011**, *9*, 1731–1760.
3. Araya, N.; Takahashi, K.; Sato, T.; Nakamura, T.; Sawa, C.; Hasegawa, D.; Ando, H.; Aratani, S.; Yagishita, N.; Fujii, R.; *et al.* Fucoidan therapy decreases the proviral load in patients with human T-lymphotropic virus type-1-associated neurological disease. *Antivir. Ther.* **2011**, *16*, 89–98.
4. Takeda, K.; Tomimori, K.; Kimura, R.; Ishikawa, C.; Nowling, T.K.; Mori, N. Anti-tumor activity of fucoidan is mediated by nitric oxide released from macrophages. *Int. J. Oncol.* **2012**, *40*, 251–260.
5. Mori, N.; Nakasone, K.; Tomimori, K.; Ishikawa, C. Beneficial effects of fucoidan in patients with chronic hepatitis C virus infection. *World J. Gastroenterol.* **2012**, *18*, 2225–2230.
6. Aisa, Y.; Miyakawa, Y.; Nakazato, T.; Shibata, H.; Saito, K.; Ikeda, Y.; Kizaki, M. Fucoidan induces apoptosis of human HS-sultan cells accompanied by activation of caspase-3 and down-regulation of ERK pathways. *Am. J. Hematol.* **2005**, *78*, 7–14.
7. Salyers, A.A.; Vercellotti, J.R.; West, S.E.; Wilkins, T.D. Fermentation of mucin and plant polysaccharides by strains of Bacteroides from the human colon. *Appl. Environ. Microbiol.* **1977**, *33*, 319–322.
8. Yang, C.; Chung, D.; Shin, I.-S.; Lee, H.; Kim, J.; Lee, Y.; You, S. Effects of molecular weight and hydrolysis conditions on anticancer activity of fucoidans from sporophyll of *Undaria pinnatifida*. *Int. J. Biol. Macromol.* **2008**, *43*, 433–437.
9. Shimizu, J.; Wada-Funada, U.; Mano, H.; Matahira, Y.; Kawaguchi, M.; Wada, M. Proportion of murine cytotoxic T cells is increased by high molecular-weight fucoidan extracted from *Okinawa mozuku* (*Cladosiphon okamuranus*). *J. Health Sci.* **2005**, *51*, 394–397.
10. Azuma, K.; Ishihara, T.; Nakamoto, H.; Amaha, T.; Osaki, T.; Tsuka, T.; Imagawa, T.; Minami, S.; Takashima, O.; Ifuku, S.; *et al.* Effects of oral administration of fucoidan extracted from *Cladosiphon okamuranus* on tumor growth and survival time in a tumor-bearing mouse model. *Mar. Drugs* **2012**, *10*, 2337–2348.
11. Cho, K.; Wang, X.; Nie, S.; Chen, Z.G.; Shin, D.M. Therapeutic nanoparticles for drug delivery in cancer. *Clin. Cancer Res.* **2008**, *14*, 1310–1316.

12. Savage, S.; Mirabello, L. Using epidemiology and genomics to understand osteosarcoma etiology. *Sarcoma* **2011**, *2011*, 548151.
13. Anninga, J.K.; Gelderblom, H.; Fiocco, M.; Kroep, J.R.; Taminiau, A.H.M.; Hogendoorn, P.C.W.; Egeler, R.M. Chemotherapeutic adjuvant treatment for osteosarcoma: Where do we stand? *Eur. J. Cancer* **2011**, *47*, 2431–2445.
14. Longhi, A.; Errani, C.; De Paolis, M.; Mercuri, M.; Bacci, G. Primary bone osteosarcoma in the pediatric age: State of the art. *Cancer Treat. Rev.* **2006**, *32*, 423–436.
15. Zhang, C.; Ao, Z.; Seth, A.; Schlossman, S.F. A mitochondrial membrane protein defined by a novel monoclonal antibody is preferentially detected in apoptotic cells. *J. Immunol.* **1996**, *157*, 3980–3987.
16. Konopleva, M.; Zhao, S.; Xie, Z.; Segall, H.; Younes, A.; Claxton, D.F.; Estrov, Z.; Kornblau, S.M.; Andreeff, M. Apoptosis. Molecules and mechanisms. *Adv. Exp. Med. Biol.* **1999**, *457*, 217–236.
17. Takahashi, M.; Inafuku, K.; Miyagi, T.; Oku, H.; Wada, K.; Imura, T.; Kitamoto, D. Efficient preparation of liposomes encapsulating food materials using lecithins by a mechanochemical method. *J. Oleo Sci.* **2007**, *56*, 35–42.
18. Tokita, Y.; Nakajima, K.; Mochida, H.; Iha, M.; Nagamine, T. Development of a fucoidan-specific antibody and measurement of fucoidan in serum and urine by sandwich ELISA. *Biosci. Biotechnol. Biochem.* **2010**, *74*, 350–357.

APS8, a Polymeric Alkylpyridinium Salt Blocks α7 nAChR and Induces Apoptosis in Non-Small Cell Lung Carcinoma

Ana Zovko, Kristina Viktorsson, Rolf Lewensohn, Katja Kološa, Metka Filipič, Hong Xing, William R. Kem, Laura Paleari and Tom Turk

Abstract: Naturally occurring 3-alkylpyridinium polymers (poly-APS) from the marine sponge *Reniera sarai*, consisting of monomers containing polar pyridinium and nonpolar alkyl chain moieties, have been demonstrated to exert a wide range of biological activities, including a selective cytotoxicity against non-small cell lung cancer (NSCLC) cells. APS8, an analog of poly-APS with defined alkyl chain length and molecular size, non-competitively inhibits α7 nicotinic acetylcholine receptors (nAChRs) at nanomolar concentrations that are too low to be acetylcholinesterase (AChE) inhibitory or generally cytotoxic. In the present study we show that APS8 inhibits NSCLC tumor cell growth and activates apoptotic pathways. APS8 was not toxic for normal lung fibroblasts. Furthermore, in NSCLC cells, APS8 reduced the adverse anti-apoptotic, proliferative effects of nicotine. Our results suggest that APS8 or similar compounds might be considered as lead compounds to develop antitumor therapeutic agents for at least certain types of lung cancer.

Reprinted from *Mar. Drugs*. Cite as: Zovko, A.; Viktorsson, K.; Lewensohn, R.; Kološa, K.; Filipič, M.; Xing, H.; Kem, W.R.; Paleari, L.; Turk, T. APS8, a Polymeric Alkylpyridinium Salt Blocks α7 nAChR and Induces Apoptosis in Non-Small Cell Lung Carcinoma. *Mar. Drugs* **2013**, *11*, 2574-2594.

1. Introduction

Lung cancer (LC) is one of the most frequently diagnosed tumor types and is also the number one when it comes to death causing tumors [1]. With respect to LC histology, two major categories are small cell lung cancers (SCLC) and non-small cell lung cancers (NSCLC); the latter is further subdivided into squamous cell carcinomas, adenocarcinomas, and large cell carcinomas [2]. NSCLC, SCLC as well as normal lung cells have been shown to express various cholinergic signaling system molecules including acetylcholine, the vesicular acetylcholine ACh transporter, and nicotinic (nAChRs) and muscarinic (mAChR) receptors [3–6].

Nicotine, the main addictive component of tobacco, as well as some of its metabolites contributes to cancer development [7]. The inhalation of tobacco smoke containing nicotine and other compounds is associated with 90% of SCLC and 60% of NSCLC cases [8]. Although nicotine has not been shown to be carcinogenic, nitrosamine metabolites of nicotine are carcinogenic and it has been estimated that 2–3 DNA mutations result from every cigarette smoked [9]. Nicotine binds to various subtypes of nicotinic acetylcholine receptors (nAChRs) that are expressed on neurons and some non-neuronal cells [10–14]. It has been shown that certain tumor cells express an elevated number of nAChRs [6,12]. The homomeric α7 nAChR subtype seems to be particularly abundant in various tumor cells of the respiratory tract. It has been reported that exposure of lung adenocarcinoma cells to nicotine or ACh enhances expression of α7 nAChRs [15]. Activation of α7

nAChRs leads to elevated intracellular calcium levels sufficient to activate signal transduction pathways that prevent apoptosis and contribute to proliferation of LC cells [7,8,16,17]. Therefore, it has been suggested that α7 nAChR antagonists may be useful as therapeutics for suppressing rapidly proliferating tumor cells including LC cells [18–20].

Marine organisms have long been a source of antitumor compounds [21–23]. A polymeric mixture of 3-alkylpyridinium salts (poly-APS) which display a broad spectrum of biological activities was isolated from a marine sponge, *Reniera sarai*, which has been recently renamed to *Haliclona* (*Rhizoneira*) *sarai* (Pulitzer-Finali, 1969) [24–27]. Relevant to the present study, the most salient poly-APS effects are those that are preferentially toxic to NSCLCs [28].

In view of the potential utility of poly-APS like compounds as anti-cancer agents, a series of synthetic analogs were prepared [29]. Preliminary results, demonstrated in this paper, revealed that at least one of these compounds, the 11.9 kDa analog APS8 (Figure 1), is a very potent α7 nAChR antagonist. Moreover, toxicity analysis in mice showed that APS12-2, a similar analog, was only moderately toxic in mice with an i.v. LD_{50} of 11.5 mg/kg [30], and the toxicity of APS8 used in this study is only slightly higher, about 8 mg/kg [31].

Figure 1. Chemical structure of APS8, the synthetic alkylpyridinium polymer, used in this study. Central monomeric unit linked to two neighboring units is shown. MW of the entire polymer is 11.9 kDa.

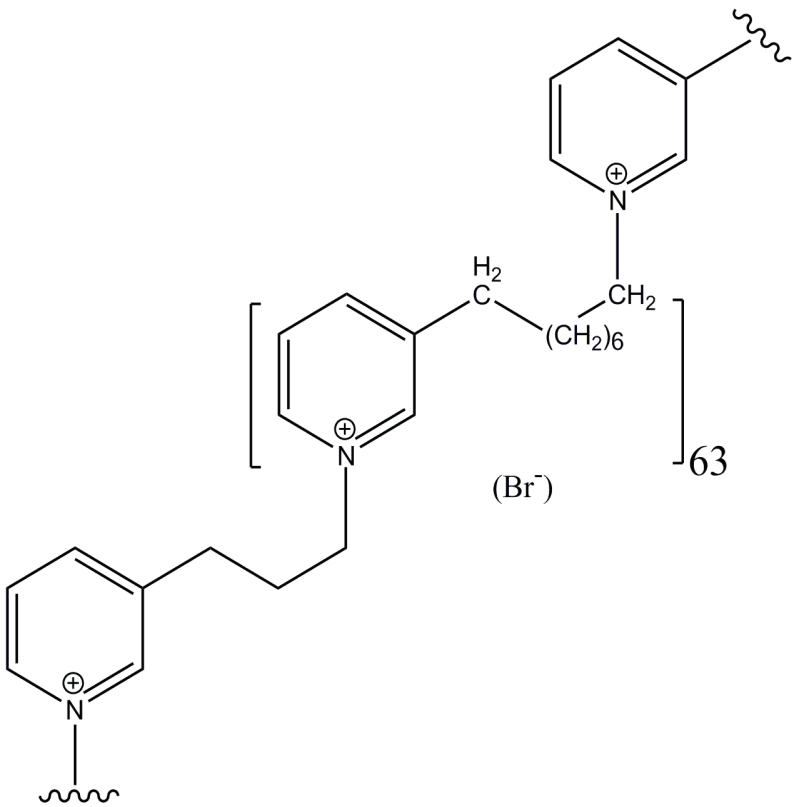

2. Results and Discussion

2.1. APS8 Induces Cytotoxicity in Lung Cancer (LC) Cells

In order to examine if APS8 is cytotoxic to LC cells the SKMES-1 and A549 cell lines were treated with various concentrations of APS8 for 48 h and analyzed for cell viability by MTT-assay (Figure 2A). The effect on normal lung fibroblasts was also examined. APS8 in a concentration dependent manner strongly decreased viability of LC cell lines (IC_{50} 375 ± 4.89 nM for A549 cells and 362 ± 9.29 nM for SKMES-1 cells). Lung fibroblast cell line MRC-5 was largely unaffected thus incubation of these cells for 48 h with APS8 only resulted in a 20% decrease in cell viability at the highest concentration (1 μM). Next, the effect of APS8 on nicotine response was examined. Nicotine alone slightly enhanced cell survival of both A549 and SKMES-1 (13% for A549 and 14% for SKMES-1) ($p < 0.05$) while only a minor effect was observed with MRC-5 normal fibroblasts (6%) (Figure 2B). Importantly, APS8 significantly counteracted nicotine-induced effects in both LC cells (about 50%) while MRC-5 normal cells were much less affected. As compared to the APS8 only treatment, a combination of APS8 with nicotine caused a statistically significant ($p < 0.05$) increase of viable SKMES-1 cells (for 28%) and statistically insignificant increase of viable A549 cells (for 22%), while normal cells were not affected.

APS8 caused a prominent induction of apoptotic cell morphology in both A549 and SKMES-1 LC cells (Figure 3A, panel b and d). Quantification of APS8-induced apoptosis revealed a statistically significant ($p < 0.05$) and comparable response in A549 and SKMES-1 cells where about 40% of cells were found to be apoptotic after exposure to 500 nM of APS8 for 48 h (Figure 3B). Importantly, no induction of apoptosis was seen in normal fibroblasts MRC-5, which displayed the same nuclear morphology in the presence or absence of APS8 (Figure 3A, panel f and Figure 3B), thus corroborating a cancer cell specific apoptotic effect of APS8. The positive control staurosporine induced apoptosis in all cell types examined with the A549 cell line being least affected with only a 30% induction of apoptosis.

Next, we investigated whether APS8 is able to induce apoptosis in nicotine treated LC and fibroblasts (Figure 3B). As expected, nicotine alone did not trigger an apoptotic response in any of the cell types examined. LC cells treated with a combination of nicotine and APS8 displayed a greater resistance to apoptosis as compared to those treated only with APS8. Moreover, a greater sensitization was observed in SKMES-1 cells relative to A549 cells. In MRC-5 cells only the highest dose of APS8 induced limited apoptosis and this was reduced by the simultaneous exposure to nicotine.

Figure 2. Viability of NSCLC (A549, SKMES-1) and normal lung fibroblast MRC-5 cells. (**A**) Viability of A549, SKMES-1 and MRC-5 cells treated with 0, 1, 10, 100, 500, and 1000 nM APS8 for 48 h was assessed by MTT assay. Each point represents the mean value of three independent experiments ± SE. Statistical analysis was performed by Student's *t*-test. * $P < 0.05$; (**B**) Viability of A549, SKMES-1 and MRC-5 cells treated with APS8 (500 nM), nicotine (1 μM) or a combination of both compounds for 48 h. The MTT assay was used. Each point represents the mean value of three independent experiments ± SE. Statistical analysis was performed by ANOVA/Tukey-Kramer multiple comparison. * $P < 0.05$, compared with control; † $P < 0.05$, compared with APS8 treatment; ‡ $P < 0.05$, compared with nicotine treatment.

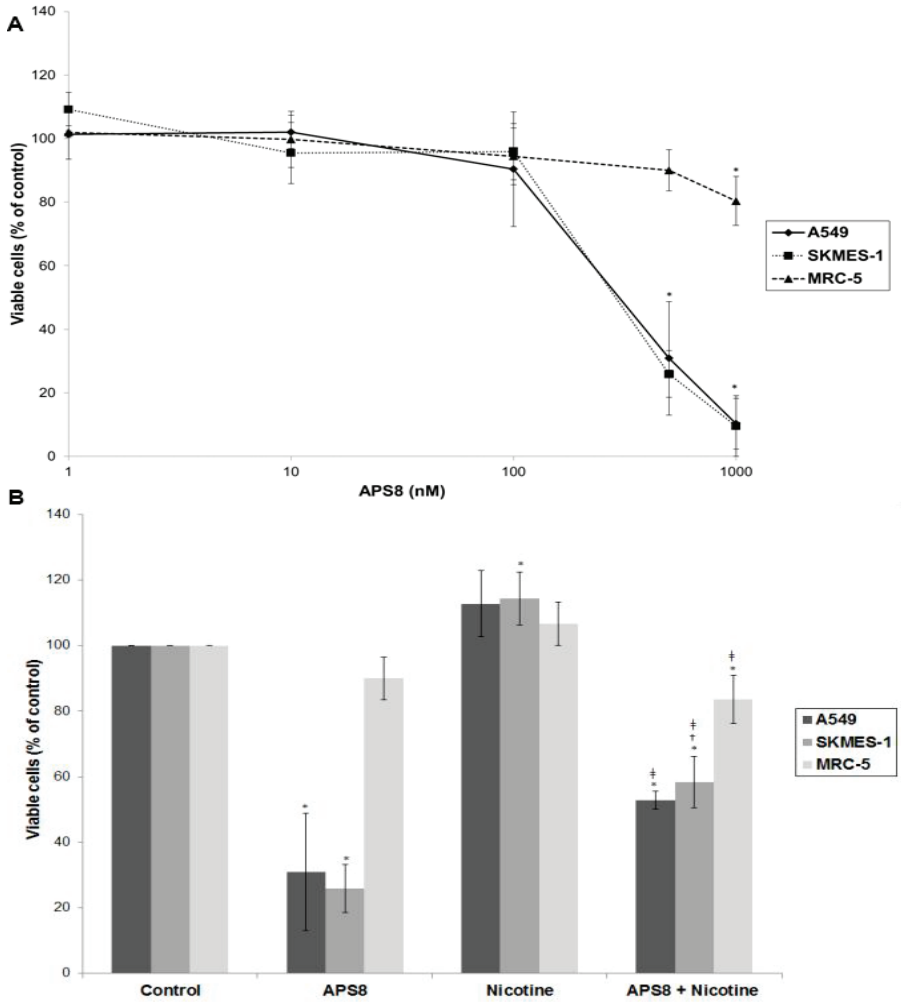

Figure 3. APS8 induces apoptosis in NSCLC but not in normal fibroblasts. (**A**) Apoptosis after APS8 treatment (500 nM, 48 h) in A549, SKMES-1, and MRC-5 were assessed by staining with acridine orange and ethidium bromide and analysis by fluorescence microscope. Photos were taken at 400× magnification. Dashed arrows indicate cells in early apoptosis and full arrows point to late apoptotic cells. Green cells are alive; (**B**) Induction of apoptosis in A549, SKMES-1, and MRC-5 lines as measured by dual staining. Cells were treated with staurosporine (2 μM), APS8 (100 nM, 500 nM, and 1000 nM), nicotine (1 μM) or combination of APS8 and nicotine. The graph indicates the percentage of cells in the single cell populations. Each point is the mean of three independent experiments. The protective effect of nicotine was significant only for A549 cancer cells treated with 500 nM of APS8 (* $P < 0.05$); (**C**) APS8 induction of apoptosis in A549, SKMES-1, and MRC-5 cell lines was measured by flow cytometric analysis of annexin V and propidium iodide stained cells at 48 h. Controls (a, c, and e) and APS8 (500 nM) treated cells (b, d, and f); (**D**) Induction of apoptosis in A549, SKMES-1 and MRC-5 lines by flow cytometry. Cells were treated with staurosporine (2 μM), APS8 (100 nM, 500 nM, and 1000 nM), nicotine (1 μM) or combination of APS8 and nicotine. The graph indicates the percentage of gated cells in each cell population. Each point is the mean of three independent experiments.

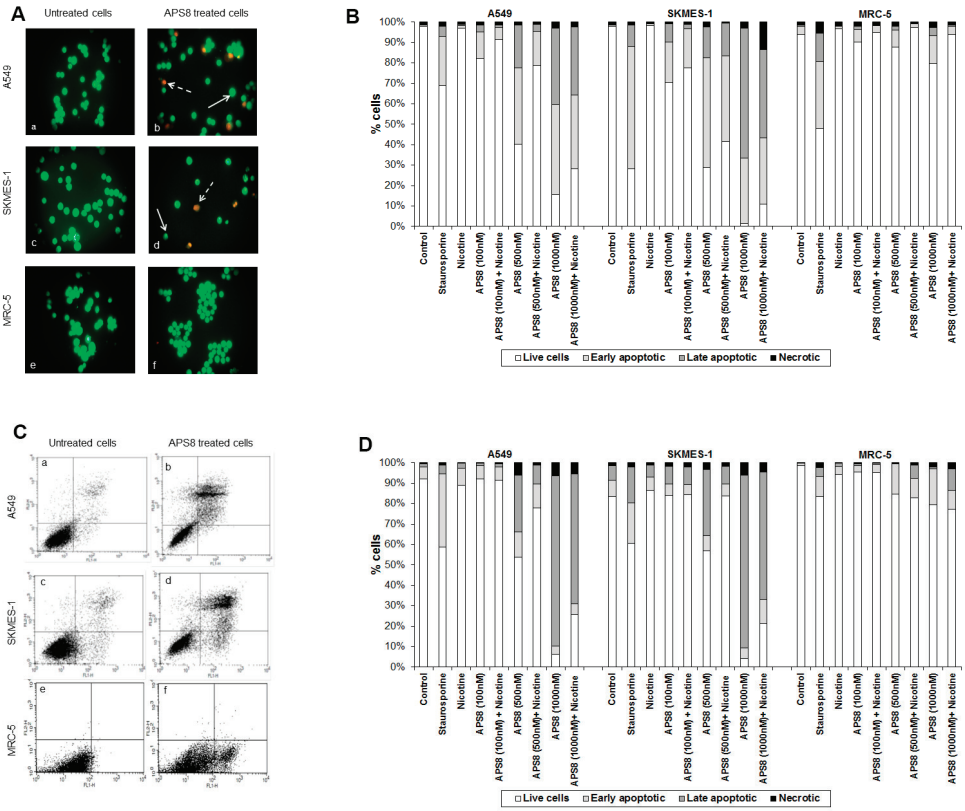

The apoptotic properties of APS8 were also examined using annexin-V/PI staining. Exposure of A549 or SKMES-1 cells to APS8 resulted in typical apoptotic cells, evident as a shift to the right quadrants of the flow diagram (Figure 3C, panels b and d). Quantification of cell populations demonstrated a concentration dependent induction of apoptosis in both A549 and SKMES-1 cells (Figure 3D). Importantly, no induction of annexin-V was observed in normal MRC-5 fibroblasts (Figure 3C, panel f). Even at the highest concentration of APS8 used (1 μM), 80% of MRC-5 cells remained non-apoptotic (Figure 3D).

We also analyzed whether nicotine attenuates APS8 induced apoptosis using this assay (Figure 3D). Although nicotine slightly reduced APS8-induced apoptosis in A549 cells, apoptosis was still evident. A minor protective effect of nicotine was also evident in SKMES-1 cells. APS8 in any of the concentrations used did not induce apoptosis in MRC-5 fibroblasts or influenced their response to nicotine. Hence, our results support that APS8 has capacity to trigger an apoptotic response in LC cells whereas normal cells remain unaffected.

Figure 4. APS8 causes depolarization of mitochondria in NSCLC cells but not in normal fibroblasts. Ratio of red and green fluorescence following exposure to staurosporine (1 μM), CCCP (50 mM), APS8 (500 nM) for 48 h. Each point is the mean of three independent experiments ± SE. Statistical analysis was performed by ANOVA/Tukey-Kramer multiple comparison. * $P < 0.05$, compared with control; ‡ $P < 0.05$, compared with staurosporine treatment.

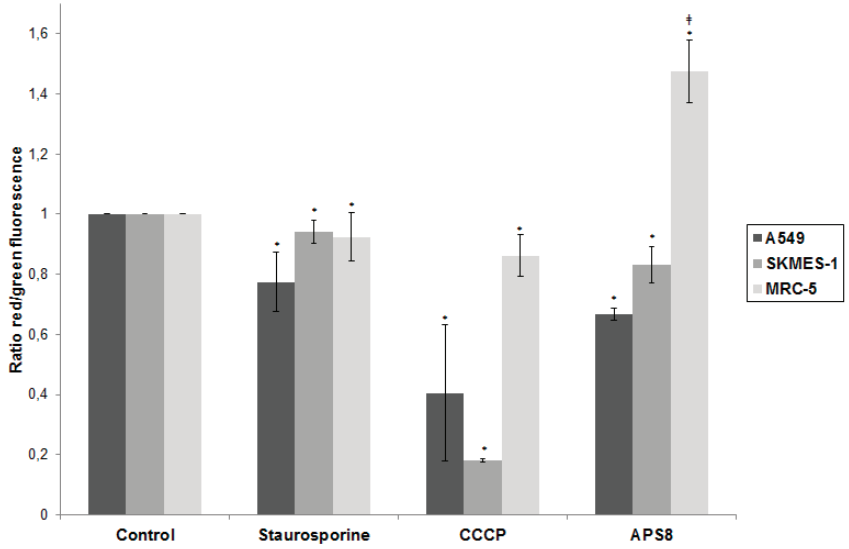

2.2. APS8 Induces Mitochondrial Depolarization in LC Cells

We analyzed if APS8 could cause depolarization of mitochondria and in this way execute an apoptotic effect (Figure 4). First, we confirmed that the system is capable of detecting alterations in mitochondrial potential as illustrated by the prominent decrease in red/green fluorescence ratio in LC

cells (60% for A549 and 80% for SKMES-1) after CCCP treatment. A substantial decrease of red/green fluorescence ratio was observed following APS8 treatment of A549 cells (about 35%) and SKMES-1 cells (about 15%) illustrating that APS8 at least in part works via mitochondrial depolarization. For comparison the staurosporine, an initiator of apoptosis, causes a 23% and 6% decrease in A549 and SKMES-1 cells respectively. There was no statistically significant difference between staurosporine and APS8 treated LC cell lines with respect to a decrease in red/green fluorescence ratio. In contrast, APS8 induced an increase in the red/green fluorescence ratio in MRC-5 cells, suggesting that APS8 does not cause mitochondrial permeabilization in normal fibroblasts (Figure 4).

2.3. APS8 Treatment Results in Increased Expression of Pro-Apoptotic Proteins and Down-Regulation of Anti-Apoptotic Proteins in LC Cells

To further understand how APS8 influenced the apoptotic propensity of LC cells we examined the effect of APS8 on the expression of a number of pro-and anti-apoptotic proteins using the Human Apoptosis Antibody Array. APS8 (500 nM) treatment of A549 cells for 48 h resulted in up-regulation of several pro-apoptotic proteins, *i.e.*, bad, bax, bim and bid, cytochrome C, SMAC, TRAIL-R1 and TRAIL-R2, Fas, FasL, caspase-8, and caspase-3 albeit to the different extent (Figure 5A). Moreover, the majority of anti-apoptotic proteins, including bcl-2 and bcl-W, c-IAP-2, XIAP, survivin, and livin were down-regulated in A549 cells after APS8 exposure (Figure 5A).

Similarly, treatment of SKMES-1 cells with APS8 (500 nM) also resulted in an increased expression of the pro-apoptotic proteins, *i.e.*, bad, bax, bim and bid, cytochrome C, SMAC, TRAIL-R1 and TRAIL-R2, Fas, caspase-8 and caspase-3, with a slighter higher expression than was observed in A549 cells (Figure 5B). In accordance with results in A549 cells also SKMES-1 cells responded to APS8 with a down-regulated expression of the anti-apoptotic proteins bcl-2, bcl-W, cIAP-2, and XIAP (Figure 5B). Importantly, treatment of normal MRC-5 fibroblasts did not show any significant change in the expression of any of the proteins known to be involved in apoptosis (data not shown).

In addition, we examined how nicotine treatment of A549 and SKMES-1 cells influenced the expression of these pro- and anti-apoptotic proteins (Figure 5A,B). A majority of pro-apoptotic proteins, including bad, bax, bid, cytochrome C, SMAC, TRAIL-R1, Fas, FasL and caspase-8, were significantly down-regulated on nicotine exposure. Moreover, an increased expression of many proteins involved in signaling pathways known to prevent apoptosis, including bcl-2, bcl-W, cIAP-2, XIAP, surviving, and livin was evident. This was further illustrated when the bax/bcl-2 ratio was compared in ASP8 and nicotine treated cells. bax/bcl-2 ratio increased after APS8 treatment in both cell lines while it decreased after nicotine treatment (Figure 5A,B, inserts). These results further emphasize the selective activation of pro-apoptotic signaling in LC cells by APS8.

Figure 5. APS8 increases the expression of pro-apoptotic proteins and represses the expression of anti-apoptotic proteins. The change in expression of anti- and pro-apoptotic proteins was examined in A549 (**A**) and SKMES-1 (**B**) cells after treatment with APS8 (500 nM) or nicotine (1 μM) for 48 h using Human Apoptosis Antibody Array. Fold values relative to untreated cells are given. For presentation proteins are divided into three groups: proteins belonging to the intrinsic pathway, inhibitors of apoptosis (IAPs), and proteins belonging to the extrinsic pathway. Each point is the mean of three independent experiments ± SE. * $P < 0.05$ compared with control. The insert shows the ratio of main pro-apoptotic and main pro-survival proteins in APS8 and nicotine treated cells.

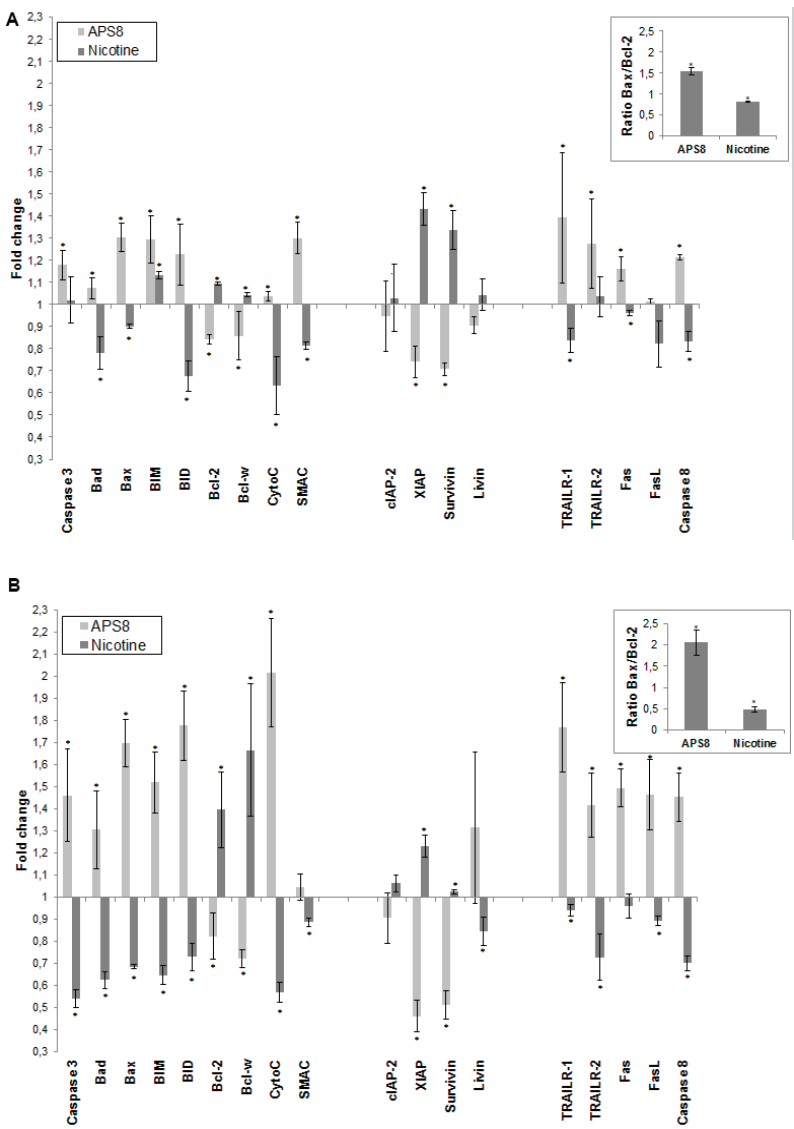

2.4. APS8 Treatment of Cancer Cell Lines Results in Activation of Caspase-9

Next, we examined caspase-9 activity, an effector molecule downstream of mitochondrial depolarization. Treatment of A549 and SKMES-1 with APS8 induced activation of caspase-9 to the similar extent as observed in positive control with staurosporine ($p < 0.05$). Nicotine treatment reduced the level of caspase-9 activity in A549 cells. In MRC-5 cells caspase-9 remained inactive after the treatment with APS8 or nicotine ($p < 0.05$) (Figure 6). These findings are in concordance with APS8 being a pro-apoptotic signaling molecule in LC cells, but not in normal fibroblasts.

Figure 6. APS8 activates the intrinsic apoptotic pathway in NSCLC cells but not in normal fibroblasts. Caspase-9 activities relative to untreated control after treatment with staurosporine (2 μM), APS8 (500 nM), and nicotine (1 μM) for 48 h in A549, SKMES-1 or MRC-5 cells are given. Each point is the mean of three independent experiments ± SE. Statistical analysis was performed by ANOVA/Tukey-Kramer multiple comparison. * $P < 0.05$, compared with control; ‡ $P < 0.05$, compared with staurosporine treatment.

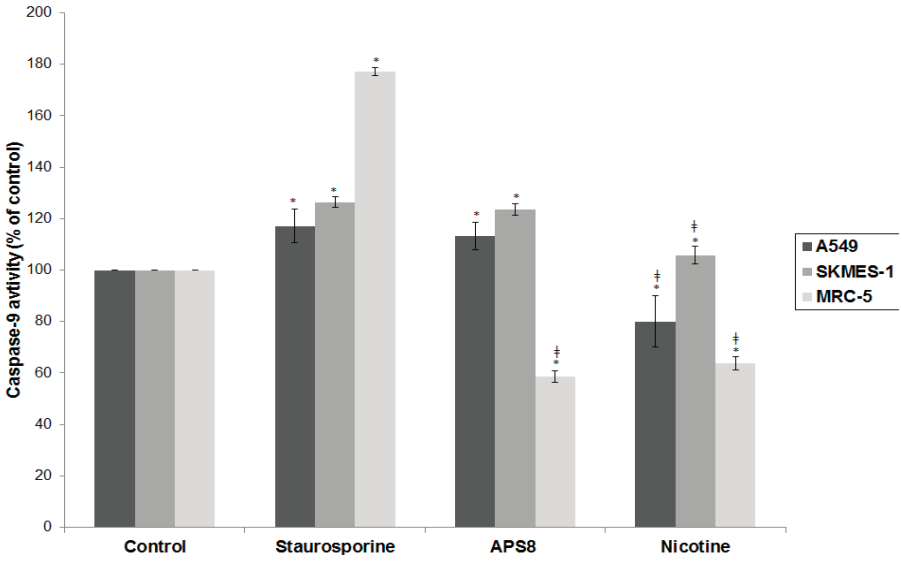

2.5. APS8 Is a Negative Regulator of Human α7 nAChRs

In order to confirm that APS8 indeed is negative regulator of α7 nAChRs we examined its capacity to inhibit α7 nAChR activity *in vitro* systems, *i.e.*, *Xenopus* oocytes and SHEP-1 cells expressing human α7 nAChR (Figure 7). APS8 potently inhibited the responses of *Xenopus* oocytes expressing human α7 nAChR in a time dependent manner (Figure 7A,B). The IC_{50} was approximately 1 nM. The action of APS8 could at least partially be slowly reversed by prolonged washing of the oocyte with frog Ringer solution (results not shown). APS8 was also able to inhibit the specific binding of the α7 nAChR antagonist ^{125}I-α-BTX in SHEP-1 cells system, but only at

concentrations which were at least two orders of magnitude higher than was required to functionally inhibit α7 nAChR when expressed in *Xenopus* oocytes (Figure 7C). In summary, these results demonstrate that APS8 indeed is an antagonist of α7 nAChRs.

Figure 7. APS8 inhibits the response of human α7 nAChRs expressed in the *Xenopus* oocyte to a near maximally activating concentration of ACh (points represent mean values for five oocytes). In part (**A**) the time course of inhibition is shown; in part (**B**) the concentration dependence of APS8 inhibition at 20 min incubation is shown; Part (**C**) shows APS8 inhibition of the specific binding of [^{125}I]-α-bungarotoxin to human α7 nAChRs expressed in cultured SHEP-1 cells. Each point is a mean value for four replicates.

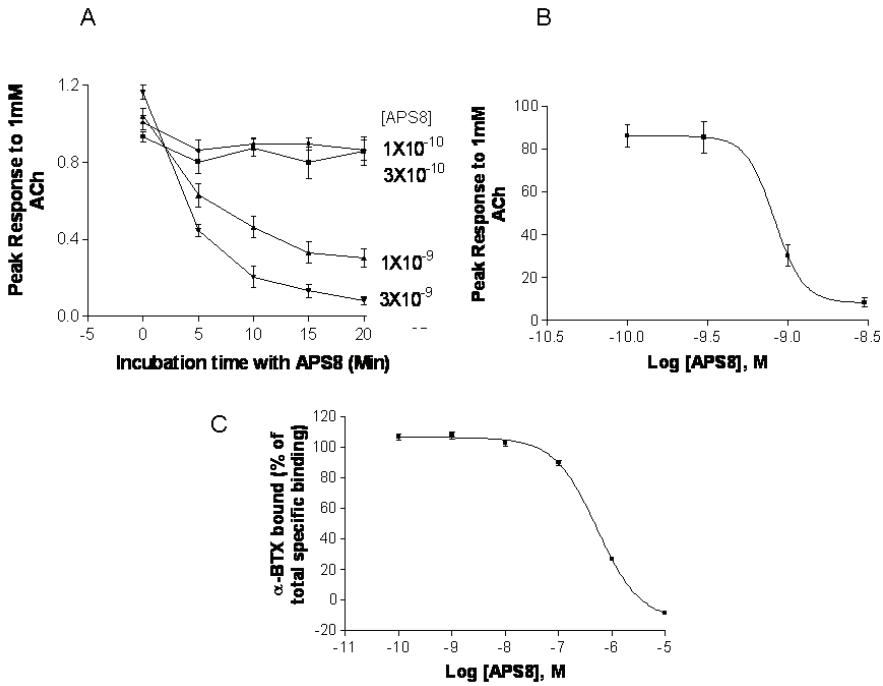

In the current study we analyzed the potential of the *Reniera sarai* derived synthetic compound APS8 as a LC antitumor agent. We show that it holds potential to selectively trigger a cytotoxic and pro-apoptotic response in NSCLC cells whereas normal fibroblasts remained unaffected. Moreover, we show that APS8 is an antagonist of the α7 nAChRs.

A variety of mAChR and nAChR subtypes are found on normal cells [3,14] but have an altered expression pattern in normal bronchial epithelial cells and airway fibroblasts of smokers, ex-smokers, and non-smokers [15]. Importantly, many cancer cell lines and primary cancer cells show a higher expression of mAChR and nAChR subtypes. Why LC cells have an increased expression of mAChR and nAChR is not completely clear but it might reflect adaption of the tissue to nicotine and other compounds inhaled by tobacco smoke [15]. Hence, α7 nAChRs might be a

therapeutic target and in light of this our findings on the selective cytotoxic effects of APS8 to LC cells but not to normal lung fibroblasts are interesting.

Cytotoxicity for lung adenocarcinoma or squamous carcinoma NSCLC cell lines and the resistance of MRC-5 cells to natural poly-APS could be explained by the lack of nAChRs on the MRC-5 cells. Albeit, we did not evaluate the expression of α7 nAChRs in A549 or SKMES-1 cells, immunohistochemistry analyses of this receptor in A549 cells by the human protein atlas project demonstrated a high expression [32]. When preparing this manuscript, Lau *et al*., in fact, demonstrated by ELISA-based assay that A549 cells, as well as multiple other bronchioalveolar carcinoma (BAC) cell lines, do express α7 nAChRs [33]. Although our results reveal a therapeutic window for APS8, siRNA experiment towards α7 nAChRs would be required in order to confirm that these receptors are the specific APS8 target.

The ability to resist apoptosis is a hallmark of almost all types of tumor cells, including NSCLC, and this hampers the efficacy of chemotherapeutics [34]. ACh and the nAChR selective agonist nicotine have been found to protect NSCLC, SCLC, and some other tumor cells expressing α7 nAChRs against apoptosis induced by chemotherapeutic agents [16,35–37]. How the anti-apoptotic effect in NSCLC is achieved by ACh, other nAChR agonists, and the two main carcinogenic metabolites of nicotine *N*-nitrosonornicotine (NNN) and (4-(methylnitrosamino)-1-(3-pyridyl)-1-butanone (NNK), was recently revealed by Schuller [7]. In smokers, nicotine and its metabolites act predominantly through the activation of Ca^{2+} permeable α7 nAChRs, possibly because the heteromeric nAChR subtypes are already desensitized by low concentrations of these compounds during smoking. The influx of Ca^{2+} and also Na^{+} ions provokes membrane depolarization, which in turn activates voltage-gated Ca^{2+} channels, leading to an additional influx of Ca^{2+} [7]. The increased intracellular concentration of calcium triggers signal-transduction cascades involved in the regulation of numerous cellular processes: proliferation, angiogenesis, migration, differentiation, and apoptosis [7,8,38–40]. Thus, the α7 nAChR appears to be a promising target for the therapy of NSCLC or at least BAC as recently was proposed. One possible therapeutical approach would be the use of α7 nAChR antagonists either alone or in combination with other chemotherapeutic drugs. Such a combination would enhance apoptosis but also impede proliferation and metastasis of tumor cells [1,20]. Indeed, snake venom polypeptide α-toxins, *i.e.*, α-cobratoxin and α-bungarotoxin, which are potent natural ACh antagonists of muscle and several other nAChR subtypes were recently proposed as possible candidates to achieve such a goal [18]. However, due to their blocking actions on neuromuscular nAChRs, these peptide toxins are also highly toxic and therefore could be problematic for clinical treatment of cancer patients. Interestingly, APS8 (i.v. LD_{50} is about 8 mg/kg in mice, [31]) is significantly less toxic than snake α-toxins and APS8 possesses a more stable chemical scaffold suggesting that this compound might be suitable as an *in vivo* probe to test the therapeutic potential of α7 nAChR antagonists.

We show here that APS8 is an extremely potent α7 nAChR antagonist. The response of human α7 nAChRs expressed in *Xenopus* oocytes to 1 mM ACh, that alone produces a near maximal response, was completely blocked by about 3 nM APS8 after 20 min of incubation. The recovery from this blockade was very slow, requiring several hours (not shown). APS8 was only able to inhibit the specific binding of the snake toxin α-bungarotoxin to human α7 nAChRs at

concentrations over 100× the function-inhibiting concentrations. These results point to a noncompetitive mode of APS8 mediated inhibition and binding of APS8 outside the actual ACh binding sites on this nAChR subtype.

We anticipated that APS8 *in vitro* would inhibit proliferation and trigger apoptosis in tumor cell lines, but not in normal fibroblasts. Our hypothesis was based on our earlier observation that the parental compound from which APS8 was derived, the natural poly-APSs from the marine sponge *Reniera sarai*, can induce apoptosis of NSCLC cells, yet being well tolerated by normal cells [28]. Exposure to APS8 induced apoptosis in both lung cancer cell lines while normal fibroblasts MRC-5 did not undergo any significant apoptosis. These results were consistent when using different methods and confirmed our hypothesis.

The cytotoxic effect is probably exerted by inducing apoptosis through the binding to α7 nAChRs, which are expressed to a greater extent by cancer than by most normal cells. As expected from previous studies in a number of laboratories, nicotine promoted cell survival of LC cells. Therefore, we expected that nicotine in combination with APS8 would reduce the APS8 cytotoxic effect on cancer cell lines. Our results show that nicotine in combination with APS8 had only moderate effect on survival of A549 cells, while slightly stronger protection was evident on SKMES-1 cells. These results are in accordance with a previous study that suggested that nicotine has higher influence on proliferation of squamous carcinomas than of adenocarcinomas [19]. Nicotine in combination with APS8 somewhat also protected LC cells from apoptosis suggesting antagonistic effect of APS8 to nicotine.

Mitochondrial permeabilization is one of the early stages of apoptosis, which leads to the release of several pro-apoptotic factors, including cytochrome c and SMAC, which in turn facilitate the activation of the apoptosome and downstream caspase-9 and caspase-3 activation. Our results show that APS8 treatment of A549 and SKMES-1 causes a mitochondrial depolarization, suggesting that APS8 in part can induce apoptosis via the apoptosome-mediated pathway. Indeed, after exposure to APS8 we observed an activation of caspase-9, a typical initiator caspase of the intrinsic apoptotic pathway.

To further test this hypothesis we used the RayBio® Human Apoptosis Antibody Array kit. Treatment of A549 and SKMES-1 cells with APS8 (500 nM) increased the expression of caspase-3 which is an effector caspase activated by both intrinsic and extrinsic apoptotic pathways. The intrinsic pathway is activated by cellular stress, involves disruption of mitochondria and is controlled by bcl-2 family proteins. Induction of apoptosis relies on the ratio between pro-apoptotic (bax, bak, bcl-Xs, bad, bid) and anti-apoptotic (bcl-2, bcl-XL, bcl-W, mcl-1, A1) members of the bcl-2 family. Upon intrinsic apoptotic signal BH3 only proteins (bid, bad, PUMA, and NOXA) interact with the bcl-2 family, leading to inhibition of anti-apoptotic proteins and activation of pro-apoptotic proteins. Bax and bak proteins insert into the outer mitochondrial membrane causing the release of cytochrome c, bim, and SMAC from mitochondria. Released proteins then induce initiator caspase-9 activation and activation of effector caspase-3 [41,42]. The ratio between the levels of bax and bcl-2 proteins, at least in part, thus determines whether apoptosis will be induced with an increase in the bax/bcl-2 ratio causing a switch towards mitochondrial membrane permeabilization and activation of apoptosis. We show that treatment of both A549 and SKMES-1

cells expressing α7 and some other nAChR subtypes with APS8 triggers an increase in the expression of pro-apoptotic proteins bax, bad, bim and bid with a concomitant decrease in the levels of anti-apoptotic proteins bcl-W and bcl-2. Hence the bax/bcl-2 is increased, which may contribute to the observed increased apoptotic response of LC cells upon APS8 exposure. The data also revealed that both cytochrome c and SMAC, which are released from mitochondria during apoptosis, have an increased expression after APS8 treatment further increasing a pro-apoptotic capacity of the NSCLC cells. In summary, these results imply that APS8 induces apoptosis through the intrinsic pathway.

Our results also show that nicotine up-regulates bcl-2 and down-regulates bax, lowering the bax/bcl-2 ratio, which would favor a reduced apoptotic propensity of the NSCLC cells. Indeed, it was earlier suggested that inactivation of bax may be an essential step in anti-apoptotic mechanism induced by nicotine [39]. Our data show strong up-regulation of bax and down regulation of bcl-2 by APS8, quite opposite effects as compared to nicotine, which suggests that APS8 may at least in part counteract the protective effect of nicotine by increasing the bax/bcl-2 ratio. This effect was more prominent in SKMES-1 than in the A549 cancer cell line.

Another large group of proteins involved in regulation of the apoptosome activity are inhibitors of apoptosis proteins (IAPs), a family of pro-survival proteins [43]. In our experiments, all tested IAPs (cIAP-2, livin, XIAP and survivin) with the sole exception of livin in SKMES-1 cells, were down-regulated after exposure to APS8, whereas an increased expression was observed after nicotine treatment. Moreover, as mentioned earlier, SMAC displayed an increased expression in APS8 treated cells. This protein is an endogenous IAP antagonist and binds to IAP proteins, preventing their binding and inactivation of caspases, and thus promoting cell death. As was shown earlier, nicotine up-regulates IAPs, particularly XIAP, and in this way enhances resistance to anti-cancer treatments [44]. Our results suggest that APS8 can circumvent nicotine-induced resistance to apoptosis by interfering with IAPs allowing proper apoptosome function and downstream caspase activation to take place.

The Fas, TNF-R1, TNF-R2, and TRAIL (TRAIL-R1, -R2, -R3, and -R4) cell membrane receptors are key molecules of the extrinsic pathway of apoptosis and are activated upon binding appropriate ligands (FasL, TNF, and TRAIL) resulting in downstream caspase-8 activation followed by effector caspases (3, 6, and 7) activation [45]. Caspase-8 activation can trigger cleavage and activation of the BH3 only protein bid, which in turn can interact with bcl-2 proteins in mitochondria, resulting in intrinsic apoptotic pathway signaling and thereby activating effector caspases [46]. In the present study we show that TRAIL-R1 and TRAIL-R2 expression are enhanced following APS8 treatment while a decreased expression was observed after nicotine treatment. Although APS8 markedly increased the expression levels of Fas in A549 cells, no significant changes of FasL were noted. In SKMES-1 cell line both Fas and FasL showed a marked increased expression following the APS8 treatment. On the contrary, nicotine in both cancer cell lines slightly decreased the levels of Fas/FasL and TRAIL receptors. These results suggest that APS8 can activate components of death receptor signaling which at least in part might be cell type specific but, nevertheless, are oppositely regulated by nicotine.

3. Experimental Section

3.1. Synthetic Poly-APS Analog and Cell Cultures

APS8 (Figure 1) was synthesized using a previously described microwave-assisted polymerization procedure. This water-soluble compound has a molecular weight of 11.9 kDa and is stable at room temperature [29]. For the current experiments, a stock concentration of 10 mg/mL APS8 in deionized water was kept at 4 °C and further diluted in cell culture media upon use.

Human lung adenocarcinoma A549 [47] squamous carcinoma SKMES-1 [48], and lung fibroblast MRC-5 [49] cells were purchased from the European Collection of Cell Cultures (ECACC). A549 and MRC-5 cells were grown in Dulbecco's Eagle's medium (DMEM) (PAA, Austria), while SKMES-1 was grown in RPMI1640 (PAA) both supplemented with 10% fetal bovine serum (FBS), L-glutamine and penicillin/streptomycin (Sigma-Aldrich, Germany). All experiments were carried out at 37 °C in 5% CO_2.

3.2. Cell Viability Assay

Cytotoxicity was determined by 3-(4,5-dimethylthiazol-2-yl)-2,5 diphenyltetrazolium bromide (MTT) assay, as previously described [50], with minor modifications. Briefly, A549 and SKMES-1 cells were seeded at a density of 2500 cells/well and MRC-5 3500 cells/well into 96-well microtiter plates in five replicates for each of the three sets of experiments. Experiments were carried out 24 h post seeding when cells were about 80% confluent, at which time the growth medium was replaced with fresh medium containing different concentrations of APS8, 1 μM nicotine, or combination of both followed by incubation for 24, 48, or 72 h. Values shown are the mean of three or five replicates in three independent experiments ± SE.

3.3. Apoptotic Morphology Assessment

Cell morphology and percentage of apoptotic cells were studied by staining cells with a combination of the fluorescent DNA-binding dyes acridine orange (AO) and ethidium bromide (EB) (Sigma-Aldrich). The method is based on differential staining, where AO stains nuclei green, while EB stains red, and in which EB is excluded from viable cells. That allows enumeration of four populations: live cells which have normal bright green nucleus, necrotic cells which have light orange nucleus, early apoptotic cells which stain green with condensed chromatin, and late apoptotic cells which have condensed and fragmented chromatin and a emit bright orange-red color.

For apoptotic morphology experiments A549, SKMES-1, and MRC-5 cells were seeded at a density of 10^5 cells/mL for 24 h and then treated with various concentrations of APS8 and/or nicotine for 48 h. Staurosporine (Sigma-Aldrich) (2 μM, 6 h) was used as a reference compound for apoptosis induction. After harvesting cells by trypsinization and centrifugation (81,614× *g*, 2 min), cell pellets were resuspended in 60 μL of medium. 50 μL of the cell suspension was mixed with 2 μL of AO/EB (1:1 w/w) dye mixture containing 100 μg/mL of AO and 100 μg/mL of EB in PBS. Cells were visualized and counted under a fluorescence microscope (Nikon Eclipse E-800, Nikon, Japan) at 400× magnification according to their color and structure. Pictures were taken with

a digital camera (Nikon Coolpix 995, Japan). The quantification data shown are from three independent experiments; each time 300 cells were examined.

3.4. Analysis of Apoptosis by Annexin V and Propidium Iodide Staining

Apoptosis was also detected by staining cells with annexin V-FITC and propidium iodide (PI) (BD Pharmingen, San Diego, CA, USA). PI is a fluorescent dye that stains DNA. As the dye does not cross intact plasma membranes, only cells with a damaged plasma membrane that already are dead or in a late stage of apoptosis are stained. Annexin V-FITC is a fluorescent dye, which binds to phosphatidylserine (PS). During the early stages of apoptosis PS translocates from the inner to the outer layer of the plasma membrane and becomes available for binding to the annexin V-FITC. Thus, living cells do not stain, cells in early apoptosis are annexin V-FITC positive and PI negative, late apoptotic cells are both annexin V-FITC and PI positive and necrotic cells are annexin V-FITC negative and PI positive. For annexin-PI staining, cells (10^5 cells/mL) were cultured for 24 h and then exposed to various concentrations of APS8 and/or nicotine for 48 h. Staurosporine (2 μM, 6 h) was used as a positive control. After treatment, cells were washed with PBS, trypsinized and resuspended in binding buffer and stained with 5 μL annexin V-FITC and 10 μL PI (50 μg/mL). The cells were incubated for 15 min at room temperature, in the dark. After incubation, 400 μL of binding buffer was added and cells were analyzed by flow cytometry (BD FACSCaliburTM, USA). Values shown are the mean of three independent experiments.

3.5. Mitochondrial Permeability

Increased mitochondrial permeability and release of pro-apoptotic proteins, e.g., cytochrome c to cytosol occurs prior to apoptosome activation. This transition is in part a result of activation and pore formation of the proapoptotic proteins (bax, bak) in the mitochondrial membrane. A specific dye, 5,5′,6,6′-tetrachloro-1,1′,3,3′-tetraethyl-benzimidazolylcarbocyanine iodide (JC-1), accumulates in mitochondria of normal cells, forming fluorescent aggregates emitting red light. When mitochondria are permeabilized the mitochondrial potential collapses and the dye is no longer concentrated within these organelles. In apoptotic cells JC-1 is dispersed throughout the cytosolic compartment in a monomeric form that emits green fluorescence. Therefore, the ratio between red and green signals indicates whether the mitochondrial potential of a cell is intact or not. To measure mitochondrial membrane potential, the Mitochondrial Permeability Transition Detection Kit JC-1 (ImmunoChemistry Technologies, Bloomington, MN, USA) was used according to the manufacturer's instructions. Briefly, cells were plated at a density of 10^6 cells/well and treated with 500 nM APS8 or 1 μM nicotine for 48 h. Staurosporine (2 μM, 6 h) and carbonylcyanide chlorophenylhydrazone (CCCP) (30 min) were used as a positive control for the induction of apoptosis and for the mitochondria depolarization, respectively. After, harvesting cells were resuspended in Mito PTTM JC-1 solution. After incubation for 15 min at 37 °C, cells were washed in assay buffer to remove any JC-1 excess and resuspended to achieve a cell suspension of 10^6 cells/mL. For each test condition, 100 μL of cell suspension was dispensed into five replicate wells of a black 96 well microtiter plate. Cells were analyzed using a fluorescence plate reader

using an excitation wavelength of 490 nm and emission wavelengths of 527 nm for green fluorescence and 590 nm for red fluorescence, respectively. Changes in mitochondrial potential were assessed by comparing the ratios of red (590 nm) and green (527 nm) fluorescence readings. A decrease of this ratio was accounted to depolarized mitochondria. Values shown are the mean of three independent experiments ± SE.

3.6. Expression of Pro-Apoptotic and Anti-Apoptotic Proteins

Expression of pro- and anti-apoptotic proteins in cells following APS8 or nicotine treatment was measured using a Human Apoptosis Antibody Array (RayBiotech Inc., USA). The Human Apoptosis Antibody Array kit simultaneously detects 43 apoptotic markers in cell lysates. Cells were seeded at a density of 10^6 cells/mL and treated with 500 nM APS8 or 1 μM nicotine. Proteins were extracted using the cell lysis buffer contained within the kit. After lysis by freeze-thawing, and subsequent homogenization, lysates were centrifuged at 10,000× *g* for 5 min at 4 °C and supernatants were stored at −20 °C until further analyses. Protein concentration was determined by BCA Protein Assay Reagent (Pierce, USA). Protein array membranes were immersed in blocking buffer and incubated with 50 μg of proteins overnight at 4 °C. After washing with the kit buffers, samples were incubated overnight with biotinylated detecting antibodies at 4 °C and, after further washing, exposed overnight to Alexa Flour 555-conjugated streptavidin. Slides were completely dried by centrifugation (81,614× *g*, 3 min). Signals in the array membranes were depicted and quantified by a chemiluminescence imaging system with an Axon GenePix laser scanner, using the cy3 channel. For each protein signal, absorbance was determined using the Antibody Array Analysis Tool (Ray Biotech Inc.). Intensities of the individual spots were normalized to the internal positive control (standardized amounts of biotinylated IgG) printed directly onto the array. The expression of proteins was determined by comparing the intensities of the signals in untreated and treated cells. Only expression data on proteins that are directly involved in apoptosis and which showed statistically relevant increase after treatment ($p < 0.05$) are shown. Values shown are the mean of three independent experiments ± SE.

3.7. Caspase-9 Activity

A Caspase-9 Colorimetric Assay Kit (BioVision, USA) was used according to the manufacturer's instructions. The assay is based on the binding of active caspase-9 to the sequence LEHD, which is labeled with a p-nitroanilide (pNA) chromophore. After cleavage from the labeled substrate, pNA absorbance can be quantified spectrophotometrically at 400 nm. Briefly, cells were plated at a density of 10^6 cells/mL and treated with 500 nM APS8 or 1 μM nicotine for 48 h. Proteins were extracted from cells using cell lysis buffer within the kit, and the lysate was centrifuged at 10,000× *g* for 1 min and supernatant was stored at −20 °C. Protein concentration was determined with BCA protein assay. To 150 μg of total protein extract 50 μL of reaction buffer containing 10 mM DTT and 5 μL of 4 mM LEHD-pNA substrate were added. After 2 h incubation at 37 °C, pNA absorbance was quantified at 400 nm (Tecan Genios, Austria). Values shown are the mean of three independent experiments ± SE.

3.8. Effect of APS8 on α7 nAChRs

Xenopus oocyte functional experiments and radioligand binding experiments were performed in order to assess the effects of APS8 to α7 nAChR. Human α7 mRNA was expressed in *Xenopus* frog oocytes, as previously described [51]. Individual oocytes were placed in a 20 μL oocyte perfusion chamber (AutomateScientific, Berkeley, CA, USA) and perfused at room temperature in Frog Ringer's solution (115 mM NaCl, 2.5 mM KCl, 10 mM HEPES, 1.8 mM $CaCl_2$, pH 7.3) containing 1 μM atropine to block potential muscarinic responses. The two-microelectrode voltage-clamp technique was used to measure current responses at a constant holding potential (−60 mV). The electric resistance of the voltage-measuring microelectrode, filled with 3 M KCl solution, was 0.5–3.0 MΩ; the resistance of the current-passing electrode (containing 250 mM CsCl, 250 mM CsF, and 100 mM EGTA) was 0.5–2.0 MΩ. Membrane currents were recorded with an AxoClamp-2 (Axon Instruments, Union City, CA, USA). Sampling rates were between 5 and 10 Hz and the data were filtered at 10 Hz. Acetylcholine (ACh) was rapidly applied using a ValveLink8.2 controller (AutoMate Scientific, Berkeley, CA, USA). ACh applications were 1.0 s in duration, unless otherwise noted. The perfusion rate was 2.0 mL/min. Initially each oocyte received two control applications of a near maximal stimulatory concentration of 1 mM ACh to achieve a consistent response. Clampfit 8.1 (Axon Instruments, USA) was used for data acquisition. The concentration-response curve for APS8 inhibition of the 1 mM ACh response was fitted with a sigmoidal dose-response curve software (Prism 3.0, La Jolla, CA, USA) allowing a variable slope.

APS8 displacement of specific binding of ^{125}I-α-bungarotoxin (α-BTX) to human α7 nAChRs expressed in SHEP-1 cells was measured according to methods essentially as previously described [51]. The membranes (50 μg per tube) were suspended in ice cold binding saline (120 mM NaCl, 5 mM KCl, 2 mM $CaCl_2$, 1 mM $MgCl_2$, 50 mM Tris-Tris-HCl buffer, pH 7.4). Measurements of α7 nAChR affinity were done by displacement of ^{125}I-α-BTX (136 Ci/mmol) binding; these experiments required incubation for three hours at 37 °C to assure equilibration [50]. The cell membranes, ^{125}I-α-BTX (final concentration ~0.2 nM) and APS8 were incubated together in 48 13 × 100 mm disposable glass culture tubes, each possessing a final volume of 0.5 mL. Nonspecific ^{125}I-α-BTX binding was measured in the presence of a final concentration of 1 mM (S)-nicotine hydrogen tartrate salt (Sigma, St. Louis, MO, USA). After incubation, the radioligand bound membranes in each of the 48 tubes were simultaneously collected by vacuum filtration (Brandel cell harvester, Gaithersburg, MD, USA) on Whatman GF/C glass fiber filters pre-soaked in 0.5% polyethylenimine for 45 min to reduce nonspecific binding. The radiolabeled membranes were rapidly washed three times with 3 mL ice-cold binding saline to separate bound from free radioligand. Filters containing ^{125}I-α-BTX bound membranes were placed in 4 mL vials and counted with a Beckman 5500B gamma counter (Fullerton, CA, USA). Displacement assay binding data were analyzed using GraphPad Prism software (San Diego, CA, USA). The mean counts per minute values for each concentration of APS8 were obtained from four replicates. The data were fitted to a sigmoidal concentration response curve from which the Hill slope (n) and IC_{50} (X) values were estimated:

$$Y = \text{Bottom} + (\text{Top} - \text{Bottom})/(1 + 10^{(X - \log(\text{IC50})n)})$$

Here, Top (top of the curve) is the maximal specific binding plateau of radioligand and Bottom (bottom of the curve) is the minimum specific binding plateau observed at high concentrations of the displacing ligand.

3.9. Statistical Analysis

All experiments were repeated three to five times. All data were expressed in terms of mean value and standard deviation. Statistical significance analysis was determined using Student's *t*-test or analysis of variance (ANOVA) followed by Tukey-Kramer multiple comparison. $P < 0.05$ was considered significant.

4. Conclusions

Our data reveal that in the tested cancer cell lines APS8 triggers the intrinsic apoptotic pathway although there is some evidence that it might be also involved in apoptotic response via the extrinsic pathway. While further studies are needed, the present work suggests that compounds with molecular characteristics similar to APS8 might represent a new molecular approach for treating certain types of lung cancer.

Acknowledgments

The authors gratefully acknowledge the Slovenian Research Agency for the financial support (grant to Tom Turk—agreement J1-4044). This research was also partially supported by grants to Rolf Lewensohn from the Swedish Cancer Society (grant agreement 120761) to Rolf Lewensohn and Kristina Viktorsson from the Stockholm Cancer Society (grant agreement 10 1493 and 11 1213) to Rolf Lewensohn from the Swedish Research Foundation (grant agreement 90266701/2009), the Swedish National Board of Health and Welfare, the Stockholm County Council, to Rolf Lewensohn and Kristina Viktorsson from the Karolinska Institutet Research Fund and the European Union (FP7/2007-2013) under grant agreement nº KBBE-2010-266033.

Conflict of Interest

The authors declare no conflict of interest.

References

1. Singhal, S.; Vachani, A.; Antin-Ozerkis, D.; Kaiser, L.; Albelda, S.M. Prognostic implications of cell cycle, apoptosis, and angiogenesis biomarkers in non-small cell lung cancer: A review. *Clin. Cancer Res.* **2005**, *11*, 3974–3986.
2. Petersen, S.; Petersen, S. Towards a genetic-based classification of human lung cancer. *Anal. Cell. Pathol.* **2001**, *22*, 111–121.
3. Wang, Y.; Pereira, E.F.; Maus, A.D.; Ostlie, N.S.; Navaneetham, D.; Lei, S.; Albuquerque, E.X.; Conti-Fine, B.M. Human bronchial epithelial and endothelial cells express a7 nicotinic acetylcholine receptors. *Mol. Pharmacol.* **2001**, *60*, 1201–1209.

4. Plummer, H.K.; Dhar, M.; Schuller, H.M. Expression of the alpha7 nicotinic acetylcholine receptor in human lung cells. *Respir. Res.* **2005**, *6*, 29.
5. Russo, P.; Catassi, A.; Cesario, A.; Servent, D. Development of novel therapeutic strategies for lung cancer: Targeting the cholinergic system. *Curr. Med. Chem.* **2006**, *13*, 3493–3512.
6. Lam, D.C.; Girard, L.; Ramirez, R.; Chau, W.S.; Suen, W.S.; Sheridan, S.; Tin, V.P.; Chung, L.P.; Wong, M.P.; Shay, J.W.; *et al*. Expression of nicotinic acetylcholine receptor subunit genes in non-small-cell lung cancer reveals differences between smokers and nonsmokers. *Cancer Res.* **2007**, *67*, 4638–4647.
7. Schuller, H.M. Is cancer triggered by altered signaling of nicotinic acetylcholine receptors? *Nat. Rev. Cancer* **2009**, *9*, 195–205.
8. Egleton, R.D.; Brown, K.C.; Dasgupta, P. Nicotinic acetylcholine receptors in cancer: Multiple roles in proliferation and inhibition of apoptosis. *Trends Pharmacol. Sci.* **2008**, *29*, 151–158.
9. Lee, W.; Jiang, Z.; Liu, J.; Haverty, P.M.; Guan, Y.; Stinson, Y.; Yue, P.; Zhang, Y.; Pant, K.P.; Bhatt, D.; *et al*. The mutation spectrum revealed by paired genome sequences from a lung cancer patient. *Nature* **2011**, *465*, 473–477.
10. Richman, D.P.; Arnason, B.G. Nicotinic acetylcholine receptor: Evidence for a functionally distinct receptor in human lymphocytes. *Proc. Natl. Acad. Sci. USA* **1979**, *76*, 4632–4635.
11. Grando, S.A.; Horton, R.M.; Pereira, E.F.; Diethelm-Okita, B.M.; George, P.M.; Albuquerque, E.X.; Conti-Fine, B.M. A nicotinic acetylcholine receptor regulating cell adhesion and motility is expressed in human keratinocytes. *J. Investig. Dermatol*. **1995**, *105*, 774–781.
12. Macklin, K.D.; Maus, A.D.; Pereira, E.F.; Albuquerque, E.X.; Conti-Fine, B.M. Human vascular endothelial cells express functional nicotinic acetylcholine receptors. *J. Pharmacol. Exp. Ther.* **1998**, *287*, 435–439.
13. Heeschen, C.; Jang, J.J.; Weis, M.; Pathak, A.; Kaji, S.; Hu, R.S.; Tsao, P.S.; Johnson, F.L.; Cooke, J.P. Nicotine stimulates angiogenesis and promotes tumor growth and atherosclerosis. *Nat. Med.* **2001**, *7*, 833–839.
14. Wessler, I.; Kirkpatrick, C.J. Acetylcholine beyond neurons: The nonneuronal cholinergic system in humans. *Br. J. Pharmacol.* **2008**, *154*, 1558–1571.
15. Carlisle, D.L.; Hopkins, T.M.; Gaither-Davis, A.; Silhanek, M.J.; Luketich, J.D.; Christie, N.A.; Siegfried, J.M. Nicotine signals through muscle-type and neuronal nicotinic acetylcholine receptors in both human bronchial epithelial cells and airway fibroblasts. *Respir. Res.* **2004**, *5*, 1–16.
16. Zeidler, R.; Albermann, K.; Lang, S. Nicotine and apoptosis. *Apoptosis* **2007**, *12*, 1927–1943.
17. Resende, R.R.; Adhikari, A. Cholinergic receptor pathways involved in apoptosis, cell proliferation and neuronal differentiation. *Cell Commun. Signal.* **2009**, *7*, 20.
18. Grozio, A.; Paleari, L.; Catassi, A.; Servent, D.; Cilli, M.; Piccardi, F.; Paganuzzi, M.; Cesario, A.; Granone, P.; Mourier, G.; *et al*. Natural agents targeting the a7-nicotinic–receptor in NSCLC: A promising prospective in anti-cancer drug development. *Int. J. Cancer* **2008**, *122*, 1911–1915.

19. Al-Wadei, H.A.; Al-Wadei, M.H.; Schuller, H.M. Cooperative regulation of non-small cell lung carcinoma by nicotinic and beta-adrenergic receptors: A novel target for intervention. *PLoS ONE* **2012**, *7*, e29915.
20. Paleari, L.; Negri, E.; Catassi, A.; Cilli, M.; Servent, D.; D'Angelillo, R.; Cesario, A.; Russo, P.; Fini, M. Inhibition of nonneuronal a7-nicotinic receptor for lung treatment. *Am. J. Respir. Crit. Care Med.* **2009**, *179*, 1141–1150.
21. Schwartsmann, G. Marine organisms and other novel natural sources of new cancer drugs. *Ann. Oncol.* **2000**, *11*, 235–243.
22. Sipkema, D.; Franssen, M.C.; Osinga, R.; Tramper, J.; Wijffels, R.H. Marine sponges as pharmacy. *Mar. Biotechnol.* **2005**, *7*, 142–162.
23. Mayer, A.M.; Glaser, K.B.; Cuevas, C.; Jacobs, R.S.; Kem, W.R.; Little, R.D.; McIntosh, J.M.; Newman, D.J.; Potts, B.C.; Shuster, D.E. The odyssey of marine pharmaceuticals: A current pipeline perspective. *Trends Pharmacol. Sci.* **2010**, *31*, 255–265.
24. Sepčić, K.; Batista, U.; Vacelet, J.; Maček, P.; Turk, T. Biological activities of aqueous extracts from marine sponges and cytotoxic effects of 3-alkylpyridinium polymers from *Reniera sarai*. *Comp. Biochem. Physiol.* **1997**, *117C*, 47–53.
25. Sepčić, K.; Guella, G.; Mancini, I.; Pietra, F.; Dalla Serra, M.; Menestrina, G.; Tubbs, K.; Maček, P.; Turk, T. Characterization of anticholinesterase-active 3-alkylpyridinium polymers from the marine sponge *Reniera sarai* in aqueous solutions. *J. Nat. Prod.* **1997**, *60*, 991–996.
26. Zovko, A.; Vaukner Gabrič, M.; Sepčić, K.; Pohleven, F.; Jaklič, D.; Gunde-Cimerman, N.; Lu, Z.; Edrada-Ebel, R.; Houssen, W.E.; Mancini, I.; *et al*. Antifungal and antibacterial activity of 3-alkylpyridinium polymeric analogues of marine toxins. *Int. Biodeterior. Biodegrad.* **2012**, *68*, 71–77.
27. Turk, T.; Frangež, R.; Sepčić, K. Mechanisms of toxicity of 3-alkylpyridinium polymers from marine sponge *Reniera sarai*. *Mar Drugs.* **2007**, *5*, 157–167.
28. Paleari, L.; Trombino, S.; Falugi, C.; Gallus, L.; Carlone, S.; Angelini, C.; Sepčić K.; Turk, T.; Faimali, M.; Noonan, D.M.; *et al*. Marine sponge-derived polymeric alkylpyridinium salts as a novel tumor chemotherapeutic targeting the cholinergic system in lung tumors. *Int. J. Oncol.* **2006**, *29*, 1381–1388.
29. Houssen, W.E.; Lu, Z.; Edrada-Ebel, R.A.; Chatzi, C.; Tucker, S.J.; Sepčić, K.; Turk, T.; Zovko, A.; Shen, S.; Mancini, I.; *et al*. Chemical synthesis and biological activities of 3-alkyl pyridinium polymeric analogues of marine toxins. *J. Chem. Biol.* **2010**, *3*, 113–125.
30. Grandič, M.; Sepčić, K.; Turk, T.; Juntes, P.; Frangež, R. *In vivo* toxic and lethal cardiovascular effects of a synthetic polymeric 1,3-dodecylpyridinium salt in rodents. *Toxicol. Appl. Pharmacol.* **2011**, *255*, 86–93.
31. Grandič, M.; Frangež, R. Veterinary Faculty, University of Ljubljana, Ljubljana, Slovenia. Unpublished work, 2012.
32. Uhlen, M.; Oksvold, P.; Fagerberg, L.; Lundberg, E.; Jonasson, K.; Forsberg, M.; Zwahlen, M.; Kampf, C.; Wester, K.; Hober, S.; *et al*. Towards a knowledge-based Human Protein Atlas. *Nat. Biotechnol.* **2010**, *28*, 1248–1250.

33. Lau, J.K.; Brown, K.C.; Thornhill, B.A.; Crabtree, C.M.; Dom, A.M.; Witte, T.W.; Hardman, W.E.; McNees, C.A.; Stover, C.A.; Carpenter, A.B.; *et al*. Inhibition of cholinergic signaling causes apoptosis in human bronchioalveolar carcinoma. *Cancer Res.* **2013**, *73*, 1328–1339.
34. Herbst, R.S.; Heymach, J.V.; Lippman, S.M. Lung cancer. *N. Engl. J. Med.* **2008**, *359*, 1367–1380.
35. Jin, Z.; Xin, M.; Deng, X. Survival function of protein kinase Cι as a novel nitrosamine 4-(methylnitrosamino)-1-(3-pyridyl)-1-butanone-activated bad kinase. *J. Biol. Chem.* **2005**, *280*, 16045–16052.
36. Zhang, Q.; Tang, X.; Zhang, Z.F.; Velikina, R.; Shi, S.; Le, A.D. Nicotine induces hypoxia-inducible factor-1alpha expression in human lung cancer cells via nicotinic acetylcholine receptor-mediated signaling pathways. *Clin. Cancer Res.* **2007**, *13*, 4686–4694.
37. Ray, M.R.; Jablons, D.; He, B. Lung cancer therapeutics that target signaling pathways: An update. *Expert Rev. Respir. Med.* **2010**, *4*, 631–645.
38. Dasgupta, P.; Rastogi, S.; Pillai, S.; Ordonez-Ercan, D.; Morris, M.; Haura, E.; Chellappan, S. Nicotine induces cell proliferation by beta-arrestin-mediated activation of Src and Rb-Raf-1 pathways. *J. Clin. Investig.* **2006**, *116*, 2208–2217.
39. Xin, M.; Deng, X. Nicotine inactivation of the proapoptotic function of bax through phosphorilation. *J. Biol. Chem.* **2005**, *280*, 10781–10784.
40. Le Novere, N.; Changeux, J.P. Molecular evolution of the nicotinic acetylcholine receptor: An example of multigene family in excitable cells. *J. Mol. Evol.* **1995**, *40*, 155–172.
41. Reed, J.C. Proapoptotic multidomain bcl-2/bax-family proteins: Mechanisms, physiological roles and therapeutic opportunities. *Cell Death Differ.* **2006**, *13*, 1378–1386.
42. Kroemer, G.; Galluzzi, L.; Brenner, C. Mitochondrial membrane permeabilization in cell death. *Physiol. Rev.* **2007**, *87*, 99–163.
43. LaCasse, E.C.; Mahoney, D.J.; Cheung, H.H.; Plenchette, S.; Baird, S.; Korneluk, R.G. IAP-targeted therapies for cancer. *Oncogene* **2008**, *27*, 6252–6275.
44. Dasgupta, P.; Kinkade, R.; Joshi, B.; DeCook, C.; Haura, E.; Chellappan, S. Nicotine inhibits apoptosis induced by chemotherapeutic drugs by up-regulating XIAP and survivin. *Proc. Natl. Acad. Sci. USA* **2006**, *103*, 6332–6337.
45. Wallach, D.; Varfolomeev, E.E.; Malinin, N.L.; Goltsev, Y.V.; Kovalenko, A.V.; Boldin, M.P. Tumor necrosis factor receptor and Fas signaling mechanisms. *Annu. Rev. Immunol.* **1999**, *17*, 331–367.
46. Li, H.; Zhu, H.; Xu, C.J.; Yuan, J. Cleavage of bid by caspase 8 mediates the mitochondrial damage in the Fas pathway of apoptosis. *Cell* **1998**, *94*, 491–501.
47. Giard, D.J.; Aaronson, S.-A.; Todaro, G.J.; Arnstein, P.; Kersey, J.H.; Dosik, H.; Parks, W.P. *In vitro* cultivation of human tumors: Establishment of cell lines derived from a series of solid tumors. *J. Natl. Cancer Inst.* **1973**, *51*, 1417–1423.
48. Jacobs, J.P.; Jones, C.M.; Baille, J.P. Characteristics of a human diploid cell designated MRC-5. *Nature* **1970**, *227*, 168–170.
49. Fogh, J. *Human Tumor Cells in Vitro*; Plenum Press: New York, NY, USA, 1975; pp. 115–141.

50. Mosmann, T. Rapid colorimetric assay for cellular growth and survival: Application to proliferation and cytotoxicity assays. *J. Immunol. Methods* **1983**, *65*, 55–63.
51. Kem, W.R.; Mahnir, V.M.; Prokai, L.; Papke, R.M.; Cao, X.F.; LeFrancois, S.; Wildeboer, K.; Porter-Papke, J.; Prokai-Tatrai, K.; Soti, F. Hydroxy metabolites of the Alzheimer's drug candidate DMXBA (GTS-21): Their interactions with brain nicotinic receptors.; and brain penetration. *Mol. Pharmacol.* **2004**, *65*, 56–67.

Proteomic Investigation of the Sinulariolide-Treated Melanoma Cells A375: Effects on the Cell Apoptosis through Mitochondrial-Related Pathway and Activation of Caspase Cascade

Hsing-Hui Li, Jui-Hsin Su, Chien-Chih Chiu, Jen-Jie Lin, Zih-Yan Yang, Wen-Ing Hwang, Yu-Kuei Chen, Yu-Hsuan Lo and Yu-Jen Wu

Abstract: Sinulariolide is an active compound isolated from the cultured soft coral *Sinularia flexibilis*. In this study, we investigated the effects of sinulariolide on A375 melanoma cell growth and protein expression. Sinulariolide suppressed the proliferation and migration of melanoma cells in a concentration-dependent manner and was found to induce both early and late apoptosis by flow cytometric analysis. Comparative proteomic analysis was conducted to investigate the effects of sinulariolide at the molecular level by comparison between the protein profiles of melanoma cells treated with sinulariolide and those without treatment. Two-dimensional gel electrophoresis (2-DE) master maps of control and treated A375 cells were generated by analysis with PDQuest software. Comparison between these maps showed up- and downregulation of 21 proteins, seven of which were upregulated and 14 were downregulated. The proteomics studies described here identify some proteins that are involved in mitochondrial dysfunction and apoptosis-associated proteins, including heat shock protein 60, heat shock protein beta-1, ubiquinol cytochrome c reductase complex core protein 1, isocitrate dehydrogenase (NAD) subunit alpha (down-regulated), and prohibitin (up-regulated), in A375 melanoma cells exposed to sinulariolide. Sinulariolide-induced apoptosis is relevant to mitochondrial-mediated apoptosis via caspase-dependent pathways, elucidated by the loss of mitochondrial membrane potential, release of cytochrome c, and activation of Bax, Bad and caspase-3/-9, as well as suppression of p-Bad, Bcl-xL and Bcl-2. Taken together, our results show that sinulariolide-induced apoptosis might be related to activation of the caspase cascade and mitochondria dysfunction pathways. Our results suggest that sinulariolide merits further evaluation as a chemotherapeutic agent for human melanoma.

Reprinted from *Mar. Drugs*. Cite as: Li, H.-H.; Su, J.-H.; Chiu, C.-C.; Lin, J.-J.; Yang, Z.-Y.; Hwang, W.-I.; Chen, Y.-K.; Lo, Y.-H.; Wu, Y.-J. Proteomic Investigation of the Sinulariolide-Treated Melanoma Cells A375: Effects on the Cell Apoptosis through Mitochondrial-Related Pathway and Activation of Caspase Cascade. *Mar. Drugs* **2013**, *11*, 2625-2642.

1. Introduction

Melanoma, the deadliest form of skin cancer, is a malignant tumor of cutaneous melanocytes. The incidence rates of melanoma continue to rapidly rise throughout the world [1]. According to an estimation of the American Cancer Society, invasive melanoma diagnoses were estimated to have reached 70,230 cases in 2011 in the United States [2]. Metastatic melanoma is mostly incurable in diagnosed patients, because melanoma does not respond to most systemic treatments [3–5].

For patients with malignant melanoma, surgery is the most essential treatment [6,7]. Other medical measures such as chemotherapy and cytokine therapy have also been investigated. However, dacarbazine, the most active single agent against melanoma, has a response rate of approximately 15%–25% [8,9]. Cytokine therapy using high-dose interleukin (IL)-2 has an overall response rate of 12.5%, but the response rate does not approach that of dacarbazine [10,11]. Hence, malignant melanoma is an urgent medical and therapeutic issue. It is important to find new drugs and develop therapies against this highly malignant tumor.

Recently, many studies have analyzed marine biologically active compounds to discover new therapeutic drugs for the prevention or inhibition of cancer development [12–17]. Sinulariolide, an active compound isolated from the cultured soft coral *Sinularia flexibilis*, has been shown to have various biological properties, including anti-microbial and anti-bladder cancer activities [18,19]. In the current investigation, the effects of sinulariolide on melanoma cells were evaluated in terms of cell viability, cell migration, and flow cytometric analysis. The results indicated anti-tumor and apoptosis-induced effects of sinulariolide on A375 melanoma cells. A comparative proteomics analysis was performed to investigate the effects of sinulariolide on A375 melanoma cells. Several differential proteins identified after sinulariolide treatment by liquid chromatography-tandem mass spectrometry (LC-MS/MS) analysis were characterized as potential anti-cancer protein markers. Western blotting analysis was carried out to confirm the changes of protein expressions, which are associated with energy metabolism and cell apoptosis. Overall, these results could provide valuable information for drug development or potential strategies against human melanoma.

2. Results

2.1. The Cytotoxicity and Anti-Migratory Effects of Sinulariolide on A375 Cells

The potential cytotoxic effects of sinulariolide on human melanoma A375 cells were examined by methylthiazoletetrazolium (MTT) assay, morphological changes and cell migration assay. Figure 1A displays the cytotoxic effects of various concentrations of sinulariolide (1, 5, 10, 15, 20 μg/mL) on A375 melanoma cells. The results of the MTT assay revealed that sinulariolide concentration-dependently inhibited the proliferation of A375 melanoma cells (* $p < 0.001$, $^{\#}$ $p < 0.05$) (Figure 1A). Morphological changes of sinulariolide-treated cells were observed by inverted light microscopy. The cell population of A375 cells obviously decreased after treatment with 10 and 15 μg/mL sinulariolide (Figure 1B). Data from the cell migration assay showed that 5–15 μg/mL sinulariolide suppressed A375 melanoma cell migration in a concentration-dependent manner, with suppression rates of approximately 21%, 42% and 72% for 5, 10 and 15 μg/mL sinulariolide treatment, respectively (Figure 1C,D).

Figure 1. Evaluation of the cell cytoxicity and anti-migratory effects of sinulariolide on A375 melanoma cells. (**A**) The cell viability of A375 melanoma cells was found to be concentration-dependently suppressed by methylthiazoletetrazolium (MTT) assay (* $p < 0.001$, # $p < 0.05$); (**B**) Reduced cell population and morphological changes of A375 melanoma cells treated with different concentrations of sinulariolide (5, 10 and 15 μg/mL); (**C** and **D**) Sinulariolide from 5 to 15 μg/mL concentration-dependently decreased A375 cell migration (* $p < 0.001$). C: control, DMSO-treated cells. Scale bar (**B**,**C**) = 20 μm.

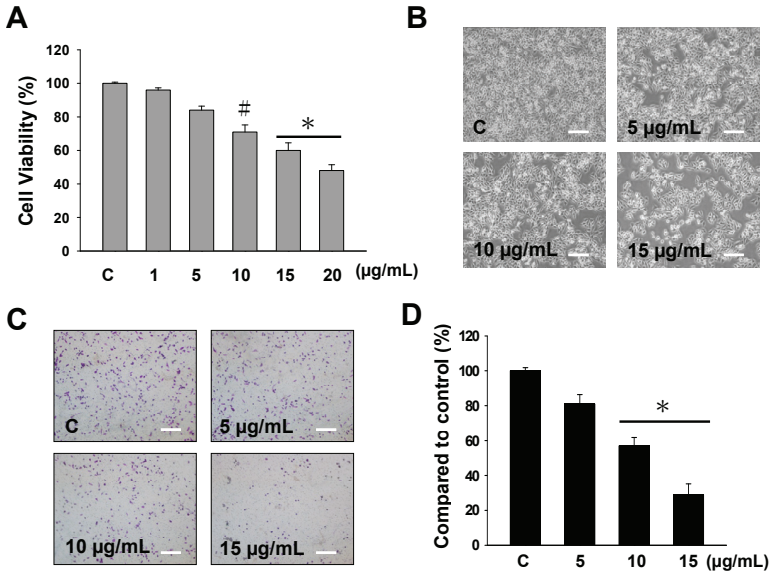

2.2. Apoptosis Was Triggered by Sinulariolide in A375 Cells

It has previously been shown that sinulariolide induced apoptosis of TSGH cells [18]. A375 cells showed growth inhibition with sinulariolide treatment in a concentration-dependent manner. To investigate whether sinulariolide also induced apoptosis in melanoma cells, A375 cells were exposed to sinulariolide and were analyzed by flow cytometry-based annexin V-fluoresceinisothiocyanate (FITC)/porpidium iodide (PI) double staining using a flow cytometer. After treatment with control, 5, 10 and 15 μg/mL of sinulariolide, the percentages of cells displaying early apoptosis/late apoptosis were 2.8%/1.7%, 7.6%/2.0%, 20.2%/5.8% and 15.6%/18.7%, respectively (Figure 2A). These data showed that sinulariolide efficiently induced apoptosis of A375 cells. To further validate the sinulariolide-induced apoptosis of A375 cells, 4′,6-diamidino-2-phenyl iodide (DAPI) and Terminal deoxynucleotidyl transferase dUTP nick end labeling (TUNEL) stained assays were performed to evaluate the apoptosis. The results showed that massive apoptotic bodies were induced in A375 cells treated with 15 μg/mL of sinulariolide (Figure 2B). Altogether, these results demonstrated that treatment with sinulariolide is able to induce both early and late apoptosis in A375 melanoma cells.

Figure 2. Sinulariolide-induced cell apoptosis of A375 melanoma cells. (**A**) Detection of apoptotic A375 cells after sinulariolide treatment by annexin V-fluoresceinisothiocyanate (FITC)/porpidium iodide (PI) analysis. Sinulariolide elevated early and late apoptosis in a concentration-dependent manner; (**B**) Detection of apoptotic cells by 4′,6-diamidino-2-phenyl iodide (DAPI) and terminal deoxynucleotidyl transferase dUTP nick end labeling (TUNEL) staining assay. A375 cells were treated with DMSO or sinulariolide at final concentrations of 5, 10 and 15 μg/mL for 24 h. Cells were harvested for DAPI and TUNEL staining as described in Materials and Methods. Scale bar = 50 μm.

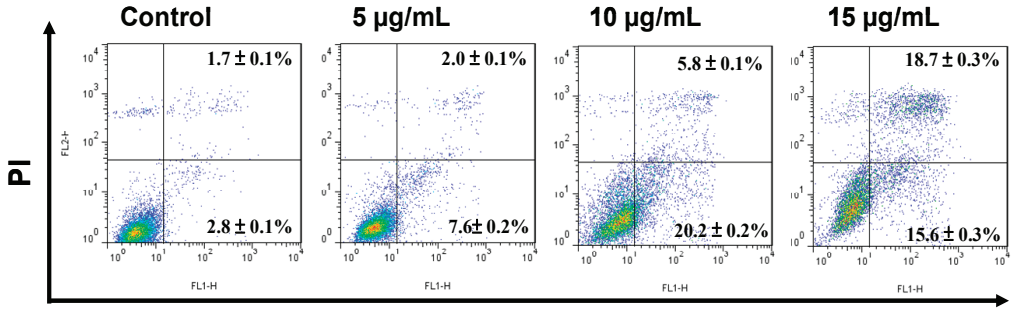

(**A**)

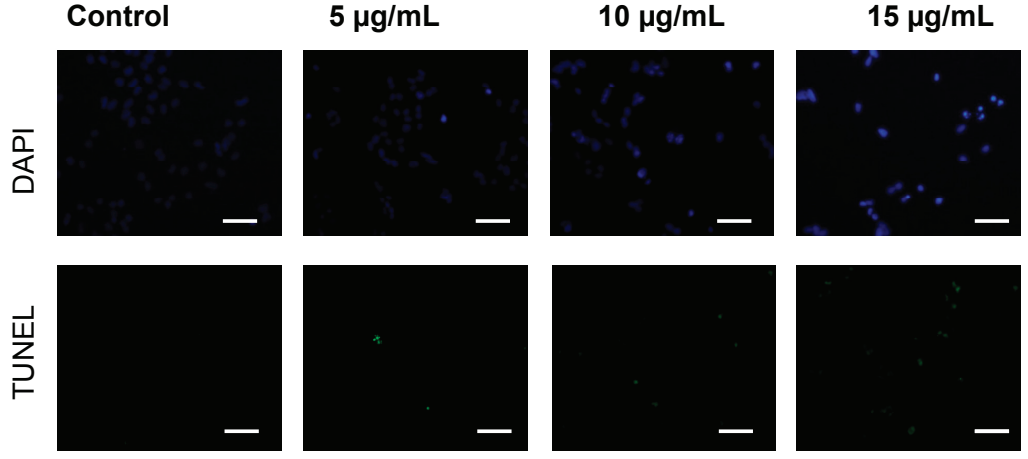

(**B**)

2.3. Proteomic Analysis of A375 Cells Treated with Sinulariolide

Proteomic analysis was used for the identification of differentially expressed proteins between control and sinulariolide-treated A375 cells. A375 cells were treated with 15 μg/mL sinulariolide for 24 h and then harvested. Total proteins were extracted from cultured cells with lysis buffer and subjected to two-dimensional gel electrophoresis (2-DE). A total of 100 μg protein was dissected with 2-DE (*p*I 4–7) and visualized by silver staining (Figure 3A). PDQuest image analysis software (Bio-Rad, Hercules, CA, USA) was employed for the detection of differential protein spots, which were defined as proteins showing a more than one and a half-fold intensity difference in 2-DE maps between the treated A375 cells and the control samples. Protein identification was carried out by LC-MS/MS analysis after gel digestion. MASCOT protein identification search software was used for the identification of the differential protein spots. A total of 21 differential protein spots were successfully identified. A list of the identified proteins with their MASCOT scores, theoretical MW/*p*I, tandem mass spectrometry (MS/MS) matched sequences, coverage, and fold changes in expression levels (upregulation or downregulation) is given in Table 1. There were seven differential proteins upregulated after sinulariolide treatment: Rho GDP-dissociation inhibitor 1, transitional endoplasmic reticulum ATPase, Lamin-A/C, stomatin-like protein 2, prohibitin, translation initiation factor eIF-2B subunit alpha and retinal dehydrogenase 2. A total of 14 differential proteins were downregulated after sinulariolide treatment: Calreticulin, vimentin, 60 kDa heat shock protein (Hsp60), ubiquinol cytochrome c reductase complex core protein 1 (UQCRC1), glutathione synthetase, DnaJ homolog subfamily B member 11, nucleophosmin, reticulocalbin-1, protein disulfide-isomerase, platelet-activating factor acetylhydrolase IB subunit beta, heterogeneous nuclear ribonucleoprotein F (hnRNP F), heat shock protein beta-1 (HspB1), isocitrate dehydrogenase (NAD) subunit alpha (IDH) and pyruvate dehydrogenase E1 component subunit beta. Differential proteins such as UQCRC1, IDH, prohibitin, Hsp60 and HspB1 are associated with anti-proliferation and induction of apoptosis, and the changes in these proteins were verified by western blot. Altogether, the differentially expressed proteins validated by western blot analysis were in agreement with the 2-DE data (Figure 3B).

Figure 3. (**A**) Protein spots marked on the maps were considered differentially expressed as identified by liquid chromatography-tandem mass spectrometry (LC-MS/MS). The results were repeated three times; (**B**) Western blotting assay to validate the selected proteins identified by 2-DE, including isocitrate dehydrogenase (NAD) subunit alpha (IDH), heat shock protein beta-1 (HspB1), prohibitin, Hsp60, and ubiquinol cytochrome c reductase complex core protein 1 (UQCRC1). T: treatment; C: control, DMSO-treated cells. β-actin was used as the internal control.

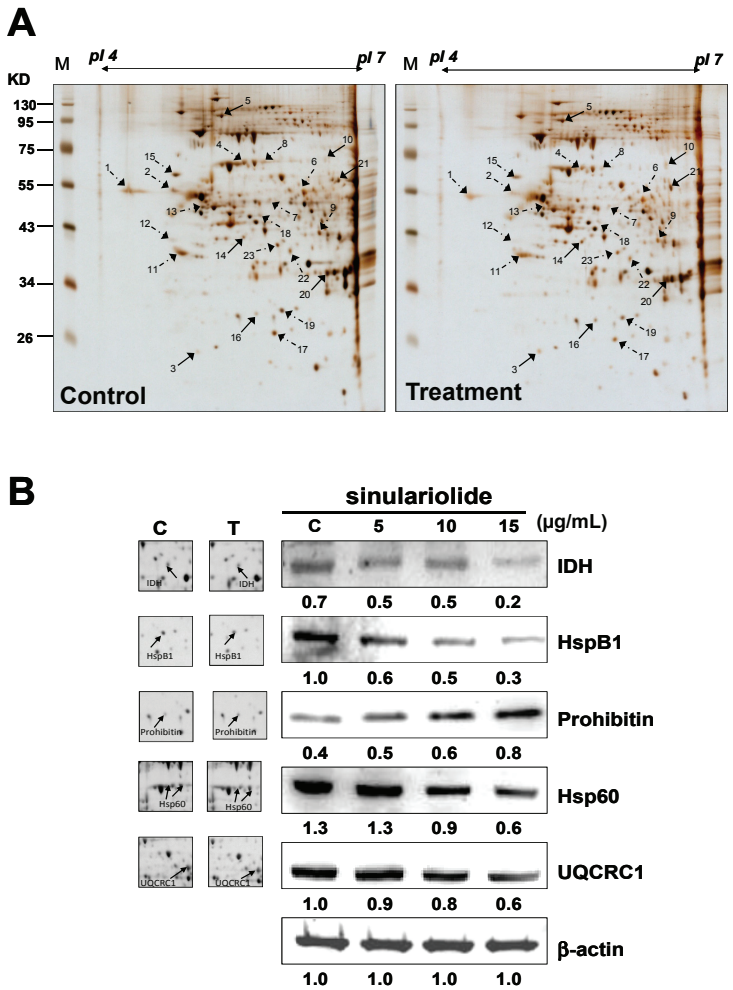

Table 1. Protein identification by LC/MS/MS.

Spot No.	Protein name	Accession No.	Calculated Mw/*p*I	Peptide matched	Sequence covered %	MASCOT score	Regulation (fold change) *
1	Calreticulin precursor	P27797	48.11/4.29	35	40	251	−1.6
2	Vimentin	P08670	53.61/5.06	26	39	272	−2.2
3	Rho GDP-dissociation inhibitor 1 (Rho-GDI)	P52565	23.19/5.02	5	26	68	+2.3
4	60 kDa heat shock protein (Hsp60)	P10809	61.01/5.7	51	47	545	−2.6
5	Transitional endoplasmic reticulum ATPase	P55072	89.26/5.14	49	47	439	+1.8
6	Ubiquinol cytochrome c reductase complex core protein 1 (UQCRC1)	P31930	52.61/5.94	5	10	53	−1.9
7	Glutathione synthetase	P48637	52.35/5.67	5	10	123	−2.8
8	60 kDa heat shock protein (Hsp60)	P10809	61.01/5.7	3	8	66	−2.5
9	DnaJ homolog subfamily B member 11 precursor	Q9UBS4	40.48/5.81	3	9	40	−2.2
10	Lamin-A/C (70 kDa lamin)	P02545	74.09/6.57	3	10	71	+1.8
11	Nucleophosmin (NPM)	P06748	32.55/4.64	28	39	216	−1.9
12	Reticulocalbin-1 precursor	Q15293	38.86/4.86	4	9	84	−2.4
13	Vimentin	P08670	53.61/5.06	7	8	101	−1.7
14	Stomatin-like protein 2	Q9UJZ1	38.51/6.88	29	46	331	+2.0
15	Protein disulfide-isomerase precursor (PDI)	P07237	57.08/4.76	23	35	205	−2.1
16	Prohibitin	P35232	29.78/5.57	45	67	660	+1.8
17	Platelet-activating factor acetylhydrolase IB subunit beta	P68402	25.55/5.57	4	9	46	−2.2
18	Heterogeneous nuclear ribonucleoprotein F	P52597	45.64/5.38	8	21	121	−1.8
19	Heat shock protein beta-1 (HspB1)	P04792	22.76/5.98	9	15	102	−2.6
20	Translation initiation factor eIF-2B subunit alpha	Q14232	33.69/6.9	1	4	47	+2.5
21	Retinal dehydrogenase 2	O94788	56.68/5.79	3	2	54	+2.3
22	Isocitrate dehydrogenase (NAD) subunit alpha (IDH)	P50213	39.56/6.47	10	17	148	−1.9
23	Pyruvate dehydrogenase E1 component subunit beta	P11177	39.19/6.2	3	10	68	−1.5

* Regulation (fold change) of differentially-expressed proteins was calculated after 24 h of sinulariolide treatment.

2.4. Sinulariolide Induced Mitochondrial Depolarization and Activated the Mitochondrial-Related Pathway, Resulting in Cell Apoptosis

From the 2-DE results, some mitochondrial-related proteins were identified upon sinulariolide treatment, such as IDH and UQCRC1, which are involved in energy production. Therefore, we measured the loss of mitochondrial membrane potential (ΔΨm) induced by sinulariolide using JC-1 dye. Fluorescence microscopy showed that untreated melanoma cells had strong red fluorescence (J-aggregation) and weak green florescence (JC-1 monomer). However, many 15 μg/mL sinulariolide-treated A375 cells showed a significant reduction in red fluorescence and increased signals of green fluorescence due to loss of ΔΨm following treatment with sinulariolide (Figure 4A). The mitochondrial-related apoptosis pathway plays an important role in apoptosis. To verify this mitochondrial-related apoptosis pathway, we further analyzed several mitochondrial-related apoptotic markers, such as Bax, Bad, p-Bad, cytosolic cytochrome c, endo G, apoptosis-inducing factor (AIF), Bcl-2, and Bcl-xL. The results are displayed in Figure 4B, and show that sinulariolide significantly increases the expression levels of Bax, Bad, AIF, endo G and cytosolic cytochrome c in A375 cells. In contrast, the expression levels of Bcl-2, Bcl-xL, and p-Bad decrease after sinulariolide treatment.

Figure 4. Sinulariolide induced apoptosis via mitochondria potential (ΔΨm) change and the mitochondria-related pathway in A375 melanoma cells. (**A**) A375 melanoma cells were treated with or without sinulariolide. The mitochondria potential change in melanoma cells was detected by staining with JC-1 and was analyzed by fluorescence microscopy; (**B**) Western blotting data showed the changes of Bcl-2, Bcl-xL, Bax, Bad, p-Bad, cytosolic cytochrome c, AIF, and endo G expression in melanoma cells treated with different concentrations of sinulariolide. Scale bar = 50 μm. β-actin was used as the internal control.

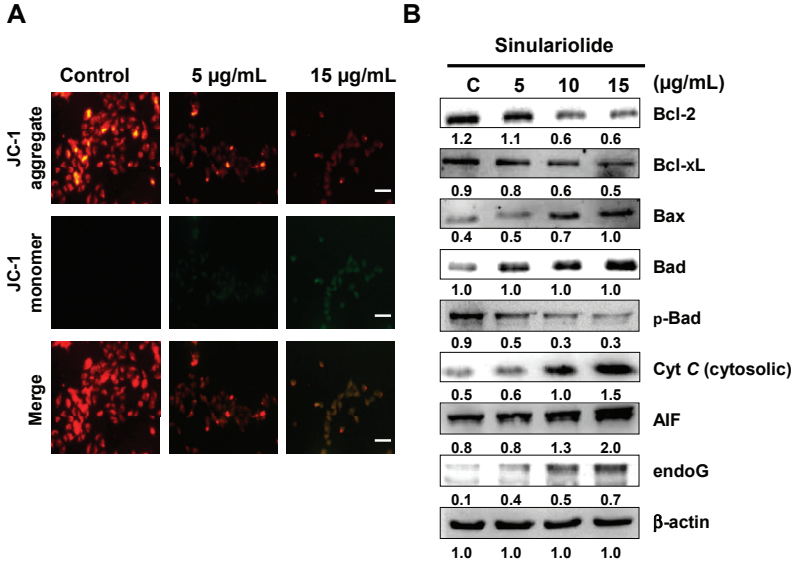

2.5. Sinulariolide Activates the Caspase-Dependent Pathway, Leading to Cell Apoptosis

Differential expression levels of caspase-3, caspase-8 and caspase-9 have been reported to be involved in the cell apoptosis pathway. In Figure 5A, western blotting data showed that the expression levels of both pro-caspase-3 and pro-caspase-9 were decreased in the sinulariolide-treated cells. The expression levels of cleaved-caspase-3 (17 kDa proteolytic fragments) and cleaved-caspased-9 (37 kDa proteolytic fragments) were elevated after sinulariolide treatment. The expression level of caspase-8 did not change. Similarly, cleaved-poly ADP ribose polymerase (PARP) (89 kDa proteolytic fragments) also increased in expression upon sinulariolide treatment (Figure 5A). These results showed that the caspase-dependent pathway was activated upon sinulariolide treatment. We examined whether caspase activation was involved in sinulariolide-induced cell apoptosis. Three caspase inhibitors, Z-DEVD-FMK (caspase-3 inhibitor), Z-IETD-FMK (caspase-8 inhibitor), and Z-LEHD-FMK (caspase-9 inhibitor), were used to examine whether they were able to block sinulariolide-induced cell apoptosis. Only Z-DEVD-FMK and Z-LEHD-FMK inhibited the sinulariolide-induced cell apoptosis (Figure 5B). These data suggest that caspase-3 and caspase-9 but not caspase-8 are involved in melanoma cell apoptosis after sinulariolide treatment.

Figure 5. Sinulariolide induced apoptosis through the caspase-dependent pathway. (**A**) Representative western blots showing changes in the apoptosis-associated protein expression levels after treatment with sinulariolide in A375 melanoma cells; (**B**) Caspase-3, -8, and -9 inhibitors affected the A375 melanoma cell viability after sinulariolide treatment. Cells were seeded on to a 24-well plate and pretreated with or without Z-DEVD-FMK, Z-IETD-FMK and Z-LEHD-FMK, followed by treatment with 15 μg/mL sinulariolide. The cells were then harvested at 24 h and subjected to MTT assay for the evaluation of cell viability. $^{\#}$ $p < 0.05$ as compared to the control groups.

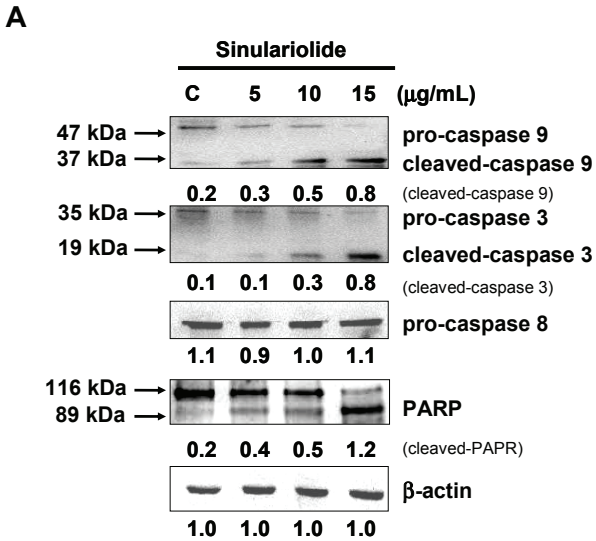

Figure 5. *Cont.*

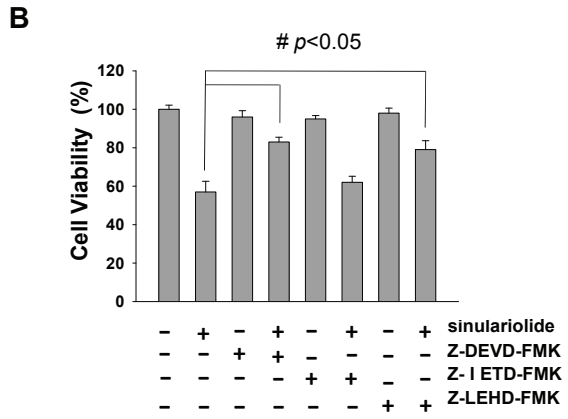

3. Discussion

In the current study, sinulariolide, isolated from the cultured soft coral *Sinularia flexibilis*, exerted cell cytotoxic and apoptosis-inducing effects on A375 melanoma cells. Our study examined the effects of sinulariolide on the cell viability. Morphological changes and migration demonstrated a concentration-dependent effect (Figure 1). The induction of apoptosis was determined by annexin V-FITC/PI staining using a flow cytometer. Treatment with sinulariolide concentration-dependently increased the early and late apoptotic rates in A375 melanoma cells (Figure 2). These results demonstrate that sinulariolide exerts anti-proliferation and apoptosis-inducing activities against melanoma cells.

The proteomic data could provide clues for the investigation of potential markers and apoptosis-inducing effects of sinulariolide on A375 melanoma cells at the molecular level. Proteins related to the effects of sinulariolide were identified by comparative proteomic analysis. We found that changes in some crucial proteins, such as Hsp60, HspB1, prohibitin, IDH, and UQCRC1, were associated with apoptosis or the mitochondrial function against melanoma cells. Hsp60 siRNA induces mitochondrial dysfunction and activates both p53-dependent and mitochondrial apoptosis [20]. HspB1, also known as heat shock protein 27, has been indicated to be a critical marker in several cancer cells [21]. Hsp B1 (Hsp27) siRNA leads to downregulation of Bcl-2 and upregulation of Bax [22]. Our previous work has shown downregulation of Hsp60 in BFTC bladder cancer cells treated with 13-acetoxysarcocrasslide and CAL-27 oral squamous cell carcinoma treated with 11-dehydrosinulariolide, which exerts anti-tumor effects *in vitro* [13,23]. Recent results have shown that treatment with sinulariolide significantly enhances apoptosis in A375 melanoma cells and reduces the Hsp60 and Hsp27 expression levels. Prohibitin, which is located in mitochondria, was found to regulate apoptosis, cellular signaling, cell migration, and cell proliferation, and stabilize mitochondria proteins [24–27]. The translocation of prohibitin to mitochondria couples with simultaneous translocation of p53, which is highly correlated with inhibition of cancer growth. Up-regulation of IDH has been reported to correlate with the metastasis of human breast cancer [28]. Inhibition of IDH resulted in curcumin-induced apoptosis in HCT116 colon cancer cells [29].

UQCRC1 is a key subunit of complex III of the mitochondrial respiratory chain. Up-regulation of UQCRC1 might contribute to the rapid proliferation of cancer cells by increased synthesis of ATP. Some anti-cancer drugs can inhibit the mitochondrial respiratory chain at complex III [30]. This suggests that the anti-cancer effects of sinulariolide may be correlated with mitochondrial function in A375 cells and associated with the reduction of IDH and UQCRC1 and enhancement of prohibitin.

The apoptosis-induced activity is a good basis for anti-cancer therapies and also a valuable guide to predict tumor response after anticancer administered treatment. The specific induction of human cancer cell apoptosis using chemotherapy critically benefits anti-cancer drug development [12]. Apoptotic processes can be divided into two major pathways: One is mediated by the plasma membrane (extrinsic pathways) and one is mediated by cells (intrinsic pathways) [31]. The intrinsic pathways that initiate apoptosis involve a large number of intracellular signals that are located in the endoplasmic reticulum or mitochondria [32]. In the mitochondria-dependent apoptotic pathway, the suppression of anti-apoptotic proteins such as Bcl-xL, Bcl-2 and Mcl-1, and activation of pro-apoptotic Bax, Bid and Bak, have been reported to alter the mitochondrial membrane potential and release mitochondrial apoptotic factors [33].

Loss of mitochondrial membrane potential leads to the release of cytochrome c, AIF and endo G from mitochondria. AIF and endo G, which are known to induce caspase-independent apoptosis, might be released into the cytosol upon loss of mitochondrial membrane potential. Cytochrome c is released from mitochondrial inter-membrane spaces and then binds to ARAF1, leading to the activation of caspase-9 and further activating the downstream effector caspase-3. Activation of caspase-3 subsequently cleaves poly (ADP-ribose) polymerase (PARP), which is further activated [34]. Thus, sinulariolide induces apoptosis in A375 cells through the mitochondria intrinsic pathway. We found that sinulariolide treatment resulted in reduced levels of mitochondrial membrane potential and led to the release of cytochrome c, AIF and endo G from mitochondria (Figure 4). Furthermore, sinulariolide also suppressed anti-apoptotic factors Bcl-2, Bcl-xL and Mcl-1 but promoted pro-apoptotic factors Bad and Bax (Figure 4). Sinulariolide treatment resulted in concentration-dependent activation of caspase-3, caspase-9 and PARP (Figure 5). The present data support that sinulariolide can induce apoptosis of A375 cells through activation of the caspase cascade.

Overall, our results indicate that sinulariolide increases apoptosis of A375 cells, which is associated with the intrinsic mitochondria dysfunction pathway and activation of the caspase cascade.

4. Materials and Methods

4.1. Materials

Immobilized pH gradient (IPG) buffer and isoelectric focusing (IEF) strips were purchased from GE Healthcare (Buckinghamshire, UK). Cell Extraction Buffer was obtained from BioSource International (Camarillo, CA, USA). Rabbit anti-human AIF, endo G and prohibitin antibodies were obtained from Epitomics (Burlingame, CA, USA). Rabbit anti-human Hsp60, HspB1, UQCRC1 and IDH antibodies were obtained from ProteinTech Group (Chicago, IL, USA). Rabbit anti-human pro-casapse-3, pro-caspase-9, pro-caspase-8, cleaved caspase-3, cleaved caspase-9, PARP, cytochrome c, Bax, Bad, p-Bad, Bcl-2 and Bcl-xL antibodies were obtained from Cell Signaling

Technology (Danvers, MA, USA). Protease inhibitor cocktail, dimethyl sulfoxide (DMSO), Z-DEVD-FMK (caspase-3 inhibitor), Z-IETD-FMK (caspase-8 inhibitor), Z-LEHD-FMK (caspase-9 inhibitor), 3-(4,5-dimethylthiazol-2-yl)-2,5-diphenyltetrazolium bromide (MTT), and rabbit anti-human β-actin antibodies were obtained from Sigma (St. Louis, MO, USA). Polyvinylidene difluoride (PVDF) membranes and goat anti-rabbit and horseradish peroxidase conjugated IgG were obtained from Millipore (Bellerica, MA, USA). Chemiliminescent horseradish peroxidase (HRP) substrate was from Pierce (Rockford, IL, USA). A DAPI fluorescent kit was obtained from Promega (Madison, WI, USA). Sinulariolide was isolated from the cultured soft coral *Sinularia flexibilis* according to the reported procedures [35]. DMSO was used to dissolve sinulariolide.

4.2. Cell Culture

A375 melanoma cells were purchased from the Food Industry Research and Development Institute (Hsinchu, Taiwan) and were grown in DMEM (Biowest, Nuaillé, France), 4 mM L-glutamine, 10% (v/v) fetal bovine serum, 100 μg/mL streptomycin, 100 U/mL penicillin and 1 mM sodium pyruvate in a humidified atmosphere of 5% CO_2 in air at 37 °C.

4.3. Determination of Cell Viability

The cell viability effect of sinulariolide against A375 cells was examined by calorimetric tetrazolium (MTT) assay [14]. Briefly, A375 cells were seeded in 96-well plates at a density of $1 \times 10^5/cm^2$ in complete medium (with 10% fetal bovine serum) and treated with different concentrations of sinulariolide (1, 5, 10, 15 and 20 μg/mL) for 24 h. Cells treated with DMSO without sinulariolide were used as a blank control. After incubation, cells were washed and 50 μL MTT solution added (1 mg/mL in phosphate buffered saline (PBS) buffer) at 37 °C for 4 h. Then, cells were lysed with 200 μL DMSO. The absorbance was determined at 595 nm on a microtiter plate ELISA reader (Bio-Rad, Hercules, CA, USA) with DMSO as the blank. All experiments were carried out in triplicate to confirm the reproducibility, and the results of three independent experiments were used for statistical analysis.

4.4. Cell Migration Assay

The cell migration assay was performed according to the methods described by Su *et al.* [36]. A375 melanoma cells were seeded onto a Boyden chamber (Neuro Probe, Cabin John, MD, USA) at 10^4 cells/well in serum-free media for 24 h. Melanoma cells with or without sinulariolide treatment were allowed to migrate for 24 h. The migrated cells on the lower site were fixed with 100% methanol and then stained with 5% Giemsa (Merck, Germany). Cell numbers were observed and counted using a 100× light microscope.

4.5. Quantitative Detection of Apoptosis by Flow Cytometry

To determine the apoptosis induced by sinulariolide in A375 melanoma cells, an annexin V-FITC Apoptosis Detection kit (Pharmingen, San Diego, CA, USA) was used and the method was as according to a previous study [37]. A total of 1×10^6 cells were seeded onto a 5-cm Petri dish and treated with or without sinulariolide for 24 h, and subsequently cells were stained with annexin V-FITC and propidium iodide (PI) for 30 min at 37 °C according to the manufacturer's protocol. Apoptotic cells were then assessed using a FACScan flow cytometer and Cell-Quest software (Becton-Dickinson, Mansfield, MA, USA).

4.6. Protein Extraction and Concentration Estimation

A375 melanoma cells were treated without or with various concentrations of sinulariolide (0, 5, 10 and 15 μg/mL) for 24 h and then lysed with Cell Extraction Buffer (BioSource). The total protein in the supernatant was then precipitated out by triple the volume of 10% trichloroacetic acid (TCA)/acetone solution overnight at −20 °C. The precipitated proteins were suspended in a rehydration buffer (6 M urea, 2 M thiourea, 0.5% IPG buffer, 0.5% 3-[(3-cholamidopropyl) dimethylammonio]-1-propanesulfonate (CHAPS), 20 mM dithiothreitol (DTT), and 0.002% bromophenol blue) at 4 °C overnight. The protein concentrations were determined using a 2-D Quant Kit (GE Healthcare).

4.7. Two-Dimensional Gel Electrophoresis, Image Analysis and Protein Identification by LC-MS/MS

Two-dimensional gel electrophoresis (2-DE), image analysis and LC-MS/MS analysis were carried out by methods similar to those used in our previous study [13,23,38]. For 2-DE, protein samples (100 μg) from control cells and cells treated with 15 μg/mL sinulariolide were applied for first dimension electrophoresis (isoelectric focusing) using a GE Healthcare Ettan IPGphor 3. Then, the equilibrated strip was loaded onto the top of a sodium dodecyl sulfate polyacrylamide gel electrophoresis (SDS-PAGE gel) (12.5%) for second dimension electrophoresis using an SE 600 Ruby (Hoeffer, Holliston, MA, USA). 2-DE images were obtained in triplicate for each sample and normalization prior to statistical analysis was performed to ensure reproducibility. The 2-DE gels were stained by silver. The silver-stained gels were then scanned and analyzed using PDQuest image analysis software (Bio-Rad). Protein spots showing more than a one and a half-fold intensity difference were considered statistically significant in 2-DE between the sinulariolide treated A375 cells and the control. The protein spots of interest were excised from the 2-DE gels. After digestion with trypsin, the excised protein spots were used for identification by LC-MS/MS analysis using an AB SCIEX QTRAP® 5500Q mass spectrometer (Applied Biosystems, Framingham, CA, USA). For the LC-MS/MS procedure, the peptide mixture was separated by a reversed phase column (Agilent Zobax 2.1 mm × 150 mm C18 column, Santa Clara, CA, USA) on a nano LC system (Agilent NanoLC 1200 System). The LC-MS/MS analysis employed a 10-mm online trapping and desalting step followed by a linear gradient from 5% to 60% acetonitrile containing 0.1% formic acid over 60 min. The scan range was from *m*/*z* 100 to1000 for MS. The

raw data were processed into the text file format of WIFF using Analyst 1.5.1. All MS/MS spectra of identified peptides were further verified by manual interpretation.

4.8. DAPI and TUNEL Stain

A375 melanoma cells (1×10^5 cells/well) in a 12-well plate were treated with 5, 10, 15 μg/mL sinulariolide for 24 h, and DMSO was added as the control. Cells in each treatment and control group were fixed with 4% paraformaldehyde in PBS solution for 15 min and stained by DAPI according to the manufacturer's instructions. The DeadEnd™ Fluorometric TUNEL System (Promega) was used to detect nuclear DNA fragmentation according to the manufacturer's manual. The cells were photographed under a fluorescence microscope (Olympus IX71 CTS, Chinetek Scientific, Hong Kong, China).

4.9. Mitochondria and Cytosol Fractionation

The mitochondria and cytosol fractions were separated using a mitochondria/cytosol fractionation kit (BioSource) by the methods described in our previous report [18].

4.10. Assessment of Mitochondrial Membrane Potential (ΔΨm)

The mitochondrial membrane potential (ΔΨm) was examined by fluorescence microscopy following staining with the cationic dye JC-1 (Biotium, Hayward, CA, USA). A375 cells (1×10^5 cells/well) in a 12-well plate were treated with different concentrations of sinulariolide (0, 5 and 15 μg/mL) and grown in 5% CO_2 at 37 °C. After incubation, cells were harvested and washed twice with PBS, then 70 μL of JC-1 staining solution were added and incubation performed at 37 °C in the dark for 30 min. After a brief wash with serum-free medium, cells were directly observed by fluorescence microscopy (Olympus IX71 CTS, Chinetek Scientific, Hong Kong, China).

4.11. Western Blot Analysis

The treated samples and control samples (25 μg) were separated by 12.5% SDS-PAGE, and then transferred to a PVDF membrane (Millipore) for 1.5 h at 400 mA using Transphor TE 62 (Hoeffer). The membranes were incubated with 5% dehydrated skim milk to block nonspecific protein binding, and then incubated with primary antibodies at 4 °C for overnight. The primary antibodies were anti-human prohibitin, IDH, UQCRC1, Hsp60, HspB1, PARP, pro-caspase-3, cleaved-caspase-3, pro-caspase-9, cleaved-caspase-9, pro-caspase-8, Cyt c, Bax, Bad, p-Bad, Bcl-2, Bxl-xL, AIF, endo G and β-actin antibodies. The secondary antibodies (horseradish peroxidase conjugated goat anti-rabbit, 1:5000 in blocking solution) were added and incubated for 2 h and then visualized using chemiluminesence (Pierce Biotechnology, Rockford, IL, USA). The western blot data were quantified using Image J software.

4.12. Statistical Analysis

Data for the MTT assay, cell migration assay and flow cytometric analysis were pooled from three independent experiments and are expressed as the mean ± standard error of mean (SEM). Data analysis of variance (ANOVA) by the Tukey-Kramer test was performed using GraphPad InStat 3 (San Diego, CA, USA) to determine the significant differences ($p \leq 0.05$) as compared with the experimental groups [14].

5. Conclusions

In conclusion, our results establish that the natural marine compound sinulariolide possesses anti-cancer activity through the induction of cellular apoptosis in A375 melanoma cells. Proteomic analysis of the differentially expressed proteins profiled indicated that energy metabolism proteins were related to the apoptotic progress. Furthermore, our findings indicate that sinulariolide performs anti-cancer activity involving induction of cellular apoptosis. Overall, this study indicates that sinulariolide-induced apoptosis can be summarized as shown in Figure 6. Sinulariolide-induced apoptosis might be related to the activation of the caspase cascade and the mitochondrial-related apoptosis pathway. Further *in vivo* evaluation of the anti-melanoma cancer activity of sinulariolide in an animal model is needed in the future. The findings of our study also benefit melanoma pharmaceutical development in the clinical setting.

Figure 6. Sinulariolide induces A375 melanoma cell apoptosis through the mitochondrial-related apoptosis pathway and activation of the caspase cascade.

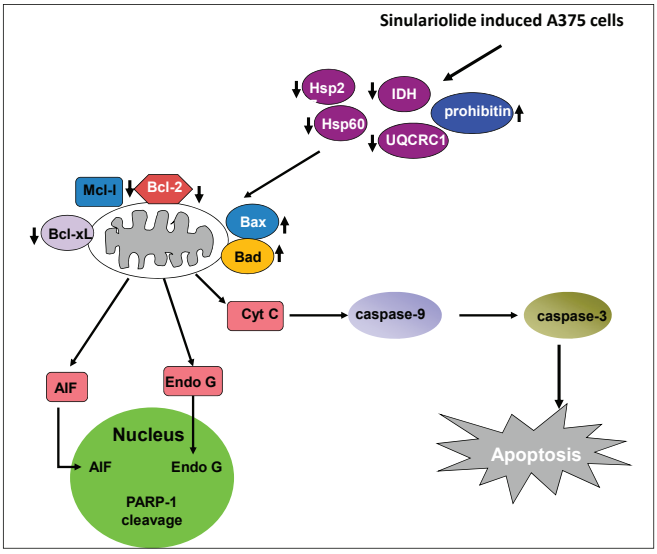

Acknowledgements

This work was supported by grants from the National Museum of Marine Biology & Aquarium and the National Science Council (NSC 98-2313-B-276-001-MY3 and NSC 101-2313-B-276-002).

Conflict of Interest

The authors declare no conflict of interest.

References

1. Parkin, D.M.; Bray, F.; Ferlay, J.; Pisani, P. Global cancer statistics, 2002. *CA Cancer J. Clin.* **2005**, *55*, 74–108.
2. Davar, D.; Tarhini, A.A.; Kirkwood, J.M. Adjuvant therapy for melanoma. *Cancer J.* **2012**, *18*, 192–202.
3. Tawbi, H.A.; Buch, S.C. Chemotherapy resistance abrogation in metastatic melanoma. *Clin. Adv. Hematol. Oncol.* **2010**, *8*, 259–266.
4. Sasse, A.D.; Sasse, E.C.; Clark, L.G.; Ulloa, L.; Clark, O.A. Chemoimmunotherapy *versus* chemotherapy for metastatic malignant melanoma. *Cochrane Database Syst. Rev.* **2007**, *1*, doi:10.1002/14651858.CD005413.pub2.
5. Fuglede, N.B.; Brinck-Claussen, U.O.; Deltour, I.; Boesen, E.H.; Dalton, S.O.; Johansen, C. Incidence of cutaneous malignant melanoma in Denmark, 1978–2007. *Br. J. Dermatol.* **2011**, *165*, 349–353.
6. Essner, R. Surgical treatment of malignant melanoma. *Surg. Clin. North Am.* **2003**, *83*, 109–156.
7. Chang, J.W. Cutaneous melanoma: Taiwan experience and literature review. *Chang Gung Med. J.* **2010**, *33*, 602–612.
8. Treisman, J.; Garlie, N. Systemic therapy for cutaneous melanoma. *Clin. Plast. Surg.* **2010**, *37*, 127–146.
9. Bleehen, N.M.; Newlands, E.S.; Lee, S.M.; Thatcher, N.; Selby, P.; Calvert, A.H.; Rustin, G.J.; Brampton, M.; Stevens, M.F. Cancer research campaign phase II trial of temozolomide in metastatic melanoma. *J. Clin. Oncol.* **1995**, *13*, 910–913.
10. Ibrahim, N.; Haluska, F.G. Molecular pathogenesis of cutaneous melanocytic neoplasms. *Annu. Rev. Pathol.* **2009**, *4*, 551–579.
11. Acquavella, N.; Kluger, H.; Rhee, J.; Farber, L.; Tara, H.; Ariyan, S.; Narayan, D.; Kelly, W.; Sznol, M. Toxicity and activity of a twice daily high-dose bolus interleukin 2 regimen in patients with metastatic melanoma and metastatic renal cell cancer. *J. Immunother.* **2008**, *31*, 569–576.
12. Liu, C.I.; Wang, R.Y.; Lin, J.J.; Su, J.H.; Chiu, C.C.; Chen, J.C.; Chen, J.Y.; Wu, Y.J. Proteomic profiling of the 11-dehydrosinulariolide-treated oral carcinoma cells Ca9–22: Effects on the cell apoptosis through mitochondrial-related and ER stress pathway. *J. Proteomics* **2012**, *75*, 5578–5589.

13. Su, C.C.; Su, J.H.; Lin, J.J.; Chen, C.C.; Hwang, W.I.; Huang, H.H.; Wu, Y.J. An investigation into the cytotoxic effects of 13-acetoxysarcocrassolide from the soft coral sarcophyton crassocaule on bladder cancer cells. *Mar. Drugs* **2011**, *9*, 2622–2642.
14. Su, T.R.; Lin, J.J.; Chiu, C.C.; Chen, J.Y.; Su, J.H.; Cheng, Z.J.; Hwang, W.I.; Huang, H.H.; Wu, Y.J. Proteomic investigation of anti-tumor activities exerted by sinularin against A2058 melanoma cells. *Electrophoresis* **2012**, *33*, 1139–1152.
15. Kondratyuk, T.P.; Park, E.J.; Yu, R.; van Breemen, R.B.; Asolkar, R.N.; Murphy, B.T.; Fenical, W.; Pezzuto, J.M. Novel marine phenazines as potential cancer chemopreventive and anti-inflammatory agents. *Mar. Drugs* **2012**, *10*, 451–464.
16. Maoka, T.; Tokuda, H.; Suzuki, N.; Kato, H.; Etoh, H. Anti-oxidative, anti-tumor-promoting, and anti-carcinogensis activities of nitroastaxanthin and nitrolutein, the reaction products of astaxanthin and lutein with peroxynitrite. *Mar. Drugs* **2012**, *10*, 1391–1399.
17. Rabelo, L.; Monteiro, N.; Serquiz, R.; Santos, P.; Oliveira, R.; Oliveira, A.; Rocha, H.; Morais, A.H.; Uchoa, A.; Santos, E. A lactose-binding lectin from the marine sponge *Cinachyrella apion* (Cal) induces cell death in human cervical adenocarcinoma cells. *Mar. Drugs* **2012**, *10*, 727–743.
18. Neoh, C.A.; Wang, R.Y.; Din, Z.H.; Su, J.H.; Chen, Y.K.; Tsai, F.J.; Weng, S.H.; Wu, Y.J. Induction of apoptosis by sinulariolide from soft coral through mitochondrial-related and p38MAPK pathways on human bladder carcinoma cells. *Mar. Drugs* **2012**, *10*, 2893–2911.
19. Aceret, T.L.; Coll, J.C.; Uchio, Y.; Sammarco, P.W. Antimicrobial activity of the diterpenes flexibilide and sinulariolide derived from *Sinularia flexibilis* Quoy and Gaimard 1833 (Coelenterata: Alcyonacea, Octocorallia). *Comp. Biochem. Physiol. C* **1998**, *120*, 121–126.
20. Ghosh, J.C.; Dohi, T.; Kang, B.H.; Altieri, D.C. Hsp60 regulation of tumor cell apoptosis. *J. Biol. Chem.* **2008**, *283*, 5188–5194.
21. Gibert, B.; Hadchity, E.; Czekalla, A.; Aloy, M.T.; Colas, P.; Rodriguez-Lafrasse, C.; Arrigo, A.P.; Diaz-Latoud, C. Inhibition of heat shock protein 27 (HspB1) tumorigenic functions by peptide aptamers. *Oncogene* **2011**, *30*, 3672–3681.
22. Kanagasabai, R.; Krishnamurthy, K.; Druhan, L.J.; Ilangovan, G. Forced expression of heat shock protein 27 (Hsp27) reverses *P*-glycoprotein (ABCB1)-mediated drug efflux and MDR1 gene expression in Adriamycin-resistant human breast cancer cells. *J. Biol. Chem.* **2011**, *286*, 33289–33300.
23. Liu, C.I.; Chen, C.C.; Chen, J.C.; Su, J.H.; Huang, H.H.; Chen, J.Y.; Wu, Y.J. Proteomic analysis of anti-tumor effects of 11-dehydrosinulariolide on CAL-27 cells. *Mar. Drugs* **2011**, *9*, 1254–1272.
24. Winter, A.; Kamarainen, O.; Hofmann, A. Molecular modeling of prohibitin domains. *Proteins* **2007**, *68*, 353–362.
25. Nijtmans, L.G.; de Jong, L.; Artal Sanz, M.; Coates, P.J.; Berden, J.A.; Back, J.W.; Muijsers, A.O.; van der Spek, H.; Grivell, L.A. Prohibitins act as a membrane-bound chaperone for the stabilization of mitochondrial proteins. *EMBO J.* **2000**, *19*, 2444–2451.

26. Fusaro, G.; Dasgupta, P.; Rastogi, S.; Joshi, B.; Chellappan, S. Prohibitin induces the transcriptional activity of p53 and is exported from the nucleus upon apoptotic signaling. *J. Biol. Chem.* **2003**, *278*, 47853–47861.
27. Rajalingam, K.; Wunder, C.; Brinkmann, V.; Churin, Y.; Hekman, M.; Sievers, C.; Rapp, U.R.; Rudel, T. Prohibitin is required for Ras-induced Raf-MEK-ERK activation and epithelial cell migration. *Nat. Cell Biol.* **2005**, *7*, 837–843.
28. Xu, S.G.; Yan, P.J.; Shao, Z.M. Differential proteomic analysis of a highly metastatic variant of human breast cancer cells using two-dimensional differential gel electrophoresis. *J. Cancer Res. Clin. Oncol.* **2010**, *136*, 1545–1556.
29. Jung, K.H.; Park, J.W. Suppression of mitochondrial NADP(+)-dependent isocitrate dehydrogenase activity enhances curcumin-induced apoptosis in HCT116 cells. *Free Radic. Res.* **2011**, *45*, 431–438.
30. Tuquet, C.; Dupont, J.; Mesneau, A.; Roussaux, J. Effects of tamoxifen on the electron transport chain of isolated rat liver mitochondria. *Cell Biol. Toxicol.* **2000**, *16*, 207–219.
31. Denicourt, C.; Dowdy, S.F. Targeting apoptotic pathways in cancer cells. *Science* **2004**, *305*, 1411–1413.
32. Liao, C.T.; Chang, J.T.; Wang, H.M.; Ng, S.H.; Hsueh, C.; Lee, L.Y.; Lin, C.H.; Chen, I.H.; Huang, S.F.; Cheng, A.J.; *et al*. Analysis of risk factors of predictive local tumor control in oral cavity cancer. *Ann. Surg. Oncol.* **2008**, *15*, 915–922.
33. Nicholson, D.W.; Thornberry, N.A. Life and death decisions. *Science* **2003**, *299*, 214–215.
34. Amarante-Mendes, G.P.; Naekyung Kim, C.; Liu, L.; Huang, Y.; Perkins, C.L.; Green, D.R.; Bhalla, K. Bcr-Abl exerts its antiapoptotic effect against diverse apoptotic stimuli through blockage of mitochondrial release of cytochrome c and activation of caspase-3. *Blood* **1998**, *91*, 1700–1705.
35. Hsieh, P.W.; Chang, F.R.; McPhail, A.T.; Lee, K.H.; Wu, Y.C. New cembranolide analogues from the formosan soft coral *Sinularia flexibilis* and their cytotoxicity. *Nat. Prod. Res.* **2003**, *17*, 409–418.
36. Su, T.R.; Tsai, F.J.; Lin, J.J.; Huang, H.H.; Chiu, C.C.; Su, J.H.; Yang, Y.T.; Chen, J.Y.; Wong, B.S.; Wu, Y.J. Induction of apoptosis by 11-dehydrosinulariolide via mitochondrial dysregulation and ER stress pathways in human melanoma cells. *Mar. Drugs* **2012**, *10*, 1883–1898.
37. Chiu, C.C.; Chen, J.Y.; Lin, K.L.; Huang, C.J.; Lee, J.C.; Chen, B.H.; Chen, W.Y.; Lo, Y.H.; Chen, Y.L.; Tseng, C.H.; Lin, S.R. p38 MAPK and NF-kappaB pathways are involved in naphtho(1,2-b)furan-4,5-dione induced anti-proliferation and apoptosis of human hepatoma cells. *Cancer Lett.* **2010**, *295*, 92–99.
38. Lu, C.M.; Wu, Y.J.; Chen, C.C.; Hsu, J.L.; Chen, J.C.; Chen, J.Y.; Huang, C.H.; Ko, Y.C. Identification of low-abundance proteins via fractionation of the urine proteome with weak anion exchange chromatography. *Proteome Sci.* **2011**, *9*, doi:10.1186/1477-5956-9-17.

Cytotoxic Anthranilic Acid Derivatives from Deep Sea Sediment-Derived Fungus *Penicillium paneum* SD-44

Chun-Shun Li, Xiao-Ming Li, Shu-Shan Gao, Yan-Hua Lu and Bin-Gui Wang

Abstract: Five new anthranilic acid derivatives, penipacids A–E (**1**–**5**), together with one known analogue (**6**), which was previously synthesized, were characterized from the ethyl acetate extract of the marine sediment-derived fungus *Penicillium paneum* SD-44. Their structures were elucidated mainly by extensive NMR spectroscopic and mass spectrometric analysis. The cytotoxicity and antimicrobial activity of the isolated compounds were evaluated. Compounds **1**, and **5** exhibited inhibitory activity against human colon cancer RKO cell line, while compound **6** displayed cytotoxic activity against Hela cell line.

Reprinted from *Mar. Drugs*. Cite as: Li, C.-S.; Li, X.-M.; Gao, S.-S.; Lu, Y.-H.; Wang, B.-G. Cytotoxic Anthranilic Acid Derivatives from Deep Sea Sediment-Derived Fungus *Penicillium paneum* SD-44. *Mar. Drugs* **2013**, *11*, 3068-3076.

1. Introduction

Marine fungi have recently attracted great attention owing to their structurally unique and biologically active metabolites [1–4]. Our previous investigation of filamentous fungi from marine habitats [5–10] enabled us to obtain a fungus *Penicillium paneum* SD-44 from the sediment sample collected from the South China Sea. Chemical investigation of this fungus by static culture in solid rice medium led to the isolation of one novel triazole and two new quinazolinone alkaloids, penipanoids A–C [11]. During our ongoing exploration of new bioactive metabolites of this fungal strain by changing fermentation conditions, we had a chance to access a large-scale bioreactor, and, as a result, six anthranilic acid derivatives including five new ones (**1**–**5**) and one previously synthesized analogue (**6**) [12] (Figure 1) were isolated from the culture broth of the dynamic fermentation in a 500-L fermentator. All the isolated new compounds possess an amidine moiety, which is rare among naturally occurring compounds [13]. Details of the isolation, structure elucidation, and biological activities are reported herein.

Figure 1. Structures of the isolated compounds **1**–**6**.

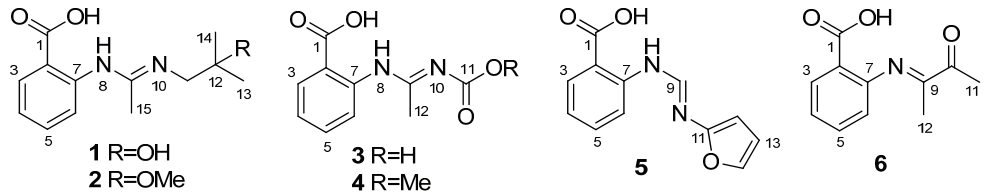

2. Results and Discussion

Structure Elucidation of the New Compounds

Penipacid A (**1**) was isolated as yellowish solid. Its molecular formula was demonstrated as $C_{13}H_{18}N_2O_3$ by HR-ESI-MS, with six degrees of unsaturation. Detailed analyses of the 1D NMR data (Tables 1 and 2) indicated the presence of one carbonyl, one *ortho*-disubstituted benzene ring, two additional quaternary carbons (one sp^2 and one sp^3), one methylene carbon and three methyls. Among them, the de-shielded sp^3 quaternary carbon resonating at δ_C 70.8 was deduced to be oxygenated, while the two sp^2 carbons at δ_C 148.3 and 148.4 and the methylene at δ_C 49.7 were ascribed to be connected with nitrogen atoms. The characters of the 1D NMR data and the UV spectrum (λ_{max} 286 and 340 nm) as well as the observed ^1H–^1H COSY and HMBC correlations (Figure 2) suggested that **1** might be an anthranilic acid derivative [14]. In the HMBC spectrum, the correlation from the double doublet aromatic proton H-3 to C-1 (δ_C 172.9) allowed the placement of the carboxyl group at C-2 (Figure 2). The observed HMBC cross-peaks from the exchangeable proton (H-8, δ_H 10.63), ascribed to nitrogenated atom, to the aromatic carbons C-2 and C-6 implied the presence of the 2-aminobenzoic acid moiety. Meanwhile, the HMBC correlations (Figure 2) from the symmetrical methyls (H_3-13 and H_3-14) to the oxygenated carbon C-12 (δ_C 70.8) and the nitrogen-bearing methylene C-11 (δ_C 49.7) and from singlet methyl H_3-15 to C-9 (δ_C 148.4/3) and C-11 as well as from H-8 to C-9 suggested the presence of *N′*-(2-hydroxy-2-methylpropyl)acetimidamide motif in the structure of **1**. The observed NOE correlation of H_2-11 with H_3-15 ascribed the imine double bond C_9=N_{10} to be *E*-configured. The structure of **1** was thus established to be (*E*)-2-(*N′*-(2-hydroxy-2-methylpropyl)acetimidamido)benzoic acid, named as penipacid A.

Penipacid B (**2**), yellowish powder, was revealed by HR-ESI-MS data to have the molecular formula $C_{14}H_{20}N_2O_3$, with a CH_2 unit more than that of **1**. Comparison of the NMR data of **2** with those of **1** indicated that the structures of these two compounds are very similar, except that one methoxy group was present in **2**. The resonance of the oxygenated quaternary carbon C-12 shifted downfield from δ_C 70.8 in **1** to δ_C 76.8 in **2**, while the adjacent methyl carbon C-13/C-14 moved upfield from δ_C 29.4 in **1** to δ_C 25.6 in the ^{13}C NMR spectrum of **2** (Table 2). Correspondingly, the methyl signal H-13/H-14 shifted from δ_H 1.35 in **1** to upfield at δ_H 1.23 in the ^1H NMR spectrum of **2** (Table 1). The observation implied that the hydroxy group at C-12 in **1** was replaced by a methoxy moiety in **2**, which was verified by the obvious HMBC correlation from the protons of the methoxy (δ_H 3.27) to C-12. The NOE correlation of H_2-11 with H_3-15 also suggested the *E*-configured of C_9=N_{10}. Thus, the structure of **2** was established as (*E*)-2-(*N′*-(2-methoxy-2-methylpropyl)acetimidamido)benzoic acid.

Table 1. ^{1}H NMR data for compounds **1**–**6** (500 MHz, δ in ppm, J in Hz).

No.	1 [a]	2 [b]	3 [c]	4 [b]	5 [b]	6 [b]
3	7.97 dd (7.9, 0.8)	7.89 dd (8.0, 1.3)	7.89 d (7.9)	7.98 d (7.7)	7.92 d (7.8)	7.99 dd (7.9, 1.2)
4	6.76 br t (7.9)	6.70 br t (8.0)	6.94 t (7.4)	6.93 t (7.5)	6.77 t (7.5)	6.94 td (8.0, 0.9)
5	7.45 td (8.2, 1.0)	7.38 td (8.5, 1.4)	7.55 t (7.4)	7.48 t (7.5)	7.42 t (7.5)	7.46 td (8.0, 1.5)
6	7.50 br d (8.2)	7.58 br d (8.5)	7.81 d (8.4)	7.80 d (8.4)	7.66 br d (8.5)	7.76 br d (8.4)
8	10.63 s	-	11.36 s	-	-	
9					7.82 s	
11	2.53 s	2.53 s				2.47 s
12			2.04 s	2.14 s	6.63 d (3.1)	2.01 s
13	1.35 s	1.23 s			6.50 dd (2.8, 1.7)	
14	1.35 s	1.23 s			7.55 br s	
15	2.00 s	1.97 s				
OMe		3.27 s				

[a] Recorded in $CDCl_3$; [b] Recorded in methanol-d_4; [c] Recorded in DMSO-d_6.

Table 2. ^{13}C NMR data for compounds **1**–**6** (125 MHz, δ in ppm).

No.	1 [a]	2 [b]	3 [c]	4 [b]	5 [b]	6 [b]
1	172.9 s	172.3 s [d]	170.4 s	172.7 s	172.2 s	173.3 s [d]
2	108.4 s	111.1 s	112.4 s	112.1 s	112.2 s	117.6 s
3	131.8 d	132.5 d	131.6 d	132.6 d	132.5 d	132.7 d
4	117.5 d	117.9 d	120.2 d	121.0 d	118.7 d	121.3 d
5	135.7 d	135.2 d	135.0 d	135.0 d	135.1 d	134.2 d
6	113.1 d	114.1 d	114.3 d	115.0 d	114.4 d	114.5 d
7	148.3 s	149.7 s	146.4 s	147.5 s	148.7 s	146.8 s
9	148.4 s	147.9 s	136.5 s	135.4 s	131.5 d	143.4 s
10						199.3 s
11	49.7 t	48.7 t	166.2 s	167.4 s	152.3 s	8.5 q
12	70.8 s	76.8 s	11.4 q	11.4 q	110.8 d	24.2 q
13	29.4 q	25.6 q			112.7 d	
14	29.4 q	25.6 q			144.5 d	
15	17.9 q	17.3 q				
OMe		49.0 q		52.7 q		

[a] Recorded in $CDCl_3$; [b] Recorded in methanol-d_4; [c] Recorded in DMSO-d_6; [d] Data deduced from HMBC.

Penipacid C (**3**) was shown to have the molecular formula of $C_{10}H_{10}N_2O_4$ (seven degrees of unsaturation) by means of HR-ESI-MS. Detailed analysis of the ^{1}H-, ^{13}C- as well as DEPT NMR data of **3** suggested that the molecule might possess the same 2-acetimidamido benzoic acid moiety as those of compounds **1** and **2**. The remaining structural unit (COOH) with the quaternary carbon atom resonated at δ_C 166.2 (C-11) was ascribed to the presence of one carbonyl group. The obvious HMBC correlations from the only methyl group (δ_H 2.04, H_3-12) to C-9 (δ_C 136.5) and C-11 established the position of the remaining carbonyl group (Figure 2). The chemical atmosphere of the methyl (C-12) might be influenced by the carboxyl group (C-11), which was correspondingly affected by the configuration of the double bond (C_9=N_{10}). When the C_9=N_{10} takes the

E configuration, the methyl group (C-12) is at the shielding area of the carboxyl group, which implied the lower chemical shift of C-12 in this mode than in that of the *Z* configured C_9=N_{10} molecule. The preliminary prediction of the chemical shift of C-12 by the software ChemBioDraw Ultra (V12.0) verified this deduction that C-12 was in a higher fielded atmosphere (δ_C 18.9) in the *E*-configured molecule, and in a lower one (δ_C 24.9) for the *Z*-configured model. The experimental value (δ_C 11.4) of the chemical shift of C-12 is closer to that of the predicted one of *E*-configured molecule than that of the *Z*-configured model. The configuration of the double bond C_9=N_{10} was thus tentatively assigned to be *E*, which was biogenetically identical to those of compounds **1** and **2**. A double bond isomer (C_9=N_{10}) of **3** was previously described in a complex with manganese [15].

Penipacid E (**4**) was isolated as yellowish solid. Its molecular formula was determined to be $C_{11}H_{12}N_2O_4$ by HR-ESI-MS, possessing one more CH_2 moiety than that of **3**. Comprehensive comparison of the 1D NMR data of **4** with those of **3** suggested that the two molecules were very similar, except that an *O*-methyl group (δ_H 3.84 and δ_C 52.7) was observed in the NMR spectra of **4**, implying one of the COOH group in **3** was replaced by a COOMe group in **4**. The HMBC correlation from the methoxy group to C-11 (δ_C 167.4) allowed the placement of the COOMe group at N-10. The geometry of the double bond (C_9=N_{10}) in **4** was also assigned by the chemical shift prediction using ChemBioDraw Ultra (version 12.0) software to be *E*-configured. The similarity of the chemical shifts of compounds **3** and **4** also implied that both of them should take the same configuration.

Penipacid G (**5**) was obtained as a yellowish solid. The molecular formula was deduced from the HR-ESI-MS data to be $C_{12}H_{10}N_2O_3$, with nine degrees of unsaturation. The similarity of the 1D NMR data of **5** with compounds **1**–**4** suggested that **5** should also be an anthranilic acid derivative. Besides the 2-aminobenzoic acid moiety, the remaining part (C_5H_4NO) of the structure was established by 2D NMR spectra. The COSY correlations from H-12 to H-13 and from H-13 to H-14 as well as the HMBC correlations from H-12 and H-13 to the oxygenated aromatic carbons C-11 (δ_C 152.3) and C-14 (δ_C 144.5) and from H-14 to C-11 and C-12 (Figure 2) implied the presence of the nitrogen substituted furan moiety. Moreover, the HMBC cross peak from H-9 to C-11 established the planar structure of compound **5** to be 2-(*N*′-(furan-2-yl)formimidamido)benzoic acid. The NOE correlation from H-9 to the furan proton H-12 implied the *E*-configuration of C_9=N_{10}.

To clarify whether the new compounds **2** and **4** are artifacts, which might be respectively derived from **1** and **3** during the purification procedures, compounds **1** and **3** were mixed with silica gel in $CHCl_3$–MeOH (1:1) for 24 hours and then checked by HPLC. Additionally, these compounds were respectively dissolved in MeOH and were stirred at room temperature for 48 hours and then also analyzed by HPLC. The results indicated that none of them showed obvious change compared with the standard samples. Based on the above experiments, compounds **2** and **4** are regarded as natural occurring products, rather than the artifacts.

Figure 2. Key HMBC (arrows) and ^{1}H–^{1}H COSY (bold lines) correlations of compounds **1**, **3**, and **5**.

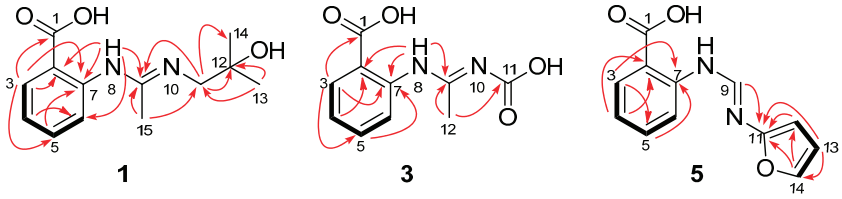

Compounds **1**–**6** were evaluated for the cytotoxicity against Hela and RKO cell lines and the antimicrobial activity on two bacteria (*Staphylococcus aureus* and *Escherichia coli*) and three plant-pathogenic fungi (*Alternaria brassicae*, *Fusarium graminearum*, and *Rhizoctonia cerealis*). In the cytotoxic assays, penipacids A (**1**) and E (**5**) exhibited inhibitory activity against RKO cell line with an IC_{50} value of 8.4 and 9.7 μM, respectively, while compound **6** displayed cytotoxic activity against Hela cell line with the IC_{50} value of 6.6 μM, which are all stronger than the positive control fluorouracil (with IC_{50} values of 25.0 and 14.5 μM, respectively). In the antimicrobial screening, no obvious activity could be observed for the tested compounds.

3. Experimental Section

3.1. General

UV Spectroscopic data were obtained on a Lengguang Gold S54. NMR Spectra were recorded at 500 and 125 MHz for ^{1}H and ^{13}C, respectively, on a Bruker Advance 500. Mass spectra were measured on a VG Autospec 3000 mass spectrometer. Column chromatography (CC) was performed with silica gel (200–300 mesh, Qingdao Marine Chemical Factory, Qingdao, China), Lobar LiChroprep RP-18 (40–63 μm; Merck), and Sephadex LH-20 (18–110 μm, Merck, Darmstadt, Germany). HPLC was performed using an Elite semi-preparative colume (10 × 300 mm, Elite, Dalian, China) on Dionex HPLC system.

3.2. Fungal Material

The procedures of isolation and identification of the fungal strain used in this experiment were described in an earlier report [11].

3.3. Extraction and Isolation

The fresh mycelium was inoculated into 500 mL flask preloaded with 200 mL liquid medium (consisting of mannitol 20 g, maltose 20 g, monosodium glutamate 10 g, glucose 10 g, yeast extract 3 g, corn steep liquor 1 g, KH_2PO_4 0.5 g, and $MgSO_4 \cdot 7H_2O$ 0.3 g, in 1 L filtered sea water) followed by a two-day culture incubation at 28 °C and 150 rpm/min. The whole liquid (15 × 200 mL) collected from the flask was inoculated into a 50-L seed fermentator containing 27 L sterilized medium for a one-day fermentation at 28 °C and 150 rpm/min. The cultured liquid was then

transferred into a 500 L fermentator preloaded with 270 L sterilized medium and cultured for another 5 days at the same conditions.

The fermented mycelia and broth were separated by centrifugation, and the mycelia were exhaustively extracted with acetone to afford the crude extract (70.0 g). The extract was fractionated by Si gel vacuum liquid chromatography (VLC) using petroleum ether (PE)–EtOAc (from 1:0 to 1:1) and $CHCl_3$–MeOH (from 20:1 to 0:1) gradient elution to afford 10 fractions (Fr.1–Fr.10). Fr.2 (6.1 g) eluted with PE–EtOAc (5:1) was further purified by column chromatography (CC) on reversed-phase silica gel C_{18} eluted with a MeOH–H_2O gradient (20% to 100%) to obtain eight parts (P.1–P.8). P.4 (170.0 mg) was further purified by semi-preparative HPLC (Elite ODS-BP column, 10 μm; 10.0 × 300 mm; 3 mL/min; 70% MeOH/H_2O with 0.1% acetic acid in mobile phases) to obtain compounds **4** (5.7 mg, t_R 10.2 min), **1** (16.7 mg, t_R 17.5 min), and **2** (9.3 mg, t_R 27.6 min;). P.5 (110.0 mg) was then subjected to Sephadex LH-20 (MeOH), which was followed by semi-preparative HPLC (73% MeOH/H_2O) to get **5** (4.1 mg, t_R 19.6 min). P.6 (180.0 mg) was fractionated by Sephadex LH-20 (MeOH) and semi-preparative HPLC to yield compound **6** (8.7 mg, t_R 15.5 min; 65% MeOH/H_2O). Fr.3 (8.43 g) eluted with PE–EtOAc (2:1) was further separated by CC on reversed-phase silica gel C_{18} eluted with a MeOH–H_2O gradient (20% to 100%) to afford eight parts (P.1–P.8). P.7 (125.0 mg) was separated by semi-preparative HPLC (75% MeOH/H_2O) to get **3** (21.2 mg, t_R 9.8 min).

Penipacid A (**1**): yellowish solid; UV (MeOH) λ_{max} (log ε) 215 (4.50), 286 (4.40), 340 (3.85) nm; ^1H and ^{13}C NMR data, see Tables 1 and 2; ESIMS *m/z* 251 $[M + H]^+$; HRESIMS *m/z* 251.1393 $[M + H]^+$ (calcd for $C_{13}H_{19}N_2O_3$, 251.1390).

Penipacid B (**2**): yellowish powder; UV (MeOH) λ_{max} (log ε) 215 (4.06), 286 (4.07), 336 (3.48) nm; ^1H and ^{13}C NMR data, see Tables 1 and 2; ESIMS *m/z* 287 $[M + Na]^+$; HRESIMS *m/z* 287.1365 $[M + Na]^+$ (calcd for $C_{14}H_{20}N_2O_3Na$, 287.1371).

Penipacid C (**3**): yellowish solid; UV (MeOH) λ_{max} (log ε) 218 (4.70) nm, 334 (4.66); ESIMS *m/z* 223 $[M + H]^+$; HRESIMS *m/z* 223.0713 (calcd for $C_{10}H_{11}N_2O_4$, 223.0714).

Penipacid D (**4**): yellowish solid; UV (MeOH) λ_{max} (log ε) 217 (4.31) nm, 334 (4.42); ^1H and ^{13}C NMR data, see Tables 1 and 2; ESIMS *m/z* 237 $[M + H]^+$; HRESIMS *m/z* 237.0869 $[M + H]^+$ (calcd for $C_{11}H_{13}N_2O_4$, 237.0870).

Penipacid E (**5**): yellowish solid; UV (MeOH) λ_{max} (log ε) 215 (4.65), 350 (4.75) nm; ^1H and ^{13}C NMR data, see Tables 1 and 2, respectively; ESIMS *m/z* 229 $[M - H]^-$; HRESIMS *m/z* 229.0629 $[M - H]^-$ (calcd for $C_{12}H_9N_2O_3$, 229.0619).

3.4. Cytotoxic Assay

The cytotoxic activity against Hela (human epithelial carcinoma) and RKO (human colon cancer) cell lines was determined according to previously reported methods [16]. Briefly, cells were seeded onto 96-well plates at a density of 4×10^3 cells/well for 24 h, and treated with gradient concentrations of the tested compounds for 48 h. MTT (100 μL, 0.5 mg/mL) was added to each well and the cells were incubated for further 4 h in the dark at 37 °C. Then, the dye crystals were

dissolved in 150 μL dimethyl sulphoxide (DMSO) after careful removal of the medium. Absorbance was measured at 570 nm using a microplate reader (BioTek, USA). The viability of the treated groups was assessed as a percentage of non-treated control groups, which was assumed to be 100%. The cytotoxicity of the compounds was expressed as an IC_{50}, defined as the concentration causing a 50% reduction of cell growth compared with untreated cells.

3.5. Antimicrobial Assays

The antimicrobial activities against two bacteria (*S. aureus* and *E. coli*) and three plant-pathogenic fungi (*A. brassicae*, *F. graminearum*, and *R. cerealis*) were carried out using the disk diffusion method [17]. Chloramphenicol and amphotericin B were used as antibacterial and antifungal positive controls, respectively.

4. Conclusions

Five new anthranilic acid derivatives, penipacids A–E (**1**–**5**), along with one known analogue (**6**), were identified from *P. paneum* SD-44 fermented in a 500 L bioreactor. Compounds **1**, **5**, and **6** exhibited cytotoxic activities. The biosynthetic potential of filamentous fungi is proven to be under exploited [18,19]. The strategy of changing culture conditions of fungi for inducing the production of new metabolites has been successfully applied in recent years [20–23]. Detailed HPLC-DAD analysis of the crude extract and VLC fractions of fungus SD-44 cultured in rice medium revealed that none of the penipacid compounds could be detected. However, the penipanoids, which were isolated from the static fermentation [11] were also isolated from the dynamic cultured products in the present investigation. Since there is no more powerful evidence to prove whether the penipacid compounds could be metabolized by SD-44 in the static fermentation, the discovery of penipacids could not be definitely ascribed to the change of fermentation condition of the fungus SD-44.

Acknowledgments

This work was financially supported by grants from National Natural Science Foundation of China (30901880) and from the Ministry of Science and Technology of China (2012AA092104 and 2013AA092901).

Conflicts of Interest

The authors declare no conflict of interest.

References

1. Rateb, M.E.; Ebel, R. Secondary metabolites of fungi from marine habitats. *Nat. Prod. Rep.* **2011**, *28*, 290–344.
2. Blunt, J.W.; Copp, B.R.; Munro, M.H.G.; Northcote, P.T.; Prinsep, M.R. Marine natural products. *Nat. Prod. Rep.* **2011**, *28*, 196–268.

3. Blunt, J.W.; Copp, B.R.; Munro, M.H.G.; Northcote, P.T.; Prinsep, M.R. Marine natural products. *Nat. Prod. Rep.* **2010**, *27*, 165–237.
4. Blunt, J.W.; Copp, B.R.; Hu, W.P.; Munro, M.H.G.; Northcote, P.T.; Prinsep, M.R. Marine natural products. *Nat. Prod. Rep.* **2009**, *26*, 170–244.
5. Liu, D.; Li, X.M.; Meng, L.; Li, C.S.; Gao, S.S.; Shang, Z.; Proksch, P.; Huang, C.G.; Wang, B.G. Nigerapyrones A–H, α-pyrone derivatives from the marine mangrove-derived endophytic fungus *Aspergillus niger* MA-132. *J. Nat. Prod.* **2011**, *74*, 1787–1791.
6. Gao, S.S.; Li, X.M.; Zhang, Y.; Li, C.S.; Cui, C.M.; Wang, B.G. Comazaphilones A–F, azaphilone derivatives from the marine sediment-derived fungus *Penicillium commune* QSD-17. *J. Nat. Prod.* **2011**, *74*, 256–261.
7. Du, F.Y.; Li, X.M.; Li, C.S.; Shang, Z.; Wang, B.G. Cristatumins A–D, new indole alkaloids from the marine-derived endophytic fungus *Eurotium cristatum* EN-220. *Bioorg. Med. Chem. Lett.* **2012**, *22*, 4650–4653.
8. Sun, H.F.; Li, X.M.; Meng, L.; Cui, C.M.; Gao, S.S.; Li, C.S.; Huang, C.G.; Wang, B.G. Asperolides A–C, tetranorlabdane diterpenoids from the marine alga-derived endophytic fungus *Aspergillus wentii* EN-48. *J. Nat. Prod.* **2012**, *75*, 148–152.
9. Zhang, Y.; Li, X.M.; Shang, Z.; Li, C.S.; Ji, N.Y.; Wang, B.G. Meroterpenoid and diphenyl ether derivatives from *Penicillium* sp. MA-37, a fungus isolated from marine mangrove rhizospheric soil. *J. Nat. Prod.* **2012**, *75*, 1888–1895.
10. An, C.Y.; Li, X.M.; Li, C.S.; Gao, S.S.; Shang, Z.; Wang, B.G. Triazoles and other N-containing metabolites from the marine-derived endophytic fungus *Penicillium chrysogenum* EN-118. *Helv. Chim. Acta* **2013**, *96*, 682–687.
11. Li, C.S.; An, C.Y.; Li, X.M.; Gao, S.S.; Cui, C.M.; Sun, H.F.; Wang, B.G. Triazole and dihydroimidazole alkaloids from the marine sediment-derived fungus *Penicillium paneum* SD-44. *J. Nat. Prod.* **2011**, *74*, 1331–1334.
12. Imran, M.; Mitu, L.; Latif, S.; Mahmood, I.N.; Zaman, S.S.; Fatima, S. Antibacterial Co (II), Ni (II), Cu (II) and Zn (II) complexes with biacetyl-derived Schiff bases. *J. Serb. Chem. Soc*. **2010**, *75*, 1075–1084.
13. Munekata, M.; Seto, H.; Tamura, G. The selective inhibitors against sv40-transformed cells. 4, isolation of ortho-acetylbenzene-amidinocarboxylic acid, a new metabolite of *Gibberella saubinetii*. *Agric. Biol. Chem.* **1982**, *46*, 1711–1713.
14. Ahmad, I.; Nawaz, S.A.; Afza, N.; Malik, A.; Fatima, I.; Khan, S.B.; Ahmad, M.; Choudhary, M.I. Isolation of onosmins A and B, lipoxygenase inhibitors from *Onosma hispida*. *Chem. Pharm. Bull.* **2005**, *53*, 907–910.
15. Abu-El-Wafa, S.M.; El-Behairy, M.A.; Issa, R.M.; Saleh, A.A. On the formation of Mn (II) antranilic acid anilide complexes, structural elucidation by TGA, IR, electronic, EPR spectra and potentiometric studies. *J. Chem. Soc. Pak.* **1988**, *10*, 464–469.
16. Mosmann, T. Rapid colorimetric assay for cellular growth and survival: Application to proliferation and cytotoxcity assays. *J. Immunol. Methods* **1983**, *65*, 55–63.

17. Al-Burtamani, S.K.S.; Fatope, M.O.; Marwah, R.G.; Onifade, A.K.; Al-Saidi, S.H. Chemical composition, antibacterial and antifungal activities of the essential oil of *Haplophyllum tuberculatum* from Oman. *J. Ethnopharmacol.* **2005**, *96*, 107–112.
18. Schroeckh, V.; Brakhage, A.A. Fungal secondary metabolites-strategies to activate silent gene clusters. *Fungal Genet. Biol.* **2011**, *48*, 15–22.
19. Scherlach, K.; Hertweck, C. Triggering cryptic natural product biosynthesis in microorganisms. *Org. Biomol. Chem.* **2009**, *7*, 1753–1760.
20. Knight, V.; Sanglier, J.J.; DiTullio, D.; Braccili, S.; Bonner, P.; Waters, J.; Hughes, D.; Zhang, L. Diversifying microbial natural products for drug discovery. *Appl. Microbiol. Biotechnol.* **2003**, *62*, 446–458.
21. Bode, H.B.; Bethe, B.; Hofs, R.; Zeeck, A. Big effects from small changes: Possible ways to explore nature's chemical diversity. *Chembiochem* **2002**, *3*, 619–627.
22. Amagata, T.; Tanaka, M.; Yamada, T.; Doi, M.; Minoura, K.; Ohishi, H.; Yamori, T.; Numata, A. Variation in cytostatic constituents of a sponge-derived *Gymnascella dankaliensis* by manipulating the carbon source. *J. Nat. Prod.* **2007**, *70*, 1731–1740.
23. Paranagama, P.A.; Wijeratne, E.M.K.; Gunatilaka, A.A.L. Uncovering biosynthetic potential of plant-associated fungi: Effect of culture conditions on metabolite production by *Paraphaeosphaeria quadriseptata* and *Chaetomium chiWersii*. *J. Nat. Prod.* **2007**, *70*, 1939–1945.

Epigonal Conditioned Media from Bonnethead Shark, *Sphyrna tiburo*, Induces Apoptosis in a T-Cell Leukemia Cell Line, Jurkat E6-1

Catherine J. Walsh, Carl A. Luer, Jennifer E. Yordy, Theresa Cantu, Jodi Miedema, Stephanie R. Leggett, Brittany Leigh, Philip Adams, Marissa Ciesla, Courtney Bennett and Ashby B. Bodine

Abstract: Representatives of Subclass Elasmobranchii are cartilaginous fish whose members include sharks, skates, and rays. Because of their unique phylogenetic position of being the most primitive group of vertebrates to possess all the components necessary for an adaptive immune system, the immune regulatory compounds they possess may represent the earliest evolutionary forms of novel compounds with the potential for innovative therapeutic applications. Conditioned medium, generated from short term culture of cells from the epigonal organ of bonnethead sharks (*Sphyrna tiburo*), has been shown to have potent reproducible cytotoxic activity against a variety of human tumor cell lines *in vitro*. Existing data suggest that epigonal conditioned medium (ECM) exerts this cytotoxic activity through induction of apoptosis in target cells. This manuscript describes apoptosis induction in a representative tumor cell line, Jurkat E6-1, in response to treatment with ECM at concentrations of 1 and 2 mg/mL. Data indicate that ECM exposure initiates the mitochondrial pathway of apoptosis through activation of caspase enzymes. Future purification of ECM components may result in the isolation of an immune-regulatory compound with potential therapeutic benefit for treatment of human cancer.

Reprinted from *Mar. Drugs*. Cite as: Walsh, C.J.; Luer, C.A.; Yordy, J.E.; Cantu, T.; Miedema, J.; Leggett, S.R.; Leigh, B.; Adams, P.; Ciesla, M.; Bennett, C.; *et al*. Epigonal Conditioned Media from Bonnethead Shark, *Sphyrna tiburo*, Induces Apoptosis in a T-Cell Leukemia Cell Line, Jurkat E6-1. *Mar. Drugs* **2013**, *11*, 3224-3257.

1. Introduction

While a few pharmaceuticals have originated from the marine environment or been derived from tissues of marine inhabitants, marine organisms represent a relatively untapped source of potentially novel compounds. In particular, elasmobranch fishes (cartilaginous fish whose members include the sharks, skates, and rays) may provide a unique and underutilized source of potential therapeutic agents. With anecdotal observations that sharks, skates, and rays have a low incidence of disease in general, but specifically a low incidence of documented malignant tumors, understanding the role of the elasmobranch immune system in this apparent resistance would open the door for new areas of research.

Although research in this area may potentially translate into applications for human health, a basic understanding of the elasmobranch immune system components and how they function is essential. Immunologically, elasmobranch fishes fill a unique niche in that they are phylogenetically the most primitive group of vertebrates to possess all the components necessary for an adaptive

immune system [1–4]. As in higher vertebrates, elasmobranchs possess thymus and spleen, but in the absence of bone marrow and lymph nodes, these fish have evolved unique lymphomyeloid tissues, namely the epigonal and Leydig organs. Because they are specific to elasmobranchs, research in our lab has focused on the epigonal and Leydig organs, with efforts focused on *in vitro* culture of cells collected from the epigonal organ. Optimization of short-term culture of elasmobranch immune cells has facilitated investigation of cytokine-like factors derived from conditioned culture medium from elasmobranch epigonal cells (epigonal conditioned medium, ECM). Specifically, media conditioned by cultures of epigonal tissue from bonnethead sharks (*Sphyrna tiburo*) contains potent growth inhibitory activity against a number of tumor cell lines [5], while only limited growth inhibitory activity against normal cells [6]. Among the cell lines tested, the Jurkat E6-1 cell line, derived from an acute T-cell leukemia [7], was shown to be among the most sensitive to growth inhibition effects resulting from exposure to ECM. Previous reports indicate that cytotoxic activity of ECM against mammalian tumor cell lines proceeded through mechanisms of apoptosis [5,6]. In this paper, pathways of apoptosis initiated by exposure to ECM in Jurkat cells are described.

Caspases (cysteine-dependent aspartate-directed proteases) belong to a highly conserved family of cysteine proteases with specificity for aspartic acid residues on their substrates. Caspase enzymes play a central role in apoptosis and are classified as initiators or effectors (executioners), depending on point of entry into the apoptotic cascade. To date, ten major caspases have been identified and broadly categorized as initiators (caspases-2, -8, -9, -10), effectors/executioners (caspases-3, -6, -7), or inflammatory caspases (caspases-1, -4, -5) (reviewed in [8]). Initiator caspases are the first to be activated, and serve as the initial steps in a cascade effect that activates downstream effector or executioner caspases. Initiator caspases (-8, -9, and -10) are closely coupled to pro-apoptotic signals and once activated, the execution phase of apoptosis is triggered and downstream effector caspases (-3, -6, and -7) are cleaved and activated, which, in turn, cleave cytoskeletal and nuclear proteins, such as PARP, and ultimately result in cell apoptosis. A schematic diagram of selected initiator and effector caspase activation pathways resulting in apoptosis is shown in Figure 1.

2. Results and Discussion

2.1. Growth Inhibition Assay

Growth inhibitory activity of ECM was assessed using a T-cell leukemia cell line, Jurkat E6-1 (ATCC TIB 152). Growth inhibition was quantified using the MTT assay [9], an assay that measures the ability of live cells to convert the tetrazolium salt MTT (3-(4,5-dimethylthiazol-2-yl)-2,5-diphenyl tetrazolium bromide) to a formazan product via mitochondrial enzymes. At ECM concentrations of 1 and 2 mg/mL, inhibition of Jurkat cell growth after 72 h was greater than 90% (Figure 2A). At 0.5 mg/mL, growth inhibition was greater than 50%. Growth inhibition in response to 1 and 2 mg/mL ECM was significantly ($P < 0.05$) greater than control. Reduction in conversion of MTT to the formazan product by ECM-treated Jurkat cells indicates that ECM induces dose-dependent inhibition of Jurkat cell growth.

Figure 1. Schematic diagram showing the activation of selected initiator and effector caspase pathways resulting in apoptosis.

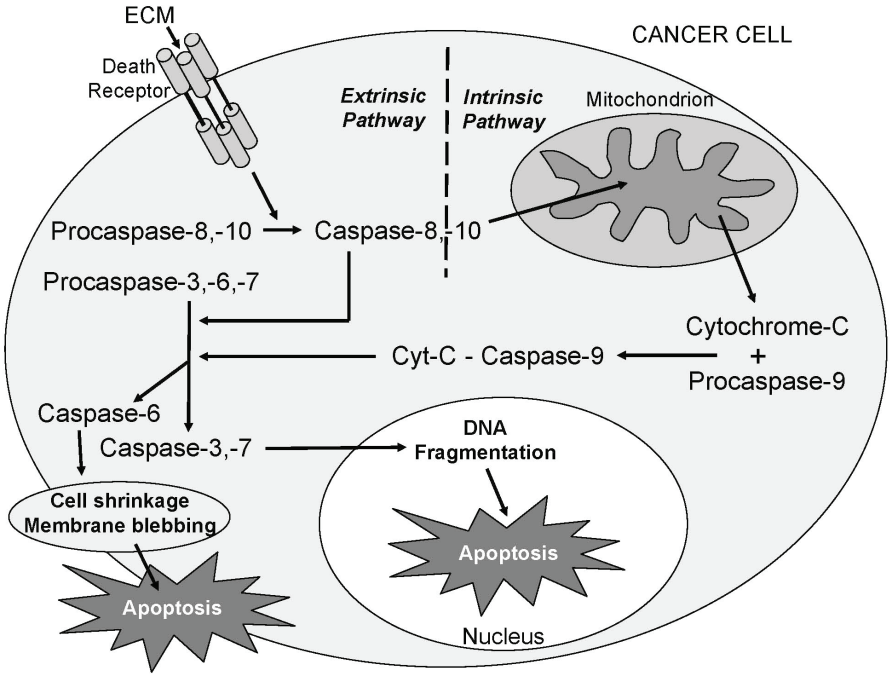

2.2. Annexin V Assay

Annexin V is a phospholipid binding protein with high affinity for phosphatidylserine. In viable cells, phosphatidylserine is located on the cytoplasmic surface of cell membranes. In cells undergoing early cell membrane changes associated with apoptosis, phosphatidylserine is translocated from the inner membrane to the outer part of the plasma membrane where it can be detected using fluorescently labeled annexin V conjugates [10]. After 24 h, 16.72% ± 2.97% (SEM) of the Jurkat cells treated with 1 mg/mL ECM and 19.97% ± 1.76% (SEM) of the cells treated with 2 mg/mL ECM were shown to bind annexin V (Figure 2B). Binding of annexin V was significantly greater in Jurkat cells treated with 1 mg/mL ECM ($P = 0.0057$) and 2 mg/mL ECM ($P = 0.0197$) compared to untreated control cells. A flow cytometry histogram indicating a shift in the percentage of cells binding annexin V in response to ECM treatment is shown in Figure 2C. These results indicate that ECM-treated Jurkat cells undergo apoptosis and that apoptotic processes are likely involved in the observed growth inhibition. In this histogram, an insignificant ($P = 0.202$) increase in the number of dead cells (Q1-UR; Figure 2C) was also observed with ECM treatment.

Figure 2. Effects of epigonal conditioned medium (ECM) on cell growth and apoptosis in Jurkat cells. (**a**) Growth inhibition of Jurkat cells ($N = 11$) treated with ECM for 72 h measured using MTT. * Significantly greater ($P < 0.05$) than control; (**b**) Apoptosis in Jurkat cells treated with ECM for 24 h ($N = 3$), measured using flow cytometric detection of annexin V binding. * Significantly greater than untreated control ($P = 0.0057$ and 0.0197, respectively); (**c**) Histogram from ECM treated Jurkat cells showing binding of annexin V in flow cytometry; untreated control (top), 2 mg/mL ECM (bottom).

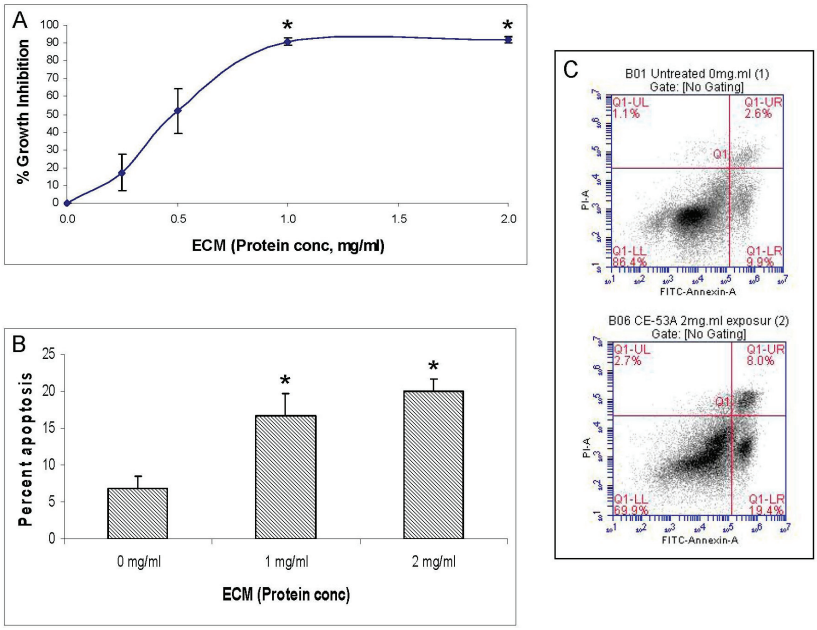

2.3. Caspase Activity Assays

To determine whether ECM exposure activates the caspase cascade in Jurkat cells, the functional activity of two initiator caspases (-8, -9) and one effector caspase (-3) was assessed in cell lysates from untreated and ECM-treated Jurkat cells. Results from enzyme activity assays are shown in Figure 3, and indicate increased caspase activity with exposure to ECM. Exposure to ECM resulted in a greater than 4-fold (4.11 ± 1.13, $N = 4$, $P < 0.05$) increase in the activity of the initiator caspase-8 (Figure 3A) in response to 1 mg/mL ECM and a greater than 2-fold (2.31 ± 0.67, $N = 4$, $P < 0.05$) increase in activity in response to 2 mg/mL ECM compared to untreated cells. Activity of the initiator caspase-9 (Figure 3B) was also significantly increased compared to untreated cells. At 1 mg/mL ECM, caspase-9 activity was 2.73 ± 0.41 (SEM)-fold and at 2 mg/mL ECM, caspase-9 activity was 2.83 ± 0.59 (SEM)-fold greater than in untreated Jurkat cells. Activity of the terminal caspase, caspase-3, was also increased in Jurkat cells treated with ECM compared to untreated controls (Figure 3C). The highest caspase-3 activity was observed in response to 2 mg/mL ECM, with a 4.8 ± 0.16-fold ($N = 3$, $P < 0.05$) increase in relative fluorescence compared with untreated controls. In response to 1 mg/mL ECM, the fold increase was 4.3 ± 0.22 ($P < 0.05$,

N = 3). These results indicate significant activation of key enzymes in the caspase cascade—caspases-8, -9, and -3—in response to exposure to ECM for 24 h. All apoptotic pathways end in activation of caspase-3, so observation of caspase-3 activation only provides additional evidence that apoptosis is occurring in target cells. Activation of caspase-8 is generally triggered through signals transmitted by death receptors (TRAIL or Fas) on the cell surface, but apoptosis can proceed either through the mitochondria (intrinsic) or bypass the mitochondria (extrinsic). Activation of caspase-9, however, can only occur in response to mediators released from the mitochondria, and thus indicates involvement of the mitochondria in apoptosis. Thus, observations reported here of significant activation of caspases-8, -9, and -3 are consistent with progression of apoptosis through the mitochondrial pathway.

Figure 3. Activation of caspase enzymes in Jurkat cells by ECM treatment. (**a**) Caspase-8; (**b**) Caspase-9; (**c**) Caspase-3. Activity of caspases-8 and -9 were measured using a colorimetric microplate assay; activity of caspase-3 was measured using a fluorimetric microplate assay. * Significantly different ($P < 0.05$) from control.

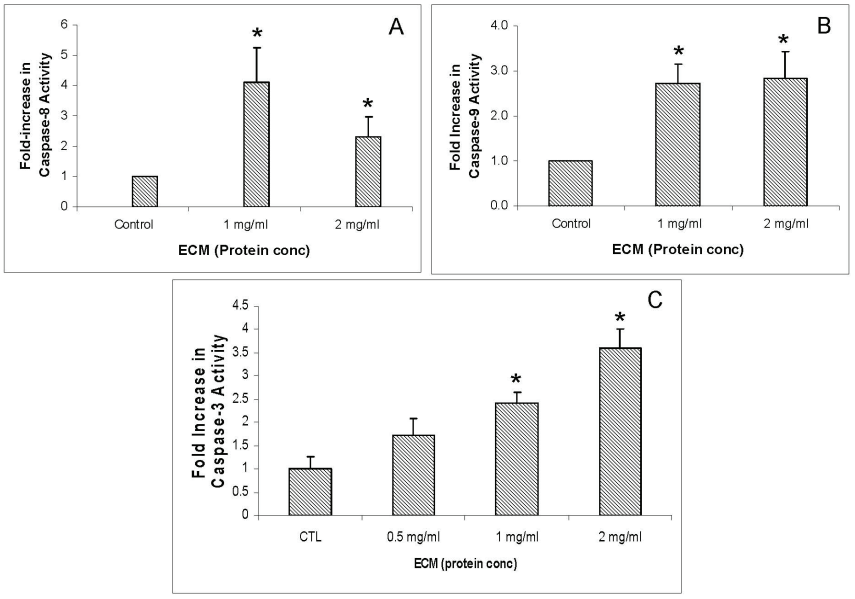

2.4. Western Blotting

In addition to functional activity assays, expression of specific apoptotic pathway intermediates at the protein level was assessed in ECM-treated Jurkat cells through Western blotting with monoclonal antibodies against caspases-3, -6, -7, -8, -9, and -10, cleaved caspases -3, -7, -8, and -9, apoptotic pathway promoters Smac/DIABLO, APAF-1, FADD, and apoptotic pathway inhibitors FLIP, PARP, and XIAP.

Western blot images demonstrating relative concentrations of initiator caspases -8 and -10, as well as cleaved caspase-8, are shown in Figure 4A. Figure 4B,C show relative band densities,

normalized to β-actin as protein loading control, of each of these molecules in ECM-treated Jurkat cell lysates compared with control. A significant ($P < 0.05$) decrease in the amount of full-length caspase-10 was observed after treatment with both 1 and 2 mg/mL ECM, which demonstrates activation of pro-caspase-10 to cleaved caspase-10. Differences in full-length and cleaved caspase-8 expression were not significant, although visually there appeared to be a difference in expression of these proteins in ECM-treated cells. These images demonstrate significant activation of caspase-10. A significant effect on protein expression of caspase-8 is not strongly observed through Western blotting. Once caspases-8 and -10 are activated, caspase-9 is cleaved, followed by activation of effector caspases-6 and -7, and finally by the terminal caspase, caspase-3. Western blot images demonstrating relative concentrations of caspase-9 and cleaved caspase-9 in Jurkat cells treated with ECM for 24 h are shown in Figure 5A. Relative band densities, using β-actin as protein loading control, are shown in Figure 5B. Full-length caspase-9 was significantly reduced in response to 2 mg ECM/mL (78.58% ± 2.36% of control; $P = 0.015$; one-way ANOVA). Production of cleaved caspase-9 is apparent, with an increase in band density over untreated cells observed following 1 mg/mL ECM treatment (125.89% ± 9.74%, $N = 4$, $P = 0.029$, *t*-test) and 2 mg/mL ECM treatment (131.20% ± 4.34%, $P = 0.029$, *t*-test). Activation of caspase-9 indicates progression of apoptosis through the mitochondrial (intrinsic) pathway.

Figure 4. Western blot analysis demonstrating relative concentrations of caspase-10, caspase-8, and cleaved caspase-8 in Jurkat cells treated with ECM for 24 h, using β-actin as protein loading control. (**a**) Western blot images and relative band densities for (**b**) caspase-10; and (**c**) caspase-8 and cleaved caspase-8. * Significantly different ($P < 0.05$) from control.

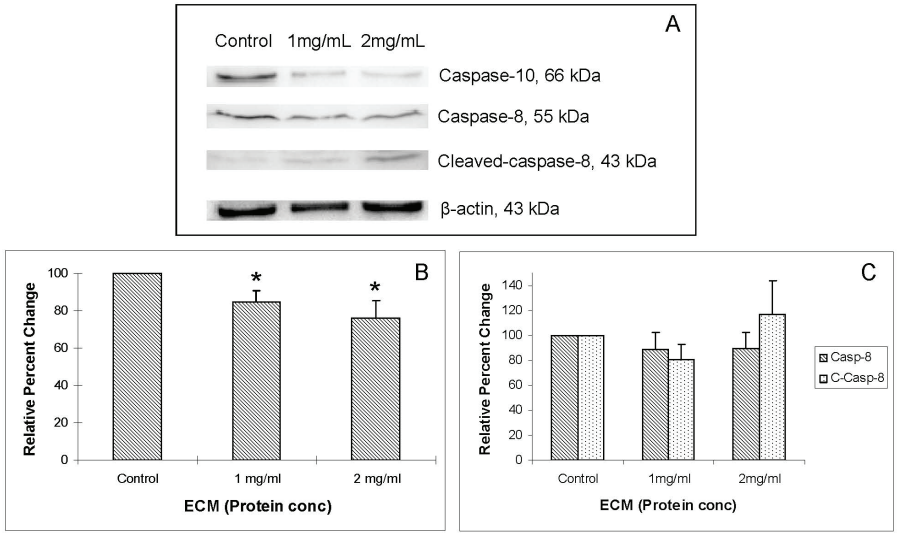

Figure 5. Western blot analysis demonstrating relative concentrations of caspase-9 and cleaved caspase-9 in Jurkat cells treated with ECM for 24 h, using β-actin as protein loading control. (**a**) Western blot images; (**b**) relative band densities for caspase-9 and cleaved caspase-9. * Significantly different ($P < 0.05$) from control.

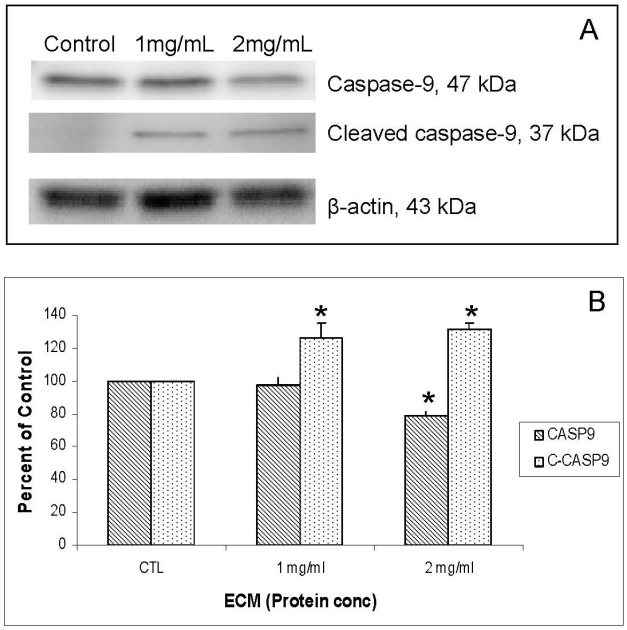

Western blot images demonstrating relative concentrations of caspase-6, -7, and -3 and cleaved caspases -7 and -3 in Jurkat cells treated with ECM for 24 h are shown in Figure 6A. Corresponding relative band densities are shown in Figure 6B,C. Caspase-6 is one of the major executioner caspases functioning in cellular apoptotic processes [11]. With full-length caspase-6 (35 kDa), there was very little detectable change in protein expression with ECM treatment (Figure 6A), although there was a slight (86.89% ± 6.52% of control), but statistically insignificant, decrease in expression at 2 mg/mL (Figure 6B). No significant differences in expression of full length caspase-6 were detected. Likewise, with caspase-7, there were no detectable changes in expression of full-length caspase-7 following ECM treatment for 24 h (Figure 6A,C). A slight increase (120% ± 15%) was seen in amount of cleaved caspase-7 in response to treatment with 2 mg/mL ECM, but this expression did not differ significantly from control. With caspase-3, there were slight decreases in amount of protein for full-length caspase protein (Figure 6A,D). Amounts of cleaved caspase-3 were increased by 117.72% ± 17.07% in response to 1 mg/mL and 205.84% ± 20.64% in response to 2 mg/mL ($P = 0.037$; one way ANOVA; Figure 6D). These observations indicate cleavage, and consequently, activation of initiator caspase-9 and terminal caspase-3. No significant differences in expression of proteins for caspase-6 or -7 were observed. Molecular pathways in Jurkat cells treated with ECM at concentrations of 1 and 2 mg protein/mL for 24 h indicate activation of apoptotic pathways and progression of cell death through apoptotic mechanisms.

Figure 6. Western blot analysis demonstrating relative concentrations of caspases -6, -7, and -3 and cleaved caspase -7 and -3 in Jurkat cells treated with ECM for 24 h, using β-actin as protein loading control. (**a**) Western blot images; and relative band densities for (**b**) caspase-6; (**c**) caspase-7 and cleaved caspase-7; and (**d**) caspase-3 and cleaved caspase-3. * Significantly different from untreated control.

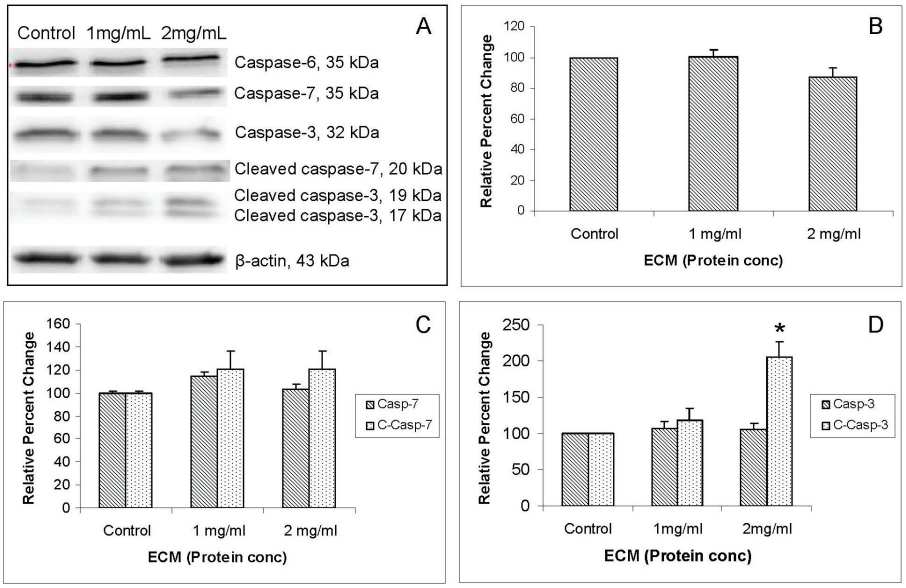

Other apoptosis pathway intermediates that were examined for their role in ECM-induced apoptosis in Jurkat cells include regulators involved in activation (FADD, APAF-1, Smac/DIABLO) as well as inhibitors of apoptosis (FLIP, XIAP, PARP). Western blotting results for FADD, APAF-1, and Smac/DIABLO are shown in Figure 7. Western blotting results for inhibitors FLIP and XIAP are shown in Figure 8. FADD (Fas-associated via death domain) functions as an apoptotic adaptor molecule that recruits caspase-8 or -10 to activated Fas (CD95) or TNFR-1 to form a death-inducing signaling complex (DISC) [12]. Relative band densities demonstrating effects of 24 h ECM on expression of FADD through Western blotting are shown in Figure 7B. With FADD, relative band density changed in response to 1 mg/mL (144.73% ± 25.45%, $N = 3$) and in response to 2 mg/mL (199.32% ± 45.2%, $N = 3$, $P < 0.05$, one-way ANOVA followed by Tukey's). APAF-1 (apoptotic protease activating factor 1) is a cytoplasmic protein involved in apoptosis by forming part of the apoptosome that binds and activates caspase-9. Relative band densities for APAF-1 are shown in Figure 7C. APAF-1 changed in relative band density by 114.79% ± 6.82% at 1 mg/mL ECM and 124.98% ± 6.07% at 2 mg/mL ECM ($P = 0.021$, one way ANOVA followed by Tukey's). Smac/DIABLO is a mitochondrial protein that functions as an apoptotic promoter by translocating to the cytosol and activating caspases in the cytochrome c/APAF-1/caspase-9 pathway and opposing inhibitory activity of inhibitor of apoptosis proteins (IAP), including XIAP [13]. No detectable change in expression of Smac/DIABLO was observed among ECM treatments. In summary, results indicate an increase in FADD and APAF-1

expression, but no change in expression of Smac/DIABLO. An increase in FADD expression indicates that ECM is involved in recruitment of FADD to the receptor, possibly through binding to TRAIL receptor [14], which would also be consistent with observed increased in caspase-8 activity. The increase in APAF-1 expression provides evidence that ECM initiates pathways that involve apoptosome formation and activation of caspase-9 [15]. Logically, a translocation of Smac/DIABLO would be involved in this process as well, but a significant change in expression of this molecule was not observed. This is not unexpected; however, since the whole cell lysate method used in these experiments does not provide information about protein localization within the cell.

Figure 7. Western blot analysis demonstrating effects of 24 h ECM treatment on expression of apoptotic pathway proteins FADD, APAF-1, and Smac/DIABLO. Western blot images (**a**) and relative band densities for (**b**) FADD; (**c**) APAF-1; and (**d**) Smac/DIABLO, using β-actin as protein loading control. *Significantly different ($P < 0.05$) from untreated control.

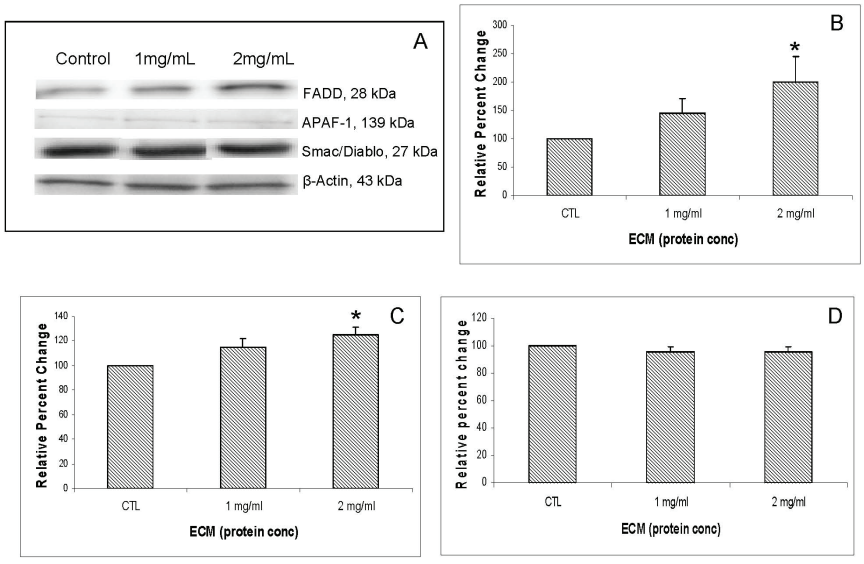

XIAP (X-linked inhibitor of apoptosis) encodes a potent apoptotic suppressor protein that functions by suppressing activities of caspases -3 and 7 [13]. FLIP (FLICE-like inhibitory protein), also known as CFLAR (CASP8 and FADD-like apoptosis regulator), is structurally similar to caspase-8 and regulates apoptosis by functioning as a crucial link between cell survival and cell death pathways by inhibiting TNFRSF6-mediated apoptosis [16,17]. As the major protein that prevents caspase-8 from activation by death receptors, c-FLIP protein can be recruited to the death-inducing signaling complex (DISC) to inhibit caspase-8 activation [18,19]. Western blot images demonstrating effects of 24 h ECM treatment on expression of apoptotic pathway inhibitor proteins, XIAP and FLIP, are shown in Figure 8A. Graphs representing relative band densities are shown in Figure 8B,C. XIAP was strongly affected by ECM treatment, with a relative band density

51.13% ± 11.29% of control at 1 mg/mL and 48.24% ± 12.14% of control at 2 mg/mL. These differences were significant at 1 mg/mL (P = 0.014, One way ANOVA Tukey's) and 2 mg/mL (P = 0.01, Tukey's). These results indicate a strong down-regulation of the key inhibitor protein, XIAP. Down-regulation of XIAP functions in facilitating progression of apoptotic pathways towards cell death by inhibiting caspase activity. Relative band density of FLIP did not change significantly in response to ECM treatment at either 1 or 2 mg/mL. Since FLIP is involved in inhibiting recruitment of caspase-8 [17], the absence of significant effects on expression of this inhibitor protein indicates no inhibition of apoptosis proceeding through caspase-8 recruitment and activation.

Figure 8. Western blot analysis demonstrating effects of 24 h ECM treatment on expression of apoptotic pathway proteins XIAP and FLIP. (**a**) Western blot images; and relative band densities for (**b**) XIAP; and (**c**) FLIP, using β-actin as protein loading control. * Significantly different (P < 0.05) from untreated control.

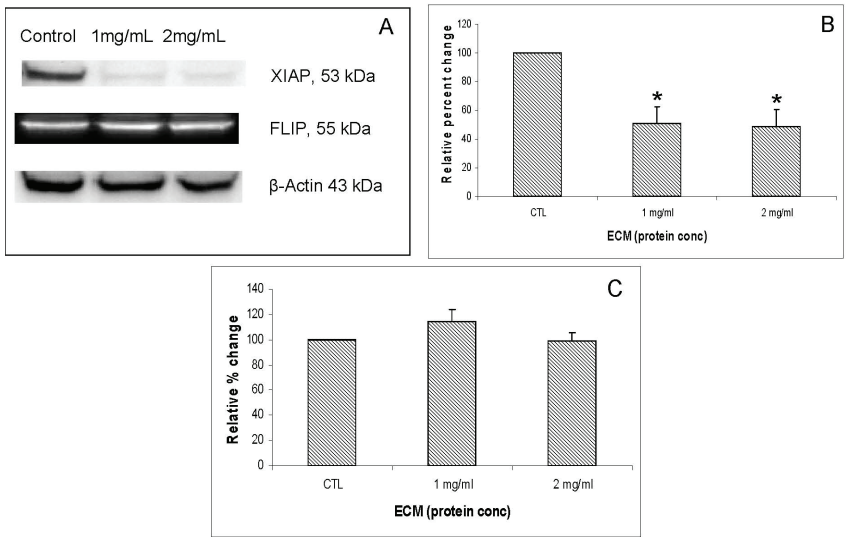

Another protein involved in inhibition of apoptosis is PARP (poly ADP-ribose polymerase), a nuclear protein that plays an important role in DNA repair [20] and is inactivated by enzymatic cleavage. Once the enzyme is inactivated by caspase-3, DNA repair is prevented, which allows DNA fragmentation, and thus apoptosis, to proceed. Effects of ECM treatment on the apoptotic inhibitor, PARP, were investigated using Western blotting, with results shown in Figure 9A (blot) and 9B (relative band densities for PARP/cleaved PARP). Cleavage of PARP was strongly observed in ECM-treated Jurkat cells, as evidenced by significant (P < 0.05) decreases in full-length PARP and significant increases in cleaved PARP at both 1 and 2 mg ECM protein/mL. These results indicate that the nuclear DNA repair protein, PARP, is inactivated in Jurkat cells treated with ECM.

Figure 9. Western blot analysis demonstrating effects of 24 h ECM treatment on expression of apoptotic pathway protein PARP. (**a**) Western blot images; (**b**) relative band densities for PARP and cleaved PARP, using β-actin as protein loading control. * Significantly different from untreated control.

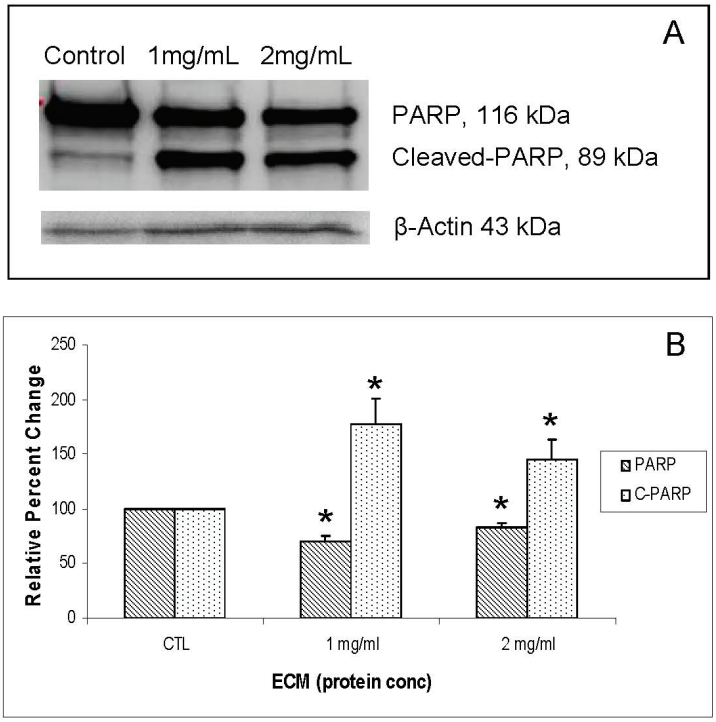

2.5. Antibody Array

An antibody array that measures 43 different apoptotic pathway intermediates was utilized to assess effects of ECM on Jurkat cells. The change in expression of apoptotic pathway proteins in Jurkat cell lysates detected on the antibody array following 24 h treatment with ECM is shown in Figure 10. Results are expressed as relative percent change compared to control (untreated) Jurkat cells using a graph representing relative band densities (Figure 10A) and a heat map (Figure 10B). A representative image of antibody arrays from control and ECM-treated (1 mg/mL) Jurkat cell lysates is also given (Figure 10C). Responses to ECM varied with concentration; of the 43 proteins that were on the array, only 9 were significantly ($P < 0.05$) changed from control in response to treatment with either 1 or 2 mg/mL ECM (ANOVA, $P < 0.05$). No pathway intermediates changed significantly in response to both ECM concentrations. The nine proteins which changed significantly at either 1 or 2 mg/mL ECM included the mitochondrial proteins BAD and BAX, apoptosis inhibitor, survivin, initiator caspase-8, death receptors DR6 and Fas, insulin growth factor binding protein IGFBP-1, and TNF family members TNF-α and sTNF-R2.

Figure 10. Relative percent change in expression of apoptotic pathway proteins in Jurkat cell lysates following 24 h treatment with ECM. Protein expression was determined using an antibody array (RayBio) containing 43 different antibodies for apoptotic pathway intermediates. Results are expressed as relative percent change compared to control (untreated) Jurkat cells using a heat map according to the color scale on the lower right. Only proteins that were significantly different ($P < 0.05$) compared to control at either 1 or 2 mg/mL ECM are shown. (**a**) Relative expression of intermediates significantly increased or decreased (d) from control at either 1 or 2 mg/mL. * Significantly different from control ($P < 0.05$); (**b**) heat map showing relative change in expression of proteins with significant increases or decreases; (**c**) representative array blot. $N = 4$ trials for the experiment.

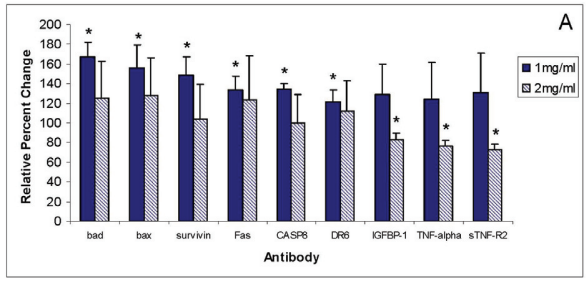

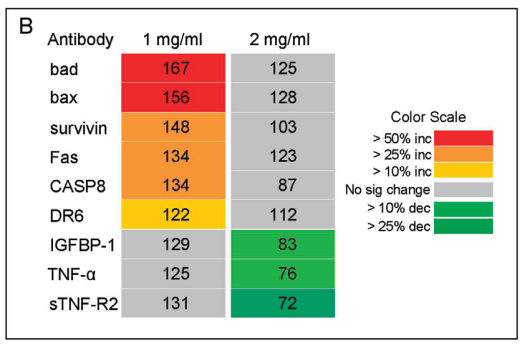

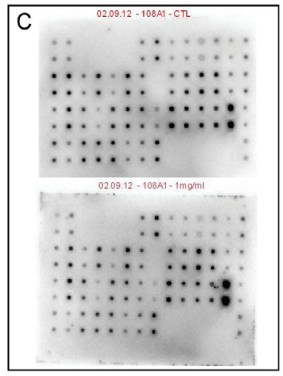

BAD and BAX are mitochondrial proteins that belong to the bcl-2 family of apoptosis regulators [21]. BAD, also known as BCL2-associated agonist of cell death, positively regulates apoptosis by forming heterodimers with BCL-XL and BCL-2 and reversing their repressor activity. BAX, also known as BCL2-associated X protein, activates apoptosis by opening mitochondrial voltage-dependent anion channel (VDAC) which leads to loss in membrane potential and subsequent release of cytochrome c from the mitochondria. BAX and BAD were both up-regulated greater than >150% in response to 1 mg/mL ECM ($P < 0.05$), but not significantly up-regulated in response to 2 mg/mL. Although an antibody for cytochrome c was included on the array, expression of cytochrome c was not significantly changed in response to ECM treatment. An increase in cytochrome c release, however, was previously demonstrated using mitochondrial and cytosolic fractions from another

cell line, a B-cell lymphoma (Daudi) exposed to ECM [5,6]. Similar to Smac/DIABLO, it is likely that no change was observed in these experiments with ECM-treated Jurkat cells because whole cell lysates rather than separated mitochondrial and cytosolic fractions were utilized.

Only two caspases (caspase-3 and caspase-8) were included on the array. Interestingly, caspase-3 was not significantly changed in response to ECM treatment on the array, although blot results with individual antibodies did show a significant change in both full-length procaspase enzyme forms as well as cleaved (active) forms of the enzyme. Levels of caspase-8 were up-regulated on the antibody array in response to 1 mg/mL ECM, a response different from the results obtained using Western blotting and individual antibodies, however, functional enzyme activity assays also indicated induction of caspase-8 activity with ECM treatment.

Several members of the TNF receptor superfamily were included on the array. DR6 and Fas are both cell surface receptors belonging to the TNF receptor superfamily that were significantly up-regulated in response to ECM. Expression of DR6 was significantly increased in response to 1 mg/mL ECM, but not 2 mg/mL. DR6 is TNF receptor superfamily member 21 (TNFRSF21) and is involved in inducing apoptosis. Through its death domain, DR6 interacts with TRADD (TNFRSF1A-associated via death domain), an adaptor molecule that mediates signal transduction occurring through TNF-receptors and triggers the caspase cascade [12,22]. DR6 also activates NF-κB and MAPK8/JNK. Fas, another member of the TNF-receptor superfamily (TNFRSF6), was also significantly up-regulated in response to 1 mg/mL ECM, but not 2 mg/mL. Fas, also known as CD95 or APO-1, plays a central role in regulation of apoptosis and contains a death domain [12]. The interaction of Fas with FasL forms a death-inducing signaling complex that includes Fas-associated death domain protein (FADD), caspase-8 and caspase-10, and leads to apoptosis [12]. Results indicate activation of Fas and DR6 by ECM, thus likely leading to induction of the caspase cascade through caspase-8. Other TNF family members on the array included soluble TNF receptors sTNF-R1 and sTNF-R2, with sTNF-R2 significantly down-regulated in response to 2 mg/mL ECM. TNF-R2 mediates most effects of TNF-α [23]. TNF-α was significantly down-regulated in response to ECM treatment at 2 mg/mL. Although several TRAIL receptors, death receptors TRAIL-R1 (DR4) and TRAIL-R2 (DR5) and decoy receptors TRAIL-R3 (DcR3) and TRAIL-R4 (DcR2), were included on the array, none of these were significantly altered in response to ECM treatment. TRAIL-R1 (DR4) is activated by TRAIL and functions in transducing cell death signals and inducing apoptosis [12]. TRAIL-R2 (DR5) is also activated by TRAIL binding and transduces apoptosis signals [12]. The decoy receptor, TRAIL-R3 (DcR1), binds TRAIL but lacks a cytoplasmic death domain and therefore is not capable of inducing apoptosis. This receptor is believed to protect against TRAIL-mediated apoptosis by competing with TRAIL-R1 and R2 for ligand binding [12]. Another decoy receptor, TRAIL-R4 (DcR2), also binds TRAIL but contains a truncated cytoplasmic death domain and thus does not transmit signals for apoptosis induction [12]. Several heat shock proteins (HSP27, HSP60, HSP70), markers of cell stress, were included on the array, although none were significantly affected by ECM treatment.

Apoptosis is tightly regulated through careful balance of pro- and anti-apoptotic factors. Survivin and IGFBP-1 are apoptotic inhibitor proteins that were present on the array. IGFBP-1 has been reported to function as a negative regulator of BAK-dependent apoptosis, and thus functions

to inhibit apoptosis [24]. In response to ECM treatment, IGFBP-1 was significantly down-regulated at 2 mg/mL. Based on its role as an inhibitor of apoptosis, this decrease in IGFBP-1 protein levels indicates ECM facilitates apoptosis by decreasing inhibitor expression. Although a number of pro-apoptotic molecules were positively up-regulated, a significant increase in the anti-apoptotic molecule, survivin, was observed in response to 1 mg/mL ECM. Survivin, also known as BIRC5, is an inhibitor of apoptosis and functions in promoting cell survival by inhibiting activities of caspase-3 and caspase-7 [25,26]. Survivin is a member of the IAP (inhibitor of apoptosis proteins) family of proteins and acts downstream of mitochondria to prevent processing of caspase-9 from the apoptosome, which prevents activation of downstream effector caspases, and is thought to modulate both extrinsic and intrinsic apoptotic pathways [25,26]. In contrast to malignant tissues, survivin is not usually expressed in normal cells, thus making it an ideal target for cancer therapy [27]. In experiments reported here, ECM treatment significantly increased survivin expression at 1 mg/mL, observations which are inconsistent with the large amount of data indicating activation of pro-apoptotic molecules. Despite up-regulation of survivin, however, ECM induces apoptosis in Jurkat cells. The explanation for this is unclear, although it appears that the pro-apoptotic signaling activated by ECM overcomes the anti-apoptotic signaling provided by survivin. Similar responses have been observed with another potential therapeutic agent, P2-341 (Bortezomib), in which survivin expression was increased in presence of apoptosis, an observation hypothesized to be a consequence of proteasome inhibition [28]. In other systems, Fas-induced apoptosis was associated with release of cytochrome c as well as up-regulation of survivin in mitochondria, nucleus, and cytosol [29]. Survivin is known to be a multifunctional protein with roles in cell division as well as apoptosis [30]. Survivin biology includes a link to multiple pathways of cellular homeostasis [31]. XIAP binds survivin that is released from mitochondria in response to cell death stimuli [32]. Since XIAP was dramatically decreased, it is possible that the increase in survivin was a reflection of lower amounts of available XIAP. Alternatively, the observed increase in survivin expression may be related to one of the other cellular roles attributed to survivin. Overexpression of survivin has been reported to be more efficient at blocking mitochondrial but not death-receptor-induced apoptosis [33]. Also of interest is that a complex between survivin and caspase-9 has been demonstrated [34]; survivin is also believed to associated with Smac/DIABLO [35].

2.6. Gene Expression

Effects of ECM treatment on the expression of APAF-1, Smac/DIABLO, XIAP, and Bcl-xL genes in Jurkat cells was investigated using both gene-specific primers and PCR arrays (described below). These results using real-time quantitative PCR are shown in Figure 11. The genes that were significantly altered included XIAP, which was significantly decreased in response to ECM treatment at 1 and 2 mg/mL and APAF-1, which was significantly decreased in response to 2 mg/mL. Genes coding for Smac/DIABLO and Bcl-xL were not significantly affected by ECM treatment. The significant decrease in gene expression for XIAP corresponds to what was observed at the protein level with the individual antibody to XIAP. The significant decrease in APAF-1 observed at the gene level, however, is contrary to what was observed at the protein level.

Figure 11. Effect of ECM treatment on gene expression on APAF-1, Smac/DIABLO, XIAP, and Bcl-xL using qPCR. * Significantly different from control (ANOVA, $P < 0.05$).

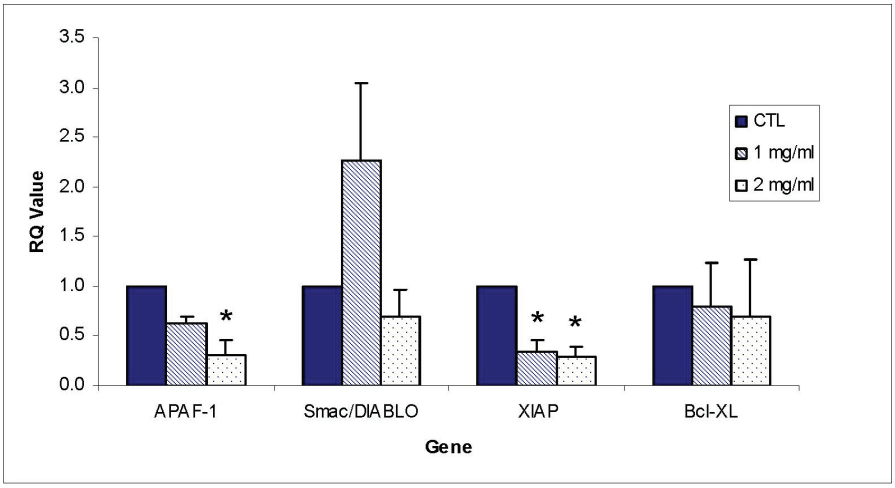

2.7. PCR Array

The relative fold change in expression of apoptotic pathway genes in Jurkat cells following 24 h treatment with ECM is shown in Figure 12. Gene expression was determined using a PCR array (Applied Biosystems) containing primers for 84 different genes coding for apoptotic pathway intermediates. Results are expressed as relative fold change compared to control (untreated) Jurkat cells using a heat map. Only genes with expression that was significantly changed ($P < 0.05$) in response to ECM treatment at 1 or 2 mg/mL were included on the heat map. Genes that encode positive inducers of apoptosis are shown in Figure 12A; inhibitors of apoptosis are shown in Figure 12B. The first several genes listed in the array data in Figure 12A encode mitochondrial proteins (BAD, BCL10 BCL2L11, BCL2L14, and BID). Expression of the genes encoding BAD, a mitochondrial protein that promotes apoptosis, was down-regulated in response to 1 and 2 mg/mL ECM treatment; an opposite effect to that observed at the protein level. Expression of mitochondrial BCL family members BCL10, BCL2L11, BCL2L14, all inducers of apoptosis, was up-regulated in response to 2 mg/mL ECM. BCL10 contains a caspase recruitment domain (CARD) and has been shown to induce apoptosis through activation of pro-caspase-9 and NF-κB. BCL2L11, also known as BIM, encodes a protein that acts as an apoptotic activator, as does BCL2L14. A gene coding for another mitochondrial protein and BCL2 family member, BID, was down-regulated in response to 1 and 2 mg/mL ECM. BID functions by mediating mitochondrial damage induced by caspase-8 and ultimately triggering cytochrome c release [21].

Figure 12. Relative fold change in expression of apoptotic pathway genes in Jurkat cells following 24 h treatment with ECM. Gene expression was determined using a PCR array (Applied Biosystems) containing primers for 84 different genes for apoptotic pathway intermediates. Results are expressed as relative fold change compared to control (untreated) Jurkat cells using a heat map according to the color scale. (**a**) relative fold change of pro-apoptotic intermediates; (**b**) relative fold change of anti-apoptotic intermediates. $N = 3$ trails for the experiment. Only genes that were significantly different among treatments ($P < 0.05$, $N = 3$) are included in the heat map.

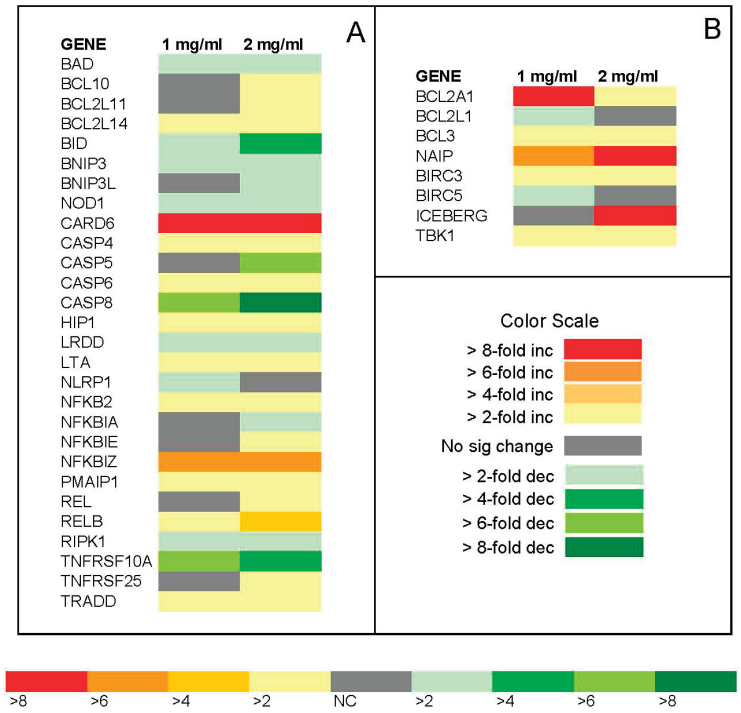

The genes BNIP3, BNIP3L, and NOD1 were all down-regulated. BNIP3 and BNIP3L are apoptosis-inducing proteins that can overcome BCL2 and BCL-XL suppression [36]. Nods, a growing family of proteins containing a nucleotide-binding oligomerization domain (NOD), are involved in regulation of programmed cell death and immune responses. APAF-1, ced-4, and Nod1 are members of this family. The NOD module is homologous to ATP-binding cassette (ABC) found in a large number of proteins with diverse biological function, and result in activation of diverse signaling pathways involved in elimination of cells via programmed cell death. NOD1 encodes a cytosolic APAF-1 like molecule that contains a caspase recruitment domain (CARD) and promotes apoptosis by enhancing caspase-9-mediated apoptosis [37]. The most strongly up-regulated molecule on the array was CARD6, with greater than 8-fold increase in expression at both 1 and 2 mg/mL ECM. The protein encoded by this gene contains a CARD with a domain structure not shared by other CARD proteins and is a microtubule-associated protein that interacts with

receptor-interacting protein kinases (RIPK) and positively modulates signal transduction pathways activating NF-κB [38,39]. Most proteins containing a CARD are involved in pathways regulating apoptosis [38,39]. Examples of prominent CARD proteins are caspase-9 and APAF-1, which are involved in the intrinsic death pathway; BCL10 and CARD11, which mediate antigen receptor-induced NF-κB activation, and receptor-interacting protein (RIP)-like interacting caspase-like apoptosis regulatory protein kinase (RICK) and the nucleotide-binding oligomerization domain (NOD) proteins, which induce NF-κB activation [38].

With regard to caspase genes on the array, the genes coding for CASP4 and CASP6 were up-regulated, whereas the genes coding for CASP5 and CASP8 were down-regulated. Caspase-8 was the only caspase that appeared on both the protein and gene arrays. CASP8 was down-regulated in the gene array and up-regulated on the protein array. CASP4, CASP5, CASP6, and CASP8 all encode caspase enzymes which are initially present in the cell as inactive precursor forms that become activated with cellular processing; overexpression of these genes promotes cell death. HIP1, also known as huntingtin interacting protein, was up-regulated. The protein encoded by this gene is important in cell filament networks and promotes apoptosis through the intrinsic apoptosis pathway [40]. The gene coding for LRDD, also known as PIDD (p53-induced death domain protein), was down-regulated. LRDD is involved in apoptosis through interaction with death domain proteins such as FADD and MADD and may function as an adaptor protein in cell death-related signaling processes and play a role as an effector of p53-dependent apoptosis by promoting apoptosis as a component of the DNA damage/stress response pathway that connects p53 to apoptosis [41]. PIDD is implicated in activation of pro-caspase-2 and may mediate apoptosis induction by tumor suppressor p53 [42]. LTA encodes a protein, lymphotoxin alpha—a member of the tumor necrosis factor family, that functions as a death receptor ligand and plays a role in promoting apoptosis by binding to TNFRs [43]. LTA was up-regulated in response to both 1 and 2 mg/mL ECM. NLRP1 is a gene that encodes a member of the ced-4 family of apoptosis proteins; ced-family members contain a CARD and are known to be key mediators of programmed cell death by enhancing APAF-1 and cytochrome c-dependent activation of pro-caspase 9. NLRP1 was up-regulated in response to 1 mg/mL ECM, but unchanged in response to 2 mg/mL ECM. The higher expression of genes for certain caspase enzymes, genes coding for death domain proteins, and genes coding for proteins that promote apoptosis through death receptors in response to ECM treatment indicates apoptosis induction in target cells by ECM, proceeding through death receptor-initiated mechanisms.

The transcription factor NFκB is activated in response to death receptor signaling [44]. The pattern of NFkB pathway activation in Jurkat cells treated with ECM was complex. In the NFκB family, some mediators were up-regulated and some were down-regulated in response to ECM treatment. NFKB2, NFKBIE, and NFKBIZ were up-regulated. NFKB2, a subunit of the NFκB transcription factor complex, was up-regulated. REL (also designated c-Rel) was up-regulated, which functions in promoting cell death [44]; RELB was also up-regulated. Certain NFkB pathway regulators, NFKBIE and NFKBIZ, were also up-regulated. PMAIP, also known as NOXA, was up-regulated. This molecule is known to promote activation of caspases, and thus induction of apoptosis. PMAIP1, REL, and RELB were up-regulated. PMAIP1 promotes activation of caspases

and mitochondrial membrane changes that result in efflux of apoptogenic proteins from the mitochondria, while REL and RELB form part of NFKB complex.

RIPK1, also known as receptor (TNFRSF)-interacting serine-threonine kinase, was down-regulated. The protein encoded by this gene induces apoptosis following death receptor ligation and forms a necroptosis inducing complex [45]. TNFRSF10A, also known as DR4 or TRAIL-R1, is activated by TRAIL and transduces cell death signals and induces apoptosis [43]. TNFRSF10A was down-regulated on the gene array in response to both 1 and 2 mg/mL ECM. TNFRSF25 was up-regulated in response to 1 mg/mL ECM and TRADD was up-regulated in response to both 1 and 2 mg/mL ECM. TNFRSF25, also known as DR3, regulates apoptosis by interacting directly with TRADD and activating NFκB [46]. Overexpression of TRADD (TNFR1-associated death domain protein) is involved in Fas-induced cell death pathway and activation of NFκB [46].

BCL2A1, an inhibitor of apoptosis, was up-regulated in response to both 1 and 2 mg/mL. BCL2A1 is a member of the BCL2 family and encodes a protein that decreases mitochondrial release of cytochrome c and blocks caspase activation [47]. Another apoptosis inhibitor, BCL2L1, was down-regulated. BCL2L1 also works by preventing release of caspase activators from the mitochondrial membrane and thus preventing activation of caspases [21]. Other inhibitors, BCL3, NAIP, and BIRC3, were up-regulated. NAIP (NLR family, apoptosis inhibitory protein) is involved in suppressing apoptosis by inhibiting activities of caspases-3, -7, and -9 [48]. BIRC3 encodes a member of the IAP family of proteins that inhibit apoptosis by binding to tumor necrosis receptor-associated factors TRAF1 and TRAF2 [49]. BIRC5, also known as survivin, was down-regulated on the PCR array in response to 1 mg/mL ECM, but was up-regulated at the protein level on the antibody array in response to treatment with the same concentration of ECM. ICEBERG was strongly (>8-fold) up-regulated in response to 2 mg/mL ECM. ICEBERG is a CARD family member that inhibits caspase-1 [50]. In other studies, ICEBERG was up-regulated in response to TNF [50]. TBK1 (TANK-binding kinase 1), which is also known as NF-kappa-B-activating kinase, was up-regulated; this molecule plays a role in mediate NFKB activation in response to certain growth factors.

2.8. Expression of TRAIL Receptors on Jurkat Cells Treated with ECM

TRAIL, tumor necrosis factor-related apoptosis-inducing ligand, is a member of the TNF family of proteins [51]. TRAIL activates apoptosis through binding to receptors known as “death receptors”. The primary known death receptors are TRAIL-R1 (also designated as DR4) and TRAIL-R2 (also known as DR5), which are members of the TNFR superfamily [52–54]. TRAIL also binds two other cell receptors which are known as “decoy” receptors. These decoy receptors are designated TRAIL-R3 (or DcR1) and TRAIL-R4 (or DcR2) and contain substantial homology in their extracellular domains to TRAIL-R1 and TRAIL-R2. Because of their homology, TRAIL readily binds to TRAIL-R3 and TRAIL-R4, but because they have either a truncated (DcR2) or absent (DcR1) intracellular death domain, binding of TRAIL to these receptors does not trigger apoptosis [12]. Unlike TRAIL-R1 and TRAIL-R2, neither TRAIL-R3 nor TRAIL-R4 contain intact cytoplasmic death domains that signal for apoptosis. TRAIL-R4 possesses a partially truncated death domain, whereas TRAIL-R3 is anchored on the membrane via glycosyl-phosphatidylinositol

linkage [55]. In cells that are sensitive to TRAIL-induced apoptosis, increased expression of decoy receptors on normal cells is believed to be a major factor responsible for resistance against TRAIL-induced apoptosis [44,56].

In these experiments, expression of two death receptors, TRAIL-R1 and TRAIL-R2, and two decoy receptors, TRAIL-R3 (DcR1) and TRAIL-R4 (DcR2) were examined. Jurkat cells are known to express high levels of TRAIL-R2 [57]. Expression of TRAIL-R1 (DR4) and/or TRAIL-R2 (DR5) was up-regulated in cancer cells in response to a number of chemotherapeutic drugs [58]. Surface expression of death receptors TRAIL-R1 (DR4) and TRAIL-R2 (DR5) on Jurkat cells in response to ECM is shown in Figure 13. Expression of TRAIL-R2 (DR5) was significantly ($P < 0.05$) up-regulated in response to 1 and 2 mg/mL ECM (25.35% ± 3.26%; 24.75% ± 1.65%) whereas expression of TRAIL-R1 (DR4) was significantly up-regulated only in response to 2 mg/mL ECM (24.84% ± 0.98% SEM). Surprisingly, expression of TRAIL-R3 (DcR1) and TRAIL-R4 (DcR2) were significantly up-regulated in response to both 1 and 2 mg/mL ECM.

Figure 13. Expression of death and decoy receptors on the surface of untreated Jurkat T cell leukemia cells (control) and Jurkat cells treated with ECM at 1 and 2 mg/mL for 24 h. (**a**) death receptor (TRAIL-R1 and TRAIL-R2) expression; (**b**) decoy receptor (TRAIL-R3 and TRAIL-R4) expression. * Significantly different ($P < 0.05$; one-way ANOVA; $N = 3$) from control.

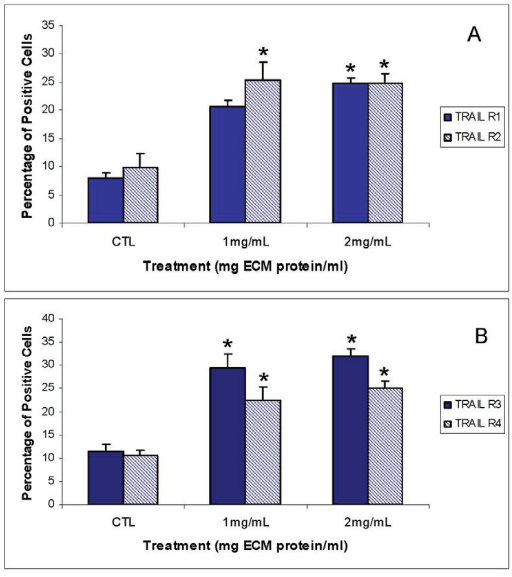

2.9. Comparison of Apoptosis Pathway Intermediates Using Different Means of Detection

Figures 14 and 15 show qualitative comparisons of effects of 1 and 2 mg/mL ECM on apoptosis mediators in Jurkat cells as measured by different methods. Observed increases or decreases of pro-apoptosis regulators (Figure 14) and anti-apoptosis regulators (Figure 15) among Western blotting with individual antibodies and antibody arrays, gene expression of pathway intermediates

using Q-PCR of individual genes and PCR arrays, functional enzyme activity assays, and surface expression of receptors using flow cytometric detection are shown.

Figure 14. Qualitative comparison of changes in 62 pro-apoptotic regulators in Jurkat T cell leukemia cells exposed to ECM at 1 and 2 mg/mL. Observed increases or decreases are based on antibody recognition of pathway intermediates using Western blotting with individual antibodies and antibody arrays, gene expression of pathway intermediates using Q-PCR of individual genes and PCR arrays, functional enzyme activity assays, and surface expression of receptors using flow cytometric detection.

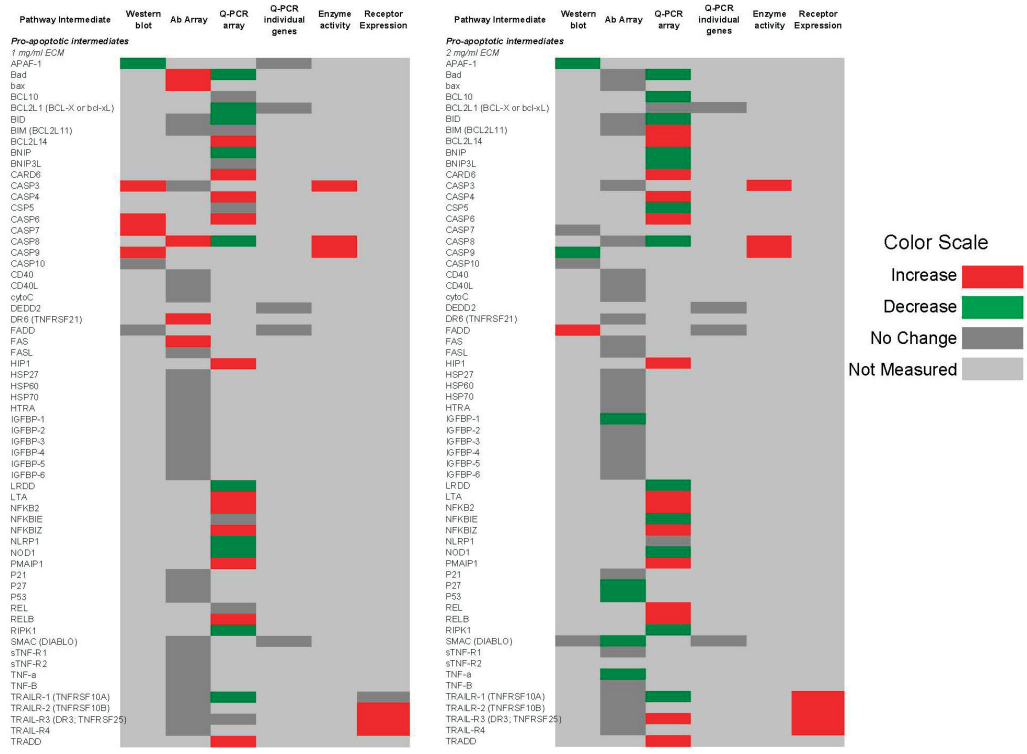

In these comparisons, inconsistencies among results obtained through different methods of analysis were observed. Some variations may be a result of the temporal nature of apoptotic signaling, with gene expression changes occurring generally earlier than changes reflected at the protein level.

With regard to mitochondrial proteins, BAD was up-regulated in response to 1 mg/mL at the protein level but down-regulated at the gene level in response to both 1 and 2 mg/mL treatments. BID showed no change in response to 1 mg/mL at the protein level, but was decreased in expression at the gene level. In response to 2 mg/mL, BIM was decreased at the protein level but increased at the gene level. BAX was up-regulated at the gene level. BAX and BAD are important pro-apoptotic in the mitochondria [59].

Figure 15. Qualitative comparison of changes in 17 anti-apoptotic regulators in Jurkat T cell leukemia cells exposed to ECM at 1 and 2 mg/mL. Observed increases or decreases are based on antibody recognition of pathway intermediates using Western blotting with individual antibodies and antibody arrays, and gene expression of pathway intermediates using Q-PCR of individual genes and PCR array.

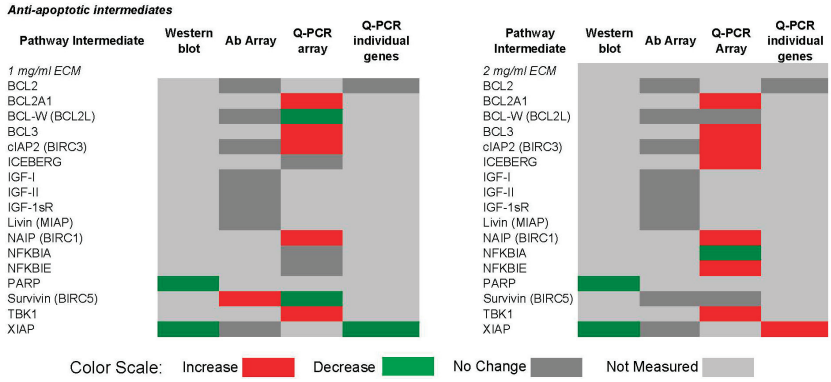

With caspase enzymes, expression of caspase-8 was increased at the protein level and at the level of functional enzyme activity. Genetic expression of caspase-8, however, was decreased in response to 1 mg/mL. With 2 mg/mL ECM treatment, caspase-8 expression was decreased at both protein and gene levels. Caspase-3 expression was not significantly changed at the protein level as determined using the antibody array, but functional enzyme activity and amount of cleaved caspase-3 at the protein level were increased in response to 2 mg/mL ECM.

Expression of TRAIL-R1 was not changed at the protein level, but was decreased at the gene level. Surface expression was also not significantly up-regulated in response to 1 mg/mL ECM. Jurkat cells express higher levels of TRAIL-R2 than TRAIL-R1 [56,57]. Surface expression of TRAIL-R1 and TRAIL-R2, however, was significantly increased with 2 mg/mL ECM. No changed was observed at the protein level in expression of the decoy receptor TRAIL-R3, but an increase in expression was observed at the gene level in response to 2 mg/mL. Surprisingly, surface expression of the decoy receptors TRAIL-R3 and TRAIL-R4 was significantly increased. The observed effects with decoy and death receptors are difficult to interpret. In other studies, decoy receptors DcR1 and DcR2 were expressed on Jurkat cells and were increased in expression with stimulation with TRAIL [60]. Generally, it has been believed that transient overexpression of DcR1 or DcR2 in TRAIL-sensitive tumor cells prevents cell death trigger by TRAIL [61,62] and recent evidence indicates that tumor and normal cells can acquire resistance to TRAIL-induced killing by up-regulating TRAIL antagonistic receptors [55,63,64]. It has been proposed that decoy receptors actually are likely to play more of a regulatory rather than inhibitory role [55].

Overall, the results obtained indicate that ECM is cytotoxic (MTT) towards cultured Jurkat cells through triggering apoptosis (annexin V). The diagram in Figure 16 can be used to illustrate proposed ECM-induced regulation of pathway intermediates resulting in apoptosis in ECM-treated Jurkat cells. Briefly, results presented here following ECM treatment are consistent with apoptotic

activation pathways that would be observed with binding to death receptors (DR4 and DR5) on the cell surface (Figure 16, Box 1). Based on the pattern of adaptor molecule (FADD; Box 2) and initiator caspase activation (caspase 8 and caspase 10; Box 3), activation of mitochondrial proteins BAD (Box 4) and BAX (Box 5), post-mitochondrial apoptosis pathway intermediates APAF-1 (Box 6) and caspase-9 (Box 7), and activation of the terminal caspase, caspase-3 (Box 9), these data are consistent with progression of apoptosis through the intrinsic (mitochondrial) pathway. Down-regulation of an important inhibitor of apoptosis (XIAP, Box 8) and cleavage of the nuclear DNA repair enzyme, PARP (Box 10) also facilitate progression of apoptosis.

Figure 16. A schematic diagram showing the proposed ECM-induced regulation of pathway intermediates resulting in apoptosis in ECM-treated Jurkat cells. In this proposed schematic, ECM binds to death receptors DR4 and DR5 on the cell surface (**Box 1**) which stimulates the adapter molecule FADD (**Box 2**) to activate initiator caspases -8 and -10 (**Box 3**), mitochondrial proteins BAD (**Box 4**) and BAX (**Box 5**), post-mitochondrial apoptosis pathway intermediate APAF-1 (**Box 6**) and initiator caspase-9 (**Box 7**), resulting in the activation of terminal effector caspase-3 (**Box 8**). These data are consistent with progression of apoptosis through the intrinsic (mitochondrial) pathway. Down-regulation of an apoptotic inhibitor XIAP (**Box 9**) and cleavage of the nuclear DNA repair enzyme PARP (**Box 10**) also facilitate progression of apoptosis.

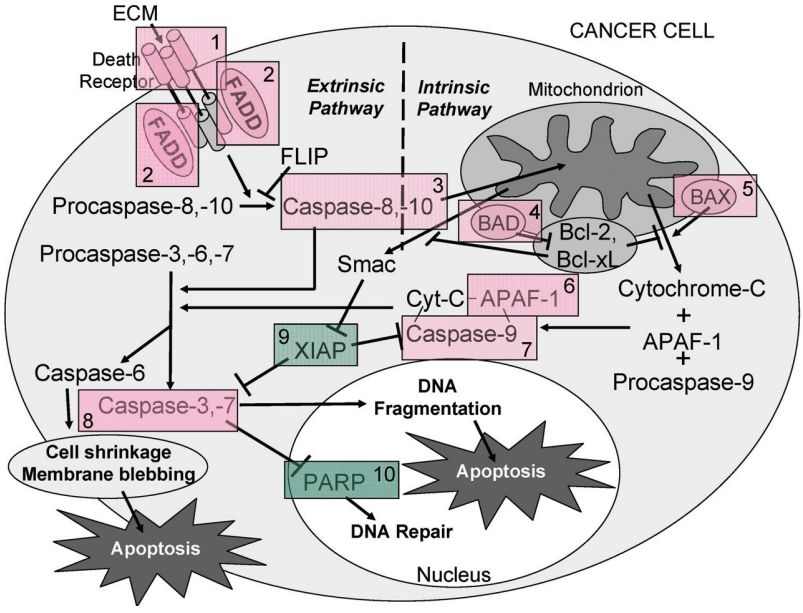

3. Experimental Section

3.1. Animals

Mature bonnethead sharks (*Sphyrna tiburo*) were collected in the Gulf of Mexico in nearshore waters off Sarasota, FL, under a Special Activities License issued to Mote Marine Laboratory by the Florida Fish and Wildlife Conservation Commission, and transported live to Mote Marine Laboratory, in Sarasota, FL, USA.

3.2. Culture of Elasmobranch Epigonal Cells

Epigonal organs were excised under aseptic conditions from sharks euthanized using methods approved by the AVMA Guidelines for the Euthanasia of Animals (2013 Edition), and following protocols approved by Mote Marine Laboratory's IACUC. Epigonal tissue was rinsed thoroughly with sterile elasmobranch-modified phosphate buffered saline (E-PBS) [65], epigonal cells were resuspended in sterile elasmobranch-modified RPMI (E-RPMI) [5,6], and cultured at 25 °C, 5% CO_2 for 2–4 days as described [6].

3.3. Preparation of Epigonal Conditioned Medium (ECM)

After 2–4 days of culture, cell-free-ECM was prepared by aspirating culture supernatants and centrifuging at 2000 × *g* for 20 min at 4 °C. Cell pellets were discarded and supernatant dialyzed against several changes of 50 mM ammonium bicarbonate at 4 °C for 4–5 days using 6–8000 MWCO dialysis tubing (Spectrum). Dialyzed conditioned media preparations were lyophilized at stored at −80 °C. Protein concentration of ECM was determined using the Bradford assay (BioRad).

3.4. Cell Line

Jurkat cells, clone E6-1, were obtained from the American Type Culture Collection (TIB-15; ATCC, Manasass, VA, USA) and maintained in RPMI-1640 (ATCC) with 10% heat-inactivated fetal bovine serum (HI-FBS; Hyclone) in a humidified atmosphere of 37 °C, 5% CO_2. Cells were subcultured by adjusting cell concentration to 2×10^5 cells/mL every 2–3 days.

3.5. Growth Inhibition Assay

Growth inhibitory activity of ECM against Jurkat cells was assessed using 1-(4,5-dimethylthiazol-2-yl)-3,5-diphenylformazan (MTT) [9]. Lyophilized ECM samples ($N = 11$) were resuspended in RPMI 1640 at a concentration of 4 mg/mL and filter-sterilized through a 0.2 µm syringe filter. Cells (2.5×10^4 cells/mL final concentration) were co-cultured with ECM in 96-well sterile microtiter plates in triplicate for concentrations ranging from 0.25 to 2 mg/mL protein in a total volume of 200 µL RPMI 1640 and 10% HI-FBS for 72 h at 37 °C, 5% CO_2 in a humidified atmosphere. After 72 h incubation, 100 µL supernatant was removed from each well, and microtiter plates were returned to the incubator for 4 h. After 4 h, 100 µL solubilizer (0.01 N HCl, 10% SDS) was added to each well and plates incubated overnight at 37 °C. MTT conversion was measured at

570 nm with background absorbance at 630 nm using a microplate reader (BioTek, Model ELx800, Winooski, VT, USA). Percent growth inhibition was calculated using the following formula: %GI = (CTL $Abs_{570-630}$ − TRT $Abs_{570-630}$ × 100).

3.6. Experimental ECM Exposures

Jurkat cells were co-cultured with ECM for 24 h and harvested as appropriate for analysis by enzyme activity assay, western blotting, antibody array, Q-PCR, PCR array, or cell flow cytometry. Jurkat cells were plated in sterile 24-well plates at concentrations of either 2 × 10^6 cells/well (Q-PCR), 5 × 10^6 cells/well (enzyme activity, Western blotting, antibody array, cell flow cytometry) or as specified below. Lyophilyzed ECM samples were resuspended in RPMI 1640 at a concentration of 4 mg/mL and filter-sterilized through a 0.2 µm syringe filter. Cells were co-cultured with ECM in concentrations of 0, 1, and 2 mg/mL protein in a total volume of 1 mL RPMI 1640 and 10% HI-FBS. Cells were incubated for 24 h at 37 °C, 5% CO_2 in a humidified atmosphere.

3.7. Annexin V

Induction of apoptosis in Jurkat cells was measured using the ApoDETECT Annexin V-FITC kit (Life Technologies, Grand Island, NY, USA) according to manufacturer's instructions. Jurkat cells were cultured as described above for flow cytometry and exposed to three different ECM (0, 1, 2 mg/mL protein) preparations or staurosporine (1 µM) in duplicate. A dead cell control was prepared by freezing cells (−80 °C) for 30 min, followed by heating (95 °C) for 30 min. Cells were incubated with ECM for 24 h at 37 °C, 5% CO_2 in RPMI 1640 containing 10% FBS. After treatment, cells were harvested by centrifugation, washed in sterile PBS, resuspended in binding buffer, and stained with FITC-labeled Annexin V (10 µL) and propidium iodide (1 µg/mL final concentration). Samples were analyzed using an Accuri C6 Flow Cytometer with CFlow PLUS software (BD Biosciences, San Jose, CA, USA), with 25,000 events collected on each sample. Compensation was adjusted to minimize overlap in fluorescence signals. Percent apoptosis was calculated as the percentage of the total cell population which stained positive for Annexin V, but not propidium iodide.

3.8. Caspase Activity

Lysates of Jurkat cells were prepared using lysis buffers specific for each activity assay provided with enzyme activity kits. Protein in cell lysates was determined using the Lowry method (BioRad DC) [66]. Activity of caspase-3, caspase-8, and caspase-9 was measured in lysates of Jurkat cells treated with ECM for 24 h as described above using fluorimetric (caspase-3) and colorimetric (caspase-8 and -9) microtiter plate based assays.

3.8.1. Caspase-3

Activity of caspase-3 was measured using a fluorescent microtiter plate assay (Invitrogen) based on cleavage of a non-fluorescent substrate, rhodamine 110 bis-(*N*-CBZ-L-aspartyl-L-glutamyl-L-

valyl-L-aspartic acid amid, Z-DEVD-R110) by active caspase-3. With enzymatic cleavage by caspase-3, the nonfluorescent bisamide substrate is converted to fluorescent R110. Jurkat cells (20,000 per well) were treated with 0, 1, and 2 mg/mL ECM for 3 and 24 h. Excitation and emission were measured at 496 nm and 520 nm, respectively. Fluorescence was measured using black microtiter plates and a fluorescence microtiter plate reader (BioTek, Flx800, Winooski, VT, USA).

3.8.2. Caspase-8

Caspase-8 activity was measured using a colorimetric microtiter plate based assay (Sigma). This assay, based on hydrolysis of the peptide substrate acetyl-Ile-Glu-Thr-Asp *p*-nitroaniline (Ac-IETD-pNA) by caspase-8, results in the release of p-nitroaniline (pNA) which is measured spectrophotometrically (405 nm, BioTek Model ELx800). Ac-IETD-pNA (caspase-8 substrate) was added at a final concentration of 2 mM. Initial absorbance was measured at 405 nm (T = 0) and then read at 5 min intervals for 90 min.

3.8.3. Caspase-9

Caspase-9 activity was measured using a colorimetric microtiter plate based assay (R&D Systems, Inc., Minneapolis, MN, USA), with release of pNA from the caspase-9 substrate, LEHD-pNA, measured spectrophotometrically (405 nm, BioTek Model ELx800). Lysates were incubated with substrate for 1, 1.5, and 2 h at 37 °C.

3.9. Western Blotting

For Western blotting, lysates of Jurkat cells were prepared using Western lysis buffer (1% Triton X-100, 50 mM Tris-HCl, pH 8.0, 150 mM NaCl, 10% glycerol, 0.1 mM EDTA, 10 mM NaF, 1 mM sodium orthovanadate) with protease inhibitors (Sigma Protease Cocktail, 1 mM PMSF) added. Cells were lysed on ice, and spun at 12,500 × *g* for 15 min to remove cell debris. Supernatants were aspirated and supernatants stored at −80 °C until analysis. For enzyme activity assays, lysates of Jurkat cells were prepared using lysis buffers specific for each activity assay and provided with the enzyme activity kits. Protein in cell lysates was determined using the Lowry method (BioRad) [66]. Cell lysates from Jurkat cells exposed to ECM were loaded onto SDS-PAGE gels (12%) at a concentration of 40 µg/lane. Proteins were separated at 200 V for approximately 1 h. Proteins were transferred from gels onto PVDF membranes (BioRad) at 70 V for 90 min via wet transfer. Blots were blocked for approximately 1 h in blocking buffer (10% non-fat dry milk, NFDM) and incubated overnight in primary antibody dilution buffer (1:1000) to prevent non-specific binding. Primary antibodies and their sources are listed in Table 1. Anti-rabbit IgG HRP-linked secondary antibody (1:2000; Santa Cruz) in 1% blocking buffer (3% NFDM, 2% BSA in TBS-T) was used with 1 µL Precision Protein™ Strep Tactin-HRP conjugate (BioRad) added for imaging of standards. Imaging of blots was accomplished using enhanced chemiluminescence (ECL) with the Immun-Star Western C Kit (BioRad). As a protein loading control, blots were stripped with stripping buffer (15 g glycine, 1 g SDS, 10 mL Tween 20, pH 2.2 in 1 L), and then re-probed with HRP-β-actin (Santa Cruz) using 1:2000 dilution (in 1% blocking buffer) for overnight incubation

(4 °C). Relative band densities on western blots were measured using ChemiDoc™ XRS$^+$ with Image Lab™ image acquisition and analysis software (BioRad). Relative band densities of each protein sample were normalized to relative band density of β-actin within each lane. β-actin has been shown not to undergo cleavage in Jurkat cells undergoing apoptosis [67].

Table 1. Primary antibodies used in Western blotting in lysates from Jurkat cells treated with ECM.

Antibody	Source
Caspase-3	Cell Signaling
Caspase-6	Cell Signaling
Caspase-7	Cell Signaling
Caspase-8	Santa Cruz
Caspase-9	Cell Signaling
Caspase-10	Cell Signaling
PARP	Cell Signaling
APAF-1	Cell Signal
FADD	Abcam
FLIP	Abcam
XIAP	Cell Signaling
Smac/DIABLO	R & D Systems

3.10. Antibody Arrays

Antibody arrays (RayBio Human Apoptosis Antibody Array) containing 43 apoptotic pathway intermediates were used to measure effects of ECM exposure on Jurkat cells. Following experimental treatments with ECM for 24 h, cells from duplicate wells (10×10^6 cells/treatment) were solubilized in lysis buffer containing protease inhibitors at 2×10^7 cells/mL for 30 min with rocking at 4 °C. Cells were pelleted at 14,000 × *g* for 15 min, and supernatants aspirated. Protein concentration in supernatants was determined using the Lowry method (BioRad) [66]. Protein load per membrane was approximately 600 μg/mL total protein diluted 5-fold with blocking buffer. Membranes were blocked with blocking buffer for 30 min at room temperature. Diluted sample was applied to membranes and incubated overnight with gentle rocking at 4 °C. Membranes were washed, and a biotin-conjugated secondary antibody added. HRP-conjugated streptavidin was added for detection through enhanced chemiluminescence (ECL). Blots were imaged using ChemiDoc XRS+ gel imager (BioRad). Relative densities of antibodies were determined by comparing to protein loading control antibodies.

3.11. Real-Time PCR (Q-PCR) and PCR Arrays

ECM-treated Jurkat cells and untreated controls were screened in triplicate for expression of 96 different genes related to cell death and cell survival using “Human Apoptosis” PCR arrays (Applied Biosystems, Carlsbad, CA, USA). RNA was isolated from ECM-treated Jurkat cells with TRIzol (Invitrogen, Grand Island, NY, USA) according to the manufacturer’s instructions. Concentration and purity of RNA was assessed using a NanoDrop spectrophotometer

(ThermoScientific, Waltham, MA, USA) and cDNA was prepared with the High Capacity cDNA Reverse Transcription kit (Applied Biosystems). Prepared cDNA was diluted with nuclease-free water and added to PCR arrays at a concentration of 25 ng/well with Taqman Gene Expression Master Mix (Applied Biosystems). Arrays were amplified using a 7500 Real time PCR system (Applied Biosystems) with the following conditions: initial denaturation step at 50 °C, 2 min and 95 °C, 10 min, followed by 40 cycles of 95 °C, 15 s, 60 °C, 1 min.

Expression of select genes was also analyzed in ECM-treated Jurkat cells and untreated control cells using gene-specific primers (Table 2). RNA was isolated as described using TRIzol (Invitrogen) and concentration and purity were determined using a NanoDrop spectrophotometer (ThermoScientific). RNA was reverse transcribed into cDNA using Superscript III First Strand Reverse Transcription kit (Invitrogen). Amplification of individual genes was conducted using specific primer sequences (Table 2). Primers for 18S, β-actin, beta-2 microglobulin (B2M), Fas, FADD, APAF-1, XIAP, Smac/DIABLO, and Bcl-xL were purchased from Integrated DNA Technologies (Coralville, IA). Copy DNA (cDNA) products were amplified by qPCR in quadruplicate wells containing 10 ng cDNA, 200 nM of each primer (combined forward and reverse sequences) and Power SYBR Green PCR Master Mix (Applied Biosystems) with a 7500 Real-Time PCR system (Applied Biosystems). Conditions for qPCR were as follows: initial denaturation step at 95 °C, 10 min, followed by 40 cycles of 95 °C, 15 s, 60 °C, 1 min. Q-PCR data (mean C_T values) for target genes was normalized to the average expression levels of three internal reference genes (18S, β-actin, and B2M) as previously recommended [68].

Table 2. Primer sequences used for real-time PCR amplification of individual genes in ECM-treated Jurkat cells.

Gene	Direction	5′-3′ sequence	Reference
18S	FWD	GCC AGG TCC TAG CCA ATG G	Applied Biosystems
	RVS	TCA GTC GCT CCA GGT CTT CA	Applied Biosystems
β-actin	FWD	TGC CGA CAG GAT GCA GAA G	
	RVS	CTC AGG AGG AGC AAT GAT CTT GA	
B2M	FWD	TGC TGT CTC CAT GTT TGA TGT ATC T	Vandesompele *et al*, 2002 [68]
	RVS	TCT CTG CTC CCC ACC TCT AAG T	
XIAP	FWD	5′ GCA CGA GCA GGG TTT CTT TAT ACT GGT G 3′	Espinosa *et al.*, 2006 [69]
	RVS	5′ CTT CTT CAC AAT ACA TGG CAG GGT TCC TC 3′	
Smac/DIABLO	FWD	5′ CCT GTG TGC GGT TCC TAT TGC 3′	Dai *et al.*, 2010 [70]
	RVS	5′ TGA TTC CTG GCG GTT ATA GAG 3′	
APAF-1	FWD	5′ CAC GTT CAA AGG TGG CTG AT 3′	Robles *et al.*, 2001 [71]
	RVS	5′ TGG TCA ACT GCA AGG ACC AT 3′	
Bcl-xl	FWD	5′ GTA AAC TGG GGT CGC ATT GT 3′	Will *et al.*, 2010 [72]
	RVS	5′ TGC TGC ATT GTT CCC ATA GA 3′	
CD95/Fas	FWD	5′-GAC CCA GAA TAC CAA GTG CAG ATG TA-3′	Petak *et al.*, 2003 [73]
	RVS	5′-CTG TTT CAG GAT TTA AGG TTG GAG ATT-3′	
FLIP	FWD	5′-GTT AGG TAG CCA GTT GG-3′	Kataoka *et al.*, 1998 [74]
	RVS	5′-CCT GCC TTG CTT CAG C-3′	

3.12. Surface Expression of TRAIL-R1 (DR4), TRAIL-R2 (DR5), TRAIL-R3 (DcR1), and TRAIL-R4 (DcR2)

The cell surface expression of death receptors (TRAIL-R1, TRAIL-R2) and decoy receptors (TRAIL-R3, TRAIL-R4) was measured in Jurkat cells ($N = 3$) treated with 0, 1, or 2 mg/mL ECM for 24 h using flow cytometry. After 24 h, cells were harvested and stained with fluorescently labeled (PE) antibodies to TRAIL-R1 (anti-hTRAILR1, FAB347P), TRAIL-R2 (anti-hTRAIL-R2, FAB311P), TRAIL-R3 (anti-hTRAIL-R3, FAB6320P), and TRAIL-R4 (anti-hTRAIL-R4, FAB633P). Mouse IgG (PE 1C002P) was used as isotype control. All antibodies were obtained from R&D Systems. Expression of cell surface receptors was measured using an Accuri C6 Flow Cytomter with CFLow PLUS software (BD Biosciences, San Jose, CA, USA), with 25,000 events collected on each sample.

3.13. Statistical Analyses

3.13.1. Growth Inhibition (MTT), Annexin V, and Receptor Expression Assays

Statistical analyses comparing untreated with ECM-treated cells were performed using Sigma-Stat Version 2.03. Means ± SEM are presented. Data that passed tests for both normality and equal variance were analyzed using either one-way analysis of variance (ANOVA) or Student's *t*-test. Data that did not satisfy requirements for normality and equal variance were analyzed using either non-parametric rank sum test or one-way ANOVA on Ranks. *P*-values less than 0.05 were considered significant.

3.13.2. Western Blots and Antibody Arrays

β-actin was used as a protein loading control. Blot images were normalized to β-actin. Percent change compared to untreated control was determined. Relative band densities from three to four individual blots were measured, and data reported as mean ± SEM. Antibody arrays were normalized to three averaged protein loading controls. Tests of significance were determined using either one-way ANOVA among ECM treatment concentrations or Student's *t*-test for comparing individual concentrations to untreated control. *P* values less than 0.05 were considered significant.

3.13.3. Q-PCR and PCR Arrays

Q-PCR array data were analyzed using the RT2 Profiler PCR Array Data Analysis web-based software (Version 3.5, Qiagen). Briefly, mean C_T values for target genes were normalized to the average expression levels of two internal reference genes (GAPDH and beta glucuronidase (GUSB)). The resulting ΔC_T values were averaged for replicates within the untreated and ECM-treated groups (1 mg/mL and 2 mg/mL). Mean ΔC_T values for ECM-treated groups were then normalized to those of the untreated control group and used to calculate the fold change in expression. Expression changes (up- or down-regulated) greater than 2-fold with $P < 0.05$ were considered significant.

Data from gene specific Q-PCR analysis (mean C_T values) for target gene expression of APAF-1, Smac/DIABLO, XIAP, and Bcl-xL were normalized to the average expression levels of three internal reference genes (18S, β-actin, and B2M) as previously recommended [68]. The resulting ΔC_T values were averaged for replicates within the untreated and ECM-treated groups (1 mg/mL and 2 mg/mL). Mean ΔC_T values for ECM-treated groups were then normalized to those of untreated control group and used to calculate the relative quantity (RQ). Differences in expression between untreated and ECM-treated groups were determined by one-way ANOVA, with $P < 0.05$ indicating significant differences.

4. Conclusions

Sharks and their skate and ray relatives (Subclass Elasmobranchii), collectively known as the elasmobranch fishes, represent a novel and untapped source of marine-derived compounds with the potential to be developed into therapeutic agents to benefit human health. Apoptosis of Jurkat T cell leukemia cells (clone E6-1, ATCC TIB-15) occurs in response to 24 h treatment with compounds present in a culture medium conditioned by shark epigonal organ cells (epigonal conditioned medium, ECM). The data presented support the conclusion that specific apoptotic pathways are targeted by ECM compounds and may have a direct role in inducing tumor cell death and/or sensitizing cancer cells to apoptosis induced through other means.

Acknowledgments

This study was supported by Henry L. and Grace Doherty Charitable Foundation and Florida High Tech Corridor Seed Grants FHT10-32, FHT11-23, and FHT12-16. Students (T. Cantu, B. Leigh, P. Adams) were supported through NSF REU Program Grant #1004181. T. Cantu was also supported by MARC U*STAR grant number GM077017. B. Leigh was also supported by USF Florida High Tech Corridor Seed Grant FHT11-23. M. Ciesla was supported by USF Florida High Tech Corridor Seed Grant FHT12-16.

Conflicts of Interest

The authors declare no conflict of interest.

References

1. Luer, C.A.; Walsh, C.J.; Bodine, A.B. The immune system of sharks, skates, and rays. In *Biology and Sharks and Their Relatives*; Carrier, J.C., Musick, J.A., Heithaus, M.R., Eds.; CRC Press: Boca Raton, FL, USA, 2004; pp. 369–395.
2. Luer, C.A.; Walsh, C.J.; Bodine, A.B. Recent advances in elasmobranch immunology. In *The Biology of Sharks and Their Relatives*; Carrier, J.C., Heithaus, M.R., Musick, J.A., Eds.; CRC Press: Boca Raton, FL, USA, 2012; pp. 403–420.
3. Litman, G.W.; Anderson, M.K.; Rast, J.P. Evolution of antigen binding receptors. *Ann. Rev. Immunol.* **1999**, *17*, 109–147.

4. Flajnik, M.F.; Rumfelt, L.L. The immune system of cartilaginous fish. *Curr. Top. Microbiol. Immunol.* **2000**, *248*, 249–270.
5. Walsh, C.J.; Luer, C.A.; Noyes, D.R.; Smith, C.A.; Gasparetto, M.; Bhalla, K.N. Characterization of shark immune cell factor (*Sphyrna tiburo* epigonal factor, STEF) that inhibits tumor cell growth by inhibiting S-phase and inducing apoptosis via the TRAIL pathway. *FASEB J.* **2004**, *18*, A60.
6. Walsh, C.J.; Luer, C.A.; Bodine, A.B.; Smith, C.A.; Cox, H.L.; Noyes, D.R.; Maura, G. Elasmobranch immune cells as a source of novel tumor cell inhibitors: Implications for public health. *Integr. Comp. Biol.* **2006**, *46*, 1072–1081.
7. Schneider, U.; Schwenk, H.U.; Bornkamm, G. Characterization of EBV-genome negative "null" and "T" cell lines derived from children with acute lymphoblastic leukemia and leukemic transformed non-Hodgkin lymphoma. *Int. J. Cancer* **1977**, *19*, 621–626.
8. Elmore, S. Apoptosis: A review of programmed cell death. *Toxicol. Pathol.* **2007**, *35*, 495–516.
9. Mosmann, T. Rapid colorimetric assay for cellular growth and survival: application to proliferation and cytotoxicity assays. *J. Immunol. Methods* **1983**, *65*, 55–63.
10. Koopman, G.; Reutelingsperger, C.P.; Kuijten, G.A.; Keehnen, R.M.; Pals, S.T.; van Oers, M.H. Annexin V for flow cytometric detection of phosphatidylserine expression on B cells undergoing apoptosis. *Blood* **1994**, *84*, 1415–1420.
11. Cohen, G.M. Caspases: The executioners of apoptosis. *Biochem. J.* **1997**, *326*, 1–16.
12. Ashkenazi, A.; Dixit, V.M. Apoptosis control by death and decoy receptors. *Curr. Opin. Cell Biol.* **1999**, *11*, 255–260.
13. Kashkar, H. X-linked inhibitor of apoptosis: a chemoresistance factor or a hollow promise. *Clin. Cancer Res.* **2010**, *16*, 4496–4502.
14. Cao, X.; Pobezinskaya, Y.L.; Morgan, M.J.; Liu, Z.G. The role of TRADD in TRAIL-induced apoptosis and signaling. *FASEB J.* **2011**, *25*, 1353–1358.
15. Bratton, S.B.; Salvesen, G.S. Regulation of the Apaf-1-caspase-9 apoptosome. *J. Cell Sci.* **2010**, *123*, 3209–3214.
16. Bagnoli, M.; Canevari, S.; Mezzanzanica, D. Cellular FLICE-inhibitory protein (c-FLIP) signalling: A key regulator of receptor-mediated apoptosis in physiologic context and in cancer. *Int. J. Biochem. Cell Biol.* **2010**, *42*, 210–213.
17. Lavrik, I.N.; Krammer, P.H. Regulation of CD95/Fas signaling at the DISC. *Cell Death Differ.* **2012**, *19*, 36–41.
18. Krueger, A.; Schmitz, I.; Baumann, S.; Krammer, P.H.; Kirchhoff, S. Cellular FLICE-inhibitory protein splice variants inhibit different steps of caspase-8 activation at the CD95 death-inducing signaling complex. *J. Biol. Chem.* **2001**, *276*, 20633–20640.
19. Wajant, H. Targeting the FLICE Inhibitory Protein (FLIP) in cancer therapy. *Mol. Interv.* **2003**, *3*, 124–127.
20. Oliver, F.J.; Menissier-de Murcia, J.; de Murcia, G. Poly(ADP-ribose) polymerase in the cellular response to DNA damage, apoptosis, and disease. *Am. J. Hum. Genet.* **1999**, *64*, 1282–1288.
21. Adams, J.M.; Cory, S. Bcl-2-regulated apoptosis: mechanism and therapeutic potential. *Curr. Opin. Immunol.* **2007**, *19*, 488–496.

22. Zeng, L.; Li, T.; Xu, D.C.; Liu, J.; Mao, G.; Cui, M.Z.; Fu, X.; Xu, X. Death receptor 6 induces apoptosis not through type I or type II pathways, but via a unique mitochondria-dependent pathway by interacting with Bax protein. *J. Biol. Chem.* **2012**, *287*, 29125–29133.
23. Aggarwal, B.B. Tumour necrosis factors receptor associated signalling molecules and their role in activation of apoptosis, JNK and NF-kappaB. *Ann. Rheum. Dis.* **2000**, *59* (Suppl. 1), i6–i16.
24. Leu, J.I.; George, D.L. Hepatic IGFBP1 is a prosurvival factor that binds to BAK, protects the liver from apoptosis, and antagonizes the proapoptotic actions of p53 at mitochondria. *Genes Dev.* **2007**, *21*, 3095–3109.
25. Altieri, D.C. Survivin in apoptosis control and cell cycle regulation in cancer. *Prog. Cell Cycle Res.* **2003**, *5*, 447–452.
26. Altieri, D.C. Survivin and apoptosis control. *Adv. Cancer Res.* **2003**, *88*, 31–52.
27. Mita, A.C.; Mita, M.M.; Nawrocki, S.T.; Giles, F.J. Survivin: key regulator of mitosis and apoptosis and novel target for cancer therapeutics. *Clin. Cancer Res.* **2008**, *14*, 5000–5005.
28. Liu, X.; Yue, P.; Chen, S.; Hu, L.; Lonial, S.; Khuri, F.R.; Sun, S.Y. The proteasome inhibitor PS-341 (bortezomib) up-regulates DR5 expression leading to induction of apoptosis and enhancement of TRAIL-induced apoptosis despite up-regulation of c-FLIP and survivin expression in human NSCLC cells. *Cancer Res.* **2007**, *67*, 4981–4988.
29. Conway, E.M.; Pollefeyt, S.; Steiner-Mosonyi, M.; Luo, W.; Devriese, A.; Lupu, F.; Bono, F.; Leducq, N.; Dol, F.; Schaeffer, P.; *et al*. Deficiency of survivin in transgenic mice exacerbates Fas-induced apoptosis via mitochondrial pathways. *Gastroenterology* **2002**, *123*, 619–631.
30. Johnson, M.E.; Howerth, E.W. Survivin: A bifunctional inhibitor of apoptosis protein. *Vet. Pathol.* **2004**, *41*, 599–607.
31. Altieri, D.C. Survivin, cancer networks and pathway-directed drug discovery. *Nature Rev. Cancer* **2008**, *8*, 61–70.
32. Dohi, T.; Xia, F.; Altieri, D.C. Compartmentalized phosphorylation of IAP by protein kinase A regulates cytoprotection. *Mol. Cell* **2007**, *27*, 17–28.
33. Grossman, D.; Kim, P.J.; Blanc-Brude, O.P.; Brash, D.E.; Tognin, S.; Marchisio, P.C.; Altieri, D.C. Transgenic expression of survivin in keratinocytes counteracts UVB-induced apoptosis and cooperates with loss of p53. *J. Clin. Invest.* **2001**, *108*, 991–999.
34. O'Connor, D.S.; Grossman, D.; Plescia, J.; Li, F.; Zhang, H.; Villa, A.; Tognin, S.; Marchisio, P.C.; Altieri, D.C. Regulation of apoptosis at cell division by p34cdc2 phosphorylation of survivin. *Proc. Natl. Acad. Sci. USA* **2000**, *97*, 13103–13107.
35. Du, C.; Fang, M.; Li, Y.; Li, L.; Wang, X. Smac, a mitochondrial protein that promotes cytochrome c-dependent caspase activation by eliminating IAP inhibition. *Cell* **2000**, *102*, 33–42.
36. Lomonosova, E.; Chinnadurai, G. BH3-only proteins in apoptosis and beyond: An overview. *Oncogene* **2008**, *27* (Suppl. 1), S2–S19.
37. Inohara, N.; Nunez, G. The NOD: A signaling module that regulates apoptosis and host defense against pathogens. *Oncogene* **2001**, *20*, 6473–6481.

38. Dufner, A.; Mak, T.W. CARD tricks: Controlling the interactions of CARD6 with RICK and microtubules. *Cell Cycle* **2006**, *5*, 797–800.
39. Dufner, A.; Pownall, S.; Mak, T.W. Caspase recruitment domain protein 6 is a microtubule-interacting protein that positively modulates NF-kappaB activation. *Proc. Natl. Acad. Sci. USA* **2006**, *103*, 988–993.
40. Banerjee, M.; Datta, M.; Majumder, P.; Mukhopadhyay, D.; Bhattacharyya, N.P. Transcription regulation of caspase-1 by R393 of HIPPI and its molecular partner HIP-1. *Nucleic Acids Res.* **2010**, *38*, 878–892.
41. Manzl, C.; Krumschnabel, G.; Bock, F.; Sohm, B.; Labi, V.; Baumgartner, F.; Logette, E.; Tschopp, J.; Villunger, A. Caspase-2 activation in the absence of PIDDosome formation. *J. Cell Biol.* **2009**, *185*, 291–303.
42. Lin, Y.; Ma, W.; Benchimol, S. Pidd, a new death-domain-containing protein, is induced by p53 and promotes apoptosis. *Nat. Genet.* **2000**, *26*, 122–127.
43. Rossi, D.; Gaidano, G. Messengers of cell death: Apoptotic signaling in health and disease. *Haematologica* **2003**, *88*, 212–218.
44. Zhang, L.; Fang, B. Mechanisms of resistance to TRAIL-induced apoptosis in cancer. *Cancer Gene Ther.* **2005**, *12*, 228–237.
45. Chan, F.K.; Shisler, J.; Bixby, J.G.; Felices, M.; Zheng, L.; Appel, M.; Orenstein, J.; Moss, B.; Lenardo, M.J. A role for tumor necrosis factor receptor-2 and receptor-interacting protein in programmed necrosis and antiviral responses. *J. Biol. Chem.* **2003**, *278*, 51613–51621.
46. Sancho-Martinez, I.; Martin-Villalba, A. Tyrosine phosphorylation and CD95: A FAScinating switch. *Cell Cycle* **2009**, *8*, 838–842.
47. Lanave, C.; Santamaria, M.; Saccone, C. Comparative genomics: the evolutionary history of the Bcl-2 family. *Gene* **2004**, *333*, 71–79.
48. Martinon, F.; Tschopp, J. Inflammatory caspases and inflammasomes: master switches of inflammation. *Cell Death Differ.* **2007**, *14*, 10–22.
49. Zheng, C.; Kabaleeswaran, V.; Wang, Y.; Cheng, G.; Wu, H. Crystal structures of the TRAF2: cIAP2 and the TRAF1: TRAF2: cIAP2 complexes: Affinity, specificity, and regulation. *Mol. Cell* **2010**, *38*, 101–113.
50. Razmara, M.; Srinivasula, S.M.; Wang, L.; Poyet, J.L.; Geddes, B.J.; DiStefano, P.S.; Bertin, J.; Alnemri, E.S. CARD-8 protein, a new CARD family member that regulates caspase-1 activation and apoptosis. *J. Biol. Chem.* **2002**, *277*, 13952–13958.
51. Wiley, S.R.; Schooley, K.; Smolak, P.J.; Din, W.S.; Huang, C.P.; Nicholl, J.K.; Sutherland, G.R.; Smith, T.D.; Rauch, C.; Smith, C.A.; *et al*. Identification and characterization of a new member of the TNF family that induces apoptosis. *Immunity* **1995**, *3*, 673–682.
52. Pan, G.; Ni, J.; Wei, Y.F.; Yu, G.; Gentz, R.; Dixit, V.M. An antagonist decoy receptor and a death domain-containing receptor for TRAIL. *Science* **1997**, *277*, 815–818.
53. Pan, G.; O'Rourke, K.; Chinnaiyan, A.M.; Gentz, R.; Ebner, R.; Ni, J.; Dixit, V.M. The receptor for the cytotoxic ligand TRAIL. *Science* **1997**, *276*, 111–113.

54. Walczak, H.; Degli-Esposti, M.A.; Johnson, R.S.; Smolak, P.J.; Waugh, J.Y.; Boiani, N.; Timour, M.S.; Gerhart, M.J.; Schooley, K.A.; Smith, C.A.; Goodwin, R.G.; Rauch, C.T. TRAIL-R2: A novel apoptosis-mediating receptor for TRAIL. *EMBO J.* **1997**, *16*, 5386–5397.
55. Clancy, L.; Mruk, K.; Archer, K.; Woelfel, M.; Mongkolsapaya, J.; Screaton, G.; Lenardo, M.J.; Chan, F.K. Preligand assembly domain-mediated ligand-independent association between TRAIL receptor 4 (TR4) and TR2 regulates TRAIL-induced apoptosis. *Proc. Natl. Acad. Sci. USA* **2005**, *102*, 18099–18104.
56. Daniels, R.A.; Turley, H.; Kimberley, F.C.; Liu, X.S.; Mongkolsapaya, J.; Ch'En, P.; Xu, X.N.; Jin, B.Q.; Pezzella, F.; Screaton, G.R. Expression of TRAIL and TRAIL receptors in normal and malignant tissues. *Cell Res.* **2005**, *15*, 430–438.
57. Ma, Y.; Yang, D.; Chen, Y. Analysis of TRAIL receptor expression using anti-TRAIL death receptor-5 monoclonal antibodies. *Chin. Med. J. (Engl.)* **2003**, *116*, 947–950.
58. LeBlanc, H.N.; Ashkenazi, A. Apo2L/TRAIL and its death and decoy receptors. *Cell Death Differ.* **2003**, *10*, 66–75.
59. Gross, A.; McDonnell, J.M.; Korsmeyer, S.J. BCL-2 family members and the mitochondria in apoptosis. *Genes Dev.* **1999**, *13*, 1899–1911.
60. Merino, D.; Lalaoui, N.; Morizot, A.; Schneider, P.; Solary, E.; Micheau, O. Differential inhibition of TRAIL-mediated DR5-DISC formation by decoy receptors 1 and 2. *Mol. Cell Biol.* **2006**, *26*, 7046–7055.
61. Degli-Esposti, M.A.; Dougall, W.C.; Smolak, P.J.; Waugh, J.Y.; Smith, C.A.; Goodwin, R.G. The novel receptor TRAIL-R4 induces NF-kappaB and protects against TRAIL-mediated apoptosis, yet retains an incomplete death domain. *Immunity* **1997**, *7*, 813–820.
62. Degli-Esposti, M.A.; Smolak, P.J.; Walczak, H.; Waugh, J.; Huang, C.P.; DuBose, R.F.; Goodwin, R.G.; Smith, C.A. Cloning and characterization of TRAIL-R3, a novel member of the emerging TRAIL receptor family. *J. Exp. Med.* **1997**, *186*, 1165–1170.
63. Davidovich, I.A.; Levenson, A.S.; Levenson Chernokhvostov, V.V. Overexpression of DcR1 and survivin in genetically modified cells with pleiotropic drug resistance. *Cancer Lett.* **2004**, *211*, 189–197.
64. Riccioni, R.; Pasquini, L.; Mariani, G.; Saulle, E.; Rossini, A.; Diverio, D.; Pelosi, E.; Vitale, A.; Chierichini, A.; Cedrone, M.; *et al*. TRAIL decoy receptors mediate resistance of acute myeloid leukemia cells to TRAIL. *Haematologica* **2005**, *90*, 612–624.
65. Walsh, C.; Luer, C.A. Elasmobranch hematology: Identification of cell types and practical applications. In *Elasmobranch Husbandry Manual*, Proceedings of the First International Elasmobranch Husbandry Symposium, Orlando, FL, USA, 2001; Warmolts, D., Thoney, D., Hueter, R., Eds.; Ohio Biological Sruvey: Columbus, OH, USA, 2004; pp. 309–326.
66. Lowry, O.H.; Rosebrough, N.J.; Farr, A.L.; Randall, R.J. Protein measurement with the Folin phenol reagent. *J. Biol. Chem.* **1951**, *193*, 265–275.
67. Cohen, L.Y.; Bourbonniere, M.; Sabbagh, L.; Bouchard, A.; Chew, T.; Jeannequin, P.; Lazure, C.; Sekaly, R.P. Notch1 antiapoptotic activity is abrogated by caspase cleavage in dying T lymphocytes. *Cell Death Differ.* **2005**, *12*, 243–254.

68. Vandesompele, J.; De Preter, K.; Pattyn, F.; Poppe, B.; Van Roy, N.; De Paepe, A.; Speleman, F. Accurate normalization of real-time quantitative RT-PCR data by geometric averaging of multiple internal control genes. *Genome Biol.* **2002**, *3*, RESEARCH0034.
69. Espinosa, M.; Cantu, D.; Herrera, N.; Lopez, C.M.; De la Garza, J.G.; Maldonado, V.; Melendez-Zajgla, J. Inhibitors of apoptosis proteins in human cervical cancer. *BMC Cancer* **2006**, *6*, 45.
70. Dai, C.H.; Li, J.; Shi, S.B.; Yu, L.C.; Ge, L.P.; Chen, P. Survivin and Smac gene expressions but not livin are predictors of prognosis in non-small cell lung cancer patients treated with adjuvant chemotherapy following surgery. *Jpn. J. Clin. Oncol.* **2010**, *40*, 327–335.
71. Robles, A.I.; Bemmels, N.A.; Foraker, A.B.; Harris, C.C. APAF-1 is a transcriptional target of p53 in DNA damage-induced apoptosis. *Cancer Res.* **2001**, *61*, 6660–6664.
72. Will, B.; Siddiqi, T.; Jorda, M.A.; Shimamura, T.; Luptakova, K.; Staber, P.B.; Costa, D.B.; Steidl, U.; Tenen, D.G.; Kobayashi, S. Apoptosis induced by JAK2 inhibition is mediated by Bim and enhanced by the BH3 mimetic ABT-737 in JAK2 mutant human erythroid cells. *Blood* **2010**, *115*, 2901–2909.
73. Petak, I.; Danam, R.P.; Tillman, D.M.; Vernes, R.; Howell, S.R.; Berczi, L.; Kopper, L.; Brent, T.P.; Houghton, J.A. Hypermethylation of the gene promoter and enhancer region can regulate Fas expression and sensitivity in colon carcinoma. *Cell Death Differ.* **2003**, *10*, 211–217.
74. Kataoka, T.; Schroter, M.; Hahne, M.; Schneider, P.; Irmler, M.; Thome, M.; Froelich, C.J.; Tschopp, J. FLIP prevents apoptosis induced by death receptors but not by perforin/granzyme B, chemotherapeutic drugs, and gamma irradiation. *J. Immunol.* **1998**, *161*, 3936–3942.

Towards the Small and the Beautiful: A Small Dibromotyrosine Derivative from *Pseudoceratina* sp. Sponge Exhibits Potent Apoptotic Effect through Targeting IKK/NFκB Signaling Pathway

Jui-Hsin Su, Yu-Cheng Chen, Mohamed El-Shazly, Ying-Chi Du, Chiang-Wen Su, Chia-Wei Tsao, Li-Lian Liu, Yalan Chou, Wen-Been Chang, Yin-Di Su, Michael Y. Chiang, Yao-Tsung Yeh and Mei-Chin Lu

Abstract: A dibromotyrosine derivative, (1′*R*,5′*S*,6′*S*)-2-(3′,5′-dibromo-1′,6′-dihydroxy-4′-oxocyclohex-2′-enyl) acetonitrile (DT), was isolated from the sponge *Pseudoceratina* sp., and was found to exhibit a significant cytotoxic activity against leukemia K562 cells. Despite the large number of the isolated bromotyrosine derivatives, studies focusing on their biological mechanism of action are scarce. In the current study we designed a set of experiments to reveal the underlying mechanism of DT cytotoxic activity against K562 cells. First, the results of MTT cytotoxic and the annexin V-FITC/PI apoptotic assays, indicated that the DT cytotoxic activity is mediated through induction of apoptosis. This effect was also supported by caspases-3 and -9 activation as well as PARP cleavage. DT induced generation of reactive oxygen species (ROS) and the disruption of mitochondrial membrane potential (MMP) as indicated by flow cytometric assay. The involvement of ROS generation in the apoptotic activity of DT was further corroborated by the pretreatment of K562 cells with *N*-acetyl-cysteine (NAC), a ROS scavenger, which prevented apoptosis and the disruption of MMP induced by DT. Results of cell-free system assay suggested that DT can act as a topoisomerase II catalytic inhibitor, unlike the clinical anticancer drug, etoposide, which acts as a topoisomerase poison. Additionally, we found that DT treatment can block IKK/NFκB pathway and activate PI3K/Akt pathway. These findings suggest that the cytotoxic effect of DT is associated with mitochondrial dysfunction-dependent apoptosis which is mediated through oxidative stress. Therefore, DT represents an interesting reference point for the development of new cytotoxic agent targeting IKK/NFκB pathway.

Reprinted from *Mar. Drugs*. Cite as: Su, J.-H.; Chen, Y.-C.; El-Shazly, M.; Du, Y.-C.; Su, C.-W.; Tsao, C.-W.; Liu, L.-L.; Chou, Y.; Chang, W.-B.; Su, Y.-D.; *et al.* Towards the Small and the Beautiful: A Small Dibromotyrosine Derivative from *Pseudoceratina* sp. Sponge Exhibits Potent Apoptotic Effect through Targeting IKK/NFκB Signaling Pathway. *Mar. Drugs* **2013**, *11*, 3168-3185.

1. Introduction

Living organisms in oceans are widely regarded as the ancestral tree of all creatures and the cradle of the first signs of uni- and multicellular life. One of the earliest manifestations of multicellular organisms is the development of marine sponges. It took millennia to develop multicellular organisms equipped with necessary tools of survival. Sponges are sessile creatures which can be attacked by different kinds of predators and fouling microorganisms [1]. These harsh

conditions led to the development of a highly sophisticated defense system of secondary metabolites. A silver line had to be established in developing such defense system, through synthesizing compounds which are extremely toxic to the predators under high dilution condition, however still tolerable by the sponges. Among these compounds which were discovered in the seventies of the last century, are bromotyrosine derivatives. These derivatives are biosynthesized from common L-tyrosine metabolites such as 3-bromo-L-tyrosine and 3,5-dibromo-L-tyrosine which serve as the basic structural elements for this class of marine alkaloids [2].

In the past four decades, over 300 different bromotyrosine derivatives were isolated from sponges and their biological activity was evaluated [3]. In 1987, a dibromotyrosine derivative was found to act on the hypothalamic centers which control thyroid function and was proposed as a potential candidate targeting certain CNS disorders [4]. Aeroplysinin-1, a dibromotyrosine acetonitrile derivative, was isolated from marine sponges along with an array of closely related analogues. The potent biological activities of these derivatives led to the development of different synthetic protocols for their synthesis [5–7]. Reports indicated that aeroplysinin-1 exhibited a myriad of biological activities including antiparasitic [5], antiinflammatory [8], antibiotic [9] and cytotoxic activities [7,10]. Moreover, it was found that this compound can be utilized as a structural template for the synthesis of antiangiogenic agents based on the docking experiments in the ATP binding site of Vascular Endothelial Growth Factor Receptors (VEGFR) [11]. Despite the wide spectrum of biological activities exhibited by bromotyrosine derivatives, only a handful of reports have focused on studying their biological mechanism of action [3].

Sponges belonging to the order Verongida are considered the richest source of naturally occurring bromotyrosine derivatives. Over 15 classes of these derivatives were isolated including fistularin, psammaplysin, aerothionin, psammaplin, purealidinand bastadin subtypes [12]. Among the widely studied genera of this order is *Pseudoceratina* sp. From this order different bromotyrosine derivatives were isolated including pseudoceramines A–D and spermatinamine [13], aplysamine 6 [14], ceratinadins A–C [15], as well as 11,19-dideoxyfistularin-3, 11-deoxyfistularin-3 and dibromoverongiaquinol [16]. The wide diversity of the separated bromotyrosine derivatives has encouraged us to subject *Pseudoceratina* sp., collected from the Green Island on the east cost of Taiwan, to an intensive chemical investigation which led to the isolation of (1′*R*,5′*S*,6′*S*)-2-(3′,5′-dibromo-1′,6′-dihydroxy-4′-oxocyclohex-2′-enyl) acetonitrile (DT) (Figure 1). This secondary metabolite is an oxidized derivative of aeroplysinin-1, suggesting that DT may possess similar cytotoxic activity. In the current study we sought to evaluate the cytotoxic activity of DT on chronic myeloid leukemia (CML) (K562) as well as to identify its underlying mechanism of action.

Figure 1. (**a**) Morphology of the Taiwanese Green Island sponge, *Pseudoceratina* sp.; (**b**) Molecular structure of (1′*R*,5′*S*,6′*S*)-2-(3′,5′-dibromo-1′,6′-dihydroxy-4′-oxocyclohex-2′-enyl) acetonitrilebased on X-ray analysis.

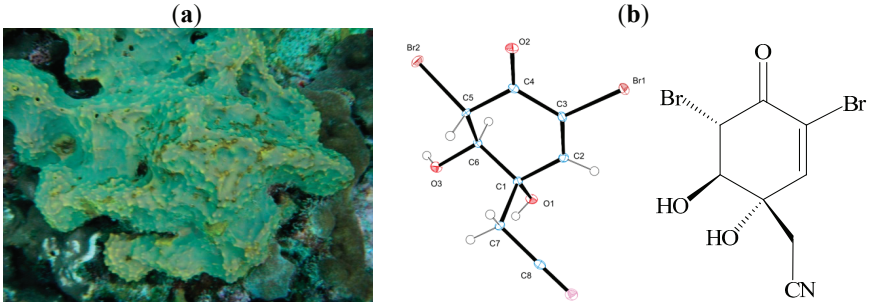

2. Results

2.1. DT Inhibits Cellular Growth and Induces Apoptosis in K562 Cells

The cytotoxic effect of DT was evaluated against several cancer cell lines and we found that DT exhibited potent activity against K562, Hela, MCF-7, and MDA-MB-231 cells, with IC_{50} values of 1.4, 4.8, 1.9, and 5.5 µg/mL, respectively, for 72 h. Leukemia K562 cell line was the most sensitive cell line to the cytotoxic effect of DT and was selected for further investigation. K562 cells and rat alveolar macrophage NR8383 cell line were treated with different doses of DT, for 24 h. DT downregulated viability of K562 cells in a dose dependent manner, but did not suppress growth of NR8383 cells. Even at the highest dose (5 µg/mL), DT treatment resulted in viability of NR8383 cells about 80% (Figure 2a). Nuclear condensation was observed after treating K562 cells with 2.5 and 5 µg/mL of DT (Figure 2b). To understand whether DT cytotoxic effect is mediated through apoptosis, we used annexin V/PI double staining and flow cytometric analysis. We found that increasing the concentration of DT (2.5, 5 and 10 µg/mL) led to a significant increase in the apoptotic population (13, 61.9 and 87.1%, respectively) after 24 h (Figure 2c). Treatment with 0.5 and 1 µg/mL of DT resulted in a significant increase in the level of caspase 3 activation and PARP cleavage, but at high concentration (5 µg/mL) it led to a decrease in caspase 3 activation, PARP cleavage and XIAP expression (Figure 2d). Furthermore, the phosphorylation of H2AX, a biomarker of DNA damage, was observed with the DT treatment. Moreover, an increase in ATM and BRCA phosphorylation was observed with the use of low doses (0.5 and 1 µg/mL) of DT, however their phosphorylation decreased at high doses (2.5 and 5 µg/mL). Also ATR phosphorylation was observed with the treatment of increasing concentrations of DT (Figure 2e). Upon DNA damage, cells activate a complex DNA-damage-response (DDR) signaling network to arrest the cell cycle and repair DNA, but if the extent of the damage is beyond the capacity of the repair system, apoptosis is induced [17]. Our results indicated that apoptosis and DNA damage induced by DT treatment were mediated through caspase activation and Chk2 phosphorylation, respectively.

2.2. DT Inhibits Topoisomerase II Catalytic Cycle

Phosphorylation of H2AX (γH2AX) is the hallmark of DNA damage which was observed in K562 cells upon DT treatment (Figure 2e). We tried to determine whether the DNA damage induced by DT is associated with the interruption of topo II activity. For this purpose, a cell-free DNA cleavage assay using an enzyme-mediated negatively supercoiled pHOT1 plasmid DNA, was applied. As shown in (Figure 3), DT at low doses (0.01, 0.1, and 1 µg) induced DNA relaxation in the presence of topo IIα (Lanes 1–3); but at high doses (2.5, 5, and 10 µg) it inhibited DNA relaxation in the presence of topo IIα (Lanes 4–6). Lane 7 is showing a linear DNA strand which was also observed upon treating the supercoiled pHOT1 plasmid DNA with etoposide, a standard topo II poison (Lane 11) [18]. These results suggested that one of the DT targets, as a DNA damaging agent, is to interfere with various steps of topoisomerase IIα catalytic cycle, which plays a critical role in DNA replication, transcription and chromosomal segregation [19].

Figure 2. DT inhibits K562 cellular growth and induces apoptosis. K562 cells were treated with different doses of DT and incubated for 24 h, (**a**) Viability of K562 and normal rat macrophage NR8383 cells were determined with different doses of DT; (**b**) Treated cells were stained with DAPI and examined with fluorescence microscope (200×); (**c**) Double staining with annexin V/propidium iodide (PI) was used to determine the induction of apoptosis following the treatment of K562 cells with different concentrations of DT (0, 0.5, 1, 2.5, 5 and 10 µg/mL) for 24 h. The histogram summarizes the apoptotic population in percentage of K562 cells. Results are presented as mean ± SD of three independent experiments; (**d**) Caspase-activated proteins; (**e**) DNA damage-related proteins were examined following the treatment with the indicated doses of DT for 24 h, as shown from the Western blots. GAPDH was the loading control.

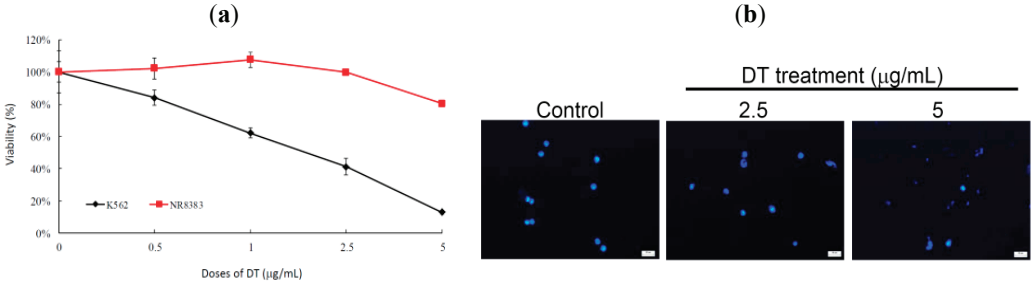

Figure 2. *Cont.*

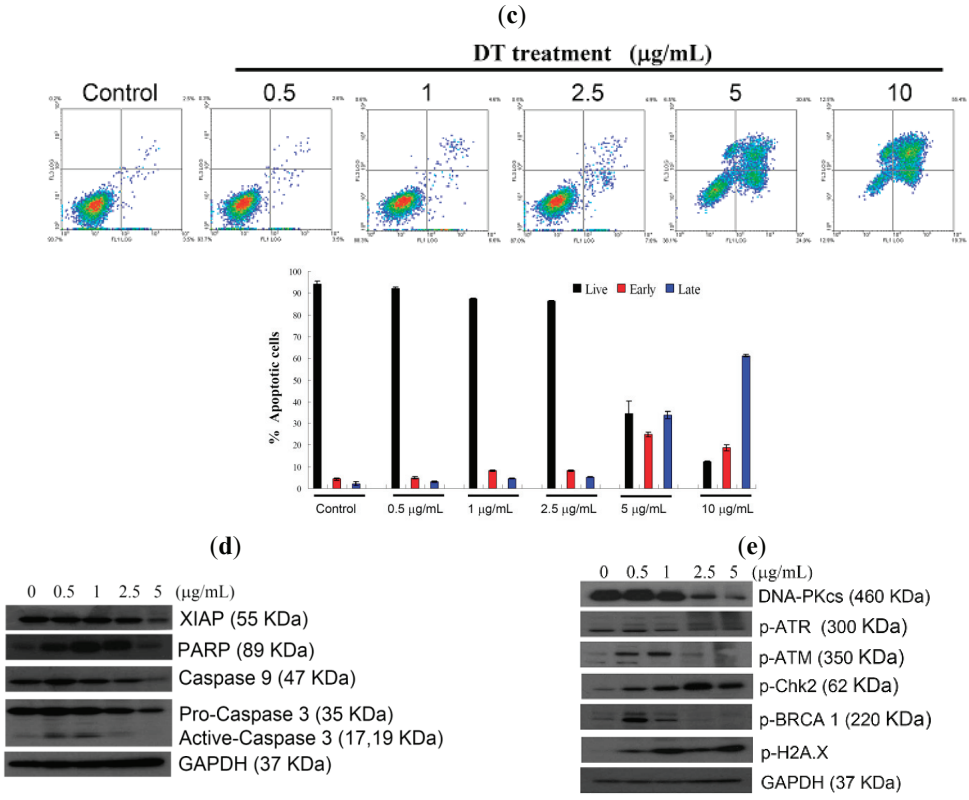

2.3. DT-Induced Apoptosis Is Mediated through Reactive Oxygen Species (ROS) Generation in K562 Cells

Mounting experimental evidence has continued to lend credence to the fact that ROS plays a critical role in the cellular homeostasis and a delicate balance should be established to avoid overproduction of ROS which may induce apoptosis and cell death [20]. Hence, we further examined whether ROS production was involved in the DT-induced apoptosis. Production of ROS was examined utilizing the carboxy derivative of fluorescein, carboxy-H_2DCFDA. As shown in Figure 4a, treatment with DT at 2.5 μg/mL for 20 and 60 min, resulted in 6.53- and 8.73-fold increase in ROS levels, respectively, and the high production of ROS persisted for the next 18 hours as compared to the mean fluorescence index (MFI) of the control. However, the use of DT (5 μg/mL) for 10, 30, 40, 50 and 60 min resulted in 1.73-, 3.11-, 3.07-, 2.88- and 1.99-folds increase of the fluorescence intensity, respectively as compared to the mean fluorescence index (MFI) of the control (Figure 4b). To clarify whether ROS generation is the major regulator in the DT-induced apoptosis, K562 cells were pretreated with NAC, a ROS scavenger, to suppress the intracellular oxidative stress. Cellular viability was measured by a trypan blue dye exclusion assay following DT treatment. As shown in Figure 4c, NAC pretreatment improved cell viability up to

37% and 58% in response to the use of 2.5 and 5 μg/mL of DT, respectively in comparison to the control group.

Figure 3. Effect of DT on topo IIα mediated supercoiled pHOT1 plasmid DNA relaxation, Lanes 1–6: DT (0.01, 0.1, 1, 2.5, 5, and 10 μg); Lane 7: Linear DNA; Lane 8: negative control plasmid DNA; Lane 9: plasmid DNA + topoisomerase IIα (induction of DNA relaxation); Lane 10: plasmid DNA + topoisomerase IIα + solvent control (induction of DNA relaxation); Lane 11: positive control, etoposide (20 mM), as topo II poison (induction of linear DNA).

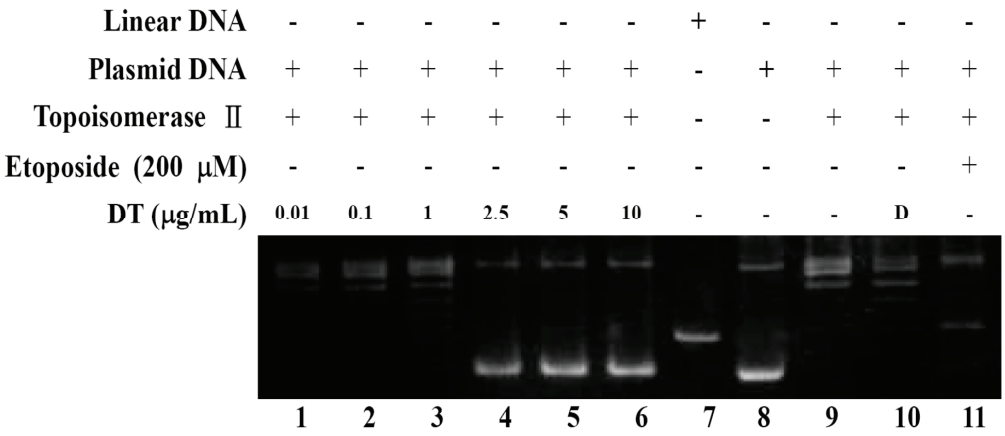

2.4. DT-Induced Oxidative Stress Disturbs Mitochondrial Membrane Potential (MMP)

The next step after showing that DT induced apoptosis in K562 cells is mediated through ROS overproduction; was to evaluate the effect of ROS overproduction on the mitochondrial membrane potential (MMP) of these cells. Flow cytometric assay with JC-1 cationic dye was used to evaluate this effect. Cells were divided into two groups, one group was treated with NAC (1.5 mM) followed by 5 μg/mL of DT and the other group was treated with DT (5 μg/mL) only. After 24 h, the change of MMP was analyzed in the two groups. DT treatment led to 46.1% disruption of MMP in K562 cells. However, NAC pretreatment maintained the integrity of MMP to the status of the control group (Figure 5a). We further determined the effect of NAC pretreatment on the expression of the DNA damage-signaling proteins. As shown in Figure 5b, NAC pretreatment abrogated PARP cleavage and H2AX phosphorylation.

Figure 4. DT-induced K562 cellular apoptosis involves ROS production, we evaluated the effect of DT treatment on the ROS generation in K562 cells; (**a**) Cells were treated with 2.5 μg/mL of DT for the indicated times; (**b**) Cells were treated with 5.0 μg/mL of DT for the indicated times. Quantitative results of the change in the ROS level showed a gradual increase in the ROS production upon DT treatment when compared with the control group; (**c**) Effect of ROS generation on DT-induced cell death in K562 cells. Following pretreatment of 1.5 mM NAC for 1.5 h, cells were treated with 2.5 and 5 μg/mL of DT, respectively, and the cellular viability was measured with trypan blue dye exclusion assay. Results are presented as mean ± SD of three independent experiments (* $P < 0.001$).

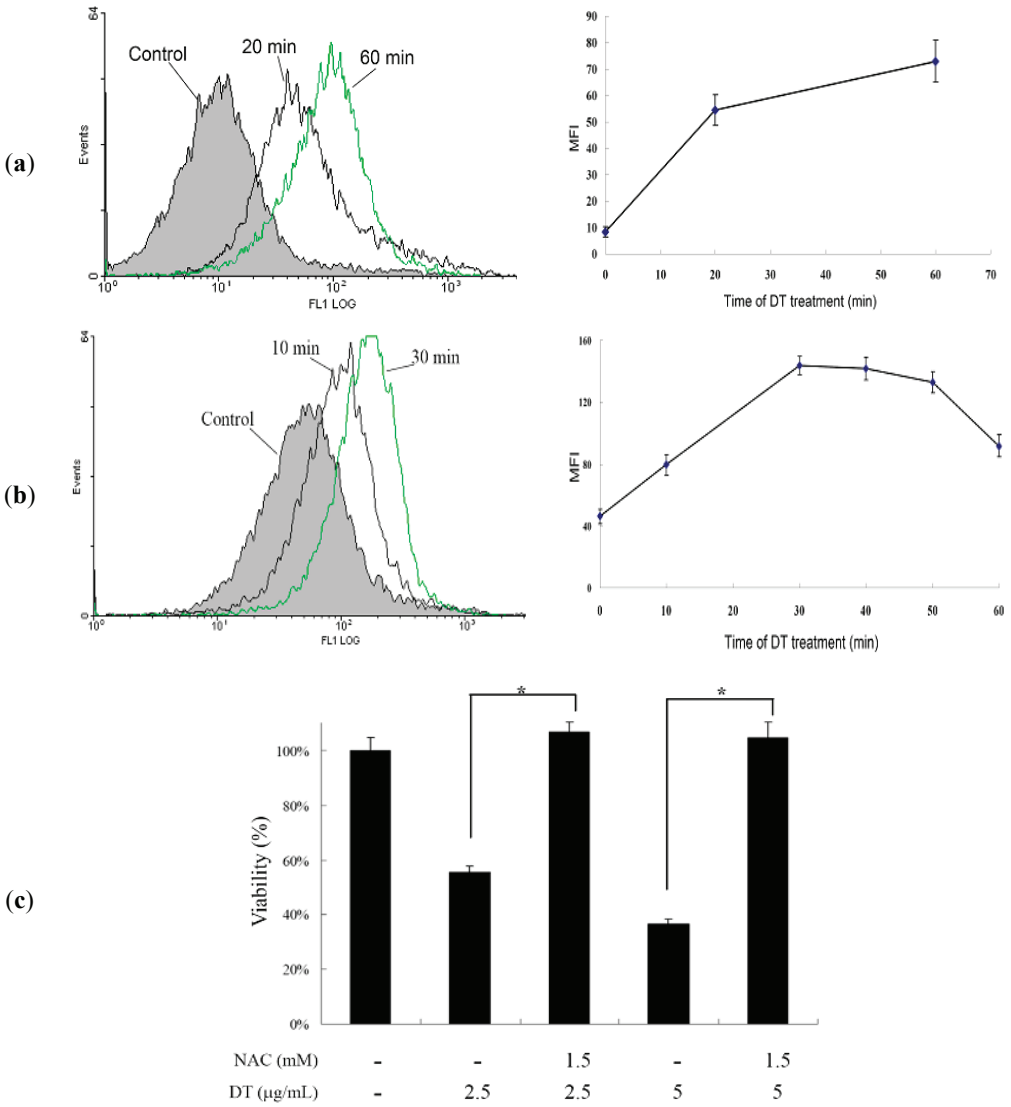

Figure 5. Effect of *N*-acetyl-cysteine (NAC) pretreatment on mitochondrial membrane potential (MMP) disruption- and DNA damage-induced by DT. Following pretreatment with NAC (1.5 mM) for 1.5 h, K562 cells were then treated with 5 μg/mL of DT for additional 24 hours. Cells were collected and analyzed; (**a**) Change of MMP with flow cytometry; (**b**) Expression of DNA damage-related proteins as shown by Western blot, results are presented as mean ± SD of three independent experiments (** P <0.001).

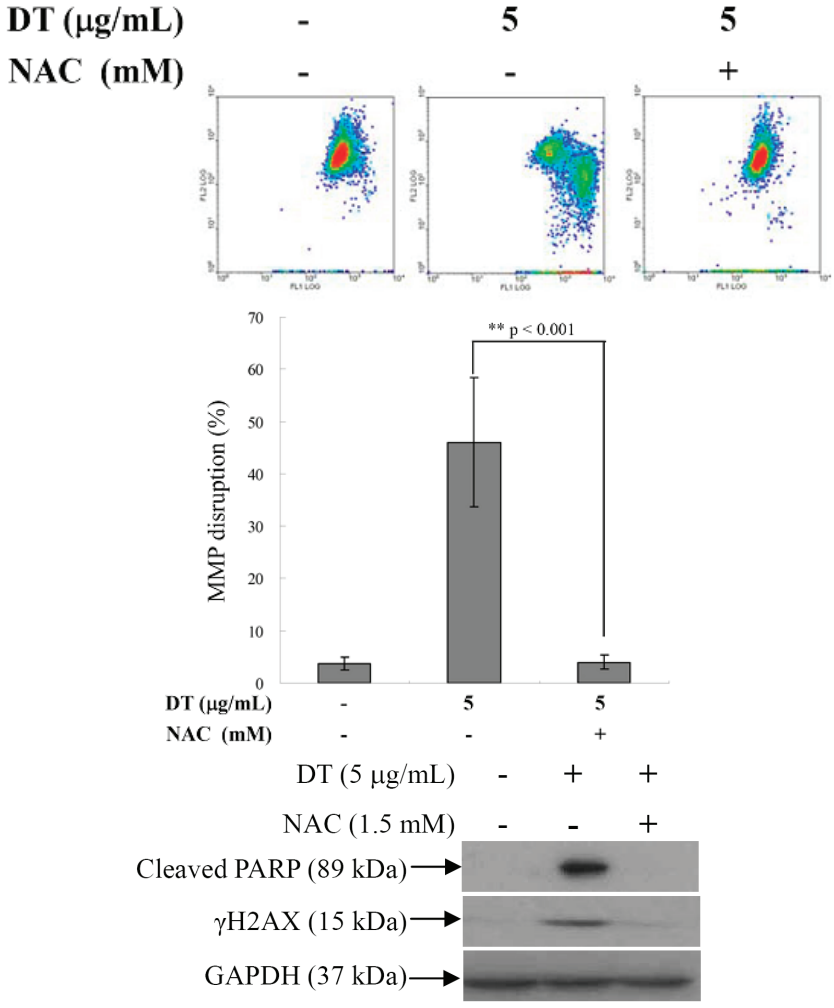

2.5. ROS Generation in DT-Induced Apoptosis is Mediated through the Inhibition of IKK/NFκB and the Activation of PI3K/Akt Pathways

Recent studies have revealed the interlocking nature of different pathways in controlling several cellular abnormalities such as inflammation and excessive cellular proliferation [21]. It was suggested that IKK/NFκB pathway is a potential therapeutic target in cancer treatment [22,23] and

the ROS-mediated apoptosis involves the inhibition of this pathway [24,25]. Additionally, it was found that phosphatidylinositol 3-kinase (PI3K)/Akt (protein kinase B, PKB) signaling pathway is overexpressed in many human malignancies and it plays a critical role in many cellular functions including cellular proliferation and survival, autophagy, metabolism, angiogenesis and motility [26]. Since our results demonstrated that the oxidative stress is the major contributor of DT-induced apoptosis in K562 cells, we further investigated whether these IKK/NFκB and PI3K/Akt pathways are associated with the ROS overproduction. To assess the involvement of IKK/NFκB and PI3K/Akt pathways, Western blot analysis was performed with specific antibodies. This allowed us to examine the effect of DT treatment on the expression of certain proteins related to these pathways. We found that treating K562 cells with DT (5 μg/mL) for 6 and 18 h diminished the expression of IKK/NFκB-related proteins and the phosphorylation of PTEN. On the other hand, an elevation of Akt and PLCγ-1 phosphorylation was observed (Figure 6a). Finally, in line with our expectation, NAC pretreatment of K562 cells abrogated the induction of Akt and PLCγ-1 phosphorylation as well as the inhibition of IKK/NFκB/TRADD, p-PTEN, PKR and HIF 1 expression caused by DT treatment (Figure 6b).

Figure 6. Effect of the oxidative stress caused by DT treatment on IκB kinases (IKK)/NFκB and phosphatidylinositol 3-kinase (PI3K)/Akt pathways; (**a**) Cells were treated with DT (5 μg/mL) for 6 and 18 h, respectively; (**b**) Other group of cells were pretreated with 1.5 mM NAC for 1.5 h, followed by the treatment with 2.5 or 5 μg/mL of DT for 18 additional hours. The expression of IKK/NFκB and PI3K/Akt pathways related proteins was examined in all groups. GAPDH was the loading control.

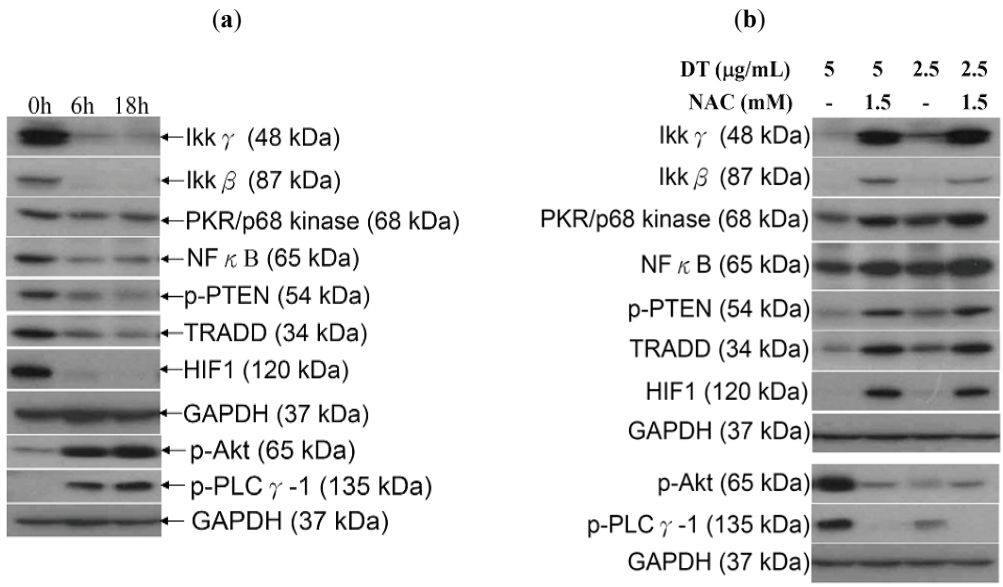

3. Discussion

In our preliminary cytotoxic screening assays against different cancer cell lines, DT exhibited a dose- and time-dependent cytotoxic effect against K562 leukemia cell line (IC_{50} of 1.4 μg/mL) (Figure 2a). K562 cells are derived from chronic myeloid leukemia (CML) patients, which are a clonal myeloproliferative disorder with constitutive tyrosine kinase (TK) activity [27,28]. Inhibition of TK has emerged as a promising target for leukemia treatment. The second generation of TK inhibitors, such as nilotinib and dasatinib, has been recently utilized as a potent class of chemotherapeutic agents. However, it was found that these inhibitors possess significant toxicities for 30%–60% of the patients [29], with high possibility of cancer relapse [30]. The significant cytotoxic activity of DT against K562 cells and the lack of efficient treatment for myeloid leukemia (CML) encouraged us to investigate its cytotoxic mechanism of action aiming to develop a safer and more potent anti-myeloid leukemia lead candidate.

We examined the induction of apoptosis by DT in K562 cells and found that ROS production is a critical factor in regulating DT cytotoxicity. Overproduction of ROS is usually accompanied with negative consequences on cellular function and integrity. It may lead to the disruption of mitochondrial membrane potential (MMP) resulting in the loss of mitochondrial membrane integrity. As shown in Figures 4 and 5, pretreatment of K562 cells with NAC, a ROS scavenger, prevented apoptosis and the disruption of MMP induced by DT. A recent report suggested that psammaplysenes A and B, dibromotyrosine-derived metabolites isolated from marine sponges, could act as potent inhibitors of FOXO1a nuclear export [31]. FOXO proteins are both sensors of oxidative stress and effectors of the cellular response [32]. These proteins are important downstream targets of the PI3K/Akt pathway. Activation of PI3K/Akt pathway directly phosphorylates FOXO proteins and inhibits their activity [33]. Our results showed that the DT induced apoptosis can be associated with the inhibition of FOXO, exerted through activation of PI3K/Akt (Figure 6a).

Reports on new cancer molecular targets indicated that some success has been achieved in the inhibition of PI3K/Akt/mTOR pathway for therapeutic purposes, but unfortunately different feedback loops were found to interrupt chemotherapeutic efficiency of the inhibitors [34]. A recent study has suggested that the loss of PTEN function, a PI3K/Akt related protein, leads to the accumulation of activated Akt, which plays a key role in the PTEN-mediated tumorigenesis via multiple mechanisms including the inhibition of apoptosis [35,36]. Our results were in harmony with previous results showing that the activation of Akt by DT is mediated through the inhibition of PTEN. Despite these preliminary results on the positive role of Akt activation in cancer therapy, its actual role is still controversial. Ahn *et al.* reported that apoptosis induced by shikonin, a secondary metabolite with a naphthoquinone skeleton, required the activation of the Akt/ASK/p38 signaling cascade via ROS generation [37]. On the other hand, chemoresistance accompanying PI3K/Akt activation was found to be regulated by the inhibition of PARP-1 [38] or the promotion of survivin [39].

Recently, several preclinical studies have focused on developing novel small molecules as inhibitors of IκB kinases (IKKs), such as Bayer "Compound A" [40], PS-1145 [41], SC-514 [42], and diarylbenzamide [43], aiming to block IKK/NFκB activation [44]. Inhibition of IKKs is

emerging as an exciting novel target for cancer therapy [44]. Moreover, hypoxia-Inducible factor-1 (HIF-1) and NFκB were found to act as pivotal regulators of cellular growth and oncogenesis [45]. Interestingly, our results indicated that the inhibition of the ROS generation with NAC pretreatment was accompanied with the recovery of HIF-1 and IKK/NFκB pathway to similar levels of the control group (Figure 6b). Kuphal *et al.* proposed that NFκB regulation in malignant melanoma under normoxic conditions is mediated through ROS. They also demonstrated that the inhibition of NFκB by adenoviral overexpression of NFκB inhibitor (IκB) led to the attenuation of HIF activity [46]. Therefore, we can propose that NFκB-attenuated HIF-1, along with ROS generation, is involved in DT-induced K562 cellular apoptosis.

4. Experimental Section

4.1. Bioassays Materials

RPMI 1640 medium, fetal calf serum (FCS), trypan blue, penicillin G, and streptomycin were obtained from GibcoBRL (Gaithersburg, MD, USA). 3-(4,5-dimethylthiazol-2-yl)-2,5-diphenyl-tetrazolium bromide (MTT), dimethyl sulfoxide (DMSO), and all other chemicals were purchased from Sigma-Aldrich (St. Louis, MO, USA). Antibodies against caspases-3, -8, and -9,TRADD, PKR, p-PTEN, p-PLCγ-1 as well as p-Akt (Ser^{473}) and PARP were purchased from Cell Signaling Technologies (Beverly, MA, USA). Antibodies of Ikkγ, Ikkβ, GAPDH, XIAP, and NFκB (p65) were obtained from Santa Cruz Biotechnology (Santa Cruz, CA, USA). HIF 1 was obtained from Enzo Life Science International, Inc. (Farmingdale, NY, USA). JC-1 cationic dye, and the carboxy derivative of fluorescein (carboxy-H_2DCFDA) were purchased from Molecular Probes and Invitrogen detection technologies (Carlsbad, CA, USA). Anti-mouse and rabbit IgG peroxidase-conjugated secondary antibody were purchased from Pierce (Rockford, IL, USA). HybondECL transfer membrane and ECL Western blotting detection kits were obtained from Amersham Life Sciences (Amersham,UK).

4.2. Preparation of (1′R,5′S,6′S)-2-(3′,5′-dibromo-1′,6′-dihydroxy-4′-oxocyclohex-2′-enyl) Acetonitrile (DT) Stock Solution

The marine sponge *Pseudoceratina* sp. was collected by scuba diving at the Green Island, which is located on the east coast of Taiwan, in March 2011, at a depth of 10 m, and the collected material was frozen immediately. A voucher sample was deposited at the National Museum of Marine Biology and Aquarium, Taiwan (specimen No. 2011-03-1). The sponge (800 g, wet wt.) was stored frozen and then freeze dried. The freeze-dried material (250 g) was minced and extracted five times with EtOAc (1 L) for 24 h each time at room temperature. The organic extract was evaporated to yield a residue (22.5 g), which was subjected to open column chromatography on silica gel eluted with gradient solution of *n*-hexane (H)–EtOAc (E), to give 11 fractions: Fr-1 (eluted by *n*-hexane), Fr-2 (eluted by H–E 100:1), Fr-3 (eluted by H–E 50:1), Fr-4 (eluted by H–E 20:1), Fr-5 (eluted by H–E 10:1), Fr-6 (eluted by H–E 5:1), Fr-7 (eluted by H–E 3:1), Fr-8 (eluted by H–E 2:1), Fr-9 (eluted by H–E 1:1), Fr-10 (eluted by H–E 1:2), and Fr-11 (eluted by EtOAc). Fraction 8 (200 mg), was subjected to normal phase HPLC, using *n*-hexane–EtOAc (3:1) as the eluent, to afford four

subfractions (A1–A4). Subfraction A1 (60 mg) was separated by normal phase HPLC using *n*-hexane–EtOAc (2:1) to afford DT (30.5 mg). The structure and the absolute configuration of this compound was unambiguously proven by X-ray diffraction analysis [47]. In the current report we isolated also aeroplysinin-1 and the other isomer of DT, (1′*R*,5′*R*,6′*S*)-2-(3′,5′-dibromo-1′,6′-dihydroxy-4′-oxo-cyclohex-2′-enyl) acetonitrile which was isolated in minute quantity [48,49].

A suitable colorless crystal was grown by slow evaporation of the EtOAc solution. Diffraction intensity data were acquired with Bruker APEX DUO single-crystal X-ray diffractometer with graphite-monochromated Mo Kα radiation (λ = 0.71073 Å). Crystal data for this compound: $C_8H_7Br_2NO_3$ (formula weight 324.97), approximate crystal size, 0.2 × 0.15 × 0.15 mm^3, monoclinic, space group, $P2_1$ (# 4), T = 100(2) K, a = 7.7217(3) Å, α = 90°, b = 8.2480(3) Å, β = 90°, c = 15.0536(6) Å, γ = 90°, V = 958.74(6) $Å^3$, Dc = 2.251 mg/m^3, Z = 4, F(000) = 624, $\mu_{(MoK\alpha)}$ = 8.433 mm^{-1}. A total of 8639 reflections were collected in the range 2.63 < θ < 26.67, with 1993 independent reflections [R(int) = 0.0202], completeness to θ_{max} was 99.6%; semi-empirical from equivalents absorption correction applied; full-matrix least-squares refinement on F^2, the number of data/restraints/parameters were 1993/0/135; goodness-of-fit on F^2 = 1.060; final R indices [I > 2 sigma (I)], R_1 = 0.0134, wR_2 = 0.0286; R indices (all data), R_1 = 0.0143, wR_2 = 0.0287, largest difference peak and hole, 0.311 and −0.282e/$Å^3$.

4.3. MTT Antiproliferative Assay

Cells were seeded at 4 × 10^4 per well in 96-well culture plates before treatment with different concentrations of the test compound. After treatment for 24, 48, or 72 h, the cytotoxicity of the test compound was determined using MTT cell proliferation assay (thiazolyl blue tetrazolium bromide, Sigma-M2128). Light absorbance values ($OD = OD_{570} - OD_{620}$) were recorded at wavelengths of 570 and 620 nm using an ELISA reader for calculating IC_{50}, *i.e.*, the cell concentration at which the light absorbance value of the experimental group is half that of the control group. These results were expressed as a percentage of the control ± SD established from n = 4 wells per one experiment from three separate experiments.

4.4. Annexin V/PI Apoptosis Assay

The externalization of phosphatidylserine (PS) and membrane integrity were quantified using an annexin V-FITC staining kit. In brief, 10^6 cells were grown in 35 mm diameter plates and were labeled with annexin V-FITC (10 µg/mL) and PI (20 µg/mL) prior to harvesting. After labeling, all plates were washed with a binding buffer and harvested. Cells were resuspended in the binding buffer at a concentration of 2 × 10^5 cells/mL before analysis by flow cytometer FACS-Calibur (Becton-Dickinson, San Jose, CA, USA) and CellQuest software. Approximately 10,000 cells were counted for each determination.

4.5. Determination of ROS Generation and MMP Disruption

These assays were performed as described previously [50]. MMP disruption and ROS generation were detected with JC-1 cationic dye (5 µg/mL) and the carboxy derivative of

fluorescein (carboxy-H_2DCFDA, 1 mM), respectively. In brief, the treated cells were labeled with a specific fluorescent dye for 30 min. After labeling, cells were washed with PBS and resuspended in PBS at a concentration of 1×10^6 cells/mL before analysis by flow cytometry.

4.6. Assay of Topoisomerase II Inhibitors and Poisons

The assay was performed as described previously [18]. Standard relaxation reaction mixtures (20 µL) containing 50 mMTris–HCl (pH 8.0), 10 mM $MgCl_2$, 200 mM potassium glutamate, 10 mM dithiothreitol, 50 µg/mL bovine serum albumin, 1 mM ATP, 0.3 µg of pHOT1 plasmid DNA, two units of human topoisomerase II (Topogen, Columbus, OH, USA) and the indicated concentrations of etoposide and 10AB were incubated at 37 °C for 30 min. Reactions were terminated by the addition of 2 µL of 10% SDS to facilitate trapping the enzyme in a cleavage complex, followed by the addition of 2.5 µL of proteinase K (50 µg/mL) to digest the bound protein (incubated 37 °C for 15 min) and finally by adding 0.1 volume of the sample loading dye. The DNA products were analyzed by electrophoresis through vertical 2% agarose gels at 2 V/cm in 0.5XTAE buffer. Gels were stained with ethidium bromide and photographed using an Eagle Eye II system (Stratagene, La Jolla, CA, USA).

4.7. Western Blotting Analysis

Cell lysates were prepared by treating the cells for 30 min in RIPAlysis buffer, 1% Nonidet P-40, 0.5% sodium deoxycholate, 0.1% sodium dodecyl sulphate (SDS), 1 mM sodium orthovanadate, 100 µg/mL phenylmethylsulfonyl fluoride and 30 µg/mL aprotinin) (all chemicals were obtained from Sigma). The lysates were centrifuged at 20,000× *g* for 30 min, and the protein concentration in the supernatant was determined using a BCA protein assay kit (Pierce, Rockford, IL, USA). Equal amounts of proteins were respectively separated by 7.5%, 10% or 12% of SDS-polyacrylamide gel electrophoresis and then were electrotransferred to a PVDF membrane. The membrane was blocked with a solution containing 5% non-fat dry milk TBST buffer (20 mMTris-HCl, pH 7.4, 150 mM NaCl and 0.1% Tween 20) for 1 h and washed with TBST buffer. The protein expressions were monitored by immunoblotting using specific antibodies. These proteins were detected by an enhanced chemiluminescence kit (Pierce).

4.8. Statistics

The results were expressed as mean ± standard deviation (SD). Comparison in each experiment was performed using an unpaired Student's *t*-test and * *P* value of less than 0.05 was considered to be statistically significant.

5. Conclusions

The purpose of this work was to elucidate the mechanism underlying the cytotoxic activity of marine dibromotyrosine, (1′*R*,5′*S*,6′*S*)-2-(3′,5′-dibromo-1′,6′-dihydroxy-4′-oxocyclohex-2′-enyl) acetonitrile (DT), against K562 cells. DT induced ROS production which resulted in mitochondrial

dysfunction and apoptosis in K562 cells. Our results suggest that this marine product may elevate the ROS-induced apoptosis in leukemia K562 cells via the blockage of IKK/NFκB/HIF/PTEN pathway and the activation of PI3K/Akt pathway. Taken together, despite the large footprint of bromotyrosine derivatives we believe that they are still under-researched and our findings will provide an impetus for future research revealing the mechanisms underlying the biological activity of these compounds.

Acknowledgments

This research was supported by grants from the National Museum of Marine Biology & Aquarium and the National Science Council (NSC101-2320-B-259-001-MY3 & NSC101-2325-B-291-001), Taiwan, awarded to Mei-Chin Lu and Ping-Jyun Sung.

Conflicts of Interest

The authors declare no conflict of interest.

References and Notes

1. Kunze, K.; Niemann, H.; Ueberlein, S.; Schulze, R.; Ehrlich, H.; Brunner, E.; Proksch, P.; Pee, K.H. Brominated skeletal components of the marine demosponges, *Aplysina cavernicola* and *Ianthella basta*: Analytical and biochemical investigations. *Mar. Drugs* **2013**, *11*, 1271–1287.
2. Ebada, S.S.; Lin, W.; Proksch, P. Bioactive sesterterpenes and triterpenes from marine sponges: Occurrence and pharmacological significance. *Mar. Drugs* **2010**, *8*, 313–346.
3. Lira, N.S.; Montes, R.C.; Tavares, J.F.; da Silva, M.S.; da Cunha, E.V.; de Athayde-Filho, P.F.; Rodrigues, L.C.; da Silva Dias, C.; Barbosa-Filho, J.M. Brominated compounds from marine sponges of the genus Aplysina and a compilation of their ^{13}C NMR spectral data. *Mar. Drugs* **2011**, *9*, 2316–2368.
4. Isidori, A. Clinical experimental evaluation of the effect of dibromotyrosine on thyroid function. *Int. J. Clin. Pharmacol. Biopharm.* **1978**, *16*, 180–182.
5. Galeano, E.; Thomas, O.P.; Robledo, S.; Munoz, D.; Martinez, A. Antiparasitic bromotyrosine derivatives from the marine sponge *Verongula rigida*. *Mar. Drugs* **2011**, *9*, 1902–1913.
6. Hinterding, K.; Knebel, A.; Herrlich, P.; Waldmann, H. Synthesis and biological evaluation of aeroplysinin analogues: A new class of receptor tyrosine kinase inhibitors. *Bioorg. Med. Chem.* **1998**, *6*, 1153–1162.
7. Cordoba, R.; Tormo, N.S.; Medarde, A.F.; Plumet, J. Antiangiogenic *versus* cytotoxic activity in analogues of aeroplysinin-1. *Bioorg. Med. Chem.* **2007**, *15*, 5300–5315.
8. Martinez-Poveda, B.; Garcia-Vilas, J.A.; Cardenas, C.; Melgarejo, E.; Quesada, A.R.; Medina, M.A. The brominated compound aeroplysinin-1 inhibits proliferation and the expression of key pro-inflammatory molecules in human endothelial and monocyte cells. *PLoS One* **2013**, *8*, e55203.

9. Teeyapant, R.; Woerdenbag, H.J.; Kreis, P.; Hacker, J.; Wray, V.; Witte, L.; Proksch, P. Antibiotic and cytotoxic activity of brominated compounds from the marine sponge *Verongia aerophoba*. *Z. Naturforsch C* **1993**, *48*, 939–945.
10. Martinez-Poveda, B.; Rodriguez-Nieto, S.; Garcia-Caballero, M.; Medina, M.A.; Quesada, A.R. The antiangiogenic compound aeroplysinin-1 induces apoptosis in endothelial cells by activating the mitochondrial pathway. *Mar. Drugs* **2012**, *10*, 2033–2046.
11. Sallam, A.A.; Ramasahayam, S.; Meyer, S.A.; El Sayed, K.A. Design, synthesis, and biological evaluation of dibromotyrosine analogues inspired by marine natural products as inhibitors of human prostate cancer proliferation, invasion, and migration. *Bioorg. Med. Chem.* **2010**, *18*, 7446–7457.
12. Kalaitzis, J.A.; Davis, R.A.; Quinn, R.J. Unequivocal ^{13}C NMR assignment of cyclohexadienyl rings in bromotyrosine-derived metabolites from marine sponges. *Magn. Reson. Chem.* **2012**, *50*, 749–754.
13. Hillgren, J.M.; Oberg, C.T.; Elofsson, M. Syntheses of pseudoceramines A–D and a new synthesis of spermatinamine, bromotyrosine natural products from marine sponges. *Org. Biomol. Chem.* **2012**, *10*, 1246–1254.
14. Buchanan, M.S.; Carroll, A.R.; Fechner, G.A.; Boyle, A.; Simpson, M.; Addepalli, R.; Avery, V.M.; Hooper, J.N.; Cheung, T.; Chen, H.; *et al*. Aplysamine 6, an alkaloidal inhibitor of isoprenylcysteine carboxyl methyltransferase from the sponge *Pseudoceratina* sp. *J. Nat. Prod.* **2008**, *71*, 1066–1067.
15. Kon, Y.; Kubota, T.; Shibazaki, A.; Gonoi, T.; Kobayashi, J. Ceratinadins A–C, new bromotyrosine alkaloids from an Okinawan marine sponge *Pseudoceratina* sp. *Bioorg. Med. Chem. Lett.* **2010**, *20*, 4569–4572.
16. Lebouvier, N.; Jullian, V.; Desvignes, I.; Maurel, S.; Parenty, A.; Dorin-Semblat, D.; Doerig, C.; Sauvain, M.; Laurent, D. Antiplasmodial activities of homogentisic acid derivative protein kinase inhibitors isolated from a Vanuatu marine sponge *Pseudoceratina* sp. *Mar. Drugs* **2009**, *7*, 640–653.
17. Herter-Sprie, G.S.; Chen, S.; Hopker, K.; Reinhardt, H.C. Synthetic lethality as a new concept for the treatment of cancer. *Ger. Med. Wkly.* **2011**, *136*, 1526–1530.
18. Du, Y.C.; Chang, F.R.; Wu, T.Y.; Hsu, Y.M.; El-Shazly, M.; Chen, C.F.; Sung, P.J.; Lin, Y.Y.; Lin, Y.H.; Wu, Y.C.; *et al*. Antileukemia component, dehydroeburicoic acid from *Antrodia camphorata* induces DNA damage and apoptosis *in vitro* and *in vivo* models. *Phytomedicine* **2012**, *19*, 788–796.
19. Nitiss, J.L. Targeting DNA topoisomerase II in cancer chemotherapy. *Nat. Rev. Cancer* **2009**, *9*, 338–350.
20. Sinha, K.; Das, J.; Pal, P.B.; Sil, P.C. Oxidative stress: The mitochondria-dependent and mitochondria-independent pathways of apoptosis. *Arch. Toxicol.* **2013**, *87*, 1157–1180.
21. Hutti, J.E.; Pfefferle, A.D.; Russell, S.C.; Sircar, M.; Perou, C.M.; Baldwin, A.S. Oncogenic PI3K mutations lead to NF-kappaB-dependent cytokine expression following growth factor deprivation. *Cancer Res*. **2012**, *72*, 3260–3269.

22. Kim, H.J.; Hawke, N.; Baldwin, A.S. NF-kappaB and IKK as therapeutic targets in cancer. *Cell Death Differ*. **2006**, *13*, 738–747.
23. Li, X.; Abdel-Mageed, A.B.; Mondal, D.; Kandil, E. The nuclear factor kappa-B signaling pathway as a therapeutic target against thyroid cancers. *Thyroid* **2013**, *23*, 209–218.
24. Lampiasi, N.; Azzolina, A.; Umezawa, K.; Montalto, G.; McCubrey, J.A.; Cervello, M. The novel NF-kappaB inhibitor DHMEQ synergizes with celecoxib to exert antitumor effects on human liver cancer cells by a ROS-dependent mechanism. *Cancer Lett*. **2012**, *322*, 35–44.
25. Madonna, G.; Ullman, C.D.; Gentilcore, G.; Palmieri, G.; Ascierto, P.A. NF-kappaB as potential target in the treatment of melanoma. *J. Transl. Med.* **2012**, *10*, 53.
26. Martelli, A.M.; Tabellini, G.; Bressanin, D.; Ognibene, A.; Goto, K.; Cocco, L.; Evangelisti, C. The emerging multiple roles of nuclear Akt. *Biochim. Biophys. Acta* **2012**, *1823*, 2168–2178.
27. Sawyers, C.L. Chronic myeloid leukemia. *N. Engl. J. Med.* **1999**, *340*, 1330–1340.
28. Rowley, J.D. Letter: A new consistent chromosomal abnormality in chronic myelogenous leukaemia identified by quinacrine fluorescence and Giemsa staining. *Nature* **1973**, *243*, 290–293.
29. Druker, B.J.; Guilhot, F.; O'Brien, S.G.; Gathmann, I.; Kantarjian, H.; Gattermann, N.; Deininger, M.W.; Silver, R.T.; Goldman, J.M.; Stone, R.M.; *et al*. Five-year follow-up of patients receiving imatinib for chronic myeloid leukemia. *N. Engl. J. Med.* **2006**, *355*, 2408–2417.
30. Ibrahim, A.R.; Eliasson, L.; Apperley, J.F.; Milojkovic, D.; Bua, M.; Szydlo, R.; Mahon, F.X.; Kozlowski, K.; Paliompeis, C.; Foroni, L.; *et al*. Poor adherence is the main reason for loss of CCyR and imatinib failure for chronic myeloid leukemia patients on long-term therapy. *Blood* **2011**, *117*, 3733–3736.
31. Georgiades, S.N.; Clardy, J. Total synthesis of psammaplysenes A and B, naturally occurring inhibitors of FOXO1a nuclear export. *Org. Lett.* **2005**, *7*, 4091–4094.
32. Myatt, S.S.; Brosens, J.J.; Lam, E.W. Sense and sensitivity: FOXO and ROS in cancer development and treatment. *Antioxid. Redox Signal.* **2011**, *14*, 675–687.
33. Greer, E.L.; Brunet, A. FOXO transcription factors at the interface between longevity and tumor suppression. *Oncogene* **2005**, *24*, 7410–7425.
34. Kryston, T.B.; Georgiev, A.B.; Pissis, P.; Georgakilas, A.G. Role of oxidative stress and DNA damage in human carcinogenesis. *Mutat. Res.* **2011**, *711*, 193–201.
35. Downward, J. PI 3-kinase, Akt and cell survival. *Semin. Cell Dev. Biol.* **2004**, *15*, 177–182.
36. Blanco-Aparicio, C.; Renner, O.; Leal, J.F.; Carnero, A. PTEN, more than the AKT pathway. *Carcinogenesis* **2007**, *28*, 1379–1386.
37. Ahn, J.; Won, M.; Choi, J.H.; Kim, Y.S.; Jung, C.R.; Im, D.S.; Kyun, M.L.; Lee, K.; Song, K.B.; Chung, K.S. Reactive oxygen species-mediated activation of the Akt/ASK1/p38 signaling cascade and p21 downregulation are required for shikonin-induced apoptosis. *Apoptosis* **2013**, *18*, 870–881.
38. Szanto, A.; Hellebrand, E.E.; Bognar, Z.; Tucsek, Z.; Szabo, A.; Gallyas, F., Jr.; Sumegi, B.; Varbiro, G. PARP-1 inhibition-induced activation of PI-3-kinase-Akt pathway promotes resistance to taxol. *Biochem. Pharmacol.* **2009**, *77*, 1348–1357.

39. Xing, H.; Weng, D.; Chen, G.; Tao, W.; Zhu, T.; Yang, X.; Meng, L.; Wang, S.; Lu, Y.; Ma, D. Activation of fibronectin/PI-3K/Akt2 leads to chemoresistance to docetaxel by regulating survivin protein expression in ovarian and breast cancer cells. *Cancer Lett.* **2008**, *261*, 108–119.
40. Ziegelbauer, K.; Gantner, F.; Lukacs, N.W.; Berlin, A.; Fuchikami, K.; Niki, T.; Sakai, K.; Inbe, H.; Takeshita, K.; Ishimori, M.; Komura, H.; Murata, T.; Lowinger, T.; Bacon, K.B. A selective novel low-molecular-weight inhibitor of IkappaB kinase-beta (IKK-beta) prevents pulmonary inflammation and shows broad anti-inflammatory activity. *Br. J. Pharmacol.* **2005**, *145*, 178–192.
41. Castro, A.C.; Dang, L.C.; Soucy, F.; Grenier, L.; Mazdiyasni, H.; Hottelet, M.; Parent, L.; Pien, C.; Palombella, V.; Adams, J. Novel IKK inhibitors: Beta-Carbolines. *Bioorg. Med. Chem. Lett.* **2003**, *13*, 2419–2422.
42. Kishore, N.; Sommers, C.; Mathialagan, S.; Guzova, J.; Yao, M.; Hauser, S.; Huynh, K.; Bonar, S.; Mielke, C.; Albee, L.; *et al*. A selective IKK-2 inhibitor blocks NF-kappa B-dependent gene expression in interleukin-1 beta-stimulated synovial fibroblasts. *J. Biol. Chem.* **2003**, *278*, 32861–32871.
43. Christopher, J.A.; Avitabile, B.G.; Bamborough, P.; Champigny, A.C.; Cutler, G.J.; Dyos, S.L.; Grace, K.G.; Kerns, J.K.; Kitson, J.D.; Mellor, G.W.; *et al*. The discovery of 2-amino-3,5-diarylbenzamide inhibitors of IKK-alpha and IKK-beta kinases. *Bioorg. Med. Chem. Lett.* **2007**, *17*, 3972–3977.
44. Gamble, C.; McIntosh, K.; Scott, R.; Ho, K.H.; Plevin, R.; Paul, A. Inhibitory kappa B Kinases as targets for pharmacological regulation. *Br. J. Pharmacol.* **2012**, *165*, 802–819.
45. Nam, S.Y.; Ko, Y.S.; Jung, J.; Yoon, J.; Kim, Y.H.; Choi, Y.J.; Park, J.W.; Chang, M.S.; Kim, W.H.; Lee, B.L. A hypoxia-dependent upregulation of hypoxia-inducible factor-1 by nuclear factor-kappa B promotes gastric tumour growth and angiogenesis. *Br. J. Cancer* **2011**, *104*, 166–174.
46. Kuphal, S.; Winklmeier, A.; Warnecke, C.; Bosserhoff, A.K. Constitutive HIF-1 activity in malignant melanoma. *Eur. J. Cancer* **2010**, *46*, 1159–1169.
47. Crystallographic data have been deposited with the Cambridge Crystallographic Data Centre (deposition number CCDC 930829). Copies of the data can be obtained, f.o.c., on application to the Director, CCDC, 12 Union Road, Cambridge CB2 1EZ, UK (Fax: +44-1223-336033 or E-Mail: deposit@ccdc.cam.ac.uk).
48. Capon, R.; Macleod, J. Two epimeric dibromo nitriles from the australian sponge *Aplysina laevis*. *Aust. J. Chem.* **1987**, *40*, 341–346.
49. Santalova, E.A.; Denisenko, V.A.; Glazunov, V.P.; Kalinovskii, A.I.; Anastyuk, S.D.; Stonik, V.A. Dibromotyrosine derivatives from the ethanol extract of the marine sponge *Aplysina* sp.: Structures, transformations and origin. *Russian Chem. Bull.* **2011**, *60*, 570–580.
50. Huang, K.-J.; Chen, Y.-C.; El-Shazly, M.; Du, Y.-C.; Su, J.-H.; Tsao, C.-W.; Yen, W.-H.; Chang, W.-B.; Su, Y.-D.; Yeh, Y.-T.; *et al*. 5-Episinuleptolide acetate, a norcembranoidal diterpene from the formosan soft coral *Sinularia* sp., induces leukemia cell apoptosis through Hsp90 inhibition. *Molecules* **2013**, *18*, 2924–2933.

Hippuristanol Reduces the Viability of Primary Effusion Lymphoma Cells both *in Vitro* and *in Vivo*

Chie Ishikawa, Junichi Tanaka, Harutaka Katano, Masachika Senba and Naoki Mori

Abstract: Primary effusion lymphoma (PEL) caused by Kaposi's sarcoma-associated herpesvirus (also known as human herpesvirus-8) shows serious lymphomatous effusion in body cavities. PEL is difficult to treat and there is no standard treatment strategy. Hippuristanol is extracted from Okinawan coral *Isis hippuris*, and inhibits translational initiation by blocking eukaryotic initiation factor 4A, an ATP-dependent RNA helicase, binding to mRNA. Recently, there has been much interest in targeting translation initiation as an anticancer therapy. Here, we show that treatment of PEL cell lines with hippuristanol resulted in cell cycle arrest at G_1 phase, and induced caspases activation and apoptosis. Hippuristanol also reduced the expression of cyclin D2, CDK2, CDK4, CDK6 and prosurvival XIAP and Mcl-1 proteins. Activation of activator protein-1, signal transducers and activators of transcription protein 3 and Akt pathways plays a critical role in the survival and growth of PEL cells. Hippuristanol suppressed the activities of these three pathways by inhibiting the expression of JunB, JunD, c-Fos, signal transducers and activators of transcription protein 3 and Akt proteins. In a xenograft mouse model that showed ascites and diffused organ invasion of PEL cells, treatment with hippuristanol significantly inhibited the growth and invasion of PEL cells compared with untreated mice. The results of the *in vitro* and *in vivo* experiments underline the potential usefulness of hippuristanol in the treatment of PEL.

Reprinted from *Mar. Drugs*. Cite as: Ishikawa, C.; Tanaka, J.; Katano, H.; Senba, M.; Mori, N. Hippuristanol Reduces the Viability of Primary Effusion Lymphoma Cells both *in Vitro* and *in Vivo*. *Mar. Drugs* **2013**, *11*, 3410-3424.

1. Introduction

The lymphoproliferative disorder, primary effusion lymphoma (PEL), afflicts mainly patients infected with human immunodeficiency virus, and exclusively involves body cavities such as the peritoneal, pleural and pericardial cavities [1,2]. PEL is caused by clonal expansion of Kaposi's sarcoma-associated herpesvirus (KSHV; also known as human herpesvirus-8) infected B cells [1,2]. Patients with PEL present with lymphomatous effusions within body cavities [1,2]. This type of lymphoma is generally aggressive, rapidly progressing and resistant to conventional chemotherapy, with a median survival time of six months and a one-year overall survival rate of 40% [3], emphasizing the need for new therapies. A number of constitutively activated signaling pathways play critical roles in the survival and growth of PEL cells. These include nuclear factor kappa B (NF-κB), activator protein-1 (AP-1), signal transducers and activators of transcription protein (STAT) and phosphatidylinositol-3-kinase (PI3K)/Akt pathways [4–7]. KSHV is a master in altering these pathways in favor of its survival [8].

Hippuristanol, a steroid isolated from coral *Isis hippuris*, has been identified as a selective and potent inhibitor of RNA helicase, eukaryotic initiation factor 4A, and RNA-binding activity [9].

The eukaryotic initiation factor 4A plays a key role in the recruitment of ribosomes to mRNA templates during the initiation of eukaryotic translation. Recently, there has been much interest in targeting translation initiation as an anticancer therapy, because deregulated translation initiation is implicated extensively in cancer initiation and progression [10].

In the present study, we investigated the effects of hippuristanol on the proliferation and apoptosis of cultured human PEL cells and analyzed the mechanisms of such effects. We also assessed the *in vivo* effects of hippuristanol in immunodeficient SCID mice inoculated with PEL cells. The results provide insights into the molecular target of hippuristanol in PEL cells and the anticancer mechanism of hippuristanol against PEL cells.

2. Results

2.1. Hippuristanol Dose-Dependently Inhibits PEL Cell Viability

First, we examined the effects of hippuristanol on PEL cell viability. Two PEL cell lines (BCBL-1 and TY-1), two KSHV-uninfected lymphoma B cell lines (BJAB and Ramos), and peripheral blood mononuclear cells (PBMCs) from three healthy volunteers were cultured for 24 h in the presence of various concentrations of hippuristanol, and their viability was analyzed by water-soluble tetrazolium (WST)-8 assays. Figure 1A shows that increasing the concentration of hippuristanol from 12.5 to 200 nM resulted in further suppression of cell viability and that this effect was dose-dependent in the two PEL cell lines. The estimated 50% inhibitory concentration (IC_{50}) values for BCBL-1 and TY-1 were 62 and 55 nM, respectively. In contrast, the IC_{50} values for BJAB and Ramos were 175 and 104 nM, respectively. We reported previously that the IC_{50} values for five human T cell leukemia virus type 1-infected T cell lines ranged from 189 to 329 nM [11]. Thus, PEL cell lines were considered more sensitive than T cell lines and KSHV-uninfected lymphoma B cell lines to hippuristanol. On the other hand, PBMCs from healthy volunteers were resistant to hippuristanol with IC_{50} of >1021 nM [11]. These results suggest that hippuristanol is less cytotoxic to normal cells than PEL cells, and most effectively inhibited cell survival of PEL cells at low nanomolar concentrations.

2.2. Effects of Hippuristanol on PEL Cell Cycle and Apoptosis

In following experiments, we determined the mechanism of the suppressive effects of hippuristanol on PEL cell viability. The effect of hippuristanol on cell cycle progression was investigated by flow cytometry analysis after propidium iodide staining. Hippuristanol accumulated cells in sub-G_1 phase (from 3.9% and 2.9% of control BCBL-1 and TY-1 cells to 17.4% and 13.9% of treated BCBL-1 and TY-1 cells, respectively). A cell cycle profile was then created by using selective gating excluding sub-G_1 population. As shown in Figure 1B, hippuristanol increased the G_1 population of PEL cells, compared with the control. This increase was accompanied by a concomitant decrease in the S phase and G_2/M phase cell populations. These results indicate that the inhibitory effects of hippuristanol on PEL cell viability were due to cell cycle arrest at G_1 phase.

Figure 1. Hippuristanol reduces viability and induces cell cycle arrest of primary effusion lymphoma (PEL) cells. (**A**) *Left:* Structure of hippuristanol. *Right:* Hippuristanol reduced PEL cell viability. PEL cell lines were treated with the indicated concentrations of hippuristanol for 24 h. The cell viability was determined by WST-8. Data are mean ± SD percentage values of triplicate experiments compared with untreated cells; (**B**) Hippuristanol causes PEL cell cycle arrest. PEL cells were treated with hippuristanol (200 nM) for 24 h and analyzed by flow cytometry. The percentages of cells in the G_1, S and G_2/M phases were calculated using MultiCycle software. Data are mean ± SD percentage values of cells at various phases of the cell cycle (n = 3). * $P < 0.05$, ** $P < 0.01$, compared with control cells.

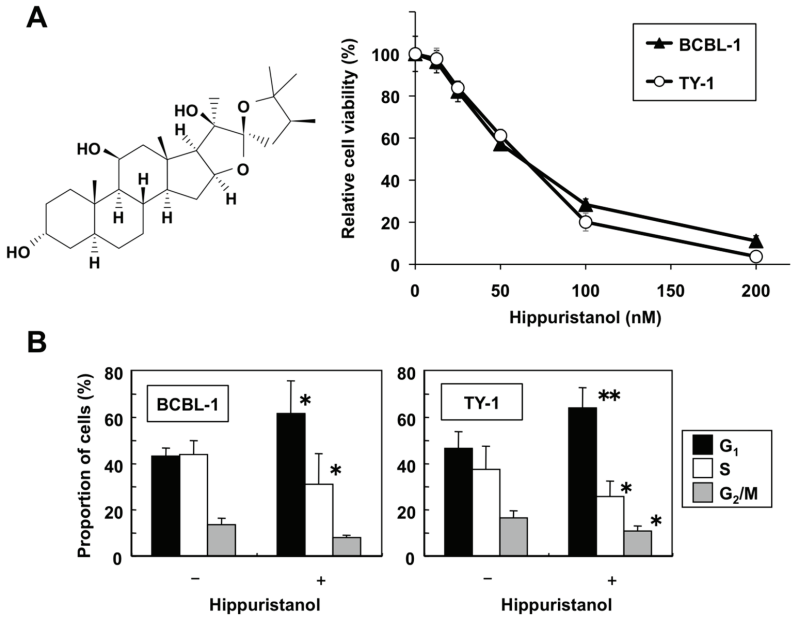

Since cells with sub-G_1 DNA content were considered apoptotic, we determined the extent of apoptosis in hippuristanol-treated PEL cells by using Apo2.7 staining. Apo2.7 specifically detects the 38-kDa mitochondrial membrane antigen 7A6 expressed on the mitochondrial outer membrane during apoptosis [12]. As shown in Figure 2A, the addition of 200 nM hippuristanol to cultures of PEL cells for 24 h resulted in apoptosis of these cells. Next, we studied the role of caspases in this process by determining cleavage of endogenous caspases. Western blot analyses carried out after treatment of PEL cells with hippuristanol showed increased levels of activated cleaved forms of caspase-3, -8 and -9, and that such increases were hippuristanol dose-dependent (Figure 2B). Caspase-3 has several substrate proteins, and the DNA damage repair enzyme polyadenosin-5′-diphosphate-ribose polymerase (PARP) is a major substrate [13]. The cleaved PARP was present as an active form and its production level was hippuristanol dose-dependent. Control experiments showed no change in the expression of the structural protein actin after the addition of hippuristanol up to 200 nM.

Immunoblotting allowed us to examine the processing of caspases, but did not indicate whether the cleavage products were enzymatically active. Therefore, we used colorimetric assays to determine caspase-3, -8 and -9 activities based on cleavage of caspase-specific-labeled substrates. Hippuristanol activated caspase-3, -8 and -9 in PEL cells (Figure 2C). The results of the above experiments confirmed that caspase activation mediates hippuristanol-induced apoptosis of PEL cells.

2.3. Effects of Hippuristanol on Expression of Cell Cycle and Apoptosis Regulatory Proteins in PEL Cells

The cell cycle process in eukaryotes is orchestrated by the function of a family of protein kinase complexes. Each complex is composed minimally of cyclins that bind to CDK to form active cyclin-CDK complexes. We next examined the effects of hippuristanol on cell cycle regulatory molecules operative in the G_1 phase of the cell cycle in PEL cells. Western blot analysis showed that treatment of BCBL-1 cells with hippuristanol resulted in a significant and dose-dependent decrease in the protein expression of cyclin D2, CDK2, CDK4 and CDK6, but not cyclin E (Figure 3A).

Figure 2. Hippuristanol induces apoptosis of PEL cells. (**A**) PEL cells were cultured in the presence or absence of hippuristanol (200 nM) for 24 h and apoptosis was determined by Apo2.7 staining. Data are mean ± SD; (**B**) Immunoblot analysis of caspases and PARP cleavage. PEL cells were treated with the indicated concentrations of hippuristanol for 24 h, and then subjected to Western blotting. Arrowheads indicate the cleaved form of caspase-8; (**C**) Changes in caspase-3, -8 and -9 activities in PEL cells. Cells were cultured in the presence or absence of hippuristanol (200 nM) for 24 h before harvesting. The activity of the indicated caspases was measured using the colorimetric caspase assay and labeled caspase substrates. Caspase activity in untreated cells was defined as 1. Data are mean ± SD of three experiments.

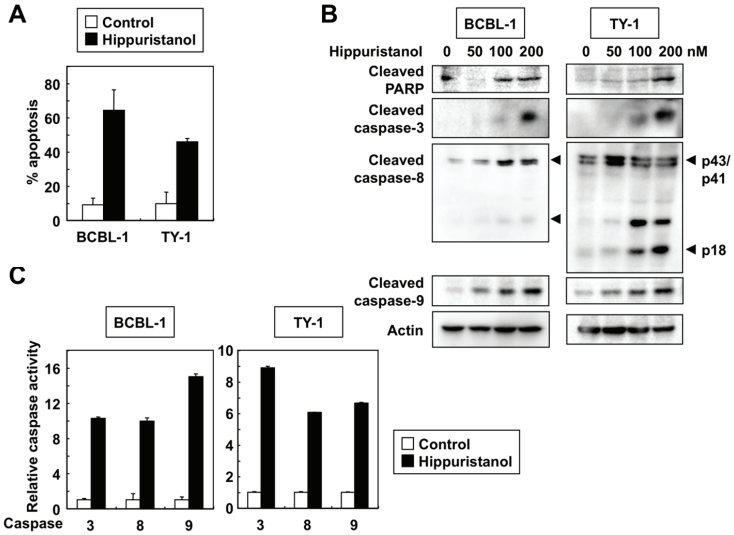

We also examined whether the effects of hippuristanol on apoptosis is mediated through the modulation of expression of inhibitors of apoptosis. Hippuristanol caused a dose-dependent downregulation of XIAP and Mcl-1, but had no effect on the expression of cIAP-2, survivin and Bcl-xL (Figure 3A). Furthermore, hippuristanol did not alter the expression of pro-apoptotic proteins, Bax and Bak. These results suggest the possible involvement of XIAP and Mcl-1 proteins in hippuristanol-induced apoptosis.

Figure 3. Hippuristanol induces downregulation of cell cycle and apoptosis regulatory proteins and suppresses AP-1 signaling in PEL cells. (**A**) Effects of hippuristanol on the expression of cell cycle (left panels) and apoptosis regulatory proteins (right panels). BCBL-1 cells were treated with the indicated concentrations of hippuristanol for 24 h and then harvested. Total cell lysates were prepared and equal amounts of protein were subjected to Western blot analysis; (**B** and **C**) Hippuristanol inhibits AP-1 activation. BCBL-1 cells were treated with hippuristanol (200 nM) for the indicated time periods and assessed for AP-1, NF-κB and Oct-1 DNA-binding activity by EMSA using each specific oligonucleotide probe; (**D**) Competition and supershift assays were performed by adding the indicated competitor oligonucleotides or antibodies (Ab), to nuclear extracts from BCBL-1 cells.

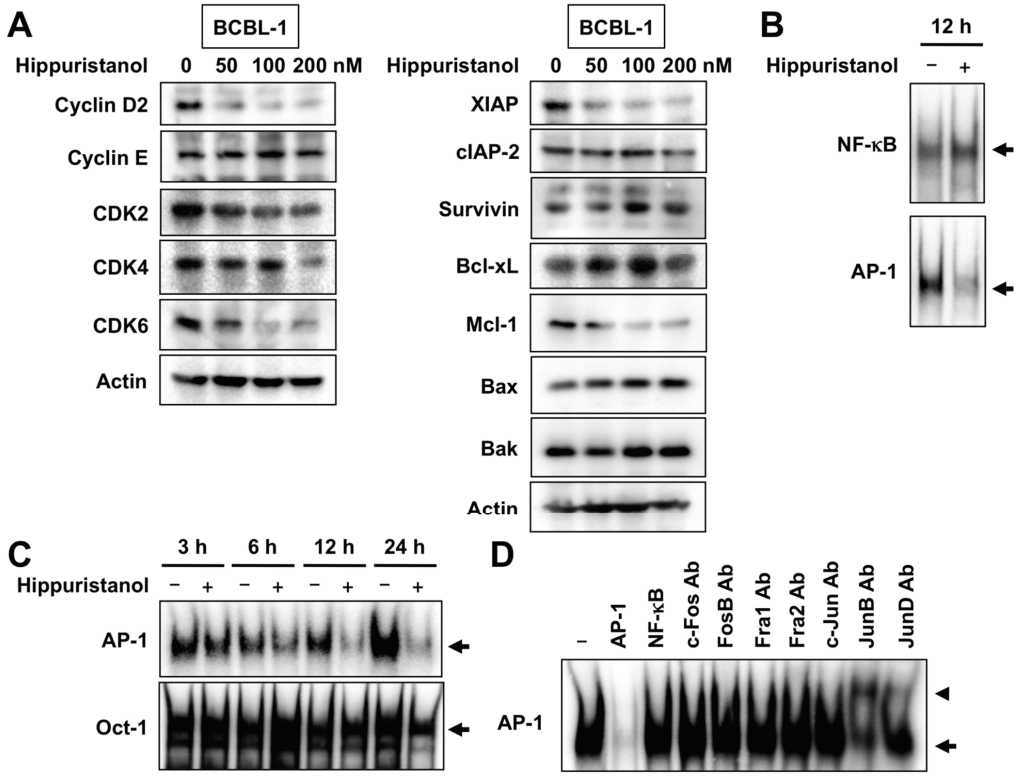

2.4. Hippuristanol Efficiently Blocks Constitutive Activation of AP-1 in PEL Cells

Several reports have suggested that NF-κB and AP-1 can act as survival factors and are required for the proliferation of PEL cells [4,7]. Because NF-κB and AP-1 are constitutively active in PEL cells [4,7], we examined whether hippuristanol inhibits NF-κB and AP-1 activation using electrophoretic mobility shift assay (EMSA). Treatment with 200 nM hippuristanol suppressed the DNA-binding activities of AP-1 but not NF-κB in BCBL-1 cells (Figure 3B). The suppression was specific to AP-1 and was not due to cell death because no significant change in binding activity of Oct-1 was observed after treatment of cells with hippuristanol (Figure 3C). The specificity of the gel retardation was demonstrated in cold competition experiments. Excess of the cold AP-1 probe abrogated the band, whereas excess of the cold NF-κB probe had no effect (Figure 3D). We next analyzed AP-1 subcomponents by supershift assays using BCBL-1 cells. Supershift analyses showed that AP-1 band was composed of JunB and JunD (Figure 3D). We then examined the effect of hippuristanol on the expression of JunB and JunD proteins in BCBL-1 cells. When incubated with hippuristanol for 24 h, BCBL-1 cells displayed decreased expression of JunB and JunD, and the decrease was hippuristanol dose-dependent (Figure 4A). c-Jun, the most potent transcription factor in AP-1 family, forms heterodimer with c-Fos. The KSHV-encoded latency-associated nuclear antigen induces binding of a c-Jun-Fos heterodimer to the AP-1 response element [14]. We also examined the effect of hippuristanol on the expression of c-Jun and c-Fos proteins. As shown in Figure 4A, hippuristanol reduced the expression of c-Fos, but not c-Jun. These results suggest that hippuristanol inhibits AP-1 activation through depletion of JunB, JunD and c-Fos.

2.5. Hippuristanol Inhibits Activation of STAT3 and Akt in PEL Cells

Aberrant STAT3 and Akt activation is also found in PEL cells [5,6]. The next series of experiments examined the inhibitory effect of hippuristanol on STAT3 and Akt activation in BCBL-1 cells using Western blot analysis. Phosphorylation of STAT3 and Akt was detected in BCBL-1 cells, and hippuristanol suppressed the levels of total and phosphorylated STAT3 and Akt proteins (Figure 4B). Phosphatidylinositol 3-kinase (PI3K) catalyzes the phosphorylation of the 3-hydroxyl position of phosphatidylinositol 4,5-diphosphate (PIP2) to phosphatidylinositol 3,4,5-triphosphate (PIP3). PIP3 facilitates the phosphorylation of Akt at Thr308 by 3-phosphoinositide-dependent protein kinase 1 (PDK1) [15]. Phosphorylation on the activation loop Ser241 by autophosphorylation is necessary for PDK1 activity [16]. The phosphorylation level of PDK1 was also examined at this time point. Hippuristanol inhibited the phosphorylation of PDK1 in a dose-dependent manner (Figure 4B), but had no effect on PDK1 total protein level. These results suggest that hippuristanol inhibits constitutive activation of STAT3 and Akt in PEL cells, and that Akt inhibition is due at least in part to PDK1 dephosphorylation.

2.6. In Vivo Effects of Hippuristanol in Immunodeficient Mice Inoculated with PEL Cells

The above *in vitro* experiments demonstrated the efficacy of hippuristanol against PEL cells. In the next series of experiments, we tested the effects of hippuristanol in immunodeficient mice. BCBL-1 cells were injected intraperitoneally into the SCID mice and hippuristanol or vehicle was

administered intraperitoneally every day. BCBL-1 produced massive ascites within 35 days of inoculation. Vehicle-treated mice developed massive abdominal distention, whereas hippuristanol-treated mice appeared normal and healthy. The body weight of hippuristanol-treated mice was significantly less than that of vehicle-treated mice at 28 and 35 days (Figure 5A). Evaluation of PEL cell infiltration in body organs on day 35 by hematoxylin and eosin (H&E) staining showed infiltration of BCBL-1 cells in the liver and spleen of vehicle-treated mice (Figure 5B). In contrast, the infiltration of BCBL-1 cells into the liver and spleen in hippuristanol-treated mice was not observed. The weight of the livers and spleens was significantly lower in hippuristanol-treated mice than in vehicle-treated mice (Figure 5B). No apparent adverse effects were observed in mice treated with hippuristanol.

Figure 4. Hippuristanol inhibits the constitutively active AP-1, STAT3 and Akt in PEL cells. (**A**) Hippuristanol reduced AP-1 family proteins, JunB, JunD and c-Fos; (**B**) Hippuristanol inhibited the activation of STAT3 and Akt. BCBL-1 cells were treated with various doses of hippuristanol for 24 h, and cell lysates were prepared. Equal amounts of protein from each sample were separated and immunoblotted with the indicated antibodies.

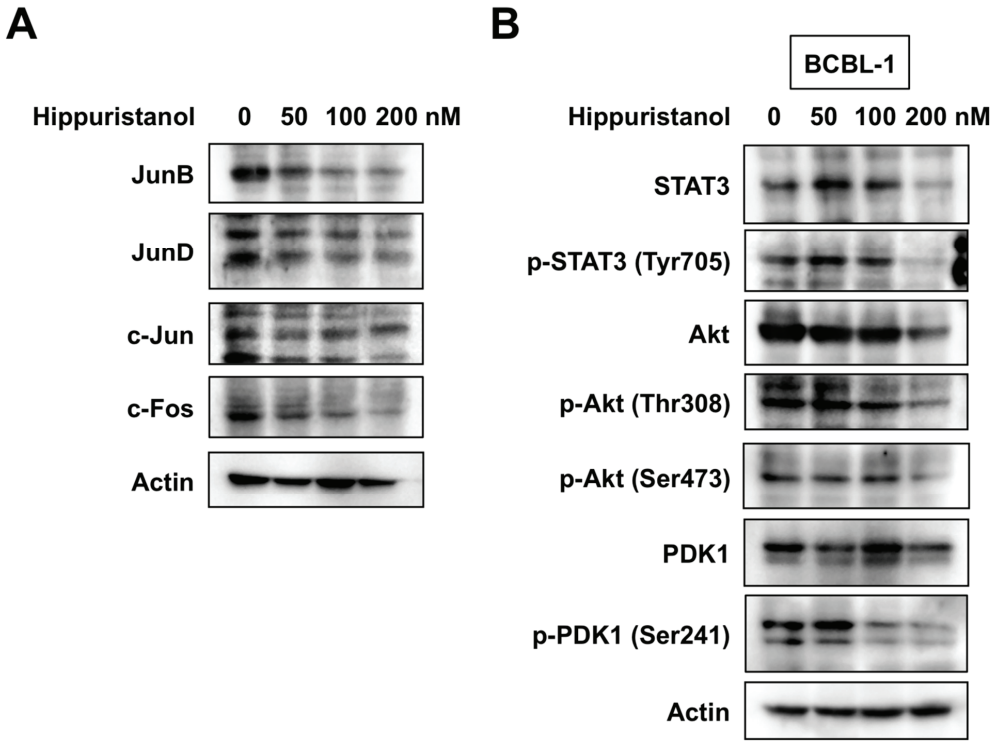

PEL cells are known to express CD30, a 120-kDa type I surface glycoprotein [1] and soluble CD30 (sCD30) is produced by PEL cells [17]. The serum level of sCD30 appears to be a useful biological tumor marker for the diagnosis and management of PEL [17]. Treatment of mice with

hippuristanol significantly reduced serum sCD30 to undetectable levels, whereas that of vehicle-treated mice was 352 ± 186 ng/mL (n = 5) (Figure 5C). These data indicate that hippuristanol significantly inhibits the growth and infiltration of PEL cells *in vivo*. Collectively, these results demonstrated that hippuristanol is effective against PEL cells.

Figure 5. Treatment of SCID mice with hippuristanol suppresses the development of PEL *in vivo*. (**A**) *Left:* Body weight of mice inoculated with BCBL-1 cells and treated or untreated with hippuristanol. Data are mean ± SD of five mice. *Right:* Photographs of hippuristanol-treated and -untreated ascites-bearing mice five weeks after intraperitoneal inoculation of BCBL-1; (**B**) Metastasis of PEL cells into the liver and spleen in BCBL-1 inoculated mice. *Left:* Weight of the indicated organs in mice inoculated with BCBL-1 cells and treated or untreated with hippuristanol. Data are mean ± SD of five mice. * $P < 0.05$, compared with the vehicle-treated group. *Top Right:* Photographs of the livers and spleens in hippuristanol- and vehicle-treated mice. *Bottom Right*: H&E staining was performed to detect BCBL-1 cells in the liver in mice untreated with hippuristanol. Original magnification, ×400; (**C**) Serum levels of sCD30 in hippuristanol-treated and -untreated mice. The sCD30 concentrations were measured by ELISA.

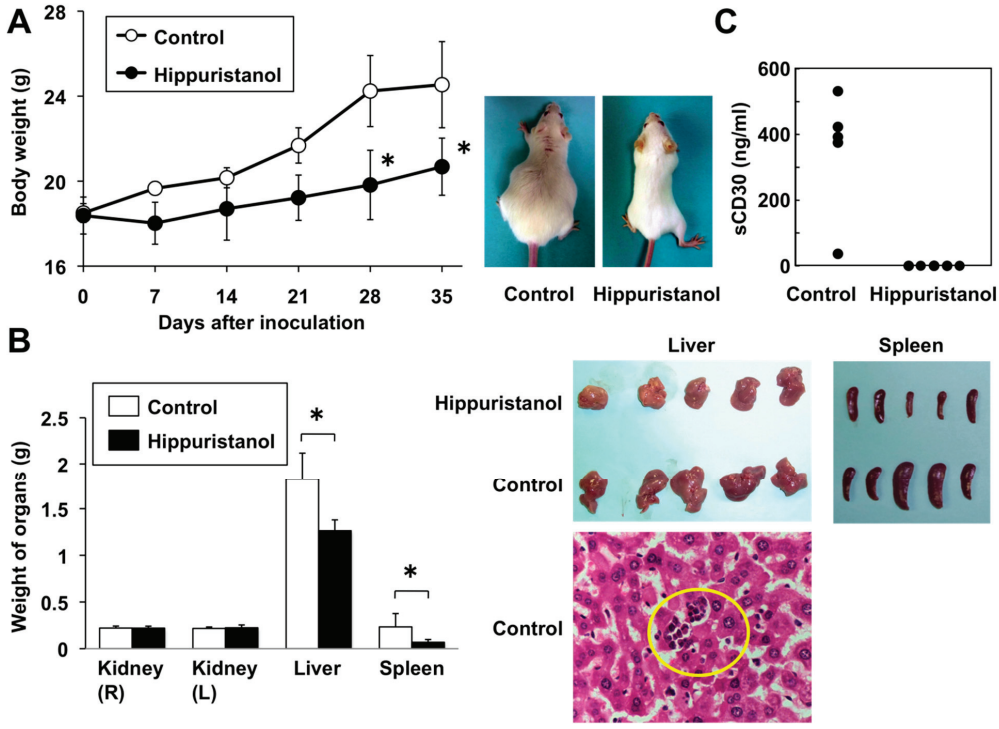

3. Discussion

In the present study, we investigated the effects of a naturally occurring eukaryotic translation initiation inhibitor, hippuristanol, on PEL cells, both *in vitro* and *in vivo*, and showed that hippuristanol is cytotoxic to these cells and this action is mediated through inhibition of the AP-1, STAT3 and Akt pathways and depletion of JunB, JunD, c-Fos, STAT3 and Akt. Since hippuristanol did not significantly alter the ratios of phosphorylated STAT3 *versus* total STAT3 and phosphorylated Akt *versus* total Akt, the decrease in phosphorylated STAT3 and Akt is possibly due to the downregulation of total STAT3 and Akt, rather than their dephosphorylation. In this study, we found that hippuristanol disrupted the phosphorylation of PDK1 in PEL cells. We also showed that hippuristanol reduced the expression of cyclin D2, CDK2, CDK4, CDK6, XIAP and Mcl-1 proteins. Cyclin D2 promoter contains AP-1 site [18]. Constitutively activated STAT3 is known to participate in oncogenesis through upregulation of STAT3 target genes encoding cyclin D2 [19] and apoptosis inhibitors such as XIAP, which is known to suppress cell death by inhibiting caspase-3 and caspase-9 [20]. Furthermore, Akt interacts with and phosphorylates XIAP, leading to inhibition of ubiquitination of XIAP [21]. A link between STAT3 activation and regulation of Bcl-2 family protein expression has been demonstrated [22]. Inhibition of STAT3 signaling resulted in apoptosis and decreased Mcl-1 expression [22]. Mcl-1 is also a PI3K-regulated protein [23]. In addition, STAT3 can regulate the AP-1 family protein, JunB [24]. Thus, AP-1, STAT3 and Akt can collaborate in PEL, depending on various of survival factors. Although hippuristanol-induced downregulation of cell cycle and apoptosis regulatory proteins depends on direct inhibition of translation, we speculate that this agent blocks the AP-1, STAT3 and Akt signaling pathways, resulting in reduced expression of their downstream effectors.

It is known that hippuristanol delays poliovirus replication in infected cells [9]. Therefore, we investigated whether hippuristanol affects KSHV lytic replication in PEL cells. The expression of two viral genes known as lytic genes (ORF50 and ORFK9) and three viral genes known as latent genes (ORF72, ORF73 and ORFK13) was examined in TY-1 cells treated with hippuristanol by reverse transcription-polymerase chain reaction. However, there was no significant change in the expression levels of lytic and latent genes after treatment (data not shown), suggesting that hippuristanol does not induce viral reactivation.

In vivo experiments showed that untreated PEL-xenografted mice tended to be heavier, both in appearance and weight. The mean body weight and weight of livers and spleens were significantly higher in the control group, which was likely due to effusion in body cavities and organ invasion. Treatment with hippuristanol reduced serum levels of the surrogate marker sCD30 to undetectable levels, compared with relatively high levels in untreated mice. Although there is still the possibility that hippuristanol directly inhibits CD30 mRNA translation, treatment with hippuristanol could induce cell death of PEL cells, a major source for sCD30, resulting in a decrease in serum sCD30. The significant reduction of ascites and organ invasion with no apparent adverse effects in mice suggests that hippuristanol could add a new direction in the treatment of refractory PEL.

4. Experimental Section

4.1. Cell Lines and Reagents

Human KSHV-infected PEL cell lines, BCBL-1 [25] and TY-1 [26], and KSHV-uninfected lymphoma B cell lines, BJAB and Ramos, were maintained in Roswell Park Memorial Institute (RPMI) 1640 medium supplemented with 10% heat inactivated fetal bovine serum, penicillin (50 U/mL) and streptomycin (50 μg/mL) in a humidified incubator. Hippuristanol was extracted from the gorgonian *I. hippuris* as described previously [9]. Final purification of hippuristanol was done by HPLC up to 97%. Its purity was confirmed by 1H NMR spectrum. Antibodies to cleaved PARP, cleaved caspase-3, cleaved caspase-8, cleaved caspase-9, survivin, Bcl-xL, Bax, Bak, c-Jun, Akt, phospho-Akt (Thr308), phospho-Akt (Ser473), PDK1, phospho-PDK1 (Ser241), STAT3 and phospho-STAT3 (Tyr705) were purchased from Cell Signaling Technology (Beverly, MA, USA). Antibodies to cyclin E, CDK2, CDK4, CDK6 and actin were purchased from NeoMarkers (Fremont, CA, USA). The antibody to XIAP was obtained from Medical & Biological Laboratories (Nagoya, Japan). Antibodies to cyclin D2, cIAP-2, Mcl-1, JunB, JunD and c-Fos were purchased from Santa Cruz Biotechnology (Santa Cruz, CA, USA).

4.2. Assesement of Cell Viability and Apoptosis

Cell viability was determined by color reaction with WST-8 (Wako Pure Chemical Industries, Osaka, Japan). Mitochondrial dehydrogenase cleavage of WST-8 to formazan dye provided a measure of cell viability. Briefly, 1×10^5 cells/mL were incubated in triplicate in a 96-well microculture plate in the presence of different concentrations of hippuristanol for 24 h. Subsequently, WST-8 was added to each well. After 4 h of additional incubation, absorption values at 450 nm were determined with an automatic microplate reader. Values were normalized to untreated control samples. The IC_{50} value was calculated by dotting the data points to a logistic curve using the CalcuSym software. Apoptotic events in cells were detected by staining with phycoerythrin-conjugated Apo2.7 antibody (Beckman Coulter, Marseille, France), which specifically detects the 38-kDa mitochondrial membrane antigen 7A6 [12], and analyzed by flow cytometry.

4.3. Cell Cycle Analysis

Log phase growing cells were treated with hippuristanol (200 nM) in complete culture medium for 24 h. Cell cycle analysis was performed with the CycleTEST PLUS DNA reagent kit (Becton Dickinson Immunocytometry Systems, San Jose, CA, USA). Cell suspensions were analyzed by flow cytometry. The population of cells in each cell cycle phase was determined with MultiCycle software.

4.4. In Vitro Measurement of Caspase Activity

Caspase activity was measured using colorimetric caspase assay kits (Medical & Biological Laboratories). Cell extracts were recovered using the cell lysis buffer supplied with the kit and

assessed for caspase-3, -8 and -9 activities using colorimetric probes. The assay kits are based on detection of chromophore ρ-nitroanilide after cleavage from caspase-specific labeled substrates. Colorimetric readings were performed in an automated microplate reader.

4.5. Western Blotting

Cells were treated with various concentrations of hippuristanol in complete medium for 24 h. Cells were lysed in a buffer containing 62.5 mM Tris-HCl (pH 6.8), 2% sodium dodecyl sulfate, 10% glycerol, 6% 2-mercaptoethanol and 0.01% bromophenol blue. For Western blotting, 20 μg protein was resolved over polyacrylamide gels and transferred to a polyvinylidene difluoride membrane, and probing with the specific antibodies. Detection was performed using Amersham Biosciences enhanced chemiluminescence kit (Piscataway, NJ, USA).

4.6. Electrophoretic Mobility Shift Assay (EMSA)

Nuclei were extracted from cells using the method described previously [27] with some modifications. EMSA was conducted as described by Mori and Prager [28]. Briefly, nuclear extracts (5 μg) were incubated with ^{32}P-labeled probes, followed by separation of the DNA-protein complex from free oligonucleotides on 4% polyacrylamide gel. The sense and antisense synthetic oligonucleotides, containing the AP-1 element from interleukin-8 gene (5′-gatcGTGATGACTCAGGTT-3′) and the NF-κB element from interleukin-2 receptor α chain gene (5′-gatcCGGCAGGGGAATCTCCCTCTC-3′), were annealed and the resultant probes were used. The oligonucleotide 5′- gatcTGTCGAATGCAAATCACTAGAA-3′, containing the consensus sequence of the octamer binding motif, was used to identify specific binding of the transcription factor Oct-1, which regulates the transcription of a number of so-called housekeeping genes. The above underlined sequences represent the AP-1, NF-κB and Oct-1 binding sites, respectively. Cold-competition experiments were performed with excess of cold AP-1 or NF-κB oligonucleotides. For supershift assays, the prepared extracts were preincubated with antibodies against c-Fos, FosB, Fra1, Fra2, c-Jun, JunB and JunD from Santa Cruz Biotechnology.

4.7. In Vivo Therapeutic Effect of Hippuristanol

Five-week-old female C.B-17/Icr-SCID mice, obtained from Kyudo, Co. (Tosu, Japan), were maintained in containment level 2 cabinets and provided with autoclaved food and water *ad libitum*. They were inoculated intraperitoneally with 5×10^6 BCBL-1 cells and then randomly placed into two cohorts of five mice each that received vehicle or hippuristanol. Treatment was initiated on the day after cell injection. Hippuristanol was dissolved in 5.2% polyethylene glycol 400 (Wako Pure Chemical Industries) and 5.2% Tween 80 (Becton Dickinson, Franklin Lakes, NJ, USA) at a concentration of 0.25 mg/mL, and hippuristanol was administered at 7.5 mg/kg body weight every day for 35 days. Tumor burden was evaluated by measuring body weight. All mice were sacrificed on day 35, and then the liver, spleen and kidneys were dissected out and their weight was measured. Organ infiltration by BCBL-1 cells was evaluated by H&E staining. Treatment efficacy was determined by measuring the serum levels of human sCD30 by ELISA

(BioVendor Inc., Brno, Czech Republic). This experiment was performed according to the guidelines for Animal Experimentation of the University of the Ryukyus and approved by the Animal Care and Use Committee of the same University.

4.8. Statistical Analysis

All values are expressed as mean ± SD. Differences between groups and between treatments were tested for statistical significance by the Mann-Whitney *U*-test and Student's *t*-test as appropriate. A confidence level of $P < 0.05$ was chosen as indication of statistical difference.

5. Conclusions

The present results indicated that hippuristanol is a potentially promising natural product for the treatment of PEL, warranting further exploration. Hippuristanol reduced cell viability through the induction of G_1 cell cycle arrest and apoptosis, and these effects were mediated, at least in part, by inactivation of AP-1, STAT3 and Akt pathways.

Acknowledgments

This work was supported by the Japan Science and Technology Agency Grant number AS231Z04853G.

Conflicts of Interest

The authors declare no conflict of interest.

References

1. Nador, R.G.; Cesarman, E.; Chadburn, A.; Dawson, D.B.; Ansari, M.Q.; Sald, J.; Knowles, D.M. Primary effusion lymphoma: A distinct clinicopathologic entity associated with the Kaposi's sarcoma-associated herpes virus. *Blood* **1996**, *88*, 645–656.
2. Green, I.; Espiritu, E.; Ladanyi, M.; Chaponda, R.; Wieczorek, R.; Gallo, L.; Feiner, H. Primary lymphomatous effusions in AIDS: A morphological, immunophenotypic, and molecular study. *Mod. Pathol.* **1995**, *8*, 39–45.
3. Boulanger, E.; Gérard, L.; Gabarre, J.; Molina, J.-M.; Rapp, C.; Abino, J.-F.; Cadranel, J.; Chevret, S.; Oksenhendler, E. Prognostic factors and outcome of human herpesvirus 8-associated primary effusion lymphoma in patients with AIDS. *J. Clin. Oncol.* **2005**, *23*, 4372–4380.
4. Keller, S.A.; Schattner, E.J.; Cesarman, E. Inhibition of NF-κB induces apoptosis of KSHV-infected primary effusion lymphoma cells. *Blood* **2000**, *96*, 2537–2542.
5. Aoki, Y.; Feldman, G.M.; Tosato, G. Inhibition of STAT3 signaling induces apoptosis and decreases survivin expression in primary effusion lymphoma. *Blood* **2003**, *101*, 1535–1542.

6. Uddin, S.; Hussain, A.R.; Al-Hussein, K.A.; Manogaran, P.S.; Wickrema, A.; Gutierrez, M.I.; Bhatia, K.G. Inhibition of phosphatidylinositol 3′-kinase/AKT signaling promotes apoptosis of primary effusion lymphoma cells. *Clin. Cancer Res.* **2005**, *11*, 3102–3108.
7. Yamamoto, K.; Ishikawa, C.; Katano, H.; Yasumoto, T.; Mori, N. Fucoxanthin and its deacetylated product, fucoxanthinol, induce apoptosis of primary effusion lymphomas. *Cancer Lett.* **2011**, *300*, 225–234.
8. Wen, K.W.; Damania, B. Kaposi sarcoma-associated herpesvirus (KSHV): Molecular biology and oncogenesis. *Cancer Lett.* **2010**, *289*, 140–150.
9. Bordeleau, M.-E.; Mori, A.; Oberer, M.; Lindqvist, L.; Chard, L.S.; Higa, T.; Belsham, G.J.; Wagner, G.; Tanaka, J.; Pelletier, J. Functional characterization of IRESes by an inhibitor of the RNA helicase eIF4A. *Nat. Chem. Biol.* **2006**, *2*, 213–220.
10. Lindqvist, L.; Pelletier, J. Inhibitors of translation initiation as cancer therapeutics. *Future Med. Chem.* **2009**, *1*, 1709–1722.
11. Tsumuraya, T.; Ishikawa, C.; Machijima, Y.; Nakachi, S.; Senba, M.; Tanaka, J.; Mori, N. Effects of hippuristanol, an inhibitor of eIF4A, on adult T-cell leukemia. *Biochem. Pharmacol.* **2011**, *81*, 713–722.
12. Zhang, C.; Ao, Z.; Seth, A.; Schlossman, S.F. A mitochondrial membrane protein defined by a novel monoclonal antibody is preferentially detected in apoptotic cells. *J. Immunol.* **1996**, *157*, 3980–3987.
13. Tewari, M.; Quan, L.T.; O'Rourke, K.; Desnoyers, S.; Zeng, Z.; Beidler, D.R.; Poirier, G.G.; Salvesen, G.S.; Dixit, V.M. Yama/CPP32β, a mammalian homolog of CED-3, is a CrmA-inhibitable protease that cleaves the death substrate poly(ADP-ribose) polymerase. *Cell* **1995**, *81*, 801–809.
14. An, J.; Sun, Y.; Rettig, M.B. Transcriptional coactivation of c-Jun by KSHV-encoded LANA. *Blood* **2004**, *103*, 222–228.
15. Chakraborty, A.; Koldobskiy, M.A.; Bello, N.T.; Maxwell, M.; Potter, J.J.; Juluri, K.R.; Maag, D.; Kim, S.; Huang, A.S.; Dailey, M.J.; *et al*. Inositol pyrophosphates inhibit Akt signaling, thereby regulating insulin sensitivity and weight gain. *Cell* **2010**, *143*, 897–910.
16. Casamayor, A.; Morrice, N.A.; Alessi, D.R. Phosphorylation of Ser-241 is essential for the activity of 3-phosphoinositide-dependent protein kinase-1: Identification of five sites of phosphorylation *in vivo*. *Biochem. J.* **1999**, *342*, 287–292.
17. Michai, M.; Goto, H.; Hattori, S.; Vaeteewoottacharn, K.; Wongkham, C.; Wongkham, S.; Okada, S. Soluble CD30: A possible serum tumor marker for primary effusion lymphoma. *Asian Pacific J. Cancer Prev.* **2012**, *13*, 4939–4941.
18. Brooks, A.R.; Shiffman, D.; Chan, C.S.; Brooks, E.E.; Milner, P.G. Functional analysis of the human cyclin D2 and cyclin D3 promoters. *J. Biol. Chem.* **1996**, *271*, 9090–9099.
19. Fukada, T.; Ohtani, T.; Yoshida, Y.; Shirogane, T.; Nishida, K.; Nakajima, K.; Hibi, M.; Hirano, T. STAT3 orchestrates contradictory signals in cytokine-induced G_1 to S cell-cycle transition. *EMBO J.* **1998**, *17*, 6670–6677.

20. Wang, X.H.; Liu, B.R.; Qu, B.; Xing, H.; Gao, S.L.; Yin, J.M.; Wang, X.F.; Cheng, Y.Q. Silencing STAT3 may inhibit cell growth through regulating signaling pathway, telomerase, cell cycle, apoptosis and angiogenesis in hepatocellular carcinoma: Potential uses for gene therapy. *Neoplasma* **2011**, *58*, 158–171.
21. Dan, H.C.; Sun, M.; Kaneko, S.; Feldman, R.I.; Nicosia, S.V.; Wang, H.G.; Tsang, B.K.; Cheng, J.Q. Akt phosphorylation and stabilization of X-linked inhibitor of apoptosis protein (XIAP). *J. Biol. Chem.* **2004**, *279*, 5405–5412.
22. Epling-Burnette, P.K.; Liu, J.H.; Catlett-Falcone, R.; Turkson, J.; Oshiro, M.; Kothapalli, R.; Li, Y.; Wang, J.-M.; Yang-Yen, H.-F.; Karras, J.; *et al*. Inhibition of STAT3 signaling leads to apoptosis of leukemic large granular lymphocytes and decreased Mcl-1 expression. *J. Clin. Invest.* **2001**, *107*, 351–362.
23. Chan, G.; Nogalski, M.T.; Bentz, G.L.; Smith, M.S.; Parmater, A.; Yurochko, A.D. PI3K-dependent upregulation of Mcl-1 by human cytomegalovirus is mediated by epidermal growth factor receptor and inhibits apoptosis in short-lived monocytes. *J. Immunol.* **2010**, *184*, 3213–3222.
24. Alvarez, J.V.; Febbo, P.G.; Ramaswamy, S.; Loda, M.; Richardson, A.; Frank, D.A. Identification of a genetic signature of activated signal transducer and activator of transcription 3 in human tumors. *Cancer Res.* **2005**, *65*, 5054–5062.
25. Renne, R.; Zhong, W.; Herndier, B.; McGrath, M.; Abbey, N.; Kedes, D.; Ganem, D. Lytic growth of Kaposi's sarcoma-associated herpesvirus (human herpesvirus 8) in culture. *Nat. Med.* **1996**, *2*, 342–346.
26. Katano, H.; Hoshino, Y.; Morishita, Y.; Nakamura, T.; Satoh, H.; Iwamoto, A.; Herndier, B.; Mori, S. Establishing and characterizing a CD30-positive cell line harboring HHV-8 from a primary effusion lymphoma. *J. Med. Virol.* **1999**, *58*, 394–401.
27. Antalis, T.M.; Godbolt, D. Isolation of intact nuclei from hematopoietic cell types. *Nucl. Acids Res.* **1991**, *19*, 4301.
28. Mori, N.; Prager, D. Transactivation of the interleukin-1α promoter by human T cell leukemia virus type I and type II Tax proteins. *Blood* **1996**, *87*, 3410–3417.

Purified Brominated Indole Derivatives from *Dicathais orbita* Induce Apoptosis and Cell Cycle Arrest in Colorectal Cancer Cell Lines

Babak Esmaeelian, Kirsten Benkendorff, Martin R. Johnston and Catherine A. Abbott

Abstract: *Dicathais orbita* is a large Australian marine gastropod known to produce bioactive compounds with anticancer properties. In this research, we used bioassay guided fractionation from the egg mass extract of *D. orbita* using flash column chromatography and identified fractions containing tyrindoleninone and 6-bromoisatin as the most active against colon cancer cells HT29 and Caco-2. Liquid chromatography coupled with mass spectrometry (LCMS) and ^{1}H NMR were used to characterize the purity and chemical composition of the isolated compounds. An MTT assay was used to determine effects on cell viability. Necrosis and apoptosis induction using caspase/LDH assay and flow cytometry (PI/Annexin-V) and cell cycle analysis were also investigated. Our results show that semi-purified 6-bromoisatin had the highest anti-cancer activity by inhibiting cell viability (IC_{50} = ~100 μM) and increasing caspase 3/7 activity in both of the cell lines at low concentration. The fraction containing 6-bromoisatin induced 77.6% apoptosis and arrested 25.7% of the cells in G2/M phase of cell cycle in HT29 cells. Tyrindoleninone was less potent but significantly decreased the viability of HT29 cells at IC_{50} = 390 μM and induced apoptosis at 195 μM by increasing caspase 3/7 activity in these cells. This research will facilitate the development of these molluscan natural products as novel complementary medicines for colorectal cancer.

Reprinted from *Mar. Drugs*. Cite as: Esmaeelian, B.; Benkendorff, K.; Johnston, M.R.; Abbott, C.A. Purified Brominated Indole Derivatives from *Dicathais orbita* Induce Apoptosis and Cell Cycle Arrest in Colorectal Cancer Cell Lines. *Mar. Drugs* **2013**, *11*, 3802-3822.

1. Introduction

Colorectal cancer (CRC) is the third most diagnosed cancer worldwide [1] with an incidence of 1.2 million new cases (9.7% of all cancers excluding non-melanoma skin cancers) and 608,000 deaths in 2008 [2]. Many therapeutic strategies are used to fight CRC. However, chemotherapy with drugs such as 5-fluorouracil and radiotherapy can expose patients to troublesome side effects [3]. Surgical treatment of CRC is associated with a high mortality and the risk of local repetition [4].

Natural products have served as the most productive source of leads for drug development for centuries [5]. In recent decades, many of the new antibiotics and new antitumor drugs approved by the US Food and Drug Administration (FDA), or comparable entities in other countries, are natural products or derived from natural products [6–8]. Protective effects against a wide range of cancers, including colon cancer, have been shown by several foods such as nuts, spices, grains, fruits, cereals, vegetables, herbs, as well as medicinal plants and their various bioactive constituents including flavonoids, alkaloids, phenolics, carotenoids, and organosulfur compounds [9]. Natural

products are usually considered to exhibit low toxicity, and are cost effective and socially acceptable alternatives to pharmaceutical chemopreventatives [10]. The marine environment is one of the major sources for novel natural products. The immeasurable chemical and biological diversity of the ocean offers a great source for new as yet undiscovered potential bioactive compounds [11–13]. Many marine secondary metabolites have shown bioactivity for application as anticancer agents [14–16].

The Muricidae (Neogastropoda) are a family of predatory marine gastropods that are historically known for the production of Tyrian purple (6,6′-dibromoindigo), an ancient dye, *de novo* biosynthesized from a choline ester precursor salt of tyrindoxyl sulphate after a series of oxidative, enzymatic and photochemical reactions in the hypobranchial gland and egg masses [17–21]. Tyrindoleninone is the main indole precursor found in the extracts, along with 6-bromoisatin, a natural oxidative by-product of Tyrian purple synthesis [18,22]. 6,6-dibromoindirubin is a structural isomer of Tyrian purple that can form from the combination of tyrindoleninone and 6-bromoisatin [19,23] and is a minor pigment found in hypobranchial and male reproductive gland extracts of some muricids [19,24]. Benkendorff [25] highlights the fact that all of these brominated indole derivatives in Muricidae molluscs conform to Lipinskis' rule of five for druglikeness and orally active drugs in humans.

Anticancer properties of egg mass extracts and the isolated brominated indoles from the Australian Muricidae *Dicathais orbita*, have been shown by several studies [25]. The extracts have been tested against a panel of cancer cell lines *in vitro* [26]. Tyrindoleninone and 6-bromoisatin purified from *D. orbita* extracts were shown to specifically decrease cell viability of female reproductive cancer cells, rather than freshly isolated human granulosa cells [27]. Furthermore, in a study by Vine *et al.* [28], some substituted isatin derivatives including 6-bromoisatin have been synthesized and show *in vitro* anticancer properties on a range of human cancer cells, including leukemia, lymphoma and colorectal (HCT-116) cell lines. Bioassay guided fractionation of secretions from hypobranchial gland of a Mediterranean Muricidae *Hexaplex (Murex*) *trunculus* showed that 6,6-dibromoindirubin is an inhibitor of protein kinases and efficiently inhibits cell proliferation by selectively targeting glycogen synthase kinase-3 (GSK-3) [29,30]. In an *in vivo* study using a rodent model for colon cancer prevention by administrating the DNA damaging agent azoxymethane, pro-apoptotic activity of a crude extract from *D. orbita* containing these brominated indoles, was demonstrated in the distal colon [22]. However, the compound or compounds responsible for the anticancer *in vivo* and *in vitro* activity have not yet been characterized.

Muricidae molluscs are subject to a small scale world-wide fisheries industry and are of growing interest in aquaculture [31,32]. Given that these edible molluscs have anticancer properties, there is growing interest in their potential use as a medicinal food for prevention of colon cancer [25,33]. The aim of this study was to perform bioassay guided fractionation on *D. orbita* extracts and to characterize these fractions *in vitro* using cell viability, apoptosis and cell cycle analysis in two human colon adenocarcinoma cell lines, Caco2 and HT29.

2. Results and Discussion

2.1. Chemical Analysis and Bioassay Guided Fractionation

LC-MS analysis of *D. orbita* egg capsule mass crude extract showed five peaks corresponding to brominated indoles (Figure 1). The dominant peak in this extract at t_R 6.39 min and major ions in ESI-MS at *m*/*z* 224, 226 was attributed to the molecular mass of 6-bromoisatin. Another dominant peak at t_R 11.03 min corresponded to the molecular weight of tyrindoleninone with major ions at *m*/*z* 255, 257. Mass spectrum of the peak at t_R 9.40 min with major ions in ESI-MS at *m*/*z* 302, 304 was indicative of tyrindolinone. The peak at t_R 8.58 min corresponds to tyrindoxyl sulphate, with major ions in ESI-MS at *m*/*z* 336, 338 and a smaller peak at t_R 11.90 min occurred with ions in ESI-MS at *m*/*z* 511, 513, 515 corresponding to the molecular mass of tyriverdin with major fragment ions at *m*/*z* 417, 419, 421 formed by the elimination of dimethyl disulphide.

Bioassay guided fractionation using the 3-(4,5-dimethylthiazol-2-yl)-2,5-diphenyltetrazolium bromide (MTT) cell viability assay revealed a statistically significant mean reduction of 27.6% and 72.4% cell viability in HT29 cells respectively at high concentrations of 1 and 2 mg/mL of crude extract compared with the solvent control (Figure 2a). Caco2 cells showed 86.4% ($p < 0.001$) mean reduction in cell viability when exposed to the highest concentration of crude extract 2 mg/mL (Figure 2b). Significant reductions in cell viability also occurred in some fractions. For example, HT29 cells treated with 0.1 and 0.05 mg/mL of fraction 2, showed 57.3% and 30.2% reduction in formazan production (Figure 2a), while this reduction was more than 90% for Caco2 cells treated with the same concentrations of fraction 2 (Figure 2b). At the highest concentration of 0.5 mg/mL, cell viability was less than 2% in both cell types. Similar activity was observed for fraction 3 (Figure 2). The highest concentration of fraction 4 (0.5 mg/mL) caused 23.9% and 24.3% reduction in cell viability of HT29 and Caco2 cells respectively. Fraction 5 at the concentrations of 0.05 and 0.1 mg/mL showed 76.3% and 91.4% reduction of cell viability for Caco2 cells respectively and the greatest reduction in cell viability for HT29 cells. Fraction 5 reduced the viability of both cell lines by over 95% at the highest concentration of 0.5 mg/mL. A mean reduction of 24.4% in the cell viability of Caco2 cells was also observed in fraction 6 with the higher concentration of 0.5 mg/mL. Significant dose effects were observed in both cancer cell lines, with lower viability rates recorded at the higher treatment concentrations. Bioassay guided fractionation using the MTT assay showed that fractions containing both tyrindoleninone and 6-bromoisatin inhibit the viability of HT29 and Caco2 cells, though tyrindoleninone was more potent towards Caco2 cells than HT29. The effect on viability of fraction 3 (mixture of tyrindoleninone and tyrinolinone) was similar to fraction 2 (tyrindoleninone), indicating the additional methyl thiol group on tyrindolinone does not increase the overall activity.

Figure 1. Liquid chromatography-mass spectrometry (LC-MS) analysis of extract from *D. orbita* egg capsules. The chromatogram obtained from diode array detection at 300 and 600 nm shows five peaks corresponding to brominated indoles where a: 6-bromoisatin (*m/z* 224, 226); b: tyrindoxylsulphate (*m/z* 336, 338); c: tyrindolinone (*m/z* 302, 304); d: tyrindoleninone (*m/z* 255, 257) and e: tyriverdin (*m/z* 511, 513, 515).

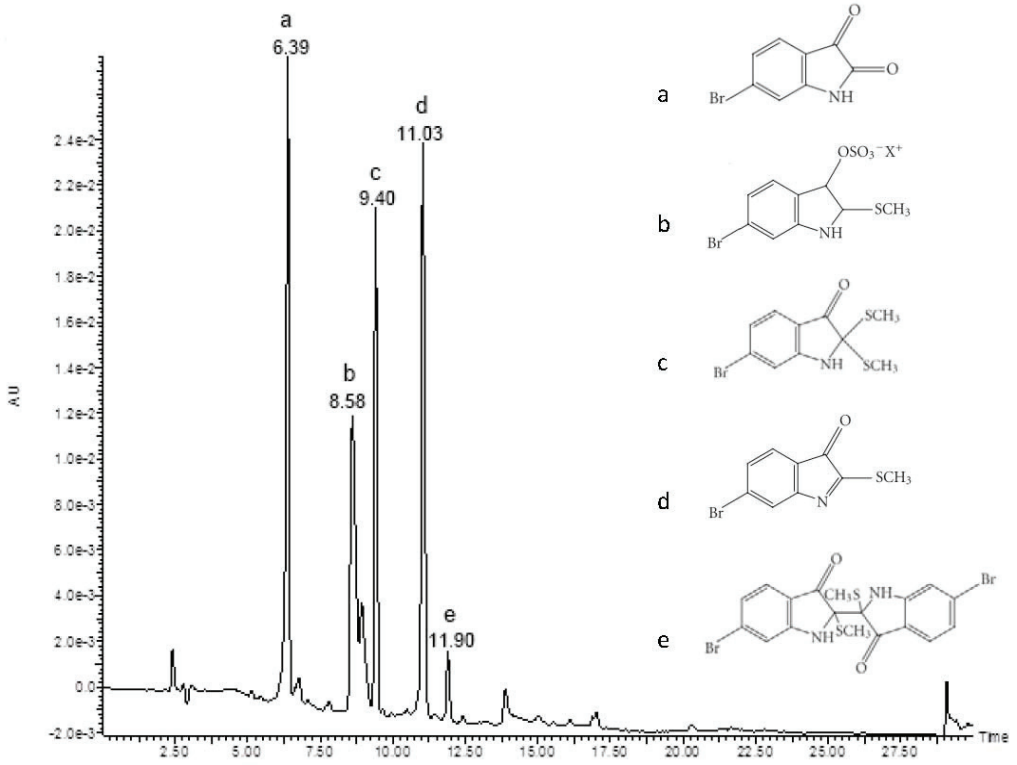

All fractions from flash chromatography of the crude egg capsule extract that were found to effect cell viability using the MTT assay, were then analyzed by LC-MS. In addition to matching the molecular mass of the isolated compounds with tyrindoleninone and 6-bromoisatin, the identity of these compounds was also confirmed by data gained from ^{1}H NMR. One purified compound was identified in fraction 2 at t_R 11.03 min, which was attributed to the molecular mass of tyrindoleninone (*m/z* 255, 257). The purity and identity of tyrindoleninone in fraction 2 was confirmed by GC/MS with one peak at t_R 11.24 min and exact MS match to tyrindoleninone in the mass spectrum library (Figure 3a). ^{1}H NMR also confirmed the identity of tyrindoleninone: ^{1}H NMR (400 MHz, CD_3CN) δ 7.46 (^{1}H, dd, J = 0.5, 1.4 Hz), 7.42 (^{1}H, dd, J = 0.5, 7.6 Hz), 7.39 (^{1}H, dd, J = 7.6, 1.4 Hz), 2.63 (3H, s). Our data for tyrindoleninone was consistent with the ^{1}H NMR results for this compound previously reported by Benkendorff *et al*. [18] and Baker and Duke [34]. LC-MS of fraction 3 revealed two major peaks at t_R 9.40 and 11.03 min corresponding to the molecular mass of tyrindolinone (*m/z* 302, 304) and tyrindoleninone (*m/z* 255, 257) respectively. LC/MS of fraction 5 identified one major compound at t_R 6.42 min which was indicative of

6-bromoisatin (*m*/*z* 224, 226). GC/MS revealed several other minor compounds (at least six peaks) in this fraction but confirmed 6-bromoisatin as the major component (90%) with a dominant peak at t_R 13.01 min (Figure 3b). The other minor compounds in fraction 6 were matched with two short chain aldehydes at t_R 11.71 min and t_R 12.35 min, two sterols at t_R 16.82 min (molecular mass of 366% and 93.7% match with cholesta-4,6-dien-3-ol (3β); $C_{27}H_{44}O$) and at t_R 17.02 min (molecular mass of 364), an unidentified ester at t_R 15.96 min (molecular mass of 302) and finally a new brominated indole with a tiny amount was found at t_R 13.61 min (molecular mass of 267/269). ^{1}HNMR confirmed the identity of the major compound in fraction 5 as 6-bromoisatin: ^{1}H NMR (400 MHz, CD_3CN) δ 8.96 (^{1}H, s), 7.44 (^{1}H, d, J = 8.08 Hz), 7.30 (^{1}H, dd, J = 1.64, 8 Hz), 7.19 (^{1}H, d, J = 1.6 Hz) despite also detecting small peaks associated with minor contaminants. Chemical analysis of the most bioactive fractions showed that a good separation for tyrindoleninone producing pure material and a semi-purification for 6-bromoisatin (90% purity) based on the GC/MS analysis.

Figure 2. MTT viability results of *D. orbita* egg mass crude extract (CE) and all fractions collected from flash column chromatography (Frac 1–7) on HT29 cells (**a**) and Caco2 cells (**b**). Fraction 1 is the most lipophilic collected with 100% hexane and fraction 7 is the most polar collected with 100% methanol. Significant difference between each group and the 1% DMSO control are shown as $p \leq 0.05$ (*), $p \leq 0.01$ (**) and $p \leq 0.001$ (***).

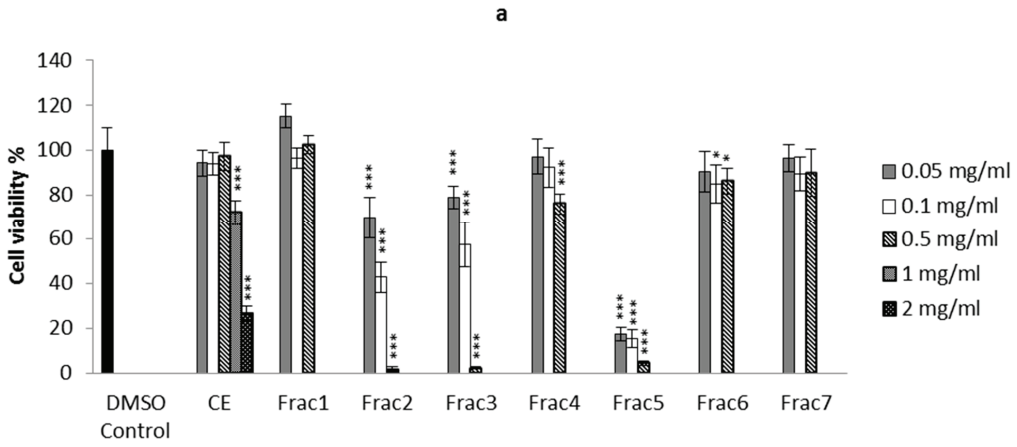

Figure 2. *Cont.*

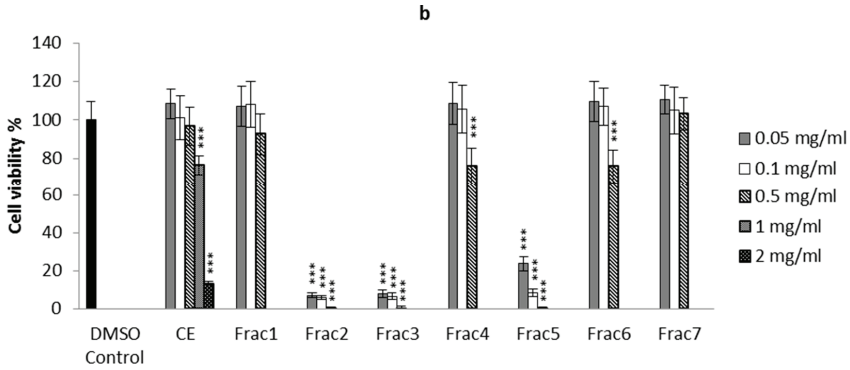

Figure 3. Gas chromatography–mass spectrometry (GC-MS) chromatogram of fractions from the egg masses extract of the Australian muricid, *D. orbita*. Fraction 2 (**a**) at t_R 11.24 min corresponds to tyrindoleninone and fraction 5 (**b**) with dominant peak at t_R 13.01 min matches the molecular mass of 6-bromoisatin. The mass spectra (ESI-MS) for the major peaks are inset.

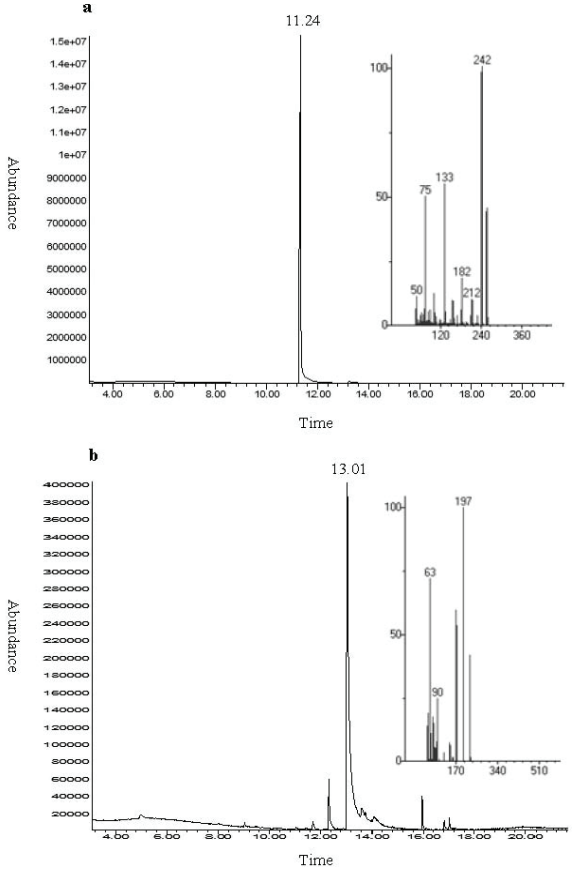

2.2. Biological Activity of the D. orbita *Compounds*

2.2.1. Apoptosis, Necrosis and Cell Viability

Death by necrosis, which may result in damage to the plasma membrane and releasing of the cytoplasmic contents, including lysosomal enzymes into the extracellular fluid, is often considered as a toxic process in comparision to apoptosis [35,36]. The most bioactive fractions from the MTT assay—fraction 2 (tyrindoleninone) and fraction 5 (semi-purified 6-bromoisatin) were examined for their ability to induce either apoptosis or necrosis.

Tyrindoleninone, was found to be more cytotoxic towards Caco2 cells (IC_{50} = 98 μM), than for the HT29 cells (IC_{50} = 390 μM; Figure 4a,d). In a study by Benkendorff *et al*. [26], greater reduction in cell viability (over 60%) was observed in Caco2 and U937 lymphoma cells treated using a semi-purified egg extract with increased concentration of tyrindoleninone, compared to crude extract, whereas less activity was observed against HT29 cells. This confirms our result that Caco2 cells are more susceptible to tyrindoleninone than HT29 cells. Edwards *et al*. [27] showed that tyrindoleninone inhibited KGN cell viability (a tumour-derived granulosa cell line), JAr and OVCAR-3 cells with the IC_{50} 39 μM, 39 μM and 156 μM respectively. In addition, Vine *et al.* [37] demonstrated that tyrindoleninone had less cytotoxic effects on untransformed human mononuclear cells (IC_{50} = 195 μM) than U937 cancer cells (IC_{50} = 4 μM) after 1 h exposure. The current study confirms the different cell line specificity of tyrindoleninone, with a four-fold difference observed here between the two adherent colon cancer cells lines. This difference in drug resistance may be due to the variations in metabolic and signaling pathways and also the difference in expression and activity of some drug-metabolizing enzymes in different cancer cells [38].

The other bioactive compound, 6-bromoisatin however, inhibited the viability of both Caco2 and HT29 cells (IC_{50} = 100 μM; Figure 4a,d). Edwards *et al.* [27] demonstrated that semi-purified 6-bromoisatin significantly reduced cell numbers of three reproductive cancer cell lines KGN, JAr and OVCAR-3, although converse to this study, it was not as potent as tyrindoleninone. The JAr cells were the most susceptible, with cell numbers halved at approximately 223 μM 6-bromoisatin. Vine *et al.* [28], on the other hand, showed that a range of isatin derivatives including 7-bromoisatin (IC_{50} = 83 μM) and 6-bromoisatin (IC_{50} = 75 μM) reduced the cell viability of lymphoma cell line U937, which was similar to the efficacy of 6-bromoisatin against Caco2 and HT29 cells in our study (IC_{50} = 100 μM). Vine *et al.* [28] also reported different specificity of isatin derivatives against different cancer cell lines. Human leukemic Jurkat cell lines were the most sensitive to isatin treatment (IC_{50} = 5–20.9 μM), the next most sensitive cells were the colon cancer cell line HCT-116 (IC_{50} = 15.9–37.3 μM) and the least sensitive cells were the prostrate PC3 cell line (IC_{50} = 25.9–101 μM). In a review by Vine *et al.* [39], small electron withdrawing groups, mono, di and tri-halogenation at positions 5, 6 and/or 7 on the isatin molecule were found to enhance cytotoxicity activity. 6-Bromoisatin is an example of this kind of halogenated isatin.

Figure 4. Effects of *D. orbita* egg mass crude extract (CE), purified tyrindoleninone (TYR) and semi-purified 6-bromoisatin (6-BRO) in mg/mL on HT29 (left panels) and Caco2 (right panels) cells. Cell viability (**a**,**d**), lactate dehydrogenase (LDH) release (**b**,**e**) and caspase-3/7 activity (**c**,**f**). LDH release was measured by fluorescence at 535EX/590EM and caspase-3/7 activity was measured at full light on a luminescence plate reader. Staurosporin (Str) (5 µM; Sigma) was used as a positive control for the MTT and caspase-3/7 assay; lysis buffer (5 µL/well; Promega) served as the positive control for the LDH assay. A final concentration of 1% DMSO was used in all control and treated cells. The results are the mean for three independent repeat assays each performed in triplicate (n = 3). Significant difference between each group and the DMSO control are shown as $p \leq 0.05$ (*); $p \leq 0.01$ (**) and $p \leq 0.001$ (***).

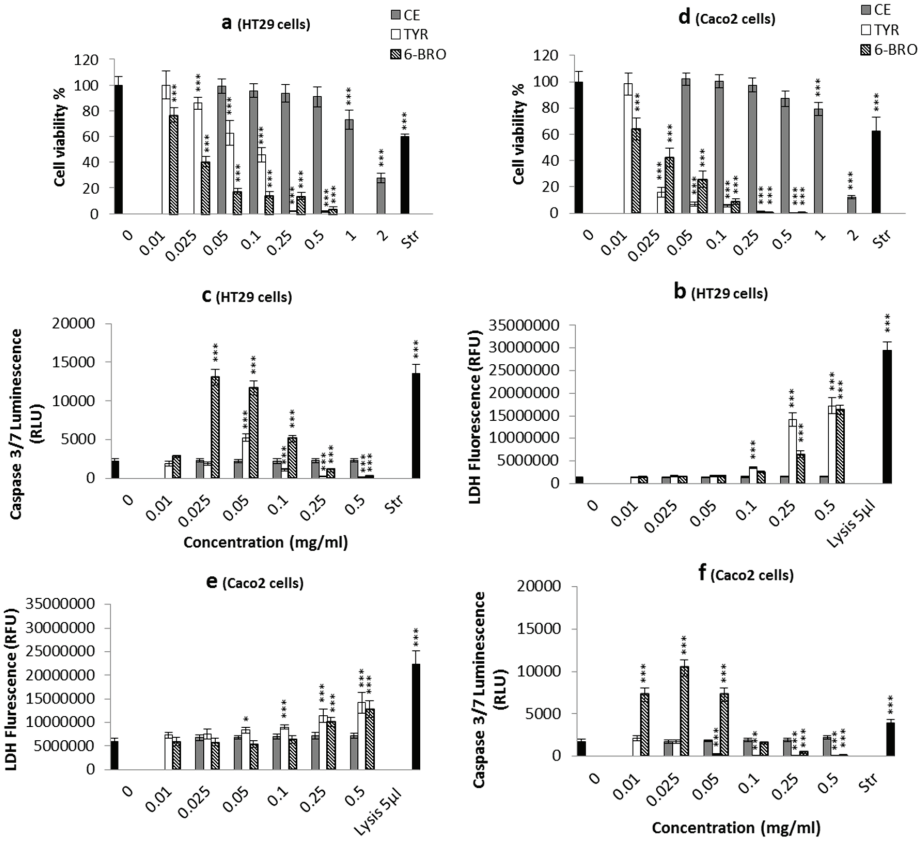

Caspase-3 and -7 activity significantly increased only in HT29 cells treated with 195 µM (0.05 mg/mL) tyrindoleninone in 1% DMSO compared to the 1% DMSO control (Figure 4c). An increase in the proportion of Annexin-V positive, PI negative cells (27.6% ± 9.25%) was also observed by flow cytometry in HT29 cells treated with 195 µM (0.05 mg/mL) tyrindoleninone; however, it was not significant (Figure 5). Despite a dose-dependent decrease in viability from Caco2 cells treated with tyrindoleninone, no significant increase in caspase-3 and -7 activity was

observed (Figure 4d). Tyrindoleninone at high concentrations appears to induce necrosis rather than apoptosis (increase in LDH observed, Figure 4e) towards Caco2 cells, whereas some apoptosis by caspase 3/7 up-regulation was observed in HT29 treated with tyrindoleninone. Apoptotic cells are characterized by particular morphological features [40,41], such as dense chromatin surrounded by a halo, which were observed in the treated HT29 cells in this study (Figure 6d). Purification of tyrindoleninone from the crude extract consistently increased the cytotoxic potency towards Caco2 cells, but resulted in induction of necrosis rather than apoptosis in these cells, whereas HT29 cells, which were more resilient to the anti-proliferation effects of tyrindoleninone, underwent apoptosis at the concentration of 195 µM. This difference in cell line specificity might be due to the phenotype of the cells, as bioactive compounds may target alternative pathways in different cells [26,42]. Edwards *et al*. [27] revealed that purified tyrindoleninone induced 66% apoptosis with 20 µM in KGN compared to 31% apoptosis (391 µM) in freshly isolated human granulosa cells (HGC) using TUNEL assay after 4 h. This study showed that reproductive cancer cell lines were ten times more susceptible than HCG to tyrindoleninone and indicated specificity of this compound toward reproductive cancer cells.

Figure 5. Flow cytometric analysis of HT29 cells (1.5×10^5) treated with (**a**) DMSO only (final concentration 1%); (**b**) 0.025 mg/mL semi-purified 6-bromoisatin; (**c**) 0.05 mg/mL semi-purified 6-bromoisatin and (**d**) 0.05 mg/mL tyrindoleninone purified from *D. orbita* egg masses. Cells were treated for 12 h and stained with Annexin-V-FITC and PI then analyzed by a FACscan flow cytometer and FlowJo analysis software. *X*-axis shows Annexin-V positive cells and *Y*-axis shows propidium iodide (PI) positive cells. (**e**) Histograms of the mean ± SE of three separate experiments for PI and annexin positive cells Significant difference between each group and the DMSO control are shown as $p \leq 0.05$ (*) and $p \leq 0.01$ (**).

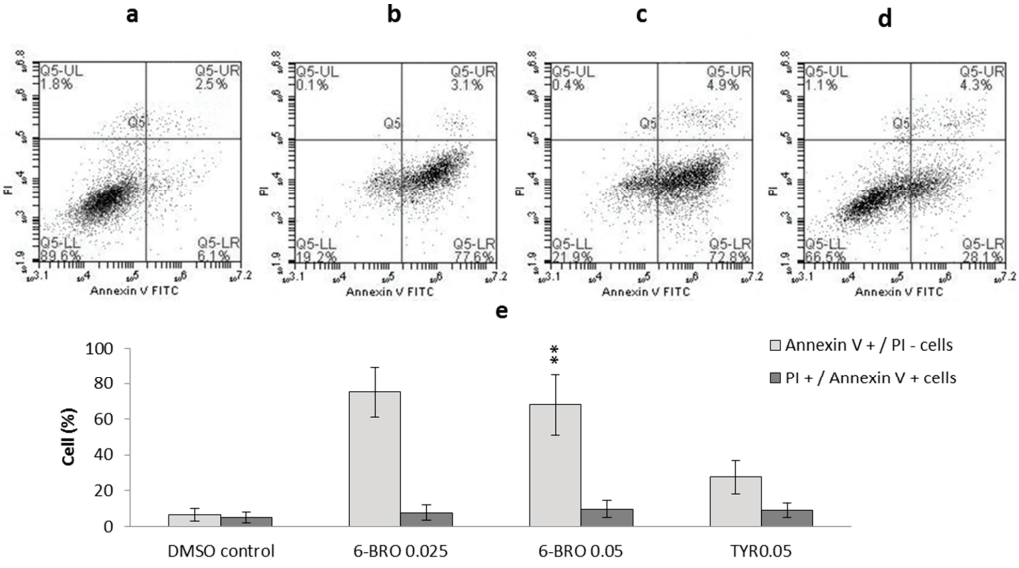

The fraction containing 6-bromoisatin considerably activated caspase-3 and -7 enzymes and induced cell death by apoptosis in both cell lines at approximately 100 μM (0.025 mg/mL) and 200 μM (0.05 mg/mL), much lower concentrations than those required to cause lactate dehydrogenase (LDH) release and necrosis (~1000 to ~2000 μM; Figure 4b,e). For example, the HT29 cells treated with 6-bromoisatin at ~100 μM and 200 μM showed significant increases in caspase-3 and -7 activity, with luminescence values greater than five times the negative (DMSO) control. The light microscopic images from the HT29 cells treated with ~200 μM 6-bromoisatin showed morphological alterations, such as chromatin condensation characteristic of the apoptotic process (Figure 6b). Flow cytometry results (Figure 5) also confirmed that HT29 cells treated with ~100 μM (0.025 mg/mL semi-purified) 6-bromoisatin underwent a significant induction of apoptosis (75.3% ± 14.03% Annexin-V positive, PI negative cells) compared with the DMSO control (6.6% ± 3.43% Annexin-V positive, PI negative). Similarly, ~200 μM 6-bromoisatin, induced apoptosis up to 68.1% ± 17.1%, but also with a 9.7% increase in the number of PI positive necrotic cells, as compared to DMSO control. In contrast, the highest concentrations of 6-bromoisatin (~1000 μM and 2000 μM) caused a high release of LDH indicating necrosis in HT29 cells (Figure 4b) without any sign of apoptosis. HT29 cells incubated with approximately 400 μM of 6-bromoisatin underwent a significant induction of apoptosis, while the increase in LDH release did not reach significance at this concentration (Figure 4b). Caco2 cells treated with the three lowest concentrations of semi-purified 6-bromoisatin (~40 μM, 100 μM and 200 μM) showed a significant induction of apoptosis (Figure 4f), but without any significant increase in the release of LDH compared to the DMSO control (Figure 4e). At the highest concentrations of 6-bromoisatin (~1000 μM and 2000 μM) Caco2 cells underwent a significant increase in LDH release (Figure 4e) with no in increase in caspase-3 and -7 activity.

Our results showed that 6-bromoisatin increased the level of caspase 3/7 in both cell lines, while tyrindoleninone only up-regulated the caspase 3/7 in HT29 cells. 6-Bromoisatin also showed more potency than tyrindoleninone producing higher levels of caspase 3/7 in HT29 cells and indicating high induction of apoptosis in these cells. The morphology of condensed chromatin and haloed areas in nearly all cells from the images was also consistent with this type of cell death. Furthermore, Caco2 cells treated with semi-purified 6-bromoisatin also underwent the induction of apoptosis. Therefore, semi-purified 6-bromoisatin in our study had the most consistent anti-cancer efficacy against both colon cancer cell lines at low concentrations. Necrosis, as indicated by LDH release, was only significantly increased with exposure to the highest concentrations of 6-bromoisatin in both cell lines. Our caspase 3/7 and LDH results suggest that 6-bromoisatin induces cell death by apoptosis at low concentrations, while the apoptotic pathway is terminated at higher concentrations and secondary necrosis or necrosis is being triggered [43,44]. It has been shown that some structurally similar isatin and indole compounds at low concentrations induce apoptosis through the activation of caspase 3 in a range of cell lines [28,45,46]. For example, caspase 3/7 was activated by 5,6,7-tribromoisatin at a concentration of 8 μM in the Jurkat cell line after 5 h [28]. Edwards *et al*. [27] showed that caspase 3/7 was up-regulated significantly with approximately 22 μM 6-bromoisatin in KGN cells and apoptosis was also confirmed by Tunnel staining in these cells.

Figure 6. HT29 cells at 400× magnification under an Olympus inverted microscope. DMSO control (**a**); cells treated with 0.05 mg/mL semi-purified 6-bromoisatin (**b**); cells treated with 0.5 mg/mL semi-purified 6-bromoisatin (**c**) and cells treated with 0.05 mg/mL tyrindoleninone (**d**) for 12 h (final concentration of 1% DMSO). Apoptotic cells with chromatin condensation characteristic are shown by arrows and necrotic cells with deformed cell shapes are shown by arrowheads.

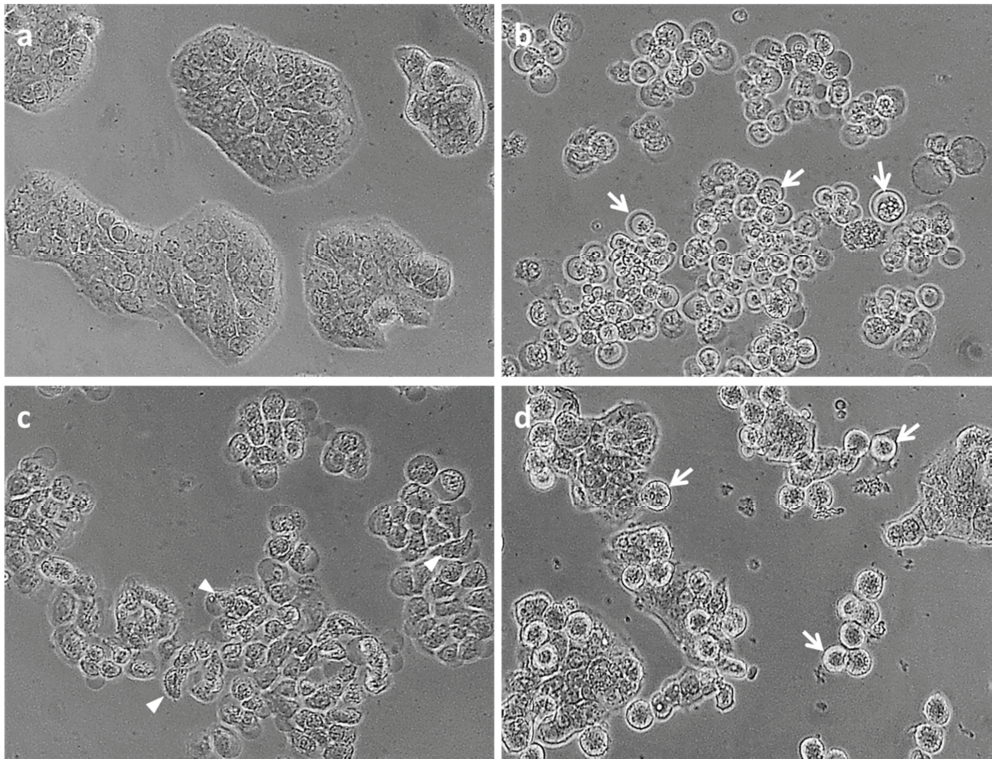

Our results suggest that both tyrindoleninone and semi-purified 6-bromoisatin induce apoptosis through caspase-dependent pathways on HT29 cells. However, more investigation on initiator caspase 8 and 9 would be required to distinguish between the extrinsic and intrinsic apoptosis pathways [36,47] induced by these brominated indoles. In a review by Vine *et al.* [39], the mode of action of some halogenated isatins, such as 6-bromoisatin, was proposed to be linked to the reduction in extracellular signal-regulated protein kinase (ERK) activity. Another study by Cane *et al*. [48] suggests that isatin and indole inhibit cell proliferation and induce apoptosis via inhibiting the signaling of ERK. Inhibition of ERK can suppress cell growth and results in induction of apoptosis in the cells [49]. Moreover, some other apoptosis pathways, including both caspase-dependent or caspase-independent, can occur via inhibition of ERK, as has been reported by Georgakis *et al*. [50]. ERK may also act through suppression of the anti-apoptotic signaling molecule Akt [51]. Therefore, further study on ERK and Akt inhibition, especially with pure 6-bromoisatin, is required to evaluate the exact mode of action of these brominated compounds.

2.2.2. Cell Cycle Analysis

Cell cycle analysis revealed three distinct cell populations in HT29 cells, which were indicative of cells in the G0/G1, S and G2/M phases of the cell cycle (Figure 7). The DMSO control showed more accumulation of the cells in G0/G1 (64% ± 1.9%) with approximately the same proportion of the cells in S and G2/M (17% *versus* 15.6%). After exposure to ~400 μM (0.1 mg/mL semi-purified) 6-bromoisatin, 26.7% of HT29 cells were in the S phase ($p \leq 0.001$). This switched to significantly more cells in G2/M at the lower and most effective concentrations (100 μM = 25.7% and 200 μM = 23.8%). There were no significant differences in the cell population analysis between the DMSO control negative and the cells treated with 6-bromoisatin at the concentration of 0.01 mg/mL. Our result revealed that the most effective concentration of 6-bromoisatin that induced the highest apoptosis in HT29 cells, also caused the accumulation of cells at G2/M phase of the cell cycle. G2 phase in the cell cycle is where DNA repair might occur in cells, along with preparation for mitosis in M phase [52].

Figure 7. Cell cycle analysis using propidium iodide (PI) staining and flow cytometry. HT29 cells (5×10^5 cells in 1 mL media/well) were treated for 12 h with (**a**) DMSO only (final concentration 1%); (**b**) 0.025 mg/mL 6-bromoisatin; (**c**) 0.05 mg/mL 6-bromoisatin; (**d**) 0.1 mg/mL 6-bromoisatin semi-purified from egg mass of *D. orbita*; (**e**) Results are the mean ± SE of three separate experiments. Significant difference between each group and the DMSO control are shown as $p \leq 0.05$ (*); $p \leq 0.01$ (**) and $p \leq 0.001$ (***).

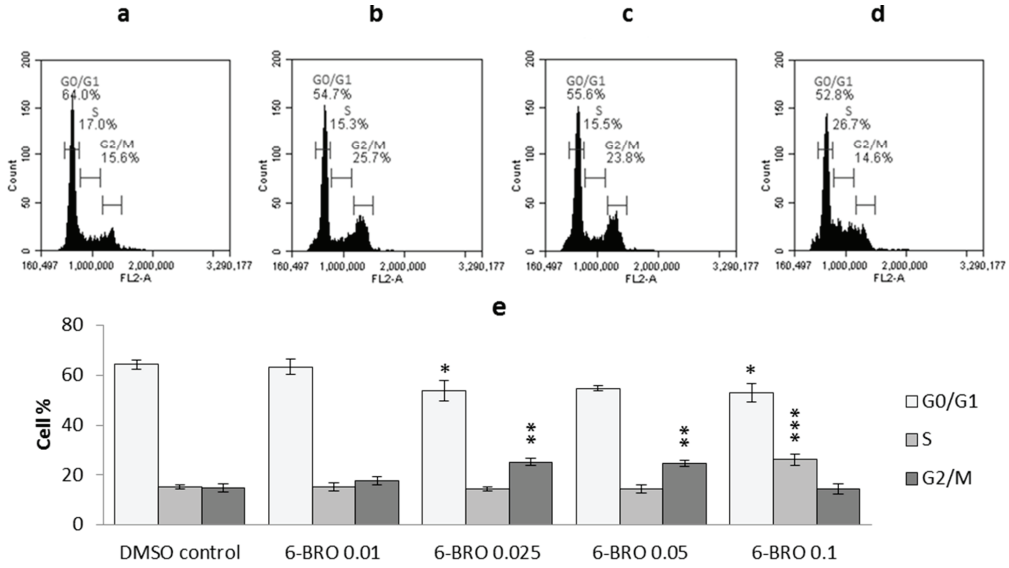

Increasing arrest of the cells in G2/M phase has been shown to be associated with enhanced apoptosis [10]. CDK1 (cyclin dependent kinase) is one of the protein kinase families that is activated by dephosphorylation and acts as a G2 checkpoint, which controls cell cycle progression

from G2 to M phase [52]. For example, in a study by Singh *et al*. [53] sulforaphane, a naturally occurring cancer chemopreventive agent, caused an irreversible arrest in the G2/M phase of human prostate cancer cells (PC-3), which was associated with a significant reduction in protein levels of cyclin B1, CDC25B, and CDC25C. In a study by Vine *et al*. [45] various *N*-alkyl isatins induced G2/M cell cycle arrest. It is known that the indole based small molecules inhibit serine/threonine kinases, glycogen synthase kinase-3 (GSK3) [30,54] and CDK5 [55,56]. Another well-known isatin derivative 6,6′-dibromoindirubin has also been identified as a specific GSK-3 inhibitor [29]. Anti-proliferative activity of indirubin has been shown via ATP-competitive inhibition of both CDK1 and CDK2 [57–59]. The modes of action associated with indirubins [58] includes the induction of apoptosis through cell cycle arrest at G2/M via the inhibition of GSK3 [30], as well as induction of the c-Src kinase and nuclear factor-κB signaling pathway and expression [60,61] and activation of the aryl hydrocarbon receptor [62,63]. Vine [37] tested the inhibitory effect of six representative *N*-alkyl isatins on a range of tyrosine-specific and serine/threonine-specific protein kinases, but found no inhibition of enzyme activity by these isatins [37]. Based on molecular modeling results, neither 6-bromoisatin or tyrindoleninone are predicted to have any kinase receptor binding or enzyme inhibiting activity [25]. However, inhibition of tubulin polymerisation in a range of cancer cell lines was shown by an array of imidazole and pyrrole containing 3-substituted isatins, resulting in cell cycle arrest at G2/M and final cell death [64,65]. Based on morphological examination of treated cells, Vine *et al*. [45] suggested that *N*-alkyl isatins may either stabilize or disrupt microtubules in a similar manner. Therefore, the finding that 6-bromoisatin increases the proportion of cells in the G2/M phase is consistent with a range of other studies on isatin derivatives and could be linked to a range of different modes of action that require further investigation.

3. Experimental Section

3.1. Egg Mass Extraction, Purification

All chemicals, HPLC grade solvents and silica gel where obtained from Sigma-Aldrich Pty Ltd. (Castle Hill, Australia) unless otherwise stated. *D. orbita* egg capsules (27 g) were collected from a recirculating aquarium in the School of Biological Sciences, Flinders University, South Australia. The eggs capsules were opened and soaked in 100 mL (per 10 g eggs) chloroform and methanol (1:1, v/v) under agitation at room temperature for 2 h, followed by overnight soaking in fresh solvent. Both extracts were combined and filtered. Then a low volume of milli-Q water (~20–30 mL) was added to facilitate the separation of methanol and chloroform into two phases. The chloroform layer was separated and dried under reduced pressure of 474 mbar on a Buchi rotary evaporator at 40 °C. The dried extracts were re-dissolved in a small volume of dichloromethane (~1 mL), transferred to amber vials, then dried under a stream of nitrogen gas, yielding 300 mg of a light brown/red oily extract which was subsequently stored at −20 °C. Previous research has shown that the dominant compounds in *D. orbita* extracts are colored and can be separated by silica chromatography [18]. Here flash column chromatography pressurized with nitrogen gas was used to separate the bioactive compounds. The stationary phase consisted of approximately 20 g silica gel (100 mesh) mixed with hexane. The chloroform extract (300 mg) was loaded onto the column

and eluted using a stepwise gradient of solvents, starting with 100% hexane (100 mL, Fraction 1). Fraction 2 was eluted using 20% DCM in hexane (50 mL), then Fraction 3 was collected using 25% DCM in hexane (200 mL), followed by Fraction 4 with 100% DCM (200 mL). The polarity of the solvent was then increased to 10% methanol in DCM to collect Fractions 5 (15 mL) and 6 (85 mL). Finally, Fraction 7 was collected by washing the column with 50 mL 100% methanol. All solvents were evaporated from the fractions under reduced pressure by rotary evaporation at 40 °C.

3.2. Chemical Analysis

All fractions affecting cell viability in the MTT assay (see below) were further analyzed using liquid chromatography coupled with mass spectrometry (LC/MS). Briefly, fractions were dissolved in acetonitrile and analyzed by HPLC (Waters Alliance) that was coupled to a mass spectrometer (MS, Micromass, Quatro micro™) with a Hydro-RP C18 column (250mm × 4.6 mm × 4 µm) and parallel UV/Vis diode-array detection at 300 and 600 nm. The flow rate was 1 mL/min of formic acid and a gradient of acetonitrile in water, according to the methods established by Westley and Benkendorff [24]. Compounds were identified using electrospray ionization-mass spectrometry (ESI-MS) with a flow rate of 300 µL/min. Mass Lynx 4.0 software was used to analyze the data. Additional analysis on bioactive fractions was facilitated by gas chromatography–mass spectrometry (GC-MS, Agilent Technologies (Mulgrave, Australia) 5975C Series GC/MS) with a capillary column (SGE HT-5, 15 m × 0.25 mm i.d.) with a 0.25 µm film thickness. The injection port temperature was set at 260 °C. The initial oven temperature was held at 50 °C for 3 min and then ramped with a rate of 15 °C/min to the final temperature of 300 °C and held for 2 min. The carrier gas was helium with a constant flow rate of 2 mL/min. Electron ionisation (EI) was used with the electron energy of 70 eV. The source temperature was set to 230 °C and the MS quadrupole was 150 °C. To confirm the identity of the bioactive compounds, ^{1}H NMR spectroscopy was also used on purified fractions on a Bruker Avance III 400 MHz spectrometer (Bruker Biosciences, Preston, Australia), operating at 294K, in deuterated acetonitrile. Chemical shifts (δ) are reported as parts per million (ppm) and referenced to residual solvent peaks. Spin multiplicities are indicated by: s, singlet; bs, broad singlet; d, doublet; t, triplet; q, quartet; m, multiplet; and dd, doublet of doublets.

3.3. Cell Culture

Two human colorectal cancer cell lines Caco2 (passage no. 26–34) and HT29 (passage no. 18–26) maintained at 37 °C in a 5% CO_2 humidified atmosphere. The cells were cultured in Dulbecco's Modified Eagle's Medium (DMEM) supplemented with 4500 mg/L L-glutamine, 10% FBS, 100 U/mL Penicillin/Streptomycin and 1% Non-essential Amino Acid (100×).

3.4. MTT Viability Assay and Cell Morphology

All fractions and purified compounds were tested using an MTT viability assay which measured the reduction of MTT tetrazolium salt to formazan [66,67]. Caco2 and HT29 cells were grown to 70% confluence, detached from flasks with 1X Trypsin-EDTA, counted using trypan blue dye

exclusion method, and plated into 96-well plates (Costar®) (2×10^4 cells in 100 µL media/well). The cells were incubated for 48 h before treatment. All extracts and purified compounds were dissolved in 100% dimethylsulphoxide (DMSO) then diluted in media and added to the cell cultures in triplicate (final DMSO concentration of 1%), with final concentrations ranging from 2 to 0.01 mg/mL. 1% DMSO controls were also included on each plate. All extracts were incubated with the cells for 12 h. The media was removed prior to adding 100 µL of 0.05% MTT with fresh media to each well. The cells were incubated for 1 h and then 80 µL of 20% SDS in 0.02 M HCl was added to each well. The absorbance of the samples was determined spectrophotometrically after 1 h by measuring the optical density at 480 and 520 nm on a FLUOstar Omega microplate reader (BMG Labtech, Mornington, Australia). This assay was repeated on three separate occasions ($n = 3$). The morphological changes in HT29 cells were also observed by Olympus (Mt Waverly, Australia) CK2 inverted optical microscope (original magnification 400×) 12 h after treatment.

3.5. Combined Caspase 3/7, Membrane Integrity and Cell Viability Assays

HT29 and Caco-2 cells (2×10^4 cells in 100 µL media/well) were seeded into sterile white (opaque) 96-well plates (Interpath, Heidelberg West, Australia) (for determination of apoptosis and necrosis) and clear sterile 96-well plates (Costar®) (for measurement of cell viability). All cells were incubated for 48 h to allow attachment of these adherent cells, then the media was removed and the cells were washed with PBS. The cells were treated with different concentrations of crude extract and purified compounds from 0.5 to 0.01 mg/mL in fresh media. Two positive controls were added to each plate in triplicate wells; staurosporin (5 µM/mL) for apoptosis and lysis solution (5 µL/well, Promega, Madison, WI, USA) for necrosis. All cells were treated for 12 h. To measure necrosis, 70 µL of supernatant from each well of the white opaque plate was transferred to another white opaque 96-well plate. The CytoTox-ONE Homogeneous Membrane Integrity Assay reagent (Promega) was applied based on the manufacturer's instructions, in equal volume to the cell culture medium (70 µL). The plates were then incubated at 22 °C for 10 min and the fluorescence recorded with an excitation wavelength of 535 nm and an emission wavelength of 590 nm on a FLUOstar Omegaplate reader (BMG Labtech, Mornington, Australia). To measure apoptosis, the Caspase-Glo 3/7® assay (Promega) was applied. 30 µL Caspase-Glo® 3/7 Reagent was added to the primary white opaque 96-well containing cells and 30 µL cell culture medium and incubated at 22 °C for 1 h. The plates were read on a FLUOstar Omega with full light to capture total luminescence. This experiment was repeated on three separate occasions ($n = 3$).

3.6. Flow Cytometric Detection of Apoptosis

To confirm the caspase assay results, the most bioactive compounds were used in flow cytometry. HT29 cells were plated in 24 well plates (Nunc®) in duplicate with 1.5×10^5 cells/well in 1 mL media, then incubated for 48 h. Media were removed and 1 mL media and treatments including 0.025 and 0.05 mg/mL semi-purified 6-bromoisatin and 0.05 mg/mL tyrindoleninone (final concentration of 1% DMSO) were added to each well. Staurosporin (5 µM/mL) was used as a positive control reagent for triggering apoptosis (data not shown). Cells were treated for 12 h and

collected from the wells after the trypsinization by 1× trypsin-EDTA, then were placed in 15 mL tubes before centrifugation (1500 rpm for 3 min). Media were removed and the cells were washed twice with sterilized phosphate buffered saline (PBS) and suspended in 1× Binding buffer (10 mM Hepes/NaOH, pH 7.4, 140 mM NaCl, 2.5 mM $CaCl_2$) at a concentration of 1×10^6 cells/mL. 100 µL of the solution (1×10^5 cells) were transferred to a 5 mL culture tube then 5 µL of FITC Annexin V (BD Biosciences, Franklin Lakes, NJ, USA) and 5 µL of propidium iodide (BD Biosciences) at 10 µg/mL final concentration were added to each tube. All cells were incubated for 15 min at RT (25 °C) in the dark and cell distribution was analyzed using FACSan Flow Cytometer (Becton Dickinson, North Ryde, Australia) and FlowJo analysis software.

3.7. Cell Cycle Analysis

Flow cytometry was used to assess whether the bioactive compounds arrested the cells at a particular stage of the cell cycle. HT29 cells (5×10^4 cells in 1 mL media/well) were seeded into 12-well plates (Costar®). The cells were incubated for 48 h before treating with different concentrations of semi-purified 6-bromoisatin for 12 h (final DMSO concentration of 1%). The supernatant and cells were then harvested by exposing the cells to 0.25%, Trypsin-EDTA solution for 10 min, then centrifuged and washed in phosphate buffered saline (PBS), fixed in 3 mL ice-cold 100% ethanol and stored overnight at −20 °C. At the time of analysis, the cells were centrifuged, washed once again in PBS and stained with a freshly made solution containing 0.1 mg/mL propidium iodide (PI), 0.1% Triton x-100 and 0.2 mg/mL ribonuclease A in PBS. All samples were incubated for 30 min at room temperature in the dark. Cell cycle distribution was determined by an analytical DNA flow cytometer (Accuri C6, BD Biosciences) and CFlow Plus software on DNA instrument settings (linear FL2) on low.

3.8. Statistical Analysis

Statistical analyses were performed using SPSS and values of $p \leq 0.05$ were considered to be statistically significant. One way ANOVA test was performed to compare between different concentrations of treatments and control. Tukey post-hoc test was applied to detect which groups significantly differ.

4. Conclusions

Our study demonstrated that both semi-purified 6-bromoisatin and purified tyrindoleninone decreased cell viability in the colon cancer cell lines HT29 and Caco2. In particular, 6-bromoisatin showed more specificity and potency than tyrindoleninone and greater induction of apoptosis toward the colon cancer cells. 6-Bromoisatin also inhibited cell cycle progression of HT29 cells by arresting some cells in the G2/M phase. This data, along with the previously reported *in-vivo* induction of apoptosis in DNA damaged cells of the colon using Muricidae extracts [22] suggests that 6-bromoisatin from Muricidae molluscs is promising as an anti-cancer drug against colon cancer.

Acknowledgments

We are grateful to Daniel Jardine from the Flinders Analytical Laboratory of Flinders University for LC/MS and GC/MS analysis of compounds. We would further like to thank Peta Macardle from the flow cytometry analysis lab, Flinders Medical Centre, Tim Chataway and Nusha Chegeni from proteomics facility, Flinders Medical Centre for their help and advice, and Kathy Schuller in the School of Biological Sciences of Flinders University for housing equipment and facilitating access to her lab.

Conflicts of Interest

The authors declare no conflict of interest.

References

1. Jemal, A.; Bray, F.; Center, M.M.; Ferlay, J.; Ward, E.; Forman, D. Global cancer statistics. *CA Cancer J. Clin.* **2011**, *61*, 69–90.
2. Ferlay, J.; Shin, H.R.; Bray, F.; Forman, D.; Mathers, C.; Parkin, D.M. Estimates of worldwide burden of cancer in 2008: GLOBOCAN 2008. *Int. J. Cancer* **2010**, *127*, 2893–2917.
3. Carnesecchi, S.; Langley, K.; Exinger, F.; Gosse, F.; Raul, F. Geraniol, a component of plant essential oils, sensitizes human colonic cancer cells to 5-fluorouracil treatment. *J. Pharmacol. Exp. Ther.* **2002**, *301*, 625–630.
4. Line-Edwige, M. Antiproliferative effect of alcoholic extracts of some Gabonese medicinal plants on human colonic cancer cells. *Afr. J. Tradit. Complement. Altern. Med.* **2009**, *6*, 112–117.
5. Harvey, A.L. Natural products as a screening resource. *Curr. Opin. Chem. Biol.* **2007**, *11*, 480–484.
6. Harvey, A. Strategies for discovering drugs from previously unexplored natural products. *Drug Discov. Today* **2000**, *5*, 294–300.
7. Esmaeelian, B.; Kamrani, Y.Y.; Amoozegar, M.A.; Rahmani, S.; Rahimi, M.; Amanlou, M. Anti-cariogenic properties of malvidin-3,5-diglucoside isolated from *Alcea longipedicellata* against oral bacteria. *Int. J. Pharmacol.* **2007**, *3*, 468–474.
8. Newman, D.J.; Cragg, G.M. Natural products as sources of new drugs over the last 25 years. *J. Nat. Prod.* **2007**, *70*, 461–477.
9. Rajamanickam, S.; Agarwal, R. Natural products and colon cancer: Current status and future prospects. *Drug Dev. Res.* **2008**, *69*, 460–471.
10. Manson, M.M.; Farmer, P.B.; Gescher, A.; Steward, W.P. Innovative agents in cancer prevention. *Recent Results Cancer Res.* **2005**, *166*, 257–275.
11. Blunt, J.W.; Copp, B.R.; Munro, M.H.; Northcote, P.T.; Prinsep, M.R. Marine natural products. *Nat. Prod. Rep.* **2006**, *30*, 237–323.
12. Benkendorff, K. Molluscan biological and chemical diversity: Secondary metabolites and medicinal resources produced by marine molluscs. *Biol. Rev.* **2010**, *85*, 757–775.

13. Blunt, J.W.; Copp, B.R.; Keyzers, R.A.; Munro, M.H.; Prinsep, M.R. Marine natural products. *Nat. Prod. Rep.* **2013**, *30*, 237–323.
14. Simmons, T.L.; Andrianasolo, E.; McPhail, K.; Flatt, P.; Gerwick, W.H. Marine natural products as anticancer drugs. *Mol. Cancer Ther.* **2005**, *4*, 333–342.
15. Sato, M.; Sagawa, M.; Nakazato, T.; Ikeda, Y.; Kizaki, M. A natural peptide, dolastatin 15, induces G2/M cell cycle arrest and apoptosis of human multiple myeloma cells. *Int. J. Oncol.* **2007**, *30*, 1453–1459.
16. Jiang, C.; Wang, M.; Liu, J.; Gan, D.; Zeng, X. Extraction, preliminary characterization, antioxidant and anticancer activities *in vitro* of polysaccharides from *Cyclina sinensis*. *Carbohydr. Polym.* **2011**, *84*, 851–857.
17. Baker, J. Tyrian purple: An ancient dye, a modern problem. *Endeavour* **1974**, *33*, 11–17.
18. Benkendorff, K.; Bremner, J.B.; Davis, A.R. Tyrian purple precursors in the egg masses of the Australian muricid, Dicathais orbita: A possible defensive role. *J. Chem. Ecol.* **2000**, *26*, 1037–1050.
19. Cooksey, C.J. Tyrian purple: 6,6′-dibromoindigo and related compounds. *Molecules* **2001**, *6*, 736–769.
20. Baker, J.T.; Duke, C.C. Isolation of choline and choline ester salts of tyrindoxyl sulphate from the marine mollusks *Dicathais orbita* and *Mancinella keineri*. *Tetrahedron Lett.* **1976**, 1233–1234.
21. Westley, C.B.; Vine, K.L.; Benkendorff, K. A Proposed Functional Role for Indole Derivatives in Reproduction and Defense of the Muricidae (Neogastropoda: Mollusca). In *Indirubin, the Red Shade of Indigo*; Meijer, L., Guyard, N., Skaltsounis, L., Eisenbrand, G., Eds.; Life in Progress Editions: Roscoff, France, 2006; pp. 31–44.
22. Westley, C.B.; McIver, C.M.; Abbott, C.A.; Le Leu, R.K.; Benkendorff, K. Enhanced acute apoptotic response to azoxymethane-induced DNA damage in the rodent colonic epithelium by Tyrian purple precursors: A potential colorectal cancer chemopreventative. *Cancer Biol. Ther.* **2010**, *9*, 371–379.
23. Cooksey, C.J. Marine Indirubins. In *Indirubin, the Red Shade of Indigo*; Meijer, L., Guyard, N., Skaltsounis, L., Eisenbrand, G., Eds.; Life in Progress Editions: Roscoff, France, 2006; pp. 23–30.
24. Westley, C.; Benkendorff, K. Sex-specific Tyrian purple genesis: Precursor and pigment distribution in the reproductive system of the marine mollusc, *Dicathais orbita*. *J. Chem. Ecol.* **2008**, *34*, 44–56.
25. Benkendorff, K. The Australian Muricidae *Dicathais orbita*: A model species for marine natural product research. *Mar. Drugs* **2013**, *11*, 1370–1398.
26. Benkendorff, K.; McIver, C.M.; Abbott, C.A. Bioactivity of the Murex homeopathic remedy and of extracts from an Australian muricid mollusc against human cancer cells. *Evid. Based Complement. Altern. Med.* **2011**, *2011*, 879585.
27. Edwards, V.; Benkendorff, K.; Young, F. Marine compounds selectively induce apoptosis in female reproductive cancer cells but not in primary-derived human reproductive granulosa cells. *Mar. Drugs* **2012**, *10*, 64–83.

28. Vine, K.L.; Locke, J.M.; Ranson, M.; Benkendorff, K.; Pyne, S.G.; Bremner, J.B. *In vitro* cytotoxicity evaluation of some substituted isatin derivatives. *Bioorg. Med. Chem.* **2007**, *15*, 931–938.
29. Meijer, L.; Skaltsounis, A.L.; Magiatis, P.; Polychronopoulos, P.; Knockaert, M.; Leost, M.; Ryan, X.P.; Vonica, C.A.; Brivanlou, A.; Dajani, R. GSK-3-selective inhibitors derived from Tyrian purple indirubins. *Chem. Biol.* **2003**, *10*, 1255–1266.
30. Leclerc, S.; Garnier, M.; Hoessel, R.; Marko, D.; Bibb, J.A.; Snyder, G.L.; Greengard, P.; Biernat, J.; Wu, Y.Z.; Mandelkow, E.M. Indirubins inhibit glycogen synthase kinase-3β and CDK5/P25, two protein kinases involved in abnormal tau phosphorylation in Alzheimer's disease. *J. Biol. Chem.* **2001**, *276*, 251–260.
31. Noble, W.J.; Cocks, R.R.; Harris, J.O.; Benkendorff, K. Application of anaesthetics for sex identification and bioactive compound recovery from wild *Dicathais orbita*. *J. Exp. Mar. Biol. Ecol.* **2009**, *380*, 53–60.
32. Benkendorff, K. *Aquaculture and the Production of Pharmaceuticals and Nutraceuticals*; Woodhead Publishing: Cambridge, UK, 2009; pp. 866–891.
33. Westley, C.B.; Benkendorff, K.; McIver, C.M.; Le Leu, R.K.; Abbott, C.A. Gastrointestinal and hepatotoxicity assessment of an anticancer extract from muricid molluscs. *Evid. Based Complement. Altern. Med.* **2013**, *2013*, 837370.
34. Baker, J.; Duke, C. Chemistry of the indoleninones. II. Isolation from the hypobranchial glands of marine molluscs of 6-Bromo-2,2-dimethylthioindolin-3-one and 6-Bromo-2-methylthioindoleninone as alternative precursors to Tyrian purple. *Aust. J. Chem.* **1973**, *26*, 2153–2157.
35. Jin, Z.; El-Deiry, W.S. Review overview of cell death signaling pathways. *Cancer Biol. Ther.* **2005**, *4*, 139–163.
36. Elmore, S. Apoptosis: A review of programmed cell death. *Toxicol. Pathol.* **2007**, *35*, 495–516.
37. Vine, K.L. An Investigation into the Cytotoxic Properties of Isatin-Derived Compounds: Potential for Use in Targeted Cancer Therapy. Ph.D. Thesis, University of Wollongong, Wollongong, Australia, 14 September 2007.
38. Rochat, B. Importance of influx and efflux systems and xenobiotic metabolizing enzymes in intratumoral disposition of anticancer agents. *Curr. Cancer Drug Targets* **2009**, *9*, 652–674.
39. Vine, K.; Matesic, L.; Locke, J.; Ranson, M.; Skropeta, D. Cytotoxic and anticancer activities of isatin and its derivatives: A comprehensive review from 2000–2008. *Anticancer Agents Med. Chem.* **2009**, *9*, 397–414.
40. Thompson, C.B. Apoptosis in the pathogenesis and treatment of disease. *Science* **1995**, *267*, 1456–1462.
41. Gamet-Payrastre, L.; Li, P.; Lumeau, S.; Cassar, G.; Dupont, M.-A.; Chevolleau, S.; Gasc, N.; Tulliez, J.; Tercé, F. Sulforaphane, a naturally occurring isothiocyanate, induces cell cycle arrest and apoptosis in HT29 human colon cancer cells. *Cancer Res.* **2000**, *60*, 1426–1433.
42. Nguyen, J.T.; Wells, J.A. Direct activation of the apoptosis machinery as a mechanism to target cancer cells. *Proc. Natl. Acad. Sci. USA* **2003**, *100*, 7533–7538.

43. Riss, T.L.; Moravec, R.A. Use of multiple assay endpoints to investigate the effects of incubation time, dose of toxin, and plating density in cell-based cytotoxicity assays. *Assay Drug Dev. Technol.* **2004**, *2*, 51–62.
44. Pozhilenkova, E.; Salmina, A.; Yamanova, M.; Ruksha, T.; Mikhutkina, S.; Trufanova, L. Disorders of folliculogenesis are associated with abnormal expression of peripheral benzodiazepine receptors in granulosa cells. *Bull. Exp. Biol. Med.* **2008**, *145*, 29–32.
45. Vine, K.L.; Locke, J.M.; Ranson, M.; Pyne, S.G.; Bremner, J.B. An investigation into the cytotoxicity and mode of action of some novel *N*-alkyl-substituted isatins. *J. Med. Chem.* **2007**, *50*, 5109–5117.
46. Weng, J.-R.; Tsai, C.-H.; Kulp, S.K.; Wang, D.; Lin, C.-H.; Yang, H.-C.; Ma, Y.; Sargeant, A.; Chiu, C.-F.; Tsai, M.-H. A potent indole-3-carbinol–derived antitumor agent with pleiotropic effects on multiple signaling pathways in prostate cancer cells. *Cancer Res.* **2007**, *67*, 7815–7824.
47. Nicholson, D. Caspase structure, proteolytic substrates, and function during apoptotic cell death. *Cell Death Differ.* **1999**, *6*, 1028–1042.
48. Cane, A.; Tournaire, M.-C.; Barritault, D.; Crumeyrolle-Arias, M. The endogenous oxindoles 5-hydroxyoxindole and isatin are antiproliferative and proapoptotic. *Biochem. Biophys. Res. Commun.* **2000**, *276*, 379–384.
49. Steinmetz, R.; Wagoner, H.A.; Zeng, P.; Hammond, J.R.; Hannon, T.S.; Meyers, J.L.; Pescovitz, O.H. Mechanisms regulating the constitutive activation of the extracellular signal-regulated kinase (ERK) signaling pathway in ovarian cancer and the effect of ribonucleic acid interference for ERK1/2 on cancer cell proliferation. *Mol. Endocrinol.* **2004**, *18*, 2570–2582.
50. Georgakis, G.V.; Li, Y.; Rassidakis, G.Z.; Martinez-Valdez, H.; Medeiros, L.J.; Younes, A. Inhibition of heat shock protein 90 function by 17-allylamino-17-demethoxy-geldanamycin in Hodgkin's lymphoma cells down-regulates Akt kinase, dephosphorylates extracellular signal–regulated kinase, and induces cell cycle arrest and cell death. *Clin. Cancer Res.* **2006**, *12*, 584–590.
51. Zhuang, S.; Schnellmann, R.G. A death-promoting role for extracellular signal-regulated kinase. *J. Pharmacol. Exp. Ther.* **2006**, *319*, 991–997.
52. DiPaola, R.S. To arrest or not to G2-M cell-cycle arrest commentary re: AK Tyagi *et al*., silibinin strongly synergizes human prostate carcinoma DU145 cells to doxorubicin-induced growth inhibition, G2-M arrest, and apoptosis. *Clin. Cancer. Res.* **2002**, *8*, 3311–3314.
53. Singh, S.V.; Herman-Antosiewicz, A.; Singh, A.V.; Lew, K.L.; Srivastava, S.K.; Kamath, R.; Brown, K.D.; Zhang, L.; Baskaran, R. Sulforaphane-induced G2/M phase cell cycle arrest involves checkpoint kinase 2-mediated phosphorylation of cell division cycle 25C. *J. Biol. Chem.* **2004**, *279*, 25813–25822.
54. Damiens, E.; Baratte, B.; Marie, D.; Eisenbrand, G.; Meijer, L. Anti-mitotic properties of indirubin-3′-monoxime, a CDK/GSK-3 inhibitor: Induction of endoreplication following prophase arrest. *Oncogene* **2001**, *20*, 3786–3797.

55. Davis, S.T.; Benson, B.G.; Bramson, H.N.; Chapman, D.E.; Dickerson, S.H.; Dold, K.M.; Eberwein, D.J.; Edelstein, M.; Frye, S.V.; Gampe, R.T., Jr. Prevention of chemotherapy-induced alopecia in rats by CDK inhibitors. *Science* **2001**, *291*, 134–137.
56. Lane, M.E.; Yu, B.; Rice, A.; Lipson, K.E.; Liang, C.; Sun, L.; Tang, C.; McMahon, G.; Pestell, R.G.; Wadler, S. A novel cdk2-selective inhibitor, SU9516, induces apoptosis in colon carcinoma cells. *Cancer Res.* **2001**, *61*, 6170–6177.
57. Hoessel, R.; Leclerc, S.; Endicott, J.A.; Nobel, M.E.; Lawrie, A.; Tunnah, P.; Leost, M.; Damiens, E.; Marie, D.; Marko, D. Indirubin, the active constituent of a Chinese antileukaemia medicine, inhibits cyclin-dependent kinases. *Nat. Cell Biol.* **1999**, *1*, 60–67.
58. Marko, D.; Schätzle, S.; Friedel, A.; Genzlinger, A.; Zankl, H.; Meijer, L.; Eisenbrand, G. Inhibition of cyclin-dependent kinase 1 (CDK1) by indirubin derivatives in human tumour cells. *Br. J. Cancer* **2001**, *84*, 283–289.
59. Jautelat, R.; Brumby, T.; Schäfer, M.; Briem, H.; Eisenbrand, G.; Schwahn, S.; Krüger, M.; Lücking, U.; Prien, O.; Siemeister, G. From the insoluble dye indirubin towards highly active, soluble CDK2-inhibitors. *ChemBioChem* **2005**, *6*, 531–540.
60. Eisenbrand, G.; Hippe, F.; Jakobs, S.; Muehlbeyer, S. Molecular mechanisms of indirubin and its derivatives: Novel anticancer molecules with their origin in traditional Chinese phytomedicine. *J. Cancer Res. Clin. Oncol.* **2004**, *130*, 627–635.
61. Sethi, G.; Ahn, K.S.; Sandur, S.K.; Lin, X.; Chaturvedi, M.M.; Aggarwal, B.B. Indirubin enhances tumor necrosis factor-induced apoptosis through modulation of nuclear factor-κB signaling pathway. *J. Biol. Chem.* **2006**, *281*, 23425–23435.
62. Adachi, J.; Mori, Y.; Matsui, S.; Takigami, H.; Fujino, J.; Kitagawa, H.; Miller Iii, C.A.; Kato, T.; Saeki, K.; Matsuda, T. Indirubin and indigo are potent aryl hydrocarbon receptor ligands present in human urine. *J. Biol. Chem.* **2001**, *276*, 31475–31478.
63. Spink, B.C.; Hussain, M.M.; Katz, B.H.; Eisele, L.; Spink, D.C. Transient induction of cytochromes P450 1A1 and 1B1 in MCF-7 human breast cancer cells by indirubin. *Biochem. Pharmacol.* **2003**, *66*, 2313–2321.
64. Andreani, A.; Granaiola, M.; Leoni, A.; Locatelli, A.; Morigi, R.; Rambaldi, M.; Garaliene, V.; Welsh, W.; Arora, S.; Farruggia, G. Antitumor activity of new substituted 3-(5-Imidazo [2,1-*b*] thiazolylmethylene)-2-indolinones and study of their effect on the cell cycle 1. *J. Med. Chem.* **2005**, *48*, 5604–5607.
65. Chen, Z.; Merta, P.J.; Lin, N.-H.; Tahir, S.K.; Kovar, P.; Sham, H.L.; Zhang, H. A-432411, a novel indolinone compound that disrupts spindle pole formation and inhibits human cancer cell growth. *Mol. Cancer Ther.* **2005**, *4*, 562–568.
66. Mosmann, T. Rapid colorimetric assay for cellular growth and survival: application to proliferation and cytotoxicity assays. *J. Immunol. Methods* **1983**, *65*, 55–63.
67. Young, F.M.; Phungtamdet, W.; Sanderson, B.J. Modification of MTT assay conditions to examine the cytotoxic effects of amitraz on the human lymphoblastoid cell line, WIL2NS. *Toxicol. In Vitro* **2005**, *19*, 1051–1059.

6-Bromoisatin Found in Muricid Mollusc Extracts Inhibits Colon Cancer Cell Proliferation and Induces Apoptosis, Preventing Early Stage Tumor Formation in a Colorectal Cancer Rodent Model

Babak Esmaeelian, Catherine A. Abbott, Richard K. Le Leu and Kirsten Benkendorff

Abstract: Muricid molluscs are a natural source of brominated isatin with anticancer activity. The aim of this study was to examine the safety and efficacy of synthetic 6-bromoisatin for reducing the risk of early stage colorectal tumor formation. The purity of 6-bromoisatin was confirmed by ^{1}H NMR spectroscopy, then tested for *in vitro* and *in vivo* anticancer activity. A mouse model for colorectal cancer was utilized whereby colonic apoptosis and cell proliferation was measured 6 h after azoxymethane treatment by hematoxylin and immunohistochemical staining. Liver enzymes and other biochemistry parameters were measured in plasma and haematological assessment of the blood was conducted to assess potential toxic side-effects. 6-Bromoisatin inhibited proliferation of HT29 cells at IC_{50} 223 μM (0.05 mg/mL) and induced apoptosis without increasing caspase 3/7 activity. *In vivo* 6-bromoisatin (0.05 mg/g) was found to significantly enhance the apoptotic index ($p \leq 0.001$) and reduced cell proliferation ($p \leq 0.01$) in the distal colon. There were no significant effects on mouse body weight, liver enzymes, biochemical factors or blood cells. However, 6-bromoisatin caused a decrease in the plasma level of potassium, suggesting a diuretic effect. In conclusion this study supports 6-bromoisatin in Muricidae extracts as a promising lead for prevention of colorectal cancer.

Reprinted from *Mar. Drugs*. Cite as: Esmaeelian, B.; Abbott, C.A.; Le Leu, R.K.; Benkendorff, K. 6-Bromoisatin Found in Muricid Mollusc Extracts Inhibits Colon Cancer Cell Proliferation and Induces Apoptosis, Preventing Early Stage Tumor Formation in a Colorectal Cancer Rodent Model. *Mar. Drugs* **2014**, *12*, 17-35.

1. Introduction

Isatin (1*H*-indole-2,3-dione) is a synthetically versatile molecule, and its derivatives possess diverse biological and pharmacological properties, including antibacterial, antifungal, antiviral, anticonvulsant, and anticancer activities [1–5]. Isatin itself has demonstrated cytotoxic and apoptotic activity. For example, Cane *et al.* [6] showed that isatin at a concentration of 100 μM reduced cell proliferation of human promyelocytic leukemia (HL60) cancer cells by 80% and induced morphological changes consistent with proapoptotic cells (including DNA fragmentation and chromatin condensation). In another study by Igosheva *et al.* [7], apoptosis was observed in human neuroblastoma SH-SY5Y cells exposed to 50 μM of isatin. A range of mono-substituted isatins have been studied by Vine *et al.* [8] for their *in vitro* cytotoxicity on a lymphoma (U937) cell line. Structure activity relationship studies have shown that substitution with halogens (5-bromo-, 5-iodo-, and 5-fluoroisatin) yielded 5–10 times more activity for killing cancer cells, than the unsubstituted isatin [8]. Sunitinib (Sutent®) is a fluorinated isatin derivative that has been

approved by FDA as a new anticancer drug to treat advanced renal carcinoma [9] and gastrointestinal stromal tumors [10].

Various substituted isatins have been found in nature including in plants [11], fungi [12] and marine molluscs [5,13]. Recently 6-bromoisatin (Figure 1) from the Australian marine mollusc *Dicathais orbita* has become of particular interest as a major compound of the bioactive extract from this species [5]. In a study by Edwards *et al.* [14], semi-purified 6-bromoisatin from *D. orbita* extracts revealed specific anticancer activity with >10 fold selective cytotoxicity towards female reproductive cancer cells compared to freshly isolated human granulosa cells. Furthermore, semi-purified 6-bromoisatin was shown to significantly reduce proliferation and induce apoptosis in human colon cancer cell lines HT29 and Caco2 cells [15]. In a short-term rodent model for the prevention of colon cancer Westley *et al.* [16] demonstrated that the crude extract of *D. orbita* increased the apoptotic index of distal colon cells significantly. Due to several contaminants in the naturally purified extract [15,16], further work using the pure synthesized compound is required to confirm the activity of 6-bromoisatin against colon cancer cells.

Figure 1. ^{1}H NMR spectrum of synthetic 6-bromoisatin on the Bruker Avance III 400 MHz spectrometer in deuterated acetonitrile. Chemical shifts (δ) are as parts per million (ppm) and referenced to residual solvent peaks. The peaks corresponding to the solvent occur below 3 ppm are not shown.

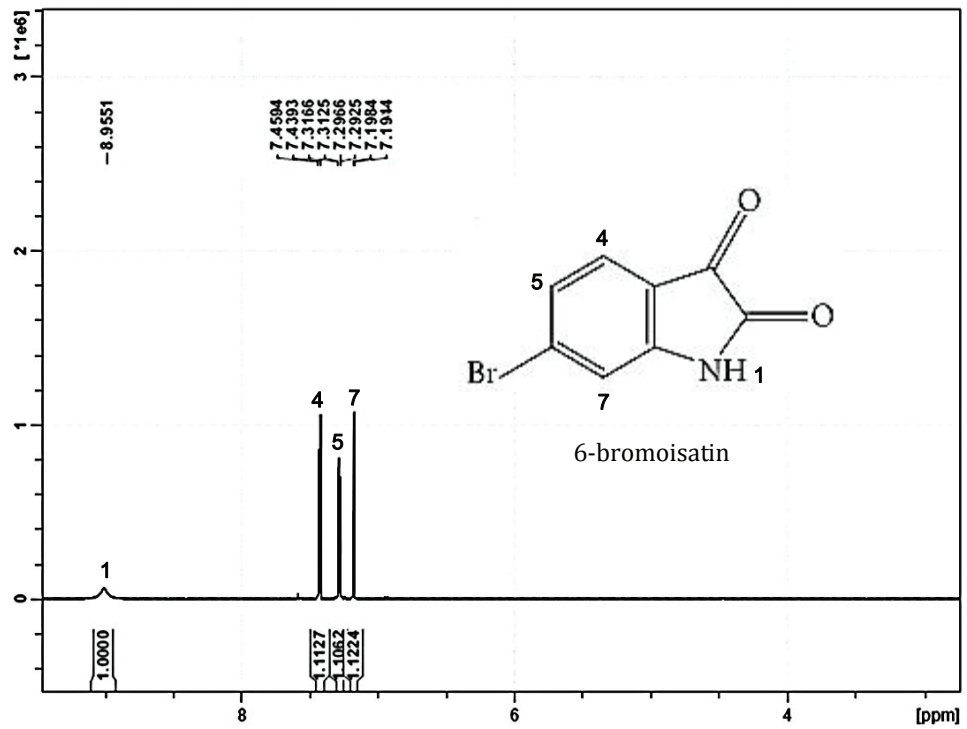

Colorectal cancer (CRC) is the third most common cancer worldwide [17] with the highest incidence rates in Australia, New Zealand, North America and Europe [18]. In the United States, CRC is the second highest cause of cancer-related mortality in both males and females [19]. Just 39% of CRCs are diagnosed at early stage and in most cases the cancer spreads to adjacent and distant organs before detection [20]. Therefore, prevention of CRC is an important priority [21]. Chemoprevention involves the use of functional foods, specific natural products or synthetic chemical agents to suppress or prevent a wide range of cancers, including colon cancer [22]. The acute apoptotic response to genotoxic carcinogens (AARGC) is a good model for chemopreventative research which has been used in several studies [16,23–27]. In this model, the carcinogen azoxymethane (AOM) is injected into mice causing DNA damage in epithelial cells in the crypts of the distal colon inducing an acute apoptotic response 6–8 h later. The AARGC model has been mainly used to identify the effect of natural products on inducing apoptosis of the damaged colon cells, with the aim of detecting early stage CRC prevention [25].

In a previous *in vivo* study using a two-week preventative treatment with the crude extract from *D. orbita*, we detected an increase in apoptosis in the colon of mice in response to AOM injection. The aim of this study is to test the *in vitro* and *in vivo* effects of pure synthetic 6-bromoisatin, to confirm whether this compound is the key factor in *D. orbita* extracts responsible for the inhibition of colon cancer cells and the induction of apoptosis in damaged colon cells in the AARGC rodent model of colon cancer prevention. We also obtained additional data to assess any potential side effects of synthetic 6-bromoisatin on blood parameters and liver toxicity in the mice.

2. Results and Discussion

2.1. Chemical Analysis

^{1}H NMR results showed four major peaks corresponding to the four hydrogen protons in the 6-bromoisatin molecule: ^{1}H NMR (400 MHz, CD3CN) δ 8.96 (^{1}H, s), 7.44 (^{1}H, d, J = 8.08 Hz), 7.30 (^{1}H dd, J = 1.64, 8 Hz), 7.19 (^{1}H, d, J = 1.6 Hz) and confirming the identity of synthetic 6-bromoisatin and its high purity (Figure 1). The ^{1}H NMR spectra for synthetic 6-bromoisatin matches our previous NMR data for semi-purified 6-bromoisatin in anticancer extracts from the marine mollusc *D. orbita* [15].

2.2. In Vitro Apoptosis, Necrosis and Cell Viability

The effects of 6-bromoisatin on proliferation, apoptosis and necrosis of HT29 cells was examined. A dose dependent effect of 6-bromoisatin on the viability of cells was observed using the 3-(4,5-dimethylthiazol-2-yl)-2 5-diphenyltetrazolium bromide (MTT) assay for inhibition of metabolic activity (Figure 2). The three highest concentrations of 6-bromoisatin (1 mg/mL, 0.05 mg/mL and 0.025 mg/mL) significantly reduced the cell viability by 64%, 53% and 26% respectively ($p < 0.001$), relative to the DMSO control, but no significant reduction was observed at the lowest dose of 0.01 mg/mL ($p > 0.05$). The IC_{50} for synthetic 6-bromoisatin was calculated at 223 μM (0.05 mg/mL) for HT29 cells (Figure 2a). However, our previous *in vitro* study using semi-purified 6-bromoistain, on both HT29 and Caco2 cells, revealed a lower IC_{50} of 100 μM [15],

suggesting possible synergistic activity with other factors in the extract. The *in vitro* cytotoxic effects of synthetic 6-bromoisatin in this study could also be due to lower bioavailability of the pure compound to the cells when compared to the natural extract, which contains trace lipids that may help dissolve this lipophylic compound and/or facilitate interactions with cell membrane lipids. Previous studies have reported lower bioavailability of some synthetic compounds, in comparison with the naturally purified compounds [28,29]. For example, the bioavailability ratio of natural Vitamin E *versus* synthetic Vitamin E was shown to be close to 2:1 [29], which is similar to our study.

No increase in the level of lactate dehydrogenase (LDH) (Figure 2b) a measure of necrosis or late stage apoptosis was observed in the cells treated with any concentration of 6-bromoisatin, in comparison with DMSO control. Unexpectedly, synthetic 6-bromoisatin did not increase caspase 3/7 activity in HT29 cells *in vitro* at concentrations <0.1 mg/mL. This is in conflict with our previous study on semi-purified 6-bromoisatin, which significantly upregulated caspase 3/7 activity in HT29 cells [15]. The positive controls, lysis buffer and staurosporine, resulted in a significant increase in LDH activity (Figure 2b, $p < 0.001$) and caspase 3/7 activity (Figure 2c, $p < 0.001$) respectively, demonstrating that the assays were working. The cells treated with the highest concentration of 6-bromoisatin (446 μM = 0.1 mg/mL) showed a minor but significant reduction of caspase3/7 activity compared to the DMSO control (Figure 2c, $p = 0.011$). Nevertheless, the light microscopic images from the HT29 cells treated with 223 μM and 112 μM 6-bromoisatin showed morphological alterations, such as chromatin condensation, characteristic of the apoptotic process (Figure 3b,c). Apoptotic cells were also observed in cultures treated with the highest dose of 6-bromoisatin 446 μM, although in lower numbers than the two other doses (Figure 3d). This indicates that synthetic 6-bromoisatin may induce apoptosis in the HT29 cells through a caspase-independent pathway. In the past few years, the existence of caspase-independent programmed cell death pathways have been reported in the literature, which are associated with executioners other than the caspases, such as cathepsins, calpains, serine proteases and also apoptosis inducing factor (AIF) protein [30].

In terms of the mode of action, the isatin molecule has been proposed to interact via extracellular signal regulated protein kinases (ERKs) to inhibit cancer cell proliferation and promote apoptosis [2]. In a study by Cane *et al.* [6], isatin at a concentration of 100 μM inhibited the phosphorylation of ERK-2 (but not ERK-1) by 35% compared to the control. ERK is attributed to a survival signaling pathway in several cell types; however, it mediates apoptosis in some cell types and organs (e.g., neuronal and renal epithelial cells) under certain conditions [31]. Although the mechanisms for mediating apoptosis by ERK is not fully understood, three mechanisms have been proposed: (1) ERK1/2 may act through the intrinsic apoptotic pathway by up-regulating Bax and p53 followed by mitochondrial cytochrome c release and activation of caspase-3 [31–33]; (2) Through the extrinsic pathway by increasing an upstream signal for death receptors, such as TNF-α followed by activation of caspase-8 and caspase-3 [31,34] or; (3) Through inhibition of Akt (Protein kinase B) mediated survival signaling [35]. As synthetic 6-bromoisatin in this study induced apoptosis in HT29 cells without activating caspase-3 and considering the fact that both intrinsic and extrinsic pathways are associated with upregulation of caspase-3, the third pathway resulting in a decrease in Akt activity is hypothesized as a caspase-independent apoptosis pathway for synthetic 6-bromoisatin.

However, further mode of action studies that specifically target Akt gene expression in colon cancer cells are required with 6-bromoisatin to confirm this.

Figure 2. Effects of synthetic 6-bromoisatin on HT29 cells: Cell viability (**a**), LDH release (**b**) and caspase-3/7 activity (**c**). LDH release was measured by fluorescence at 535EX/590EM and caspase-3/7 activity was measured at full light on a luminescence plate reader. The positive controls are lysis buffer (5 µL/well) for the LDH assay and staurosporine (Str) (5 µM) for apoptosis. A final concentration of 1% DMSO was used in all control and treated cells. The results are mean for three independent repeat assays (n = 3) each performed in triplicate. Significant differences between each group and the DMSO control are shown as $p \leq 0.05$ (*) and $p \leq 0.001$ (***).

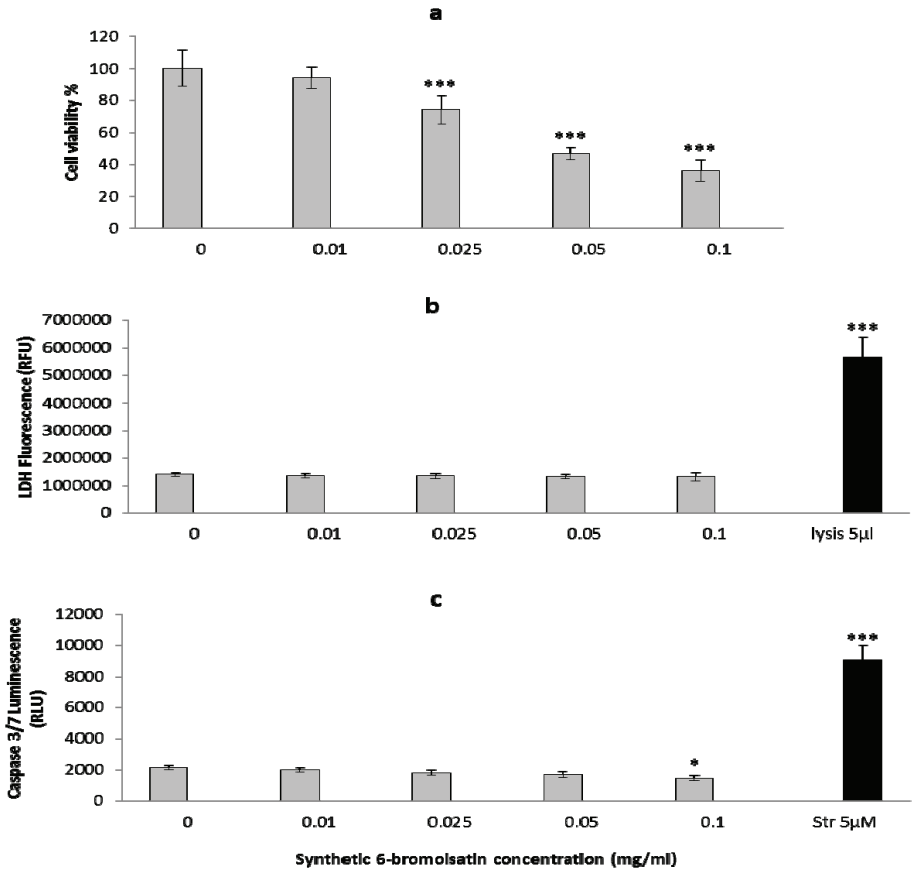

Figure 3. HT29 cells at 400× magnification under the Olympus inverted microscope. One percent dimethylsulphoxide (DMSO) control (**a**); cells treated with 0.025 mg/mL synthetic 6-bromoisatin (**b**); cells treated with 0.05 mg/mL synthetic 6-bromoisatin (**c**) and cells treated with 0.1 mg/mL synthetic 6-bromoisatin (**d**) for 12 h (final concentration of 1% DMSO). Examples of apoptotic cells with chromatin condensation and surrounded by a halo are indicated by the arrows.

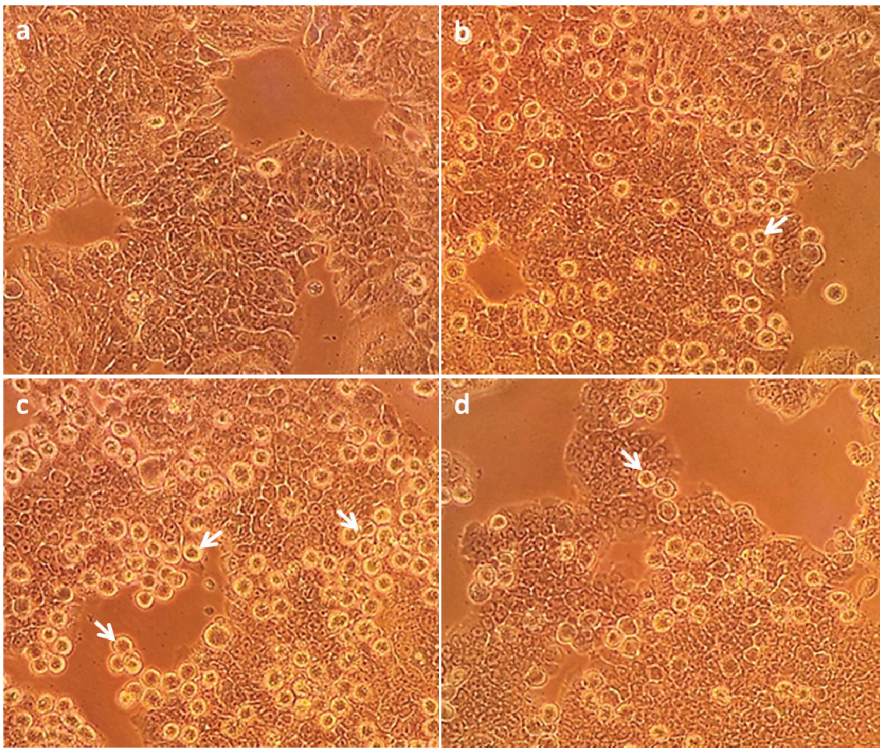

2.3. In Vivo Mouse Model

2.3.1. Mice; General Observations

Given synthetic 6-bromoisatin reduced the cell viability of a colon cancer cell line *in vitro*, we tested its effects on the AARGC response in a mouse model of CRC. The mice did not show any signs of illness in the treatment groups or the control group during the study. The body weights of all mice increased steadily over the trial duration, without any significant differences in mean total weight gain between the treatment groups and the control (Table 1, $p = 0.999$). No significant change in the liver weight or the percentage liver to body weight ($p = 0.098$) was revealed between treatment groups and the control (Table 1).

Table 1. Comparison of mean (±S.E.) progressive body weight (g) in controls and mice treated with different concentrations of 6-bromoisatin on different days of the experiment. All treatments and the control were injected with 10 mg/kg AOM 6 h prior to kill. Liver weight (g) and percentage liver weight/body weight were calculated on the day of kill. n = 10 mice in treatment groups and n = 8 mice in the control.

	Weight (g)						
Concentration	**Body (Day1)**	**Body (Day5)**	**Body (Day10)**	**Body (Day14)**	**Total weight Gain**	**Liver**	**Liver/Body (%)**
Control	22.0 ± 1.6	22.6 ± 1.6	22.8 ± 1.9	23.5 ± 1.9	1.4 ± 0.7	1.1 ± 0.3	4.8 ± 1.2
0.025 mg/g	22.2 ± 1.3	22.7 ± 1.3	23.0 ± 1.3	23.6 ± 1.4	1.4 ± 0.8	1.0 ± 0.1	4.4 ± 0.6
0.05 mg/g	22.6 ± 1.2	23.4 ± 1.2	23.4 ± 1.5	24.1 ± 1.6	1.4 ± 1.0	1.2 ± 0.1	5.2 ± 0.6
0.1 mg/g	22.3 ± 1.3	22.6 ± 1.3	23.3 ± 1.3	23.8 ± 1.6	1.4 ± 0.8	1.3 ± 0.1	5.3 ± 0.4

2.3.2. Apoptotic Index, Crypt Height and Cell Proliferation

Synthetic 6-bromoisatin was found to significantly increase apoptosis in response to AOM injection (ANOVA F = 14.660, $p < 0.001$, df = 3), but had no significant effect on colon crypt height (ANOVA F = 1.013, p = 0.403, df = 3); (Figure 4). The mice treated for two weeks daily with 0.05 mg/g 6-bromoisatin showed the greatest increase in apoptotic index in the distal colon (Figure 4a), with a 2.3 fold increase over the oil control ($p \leq 0.001$). The highest dose of 6-bromoisatin (0.1 mg/g) also significantly induced apoptosis (p = 0.007) in the distal colon of the mice compared with the control group. However, this effect was significantly lower, by 40%, than the dose of 0.05 mg/g (p = 0.031). In contrast, although the distal colon of the mice administered with the lowest concentration of 6-bromoisatin showed a slightly increased apoptosis index, there was not a significant difference when compared to the AOM injected control (Figure 4a, p = 0.158). Apoptosis in the distal colon of the mice occurred mostly in basal crypt cells (Figure 5).

Figure 4. Apoptotic response and crypt height in the distal colon of mice after 14 day oral gavage with different concentrations of synthetic 6-bromoisatin, showing: apoptotic index (**a**) and crypt height (**b**). All treatments and the oil only control were injected with 10 mg/kg AOM 6 h prior to kill. Data are means ± S.E. for 10 full crypts/animal (n = 10 mice in treatment groups and n = 8 mice in control group). Significant differences between each group and the control are shown as $p \leq 0.01$ (**) and $p \leq 0.001$ (***).

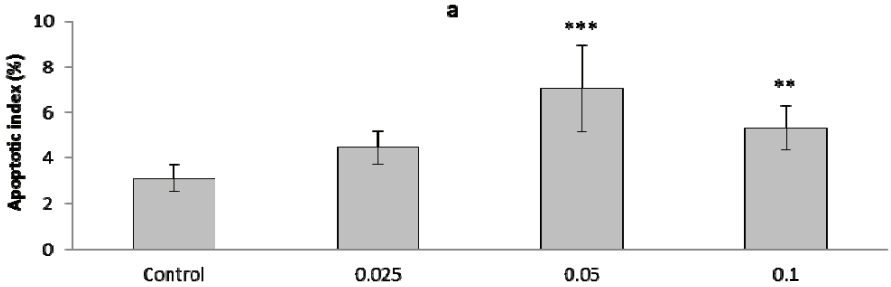

Figure 5. *Cont.*

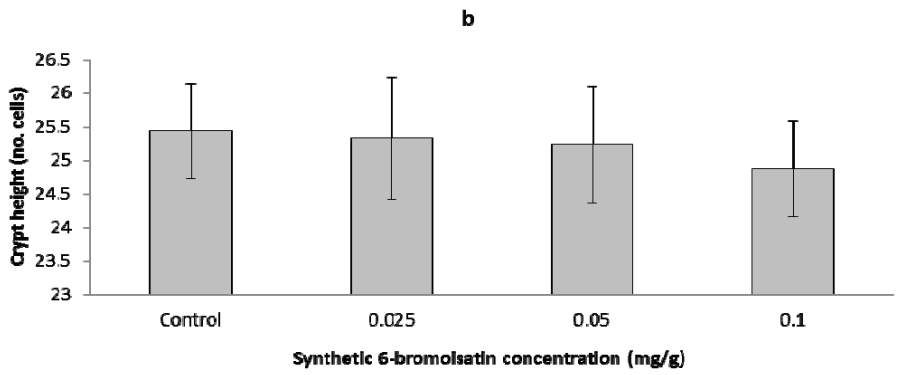

Figure 5. Apoptosis in the basal crypt cells of the distal colon of mice 6 h post AOM injection (10 mg/kg). Mice were oral gavaged daily for two weeks prior with oil. (**a**) control; (**b**) 6-bromoisatin 0.025 mg/g; (**c**) 6-bromoisatin 0.05 mg/g; (**d**) 6-bromoisatin 0.1 mg/g. Apoptotic cells with chromatin condensation characteristics are shown by arrows.

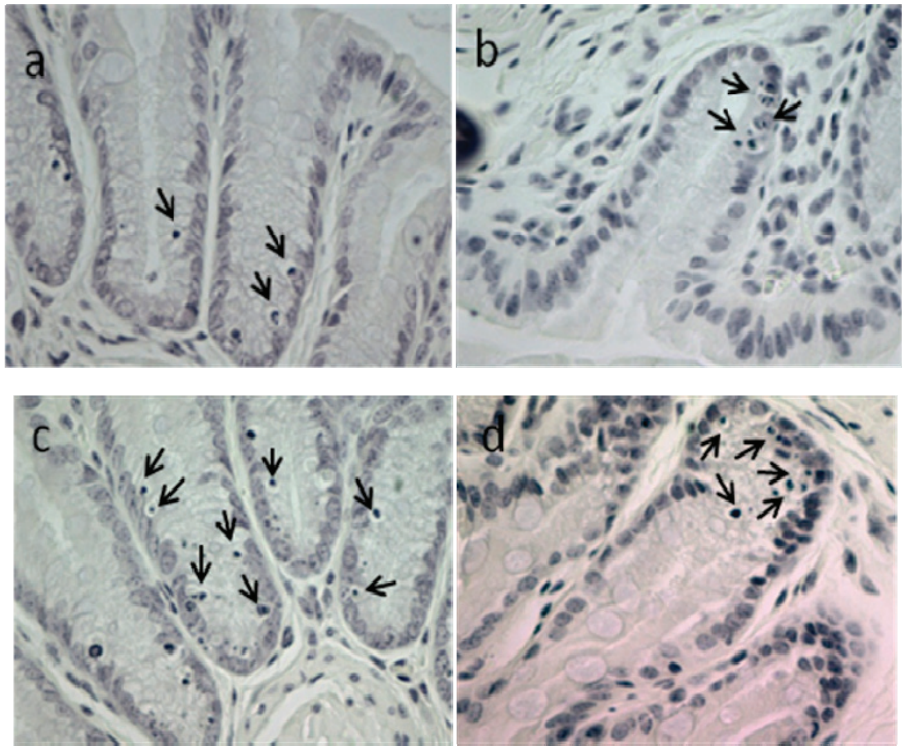

Ki-67 immunohistochemistry showed evidence for cell proliferation, also in the basal cells of colon crypts of mice, in response to AOM injection (Figure 6). After two weeks daily oral gavage, synthetic 6-bromoisatin was found to significantly reduce this cell proliferation in the distal colon

of mice (ANOVA $F = 41.273$, $p < 0.001$, $df = 3$); (Figure 7). After AOM injection, the mice treated with the highest concentration of 6-bromoisatin (0.1 mg/g) had the greatest reduction in cell proliferation in the distal colon, by more than 50% compared to control mice gavaged with oil alone ($p \leq 0.001$). Similarly, the dose of 0.05mg/g significantly reduced the proliferation in the distal colon compared to the oil alone control ($p = 0.006$), and was not significantly different to the higher dose of 0.1 mg/g ($p = 0.652$). In contrast, the lowest dose of 6-bromoisatin (0.025 mg/g) did not show a significant anti-proliferative effect in the distal colon as compared to the oil alone control (Figures 6 and 7, $p = 0.052$).

Figure 6. Proliferative activity of distal colonic epithelial cells in mice 6 h after AOM injection (10 mg/kg), shown using an antibody specific for the ki-67 antigen. Mice were oral gavaged daily for two weeks prior with oil; (**a**) control; (**b**) 6-bromoisatin 0.025 mg/g; (**c**) 6-bromoisatin 0.05 mg/g; (**d**) 6-bromoisatin 0.1 mg/g. Proliferating cells are shown by arrowheads.

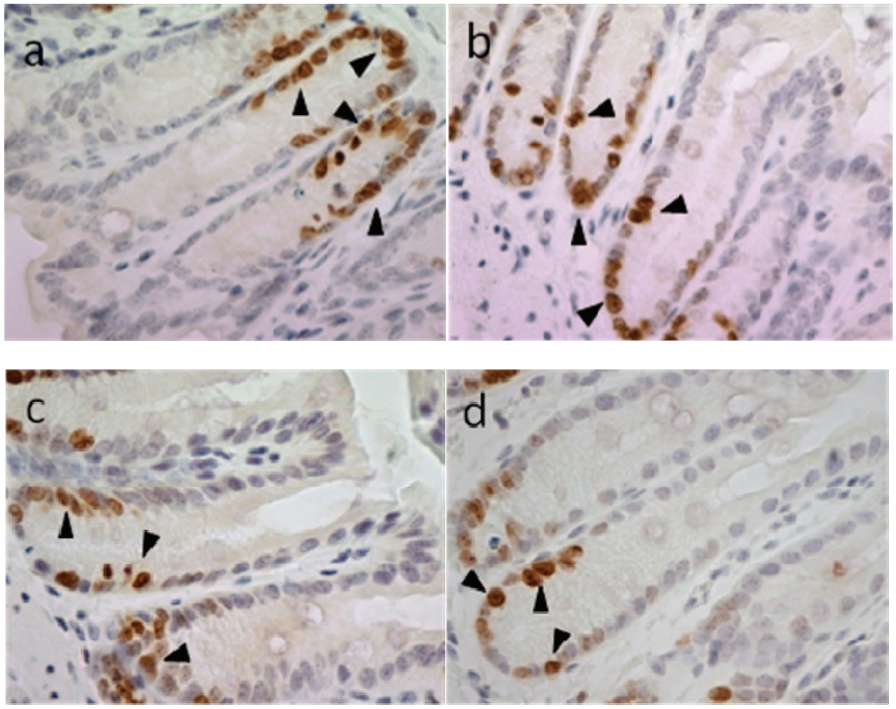

Figure 7. Proliferation index in the distal colon of oil control mice and mice treated with different concentrations of 6-bromoisatin by daily oral gavage for 2 weeks, followed by 10 mg/kg AOM injection 6 h prior to kill. Significant differences between each group and the control are shown as $p \leq 0.01$ (**) and $p \leq 0.001$ (***).

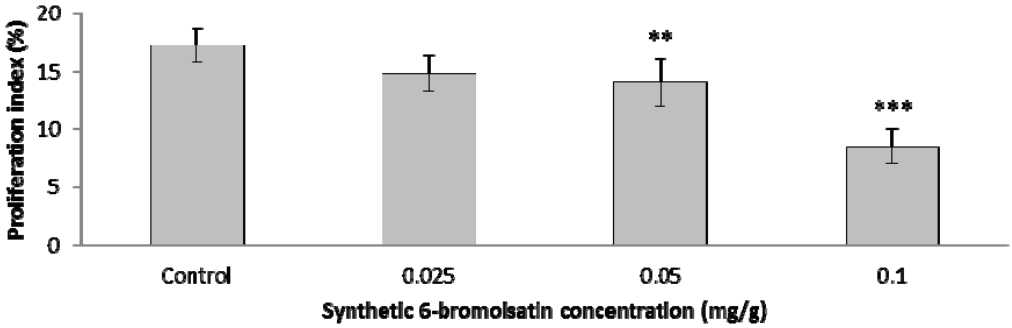

A connection between AARGC stimulation and the inhibition of oncogenesis in the distal colon has been previously shown in mice [36,37]. In our study, synthetic 6-bromoisatin at the concentration of 0.05 mg/g had the greatest effect in facilitating apoptosis in the distal colon of mice. Interestingly, the apoptotic index at the highest dose of synthetic 6-bromoisatin (0.1 mg/g) was lower than the middle dose of 0.05 mg/g, which is consistent with a previous study using the crude extract from *D. orbita* [16]. This could be related to the fact that cell proliferation in the colon showed the highest reduction at the highest dose of 0.1 mg/g 6-bromoisatin, indicating that fewer DNA damaged cells may have been present that required removal by the initiation of programmed cell death. In a study by Saini *et al.* [38] the cytotoxic effect of streptozotocin, at low doses, was shown to be associated with the activation of the apoptotic pathway on beta cells, whereas this predominantly changed to necrosis at high doses. Therefore the lower apoptosis index with the highest dose of 6-bromoisatin may indicate that some necrosis or cell cycle arrest occurred in the crypt cells at this high dose. However, the *in vitro* LDH assays found no evidence of an increase in cell membrane permeability that would suggest necrosis at this concentration.

2.3.3. Blood Biochemistry and Hematology

To be useful as a future drug or nutraceutical for the prevention of colon cancer, 6-bromoisatin and/or *D. orbita* extracts must also be safe for oral use. The plasma level of the liver enzymes aspartate aminotransferase (AST), alanine aminotransferase (ALT) and alkaline phosphatase (ALP) are indicators of hepatotoxicity [39]. No significant difference was revealed in the plasma level of these enzymes in the oil control, as compared to treatment groups gavaged for two weeks daily with 6-bromoisatin (Figure 8, $p > 0.6$), providing evidence that synthetic 6-bromoisatin is not hepatotoxic at these concentrations. In a study by Westley *et al.* [40], mice treated with the crude *D. orbita* extracts containing 6-bromoisatin showed some idiosyncratic toxicity in the liver, whereas pure 6-bromoisatin did not exhibit this hepatotoxicity.

Figure 8. Liver enzymes *aspartate aminotransferase* (AST), *alanine aminotransferase* (ALT) and *alkaline phosphatase* (ALP) levels in serum (U/L) of oil control mice and mice treated with different concentrations of 6-bromoisatin by daily oral gavage for two weeks.

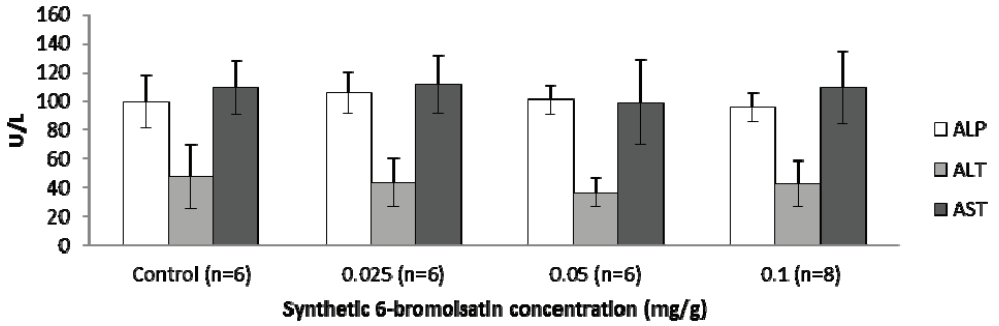

In the plasma there were no significant differences in sodium, urea, creatinine, calcium, protein, albumin and globulin levels in the mice treated with 6-bromoisatin in comparison to the oil control (Table 2; $p > 0.05$). However, a significant dose dependent reduction in potassium plasma levels (Hypokalemia) was observed in the mice administered with both 0.05 mg/g ($p = 0.005$) and 0.1 mg/g 6-bromoisatin ($p = 0.001$), as compared to the oil control (Table 2). Consequently, the sodium/potassium ratio (Na/K) increased significantly in these groups compared to the oil control (Table 2, $p < 0.005$).

The most common reason for a potassium deficiency is diuretic therapy (loop diuretics, thiazides) that causes urinary potassium excretion [41,42], and gastrointestinal potassium wasting from diarrhea [41,43]. In this study, no diarrhea or change in stool consistency was observed in either the oil control or 6-bromoisatin treatment groups. Therefore, the potassium deficiency in the treatment groups might be due to a diuretic effect of 6-bromoisatin leading to an increase in urinary potassium excretion. Diuretic effects of some novel isatin derivatives, especially the derivatives of bromoisatin, were previously shown by Nataraj *et al.* [44]. Consequently, future *in vivo* studies using 6-bromoisatin should carefully monitor this possible diuretic effect.

Table 2. Plasma biochemistry and blood hematology from mice in the oil only control group and mice treated with different concentrations of 6-bromoisatin, 6 h after injection of 10 mg/kg AOM. Significant differences between each group and the oil control are shown as $p \leq 0.05$ (*), $p \leq 0.01$ (**) and $p \leq 0.001$ (***). Significant differences between 6-bromoistain doses are shown as $p \leq 0.05$ ($^{\#}$) relative to 0.1 mg/mL. Na/K = Sodium/Potassium ratio, Creat = Creatinine, Hct = Hematocrit, MCV = Mean Corpuscular Volume, MCH = Mean Corpuscular Hemoglobin, MCHC = Mean Corpuscular Hemoglobin Concentration.

	Oil Control (n = 6)	6-Bromoisatin (0.025 mg/g, n = 6)	6-Bromoisatin (0.05 mg/g, n = 6)	6-Bromoisatin (0.1 mg/g, n = 8)
Biochemistry				
Sodium (mmol/L)	146.5 ± 1.2	147.7 ± 0.5	149.7 ± 1.4	149.7 ± 1.2
Potassium (mmol/L)	5.4 ± 0.3	5.1 ± 0.2 #	4.5 ± 0.4 *	4.3 ± 0.4 **
NA/K	27.0 ± 2.2	29.1 ± 1.2 #	33.5 ± 2.7 **	34.1 ± 3.6 ***
Urea (mmol/L)	10.6 ± 1.2	9.7 ± 1.6	9.9 ± 1.4	9.6 ± 1.2
Creat. (umol/L)	14.2 ± 1.2	13.3 ± 0.8	14.7 ± 0.5	14.6 ± 1.2
Calcium (mmol/L)	2.2 ± 0.03	2.2 ± 0.1	2.2 ± 0.04	2.2 ± 0.1
Protein (g/L)	45.8 ± 3.0	46.7 ± 2.8	46.2 ± 1.9	46.1 ± 2.2
Albumin (g/L)	28.2 ± 1.7	28.7 ± 1.5	27.8 ± 1.5	28.2 ± 1.5
Globulin (g/L)	17.7 ± 1.5	18.0 ± 1.4	18.3 ± 0.8	17.9 ± 1.2
Hematology				
Red cell count ($\times 10^{12}$/L)	9.0 ± 0.4	9.3 ± 0.4	9.1 ± 0.4	9.4 ± 0.5
Hemoglobin (g/L)	135.2 ± 2.7	139.7 ± 5.1	135.0 ± 3.5	138.4 ± 5.7
Hct (L/L)	0.4 ± 0.01	0.4 ± 0.01	0.4 ± 0.01	0.4 ± 0.02
MCV (FL)	46.0 ± 1.2	46.5 ± 0.8	46.7 ± 1.2	46.4 ± 0.7
MCH (Pg)	15.2 ± 0.4	15.0 ± 0.0	15.0 ± 0.0	15.0 ± 0.0
MCHC (g/L)	323.7 ± 4.5	322.7 ± 1.5	319.0 ± 2.8	319.8 ± 3.0
White cell count ($\times 10^9$/L)	4.8 ± 0.9	5.2 ± 1.8	5.8 ± 1.5 #	3.2 ± 1.1
Neutrophils ($\times 10^9$/L)	1.9 ± 0.3	1.6 ± 0.8	2.2 ± 1.3	0.8 ± 0.7
Lymphocytes ($\times 10^9$/L)	2.8 ± 0.9	3.3 ± 1.1	3.4 ± 0.8	2.3 ± 0.9
Monocytes ($\times 10^9$/L)	0.2 ± 0.1	0.2 ± 0.3	0.2 ± 0.1	0.1 ± 0.1

The hematological factors including white blood count, red blood count, hemoglobin, hematocrit (Hct), mean corpuscular volume (MCV), mean corpuscular hemoglobin (MCH), mean corpuscular hemoglobin concentration (MCHC), band form neutrophils, lymphocytes and monocytes were not significantly altered in treatment groups, in comparison to the oil only control (Table 2, $p > 0.05$). However, there was a significant increase in the white blood cell count of mice treated with 0.05 mg/g 6-bromoistain, compared to mice treated with the higher dose of 0.1 mg/g (Table 2, $p = 0.037$). This may indicate some mild anti-inflammatory effects at the higher dose of 6-bromoistain. Isatin has been previously found to inhibit NO production, COX-2, TNF and PGE2 in mouse macrophages [45]. Furthermore, indirubin derivatives exhibit inflammatory activity in RAW 264.7 cells [46] and in rat brain microglia [47].

Overall, this study demonstrates that 6-bromoisatin, a dominant compound found in muricid mollusc extract, has anticancer effects and low toxicity *in vivo*. Pure synthetic 6-bromoisatin

effectively reduced the proliferation of colon cells, both *in vitro* against the HT29 colorectal cancer cell line and *in vivo* in mice administered AOM, which causes DNA damage in colon cells. 6-Bromoisatin also enhanced the apoptotic response in DNA damaged colon cells *in vivo*, with 0.05 mg/g found to be the most effective dose, with the only sign of toxicity after two weeks administration being a possible diuretic effect. Although synthetic 6-bromoisatin did not increase caspase 3/7 activity in HT29 cells, light microscopy confirmed the presence of many cells with the morphological appearance of apoptosis, such as a condensed nucleus surrounded by a halo. Consequently it can be concluded that 6-bromoisatin is the main factor in the *D. orbita* anticancer extracts contributing to enhancing the apoptotic response to the genotoxic insult of AOM. Although the effective doses of 6-bromoistain used in this study were high relative to common chemotherapeutic drugs, cancer prevention strategies are more likely to utilize dietary supplements or nutraceuticals containing higher doses of bioactive secondary metabolites with demonstrated low toxicity. 6-Bromoisatin is the dominant compound in oxidized extracts from the hypobranchial glands of *D. orbita*, an edible marine mollusc [40], This compound is stable at low pH in simulated digestive fluid [16] and appears to be bioavailable in the distal colon. Therefore, this paper supports the further development of a nutraceutical from Muricidae molluscs with potential application for the prevention of early stage colon cancer, by specifically targeting the 6-bromoisatin fraction.

3. Experimental Section

3.1. Synthetic 6-Bromoisatin and Chemical Analysis

Synthetic 6-bromoisatin (6-Bromoindole-2,3-dione) was purchased from TCI AMERICA (Portland, OR, USA) (purity of >97.0% GC). To confirm the identity and purity of the compound, ^{1}H NMR spectroscopy (Bruker Avance III 400 MHz spectrometer, Preston, VIC, Australia) was performed in deuterated acetonitrile (Sigma Aldrich, Castle Hill, NSW, Australia). Chemical shifts (δ) are reported as parts per million (ppm) and referenced to residual solvent peaks. Spin multiplicities are indicated by: s, singlet; bs, broad singlet; d, doublet; t, triplet; q, quartet; m, multiplet; and dd, doublet of doublets.

3.2. In Vitro Experiments Using HT29 Colorectal Cancer Cells

All media and chemicals were purchased from Sigma Aldrich (Castle Hill, NSW, Australia) unless otherwise stated. HT29 human colorectal cancer cell line (passage no. 36-42) were cultured (37 °C and 5% CO_2) in Dulbecco's Modified Eagle's Medium (DMEM) supplemented with 4500 mg/L L-glutamine, 10% FBS, 100 U/mL Penicillin/Streptomycin and 1% Non-essential Amino Acid (100×), until the cells reached 70% confluence.

The cells were harvested from flasks by trypsinization (1× Trypsin-EDTA) and were seeded (20,000 cells/well) into clear 96-well plates (Costar®, Mt Martha, VIC, Australia) for measurement of cell viability and white (opaque) 96-well plates (Interpath, Heidelberg West, VIC, Australia) for determination of apoptosis and necrosis. HT29 cells were incubated for 48 h, then the media was removed and the cells were washed with PBS. To treat the cells, synthetic 6-bromoisatin was dissolved in 100% dimethylsulphoxide (DMSO) then diluted in media and added to the cells at a

range of concentrations from 0.1 to 0.01 mg/mL, in triplicate (final DMSO concentration of 1%). 1% DMSO controls were also included on each plate. Staurosporine (5 μM) for apoptosis and lysis solution (5 μL/well, Promega, Alexandria, NSW, Australia) for necrosis were added to the white plates in triplicate, as positive controls. All cells were treated for 12 h.

Morphological changes in the cells were observed on an Olympus CK2 inverted optical microscope (×400 magnification) 12 h after treatment. To measure cell viability, the MTT assay was applied, which measures the reduction of MTT tetrazolium salt to formazan, as previously described [15]. To measure necrosis and apoptosis, CytoTox-ONE Homogeneous Membrane Integrity Assay reagent (Promega) and Caspase-Glo 3/7® assay (Promega) were applied respectively, according to our previous study [15]. These assays were all repeated in triplicate on three separate occasions (n = 3).

3.3. In Vivo Model for Early Stage Colon Cancer Prevention

This experiment was conducted under Flinders animal welfare approval number 751-10. A total of 38 wild-type (C57BL/6J) male mice aged 10 weeks were obtained from the Animal Resource Centre, Perth, Western Australia. Mice were divided randomly into 4 groups (ten mice in each treatment group and 8 mice in the sunflower oil only control group) and housed in 8 cages (four to five mice per cage). The mice were given water and food (rodent chow) *ad libitum* and maintained at the temperature of 22 ± 2 °C and humidity of 80% ± 10% with a 12 h light/dark cycle. Mice were weighed every five days and on the day of kill, and monitored daily for signs of illness, such as weight and hair loss, diarrhea, constipation, rectal bleeding, labored breathing, lethargy, eye and nose discharge.

To detect the early stage prevention of colon cancer, an established AARGC rodent model with injection of the carcinogen AOM was used [16,25,26,48]. Synthetic 6-bromoisatin at 3 different dosages (0.025, 0.05 and 0.1 mg/g body weight) was administered to mice by daily oral gavage in 100 μL sunflower oil, containing 0.02% Vitamin E, for two weeks. The control group was gavaged with sunflower oil (containing 0.02% Vitamin E) only. After two weeks, all mice were injected with a single intraperitoneal (i.p.) injection of AOM at a dosage of 10 mg/kg bodyweight and euthanized 6 h later by cervical dislocation under anesthesia. Our previous studies have shown that the peak time for the acute apoptotic response to carcinogen occurs between 6 h and 8 h post AOM injection (25), hence 6 h post AOM was chosen in the current study. The distal colon of each mouse was excised and fixed in 10% buffered formalin for 24 h and then embedded in paraffin for histological and immunohistological examination.

Distal colon segments were embedded in paraffin and sectioned at 4 μm (3–4 sections per mouse), then stained with hematoxylin, to evaluate apoptosis in epithelial cells of distal colon sections [48]. The slides were examined under a light microscope (Olympus BH-2, Mt Waverly, VIC, Australia, 400× magnification) to identify the apoptotic cells, by characteristic morphological changes such as cell shrinkage, condensed chromatin and sharply delineated cell borders surrounded by an unstained halo [26,49]. Twenty randomly chosen crypts were used to calculate the percent of apoptotic cells per crypt. The mean crypt column height was also determined.

Ki-67 is a cell cycle associated antigen and regarded as a useful proliferation marker [50]. Proliferative activity of distal colonic epithelial cells was measured using an antibody specific for the nuclear proliferating antigen ki-67 (rat-anti-mouse clone TEC-3, Dako, Campbellfield, VIC, Australia) in combination with an immunohistochemistry detection method in paraffin embedded sections, as previously described [15]. Sections of 4 μm were examined under a light microscope (Zeiss, Axio Imager A1, North Ryde, NSW, Australia) at 400× magnification to calculate the proliferation index as a percent of proliferated cells per crypt.

3.4. Liver Enzymes, Blood Biochemistry and Hematology

Blood samples (0.5–1 mL) were obtained from the mice under anesthesia by cardiac puncture at time of kill and transferred to Gribbles Veterinary Pathology laboratory, Adelaide within heparinized vacutainer tubes then centrifuged to separate into the cell layer for hematology analysis (Abbott Cell Dyn 3700 analyzer, North Ryde, NSW, Australia) and plasma for biochemistry analysis (Siemens Advia 1800 chemistry analyzer, Erlangen, Germany). The plasma levels of the liver enzymes AST, ALT and ALP were assessed as indicators of hepatotoxicity [39].

3.5. Statistical Analysis

Statistical analyses were performed using SPSS and values of $P \leq 0.05$ were considered to be statistically significant. One way ANOVAs with post hoc Tukey HSD multiple comparisons were performed to determine which concentrations of 6-bromoisatin were significantly different to each other and the control.

4. Conclusions

In conclusion, this study supports the efficacy of synthetic 6-bromoisatin, at the concentration of 0.05 mg/g, for enhancing the apoptotic response to a genotoxic carcinogen and reducing cell proliferation in the distal colon of mice, without significant toxic effects detected in the liver or blood. The highest dose of 0.1 mg/g 6-bromoisatin showed a saturated dose–response for the induction of apoptosis, but had a stronger effect of inhibiting cell proliferation in the crypt of the distal colon and appears to also reduce the number of circulating white blood cells relative to the lower dose. Synthetic 6-bromoisatin appears to induce apoptosis in HT29 cells by a caspase-independent pathway. Although there was evidence of hypokalemia in the mice, due to the possible diuretic effect of 6-bromoisatin, no further toxicity in the liver or blood cells were observed. Longer term studies in mice are required to assess the effect of 6-bromoisatin on colonic aberrant crypt foci formation and/or tumor formation and also any possible side-effects associated with longer term use of this compound.

Acknowledgments

We appreciate the assistance of Martin Johnston (School of Chemistry and Physical Sciences, Flinders University, Adelaide, Australia) with the NMR analysis of 6-bromoistain. Hanna

Krysinska and Lisa Pogson (School of Biological Sciences, Flinders University, Adelaide, Australia) and Roshini Somashekar, Joanne Wilkins and Jean Winter (Flinders Centre for Innovation in Cancer, Adelaide, Australia) provided valuable technical assistance.

Conflicts of Interest

The authors declare no conflict of interest.

References

1. Medvedev, A.; Buneeva, O.; Glover, V. Biological targets for isatin and its analogues: Implications for therapy. *Biol. Targets Ther.* **2007**, *1*, 151–162.
2. Vine, K.L.; Matesic, L.; Locke, J.; Ranson, M.; Skropeta, D. Cytotoxic and anticancer activities of isatin and its derivatives: A comprehensive review from 2000–2008. *Anticancer Agents Med. Chem.* **2009**, *9*, 397–414.
3. Pal, M.; Sharma, N.K.; Priyanka, J.K. Synthetic and biological multiplicity of isatin: A review. *J. Adv. Sci. Res.* **2011**, *2*, 35–44.
4. Akgul, O.; Tarikogullari, A.H.; Kose, F.A.; Ballar, P.; Pabuccuoglu, V. Synthesis and cytotoxic activity of some 2-(2,3-dioxo-2, 3-dihydro-1*H*-indol-1-yl) acetamide derivatives. *Turk. J. Chem.* **2013**, *37*, 204–212.
5. Benkendorff, K. The Australian Muricidae Dicathais orbita: A model species for marine natural product research. *Mar. Drugs* **2013**, *11*, 1370–1398.
6. Cane, A.; Tournaire, M.-C.; Barritault, D.; Crumeyrolle-Arias, M. The endogenous oxindoles 5-hydroxyoxindole and isatin are antiproliferative and proapoptotic. *Biochem. Biophys. Res. Commun.* **2000**, *276*, 379–384.
7. Igosheva, N.; Lorz, C.; O'Conner, E.; Glover, V.; Mehmet, H. Isatin, an endogenous monoamine oxidase inhibitor, triggers a dose-and time-dependent switch from apoptosis to necrosis in human neuroblastoma cells. *Neurochem. Int.* **2005**, *47*, 216–224.
8. Vine, K.L.; Locke, J.M.; Ranson, M.; Benkendorff, K.; Pyne, S.G.; Bremner, J.B. *In vitro* cytotoxicity evaluation of some substituted isatin derivatives. *Bioorg. Med. Chem.* **2007**, *15*, 931–938.
9. Motzer, R.J.; Michaelson, M.D.; Redman, B.G.; Hudes, G.R.; Wilding, G.; Figlin, R.A.; Ginsberg, M.S.; Kim, S.T.; Baum, C.M.; DePrimo, S.E. Activity of SU11248, a multitargeted inhibitor of vascular endothelial growth factor receptor and platelet-derived growth factor receptor, in patients with metastatic renal cell carcinoma. *J. Clin. Oncol.* **2006**, *24*, 16–24.
10. Prenen, H.; Cools, J.; Mentens, N.; Folens, C.; Sciot, R.; Schöffski, P.; Van Oosterom, A.; Marynen, P.; Debiec-Rychter, M. Efficacy of the kinase inhibitor SU11248 against gastrointestinal stromal tumor mutants refractory to imatinib mesylate. *Clin. Cancer Res.* **2006**, *12*, 2622–2627.
11. Kapadia, G.; Shukla, Y.; Basak, S.; Sokoloski, E.; Fales, H. The melosatins—A novel class of alkaloids from *Melochia tomentosa*. *Tetrahedron* **1980**, *36*, 2441–2447.

12. Gräfe, U.; Radics, L. Isolation and structure elucidation of 6-(3′-methylbuten-2′-yl) isatin, an unusual metabolite from *Streptomyces albus*. *J. Antibiot.* **1986**, *39*, 162–163.
13. Cooksey, C. J. Tyrian purple: 6,6′-dibromoindigo and related compounds. *Molecules* **2001**, *6*, 736–769.
14. Edwards, V.; Benkendorff, K.; Young, F. Marine compounds selectively induce apoptosis in female reproductive cancer cells but not in primary-derived human reproductive granulosa cells. *Mar. Drugs* **2012**, *10*, 64–83.
15. Esmaeelian, B.; Benkendorff, K.; Johnston, R.M.; Abbott, C.A. Purified brominated indole derivatives from *Dicathais orbita* induce apoptosis and cell cycle arrest in colorectal cancer cell lines. *Mar. Drugs* **2013**, *11*, 3802–3822.
16. Westley, C.B.; McIver, C.M.; Abbott, C.A.; Le Leu, R.K.; Benkendorff, K. Enhanced acute apoptotic response to azoxymethane-induced DNA damage in the rodent colonic epithelium by Tyrian purple precursors: A potential colorectal cancer chemopreventative. *Cancer Biol. Ther.* **2010**, *9*, 371–379.
17. McLeod, R.; Schmocker, S.; Kennedy, E. Management of primary colon cancer in older adults. *Geriat. Aging* **2009**, *12*, 374–381.
18. Jemal, A.; Bray, F.; Center, M.M.; Ferlay, J.; Ward, E.; Forman, D. Global cancer statistics. *CA Cancer J. Clin.* **2011**, *61*, 69–90.
19. Chan, A.T.; Giovannucci, E.L. Primary prevention of colorectal cancer. *Gastroenterology* **2010**, *138*, 2029–2043.e10.
20. ACS, American Cancer Society. *Colorectal Cancer Facts & Figures 2011–2013*; American Cancer Society: Atlanta, GA, USA, 2013.
21. IARC, International Agency for Research on Cancer (IARC). *World Cancer Report 2008*; World Health Organization Press: Geneva, Switzerland, 2008; pp. 192–193.
22. Rajamanickam, S.; Agarwal, R. Natural products and colon cancer: Current status and future prospects. *Drug Dev. Res.* **2008**, *69*, 460–471.
23. Hong, M.Y.; Chapkin, R.S.; Wild, C.P.; Morris, J.S.; Wang, N.; Carroll, R.J.; Turner, N.D.; Lupton, J.R. Relationship between DNA adduct levels, repair enzyme, and apoptosis as a function of DNA methylation by azoxymethane. *Cell Growth Differ.* **1999**, *10*, 749–758.
24. Reddy, B.S.; Hirose, Y.; Cohen, L.A.; Simi, B.; Cooma, I.; Rao, C.V. Preventive potential of wheat bran fractions against experimental colon carcinogenesis: implications for human colon cancer prevention. *Cancer Res.* **2000**, *60*, 4792–4797.
25. Hu, Y.; Martin, J.; Le Leu, R.; Young, G. The colonic response to genotoxic carcinogens in the rat: regulation by dietary fibre. *Carcinogenesis* **2002**, *23*, 1131–1137.
26. Le Leu, R.; Hu, Y.; Young, G. Effects of resistant starch and nonstarch polysaccharides on colonic luminal environment and genotoxin-induced apoptosis in the rat. *Carcinogenesis* **2002**, *23*, 713–719.
27. Le Leu, R.K.; Brown, I.L.; Hu, Y.; Young, G.P. Effect of resistant starch on genotoxin-induced apoptosis, colonic epithelium, and lumenal contents in rats. *Carcinogenesis* **2003**, *24*, 1347–1352.
28. Vinson, J.; Bose, P. Comparative bioavailability of synthetic and natural Vitamin C in guinea pigs. *Nutr. Rep .Int.* **1983**, *27*, 1–5.

29. Lodge, J. K. Vitamin E bioavailability in humans. *J. Plant Physiol.* **2005**, *162*, 790–796.
30. Constantinou, C.; Papas, K.; Constantinou, A. Caspase-independent pathways of programmed cell death: The unraveling of new targets of cancer therapy? *Curr. Cancer Drug Targets* **2009**, *9*, 717–728.
31. Zhuang, S.; Schnellmann, R.G. A death-promoting role for extracellular signal-regulated kinase. *J. Pharmacol. Exp. Ther.* **2006**, *319*, 991–997.
32. Wang, X.; Martindale, J.L.; Holbrook, N.J. Requirement for ERK activation in cisplatin-induced apoptosis. *J. Biol. Chem.* **2000**, *275*, 39435–39443.
33. Kim, Y.K.; Kim, H.J.; Kwon, C.H.; Kim, J.H.; Woo, J.S.; Jung, J.S.; Kim, J.M. Role of ERK activation in cisplatin-induced apoptosis in OK renal epithelial cells. *J. Appl. Toxicol.* **2005**, *25*, 374–382.
34. Jo, S.-K.; Cho, W.Y.; Sung, S.A.; Kim, H.K.; Won, N.H. MEK inhibitor, U0126, attenuates cisplatin-induced renal injury by decreasing inflammation and apoptosis. *Kidney Int.* **2005**, *67*, 458–466.
35. Sinha, D.; Bannergee, S.; Schwartz, J.H.; Lieberthal, W.; Levine, J.S. Inhibition of ligand-independent ERK1/2 activity in kidney proximal tubular cells deprived of soluble survival factors up-regulates Akt and prevents apoptosis. *J. Biol. Chem.* **2004**, *279*, 10962–10972.
36. Hu, Y.; McIntosh, G.H.; Le Leu, R.K.; Woodman, R.; Young, G.P. Suppression of colorectal oncogenesis by selenium-enriched milk proteins: apoptosis and K-ras mutations. *Cancer Res.* **2008**, *68*, 4936–4944.
37. Le Leu, R.K.; Hu, Y.; Brown, I.L.; Woodman, R.J.; Young, G.P. Synbiotic intervention of Bifidobacterium lactis and resistant starch protects against colorectal cancer development in rats. *Carcinogenesis* **2010**, *31*, 246–251.
38. Saini, K.S.; Thompson, C.; Winterford, C.M.; Walker, N.I.; Cameron, D.P. Streptozotocin at low doses induces apoptosis and at high doses causes necrosis in a murine pancreatic β cell line, INS-1. *IUBMB Life* **1996**, *39*, 1229–1236.
39. Hewawasam, R.; Jayatilaka, K.; Pathirana, C.; Mudduwa, L. Hepatoprotective effect of *Epaltes divaricata* extract on carbon tetrachloride induced hepatotoxicity in mice. *Indian J. Med. Res.* **2004**, *120*, 30–34.
40. Westley, C.B.; Benkendorff, K.; McIver, C.M.; Le Leu, R.K.; Abbott, C.A. Gastrointestinal and hepatotoxicity assessment of an anticancer extract from muricid molluscs. *Evid.-Based Comp. Alt. Med.* **2013**, *2013*, 1–12.
41. Lindeman, R.D. Hypokalemia: causes, consequences and correction. *Am. J. Med. Sci.* **1976**, *272*, 5–17.
42. Weiner, I.D.; Wingo, C.S. Hypokalemia—consequences, causes, and correction. *J. Am. Soc. Nephrol.* **1997**, *8*, 1179–1188.
43. Gennari, F.J. Disorders of potassium homeostasis: Hypokalemia and hyperkalemia. *Crit. Care Clin.* **2002**, *18*, 273–288.
44. Nataraj, K.S.; Rao, J.V.; Jayaveera, K.N. Diuretic activity of some novel isatin derivatives. *J. Pharm. Res.* **2010**, *3*, 863.

45. Matheus, M.E.; de Almeida Violante, F.; Garden, S.J.; Pinto, A.C.; Dias Fernandes, P. Isatins inhibit cyclooxygenase-2 and inducible nitric oxide synthase in a mouse macrophage cell line. *Eur. J. Pharm.* **2007**, *556*, 200–206.
46. Kim, J.-K.; Park, G.-M. Indirubin-3-monoxime exhibits anti-inflammatory properties by down-regulating NF-κB and JNK signaling pathways in lipopolysaccharide-treated RAW264.7 cells. *Inflamm. Res.* **2012**, *61*, 319–325.
47. Jung, H.-L.; Nam, K.N.; Son, M.S.; Kang, H.; Hong, J.W.; Kim, J.W.; Lee, E.H. Indirubin-3′-oxime inhibits inflammatory activation of rat brain microglia. *Neurosci. Lett.* **2011**, *487*, 139–143.
48. Hu, Y.; Le Leu, R.K.; Young, G.P. Sulindac corrects defective apoptosis and suppresses azoxymethane-induced colonic oncogenesis in p53 knockout mice. *Int. J. Cancer* **2005**, *116*, 870–875.
49. Potten, C.S.; Li, Y.; O'Connor, P.J.; Winton, D. A possible explanation for the differential cancer incidence in the intestine, based on distribution of the cytotoxic effects of carcinogens in the murine large bowel. *Carcinogenesis* **1992**, *13*, 2305–2312.
50. Cordes, C.; Munzel, A.N.N.K.; Rudolph, P.; Hoffmann, M.; Leuschner, I.; Gottschlich, S. Immunohistochemical staining of Ki-67 using the monoclonal antibody Ki-S11 is a prognostic indicator for laryngeal squamous cell carcinoma. *Anticancer Res.* **2009**, *29*, 1459–1465.

Hypoxia Reduces the Efficiency of Elisidepsin by Inhibiting Hydroxylation and Altering the Structure of Lipid Rafts

Anna Király, Tímea Váradi, Tímea Hajdu, Ralph Rühl, Carlos M. Galmarini, János Szöllősi and Peter Nagy

Abstract: The mechanism of action of elisidepsin (PM02734, Irvalec®) is assumed to involve membrane permeabilization via attacking lipid rafts and hydroxylated lipids. Here we investigate the role of hypoxia in the mechanism of action of elisidepsin. Culturing under hypoxic conditions increased the half-maximal inhibitory concentration and decreased the drug's binding to almost all cell lines which was reversed by incubation of cells with 2-hydroxy palmitic acid. The expression of fatty acid 2-hydroxylase was strongly correlated with the efficiency of the drug and inversely correlated with the effect of hypoxia. Number and brightness analysis and fluorescence anisotropy experiments showed that hypoxia decreased the clustering of lipid rafts and altered the structure of the plasma membrane. Although the binding of elisidepsin to the membrane is non-cooperative, its membrane permeabilizing effect is characterized by a Hill coefficient of ~3.3. The latter finding is in agreement with elisidepsin-induced clusters of lipid raft-anchored GFP visualized by confocal microscopy. We propose that the concentration of elisidepsin needs to reach a critical level in the membrane above which elisidepsin induces the disruption of the cell membrane. Testing for tumor hypoxia or the density of hydroxylated lipids could be an interesting strategy to increase the efficiency of elisidepsin.

Reprinted from *Mar. Drugs*. Cite as: Király, A.; Váradi, T.; Hajdu, T.; Rühl, R.; Galmarini, C.M.; Szöllősi, J.; Nagy, P. Hypoxia Reduces the Efficiency of Elisidepsin by Inhibiting Hydroxylation and Altering the Structure of Lipid Rafts. *Mar. Drugs* **2013**, *11*, 4858-4875.

1. Introduction

Although significant progress has been made in the understanding of cancer at the molecular and cellular level, the potency of chemotherapy of advanced malignant tumors is still limited and based on conventional cytotoxic drugs calling for medications with new mechanism of action [1]. Elisidepsin (Irvalec®, PM02734) is a synthetic cyclodepsipeptide closely related to Kahalalide F, a natural antitumor compound isolated from the Hawaiian marine mollusk Elysia rufescens [2–4]. Preclinically, elisidepsin showed antiproliferative activity against a broad spectrum of tumor types [5]. Additionally, elisidepsin has been found to have synergistic effects when combined with several different conventional chemotherapeutic agents and tyrosine kinase inhibitors in cell lines and mouse xenograft models most likely due to its unique mechanism of action [6,7]. In clinical trials, elisidepsin has been shown to have a low toxicity profile [8–11] and preliminary assessment of its clinical efficacy showed interesting results in different solid tumors [8–12].

Although ErbB proteins have been implicated as the target of elisidepsin based on weak correlations between the drug's efficiency and ErbB protein expression levels [6,7,13], we have refuted this hypothesis by showing that the expression of ErbB1, ErbB2 or ErbB3 proteins have no

influence on the sensitivity of cell lines to elisidepsin [14]. According to the most widely accepted view the primary mechanism of action of elisidepsin involves a direct hit on the membrane by binding to lipid rafts [5,14]. Based on experiments with RNA interference-mediated knock-down of fatty acid 2-hydroxylase (FA2H) and incorporation of exogenous hydroxylated fatty acids, 2-hydroxylated sphingolipids have been suggested as the binding site of elisidepsin [15]. It has been postulated that elisidepsin binds to hydroxylated lipids in rafts and induces rapid permeabilization of the cell membrane [14]. All other effects of the drug, including autophagy [16], necrosis [2,13], disruption of lysosomal membranes [17], inhibition of Akt signaling [6,16] and downregulation of ErbB3 expression and activation [13,14], are thought to be secondary effects pursuant to the primary hit on the membrane.

As FA2H, the enzyme thought to be responsible for the generation of the target of elisidepsin [15], is oxygen dependent [18,19] and tumor hypoxia is widespread in advanced tumors [20], we have decided to investigate its role in the mechanism of action of elisidepsin. In the current paper, we show that the sensitivity of cell lines to elisidepsin is proportional to their FA2H level and hypoxia reduces the efficiency of the drug. The effect of hypoxia was reversed by the addition of exogenous hydroxylated fatty acid. Hypoxia was found to induce changes in the organization of lipid rafts. Our results suggest that testing for tumor hypoxia or the density of hydroxylated lipids could potentially increase the efficacy of elisidepsin.

2. Results

2.1. The Elisidepsin Sensitivity of Cell Lines is Reduced under Hypoxic Conditions

We suspected that hypoxia would lead to a diminished synthesis of hydroxylated fatty acids thereby reducing the sensitivity of cells to elisidepsin. In order to test the aforementioned assumption different cell types were cultured under hypoxic conditions for four days followed by testing their elisidepsin sensitivity. Four of the seven investigated cell lines (A431, CHO, HaCaT, HeLa) displayed significantly reduced elisidepsin sensitivity while the other three cell types (MCF-7, MDA-MB-453, SKBR-3) were resistant to the hypoxia-induced effects (Table 1, Supplementary Figure S1). We reasoned that the applied four-day hypoxia may be insufficient to deplete the pool of hydroxylated fatty acids in those cells which did not show any change in elisidepsin sensitivity in conditions of reduced oxygen partial pressure. Therefore, these cell types were cultured under hypoxic conditions for fourteen days followed by testing their elisidepsin sensitivity. Extensive hypoxia slightly increased the IC_{50} values in two of the cell lines (MDA-MB-453, SKBR-3), whereas MCF-7 cells did not show any change under these experimental conditions either (Table 1, Supplementary Figure S2). We conclude that hypoxic conditions generally lead to diminished sensitivity of cells to elisidepsin.

Table 1. Sensitivity of cell lines to elisidepsin under hypoxic and normoxic conditions. Cells plated in 96-well plates were kept under hypoxic conditions for four days or fourteen days followed by elisidepsin treatment. The normoxic control samples were plated one day before adding elisidepsin. Both normoxic and hypoxic cells were treated with the drug for 30 min and allowed to grow for another three days under normoxic and hypoxic conditions. The mean IC_{50} values (±standard error of the mean), determined from three independent measurements, are shown in the table. Two-way ANOVA indicated a significant effect of hypoxia. Pairwise comparisons between normoxic and hypoxic samples were carried out by Tukey's HSD test. * Asterisks indicate significant difference compared to the normoxic values ($p < 0.05$). Representative dose-response curves from which the IC_{50} values were determined are shown in Supplementary Figures S1 and S2 (n. d. = not determined).

Cell lines	IC_{50} (μM)		
	Normoxia	4-day hypoxia	14-day hypoxia
A431	7.8 ± 0.8	15.4 ± 1.8 *	n. d.
CHO	15 ± 0.8	66 ± 9.3 *	n. d.
HaCaT	7.5 ± 0.9	27.6 ± 4.2 *	n. d.
HeLa	9.1 ± 1.2	16.5 ± 1.7 *	n. d.
MCF-7	1.4 ± 0.3	1.6 ± 0.5	1.7 ± 0.6
MDA-MB-453	3.6 ± 0.5	3.9 ± 0.7	6.1 ± 0.5 *
SKBR-3	2.4 ± 0.4	2.3 ± 0.5	5.2 ± 0.2 *

2.2. The Expression of FA2H Correlates with Elisidepsin Sensitivity in Normoxia and Determines the Hypoxia-Induced Increase in the IC_{50} Values

We assumed that the complete absence of hypoxia-induced changes in MCF-7 may be the consequence of the high expression level of FA2H in these cells. Therefore, we measured the expression level of FA2H by fluorescent staining followed by flow cytometry and correlated the fluorescence intensities with the IC_{50} values measured in normoxic conditions (Figure 1A). The IC_{50} values and the expression level of FA2H showed strong negative correlation (Pearson correlation coefficient: −0.9, 95% confidence interval: [−0.96, −0.78], Spearman rank correlation coefficient: −0.86, 95% confidence interval: [−0.94, −0.68]; confidence intervals determined by Fisher's *z*-transform). These results confirmed previous data implying the role of FA2H in determining elisidepsin sensitivity [15]. Next, we compared the magnitude of the hypoxia-induced changes to the expression of FA2H (Figure 1B). The analysis revealed a strong correlation between the parameters (Pearson correlation coefficient: −0.85, 95% confidence interval: [−0.94, −0.66], Spearman rank correlation coefficient: −0.89, 95% confidence interval: [−0.96, −0.75], Figure 1B) indicating that high levels of FA2H (indicative of a higher density of hydroxylated lipids and thus high cytotoxic activity of elisidepsin) counteracts the effect of hypoxia in reducing the sensitivity of cells to the drug.

Figure 1. FA2H expression determines the sensitivity of cell lines to elisidepsin under normoxic conditions and the hypoxia-induced decrease in elisidepsin responsiveness. (**A**) The IC_{50} values shown in Table 1 were correlated with the expression level of FA2H determined by flow cytometry. The means (±standard error of the mean) of three independent measurements are shown; (**B**) The sensitivity of cell lines was determined under normoxic and hypoxic conditions as shown in Table 1. The FA2H expression level is plotted as a function of the ratio of the IC_{50} values determined under hypoxic and normoxic conditions. The means (±standard error of the mean) of three independent measurements are shown.

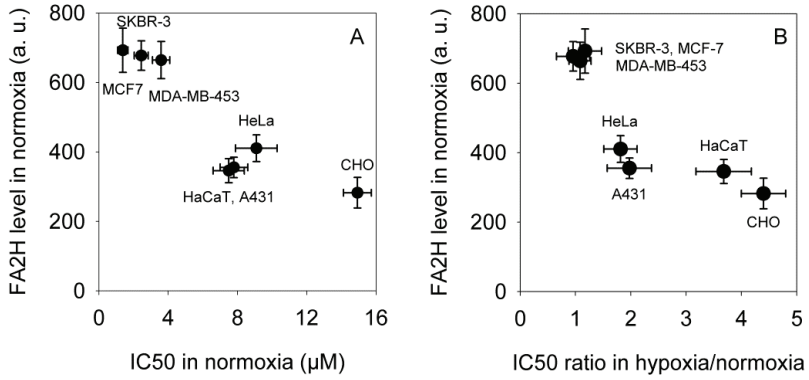

In order to show that hypoxia indeed decreases the amount of the product of FA2H we quantified 2-hydroxy fatty acids in normoxic and hypoxic cells using mass spectrometry. The results showed that culturing cells for four days under hypoxic conditions significantly decreased the amount of 2-hydroxylated palmitic and stearic acids without significantly affecting their 3-hydroxylated counterparts. Representative mass spectrometry tracks are shown in Supplementary Figure S3.

2.3. 2-Hydroxy Palmitic Acid Reverses the Effect of Hypoxia on Elisidepsin Sensitivity

Hypoxia may have resulted in a reduced concentration of hydroxylated fatty acids in the plasma membrane thereby bringing about the observed reduced efficiency of elisidepsin. In order to test the aforementioned assumption hypoxia-responsive cell lines (A431, CHO, HaCaT, HeLa) were incubated in the presence of 2-hydroxy palmitic acid during the last 24 hours of their hypoxic culture followed by testing their elisidepsin sensitivity. Hypoxia reduced the efficiency of elisidepsin compared to normoxia in this series of experiments as well, while 2-hydroxy palmitic acid reversed the hypoxia-induced changes (Table 2, Supplementary Figure S4). We also tested the effect of 3-hydroxy palmitic acid on one of the cell lines (A431), but it could not restore the elisidepsin sensitivity of hypoxic cells (data not shown). This finding is in accordance with the lack of any significant hypoxia-induced change in the levels of 3-hydroxy fatty acids (Supplementary Figure S3). These results imply that 3-hydroxy fatty acids do not play an important role in determining elisidepsin sensitivity. The fact that methanol, the solvent of the hydroxylated fatty

acid, was without any significant effect allowed us to conclude that 2-hydroxy palmitic acid abolishes the effect of hypoxia on the elisidepsin sensitivity of the cell lines tested.

Table 2. The effect of hydroxylated palmitic acid on the sensitivity of cell lines to elisidepsin in hypoxia. Cells plated in 96-well plates were kept under hypoxic conditions for four days. On the third day, they were treated with 100 μM 2-hydroxy palmitic acid (2-OH-PA) or its solvent, methanol (MeOH). The normoxic control samples were plated one day before adding elisidepsin. Both normoxic and hypoxic cells were treated with the drug for 30 min and allowed to grow for another three days under normoxic and hypoxic conditions. The mean IC_{50} values (±standard error of the mean), determined from three independent measurements, are shown in the table. Representative dose-response curves from which the IC_{50} values were determined are shown in Supplementary Figure S4.

Cell lines	IC_{50} (μM)			
	Normoxia	Hypoxia	MeOH in hypoxia	2-OH-PA in hypoxia
A431	9.0 ± 1.7	17.9 ± 2.8	15.6 ± 3.1	7.75 ± 2.0
CHO	15.6 ± 2.1	34.6 ± 4.7	38.9 ± 5.3	12.3 ± 2.4
HaCaT	7.6 ± 1.9	18.7 ± 2.5	16.4 ± 2.8	9.5 ± 1.7
HeLa	9.4 ± 1.0	21.0 ± 3.3	19.0 ± 2.4	10.1 ± 1.8

2.4. Hypoxia Reduces the Binding of Fluorescent Elisidepsin

The results presented so far imply that hypoxia leads to diminished binding of elisidepsin to the cell membrane. In order to test this idea normoxic and hypoxic A431 cells were incubated in the presence of a 1:4 mixture of fluorescent and unlabeled elisidepsin for 2 min followed by removal of unbound elisidepsin and confocal microscopy. Dilution of fluorescent and non-fluorescent elisidepsin was necessary since it has been shown previously that fluorescent elisidepsin displays vague or no fluorescence in the membrane in the absence of unlabeled drug molecules most likely due to the formation of clusters and fluorescence quenching [5]. The fluorescence intensity was evaluated in the membrane after image segmentation showing a significant reduction in the binding of elisidepsin by hypoxia (mean fluorescence intensity in normoxic cells: 79 ± 7, in hypoxic cells: 27 ± 5; p = 0.0002; Figure 2A). Since generation of statistically reliable data is more straightforward in flow cytometry, we repeated the binding experiment using this technique. Elisidepsin binds to cells and is internalized very rapidly [14], therefore fluorescence intensities reported by the flow cytometer do not represent the amount of membrane-bound drug. In order to get around this problem we developed an approach to measure the kinetics of binding of fluorescent elisidepsin to the cells (see Supplementary Materials and Methods for details). According to this model, the very first part of the curve represents membrane-bound elisidepsin without significant contribution from the intracellular space. The slope of the initial part of the curve was shown to be proportional to the amount of membrane-bound elisidepsin. We compared the uptake of fluorescent elisidepsin in a panel of seven cell lines and calculated the fold-reduction induced by hypoxia, which was correlated with the IC_{50} values observed under normoxic

conditions (Figure 2B). According to this analysis, hypoxia significantly reduced the binding of elisidepsin in those cell lines (A431, CHO, HaCaT, HeLa) whose IC_{50} values were increased under hypoxic conditions. The hypoxia-induced reduction in elisidepsin binding displayed a negative correlation with the normoxic IC_{50} values. We can conclude that the hypoxia-induced reduction in elisidepsin sensitivity is caused by reduced binding of the drug to the cell membrane under hypoxic conditions.

Figure 2. The binding of fluorescent elisidepsin is reduced by hypoxia. (**A**) A431 cells kept under hypoxic conditions for four days and their normoxic counterparts were labeled with a mixture of elisidepsin containing OregonGreen488-conjugated and unlabeled elisidepsin at a molar ratio of 1:4 for two min followed by washing and confocal microscopy in five min. The total concentration of elisidepsin was 2 µM, approximately 5-times smaller than the IC_{50} of A431 cells. The fluorescence intensity was evaluated in the membrane mask determined by manually-seeded watershed transformation after subtracting the background determined in a cell-free area of an image; (**B**) A mixture of OregonGreen488-elisidepsin and unlabeled elisidepsin (molar ratio of 1:4) was added to the cell suspension and the fluorescence intensity was immediately measured by flow cytometry. The total concentration of elisidepsin was 0.5 µM. The slope of cell-bound elisidepsin fluorescence intensity as a function of time was estimated in the first ~30 s of uptake and the relative reduction of the rate of elisidepsin binding in hypoxia is plotted against the IC_{50} of elisidepsin in normoxia (mean ± standard error of the mean, $n = 3$).

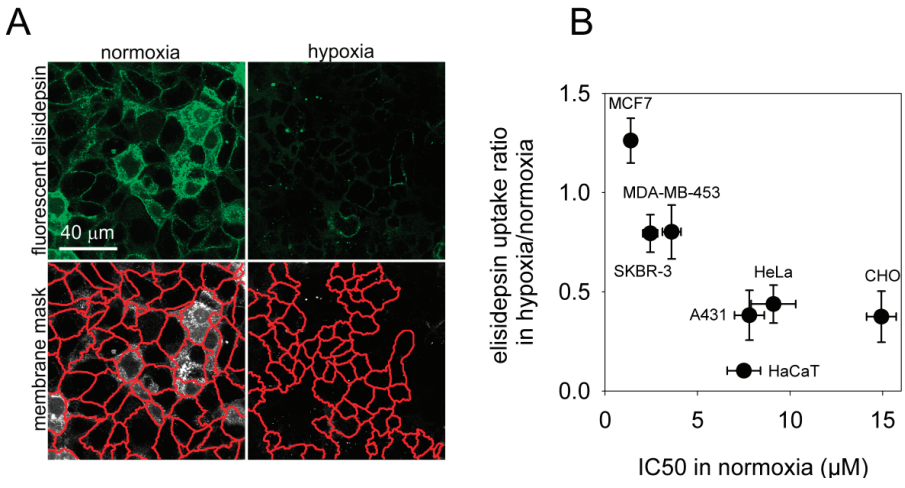

2.5. Elisidepsin Induces Clustering of GPI-Anchored GFP

All of the current results and evidence presented elsewhere [5,14,15] point at elisidepsin binding to the membrane, more specifically to lipid rafts. Therefore, we wanted to investigate the effect of elisidepsin on the distribution of lipid rafts in the membrane. To this aim, normoxic and hypoxic

A431 cells were transfected with GPI-anchored GFP (GFP-GPI) followed by elisidepsin treatment in two days. The fluorescence of GFP-GPI was unevenly distributed in the membrane of both normoxic and hypoxic cells. Elisidepsin treatment induced the formation of bright fluorescent spots in normoxic cells while it was without any significant effect in hypoxic cells (Figure 3A). The number of bright fluorescent clusters, enumerated by an algorithm, was shown to be significantly higher in elisidepsin-treated normoxic cells than under other conditions (two-way ANOVA followed by Tukey's HSD test, $p < 0.01$). Next, we incubated GFP-GPI-transfected cells in the presence of a fluorescent analog of elisidepsin for two min followed by determining the colocalization between the two fluorescent signals. Quantitative analysis revealed a strong correlation between the distribution of GFP-GPI and elisidepsin (Figure 3B, correlation coefficient = 0.92, 95% confidence interval = [0.78,0.97]).

Figure 3. Elisidepsin induces the clustering of GPI-anchored GFP. (**A**) A431 cells were kept under hypoxic conditions for two days followed by transfection with GFP-GPI and another two days in hypoxia. Control normoxic cells were also transfected with GFP-GPI and kept under normoxic conditions for another two days. Confocal microscopic images were taken before and after treating the cells with 10 μM elisidepsin for five min. The representative images show the membrane adjacent to the coverslip. The insert in the lower left panel displays another normoxic cell treated with elisidepsin. Numbers in the lower right corner of images represent the mean (±standard error of the mean) number of bright fluorescent spots in an image determined from six images; (**B**) Normoxic A431 cells transfected with GFP-GPI were labeled with 2 μM elisidepsin containing AlexaFluor555-tagged and unlabeled elisidepsin at a molar ratio of 1:4 for two min followed by washing twice. Confocal microscopic images taken five min after the washing in the GFP and AlexaFluor555 channels and their overlay (green–GFP-GPI; red–elisidepsin) are shown in the figure.

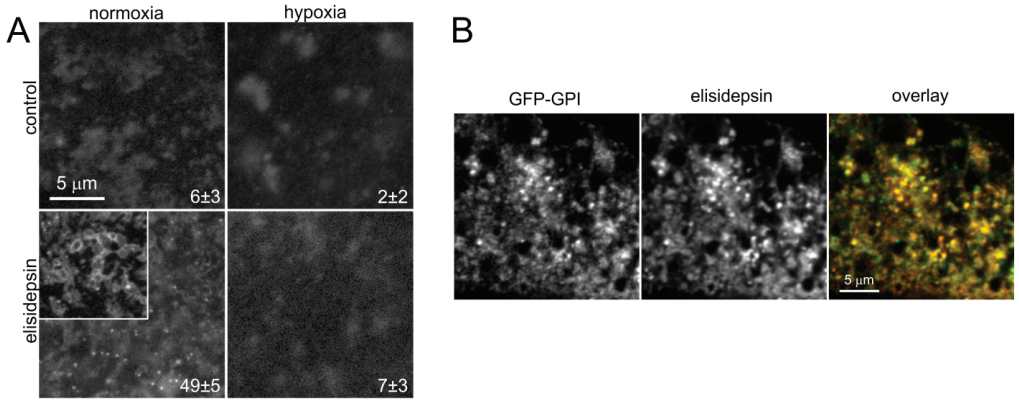

Since we observed binding of fluorescent elisidepsin at concentrations that did not induce any killing, we systematically analyzed the reason for this discrepancy. As the IC_{50} of fluorescent elisidepsin was found to be identical to that of the unconjugated drug within experimental error

(IC_{50} of unconjugated drug in A431 cells: 8.8 ± 1.6 µM, fluorescent analog: 9.2 ± 1.8 µM; $p > 0.1$), we compared the concentration dependence of killing and the binding of fluorescent elisidepsin. Killing was quantitated as the fraction of propidium iodide-positive cells and binding of fluorescent elisidepsin was determined in the membrane. The curves were fitted separately allowing for different half-maximal effective or inhibitory concentrations (K_d of binding and IC_{50} for killing) and Hill coefficients. The K_d of binding turned out to be 5.1 µM, whereas the IC_{50} value was found to be 10.2 µM in agreement with previous analyses. As opposed to the binding of fluorescent elisidepsin, which was non-cooperative characterized by a Hill coefficient of 1.1, the killing curve was fitted with an equation with a Hill coefficient of 3.2 (Figure 4, Supplementary Figure S5). These observations support the assumption that elisidepsin undergoes oligomerization in the membrane accompanied by increased clustering of lipid raft-associated proteins.

Figure 4. Difference in the concentration dependence of the binding and killing effect of elisidepsin. A431 cells were treated with six different concentrations of elisidepsin containing OregonGreen488-elisidepsin and unlabeled elisidepsin mixed at a molar ratio of 1:4 in the presence of 10 µg/mL propidium iodide. After a 20-min treatment, cells were washed and imaged using confocal microscopy. The background-corrected fluorescence intensity of membrane-bound elisidepsin (triangles) and the fraction of propidium iodide-positive cells (circles) were determined and plotted as a function of elisidepsin concentration. Error bars represent the standard error of the mean. The continuous lines are fits of the Hill equation to the measurement points. A representative image series is shown in Supplementary Figure S5.

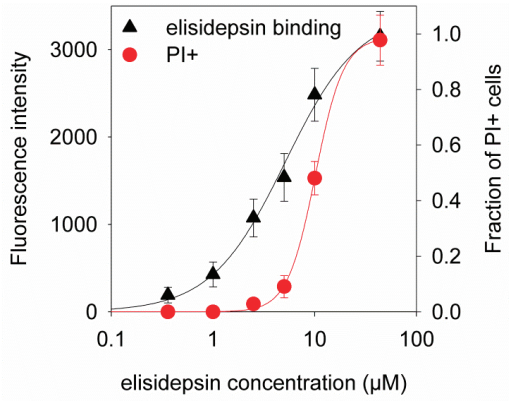

2.6. Hypoxia Decreases the Clustering of Lipid Rafts and Induces Changes in the Fluidity and Compactness of the Membrane

Results presented in the previous sections imply that elisidepsin alters the distribution and clustering of lipid rafts. In order to test this hypothesis directly we carried out N&B analysis to determine the mean number of GPI-GFP molecules in a cluster. We did not find any significant difference between the molecular brightness of GPI-GFP in elisidepsin-treated and control cells

implying that the drug did not significantly change the average number of GPI-GFP molecules per cluster (Figure 5).

Hypoxia is expected to decrease the amount of hydroxylated lipids in the membrane thereby reducing the number of hydrogen bond donors and acceptors, which may cause measurable changes in the clustering of membrane proteins as well as in the fluidity and compactness of the membrane. According to N&B analysis carried out on GPI-GFP-transfected normoxic and hypoxic A431 cells the molecular brightness of GPI-GFP was indicative of molecular dimers in normoxic cells while a pure monomeric population was present in hypoxic cells (Figure 5). Since our previous results pointed at an effect of elisidepsin on the structure of the plasma membrane [14], we analyzed whether hypoxia modifies the fluidity and compactness of the membrane. Both the viscosity (measured by fluorescence anisotropy) and the order (measured by the generalized polarization of Laurdan) of the plasma membrane increased in A431 cells cultured under hypoxic conditions for four days, while there was no change in these parameters in SKBR-3 cells which did not show any alteration in elisidepsin sensitivity after four days of hypoxia either (Supplementary Figure S6). These results imply that hypoxia is associated with alterations in the structure of the membrane and the clustering of lipid raft-associated proteins.

Figure 5. (**A**) A431 cells were cultured under normoxic conditions or kept in a hypoxic atmosphere for four days. Both normoxic and hypoxic cells were transfected with GPI-anchored GFP two days before N&B analysis using confocal microscopy. Cells were left untreated or incubated in the presence of 10 µg/mL elisidepsin for three min. The molecular brightness of GPI-GFP (mean ± standard error of the mean), determined from ten cells, is shown in the graph. Asterisks indicate a significant difference between normoxic and hypoxic cells ($p < 0.05$, ANOVA followed by Tukey's HSD test). The molecular brightness of monomeric soluble GFP is shown as a reference; (**B**) Representative brightness curves of pixels in normoxic (blue) and hypoxic (red) cells and in a sample containing soluble monomeric GFP (black).

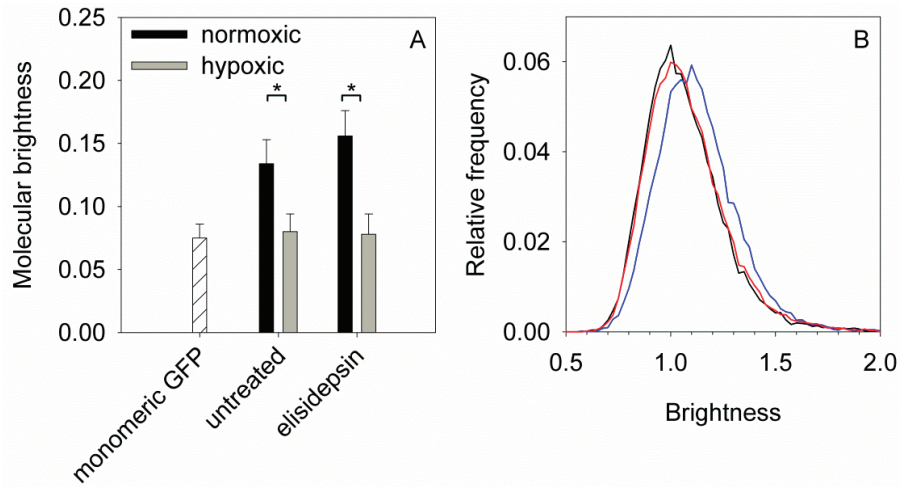

3. Discussion

The results presented in the paper reveal insight into the mechanism of action of elisidepsin which can be summarized in the following three points: (a) elisidepsin binds to lipid rafts; (b) elisidepsin induces oligomerization of lipid rafts detected in confocal microscopic images and also supported by the fact that elisidepsin-induced membrane permeabilization is characterized by a Hill coefficient of 3–4 while its binding follows a non-cooperative concentration dependence; (c) hypoxia reduces the efficiency of elisidepsin by decreasing its binding to the membrane.

Our results implying the formation of elisidepsin oligomers are in accordance with previous fluorescence resonance energy transfer (FRET) experiments [5]. Here we not only present evidence for the formation of elisidepsin oligomers, but also for elisidepsin-lipid raft interactions and elisidepsin-induced raft clustering. Similar to membrane permeabilization elisidepsin-induced raft associations were induced rapidly, within five min of elisidepsin application followed by the internalization of lipid rafts in 30 min shown in a previous publication [14]. We failed to detect elisidepsin-induced oligomerization of lipid rafts by N&B experiments. We suspect that clusters of GPI-anchored, raft-associated proteins occupy only a small fraction of pixels; therefore, their contribution to the average molecular brightness is negligible. Since they are not immobile for the whole duration of a N&B experiment, they cannot be resolved as pixels with a different molecular brightness either.

Based on the key findings of the paper we propose a model in which elisidepsin binds in a non-cooperative fashion to membrane regions enriched in hydroxylated lipids followed by oligomerization and membrane permeabilization. It was further assumed that elisidepsin oligomers generate the pores responsible for membrane permeabilization and their concentration has to reach a threshold so that necrosis takes place. A quantitative elaboration of the model, provided as Supplementary material, shows that cooperativity in the dose dependence of cell death is the consequence of attributing membrane permeabilization to elisidepsin oligomers [21]. Quantitative predictions of the model which are in accordance with our experimental observations are: (a) elisidepsin binds to the membrane at much lower concentrations than expected based on the killing curves; (b) membrane permeabilization takes place in a narrow concentration range characterized by high cooperativity; (c) the lower the number of elisidepsin binding sites (e.g., in hypoxia or in cells with low FA2H expression), the higher the free concentration of the drug has to be so that the concentration of elisidepsin oligomers in the membrane reaches the critical level; (d) a certain fold-reduction in the number of elisidepsin binding sites results in negligible changes in the IC_{50} if the original number of bindings sites was much higher than the critical level, while the same fold-decrease causes substantial increase in the IC_{50} if the original number of binding sites was close to the critical level (Supplementary Figure S7).

Several lines of evidence support the conclusion that the presence of a membrane environment enriched in hydroxylated lipids is necessary for the binding of elisidepsin: (a) FA2H expression level correlates with elisidepsin sensitivity; (b) hypoxia reduces the efficiency of elisidepsin which is reversed by 2-hydroxy palmitic acid; (c) FA2H expression predicts how much hypoxia increases the IC_{50} of elisidepsin. The last statement can be rationalized by the proposed model since highly

expressed FA2H generates more “elisidepsin-friendly” plasma membrane requiring more pronounced hypoxia to reduce the amount of hydroxylated lipids to a level close to the critical concentration. Our results about the role of FA2H in determining elisidepsin sensitivity are in agreement with previous findings [15]. The fact that hydroxylated lipids are primarily present in lipid rafts explains that elisidepsin binds to these membrane microdomains [22]. It has recently been shown that FA2H specifically generates the R-stereoisomer of fatty acids and only the R-enantiomer is able to reverse the effect of FA2H knock-down on membrane viscosity [23]. These findings can be rationalized by the fact that (*S*)-hydroxy fatty acids preferentially form intramolecular hydrogen bonds, while the *R*-stereoisomer is usually involved in intermolecular hydrogen bonds. Therefore, we expect that the (*R*)-2-hydroxy palmitic acid component of the racemic mixture used in our experiments was responsible for restoring the effect of elisidepsin in hypoxic cells.

Hypoxia was found to change the clustering of lipid rafts and the dynamic properties of the cell membrane. Although decreased hydrogen bonding resulting from inhibited hydroxylation is expected to increase membrane fluidity [22], hypoxia decreased the fluidity of the plasma membrane and increased its compactness shown by decreased hydration of Laurdan. These findings are in agreement with previous results showing that hypoxia-induced lipid peroxidation results in decreased membrane fluidity [24,25]. Decreased clustering of GPI-anchored proteins in hypoxic cells may be the consequence of decreased hydrogen bonding or increased viscosity which has been shown to be associated with decreased protein clustering [26].

Lipid hydroxylation is important for the stability of the cell membrane, lipid rafts, myelin sheaths and cornified epithelia [18,22]. The role of FA2H-mediated lipid hydroxylation in maintaining the integrity of certain membranes is supported by observations linking the loss of FA2H expression to late-onset demyelination [27,28]. Cancer cells display characteristic changes in their fatty acid and ganglioside composition [29–31]. An increase in the ratio of saturated/non-saturated fatty acids and accumulation of less-complex gangliosides have been observed. In addition, upregulation of FA2H in malignant tumors has been reported which may lead to cancer specific cytotoxic effects of elisidepsin [18,31]. However, tumor hypoxia is known to decrease the rate of hydroxylation due to shortage of oxygen, which acts against the tumor-specificity of elisidepsin by reducing the activity of FA2H [31]. The balance between hypoxia-induced increased FA2H expression and its decreased catalytic activity due to oxygen shortage is unpredictable, but these parameters must be predictive of the sensitivity of tumors to elisidepsin. Although tumor hypoxia is readily detectable *in vivo* [20,32], FA2H expression and the amount of 2-hydroxy fatty acids in the membrane are not amenable to clinical investigations and none of these parameters is routinely measured in clinical practice. But future clinical trials could define the true potential of this drug with a unique mechanism of action in the treatment of human cancer.

4. Experimental Section

4.1. Cell Culture and Transfection

SKBR-3, HeLa, A431, MCF-7, MDA-MB-453 and CHO cells were obtained from the American Type Culture Collection (ATCC, Manassas, VA, USA) and grown according to their specifications. The immortalized human keratinocyte cell line HaCaT was obtained from the Department of Physiology, University of Debrecen, and cultured in DMEM supplemented with 10% FCS and antibiotics. For generating hypoxic conditions cells plated in a flask or chambered coverglass were kept in a modular hypoxia chamber (Billups-Rothenberg, Del Mar, CA, USA) flushed with a gas mixture containing 1% O_2, 5% CO_2 and 94% N_2 (Linde, Munich, Germany) at a rate of 25 L/min for 4 min. During 4-day hypoxic culturing the cells were not harvested, but they were harvested and split when reaching confluency during 2-week hypoxic culturing. The GFP-GPI plasmid was a kind gift from Jennifer Lippincott-Schwartz (NIH, Bethesda, MD, USA). Cells were transfected with the Amaxa Nucleofector device (Lonza, Basel, Switzerland). The transfection solution and the program were selected according to the "Cell & Transfection Database" of the manufacturer.

4.2. Antibodies and Chemicals

The polyclonal antibody against fatty acid 2-hydroxylase (sc161045) and the blocking peptide (sc161045-P) were purchased from Santa Cruz (Santa Cruz, CA, USA). 2-hydroxy and 3-hydroxy palmitic acid were from Sigma-Aldrich (St. Louis, MO, USA). 4′-(trimethylammonio)-diphenylhexatriene (TMA-DPH) and Laurdan (6-dodecanoyl-*N*,*N*-dimethyl-2-naphthylamine) were purchased from Sigma-Aldrich. Elisidepsin was manufactured by PharmaMar (Madrid, Spain) and dissolved in dimethyl sulfoxide at a concentration of 1 mg/mL.

4.3. Determination of Elisidepsin Sensitivity

Cells were plated into 96-well plates 24 h before the experiment carried out under normoxic conditions or were kept in hypoxia for 96 h. They were treated with a dilution series of elisidepsin for 30 min in triplicate followed by incubation for 72 h in cell culture medium in a CO_2 incubator at 37 °C. The viability of cells was determined by measuring the absorbance of WST-1 reagent (Roche Diagnostics GmbH, Mannheim, Germany) with an ELISA reader at 450 nm and 620 nm. The IC_{50} value was determined by fitting the Hill equation to the measurement data using Matlab (Mathworks Inc., Natick, MA, USA).

4.4. Flow Cytometric Measurement of Fatty Acid 2-Hydroxylase Expression

Cells were fixed with 3.7% formaldehyde for 30 min on ice followed by washing and labeling with a polyclonal antibody against fatty acid 2-hyroxylase (FA2H) dissolved in PBS containing 0.1% BSA and 0.1% Triton X-100 for 30 min. Unbound antibodies were removed by washing twice in PBS followed by staining with fluorescent secondary antibody. The fluorescence intensity

was measured with a FacsArray flow cytometer (Becton Dickinson, Franklin Lakes, NJ, USA). Evaluation was performed with FCS Express (De Novo Software, Los Angeles, CA, USA) and the FA2H levels are reported as the mean intensity of the sample labeled by the primary and the secondary antibodies corrected by subtracting the mean fluorescence intensity of the sample, which was also incubated with the blocking peptide.

4.5. Confocal Microscopy

An Olympus FV1000 confocal microscope was used to acquire images using a 60× oil immersion objective (NA = 1.35). GFP-GPI and OregonGreen488 were excited at 488 nm and their emission was measured above 510 nm when the sample was not labeled by any other dye. It was essential to increase the lower cutoff value of the detected emission wavelength range from the default value of 500 nm due to strong light scattering from the glass surface when the membrane adjacent to the coverslip was imaged. AlexaFluor555 was excited at 543 nm and detected above 555 nm. When GFP-GPI and AlexaFluor555 were both present in the sample, the fluorescence of GFP was detected in the spectral region of 510–540 nm. For dual imaging of OregonGreen488-elisidepsin and propidium iodide they were excited at 488 and 543 nm, respectively. The fluorescence of OregonGreen488 was detected in the spectral region of 520 ± 15 nm, whereas propidium iodide was measured at 620 ± 50 nm. Image analysis was carried out with DipImage (Delft University of Technology, Delft, The Netherlands) in a Matlab environment. For quantitative evaluation of membrane-associated fluorescence intensity the cell membrane was identified with the manually-seeded watershed algorithm [33,34] and the mean background corrected fluorescence intensity was calculated. The background was measured in a cell-free area of images. In order to count the number of localized bright spots images were smoothed with a Gauss filter and normalized to their maximum intensity followed by top-hat filtering to remove objects larger than the observed spots. Local maxima were identified by the extended maxima transform followed by filling the holes and shrinking the spots to single points which were enumerated.

4.6. Determination of the Binding of Fluorescent Elisidepsin to the Membrane

For confocal microscopic measurements cells, cultured on chambered coverglass, were labeled with a mixture containing fluorescent and unlabeled elisidepsin at a molar ratio of 1:4 for 20 min in the presence of 10 μg/mL propidium iodide followed by washing to remove unbound elisidepsin. For flow cytometry trypsinized cells were labeled with the same mixture of elisidepsin and measured immediately without washing using a FacsAria instrument (Becton Dickinson). Fluorescent elisidepsin was prepared by labeling the drug with OregonGreen488 or AlexaFluor555 (both from Invitrogen, Carslbad, CA, USA) according to the manufacturer's specifications. Details of the data analysis are described in Supplementary Materials and Methods (Supplementary Figures S8 and S9).

4.7. Number and Brightness (N&B) Analysis of Cells Transfected by GFP-GPI

An Olympus FV1000 confocal microscope running in pseudo photon-counting mode was used to carry out N&B analysis according to Digman *et al*. [35]. Live cells were analyzed at room temperature in Tyrode's buffer with 10 mM glucose and 0.1% BSA. Image series of 100 optical slices of the cell membrane adjacent to the coverslip were acquired with a pixel size of 82 nm and pixel dwell time of 10 µs. A single image consisted of 256 × 256 pixels and the central part of images was used for analysis to eliminate artifacts arising from scanner speed nonlinearity at the borders. The image stack was analyzed with a custom-written Matlab program incorporating functions of the DipImage toolbox. The images were first registered (*i.e*., corrected for lateral shift) followed by calculating the mean and variance of every pixel. The apparent brightness was calculated according to the following equation:

$$B = \frac{\sigma^2}{\langle k \rangle} = \varepsilon + 1 \tag{1}$$

where σ^2 and $\langle k \rangle$ are the variance and the mean, respectively, of a given pixel. The molecular brightness (ε) characterizes the clustering state of a fluorescent molecule by giving the number of photons detected from a single diffusing unit during the pixel dwell time. If the image mean decreased by more than 10% due to stage shift or photobleaching or if the pixel variance did not converge to zero with increasing stack size, the stack was discarded.

4.8. Measurement of Fluorescence Anisotropy and Generalized Polarization

Trypsinized cells were resuspended in Hank's buffer at a concentration of 10^7/mL and labeled with 2 µM TMA-DPH or 2.5 µM Laurdan at room temperature for 20 min. After TMA-DPH labeling cells were diluted in Hank's buffer without washing to a concentration of 10^6/mL for fluorescence anisotropy measurements, whereas Laurdan-labeled cells were washed once and resuspended at a concentration of 10^6/mL in Hank's buffer. Fluorescence measurements were carried out with a Fluorolog-3 spectrofluorimeter (Horiba Jobin Yvon, Edison, NJ, USA). The temperature of the cuvette holder was adjusted to 37 °C by a circulating water bath. TMA-DPH was excited at 352 nm and its emission was measured at 430 nm. The fluorescence anisotropy (r) of TMA-DPH was measured in the L-format according to the following formula [36,37]:

$$r = \frac{I_{vv} - GI_{vh}}{I_{vv} + 2GI_{vh}} \tag{2}$$

where I_{vv} and I_{vh} are the vertical and horizontal components, respectively, of the fluorescence excited by vertically polarized light, and G is a correction factor characterizing the different sensitivity of the detection system for vertically and horizontally polarized light.

Laurdan was excited at 350 nm and its emission was detected in the blue range of its emission spectrum at 435 nm (I_{blue}) and at the red edge at 500 nm (I_{red}). Generalized polarization (GP) of Laurdan fluorescence was calculated according to the following formula [38–40]:

$$GP = \frac{I_{blue} - I_{red}}{I_{blue} + I_{red}} \quad (3)$$

4.9. Determination of 2-Hydroxylated Fatty Acids Using Mass Spectrometry

We used an existing high performance liquid chromatography/mass spectrometry/mass spectrometry (HPLC MS-MS) configuration similar to that already published [41,42]. The separation using HPLC was performed in a manner similar to what has been reported previously [41]. For the detection of 2-hydroxy-palmitate, 3-hydroxy-palmitate and 2-hydroxy-stearate (all chemical reference standards were from Sigma-Aldrich) we established a specific MS-MS method using ESI (−) setting with 271 → 271 *m/z* for 2/3-hydroxy-palmitate with a collision energy of 5 V, a dwell time of 0.1 s and 299 → 299 *m/z* for 2/3-hydroxy-stearate with a collision energy of 5 V, a dwell time of 0.1 s and a cone voltage of 50 V in each case as parameters for multiple reaction monitoring (MRM) measurements.

5. Conclusions

In summary, we have shown that the necrotic effect of elisidepsin is highly cooperative which is most likely explained by membrane permeabilization resulting from elisidepsin oligomers. Moreover, we have shown that hypoxia significantly inhibits the anti-tumor effect of elisidepsin in some experimental models, apparently by reducing the level of 2-hydroxy lipids in the membrane of tumor cells. Our results identify tumor hypoxia and the density of 2-hydroxy lipids as factors predicting elisidepsin sensitivity.

Acknowledgments

This work was supported by the Hungarian Scientific Research Fund (K103906, NK101337); the European Union and the European Social Fund (TÁMOP-4.2.2.A-11/1/KONV-2012-0025).

Conflicts of Interest

One of the authors, Carlos M. Galmarini, is a shareholder of Pharmamar, the producer of the drug investigated in the study.

References

1. Albreht, T.; McKee, M.; Alexe, D.M.; Coleman, M.P.; Martin-Moreno, J.M. Making progress against cancer in europe in 2008. *Eur. J. Cancer* **2008**, *44*, 1451–1456.
2. Suarez, Y.; Gonzalez, L.; Cuadrado, A.; Berciano, M.; Lafarga, M.; Munoz, A. Kahalalide f, a new marine-derived compound, induces oncosis in human prostate and breast cancer cells. *Mol. Cancer Ther.* **2003**, *2*, 863–872.
3. Faircloth, G.; Cuevas, C. Kahalalide f and es285: Potent anticancer agents from marine molluscs. *Prog. Mol. Subcell Biol.* **2006**, *43*, 363–379.

4. Provencio, M.; Sanchez, A.; Gasent, J.; Gomez, P.; Rosell, R. Cancer treatments: Can we find treasures at the bottom of the sea? *Clin*. *Lung Cancer* **2009**, *10*, 295–300.
5. Molina-Guijarro, J.M.; Macias, A.; Garcia, C.; Munoz, E.; Garcia-Fernandez, L.F.; David, M.; Nunez, L.; Martinez-Leal, J.F.; Moneo, V.; Cuevas, C.; *et al*. Irvalec inserts into the plasma membrane causing rapid loss of integrity and necrotic cell death in tumor cells. *PLoS One* **2011**, *6*, e19042.
6. Ling, Y.H.; Aracil, M.; Jimeno, J.; Perez-Soler, R.; Zou, Y. Molecular pharmacodynamics of pm02734 (elisidepsin) as single agent and in combination with erlotinib; synergistic activity in human non-small cell lung cancer cell lines and xenograft models. *Eur*. *J*. *Cancer* **2009**, *45*, 1855–1864.
7. Teixido, C.; Arguelaguet, E.; Pons, B.; Aracil, M.; Jimeno, J.; Somoza, R.; Mares, R.; Ramon, Y.C.S.; Hernandez-Losa, J. Erbb3 expression predicts sensitivity to elisidepsin treatment: *In vitro* synergism with cisplatin, paclitaxel and gemcitabine in lung, breast and colon cancer cell lines. *Int*. *J*. *Oncol*. **2012**, *41*, 317–324.
8. Martin-Algarra, S.; Espinosa, E.; Rubio, J.; Lopez Lopez, J.J.; Manzano, J.L.; Carrion, L.A.; Plazaola, A.; Tanovic, A.; Paz-Ares, L. Phase ii study of weekly kahalalide f in patients with advanced malignant melanoma. *Eur*. *J*. *Cancer* **2009**, *45*, 732–735.
9. Pardo, B.; Paz-Ares, L.; Tabernero, J.; Ciruelos, E.; Garcia, M.; Salazar, R.; Lopez, A.; Blanco, M.; Nieto, A.; Jimeno, J.; *et al*. Phase i clinical and pharmacokinetic study of kahalalide f administered weekly as a 1-hour infusion to patients with advanced solid tumors. *Clin*. *Cancer Res*. **2008**, *14*, 1116–1123.
10. Rademaker-Lakhai, J.M.; Horenblas, S.; Meinhardt, W.; Stokvis, E.; de Reijke, T.M.; Jimeno, J.M.; Lopez-Lazaro, L.; Lopez Martin, J.A.; Beijnen, J.H.; Schellens, J.H. Phase i clinical and pharmacokinetic study of kahalalide f in patients with advanced androgen refractory prostate cancer. *Clin*. *Cancer Res*. **2005**, *11*, 1854–1862.
11. Salazar, R.; Jones, R.J.; Oaknin, A.; Crawford, D.; Cuadra, C.; Hopkins, C.; Gil, M.; Coronado, C.; Soto-Matos, A.; Cullell-Young, M.; *et al*. A phase i and pharmacokinetic study of elisidepsin (pm02734) in patients with advanced solid tumors. *Cancer Chemother*. *Pharmacol*. **2012**, *70*, 673–681.
12. Salazar, R.; Cuadra, C.; Gil-Martin, M.; Vandermeeren, A.; Alfaro, V.; Coronado, C. Complete and sustained objective response per recist to irvalec (pm02734) in undifferentiated large cell esophageal adenocarcinoma: A case report and a review of the literature. *Case Rep*. *Oncol*. **2012**, *5*, 354–358.
13. Janmaat, M.L.; Rodriguez, J.A.; Jimeno, J.; Kruyt, F.A.; Giaccone, G. Kahalalide f induces necrosis-like cell death that involves depletion of erbb3 and inhibition of akt signaling. *Mol*. *Pharmacol*. **2005**, *68*, 502–510.
14. Váradi, T.; Roszik, J.; Lisboa, D.; Vereb, G.; Molina-Guijarro, J.M.; Galmarini, C.M.; Szöllősi, J.; Nagy, P. Erbb protein modifications are secondary to severe cell membrane alterations induced by elisidepsin treatment. *Eur*. *J*. *Pharmacol*. **2011**, *667*, 91–99.

15. Herrero, A.B.; Astudillo, A.M.; Balboa, M.A.; Cuevas, C.; Balsinde, J.; Moreno, S. Levels of scs7/fa2h-mediated fatty acid 2-hydroxylation determine the sensitivity of cells to antitumor pm02734. *Cancer Res*. **2008**, *68*, 9779–9787.
16. Ling, Y.H.; Aracil, M.; Zou, Y.; Yuan, Z.; Lu, B.; Jimeno, J.; Cuervo, A.M.; Perez-Soler, R. Pm02734 (elisidepsin) induces caspase-independent cell death associated with features of autophagy, inhibition of the akt/mtor signaling pathway, and activation of death-associated protein kinase. *Clin*. *Cancer Res*. **2011**, *17*, 5353–5366.
17. Garcia-Rocha, M.; Bonay, P.; Avila, J. The antitumoral compound kahalalide f acts on cell lysosomes. *Cancer Lett*. **1996**, *99*, 43–50.
18. Hama, H. Fatty acid 2-hydroxylation in mammalian sphingolipid biology. *Biochim*. *Biophys*. *Acta* **2010**, *1801*, 405–414.
19. Hoshi, M.; Kishimoto, Y. Synthesis of cerebronic acid from lignoceric acid by rat brain preparation. Some properties and distribution of the -hydroxylation system. *J*. *Biol*. *Chem*. **1973**, *248*, 4123–4130.
20. Davda, S.; Bezabeh, T. Advances in methods for assessing tumor hypoxia *in vivo*: Implications for treatment planning. *Cancer Metastasis Rev*. **2006**, *25*, 469–480.
21. Goldstein, R.F.; Stryer, L. Cooperative polymerization reactions. Analytical approximations, numerical examples, and experimental strategy. *Biophys*. *J*. **1986**, *50*, 583–599.
22. Guo, L.; Zhou, D.; Pryse, K.M.; Okunade, A.L.; Su, X. Fatty acid 2-hydroxylase mediates diffusional mobility of raft-associated lipids, glut4 level, and lipogenesis in 3t3-l1 adipocytes. *J*. *Biol*. *Chem*. **2010**, *285*, 25438–25447.
23. Guo, L.; Zhang, X.; Zhou, D.; Okunade, A.L.; Su, X. Stereospecificity of fatty acid 2-hydroxylase and differential functions of 2-hydroxy fatty acid enantiomers. *J*. *Lipid Res*. **2012**, *53*, 1327–1335.
24. Behn, C.; Araneda, O.F.; Llanos, A.J.; Celedon, G.; Gonzalez, G. Hypoxia-related lipid peroxidation: Evidences, implications and approaches. *Respir*. *Physiol*. *Neurobiol*. **2007**, *158*, 143–150.
25. Bagchi, M.; Prasad, M.R.; Engelman, R.M.; Das, D.K. Effects of free radicals on the fluidity of myocardial membranes. *Free Radic*. *Res*. *Commun*. **1989**, *7*, 375–380.
26. Park, J.S.; Jung, T.S.; Noh, Y.H.; Kim, W.S.; Park, W.I.; Kim, Y.S.; Chung, I.K.; Sohn, U.D.; Bae, S.K.; Bae, M.K.; *et al*. The effect of lidocaine. Hcl on the fluidity of native and model membrane lipid bilayers. *Korean J*. *Physiol*. *Pharmacol*. **2012**, *16*, 413–422.
27. Edvardson, S.; Hama, H.; Shaag, A.; Gomori, J.M.; Berger, I.; Soffer, D.; Korman, S.H.; Taustein, I.; Saada, A.; Elpeleg, O. Mutations in the fatty acid 2-hydroxylase gene are associated with leukodystrophy with spastic paraparesis and dystonia. *Am*. *J*. *Hum*. *Genet*. **2008**, *83*, 643–648.
28. Zoller, I.; Meixner, M.; Hartmann, D.; Bussow, H.; Meyer, R.; Gieselmann, V.; Eckhardt, M. Absence of 2-hydroxylated sphingolipids is compatible with normal neural development but causes late-onset axon and myelin sheath degeneration. *J*. *Neurosci*. **2008**, *28*, 9741–9754.
29. Lopez, P.H.; Schnaar, R.L. Gangliosides in cell recognition and membrane protein regulation. *Curr*. *Opin*. *Struct*. *Biol*. **2009**, *19*, 549–557.

30. Yin, J.; Hashimoto, A.; Izawa, M.; Miyazaki, K.; Chen, G.Y.; Takematsu, H.; Kozutsumi, Y.; Suzuki, A.; Furuhata, K.; Cheng, F.L.; *et al*. Hypoxic culture induces expression of sialin, a sialic acid transporter, and cancer-associated gangliosides containing non-human sialic acid on human cancer cells. *Cancer Res*. **2006**, *66*, 2937–2945.
31. Yin, J.; Miyazaki, K.; Shaner, R.L.; Merrill, A.H., Jr.; Kannagi, R. Altered sphingolipid metabolism induced by tumor hypoxia—New vistas in glycolipid tumor markers. *FEBS Lett*. **2010**, *584*, 1872–1878.
32. Young, R.J.; Moller, A. Immunohistochemical detection of tumour hypoxia. *Methods Mol*. *Biol*. **2010**, *611*, 151–159.
33. Pályi-Krekk, Z.; Barok, M.; Isola, J.; Tammi, M.; Szöllősi, J.; Nagy, P. Hyaluronan-induced masking of erbb2 and cd44-enhanced trastuzumab internalisation in trastuzumab resistant breast cancer. *Eur*. *J*. *Cancer* **2007**, *43*, 2423–2433.
34. Gonzalez, R.C.; Woods, R.E.; Eddins, S.L. Segmentation Using the Watershed Algorithm. In *Digital Image Processing Using Matlab*; Gonzalez, R.C., Woods, R.E., Eddins, S.L., Eds.; Pearson Prentice Hall: Upper Saddle River, NJ, USA, 2004; pp. 417–425.
35. Digman, M.A.; Dalal, R.; Horwitz, A.F.; Gratton, E. Mapping the number of molecules and brightness in the laser scanning microscope. *Biophys*. *J*. **2008**, *94*, 2320–2332.
36. Kuhry, J.G.; Fonteneau, P.; Duportail, G.; Maechling, C.; Laustriat, G. Tma-dph: A suitable fluorescence polarization probe for specific plasma membrane fluidity studies in intact living cells. *Cell Biophys*. **1983**, *5*, 129–140.
37. Lakowicz, J.R. Fluorescence Anisotropy. In *Principles of Fluorescence Spectroscopy*, 3rd ed.; Springer: New York, NY, USA, 2006; pp. 353–382.
38. Harris, F.M.; Best, K.B.; Bell, J.D. Use of laurdan fluorescence intensity and polarization to distinguish between changes in membrane fluidity and phospholipid order. *Biochim*. *Biophys*. *Acta* **2002**, *1565*, 123–128.
39. Sanchez, S.A.; Tricerri, M.A.; Gunther, G.; Gratton, G. Laurdan Generalized Polarization: From Cuvette to Microscope. In *Modern Research and Educational Topics in Microscopy*. *Applications in Biology and Medicine*; Méndez-Vilas, A., Díaz, J., Eds.; Formatex: Badajoz, Spain, 2007; Volume 1, pp. 1007–1014.
40. Parasassi, T.; de Stasio, G.; Ravagnan, G.; Rusch, R.M.; Gratton, E. Quantitation of lipid phases in phospholipid vesicles by the generalized polarization of laurdan fluorescence. *Biophys*. *J*. **1991**, *60*, 179–189.
41. Szklenar, M.; Kalkowski, J.; Stangl, V.; Lorenz, M.; Rühl, R. Eicosanoids and docosanoids in plasma and aorta of healthy and atherosclerotic rabbits. *J*. *Vasc*. *Res*. **2013**, *50*, 372–382.
42. Rühl, R. Method to determine 4-oxo-retinoic acids, retinoic acids and retinol in serum and cell extracts by liquid chromatography/diode-array detection atmospheric pressure chemical ionisation tandem mass spectrometry. *Rapid Commun*. *Mass Spectrom*. **2006**, *20*, 2497–2504.

Fumigaclavine C from a Marine-Derived Fungus *Aspergillus Fumigatus* Induces Apoptosis in MCF-7 Breast Cancer Cells

Yong-Xin Li, S.W.A. Himaya, Pradeep Dewapriya, Chen Zhang and Se-Kwon Kim

Abstract: Recently, much attention has been given to discovering natural compounds as potent anti-cancer candidates. In the present study, the anti-cancer effects of fumigaclavine C, isolated from a marine-derived fungus, *Aspergillus fumigatus*, was evaluated *in vitro*. In order to investigate the impact of fumigaclavine C on inhibition of proliferation and induction of apoptosis in breast cancer, MCF-7 cells were treated with various concentrations of fumigaclavine C, and fumigaclavine C showed significant cytotoxicity towards MCF-7 cells. Anti-proliferation was analyzed via cell mobility and mitogen-activated protein kinase (MAPK) signaling pathway. In addition, fumigaclavine C showed potent inhibition on the protein and gene level expressions of MMP-2, -9 in MCF-7 cells which were manifested in Western blot and reverse transcription polymerase chain reaction (RT-PCR) results. The apoptosis induction abilities of the fumigaclvine C was studied by analyzing the expression of apoptosis related proteins, cell cycle analysis, DNA fragmentation and molecular docking studies. It was found that fumigaclavine C fragmented the MCF-7 cell DNA and arrested the cell cycle by modulating the apoptotic protein expressions. Moreover, fumigaclavine C significantly down-regulated the NF-kappa-B cell survival pathway. Collectively, data suggest that fumigaclavine C has a potential to be developed as a therapeutic candidate for breast cancer.

Reprinted from *Mar. Drugs*. Cite as: Li, Y.-X.; Himaya, S.W.A.; Dewapriya, P.; Zhang, C.; Kim, S.-K. Fumigaclavine C from a Marine-Derived Fungus *Aspergillus Fumigatus* Induces Apoptosis in MCF-7 Breast Cancer Cells. *Mar. Drugs* **2013**, *11*, 5063-5086.

1. Introduction

Breast cancer is one of the most common causes of cancer-related death in women. According to the World Health Organization, more than 1.2 million women are diagnosed with breast cancer each year worldwide [1,2]. Most of the present breast cancer chemopreventive and chemotherapeutic agents lead to undesirable side effects [3]. Therefore, the search for new agents derived from natural products with a fewer side effects should continue.

Marine fungi are a rich source of bioactive secondary metabolites including novel compounds that have unique structural features. Marine fungi have been widely studied for their bioactive metabolites, and these organisms have proved to be a rich, promising source of novel anticancer, antibacterial, antiplasmodial, anti-inflammatory and antitumor agents [4–7]. Therefore, bioactive compounds produced by marine fungi are of interest as new lead compounds in medicine.

Aspergillus fumigatus is a common environmental fungus and a significant cause of disease in immune-compromised patients and is responsible for up to 4% of deaths in tertiary hospitals in Europe [8]. Nevertheless, a number of bioactive compounds such as dioxopiperazine, alkaloids, dibenzofurans, and indole diketopiperazine have been isolated from *Aspergillus fumigatus* [9,10].

In this study, subsequent culturing and fractionation of the ethyl acetate (EtOAc) extract of *Aspergillus fumigatus* culture led to the isolation of fumigaclavine C as a major secondary metabolite. Fumigaclavine C is an indole alkaloid which was first isolated from the culture of *Cephalosporium* sp. IFB-018, an endophytic fungus from the rhizoma of a salinity-tolerant medicinal plant *Imperata cylindrica* by a column chromatography fraction of chloroform-methanol (1:1) extract [11,12]. Although this compound was discovered as early as 1977, its biological activity is seldom reported [13]. Its immunosuppressive activity against concanavalin A-induced hepatitis in mice by the mechanisms of inhibiting T cell proliferation, adhesion and TNF-α production has been reported previously, suggesting that fumigaclavine C may have a characteristic to inhibit the T-cell mediated immune response [14].

It is a well-known fact that alkaloids often possess significant physiological activities including anticancer and antitumor activity, and some of them are currently being used in clinical treatments. Moreover, in the broad range of alkaloids, indole-containing alkaloids have been reported as an interesting group of bioactive alkaloids and have frequently been isolated form marine organisms [15]. Ge and his research team [10] reported that two new alkaloids, which have a close similarity to fumigaclavine C in structure, showed selectively potent cytotoxicity against human leukemia cells (K562) with an IC_{50} value of 3.1 μM; however, detailed studies have not been reported yet. Therefore, in this study, we aimed to investigate the anti-cancer potential of fumigaclavine C while revealing the underlying molecular signaling pathways using a MCF-7 breast cancer cell model.

2. Results

2.1. Structural Elucidation of Fumigaclavine C

The chemical structure of the isolated compound from broth extract of the marine-derived fungus was determined according to **1D**, **2D** nuclear magnetic resonance (NMR), and low-resolution electron ionization mass spectrometry (LREIMS) data, together with comparison with the data published previously [10]. The compound was identified as fumigaclavine C (15.8 mg), illustrated in Figure 1A.

Fumigaclavine C (15.8 mg): white powder; ^{1}H-NMR (CD_3OD, 400 MHz) δ 7.06 (1H, d, J = 8.0 Hz, H-12), 6.93 (1H, dt, H-13), 6.57 (1H, d, J = 7.1 Hz, H-14), 6.12 (1H, dd, J = 10.6 Hz, J = 6.5 Hz, H-22), 5.61 (1H, t, H-9), 5.03 (1H, dd, H-23), 5.06 (1H, t, H-23), 3.55 (1H, dd, H-10), 3.19 (1H, m, H-5), 2.71 (2H, m, H-7), 2.55 (2H, m, H-4), 2.41 (3H, brs, H-17), 2.07 (1H, m, H-8), 1.83 (3H, brs, H-25), 1.51 (6H, d, H-20, 21), 1.31 (3H, d, J =7.5 Hz, H-18); ^{13}C-NMR (CD_3OD, 100 MHz) δ 172.6 (C-24), 147.6 (C-22), 138.5 (C-2), 134.5 (C-15), 129.3 (C-11), 129.0 (C-16), 122.5 (C-14), 112.8 (C-12), 111.4 (C-23), 109.1 (C-13), 106.1 (C-3), 72.8 (C-9), 63.3 (C-5), 58.9 (C-7), 43.9 (C-17), 40.5 (C-10), 40.3 (C-19), 34.5 (C-8), 28.9 (C-4), 28.1 (C-20), 28.0 (C-21), 20.9 (C-25), 16.9 (C-18). LREIMS *m/z*: 366.20 $[M]^+$ ($C_{23}H_{30}N_2O_2$).

Figure 1. (**A**) Chemical structure of fumigaclavine C isolated from the marine-derived fungus *Aspergillus fumigatus*; (**B**) cytotoxic and anti-proliferation effect of fumigaclavine C on MCF-7 breast cancer cells. Briefly, MCF-7 cells were cultured in 96-well plates at a density of 5 × 10^3 cells per well and treated with different concentrations (20 μM, 40 μM, and 60 μM) of fumigaclavine C for 24 h and 36 h; (**C**) and (**D**) effect of fumigaclavine C on MCF-7 cells migration and invasion. The results were observed with a microscope at 200× and the relatively blocked percentage (%) of migrated and invaded cells per field was assessed. Each value was expressed as the mean ± SD of triplicate experiments. * $p < 0.05$ as compared with blank groups.

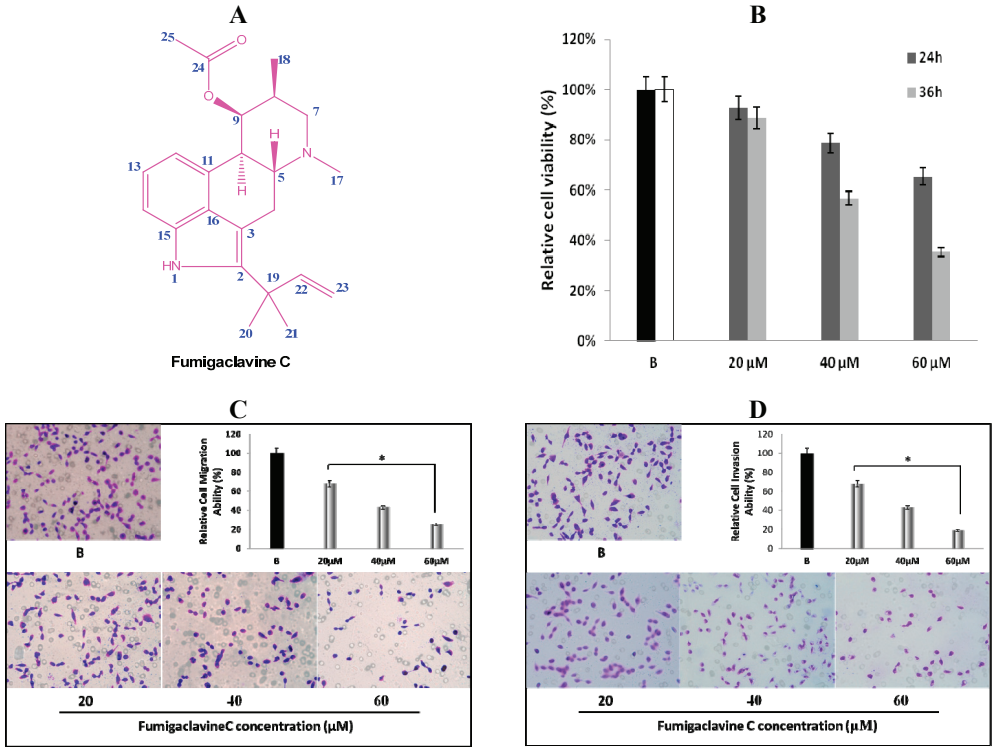

2.2. Anti-Proliferative Effect of Fumigaclavine C on MCF-7 Cells

The anti-proliferative effect of fumigaclavine C was tested on a cultured MCF-7 breast cancer cell line. Comparisons of the cell growth for 24 and 36 h with various concentrations of fumigaclavine C (20 μM, 40 μM, and 60 μM) are shown in Figure 1B. In a comparative analysis, fumigaclavine C showed significant high growth inhibitory effects on the MCF-7 cell line in a dose-dependent and time-dependent manner ($p < 0.05$). Fumigaclavine C inhibited the proliferation of MCF-7 cells with the viability percentages of 93%, and 89% (20 μM), 79%, and 57% (40 μM), and 65% and 35% (60 μM) at 24 h and 36 h, respectively, compared to the vehicle treated blank. Therefore, it was clear that fumigaclavine C had anti-proliferative effects on MCF-7 cells.

Fumigaclavine C treatment (60 μM for 36 h) reduced the viable cell population up to 35% and thus fumigaclavine C treatment for 24 h was selected for further analysis.

2.3. Effects of Fumigaclavine C on Migration and Invasion of MCF-7 Cells

MCF-7 cells were treated with different concentrations (20 μM, 40 μM, and 60 μM) of fumigaclavine C for 24 h. It was observed that fumigaclavine C treatment reduced the cancer cell migration and invasion in a dose-dependent manner (Figure 1C,D). Interestingly, it was also observed that at the highest concentration (60 μM), fumigaclavine C almost completely blocked MCF-7 cell migration and invasion. Fumigaclavine C blocked the migration and invasion of MCF-7 cells with the blocking percentages of 38%, 29% (60 μM), and 25%, 19% (60 μM) at 24 h, respectively. The results indicate that fumigaclavine C has the ability to suppress MCF-7 cell migration and invasion.

2.4. Effect of Fumigaclavine C on MMP-2 and -9 Expressions in MCF-7 Breast Cancer Cells

Western blot results revealed that fumigaclavine C treatment of the MCF-7 cells resulted in an inhibition of protein expression of both MMP-2 and MMP-9. At the highest concentration (60 μM) of the compound there was a significant inhibition in both MMP-2 and MMP-9 and the inhibitory activity was significant ($p < 0.05$) from the concentrations of 20 to 60 μM (Figure 2A). These results suggest that fumigaclavine C effectively inhibits the MMP-2 and -9 activities and that this probably contributes to the anti-proliferative effects of fumigaclavine C.

To find out whether this inhibition of MMP-2 and -9 by fumigaclavine C are apparent at their gene levels, a reverse transcription polymerase chain reaction (RT-PCR) experiment was carried out using RNA isolated from MCF-7 cells treated with fumigaclavine C at different concentrations (20 μM, 40 μM, and 60 μM). Fumigaclavine C showed a clear inhibitory activity on the expression of both MMP-2 and -9 mRNAs in MCF-7 cells. The inhibition of MMP-2 and -9 gene expressions were observed in a concentration-dependent manner, where the inhibition was even lower than the blank group in MCF-7 cells at the highest concentration (60 μM) of the compound (Figure 2B). These results of the inhibition of MMP-2 and -9 mRNA expressions coincide with protein expression results suggesting that the MMP-2 and -9 were inhibited by the fumigaclavine C at both the protein and gene level. This clear inhibition of MMP-2 and -9 may be involved in the suppression of cell proliferation and migration.

Figure 2. Inhibitory effect of fumigaclavine C on MMP-2 and -9 protein and mRNA expressions in MCF-7. (**A**) Protein expression level of MMP-2 and -9 in treated MCF-7 cells. Cell lysates were collected and subjected to sodium dodecyl sulfate polyacrylamide gel electrophoresis (SDS-PAGE) Western blot analysis using antibodies specific for MMP-2 and -9. Beta-actin was used as an internal control. (**B**) mRNA expression levels of MMP-2 and -9 in treated MCF-7 cells were analyzed by RT-PCR. Each value was expressed as the mean ± SD of triplicate experiments. * $p < 0.05$ as compared with blank groups.

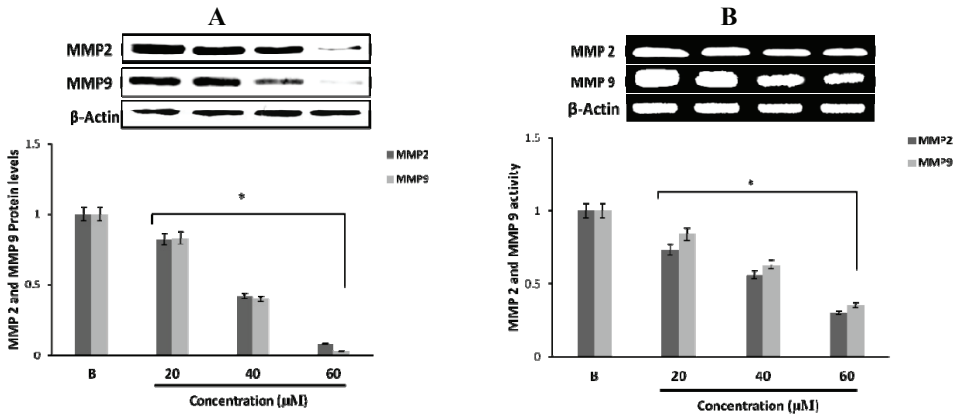

2.5. Effect of Fumigaclavine C on ERK, JNK, and p38 MAPK Signaling Pathway

To find out through which pathway fumigaclavine C blocked the expression of MMP, the effect of fumigaclavine C on the ERK 1/2, JNK, and p38 MAPK signaling pathways was analyzed. Treatment with fumigaclavine C at various concentrations (20 μM, 40 μM, and 60 μM) showed a dose-dependent inhibitory effect on the phosphorylation of ERK 1/2, JNK, p38 in MCF-7 cell line (Figure 3A–C).

These results demonstrated that the anti-proliferative effect of fumigaclavine C was mediated by blocking the signal transduction of MAPK pathway molecules, *i.e.*, ERK, JNK, and p38 MAPK signaling pathways in activated MCF-7 cells. Therefore it was clear that the possible molecular mechanism for the fumigaclavine C mediated inhibition of proteinases is probably the inhibition of the activation of these signaling cascades.

Figure 3. Effect of fumigaclavine C on expression of (**A**) p-ERK 1/2, ERK 1/2, (**B**) p-JNK, JNK, (**C**) p-p38, and p38 MAPK signaling pathways. Expression levels were assayed using Western blot following treatment with fumigaclavine C at different concentrations (20 μM, 40 μM, and 60 μM) for 24 h. Each value is expressed as the mean ± SD of triplicate experiments. *$p < 0.05$ as compared with blank groups.

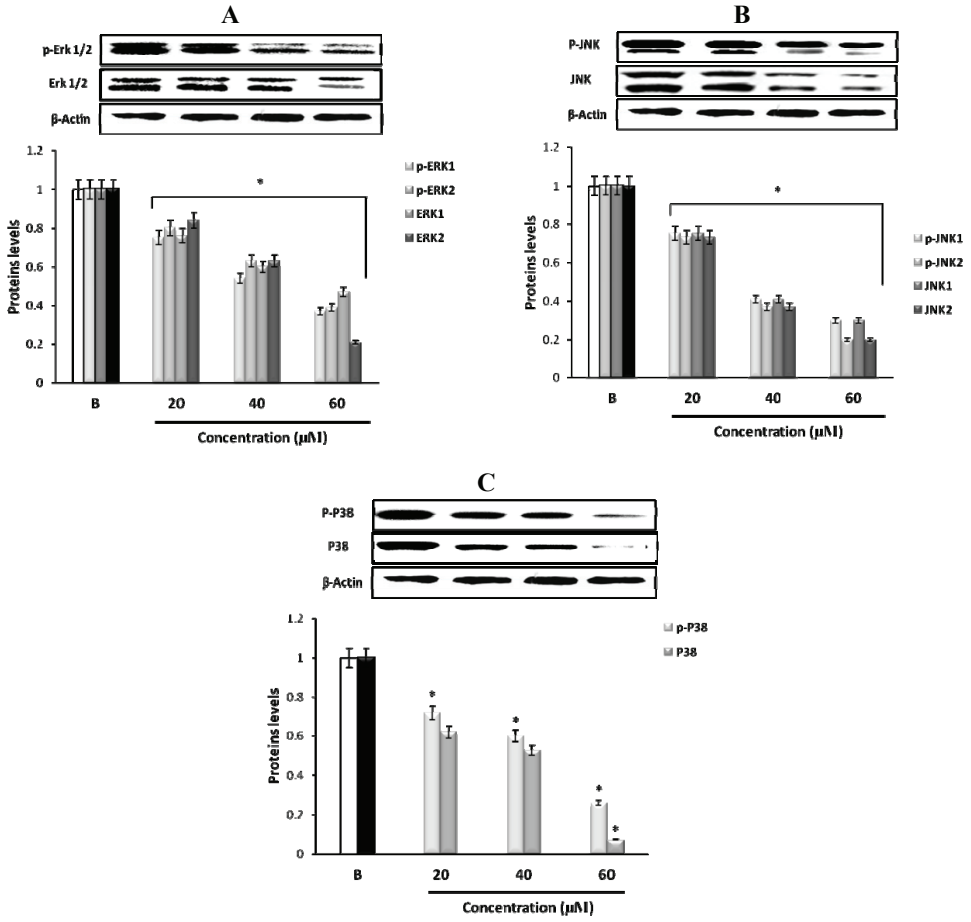

2.6. The Effects of Fumigaclavine C on the Cell Cycle of MCF-7 Cells

To further study the mechanism responsible for fumigaclavine C induced growth inhibition, the effect of fumigaclavine C on the cell cycle distributions was analyzed by flow cytometry. As shown in Figure 4A, treatment of the MCF-7 breast cancer cells with various concentrations of fumigaclavine C for 24 h resulted in a significant dose-dependent induction of sub-G1 cell population. It indicated that fumigaclavine C induced apoptosis in MCF-7 cells where the sub-G1 cell percentages were 15.6% (20 μM), 21.5% (40 μM), and 46.6%, (60 μM) at 24 h, respectively.

Figure 4. Effect of fumigaclavine C on cell cycle progression and cell cycle apparatus. (**A**) Cell cycle distribution pattern of fumigaclavine C treated (24 h) MCF-7 cells analyzed by fluorescence-activated cell sorting (FACS). Cells were fixed in 70% ethanol, re-suspended in PBS and stained with PI. After 24 h, a prominent sub-G1 peak could be seen in the histogram. (**B**) and (**C**) protein and gene expressions of p53, and p21 in MCF-7 cells treated with fumigaclavine C. MCF-7 cells were treated with various concentrations of fumigaclavine C for 24 h under serum-free conditions. (**D**) Protein expressions of CDK2, CDK4, cyclin B1, and cyclin E in fumigaclavine C treated MCF-7 cells. The antibody bindings were detected by enhanced chemiluminescence reagent using luminoimager. Each value was expressed as the mean ± SD of triplicate experiments. * $p < 0.05$ as compared with blank groups.

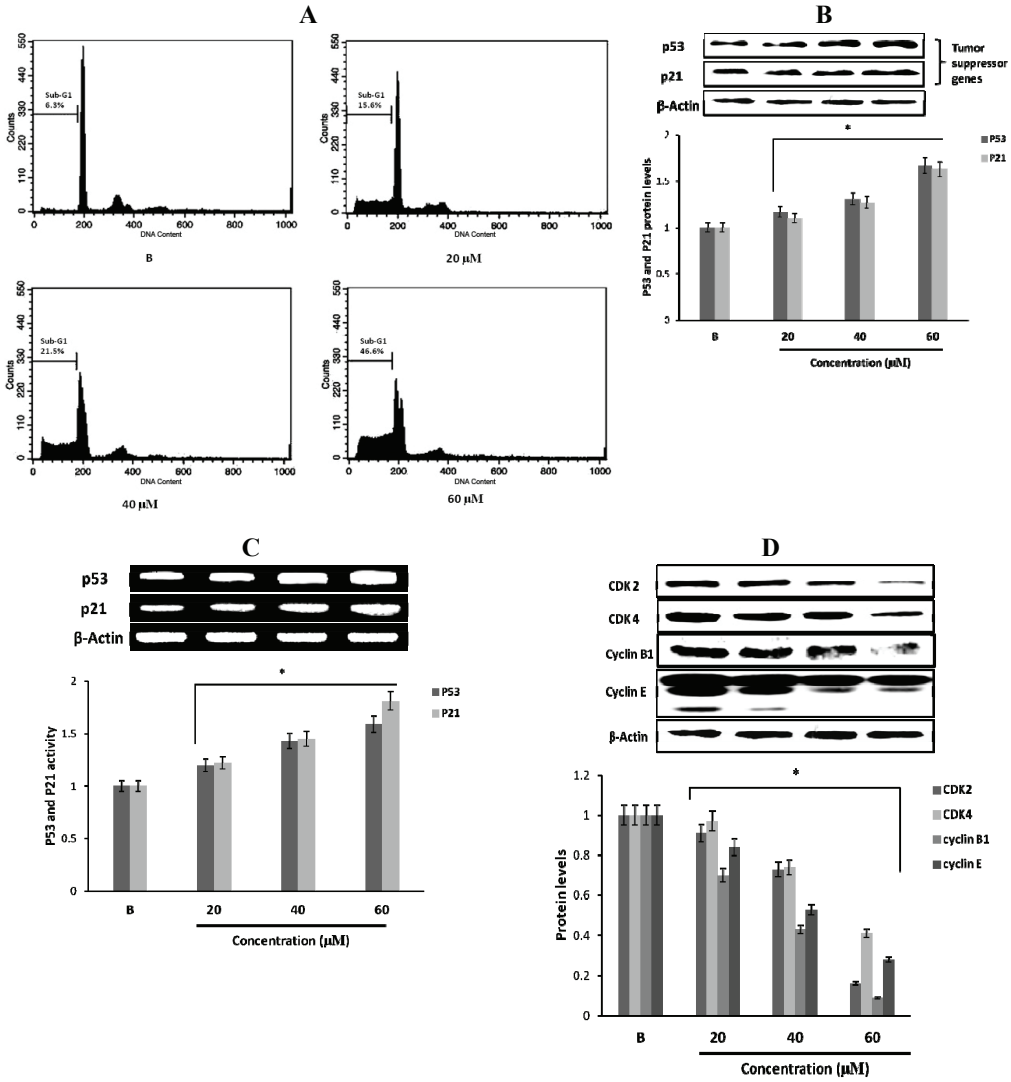

2.7. Effect of Fumigaclavine C on p53 Family Gene Expression in MCF-7 Breast Cancer Cells

The tumor suppressor gene p53 plays an essential role in various types of anti-proliferation and apoptosis. And the induction of p21 is mostly mediated through a p53-dependent pathway. Therefore, we determined whether the tumor suppressor factors, p53 and p21, were involved in the anti-proliferative effect of fumigaclavine C. Treatment with different concentrations of fumigaclavine C activated p53 and p21 proteins and gene levels in a dose-dependent manner (Figure 4B,C). These results imply that a part of the anti-proliferative activity of fumigaclavine C is related to apoptosis through up-regulation of p53 and p21 levels.

2.8. Effect of Fumigaclavine C on Cyclin B1, Cyclin E, CDK2, and CDK4 Expression in MCF-7 Breast Cancer Cells

To further explore the underlying mechanism by which fumigaclavine C mediates cell cycle arrest, we examined the regulatory effects of fumigaclavine C on the expression of CDK2, CDK4, cyclin B1 and cyclin E, which control the cell cycle progression. As shown in Figure 4D, CDK2, CDK4, cyclin B1, and cyclin E were down-regulated to varying degrees by fumigaclavine C treatment. These results demonstrated that fumigaclavine C induced cell cycle arrest by changing the CDK2, CDK4, cyclin B1 and cyclin E protein expression levels.

2.9. The Morphological Changes and DNA Damages of MCF-7 Cells Observed with Hoechst 33258 Staining

To observe the morphological changes and DNA damage induced by the fumigaclavine C in MCF-7 cells, Hoechst 33258 staining was used as described earlier. The results are depicted in Figure 5A. MCF-7 cells were cultured in 24-well plate and treated with different concentrations (20 μM, 40 μM, and 60 μM) of fumigaclavine C for 24 h. The results were observed under fluorescence inverted microscope at 100× magnification. Clear morphological changes and DNA damage were observed with the treatment of the compound. Moreover, the DNA damage was dose dependently increased. The results indicate that fumigaclavine C potently damages DNA and thereby induces apoptosis in MCF-7 cells.

2.10. Fumigaclavine C Induced DNA Fragmentation in MCF-7 Cells

For further confirmation of the effect of fumigaclavine C on nuclear damage, DNA fragmentation of MCF-7 breast cancer cells was analyzed by an agarose gel electrophoresis. There was a dose dependant DNA fragmentation or laddering pattern in the cells treated with various concentrations of fumigaclavine C compared to the blank (Figure 5B). Hence, the results could imply that fumigaclavine C may have induced apoptosis and subsequent DNA damage.

Figure 5. Effect of fumigaclavine C treatment on nuclear damage of MCF-7 cells. (**A**) Hoechst staining of MCF-7 cells treated with fumigaclavine C. For Hoechst staining, MCF-7 cells were cultured in 24-well plate and treated with fumigaclavine C for 24 h. (**B**) The effects of fumigaclavine C on the DNA fragmentation. (**C**) Western blot analysis of the expressions of PI3K, p-Akt, and Akt in MCF-7 cells treated with fumigaclavine C. MCF-7 cells were grown at 5 × 10^5 cells/dish and treated with different concentrations of fumigaclavine C. Each value was expressed as the mean ± SD of triplicate experiments. * $p < 0.05$ as compared with blank groups.

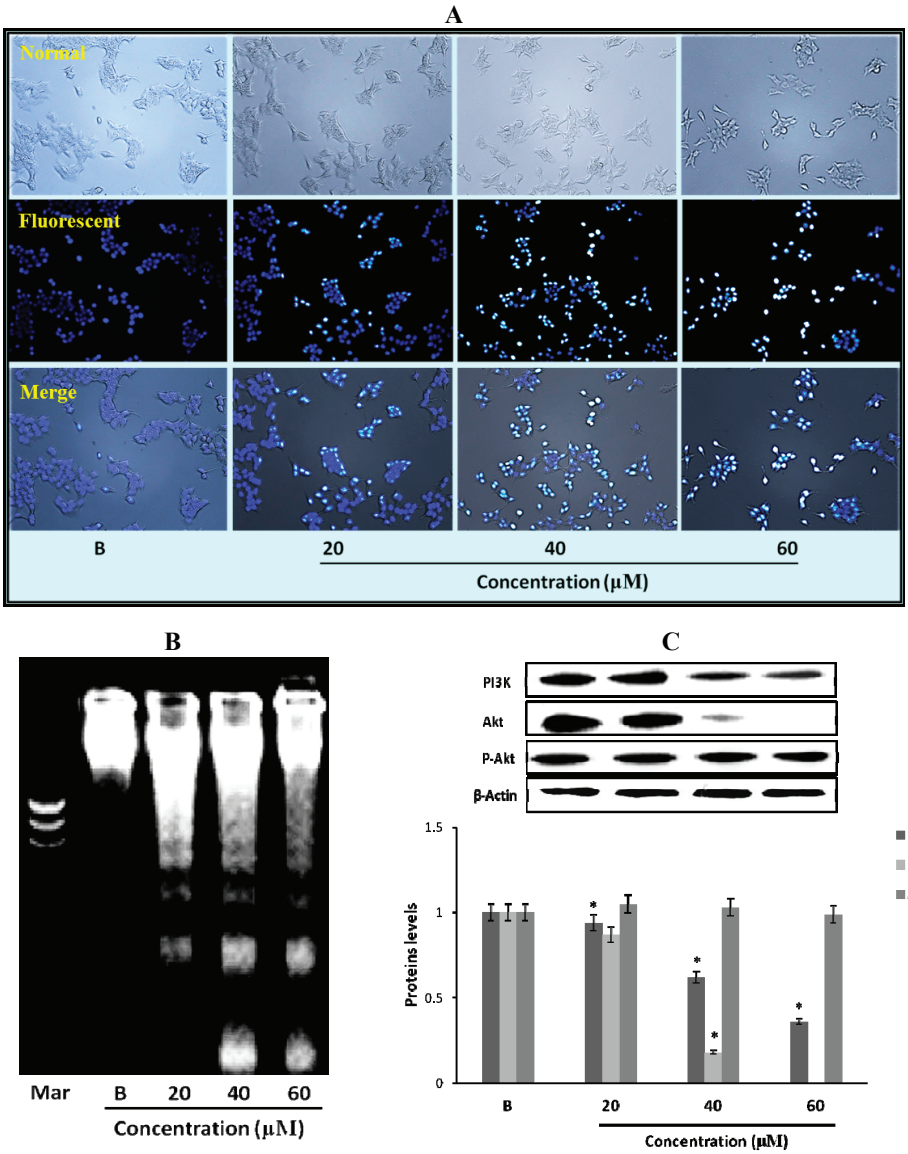

2.11. Effect of Fumigaclavine C on PI3K/Akt Pathway in MCF-7 Breast Cancer Cells

In order to elucidate the specific intracellular signaling pathways involved in the growth inhibitory effects of fumigaclavine C in MCF-7 cells, the effect of fumigaclavine C on the expression of PI3K, p-Akt, and Akt, which can control cell apoptosis progression was investigated. As shown in Figure 5C, PI3K and Akt were down-regulated by the treatment of fumigaclavine C. These results demonstrate that fumigaclavine C induces cell apoptosis most probably via regulating the PI3Kand p-Akt protein levels.

2.12. Effect of Fumigaclavine C on Bcl-2 Family Protein Expression in MCF-7 Breast Cancer Cells

Apoptotic genes regulate apoptosis by the activation of their pro- and anti-apoptotic products. Among them, Bcl-2 proteins are very important in apoptosis regulation. In order to confirm the expression levels of proteins and genes related to the induction of apoptosis, expression of Bcl-2, Bcl-xl, Bax and Bad in fumigaclavine C treated MCF-7 cells were analyzed using Western blot and RT-PCR analysis. As per the results fumigaclavine C exhibited the induction of apoptosis in MCF-7 cells by down-regulating the anti-apoptotic Bcl-2 and Bcl-xl levels as well as up-regulating the pro-apoptotic Bax and Bad levels at protein and gene levels (Figure 6A,B).

2.13. Effect of Fumigaclavine C on Caspase-3, -8, and -9 Expression in MCF-7 Breast Cancer Cells

To find out whether apoptosis is induced as an underlying mechanism of anti-proliferation of fumigaclavine C treatment, Western blot analysis was carried out to investigate the activation of caspase-3, -8 and -9. The results showed that the active caspase levels were increased by treatment with fumigaclavine C in a dose-dependent manner (Figure 6C). Furthermore, fumigaclavine C treatment more potently induced the expression of caspase-9 protein in MCF-7 cells compared to caspase-3 protein.

In order to analyze whether this activation of caspase-3, -8 and -9 and by fumigaclavine C occurs at their gene levels, a RT-PCR experiment was carried out using RNA collected from MCF-7 cells treated with fumigaclavine C at different concentrations (20 μM, 40 μM, and 60 μM). Fumigaclavine C showed a clear elevation in expression of caspase-9 and -3 mRNAs in MCF-7 cells. The activities of caspase-3, -8 and -9 gene expressions were observed in a concentration-dependent manner (Figure 6D). These expression levels of caspase-3, -8 and -9 mRNA coincide with protein expressions results, suggesting that the caspase-3, -8 and -9 were activated by the fumigaclavine C at both protein and gene levels. This clear activation of caspase-3, -8 and -9 may be involved in the induction of apoptosis.

Figure 6. Effect of fumigaclavine C treatment on protein and gene expression in the apoptotic signaling cascade. (**A**) and (**B**) Protein and gene expressions of Bcl-2 family proteins in MCF-7 cells treated with fumigaclavine C. (**C**) and (**D**) effect of fumigaclavine C on the protein and gene expressions of caspase-3, -8, and -9 in MCF-7. Each value is expressed as the mean ± SD of triplicate experiments. *$p < 0.05$ as compared with blank groups.

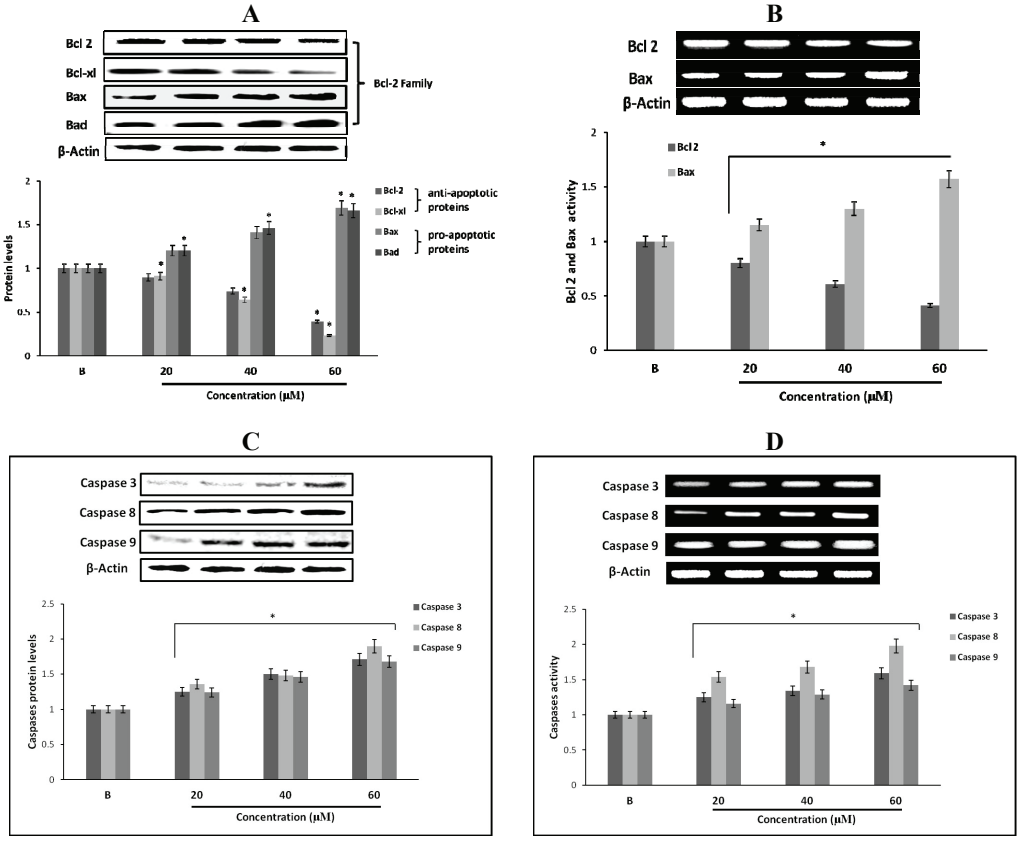

2.14. Effect of Fumigaclavine C on Cytochrome C and Apaf-1 Protein Expression in MCF-7 Breast Cancer Cells

In order to examine whether the activities of casapase-3 and caspase-9 were initiated due to mitochondrial release of cytochrome C and Apaf-1, the MCF-7 cells were exposed to fumigaclavine C in different concentrations (20 μM, 40 μM, and 60 μM). As shown in Figure 7A, we observed an increase of cytochrome C and Apaf-1 in the cytosolic fraction of fumigaclavine C treated MCF-7 cells. Mitochondrial release of cytochrome C and Apaf-1 resulted in the activation of caspase-9-mediated apoptosis.

Figure 7. Protein expression levels of cell survival signaling molecules of MCF-7 cells. (**A**) Western blot analysis of the expression of cytochrome C and Apaf-1 in MCF-7 cells by fumigaclavine C. After incubation for 24 h, cell lysates were collected from tread and the same amount of proteins were subjected to Western blot using antibodies specific for cytochrome C and Apaf-1. β-actin was used as an internal standard. (**B**) Protein expressions of p50, p65, and IKK in MCF-7 cells by fumigaclavine C. Western blot analysis confirmed that the p50, p65, and IKK protein levels were down-regulated. MCF-7 cells were grown at 5×10^5 cells/dish and treated with different concentrations of fumigaclavine C. The antibody bindings were detected by enhanced chemiluminescence reagent using luminoimager. Each value was expressed as the mean ± SD of triplicate experiments. * $p < 0.05$ as compared with blank groups.

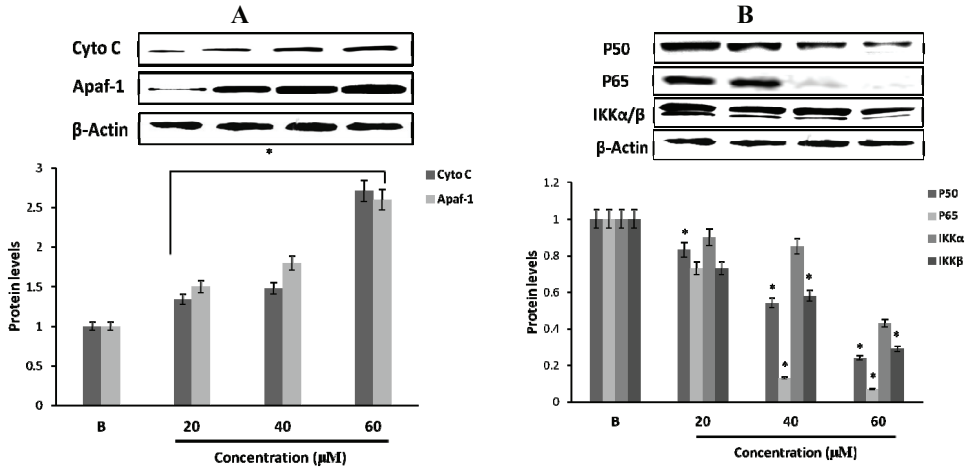

2.15. Effect of Fumigaclavine C on p50, p65 and IKK Expression in MCF-7 Breast Cancer Cells

Transcription factor NF-κB (p50 and p65) is generally localized in the cytoplasm with its inhibitor IκB kinase (IKK). We investigated whether fumigaclavine C is associated with the inhibition of the activation of NF-κB and the NF-κB-dependent genes. The treatment with different concentrations (20 μM, 40 μM, and 60 μM) of fumigaclavine C inhibited the expression levels of p50 and p65 in a dose-dependent manner at transcriptional levels (Figure 7B). Down-regulation of IKK and up-stream activating kinases of NF-κB was also observed. Fumigaclavine C strongly suppressed NF-κB and IKK activation and this might have also been involved in the initiation of apoptosis.

2.16. Computational Modeling of the Fumigaclavine C Apoptosis Activity

The compound of fumigaclavine C was docked at the active site of the crystal structure of apoptosis regulator Bcl-2 (2w3L-Apoptosis). The computational docking study results are presented in Figure 8A,B. The schematic 2D plot shows intermolecular interactions of the representative fumigaclavine C with 2w3L-Apoptosis (Figure 8B). The nitrogen atoms of

fumigaclavine C show an ionic interaction with GLU95 (2w3L-Apoptosis). The data show that fumigaclavine C has the lowest estimated (est.) energy of binding (−6.97) and est. inhibition constant (Ki = 7.75 μM) (Table 1), which is necessary for a strong interaction. In the binding mode (fumigaclavine C to 2w3L-Apoptosis), GLU95 residues in Bcl-2 were responsible for the hydrogen bonding and GLU95 alone was expected to make a polar interaction with fumigaclavine C. A hydrophobic interaction was the major interacting force brought up by MET74, LEU78, VAL92, LEU96, and PHE112 amino acid residues. The experimental results suggest that the fumigaclavine C can bind to the cleft of 2w3l-Apoptosis and interact with the key active-site residues GLU95, which can result in induced apoptosis activity.

Figure 8. (**A**) The binding mode between Fumigaclavine C and 2w3l-Apoptosis. The interacting side chains of 2w3l-Apoptosis are displayed in surface mode. Fumigaclavine C is represented using balls and stick. The atoms of fumigalavine C are color-coded as follows: O, red; N, blue; C, green; H, white. (**B**) Schematic 2D plot showing intermolecular interactions.

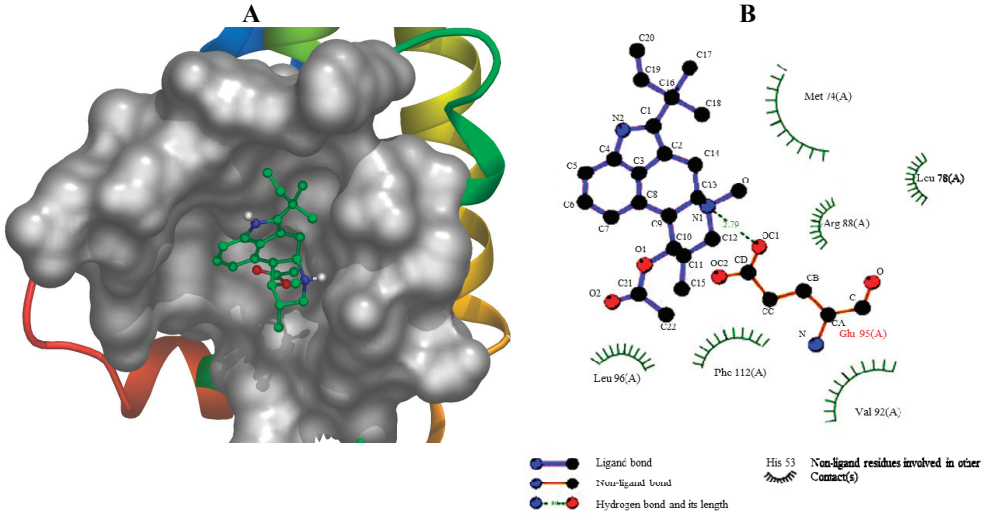

Table 1. Docking results (fumigaclavine C was docked at the crystal structure of apoptosis regulator (2w3L-Apoptosis)).

Rank	Est. Free Energy of Binding	Est. Ingibition Constant, Ki	vdW + Hbond + desolv Energy	Electrostatic Energy	Total Internoiec. Energy	Frequency	Interact Surface
1	−6.97 kcal/mol	7.75 μM	−6.74 kcal/mol	−0.92 kcal/mol	−7.66 kcal/mol	40%	690.553
2	−6.60 kcal/mol	14.57 μM	−7.24 kcal/mol	−0.11 kcal/mol	−7.35 kcal/mol	10%	671.602
3	−6.56 kcal/mol	15.59 μM	−7.06 kcal/mol	−0.23 kcal/mol	−7.29 kcal/mol	10%	671.075
4	−6.34 kcal/mol	22.62 μM	−6.78 kcal/mol	−0.29 kcal/mol	−7.07 kcal/mol	30%	650.265
5	−5.85 kcal/mol	51.78 μM	−6.26 kcal/mol	−0.30 kcal/mol	−6.55 kcal/mol	10%	639.255

3. Discussions

Apoptosis is a programmed cell death mechanism recognized as a vital process in the regulation of tissue development and homeostasis, and a highly conserved mechanism throughout evolution [16,17]. Homeostasis between cell death and cell proliferation is required to maintain a normal state in all tissues [18,19]. The present study was designed to determine the anti-proliferative and apoptotic effects of fumigaclavine C isolated from a marine-derived fungus, *Aspergillus fumigatus*, on MCF-7 human breast cancer cells.

In recent years, interest in bioactive ingredients of marine fungi has been growing rapidly, as most of the fungal derived compounds are capable of inhibiting the growth and proliferation of cancer cells [20]. As shown in Figure 1B, fumigaclavine C showed significant cytotoxicity towards MCF-7 breast cancer cells and arrested progression of cell cycle at the G1 level inducing apoptosis in the cell. Even though similar cytotoxicity studies of effects of this compound on other cell lines have not been reported in the literature, Ge and colleagues [10] showed that 9-deacetylfumigaclavine C and 9-deacetoxyfumigaclavine C, which have a close similarity to fumigaclavine C in structure, have potent cytotoxicity towards human leukemia (K562), human nasopharynyeal epidermoid tumor (KB), and human breast adenocarcinoma (MCF-7) cells. Furthermore, previous studies have reported that fumigaclavine C acts against Con A-induced hepatitis in mice by inhibiting T cell proliferation, adhesion and TNF-α production [14]. Hence, it may be expected that fumigaclavine C might have more or less similar cytotoxic effects on other cancer cell lines. Moreover, Du and colleagues revealed that the compound does not exert any detectable cytotoxicity on RAW 264.7 cells at concentrations up to 100 μM [21]. These findings indicate that fumigaclavine C shows a selective toxicity towards cells, which is an interesting characteristics in chemo preventive agents, as most potent cytotoxic compounds result in several side effects due to lack of selectivity.

Here, we show that fumigaclavine C induces apoptosis in MCF-7 cells while inhibiting expression of relevant matrix metalloproteases (MMPs). Anti-apoptotic actions along with inhibition of MMP expression depend on the activation of the MAPK signaling pathway [22]. Several studies have shown that MMPs promote tumor proliferation and migration and therefore an anti-cancer compound with MMP inhibitory activity provides added advantage in chemoprevention. It has been found that metalloproteinase MMP-2 is responsible for increased invasiveness while MMP-9 expression in carcinoma cells offers survival advantage [23]. Our data clearly demonstrates that fumigaclavine C can inhibit MMP-2 and -9, which are known to be highly expressed in invasive cancer cells while suppressing the survival of cancer cell. A number of articles have shown that the MAPK signaling pathways play a considerable role in MMP expression and apoptosis related to cancer signaling cascades [24–28]. The results indicate that the inhibitory effect of fumigaclavine C on cell mobility, invasion and MMP-2, -9 expressions are due to the compound-mediated suppression of phosphorylation of the MAPK signaling molecules ERK, JNK and p38.

Tumor suppressor gene p53 plays an essential role in cell death and apoptosis [29]. When MAP kinases are activated, they function as effector protein kinases to phosphorylate a number of

substrates including p53. The p53 is the up-stream molecule of cyclin dependent kinase inhibitor p21, and leads to many changes in cells such as cell growth differentiation and apoptosis [30,31]. Therefore, the p53 family was examined to determine apoptotic mechanisms in MCF-7 cells. Treatment with fumigaclavine C induced the up-regulation of cyclin dependent kinase inhibitor p21 as well as the down-regulation of cyclin B1, cyclin E, CDK2 and CDK4 levels.

Interestingly, recent findings have revealed that MAPK inhibitory compounds have a high potential to strengthen their apoptotic activity via regulating Bcl-2 family proteins, phosphatidylinositol PI3K/Akt and nuclear factor kappa B (NF-κB) [32,33]. Akt is an up-stream signaling intermediate molecule of NF-κB dependent cell survival gene expression, and activation of NF-κB and subsequent signaling molecules plays an important role in tumor cell growth, cell proliferation, tumor cell invasion and survival [34–36]. Inhibition of NF-κB activity has been identified as an apoptotic stimulus in a number of human cell lines [37]. NF-κB activation requires phosphorylation of IκBα by IκB kinases (IKKs). IκBα phosphorylation targets IκBα for ubiquitination and proteolytic degradation, releasing p50-p65 heterodimers to migrate into the nucleus and activate transcription [38,39]. In our results, it was clear that fumigaclavine C potently inhibited the activation of NF-κB and responsible gene expressions. A previous study reported a similar result, *i.e.*, that MMP-2 inhibitory apigenin isolated from *Anisomeles indica* showed a significant inhibition of NF-κB activation in MCF-7 cells [40].

Bcl-2 family proteins including Bcl-xl and pro-apoptotic members Bax and Bad are the most important regulators of apoptosis, and the activation of the signaling partly depends on the Akt-NF-κB activation. The results indicated that fumigaclavine C markedly reduced the expression of anti-apotoic protein Bcl-2 and Bcl-xl while upregulating Bax and Bad expressions. In the literature, it could be found that many indole alkaloid induced apoptosis in cancer cells by down-regulating apoptotic Bcl-2 family proteins in a NF-κB-dependent manner [41,42]. In addition, many researchers have found that Bcl-2 protein is a promising small molecular anticancer target because active compounds that can bind to hydrophobic surface pockets in Bcl-2 protein can promote apoptosis. A computational docking study was performed to evaluate the affinity of fumigaclavine C to Bcl-2 protein. In the field of molecular modeling, docking is a method which predicts the preferred orientation of one molecule to a second when bound to each other to form a stable complex. Docking is frequently used to predict the binding orientation of small molecular drug candidates to their protein targets in order to predict the affinity and activity of the small molecule. Hence docking plays an important role in the rational design of drugs [43]. Interestingly, our molecular docking study showed that fumigaclavine C had a comparatively high capacity to bind with GLU95 (2w3L-Apoptosis) having the lowest est. energy of binding (−6.97) and est. inhibition constant (Ki = 7.75 μM). This might be the reason why fumigaclavine C showed a considerably high apoptotic effect on MCF-7 cells. Several findings support this argument showing that small molecules such as tetrocarcin A and antimycin A may have the ability to recognize surface pockets of Bcl-2 and Bcl-xl, respectively, and expedite apoptosis [44].

Activation of caspases is affected by Bcl-2 family proteins, which play a central role in the mitochondrial apoptosis pathway [45,46]. Apoptosis is induced via two main pathways involving either the mitochondria (the intrinsic pathway) or the activation of death receptors (the extrinsic

pathway). Both pathways converge to induce the activation of caspases, the final executioners of cell death [47]. Caspases play essential roles in cells for apoptosis and have been termed "executioner" proteins for their roles in the cell [48]. The apoptosome is a multiprotein complex comprising cytochrome C, Apaf-1, and caspase-9 that functions to activate caspase-3, down-stream of the mitochondria apoptosis pathway in response to apoptotic signals. Binding of cytochrome C and dATP to Apaf-1 in the cytosol leads to the assembly of a heptameric complex in which each Apaf-1 subunit is bound non-covalently to a pro-caspase-9 subunit via its respective CARD domains [49]. Caspase-9 is activated very early in the apoptotic cascade by cytochrome C, which is released from the mitochondria in response to apoptotic stimuli [50]. Activated caspase-9 then initiates the proteolytic activity of other down-stream caspases such as caspase-3. The results of this study indicate that fumigaclavine C induces executor caspases-3, -8 and -9 leading to apoptosis. The western blot analysis may suggest that activation of apoptotic caspases is mainly due to induced expression of apoptotic Bax and Bid proteins, which leads to the mitochondrial cell death pathway. As showed in the data reducing the expression of Bcl-2 promotes the activity of Bax and Bak that mediate apoptosis by triggering destabilization of the mitochondrial membrane and consequently release the cytochrome c from the mitochondria to the cytosol. The release of cytochrome c is the leading factor for the higher expression of apoptotic caspases, which was manifested in our data after treatment with fumigaclavine C [45]. Furthermore, the result was confirmed by characteristic patterns of DNA fragmentation and cell cycle arrest.

4. Materials and Methods

4.1. Materials

Aspergillus fumigatus was isolated from the surface of marine green algae, collected at Seosaeng-myeon, Ulsan in the Republic of Korea in 2009. The fungal strain was cultured in YPG medium (1% yeast extract, 2% peptone, 10% glucose, 60% seawater, and 40% distilled water), and the fungal strain stored in 10% glycerol with the YPG medium at −78 °C for further experiments.

4.2. Chemicals

Extraction of the bioactive compound from *Aspergillus fumigatus* was performed using the extraction unit (Dongwon Scientific Co, Seoul, Korea). Silica gel 60 (230–400 mesh, Merck KGaA, Darmstadt, Germany), sephadex LH-20 (Sigma, St. Louis, MO, USA), YMC gel ODS-A 12 nm S-150 μm (YMC Co. Ltd., Kyoto, Japan) and thin-layer chromatography (TLC) plates (Kieselgel 60 F254, 0.25 mm, Merck KGaA, Darmstadt, Germany) were used for column chromatography and analytical TLC, respectively. The culture medium: Yeast extract (Lab M Limited, Lancashire, UK), peptone (Lab M Limited, Lancashire, UK), D-(+)-glucose (Yakuri, Sendai, Japan), agar powder (Lab M Limited, Lancashire, UK), glycerol (Sigma, 99%, St. Louis, MO, USA), penicillin G (Sigma, St. Louis, MO, USA). Organic solvent: *n*-hexane, EtOAc, CH_2Cl_2, MeOH, (Duksan Pure Chemical, Ansan-si, Korea, 99.5%) were used for the extraction. Coloring reagent used for visualization of TLC was $Ce(SO_4)_2$ (Sigma, St. Louis, MO, USA). ^1H NMR (400 MHz) and ^{13}C NMR (100 MHz) spectra were recorded on a JEOL JNM-ECP 400 NMR

spectrometer (JEOL, Tokyo, Japan), using the CD_3OD (3.34 ppm in ^1H and 49.86 ppm in ^{13}C NMR) solvent peak as an internal reference standard. Mass spectra were recorded on a JEOLJMS-700 spectrometer (JEOL).

4.3. Extraction and Isolation

The fungal strain was cultured in YPG medium (1% yeast extract, 2% peptone, 10% glucose, 4% agar, 60% seawater, and 40% distill water). Further culturing for extraction of metabolites was completed on YPG broth which was inoculated with 20 mL of fungal spore into 1 L long-neck flat bottom flask. The fungus was cultured (30 L) at 25 °C pH 7.6 in YPG medium for 30 days. The culture broth was extracted (2.3 g) with EtOAc (1:1.5 v/v, 1:1 v/v, broth–EtOAc) two times. The extract was fractionated by silica gel flash chromatography (*n*-hexane:EtOAc and CH_2Cl_2:MeOH) to generate five fractions. Final purification of each fraction was performed using ODS column chromatography (H_2O:MeOH), followed by HPLC (YMC ODS-A, MeOH) and obtained fumigaclavine C (15.8 mg) as a pure compound.

4.4. Cell Culture

Human breast cancer cells MCF-7 were obtained from American Type Culture Collection (ATCC). The cells were routinely grown in Dulbecco's modified Eagle's medium (Gibco, New York, NY, USA) supplemented with 10% FBS (Gibco, New York, NY, USA), 100 µg/mL penicillin, 100 µg/mL streptomycin, at 37 °C in humidified incubator under 5% CO_2. For experiments, cells were passaged at least for 5 times and detached with trypsin-EDTA.

4.5. Cell Viability (MTT) Assay

Cytotoxicity levels and anti-proliferative effects of the isolated compound from *Aspergillus fumigatus* on MCF-7 cells were measured using MTT (3-(4,5-dimethyl-2-yl)-2,5-diphenyl-tetrazoliumbromide) assay as described by Carmichael *et al.* [51]. In the testing, MCF-7 cells were cultured in 96-well plates at a density of 5×10^3 cells/well. After incubation for 24 h, cells were washed with fresh medium and were treated with different concentrations of fumigaclavine C. After 24 h or 36 h, 100 µL of MTT (0.5 mg/mL, final concentration) solution was added to each well and incubated for another 4 h at 37 °C under 5% CO_2. The MTT solution was removed and DMSO (100 µL) was added to each well. The amount of formazan salt was determined by measuring the OD at 570 nm wavelength by GENios® microplate reader (Tecan Austria GmbH, Grödig, Austria). The data were expressed as means of at least three independent experiments. Each value was expressed as the mean ± SD of triplicate experiments.

4.6. Cell Migration and Invasion Assay

The migration and invasion assay was performed using a 24-well transwell chamber with polyvinylpyrrolidone-free polycarbonate membranes (8 µm pore size) as previously reported [52]. For migration assay, 200 µL cells (2.5×10^5/mL in serum-free medium) were placed in the upper

compartment of the migration chamber and placed in 750 µL culture medium (with 10% FBS) in the lower chamber. The transwell was placed into the lower chamber to incubate at 37 °C in 5% CO_2 for 12 h. Then it was incubated in a FBS-free medium containing 0.2% BSA in the presence or absence of various concentrations (20 µM, 40 µM, and 60 µM) of fumigaclavine C, dissolved in 10% DMSO for 36 h at 37 °C. In 5% CO_2, the invasive cells attached to the lower surface of the inserted membrane and were fixed with 4% formaldehyde, methanol and stained with 0.5% crystal violet for 10 min [53]. After incubation, the filter inserts were removed from the wells, and the cells on the upper side of the filter were removed using cotton swabs. For the invasion assay, cells were measured in 24-well matrigel-coated (BD, New Jersey, NJ, USA) invasion chambers, other experiment steps were done with same with migration assay. Finally, the migrating and invading cells were observed with an optical microscope (Leica Microsystems Wetzlar GmbH, Wetzlar, Germany) at 100× magnification and the number of cells in four randomly selected microscopic bright fields per membrane was counted.

4.7. Hoechst 33258 Staining Assay

MCF-7 cells were cultured in 24-well plates at a density of 2×10^5 cells/well. After the cells were treated with fumigaclavine C for 24 h, cells were fixed with 3.7% formaldehyde in PBS at room temperature for 20 min, the formaldehyde was aspirated and the cells were washed three times with PBS, cold (−20 °C) methanol (100%) was added and then left at room temperature for 20 min, then stained with Hoechst 33258 (0.12 µg/mL), and then subjected to fluorescence microscopy.

4.8. Cell Cycle Assay

Cell cycle analyses were performed on propidium iodide-stained nuclei by using CellQuest software on a FACSCalibur flow cytometer (Becton-Dickinson Biosciences, San Jose, CA, USA). MCF-7 cells were cultured in six-well plates at a density of 5×10^5 cells/well. After the cells were treated with fumigaclavine C for 36 h, cells were harvested by trypsinizing, pelleted by centrifugation for 5 min at 1000 rpm, and 1×10^6 cells were resuspended in 0.5 mL ice cold PBS. Cells were then fixed by drop-wise addition to 70% ice-cold ethanol and stored overnight at 4 °C. The cell pellet was then resuspended in 0.5 mL staining solution containing 50 µg/mL of RNase A (Sigma, St. Louis, MO, USA) in 0.1% Triton X-100 and 100 µg/mL of propidium iodide (Molecular Probes, Eugene, OR, USA). Data were analyzed by single histogram statistics as described [54].

4.9. DNA Laddering Assay

DNA was isolated according to the method described by Shinzawa *et al.* [55]. Briefly, MCF-7 cells (1×10^6 cells/mL) were cultured in 10 cm2 culture disks for 24 h and treated with different concentrations (20 µM, 40 µM, and 60 µM) of fumigaclavine C. The amount of 1×10^6 cells/mL was incubated with the tail lysis buffer (20 µg/mL of protease K, 1 mM of Tris pH 8.0, 100 mM of NaCl, 10 mM of EDTA, and 0.5% of SDS) for 24 h at 37 °C. Chromosomal DNA was obtained by phenol/chloroform/isoamyl alcohol (25:24:1) extraction and ethanol (100%) precipitation. The

samples in TE solution (10 mM of Tris-HCl (pH 8.0) and 1 mM of EDTA) with 1 μg/mL of RNase A were incubated for 1 h at 37 °C. Ten micrograms of DNA from each sample were subjected to electrophoresis on 1.5% agarose gel for 2 h at 100 V and the gel stained with 1 mg/mL ethidium bromide and visualized by UV light using AlphaEase gel image analysis software (Alpha Innotech, Santa Clara, CA, USA).

4.10. Reverse Transcription-PCR (Polymerase Chain Reaction)

The total RNA from the MCF-7 cell line cultured in 10 cm dishes for 36 h was isolated using Trizol reagent (Invitrogen Co., Carlsbad, CA, USA) according to the supplier's protocol and measured at 260 nm. In brief, 2 μg of total RNA was used to synthesize first-strand cDNAs with a kit (Promega, Madison, WI, USA), which synthesis cDNA with long mRNA templates (>5 kb) [56]. PCR was then carried out in 50 μL of reaction volumes containing RNA PCR buffer, 2.5 mM $MgCl_2$, 0.2 μM of each primer, and 2.5 units of Taqpolymerase. Samples were pre-denatured at 94 °C for 4 min, followed by amplification at 94 °C for 1 min, at 55 °C for 30 s, and at 72 °C for 1 min for 30 cycles, followed by a final 10 min extension step at 72 °C. The primers for β-actin were forward primer 5′-AGC-CAT-GTA-CGT-AGC-CAT-CC-3′ and reverse primer 5′-TCC-CTC-TCA-GCT-GTG-GTG-GTG-AA-3′; the primers for MMP-2 were forward primer 5′-CAC-CTA-CAC-CAA-GAA-CTT-C-3′ and reverse primer 5′-AAC-ACA-GCC-TTC-TCC-TCC-TG-3′; the primers for MMP-9 were forward primer 5′-TTG-AGT-CCG-GCA-GAC-AAT-CC-3′ and reverse primer 5′-CCT-TAT-CCA-CGC-GAA-TGA-CG-3′; the primers for caspase-3 were forward primer 5′-GAA-CTG-GAC-TGT-GGC-ATT-GA-3′ and reverse primer 5′-TGT-CGG-CAT-ACT-GTT-TCA-GC-3′; the primers for caspase-8 were forward primer 5′-CAT-CCA-GTC-ACT-TTG-CCA-GA-3′ and reverse primer 5′-GCA-TCT-GTT- TCC-CCA-TGT-TT-3′; the primers for caspase-9 were forward primer 5′-TGG-ACG-ACA-TCT-TTG-AGC-AG-3′ and reverse primer 5′-GCA-AGA-TAA-GGC-AGG-GTG-AG-3′; the primers for Bax were forward primer 5′-TGC-CAG-CAA-ACT-GGT-GCT-CA-3′ and reverse primer 5′-GCA-CTC-CCG-CCA-CAA-AGA-TG-3′; the primers for Bcl-2 were forward primer 5′-CGC-ATC-AGG-AAG-GCT-AGA-GT-3′ and reverse primer 5′-AGC-TTC-CAG-ACA-TTC-GGA-GA-3′; the primers for p53 were forward primer 5′-GCG-CAC-AGA-GGA-AGA-GAA-TC-3′ and reverse primer 5′-CTC-TCG-GAA-CAT-CTC-GAA-GC-3′; the primers for p21 were forward primer 5′-CTG-TCA-CAG-GCG-GTT-ATG-AA-3′ and reverse primer 5′-TGT-GCT-CAC-TTC-AGG-GTC-AC-3′. Polymerase chain reaction products electrophoresed on 1.5% argarose gels were visualized by ethidium bromide staining and quantified using AlphaEase® gel image-analysis software (Alpha Innotech, San Leandro, CA, USA).

4.11. Western Blot Analysis

Western blotting was performed according to standard procedures [57]. A total amount of 1×10^6 of MCF-7 cells was treated with different concentrations (20 μM, 40 μM, and 60 μM) of the fumigaclavine C. The cells were lysed in RIPA lysis buffer containing 50 mM Tris-HCl (pH 7.5), 0.4% Nonidet P-40, 120 mM NaCl, 1.5 mM $MgCl_2$, 2 mM phenylmethylsulfonyl fluoride, 80 μg/mL of leupeptin, 3 mM NaF and 1 mM DTT at 4 °C for 30 min. Cell lysates (about 20 μg of

total proteins) were resolved on a 4%–20% SDS-page gel, electrotransferred onto a nitrocellulose membrane and blocked with 5% (w/v) non-fat dry milk in Tris-buffered saline and 0.1% Tween 20 for 1 h at room temperature. Different antibodies (Santa Cruz Biotechnology, Inc., Dallas, TX, USA) were used to detect the respective proteins using a chemiluminescent ECL assay kit (Amersham Pharmacia Biosciences, Buckinghamshire, UK), according to the manufacturer's instructions. Blots were visualized using an LAS3000® Luminescent image analyzer and protein expression was quantified by MULTI GAUGE V3.0 software (Fujifilm Life Science, Tokyo, Japan).

4.12. Docking Calculations

Docking calculations were carried out using DockingServer [58]. The MMFF94 force field was used for energy minimization of ligand molecule (Fumigaclavine C) using DockingServer [59]. Gasteiger partial charges were added to the ligand atoms. Non-polar hydrogen atoms were merged and rotatable bonds were defined.

Docking calculations were carried out on the crystal structure of apoptosis regulator Bcl-2 (2w3L-Apoptosis) protein model. Essential hydrogen atoms, Kollman united atom type charges, and solvation parameters were added with the aid of AutoDock tools. Affinity (grid) maps of 20 × 20 × 20 Å grid points and 0.375 Å spacing were generated using the Autogrid program [60]. AutoDock parameter set- and distance-dependent dielectric functions were used in the calculation of the van der Waals and the electrostatic terms, respectively.

Docking simulations were performed using the Lamarckian genetic algorithm (LGA) and the Solis & Wets local search method [61]. Initial position, orientation, and torsions of the ligand molecules were set randomly. Each docking experiment was derived from 10 different runs that were set to terminate after a maximum of 250,000 energy evaluations. The population size was set to 150. During the search, a translational step of 0.2 Å, and quaternion and torsion steps of five were applied.

5. Conclusions

In summary, it was found in this study that fumigaclavine C isolated from a marine-derived fungus, *Aspergillus fumigatus*, shows potent anti-cancer activity. *In vitro* screening in MCF-7 human cancer cells showed that the compound induced apoptosis in the cells most probably via PI3/Akt and NF-κB signaling which lead to the activation of the mitochondrial cell death pathway. Moreover, the correlative mechanisms behind the anti-proliferation and apoptosis induction of fumigaclavine C were studied in detail (Figure 9). Collectively, it could be suggested that fumigaclavine C could be developed as potential therapeutic candidate in the treatment of breast cancer.

Figure 9. Fumigaclavine C-induced apoptosis in MCF-7 breast cancer cells through the mitochondrial pathway.

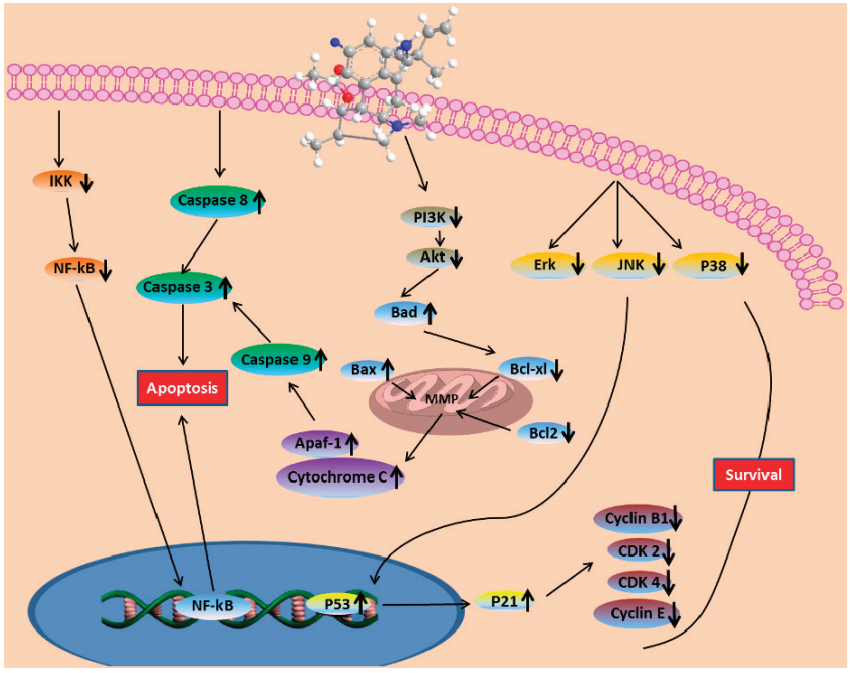

Acknowledgments

This research was supported by a grant from Marine Bioprocess Research Center of the Marine Biotechnology Program funded by the Ministry of Oceans and Fisheries, Seoul, Korea.

Conflicts of Interest

Authors declare that there is no conflict of interest.

References

1. Jemal, A.; Thomas, A.; Murry, T.; Thun, M. Cancer statistics. *CA Cancer J. Clin*. **2002**, *52*, 23–37.
2. Jemal, A.; Siegel, R.; Ward, E.; Murray, T.; Xu, J.; Thun, M.J. Cancer statistics. *CA. Cancer J. Clin*. **2007**, *57*, 43–66.
3. Aggarwal, B.B.; Takada, Y.; Oommen, O.V. From chemoprevention to chemotherapy: Common targets and common goals. *Expert Opin. Investig. Drugs* **2004**, *13*, 1327–1338.
4. Xin, Z.H.; Fang, Y.C.; Du, L.; Zhu, T.J.; Duan, L.; Chen, J.; Gu, Q.Q.; Zhu, W.M. Aurantiomides A–C, quinazoline alkaloids from the sponge-derived fungus *Penicillium aurantiogriseum* SP0-19. *J. Nat. Prod*. **2007**, *70*, 853–855.

5. Osterhage, C.; Kaminsky, R.; Konig, G.M.; Wright, A.D. Ascosali-pyrrolidinone A, an antimicrobial alkaloid, from the obligate marine fungus *Ascochyta salicorniae*. *J. Org. Chem*. **2000**, *65*, 6412–6417.
6. Lu, X.H.; Shi, Q.W.; Zheng, Z.H.; Ke, A.B.; Zhang, H.; Huo, C.H.; Ma, Y.; Ren, X.; Li, Y.Y.; Lin, J.; *et al.* Oxepinamides: Novel liver X receptor agonists from *Aspergillus puniceus*. *Eur. J. Org. Chem*. **2011**, *2011*, 802–807.
7. Du, L.; Li, D.H.; Zhu, T.J.; Cai, S.X.; Wang, F.P.; Xiao, X.; Gu, Q.Q. New alkaloids and diterpenes from a deep ocean sediment derived fungus *Penicillium* sp. *Tetrahedron* **2009**, *65*, 1033–1039.
8. Fallon, J.P.; Reeves, E.P.; Kavanagh, K. Inhibition of neutrophil function following exposure to the *Aspergillus fumigatus* toxin fumagillin. *J. Med. Microbiol*. **2010**, *59*, 625–633.
9. Fujiki, H.; Mori, M.; Nakayasu, M.; Terada, M.; Sugimura, T.; Mooret, R.E. Indole alkaloids: Dihydroteleocidin B, teleocidin, and lyngbyatoxin A as members of a new class of tumor promoters. *Proc. Natl. Acad. Sci. USA* **1981**, *78*, 3872–3876.
10. Ge, H.M.; Yu, Z.G.; Zhang, J.; Wu, J.H.; Tan, R.X. Bioactive alkaloids from endophytic *Aspergillus fumigatus*. *J. Nat. Prod*. **2009**, *72*, 753–755.
11. Shu, R.G.; Wang, F.W.; Yang, Y.M.; Liu, Y.X.; Tan, R.X. Antibacterial and xanthine oxidase inhibitory cerebrosides from *Fusarium* sp. IFB-121, an endophytic fungus in *Quercus variabilis*. *Lipids* **2004**, *39*, 667–673.
12. Lu, H.; Zou, W.X.; Meng, J.C.; Hu, J.; Tan, R.X. New bioactive metabolites produced by *Colletotrichum* sp., an endophytic fungus in *Artemisia annua*. *Plant Sci*. **2000**, *151*, 67–73.
13. Cole, R.J.; Kirksey, J.W.; Dorner, J.W.; Wilson, D.V.; Johnson, J.C.; Bedell, D. Mycotoxins produced by *Aspergillus fumigatus* species isolated from molded silage. *J. Agric. Food Chem*. **1977**, *25*, 826–830.
14. Zhao, Y.; Liu, J.; Wang, J.; Wang, L.; Yin, H.; Tan, R. Fumigaclavine C improves concanavalin A-induced liver injury inmicemainly via inhibiting TNF-α production and lymphocyte adhesion to extracellular matrices. *J. Pharm. Pharmacol*. **2004**, *56*, 775–784.
15. Kuramoto, M.; Arimoto, H.; Uemura, D. Bioactive alkaloids from the sea: a review. *Mar. Drugs* **2004**, *2*, 39–54.
16. Ghobrial, I.M.; Witzig, T.E.; Adjei, A.A. Targeting apoptosis pathways in cancer therapy. *CA Cancer J. Clin*. **2005**, *55*, 178–194.
17. Hetz, C.A.; Torres, V.; Quest, A.F. Beyond apoptosis: nonapoptotic cell death inphysiology and disease. *Biochem. Cell Biol*. **2005**, *83*, 579–588.
18. Thompson, C.B. Apoptosis in the pathogenesis and treatment of disease. *Science* **1995**, *267*, 1456–1462.
19. Williams, G.T.; Smith, C.A. Molecular regulation of apoptosis: genetic controls on cell death. *Cell* **1993**, *74*, 777–779.
20. Pereira, D.M.; Cheel, J.; Areche, C.; San-Martin, A.; Rovirosa, J.; Silva, L.R.; Valentao, P.; Andrade, P.B. Anti-proliferative activity of meroditerpenoids isolated from the brown alga *Stypopodium flabelliforme* against several cancer cell lines. *Mar. Drugs* **2011**, *9*, 852–862.

21. Du, R.H.; Li, E.G.; Cao, Y.; Song, Y.C.; Tan, R.X. Fumigaclavine C inhibits tumor necrosis factor α production via suppression of toll-like receptor 4 and nuclear factor κB activation in macrophages. *Life Sci*. **2011**, *89*, 235–240.
22. Adya, R.; Tan, B.K.; Punn, A.; Chen, J.; Randeva, H.S. Visfatin induces human endothelial VEGF and MMP-2/9 production via MAPK and PI3K/Akt signalling pathways: novel insights into visfatin-induced angiogenesis. *Cardiovasc. Res.* **2008**, *78*, 356–365.
23. Newby, A.C. Matrix metalloproteinases regulate migration, proliferation, and death of vascular smooth muscle cells by degrading matrix and non-matrix substrates. *Cardiovasc. Res.* **2006**, *69*, 614–624.
24. Yang, G.H.; Jarvis, B.B.; Chung, Y.J.; Pestka, J.J. Apoptosis Induction by the satratoxins and other trichothecene mycotoxins: Relationship to ERK, p38 MAPK, and SAPK/JNK activation. *Toxicol. Appl. Pharmacol.* **2000**, *164*, 149–160.
25. Seger, R.; Krebs, E.G. The MAPK signaling cascade. *FASEB J*. **1995**, *9*, 726–735.
26. Tibbles, L.A.; Woodgett, J.R. The stress-activated protein kinase pathways. *Cell. Mol. Life Sci*. **1999**, *55*, 1230–1254.
27. Tournier, C.; Hess, P.; Yang, D.D.; Xu, J.; Turner, T.K.; Nimnual, A.; Bar-Sagi, D.; Jones, S.N.; Flavell, R.A.; Davis, R.J. Requirement of JNK for stress-induced activation of the cytochrome
C-mediated death pathway. *Science* **2000**, *288*, 870–874.
28. Chang, L.; Karin, M. Mammalian MAP kinase signalling cascades. *Nature* **2001**, *410*, 37–40.
29. Fridman, J.S.; Lowe, S.W. Control of apoptosis by p53. *Oncogene* **2003**, *22*, 9030–9040.
30. Wu, G.S. The functional interactions between the p53 and MAPK signaling pathways. *Cancer Biol. Ther.* **2004**, *2*, 156–161.
31. Bunz, F.; Dutriaux, A.; Lengauer, C.; Waldman, T.; Zhou, S.; Brown, J.P.; Sedivy, J.M.; Kinzler, K.W.; Vogelstein, B. Requirement for p53 and p21to sustain G2 arrest after DNA damage. *Science* **1998**, *282*, 1497–1501.
32. Wang, J.H.; Yu, B.; He, P.; Bai, X. Roles of Bcl-2 family members, PI3K and NF-κB pathways in *Escherichia* coli-induced apoptosis in human monocytic U937 cells. *World J. Microb. Biot.* **2011**, *27*, 1827–1838.
33. Lin, M.L.; Lu, Y.C.; Chung, J.G.; Wang, S.G.; Lin, H.T.; Kang, S.E.; Tang, C.H.; Ko, J.L.; Chen, S.S. Down-regulation of MMP-2 through the p38 MAPK-NF-κB-dependent pathway by aloe-emodin leads to inhibition of nasopharyngeal carcinoma cell invasion. *Mol. Carcinog*. **2010**, *49*, 783–797.
34. Datta, S.R.; Brunet, A.; Greenberg, M.E. Cellular survival: A play in three Akts. *Genes Dev*. **1999**, *13*, 2905–2927.
35. Rahman, K.W.; Ali, S.; Aboukameel, A.; Sarkar, S.H.; Wang, Z.; Philip, P.A.; Sakr, W.A.; Raz, A. Inactivation of NF-κB by 3, 3′-diindolylmethane contributes to increased apoptosis induced by chemotherapeutic agent in breast cancer cells. *Mol. Cancer Ther.* **2007**, *6*, 2757–2765.

36. Kong, C.S.; Kim, J.A.; Yoon, N.Y.; Kim, S.K. Induction of apoptosis by phloroglucinol derivative from *Ecklonia Cava* in MCF-7 human breast cancer cells. *Food Chem. Toxicol*. **2009**, *47*, 1653–1658.
37. Cahir-McFarland, E.D.; Davidson, D.M.; Schauer, S.L.; Duong, J.; Kieff, E. NF-κB inhibition causes spontaneous apoptosis in Epstein-Barr virus-trans formed lympho blastoid cells. *Proc. Natl. Acad. Sci. USA* **2000**, *97*, 6055–6060.
38. Baldwin, A.S.J. The NF-kappa B and I kappa B proteins: new discoveries and insights. *Annu. Rev. Immunol*. **1996**, *14*, 649–683.
39. Beg, A.A.; Baldwin, A.S.J. The I kappa B proteins: multifunctional regulators of Rel/NF-kappa B transcription factors. *Genes Dev*. **1993**, *7*, 2064–2070.
40. Liao, Y.F.; Rao, Y.K.; Tzeng, Y.M. Aqueous extract of Anisomeles indica and its purified compound exerts anti-metastatic activity through inhibition of NF-κB/AP-1-dependent MMP-9 activation in human breast cancer MCF-7 cells. *Food Chem. Toxicol*. **2012**, *50*, 2930–2936.
41. Roy, N.; Deveraux, O.L.; Takahashi, R.; Salvesen, G.S.; Reed, J.C. The c-IAP-1 and c-IAP-2 proteins are direct inhibitors of specific caspases. *EMBO J*. **1997**, *16*, 6914–6925.
42. Deveraux, Q.L.; Reed, J.C. IAP family proteins suppressors of apoptosis. *Genes Dev*. **1999**, *13*, 239–252.
43. Kitchen, D.B.; Decornez, H.; Furr, J.R.; Bajorath, J. Docking and scoring in virtual screening for drug discovery: methods and applications. *Nat. Rev. Drug Discov*. **2004**, *3*, 935–949.
44. Huang, Z. Bcl-2 family proteins as targets for anticancer drug design. *Oncogene* **2000**, *19*, 6627–6631.
45. Antonsson, B. Bax and other pro-apoptotic Bcl-2 family ‘‘killer-proteins” and their victim the mitochondrion. *Cell Tissue Res.* **2001**, *306*, 347–361.
46. Zornig, M.; Hueber, A.; Baum, W.; Evan, G. Apoptosis regulators and their role in tumorigenesis. *Biochem. Biophys. Acta* **2001**, *1551*, 1–37.
47. Leist, M.; Jaattela, M. Four deaths and a funeral: From caspases to alternative mechanism. *Nat. Rev. Mol. Cell Biol*. **2001**, *2*, 589–598.
48. Nagy, G.; Szarka, A.; Lotz, G.; Dóczi, J.; Wunderlich, L.; Kiss, A.; Jemnitz, K.; Veres, Z.; Bánhegyi, G.; Schaff, Z.; *et al.* BGP-15 inhibits caspase-independent programmed cell death in acetaminophen-induced liver injury. *Toxicol. Appl. Pharmacol*. **2010**, *243*, 96–103.
49. Zou, H.; Yang, R.M.; Hao, J.S.; Wang, J.; Sun, C.H.; Fesik, S.W.; Wu, J.C.; Tomaselli, K.J.; Armstrong, R.C. Regulation of the apaf-1/caspase-9 apoptosome bycaspase-3 and XIAP. *J. Biol. Chem*. **2003**, *278*, 8091–8098.
50. Kuida, K.; Haydar, T.F.; Kuan, C.Y.; Gu, Y.; Taya, C.J.; Karasuyama, H.; Su, M.S.; Rakic, P.; Flavell, R.A. Reduced apoptosis and cytochrome C-mediated caspase activation in mice lacking caspase 9. *Cell* **1998**, *94*, 325–337.
51. Carmichael, J.; DeGraff, W.G.; Gazdar, A.F. Evaluation of a tetrazolium-based semiautomated colorimetric assay: Assessment of chemosensitivity testing. *Cancer Res*. **1987**, *47*, 936–942.

52. Jin, U.H.; Suh, S.J.; Chang, H.W.; Son, J.K.; Lee, S.H.; Son, K.H.; Chang, Y.C.; Kim, C.H. Tanshinone IIA from salvia miltiorrhiza bungeinhibits human aortic smooth muscle cell migration and MMP-9 activity through AKT signaling pathway. *J. Cell. Biochem*. **2008**, *104*, 15–26.
53. Frisk, T.; Rydholm, S.; Liebmann, T.; Svahn, H.A.; Stemme, G.; Brismar, H. A microfluidic device for parallel 3-D cell cultures in asymmetric environments. *Electrophoresis* **2007**, *28*, 4705–4712.
54. Yin, X.Y.; Grove, L.; Datta, N.S.; Long, M.W.; Prochownik, E.V. C-myc overexpression and p53 loss cooperate to promote genomic instability. *Oncogene* **1999**, *18*, 1177–1184.
55. Shinzawa, K.; Watanabe, Y.; Akaike, T. Primary cultured murine hepatocytes but not hepatoma cells regulate the cell number through density-dependent cell death. *Cell Death Differ*. **1995**, *2*, 133–140.
56. Roth, M.J.; Tanese, N.; Goff, S.P. Purification and characterization of murine retroviral reverse transcriptase expressed in *Escherichia coli*. *J. Biol. Chem*. **1985**, *26*0, 9326–9335.
57. Towbin, H.; Staehelin, T.; Gordon, J. Electrophoretic transfer of proteins from polyacrylamide gels to nitrocellulose sheets: Procedure and some applications. *Proc. Natl. Acad. Sci. USA* **1979**, *76*, 4350–4354.
58. Bikadi, Z.; Hazai, E. Application of the PM6 semi-empirical method to modeling proteins enhances docking accuracy of AutoDock. *J. Cheminform*. **2009**, *1*, 15.
59. Halgren, E.; Marinkovic, K.; Chauvel, P. Generators of the late cognitive potentials in auditory and visual oddball tasks. *Electroencephalogr. Clin. Neurophysiol.* **1998**, *106*, 156–164.
60. Morris, G.M.; Goodsell, D.S.; Halliday, R.S.; Huey, R.; Hart, W.E.; Belew, R.K.; Olson, A.J. Automated docking using a lamarckian genetic algorithm and and empirical binding free energy function. *J. Comput. Chem*. **1998**, *19*, 1639–1662.
61. Solis, F.J.; Wets, R.J.B. Minimization by Random Search Techniques. *Math. Oper. Res.* **1981**, *6*, 19–30.

Palmitic Acid and Ergosta-7,22-dien-3-ol Contribute to the Apoptotic Effect and Cell Cycle Arrest of an Extract from *Marthasterias glacialis* L. in Neuroblastoma Cells

David M. Pereira, Georgina Correia-da-Silva, Patrícia Valentão, Natércia Teixeira and Paula B. Andrade

Abstract: We describe the effect of a chemically characterized lipophilic extract obtained from *Marthasterias glacialis* L. against human breast cancer (MCF-7) and human neuroblastoma (SH-SY5Y) cell lines. Evaluation of DNA synthesis revealed that both cell lines were markedly affected in a concentration-dependent way, the SH-SY5Y cell line being more susceptible. Cell cycle arrest was observed, an effect induced by the sterol, ergosta-7,22-dien-3-ol, present in the extract. Morphological evaluation of treated cells showed the advent of lipid droplets and chromatin condensation compatible with apoptosis, which was confirmed by the evaluation of caspase-3 and -9 activities. Palmitic acid was the main compound responsible for this apoptotic effect by a ceramide-independent mechanism that involved endoplasmic reticulum (ER)-stress with upregulation of CCAAT/-enhancer-binding protein homologous protein (CHOP).

Reprinted from *Mar. Drugs*. Cite as: Pereira, D.M.; Correia-da-Silva, G.; Valentão, P.; Teixeira, N.; Andrade, P.B. Palmitic Acid and Ergosta-7,22-dien-3-ol Contribute to the Apoptotic Effect and Cell Cycle Arrest of an Extract from *Marthasterias glacialis* L. in Neuroblastoma Cells. *Mar. Drugs* **2014**, *12*, 54-68.

1. Introduction

Nature is an indisputable source of drugs for the human pharmacotherapeutical arsenal [1–3]. In recent years, marine-derived drugs have received great attention, with a steady increase in the number of molecules in clinical trials [4–7].

The chemical composition of *Marthasterias glacialis* L. has been described before, and amino acids, fatty acids, carotenoids and sterols have been identified [8–10]. In addition, the effect of a purified extract upon several human cancer and non-cancer cells was reported [8,11], though the mechanism responsible for the anticancer activity has not been investigated.

Nowadays, there has been increasing awareness regarding the role of the endoplasmic reticulum (ER) in the homeostasis of the cell. When ER homeostasis is disturbed, the unfolded protein response (UPR) can be activated, and the associated ER stress is known to be the basis of several cellular aggressions, namely apoptosis. In order to monitor ER status, three stress sensor proteins are known: double-stranded RNA-dependent protein kinase PKR-like ER kinase (PERK), inositol-requiring 1α (IRE1α) and activating transcription factor 6 (ATF6). In the particular case of PERK, its active form phosphorylates eIF2, which inhibits protein translation. In this branch of UPR, the DNA-damage-inducible gene 153 (GADD153), also known as C/EBP homologous protein (CHOP, a member of the C/EBP transcription factor family that heterodimerizes with other C/EBPs), is upregulated, and for this reason, it is a widely used marker of ER-stress [12–14]. Increased levels

of CHOP have been associated with pro-apoptotic effects in several cancer cell lines, an effect attributed to CHOP-mediated repression of BCL2 gene family.

In this work, we evaluated the activity of a purified lipophilic extract from *M. glacialis* on the cancer cell lines, MCF-7 (estrogen receptor positive human breast cancer cells) and SH-SY5Y (human neuroblastoma cells), and investigated the mechanism involved in cell death and cell cycle arrest. The contribution of the main compounds present in the extract (20 µM palmitic acid, 30 µM *cis* 11-eicosenoic acid, 10 µM *cis* 11,14-eicosadienoic acid and 25 µM ergosta-7,22-dien-3-ol) is discussed.

2. Results and Discussion

2.1. Screening of M. glacialis *Lipophilic Extract Effect on Cell Morphology and DNA Synthesis*

We evaluated the effect of a broad range of concentrations (78–625 µg/mL) of *M. glacialis* lipophilic extract in DNA synthesis. As shown in Figure 1, the extract caused a concentration-dependent reduction of DNA synthesis in both cell lines. However, in neuroblastoma cells, the effect was stronger and time-independent, while in MCF-7, it was time-dependent. These results are in line with previous reports that point to a similar behavior with regards to cell viability [11]. The lowest concentrations that elicited a biological effect were selected for morphological studies, 156 and 312 µg/mL for the SH-SY5Y and MCF-7 cell lines, respectively.

Figure 1. Rate of DNA synthesis in MCF-7 and SH-SY5Y cells treated with the extract (78–625 µg/mL for 24 or 48 h) by the ^{3}H-thymidine incorporation assay. The results correspond to the mean ± standard deviation of three independent experiments performed in triplicate.

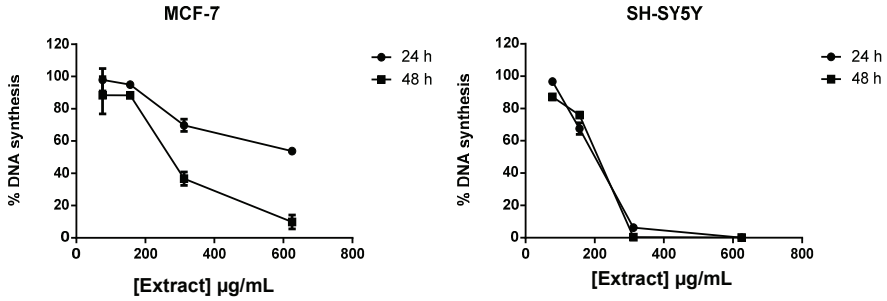

Several techniques were employed for the study of the effect of *M. glacialis* extract on cytoplasmic and nuclear morphology. After incubation with the extract for 48 and 24 h, both Giemsa and Hoechst 33342 stainings showed chromatin condensation in MCF-7 and SH-SY5Y, respectively, the latter presenting structures compatible with apoptotic bodies (Figures 2 and 3). In both cell lines, exposure to the extract resulted in cytoplasmic vesicles. Given the lipophilic nature of the extract, we hypothesized that these vesicles could be the result of the accumulation of lipid compounds in the cell. For this reason, Oil Red O staining was performed. As shown in Figures 2 and 3, Oil Red O successfully stained the cytoplasmic vesicles, which is compatible with lipid

droplets. This result was further confirmed by transmission electron microscopy, which showed that these structures displayed the homogeneous grey opacity commonly found in lipid-containing organelles (Figure 2). By evaluating the effect of individual compounds on lipid droplets accumulation, we found that *cis* 11,14-eicosadienoic acid was able to elicit a similar effect regarding lipid vesicles in cytoplasm (data not shown), being likely responsible for the same effect presented by the extract. However, we cannot rule out the possibility that the accumulation of lipids in cytoplasm is related to the impact of these compounds in lipid metabolism. As the SH-SY5Y cell line showed higher susceptibility and morphological changes, it was selected for subsequent studies.

Figure 2. Morphological assessment of MCF-7 cells (control *vs.* treatment, 48 h of incubation). Giemsa and Hoechst 33342 stainings show chromatin condensation (red and white arrows, respectively) following incubation with the extract. Cytoplasmic vesicles, visible in Giemsa staining, proved to harbor lipophilic compounds, as shown with Oil Red O staining and transmission electron microscopy (yellow arrows).

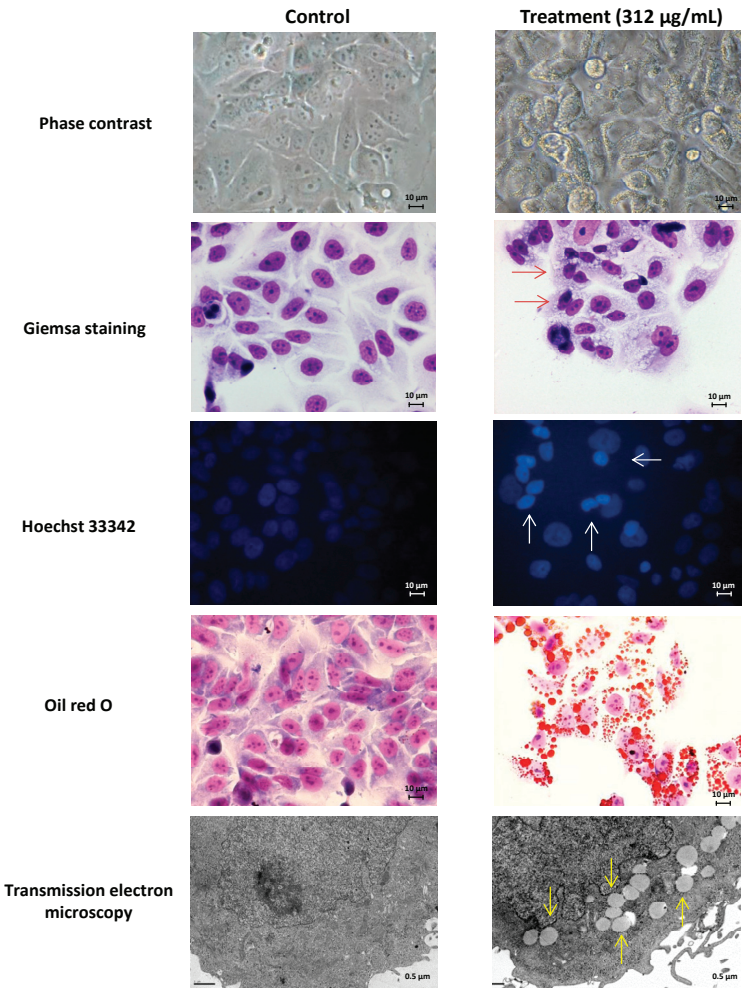

Figure 3. Morphological assessment of SH-SY5Y cells (control *vs.* treatment, 24 h of incubation). Giemsa and Hoechst 33342 stainings show chromatin condensation and fragmentation (red and white arrows). The advent of lipophilic cytosolic vesicles is demonstrated by the Oil Red O staining.

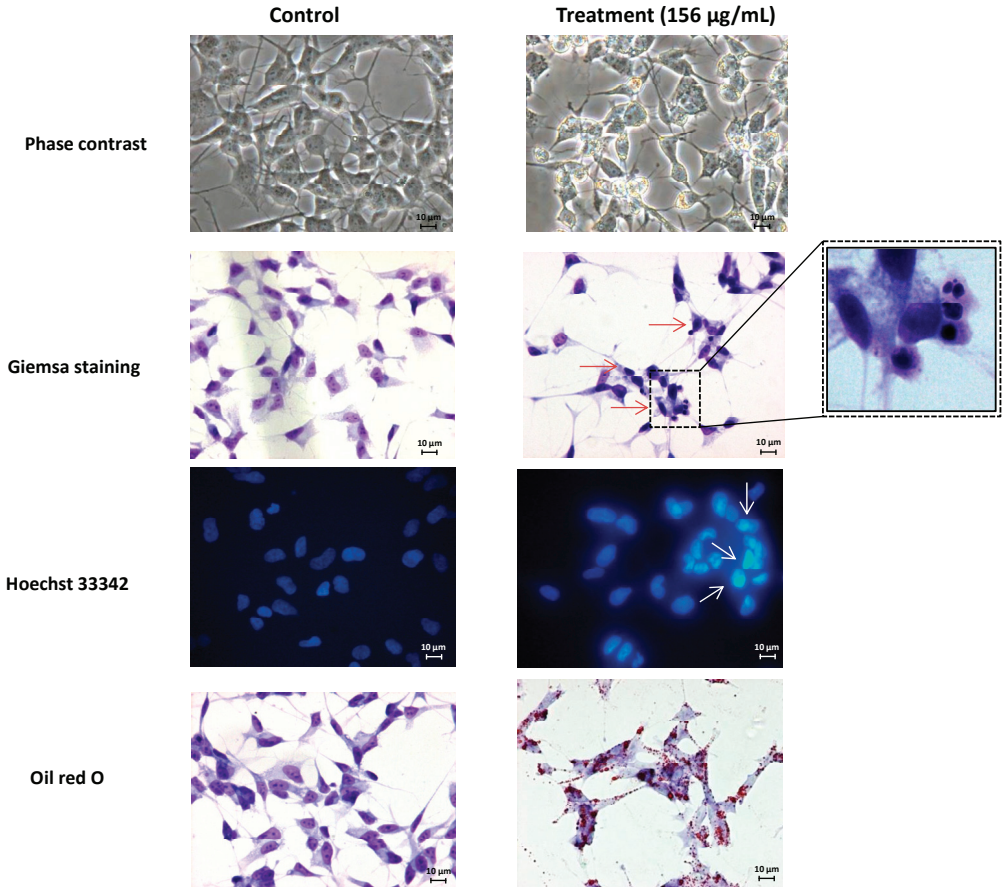

2.2. Ergosta-7,22-dien-3-ol Is Responsible for Cell Cycle Arrest

In light of the results from the thymidine incorporation assay, we evaluated the impact of the *M. glacialis* lipophilic extract and of the pure compounds that were present in higher amounts in the extract on the neuroblastoma cells' cell cycle. At a concentration of 156 µg/mL, the purified extract caused a G0/G1 arrest, which resulted in an increase of 10% of the number of cells in this phase (Figure 4).

Figure 4. Representative histograms of the effect of *M. glacialis* lipophilic extract and pure compounds on SH-SY5Y cell cycle. The extract caused a cell cycle arrest in the G0/G1 phase, an effect attributed to ergosta-7,22-dien-3-ol. Other major compounds found in the extract had no appreciable effect. Results are expressed as the mean ± standard deviation of three experiments. * $p < 0.05$; ** $p < 0.01$; *** $p < 0.001$ (*vs.* control). PA: 20 µM palmitic acid; *cis* 11: 35 µM *cis* 11-eicosenoic acid; *cis* 11,14: 10 µM *cis* 11,14-eicosadienoic acid; E-7,22: 25 µM ergosta-7,22-dien-3-ol; combination: Palmitic acid + *cis* 11-eicosenoic acid + *cis* 11,14-eicosadienoic + ergosta-7,22-dien-3-ol.

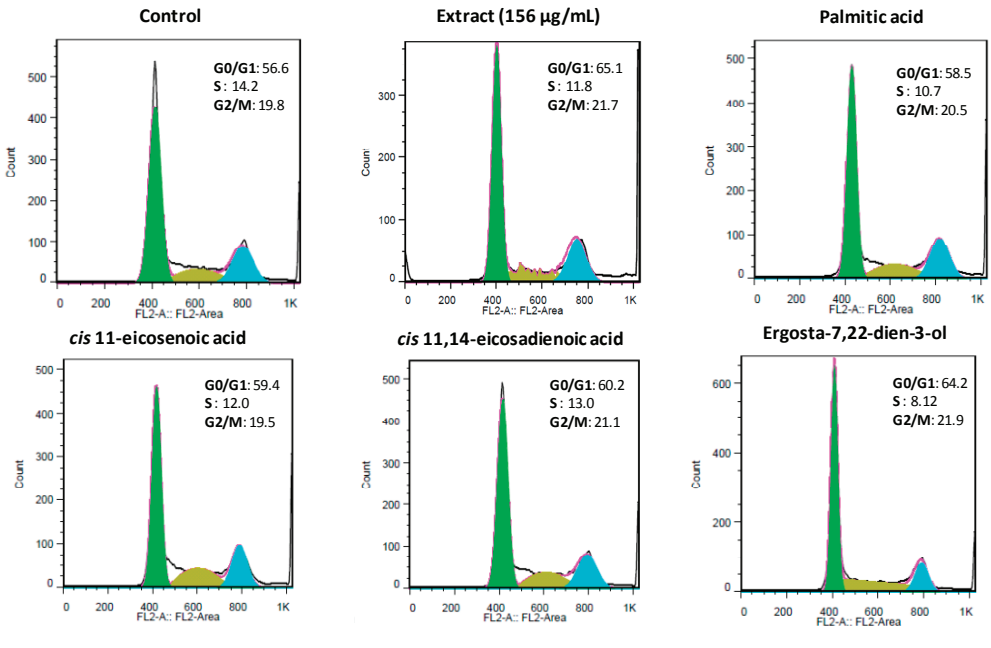

	G0/G1	S	G2/M
Control	56.7 ± 0.1	15.1 ± 1.3	20.9 ± 1.5
Ext 156 µg/mL	65.1 ± 1.0**	11.8 ± 0.6	21.7 ± 0.7
PA	59.9 ± 2.0	9.63 ± 1.5*	21.1 ± 0.9
cis 11	58.3 ± 1.6	12.6 ± 0.8	20.0 ± 0.6
cis 11,14	61.1 ± 1.3	11.9 ± 1.6	21.2 ± 0.1
E-7,22-dien-3-ol	66.2 ± 2.8**	8.6 ± 0.6**	20.1 ± 2.5
Combination	68.3 ± 1.8***	4.9 ± 1.0***	19.9 ± 1.2

In previous work, we have established the identity of major compounds and their concentrations in the purified extract from *M. glacialis* [11]. At the working concentration of 156 µg/mL, the major candidates to exert a biological effect were palmitic acid (20 µM), *cis* 11-eicosenoic acid (30 µM), *cis* 11,14-eicosadienoic acid (10 µM) and ergosta-7,22-dien-3-ol (25 µM). In order to evaluate the compounds responsible for the cell cycle arrest capacity of the extract, these compounds were evaluated individually and in combination after 24 h of incubation (Figure 4).

None of the fatty acids tested showed significant effect in these values, while the sterol, ergosta-7,22-dien-3-ol, was able to cause an effect similar to that of the extract. When all compounds were tested in combination, similar values were found. Our data show that cell cycle arrest caused by the extract can be mostly attributed to the sterol, ergosta-7,22-dien-3-ol.

2.3. Palmitic Acid Is Responsible for the Extract-Induced Ceramide-Independent Apoptosis via the Intrinsic Pathway

In previous work, we have described the impact of the purified lipophilic extract from *M. glacialis* in the cell density, viability and membrane integrity of SH-SY5Y cells [11]. At the concentration of 156 µg/mL, the extract elicited about 30% of a reduction in cell viability. Palmitic acid was the likely candidate for this activity; however, the mechanism of action was not investigated. In the work herein, we confirmed these results and showed that, apart from palmitic acid, the other compounds had no impact on cell viability. When all compounds were tested in combination, an inhibitory effect was found, albeit slightly lower than palmitic acid alone (Figure 5).

Figure 5. Cell viability was evaluated following incubation with the compounds present in the extract for 24 h. PA: Palmitic acid (20 µM); Cis 11: *cis* 11-eicosenoic acid (30 µM); Cis 11,14: *cis* 11,14-eicosadienoic acid (10 µM); E-7,22: Ergosta-7,22-dien-3-ol (25 µM); Combination: All compounds. Results are expressed as the mean ± standard deviation of three experiments. *** $p < 0.001$ (*vs.* control).

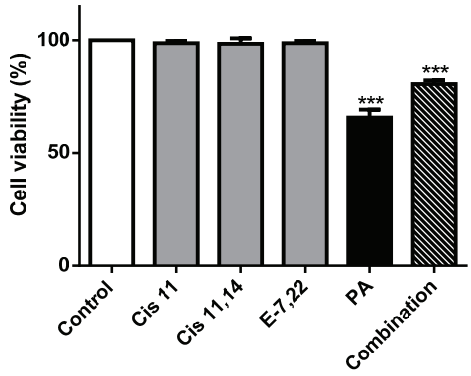

The above-mentioned morphological findings, which included apoptotic bodies in the case of SH-SY5Y cells, led us to confirm that apoptosis was taking place by evaluating the activity of caspase-3/-7, and -9. After 24 h of incubation, the extract caused an increase of about 30% in both caspase-3/-7 and -9 activity (Figure 6). While *cis* 11-eicosenoic and *cis* 11,14-eicosadienoic acids and ergosta-7,22-dien-3-ol had no impact on caspases activity (data not shown), palmitic acid elicited an increase in caspase-9 and -3/-7 activity of approximately 12 and 20%, respectively. However, when all compounds were tested in combination, higher values, closer to those displayed by the extract (18% and 25%, respectively), were found. Taken together, these results suggest that, although palmitic acid is the main compound responsible for the pro-apoptotic activity of the

extract, its effect is enhanced by the presence of the unsaturated fatty acids and sterol. The pro-apoptotic effect of palmitic acid has been described in several cell lines, the concentrations used being highly dependent on cell type and as variable as 100 µM [15] and 1 mM [16]. Although our study does, indeed, use lower palmitate concentrations, it should be taken into account that the values of caspase activation found were 12% and 20%, for caspase-9 and -3, respectively.

Figure 6. Caspase-3/-7 and -9 activity. Ext: 156 µg/mL extract; PA: Palmitic acid (20 µM); Combination: PA (20 µM) + *cis* 11-eicosenoic acid (30 µM) + *cis* 11,14-eicosadienoic acid (10 µM) + ergosta-7,22-dien-3-ol (25 µM). The results are expressed as the mean ± standard deviation of three experiments. ** $p < 0.01$; *** $p < 0.001$ (*vs.* control).

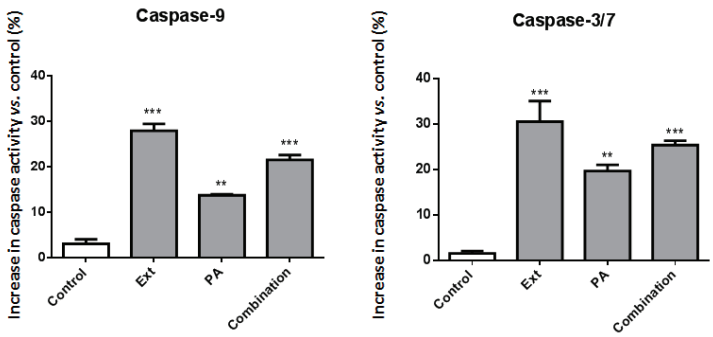

Palmitic acid plays several physiological roles in cells, from energy production to structural support in membranes. In addition, it can be the biosynthetic precursor of ceramide. Ceramide is an intra-cellular lipid signaling molecule that is involved in several cellular processes, including differentiation, growth arrest and apoptosis [17,18]. This process has been widely studied in neuronal cells [19,20]. Ceramide can be synthesized from palmitic acid via the *de novo* pathway, by the action of serine-palmitoyl transferase (SPT), and also from sphingomyelin, by the enzyme, sphingomyelinase [21]. The importance of ceramide to the pro-apoptotic effects of palmitic acid is still in discussion, and two distinct mechanisms are known: ceramide-mediated/caspase-3-independent cell death and ceramide-independent/caspase-3-dependent apoptosis [20]. We hypothesized that the high amount of palmitate in the purified extract could induce an increase of intra-cellular levels of ceramide, thus explaining the pro-apoptotic effect of the extract. In order to test this hypothesis, we evaluated the effect of two inhibitors of the key enzymes involved in the *de novo* biosynthesis of ceramide: L-cycloserine and fumonisin B1. As shown in Figure 7, the co-incubation of the extract with the two inhibitors had no significant impact on viability, and hence, we can conclude that the effects of palmitic acid are ceramide-independent. Taken together, these results show that the mechanism of cell death taking place is ceramide-independent and caspase-dependent.

Figure 7. Cell viability of SH-SY5Y cells treated with the extract (Ext, 156 µg/mL) for 24 h. The ability of L-cycloserine (CSer, 500 µM) and fumonisin B1 (FumB1, 50 µM) to prevent the extract-induced loss of viability was evaluated. Both inhibitors were not cytotoxic. Results are expressed as the mean ± standard deviation of three experiments. * $p < 0.05$ (*vs.* control).

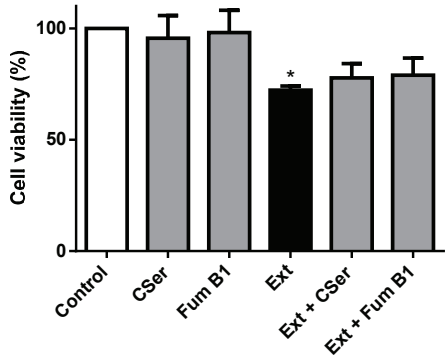

2.4. The Extract and Palmitic Acid Cause ER-Stress Involving CHOP

There has been increasing awareness regarding the role of the ER in the homeostasis of the cell. In particular, ER stress is known to be the basis of several cellular aggressions, namely apoptosis. In order to monitor ER status, several markers can be used. Nowadays, CHOP is widely used, due to its downstream involvement in several pathways of ER stress, namely PERK-eIF2a-ATF4 and ATF6 [12–14]. As can be found in Figure 8, incubation with the extract resulted in a marked increase of CHOP levels. Palmitic acid has been associated with ER-stress and apoptosis via ER-stress in pancreatic β-cells [16], liver cells [22] and neuronal cells [23]. Given the presence of this compound in the extract, it was also tested, and as seen in Figure 8, the CHOP protein levels were also increased in palmitic acid-treated cells. However, we cannot rule out the possibility that other compounds may contribute to the activity displayed or that other signaling pathways may also be involved in the induction of apoptosis.

Figure 8. Effect of the extract (Ext, 156 µg/mL) and palmitic acid (PA, 20 µM) on the expression of CHOP by Western blot.

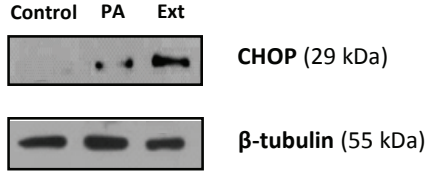

Nowadays, the link between ER stress and apoptosis has been established; however, the precise mechanisms underlying this is not completely understood. Several studies suggest that CHOP-triggered apoptosis is a result of the repression of the BCL2 gene family, thus favoring

pro-apoptotic proteins, which ultimately leads to the activation of caspase-9 and, subsequently, caspase-3. This result is in line with the caspase activation reported above, and for this reason, we suggest that extract/palmitic acid-induced apoptosis is a consequence of ER-stress via the CHOP pathway (Figure 9). Although, in this work, we studied the intrinsic pathway of apoptosis, nowadays it is also known that, in some situations, CHOP can result in the activation of the extrinsic pathway as a consequence of DR5 upregulation caused by the modulation of CHOP on the promoter of this superfamily. Another player, caspase-12, has been implicated before in mice, however the fact that most humans do not possess an active caspase-12 gene [24,25] hinders our current understanding of its importance in ER-mediated apoptosis.

Figure 9. Proposed mechanism for the effect of the purified extract from *M. glacialis*. The anti-proliferative effect is caused by ergosta-7,22-dien-3-ol, which triggers cell cycle arrest. Palmitic acid is not involved in ceramide biosynthesis; instead, it causes ER-stress, as depicted by the increase in CHOP expression levels. This protein then triggers apoptosis by interacting with mitochondrial proteins. SPT: Serine palmitoyl transferase; CERase: Ceramidase; SM: Sphingomyelin; SM synthase: Sphingomyelin synthase; CS: Ceramide synthase; SMase: Sphingomyelinase; ER: Endoplasmic reticulum.

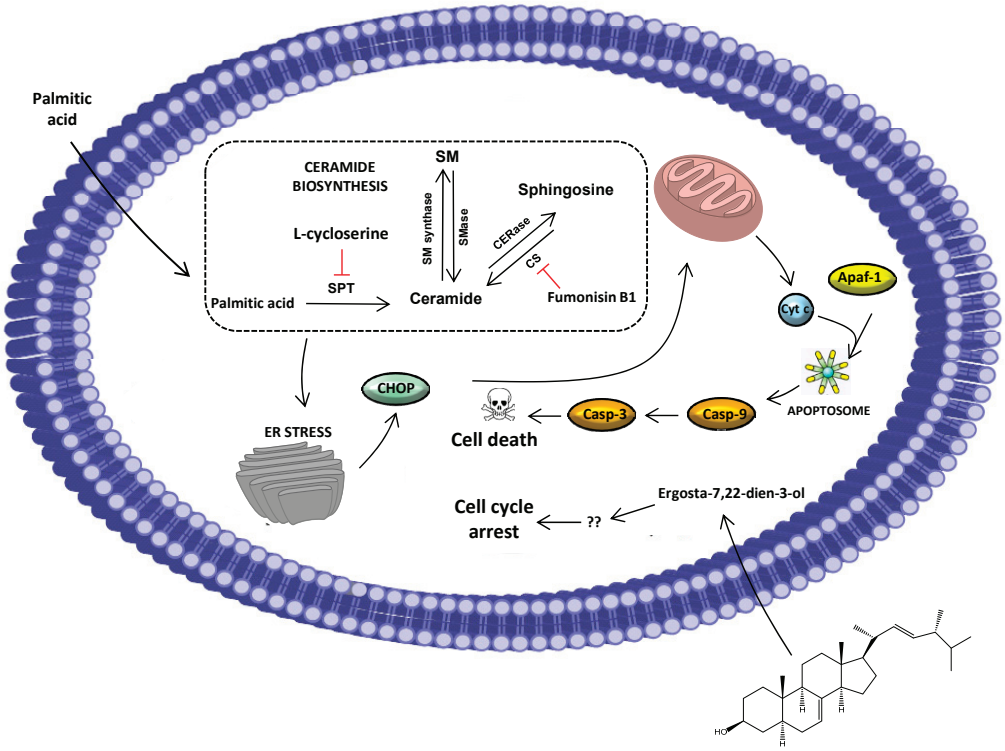

3. Experimental Section

3.1. Reagents and Standards

Dulbecco's Modified Eagle Medium (DMEM), trypsin, fetal bovine serum (FBS), phosphate buffer saline (PBS), fungizone and penicillin were from GIBCO (Invitrogen, Warrington, UK). Oil Red O, glutaraldehyde, *p*-formaldehyde, DNase-free RNase A, palmitic acid (≥99%), *cis* 11-eicosenoic acid (≥99%), *cis* 11,14-eicosadienoic acid (≥98%), Triton X-100 and propidium iodide were from Sigma-Aldrich (St. Louis, MO, USA). Thymidine was from PerkinElmer (Waltham, MA, USA). Ergosta-7,22-dien-3-ol (≥98%) was from BioBioPha Co., Ltd (Yunnan, China). L-cycloserine, fumonisin B1, CHOP and β-tubulin primary antibodies, as well as anti-rabbit secondary antibody were from Santa Cruz (Heidelberg, Germany).

3.2. Extract Preparation

M. glacialis individuals were collected in Cabo Carvoeiro, Portugal, in September, 2009. Samples were frozen, transported to the laboratory, lyophilized (Labconco 4.5 Freezone apparatus, Kansas, MO, USA) and powdered using an electric blender.

The lyophilized powder (15 g) was extracted with acetone:methanol (7:3), and the extract was added to a separating funnel with 20 mL of an ether:hexane mixture (1:1). An equivalent volume of 5% NaCl was then added. The mixture was separated into two phases, and the aqueous hypophase was collected and re-extracted with the ether:hexane mixture. The organic epiphases were then collected, washed with water in order to remove traces of acetone and evaporated until dryness in a rotary evaporator. All procedures were conducted at room temperature, and the final residue was kept at −80 °C in an inert atmosphere (nitrogen).

3.3. Compounds Preparation

Stock solutions of all compounds were prepared in ethanol. Working concentrations were prepared by diluting stock solutions with culture medium. Controls consisting of ethanol in culture medium (0.1%–1%) were used in all cases.

3.4. Cell Culture

SH-SY5Y and MCF-7 cells were maintained in DMEM and MEM, respectively, with 10% FBS and 1% penicillin/streptomycin. In the case of SH-SY5Y, the cell media was also supplemented with 1% non-essential amino acids. All cells were grown in an incubator at 37 °C and 5% CO_2.

3.5. Morphological Studies

For Giemsa staining cells were seeded at a density of 2×10^4 cells/well in 24-well plates. After incubation with different concentrations of the extract, cells were washed twice with PBS and fixed with cold methanol, at 4 °C, for 30 min. Diluted Giemsa dye (1:10) was then added and kept for

20 min, after which cells were repeatedly washed and then mounted in DPX mountant (Sigma-Aldrich, St. Louis, MO, USA).

Changes in nuclear morphology were studied by employing Hoechst 33342 staining. Cells were fixed as described for Giemsa staining, but 4% *p*-formaldehyde was used as the fixing agent. Cells were exposed to 0.5 mg/mL Hoechst 33342 for 20 min at room temperature and mounted in Vectashield mounting medium. Preparations were examined under a fluorescence microscope (Eclipse E400, Nikon, Japan), equipped with an excitation filter with maximum transmission at 360/400 nm, and processed by Nikon ACT-2U image software.

In order to study lipid bodies, methanol-fixed cells were rinsed with propylene glycol and exposed to Oil Red O (0.7% in propylene glycol) for 7 min, with agitation. Oil red O solution was removed, and 85% propylene glycol was added and maintained for 3 min, after which, cells were washed with distilled water and mounted with aqueous mounting media.

For electron microscopy studies, cells were harvested by trypsinization after 24 and 48 h of incubation with the extract, washed with phosphate buffer fixed with 1.25% glutaraldehyde/4% *p*-formaldehyde and preserved at 4 °C for further processing. The cells were post-fixed in 1% osmium tetroxide in the same buffer, dehydrated in graded alcohols and embedded in Epon 812. Ultra-thin sections obtained with a Reichert Supra Nova ultra-microtome were collected on copper grids, stained with uranyl acetate/lead citrate and examined in a Zeiss 902A transmission electron microscope.

3.6. ^{3}H-Thymidine Incorporation Assay

Cells were seeded in 96-well plates (2×10^4/well) and incubated with different concentrations of extract. Incubations were maintained for 24–48 h, and for each exposure time, ^{3}H-thymidine (0.5 μCi) was added to each well and incubated at 37 °C in 5% CO_2 for the last 8 h. After two cycles of freezing/thawing, cells were harvested using a cell harvester (Skatron Instruments, Brønnøysund, Norway), and a 1 mL scintillation cocktail was added. Incorporated ^{3}H-thymidine was determined in a scintillation counter (LS 6500, Beckman Instruments, Fullerton, CA, USA). Assays were carried out in triplicate, and the results are representative of three independent experiments.

3.7. Cell Cycle Analysis

Cell cycle analysis was performed by flow cytometry. Cells were seeded in 6-well plates (7×10^5/well) and cultured with or without extract at different concentrations or with the compounds. After 24 h of treatment, cells were harvested using 0.25% trypsin in ethylenediamine tetraacetic acid (EDTA), washed twice with PBS and fixed in 70% cold ethanol. Fixed cells were finally re-suspended in 0.5 mL DNA staining solution (5 μg/mL iodide propidium [PI], 0.1% Triton X-100 and 200 μg/mL DNase-free RNase A in PBS) and kept 30 min at room temperature, in the dark.

Flow cytometric analysis of DNA content was based on the acquisition of 20,000 events in a Becton Dickinson FACSCalibur (San Jose, CA, USA) equipped with CELLQuest Pro software. Debris, cell doublets, sub-G1 population and aggregates were gated out using a two-parameter plot

of FL-2-Area to FL-2-Width of PI fluorescence. Detectors for forward and side light scatter (FSC and SSC, respectively) and the three fluorescence channels (FL-1, FL-2 and FL-3) were set on a linear scale. Cell cycle histograms were analyzed using FlowJo Software (Tree Star, Inc., Ashland, OR, USA). Assays were carried out in triplicate, and the results are representative of three independent experiments.

3.8. Cell Viability

Cells were cultured in 96-well plates (2×10^4 cells/well) and allowed to attach for 24 h. Cells were pre-incubated with the extract/compounds for 2 h, after which, lipopolysaccharide (LPS) was added and further incubated for 24 h. After incubation, 3-(4,5-dimethylthiazol-2-yl)-2,5-diphenyltetrazolium bromide (MTT) (0.5 mg/mL, final concentration) was added to each well and incubated for 2 h at 37 °C. The formazan was dissolved by the addition of a dimethyl sulfoxide (DMSO): isopropanol mixture (3:1) and quantified spectrophotometrically at 560 nm. The results of cell viability correspond to the mean of three independent experiments performed in triplicate and are expressed as the percentage of the untreated control cells.

3.9. Caspase-3/-7 and -9 Activity Assay

For the evaluation of caspase-3/-7 and -9 activity, the luminescent assay kits, Caspase-GloH 9, and Caspase-GloH 3/7 (Promega Corporation, Fitchburg, WI, USA), were used. Cells were seeded in white 96-well plates in the conditions reported above for MTT. As positive control, cells were incubated with staurosporine (STS) (1 μM) for 12 h. Luminescence was measured in a 96-well Microplate Luminometer (BioTek Instruments) and presented as relative light units (RLU). Assays were carried out in triplicate, and the results are representative of three independent experiments.

3.10. Western Blot

Cells were seeded in 6-well plates with a density of 3.5×10^5 cells/well. Cells were treated for 24 h with the extract or palmitic acid. After this period, cells were washed with PBS, scraped and incubated with a lysis solution (20 mM Tris-HCl, 150 mM NaCl, 5 mM EDTA, 1% Triton) and a protease inhibitors cocktail (1 mM 4-(2-aminoethyl)benzenesulfonyl fluoride (AEBSF), 15 μM pepstatin A, 14 μM E-64, 40 μM bestatin, 20 μM leupeptin and 0.8 μM aprotinin) for 20 min on ice. The solution was then centrifuged at 14,000 × *g* for 15 min; the supernatant was collected, and protein content was determined by the Bradford method. Samples (40 μg) were subjected to 10% SDS-PAGE, and proteins were transferred onto nitrocellulose membranes and blocked for one hour at room temperature with a solution of 5% non-fat milk in 0.1% Triton X-100. Overnight incubation at 4 °C was performed with anti-CHOP (1:100) and anti-tubulin (1:1000) and, then, with peroxidase-conjugated secondary antibody (1:3000) at room temperature for 1 hour. β-Tubulin was used as a loading control. Finally blots were subjected to a chemiluminescence detection kit (Super Signal West Pico; Pierce, Rockford, IL, USA).

4. Conclusions

In this work, we described the effect of a lipophilic extract obtained from *M. glacialis* against the human cancer cell lines, MCF-7 and SH-SY5Y. Evaluation of DNA synthesis revealed that both cell lines were markedly affected in a concentration-dependent way, the latter being more susceptible. We showed that the extract was responsible for two distinct effects: cell cycle arrest and apoptosis. We evaluated the contribution of the main compounds and demonstrated that while ergosta-7-dien-3-ol was responsible for the cell cycle arrest, palmitic acid was responsible for the apoptotic effect via the CHOP-mediated pathway of ER-stress. A proposed mechanism of the activity displayed by the extract can be found in Figure 9.

Acknowledgments

This work has been supported by Fundação para a Ciência e a Tecnologia (FCT) through grant no. PEst-C/EQB/LA0006/2011. David M. Pereira is grateful to FCT for the grant (SFRH/BD/62663/2009).

Conflicts of Interest

The authors declare no conflict of interest.

References

1. Altmann, K.-H.; Gertsch, J. Anticancer drugs from nature—natural products as a unique source of new microtubule-stabilizing agents. *Nat. Prod. Rep.* **2007**, *24*, 327–357.
2. Itokawa, H.; Morris-Natschke, S.L.; Akiyama, T.; Lee, K.-H. Plant-derived natural product research aimed at new drug discovery. *J. Nat. Med.-Tokyo* **2008**, *62*, 263–280.
3. Pereira, D.M.; Valentão, P.; Correia-da-Silva, G.; Teixeira, N.; Andrade, P.B. Plant secondary metabolites in cancer chemotherapy: Where are we? *Curr. Pharm. Biotechnol.* **2012**, *13*, 632–650.
4. Mayer, A.; Glaser, K.B.; Cuevas, C.; Jacobs, R.S.; Kem, W.; Little, R.D.; McIntosh, J.M.; Newman, D.J.; Potts, B.C.; Shuster, D.E. The odyssey of marine pharmaceuticals: A current pipeline perspective. *Trends Pharmacol. Sci.* **2010**, *31*, 255–265.
5. Montaser, R.; Luesch, H. Marine natural products: A new wave of drugs? *Future Med. Chem.* **2011**, *3*, 1475–1489.
6. Pereira, D.M.; Valentão, P.; Andrade, P.B. Lessons from the Sea: Distribution, SAR and Molecular Mechanisms of Anti-inflammatory Drugs from Marine Organisms. In *Studies in Natural Products Chemistry (Bioactive Natural Products)*; Atta-ur-Rahman, Ed.; Elsevier Science Publishers: Amsterdam, The Netherlands, 2013.
7. Schumacher, M.; Kelkel, M.; Dicato, M.; Diederich, M. Gold from the sea: marine compounds as inhibitors of the hallmarks of cancer. *Biotechnol. Adv.* **2011**, *29*, 531–547.

8. Ferreres, F.; Pereira, D.M.; Gil-Izquierdo, A.; Valentao, P.; Botelho, J.; Mouga, T.; Andrade, P.B. HPLC-PAD-atmospheric pressure chemical ionization-MS metabolite profiling of cytotoxic carotenoids from the echinoderm *Marthasterias glacialis* (spiny sea-star). *J. Sep. Sci.* **2010**, *33*, 2250–2257.
9. Mariutti, L.R.B.; Pereira, D.M.; Mercadante, A.Z.; Valentão, P.; Teixeira, N.; Andrade, P.B. Further insights on the carotenoid profile of the echinoderm *Marthasterias glacialis*. *Mar. Drugs* **2012**, *10*, 1498–1510.
10. Pereira, D.M.; Vinholes, J.; Guedes de Pinho, P.; Valentão, P.; Mouga, T.; Teixeira, N.; Andrade, P.B. A gas chromatography-mass spectrometry multi-target method for the simultaneous analysis of three classes of metabolites in marine organisms. *Talanta* **2012**, *100*, 391–400.
11. Pereira, D.M.; Correia-da-Silva, G.; Valentão, P.; Mouga, T.; Teixeira, N.; Andrade, P.B. A lipidomic approach to drug discovery from marine organisms: Effect of a purified fraction of the lipidome of the echinoderm *Marthasterias glacialis* L. against human cancer cells. *Comb. Chem. High Throughput Screen.* 2013, in press.
12. Ron, D.; Walter, P. Signal integration in the endoplasmic reticulum unfolded protein response. *Nat. Rev. Mol. Cell Biol.* **2007**, *8*, 519–529.
13. Schroder, M.; Kaufman, R.J. The mammalian unfolded protein response. *Annu. Rev. Biochem.* **2005**, *74*, 739–789.
14. Zhang, K.; Kaufman, R.J. From endoplasmic-reticulum stress to the inflammatory response. *Nature* **2008**, *454*, 455–462.
15. Kong, J.Y.; Rabkin, S.W. Palmitate-induced cardiac apoptosis is mediated through CPT-1 but not influenced by glucose and insulin. *Am. J. Physiol.-Heart Circ. Physiol.* **2002**, *282*, H717–H725.
16. Karaskov, E.; Scott, C.; Zhang, L.; Teodoro, T.; Ravazzola, M.; Volchuk, A. Chronic palmitate but not oleate exposure induces endoplasmic reticulum stress, which may contribute to INS-1 pancreatic β-cell apoptosis. *Endocrinology* **2006**, *147*, 3398–3407.
17. Kolensnick, R.; Hannun, Y.A. Ceramide and apoptosis. *Trends Biochem. Sci.* **1999**, *24*, 224–225.
18. Morad, S.A.F.; Cabot, M.C. Ceramide-orchestrated signalling in cancer cells. *Nat. Rev. Cancer* **2013**, *13*, 51–65.
19. Movsesyan, V.A.; Yakovlev, A.G.; Dabaghyan, E.A.; Stoica, B.A.; Faden, A.I. Ceramide induces neuronal apoptosis through the caspase-9/caspase-3 pathway. *Biochem. Biophys. Res. Commun.* **2002**, *299*, 201–207.
20. Suzuki, J.; Akahane, K.; Nakamura, J.; Naruse, K.; Kamiya, H.; Himeno, T.; Nakamura, N.; Shibata, T.; Kondo, M.; Nagasaki, H.; *et al.* Palmitate induces apoptosis in Schwann cells via both ceramide-dependent and independent pathways. *Neuroscience* **2011**, *176*, 188–198.
21. Holland, W.L.; Summers, S.A. Sphingolipids, insulin resistance, and metabolic disease: New insights from *in vivo* manipulation of sphingolipid metabolism. *Endocr. Rev.* **2008**, *29*, 381–402.

22. Wei, Y.; Wang, D.; Topczewski, F.; Pagliassotti, M.J. Saturated fatty acids induce endoplasmic reticulum stress and apoptosis independently of ceramide in liver cells. *Am. J. Physiol.-Endocrinol. Metab.* **2006**, *291*, E275–E281.
23. Bolognesi, A.; Chatgilialoglu, A.; Polito, L.; Ferreri, C. Membrane lipidome reorganization correlates with the fate of neuroblastoma cells supplemented with fatty acids. *PLoS One* **2013**, *8*, e55537.
24. Saleh, M.; Vaillancourt, J.P.; Graham, R.K.; Huyck, M.; Srinivasula, S.M.; Alnemri, E.S.; Steinberg, M.H.; Nolan, V.; Baldwin, C.T.; Hotchkiss, R.S. Differential modulation of endotoxin responsiveness by human caspase-12 polymorphisms. *Nature* **2004**, *429*, 75–79.
25. Yavari, M.; Brinkley, G.; Klapstein, K.; Hartwig, W.; Rao, R.; Hermel, E. Presence of the functional CASPASE-12 allele in Indian subpopulations. *Int. J. Immunogol.* **2012**, *39*, 389–393.

The Marine Fungal Metabolite, AD0157, Inhibits Angiogenesis by Targeting the Akt Signaling Pathway

Melissa García-Caballero, Librada Cañedo, Antonio Fernández-Medarde, Miguel Ángel Medina and Ana R. Quesada

Abstract: In the course of a screening program for the inhibitors of angiogenesis from marine sources, AD0157, a pyrrolidinedione fungal metabolite, was selected for its angiosupressive properties. AD0157 inhibited the growth of endothelial and tumor cells in culture in the micromolar range. Our results show that subtoxic doses of this compound inhibit certain functions of endothelial cells, namely, differentiation, migration and proteolytic capability. Inhibition of the mentioned essential steps of *in vitro* angiogenesis is in agreement with the observed antiangiogenic activity, substantiated by using two *in vivo* angiogenesis models, the chorioallantoic membrane and the zebrafish embryo neovascularization assays, and by the *ex vivo* mouse aortic ring assay. Our data indicate that AD0157 induces apoptosis in endothelial cells through chromatin condensation, DNA fragmentation, increases in the subG1 peak and caspase activation. The data shown here altogether indicate for the first time that AD0157 displays antiangiogenic effects, both *in vitro* and *in vivo*, that are exerted partly by targeting the Akt signaling pathway in activated endothelial cells. The fact that these effects are carried out at lower concentrations than those required for other inhibitors of angiogenesis makes AD0157 a new promising drug candidate for further evaluation in the treatment of cancer and other angiogenesis-related pathologies.

Reprinted from *Mar. Drugs*. Cite as: García-Caballero, M.; Cañedo, L.; Fernández-Medarde, A.; Medina, M.Á.; Quesada, A.R. The Marine Fungal Metabolite, AD0157, Inhibits Angiogenesis by Targeting the Akt Signaling Pathway. *Mar. Drugs* **2014**, *12*, 279-299.

1. Introduction

Angiogenesis, a physiological process involving the generation of new capillaries from pre-existing vessels, is strictly controlled by a balance of stimulators and inhibitors, being restricted in adults to some processes related to the reproductive cycle and wound repair. However, angiogenesis is now widely recognized as one of the hallmarks of cancer, a crucial step in the transition of tumors from a dormant state to a malignant state, and playing an essential role in tumor growth, invasion and metastasis [1]. Furthermore, a continuously increasing number of other non-neoplastic diseases are being related to an upregulated angiogenesis. They include diabetic retinopathy, age-related macular degeneration, hemangioma, arthritis and psoriasis, among others [2]. Currently, angiogenesis inhibitors are likely to change the face of medicine, arising as an attractive approach for the treatment of cancer and other angiogenesis-dependent diseases, with some antiangiogenic compounds approved by the Food and Drug Administration (FDA) for the treatment of cancer, blindness and other angiogenesis-dependent diseases, encouraging expectations in their therapeutic potential [3,4].

In response to the angiogenic stimulus, the normally quiescent endothelial cells become activated and undergo a series of phenotypic changes, including the release of proteases that will allow them to degrade the extracellular matrix and migrate. Activated endothelial cells will proliferate and avoid apoptosis, which could be triggered by the loss of survival signals and, finally, will differentiate, rendering a new capillary. Any of these steps could be a target for the pharmacological inhibition of angiogenesis [5].

Marine species are being demonstrated to be an unexplored and prolific source of molecular diversity, yielding an increasing number of products for biotechnological applications, including the production of bioactive compounds for pharmaceutical use [6,7]. Our group is actively involved in the search for new modulators of angiogenesis from marine origin [8–11]. In the course of a screening program, the pyrrolidinedione, AD0157 (Figure 1), isolated and purified from the fermentation broth of a marine fungi, was selected for its ability to inhibit endothelial cell differentiation *in vitro* [12]. In the present study, we provide evidence that AD0157 is a potent inhibitor of angiogenesis *in vitro*, interfering with several key steps of the angiogenic process. AD0157 inhibits the growth of both endothelial and tumor cells. The growth inhibitory activity of this compound may be related in endothelial cells to an induction of apoptosis. AD0157 reduces the migratory and proteolytic activities of endothelial cells and their ability to form a network of tubular-like structures on Matrigel at micromolar concentrations. The data presented here show that this compound represses the phosphorylation of endothelial serum-stimulated Akt-phosphorylation, suggesting that AD0157 interferes with the molecular mechanisms of cell proliferation, migration and survival. The *in vitro* antiangiogenic effect of AD0157 was confirmed by means of one *ex vivo* and two *in vivo* models. Our results indicate the potential of AD0157 for the treatment of cancer and other angiogenesis-related malignancies and reinforce the concept that marine compounds are a valuable source of new inhibitors of angiogenesis.

Figure 1. Chemical structure of AD0157.

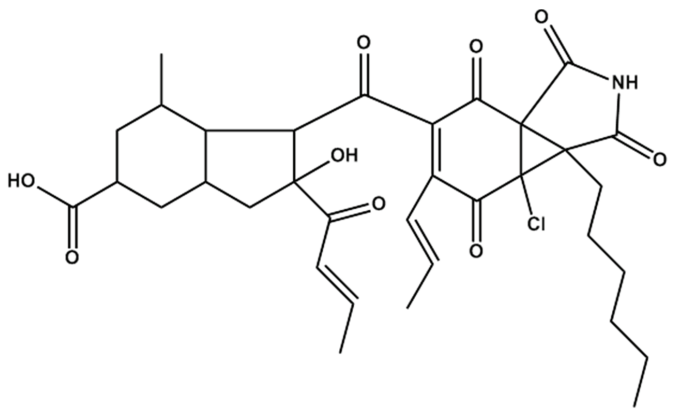

2. Results and Discussion

2.1. AD0157 Inhibits the Growth of Endothelial and Tumor Cells

Angiogenesis involves the local proliferation of endothelial cells. We first investigated the ability of AD0157 to inhibit the growth of serum-activated endothelial and tumor cells. As shown in Figure 2, AD0157 inhibited the growth of cultured bovine aortic endothelial cells (BAECs) with a half-maximal inhibitory concentration (IC_{50}) value of 10.9 µM for subconfluent BAECs stimulated to grow with 10% FBS. The data obtained with the HT-1080 fibrosarcoma cell line, HT-29 colon adenocarcinoma cell line, MDA-MB-231 breast carcinoma cell line and U2OS osteosarcoma cell line are in the same range of concentrations as that of BAEC, suggesting that AD0157 is not a specific inhibitor of endothelial cell growth.

Figure 2. (**A**) Dose-dependent effect of AD0157 on the *in vitro* growth of bovine aortic endothelial cells (BAEC) (▲), MDA-MB-231 (x), HT-29 (♦), HT-1080(■) and U2OS (●). Cell survival is represented as a percentage of control-cell growth in cultures containing no drug. Each point represents the mean of quadruplicates; SD values were typically lower than 10% of the mean values and are omitted for clarity; (**B**) Half-maximal inhibitory concentration (IC_{50}) values calculated from dose-response curves as the concentration of compound yielding 50% of control cell survival. They are expressed as means ± SD of three independent experiments.

(**A**)

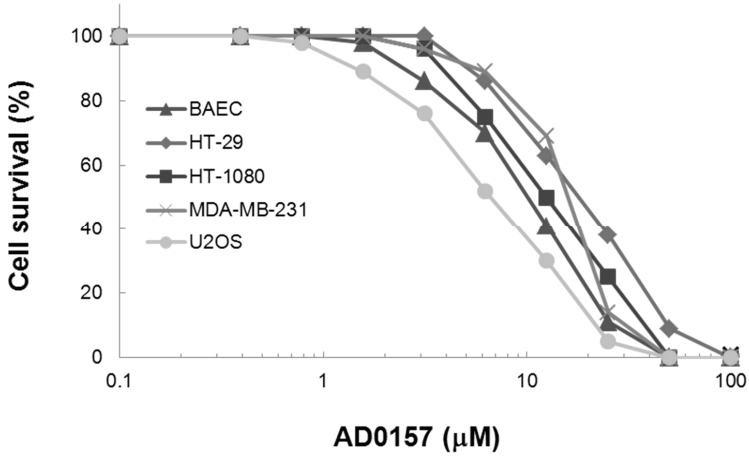

(**B**)

IC_{50} (µM)	BAEC	MDA-MB231	HT-29	HT-1080	U2OS
AD0157	10.9 ± 1.5	15.0 ± 1.7	20.0 ± 4.2	11.0 ± 2.5	5.1 ± 1.6

2.2. AD0157 Inhibits Capillary Tube Formation by Endothelial Cells

The final event during angiogenesis is the organization of endothelial cells in a three-dimensional network of tubes. *In vitro*, endothelial cells plated on Matrigel align themselves, forming cords, already evident a few hours after plating (Figure 3A, left panel). Figure 3A shows that AD0157, at a concentration of 5 μM or higher, was able to completely inhibit the morphogenesis of endothelial cells on Matrigel, with a partial inhibition of the tube-like structure formation observed at 1 μM. To check the viability of endothelial cells after treatment with the compounds in this assay, BAE cells were incubated in a 96-well plate in the same conditions employed for the tube formation assay. After 7 h, cell viability in comparison to control (untreated cells) was determined by the addition of MTT (3-(4,5-dimethylthiazol-2-yl)-2,5-diphenyltetrazolium bromide), essentially as described for the cell growth assay. The treatment with AD0157, at the concentrations used to inhibit the differentiation of BAE cells, did not affect the viability of those cells after 7 h (results not shown).

2.3. AD0157 Inhibits the Migratory Capacity of Endothelial Cells

The acquisition by endothelial cells of the capability to migrate through extracellular matrix is essential for the formation of new blood vessels. To investigate the effect of AD0157 on endothelial cell migration, the so-called “wound healing” assay was used. Figure 3B shows the effects of five and 10 μM AD0157 on endothelial cell migration after 7 h of treatment. Quantitative determination of the invaded area shows a significant dose-dependent inhibition of the migratory capability of BAECs by treatment with subtoxic concentrations of AD0157.

2.4. AD0157 Inhibits the Extracellular Matrix Degrading Potential of Endothelial Cells

Angiogenesis involves the acquisition by endothelial cells of the capability to degrade the basement membrane and, in general, to remodel the extracellular matrix. MMP-2 (gelatinase A), a matrix metalloproteinase expressed by endothelial cells, plays a relevant role in angiogenesis. Gelatin zymography of conditioned media and cell extracts of BAE cells untreated and treated with different concentrations of AD0157 for 24 h showed that this compound exerted a dose-dependent inhibition of the MMP-2 production by endothelial cells (Figure 4A). Nevertheless, our results show that no effect on the MMP-2 and MMP-9 levels is observed when the HT-1080 tumor cells were treated with AD0157 (Figure 4B), suggesting some endothelial-specificity for the inhibition of the cell proteolytic capabilities by this compound.

Figure 3. AD0157 inhibits endothelial cell tube formation and migration. (**A**) BAEC seeded on Matrigel formed tubes. AD0157 inhibited endothelial cell tubulogenesis *in vitro* in a dose-dependent manner at non-toxic doses. Cells were photographed 7 h after seeding under an inverted microscope (bar = 100 µm); (**B**) Top panel: confluent BAEC monolayers were wounded, and fresh culture medium was added either in the absence or presence of the indicated concentrations of the compound. Photographs were taken at 7 h of incubation. Broken lines indicate the wound edges (bar = 100 µm); Bottom panel: The regrowth of BAEC into the cell-free area was measured after 7 h, and percentages of the recovered area are expressed as the mean ± SD, * $p < 0.05$ *versus* the control ($n = 3$).

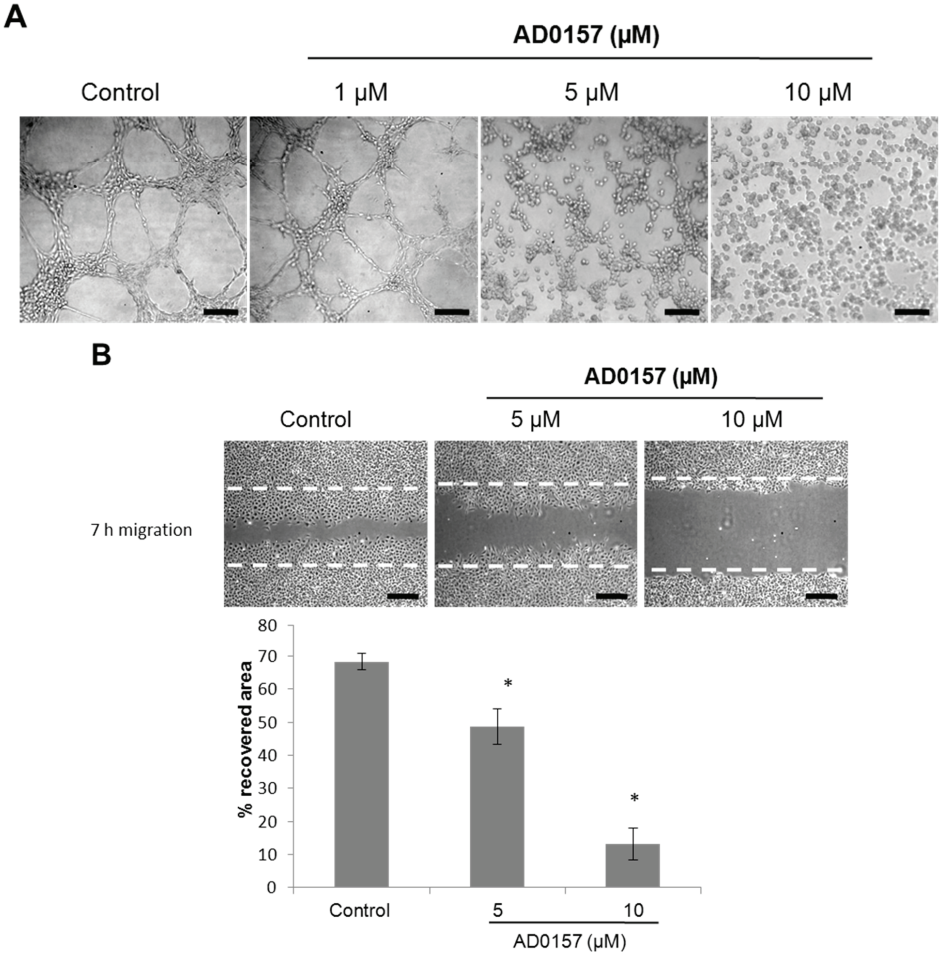

Figure 4. AD0157 inhibits endothelial MMP-2 production. Conditioned media and cellular extracts from BAE cells (**A**) or HT1080 cells (**B**) were treated during 24 h with the indicated concentrations of AD0157, were normalized for equal cell density and used for gelatin zymography. The graphics show the quantification of the normalized relative inhibitory effect on BAEC MMP-2 activity or HT1080 MMP-2 and MMP-9 activities. Data are given as the percentage of the untreated control, and they are the means ± SD of three experimental values. * $p < 0.05$ *versus* the control and ** $p < 0.005$ *versus* the control.

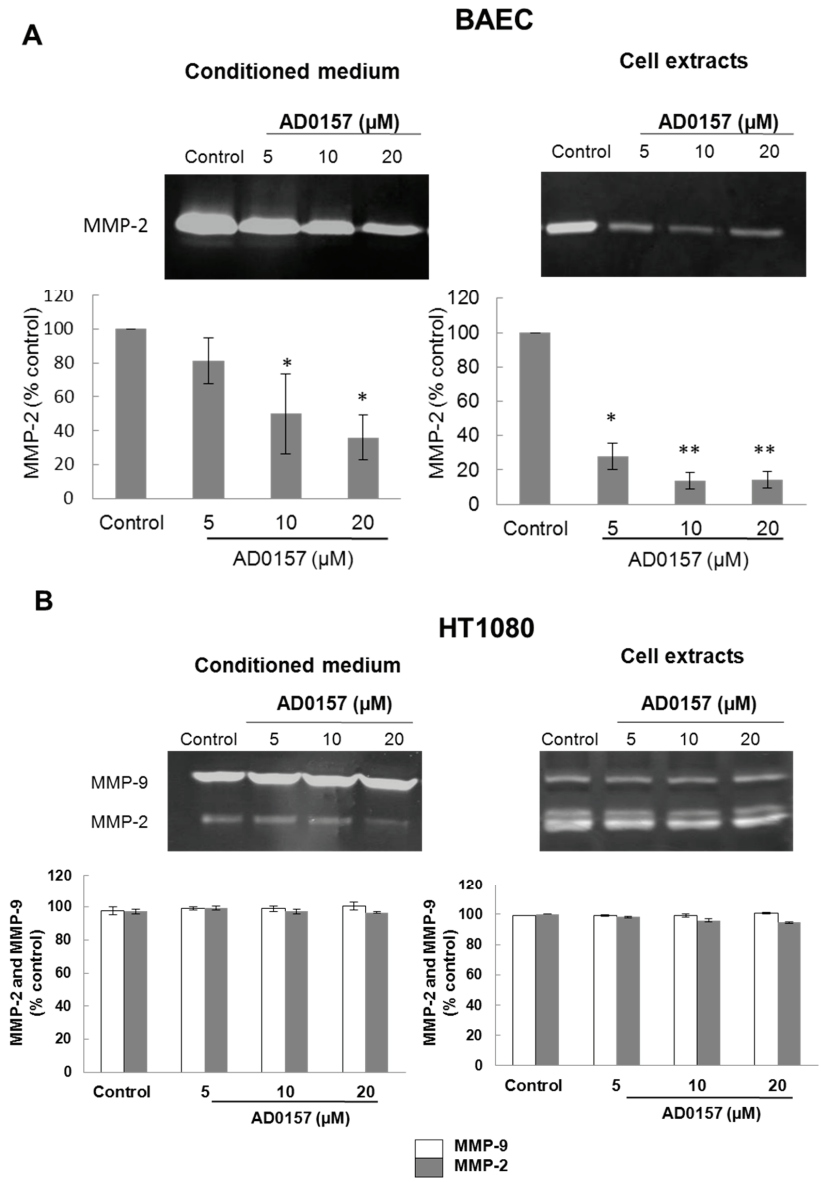

2.5. AD0157 Inhibits Angiogenesis in Vivo

The chicken chorioallantoic membrane (CAM) assay, a widely used and accessible system to study angiogenesis, was used to determine the *in vivo* antiangiogenic activity of AD0157 [13]. As shown in Table 1, treatment with AD0157 caused a dose-dependent antiangiogenic effect, which is maintained as low as 0.5 nmol (0.32 μg) per CAM, where 83% of the eggs scored positive, and reaching a maximum activity at 1 nmol (0.64 μg) per CAM, with 100% positive. As shown in Figure 5A, in untreated chorioallantoic membranes (controls), blood vessels form a dense and spatially-oriented branching network composed of vascular structures of progressively smaller diameter as they branch. The inhibition of angiogenesis by AD0157 in this assay was observed as an inhibition of the ingrowth of new vessels in the area covered by the methylcellulose discs. It could also be observed that the peripheral vessels (relative to the position of the disc) grew centrifugally, avoiding the treated area, with an overall decrease in the vascular density. When CAMs were treated with AD0157 at concentrations above 5 nmol (3.2 μg) per CAM, some intratissue hemorrhages in the treated area could be occasionally observed (Figure 5A, bottom right panel).

Table 1. Inhibition of *in vivo* angiogenesis by AD0157.

	AD0157 (nmol/CAM)	**Positive/Total**	**% inhibition**
CAM assay	0.1	1/5	20
	0.5	5/6	83
	1	6/6	100
	5	6/6	100
	AD0157 (μM)	**Positive/Total**	**% inhibition**
Zebrafish embryo assay	5	5/20	25
	10	12/25	48
	25	17/20	85

In vivo chorioallantoic membrane (CAM) and live fluorescent zebrafish embryo assays were carried out with different doses of AD0157, as described in the Methods section; data are given as the percentage of eggs with inhibited angiogenesis in their CAMs per total number of treated egg CAMs or as the percentage of embryos with inhibited angiogenesis per total number of treated zebrafish embryos.

A second experimental approach used to evaluate the effects of AD0157 on angiogenesis *in vivo* was the use of the model of transgenic zebrafish. Embryos from a transgenic (*TG(fli1:EGFP)y1*) zebrafish line that carries a 15-kb promoter of the transcription factor friend leukemia virus integration-1 (fli-1), which drives the green fluorescent protein (GFP) expression in the endothelium, were treated with different concentrations of AD0157 [14]. Along the development of the zebrafish, intersegmental vessels sprout and grow upward from the aorta, and then, the tips join by anastomosis to form a dorsal vein. Our results show that AD0157, when added to water, inhibited the formation of the last zebrafish intersegmental blood vessels in a dose-response manner, with 85% of zebrafish embryos incubated with 25 μM AD0157 being scored as positive in this assay (Table 1). Inhibition of embryo angiogenesis was observed by a decrease in the width of some vessels and interruptions in the last intersegmental vessels (Figure 5B). The embryos remained viable during the 24-h period of the study, and their overall morphology was similar to

control embryos, indicating that development was unaffected and suggesting a low toxicity of this compound.

Figure 5. AD0157 inhibits angiogenesis *in vivo*. (**A**) Chorioallantoic membrane assay (CAM). The methylcellulose disc containing the substance vehicle alone and the methylcellulose disc containing 0.5, one and 5 nmol of AD0157. Circles show the locations of the methylcellulose discs (bar = 1 mm); (**B**) Inhibition of the zebrafish neovascularization by AD0157. Transgenic *TG(fli1:EGFP)y1* zebrafish embryos that show green fluorescent protein (GFP) expression in endothelial cells were incubated without or with 10 µM AD0157 (bars represent 50 µm).

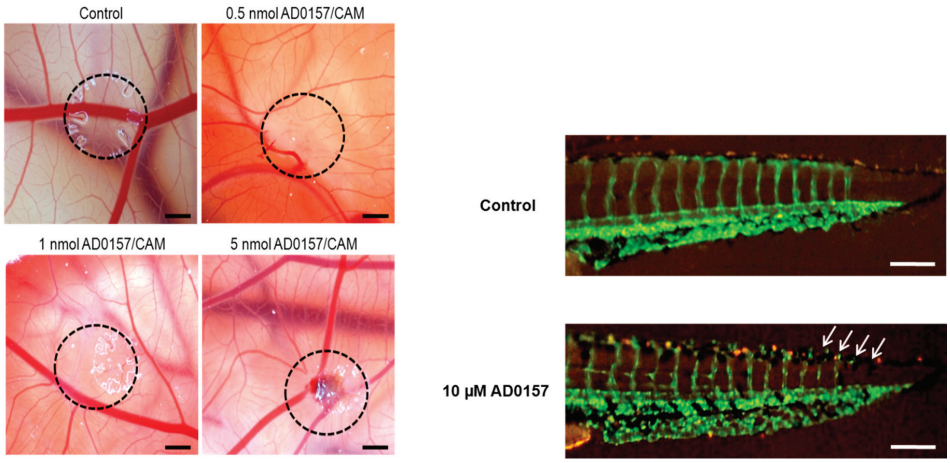

2.6. AD0157 Inhibits Microvessel Outgrowth in Mouse Aortic Rings

An additional line of evidence showing the potential of AD0157 to inhibit overall angiogenesis is provided by the *ex vivo* model of the mouse aortic ring assay [15]. In this assay, the capability of new vessel formation from explants was evaluated after 7 days of incubation of the aortic rings with different concentrations of the compound. As seen in Figure 6A, in the absence of AD0157 (controls), aortic rings were able to generate a dense microvessel outgrowth in a collagen matrix. Our results indicate that AD0157 at concentrations above 2 µM inhibited microvessel formation in a dose-response fashion.

2.7. AD0157 Induces Apoptosis in Endothelial Cells

As the first approach to determine whether the growth inhibitory activity of AD0157 could be, at least in part, due to the induction of apoptosis, the nuclear morphology of endothelial cells was investigated after 14 h of treatment with different concentrations of this compound. Figure 7A shows that AD0157, at a concentration of 5 µM or higher, induced chromatin condensation in endothelial cells.

Figure 6. AD0157 inhibits microvessel outgrowth in the mouse aortic ring assay. (**A**) Representative samples of the aortic ring without or with treatment. In the top panel, the whole ring is photographed, and in the bottom panel, only one side is detailed (bar = 500 µm). (**B**) The results were calculated as the area occupied by new microvessels expressed as a percentage by the outgrowth observed in the controls, which we considered as having 100% vessel formation. The results are the mean ± SD of four aortic rings from different mice, * $p < 0.005$ *versus* the control.

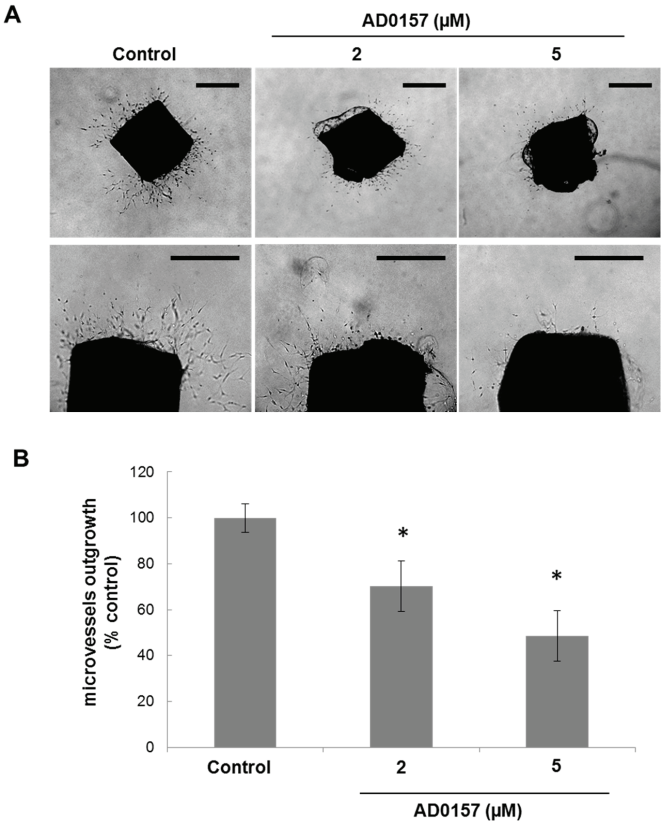

The apoptogenic activity of AD0157 was confirmed by the terminal deoxynucleotidyl transferase mediated dUTP-biotin nick end-labeling (TUNEL) assay, showing that this compound induces DNA fragmentation in BAE cells (Figure 7B). In addition, cell cycle analysis was performed in AD0157-treated BAEC after propidium iodide staining. Flow cytometric analysis showed that AD0157 significantly increased the apoptotic subG1 population at five, 10 and 20 µM (Figure 7C).

Figure 7. AD0157 induces apoptosis in BAECs. (**A**) AD0157 induces chromatin condensation in endothelial cells (Hoechst staining, bar = 50 µm). Cells with condensed chromatin are highlighted; (**B**) AD0157 induces DNA fragmentation in endothelial terminal deoxynucleotidyl transferase dUTP-biotin nick end-labeling (TUNEL assay, bar = 50 µm); (**C**) The effect of AD0157 on the endothelial cell cycle distribution. After incubation with AD0157, cells were stained with propidium iodide, and the percentage of subG1, G1, and S/G2/M subpopulations were determined using a MoFlo Dako Cytomation cytometer. A representative result and the calculated values for cell subpopulations, expressed as the means ± SD of three independent experiments, are shown, * $p < 0.05$, # $p < 0.005$ *versus* the untreated control; (**D**) The effect of AD0157 on the endothelial cells caspase-3-like activity. Ten micromolar 2-methoxyestradiol (2-ME) was used as a positive control of caspase induction. The results are the mean ± SD of three independent experiments, * $p < 0.005$ *versus* control. In all experiments, BAECs were incubated for 14 h with or without the indicated concentrations of AD0157 in complete medium, as detailed in the Methods section.

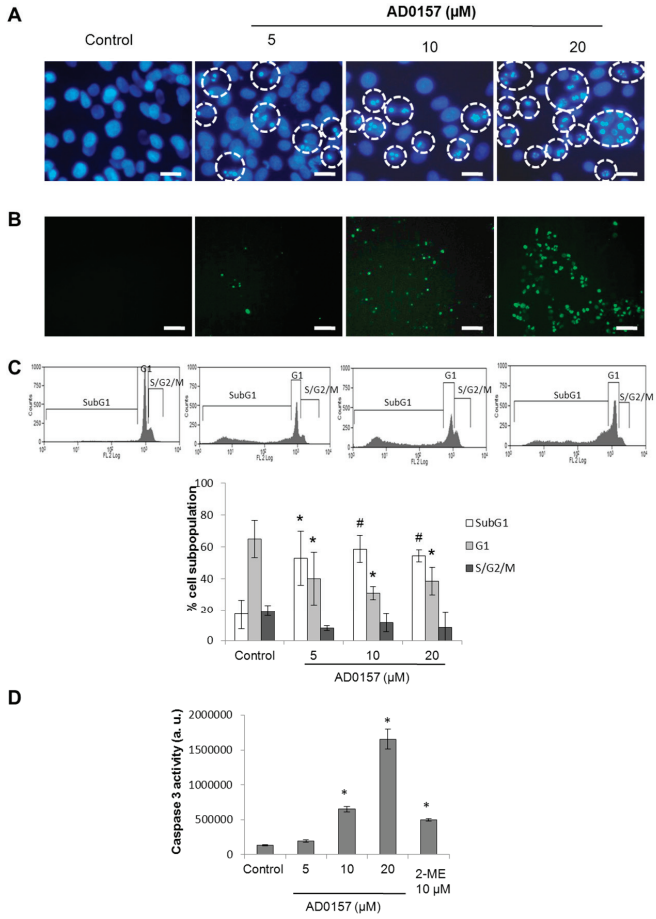

The activation of caspases plays a central role in the induction of apoptosis. To evaluate if endothelial cells caspases could be activated after cell treatment with AD0157, a caspase-3/7 substrate, N-Acetyl-Asp-Glu-Val-Asp-7-amino-4-methylcoumarin or Ac-DEVD-AMC, which is cleaved to a luminescent product by caspase-3, was used. The results shown in Figure 7D indicate that the "effector caspase-3" was significantly activated in a dose-dependent pattern in BAE cells after treatment with AD0157. In this assay, 10 μM 2-methoxyestradiol was used as the positive control of caspase activation.

2.8. AD0157 Interference on the ERK1/2 and Akt Pathways

MAPK/ERK1/2 and PI3K/Akt are two of the most relevant signaling pathways controlling angiogenesis [16]. Therefore, we examined the effect of AD0157 on the serum-induced phosphorylation of ERK1/2 and Akt in BAECs. As shown in Figure 8A, treatment of the BAEC with serum resulted in a significant enhancement of both Akt and ERK-1/2 phosphorylation. Akt phosphorylation was significantly inhibited in BAECs by the presence of 1 μM AD0157 (Figure 8B). A similar effect was observed for ERK-1/2 phosphorylation when endothelial cells were serum-activated in the presence of 10 μM AD0157 (Figure 8A).

Figure 8. The effect of AD0157 on the ERK1/2 and Akt pathways (**A**) A representative Western blot showing the effects of AD0157 on the content of phosphorylated Akt, phosphorylated ERK-1/2, total Akt and total ERK-1/2 in protein extracts from BAECs; (**B**) Western blots were quantified by densitometry, and the pAkt/total Akt ratio and P-ERK-1/2/ERK-1/2 are expressed as the percentage of the pAkt/total Akt ratio or the P-ERK/total ERK ratio in serum-stimulated BAECs (in the presence of serum, in the absence of AD0157) the means ± SD of four independent experiments), * $p < 0.001$ *versus* the control (in the presence of serum, in the absence of AD0157).

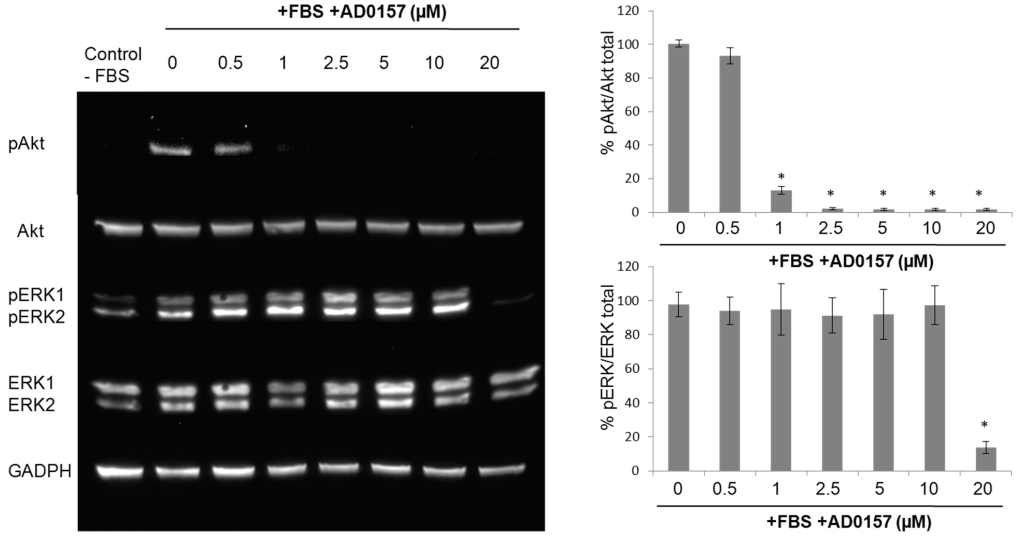

(**A**) (**B**)

2.9. Global Discussion

For angiogenesis to take place, activated endothelial cells must proliferate, migrate and invade through the basement membrane and the extracellular matrix and, finally, differentiate to yield a new capillary vessel. Any of these steps can be considered a target for the pharmaceutical inhibition of angiogenesis [5].

The vast majority of the natural compounds that have been previously described as inhibitors of angiogenesis have been isolated from plants and terrestrial microorganisms, mainly due to their higher availability and because their therapeutic effects had been previously known in folk traditional medicines [17]. However, increasing attention is being paid to the development of marine-derived antiangiogenic agents, probably fuelled by the increase in the number of marine-derived anticancer drugs, which are being successfully used for cancer therapy [18,19]. Nowadays, it is widely acknowledged that marine organisms produce interesting and singular pharmacological lead compounds, derived from the large diversity of marine habitats and environmental conditions. Marine organisms produce metabolites that allow them to adapt and survive in extreme environments, unique molecules of the highest interest for drug discovery [20]. In this regard, some angiogenesis inhibitors from marine origin have been described by us and others [8–11,21].

In this paper, we show that AD0157, a pyrrolidinedione isolated from the fermentation broth of a marine fungus, is a new inhibitor of angiogenesis *in vitro*, *in vivo* and *ex vivo*. This compound was first detected in a blind screening of compounds from marine origin that were able to inhibit, at nontoxic doses, the endothelial cell tube formation *in vitro*. AD0157 is able to abrogate the formation of "tubule-like" structures on Matrigel at concentrations that are lower than those required to inhibit endothelial cell growth. Our results also show that similar concentrations of AD0157 produced a significant inhibition of the migratory capability of BAECs, which could contribute to its antiangiogenic activity. These concentrations are in the same range as those required for other previously described inhibitors of angiogenesis, including a number of marine and plant-derived antiangiogenic compounds [8,11,22–26]. Moreover, the mentioned biological activities of AD0157 are exerted at one or two orders of magnitude lower than those required for some other natural compounds that have been previously described as inhibitors of angiogenesis [27–30].

Some of the best characterized anti-angiogenic compounds were initially detected and selected for their capability to interfere with endothelial cell growth, although the desirable endothelial cell specificity of this effect is not a common feature [31]. Our data indicate a non-specific cell growth inhibitory effect in long-term (three days) treatments with micromolar concentrations of AD0157 for endothelial and tumor cells, suggesting that this compound could also behave as a potential anti-tumor drug. The fact that the growth inhibitory activity is exerted at higher concentrations of AD0157 than those required to inhibit the endothelial tube formation suggests that the antiangiogenic activity of this compound is dependent on the prevention of capillary-like tube formation or endothelial cell migration rather than proliferation.

A positive proteolytic balance is required for capillary sprouting and lumen formation during angiogenesis. Matrix metalloproteinases (MMPs) are essential in the angiogenesis process [32].

MMP-2, also called gelatinase A, is constitutively secreted by endothelial cells contributing to the triggering of tumor angiogenesis *in vitro* and *in vivo* [33,34]. Our data show that incubation with AD0157 inhibits MMP-2 secretion in BAEC-conditioned media and cell lysates, which could contribute to the anti-angiogenic effect of this compound. The inhibition of gelatinases production by AD0157 seems to be endothelial-specific, since no effect on the levels of MMP-2 and MMP-9 (gelatinase B) produced by HT1080 tumor cells was observed after treatment with this compound. Nevertheless, further investigation is needed to confirm and characterize this suggested specificity.

Inhibition by AD0157 of *in vitro* angiogenesis agrees well with the observed effect on the *in vivo* angiogenesis, substantiated by using two widely employed and independent experimental models: the chick chorioallantoic membrane and the live fluorescent zebrafish embryo neovascularization assays. Our data show that AD0157 is a potent inhibitor of angiogenesis *in vivo*, these activities being exhibited in a concentration-dependent fashion at doses that are below those required for other previously described inhibitors of angiogenesis, including the marine natural compounds, aeroplysinin-1, 8-epipuupehedione and toluquinol, among others [8,9,11]. AD0157 *in vivo* antiangiogenic activity was confirmed by means of an *ex vivo* aortic ring assay illustrating the endothelial cell proliferation, migration and the capillary-like tube formation from aortic explants in a collagen matrix [35].

Growing evidence indicates that the induction of apoptosis in endothelial cells is a mechanism that could contribute to the biological activity of some antiangiogenic compounds [8–11]. The results obtained with BAEC indicate that after being exposed to AD0157, endothelial cells exhibit some typical hallmarks of apoptosis, including apoptotic cell morphology and DNA fragmentation. Cell cycle studies clearly show a significant increase in the percentage of cells with sub-diploid DNA content in AD0157-treated BAEC, indicating that the growth inhibitory effect produced by this compound on activated endothelial cells could be due to an induction of apoptosis. Caspases are critical components of the apoptotic machinery [36]. Measurement of the activity of the effector caspase 3 in endothelial cells shows a dose-dependent activation of the caspase proteolytic cascade after treatment with AD0157, suggesting that this compound induces apoptosis in BAEC through a caspase-dependent pathway.

The angiogenic transformation of the endothelium involves the activation of diverse intracellular signaling pathways. The knowledge about them may provide new targets of antiangiogenic therapies [16]. The PI3K/Akt pathway plays a central role in regulating cell survival, proliferation, migration, regulating normal vascularization and pathological angiogenesis, which makes this pathway an exciting target for molecular therapeutics [37,38]. Our data reveal that AD0157 caused the repression of Akt phosphorylation in serum-stimulated endothelial cells, which indicates that components of this pathway, particularly essential for the survival of the angiogenic endothelium, could be major targets in the molecular mechanism of this compound. The MAPK/ERK1-2 pathway, the main controller of the transduction of proliferation signals, is the molecular target of some successfully developed inhibitors of angiogenesis [39]. The kinase domain phosphorylation of ERK isoforms p44 (ERK-1) and p42 (ERK-2) is stimulated by a wide variety of growth factors and mitogens, including FGF and VEGF [16]. Although our results show that incubation with AD0157 abrogates the serum-stimulated ERK1-2 phosphorylation, the fact that this activity is only

observed at concentrations that are ten times higher than those required to inhibit Akt phosphorylation is in agreement with the cell cycle studies showing that this compound is preferentially acting on endothelial cell survival, rather than on endothelial proliferation. Nevertheless, deactivation of the ERK pathway in activated endothelial cells by high concentrations of AD0157 could explain the observed downregulation of MMP-2, mediated by the mentioned signaling pathway [40].

3. Experimental Section

3.1. Materials

Cell culture media, penicillin, streptomycin and amphotericin B were purchased from Biowhittaker (Walkersville, MD, USA). Fetal bovine serum (FBS) was a product of Harlan-Seralab (Belton, UK). Matrigel was purchased from Becton–Dickinson (Bedford, MA, USA). Plastics for cell culture were supplied by NUNC (Roskilde, Denmark) and VWR (West Chester, PA, USA). Hanks' Balanced Salt Solution (HBSS) and MCDB131 medium were obtained from Gibco (Grand Island, New York, NY, USA). Collagen was provided by SERVA Electrophoresis (Heidelberg, Germany). Fertilized chick eggs were obtained from Granja Santa Isabel (Córdoba, Spain). The antibodies used in this work were purchased from Cell Signaling Technology (Danvers, MA, USA). Supplements and other chemicals not listed in this section were obtained from Sigma Chemicals Co. (St. Louis, MO, USA). AD0157, kindly supplied by Biomar S.A. (León, Spain), was purified as a colorless powder from the mycelium of a fungal strain, *Paraconiothyrium* sp. HL-78-gCHSP3-B005, isolated from a marine Chordata sample collected in Guatemala, by extraction with EtOAc/MeOH [12]. The organic extract was purified by VFC (vacuum flash chromatography), flash-column chromatography on silica gel and by reverse phase HPLC. Data regarding the fermentation of this fungus, extraction, isolation and structural determination of AD0157 are available as Supplementary Information.

3.2. Cell Culture

Bovine aortic endothelial cells (BAEC) were isolated from bovine aortic arches, as previously described [41], and maintained in Dulbecco's modified Eagle's medium (DMEM) containing glucose (1 g/L), glutamine (2 mM), penicillin (50 IU/mL), streptomycin (0.05 mg/mL) and amphotericin (1.25 mg/L) supplemented with 10% FBS (DMEM/10% FBS). Human fibrosarcoma HT-1080 cells were maintained in DMEM containing glucose (4.5 g/L), glutamine (2 mM), penicillin (50 IU/mL), streptomycin (0.05 mg/mL) and amphotericin (1.25 mg/L) supplemented with 10% FBS. Human colon adenocarcinoma HT-29 cells and human osteosarcoma U2OS cells were maintained in McCoy's 5A medium containing glutamine (2 mM), penicillin (50 IU/mL), streptomycin (50 μg/mL) and amphotericin (1.25 μg/mL) supplemented with 10% FBS. Human breast cancer carcinoma MDA-MB-231 was maintained in RPMI1640 medium (medium developed at Roswell Park Memorial Institute) containing glutamine (2 mM), penicillin (50 IU/mL), streptomycin (50 μg/mL) and amphotericin (1.25 μg/mL) supplemented with 10% FBS. All cell lines were maintained at 37 °C and humidified 5% CO_2 atmosphere.

3.3. Cell Growth Assay

The 3-(4,5-dimethylthiazol-2-yl)-2,5-diphenyltetrazolium bromide or MTT dye reduction assay in 96-well microplates was used. This assay is dependent on the reduction of MTT by mitochondrial dehydrogenases of a viable cell to a blue formazan product, which can be measured spectrophotometrically. Three times ten to the power of three BAEC, 2×10^3 HT-1080, HT-29, MDA-MB-231 and U2OS cells in a total volume of 100 µL of their respective growth media were incubated with serial dilutions of AD0157. After 3 days of incubation (37 °C and 5% CO_2 in a humid atmosphere), 10 µL of MTT (5 mg/mL in phosphate-buffered saline (PBS)) were added to each well, and the plate was incubated for a further 4 h at 37 °C. The resulting formazan was dissolved in 150 µL of 0.04 N HCl/2-propanol and read at 550 nm. All determinations were carried out in quadruplicate, and three independent experiments were carried out. IC_{50} values were calculated as those concentrations of AD0157 yielding 50% cell survival, taking the values obtained for the control to be 100%.

3.4. Endothelial Cell Differentiation Assay: Tube Formation on Matrigel

Wells of 96-well microplate were coated with 50 µL of Matrigel (10.5 mg/mL) at 4 °C and allowed to polymerize at 37 °C for a minimum of 30 min. Some 5×10^4 BAE cells were added in 200 µL of complete medium. Finally, different amounts of AD0157 were added and incubated at 37 °C in a humidified chamber with 5% CO_2. After incubation for 7 h, cultures were observed and photographed with a Nikon DIAPHOT-TMD inverted microscope (Tokyo, Japan). Each concentration was tested in duplicate, and two different observers evaluated the results of chord formation inhibition. Those assays where no tubular structure could be observed were considered as positive in this assay.

3.5. Endothelial Cell Migration Assay

The migratory activity of BAEC was assessed using a wounded migration assay. Confluent monolayers in 6-well plates were wounded with pipet tips with 2 perpendicular diameters, giving rise to 2 acellular 1 mm-wide lanes per well. After washing, cells were supplied with 1.5 mL complete medium in the absence (controls) or presence of different concentration of AD0157. Wounded areas were photographed. After an additional 4, 7 and 24 h of incubation, plates were observed under the microscope, and photos were taken of the same areas as those recorded at time zero. The amount of migration at 7 h was determined by image analysis in both controls and treated wells and normalized with respect to their respective values at time zero, using the NIH Image 1.6 software. The regrowth of BAEC into the cell-free area was calculated as the percentage of the initial wounded area (time 0) that had been recovered by endothelial cells after 7 h.

3.6. Gelatinolytic Activity

To prepare conditioned media and cell lysates, BAEC and HT1080 cells were grown at 75% confluency in 6-well plates. After 2 washes with PBS, each well received the indicated

concentration of AD0157 in 1.5 mL of DMEM/0.1% bovine serum albumin (BSA) containing 200 kallikrein inhibitor units (KIU) of aprotinin/mL. After 24 h of incubation, the conditioned media were collected, and the cells were washed twice with PBS and harvested by scrapping into 0.5 mL of 0.2% Triton X-100 in 0.1 M Tris/HCl containing 200 KIU of aprotinin. Duplicates were used to determine the cell number by using a Coulter counter. The media and cell lysates were centrifuged at 1000× *g* at 4 °C for 20 min, and the supernatants were collected and used for assayed gelatinolytic activity.

The gelatinolytic activities of MMP-2 and MMP-9 delivered to the conditioned media or present in cell lysates were detected in gelatinograms. Aliquots of conditioned media and cell lysates normalized for equal cell numbers were subjected to non-reducing SDS-PAGE with gelatin (1 mg/mL) added to the 10% resolving gel. After electrophoresis, gels were washed twice with 50 mM Tris/HCl, pH 7.4, supplemented with 2% Triton X-100, and twice with 50 mM Tris/HCl, pH 7.4. Each wash was for 10 min and with continuous shaking. After the washes, the gels were incubated overnight at 37 °C immersed in a substrate buffer (50 mM Tris/HCl, pH 7.4, supplemented with 1% Triton X-100, 5 mM $CaCl_2$ and 0.02% Na_3N). Then, the gels were stained with Commassie Blue R-250, and the bands of gelatinase activity could be detected as non-stained bands in a dark, stained background. Quantitative analysis of gelatinograms was performed with the NIH Image 1.6 program.

3.7. Chorioallantoic Membrane (CAM) Assay

Fertilized chick eggs were incubated horizontally at 38 °C in a humidified incubator, windowed by day 3 of incubation and processed by day 8. The compound AD0157 were added to a 1.2% solution of methylcellulose in water, and 10 µL drops of this solution were allowed to dry on a Teflon-coated surface in a laminar flow hood and implanted on the CAM. After 48 h reincubation, the CAM was examined under a stereomicroscope by two different observers. The assay was scored as positive when both of them reported a significant reduction of vessels in the treated area [8].

3.8. Zebrafish Embryo Assay

Transgenic fli-EGFP fish (*TG(fli1:EGFP)y1*) had a vasculature labeled with GFP and were purchased from the Zebrafish International Resource Center (ZIRC, Eugene, OR, USA). Zebrafish embryos were generated via natural pairwise mating and maintained in embryo water at 28.5 °C. Embryos were manually dechorionated with forceps at 24 h postfertilization (hpf), arrayed in a 96-well plate (one embryo per well) and incubated with different concentrations of AD0157 in 100 µL of water at 28.5 °C for 24 h. DMSO was used as both the carrier of drugs and control. After incubation, fish embryos were anesthetized with tricaine (0.02%), placed on slides and examined under an epifluorescence Nikon microscope equipped with a DS-L1 Nikon (Chiyoda-Ku, Tokyo, Japan) digital Leica DM IL inverted microscope (Leica Microsystems, Wetzlar, Germany) at low and high magnification [27].

3.9. Mouse Aortic Ring Assay

Thoracic aortas were removed from 2 to 4 month-old C57BL/6 mice and immediately transferred to a culture dish containing Dulbecco's modified Eagle's medium (DMEM). The periaortic fibroadipose tissue was carefully removed with fine microdissecting forceps and iridectomy scissors paying special attention not to damage the aortic wall. One-millimeter aortic rings (approximately 15 per aorta) were sectioned and embedded in a rat tail interstitial collagen gel (1.5 mg/mL) prepared by mixing 7.5 volumes of 2 mg/mL collagen, 1 volume of 10× Hank's Balanced Salt Solution (HBBS), 1.5 volume of 186 mM $NaHCO_3$ and 0.1 volume of 1 M NaOH to adjust the pH to 7.4. The collagen gels containing the aortic rings were polymerized in cylindrical agarose wells and kept in quadruplicate at 37 °C in 60 mm diameter Petri dishes (bacteriological polystyrene, Falcon, Becton Dickinson, Lincoln Park, NJ, USA). Each Petri dish contained 6 mL of MCDB131 medium supplemented with 1% L-glutamine, 25 mM $NaHCO_3$, 100 U/mL penicillin, 100 µg/mL streptomycin and 2.5% mouse serum, in the presence or absence of AD0157 or DMSO. The cultures were kept at 37 °C in a humidified environment for a week and examined every second day with a phase contrast microscope (Zeiss, Axiovert 25) at appropriate magnification.

The quantification of aortic rings was done with NIH Image 1.6 software. The results were calculated as the area occupied by new microvessels expressed as a percentage by the outgrowth observed in the controls, which we considered to have 100% vessel formation. Four aortic rings from different mice were quantified in each experimental condition.

3.10. Apoptosis and Cell Cycle Assays

For Hoechst staining experiments, cells were plated on 8-well chamber slides and grown to sub-confluence. After treatments for 14 h with the indicated concentrations of AD0157 in complete medium, cells were washed with PBS and fixed with formalin solution. Chamber slides were stained with 1 mg/mL Hoechst in PBS for 2 min, washed twice with PBS and mounted (Dako Cytomation Fluorescent Mounting Medium, Denmark). Samples were observed under a fluorescence microscope (Leica, TCS-NT, Heidelberg, Germany).

For DNA fragmentation studies, cells were grown to sub-confluence in complete medium on 8-well Falcon humidified chamber slides and incubated for 14 h with or without the indicated concentrations of AD0157. After incubation, cells were washed with PBS, fixed with formalin solution, washed with PBS again and permeabilized with 0.1% Triton X-100 in PBS. The TUNEL (terminal deoxynucleotidyl transferase mediated dUTP-biotin nick end-labeling) assay was performed with the use of the *In Situ* Cell Death Detection Kit (Roche Diagnostics, Barcelona, Spain), according to the manufacturer's instructions. Finally, cells were mounted using Dako Cytomation Fluorescent Mounting Medium and observed under a fluorescence microscope (Leica, TCS-NT).

For cell cycle analysis, BAECs were grown in complete medium in a 6-well plate to 75% confluency. After treatment with different concentrations of AD0157 during 14 h, attached and detached cells were harvested and centrifuged at 1000× *g*. Pellets were washed whit PBS and resuspended in 250 µL of ice-cold PBS. For fixation, 70% ice-cold ethanol was added while

continuous gentle vortexing, and samples were maintained on ice for 1 h. Finally, cells were centrifuged and washed twice with PBS, resuspended in 500 µL propidium iodide staining solution (40 µg/mL propidium iodide and 0.1 mg/mL RNase-A in PBS) and incubated for 1 h with shaking and protection from light. Percentages of the subG1, G1 and S/G2/M populations were determined using a MoFlo Dako Cytomation cytometer and the software, Summit 4.3.

For the determination of caspase 3/7 activity, BAECs were plated in 96-well plates (13,000 cells/well) and treated with or without different concentrations of AD0157 for 14 h. Then, Caspase-Glo® 3/7 reagent (Promega Biotech Ibérica, Madrid, Spain) was added to the wells, according to the manufacturer's instructions, and the luminescence was recorded at 30 minutes with a GLOMAX 96 microplate luminometer (Promega Biotech Ibérica, Madrid, Spain). The assay provides a proluminescent caspase-3/7 DEVD-aminoluciferin substrate and a proprietary thermostable luciferase in a reagent optimized for caspase-3/7 activity, luciferase activity and cell lysis.

3.11. Western Blot Analysis

Subconfluent BAEC cultures were incubated in DMEM medium supplemented with 1% fetal bovine serum (FBS) for 24 h. After that, the medium was replaced, and the cells were incubated with different doses of AD0157 or vehicle (DMEM) for 30 min and, then, challenged for 20 additional minutes with FBS or the vehicle (DMEM medium). The protein lysates were obtained by scrapping the cells in a lysis buffer (50 mM Tris, pH 7.4, 150 mM NaCl, 1% Triton X-100, 0.25% sodium deoxycholate, 1 mM EDTA, 1 mM sodium orthovanadate and 5 mg/mL of a protease inhibitors mixture). Afterwards, the extracts were centrifuged at 13,000 rpm for 15 min at 4 °C, evaluated for protein concentration by the Bradford test and stored at −80 °C until the moment of analysis. These samples were denatured for 5 min at 95 °C and subjected to SDS-PAGE, loading some 20 µL of sample per well. After electrophoresis, samples were electrotransferred to nitrocellulose membranes, blocked with 5% dried skimmed milk in 50 mM Tris pH 8.4, 0.9% NaCl, 0.05% Tween 20 (Tris buffered saline-Tween 20, TBST) and incubated overnight in the presence of an anti-human phosphorylated Akt or an anti-human phosphorylated ERK-1/2 at a dilution of 1:1000 in TBST or an anti-human total Akt or an anti-human total ERK-1/2 at a dilution of 1:1000 in TBS-T with 5% BSA. After three washing steps with TBST, the membranes were incubated with horseradish peroxidase-conjugated anti-rabbit secondary antibody at a dilution of 1:5000 in blocking buffer for 2 h at room temperature. After three washing steps with TBST, the immunoreactive bands were detected using a chemiluminescence system (SuperSignal West Pico Chemiluminescent Substrate, Pierce, Rockford, IL, USA) with an imaging system (Chemidoc XRS System, Bio-Rad, Hercules, CA, USA) and were quantified by using ImageLab version 3.0 software. The membranes were incubated with an anti-GAPDH primary antibody at a dilution of 1:1000 to ensure equal loading. Akt or ERK-1/2 activation was calculated as the p-Akt/total Akt and p-ERK-1/2/ERK-1/2 ratio and expressed as the mean ± SD of 3 independent experiments.

3.12. Statistical Analysis

All data are expressed as the means ± standard deviation (SD). A one-tailed Student's *t*-test was used for evaluations of the pairs of means, to establish which groups differed from the control group. $p < 0.05$ was considered to be statistically significant.

3.13. Animal Testing Regulations

Experimentation animals were kept at the animal house facilities of the University of Málaga. Experiments on animals were subjected to the European Directive 86/609/EEC on the protection of animals used for experimental and other scientific purposes, under the approval of the Bioethics Committee of the University of Málaga.

4. Conclusions

In conclusion, in this paper, we show evidence that the marine pyrrolidinedione, AD0157, is a potent inhibitor of angiogenesis *in vitro*, *in vivo* and *ex vivo*. AD0157 abrogates certain functions of endothelial cells, namely, differentiation, migration, growth and proteases production. The induction of endothelial cell apoptosis by AD0157 could be related to an inhibition of the Akt signaling pathway in activated endothelial cells. Although additional studies will be needed to elucidate the molecular mechanisms underlying the antiangiogenic activity of AD0157 and the pharmaceutical toxicological profile of this compound, the data presented here suggest a potential therapeutic application of AD0157 for the treatment of angiogenesis-related malignances. These data reinforce the great value of marine products as candidates for further pharmaceutical studies for feeding the anti-angiogenesis drug pipeline. Further efforts to determine the pharmacological potential of AD0157 are warranted.

Acknowledgments

Melissa García has been a recipient of a predoctoral "Formación de Profesorado Universitario" (FPU) grant from the Spanish Ministry of Science and Innovation, and her work is at present funded by "III Plan propio de Investigación" (University of Málaga). This work was supported by grants PS09/02216 and PT2008-0145 (Spanish Ministry of Science and Innovation, ISCIII and FEDER), Fundación Ramón Areces and PIE P08-CTS-3759 and P12-CTS-1507 (Andalusian Government and "Fondo Europeo de Desarrollo Regional" (FEDER)). The "Centros de Investigación Biomédica en Red" or CIBER de Enfermedades Raras" is an initiative from the "Instituto de Salud Carlos III" (ISCIII) (Spain). The funders had no role in the study design, data collection and analysis, decision to publish or preparation of the manuscript. The authors are indebted to Auxiliadora López Jiménez for her excellent technical assistance.

Conflicts of Interest

The authors declare no conflict of interest.

References

1. Hanahan, D.; Weinberg, R.A. Hallmarks of cancer: The next generation. *Cell* **2011**, *144*, 646–674.
2. Chung, A.S.; Ferrara, N. Developmental and pathological angiogenesis. *Annu. Rev. Cell. Dev. Biol.* **2011**, *27*, 563–584.
3. Carmeliet, P. Angiogenesis in life, disease and medicine. *Nature* **2005**, *438*, 932–936.
4. Quesada, A.R.; Medina, M.Á.; Muñoz-Chápuli, R.; Ponce, Á.L. Do not say ever never more: The ins and outs of antiangiogenic therapies. *Curr. Pharm. Des.* **2010**, *16*, 3932–3957.
5. Quesada, A.R.; Muñoz-Chápuli, R.; Medina, M.A. Anti-angiogenic drugs: From bench to clinical trials. *Med. Res. Rev.* **2006**, *26*, 483–530.
6. Bhatnagar, I.; Kim, S.K. Immense essence of excellence: Marine microbial bioactive compounds. *Mar. Drugs* **2010**, *8*, 2673–2701.
7. Imhoff, J.F.; Labes, A.; Wiese, J. Bio-mining the microbial treasures of the ocean: New natural products. *Biotechnol. Adv.* **2011**, *29*, 468–482.
8. Rodríguez-Nieto, S.; González-Iriarte, M.; Carmona, R.; Muñoz-Chápuli, R.; Medina, M.A.; Quesada, A.R. Antiangiogenic activity of aeroplysinin-1, a brominated compound isolated from a marine sponge. *FASEB J.* **2002**, *16*, 261–263.
9. Castro, M.E.; González-Iriarte, M.; Barrero, A.F.; Salvador-Tormo, N.; Muñoz-Chápuli, R.; Medina, M.A.; Quesada, A.R. Study of puupehenone and related compounds as inhibitors of angiogenesis. *Int. J. Cancer* **2004**, *110*, 31–38.
10. Martínez-Poveda, B.; Rodríguez-Nieto, S.; García-Caballero, M.; Medina, M.Á.; Quesada, A.R. The antiangiogenic compound aeroplysinin-1 induces apoptosis in endothelial cells by activating the mitochondrial pathway. *Mar. Drugs* **2012**, *10*, 2033–2046.
11. García-Caballero, M.; Marí-Beffa, M.; Cañedo, L.; Medina, M.Á.; Quesada, A.R. Toluquinol, a marine fungus metabolite, is a new angiosuppresor that interferes with the Akt pathway. *Biochem. Pharmacol.* **2013**, *85*, 1727–1740.
12. Fernández-Medarde, A.; Cañedo, L.; Vinuesa, M.A.; Sánchez-López, J.M.; Calvo, B.; Martínez-Insua, M.; Quesada, A.R.; García-Caballero, M.; Medina, M.A. Compounds, Their Preparation And Use in Medicaments. European Patent Application 13382284, 9 July 2013.
13. Staton, C.A.; Reed, M.W.; Brown, N.J. A critical analysis of current *in vitro* and *in vivo* angiogenesis assays. *Int. J. Exp. Pathol.* **2009**, *90*, 195–221.
14. Lawson, N.D.; Weinstein, B.M. *In vivo* imaging of embryonic vascular development using transgenic zebrafish. *Dev. Biol.* **2002**, *248*, 307–318.
15. Nicosia, R.F.; Zorzi, P.; Ligresti, G.; Morishita, A.; Aplin, A.C. Paracrine regulation of angiogenesis by different cell types in the aorta ring model. *Int. J. Dev. Biol.* **2011**, *55*, 447–453.
16. Muñoz-Chápuli, R.; Quesada, A.R.; Medina, M.Á. Angiogenesis and signal transduction in endothelial cells. *Cell. Mol. Life Sci.* **2004**, *61*, 2224–2243.
17. Fan, T.P.; Yeh, J.C.; Leung, K.W.; Yue, P.Y.; Wong, R.N. Angiogenesis: From plants to blood vessels. *Trends Pharmacol. Sci.* **2006**, *27*, 297–309.

18. Bhatnagar, I.; Kim, S.K. Marine Antitumor drugs: Status, shortfalls and strategies. *Mar. Drugs* **2010**, *8*, 2702–2720.
19. Nastrucci, C.; Cesario, A.; Russo, P. Anticancer drug discovery from the marine environment. *Recent Pat. Anticancer Drug Discov.* **2012**, *7*, 218–232.
20. Blunt, J.W.; Copp, B.R.; Munro, M.H.; Northcote, P.T.; Prinsep, M.R. Marine natural products. *Nat. Prod. Rep.* **2011**, *28*, 196–268.
21. Wang, Y.Q.; Miao, Z.H. Marine-derived angiogenesis inhibitors for cancer therapy. *Mar. Drugs* **2013**, *11*, 903–933.
22. Kong, D.; Yamori, T.; Kobayashi, M.; Duan, H. Antiproliferative and antiangiogenic activities of smenospongine, a marine sponge sesquiterpene aminoquinone. *Mar. Drugs* **2011**, *9*, 154–161.
23. Kim, G.D.; Cheong, O.J.; Bae, S.Y.; Shin, S.J.; Lee, S.K. 6″-Debromohamacanthin A, a Bis (Indole) alkaloid, inhibits angiogenesis by targeting the VEGFR2-mediated PI3K/AKT/mTOR signaling pathways. *Mar. Drugs* **2013**, *11*, 1087–1103.
24. Martínez-Poveda, B.; Quesada, A.R.; Medina, M.A. Hypericin in the dark inhibits key steps of angiogenesis *in vitro*. *Eur. J. Pharmacol.* **2005**, *516*, 97–103.
25. López-Jiménez, A.; García-Caballero, M.; Medina, M.A.; Quesada, A.R. Anti-angiogenic properties of carnosol and carnosic acid, two major dietary compounds from rosemary. *Eur. J. Nutr.* **2013**, *52*, 85–95.
26. Kim, Y.H.; Shin, E.K.; Kim, D.H.; Lee, H.H.; Park, J.H.; Kim, J.K. Antiangiogenic effect of licochalcone A. *Biochem. Pharmacol.* **2010**, *80*, 1152–1159.
27. García-Caballero, M.; Marí-Beffa, M.; Medina, M.A.; Quesada, A.R. Dimethylfumarate inhibits angiogenesis *in vitro* and *in vivo*: A possible role for its antipsoriatic effect? *J. Investig. Dermatol.* **2011**, *131*, 1347–1355.
28. Fortes, C.; García-Vilas, J.A.; Quesada, A.R.; Medina, M.A. Evaluation of the anti-angiogenic potential of hydroxytyrosol and tyrosol, two bio-active phenolic compounds of extra virgin olive oil, in endothelial cell cultures. *Food Chem.* **2012**, *134*, 134–140.
29. Igura, K.; Ohta, T.; Kuroda, Y.; Kaji, K. Resveratrol and quercetin inhibit angiogenesis *in vitro*. *Cancer Lett.* **2001**, *171*, 11–16.
30. Cárdenas, C.; Quesada, A.R.; Medina, M.A. Evaluation of the anti-angiogenic effect of aloe-emodin. *Cell. Mol. Life Sci.* **2006**, *63*, 3083–3089.
31. Rodriguez-Nieto, S.; Medina, M.A.; Quesada, A.R. A re-evaluation of fumagillin selectivity towards endothelial cells. *Anticancer Res.* **2001**, *21*, 3457–3460.
32. Nguyen, M.; Arkell, J.; Jackson, C.J. Human endothelial gelatinases and angiogenesis. *Int. J. Biochem. Cell. Biol.* **2001**, *33*, 960–970.
33. Fang, J.; Shing, Y.; Wiederschain, D.; Yan, L.; Butterfield, C.; Jackson, G.; Harper, J.; Tamvakopoulos, G.; Mosess, M.A. Matrix metalloproteinase-2 is required for the switch to the angiogenic phenotype in a tumor model. *Proc. Natl. Acad. Sci. USA* **2000**, *97*, 3884–3889.
34. Itoh, T.; Tanioka, M.; Yoshida, H.; Yoshioka, T.; Nishimoto, H.; Itohara, S. Reduced angiogenesis and tumor progression in gelatinase A-deficient mice. *Cancer Res.* **1998**, *58*, 1048–1051.

35. Masson, V.E.; Devy, L.; Grignet-Debrus, C.; Bernt, S.; Bajou, K.; Blacher, S.; Roland, G.; Chang, Y.; Fong, T.; Carmeliet, P.; *et al*. Mouse aortic ring assay: A new approach of the molecular genetics of angiogenesis. *Biol. Proced. Online* **2002**, *4*, 24–31.
36. Yi, C.H.; Yuan, J. The Jekyll and Hyde functions of caspases. *Dev. Cell* **2009**, *16*, 21–34.
37. Cheng, J.Q.; Lindsley, C.W.; Cheng, G.Z.; Yang, H.; Nicosia, S.V. The Akt/PKB pathway: Molecular target for cancer drug discovery. *Oncogene* **2005**, *24*, 7482–7492.
38. Jiang, B.H.; Liu, L.Z. AKT signaling in regulating angiogenesis. *Curr. Cancer Drug Targets* **2008**, *8*, 19–26.
39. Kim, E.K.; Choi, E.J. Pathological roles of MAPK signaling pathways in human diseases. *Biochim. Biophys. Acta* **2010**, *1802*, 396–405.
40. Chakraborti, S.; Mandal, M.; Das, S.; Mandal, A.; Chakraborti, T. Regulation of matrix metalloproteinases: An overview. *Mol. Cell. Biochem.* **2003**, *253*, 269–285.
41. Gospodarowicz, D.; Moran, J.S. Mitogenic effect of fibroblast growth factor on early passage cultures of human and murine fibroblasts. *J. Cell. Biol.* **1975**, *66*, 451–457.

Cytotoxic Effects of Fascaplysin against Small Cell Lung Cancer Cell Lines

Gerhard Hamilton

Abstract: Fascaplysin, the natural product of a marine sponge, exhibits anticancer activity against a broad range of tumor cells, presumably through interaction with DNA, and/or as a highly selective cyclin-dependent kinase 4 (CDK4) inhibitor. In this study, cytotoxic activity of fascaplysin against a panel of small cell lung cancer (SCLC) cell lines and putative synergism with chemotherapeutics was investigated. SCLC responds to first-line chemotherapy with platinum-based drugs/etoposide, but relapses early with topotecan remaining as the single approved therapeutic agent. Fascaplysin was found to show high cytotoxicity against SCLC cells and to induce cell cycle arrest in G1/0 at lower and S-phase at higher concentrations, respectively. The compound generated reactive oxygen species (ROS) and induced apoptotic cell death in the chemoresistant NCI-H417 SCLC cell line. Furthermore, fascaplysin revealed marked synergism with the topoisomerase I-directed camptothecin and 10-hydroxy-camptothecin. The Poly(ADP-ribose)-Polymerase 1 (PARP1) inhibitor BYK 204165 antagonized the cytotoxic activity of fascaplysin, pointing to the involvement of DNA repair in response to the anticancer activity of the drug. In conclusion, fascaplysin seems to be suitable for treatment of SCLC, based on high cytotoxic activity through multiple routes of action, affecting topoisomerase I, integrity of DNA and generation of ROS.

Reprinted from *Mar. Drugs*. Cite as: Hamilton, G. The Distribution and Identity of Edaphic Fungi in the McMurdo Dry Valleys. *Mar. Drugs* **2014**, *12*, 1377-1389.

1. Introduction

Fascaplysin (12,13-Dihydro-13-oxopyrido[1,2-*a*:3,4-*b*′]diindol-5-ium chloride), a red bis-indole alkaloid of the marine sponge *Fascaplysinopsis* Bergquist sp., was first isolated in 1988, by Roll *et al.* [1]. This compound exhibited a broad range of activities including antibacterial, antifungal, antiviral, antimalarial, antiangiogenic and antiproliferative activity against numerous cancer cell lines [2–4]. Fascaplysin also showed DNA-intercalating capability with binding mode and affinity constants comparable to those of other typical DNA intercalators [5]. Additionally, significantly weaker non-intercalative DNA interactions were observed at high drug concentrations, pointing to its mechanism of biological activity via interference with genetic material. Furthermore, fascaplysin showed promising specific cyclin-dependent kinase 4 (CDK4) inhibitory activity with IC_{50} of 0.35 μM and it correspondingly blocked the growth of various cancer cells at the G0/1 phase of cell cycle [6,7]. Low activity was observed against other CDKs with IC_{50} of >100 μM for CDK1, >50 μM for CDK2, as well as 20 μM for CDK5. Recently, Shafiq and co-workers confirmed the specific effect of this compound on CDK4, which is known to play a key role in cell cycle control and is an important target for anticancer drugs [8]. Fascaplysin was reported to show cytotoxicity toward a panel of 60 cancer cell lines (IC_{50} values 0.6–4 μM), although testing was actually restricted to 36/60 of these cell lines [3]. The NCI60 panel misses

small cell lung cancer (SCLC) cell lines altogether, a tumor entity that accounts for a significant fraction of lung cancer deaths [9].

A range of studies reported the anticancer activities of fascaplysin in cell lines *in vitro* and in experimental animal models. Fascaplysin did not provoke G1 phase arrest in HeLa cells although it led to downregulation of CDK4, cyclin D1 and CDK4-specific Ser795 retinoblastoma phosphorylation [10]. The molecular mechanism of fascaplysin-induced apoptosis was characterized as activation of caspase-3, -8, and -9, cleavage of Bid, release of cytochrome c into cytosol and downregulation of the level of Bcl-2. Fascaplysin can block VEGF, inhibit proliferation and induce apoptosis of human umbilical vein endothelial cells (HUVECs) [11,12]. The results showed that G1 cell cycle arrest was induced by 2.6 μM fascaplysin in a time-dependent manner, and HUVECs exhibited more chemosensitivity than hepatocarcinoma cells BeL-7402 and Hela cells. Apoptosis of HUVEC cells was induced by 1.3 μM fascaplysin and this response was further confirmed by the detection of active caspase-3, indicating involvement of a mitochondrial pathway. Microarray analysis show that the TNF and TNF receptor superfamily in HUVECs and BEL-7402 were significantly regulated by fascaplysin and this tumor necrosis-related apoptosis-inducing ligand-(TRAIL)-induced apoptosis resulted in activation of caspases 3 and 9 and decreases in Bid [13].

Fascaplysin was tested in a murine sarcoma S180 experimental animal model [14]. Treatment of the mice suppressed tumor growth significantly. Tumor sections showed hallmarks of apoptosis and the decreased expression of proliferating cell nuclear antigen (PCNA) and CD31 indicated cytostasis and antiangiogenesis. In another study involving fascaplysin, HCT-116 colon cancer cells were injected subcutaneously into severe combined immunodeficiency (SCID) mice [15]. At a tumor size of 250 mm^3, mice received 4 mg/kg fascaplysin daily for five days. No toxicity was observed over the subsequent 30 days. At day 15, tumor size of the treated group was approximately 60% less than that of untreated control mice. Thus, even at this less than optimal dose, because a maxiumum tolerated dose (MTD) could not be obtained for fascaplysin, a therapeutic effect was observed.

In conclusion, cell line screening of the anticancer activity of fascaplysin is not complete and the mechanism inducing cell death in response to this drug, which may comprise different molecular mechanisms, is not clear. Interaction with other chemotherapeutic drugs to detect possible synergism was not described so far. Thus, in the present study, we screened SCLC cell lines, investigated cell cycle and cytotoxic effects of fascaplysin and used different drug combinations to screen putative synergistic action with established chemotherapeutics. In particular, fascaplysin was combined with camptothecins (CPTs) since we have reported enhancement of the cytotoxicity of the CPT analog topotecan against SCLC cell lines employing CDK4 inhibitors such as roscovitine and olomoucine [16].

Figure 1. Screening of fascaplysin toxicity against small cell lung cancer (SCLC), non-small cell lung cancer (NSCLC), HEK293 and unrelated cell lines (mean values ± SD; $n = 3$).

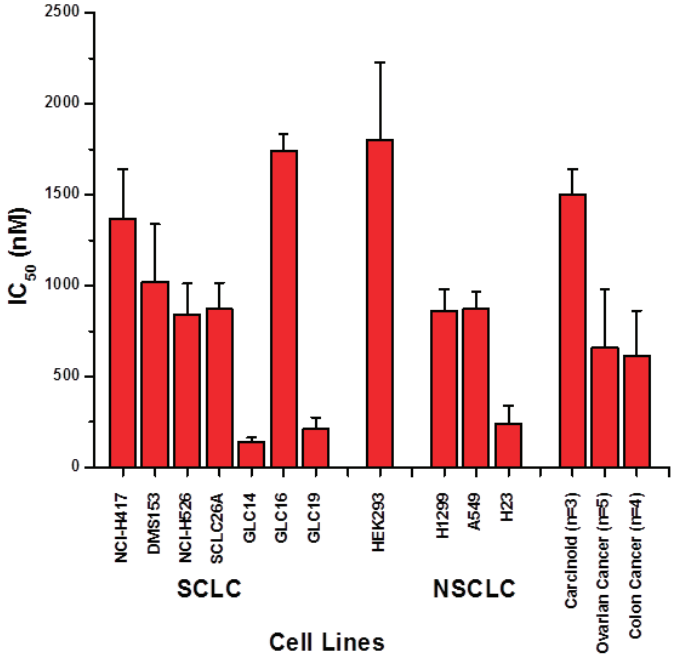

2. Results and Discussion

2.1. Screening of Cytotoxic Activity against Lung Cancer Cell Lines

The cytotoxic activity of fascaplysin was assessed using a panel of SCLC cell lines using MTT assays (Figure 1). IC_{50} values measured ranged from 134 to 1740 nM fascaplysin. GLC14, 16 and 19 comprise a series of SCLC cell lines obtained from a single patient prior to chemotherapy and after first-line and second-line therapy, respectively. Whereas SCLC26A is an untreated chemosensitive SCLC cell line with IC_{50} values (μM ± SD) for cisplatin of 1.2 ± 0.6 and for etoposide of 0.5 ± 0.2, respectively, NCI-H417 and DMS153 are chemoresistant with IC_{50} values of 12.0 ± 2.8/3.3 ± 0.9 for cisplatin and 15.1 ± 2.2/12.9 ± 0.5 for etoposide, respectively. Therefore, sensitivity for fascaplysine differs by a factor of 1.2–1.6 between SCLC26A and DMS153/NCI-H417, but cisplatin and etoposide sensitivities differ 2.75–10 fold and 25.8–30 fold, respectively. These IC_{50} values observed did not exceed the corresponding value for the HEK293 cell line, representing normal kidney epithelial tissue. Fascaplysin IC_{50} values measured in SCLC cell lines are similar to the two chemoresistant NSCLC cell lines H1299 and A549 and the chemosensitive H23 cell line, respectively. Two pulmonary carcinoid cell lines showed sensitivities in the range of the SCLC cell lines and mean IC_{50} values for a panel of seven ovarian (PA-1, CaOV3, OV90, TUVGH211,

A2780, A2780ADR) and five colon cancer (Colo205, HCT116, HCT116 p53 knockout, Colo320DM and HT29) cell lines indicated high chemosensitivity for fascaplysin.

Figure 2. Cell cycle distribution of fascaplysin-treated NCI-H417 and DMS153 SCLC cells (mean ± SD; $n = 3$).

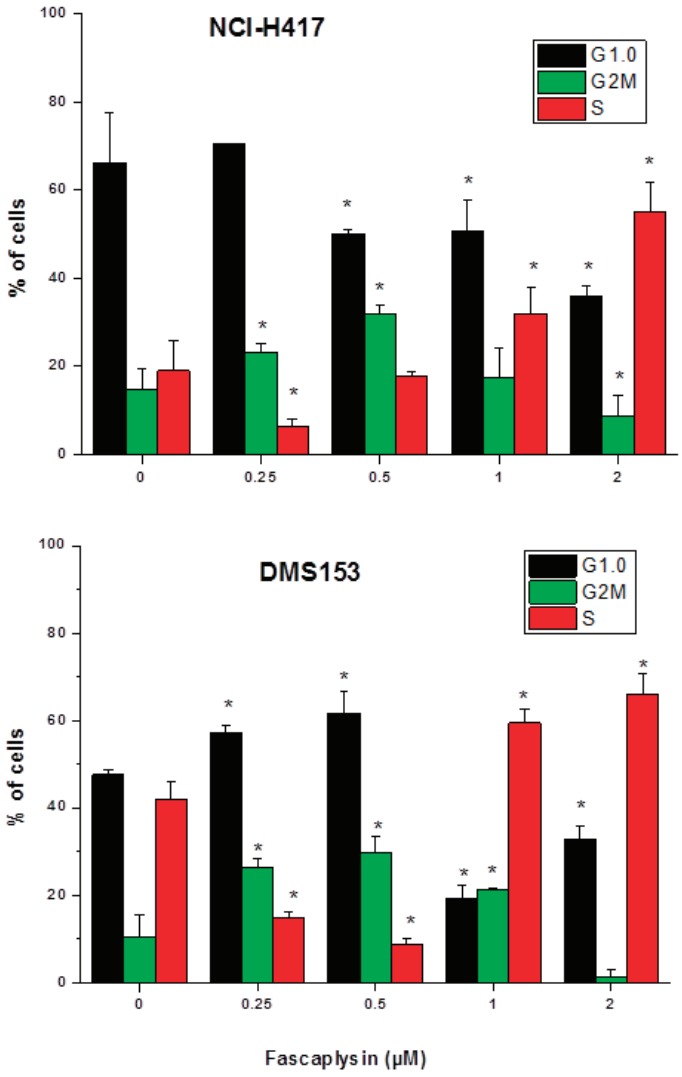

2.2. Effects of Fascaplysin on Cell Cycle Distribution of NCI-H417 and DMS153 Cells

For the assessment of effects of fascaplysin on cell cycle distribution in SCLC cells, NCI-H417 and DMS153 cells were treated with 0.25–2 μM of the compound and propidium iodide-stained cells analyzed in flow cytometry (Figure 2). The two lower concentrations of fascaplysin applied

(0.25 and 0.5 μM) caused accumulation of cells in G2M and G1/0 phases, whereas the higher concentrations (0.5 and 1 μM) arrested cells preferentially in S-phase.

Figure 3. AnnexinV-propidium iodide staining of fascaplysin-induced apoptotic cell death in NCI-H417 cells (**A**) and effects of fascaplysin on intracellular ROS levels as detected by dichlorodihydrofluorescein (DCF) fluorescence in flow cytometry (**B**; mean ± SD; n = 3). For the apoptosis assay all differences to the control are significant, except for necrotic cells and late apoptotic cells at 0.25 nM fascaplysin. In the case of the ROS assay, all values are significantly different from those of untreated cells and values were calculated relative to the DCF fluorescence signal of untreated control cells.

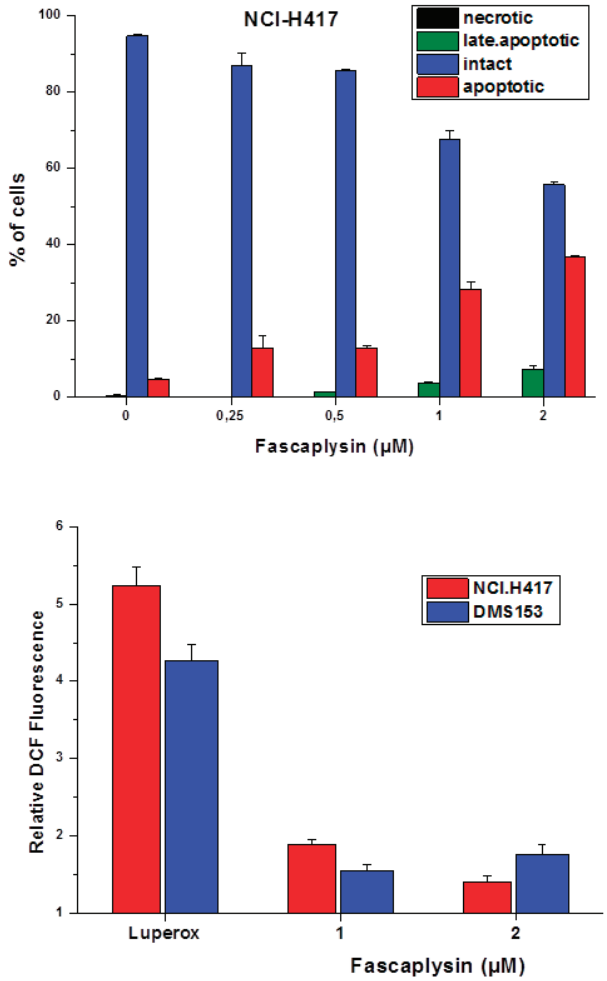

2.3. Fascaplysin-Induced Apoptosis and Generation of ROS in SCLC Lines

Fascaplysin-induced apoptotic cell death was investigated in NCI-H417 cells using annexinV-propidium iodide double staining and flow cytometry (Figure 3A). Treatment of the cells with increasing concentrations of fascaplysin (0.25–2 μM) for four days resulted in the appearance of apoptotic and a small fraction of late apoptotic/necrotic tumor cells.

Fascaplysin-induced generation of reactive oxygen species (ROS) in NCI-H417 and DMS153 cells was tested using fluorescence detection with the DCF dye (Figure 3B). A stabilized slow-release source of ROS, namely Di-tert-butyl peroxide/Luperox was included as positive control. Fascaplysin in concentrations of 1–2 μM was found to generate a limited but significant amount of ROS in both SCLC cell lines. *N*-acetyl-L-cysteine (NAC) is suitable for inactivating ROS and, accordingly, inclusion of 2.5–5 mM NAC in NCI-H417 fascaplysin cytotoxicity tests resulted in a twofold reduction of cell death (data not shown).

2.4. Synergistic Interaction of Fascaplysin and Camptothecins in NCI-H417 Cells

Fascaplysin was tested for a possible interaction with camptothecin (CPT) and 10-hydroxycamptothecin (HOCPT) in MTT assays using chemoresistant NCI-H417 SCLC cells (Figure 4). Fascaplysin synergistically enhanced both CPT- and HOCPT-induced tumor cell death at specific drug concentrations. Combination indices (CI) were calculated using the CompuSyn software and yielded 0.73 and 0.56 for CPT concentrations of 1000 and 500 nM and 0.82 and 0.95 for HOCPT concentrations of 2000 and 1000 nM, respectively. A similar albeit weaker synergistic interaction was detected with the camptothecin analog, topotecan (data not shown). A range of other chemotherapeutic drugs comprising cisplatin, carboplatin and etoposide revealed no interaction with fascaplysin. Additionally, the P-glycoprotein (ABCB1) inhibitor PSC833 (1 and 2.5 μM) exhibited no effect on fascaplysin cytotoxicity against DMS153 cells. No interaction or minor antagonism was detected using combinations of fascaplysin with doxorubicin, etoposide, vinblastine, oxaliplatin, gemcitabine, docetaxel, mitomycin and cytarabin (data not shown).

2.5. Effects of the BYK 204165 PARP Inhibitor on Fascaplysin-Induced Cell Death in SCLC Cell Lines

Cytotoxicity assays using a combination of fascaplysin with the BYK 204165 PARP1 inhibitor were performed using a panel of SCLC cell lines. Whereas in chemosensitive NCI-H526 cells 50 and 25 μM BYK204165, respectively, yielded a minor chemosensitizing effect (factor 0.66; IC_{50} in presence of fascaplysin plus BYK204165 inhibitor/IC_{50} value in presence of fascaplysin), all other cell lines (NCI-H417, DMS153, GLC14 and GLC19) used showed strong antagonism for this combination with 2.9 ± 1.13 (range 1.83–4.46) and 1.9 ± 0.51 (range 1.48–2.6) increased chemoresistance compared to fascaplysin alone.

Figure 4. Combination of fascaplysin (initial concentration 2000 nM) with camptothecin (CPT, initial concentration 2000 nM; upper panel) or 10-hydroxy-camptothecin (HOCPT, initial concentration 4000 nM; lower panel) cytotoxicity assays using NCI-H417 cells (mean ± SD, $n = 3$).

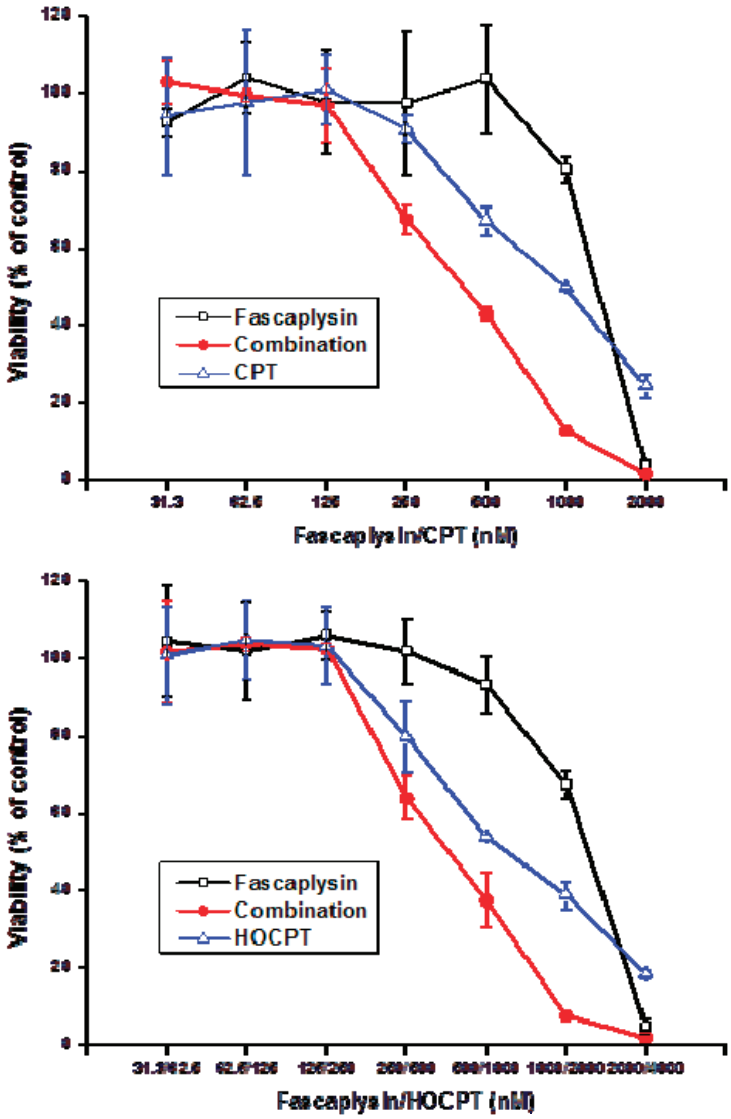

2.6. Discussion

Fascaplysin was demonstrated to show cytotoxicity towards a large panel of cell lines in low μM concentrations. Similar anticancer activity was found in the present study against SCLC cell lines, yielding IC_{50} values comparable to those found in melanoma, colon cancer and ovarian cancer cell

lines, among others. This compound exhibits high cytotoxicity independently of tissue origin and chemoresistance to unrelated drugs with few exceptions. Of the GLC14/16/19 series of SCLC cell lines, stemming from a single patient before and during two cycles of therapy failure, the GLC16 cells obtained after initial CHOP therapy showed highest resistance [17]. Likewise the H1299 and A549 NSCLC cell lines established from pretreated patients exhibited higher chemoresistance than H23, derived from tissue of an untreated patient [18,19]. However, the IC_{50} value obtained for the HEK293 epithelial kidney cell line exceeded those measured for most tumor cell lines, indicating a favorable toxicity profile. For further experiments, NCI-N417, a variant SCLC cell line known to be more aggressive and refractory to treatment although derived from a female patient with no prior treatment and DMS153, a line established from metastatic cells of a SCLC patient after therapy with cytoxan and methotrexate, were selected as chemoresistant cell lines [20,21].

As highly selective CDK4 inhibitor fascaplysin is expected to induce cell cycle arrest in G1/0 [6,7]. The activity of CDK-4 is restricted to the G1-S phases and is regulated by the attachment of the cyclin D and the endogenous CDK inhibitor p16INK4a. Both CDK4 and CDK6 encode cyclin-dependent serine-threonine kinases that, complex with D-type cyclines to phosphorylate the RB tumor suppressor protein, in turn resulting in transcription of genes required for G1-S phase cell cycle progression [22]. Fascaplysin-induced cell cycle perturbations in NCI-H417 and DMS153 are not restricted to G1/0 and seem to be insufficient to trigger apoptosis via inhibition of CDK4. In SCLC the tumor suppressor circuit comprising p16INK4, which specifically binds and inhibits CDK4/6, and RB is inactivated [23,24]. A minor fraction of SCLC tumors have absent p16INK4 protein and wildtype RB expression, whereas the majority of tumors which possess detectable levels of p16INK4 protein hold absent or mutant RB. Fascaplysin-induced G1 arrest is dependent on intact Rb protein. Absence of Rb protein was published for DMS153 cells [25] and the same result was found here for NCI-H417 cells with help of the Poly6146 rabbit antibody (Biolegend, San Diego, CA, USA) and paraformaldehyde-fixed cells (data not shown). Additionally, both SCLC cell lines, NCI-H417 and DMS153, feature mutated p53 [26,27].

Fascaplysin induces apoptotic cell death in NCI-H417 cells dose-dependently and the generation of ROS seems to support this cytotoxicity since addition of *N*-acetyl-L-cysteine (NAC) to MTT tests partially reverse the cytotoxic effect of this compound. NAC can interact directly with reactive oxygen species (ROS) because it is a scavenger of oxygen free radicals [28,29]. Drug combinations comprising fascaplysin and a range of chemotherapeutics yielded synergism with CPT and HOCPT solely. This finding may be explained either as fascaplysin acting as CDK4 inhibitor or, more likely in the two SCLC lines studied, as interfering with the camptothecin-toposiomerase I-DNA cleavable complex. We have described the chemosensitizing effects of CDK4 inhibitors in conjunction with CPTs recently [16]. In limited support of the role of fascaplysin as CDK4 inhibitor we found antagonism with a CDK4 inhibitor (EMD/Millipore, Darmstadt, Germany), no interaction with roscovitine/olomoucine and synergism with the pan-CDK inhibitor flavopiridol in MTT cytotoxicity assays (data not shown).

In order to further check possible DNA damage and repair we applied the isoquinolindione BYK204165 selective PARP1 inhibitor to fascaplysin cytotoxicity tests against different SCLC cell lines [30]. The basal activity of PARP1 is very low, but is stimulated markedly under cellular

stress/oxidative damage. Under conditions of low to moderate DNA damage, PARP provides cytoprotection, but in case of extended damage and high PARP activation cells are eliminated by apoptosis [31,32]. Consequently, depending on the circumstances, inhibitors of PARP either enhance the cytotoxicity of drugs or provide protection [33]. In the presence of a PARPi, PARP-1 binds DNA strand breaks but cannot produce poly(ADP-ribose) polymers and since DNA binding is persistent repair is impaired. The cytotoxicity of fascaplysin is impaired by the PARP1 inhibitor in the SCLC cell lines tested, except the chemosensitive NCI-H526 cells. This effect may be partially due to the fascaplysin-induced cell cycle arrest in S-phase. The increased resistance of the SCLC cell lines in presence of the PARP1 inhibitor point to an inhibition of the fascaplysin-triggered induction of cell death, possibly by prevention of NAD^+ resynthesis and ATP depletion and/or translocation of apoptosis-inducing factor (AIF) from the mitochondria to the nucleus [34].

3. Experimental Section

3.1. Reagents and Cell Lines

Stock solutions of all compounds were prepared in DMSO. All other chemicals were purchased from Sigma-Aldrich (St. Louis, MO, USA), except indicated otherwise. The BYK 204165 PARP1 inhibitor was obtained from Tocris Bioscience (Bristol, UK). Cell lines were obtained from ATCC (Rockville, MD, USA), except DMS153 cells from ECACC (Porton Down, Salisbury, UK), the GLC14/16/19 series from Dr. Nina Pedersen from the Department of Radiation Biology, The Finsen Centre, National University Hospital, Copenhagen, Denmark and H1299 and H23 from the University of Graz. The SCLC26A line was established from a pleural effusion of an untreated patient with SCLC at our institution. Cells were grown in RPMI-1640 bicarbonate medium (Seromed, Berlin, Germany) supplemented with 10% fetal bovine serum (Seromed, Berlin, Germany), 4 mM glutamine and antibiotics (10× stock formulated to contain ~5000 units penicillin, 5 mg streptomycin and 10 mg neomycin/mL) under tissue culture conditions (37 °C, 5% CO_2, 95% humidity) and checked for mycoplasma contamination (Mycoplasma PCR ELISA, Roche Diagnostics, Vienna, Austria).

3.2. Chemosensitivity Assay

1×10^4 cells in 100 µL medium per well were distributed in 96-well microtiter plates (Greiner, Kremsmuenster, Austria) and the test compound added in another 100 µL. Drugs and solute controls were serially diluted in twofold steps in triplicate. The microtiter plates were incubated under tissue culture conditions for four days and cell viability was measured using a modified MTT (3-(4,5-dimethylthiazol-2-yl)-2,5-diphenyl-tetrazolium bromide) assay (EZ4U, Biomedica, Vienna, Austria). Optical density was measured using a microplate reader at 450 nm with an empty well as reference. Values obtained from control wells containing cells and media alone were set to 100% proliferation. For tests of synergy, compounds were diluted individually and in combination, using the same (CPT) or double (HOCPT) initial concentrations. The synergistic effect of drug combinations was assessed using CompuSyn (V 1.03; CompuSyn Inc., Paramus, NJ, USA), a

software program based on the calculations for synergism developed by Chou *et al.* [35]. Combinations with a combination index (CI) <1 were considered synergistic.

3.3. Measurement of Cell Cycle Distribution

1×10^6 cells per well were incubated with the respective compound in six-well plates for three days. Harvested cells were washed with PBS and fixed with 70% ethanol at −20 °C for 30 min, washed again, transferred into staining solution (20 µg/mL propidium iodide (PI), 5 µg/mL ribonuclease A, 0.05% Nonidet P40 in PBS) and incubated at room temperature overnight. Washed cells were analyzed by acquisition of 1×10^4 cells by flow cytometry (Cytomics FC500, Beckman Coulter, Krefeld, Germany) at excitation and emission wavelengths of 488 and 675 nm, respectively. The proportion of subG1 (apoptotic) cells was obtained from the logarithmic PI histograms, and percentages of cells in cell cycle phases G1/0 (resting), S (DNA synthesis) and G2M (mitotic) were calculated from linear PI histograms using MultiCycle AV software (Phoenix Flow Systems, San Diego, CA, USA). Experiments were done in duplicate.

3.4. Detection of Reactive Oxygen Species (ROS)

1×10^6 washed cells were preincubated with 5 µg/mL 2′,7′-dichlorodihydrofluorescein diacetate (DCF), a chemically reduced, acetylated form of fluorescein, in phosphate buffered saline (PBS) at 37 °C for 15 min. This indicator is readily converted to a green-fluorescent form following removal of the acetate groups by intracellular esterases and oxidation by ROS. Cells which were washed again were then treated with fascaplysin under tissue culture conditions at 37 °C for 4 h. Identical treatment of the cells with Luperox® TBH70X, Di-tert-butyl peroxide solution, gave the positive controls. Samples were subsequently analyzed by flow cytometry.

3.5. Statistical Analysis

Statistical differences were calculated using student's paired *t*-test at significance levels of $p < 0.05$ (indicated in the figures by an asterisk).

4. Conclusions

Fascaplysin exhibits cytotoxicity against chemoresistant SCLC cell lines via several contributing pathways comprising, among others, generation of ROS and cellular mechanisms affecting topoisomerase I-activity and activation of PARP, possibly linked to its interaction with DNA in absence of a functional CDK4-RB1 axis in SCLC cell lines. Synergistic interaction with camptothecins is of special interest for second-line treatment of SCLC relying on the camptothecin analog topotecan.

Acknowledgement

This work was supported in part by a grant from the "Medical Scientific Fund of the Mayor of the City of Vienna", project number 11016. Furthermore, I wish to thank U. Olszewski for help in some experiments.

Author Contributions

The author carried out all work regarding design, experimentation and preparation of the manuscript.

Conflicts of Interest

The authors declare no conflict of interest.

References

1. Roll, D.M.; Ireland, C.M.; Lu, H.S.M.; Clardy, J. Fascaplysin, an unusual antimicrobial pigment from the marine sponge *Fascaplysinopsis* sp. *J. Org. Chem.* **1988**, *53*, 3276–3278.
2. Segraves, N.L.; Robinson, S.J.; Garcia, D.; Said, S.A.; Fu, X.; Schmitz, F.J.; Pietraszkiewicz, H.; Valeriote, F.A.; Crews, P. Comparison of fascaplysin and related alkaloids: A study of structures, cytotoxicities, and sources. *J. Nat. Prod*. **2004**, *67*, 783–792.
3. Segraves, N.L.; Lopez, S.; Johnson, T.A.; Said, S.A.; Fu, X.; Schmitz, F.J.; Pietraszkiewicz, H.; Valeriote, F.A.; Crews, P. Structures and cytotoxicities of fascaplysin and related alkaloids from two marine phyla—*Fascaplysinopsis* sponges and *Didemnum tunicates*. *Tetrahedron Lett*. **2003**, *44*, 3471–3475.
4. Bharate, S.B.; Manda, S.; Mupparapu, N.; Battini, N.; Vishwakarma, R.A. Chemistry and biology of fascaplysin, a potent marine-derived CDK-4 inhibitor. *Mini Rev. Med. Chem*. **2012**, *12*, 650–664.
5. Hormann, A.; Chaudhari, B.; Fretz, H. DNA binding properties of marine sponge pigment fascaplysin. *Bioorg. Med. Chem.* **2001**, *9*, 917–921.
6. Soni, R.; Muller, L.; Furet, P.; Schoepfer, J.; Stephan, C.; Zumstein-Mecker, S.; Fretz, H.; Chaudhuri, B. Inhibition of cyclindependent kinase 4 (Cdk4) by fascaplysin, a marine natural product. *Biochem. Biophys. Res. Commun.* **2000**, *275*, 877–884.
7. Soni, R.; O'Reilly, T.; Furet, P.; Muller, L.; Stephan, C.; Zumstein- Mecker, S.; Fretz, H.; Fabbro, D.; Chaudhuri, B. Selective *in vivo* and *in vitro* effects of a small molecule inhibitor of cyclindependent kinase-4. *J. Natl. Cancer Inst.* **2001**, *93*, 436–446.
8. Shafiq, M.I.; Steinbrecher, T.; Schmid, R. Fascaplysin as a specific inhibitor for CDK4: Insights from molecular modelling. *PLoS One* **2012**, *7*, e42612.
9. Goldberg, S.B.; Willers, H.; Heist, R.S. Multidisciplinary management of small cell lung cancer. *Surg. Oncol. Clin. N. Am.* **2013**, *22*, 329–343.

10. Lu, X.L.; Zheng, Y.L.; Chen, H.M.; Yan, X.J.; Wang, F.; Xu, W.F. Anti-proliferation of human cervical cancer HeLa cell line by fascaplysin through apoptosis induction. *Yao Xue Xue Bao* **2009**, *44*, 980–986.
11. Zheng, Y.L.; Lu, X.L.; Lin, J.; Chen, H.M.; Yan, X.J.; Wang, F.; Xu, W.F. Direct effects of fascaplysin on human umbilical vein endothelial cells attributing the anti-angiogenesis activity. *Biomed. Pharmacother.* **2010**, *64*, 527–533.
12. Lin, J.; Yan, X.J.; Chen, H.M. Fascaplysin, a selective CDK4 inhibitor, exhibit anti-angiogenic activity *in vitro* and *in vivo*. *Cancer Chemother. Pharmacol.* **2007**, *59*, 439–445.
13. Wang, F.; Chen, H.; Yan, X.; Zhen, Y. Fascaplysin sensitizes cells to TRAIL-induced apoptosis through upregulating DR5 expression. *Chin. J. Oceanol. Limnol.* **2013**, *31*, 560–569.
14. Yan, X.; Chen, H.; Lu, X.; Wang, F.; Xu, W.; Jin, H.; Zhu, P. Fascaplysin exert anti-tumor effects through apoptotic and anti-angiogenesis pathways in sarcoma mice model. *Eur. J. Pharm. Sci*. **2011**, *43*, 251–259.
15. Subramanian, B.; Nakeff, A.; Tenney, K.; Crews, P.; Gunatilaka, L.; Valeriote, F. A new paradigm for the development of anticancer agents from natural products. *J. Exp. Ther. Oncol.* **2006**, *5*, 195–204.
16. Hamilton, G.; Olszewski, U.; Klameth, L.; Ulsperger, E.; Geissler, K. Synergistic anticancer activity of topotecan—cyclin-dependent kinase inhibitor combinations against drug-resistant small cell lung cancer (SCLC) cell lines. *J. Cancer Ther*. **2013**, *4*, 47–53.
17. Berendsen, H.H.; de Leij, L.; de Vries, E.G.; Mesander, G.; Mulder, N.H.; de Jong, B.; Buys, C.H.; Postmus, E.P.; Poppema, S.; Sluiter, H.S.; *et al.* Characterization of three small cell lung cancer cell lines established from one patient during longitudinal follow-up. *Cancer Res*. **1988**, *48*, 6891–6899.
18. Giaccone, G.; Battey, J.; Gazdar, A.F.; Oie, H.; Draoui, M.; Moody, T.W. Neuromedin B is present in lung cancer cell lines. *Cancer Res*. **1992**, *52*, 2732s–2736s.
19. Little, C.D.; Nau, M.M.; Carney, D.N.; Gazdar, A.F.; Minna, J.D. Amplification and expression of the c-myc oncogene in human lung cancer cell lines. *Nature* **1983**, *306*, 194–196.
20. Jiang, T.; Collins, B.J.; Jin, N.; Watkins, D.N.; Brock, M.V.; Matsui, W.; Nelkin, B.D.; Ball, D.W. Achaete-scute complex homologue 1 regulates tumor-initiating capacity in human small cell lung cancer. *Cancer Res.* **2009**, *69*, 845–854.
21. Pettengill, O.S.; Sorenson, G.D.; Wurster-Hill, D.H.; Curphey, T.J.; Noll, W.W.; Cate, C.C.; Maurer, L.H. Isolation and growth characteristics of continuous cell lines from small-cell carcinoma of the lung. *Cancer* **1980**, *45*, 906–918.
22. Musgrove, E.A.; Caldon, C.E.; Barraclough, J.; Stone, A.; Sutherland, R.L. Cyclin D as a therapeutic target in cancer. *Nat. Rev. Cancer* **2011**, *11*, 558–572.
23. Otterson, G.A.; Kratzke, R.A.; Coxon, A.; Kim, Y.W.; Kaye, F.J. Absence of p16INK4 Protein Is Restricted to the Subset of Lung Cancer Lines that Retains Wildtype RB. *Oncogene* **1994**, *9*, 3375–3378.
24. Wikman, H.; Kettunen, E. Regulation of the G1/S Phase of the Cell Cycle and Alterations in the RB Pathway in Human Lung Cancer. *Expert Rev. Anticancer Ther.* **2006**, *6*, 515–530.

25. Rygaard, K.; Sorenson, G.D.; Pettengill, O.S.; Cate, C.C.; Spang-Thomsen, M. Abnormalities in structure and expression of the retinoblastoma gene in small cell lung cancer cell lines and xenografts in nude mice. *Cancer Res*. **1990**, *50*, 5312–5317.
26. Okamoto, A.; Hussain, S.P.; Hagiwara, K.; Spillare, E.A.; Rusin, M.R.; Demetrick, D.J.; Serrano, M.; Hannon, G.J.; Shiseki, M.; Zariwala, M.; *et al.* Mutations in the p16INK4/MTS1/CDKN2, p15INK4B/MTS2, and p18 Genes in Primary and Metastatic Lung Cancer. *Cancer Res*. **1995**, *55*, 1448–1451.
27. Zandi, R.; Selivanova, G.; Christensen, C.L. PRIMA-1Met/APR-246 Induces apoptosis and tumor growth delay in small cell lung cancer expressing mutant p53. *Clin. Cancer Res.* **2011**, *17*, 2830–2841.
28. Zhang, F.; Lau, S.S.; Monks, T.J. The cytoprotective effect of *N*-acetyl-L-cysteine against ROS-induced cytotoxicity is independent of its ability to enhance glutathione synthesis. *Toxicol. Sci.* **2011**, *120*, 87–97.
29. Caputo, F.; Vegliante, R.; Ghibelli, L. Redox modulation of the DNA damage response. *Biochem. Pharmacol*. **2012**, *84*, 1292–1306.
30. Eltze, T.; Boer, R.; Wagner, T.; Weinbrenner, S.; McDonald, M.C.; Thiemermann, C.; Bürkle, A.; Klein, T. Imidazoquinolinone, imidazopyridine, and isoquinolindione derivatives as novel and potent inhibitors of the poly(ADP-ribose) polymerase (PARP): A comparison with standard PARP inhibitors. *Mol. Pharmacol.* **2008**, *74*, 1587–1598.
31. Amé, J.C.; Spenlehauer, C.; de Murcia, G. The PARP superfamily. *Bioessays* **2004**, *26*, 882–893.
32. Schreiber, V.; Dantzer, F.; Ame, J.C.; de Murcia, G. Poly(ADP-ribose): Novel functions for an old molecule. *Nat. Rev. Mol. Cell Biol*. **2006**, *7*, 517–528.
33. Horton, J.K.; Wilson, S.H. Strategic combination of DNA-damaging agent and PARP inhibitor results in enhanced cytotoxicity. *Front. Oncol.* **2013**, *3*, doi:10.3389/fonc.2013.00257.
34. Wang, Y.; Dawson, V.L.; Dawson, T.M. Poly(ADP-ribose) signals to mitochondrial AIF: A key event in parthanatos. *Exp. Neurol*. **2009**, *218*, 193–202.
35. Chou, T.C. Theoretical basis, experimental design, and computerized simulation of synergism and antagonism in drug combination studies. *Pharmacol. Rev*. **2006**, *58*, 621–681.

Programmed Cell Death Induced by (−)-8,9-Dehydroneopeltolide in Human Promyelocytic Leukemia HL-60 Cells under Energy Stress Conditions

Haruhiko Fuwa, Mizuho Sato and Makoto Sasaki

Abstract: (+)-Neopeltolide is a marine macrolide natural product that exhibits potent antiproliferative activity against several human cancer cell lines. Previous study has established that this natural product primarily targets the complex III of the mitochondrial electron transport chain. However, the biochemical mode-of-actions of neopeltolide have not been investigated in detail. Here we report that (−)-8,9-dehydroneopeltolide (8,9-DNP), a more accessible synthetic analogue, shows potent cytotoxicity against human promyelocytic leukemia HL-60 cells preferentially under energy stress conditions. Nuclear morphology analysis, as well as DNA ladder assay, indicated that 8,9-DNP induced significant nuclear condensation/fragmentation and DNA fragmentation, and these events could be suppressed by preincubating the cells with a pan-caspase inhibitor, *N*-benzyloxycarbonyl-Val-Ala-Asp(OMe)-fluoromethylketone (zVAD). Immunoblot analysis demonstrated the release of cytochrome *c* from the mitochondria and the cleavage of full-length caspase-3 and poly(ADP-ribose) polymerase (PARP). These results indicated that 8,9-DNP induced caspase-dependent apoptotic programmed cell death under energy stress conditions. It was also found that 8,9-DNP induced non-apoptotic cell death in the presence/absence of zVAD under energy stress conditions. Immunoblot analysis showed the intracytosolic release of apoptosis-inducing factor (AIF), although it did not further translocate to the nucleus. It appears most likely that, in the presence of zVAD, 8,9-DNP triggered necrotic cell death as a result of severe intracellular ATP depletion.

Reprinted from *Mar. Drugs*. Cite as: Fuwa, H.; Sato, M.; Sasaki, M. Programmed Cell Death Induced by (−)-8,9-Dehydroneopeltolide in Human Promyelocytic Leukemia HL-60 Cells under Energy Stress Conditions. *Mar. Drugs* **2014**, *12*, 5576-5589.

1. Introduction

(+)-Neopeltolide (**1**, Figure 1), a 14-membered macrolide natural product, was isolated from a deep-water sponge that belongs to the family Neopeltidae, collected off the coast of Jamaica [1]. The gross structure, including relative configuration of this natural product was assigned on the basis of extensive 2D NMR analyses. Later, Panek [2] and Scheidt [3,4] independently reassigned the relative configuration and simultaneously established the absolute configuration of **1** through total synthesis. Wright and co-workers have reported potent antiproliferative activity of **1** against several human cancer cell lines, including the A549 human lung adenocarcinoma and the NCI/ADR-RES human ovarian sarcoma cell lines [1]. In addition, Wright *et al*. have described that **1** exhibits antifungal activity against pathogenic yeast *Candida albicans* [1]. Kozmin and co-workers have established that **1** binds to the complex III of the mitochondrial electron transport

chain (mETC) as primary molecular target [5]. However, the biochemical mode-of-action and cellular effect of **1** and its synthetic analogues remain largely underexplored.

Figure 1. Structures of (+)-neopeltolide (**1**) and (−)-8,9-dehydroneopeltolide (8,9-DNP, **2**).

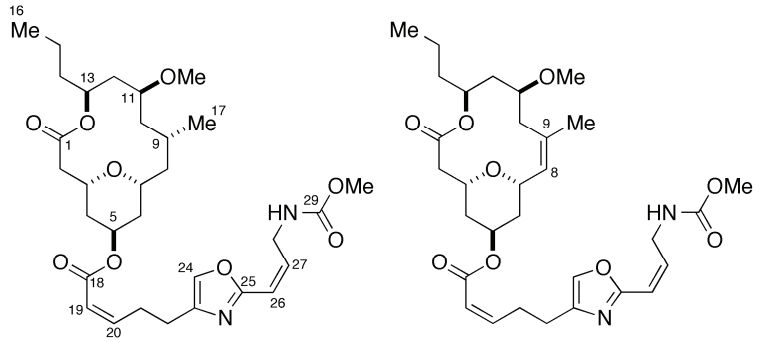

1: (+)-neopeltolide **2**: (–)-8,9-dehydroneopeltolide

We have previously reported the total synthesis of **1** and its synthetic analogues to elucidate the structure-activity relationships in detail [6–10]. During our synthetic campaign, we identified the pharmacophoric elements of **1** and discovered several highly potent and synthetically accessible analogues, as exemplified by (−)-8,9-dehydroneopeltolide (8,9-DNP, **2**) [9,11]. Here we report that 8,9-DNP induced caspase-dependent apoptotic cell death in HL-60 human promyelocytic leukemia cells under energy stress conditions. We also describe that 8,9-DNP triggered necrotic death in HL-60 cells when caspase-dependent apoptotic pathway was impaired.

2. Results

2.1. 8,9-DNP Exhibits Cytotoxicity against HL-60 Cells under Energy Stress Conditions

The effect of 8,9-DNP in human leukemic cells has not been reported so far. Initially, we examined the viability of HL-60 cells upon treatment with various concentrations of 8,9-DNP by WST-8 assay [12] (Figure 2A). We found that 8,9-DNP did not show appreciable antiproliferative activity against cells cultured in normal medium for 24 h. In contrast, the cell viability decreased when cells were treated with 8,9-DNP under energy stress conditions. Specifically, the cell viability fell below 50% by combined treatment of cells with 8,9-DNP and a glycolysis inhibitor, 2-deoxy-D-glucose (2-DG, 10 mM), in normal medium. Furthermore, marked dose-dependent decrease in cell viability was observed when cells were treated with 8,9-DNP in glucose-deprived medium. These results showed that the cells became sensitized to 8,9-DNP upon inhibition of glycolysis. We also determined that intracellular ATP concentration of HL-60 cells decreased significantly upon exposure to 8,9-DNP in glucose-deprived medium for 6 h (Figure 2B). Hereafter, we investigated the effect of 8,9-DNP on HL-60 cells in glucose-deprived medium as an *in vitro* model of energy stress conditions.

Figure 2. (**A**) Viability of HL-60 cells treated with 8,9-DNP for 24 h. Blue circles: normal medium; green triangles: normal medium + 10 mM 2-DG; red squares: glucose-deprived medium. Data are expressed as mean ± SD of three independent experiments; (**B**) Intracellular ATP concentration of HL-60 cells treated with 8,9-DNP in glucose-deprived medium for 6 h. Data are expressed as mean ± SD of three independent experiments.

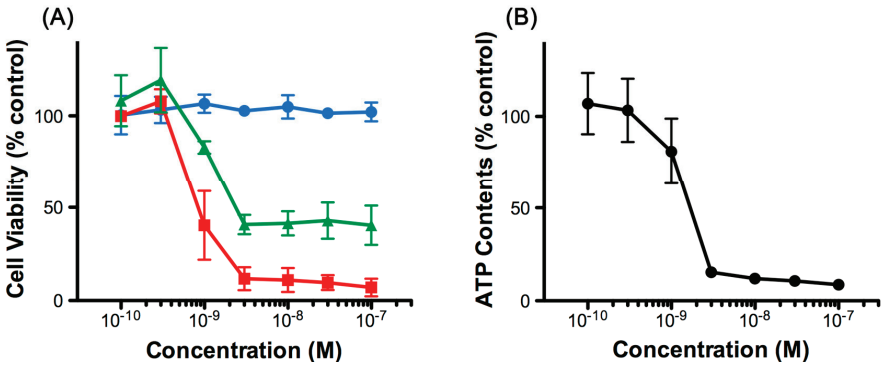

Next, we performed nuclear morphology analysis using Höechst 33342/propidium iodide (PI) double staining technique (Figure 3A). After treatment of HL-60 cells with 8,9-DNP (100 nM) in glucose-deprived medium for 6 h, a significant portion (35%) of the cells showed nuclear fragmentation without PI staining. A similar result was obtained when cells were treated with 8,9-DNP (100 nM) in the presence of 2-deoxy-D-glucose (10 mM) in normal medium for 6 h (data not shown). In addition, the nuclear fragmentation was suppressed by pretreatment of cells with a pan-caspase inhibitor, *N*-benzyloxycarbonyl-Val-Ala-Asp(OMe)-fluoromethylketone (zVAD) (25 μM) [13,14]. These results were indicative of apoptotic programmed cell death. Meanwhile, almost all the cells treated with 8,9-DNP (100 nM) became PI positive after 24 h in glucose-deprived medium even in the presence of zVAD, whereas control cells did not show appreciable morphological changes and remained PI negative.

Significant DNA laddering was observed in the cells treated with 8,9-DNP under energy stress conditions, which was prevented by co-incubation with zVAD (25 μM) (Figure 3B). These results suggested that internucleosomal cleavage of DNA, one of the characteristics of apoptosis, occurred by the action of 8,9-DNP.

2.2. Apoptotic Cell Death Induced by 8,9-DNP Depends on the Intrinsic Pathway

Because it has been shown that neopeltolide inhibits the complex III of isolated mitochondria [5], we envisioned that the apoptotic cell death induced by 8,9-DNP in HL-60 cells might be attributed to the intrinsic mitochondrial pathway [15–17], which is known to involve the release of cytochrome *c* (Cyt *c*) from the intermembrane space of the mitochondria to the cytosol [18,19], the activation of caspase-3 by proteolytic processing [20], and the cleavage of poly(ADP-ribose) polymerase (PARP) as characteristic biochemical events [21].

Figure 3. (**A**) Nuclear morphology analysis by Höechst 33342/PI double staining. Each experiment was performed independently two times. Nuclear fragmentation was observed for the cells treated with 8,9-DNP (35% at 6 h and 46% at 24 h); (**B**) DNA electrophoresis on 2% agarose gel, developed with ethidium bromide. Each experiment was performed independently three times.

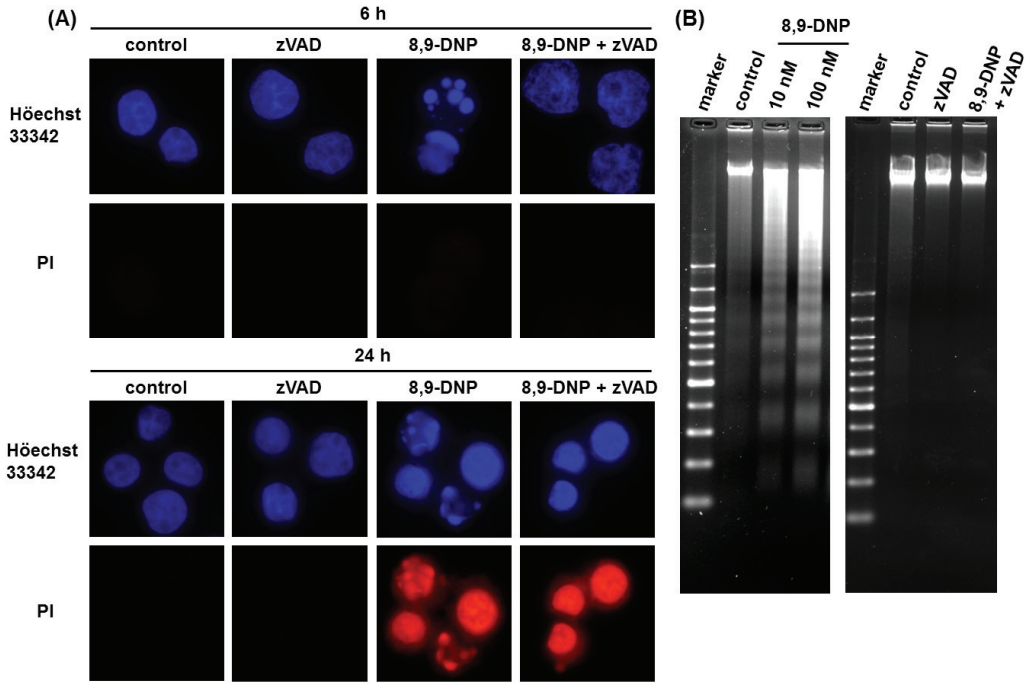

Initially, we assessed the inhibition of the mETC with 8,9-DNP by using rhodamine 123 as a fluorescent probe sensitive to mitochondrial membrane potential ($\Delta\Psi_m$) [22] (Figure 4A). Carbonyl cyanide *m*-chlorophenyl hydrazone (CCCP), an uncoupler of mETC, was used as a positive control. While the untreated cells showed bright punctate signals, the cells treated with 8,9-DNP (100 nM) only showed a dispersed pattern of weak fluorescence, indicating depolarization of $\Delta\Psi_m$. This result confirmed the inhibition of the mETC of HL-60 cells with 8,9-DNP.

Next, we performed immunoblot analysis to gain insight into the mode-of-action of 8,9-DNP. As summarized in Figure 4B, the cytosolic extract of the HL-60 cells treated with 8,9-DNP (100 nM) in glucose-deprived medium for different periods of time (1, 3, and 6 h) showed the presence of cytosolic Cyt *c* after 3 h. Furthermore, in the whole cell extract, the decrease of full-length caspase-3 (procaspase-3) and the cleavage of PARP were observed after 3 h. The PARP cleavage was abolished by co-incubation with zVAD (25 μM) prior to 8,9-DNP treatment. Taken together, these results strongly suggested that the release of Cyt *c* from the mitochondria, triggered by 8,9-DNP, induced apoptotic cell death via the intrinsic pathway involving caspase activation and PARP cleavage.

Figure 4. (**A**) Evaluation of $\Delta\Psi_m$ by rhodamine 123 staining. Each experiment was performed independently two times; (**B**) Immunoblot analysis of cell extracts to detect intracytosolic release of Cyt *c* and cleavage of full-length caspase-3 and PARP. The cytosolic extract was probed with anti-VDAC1 antibody to ensure that it was free of mitochondrial component. Each experiment was performed independently three times.

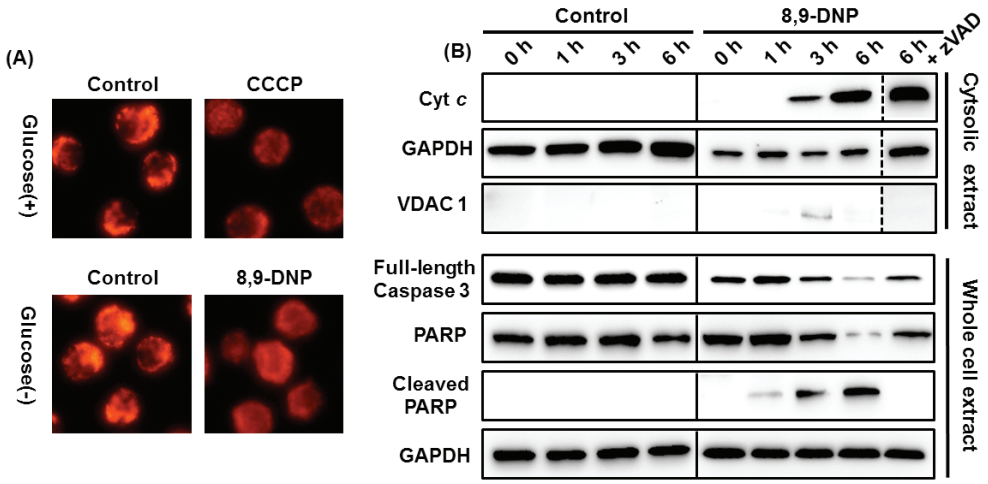

2.3. 8,9-DNP also Induces Intracytosolic Release of AIF but It Does Not Translocate to the Nucleus

The results of the nuclear morphology analysis, DNA laddering experiments, and immunoblot analysis clearly indicated that zVAD successfully inhibited caspases in the cells treated with 8,9-DNP under energy stress conditions and rescued the cells from apoptotic death. However, Höechst 33342/PI double staining analysis showed that zVAD could not prevent cell death after 24 h treatment with 8,9-DNP (Figure 3A). Neither nuclear fragmentation nor condensation were apparent for the cells treated with 8,9-DNP in the presence of zVAD in glucose-deprived medium for 24 h. Nonetheless, all the cells were clearly stained with PI.

Accordingly, we performed further immunoblot analysis of the cytosolic extract of the cells treated with 8,9-DNP in glucose-deprived medium for different periods of time (1, 3, and 6 h). Apoptosis-inducing factor (AIF) [23,24] and endonuclease G (Endo G) [25,26] are known to induce caspase-independent programmed cell death upon translocation to the nucleus. High-temperature requirement protein A2 (HtrA2)/Omi [27] is a serine protease that contributes to apoptosis by antagonizing inhibitor of apoptosis (IAP) proteins. The intracytosolic release of AIF and HtrA2/Omi, but not Endo G, was observed after 6 h, regardless of the presence of zVAD (Figure 5A). These results indicated that the intracytosolic release of AIF and HtrA2/Omi was specifically induced by the action of 8,9-DNP and that zVAD did not block the release of AIF and HtrA2/Omi to the cytosol but merely inhibited downstream caspase-dependent events. At this stage, it was envisaged that AIF might be a primary executor of the caspase-independent cell death in 8,9-DNP-treated cells. However, translocation of AIF to the nucleus was not detected by immunoblot analysis of the

nuclear extract of the cells exposed to 8,9-DNP in glucose-deprived medium for 6 h (Figure 5B). This result indicated that AIF is not responsible for the caspase-independent cell death induced by 8,9-DNP.

Figure 5. (**A**) Immunoblot analysis of cytosolic extract showed intracytosolic release of AIF and HtrA2/Omi, but not EndoG. The cytosolic extract was also probed with anti-VDAC1 antibody to ensure that it was free of mitochondrial proteins. The whole cell extract of untreated cells was used as positive control; (**B**) Immunoblot analysis of nuclear extract showed that AIF did not translocate to the nucleus. The nuclear extract was also probed with anti-GAPDH and anti-COX IV antibodies to ensure that it was free of cytosolic and mitochondrial proteins. The whole cell extract of untreated cells was used as positive control. Each experiment was performed independently three times.

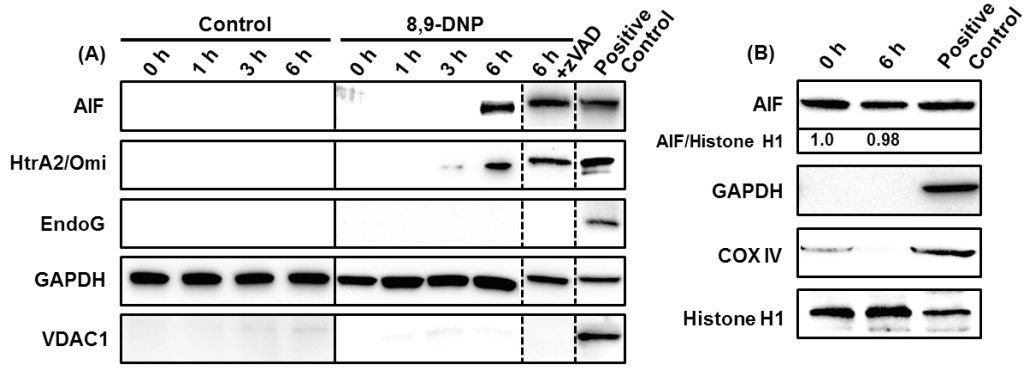

3. Discussion

The mitochondrial electron transport chain (mETC), consists of four transmembrane complexes, I, II, III, and IV, generates electrochemical proton gradient across the inner membrane of the mitochondria to facilitate ATP production by F_1F_o ATP synthase (complex V). The mitochondrial complex III is known to transfer electrons from ubiquinol to Cyt *c* and pump protons from the inner matrix to the intermembrane space using the Q-cycle. Naturally occurring antibiotics, such as antimycin A, stigmatellin, and myxothiazol, have contributed to the characterization of the structure and functions of the mitochondrial complex III at the molecular level [28,29]. It has been shown that antimycin A binds to the Q_o-site, whereas stigmatellin and myxothiazol bind to the Q_i-site [28,29]. (+)-Neopeltolide is a new potent inhibitor of the complex III of the mETC, recently identified from a deep-water sponge of the family Neopeltidae [1,5]. However, the precise location of its binding site has not been established.

The mitochondria play a key role in programmed cell death [16,17]. In response to apoptotic stimuli, the mitochondria release Cyt *c* from the intermembrane space to the cytosol via outer membrane permeabilization. Cyt *c* binds to apoptotic protease activating factor-1 (Apaf-1) in the cytosol to form apoptosome, which triggers activation of the caspase cascade [18,19]. Several

mitochondrial proteins, such as AIF, EndoG, and HtrA2/Omi, are also known to induce programmed cell death [20–27].

In this study, we investigated the effect of (−)-8,9-DNP [9,11], a potent synthetic analogue of (+)-neopeltolide, on HL-60 human promyelocytic leukemia cells. We found that 8,9-DNP decreased cell viability preferentially under the conditions in which glycolytic ATP generation was inhibited by 2-deoxy-D-glucose or by withdrawal of D-glucose from culture medium (Figure 2). Clearly, the inhibition of glycolysis made the cells significantly sensitive to 8,9-DNP [30,31]. Under these energy stress conditions, internucleosomal DNA fragmentation occurred significantly in the cells treated with 8,9-DNP, as indicated by the nuclear morphology characterization and DNA laddering experiment (Figure 3). These phenotypes are the hallmarks of caspase-dependent programmed cell death [15–17], and they were specifically suppressed by preincubating cells with a pan-caspase inhibitor zVAD [13,14]. Furthermore, immunoblot analysis of the cells treated with 8,9-DNP in glucose-deprived medium showed the leakage of Cyt *c*, an apoptogenic protein, from the intermembrane space of the mitochondria to the cytosol, the activation of caspase-3, and the cleavage of PARP (Figure 4B). Collectively, these results indicated that the cells exposed to 8,9-DNP under energy stress conditions underwent caspase-dependent apoptotic programmed cell death via the mitochondrial intrinsic pathway.

Additional immunoblot analysis showed that the intracytosolic release of AIF and HtrA2/Omi occurred after 6 h treatment of cells with 8,9-DNP in glucose-deprived medium (Figure 5A). Presumably, the release of these mitochondrial proteins could be ascribed to mitochondrial outer membrane permeabilization induced by the loss of $\Delta\Psi_m$ [32]. Moreover, prolonged treatment of HL-60 cells with 8,9-DNP induced cell death even in the presence of zVAD. We initially speculated that AIF might be responsible for the observed cell death, since AIF is known to contribute to programmed cell death when caspases are inhibited or not activated [32]. Ogita *et al*. have recently reported that antimycin A, a potent complex III inhibitor, induces nuclear translocation of AIF in a caspase 3-independent manner to show cytotoxicity against HL-60 cells [33]. However, in the present case, nuclear translocation of AIF was not observed (Figure 5B). Thus, it is most likely that AIF is not responsible for the caspase-independent cell death triggered by 8,9-DNP.

Meanwhile, it is known that ATP is required for executing caspase-dependent apoptotic cell death and that severe intracellular ATP depletion causes necrotic, programmed cell death [34,35]. In addition, inhibitors of the mETC have been shown to be cytotoxic against the PANC-1 human pancreatic carcinoma cell line under nutrient-deprived conditions, where marked decrease of intracellular ATP concentration was observed [36]. Actually, intracellular ATP concentration of HL-60 cells considerably decreased after 6 h treatment with 8,9-DNP in glucose-deprived medium (Figure 2B), implying that the cells might undergo necrotic programmed cell death because of energetic impairment induced by dual inhibition of glycolysis and oxidative phosphorylation (OXPHOS).

Because of metabolic requirements for rapid proliferation, the energy metabolism of cancer cells depends heavily on glycolysis even when sufficient oxygen is available (“aerobic glycolysis”), and hence differs significantly from that of normal cells [37–39]. It is known that leukemic cells are highly glycolytic [40], and that inhibition of the glycolytic activity sensitizes them to chemotherapeutic agents [30,31,41,42]. It has been reported that the combination of 2-deoxy-D-glucose and an

AMP-activated protein kinase (AMPK) agonist metformin is effective against human solid tumor cells [43,44] and leukemic cells [45] *in vitro* and *in vivo*. Metformin compromises mitochondrial ATP synthesis by inhibiting complex I of the mETC and depolarizing $\Delta\Psi_m$ [43–45]. Thus, dual inhibition of glycolysis and OXPHOS is an effective means to target the bioenergetics of cancer cells. It would be of interest to investigate whether 8,9-DNP shows cytotoxicity against solid tumor cells under energy stress conditions, because cancer cells in tumor microenvironment are often exposed to low-nutrient, hypoxic conditions due to their rapid proliferation and insufficient angiogenesis within solid tumors [46]. Work toward this end is underway.

4. Experimental Section

4.1. Materials

The HL-60 human promyelocytic leukemia cell line was provided from RIKEN BRC through the National Bio-Resource Project of the MEXT, Japan. Primary antibodies were obtained as follows: rabbit anti-caspase-3 monoclonal antibody, rabbit anti-PARP monoclonal antibody, rabbit anti-COX IV monoclonal antibody (Cell Signaling Technology, Danvers, MA, USA); rabbit anti-AIF polyclonal antibody, mouse anti-histone H1 monoclonal antibody, and mouse anti-VDAC1 monoclonal antibody (Santa Cruz Biotechnology, Dallas, TX, USA); mouse anti-Cyt *c* monoclonal antibody (BD Biosciences, San Jose, CA, USA); rabbit anti-endonuclease G polyclonal antibody (EMD Millipore, Temecula, CA, USA); mouse anti-HtrA2/Omi monoclonal antibody (R&D Systems, Minneapolis, MN, USA); HRP-conjugated mouse anti-GAPDH monoclonal antibody (MBL, Nagoya, Japan). Höechst 33342 and propidium iodide were obtained from Life Technologies (Carlsbad, CA, USA). zVAD was purchased from Peptide Institute (Osaka, Japan). (−)-8,9-Dehydroneopeltolide (8,9-DNP) was synthesized as described previously [9] and purified by preparative high-performance liquid chromatography performed on a Shimadzu Prominence HPLC System equipped with a COSMOSIL 5C18AR-II column (250 mm × 20 mm I.D., Nacalai Tesque, Kyoto, Japan). All other chemicals were purchased from Nacalai Tesque (Kyoto, Japan), Wako Pure Chemicals (Osaka, Japan), Dojindo Laboratories (Kumamoto, Japan), or Sigma-Aldrich (St. Louis, MO, USA). All cell culture media used in this study were supplemented with 10% fetal bovine serum, 100 units/mL of penicillin, and 100 μg/mL of streptomycin and filter-sterilized before use.

4.2. Cell Viability Assay

Cells were cultured for 2–3 days in RPMI1640 medium maintaining under a 5% CO_2/air atmosphere in a CO_2 incubator at 37 °C. Exponentially growing cells were harvested and re-suspended in RPMI1640, RPMI1640 containing 10 mM 2-deoxy-D-glucose, or RPMI1640 without D-glucose at a density of 2.5×10^5 cells/mL. The cell suspension (198 μL) was distributed to wells of a 96-well microtiter plate. The cells were then treated with various concentrations of 8,9-DNP (2 μL) and incubated in a CO_2 incubator at 37 °C for 24 h. At this point, WST-8 (5 μL) was added to each well. After incubation in a CO_2 incubator at 37 °C for additional 5 h, the UV absorbance at 405 nm and 650 nm, respectively, was measured by a microplate reader

(Synergy®HT Multi-Mode Microplate Reader, BioTek Instruments, Winooski, VT, USA). The relative absorbance values, calculated by subtracting UV absorbance at 650 nm from that at 450 nm, were plotted against sample concentrations (the relative absorbance values for 0% and 100% cell viability were obtained with blank and 10% MeOH/H_2O, respectively). IC_{50} values were calculated with a non-linear regression model of standard slope by using the GraphPad Prism software (GraphPad Software, La Jolla, CA, USA).

4.3. Measurement of Intracellular ATP Concentration

Intracelluar ATP concentration of HL-60 cells was determined by using CellTiter-Glo assay kit (Promega, Madison, WI, USA) according to the manufacturer's protocol.

4.4. Nuclear Morphology Analysis

The Höechst 33342/propidium iodide double staining technique was used to observe nuclear morphology and to discriminate living and dead cells. In cases where zVAD was used as an additive, cells were incubated with zVAD (25 μM) at 37 °C for 30 min prior to 8,9-DNP treatment. After treatment of HL-60 cells with 8,9-DNP (100 nM) in RPMI1640 without D-glucose at 37 °C for 6 or 24 h, the cells were harvested, washed once with PBS, and then treated with 10 μg/mL Höechst 33342 and 5 μg/mL propidium iodide in PBS at room temperature for 30 min. The cells were washed once with PBS and fixed with 4% paraformaldehyde in PBS at room temperature for 20 min. The cells were washed once with PBS and then observed under an inverted fluorescence microscope (IX-73, Olympus, Tokyo, Japan) equipped with a 60× objective.

4.5. Mitochondrial Membrane Potential Assay

After treatment of exponentially growing HL-60 cells with 8,9-DNP (100 nM) in glucose-deprived medium for 1 h, the cells were washed with PBS and stained with rhodamine 123 (10 μg/mL) in PBS at room temperature for 15 min. The cells were washed with PBS, and observed under an inverted fluorescence microscope (IX-73, Olympus, Tokyo, Japan) equipped with a 40× objective.

4.6. DNA Laddering Assay

Exponentially growing HL-60 cells were treated with 8,9-DNP (100 nM) in RPMI1640 without D-glucose at 37 °C for 6 h. DNA was extracted from the cells by using SepaGene kit (Eidia, Tokyo, Japan) according to the manufacturer's protocol. The extracted DNA was dissolved in 20 μg/mL RNase/TE buffer, incubated at 37 °C for 30 min, and then electrophoresed on a 2% agarose gel in TAE buffer. The gel was stained with 1 μg/mL ethidium bromide, rinsed with distilled water, and then visualized under UV light (ChemiDoc XRS+ Imaging System, Bio-Rad, Hercules, CA, USA).

4.7. Preparation of Cytosolic Extract

After treatment of exponentially growing HL-60 cells with 8,9-DNP (100 nM) in RPMI1640 medium without D-glucose at 37 °C for 1, 3, or 6 h, cells were harvested, washed once with PBS,

and then incubated on ice for 5 min with a buffer containing 75 mM KCl, 1 mM NaH_2PO_4, 8 mM Na_2HPO_4, 250 mM sucrose, 200 μg/mL digitonin, and protease inhibitor cocktail (Nacalai Tesque, Kyoto, Japan). After centrifugation (1500× *g*, 4 °C, 5 min; then 16,000× *g*, 4 °C, 5 min), the supernatant was saved as the cytosolic extract and stored at −80 °C before use. Protein concentration was determined by using Protein Assay Rapid kit (Wako Pure Chemical, Osaka, Japan).

4.8. Preparation of Whole Cell Extract

After treatment of exponentially growing HL-60 cells with 8,9-DNP (100 nM) in RPMI1640 medium without D-glucose at 37 °C for 1, 3, or 6 h, cells were harvested, washed once with PBS, and then incubated on ice with RIPA buffer (Wako Pure Chemicals, Osaka, Japan) supplemented with protease inhibitor cocktail (Nacalai Tesque, Kyoto, Japan) for 30 min. After centrifugation (10,000× *g*, 4 °C, 10 min), the supernatant was saved as the whole cell extract and stored at −80 °C before use. Protein concentration was determined by using Protein Assay Rapid kit (Wako Pure Chemical, Osaka, Japan).

4.9. Preparation of Nuclear Extract

HL-60 cells treated with or without 8,9-DNP (100 nM) were harvested, washed twice with ice-cold PBS, and incubated with ice-cold hypotonic buffer (10 mM HEPES/KOH (pH 7.9), 2 mM $MgCl_2$, 0.1 mM EDTA, 10 mM KCl, 1 mM DTT, and 0.5% Triton X-100) supplemented with protease inhibitor cocktail (Nacalai Tesque, Kyoto, Japan) on ice for 10 min. After centrifugation (800× *g*, 4 °C, 8 min), the supernatant was removed and the pellet gently suspended in the ice-cold hypotonic buffer. After centrifugation (800× *g*, 4 °C, 8 min), the supernatant was removed and the pellet gently suspended in SDS buffer (0.1 M Tris·HCl (pH 6.8), 2% SDS, and 20% glycerol) supplemented with protease inhibitor cocktail (Nacalai Tesque, Kyoto, Japan). The resultant solution was briefly sonicated in an ice-cold bath, diluted with an equal volume of 200 mM DTT plus 0.04% bromophenol blue, and boiled at 95 °C for 5 min. The nuclear extract thus obtained was stored at −80 °C before use.

4.10. Immunoblot Analysis

The cellular extract prepared above was diluted with 2× Sample Buffer Solution (Nacalai Tesque, Kyoto, Japan) containing 100 mM DTT and boiled at 95 °C for 3 min. After cooling on ice, the resultant mixture was resolved on a 12% SDS-polyacrylamide gel and then transferred onto a PVDF membrane. The membrane was blocked with Blocking One (Nacalai Tesque, Kyoto, Japan) at room temperature for 30 min and probed with an appropriate primary antibody at room temperature for 1–4 h or at 4 °C overnight. The membrane was then probed with an appropriate HRP-conjugated secondary antibody at room temperature for 1 h and then developed with Chemi-Lumi One (Nacalai Tesque, Kyoto, Japan). Chemiluminescence was detected on a ChemiDoc XRS+ Imaging System (Bio-Rad, Hercules, CA, USA).

5. Conclusions

This study has demonstrated that 8,9-DNP, a potent synthetic analogue of (+)-neopeltolide, induces apoptotic cell death in HL-60 human promyelocytic leukemia cells under energy stress conditions. The mechanism of the apoptotic cell death involves the release of Cyt *c* from the mitochondria to the cytosol, activation of caspase-3, cleavage of PARP, and DNA fragmentation. The apoptotic cell death induced by 8,9-DNP could be suppressed by co-incubation of cells with a pan-caspase inhibitor zVAD. It was also found that 8,9-DNP caused non-apoptotic cell death in the presence of zVAD. Immunoblot analysis of the cytosolic extract of the cells exposed to 8,9-DNP showed the release of AIF and HtrA2/Omi from the intermembrane space of the mitochondria to the cytosol, although the nuclear level of AIF did not increase under these conditions. It seems most likely that significant decrease of intracellular ATP concentration caused by 8,9-DNP resulted in necrotic cell death where caspases were inhibited or not activated. Further studies on the biological activity and mode-of-action of 8,9-DNP are currently underway and will be reported shortly.

Acknowledgments

This work was supported in part by a Grant-in-Aid for Young Scientists (A) from the Japan Society for Promotion of Science (No. 23681045) and by Grants-in-Aid for Scientific Research on Innovative Areas “Chemical Biology of Natural Products” from the Ministry of Education, Culture, Sports, Science and Technology, Japan (Nos. 24102507 and 26102708).

Author Contributions

H.F. designed the research and performed the experiments, M. Sato performed the experiments and analyzed the data, H.F. and M. Sasaki co-supervised the research. All the authors contributed to the preparation of the manuscript.

Conflict of Interest

The authors declare no conflict of interest.

References

1. Wright, A.E.; Botelho, J.C.; Guzmán, E.; Harmody, D.; Linley, P.; McCarthy, P.J.; Pitts, T.P.; Pomponi, S.A.; Reed, J.K. Neopeltolide, a macrolide from a lithistid sponge of the family Neopeltidae. *J. Nat. Prod.* **2007**, *70*, 412–416.
2. Youngsaye, W.; Lowe, J.T.; Pohlki, F.; Ralifo, P.; Panek, J.S. Total synthesis and stereochemical reassignment of (+)-neopeltolide. *Angew. Chem. Int. Ed.* **2007**, *46*, 9211–9214.
3. Custar, D.W.; Zabawa, T.P.; Scheidt, K.A. Total synthesis and structural revision of the marine macrolide neopeltolide. *J. Am. Chem. Soc.* **2008**, *130*, 804–805.
4. Custar, D.W.; Zabawa, T.P.; Hines, J.; Crews, C.M.; Scheidt, K.A. Total synthesis and structure-activity investigation of the marine natural product neopeltolide. *J. Am. Chem. Soc.* **2009**, *131*, 12406–12414.

5. Ulanovskaya, O.A.; Janjic, J.; Suzuki, M.; Sabharwal, S.S.; Schumacker, P.T.; Kron, S.J.; Kozmin, S.A. Synthesis enables identification of the cellular target of leucascandrolide A and neopeltolide. *Nat. Chem. Biol.* **2008**, *4*, 418–424.
6. Fuwa, H.; Naito, S.; Goto, T.; Sasaki, M. Total synthesis of (+)-neopeltolide. *Angew. Chem. Int. Ed.* **2008**, *47*, 4737–4739.
7. Fuwa, H.; Saito, A.; Naito, S.; Konoki, K.; Yotsu-Yamashita, M.; Sasaki, M. Total synthesis and biological evaluation of (+)-neopeltolide and its analogues. *Chem. Eur. J.* **2009**, *15*, 12807–12818.
8. Fuwa, H.; Saito, A.; Sasaki, M. A concise total synthesis of (+)-neopeltolide. *Angew. Chem. Int. Ed.* **2010**, *49*, 3041–3044.
9. Fuwa, H.; Kawakami, M.; Noto, K.; Muto, T.; Suga, Y.; Konoki, K.; Yotsu-Yamashita, M.; Sasaki, M. Concise synthesis and biological assessment of (+)-neopeltolide and a 16-membered stereoisomer library of 8,9-dehydroneopeltolide: Identification of pharmacophoric elements. *Chem. Eur. J.* **2013**, *19*, 8100–8110.
10. Fuwa, H.; Noguchi, T.; Kawakami, M.; Sasaki, M. Synthesis and biological evaluation of (+)-neopeltolide analogues: Importance of the oxazole-containing side chain. *Bioorg. Med. Chem. Lett.* **2014**, *24*, 2415–2419.
11. Cui, Y.; Balachandran, R.; Day, B.W.; Floreancig, P.E. Synthesis and biological evaluation of neopeltolide and analogues. *J. Org. Chem.* **2012**, *77*, 2225–2235.
12. Tominaga, H.; Ishiyama, M.; Ohseto, F.; Sasamoto, K.; Hamamoto, T.; Suzuki, K.; Watanabe, M. A water-soluble tetrazolium salt useful for colorimetric cell viability assay. *Anal. Commun.* **1999**, *36*, 47–50.
13. Slee, E.A.; Zhu, H.; Chow, S.C.; MacFarlane, M.; Nicholson, D.W.; Cohen, G.M. Benzyloxycarbonyl-Val-Ala-Asp (OMe) fluoromethylketone (Z-VAD.FMK) inhibits apoptosis by blocking the processing of CPP32. *Biochem. J.* **1996**, *315*, 21–24.
14. Polverino, A.J.; Patterson, S.D. Selective activation of caspases during apoptotic induction in HL-60 cells: Effects of a tetrapeptide inhibitor. *J. Biol. Chem.* **1997**, *272*, 7013–7021.
15. Hengartner, M.O. The biochemistry of apoptosis. *Nature* **2000**, *407*, 770–776.
16. Desagher, S.; Martinou, J.-C. Mitochondria as the central control point of apoptosis. *Trends Cell. Biol.* **2000**, *10*, 369–377.
17. Green, D.R.; Reed, J.C. Mitochondria and apoptosis. *Science* **1998**, *281*, 1309–1312.
18. Yang, J.; Liu, X.; Bhalla, K.; Kim, C.N.; Ibrado, A.M.; Cai, J.; Peng, T.-I.; Jones, D.P.; Wang, X. Prevention of apoptosis by Bcl-2: Release of cytochrome *c* from mitochondria blocked. *Science* **1997**, *275*, 1129–1132.
19. Kluck, R.M.; Bossy-Wetzel, E.; Green, D.R.; Newmeyer, D.D. The release of cytochrome *c* from mitochondria: A primary site for Bcl-2 regulation of apoptosis. *Science* **1997**, *275*, 1132–1136.
20. Jänicke, R.U.; Sprengart, M.L.; Wati, M.R.; Porter, A.G. Caspase-3 is required for DNA fragmentation and morphological changes associated with apoptosis. *J. Biol. Chem.* **1998**, *273*, 9357–9360.

21. Lazebnik, Y.A.; Kaufmann, S.H.; Desnoyers, S.; Poirer, G.G.; Earnshaw, W.C. Cleavage of poly(ADP-ribose) polymerase by a proteinase with properties like ICE. *Nature* **1994**, *371*, 346–347.
22. Nicholls, D.G. Methods in molecular biology. In *Mitochondrial Bioenergetics: Methods and Protocols*; Palmeira, C.M., Moreno, A.J., Eds.; Humana Press: New York, NY, USA, 2012; Volume 810.
23. Susin, S.A.; Lorenzo, H.K.; Zamzami, N.; Marzo, I.; Snow, B.E.; Brothers, G.M.; Mangion, J.; Jacotot, E.; Costantini, P.; Loeffler, M.; *et al.* Molecular characterization of mirochondrial apoptosis-inducing factor. *Nature* **1999**, *397*, 441–446.
24. Joza, N.; Susin, S.A.; Daugas, E.; Stanford, W.L.; Cho, S.K.; Li, C.Y.J.; Sasaki, T.; Elia, A.J.; Cheng, H.-Y.M.; Ravagnan, L.; *et al.* Essential role of the mitochondrial apoptosis-inducing factor in programmed cell death. *Nature* **2001**, *410*, 549–554.
25. Li, L.Y.; Luo, X.; Wang, X. Endonuclease G is an apoptotic DNase when released from mitochondria. *Nature* **2001**, *412*, 95–99.
26. Parrish, J.; Li, L.; Klotz, K.; Ledwich, D.; Wang, X.; Xue, D. Mitochondrial endonuclease G is important for apoptosis in *C. elegans*. *Nature* **2001**, *412*, 90–94.
27. Suzuki, Y.; Imai, Y.; Nakayama, H.; Takahashi, K.; Takio, K.; Takahashi, R. A serine protease, HtrA2, is released from the mitochondria and interacts with XIAP, inducing cell death. *Mol. Cell* **2001**, *8*, 613–621.
28. Xia, D.; Yu, C.-A.; Kim, H.; Xia, J.-Z.; Kachurin, A.M.; Zhang, L.; Yu, L.; Deisenhofer, J. Crystal structure of the cytochrome bc_1 complex from bovine heart mitochondria. *Science* **1997**, *277*, 60–66.
29. Zhang, Z.; Huang, L.; Shulmeister, V.M.; Chi, Y.-I.; Kim, K.K.; Hung, L.-W.; Crofts, A.R.; Berry, E.A.; Kim, S.-H. Electron transfer by domain movement in cytochrome bc_1. *Nature* **1998**, *392*, 677–684.
30. Xu, R.-H.; Pelicano, H.; Zhou, Y.; Carew, J.S.; Feng, L.; Bhalla, K.N.; Keating, M.J.; Huang, P. Inhibition of glycolysis in cancer cells: A novel strategy to overcome drug resistance associated with mitochondrial respiratory defect and hypoxia. *Cancer Res*. **2005**, *65*, 613–621.
31. Suganuma, K.; Miwa, H.; Imai, N.; Shikami, M.; Gotou, M.; Goto, M.; Mizuno, S.; Takahashi, M.; Yamamoto, H.; Hiramatsu, A.; *et al.* Energy metabolism of leukemia cells: Glycolysis *versus* oxidative phosphorylation. *Leuk. Lymphoma* **2010**, *51*, 2112–2119.
32. Modjtahedi, N.; Giordanetto, F.; Madeo, F.; Kroemer, G. Apoptosis-inducing factor: Vital and lethal. *Trends Cell Biol.* **2006**, *16*, 264–272.
33. Ogita, M.; Ogita, A.; Usuki, Y.; Fujita, K.; Tanaka, T. Antimycin A-induced cell death depends on AIF translocation through NO production and PARP activation and is not involved in ROS generation, cytochrome *c* release and caspase-3 activation in HL-60 cells. *J. Antibiot.* **2009**, *62*, 145–152.
34. Leist, M.; Single, B.; Castoldi, A.F.; Kühnle, S.; Nicotera, P. Intracellular adenosine triphosphate (ATP) concentration: A switch in the decision between apoptosis and necrosis. *J. Exp. Med.* **1997**, *185*, 1481–1486.

35. Eguchi, Y.; Shimizu, S.; Tsujimoto, Y. Intracellular ATP levels determine cell death fate by apoptosis or necrosis. *Cancer Res.* **1997**, *57*, 1835–1840.
36. Momose, I.; Ohba, S.-I.; Tatuda, D.; Kawada, M.; Masuda, T.; Tsujiuchi, G.; Yamori, T.; Esumi, H.; Ikeda, D. Mitochondrial inhibitors show preferential cytotoxicity to human pancreatic cancer PANC-1 cells under glucose-deprived conditions. *Biochem. Biophys. Res. Commun.* **2010**, *392*, 460–466.
37. Hsu, P.P.; Sabatini, D.M. Cancer cell metabolism: Warburg and beyond. *Cell* **2008**, *134*, 703–707.
38. Kroemer, G.; Pouyssegur, J. Tumor cell metabolism: Cancer's Achilles' heel. *Cancer Cell* **2008**, *13*, 472–482.
39. Heiden, M.G.V.; Cantley, L.C.; Thompson, C.B. Understanding the Warburg effect: The metabolic requirements of cell proliferation. *Science* **2009**, *324*, 1029–1033.
40. Elstrom, R.L.; Bauer, D.E.; Buzzai, M.; Karnauskas, R.; Harris, M.H.; Plas, D.R.; Zhuang, H.; Cinalli, R.M.; Alavi, A.; Rudin, C.M.; *et al.* Akt stimulates aerobic glycolysis in cancer cells. *Cancer Res.* **2004**, *64*, 3892–3899.
41. Porporato, P.E.; Dhup, S.; Dadhich, R.K.; Copetti, T.; Sonveaux, P. Anticancer targets in the glycolytic metabolism of tumors: A comprehensive review. *Front. Pharmacol.* **2011**, *2*, 49.
42. Granchi, C.; Minutolo, N. Anticancer agents that counteract tumor glycolysis. *ChemMedChem* **2012**, *7*, 1318–1350.
43. Sahra, I.B.; Laurent, K.; Giuliano, S.; Larbret, F.; Ponzio, G.; Gounon, P.; Le Marchand-Brustel, Y.; Giorgetti-Peraldi, S.; Cormont, M.; Bertolotto, C.; *et al.* Targeting cancer cell metabolism: The combination of metformin and 2-deoxyglucose induces p53-dependent apoptosis in prostate cancer cells. *Cancer Res.* **2010**, *70*, 2465–2475.
44. Cheong, J.-H.; Park, E.S.; Liang, J.; Dennison, J.B.; Tsavachidou, D.; Nguyen-Charles, C.; Cheng, K.W.; Hall, H.; Zhang, D.; Lu, Y.; *et al.* Dual inhibition of tumor energy pathway by 2-deoxyglucose and metformin is effective against a broad spectrum of preclinical cancer models. *Mol. Cancer Ther.* **2011**, *10*, 2350–2362.
45. Scotland, S.; Saland, E.; Skuli, N.; de Toni, F.; Boutzen, H.; Micklow, E.; Sénégas, I.; Peyraud, R.; Peyriga, L.; Théodoro, F.; *et al.* Mitochondrial energetic and AKT status mediate metabolic effects and apoptosis of metformin in human leukemic cells. *Leukemia* **2013**, *27*, 2129–2138.
46. Izuishi, K.; Kato, K.; Ogura, T.; Kinoshita, T.; Esumi, H. Remarkable tolerance of tumor cells to nutrient deprivation: Possible new biochemical target for cancer therapy. *Cancer Res.* **2000**, *60*, 6201–6207.

Araguspongine C Induces Autophagic Death in Breast Cancer Cells through Suppression of c-Met and HER2 Receptor Tyrosine Kinase Signaling

Mohamed R. Akl, Nehad M. Ayoub, Hassan Y. Ebrahim, Mohamed M. Mohyeldin, Khaled Y. Orabi, Ahmed I. Foudah and Khalid A. El Sayed

Abstract: Receptor tyrosine kinases are key regulators of cellular growth and proliferation. Dysregulations of receptor tyrosine kinases in cancer cells may promote tumorigenesis by multiple mechanisms including enhanced cell survival and inhibition of cell death. Araguspongines represent a group of macrocyclic oxaquinolizidine alkaloids isolated from the marine sponge *Xestospongia* species. This study evaluated the anticancer activity of the known oxaquinolizidine alkaloids araguspongines A, C, K and L, and xestospongin B against breast cancer cells. Araguspongine C inhibited the proliferation of multiple breast cancer cell lines *in vitro* in a dose-dependent manner. Interestingly, araguspongine C-induced autophagic cell death in HER2-overexpressing BT-474 breast cancer cells was characterized by vacuole formation and upregulation of autophagy markers including LC3A/B, Atg3, Atg7, and Atg16L. Araguspongine C-induced autophagy was associated with suppression of c-Met and HER2 receptor tyrosine kinase activation. Further *in-silico* docking studies and cell-free Z-LYTE assays indicated the potential of direct interaction between araguspongine C and the receptor tyrosine kinases c-Met and HER2 at their kinase domains. Remarkably, araguspongine C treatment resulted in the suppression of PI3K/Akt/mTOR signaling cascade in breast cancer cells undergoing autophagy. Induction of autophagic death in BT-474 cells was also associated with decreased levels of inositol 1,4,5-trisphosphate receptor upon treatment with effective concentration of araguspongine C. In conclusion, results of this study are the first to reveal the potential of araguspongine C as an inhibitor to receptor tyrosine kinases resulting in the induction of autophagic cell death in breast cancer cells.

Reprinted from *Mar. Drugs*. Cite as: Akl, M.R.; Ayoub, N.M.; Ebrahim, H.Y.; Mohyeldin, M.M.; Orabi, K.Y.; Foudah, A.I.; El Sayed, K.A. Araguspongine C Induces Autophagic Death in Breast Cancer Cells through Suppression of c-Met and HER2 Receptor Tyrosine Kinase Signaling. *Mar. Drugs* **2015**, *13*, 288-311.

1. Introduction

Receptor tyrosine kinases (RTKs) are key regulators of critical cellular processes including cell growth, differentiation, survival, and repair [1]. Multiple RTKs were identified for their oncogenic potential in breast cancer. It is well-established that aberrations in epidermal growth factor (EGF) receptor and HER2 signaling are associated with worse prognosis and more aggressive phenotypes of breast cancer [2]. Recently, strong evidence supports the role for the hepatocyte growth factor (HGF) and its receptor, c-Met, in the development and progression of breast carcinoma [2]. Abnormally increased expression of c-Met has been detected in human breast cancer and is associated with poor

prognosis [3]. RTKs are often selectively altered on malignant cells. Therefore, they represent attractive targets for cancer therapy, with a number of agents already approved for clinical use [4].

Autophagy is a catabolic process that digests cellular contents within lysosomes [5,6]. Autophagy is characterized by the formation of double-membrane vesicles, known as autophagosomes, which are engulfed by cytoplasmic molecules (Figure 1). Subsequently, the autophagosome fuses with the lysosome, which provides hydrolases and the sequestered contents undergo degradation and/or recycling (Figure 1). To date, the mammalian target of rapamycin (mTOR) is the most well-characterized autophagy regulator [7,8]. Recently, there has been growing evidence to suggest that decreased autophagic activity is related to tumorigenesis [6]. Therefore, induction of autophagic cell death may represent a promising tool for cancer cell eradication.

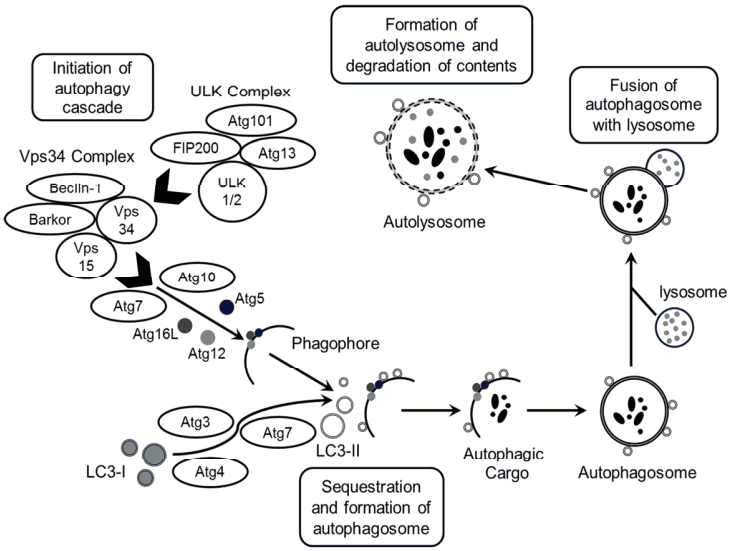

Figure 1. Schematic illustration of autophagy. The process of autophagosome formation consists of several stages, namely initiation, elongation and maturation and fusion. ULK complex (comprising ULK1/2–Atg13–FIP200–Atg101) is responsible for initiation of autophagy, in response to certain signals. In addition to initiation signals by the ULK complex, formation of double-layered membrane (phagophore) within the cytosol requires the action of the Vps34 complex (Vps34–Vps15, Beclin-1 (Atg6)–Barkor). The elongation stage requires cleavage of the microtubule-associated protein 1 light chain 3 (Atg8/LC3) by Atg4, resulting in the formation of cytosolic LC3-I protein, which is conjugated to phosphatidylethanolamine (PE) to form membrane bound LC3-II. In the meantime, the formation of Atg5–Atg12–Atg16L1 protein complex associates with the membrane and facilitates LC3 conjugation to PE and determines the sites of LC3 lipidation. The membrane grows to enwrap a portion of the cytosol, forming an autophagosome containing autophagic cargo. Next, lysosomes fuse with the autophagosome, releasing lysosomal hydrolases resulting in degradation of the vesicle contents and formation of autolysosome.

Marine sponges are rich sources of bioactive, unique, and chemically diverse natural products [9]. Xestospongins are marine natural products first isolated from the Pacific sponge *Xestospongia exigua* (Kirkpatrick) [10]. Chemically, araguspongines/xestospongins are dimeric 2,9-disubstituted 1-oxaquinolizidines (Figure 2). Stereochemically, the *trans*-2,9-disubstituted 1-oxaquinolizidine rings predominantly maintain a *trans*-decaline-like conformation, unlike the *cis*-disubstituted rings, which adapt a *cis*-decaline-like conformer [10]. Conformational variations of araguspongine/xestospongin alkaloids can significantly affect their biological activities and molecular targets [11]. Bioactivities reported for araguspongines and xestospongins include vasodilatory [12], cytotoxic [13], antifungal [11], antimalarial and antituberculosis [10], as well as antiplatelet activities [14]. Xestospongins and araguspongines have been extensively evaluated for their potential to modulate calcium release by multiple cellular calcium channels [15–17]. Xestospongins/araguspongines are powerful inhibitors of inositol 1,4,5-trisphosphate (IP3) receptor, a calcium channel mainly located at the endoplasmic reticulum [15–17].

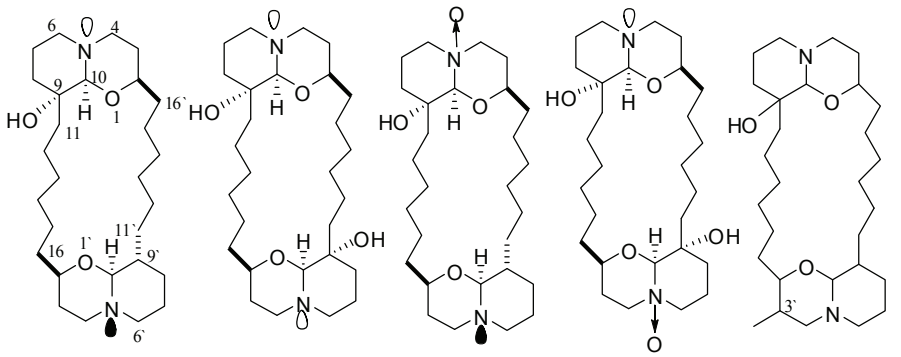

Figure 2. Chemical structures of araguspongines A, C, L, K, and xestospongin B.

Some marine-derived xestospongins and araguspongines were patented for modest antitumor activities in 1997 but little is known about their anticancer properties [18]. Therefore, the goal of this study was to evaluate the anticancer activity of araguspongines in multiple breast cancer cell lines *in vitro* and to characterize the mechanisms associated with the anticancer activity of araguspongine C in breast cancer cells.

2. Results

2.1 Chemical Diversity of Tested Oxaquinolizidine Alkaloids and Their Effect on Breast Cancer Cell Viability

Five known oxaquinolizidine alkaloids (Figure 2) have been identified and screened for their anticancer activity using the HER2-overexpressing breast cancer cell line BT-474 cells. The structures represent diverse dimeric *trans*-2,9-disubstituted 1-oxaquinolizidines, with mono and dihydroxy substitutions (araguspongines A and C, respectively), *N*-oxides (araguspongines K and

L), and monohydroxy and C-3′ methyl substitution (xestospongin B). Two day treatment of BT-474 cells resulted in antiproliferative activity and inhibition of breast cancer cell growth. The effect of oxaquinolizidine alkaloids treatment on breast cancer cells is shown in Table 1. Suppression of BT-474 cell viability was most remarkable with araguspongine A and araguspongine C treatments, with IC_{50} values of 9.3 and 15.2 μM, respectively (Table 1). Alternatively, xestospongin B and araguspongine L were the least active inhibitors of BT-474 cell growth when compared with other araguspongines used for this screening (Table 1).

Table 1. IC_{50} values for oxaquinolizidine alkaloids after 48 h treatment of BT-474 breast cancer cells in culture. Cells were plated at a density of 1×10^4 cells per well in 96-well culture plates and maintained in RPMI-1640 media supplemented with 10% FBS and allowed to adhere overnight. The next day, cells were divided into different treatment groups and then given various treatments in RPMI-1640 medium containing 40 ng/mL HGF for 48 h. Viable cell number was determined using the MTT assay. IC_{50} values were calculated using non-linear regression curve fit analysis using GraphPad Prism software.

Compound	IC_{50} (μM) ± SEM
Araguspongine A	9.3 ± 3.2
Araguspongine C	15.2 ± 2.1
Araguspongine K	29.5 ± 3.8
Araguspongine L	35.6 ± 3.7
Xestospongin B	52.5 ± 4.5

2.2. Effects of Araguspongine C on Viability, Morphology, and Colony Formation of Breast Cancer Cells

Araguspongine C exerted antiproliferative effects when applied to multiple breast cancer cell lines *in vitro*. Five breast cancer cell lines with different phenotypes and molecular characteristics were used for the evaluation of araguspongine C treatment over two days in culture. Results showed that it effectively suppressed the growth of all breast cancer cell lines used in a dose-dependent manner (Figure 3). However, growth inhibition of breast cancer cell lines showed a range of IC_{50} values (Table 2). MDA-MB-231 and MCF-7 cells were the most sensitive while T-47D cells were the least sensitive to the antiproliferative activity of araguspongine C (Table 2). Araguspongine C was not toxic in the non-tumorigenic MCF10A mammary epithelial cells at the used treatment doses. Interestingly, araguspongine C-induced antiproliferative activity in BT-474 cells was associated with a characteristic change of cellular phenotype indicated by vacuole accumulation in all colonies of BT-474 cells exposed to the compound treatment as compared to their vehicle-treated control group (Figure 4A). Vacuole accumulation in BT-474 cells was observed with araguspongine C concentration of 10 μM within three hours of treatment exposure. Furthermore, these alterations in cancer cell phenotype were exclusively noticed upon araguspongine C treatment of BT-474 cells, but not with other breast cancer cell lines concomitantly treated with the compound or with other oxaquinolizidine alkaloids previously used in BT-474 cell treatment.

Table 2. IC_{50} values for araguspongine C after 48 h treatment of multiple breast cancer cell lines in culture. IC_{50} values were calculated using non-linear regression curve fit analysis using GraphPad Prism software (GraphPad Software Inc., La Jolla, CA USA).

Cell Line	IC_{50} (μM) ± SEM
MDA-MB-231	10.1 ± 2.3
MCF-7	8.5 ± 1.6
BT-474	15.2 ± 2.1
SKBR3	18.3 ± 2.5
T-47D	46.1 ± 4.8

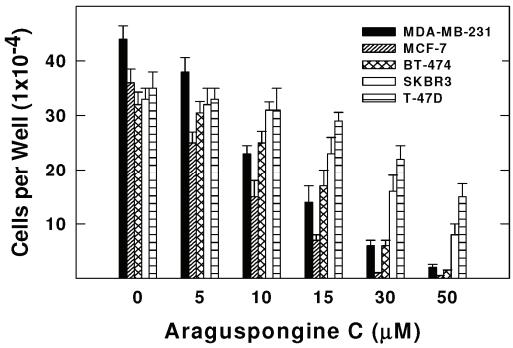

Figure 3. Effect of araguspongine C treatment on viability of breast cancer cell lines *in vitro*. MDA-MB-231, MCF-7, BT-474, SKBR3, and T-47D human breast cancer cells were plated at a density ~1 × 10^4 cells per well in 96-well culture plates and maintained in RPMI-1640 media supplemented with 10% FBS and allowed to adhere overnight. The next day, cells were divided into different treatment groups and then given various treatments in RPMI-1640 medium containing 40 ng/mL HGF for 48 h. Viable cell number was determined using the MTT assay. The data represent the mean ± SEM for three independent experiments.

For further evaluation of araguspongine C effects on BT-474 cells, cytotoxic and anchorage-independent growth studies were considered (Figure 4B,D). Araguspongine C treatment at 10 μM concentration was able to inhibit BT-474 cell anchorage-independent growth in soft agar assay compared to the vehicle-treated control cells (Figure 4B). In addition, araguspongine C treatment at 10 μM concentration induced apoptosis (cell death) in BT-474 cells treated for 48 h as compared to their vehicle-treated counterparts. Apoptosis was assessed by measuring the levels of Poly (ADP-ribose) polymerase (PARP) cleavage as shown by Western blot results (Figure 4C). Moreover, araguspongine C-induced cell death was additionally confirmed by determination of annexin V (apoptotic marker) and PI (oncotic marker) binding using flow cytometry in BT-474 cancer cells (Figure 4D). Araguspongine C at a concentration of 10 μM resulted in modest increase (17%) for the number of apoptotic cells (annexin V-positive) when compared to 25 μM (−)-oleocanthal (>60%) which was used as a positive control known to exert potent cytotoxic activity at the concentration used for this assay [19].

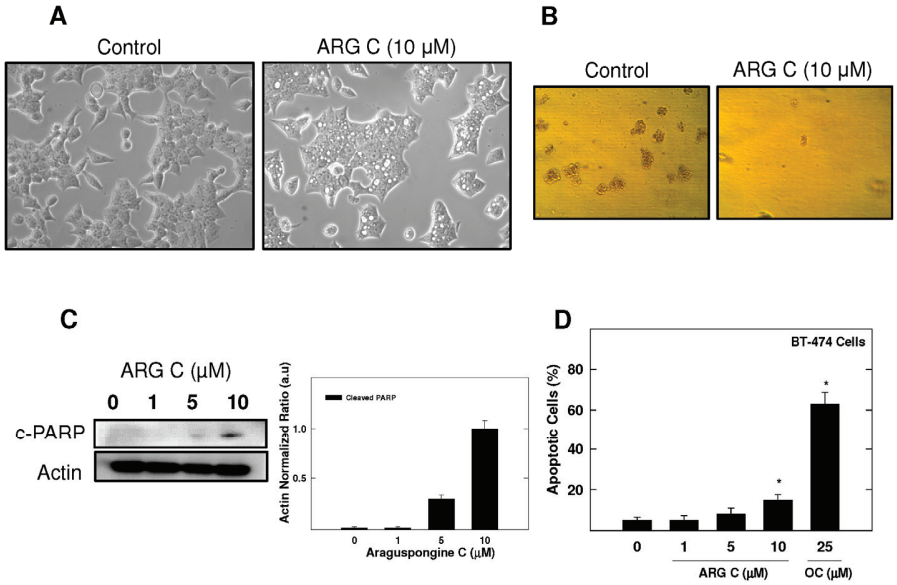

Figure 4. BT-474 breast cancer cells show characteristic vacuoles upon treatment with aragusponge C associated with cytotoxic effects. (**A**) Phase-contrast microscopy of BT-474 cells after aragusponge C treatment. BT-474 cells were treated with vehicle or aragusponge C at 10 μM for 24 h. The morphology of the cells was observed under an inverted phase contrast microscope. Magnification 100×; (**B**) Soft agar assay shows inhibition of BT-474 cell anchorage-independent growth by ARG C. BT-474 cells were cultured for 8 days in the absence (**left**) or presence (**right**) of 10 μM aragusponge C according to assay protocol and colony formation was observed under light microscope; (**C**) Western blot analysis of relative levels of c-PARP after aragusponge C treatment for 48 h in BT-474 breast cancer cells. Cells were plated at a density of 1×10^6 cells/100 mm culture plate and maintained in RPMI-1640 media supplemented with 10% FBS and allowed to adhere overnight. The next day, cells were divided into different treatment groups and then given various treatments in RPMI-1640 medium containing 40 ng/mL HGF for 48 h. At the end of treatment period, cells were lysed and equal amounts of whole cell extracts were fractionated on SDS-PAGE gels and immunoblotted as described in Materials and Methods. The visualization of β-actin was used as a loading control. Representative blots are from one of the three experiments; (**D**) Flow cytometry analysis. Cells were plated at a density of 1×10^6 cells/100 mm culture plates, allowed to attach overnight. Afterwards, cells were incubated in the respective control or aragusponge C-treated RPMI-1640 medium containing 40 ng/mL HGF for 48 h. Analysis of annexin V was determined using Annexin V-FITC Early Apoptosis Detection Kit as described in the Methods section. (−)-Oleocanthal was used as a positive control known to induce apoptosis at the dose used in this experiment. * $p < 0.05$ indicates values significantly different from non-treated cells. ARG C: Aragusponge C, c-PARP: cleaved Poly (ADP-ribose) polymerase, OC: (−)-Oleocanthal.

2.3. Autophagic Activity of Araguspongine C in BT-474 Breast Cancer Cells

A concentration of 10 μM araguspongine C caused accumulation of vacuoles in BT-474 cells and showed an increase of apoptotic cells. Therefore, the potential to induce toxic autophagy in BT-474 cells was examined. Cyto-ID Green reagent staining showed the relative fluorescence intensity of cells was increased in a dose-dependent manner, indicating the occurrence of autophagy (Figure 5A). Treatment with 5, 10, and 15 μM resulted in 18.2%, 45.5%, and 69.8% autophagy induction in BT-474 cells (Figure 5A). However, applied at the same concentration, araguspongine A showed a weaker autophagic activity in BT-474 cells (19.9%). In order to further evaluate the occurrence of cellular autophagy, Western blot studies were considered to assess araguspongine C effects on autophagy molecular modulators in BT-474 cancer cells. Treatment caused a dose-dependent increase in the total protein levels of LC3A/B, Beclin-1 (Atg6), Atg5, Atg7, and Atg16L1 in BT-474 breast cancer cells (Figure 5B). The increase in the expression of previously mentioned autophagy markers followed a dose-dependent manner and was clearly prominent at 10 μM. Taken together, these findings support the fact that araguspongine C molecular actions in BT-474 cells are mediated through the induction of autophagic cell death.

2.4. Effect of Araguspongine C on c-Met and HER2 Receptor Tyrosine Kinase Activation

Given the critical role of RTKs in controlling cell survival and death in response to external stimuli, we investigated the potential that araguspongine C-induced autophagic death to be associated with suppression of c-Met and/or HER2 signaling in BT-474 cancer cells. The Z-LYTE Kinase Assay-Tyr6 Peptide kit (Invitrogen) was used to assess the ability of araguspongines A and C to inhibit c-Met phosphorylation (activation) [19]. In these experiments, the olive phenolic (−)-oleocanthal was used as a positive standard control for activity comparison [20]. Araguspongine C was able to inhibit c-Met phosphorylation in a dose-dependent manner, with an IC_{50} value of 19.9 μM (Figure 6A). On the other hand, araguspongine A did not show significant inhibition of c-Met phosphorylation even when applied in concentrations up to 40 μM. The calculated IC_{50} of (−)-oleocanthal in this assay was 5.0 μM, which was consistent with the reported value (~4.8 μM) validating the results of this study [20]. The remarkable difference in the activity between araguspongines A and C as c-Met inhibitors can be explained based on their chemical structures and molecular modeling studies. Molecular modeling experiments were used to investigate the possible binding modes of araguspongines within the catalytic domain of unphosphorylated c-Met using the Schrödinger molecular modeling software package (Figure 6B). Araguspongine C assumed a shallow U-shaped binding mode with partial wrapping around Met 1211 at the c-Met kinase domain's activation loop (Figure 6B). The C-9′-hydroxyl group of araguspongine C's oxaquinozolidine ring participated in a critical single-point hydrogen bonding interaction with the side chain phenolic hydroxyl group of the Tyr 1159 at the hinge region (Figure 6B). This might explain, at least in part, its moderate micromolar activity level in Z-LYTE kinase biochemical assay. Additionally, the six-carbon aliphatic linker tethered the dimeric oxaquinolizidine ring system exerted hydrophobic interactions with the side chains of Ile 1084, Val 1092, Ala 1108 and Leu 1140 at the c-Met kinase domain hydrophobic sub-pocket. Alternatively, araguspongine A, which lacks C-9′-hydroxyl group, failed to satisfy such critical hydrogen bonding

interactions within the hinge region and subsequently showed poor activity in the c-Met biochemical assay. These results indicated the importance of the C-9′-hydroxyl functionality in araguspongine C chemical structure for binding the kinase domain of c-Met promoting enhanced c-Met inhibitory activity compared to oxaquinolizidine alkaloids lacking this functionality. Western blot analysis for the total and phosphorylated levels of c-Met in BT-474 and MDA-MB-231 cancer cells was considered in order to validate the c-Met inhibitory activity of araguspongine C in breast cancer cell lines. Western blot experiments showed that araguspongine C treatment resulted in a dose-dependent reduction of the total c-Met levels with a subsequent decrease in phosphorylated (active) levels in BT-474 cells. Interestingly, araguspongine C treatment caused suppression of c-Met receptor activation (phosphorylation) without changing the total levels of the receptor in MDA-MB-231 human breast cancer cells (Figure 6C).

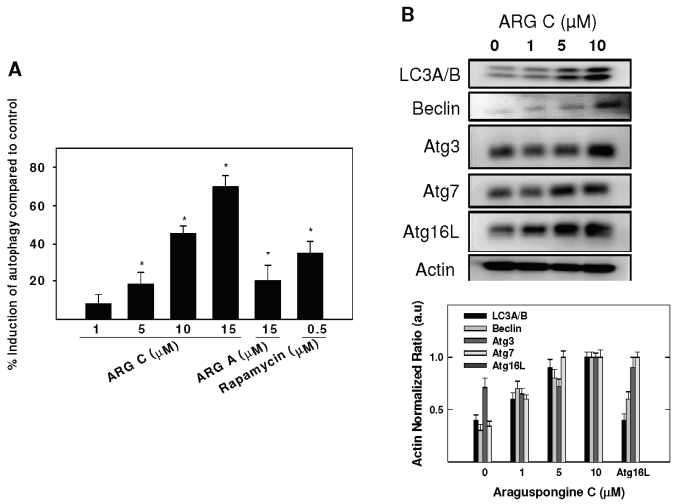

Figure 5. Araguspongine C-induced autophagy is associated with upregulation of autophagy-related proteins in BT-474 cancer cells. (**A**) Cyto-ID-coated autophagosomes in araguspongine C treated breast cancer cells. BT-474 cells were incubated with araguspongine C, araguspongine A or rapamycin (positive control) for 18 h and stained with Cyto-ID for 30 min at 37 °C. Intracellular Cyto-ID fluorescence was analyzed by microplate reader; (**B**) Western blot analysis of relative levels LC3A/B, Beclin-1, Atg3, Atg7, Atg16L after araguspongine C treatment for 24 h in BT-474 breast cancer cells. Cells were plated at a density of 1×10^6 cells/100 mm culture plate and maintained in RPMI-1640 media supplemented with 10% FBS and allowed to adhere overnight. The next day, cells were divided into different treatment groups and then given various treatments in RPMI-1640 medium containing 40 ng/mL HGF for 24 h. At the end of treatment period, cells were lysed and equal amounts of whole cell extracts were fractionated on SDS-PAGE gels and immunoblotted as described in Materials and Methods. The visualization of β-actin was used as a loading control. Representative blots are from one of the three experiments. ARG C: Araguspongine C, ARG A: Araguspongine A.

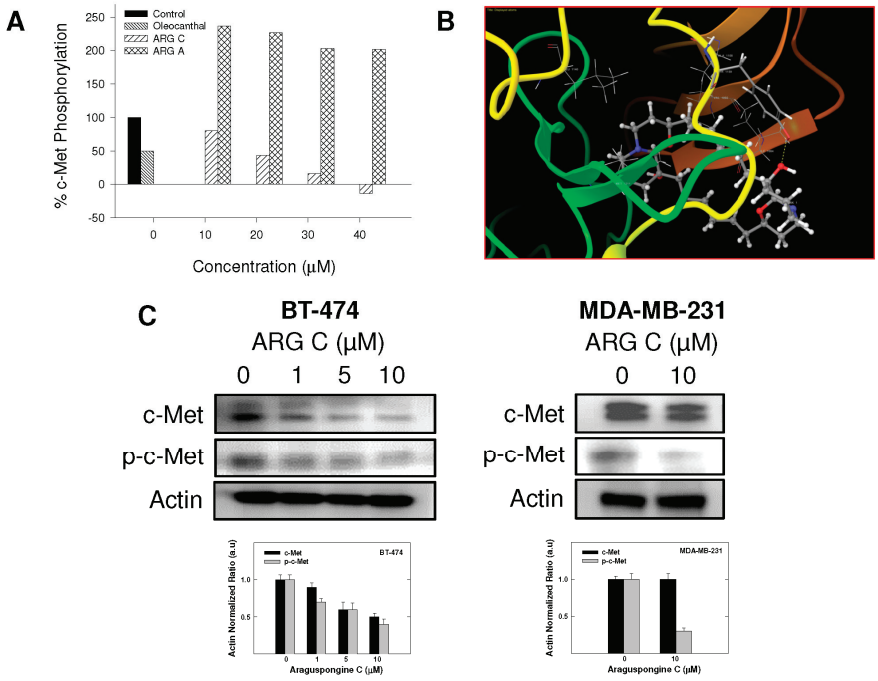

Figure 6. *In vitro* and *in-silico* c-Met receptor tyrosine kinase inhibition by araguspongine C. (**A**) Z-LYTE c-Met Kinase Assay. Araguspongine C was able to inhibit c-Met phosphorylation in a dose-dependent manner. 20 µL/well reactions were set up in 96-well plates containing kinase buffer, ATP, Z-LYTE Tyr6 Peptide substrate, c-Met kinase and, compound of interest as an inhibitor. After incubation at room temperature, development solution containing site-specific protease was added to each well. After another incubation period, the reaction was stopped, and the fluorescent signal was determined on a plate reader. (−)-Oleocanthal was used as a positive control in this experiment [21]; (**B**) *In-silico* binding mode of araguspongine C (ball and stick) in c-Met kinase domain (secondary structure and surface representation). Araguspongine C assumes a shallow U-shaped binding mode with partial wrapping around Met 1211 and the C-9′-hydroxyl on the oxaquinozolidine ring of araguspongine C contributes a critical single-point hydrogen bonding interaction with the side chain phenolic hydroxyl of Tyr 1159 in the hinge region. Araguspongine C's six-carbon aliphatic linker tethered the dimeric oxaquinolizidine ring system participates in hydrophobic interactions with the side chains of Ile 1084, Val 1092, Ala 1108 and Leu 1140 in the hydrophobic sub-pocket; (**C**) Western blot analysis of relative levels of total c-Met and phosphorylated-c-Met (p-c-Met) protein levels after araguspongine C treatment for 48 h in BT-474 and MDA-MB-231 breast cancer cells. Treatment was done according to the previously described protocol [19]. The visualization of β-actin was used as a loading control. Representative blots are from one of the three experiments. ARG C: Araguspongine C, ARG A: Araguspongine A, p-c-Met: Phosphorylated c-Met.

BT-474 is a HER2-overexpressing breast cancer cell line. Thus, further docking studies were conducted for araguspongine C on the crystal structure of HER2. Molecular docking study of araguspongine C on HER2 crystal structure (PDB: 3RCD [22]) suggested a hydrogen bonding interaction between C-9'-tertiary hydroxyl group of the quinazolidine scaffold with the carboxylate side chain of Asp 863 in the DFG motif (Figure 7A). The DFG motif (Asp863-Phe864-Gly365) of HER2 is located at the regulatory activation loop of the ATP binding pocket and is critical for HER2 protein kinase activity [23]. In active kinase conformation, the DFG motif is oriented towards the bound ATP, with the carboxylate side chain of Asp 863 residue able to coordinate with the magnesium ions bound to the β- and γ-phosphate groups of the ATP [23]. While in the inactive conformation, the DFG motif is flipped in such a way that Asp 863 no longer coordinates magnesium ion in the catalytic cleft [24]. Additionally, the importance of hydrogen bonding interaction of araguspongine C with Asp 863 at the DFG motif was obvious when the C-9'-hydroxyl group was replaced by hydrogen as in araguspongine A. Therefore, C-9'-hydroxyl of araguspongine C is an important pharmacophoric group to retain HER2 inhibitory and anticancer activities. Western blot experiments showed that araguspongine C treatment resulted in a dose-dependent reduction of the total HER2 levels with a subsequent decrease in phosphorylated (active) levels in BT-474 cells, confirming the molecular modeling results (Figure 7B). Further expression studies in BT-474 cells revealed no alterations to the total and the phosphorylated (active) levels of EGF receptor in response to araguspongine C treatment (Figure 7C). Similarly, Western blot experiments to examine the effects of araguspongine C treatment (10 μM) in MDA-MB-231 cancer cells did not result in changes in the total and the phosphorylated levels of EGF receptor (data not shown). Lack of activity of araguspongine C towards EGF receptor in both BT-474 and MDA-MB-231 cell lines may suggest some degree of selectivity toward c-Met and HER2 kinases. In addition, Western blot results showed no alterations to the total levels of estrogen receptor in BT-474 cells treated with araguspongine C for two days in culture (Figure 7C).

2.5. Effect of Araguspongine C on PI3K/Akt/mTOR Signaling Pathway and IP3 Receptor Levels

PI3K/Akt/mTOR signaling cascade is an essential pathway that is activated in response to ligand binding and activation of RTKs. Western blot studies showed that araguspongine C treatment caused a dose-dependent reduction of the levels p-PDK, p-Akt and p-mTOR in BT-474 cells (Figure 8A). In addition, araguspongine C treatment (10 μM) caused a reduction of total levels of IP3 receptor isoforms in BT-474 cells (Figure 8B). However, treatment of BT-474 cells with growth inhibitory concentration of araguspongine A (10 μM) did not cause a reduction of IP3 receptor level as compared to araguspongine C treatment (Figure 8B). These results suggest explanatory mechanisms to the autophagic activity of araguspongine C to be mediated, at least in part, through suppression of PI3K/Akt/mTOR pathway, and reduced IP3 receptor levels, which are both pathways recognized as major regulators of autophagy.

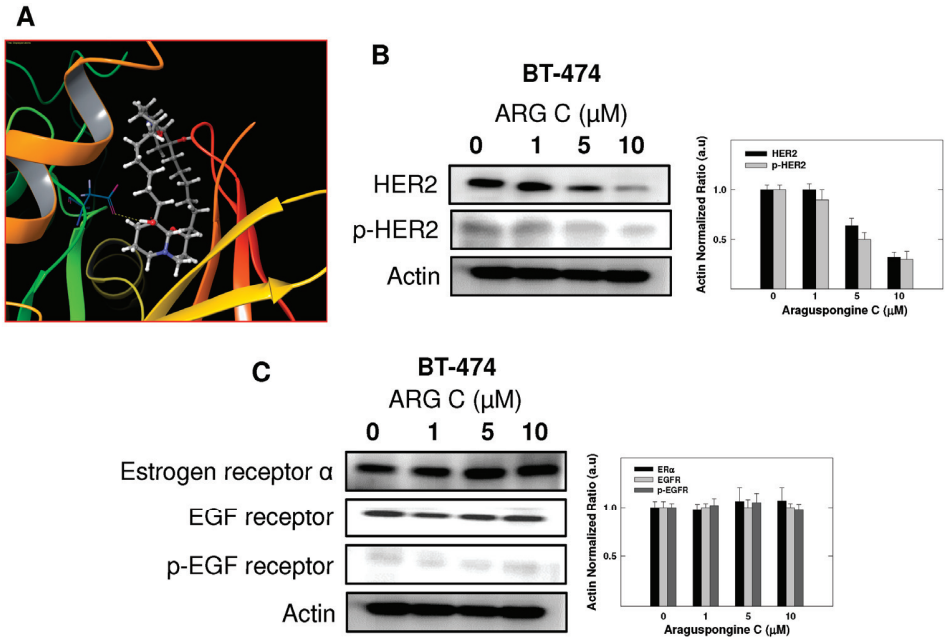

Figure 7. *In vitro* and *in-silico* ability of araguspongine C to downregulate HER2 levels and suppresses receptor activation in BT-474 breast cancer cell. (**A**) Molecular docking study of araguspongine C at the HER2 crystal structure. Docking studies suggested a hydrogen bonding interaction between araguspongine's C-9′-tertiary hydroxyl group on the quinazolidine scaffold with the carboxylate side chain of Asp863 at the DFG motif; (**B**) Western blot analysis of relative levels of total and phosphorylated HER2 after treatment with araguspongine C for 48 h in BT-474 cancer cells. Treatment was done according to the previously discussed protocol [21]. The visualization of actin was used as a loading control. Representative blots are from one of the three experiments; (**C**) Western blot analysis of the relative levels of estrogen receptor, EGF receptor, and phosphorylated-EGF receptor after araguspongine C treatment for 48 h. Treatment was done according to the previously described protocol. The visualization of β-actin was used as a loading control. Representative blots are from one of three experiments. ARG C: Araguspongine C, p-HER2: Phosphorylated HER2, EGF receptor: Epidermal growth factor receptor, p-EGF receptor: Phosphorylated epidermal growth factor receptor.

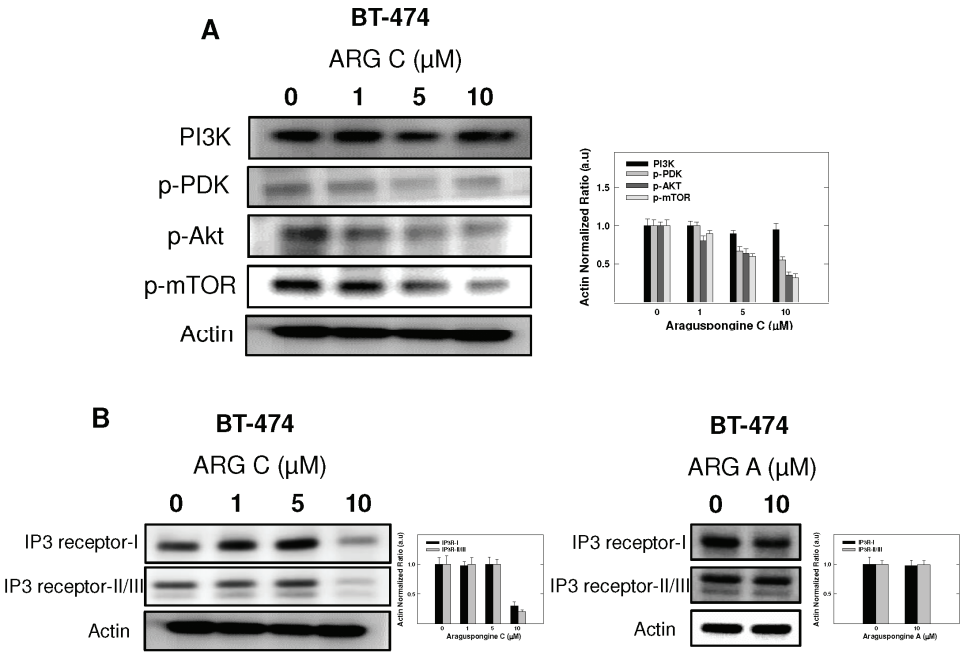

Figure 8. Cytotoxic autophagy induced by araguspongine C treatment in BT-474 cancer cells is associated with suppression of mTOR activation and downregulation of IP3 receptor levels. (**A**) Western blot analysis of relative levels of PI3K, p-PDK, p-AKT, and p-mTOR levels after araguspongine C treatment for 48 h. Treatment was done according to the protocol described previously. The visualization of β-actin was used as a loading control. Representative blots are from one of the three experiments; (**B**) Western blot analysis for the total levels of IP3 receptor-I/II/III upon treatment of BT-474 cells with araguspongine C or araguspongine A for 48 h in cell culture. Treatments were done according to the protocol described previously in the Methods section. The visualization of β-actin was used as a loading control. Representative blots are from one of the three experiments. ARG C: Araguspongine C, ARG A: Araguspongine A.

3. Discussion

Five known oxaquinolizidine alkaloids were tested for antiproliferative activity against the HER2-overexpressing breast cancer cell line BT-474 cells. Results suggest the need for two basic nitrogens of both araguspongine oxaquinolizidine rings for activity. This was based on the lower activity of the *N*-oxide-containing araguspongines K and L due to the loss of one oxaquinolizidine nitrogen lone pair of electrons to form the *N*-oxide bond. Xestospongin B also showed modest activity, possibly due to different oxaquinolizidine ring geometry and stereochemistry. Chemically, araguspongine C has C-9,9′-dihydroxylated groups, unlike the C-9 monohydroxylated araguspongines A and B. The additional C-9'-hydroxyl was virtually proved to be the main binding

and anchoring pharmacophoric group at the c-Met and HER2 kinase domains (Figures 6B and 7A). This may justify the additional c-Met and HER2 inhibitory activity as previously described in the Results section. Although araguspongine C's basic nitrogens N-5 and N-5′ did not play direct binding roles, they ultimately play crucial roles in properly aligning binding pharmacophores at the c-Met and HER2 kinase domains. They certainly play critical binding roles at IP3 receptor since some xestospongins and araguspongines lacking hydroxyl groups were reported to be active IP3 receptor antagonists. Araguspongines and xestospongins with C-7 or C-9 oxaquinolizidine ring hydroxylated groups like araguspongine C, 9-hydroxyxestospongin C, and 7-hydroxyxestospongin A showed enhanced IP3 receptor antagonistic activity, inhibiting IP3-mediated calcium release, weakly inhibiting ryanodine receptor-1 but lacking activity toward endoplasmic/sarcoplasmic reticulum calcium-ATPase (SERCA) [16]. Results of this study demonstrated that the marine-derived araguspongine C treatment inhibited HGF-induced growth and proliferation of multiple breast cancer cell lines *in vitro*. Interestingly, growth inhibition observed in BT-474 cells was associated with the suppression of HER2 and c-Met RTK activity and subsequent induction of autophagy. Autophagic death was also associated with the suppression of PI3K/Akt/mTOR signaling pathway as well as a reduction in the total levels of IP3 receptor in BT-474 cancer cells.

HER2 is a proto-oncogene encoding for HER2 receptor tyrosine kinase. HER2 is amplified in 20%–25% of breast cancers leading to HER2 protein overexpression and aggressive tumor phenotype associated with reduced survival and high risk of metastasis [25]. c-Met is a high-affinity receptor for HGF expressed mostly in epithelial cells [21]. Solid clinical evidence showed that c-Met is overexpressed in 20%–30% of breast cancer cases and is a strong and independent predictor of decreased survival and poor patient outcome [26,27]. This study indicates that araguspongine C treatment resulted in dose-dependent antiproliferative effects in different breast cancer cell lines. Few studies had evaluated the anticancer effects of araguspongines in literature. Araguspongine E (xestospongin C) inhibited the growth of MCF-7 breast cancer cells stimulated by 5% fetal calf serum or 10 nM estradiol [28]. In addition, xestospongin D has been reported to inhibit the growth of human leukemia and breast cancer cell lines comprising the NCI panel [13]. Initial screening for the anticancer effects of five different known *bis*-1-oxaquinolizidine alkaloids in BT-474 breast cancer cells showed a spectrum of variable activity, with araguspongines A and C being the most effective inhibitors of cancer cell growth. Of these, araguspongine C was the only autophagy inducer of BT-474 cells and therefore was selected for further examination in a panel of breast cancer cell lines *in vitro*.

Autophagy can function as a unique caspase-independent mechanism of cell death that is distinct from apoptosis and necrosis [29]. Autophagy is characterized by the formation of double-membrane vesicles (autophagosomes) that engulf cellular components targeted for destruction (Figure 1) [29]. The important component proteins involved in the execution of autophagy have been grouped as autophagy-related proteins (Atgs) [8,30,31]. Nearly 30 autophagy-related genes are identified so far and are implicated in different stages of autophagy [6]. One of the complexes first involved in the autophagy process is the ULK complex which triggers autophagy upon the input of certain induction signals [32]. Next in the process, autophagosome formation requires the activity of class III PI3K as vacuolar sorting protein forms a complex with Beclin-1 (Atg6) [32].

The elongation stage requires cleavage of the microtubule-associated protein 1 light chain 3 (Atg8/LC3) by Atg4, resulting in the formation of cytosolic LC3-I protein, which is conjugated to phosphatidylethanolamine to form membrane bound LC3-II [31,32]. Eventually, autophagosomes fuse with lysosomes to form autolysosomes, in which their autophagic cargo is degraded by lysosomal proteases (Figure 1) [29,31]. Compared to apoptosis, features of autophagic cell death include massive autophagic vacuolization inside the cytoplasm and the absence of chromosome condensation and nuclear fragmentation [33]. Besides autophagic vacuoles, the specific features of autophagic cell death also include Beclin-1 (Atg6), Atg5, Atg12, or Atg7 involvement and LC3-I to LC3-II conversion [33]. This study clearly showed that araguspongine C treatment of BT-474 cells induced autophagic death as indicated by the accumulation of autophagic vacuoles inside the cells and upregulation of autophagic markers LC3, Beclin-1, Atg3, Atg7, and Atg16L (Figures 4 and 5).

Autophagy is tightly regulated by upstream modulators, most essentially the PI3K/Akt/mTOR signaling pathway [30]. PI3K/Akt/mTOR signaling cascade is a major intracellular mediator of growth and survival [8,29]. Regularly, PI3K/Akt/mTOR signaling is activated by growth factors and nutrients; however, this pathway is constitutively active in many cancer types [29,30]. Since activation of the PI3K/Akt cascade promotes mTOR activity, this pathway is an important regulator of cellular autophagy. mTOR is known to suppress autophagy while promoting tumor cell growth, proliferation and survival [34]. Growth factor receptors such as c-Met and HER2 can activate PI3K/Akt/mTOR signaling cascade promoting cellular growth and survival. Earlier studies showed that inhibition of mTOR is sufficient to block cell survival induced by HGF/c-Met *in vitro* [35]. In the current study, araguspongine C treatment resulted in significant suppression of c-Met and HER2 receptor activation in BT-474 cancer cells. Further analysis showed that araguspongine C can directly inhibit c-Met and HER2 receptor activation (kinase domain phosphorylation) and that it can fit into the kinase domains of both c-Met and HER2 RTKs. In addition, suppression of c-Met and HER2 signaling by araguspongine C treatment resulted in the inhibition of PI3K/Akt/mTOR cascade, a major negative regulator of autophagy.

In cancer cell biology, autophagy is known to display a dual contrasting function [29,34,36]. Autophagic response can function as a protective mechanism allowing the recycling of proteins and cellular components to survive cell injuries induced by cytotoxic agents. Alternatively, cancer cells may undergo autophagic cell death following extreme autophagic degradation [36]. Recently, Han and colleagues identified potential interaction between Beclin-1 and HER2 in HER2-overexpressing BT-474 and SKBR3 breast cancer cells. Interestingly, the study identified a novel complex between HER2 and Beclin-1 that is disrupted by concurrent treatment with lapatinib resulting in cytoprotective autophagic response in these cells [37]. In contrast, other study showed that Ras-induced expression of Beclin-1 to promote autophagic cell death in MCF-7 breast cancer cells [38]. Thus, the induction of autophagic cell death may serve as a novel therapeutic strategy for eliminating cancer cells, especially those with high thresholds to apoptosis [34]. However, the complex role of autophagy in tumorigenesis requires specific pharmacological modulation of autophagy taking into consideration context- and cell-specific approaches [34]. In this study, exposure to araguspongine C resulted in a dose-dependent inhibition of breast cancer cell growth in culture,

however, autophagic activity was a finding specific to BT-474 cells. These observations further confirm that induction of autophagy can vary based on cancer cell type and other potential settings.

Recent findings identified intracellular calcium as a key regulator of both basal and induced autophagy [31]. The inositol 1,4,5-trisphosphate (IP3) receptor, a calcium channel mainly located at the endoplasmic reticulum, plays a vital role in regulating calcium-dependent autophagy [7]. Identification of IP3 as a regulator of autophagy goes back to studies by Sarkar and colleagues who described an mTOR-independent pathway for regulation of autophagy in mammalian cells [39]. Consequent studies revealed that xestospongins and araguspongines are potent inhibitors of IP3 receptor [16,40]. In Hela cells, xestospongin B (araguspongine B)-induced autophagy was mediated through inhibition of IP3 receptor [15]. As shown in the Results section, araguspongine C treatment of BT-474 cells resulted in a reduction in the total levels of IP3 receptor expression at doses known to induce autophagic response (10 μM). Accordingly, it can be concluded that autophagic activity of araguspongine C in BT-474 cell line is mediated, in part, by downregulation of IP3 receptor levels as well as the inhibition of mTOR signaling pathway as (Figure 9) discussed earlier.

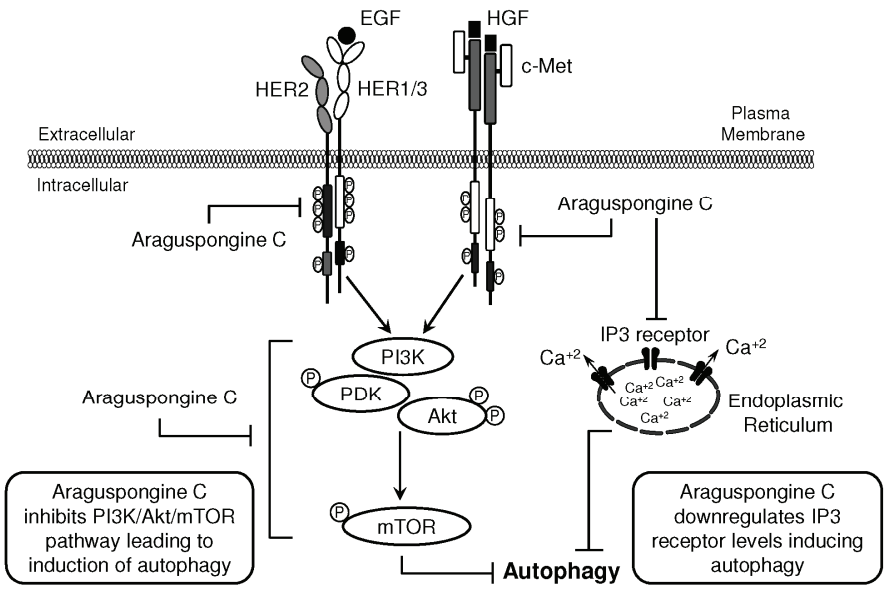

Figure 9. Schematic presentation for araguspongine C-induced autophagic death in breast cancer cells. Proposed direct inhibition of c-Met and HER2 receptor tyrosine kinases by araguspongine C. The inhibition of c-Met and HER2 activation in BT-474 breast cancer cells resulted in suppression of downstream molecular transducers, as indicated by suppression of PI3K/Akt/mTOR pathway. In addition, araguspongine C treatment resulted in a reduction in the total levels of IP3 receptor expressed by BT-474 cells. Taken together, araguspongine C inhibition of mTOR signaling pathway and inhibition of IP3 receptor resulted in the induction of autophagy in BT-474 cancer cells and subsequent inhibition of cell growth and proliferation.

4. Experimental Section

4.1. Chemicals, Reagents and Antibodies

All chemicals and reagents were purchased from Sigma-Aldrich (St. Louis, MO, USA), unless otherwise stated. Araguspongines A, C, K, L and xestospongin B were isolated from the Red Sea sponge *Xestospongia exigua* (Kirkpatrick) (Demospongiae: Haplosclerida) and identified by spectral analyses [10]. A purity of >95% was established for each compound using ^{1}H NMR and TLC analyses. Primary antibodies were purchased from Cell Signaling Technology (Beverly, MA, USA), except for IP3 receptor primary antibody which was purchased from Santa Cruz Biotechnology, Inc. (Dallas, TX, USA). Secondary antibodies were purchased from Cell Signaling Technology (Beverly, MA, USA).

4.2. Cell Lines and Culture Conditions

The human breast cancer cell lines MDA-MB-231, MCF-7, BT-474, T-47D, and SKBR3 cells were purchased from ATCC (Rockville, MD, USA). Breast cancer cell lines were maintained in RPMI-1640 media supplemented with 10% FBS, 100 U/mL penicillin G, and 0.1 mg/mL streptomycin. All cell lines were maintained in a humidified atmosphere of 5% CO_2 at 37 °C. Araguspongines and xestospongin B were first dissolved in a volume of DMSO to provide final 10 mM stock solutions which were used to prepare various concentrations of treatment media. Final concentration of DMSO was maintained as the same in all treatment groups within a given experiment and never exceeded 0.1%.

4.3. Measurement of Viable Cell Number

Viable cell count was determined using the 3-(4,5-dimethylthiazol-2yl)-2,5-diphenyl tetrazolium bromide (MTT) colorimetric assay [19]. The optical density of each sample was measured at 570 nm on a microplate reader (BioTek, Winooski, VT, USA). The number of cells/well was calculated against a standard curve prepared by plating various concentrations of cells, as determined using a hemocytometer at the start of each experiment.

4.4. Cell Viability Assays

Cells were plated at a density of 1×10^4 cells per well (6 wells/group) in 96-well culture plates and maintained in RPMI-1640 media supplemented with 10% FBS and allowed to adhere overnight. The next day, cells were divided into different treatment groups and given various treatments in RPMI-1640 medium containing 40 ng/mL HGF. Viable cell number after 48 h treatment was determined using the MTT assay.

4.5. Soft Agar Assay

The colony-forming capacity of BT-474 breast cancer cells was assessed using the CytoSelect 96-Well *in Vitro* Tumor Sensitivity Assay (Soft Agar Colony Formation) Kit (Cell Biolabs Inc.,

San Diego, CA, USA), according to manufacturer's protocol. Briefly, 50 µL of Base Agar Matrix Layer was dispensed into each well of a 96-well tissue culture plate. Cells (5×10^3) in 75 µL of Cell Suspension/Agar Matrix Layer were dispensed into each well. The cells were treated with 50 µL of culture medium containing DMSO or 10 µM of araguspongine C. After 8 days' incubation, visible colonies were photographed under an inverted phase-contrast microscope.

4.6. Western Blot Analysis

Cells were treated according to the methods described previously [19]. At the end of the treatment period, cells were lysed in RIPA buffer (Qiagen Sciences Inc., Valencia, CA, USA) and protein concentration was determined by the BCA assay (Bio-Rad Laboratories, Hercules, CA, USA). Equivalent amounts of protein (30 µg) were electrophoresed on SDS–polyacrylamide gels. The gels were then electroblotted onto PVDF membranes. These PVDF membranes were then blocked with 2% BSA in 10 mM Tris-HCl containing 50 mM NaCl and 0.1% Tween 20, pH 7.4 (TBST) and then, incubated with specific primary antibodies overnight at 4 °C. At the end of the incubation period, membranes were washed 5 times with TBST and then incubated with respective horseradish peroxide-conjugated secondary antibody in 2% BSA in TBST for 1 h at room temperature followed by rinsing with TBST for 5 times. Blots were then visualized by chemiluminescence according to the manufacturer's instructions (Pierce, Rockford, IL, USA). Images of protein bands from all treatment groups within a given experiment and scanning densitometric analysis were acquired using Kodak Gel Logic 1500 Imaging System (Carestream Health Inc., New Haven, CT, USA). All experiments were repeated at least three times.

4.7. Apoptosis Analysis with Annexin V Staining by Flow Cytometry

Induction of apoptosis was assessed by the binding of annexin V to phosphatidylserine, which is externalized to the outer leaflet of plasma membrane early during induction of apoptosis. Analysis of annexin V was determined using Annexin V-FITC Early Apoptosis Detection Kit (Cell Signaling Technology, Beverly, MA, USA). BT-474 cells were plated at a density of 5×10^6 cells/100 mm culture plates, allowed to attach overnight. Afterwards, cells were incubated in the respective control or araguspongine C treated with defined serum-free medium containing 40 ng/mL of HGF for 48 h. At the end of the experiment, cells in each treatment group were isolated with trypsin and then washed twice with ice cold PBS. Cells were then resuspended in 96 µL of ice-cold 1× Annexin V Binding Buffer. Afterwards, 1 µL Annexin V-FITC Conjugate and 12.5 µL Propidium Iodide (PI) Solution were added to each 96 µL cell suspension. The cells were then incubated for 10 min on ice in the dark. The cell suspension was then diluted to a final volume of 250 µL per assay with ice-cold, 1× Annexin V Binding Buffer. Dot plots were generated using CellQuest software (BD Biosciences, San Jose, CA, USA), and they were divided into 4 quadrants (LL: lower left; LR: lower right; UL: upper left; UR: upper right). The LL quadrant shows cells negative for both annexin V and PI (living, non-apoptotic cells). The LR quadrant shows cells positive for annexin V, but negative for PI (living, early apoptotic). The UL quadrant shows cells

positive for PI, but negative to annexin V (dead), whereas the UR quadrant shows cells positive for both annexin V and PI (late apoptotic). All experiments were repeated at least three times.

4.8. Cyto-ID Staining Assay

Cyto-ID is a proprietary reagent specifically labels autophagic vacuoles and co-localizes with light chain 3 (LC3). Cyto-ID Autophagy detection kit (Enzo Life Sciences, Farmingdale, NY, USA) was used according to the manufacturer's protocol. The fluorescence was measured by a plate reader (BioTek, Winooski, VT, USA). Cyto-ID Green reagent staining showed the relative fluorescence intensity of cells was increased in a dose-dependent manner, indicating the occurrence of autophagy. Rapamycin was used as a positive control [39].

4.9. Z-LYTE c-Met Kinase Assay

Z-LYTE Kinase Assay-Tyr6 Peptide kit (Invitrogen, Carlsbad, CA, USA) was used to assess the ability of araguspongines A and C to inhibit c-Met phosphorylation. Briefly, 20 µL/well reactions were set up in 96-well plates containing kinase buffer, 200 µM ATP, 4 µM Z-LYTE Tyr6 Peptide substrate, 2500 ng/mL c-Met kinase and compound of interest as an inhibitor. After 1 h of incubation at room temperature, 10 µL development solution containing site-specific protease was added to each well. Incubation was continued for 1 h. The reaction was then stopped, and the fluorescent signal ratio of 445 nm (coumarin)/520 nm (fluorescein) was determined on a plate reader (BioTek, Winooski, VT, USA) which reflects the peptide substrate cleavage status and/or the kinase inhibitory activity in the reaction.

4.10. Molecular Modeling

The *in-silico* experiments were carried out using Schrödinger molecular modeling software package installed on an iMac 27-inch Z0PG workstation with a 3.5 GHz Quad-core Intel Core i7, Turbo Boost up to 3.9 GHz, processor and 16 GB RAM (Apple, Cupertino, CA, USA).

4.10.1. Protein Structure Preparation

The X-ray crystal structure of the human c-Met kinase domain; residues 1048–1350, (PDB code: 3IN5, [41]) was retrieved from the Protein Data Bank [42]. The Protein Preparation Wizard of the Schrödinger suite was implemented to prepare the c-Met kinase domain [43]. The protein was reprocessed by assigning bond orders, adding hydrogens, creating disulfide bonds and optimizing H-bonding networks using PROPKA (Jensen Research Group, Copenhagen, Denmark). Finally, energy minimization with a root mean square deviation (RMSD) value of 0.30 Å was applied using an Optimized Potentials for Liquid Simulation (OPLS_2005, Schrödinger, New York, NY, USA) force field.

4.10.2. Ligand Structure Preparation

The structure of each araguspongine was sketched in the Maestro 9.3 panel (Maestro, version 9.3, 2012, Schrödinger, New York, NY, USA). The Lig Prep 2.3 module (Lig Prep, version 2.3, 2012, Schrödinger, New York, NY, USA) of the Schrödinger suite was utilized to generate the 3D structure and to search for different conformers. The Optimized Potentials for Liquid Simulation (OPLS_2005, Schrödinger, New York, NY, USA) force field was applied to geometrically optimize the ligand and to compute partial atomic charges. Finally, at most, 32 poses per ligand were generated with different steric features for the subsequent docking studies.

4.11. Molecular Docking

The prepared X-ray crystal structure of c-Met kinase domain was employed to generate receptor energy grids using the default value of the protein atomic scale (1.0 Å) within the cubic box centered on the cocrystallized ligand. After receptor grid generation, the prepared ligands were docked using the Glide 5.8 module (Glide, version 5.8, 2012, Schrödinger, New York, NY, USA) in extra precision (XP) mode [44].

4.12. Statistics

The results are presented as means ± SEM of at least three independent experiments. Differences among various treatment groups were determined by the analysis of variance (ANOVA) followed by Dunnett's test using PASW statistics® version 18. A difference of $P < 0.05$ was considered statistically significant as compared to the vehicle-treated control group. The IC_{50} values (concentrations that induce 50% cell growth inhibition) were determined using non-linear regression curve fit analysis using GraphPad Prism software version 6.

5. Conclusions

This is the first study to comprehensively characterize and evaluate the anticancer properties of the oxaquinolizidine alkaloids in breast cancer models. Results showed that araguspongine C-induced suppression of BT-474 cancer cell growth is mediated by induction of autophagic cell death. Autophagic activity of araguspongine C was associated with downregulation of c-Met and HER2 RTKs and suppression of receptor activation (Figure 9). Inhibition of these receptors was further confirmed by cell-free kinase assays and *in-silico* docking analysis. Suppression of RTK activity was also linked to PI3K/Akt/mTOR pathway inhibition (Figure 9). In addition, araguspongine C caused a reduction in the expression levels of IP3 receptor. Collectively, these results support the potential of araguspongine C as an inhibitor for RTKs and provide evidence for its anticancer activity in mammary tumor cells.

Acknowledgments

Research reported in this publication was supported by the National Cancer Institute of the National Institutes of Health under Award Number R15CA167475. The content is solely the

responsibility of the authors and does not necessarily represent the official views of the National Institutes of Health. The funders had no role in study design, data collection and analysis, decision to publish, or preparation of the manuscript.

Author Contributions

Conception and design: M.R. Akl, K.A. El Sayed. Development of methodology: M.R. Akl, N.M. Ayoub. Acquisition of data: M.R. Akl, N.M. Ayoub, H.Y. Ebrahim, M.M. Mohyeldin, A.I. Foudah. Analysis and interpretation of data (e.g., statistical analysis, biostatistics, computational analysis): M.R. Akl, N.M. Ayoub. Writing, review and/or revision of the manuscript: M. Akl, N.M. Ayoub, H.Y. Ebrahim, K.A. El Sayed. Administrative, technical or material support (*i.e.*, reporting or organizing data, constructing databases): M. Akl, N.M. Ayoub, H.Y. Ebrahim. Study supervision: K.A. El Sayed.

Abbreviations

ER, estrogen receptor; EGFR, epidermal growth factor receptor; HER-2, human epidermal growth factor receptor 2; HGF, hepatocyte growth factor; PDB, protein data bank; H & E, hematoxylin and eosin; ATCC, American Type Culture Collection; RPMI, Roswell Park Memorial Institute; DMSO, dimethyl sulfoxide; FBS, fetal bovine serum; RIPA, radioimmunoprecipitation assay; BCA, bicinchoninic acid assay; PVDF, polyvinylidene fluoride; BSA, bovine serum albumin; NIH, National Institutes of Health; HRP, horseradish peroxidase; MAPK, mitogen-activated protein kinase, PI3K, phosphatidylinositol 3-kinase; PLC-γ, phospholipase C-γ; STATs, transcription factors like the signal transducers and activators of transcription.

Conflicts of Interest

The authors declare no conflict of interest.

References

1. Eder, J.P.; Vande Woude, G.F.; Boerner, S.A.; LoRusso, P.M. Novel therapeutic inhibitors of the c-Met signaling pathway in cancer. *Clin. Cancer Res*. **2009**, *15*, 2207–2214.
2. Rho, O.; Kim, D.J.; Kiguchi, K.; Digiovanni, J. Growth factor signaling pathways as targets for prevention of epithelial carcinogenesis. *Mol. Carcinog*. **2011**, *50*, 264–279.
3. Kim, E.S.; Salgia, R. MET pathway as a therapeutic target. *J. Thorac. Oncol*. **2009**, *4*, 444–447.
4. Mendrola, J.M.; Shi, F.; Park, J.H.; Lemmon, M.A. Receptor tyrosine kinases with intracellular pseudokinase domains. *Biochem. Soc. Trans*. **2013**, *41*, 1029–1036.
5. Sharma, K.; Le, N.; Alotaibi, M.; Gewirtz, D.A. Cytotoxic autophagy in cancer therapy. *Int. J. Mol. Sci*. **2014**, *15*, 10034–10051.
6. Shimizu, S.; Yoshida, T.; Tsujioka, M.; Arakawa, S. Autophagic cell death and cancer. *Int. J. Mol. Sci*. **2014**, *15*, 3145–3153.

7. Parys, J.B.; Decuypere, J.P.; Bultynck, G. Role of the inositol 1,4,5-trisphosphate receptor/Ca^{2+}-release channel in autophagy. *Cell Commun. Signal*. **2012**, *10*, 17.
8. Wang, Z.; Han, W.; Sui, X.; Fang, Y.; Pan, H. Autophagy: A novel therapeutic target for hepatocarcinoma (Review). *Oncol. Lett*. **2014**, *7*, 1345–1351.
9. Akl, M.R.; Foudah, A.I.; Ebrahim, H.Y.; Meyer, S.A.; El Sayed, K.A. The marine-derived sipholenol A-4-*O*-3′,4′-dichlorobenzoate inhibits breast cancer growth and motility *in vitro* and *in vivo* through the suppression of Brk and FAK signaling. *Mar. Drugs* **2014**, *12*, 2282–2304.
10. Orabi, K.Y.; El Sayed, K.A.; Hamann, M.T.; Dunbar, D.C.; Al-Said, M.S.; Higa, T.; Kelly, M. Araguspongines K and L, new bioactive *bis*-1-oxaquinolizidine *N*-oxide alkaloids from Red Sea specimens of *Xestospongia exigua*. *J. Nat. Prod*. **2002**, *65*, 1782–1785.
11. Moon, S.S.; MacMillan, J.B.; Olmstead, M.M.; Ta, T.A.; Pessah, I.N.; Molinski, T.F. (+)-7*S*-Hydroxyxestospongin A from the marine sponge *Xestospongia* sp. and absolute configuration of (+)-xestospongin D. *J. Nat. Prod*. **2002**, *65*, 249–254.
12. Nakagawa, M.; Endo, M.; Tanaka, N.; Gen-Pei, L. Structures of xestospongin A, B, C and D, novel vasodilativecompounds from marine sponge *Xestospongia exigua*. *Tetrahedron Lett.* **1984**, *25*, 3227–3230.
13. Pettit, G.R.; Herald, O.B.; Doubek, D.L.; Tackett, L.; Schmidt, J.M.; Boyd, M.R.; Pettit, R.K.; Hooper, J.N.A. Isolation and X-ray crystal structure of racemic xestospongin D from the Singapore marine sponge *Niphates* sp. *Bioorg. Med. Chem. Lett*. **1996**, *6*, 1313–1318.
14. Pimentel, S.M.; Bojo, Z.P.; Roberto, A.V.; Lazaro, J.E.; Mangalindan, G.C.; Florentino, L.M.; Lim-Navarro, P.; Tasdemir, D.; Ireland, C.M.; Concepcion, G.P. Platelet aggregation inhibitors from Philippine marine invertebrate samples screened in a new microplate assay. *Mar. Biotechnol. (NY).* **2003**, *5*, 395–400.
15. Jaimovich, E.; Mattei, C.; Liberona, J.L.; Cardenas, C.; Estrada, M.; Barbier, J.; Debitus, C.; Laurent, D.; Molgo, J. Xestospongin B, a competitive inhibitor of IP3-mediated Ca^{2+} signalling in cultured rat myotubes, isolated myonuclei, and neuroblastoma (NG108–15) cells. *FEBS Lett*. **2005**, *579*, 2051–2057.
16. Ta, T.A.; Feng, W.; Molinski, T.F.; Pessah, I.N. Hydroxylated xestospongins block inositol-1,4,5-trisphosphate-induced Ca^{2+} release and sensitize Ca^{2+}-induced Ca^{2+} release mediated by ryanodine receptors. *Mol. Pharmacol*. **2006**, *69*, 532–538.
17. Vicencio, J.M.; Ortiz, C.; Criollo, A.; Jones, A.W.; Kepp, O.; Galluzzi, L.; Joza, N.; Vitale, I.; Morselli, E.; Tailler, M.; *et al*. The inositol 1,4,5-trisphosphate receptor regulates autophagy through its interaction with Beclin 1. *Cell Death Differ* **2009**, *16*, 1006–1017.
18. Tanaka J, Higa T.; Garcia G.D.; Ruffles, G.K. *bis*-1-Oxaquinolizidine Alkaloids from a Marine Sponge with Antitumor Activity. PCT International Application WO 9704783 CAN 126, 207511, 13 February 1997.
19. Akl, M.R.; Ayoub, N.M.; Mohyeldin, M.M.; Busnena, B.A.; Foudah, A.I.; Liu, Y.Y.; El Sayed, K.A. Olive phenolics as c-Met inhibitors: (−)-Oleocanthal attenuates cell proliferation, invasiveness, and tumor growth in breast cancer models. *PLoS One* **2014**, *9*, e97622.

20. Elnagar, A.Y.; Sylvester, P.W.; El Sayed, K.A. (−)-Oleocanthal as a c-Met inhibitor for the control of metastatic breast and prostate cancers. *Planta Med.* **2011**, *77*, 1013–1019.
21. Liu, Y.; Liu, J.H.; Chai, K.; Tashiro, S.; Onodera, S.; Ikejima, T. Inhibition of c-Met promoted apoptosis, autophagy and loss of the mitochondrial transmembrane potential in oridonin-induced A549 lung cancer cells. *J. Pharm. Pharmacol*. **2013**, *65*, 1622–1642.
22. Nakayama, A.; Miki, H.; Kamiguchi, H.; Tanaka, T.; Habuka, N.; Sogabe, S.; Yano, J.; Aertgeerts, K.; Kamiyama, K. Design and synthesis of novel human epidermal growth factor receptor 2 (HER2)/epidermal growth factor receptor (EGFR) dual inhibitors bearing a pyrrolo[3,2-*d*]pyrimidine scaffold. *J. Med. Chem*. **2011**, *54*, 8030–8050.
23. Hubbard, S.R. Crystal structure of the activated insulin receptor tyrosine kinase in complex with peptide substrate and ATP analog. *EMBO J*. **1997**, *16*, 5572–5581.
24. Hubbard, S.R.; Wei, L.; Ellis, L.; Hendrickson, W.A. Crystal structure of the tyrosine kinase domain of the human insulin receptor. *Nature* **1994**, *372*, 746–754.
25. Vassilakopoulou, M.; Togun, T.; Dafni, U.; Cheng, H.; Bordeaux, J.; Neumeister, V.M.; Bobos, M.; Pentheroudakis, G.; Skarlos, D.V.; Pectasides, D.; *et al*. *In situ* quantitative measurement of HER2mRNA predicts benefit from trastuzumab-containing chemotherapy in a cohort of metastatic breast cancer patients. *PLoS One* **2014**, *9*, e99131.
26. Graveel, C.R.; DeGroot, J.D.; Su, Y.; Koeman, J.; Dykema, K.; Leung, S.; Snider, J.; Davies, S.R.; Swiatek, P.J.; Cottingham, S.; *et al*. Met induces diverse mammary carcinomas in mice and is associated with human basal breast cancer. *Proc. Natl. Acad. Sci. USA* **2009**, *106*, 12909–12914.
27. Ponzo, M.G.; Lesurf, R.; Petkiewicz, S.; O'Malley, F.P.; Pinnaduwage, D.; Andrulis, I.L.; Bull, S.B.; Chughtai, N.; Zuo, D.; Souleimanova, M.; *et al*. Met induces mammary tumors with diverse histologies and is associated with poor outcome and human basal breast cancer. *Proc. Natl. Acad. Sci. USA* **2009**, *106*, 12903–12908.
28. Szatkowski, C.; Parys, J.B.; Ouadid-Ahidouch, H.; Matifat, F. Inositol 1,4,5-trisphosphate-induced Ca^{2+} signalling is involved in estradiol-induced breast cancer epithelial cell growth. *Mol. Cancer* **2010**, *9*, 156.
29. Carew, J.S.; Kelly, K.R.; Nawrocki, S.T. Autophagy as a target for cancer therapy: New developments. *Cancer Manag. Res*. **2012**, *4*, 357–365.
30. Jain, K.; Paranandi, K.S.; Sridharan, S.; Basu, A. Autophagy in breast cancer and its implications for therapy. *Am. J. Cancer Res*. **2013**, *3*, 251–265.
31. Kondratskyi, A.; Yassine, M.; Kondratska, K.; Skryma, R.; Slomianny, C.; Prevarskaya, N. Calcium-permeable ion channels in control of autophagy and cancer. *Front. Physiol.* **2013**, *4*, 272.
32. Fleming, A.; Noda, T.; Yoshimori, T.; Rubinsztein, D.C. Chemical modulators of autophagy as biological probes and potential therapeutics. *Nat. Chem. Biol*. **2011**, *7*, 9–17.
33. Chen, Y.J.; Chi, C.W.; Su, W.C.; Huang, H.L. Lapatinib induces autophagic cell death and inhibits growth of human hepatocellular carcinoma. *Oncotarget* **2014**, *5*, 4845–4854.
34. Choi, K.S. Autophagy and cancer. *Exp. Mol. Med*. **2012**, *44*, 109–120.

35. Moumen, A.; Patane, S.; Porras, A.; Dono, R.; Maina, F. Met acts on Mdm2 via mTOR to signal cell survival during development. *Development* **2007**, *134*, 1443–1451.
36. Vazquez-Martin, A.; Oliveras-Ferraros, C.; Menendez, J.A. Autophagy facilitates the development of breast cancer resistance to the anti-HER2 monoclonal antibody trastuzumab. *PLoS One* **2009**, *4*, e6251.
37. Han, J.; Hou, W.; Lu, C.; Goldstein, L.A.; Stolz, D.B.; Watkins, S.C.; Rabinowich, H. Interaction between Her2 and Beclin-1 proteins underlies a new mechanism of reciprocal regulation. *J. Biol. Chem.* **2013**, *288*, 20315–20325.
38. Elgendy, M.; Sheridan, C.; Brumatti, G.; Martin, S.J. Oncogenic Ras-induced expression of Noxa and Beclin-1 promotes autophagic cell death and limits clonogenic survival. *Mol. Cell*. **2011**, *42*, 23–25.
39. Sarkar, S.; Floto, R.A.; Berger, Z.; Imarisio, S.; Cordenier, A.; Pasco, M.; Cook, L.J.; Rubinsztein, D.C. Lithium induces autophagy by inhibiting inositol monophosphatase. *J. Cell Biol*. **2005**, *170*, 1101–1111.
40. De Smet, P.; Parys, J.B.; Callewaert, G.; Weidema, A.F.; Hill, E.; de Smedt, H.; Erneux, C.; Sorrentino, V.; Missiaen, L. Xestospongin C is an equally potent inhibitor of the inositol 1,4,5-trisphosphate receptor and the endoplasmic-reticulum Ca^{2+} pumps. *Cell Calcium.* **1999**, *26*, 9–13.
41. Boezio, A.A.; Berry, L.; Albrecht, B.K.; Bauer, D.; Bellon, S.F.; Bode, C.; Chen, A.; Choquette, D.; Dussault, I.; Fang, M.; *et al*. Discovery and optimization of potent and selective triazolopyridazine series of c-Met inhibitors. *Bioorg. Med. Chem. Lett*. **2009**, *19*, 6307–6312.
42. Protein Data Bank. Available online: http://www.rcsb.org/pdb/home/home.do (accessed on 1 September 2014).
43. Olsson, M.H.; Søndergaard, C.R.; Rostkowski, M.; Jensen, J.H. PROPKA3: Consistent treatment of internal and surface residues in empirical pKa predictions. *J. Chem. Theory Comp*. **2011**, *7*, 525–537.
44. Friesner, R.A.; Murphy, R.B.; Repasky, M.P.; Frye, L.L.; Greenwood, J.R.; Halgren, T.A.; Sanschagrin, P.C.; Mainz, D.T. Extra precision glide: Docking and scoring incorporating a model of hydrophobic enclosure for protein-ligand complexes. *J. Med. Chem*. **2006**, *49*, 6177–6196.

Combination of Trabectedin and Gemcitabine for Advanced Soft Tissue Sarcomas: Results of a Phase I Dose Escalating Trial of the German Interdisciplinary Sarcoma Group (GISG)

Bernd Kasper, Peter Reichardt, Daniel Pink, Michaela Sommer, Monika Mathew, Geraldine Rauch and Peter Hohenberger

Abstract: Background: Evaluation of the potential efficacy and safety of combination therapies for advanced soft tissue sarcomas (STS) has increased substantially after approval of trabectedin and pazopanib. Trabectedin's introduction in Europe in 2007 depended mainly on its activity in so-called L-sarcomas (liposarcoma and leiomyosarcoma); combination of trabectedin with other chemotherapies used in STS seems of particular interest. Methods: We initiated within the German Interdisciplinary Sarcoma Group (GISG) a phase I dose escalating trial evaluating the combination of trabectedin and gemcitabine in patients with advanced and/or metastatic L-sarcomas (GISG-02; ClinicalTrials.gov NCT01426633). Patients were treated with increasing doses of trabectedin and gemcitabine. The primary endpoint was to determine the maximum tolerated dose. Results: Five patients were included in the study. Two patients were treated on dose level 1 comprising trabectedin 0.9 mg/m^2 on day 1 and gemcitabine 700 mg/m^2 on days 1 + 8, every 3 weeks. Due to dose-limiting toxicity (DLT) in both patients (elevated transaminases and thrombocytopenia), an additional three patients were treated on dose level −1 with trabectedin 0.7 mg/m^2 plus gemcitabine 700 mg/m^2. Of these three patients, two demonstrated another DLT; therefore, the trial was stopped and none of the dose levels could be recommended for phase II testing. Conclusion: The GISG-02 phase I study was stopped with the conclusion that the combination of gemcitabine and trabectedin is generally not recommended for the treatment of patients with advanced and/or metastatic leiomyosarcoma or liposarcoma. Also, this phase I study strongly supports the necessity for careful evaluation of combination therapies.

Reprinted from *Mar. Drugs*. Cite as: Kasper, B.; Reichardt, P.; Pink, D.; Sommer, M.; Mathew, M.; Rauch, G.; Hohenberger, P. Combination of Trabectedin and Gemcitabine for Advanced Soft Tissue Sarcomas: Results of a Phase I Dose Escalating Trial of the German Interdisciplinary Sarcoma Group (GISG). *Mar. Drugs* **2015**, *13*, 379-388.

1. Introduction

Soft tissue sarcomas (STS) are a heterogeneous group of rare malignancies characterized by their mesenchymal origin and their poor prognosis. Around 50% of all patients diagnosed with STS will develop metastases at some point in the history of their disease. The most active drugs, doxorubicin and ifosfamide, achieve response rates around 15%–20% [1,2]. The limited efficacy of systemic treatment options results in a poor median overall survival for STS patients of about 12 months [3]. The introduction of new agents into the treatment armamentarium such as trabectedin [4] and pazopanib [5] may improve these results and suggests that longer survival could be achieved. With

the aim to further improve patients' survival, a combination of the new drugs with conventional chemotherapies used in STS has become a focus of clinical research.

The so called L-sarcomas represent about one fourth of all adult STS (15% liposarcomas and 11% leiomyosarcomas) [6]. Approval of trabectedin after treatment failure with anthracyclines and/or ifosfamide depended mainly on its activity in these L-sarcomas [7,8]. On the other hand, significant activity has been described for the use of gemcitabine and especially for the combination of gemcitabine and docetaxel, mainly in leiomyosarcomas [9]. The Sarcoma Alliance for Research through Collaboration (SARC) performed a randomized phase II study evaluating the efficacy of the combination of gemcitabine and docetaxel *versus* gemcitabine alone. This study favoured the combination with an increased response rate of 16% *versus* 9% for gemcitabine alone [10]. However, the combination of gemcitabine and docetaxel is associated with significant toxicity; pulmonary toxicity and refractory peripheral oedema are the most common severe adverse events. Thrombocytopenia and neutropenia are common, even with the use of growth factor support. Based on these data, the combination of trabectedin and gemcitabine became of interest, also for a possible later randomized comparison *versus* gemcitabine and docetaxel. Until now, safety and efficacy data using the combination of trabectedin and gemcitabine is scarce. One phase I trial evaluated weekly trabectedin and gemcitabine in patients with advanced solid tumors. The study demonstrated no pharmacokinetic interaction, and the recommended phase II dose for trabectedin was 0.4 mg/m^2 and for gemcitabine 1000 mg/m^2 for the weekly schedule. Seven out of 15 patients maintained stable disease after two cycles [11]. To formally evaluate the safety and efficacy of a possible combination treatment using trabectedin and gemcitabine, we initiated within the German Interdisciplinary Sarcoma Group (GISG) a phase I dose escalating trial in patients with advanced and/or metastatic L-sarcomas (GISG-02).

The aim of the present paper is to present the results of this trial which was stopped due to DLT as well as to discuss toxicities of combining new agents such as trabectedin and pazopanib with established chemotherapies for the treatment of advanced and metastatic STS.

2. Methods

2.1. Patient Population

Patients ≥18 years of age with a histological confirmed leiomyosarcoma or liposarcoma were eligible for enrollment. Any prior treatment was possible except adjuvant chemotherapy. Patients with evidence of newly diagnosed metastatic disease or disease progression during prior chemotherapy within the last six months in computed tomography or magnetic resonance imaging could be included. Patients were required to have a World Health Organisation (WHO) performance status of 0 or 1, an adequate haematological function (haemoglobin ≥9 g/dL, absolute neutrophil count (ANC) ≥ 1.5 × 10^3/mm^3, platelets ≥100.000/mm^3), an adequate hepatic function (serum total bilirubin ≤·upper limit of normal (ULN), serum total ALP ≤ 2.5 × ULN, serum AST and ALT ≤ 2.5 × ULN), and an adequate renal function (glomerular filtration rate (calculated by Cockroft-Gault) ≥ 60 mL/min). The trial was conducted between January 2012 and August 2014.

2.2. Study Design and Treatment

The phase I, open-label, dose-escalating combination study was conducted at two GISG centers, the Sarcoma Unit at the Interdisciplinary Tumor Center Mannheim of the Mannheim University Medical Center, University of Heidelberg and the Sarcoma Center Berlin-Brandenburg at HELIOS Klinikum Bad Saarow, Germany. The clinical protocol was approved by the local ethics committees, and all patients provided written informed consent prior to study inclusion. Trabectedin and gemcitabine were administered by intravenous (IV) infusion in a 21-day cycle. Patients were premedicated with IV dexamethason 20 mg prior to trabectedin administration. Gemcitabine was given as a 30-min. peripheral or central infusion on days 1 and 8, followed by a 3-h central infusion of trabectedin on day 1. Planned dose levels were trabectedin 0.7, 0.9, 1.1, 1.3, and 1.5 mg/m^2 and gemcitabine 700 and 900 mg/m^2.

2.3. Safety

Adverse events (AEs) were graded using the National Cancer Institute Common Toxicity Criteria (NCI-CTC), version 4.0. DLT was defined as any of the following: grade 4 neutropenia (ANC < 0.5 × 10^9/L) over 5 days, febrile neutropenia (ANC < 1.0 × 10^9/L over 5 days or with fever [body temperature ≥ 38.5 °C]), platelets < 25 × 10^9/L, grade ≥ 3 thrombocytopenia accompanied by bleeding, diarrhea ≥ grade 3 despite optimal loperamide use, rash ≥ grade 3, grade 3 transaminases (ALT/AST) increase longer than 7 days duration or grade 4 of any duration and other effects ≥ grade 3 thought to be treatment related (except nausea/vomiting, alopecia grade 2, fatigue lasting less than 48 h, and non-clinically relevant biochemical abnormalities). AEs and toxicity were assessed weekly.

2.4. Response Assessments and Statistical Analysis

Treatment responses were determined radiologically every three months based on the Response Evaluation Criteria in Solid Tumors (RECIST version 1.1). All patients who received ≥1 dose of each study drug were included in the toxicity and efficacy analyses. A standard phase I "3 + 3" dose escalation design was used.

3. Results

3.1. Patients

Five patients received ≥1 dose of study medication and were included in the study analysis population. Relevant patients' characteristics are summarized in Table 1. Four female and one male patient had a median age at study inclusion of 66 years (range: 50–76). There were four patients with a leiomyosarcoma, three of them of uterine origin, one in the gluteal region; and one patient with a retroperitoneal liposarcoma. All five patients were treated with prior surgery for the primary tumor; two of them received additional adjuvant radiotherapy. Four patients were treated with prior systemic therapy: three of them received first line therapy for metastatic disease consisting of single-agent doxorubicin; one patient was treated with letrozole.

Table 1. Patients' characteristics (n = 5).

Gender	Female	4
	Male	1
Age	Median (years)	66 (range: 50–76)
Histology	Leiomyosarcoma	4
	Liposarcoma	1
Tumor site at initial diagnosis	Uterus	3
	Abdomen/Retroperitoneum	2
Metastatic localizations	Lung	2
	Liver	3
	Abdomen	2
Previous treatments	Surgery alone	3
	Surgery plus radiotherapy	2
	Systemic therapy	4

3.2. Treatment and Safety

The median duration of combination treatment within the study was 89 days (range: 22–253). The study was stopped due to an unacceptable frequency of DLT in four of five patients. At dose level 1 (trabectedin 0.9 mg/m^2 plus gemcitabine 700 mg/m^2), two patients were included and exhibited DLT leading to an amendment of the study protocol enabling the treatment of patients on dose level −1 consisting of trabectedin 0.7 mg/m^2 and gemcitabine 700 mg/m^2. An additional two patients experienced a DLT on this dose level. The type of DLT was as follows: two patients demonstrated a platelet count $<25 \times 10^9$/L on day 15 of the first (patient No. 1) and the fifth treatment cycle (No. 5), respectively; the other two patients (patients No. 2 and 3) stopped treatment due to an increase of transaminases (ALT/AST) grade 3 lasting for more than seven days. An overview of the dose levels, the reason for the end of treatment and the types of DLT is depicted in Table 2. None of these patients had significant clinical problems or symptoms; only one of the patients (No. 1) with thrombocytopenia was hospitalized with fatigue and received a single platelet infusion during hospitalization. This was recorded as one of the three SAEs of the study; the other two SAEs were recorded due to an increased ALT and fever (Table 3). A list of all reported adverse events is depicted in Table 4. No further dose escalation could be performed and, therefore, no maximum tolerated dose could be recommended for phase II, concluding that the combination of gemcitabine and trabectedin is generally not recommended for the treatment of patients with advanced and/or metastatic leiomyosarcoma or liposarcoma.

Table 2. Dose levels and Dose-limiting toxicities (DLTs).

Patient No.	Dose Level	Duration of Treatment	Reason for End of Treatment		Type of DLT
			Disease Progression	DLT	
001	1	36 days	no	yes	hematologic
002	1	22 days	yes	yes	non-hematologic
003	−1	30 days	no	yes	non-hematologic
004	−1	253 days	yes	no	-
005	−1	106 days	no	yes	hematologic

Table 3. List of all Serious Adverse Events (SAEs).

Patient No.	Dose Level	Type of SAE	DLT	CTCAE-Grade	Related to Study Drug	Action Taken Related to Study Drug	Other Action Taken
1	1	Fatigue	No	2	Possible	Dose not changed	None
2	1	ALT increase	Yes	3	Definite	Dose reduced	Drug treatment
5	−1	Fever	No	1	Unrelated	Not applicable	Drug treatment

Table 4. List of all Adverse Events (AEs) *.

	Dose Level 1 (n = 2)		Dose Level −1 (n = 3)	
Adverse Events	**All Grades**	**Grade 3/4**	**All Grades**	**Grade 3/4**
WBC decreased	8	5	0	0
Neutrophil count decreased	6	4	0	0
Anaemia	6	0	0	0
Platelet count decreased	6	2	1	1
ALT increased	3	2	8	2
AST increased	2	0	6	1
Alkaline phosphatase increased	1	0	0	0
GGT increased	1	1	0	0
Fever	0	0	13	0
Urinary tract infection	0	0	1	0
Bladder infection	0	0	1	0
Infection ankle bone	0	0	1	0
Skin infection leg	0	0	1	0
Refluxesophagitis	0	0	1	0
Common cold	1	0	0	0
Fatigue	2	0	2	0
Nausea	1	0	1	0
Oedema	0	0	6	0
Circulatory disorder	0	0	1	0
Constipation	0	0	1	0
Pain sternum	0	0	2	0
Troponin T increased	0	0	1	0

Abbreviations: WBC = white blood cells/leucocytes count; ALT = alanin-aminotransferase; AST = aspartat-aminotransferase; GGT = gamma-glutamyltransferase.; * More than one AE may be observed per patient; percentages are not reported due to the low number of patients per dose level.

3.3. Efficacy

There were no complete or partial responses in our patient cohort. However, four patients maintained stable disease; so the rate of patients with stable disease is estimated to be 80% at three months and 50% at six months, respectively. Two patients demonstrated prolonged disease stabilization for nine months. One patient (No. 4) with a leiomyosarcoma benefited the longest from

the combination treatment, showed no DLT and had to stop study medication due to disease progression nine months after study inclusion.

4. Discussion

Standard systemic chemotherapy such as doxorubicin and/or ifosfamide still forms the backbone of palliative treatment in advanced STS. More recently, newer compounds have been added to the treatment armamentarium of STS such as gemcitabine (plus or minus docetaxel), trabectedin and pazopanib. Strategies to improve patients' outcome are urgently needed; one of these strategies is to combine "targeted" agents with the established chemotherapeutic compounds. Trabectedin gained approval in Europe in 2007 for the treatment of advanced and/or metastatic STS. Administered as single-agent therapy, it has a favorable toxicity profile. The most common side effects such as fatigue and myelosuppression are usually mild. It lacks cumulative and organ-specific toxicity and does not cause many of the problems that have an adverse effect on the quality of life of patients such as severe acute nausea, mucositis, alopecia or skin toxicity. Specific adverse events like transaminitis and rhabdomyolysis have no clinical implications in the majority of patients and are easily manageable [12].

The present GISG phase I trial formally evaluated the combination of trabectedin and gemcitabine in patients with L-sarcomas. Unexpectedly, dose-limiting toxicity occurred on two dose levels so that no further dose escalation could be performed and no recommended dose for phase II testing could be defined. Hence, the results of our trial suggest that the combination of gemcitabine and trabectedin is not recommended for the treatment of patients with advanced and/or metastatic leiomyosarcoma or liposarcoma.

In a phase I trial, the combination of trabectedin and cisplatin given every three weeks in patients with advanced solid tumors has been evaluated [13]. The regimen consisted of cisplatin at a fixed dose of 75 mg/m^2 1-h IV infusion followed by escalating doses of trabectedin 3-h IV infusion, both administered on day 1 every 3 weeks. Two DLTs, grade 4 neutropenia longer than 7 days' duration and grade 3 vomiting despite standard antiemetic therapy, occurred at the starting dose of trabectedin (0.75 mg/m^2). The immediate lower dose (trabectedin 0.60 mg/m^2) was evaluated in a total of eight patients; no DLTs occurred and this was declared the recommended dose. The safety profile at this dose and schedule was consistent with the known side effects of each agent alone: nausea, fatigue, transient transaminase elevations and neutropenia; no new or unexpected adverse reactions were observed. The authors concluded that, although the trabectedin dose achieved with this combination was rather low (40% of single-agent when given every three weeks), this combination regimen of trabectedin plus cisplatin was feasible and showed a tolerable safety profile.

To determine the dose of trabectedin plus doxorubicin a phase I combination study was performed in patients with STS treated with 0–1 prior chemotherapy regimen excluding doxorubicin [14]. The regimen consisted of a 10–15-min. IV infusion of doxorubicin 60 mg/m^2 followed by a 3-h IV infusion of trabectedin 0.9–1.3 mg/m^2 on day 1 of a 3 week cycle. Because four of the first six patients experienced DLT-defining neutropenia during cycle 1, all subsequent patients received primary prophylactic granulocyte colony-stimulating factor. No DLTs were

observed at dose level 1 (trabectedin 0.9 mg/m^2) and dose level 2 (trabectedin 1.1 mg/m^2). At dose level 3 (trabectedin 1.3 mg/m^2) two patients experienced DLTs which were grade 4 neutropenia and grade 4 thrombocytopenia making this dose level unacceptable. The maximum tolerated dose was trabectedin 1.1 mg/m^2 and doxorubicin 60 mg/m^2. Common grade 3/4 adverse events were neutropenia (71%), ALT increase (46%), and thrombocytopenia (37%). The authors concluded that the combination of doxorubicin 60 mg/m² followed by trabectedin 1.1 mg/m² every 21 days is safe and active in patients with STS. Promising phase II data in 61 leiomyosarcoma patients demonstrated one complete response, 13 partial responses and 20 stable diseases accounting for a disease control rate of 94%. Common grade 3/4 toxicities were neutropenia (41%), febrile neutropenia (4%), thrombocytopenia (20%), anemia (9%), fatigue (6%), vomiting (4%), and transaminases elevation (9%) [15]. Another phase II study from the Spanish Group for Sarcoma Research (GEIS) evaluating the combination of trabectedin and doxorubicin did not add any further information regarding toxicities [16].

Discussing the phase I/II combination studies, hematologic toxicity (neutropenia and thrombocytopenia) seems to be the major problem when combining trabectedin with cisplatin, doxorubicin or gemcitabine. In combination with cisplatin this DLT led to a rather low dose of trabectedin (only 40% of the approved single-agent treatment dose) questioning the efficacy of this combination. In the combination studies with doxorubicin, hematologic toxicity could be overcome through the use of granulocyte colony-stimulating factor. In our combination trial with gemcitabine, thrombocytopenia was the major limiting factor regarding hematologic toxicity. Notably, both patients with thrombocytopenia were treated previously with adjuvant radiation in the pelvic region which could have had an implication on the occurrence of that type of DLT. Hepatic toxicity was observed quite frequently; however, in the combination with cisplatin and doxorubicin it did not classify for a DLT (grade 3/4 transaminitis lasting ≥7 days). Therefore, prolongation of the elevation of transaminases as observed in our trial seems to be particularly related to the addition of gemcitabine. As described in the literature, gemcitabine may lead to common transient rises in transaminases. However, these laboratory abnormalities are rarely clinically significant [17]. Gemcitabine is also being evaluated in the combination with the anti-angiogenetic agent pazopanib in several phase I and II trials (NCT01593748, NCT01532687, and NCT01442662); however, no data is available yet. Nevertheless, a fatal hepatic serious adverse event occurred in one US study investigating the combination of gemcitabine and pazopanib for the treatment of advanced STS with the consequence to temporarily hold enrolment in all studies of gemcitabine in combination with pazopanib. The fatal hepatic event occurred in a patient with metastatic leiomyosarcoma with multiple liver metastases, with marked elevation of liver enzymes after one dose of gemcitabine and two doses of pazopanib leading to a hepatorenal syndrome and death. Fatal hepatotoxicity is a recognized adverse event associated with both pazopanib and gemcitabine. However, the rapidity of onset and the degree of enzyme elevation in this case is not consistent with the known safety profile of either drug. It seems that gemcitabine prolongs or increases the elevation of liver enzymes significantly.

Taken together, although clinical benefit in the form of disease stabilization was quite promising in our small patient cohort, due to dose-limiting toxicity, the combination of gemcitabine plus

trabectedin could generally not be recommended for the treatment of patients with advanced and/or metastatic leiomyosarcoma or liposarcoma. Drug combinations still seem promising, but require careful evaluation in terms of safety.

5. Conclusions

The present study of the German Interdisciplinary Sarcoma Group (GISG-02) represents the formal evaluation of the safety and efficacy of trabectedin combined with gemcitabine in so-called L-sarcomas. The study was stopped due to four dose-limiting toxicities in five treated patients. Therefore, the results of our trial suggest that the combination of gemcitabine and trabectedin is not recommended for patients with L-sarcomas. This phase I study strongly supports the necessity for careful evaluation of combination therapies.

Acknowledgments

The study was supported by a research fund from PharmaMar.

Author Contributions

BK conceived the study and participated in its design and coordination, included patients and drafted the manuscript; PR participated in the study design and coordination and included patients; DP included patients in the study; MS participated in the administrative study coordination and data acquisition; MM participated in the administrative study coordination and data acquisition; GR participated in the design of the study and performed the statistical analysis; PH participated in the study design and coordination and included patients; All authors read and approved the manuscript.

Conflicts of Interest

BK: honoraria and research funding from PharmaMar; PR: honoraria from PharmaMar; PH: research funding and honoraria from PharmaMar. All remaining authors have declared no conflict of interest.

References

1. Van Glabekke, M.; van Oosterom, A.T.; Oosterhuis, J.W.; Mouridsen, H.; Crowther, D.; Somers, R.; Verweij, J.; Santoro, A.; Buesa, J.; Tursz, T. Prognostic factors for the outcome of chemotherapy in advanced soft tissue sarcoma: An analysis of 2.185 patients treated with anthracycline-containing first-line regimens—A European Organization for Research and treatment of Cancer Soft Tissue and Bone Sarcoma Group Study. *J. Clin. Oncol.* **1999**, *17*, 150–157.

2. Van Oosterom, A.T.; Mouridsen, H.T.; Nielsen, O.S.; Dombernowsky, P.; Krzemieniecki, K.; Judson, I.; Svancarova, L.; Spooner, D.; Hermans, C.; van Glabbeke, M.; *et al*. EORTC Soft Tissue and Bone Sarcoma Group. Results of randomised studies of the EORTC Soft Tissue and Bone Sarcoma Group (STBSG) with two different ifosfamide regimens in first- and second-line chemotherapy in advanced soft tissue sarcoma patients. *Eur. J. Cancer* **2002**, *38*, 2397–2406.
3. Leahy, M.; Garcia, Del Muro X.; Reichardt, P.; Judson, I.; Staddon, A.; Verweij, J.; Baffoe-Bonnie, A.; Jönsson, L.; Musayev, A.; Justo, N.; *et al*. SABINE Investigators. Chemotherapy treatment patterns and clinical outcomes in patients with metastatic soft tissue sarcoma. The Sarcoma treatment and Burden of Illness in North America and Europe (SABINE) study. *Ann. Oncol.* **2012**, *23*, 2763–2770.
4. Demetri, G.D.; Chawla, S.P.; von Mehren, M.; Ritch, P.; Baker, L.H.; Blay, J.Y.; Hande, K.R.; Keohan, M.L.; Samuels, B.L.; Schuetze, S.; *et al*. Efficacy and safety of trabectedin in patients with advanced or metastatic liposarcoma or leiomyosarcoma after failure of prior anthracyclines and ifosfamide: results of a randomized phase II study of two different schedules. *J. Clin. Oncol.* **2009**, *27*, 4188–4196.
5. Van der Graaf, W.T.A.; Blay, J.Y.; Chawla, S.P.; Kim, D.W.; Bui-Nguyen, B.; Casali, P.G.; Schöffski, P.; Aglietta, M.; Staddon, A.P.; Beppu, Y.; *et al*. EORTC Soft Tissue and Bone Sarcoma Group. PALETTE study group. Pazopanib for metastatic soft-tissue sarcoma (PALETTE): A randomised, double-blind, placebo-controlled phase 3 trial. *Lancet* **2012**, *379*, 1879–1886.
6. Ducimetiere, F.; Lurkin, A.; Ranchere-Vince, D.; Decouvelaere, A.V.; Péoc'h, M.; Istier, L.; Chalabreysse, P.; Muller, C.; Alberti, L.; Bringuier, P.P.; *et al*. Incidence of sarcoma histotypes and molecular subtypes in a prospective epidemiological study with central pathology review and molecular testing. *PLoS One* **2011**, *6*, e20294.
7. Garcia-Carbonero, R.; Supko, J.G.; Manola, J.; Seiden, M.V.; Harmon, D.; Ryan, D.P.; Quigley, M.T.; Merriam, P.; Canniff, J.; Goss, G.; *et al*. Phase II and pharmacokinetic study of ecteinascidin 743 in patients with progressive sarcomas of soft tissues refractory to chemotherapy. *J. Clin. Oncol.* **2004**, *22*, 1480–1490.
8. Le Cesne, A.; Blay, J.Y.; Judson, I.; van Oosterom, A.; Verweij, J.; Radford, J.; Lorigan, P.; Rodenhuis, S.; Ray-Coquard, I.; Bonvalot, S.; *et al*. Phase II study of ET-743 in advanced soft tissue sarcomas: A European Organisation for the Research and Treatment of Cancer (EORTC) soft tissue and bone sarcoma group trial. *J. Clin. Oncol.* **2005**, *23*, 576–584.
9. Hensley, M.L.; Maki, R.; Venkatraman, E.; Geller, G.; Lovegren, M.; Aghajanian, C.; Sabbatini, P.; Tong, W.; Barakat, R.; Spriggs, D.R. Gemcitabine and docetaxel in patients with unresectable leiomyosarcoma: Results of a phase II trial. *J. Clin. Oncol.* **2002**, *20*, 2824–2831.
10. Maki, R.; Wathen, J.K.; Patel, S.R.; Priebat, D.A.; Okuno, S.H.; Samuels, B.; Fanucchi, M.; Harmon, D.C.; Schuetze, S.M.; Reinke, D.; *et al*. Randomized phase II study of gemcitabine and docetaxel compared with gemcitabine alone in patients with metastatic soft tissue sarcomas: Results of sarcoma alliance for research through collaboration study 002. *J. Clin. Oncol.* **2007**, *25*, 2755–2763.

11. Messersmith, W.A.; Jimeno, A.; Ettinger, D.; Laheru, D.; Brahmer, J.; Lansey, D.; Khan, Y.; Donehower, R.C.; Elsayed, Y.; Zannikos, P.; *et al*. Phase I trial of weekly trabectedin (ET-743) and gemcitabine in patients with advanced solid tumors. *Cancer Chemother. Pharmacol.* **2008**, *63*, 181–188.
12. Kasper, B. Therapie des fortgeschrittenen Weichgewebesarkoms: Neue Perspektiven mit Trabectedin (Yondelis®). *J. Med. Drug Rev.* **2013**, *3*, 35–43.
13. Sessa, C.; del Conte, G.; Christinat, A.; Cresta, S.; Perotti, A.; Gallerani, E.; Lardelli, P.; Kahatt, C.; Alfaro, V.; Iglesias, J.L.; *et al*. Phase I clinical and pharmacokinetic study of trabectedin and cisplatin given every three weeks in patients with advanced solid tumors. *Invest. New Drugs* **2013**, *31*, 1236–1243.
14. Blay, J.Y.; van Mehren, M.; Samuels, B.L.; Fanucchi, M.P.; Ray-Coquard, I.; Buckley, B.; Gilles, L.; Lebedinsky, C.; Elsayed, Y.A.; le Cesne, A. Phase I combination study of trabectedin and doxorubicin in patients with soft-tissue sarcoma. *Clin. Cancer Res.* **2008**, *14*, 6656–6662.
15. Pautier, P.; Chevreau, C.; le Cesne, A.; Penel, N.; Bui, B.; Guillemet, C.; Delcambre, C.; Rey, A.; Duffaud, F. LMS-02: A phase II single-arm multicenter study to determine the efficacy of doxorubicin in combination with trabectedin as a 1st line treatment of metastatic and/or locally advanced leiomyosarcoma of uterine (U-LMS) or soft tissue (ST-LMS) origin: Results of the soft tissue group. *Eur. J. Cancer* **2013**, *49*, s3834.
16. Broto, J.M.; Lopez-Pousa, A.; Garcia del Muro, X.; de Las Peñas, R.; Martinez-Trufero, J.; Cruz, J.; Alvarez, R.; Cubedo, R.; Redondo, A.; Poveda, A. Randomized phase II trial of doxorubicin *vs.* trabectedin plus doxorubicin in first line treatment of patients with advanced non-resectable or metastatic soft tissue sarcomas: A Spanish Group for Sarcoma Research (GEIS) study. *Eur. J. Cancer* **2013**, *49*, s3800.
17. Aapro, M.S.; Martin, C.; Hatty, S. Gemcitabine—A safety review. *Anticancer Drugs* **1998**, *9*, 191–201.

Synthesis and Biological Evaluation of Carbocyclic Analogues of Pachastrissamine

Yongseok Kwon, Jayoung Song, Hoon Bae, Woo-Jung Kim, Joo-Youn Lee, Geun-Hee Han, Sang Kook Lee and Sanghee Kim

Abstract: A series of carbocyclic analogues of naturally-occurring marine sphingolipid pachastrissamine were prepared and biologically evaluated. The analogues were efficiently synthesized via a tandem enyne/diene-ene metathesis reaction as a key step. We found that the analogue **4b** exhibited comparable cytotoxicity and more potent inhibitory activity against sphingosine kinases, compared to pachastrissamine. Molecular modeling studies were conducted to provide more detailed insight into the binding mode of **4b** in sphingosine kinase. In our docking model, pachastrissamine and **4b** were able to effectively bind to the binding pocket of sphingosine kinase 1 as co-crystalized sphingosine. However, **4b** showed a hydrophobic interaction with Phe192, which suggests that it contributes to its increased inhibitory activity against sphingosine kinase 1.

Reprinted from *Mar. Drugs*. Cite as: Kwon, Y.; Song, J.; Bae, H.; Kim, W.-J.; Lee, J.-Y.; Han, G.-H.; Lee, S.K.; Kim, S. Synthesis and Biological Evaluation of Carbocyclic Analogues of Pachastrissamine. *Mar. Drugs* **2015**, *13*, 824-837.

1. Introduction

Pachastrissamine (jaspine B, **1**; Figure 1) is a natural anhydrous derivative of phytosphingosine **2**, possessing a tetrahydrofuran core with three contiguous stereogenic centers. It was first isolated by Higa *et al.* from marine sponge *Pachastrissa* sp. in 2002 [1] and subsequently isolated from the Vanuatuan marine sponge *Jaspis* sp. by Debitus *et al.* in 2003 [2]. This marine natural product showed significant cytotoxicity against various cancer cell lines, such as P388, MEL28, A549, HT29 and HeLa [1,3]. It was found to have an inhibitory activity against sphingomyelin synthase, which, in turn, triggers apoptosis in tumor cells via a caspase-dependent pathway [4]. It was also reported that pachastrissamine and its stereoisomers inhibit sphingosine kinases (SphKs) and atypical protein kinase C [5]. Because of its intriguing biological activity, it has been an interesting target for synthetic chemists, and various synthetic routes to pachastrissamine have been reported [6–16]. However, the structure-activity relationship (SAR) of pachastrissamine remains relatively unreported. Génisson *et al.* described analogues with a modified aliphatic chain, which exhibited cytotoxicity comparable to or lower than pachastrissamine on two distinct cancer cell lines (B16 and A375 melanoma cell lines) [17,18]. Delgado *et al.* reported the stereoisomers of pachastrissamine as being 10- to 20-times less potent than the natural one [19]. Recently, Liu *et al.* reported pachastrissamine analogues containing a 1,2,3-triazole ring in the alkyl chain [20]. One analogue showed better increased cytotoxicity than the natural compound. These results suggest that the configuration and aliphatic chain of pachastrissamine would be essential to retain biological activity. The contribution of the tetrahydrofuran ring to its biological profile has been explored. The aza-analogues of pachastrissamine **3a** were reported by Génisson *et al.* [21], and the

sulfur and selenium analogues **3b**–**c** were previously reported by our group [22]. They exhibited comparable potency to natural pachastrissamine, indicating that the ring oxygen atom of pachastrissamine could be replaced with bioisosteres.

In this regard, we designed carbocyclic analogues, replacing the ethereal oxygen (–O–) with a methylene group (–CH_2–) as a divalent bioisostere [23]. The advantages of carbocyclic analogues of natural product have already been demonstrated by several successful examples, such as carbasugars and carbocyclic nucleosides [24,25]. As seen in these successful precedents, we expected that the carbocyclic analogue would show enhanced chemical and metabolic stability compared to the parent natural product. In addition, from this study, we would be able to decipher the SAR involved in the role of ethereal oxygen, which is valuable information in the development of new anti-cancer therapeutic agents. Herein, we report the synthesis and biological evaluation of a series of carbocyclic pachastrissamine analogues **4** (Figure 1) in which the alkyl-chain lengths have been varied.

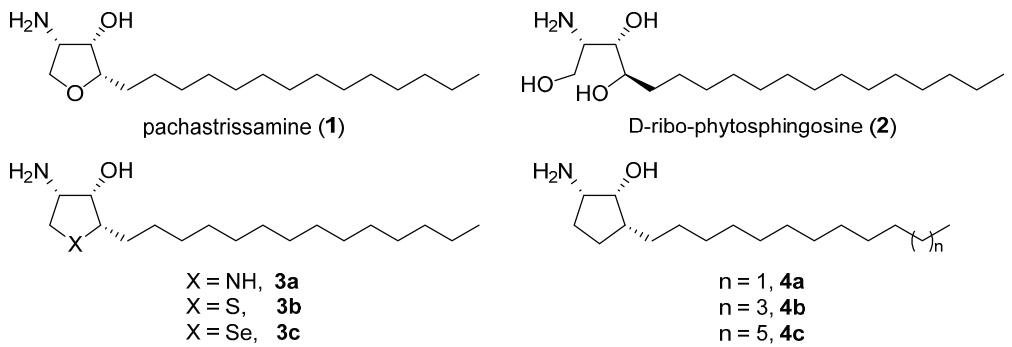

Figure 1. Chemical structures of Compounds **1**–**4**.

2. Results and Discussion

2.1. Chemistry

2.1.1. Retrosynthetic Analysis

Our retrosynthetic plan for the synthesis of **4** is shown in Scheme 1. The designed analogues **4** would be accessed from diene **5** using catalytic hydrogenation and hydrolysis. We expected catalytic hydrogenation of **5** would occur from the convex face of the bicyclic system to afford the desired stereochemistry [6]. The requisite diene **5** would be derived from the ring-closing metathesis (RCM) of enyne **6** and subsequent cross-metathesis (CM) between the resulting diene and the appropriate olefin in a tandem fashion [26–29]. Substrate **6** would be derived from a known amide **7**, which, in turn, can be easily prepared from commercially available (*S*)-allylglycine.

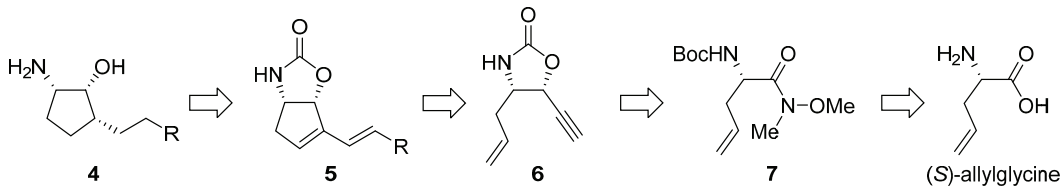

Scheme 1. Retrosynthetic plan.

2.1.2. Synthesis

Our synthesis, as shown in Scheme 2, commenced with the preparation of a known Weinreb amide **7** from commercially available (*S*)-allylglycine in two steps using a previously reported procedure [30]. Treatment of amide **7** with lithium acetylide in THF yielded ynone **8** in a 71% yield. The stereoselective reduction of ynone **8** was explored with various hydride reagents. After several trials, it was found that the treatment of **8** with sodium borohydride and cerium chloride at low temperature gave an inseparable diastereomeric mixture of alcohol **9** with the best selectivity (diastereomeric ratio = 6:1) in 87% yield. The obtained alcohol **9** was treated with lithium hexamethyldisilazide in hot toluene to provide oxazolidinone **10** in a high yield (90%). At this stage, both diastereomers (**10a** and **10b**) were separated via column chromatography, and the relative configuration of the diastereomers was assigned by a 2D-NOESY experiment (Figures S7 and S10 in the Supplementary Materials). The triisopropylsilyl group of major diastereomer **10a** was easily removed with tetrabutylammonium fluoride to give the terminal acetylene **6** in a 95% yield.

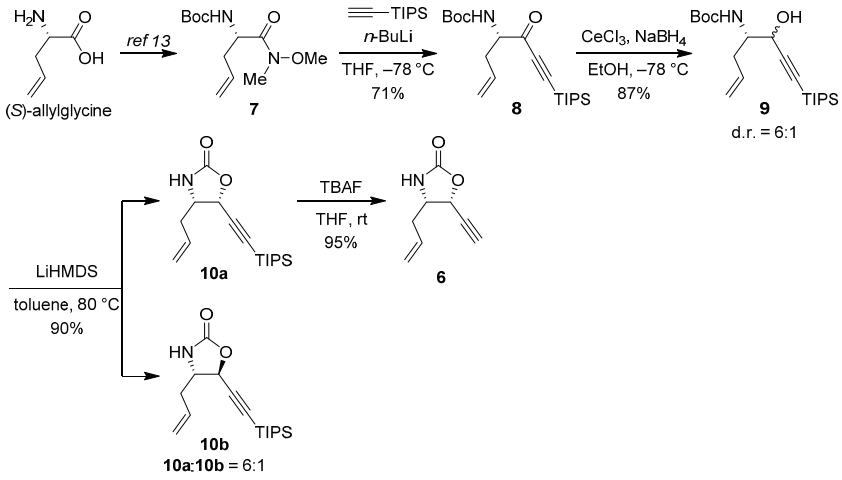

Scheme 2. Synthesis of enyne **6**. TIPS: triisopropylsilyl; LiHMDS: lithium hexamethyldisilazide; TBAF: tetrabutylammonium fluoride.

With the terminal enyne **6** in hand, the tandem enyne/diene-ene metathesis reaction was carried out (Scheme 3). The reaction of **6** with the appropriate alkenes in the presence of second-generation

Grubbs catalyst (3 mol%) afforded the desired diene **5a–c** with exclusive (*E*)-geometry. The catalytic hydrogenation of diene **5a–c** was accomplished to give cyclopentane **11a–c** as the only stereoisomers detected by ^{1}H NMR. Finally, hydrolysis of the oxazolidinone with KOH in refluxing EtOH afforded the desired carbocyclic analogues, **4a–c**.

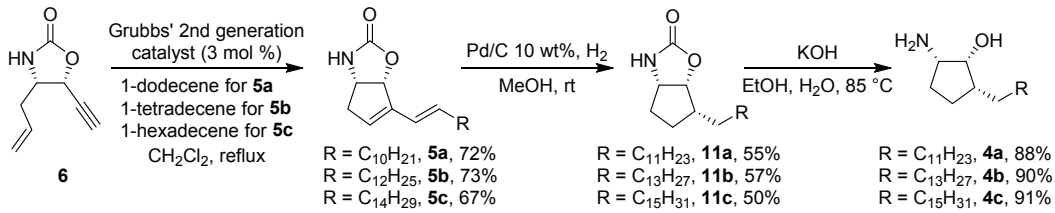

Scheme 3. Synthesis of carbocyclic analogues, **4a–c**.

2.2. Biological Evaluation

2.2.1. Cell Viability

The cytotoxic activity of analogues **4a–c** was examined in various cancer cell lines (Table 1) by the sulforhodamine B (SRB) assay [31]. For a direct comparison, natural pachastrissamine (**1**) was employed as a positive control. It was found that the cytotoxic activities of carbocyclic analogues **4** were influenced by the length of the alkyl chain. The analogue, **4b**, which has the same chain length as pachastrissamine, exhibited a comparable potency to the parent natural product, **1**, against various cell lines. However, both the shorter and longer chain analogues, **4a** and **4c**, were less effective than pachastrissamine.

Table 1. Cytotoxic activity of pachastrissamine (**1**) and its carbocyclic analogues, **4a–c**.

Compound	IC_{50} (μM) [a]				
	HCT-116 [b]	SNU-638 [c]	MDA-MB-231 [d]	PC-3 [e]	Caki-1 [f]
1	1.0	1.2	0.7	0.7	1.7
4a	9.7	12.8	6.1	7.6	12.1
4b	1.0	1.7	1.8	1.0	3.2
4c	3.2	4.4	4.1	3.1	6.6

[a] 50% inhibition concentration; [b] HCT-116, human colon cancer cell line; [c] SNU-638, human stomach cancer cell line; [d] MDA-MB-231, human breast cancer cell line; [e] PC-3, human prostate cancer cell line; [f] Caki-1, human renal cancer cell line.

2.2.2. Inhibitory Activity against Sphingosine Kinases

Because pachastrissamine was reported as an inhibitor of sphingosine kinases (SphKs), the inhibitory activity of analogues **4** against SphKs were examined using a sphingosine kinase inhibition assay (Table 2). There are two isoforms of mammalian SphKs (SphK1 and SphK2) catalyzing the phosphorylation of sphingosine to sphingosine 1-phosphate (S1P). S1P regulates

diverse cellular processes, including cell growth, survival and differentiation [32]. In our experiments, *N*,*N*-dimethylsphingosine (DMS), as well as pachastrissamine (**1**) were used as a positive control [33]. It was revealed that the inhibitory activity of **4** against SphKs was influenced by the length of the attached chain. The analogue **4b** showed a similar inhibitory activity to DMS, which, in turn, was more effective than **1**. However, the other analogues, **4a** and **4c**, were found to be less effective at the inhibition of SphKs. These results suggest that the ring oxygen atom of pachastrissamine is dispensable, but the appropriate chain length is apparently required to retain its biological properties.

Table 2. Inhibitory activity of pachastrissamine (**1**) and its carbocyclic analogues, **4a**–**c**, against sphingosine kinases.

Compound	IC_{50} (μM) [a]	
	SphK1	SphK2
1	12.0	41.8
4a	58.2	>100
4b	7.5	20.1
4c	41.3	>100
DMS [b]	6.6	19.9

[a] 50% inhibition concentration; [b] *N*,*N*-dimethylsphingosine.

2.3. Molecular Modeling

To understand the molecular interaction between **4b** and the sphingosine kinase, a molecular modeling study was performed using the crystal structure of human SphK1 in complex with sphingosine (PDB Code 3VZB) [34]. As shown in Figure 2, pachastrissamine (**1**) and its carbocyclic analogue **4b** are able to effectively bind to the binding pocket of SphK1 in virtually the same pose. They occupy nearly the same position as sphingosine. In our docking model, the alkyl chain of **4b** is buried in the hydrophobic J-shaped tunnel constituted of hydrophobic residues Leu268, Ala274, His311, Phe173, Phe303, Val177 and Phe192. The hydroxyl group forms a hydrogen bond with Asp178 and a water-mediated hydrogen bond with Ser168, in the same manner as the 3-hydroxyl group of sphingosine. The amino group makes a hydrogen bond interaction with Ser168. In the hydrophilic recognition site, pachastrissamine (**1**) and its analogue **4b** formed the same set of hydrogen bonds. However, carbocyclic analogue **4b** exhibits an additional interaction with the hydrophobic residue, Phe192 (Figure 2B). This pi-alkyl interaction seems to contribute to the increased activity of **4b** toward SphK1 compared to **1** [35].

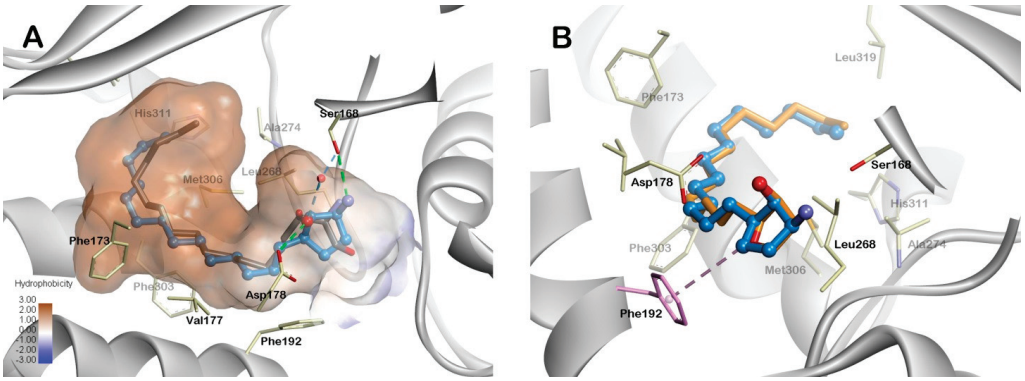

Figure 2. Docking model of the carbocyclic analogue **4b** and pachastrissamine (**1**). (**A**) The overlay of the proposed binding model of carbocyclic analogue **4b** (blue) and X-ray complex sphingosine (gray). A water molecule is shown as a red sphere. The direct H-bonds and water-mediated H-bonds are shown as green and blue dashed lines, respectively. The ligand binding surface of the binding pocket was colored according to hydrophobicity (brown: hydrophobic, blue: hydrophilic); (**B**) The overlay of the proposed binding model of **4b** (blue) and **1** (orange). Hydrophobic interaction with Phe192 is shown as a pink dashed line.

3. Experimental Section

3.1. Chemistry

3.1.1. General

All chemicals were reagent grade and used as purchased. All reactions were performed under an inert atmosphere of dry nitrogen using distilled dry solvents. Reactions were monitored through thin layer chromatography (TLC) analysis using silica gel 60 F-254 thin layer plates. Compounds were visualized on the TLC plates under UV light and by spraying with either $KMnO_4$ or anisaldehyde staining solutions. Flash column chromatography was conducted on silica gel 60 (230–400 mesh). Melting points were measured using a Buchi B-540 melting point apparatus without correction. ^{1}H NMR (400, 500 or 600 MHz) and ^{13}C NMR (100, 125 or 150 MHz) spectra were recorded in δ units relative to the deuterated solvent. The IR spectra were measured on a Fourier transform infrared spectrometer. High-resolution mass spectra (HRMS) were recorded using FAB.

3.1.2. *tert*-Butyl (*S*)-(5-oxo-7-(triisopropylsilyl)hept-1-en-6-yn-4-yl)carbamate (**8**)

To a solution of (triisopropylsilyl)acetylene (17.4 mL, 77.4 mmol) in THF (80 mL) was added *n*-BuLi (48.4 mL, 77.4 mmol, 1.6 M solution in hexane) at −78 °C under nitrogen. After the reaction mixture was stirred for 30 min at −78 °C, known amide **7** (10 g, 38.7 mmol) in dry THF (20 mL) was added at 0 °C. The reaction mixture was stirred for 1.5 h at 0 °C. The reaction was quenched with a saturated NH_4Cl aqueous solution and extracted with EtOAc. The organic layer

was washed twice with brine, dried over $MgSO_4$, filtered and concentrated. The crude product was purified using column chromatography on silica gel (hexane/EtOAc, 20:1), to afford the desired ynone **8** (10.4 g, 71%) as a yellow oil. $[\alpha]_D^{20}$ +8.20 (c 1.0, $CHCl_3$); ^{1}H NMR (400 MHz, $CDCl_3$) δ 5.70–5.61 (m, 1H), 5.13 (d, *J* = 17.2 Hz, 1H), 5.12 (d, *J* = 9.2 Hz, 1H), 5.10 (brs, 1H), 4.48 (d, *J* = 5.7 Hz, 1H), 2.70–2.59 (m, 2H), 1.42 (s, 9H), 1.17–1.01 (m, 21H); ^{13}C NMR (100 MHz, $CDCl_3$) δ 185.4, 155.1, 131.7, 119.5, 102.2, 100.1, 80.0, 60.8, 36.0, 28.3 (3C), 18.5 (6C), 11.0 (3C); IR ($CHCl_3$) ν_{max} 3358, 2947, 2869, 2150, 1719, 1682, 1495, 1368, 1171 (cm^{-1}); HRMS (FAB) calcd. for $C_{21}H_{38}NO_3Si$ ($[M + H]^+$), 380.2621; found, 380.2614.

3.1.3. *tert*-Butyl ((4*S*)-5-hydroxy-7-(triisopropylsilyl)hept-1-en-6-yn-4-yl)carbamate (**9**)

To a solution of ynone **8** (10 g, 26.3 mmol) in EtOH (100 mL) was added anhydrous $CeCl_3$ (13 g, 52.6 mmol) at room temperature under nitrogen. After the reaction mixture was stirred for 15 min, $NaBH_4$ (2.0 g, 52.6 mmol) was added at −78 °C. The reaction mixture was stirred for 3 h at −78 °C. The reaction was quenched with a saturated NH_4Cl aqueous solution and extracted with EtOAc. The organic layer was washed twice with brine, dried over $MgSO_4$, filtered and concentrated. The crude product was purified using column chromatography on silica gel (hexane/EtOAc, 5:1), to afford the desired alcohol **9** (8.7 g, 87%) as a diastereomeric mixture (6:1) as a colorless oil. $[\alpha]_D^{20}$ −18.3 (c 1.0, $CHCl_3$); ^{1}H NMR (400 MHz, $CDCl_3$) δ 5.82–5.72 (m, 1H), 5.08 (d, *J* = 15.2 Hz, 1H), 5.06 (d, *J* = 8.9 Hz, 1H), 4.74–4.72 (m, 0.85H), 4.45–4.44 (m, 1H), 3.82 (brs, 0.85H), 3.72 (brs, 0.15H), 3.38 (brs, 0.85H), 2.56–2.46 (m, 0.15H), 2.42–2.22 (m, 1.85H), 1.40 (s, 9H), 1.04 (s, 21H); ^{13}C NMR (100 MHz, $CDCl_3$) δ 156.5, 134.0, 118.0, 105.2, 87.6, 79.9, 66.1, 55.1, 35.7, 28.2 (3C), 18.5 (6C), 11.1 (3C); IR ($CHCl_3$) ν_{max} 3428, 2945, 2868, 2170, 1696, 1504, 1170 (cm^{-1}); HRMS (FAB) calcd. for $C_{21}H_{40}NO_3Si$ ($[M + H]^+$), 382.2777; found, 382.2770.

3.1.4. (4*S*)-4-Allyl-5-((triisopropylsilyl)ethynyl)oxazolidin-2-one (**10**)

To a solution of alcohol **9** (8 g, 21 mmol) in toluene (100 mL) was added lithium hexamethyldisilazide (46.2 mL, 46.2 mmol, 1 M solution in THF) at room temperature under nitrogen. After stirring for 1.5 h at 80 °C, the reaction mixture was cooled to 0 °C. The reaction was quenched with a saturated NH_4Cl aqueous solution and extracted with EtOAc. The organic layer was washed twice with brine, dried over $MgSO_4$, filtered and concentrated. The crude product was purified using column chromatography on silica gel (hexane/EtOAc, 1.5:1), to afford the desired oxazolidinone **10a** (5.0 g, 77%) and **10b** (850 mg, 13%).

(4*S*,5*R*)-4-Allyl-5-((triisopropylsilyl)ethynyl)oxazolidin-2-one (**10a**): a white solid; m.p. 91.2–93.3 °C; $[\alpha]_D^{20}$ −4.12 (c 0.35, $CHCl_3$); ^{1}H NMR (400 MHz, $CDCl_3$) δ 5.80–5.72 (m, 1H), 5.33–5.31 (d, *J* = 7.8 Hz, 1H), 5.20 (d, *J* = 10.4 Hz, 1H), 5.19 (d, *J* = 16.8 Hz, 1H), 5.17 (brs, 1H), 3.88 (td, *J* = 4.1 Hz, 8.6 Hz, 1H), 2.59–2.53 (m, 1H), 2.44–2.36 (m, 1H), 1.07 (s, 21H); ^{13}C NMR (100 MHz, $CDCl_3$) δ 159.6, 132.7, 119.8, 98.5, 93.5, 70.1, 54.1, 36.8, 18.5 (6C), 11.0 (3C); IR ($CHCl_3$) ν_{max} 3276, 2946, 2868, 1759, 1464, 1334, 1048, 758, 676 (cm^{-1}); HRMS (FAB) calcd. for $C_{17}H_{30}NO_2Si$ ($[M + H]^+$), 308.2046; found, 308.2039.

(4*S*,5*S*)-4-Allyl-5-((triisopropylsilyl)ethynyl)oxazolidin-2-one (**10b**): a yellow oil; $[\alpha]_D^{20}$ −36.2 (c 1.4, $CHCl_3$); ^1H NMR (600 MHz, $CDCl_3$) δ 6.12 (d, *J* = 9.2 Hz, 1H), 5.77–5.70 (m, 1H), 5.19 (d, *J* = 11.5 Hz, 1H), 5.18 (d, *J* = 16.1 Hz, 1H), 4.80 (d, *J* = 6.4 Hz, 1H), 3.87 (q, *J* = 6.4 Hz, 1H), 2.40 (q, *J* = 6.7 Hz, 1H), 2.33 (q, *J* = 7.1 Hz, 1H), 1.05 (s, 21H); ^{13}C NMR (150 MHz, $CDCl_3$) δ 158.2, 131.5, 119.8, 101.7, 90.8, 70.9, 59.2, 38.7, 18.5 (6C), 11.0 (3C); IR ($CHCl_3$) ν_{max} 3282, 2946, 2869, 1760, 1464, 1323, 1071, 992, 883, 675 (cm^{-1}); HRMS (FAB) calcd. for $C_{17}H_{30}NO_2Si$ ($[M + H]^+$), 308.2046; found, 308.2042.

3.1.5. (4*S*,5*R*)-4-Allyl-5-ethynyloxazolidin-2-one (**6**)

To a solution of alcohol **10a** (4.0 g, 13.0 mmol) in THF (60 mL) was added tetrabutylammonium fluoride (15.6 mL, 15.6 mmol, 1 M solution in THF) at room temperature under nitrogen. The reaction mixture was stirred for 1 h at room temperature. The reaction was quenched with a saturated NH_4Cl aqueous solution and extracted with EtOAc. The organic layer was washed twice with brine, dried over $MgSO_4$, filtered and concentrated. The crude product was purified using column chromatography on silica gel (hexane/EtOAc, 1:1), to afford the desired terminal acetylene **6** (1.87 g, 95%) as a white solid. m.p. 42.0–44.0 °C; $[\alpha]_D^{20}$ −6.32 (c 0.54, $CHCl_3$); ^1H NMR (400 MHz, $CDCl_3$) δ 5.81–5.70 (m, 1H), 5.28 (dd, *J* = 2.2 Hz, 7.8 Hz, 2H), 5.22 (d, *J* = 0.7 Hz, 1H), 5.19–5.18 (m, 1H), 3.91 (td, *J* = 4.1 Hz, 8.6 Hz, 1H) 2.72 (d, *J* = 2.1 Hz, 1H), 2.58–2.52 (m, 1H), 2.44–2.36 (m, 1H); ^{13}C NMR (150 MHz, $CDCl_3$) δ 157.2, 132.4, 120.0, 79.0, 75.8, 69.3, 53.9, 36.5; IR ($CHCl_3$) ν_{max} 3292, 2128, 1755, 1644, 1338, 1243, 1041 (cm^{-1}); HRMS (FAB) calcd. for $C_8H_{10}NO_2$ ($[M + H]^+$), 152.0712; found, 152.0714.

3.1.6. General Procedure for the Preparation of **5**

To a solution of **6** (300 mg, 2.0 mmol) with the appropriate alkene (2 mL) in CH_2Cl_2 (20 mL) was added Grubbs' second-generation catalyst (50 mg, 0.059 mmol) at room temperature. The resulting mixture was refluxed for 20 h. After the mixture was cooled to room temperature, the solvent was removed under reduced pressure. The crude product was purified by column chromatography on silica gel (hexane/EtOAc, 1:3) to give diene **5**.

3.1.7. (3a*S*,6a*R*)-6-((*E*)-Dodec-1-en-1-yl)-3,3a,4,6a-tetrahydro-2*H*-cyclopenta[*d*]oxazol-2-one (**5a**)

A white solid (420 mg, 72%); m.p. 83.6–84.5 °C; $[\alpha]_D^{20}$ +23.7 (c 1.1, $CHCl_3$); ^1H NMR (500 MHz, $CDCl_3$) δ 6.12 (d, *J* = 16.0 Hz, 1H), 5.94 (td, *J* = 7.4 Hz, 15.2 Hz, 1H), 5.68 (s, 1H), 5.63 (brs, 1H), 5.59 (d, *J* = 7.8 Hz, 1H), 4.44 (t, *J* = 7.2 Hz, 1H), 2.71 (dd, *J* = 6.1 Hz, 18.1 Hz, 1H), 2.47 (d, *J* = 18.2 Hz, 1H), 2.15–2.02 (m, 2H), 1.40–1.35 (m, 2H), 1.24 (s, 14H), 0.86 (t, *J* = 6.9 Hz, 3H); ^{13}C NMR (125 MHz, $CDCl_3$) δ 158.9, 139.8, 135.0, 128.8, 123.0, 84.9, 53.7, 40.2, 33.1, 31.9, 29.62, 29.58, 29.48, 29.33, 29.25, 29.0, 22.7, 14.1; IR ($CHCl_3$) ν_{max} 3270, 2922, 2854, 1739, 1716, 1385, 1238, 1018, 756 (cm^{-1}); HRMS (FAB) calcd. for $C_{18}H_{30}NO_2$ ($[M + H]^+$), 292.2277; found, 292.2279.

3.1.8. (3a*S*,6a*R*)-6-((*E*)-Tetradec-1-en-1-yl)-3,3a,4,6a-tetrahydro-2*H*-cyclopenta[*d*]oxazol-2-one (**5b**)

A white solid (466 mg, 73%); m.p. 93.1–94.5 °C; $[\alpha]_D^{20}$ +33.0 (c 0.43, $CHCl_3$); ^1H NMR (400 MHz, $CDCl_3$) δ 6.12 (d, *J* = 15.9 Hz, 1H), 5.94 (td, *J* = 7.3 Hz, 15.1 Hz, 1H), 5.68 (s, 1H), 5.59 (d, *J* = 7.7 Hz, 1H), 5.51 (brs, 1H), 4.44 (t, *J* = 7.1 Hz, 1H), 2.72 (dd, *J* = 6.0 Hz, 18.3 Hz, 1H), 2.47 (d, *J* = 18.2 Hz, 1H), 2.13–2.04 (m, 2H), 1.40–1.37 (m, 2H), 1.24 (s, 18H), 0.86 (t, *J* = 6.7 Hz, 3H); ^{13}C NMR (100 MHz, $CDCl_3$) δ 158.8, 139.8, 135.1, 128.7, 123.0, 84.9, 53.7, 40.2, 33.1, 31.9, 29.7 (2C), 29.64, 29.58, 29.48, 29.35, 29.3, 29.0, 22.7, 14.1; IR ($CHCl_3$) ν_{max} 3244, 2917, 2852, 1735, 1471, 1386, 1248, 1016, 716 (cm^{-1}); HRMS (FAB) calcd. for $C_{20}H_{34}NO_2$ ($[M + H]^+$), 320.2590; found, 320.2584.

3.1.9. (3a*S*,6a*R*)-6-((*E*)-Hexadec-1-en-1-yl)-3,3a,4,6a-tetrahydro-2*H*-cyclopenta[*d*]oxazol-2-one (**5c**)

A white solid (466 mg, 67%); m.p. 90.1–91.6 °C; $[\alpha]_D^{20}$ +38.4 (c 0.95, $CHCl_3$); ^1H NMR (600 MHz, $CDCl_3$) δ 6.12 (d, *J* = 16.0 Hz, 1H), 5.94 (td, *J* = 7.4 Hz, 15.3 Hz, 1H), 5.86 (brs, 1H), 5.68 (s, 1H), 5.59 (d, *J* = 8.2 Hz, 1H), 4.44 (t, *J* = 7.1 Hz, 1H), 2.70 (dd, *J* = 6.4 Hz, 17.9 Hz, 1H), 2.47 (d, *J* = 18.3 Hz, 1H), 2.15–2.02 (m, 2H), 1.39–1.34 (m, 2H), 1.24 (s, 22H), 0.86 (t, *J* = 7.1 Hz, 3H); ^{13}C NMR (150 MHz, $CDCl_3$) δ 159.0, 139.8, 135.0, 128.9, 123.0, 84.9, 53.8, 40.2, 33.1, 31.9, 29.67 (3C), 29.64 (2C), 29.58, 29.48, 29.35, 29.26, 29.0, 22.7, 14.1; IR ($CHCl_3$) ν_{max} 3284, 2922, 2853, 1737, 1716, 1385, 1237, 1015 (cm^{-1}); HRMS (FAB) calcd. for $C_{22}H_{38}NO_2$ ($[M + H]^+$), 348.2903; found, 348.2905.

3.1.10. General Procedure for the Preparation of **11**

To a solution of diene **5** (0.72 mmol) in MeOH (30 mL) was added Pd/C (40 mg, 10 wt.% Pd) at room temperature. The reaction mixture was shaken in a Parr hydrogenator for 10 h at an initial pressure of 35 psi. The catalyst was filtered off with Celite® (OCI Company Ltd., Seoul, Korea), and the solvent was removed under reduced pressure. The crude product was purified by column chromatography on silica gel (hexane/EtOAc, 1:3) to give the desired product, **11**.

3.1.11. (3a*S*,6*R*,6a*R*)-6-Dodecylhexahydro-2*H*-cyclopenta[*d*]oxazol-2-one (**11a**)

A white solid (117 mg, 55%). m.p. 67.8–69.1 °C; $[\alpha]_D^{20}$ +10.6 (c 0.50, $CHCl_3$); ^1H NMR (400 MHz, $CDCl_3$) δ 5.71 (brs, 1H), 4.88 (t, *J* = 6.1 Hz, 1H), 4.22 (t, *J* = 6.5 Hz, 1H), 1.76–1.69 (m, 3H), 1.63–1.55 (m, 2H), 1.53–1.39 (m, 2H), 1.23 (s, 20H), 0.86 (t, *J* = 6.7 Hz, 3H); ^{13}C NMR (100 MHz, $CDCl_3$) δ 160.1, 83.2, 56.6, 46.0, 33.8, 31.9, 29.8, 29.62 (4C), 29.56, 29.3, 28.4, 28.2, 28.0, 22.7, 14.1; IR ($CHCl_3$) ν_{max} 3306, 2923, 2854, 1736, 1713, 1423, 1242 (cm^{-1}); HRMS (FAB) calcd. for $C_{18}H_{34}NO_2$ ($[M + H]^+$), 296.2590; found, 296.2588.

3.1.12. (3a*S*,6*R*,6a*R*)-6-Tetradecylhexahydro-2*H*-cyclopenta[*d*]oxazol-2-one (**11b**)

A white solid (127 mg, 57%). m.p. 88.7–89.6 °C; $[\alpha]_D^{20}$ +8.56 (c 0.52, $CHCl_3$); ^1H NMR (400 MHz, $CDCl_3$) δ 5.59 (brs, 1H), 4.88 (t, *J* = 6.1 Hz, 1H), 4.23 (t, *J* = 6.5 Hz, 1H), 1.77–1.70 (m, 3H), 1.60–1.54 (m, 2H), 1.48–1.42 (m, 2H), 1.23 (s, 24H), 0.86 (t, *J* = 6.8 Hz, 3H); ^{13}C NMR (100 MHz, $CDCl_3$) δ 160.0, 83.2, 56.6, 46.1, 33.9, 31.9, 29.8, 29.67 (3C), 29.64 (3C), 29.57, 29.3, 28.4, 28.3, 28.0, 22.7, 14.1; IR ($CHCl_3$) ν_{max} 3255, 2919, 2852, 1723, 1469, 1248 (cm^{-1}); HRMS (FAB) calcd. for $C_{20}H_{38}NO_2$ ($[M + H]^+$), 324.2903; found, 324.2903.

3.1.13. (3a*S*,6*R*,6a*R*)-6-Hexadecylhexahydro-2*H*-cyclopenta[*d*]oxazol-2-one (**11c**)

A white solid (122 mg, 50%). m.p. 91.9–92.1 °C; $[\alpha]_D^{20}$ +7.91 (c 0.46, $CHCl_3$); ^1H NMR (400 MHz, $CDCl_3$) δ 5.51 (brs, 1H), 4.89 (t, *J* = 6.1 Hz, 1H), 4.23 (t, *J* = 6.5 Hz, 1H), 1.77–1.70 (m, 3H), 1.61–1.55 (m, 2H), 1.48–1.40 (m, 2H), 1.23 (s, 28H), 0.86 (t, *J* = 6.8 Hz, 3H); ^{13}C NMR (100 MHz, $CDCl_3$) δ 159.9, 83.2, 56.6, 46.1, 33.9, 31.9, 29.8, 29.68 (5C), 29.65 (3C), 29.58, 29.3, 28.4, 28.3, 28.0, 22.7, 14.1; IR ($CHCl_3$) ν_{max} 3262, 2918, 2851, 1725, 1469, 1245 (cm^{-1}); HRMS (FAB) calcd. for $C_{22}H_{42}NO_2$ ($[M + H]^+$), 352.3216; found, 352.3216.

3.1.14. General Procedure for the Preparation of **4**

To a solution of **11** (0.071 mmol) in EtOH (1 mL) was added 1 M aq KOH (1 mL) at room temperature. The reaction mixture was stirred for 20 h at 85 °C. After the reaction mixture was cooled to room temperature, the solvent was removed under reduced pressure. The crude product was purified by column chromatography on silica gel (CH_2Cl_2/MeOH/NH_4OH, 100:10:1) to give the desired product, **4**.

3.1.15. (1*R*,2*S*,5*R*)-2-Amino-5-dodecylcyclopentan-1-ol (**4a**)

A white solid (17 mg, 88%). m.p. 93.2–96.2 °C; $[\alpha]_D^{20}$ +3.96 (c 0.36, EtOH); ^1H NMR (400 MHz, $CDCl_3$) δ 3.68 (t, *J* = 3.5 Hz, 1H), 3.30 (td, *J* = 3.8 Hz, 8.4 Hz, 1H), 2.10 (brs, 2H), 1.91–1.86 (m, 1H), 1.74–1.66 (m, 2H), 1.56–1.34 (m, 1H), 1.23 (s, 23H), 0.86 (t, *J* = 6.8 Hz, 3H); ^{13}C NMR (100 MHz, $CDCl_3$) δ 74.4, 55.4, 44.2, 31.9, 30.9, 29.95, 29.93, 29.68 (3C), 29.64, 29.3, 28.5, 28.0, 22.7, 14.1; IR ($CHCl_3$) ν_{max} 3054, 2922, 2852, 2727, 1469, 992 (cm^{-1}); HRMS (FAB) calcd. for $C_{17}H_{36}NO$ ($[M + H]^+$), 270.2797; found, 270.2794.

3.1.16. (1*R*,2*S*,5*R*)-2-Amino-5-tetradecylcyclopentan-1-ol (**4b**)

A white solid (19 mg, 90%). m.p. 100.1–101.0 °C; $[\alpha]_D^{20}$ +3.29 (c 0.25, EtOH); ^1H NMR (400 MHz, $CDCl_3$) δ 3.70 (t, *J* = 3.4 Hz, 1H), 3.30 (td, *J* = 3.9 Hz, 8.5 Hz, 1H), 2.44 (brs, 3H), 1.91–1.85 (m, 1H), 1.75–1.65 (m, 2H), 1.54–1.34 (m, 1H), 1.23 (s, 27H), 0.86 (t, *J* = 6.8 Hz, 3H); ^{13}C NMR (100 MHz, $CDCl_3$) δ 74.4, 55.4, 44.1, 31.9, 30.8, 30.0, 29.9, 29.69 (5C), 29.65 (2C), 29.3, 28.5, 28.0, 22.7, 14.1; IR ($CHCl_3$) ν_{max} 3049, 2921, 2852, 2729, 1469, 994 (cm^{-1}); HRMS (FAB) calcd. for $C_{19}H_{40}NO$ ($[M + H]^+$), 298.3110; found, 298.3117.

3.1.17. (1*R*,2*S*,5*R*)-2-Amino-5-hexadecylcyclopentan-1-ol (**4c**)

A white solid (21 mg, 91%). m.p. 102.1–103.0 °C; $[\alpha]_D^{20}$ +1.89 (c 0.51, $CHCl_3$); ^1H NMR (400 MHz, $CDCl_3$) δ 3.70 (t, *J* = 3.5 Hz, 1H), 3.30 (td, *J* = 3.8 Hz, 8.2 Hz, 1H), 2.41 (brs, 3H), 1.89–1.85 (m, 1H), 1.75–1.65 (m, 2H), 1.54–1.34 (m, 1H), 1.23 (s, 31H), 0.86 (t, *J* = 6.8 Hz, 3H); ^{13}C NMR (100 MHz, $CDCl_3$) δ 74.5, 55.5, 44.2, 31.9, 30.9, 30.0, 29.9, 29.69 (7C), 29.65 (2C), 29.4, 28.5, 28.0, 22.7, 14.1; IR ($CHCl_3$) ν_{max} 3057, 2921, 2852, 2728, 1468, 995 (cm^{-1}); HRMS (FAB) calcd. for $C_{21}H_{44}NO$ ($[M + H]^+$), 326.3423; found, 326.3433.

3.2. Biological Evaluation

3.2.1. Sulforhodamine B (SRB) Assay

Cells (5×10^4 cells/mL) were treated with various concentrations of test compounds in 96-well culture plates for 72 h. After incubation, cells were fixed with 10% trichloroacetic acid (TCA), dried and stained with 0.4% SRB in 1% acetic acid. The unbound dye was washed out, and the stained cells were dried and resuspended in 10 mM Tris (pH 10.0). The absorbance at 515 nm was measured, and cell proliferation was determined as follows: cell proliferation (%) = (average $absorbance_{compound}$ − average $absorbance_{day\ zero}$)/(average $absorbance_{control}$ − average $absorbance_{day\ zero}$) × 100. IC_{50} values were calculated by nonlinear regression analysis using TableCurve 2D v5.01 (Systat Software Inc., Richmond, CA, USA).

3.2.2. Sphingosine Kinase Inhibition Assay

In 384-well polystyrene plates, Sphk1 and Sphk2 (BPS Bioscience, San Diego, CA, USA) were incubated in kinase buffer (5 mM MOPS, pH 7.2, 2.5 mM β-glycerol-phosphate, 5 mM $MgCl_2$, 1 mM EGTA, 0.4 mM EDTA, 0.5 mM DTT) containing 1 μM sphingosine, ATP (50 μM for SphK1; 150 μM for SphK2) and test compounds with a final concentration of 1% DMSO for 1 h at room temperature. The amount of ATP transferred was measured with the ADP-Glo™ kinase assay kit (Catalog #V9101, Promega, Madison, WI, USA) according to the manufacturer's instructions. IC_{50} values were calculated using GraphPad Prism 5 software (GraphPad Software Inc., La Jolla, CA, USA).

3.3. Molecular Modeling

To understand the binding mode of the pachastrissamine and its analogue, we performed a flexible docking study using the Schrödinger Glide program with standard precision settings (Schrödinger, LLC, New York, NY, USA, http://www.schrodinger.com). The X-ray crystal structure of the human SphK1 (PDB Code 3VZB) was obtained from the Protein Data Bank (PDB, [36]). The pachastrissamine and **4b** were minimized using a Merck Molecular Force Field (MMFF) with a dielectric constant of 80.0 using the MacroModel program suite. The initial structure of pachastrissamine and **4b** were built based on the sphingosine structure co-crystallized with SphK1. The best docking result was visualized using Discovery Studio 4.1 (Accelrys

Software, Inc., San Diego, CA, USA). The hydrogen bonding interactions were displayed as green dashed lines between the ligand and the SphK1.

4. Conclusions

We have reported the synthesis and biological evaluation of the carbocyclic analogues of pachastrissamine with varying chain lengths. The designed carbocyclic analogues were efficiently synthesized in good overall yield by the tandem ene/yne-ene metathesis as a key step. Among them, the analogue **4b** exhibits comparable cytotoxic activity and more potent inhibitory activity against sphingosine kinases, compared to the parent natural product. In our docking model, **4b** showed an additional interaction caused by the adjacent hydrophobic amino acid residue, which could explain its increased inhibitory activity. These results imply that bioisosteric replacement of the ethereal oxygen in the cyclic core to the methylene carbon is possible. Our findings are valuable in the development of sphingosine kinase inhibitors, which may lead to the development of promising new anti-cancer therapeutic agents. Further studies toward the biochemical and pharmacological properties of the carbocyclic analogue, based on these findings, are worthy of pursuing in the future.

Acknowledgments

This work was supported by the Mid-Career Researcher Program (No. 2013R1A2A1A01015998) of the National Research Foundation of Korea (NRF) grant funded by the Korean government (MSIP). This work was also supported by an NRF (National Research Foundation of Korea) grant funded by the Korean Government (NRF-2012-Fostering Core Leaders of the Future Basic Science Program).

Author Contributions

Yongseok Kwon, Hoon Bae and Geun-Hee Han performed the synthetic experiments. Jayoung Song and Sang Kook Lee performed the biological experiments. Joo-Youn Lee performed the molecular modeling. Yongseok Kwon, Woo-Jung Kim and Sanghee Kim wrote the manuscript. Sanghee Kim designed and developed the study.

Conflicts of Interest

The authors declare no conflict of interest.

References

1. Kuroda, I.; Musman, M.; Ohtani, I.I.; Ichiba, T.; Tanaka, J.; Gravalos, D.G.; Higa, T. Pachastrissamine, a cytotoxic anhydrophytosphingosine from a marine sponge, *Pachastrissa* sp. *J. Nat. Prod.* **2002**, *65*, 1505–1506.

2. Ledroit, V.; Debitus, C.; Lavaud, C.; Massiot, G. Jaspines A and B: Two new cytotoxic sphingosine derivatives from the marine sponge *Jaspis* sp. *Tetrahedron Lett.* **2003**, *44*, 225–228.
3. Liu, J.; Du, Y.; Dong, X.; Meng, S.; Xiao, J.; Cheng, L. Stereoselective synthesis of jaspine B from D-xylose. *Carbohydr. Res.* **2006**, *341*, 2653–2657.
4. Salma, Y.; Lafont, E.; Therville, N.; Carpentier, S.; Bonnafé, M.-J.; Levade, T.; Génisson, Y.; Andrieu-Abadie, N. The natural marine anhydrophytosphingosine, jaspine B, induces apoptosis in melanoma cells by interfering with ceramide metabolism. *Biochem. Pharmacol.* **2009**, *78*, 477–485.
5. Yoshimitsu, Y.; Oishi, S.; Miyagaki, J.; Inuki, S.; Ohno, H.; Fujii, N. Pachastrissamine (jaspine B) and its stereoisomers inhibit sphingosine kinases and atypical protein kinase C. *Biorg. Med. Chem.* **2011**, *19*, 5402–5408.
6. Inuki, S.; Yoshimitsu, Y.; Oishi, S.; Fujii, N.; Ohno, H. Ring-construction/stereoselective functionalization cascade: Total synthesis of pachastrissamine (jaspine B) through palladium-catalyzed bis-cyclization of propargyl chlorides and carbonates. *J. Org. Chem.* **2010**, *75*, 3831–3842.
7. Passiniemi, M.; Koskinen, A.M.P. Asymmetric synthesis of pachastrissamine (jaspine B) and its diastereomers via η^3-allylpalladium intermediates. *Org. Biomol. Chem.* **2011**, *9*, 1774–1783.
8. Srinivas Rao, G.; Venkateswara Rao, B. A common strategy for the stereoselective synthesis of anhydrophytosphingosine pachastrissamine (jaspine B) and *N*,*O*,*O*,*O*-tetra-acetyl D-lyxo-phytosphingosine. *Tetrahedron Lett.* **2011**, *52*, 6076–6079.
9. Llaveria, J.; Díaz, Y.; Matheu, M.I.; Castillón, S. Enantioselective synthesis of jaspine B (pachastrissamine) and its C-2 and/or C-3 epimers. *Eur. J. Org. Chem.* **2011**, 1514–1519.
10. Zhao, M.-L.; Zhang, E.; Gao, J.; Zhang, Z.; Zhao, Y.-T.; Qu, W.; Liu, H.-M. An efficient and convenient formal synthesis of jaspine B from D-xylose. *Carbohydr. Res.* **2012**, *351*, 126–129.
11. Schmiedel, V.M.; Stefani, S.; Reissig, H.-U. Stereodivergent synthesis of jaspine B and its isomers using a carbohydrate-derived alkoxyallene as C3-building block. *Beilstein J. Org. Chem.* **2013**, *9*, 2564–2569.
12. Ghosal, P.; Ajay, S.; Meena, S.; Sinha, S.; Shaw, A.K. Stereoselective total synthesis of jaspine B (pachastrissamine) utilizing iodocyclization and an investigation of its cytotoxic activity. *Tetrahedron Asymmetry* **2013**, *24*, 903–908.
13. Jana, A.K.; Panda, G. Stereoselective synthesis of jaspine B and its C2 epimer from garner aldehyde. *RSC Adv.* **2013**, *3*, 16795–16801.
14. Dhand, V.; Chang, S.; Britton, R. Total synthesis of the cytotoxic anhydrophytosphingosine pachastrissamine (jaspine B). *J. Org. Chem.* **2013**, *78*, 8208–8213.
15. Lin, C.-W.; Liu, S.-W.; Hou, D.-R. Formation of tetrahydrofurans via a 5-endo-tet cyclization of aziridines—Synthesis of (−)-pachastrissamine. *Org. Biomol. Chem.* **2013**, *11*, 5292–5299.
16. Martinková, M.; Mezeiová, E.; Gonda, J.; Jacková, D.; Pomikalová, K. Total synthesis of (−)-jaspine B and its 4-epi-analogue from D-xylose. *Tetrahedron Asymmetry* **2014**, *25*, 750–766.

17. Génisson, Y.; Lamandé, L.; Salma, Y.; Andrieu-Abadie, N.; André, C.; Baltas, M. Enantioselective access to a versatile 4-oxazolidinonecarbaldehyde and application to the synthesis of a cytotoxic jaspine B truncated analogue. *Tetrahedron Asymmetry* **2007**, *18*, 857–864.
18. Salma, Y.; Ballereau, S.; Maaliki, C.; Ladeira, S.; Andrieu-Abadie, N.; Génisson, Y. Flexible and enantioselective access to jaspine B and biologically active chain-modified analogues thereof. *Org. Biomol. Chem.* **2010**, *8*, 3227–3243.
19. Canals, D.; Mormeneo, D.; Fabriàs, G.; Llebaria, A.; Casas, J.; Delgado, A. Synthesis and biological properties of pachastrissamine (jaspine B) and diastereoisomeric jaspines. *Biorg. Med. Chem.* **2009**, *17*, 235–241.
20. Xu, J.-M.; Zhang, E.; Shi, X.-J.; Wang, Y.-C.; Yu, B.; Jiao, W.-W.; Guo, Y.-Z.; Liu, H.-M. Synthesis and preliminary biological evaluation of 1,2,3-triazole-jaspine B hybrids as potential cytotoxic agents. *Eur. J. Med. Chem.* **2014**, *80*, 593–604.
21. Rives, A.; Ladeira, S.; Levade, T.; Andrieu-Abadie, N.; Génisson, Y. Synthesis of cytotoxic aza analogues of jaspine B. *J. Org. Chem.* **2010**, *75*, 7920–7923.
22. Jeon, H.; Bae, H.; Baek, D.J.; Kwak, Y.-S.; Kim, D.; Kim, S. Syntheses of sulfur and selenium analogues of pachastrissamine via double displacements of cyclic sulfate. *Org. Biomol. Chem.* **2011**, *9*, 7237–7242.
23. Patani, G.A.; LaVoie, E.J. Bioisosterism: A rational approach in drug design. *Chem. Rev.* **1996**, *96*, 3147–3176.
24. Arjona, O.; Gómez, A.M.; López, J.C.; Plumet, J. Synthesis and conformational and biological aspects of carbasugars. *Chem. Rev.* **2007**, *107*, 1919–2036.
25. Ferrero, M.; Gotor, V. Biocatalytic selective modifications of conventional nucleosides, carbocyclic nucleosides, and C-nucleosides. *Chem. Rev.* **2000**, *100*, 4319–4348.
26. Villar, H.; Frings, M.; Bolm, C. Ring closing enyne metathesis: A powerful tool for the synthesis of heterocycles. *Chem. Soc. Rev.* **2007**, *36*, 55–66.
27. Grubbs, R.H. Olefin metathesis. *Tetrahedron* **2004**, *60*, 7117–7140.
28. Royer, F.; Vilain, C.; Elkaïm, L.; Grimaud, L. Selective domino ring-closing metathesis–cross-metathesis reactions between enynes and electron-deficient alkenes. *Org. Lett.* **2003**, *5*, 2007–2009.
29. Lee, H.-Y.; Kim, H.Y.; Tae, H.; Kim, B.G.; Lee, J. One-pot three-component tandem metathesis/Diels−alder reaction. *Org. Lett.* **2003**, *5*, 3439–3442.
30. Borzilleri, R.M.; Zheng, X.; Schmidt, R.J.; Johnson, J.A.; Kim, S.-H.; DiMarco, J.D.; Fairchild, C.R.; Gougoutas, J.Z.; Lee, F.Y.F.; Long, B.H.; *et al.* A novel application of a Pd(0)-catalyzed nucleophilic substitution reaction to the regio- and stereo-selective synthesis of lactam analogues of the epothilone natural products. *J. Am. Chem. Soc.* **2000**, *122*, 8890–8897.
31. Lee, S.K.; Nam, K.-A.; Heo, Y.-H. Cytotoxic activity and G2/M cell cycle arrest mediated by antofine, a phenanthroindolizidine alkaloid isolated from *cynanchum paniculatum*. *Planta Med.* **2003**, *69*, 21–25.
32. Pyne, N.J.; Pyne, S. Sphingosine 1-phosphate and cancer. *Nat. Rev. Cancer* **2010**, *10*, 489–503.

33. Yatomi, Y.; Ruan, F.; Megidish, T.; Toyokuni, T.; Hakomori, S.-I.; Igarashi, Y. *N*,*N*-dimethylsphingosine inhibition of sphingosine kinase and sphingosine 1-phosphate activity in human platelets. *Biochemistry* **1996**, *35*, 626–633.
34. Wang, Z.; Min, X.; Xiao, S.-H.; Johnstone, S.; Romanow, W.; Meininger, D.; Xu, H.; Liu, J.; Dai, J.; An, S.; *et al.* Molecular basis of sphingosine kinase 1 substrate recognition and catalysis. *Structure* **2013**, *21*, 798–809.
35. Bissantz, C.; Kuhn, B.; Stahl, M. A medicinal chemist's guide to molecular interactions. *J. Med. Chem.* **2010**, *53*, 5061–5084.
36. Protein Data Bank. Available online: http://www.rcsb.org (accessed on 27 November 2014).

Marine Bromophenol Bis (2,3-Dibromo-4,5-dihydroxy-phenyl)-methane Inhibits the Proliferation, Migration, and Invasion of Hepatocellular Carcinoma Cells via Modulating β1-Integrin/FAK Signaling

Ning Wu, Jiao Luo, Bo Jiang, Lijun Wang, Shuaiyu Wang, Changhui Wang, Changqing Fu, Jian Li and Dayong Shi

Abstract: Bis (2,3-dibromo-4,5-dihydroxy-phenyl)-methane (BDDPM) is a natural bromophenol compound derived from marine algae. Previous reports have shown that BDDPM possesses antimicrobial activity. In the present study, we found that BDDPM has cytotoxic activity on a wide range of tumor cells, including BEL-7402 cells (IC_{50} = 8.7 μg/mL). Further studies have shown that prior to the onset of apoptosis, the BDDPM induces BEL-7402 cell detachment by decreasing the adherence of cells to the extracellular matrix (ECM). Detachment experiments have shown that the treatment of BEL-7402 cells with low concentrations of BDDPM (5.0 μg/mL) significantly inhibits cell adhesion to fibronectin and collagen IV as well as cell migration and invasion. High doses of BDDPM (10.0 μg/mL) completely inhibit the migration of BEL-7402 cells, and the expression level of MMPs (MMP-2 and MMP-9) is significantly decreased. Moreover, the expression of β1-integrin and focal adhesion kinase (FAK) is found to be down-regulated by BDDPM. This study suggests that BDDPM has a potential to be developed as a novel anticancer therapeutic agent due to its anti-metastatic activity and also indicates that BDDPM, which has a unique chemical structure, could serve as a lead compound for rational drug design and for future development of anticancer agents.

Reprinted from *Mar. Drugs*. Cite as: Wu, N.; Luo, J.; Jiang, B.; Wang, L.; Wang, S.; Wang, C.; Fu, C.; Li, J.; Shi, D. Marine Bromophenol Bis (2,3-Dibromo-4,5-dihydroxy-phenyl)-methane Inhibits the Proliferation, Migration, and Invasion of Hepatocellular Carcinoma Cells via Modulating β1-Integrin/FAK Signaling. *Mar. Drugs* **2015**, *13*, 1010-1025.

1. Introduction

Bromophenol compounds are frequently isolated from various marine red algae and have been reported to exhibit a wide spectrum of pharmacological activities including antibacterial, antimicrobial, and antitumor activities [1–4]. Due to their multiple bioactivities, bromophenol compounds, which usually exist in marine sponges and algae, have attracted much attention from the researchers in the field of functional food and pharmaceutical agents. Previous studies have reported that some marine bromophenols, together with their derivatives, can inhibit the proliferation of many types of cancer cell lines *in vitro* [3,5–7]. Bromophenols isolated form red algae, as well as some synthesized isomers, have been reported to be cytotoxic against k562 cell lines [2]. The *Leathesia nana* extract containing large amounts of bromophenol derivatives inhibited the growth of Sarcoma 180 tumors in mice [7]. Accumulated evidence, both *in vitro* and *in vivo*, indicates that marine bromophenols may be a promising group of anticancer compounds.

Bis (2,3-dibromo-4,5-dihydroxy-phenyl)-methane (BDDPM, Figure 1A), isolated from marine algae *L. nana* and *Rhodomela confervoides*, possesses various bioactivities, such as antimicrobial and antifungal activities [8]. We recently isolated and synthesized Bis (2,3-dibromo-4,5-dihydroxy-phenyl)-methane and found that it had PTP1B-inhibiting activity [9]. In the present research, we found that, among natural bromophenols, BDDPM displayed the highest anti-tumor activity against several cancer cell lines based on the 3-(4,5-dimethylthiazol-2-yl)-2,5-diphenyltetrazolium bromide (MTT) assay. However, the cytotoxic activity and the related molecular mechanism remain elusive.

The interaction between cells and extracellular matrix (ECM) plays a crucial role in cancer initiation and progression. The integrin family of cell adhesion receptors is the major mediator of cell adhesion to ECM, which links ECM to actin cytoskeleton at cellular structures called focal adhesions (or focal contacts) [10–12]. Besides integrins themselves, multiple structural and signaling molecules have been identified to be associated with focal adhesions, which highlight the importance of focal adhesions in the regulation of cellular structure and functions. Focal adhesion kinase (FAK), a non-receptor tyrosine kinase, is the first identified signaling molecule in focal adhesions. FAK-associated cell signaling plays an important role in cell motility and invasion. Integrin/FAK signaling has been shown to activate many signaling pathways through phosphorylation and protein-protein interactions to promote tumorigenesis [13–16]. FAK also plays a critical role in tumor progression and metastasis through its regulation of cancer cell migration, invasion, epithelial to mesenchymal transition, and angiogenesis, which are involved with both cancer cells and their microenvironment [17–19]. Here, we found that BDDPM could disturb the Integrin-FAK signaling, detach hepatocellular carcinoma cells from ECM, and abrogate their motility and invasiveness. BDDPM will be a potential novel Integrin-FAK inhibitor.

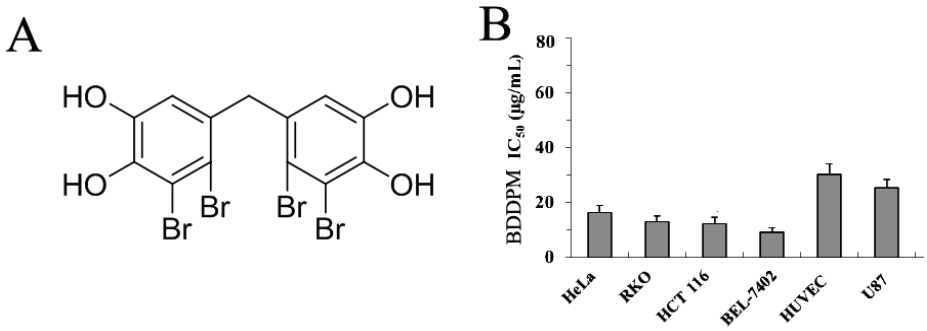

Figure 1. The structure of Bis-(2,3-dibromo-4, 5-dihydroxy-phenyl)-methane (BDDPM) and its cytotoxic activity in cancer cell lines. Human cervical cancer cells (Hela), human colon cancer cells (RKO and HCT-116), human hepatoma cells (BEL-7402), and human vascular endothelial cells (HUVEC), as well as human glioblastoma cells (U87) were incubated in the absence or presence of certain concentrations of BDDPM for 24 h at 37 °C. MTT assay was performed to determine the growth inhibition of different cancer cells and HUVEC cells by BDDPM. The experiments were performed more than three times.

2. Results

2.1. BDDPM Inhibits Cancer Cell Proliferation

MTT assays were performed to investigate the effects of BDDPM on the proliferation of six cell lines. As shown in Figure 1B, BDDPM had a significant growth-inhibiting effect on Hela (IC_{50} = 17.63 μg/mL), RKO (IC_{50} = 11.37 μg/mL), HCT-116 (IC_{50} = 10.58 μg/mL), BEL-7402 (IC_{50} = 8.7 μg/mL) and U87 (IC_{50} = 23.69 μg/mL) cancer cell lines, and a minimal growth-inhibiting effect on the HUVEC (IC_{50} = 30.15 μg/mL) cell line. The results indicated that BDDPM had a significant growth-inhibiting effect on the cancer cell lines (Figure 1B). Among these cell lines, BEL-7402 cells were much more sensitive than the other cell lines. Based on this result, BEL-7402 cells were chosen for the subsequent experiments.

2.2. BDDPM Induces Morphological Changes and Apoptosis in BEL-7402 Cell

Morphological changes were observed in cells under an invert microscope. The results showed that the BEL-7402 cells without treatment had the typical characters of human liver cancer cells, most of which were spindle-shaped with smooth edges and firmly attached to the surfaces of the cell culture dish (Figure 2A). However, the cells treated with BDDPM became spherical and detached from the plate surface, and most of them gradually became round with the increase in BDDPM concentration. The number of round cells increased in a dose-dependent manner. Cytoplasmic vacuoles could be detected in the rounded damaged cells under the high power microscope (Figure 2A).

The morphologic changes in the cell membrane were clearly visualized by scanning electronic microscopy (SEM). Remarkable alterations in the cell membrane of BEL-7402 cells were observed after BDDPM treatment. The architecture of untreated BEL-7402 cells displayed a typical polygonal shape (Figure 2B-I). However, the morphology of cells started to change after incubation with BDDPM. The cells were detached from the substratum, separated from each other, and became spindle-shaped (Figure 2B-II) after their exposure to 2.5 μg/mL of BDDPM. Membrane bulging and detachment from cytoplasmic inclusion were also observed in the cells with 5.0 μg/mL and 10.0 μg/mL BDDPM treatments (Figures 2B-III and 2B-IV).

2.3. BDDPM Induces Apoptosis in BEL-7402 Cells

We further investigated the role of BDDPM in the apoptosis of BEL-7402 cells. Cells were treated with 0, 2.5, 5.0, and 10.0 μg/mL of BDDPM. After being cultured for 24–48 h, cells were collected, and AnnexinV-FITC and PI staining assays were performed to quantify the number of apoptotic cells. As shown in Figure 3A, BDDPM exposure resulted in an increase in the number of early apoptotic cells (AnnexinV-FITC-positive/PI-negative) in BEL-7402 in a dose-dependent manner. When treated with BDDPM at 2.5 and 10.0 μg/mL, the percentage of apoptotic cells was increased from 25.68% to 87.47%, respectively (Figure 3B). Subsequently, Hoechst 33342 staining was also performed to detect the apoptotic cells. Cell nuclear pyknosis, chromosome condensation and formation of apoptotic bodies were observed in BEL-7402 cells treated with BDDPM as

detected by Hoechst 33342 staining. However, no apoptosis was found in cells treated with DMSO (Figure 3C). Cleavages of Caspase 3, 9, and poly ADP ribose polymerase (PARP) are important events for the activation of the intrinsic apoptotic pathway. Western blot analysis was performed to determine if BDDPM treatment resulted in cleavages of Caspases and PARP. The results showed that BDDPM promoted the cleavages of Caspase 3, 9, and PARP expression in a dose-dependent manner (Figure 3D). These results suggest that BDDPM induces cell death via the intrinsic apoptotic pathway.

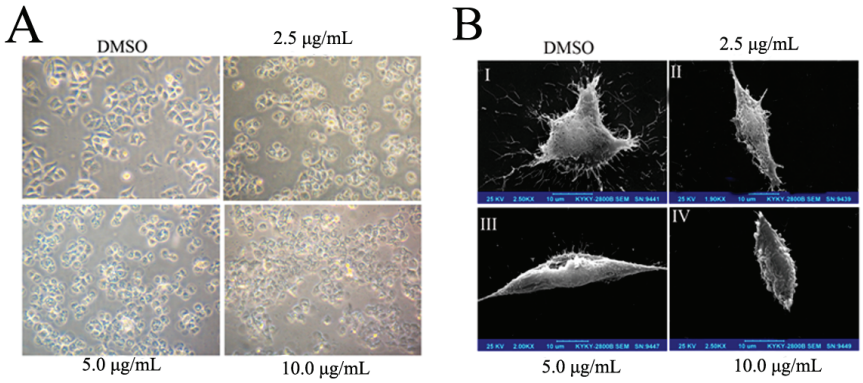

Figure 2. The morphological change of BEL-7402 cells upon treatment with BDDPM. (**A**) Cells were seeded in six-well plates (2×10^5 cells/well) and allowed to adhere overnight. Then the cells were treated without or with 2.5, 5.0 and 10.0 μg/mL BDDPM for 12 h and subsequently observed under an inverted phase-contrast microscope (magnification, 100×); (**B**) For scanning electron microscopic observation, the BEL-7402 cells were grown on poly-L-lysine-coated cover slips for 24 h to allow firm attachment and treated with 2.5, 5.0, and 10.0 μg/mL BDDPM for 12 h. Cells were fixed on cover slips coated with gold and analyzed using the KYKY-2800B SEM. Cells were treated with DMSO were considered as negative controls (I). The remaining cells were treated with 2.5 μg/mL (II), 5.0 μg /mL (III) or 10.0 μg/mL (IV) of BDDPM. The BEL-7402 cells treated with DMSO showed a normal smooth surface with a lot of apophysis. In contrast, the cells treated with BDDPM became rounded, and the surface of the cell membrane was markedly disrupted (Scale bar = 10 μm).

2.4. BDDPM Affects the Migration and Invasion of BEL-7402 Cells

Cell migration and invasion play crucial roles in tumor metastasis [11,18,20]. To further investigate the anti-metastatic effect of BDDPM, the ability of BEL-7402 cell migration was assessed by scratch-wound assay and transwell assays. The results from the scratch-wound assay showed that wound healing gradually reduced as the concentration of the BDDPM increased (Figure 4A).

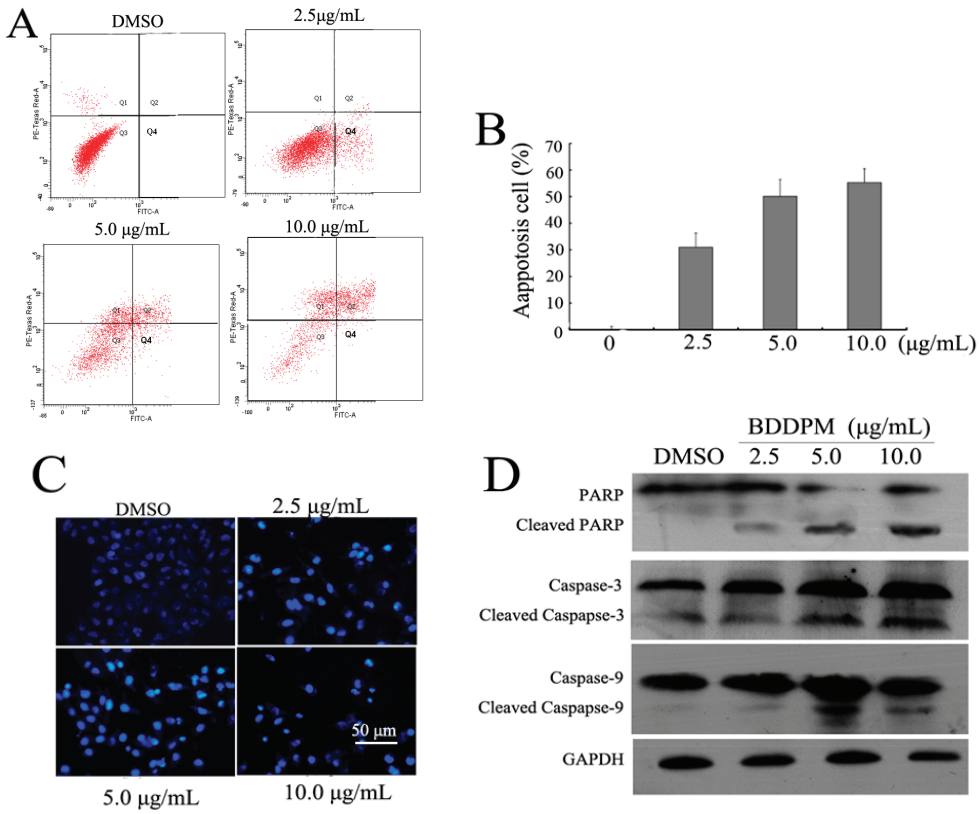

Figure 3. BDDPM induces BEL-7402 cell apoptosis. (**A**) Flow cytometric analysis of BDDPM-induced apoptosis in BEL-7402 cells. The percentage of Annexin V-FITC positive cells in the top (PI negative) and bottom (PI positive) right quadrant are indicated. Cells were treated with DMSO or treated with 2.5, 5.0, and 10.0 μg/mL of BDDPM for 48 h, respectively; (**B**) The histogram shows the percentage of early and late apoptosis and necrosis induced by BDDPM; (**C**) Analysis of apoptosis by staining with Hoechst 33342. The BEL-7402 cells were treated with DMSO or treated with 2.5, 5.0, or 10.0 μg/mL of BDDPM for 48 h. Cells were stained with Hoechst 33342 and observed under a fluorescence microscope; (Scale bar = 50 μm); (**D**) Immunoblot assays were applied to reveal the cleavages of Caspase 3, 9, and PARP in BEL-7402 treated with BDDPM. Glyceraldehyde 3-phosphate dehydrogenase (GAPDH) was used as loading control.

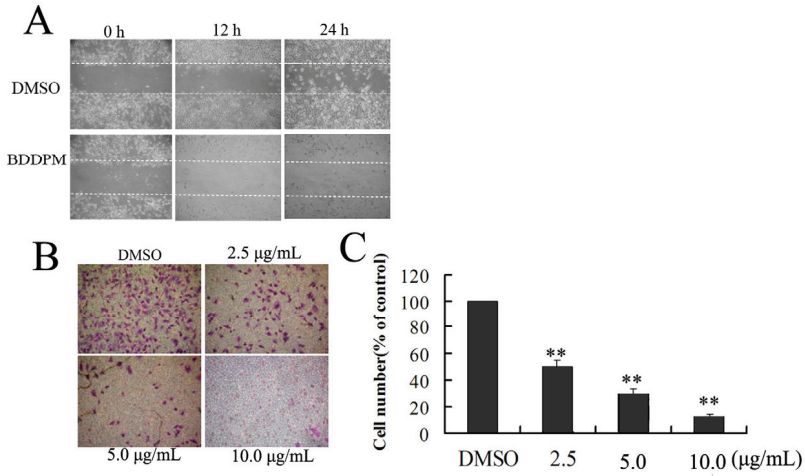

Figure 4. BDDPM inhibits BEL-7402 migration and invasion. (**A**) For the cell migration assay, BEL-7402 cells were treated with DMSO or 5.0 μg/mL BDDPM. After incubation for 12 h and 24 h, cell migration was analyzed using a scratch-wound assay; (**B**) For cell the invasion assay, BEL-7402 cells were treated with DMSO or with 2.5, 5.0 or 10.0 μg/mL BDDPM. After incubation for 24 h, non-invading cells on the upper surface of the membrane were removed and the invasive cells on the lower surface were stained with 0.1% crystal violet. The stained invasive cells were photographed under an inverted light microscope (100× magnifications); (**C**) Quantitative results of BEL-7402 cell invasion. Invasive cells were quantified by manual counting. The number represents the mean of six counting sights. Results are normalized to DMSO treated cells. All experiments were repeated more than three times. ** $p < 0.01$ *vs.* control.

We next investigated the anti-invasion activity of BDDPM on BEL-7402 cells using a transwell system. As shown in Figure 4B, treatment of BEL-7402 cells with BDDPM significantly inhibited the invasion of the cancer cells in a dose-dependent manner. When BEL-7402 was exposed to BDDPM at a concentration of 2.5, 5.0 and 10.0 μg/mL, the cell invasion to transwell was inhibited by 47.8%, 70.7%, and 86.2%, respectively (Figure 4B,C). These results suggested that BDDPM affected the ability of cell migration and invasion.

Both of the above findings indicated that BDDPM could significantly prevent BEL-7402 migration and invasion. Since inhibition of cell migration by BDDPM occurred before its inhibitory effect on cell proliferation was observed, the results suggest that BDDPM might indeed affect BEL-7402 cell migration and invasion, regardless of its effect on cell proliferation.

2.5. BDDPM Inhibits the Ability of BEL-7402 Cells to Adhere to ECM

It is well known that some extracellular matrix (ECM) proteins, such as collagen IV, fibronectin (FN), and laminin (LN) play an important role in cell adhesion. To determine whether BDDPM affects some molecular events associated with cell attachment. The anti-adhesion effect of BDDPM

on BEL-7402 cells was assessed by testing the adhesion ability of the cells to a cell matrix containing Col IV, FN, or LN. As shown in Figure 5, BDDPM remarkably reduced the adhesive ability of BEL-7402 cells to Col IV, FN or LN. Approximately 86.74% reduction in the number of cells adhering to Col IV gel was detected under the treatment of BDDPM (5.0 μg/mL), while exposure to the same concentration of BDDPM led to an adhesion of the BEL-7402 cells to the FN-containing matrix and a reduction of LN by 70.31% and 61.23%, respectively. However, BDDPM did not inhibit BEL-7402 cell adhesion to poly-L-lysine ($p > 0.05$), a non-ECM matrix. These results demonstrate that the treatment of BEL-7402 cells with BDDPM could inhibit the ability of these cells to adhere to ECM and result in cell detachment.

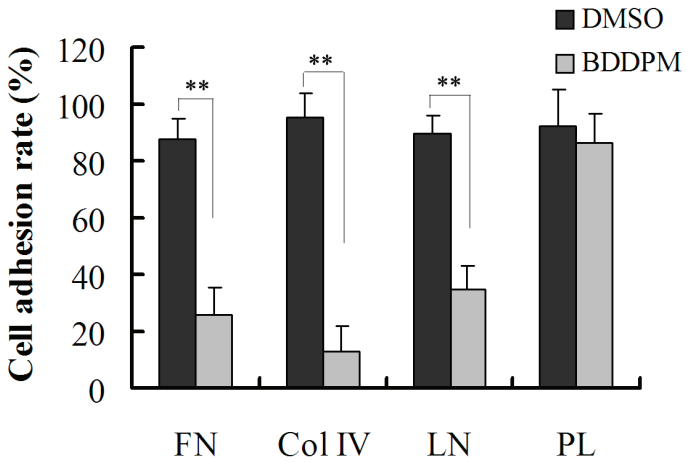

Figure 5. BDDPM affects Bel-7402 cell attachment to some extracellular matrix (ECM) proteins. Bel-7402 cells were suspended in serum-free medium containing 0.2% BSA without or with 5.0 μg/mL BDDPM and then seeded into pre-coated 96-well plates with 2.5 μg/mL fibronectin (FN), laminin (LN), poly-L-lysine (PL) or 5.0 μg/mL collagen IV (Col IV), respectively, and allowed to adhere for 1 h at 37 °C. After washing with PBS, the adhering cells were measured using an MTT assay. The adhesion rate of the treated cells was normalized to the control group. Data is shown as Mean ± SD from three independent experiments. ** $p < 0.01$ *vs.* control.

2.6. BDDPM Disrupts the Cytoskeleton and Changes the Morphology of BEL-7402

The effect of BDDPM on F-actin cytoskeleton organization was examined by immunofluorescence. As shown in Figure 6, BDDPM led to a dramatic disruption of the BEL-7402 cell cytoskeleton, producing a diffuse microtubule network and an increase in actin stress fibers and membrane blebbing. At the same time, cell morphology was significantly changed, with a rounded and retracted shape following exposure to BDDPM (Figure 6).

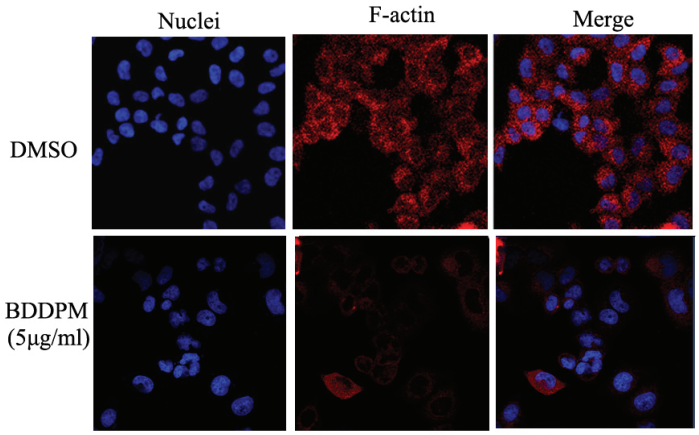

Figure 6. Effects of BDDPM on the BEL-7402 cell cytoskeleton. Human BEL-7402 cells were seeded onto cover slips coated with fibronectin and incubated over night prior to treatment (12 h, with or without 5.0 μg/mL BDDPM). Cells were then fixed and stained for F-actin (red) and the nuclei of the cells were stained using 4′,6-diamidino-2-phenylindole (DAPI) (blue); fluorescence images were viewed using a Zeiss confocal microscope (20×).

2.7. BDDPM Inhibits the Expression of β1-Integrin and FAK

To investigate the possible molecular mechanism underlying the effects of BDDPM on BEL-7402 cell behaviors, we performed flow cytometry and Western blot analysis to detect the expression of β1-integrin. Flow cytometrical analysis showed that, when the cells were treated with 5.0 μg/mL of BDDPM, the β1-integrin expression on the cell surface was significantly down-regulated in a dose-dependent manner (Figure 7A) compared to control cells. Accordingly, FAK, which is activated by β-integrin in normal and cancer cells, was significantly inhibited by BDDPM. Exposure to BDDMP resulted in the decrease in both total FAK protein and the activated FAK (phosphorylated FAK) expression levels (Figure 7A). Next, we detected the expression levels of MMP-2 and MMP-9, which are regulated by FAK and are critical for cancer cell invasion. The results revealed that treatment with BDDPM resulted in a significant decrease in the expression levels of MMP2 and MMP-9 in a dose-dependant manner (Figure 7B). PI3K/Akt and ERK are also in the downstream cascades of FAK signaling, and FAK phosphorylation of Akt/ERK suggests Akt and ERK activation. In the present study we examined the effects of BDDPM on Akt/ERK phosphorylation using antibodies recognizing phospho-serine 473 of Akt and phospho-Thr202/Tyr204 of ERK. The cells were incubated for 1 h in a medium containing 2.5–10.0 μg/mL of BDDPM. Drug treatment decreased the normalized levels of phospho-Akt and phospho-ERK in BEL-7402 cells (Figure 7C). This observation demonstrated that BDDPM inhibition of FAK kinase activity could decrease Akt and ERK activity. These results indicate that BDDPM inhibits proliferation, migration, and invasion of BEL-7402 cells by disturbing the β1-integrin/FAK signaling pathway.

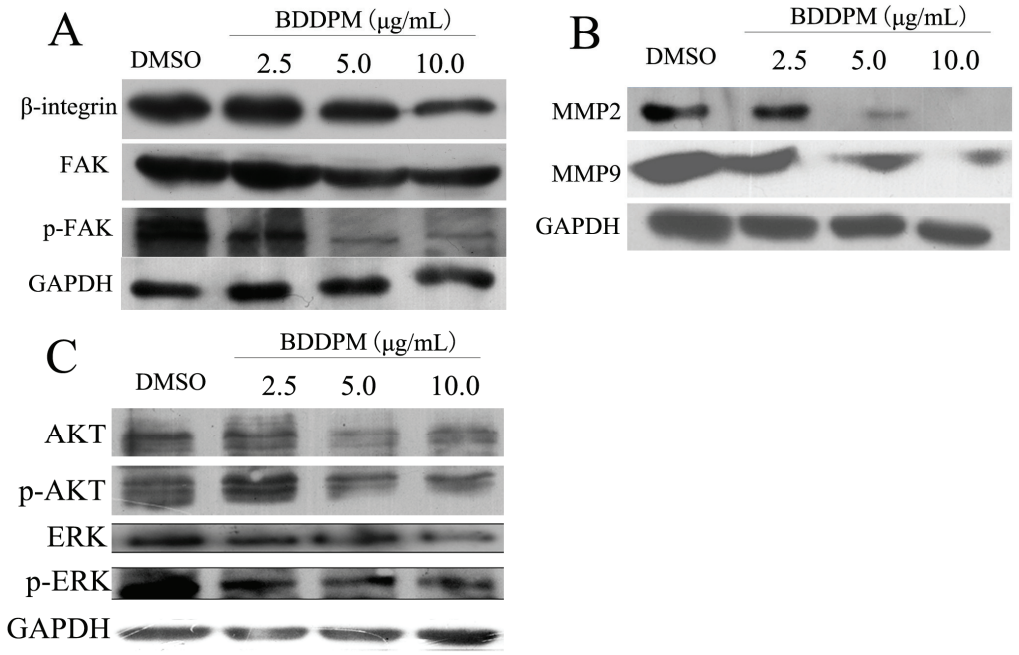

Figure 7. BDDPM disturbs β1-integrin/FAK signaling in BEL-7402 cells. BEL-7402 cells were treated with 2.5, 5.0 or 10.0 μg/mL BDDPM. After incubation for 24 h, cells were collected and the cell protein was isolated. (**A**) The expression level of β1-integrin, FAK, p-FAK were detected by Western blot; (**B**) The expression levels of MMP-2 and MMP-9 were measured by Western blot; (**C**) BDDPM inhibition of AKT and ERK phosphorylation. The anti-phospho-AKT antibody and anti-phospho-ERK antibody were used. The same membrane was stripped and re-probed using the anti-AKT, anti-ERK or anti-GAPDH antibody to detect total AKT and ERK levels. The cells treated with DMSO were used as negative control and the expression of GAPDH was used as a loading control.

3. Discussion

Tumor metastasis is a multistep process that involves tumor cell detachment from the primary tumor, adhesion to ECM or basement membrane, migration, invasion, angiogenesis, and metastatic tumor cell growth [20]. Tumor metastasis is also a major cause of death of cancer patients, and its blockage has been considered to benefit the survival of cancer patients [21]. Thus, it is crucial to identify new promising agents with anti-metastatic activity, which can disrupt or block metastasis. In this study, we found that the natural product BDDPM has antitumor activity on many types of cancer cells, and it has a potential to be developed as an anti-metastasis agent. Several lines of evidence suggest that BDDPM has anti-metastasis activity *in vitro*. Firstly, BDDPM has been found to induce cancer cell detachment and cause their apoptotic death. Secondly, BDDPM inhibits BEL-7402 cell adhesion to ECM and the major ECM proteins FN, LN, and Col IV. The promotion

of detachment and inhibition of adhesion in BEL-7402 cancer cells mediated by BDDMP indicates that it disrupts the dynamic balance between attachment and detachment of cancer cells, whereas such dynamic balance regulates cell motility and is a fundamental premise for the metastasis of cancer cells [22,23]. It is assumed that BDDMP possesses anti-metastasis activity *in vitro*. Thirdly, wound a healing assay and a Boyden chamber assay revealed that BDDMP inhibites the migration and invasion of BEL-7402 cancer cells. Thus, BDDMP possesses anti-metastasis activity *in vitro* and could be developed as a novel anticancer agent.

Integrins are the major cell adhesion receptors that mediate cell adhesion to ECM proteins and influence diverse cellular functions crucial for the initiation, progression, and metastasis of solid tumors [24]. The importance of integrins for tumor progression has made them an appealing target for cancer therapy. In recent years, various integrin antagonists or inhibitors have been developed. Cilengitide, an inhibitor of both αvβ3 and αvβ5 integrins, has been tested in Phase II trials in patients with lung and prostate cancer [25], and Phase II and Phase III trials are currently underway for glioblastoma treatment [26–28]. Volociximab, a function-blocking antibody against σ5β1 integrin, is currently undergoing Phase II clinical trials for solid tumors [29]. In the present study, we also found that BDDMP had a direct effect on the expression of β1-integrin (Figure 6). The β1-integrin is a candidate target well known for mediating cell-ECM interactions. Recent studies have shown that its aberrant expression is implicated in cancer progression and the resistance to cytotoxic therapy [30]. With the down-regulation of β1-integrin by siRNA or miR-134, the cell adhesion and invasiveness were highly inhibited [31,32]. Our findings indicate that BDDPM could be developed into a novel inhibitor of β1-integrin. However, further studies are needed to verify BDDPM-induced down-regulation of β1-integrin in BEL-7402 cancer cells, as well as in other cancer cell lines. A study is in progress in our laboratory to investigate if the treatment of cancer cells with BDDPM affects the expression of other types of integrins.

FAK activation and phosphorylation stimulated by integrins is critical for anchorage-independent growth of cancer cells. Several studies have revealed that increased FAK expression is correlated with enhanced tumor malignancy and poor prognosis [33]. Recent studies that employed RNAi to inhibit FAK expression in carcinoma cells have been yielding insights into FAK's role for tumor growth and spreading, and have also revealed that FAK expression and activity are essential for cell invasiveness [12]. FAK is required for cell transformation and invasion [13,23,34], which has become an attractive target for drug discovery. To determine the effects of BDDPM-inhibited FAK on downstream signaling and cell phenotypes, the important downstream genes including AKT/ERK were also investigated in the present study, and we found that BDDPM inhibition of FAK activity in BDDPM cells resulted in a lower AKT/ERK phosphorylation/activity, which is correlated with decreased survival and increased apoptosis (cleaved PARP and Caspases increased). Besides, BDDPM inhibits cell migration by downregulation of the MMP-2 and MMP-9. All the results indicate that BDDPM targets FAK kinase activity and inhibits FAK-related AKT/ERK activation, which impacts cell viability, and decreases anchorage-independent growth and motility. In summary, the present study found that BDDPM could disturb the integrin-FAK signal transduction and that the FAK expression level was decreased by BDDPM treatment, indicating that BDDPM has a potential to be developed as an intergrin-FAK inhibitor.

4. Experimental Section

4.1. Materials

BDDPM was first isolated from *Rhodomelaceae confervoides*, and was subsequently synthesized by our lab (purity, 98%) [9]. The Dulbecco's modified Eagle's medium (DMEM), fetal bovine serum (FBS), and other cell culture reagents were purchased from Invitrogen (Carlsbad, CA, USA). The high concentration ECM gel was purchased from BD Biosciences (BD Biosciences, Bedford, MA, USA).

4.2. MTT Assay

MTT assay was performed as previously reported [35]. Briefly, cells were seeded in 96-well plates (5×10^3 cells/well) and allowed to adhere overnight. After the cells were treated with specific doses of samples for 24 h at 37 °C, a MTT solution (30 μL, 5 mg/mL) was added into each well and the plates were incubated for 4 h before the MTT-containing solution was removed and replaced with 150 μL of DMSO. The absorbance at 490 nm was then determined with an ELx808 microplate reader (BioTek, Winooski, VT, USA). The viability rate of the treated cells was calculated by the formula: cell viability rate (%) = [(A490 sample)/(A490 control)] × 100%. The IC50 value was deduced from the MTT dose-response curves of cell viability against drug concentration.

4.3. Cell Morphological Observation

Morphologic alterations in BEL-7402 cells after BDDPM treatment were observed and photographed under an inverted microscope (Carl Zeiss, Oberkochen, Germany) or scanning electron microscope (SEM). For inverted microscope observation, cells in logarithmic phase were suspended in 1640 medium with 10% FBS and seeded into 24-well plates (50,000 cells/well). After incubation for 24 h, cells were treated with BDDPM (0, 2.5, 5.0, 10.0 μg/mL) and cultured for 12 h. Cell morphological changes were observed and photographed under an inverted microscope (Carl Zeiss, Oberkochen, Germany). For scanning electron microscope assay, the cells were grown on poly-L-lysine-coated coverslips in six-well plates for 24 h to allow firm attachment. Cells were then treated with 2.5, 5.0, 10.0 μg/mL BDDPM and incubated for 12 h. The medium containing BDDPM was removed, and the cells were subsequently fixed in 0.25% glutaraldehyde. After fixation overnight at 4 °C, the coverslips were dehydrated with ethanol and dried in a critical point dryer. Cells on cover slips were coated with gold and analyzed with the S-3400N SEM (Hitachi, Lexington, KY, USA).

4.4. Hoechst33342/Propidium Iodide (PI) Dual Staining Assays

The apoptotic cells were stained using Hoechst33342/PI double staining as we described previously [35]. The BEL-7402 cells were seeded in six-well plates (2×10^5 cells/well) and treated with certain concentrations of BDDPM (2.5, 5.0, 10.0 μg/mL). After incubation for 24 h, the cells were collected and washed with PBS. Cells were stained with Hoechst33342 and PI using the dual

staining kit (Beyond, Beijing, China). Then the cells were spread on slides and observed under the fluorescence microscope (Carl Zeiss, Oberkochen, Germany).

4.5. Apoptosis Assay

Cell apoptosis was detected by Annexin V-FITC assay. Apoptotic cell death was quantified by flow cytometry with Annexin V-FITC and propidium iodide (PI) staining. Annexin V-FITC apoptosis detection kit (Invitrogen, Carlsbad, CA, USA) was used according to the manufacturer's instructions. Briefly, both attached and floating cells were collected and resuspended in binding buffer before adding the Annexin V-FITC antibody and PI. Stained cells were analyzed by flow cytometry (Beckman Coulter,Brea, CA, USA).

4.6. Cell Adhesion Assay

The cell adhesion assay was performed as described previously [19]. Briefly, Bel-7402 cells were suspended in serum-free medium containing 0.2% BSA without or with 5 μg/mL BDDPM and then seeded in precoated 96-well plates with 2.5 μg/mL fibronectin (FN) and laminin (LN), poly-L-lysine (PL) or 5 μg/mL collagen IV (Col IV), respectively, and allowed to adhere for 1 h at 37 °C. After washing with PBS, the adherent cells were measured using an MTT assay. The adherent rate of the treated cells was normalized to the control group.

4.7. Cell Migration Assay

The migration ability of BEL-7402 cells was assessed using a modified version of a previously described protocol [34] with a transwell system (Corning, Tewksbury, MA, USA). Cells (10,000 cells/well) were added to the upper chamber of the transwell culture plates, in the presence and absence of certain concentrations of BDDPM (0.0–10.0 μg/mL). The lower chamber was filled with 500 μL F-12K medium containing 10% FBS as a chemo-attractant. After incubation for 12 h, non-migrating cells on the upper surface of the membrane were scrubbed gently with a cotton-tipped swab. The migratory cells on the lower surface of the membrane were fixed with 95% methanol, stained with 0.1% crystal violet (Sigma-Aldrich, St. Louis, MO, USA), counted with inverted microscope and quantified by manual counting in three randomly selected areas.

4.8. Cell Invasion Assay

The effect of BDDPM on BL-7402 cell invasion was measured by a transwell system with a diameter of 6.5 mm and a pore size of 8 μm. ECM gel was applied to the top side of the filter to form a thin gel layer. As described above for the cell migration assay, cells that penetrated to the lower chamber were fixed and stained. The stained invasive cells were photographed under an inverted light microscope and quantified by manual counting in three randomly selected areas.

4.9. Cytoskeleton Immunofluorescence

BEL-7402 cells were seeded on ploy lysine-coated chamber slides before exposure to BDDPM (10 μg/mL) for 4 h. The cells were then harvested and fixed with 4% paraformaldehyde, permeabilized with 0.1% Triton X-100, and blocked with 5% BSA solution. The microtubules were then labeled with mouse monoclonal anti-F-actin antibody (1:500, Santa Cruz, Dallas, TX, USA), followed by incubated with the second antibody (Alexa Fluor549-anti-Rabbit IgG, 1:1000, Life science, St. Louis, MO, USA), after that the cell nuclei were stained with DAPI (5 mg/mL) for five minutes and the Fluorescence images were obtained by using confocal microscope (Zeiss, Oberkochen, Germany).

4.10. Western Blot Analysis

Cells were lysed in RIPA buffer (Solaibo, Beijing, China). Proteins were separated by a 10% polyacrylamide gel and transferred to a methanol-activated PVDF membrane (GE Healthcare, Little Chalfont, Buckinghamshire, UK). The membrane was blocked in blocking solution (5% nonfat dry milk powder) for 2 h at room temperature and subsequently probed with primary antibodies; including ILK, β1- integrin, PARP, Caspase-3, Caspase-9, total/phospho FAK, total/phospho-Akt, total/phospho-ERK, (used at a 1/1000 dilution, Santa Cruz Biotechnology, Santa Cruz, CA, USA), MMP2, MMP9 (used at a 1/1000 dilution, AbClonal, USA) Or GAPDH (used at a 1/5000 dilution, AbClonal, Cambridge, MA, USA). After three 10 min washes with 0.1% Tween-20 in PBS buffer, membranes were incubated with rabbit anti mouse or goat anti rabbit HRP-conjugated secondary antibody (Santa Cruz) for 1 h. After an additional three 10 min washes with 0.1% Tween-20 in PBS buffer, the chemiluminescence method was employed to detect the signals using Super Signal West Dura (Thermo Scientific, Waltham, MA, USA) and protein bands were visualized by autoradiography.

4.11. Statistical Analysis

Statistical significance of the data was analyzed by the two-tail Student's *t*-test with a minimum significance level set at $p < 0.05$ (marked as * $p < 0.05$ and ** $p < 0.01$).

5. Conclusions

This study suggests that the natural marine bromphenol compound Bis (2,3-dibromo-4,5-dihydroxy-phenyl)-methane (BDDPM) induces cancer cell detachment and causes their apoptotic death, and it has a potential to be developed as a novel anticancer therapeutic agent due to its anti-metastatic activity. BDDPM inhibits cell migration and invasion by targeting β1-integrin/FAK signaling.

Acknowledgments

This study was supported by the National Natural Science Foundation of China (41306157, 41276167 and 41206066) and Basic research projects of Qingdao Science and Technology plan (12-1-4-8-(4)-jch).

Author Contributions

Ning Wu and Dayong Shi designed the experiments; Ning Wu, Jiao Luo, Bo Jiang, Changhui Wang, Changqing Fu and Jian Li Performed the experiments; Lijun Wang and Shuaiyu Wang Analyzed the data; Ning Wu and Dayong Shi Wrote the paper.

Conflicts of Interest

The authors declare no conflict of interest.

References

1. Liu, M.; Wang, G.; Xiao, L.; Xu, X.; Liu, X.; Xu, P.; Lin, X. Bis(2,3-dibromo-4,5-dihydroxybenzyl) ether, a marine algae derived bromophenol, inhibits the growth of botrytis cinerea and interacts with DNA molecules. *Mar. Drugs* **2014**, *12*, 3838–3851.
2. Liu, M.; Zhang, W.; Wei, J.; Qiu, L.; Lin, X. Marine bromophenol bis(2,3-dibromo-4,5-dihydroxybenzyl) ether, induces mitochondrial apoptosis in k562 cells and inhibits topoisomerase I *in vitro*. *Toxicol. Lett.* **2012**, *211*, 126–134.
3. Ma, M.; Zhao, J.; Wang, S.; Li, S.; Yang, Y.; Shi, J.; Fan, X.; He, L. Bromophenols coupled with methyl gamma-ureidobutyrate and bromophenol sulfates from the red alga rhodomela confervoides. *J. Nat. Prod.* **2006**, *69*, 206–210.
4. Wang, B.G.; Gloer, J.B.; Ji, N.Y.; Zhao, J.C. Halogenated organic molecules of rhodomelaceae origin: Chemistry and biology. *Chem. Rev.* **2013**, *113*, 3632–3685.
5. Liu, M.; Zhang, W.; Wei, J.; Lin, X. Synthesis and alpha-glucosidase inhibitory mechanisms of bis(2,3-dibromo-4,5-dihydroxybenzyl) ether, a potential marine bromophenol alpha-glucosidase inhibitor. *Mar. Drugs* **2011**, *9*, 1554–1565.
6. Pereira, R.; Benedetti, R.; Perez-Rodriguez, S.; Nebbioso, A.; Garcia-Rodriguez, J.; Carafa, V.; Stuhldreier, M.; Conte, M.; Rodriguez-Barrios, F.; Stunnenberg, H.G.; *et al.* Indole-derived psammaplin a analogues as epigenetic modulators with multiple inhibitory activities. *J. Med. Chem.* **2012**, *55*, 9467–9491.
7. Shi, D.Y.; Li, J.; Guo, S.J.; Su, H.; Fan, X. The antitumor effect of bromophenol derivatives *in vitro* and *Leathesia nana* extract *in vivo*. *Chin. J. Oceanol. Limn.* **2009**, *27*, 277–282.
8. Oh, K.B.; Lee, J.H.; Lee, J.W.; Yoon, K.M.; Chung, S.C.; Jeon, H.B.; Shin, J.; Lee, H.S. Synthesis and antimicrobial activities of halogenated bis(hydroxyphenyl)methanes. *Bioorg. Med. Chem. Lett.* **2009**, *19*, 945–948.
9. Li, J.; Guo, S.J.; Su, H.; Han, L.J.; Shi, D.Y. Total synthesis of bis-(2,3-dibromo-4,5-dihydroxyphenyl)-methane as potent PTP1B inhibitor. *Chin. Chem. Lett.* **2008**, *19*, 1290–1292.

10. Bauvois, B. New facets of matrix metalloproteinases mmp-2 and mmp-9 as cell surface transducers: Outside-in signaling and relationship to tumor progression. *Bba-Rev. Cancer* **2012**, *1825*, 29–36.
11. Ma, W.L.; Jeng, L.B.; Lai, H.C.; Liao, P.Y.; Chang, C. Androgen receptor enhances cell adhesion and decreases cell migration via modulating beta 1-integrin-Akt signaling in hepatocellular carcinoma cells. *Cancer Lett.* **2014**, *351*, 64–71.
12. Mitra, S.K.; Schlaepfer, D.D. Integrin-regulated FAK-Src signaling in normal and cancer cells. *Curr. Opin. Cell Biol.* **2006**, *18*, 516–523.
13. Yao, W.L.; Ko, B.S.; Liu, T.A.; Liang, S.M.; Liu, C.C.; Lu, Y.J.; Tzean, S.S.; Shen, T.L.; Liou, J.Y. Cordycepin suppresses integrin/FAK signaling and epithelial-mesenchymal transition in hepatocellular carcinoma. *Anti-Cancer Agent Me* **2014**, *14*, 29–34.
14. Eke, I.; Deuse, Y.; Hehlgans, S.; Gurtner, K.; Krause, M.; Baumann, M.; Shevchenko, A.; Sandfort, V.; Cordes, N. Beta(1) integrin/FAK/cortactin signaling is essential for human head and neck cancer resistance to radiotherapy. *J. Clin. Invest.* **2012**, *122*, 1529–1540.
15. Saleem, S.; Li, J.M.; Yee, S.P.; Fellows, G.F.; Goodyer, C.G.; Wang, R.N. Beta 1 integrin/FAK/Erk signalling pathway is essential for human fetal islet cell differentiation and survival. *J. Pathol.* **2009**, *219*, 182–192.
16. Bouchard, V.; Harnois, C.; Demers, M.J.; Thibodeau, S.; Laquerre, V.; Gauthier, R.; Vezina, A.; Noel, D.; Fujita, N.; Tsuruo, T.; *et al*. Beta 1 integrin/FAK/Src signaling in intestinal epithelial crypt cell survival: Integration of complex regulatory mechanisms. *Apoptosis* **2008**, *13*, 531–542.
17. Han, J.W.; Lee, H.J.; Bae, G.U.; Kang, J.S. Promyogenic function of integrin/FAK signaling is mediated by Cdo, Cdc42 and MyoD. *Cell Signal.* **2011**, *23*, 1162–1169.
18. Huttenlocher, A.; Sahai, E. Editorial overview: Cell adhesion and migration. *Curr. Opin. Cell Biol.* **2014**, *30*, V–Vi.
19. Wang, F.X.; Wu, N.; Wei, J.T.; Liu, J.; Zhao, J.; Ji, A.G.; Lin, X.K. A novel protein from eupolyphaga sinensis inhibits adhesion, migration, and invasion of human lung cancer A549 cells. *Biochem. Cell Biol.* **2013**, *91*, 244–251.
20. Woodhouse, E.C.; Chuaqui, R.F.; Liotta, L.A. General mechanisms of metastasis. *Cancer* **1997**, *80*, 1529–1537.
21. Lee, Y.S.; Nam, K.T.; Lee, S.; Yu, D.; Choi, G.; Shin, S.K.; Lee, Y.C. Regulation of epithelial mesenchymal transition through protein kinase CK2 in helicobacter pylori infected gastric cancer cells. *Gastroenterology* **2012**, *142*, S515–S516.
22. Lauffenburger, D.A. Cell motility. Making connections count. *Nature* **1996**, *383*, 390–391.
23. Lauffenburger, D.A.; Horwitz, A.F. Cell migration: A physically integrated molecular process. *Cell* **1996**, *84*, 359–369.
24. Desgrosellier, J.S.; Cheresh, D.A. Integrins in cancer: Biological implications and therapeutic opportunities. *Nat. Rev. Cancer* **2010**, *10*, 9–22.
25. Beekman, K.W.; Colevas, A.D.; Cooney, K.; Dipaola, R.; Dunn, R.L.; Gross, M.; Keller, E.T.; Pienta, K.J.; Ryan, C.J.; Smith, D.; *et al.* Phase II evaluations of cilengitide in asymptomatic patients with androgen-independent prostate cancer: Scientific rationale and study design. *Clin. Genitourin Cancer* **2006**, *4*, 299–302.

26. Manegold, C.; Vansteenkiste, J.; Cardenal, F.; Schuette, W.; Woll, P.J.; Ulsperger, E.; Kerber, A.; Eckmayr, J.; von Pawel, J. Randomized phase II study of three doses of the integrin inhibitor cilengitide *vs.* docetaxel as second-line treatment for patients with advanced non-small-cell lung cancer. *Invest. New Drugs* **2013**, *31*, 175–182.
27. Kim, K.B.; Prieto, V.; Joseph, R.W.; Diwan, A.H.; Gallick, G.E.; Papadopoulos, N.E.; Bedikian, A.Y.; Camacho, L.H.; Hwu, P.; Ng, C.S.; *et al.* A randomized phase II study of cilengitide (EMD 121974) in patients with metastatic melanoma. *Melanoma Res.* **2012**, *22*, 294–301.
28. Reardon, D.A.; Fink, K.L.; Mikkelsen, T.; Cloughesy, T.F.; O'Neill, A.; Plotkin, S.; Glantz, M.; Ravin, P.; Raizer, J.J.; Rich, K.M.; *et al*. Randomized phase II study of cilengitide, an integrin-targeting arginine-glycine-aspartic acid peptide, in recurrent glioblastoma multiforme. *J. Clin. Oncol.* **2008**, *26*, 5610–5617.
29. Besse, B.; Tsao, L.C.; Chao, D.T.; Fang, Y.; Soria, J.C.; Almokadem, S.; Belani, C.P. Phase IB safety and pharmacokinetic study of volociximab, an anti-alpha5beta1 integrin antibody, in combination with carboplatin and paclitaxel in advanced non-small-cell lung cancer. *Ann. Oncol.* **2013**, *24*, 90–96.
30. Park, C.C.; Zhang, H.; Pallavicini, M.; Gray, J.W.; Baehner, F.; Park, C.J.; Bissell, M.J. Beta1 integrin inhibitory antibody induces apoptosis of breast cancer cells, inhibits growth, and distinguishes malignant from normal phenotype in three dimensional cultures and *in vivo*. *Cancer Res.* **2006**, *66*, 1526–1535.
31. Zha, R.; Guo, W.; Zhang, Z.; Qiu, Z.; Wang, Q.; Ding, J.; Huang, S.; Chen, T.; Gu, J.; Yao, M.; *et al.* Genome-wide screening identified that miR-134 acts as a metastasis suppressor by targeting integrin beta1 in hepatocellular carcinoma. *PLoS One* **2014**, *9*, e87665.
32. Speicher, T.; Siegenthaler, B.; Bogorad, R.L.; Ruppert, R.; Petzold, T.; Padrissa-Altes, S.; Bachofner, M.; Anderson, D.G.; Koteliansky, V.; Fassler, R.; *et al*. Knockdown and knockout of beta1-integrin in hepatocytes impairs liver regeneration through inhibition of growth factor signalling. *Nat. Commun.* **2014**, *5*, 3862.
33. Hsia, D.A.; Mitra, S.K.; Hauck, C.R.; Streblow, D.N.; Nelson, J.A.; Ilic, D.; Huang, S.; Li, E.; Nemerow, G.R.; Leng, J.; *et al.* Differential regulation of cell motility and invasion by FAK. *J. Cell Biol.* **2003**, *160*, 753–767.
34. Wu, X.; Gan, B.; Yoo, Y.; Guan, J.L. Fak-mediated src phosphorylation of endophilin A2 inhibits endocytosis of MT1-MMP and promotes ECM degradation. *Dev. Cell* **2005**, *9*, 185–196.
35. Wu, N.; Lin, X.; Zhao, X.; Zheng, L.; Xiao, L.; Liu, J.; Ge, L.; Cao, S. miR-125b acts as an oncogene in glioblastoma cells and inhibits cell apoptosis through p53 and p38MAPK-independent pathways. *Br. J. Cancer* **2013**, *109*, 2853–2863.

The Anticancer Effect of (1*S*,2*S*,3*E*,7*E*,11*E*)-3,7,11, 15-Cembratetraen-17,2-olide(LS-1) through the Activation of TGF-β Signaling in SNU-C5/5-FU, Fluorouracil-Resistant Human Colon Cancer Cells

Eun-Ji Kim, Jung-Il Kang, Jeon-Won Kwak, Chan-Hee Jeon, Nguyen-Huu Tung, Young-Ho Kim, Cheol-Hee Choi, Jin-Won Hyun, Young-Sang Koh, Eun-Sook Yoo and Hee-Kyoung Kang

Abstract: The anticancer effect of (1*S*,2*S*,3*E*,7*E*,11*E*)-3,7,11,15-cembratetraen-17,2-olide (LS-1) from *Lobophytum* sp. has been already reported in HT-29 human colorectal cancer cells. In this study, we examined the effect of LS-1 on the apoptosis induction of SNU-C5/5-FU, fluorouracil-resistant human colon cancer cells. Furthermore, we investigated whether the apoptosis-induction effect of LS-1 could arise from the activation of the TGF-β pathway. In SNU-C5/5-FU treated with LS-1 of 7.1 μM (IC_{50}), we could observe the various apoptotic characteristics, such as the increase of apoptotic bodies, the increase of the sub-G1 hypodiploid cell population, the decrease of the Bcl-2 level, the increase of procaspase-9 cleavage, the increase of procaspase-3 cleavage and the increase of poly(ADP-ribose) polymerase cleavage. Interestingly, the apoptosis-induction effect of LS-1 was also accompanied by the increase of Smad-3 phosphorylation and the downregulation of c-Myc in SNU-C5/5-FU. LS-1 also increased the nuclear localization of phospho-Smad-3 and Smad-4. We examined whether LS-1 could downregulate the expression of carcinoembryonic antigen (CEA), a direct inhibitor of TGF-β signaling. LS-1 decreased the CEA level, as well as the direct interaction between CEA and TGF-βR1 in the apoptosis-induction condition of SNU-C5/5-FU. To examine whether LS-1 can induce apoptosis via the activation of TGF-β signaling, the SNU-C5/5-FU cells were treated with LS-1 in the presence or absence of SB525334, a TGF-βRI kinase inhibitor. SB525334 inhibited the effect of LS-1 on the apoptosis induction. These findings provide evidence demonstrating that the apoptosis-induction effect of LS-1 results from the activation of the TGF-β pathway via the downregulation of CEA in SNU-C5/5-FU.

Reprinted from *Mar. Drugs*. Cite as: Kim, E.-J.; Kang, J.-I.; Kwak, J.-W.; Jeon, C.-H.; Tung, N.-H.; Kim, Y.-H.; Choi, C.-H.; Hyun, J.-W.; Koh, Y.-S.; Yoo, E.-S.; *et al*. The Anticancer Effect of (1*S*,2*S*,3*E*,7*E*,11*E*)-3,7,11,15-Cembratetraen-17,2-olide(LS-1) through the Activation of TGF-β Signaling in SNU-C5/5-FU, Fluorouracil-Resistant Human Colon Cancer Cells. *Mar. Drugs* **2015**, *13*, 1340-1359.

1. Introduction

Colon cancer is one of the most prevalent cancers in the United States, and incidence rates of colon cancer have been increasing steadily worldwide [1]. There have been remarkable advances in chemotherapy for colon cancer in recent years. Especially, 5-fluorouracil (5-FU), oxaliplatin and irinotecan are often used in combination for the chemotherapy of colon cancer [2,3]. Among them, 5-FU is the anti-metabolite of DNA synthesis by inhibiting thymidylate synthase and was used as

the most basic anti-cancer drug in colon cancer and other cancers [4]. However, the increased resistance to anti-cancer drugs is an important factor disturbing cancer treatment. Overcoming drug-resistance is important for the improvement of chemotherapy response and the increase of the survival rate. Interestingly, recent studies indicated that the drug-resistant colon cancer cells could induce a high carcinoembryonic antigen (CEA) level [5]. Moreover, it has been reported that CEA could be upregulated after exposure to 5-fluorouracil in colon and breast cancer cells [6,7].

CEA is a glycosyl phosphatidyl inositol (GPI)-anchored glycoprotein. Normally, CEA is found in both colon and gastrointestinal tissues of a developing fetus in the womb, but the synthesis of CEA stops before birth. Thus, a low level of CEA is maintained in the blood of healthy adults. If the CEA level is raised in the blood of adults, this means that the possibility of developing cancer increases. In cancer patients, an elevated CEA level in blood has also shown poor prognosis and metastasis. Recent studies reported that CEA could contribute to the inhibition of anoikis, a form of apoptosis induced by cell detaching, via interfering with TRAIL-R2 signaling [8] or inactivation of the intrinsic apoptosis pathway [9]. Furthermore, overexpression of CEA has been reported to inhibit apoptosis and transforming growth factor-beta (TGF-β) signaling via CEA directly binding to TGF-β receptor I (TGF-βRI) [10].

The TGF-β signaling pathway is involved in many cellular processes, including cell differentiation, apoptosis and other cellular functions [11]. In fact, the TGF-β signaling pathway shows dual roles, such as being a promoter of tumor metastasis and a suppressor of tumor in human cancers [12]. The promotion of tumor metastasis includes the induction of epithelial-mesenchymal transition (EMT), which is improved by TGF-β overexpressed tumor cells at the invasion. The effect of the TGF-β signaling pathway in EMT has been well characterized [13]. Blocking of TGF-β signaling using dominant-negative TGF-βRII prevents mouse skin carcinoma cells from EMT *in vivo* [14]. On the other hand, paradoxically, the activation of the TGF-β signaling pathway has been known to induce tumor suppression [15]. Moreover, the TGF-β signaling pathway is correlated with tumor suppression in the early stages of tumor development [16].

(1*S*,2*S*,3*E*,7*E*,11*E*)-3,7,11,15-Cembratetraen-17,2-olide(LS-1), a marine cembrenolide diterpene, from *Lobophytum sp*. (Figure 1) has been reported to have anticancer effects in HT-29 human colorectal cancer cells via reactive oxygen species (ROS) generation [17,18]. Recent studies reported that overexpression of CEA could inhibit the tumor suppresser effect of the TGF-β signaling pathway via CEA direct interaction with TGF-β receptor I [10]. In the study, we examined the effect of LS-1 on the apoptosis induction of SNU-C5/5-FU, 5-FU-resistant human colon cancer cells. Furthermore, we investigated whether the apoptosis-induction effect of LS-1 could arise from the activation of the TGF-β pathway via the downregulation of CEA.

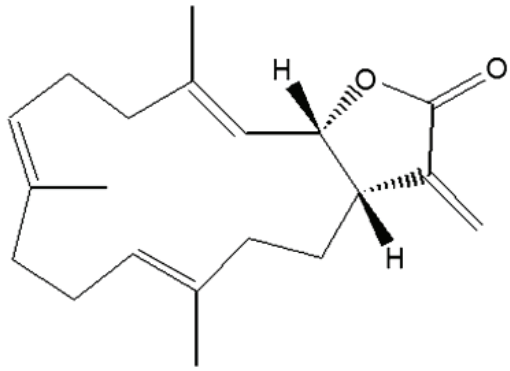

Figure 1. Chemical structure of cembrenolide LS-1.

2. Results and Discussion

2.1. Results

2.1.1. Effect of LS-1 on the Growth of SNU-C5/5-FU

To ascertain whether SNU-C5/5-FU cells have stable resistance to 5-FU, we examined the IC_{50} values for 5-FU in SNU-C5/5-FU and SNU-C5/WT. When 5-FU was treated for 72 h in various concentrations (1, 10, 50, 100 and 200 μM), the IC_{50} (the concentration resulting in 50% inhibition of growth) values of 5-FU in SNU-C5/WT and SNU-C5/5-FU were 4.84 μM and 182.66 μM, respectively (Figure 2). These results indicate that SNU-C5/5-FU is potentially resistant to 5-FU.

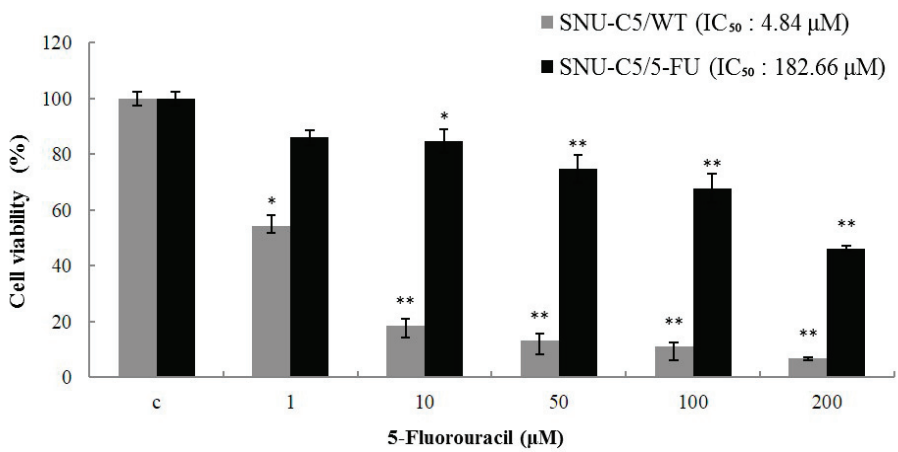

Figure 2. Cytotoxicity of 5-FU in SNU-C5/5-FU and SNU-C5/WT. The cytotoxicity of 5-FU on the cell lines was measured using the methylthiazol tetrazolium (MTT) assay. The data are presented as the mean value ± SD from three independent trials. * $p < 0.05$ and ** $p < 0.01$ compared with the control.

To evaluate the effect of LS-1 on the proliferation of SNU-C5/5-FU, SNU-C5/WT and HEL-299, a normal fibroblast cell, SNU-C5/5-FU, SNU-C5/WT and HEL-299 were treated with LS-1 (0.1, 1, 10 and 50 μM) for 72 h. Treatment of LS-1 significantly induced cell death of SNU-C5/5-FU and SNU-C5/WT in a dose-dependent manner (IC_{50} = 7.10 and 5.65 μM, respectively), whereas cell death of HEL-299 was scarcely induced even over a 10 μM concentration compared to SNU-C5/5-FU (IC_{50} = 43.07 μM) (Figure 3). The results show that the effect of LS-1 on the induction of cell death affects the cancer cells, including chemotherapeutic agent-resistant cancer cells, such as SNU-C5/5-FU.

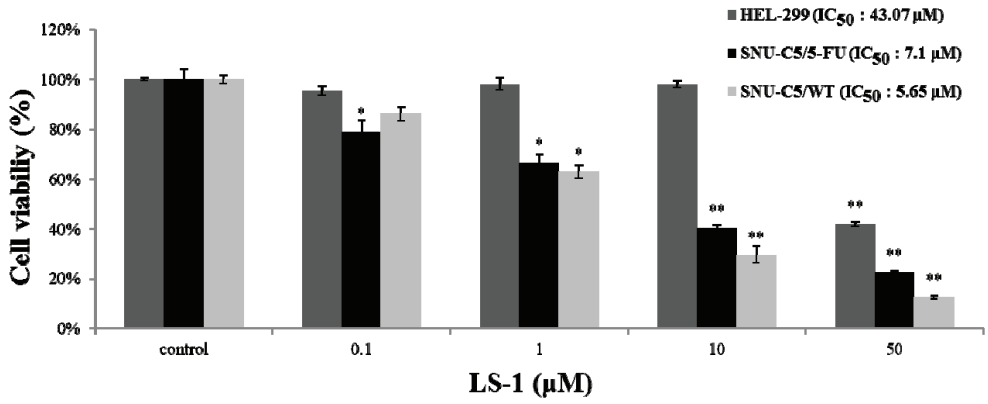

Figure 3. Cytotoxicity of LS-1 in SNU-C5/5-FU, SNU-C5/WT and HEL-299. The cytotoxicity of LS-1 on the cell lines was measured using the MTT assay. The data are presented as the mean value ± SD from three independent trials. * $p < 0.05$ and ** $p < 0.01$ compared with the control.

2.1.2. Effect of LS-1 on the Apoptosis Induction of SNU-C5/5-FU Cells

Cell death via apoptosis has typical characteristics, such as apoptotic bodies and the increase of sub-G1 hypodiploid cells [19,20]. We thus examined whether the inhibitory effect of LS-1 on the proliferation of SNU-C5/5-FU could result from the induction of apoptosis.

When treated with LS-1 of 7.1 μM for 24 h, we could observe the increase of apoptotic bodies (Figure 4A). As shown in Figure 4B, the sub-G1 phase population increased significantly from 1.19% to 8.55% after 24 h of 7.1 μM LS-1 treatment, while the percentages of S and G2/M phase decreased (Figure 4B). Furthermore, treatment with LS-1 regulated the levels of apoptosis-related proteins, such as a decrease of the Bcl-2 level, increase of procaspase-9 cleavage, increase of procaspase-3 cleavage and increase of poly(ADP-ribose) polymerase (PARP) cleavage (Figure 4C). To determine whether LS-1 induced the mitochondrial apoptotic pathway, we measured the effect of LS-1 on the release of cytochrome *c* from mitochondria to the cytosol. As shown in Figure 4D, treatment of LS-1 increased the cytosolic release of cytochrome *c*. These results indicate that LS-1 could inhibit the proliferation of SNU-C5/5-FU via the induction of apoptosis.

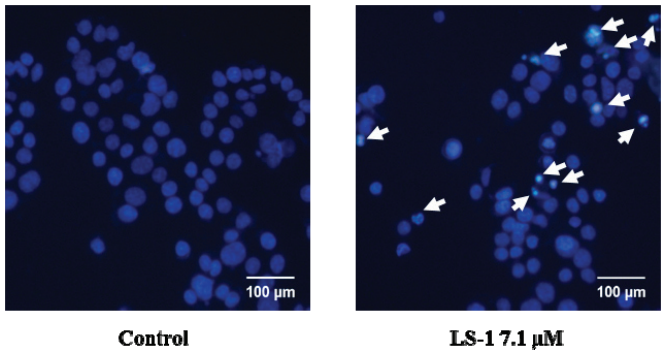

(A)

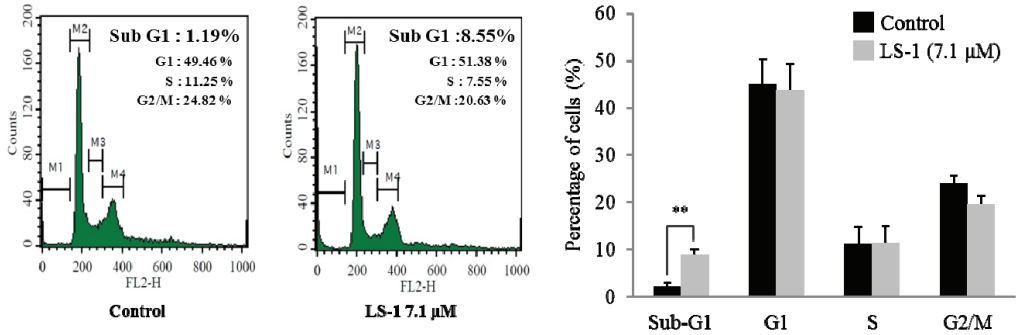

(B)

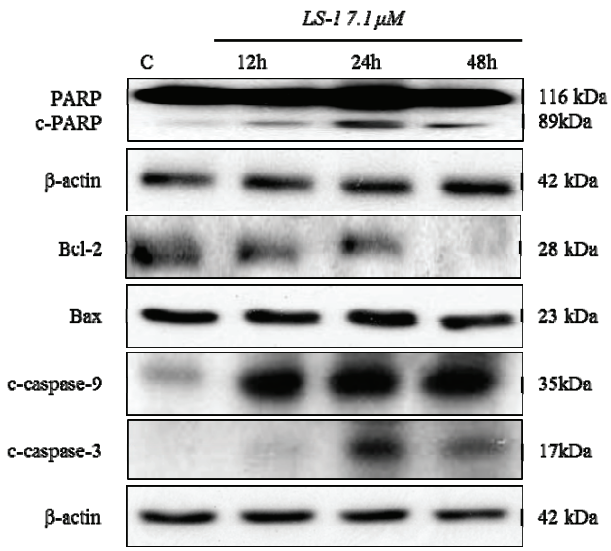

(C)

Figure 4. *Cont.*

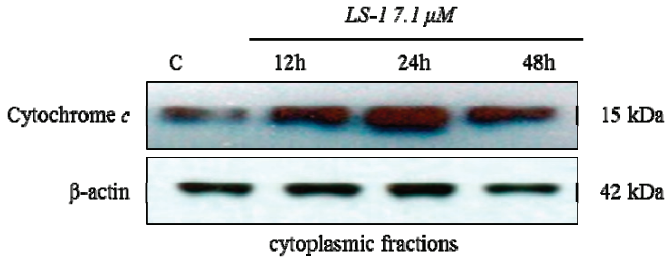

(**D**)

Figure 4. Effect of LS-1 on the induction of apoptosis in SNU-C5/5-FU. (**A**) The SNU-C5/5-FU was treated with LS-1 for 24 h and stained with Hoechst 33,342, which is a DNA-specific fluorescent (10 μg/mL medium at final). Apoptotic bodies were observed in an inverted fluorescent microscope equipped with an IX-71 Olympus camera. (magnification: ×20); (**B**) The SNU-C5/5-FU were treated with LS-1 for 24 h. The cell cycle analysis was performed by flow cytometry. The experiments were performed four times. The data shown are the percentage of cells at that phase of the cell cycle (mean ± SD). ** $p < 0.01$ *versus* control; (**C**) The levels of apoptosis-related proteins were examined by Western blot; (**D**) The levels of cytochrome *c* in the cytoplasmic fractions were examined by Western blot.

2.1.3. Effect of LS-1 on the TGF-β Signaling in SNU-C5/5-FU

The TGF-β signaling pathway has been known to show the promotion of tumor metastasis or the suppression of tumor, depending on the tumors [12]. On the other hand, recent studies reported that TGF-β could regulate CEA expression [21,22]. Thus, to elucidate the action mechanism of LS-1 on the apoptosis induction of SNU-C5/5-FU, we investigated whether LS-1 could affect the TGF-β signaling in SNU-C5/5-FU. Firstly, we thus examined the characteristics of SNU-C5/5-FU on the TGF-β signaling activation and CEA expression. The activation level of TGF-β signaling was examined as the phosphorylation of Smad-2/3. We also evaluated the CEA level of SNU-C5/5-FU compared with LOVO, CEA high-expressed human colon cancer cells, HT-29, CEA low-expressed human colon cancer cells, HCT-116, CEA none-expressed human colon cancer cells [10], and SNU-C5/WT. The result showed that high-expression of CEA was also accompanied by low activation of TGF-β signaling in LOVO cells, as expected (Figure 5A,B). Relatively speaking, HT-29 and HCT-116 cells showed high activation of TGF-β signaling with low or no CEA expression (Figure 5A,B). Interestingly, SNU-C5/5-FU showed high expression of CEA with low activation of TGF-β signaling compared with SNU-C5/WT (Figure 5A,B). Furthermore, SNU-C5/5-FU and LOVO showed a similar pattern with regard to the expression of CEA, Smad-2/3 and phospho-Smad-3 (Figure 5B). These results suggest that SNU-C5/5-FU has the characteristic of low TGF-β signaling with high-expressed CEA.

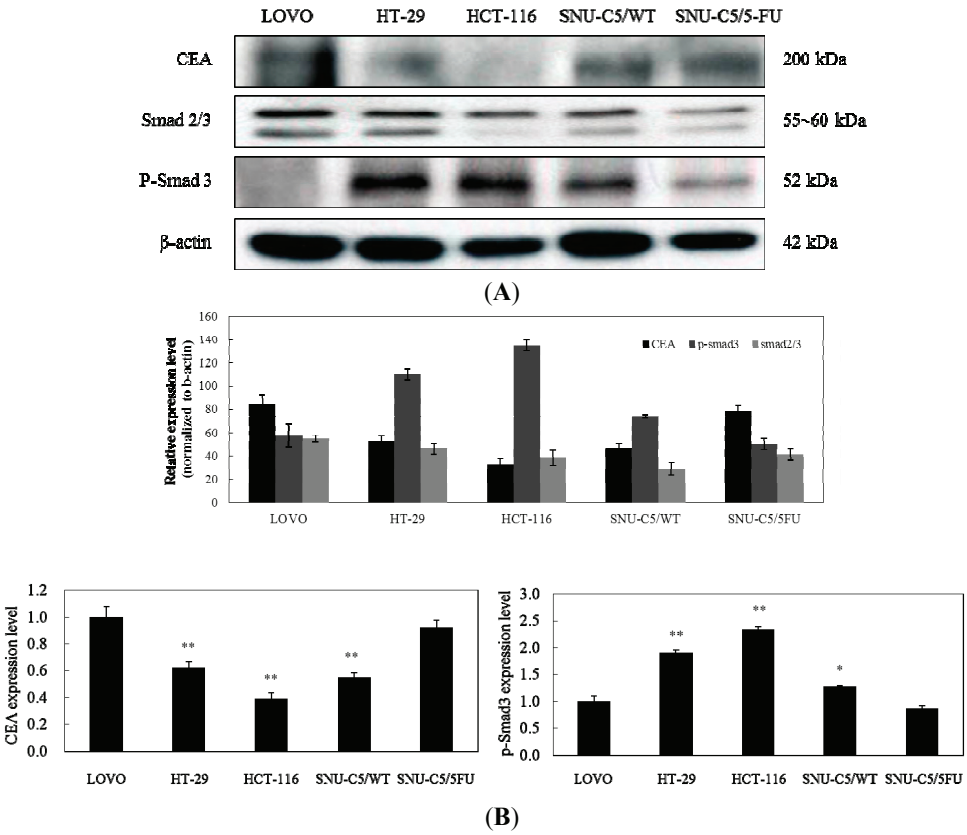

Figure 5. Comparison of CEA and Smad levels in LOVO, HT-29, HCT-116, SNU-C5/WT and SNU-C5/5-FU. (**A**) Levels of CEA and Smad proteins in the cell lines were examined by Western blot. (**B**) Data represent the relative expression percentage of CEA, Smad-2/3 and p-Smad-3 in the cell lines. The data are presented as the mean value ± SD from three independent trials. * $p < 0.05$ and ** $p < 0.01$ compared with the control.

When treated with LS-1 of 7.1 μM, we could observe the increase of Smad-3 phosphorylation and the decrease of c-Myc and CEA, the target proteins of TGF-β signaling (Figure 6A). During activation of TGF-β signaling, phosphorylated Smad-3 combines the Smad-4 and moves into the nucleus [23]. The LS-1 increased the levels of phospho-Smad-3, as well as Smad-4 in the nucleus (Figure 6B,C). These results suggest that LS-1 could induce the activation of TGF-β signaling in SNU-C5/5-FU.

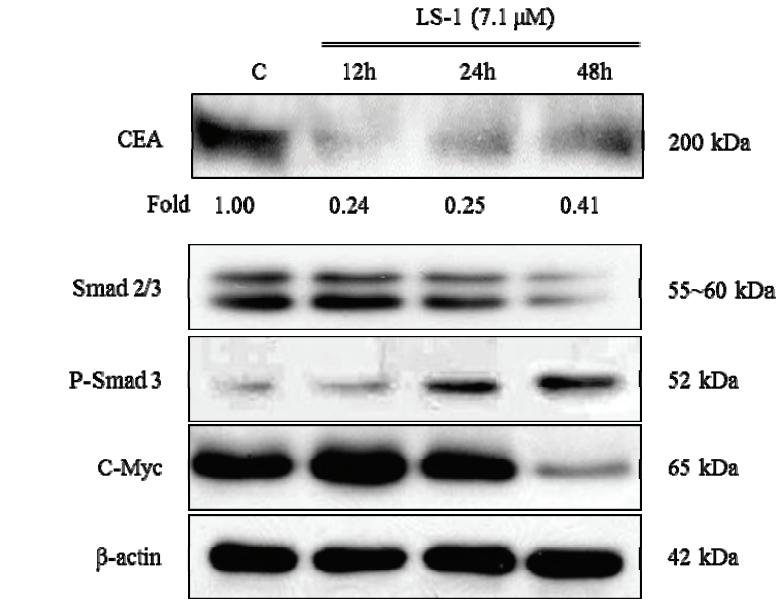

(A)

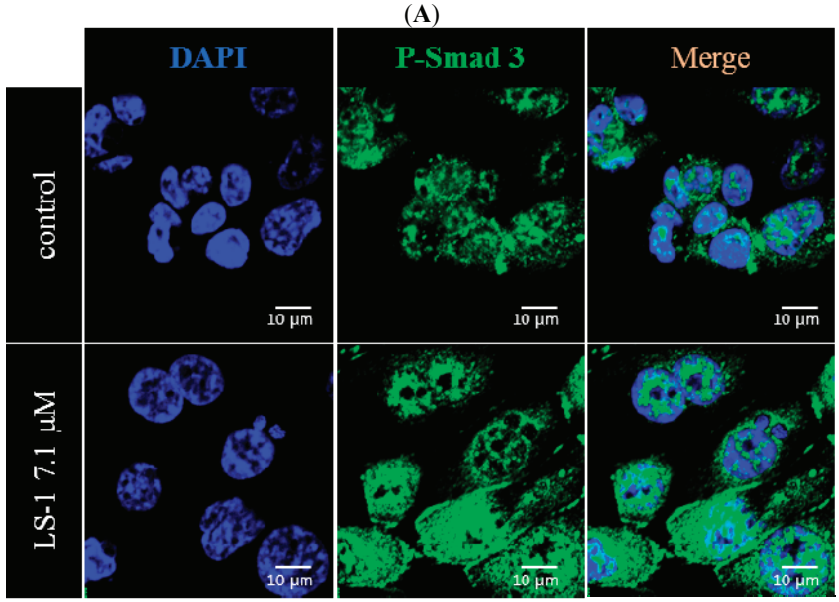

(B)

Figure 6. *Cont.*

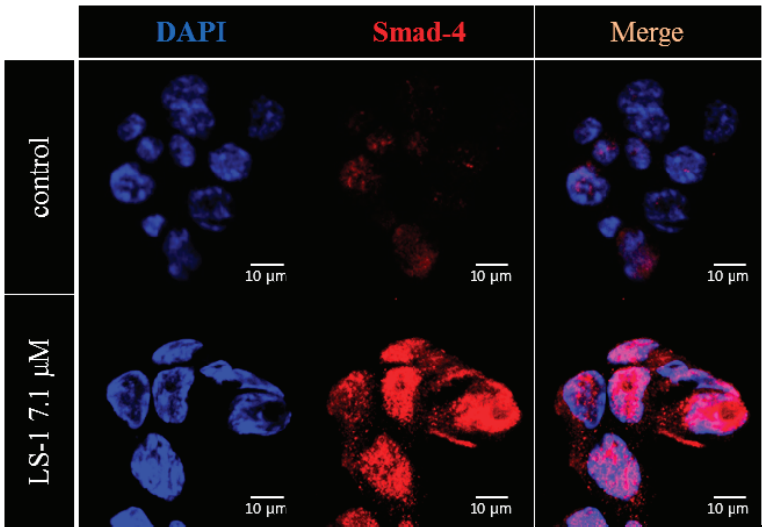

(**C**)

Figure 6. The effect of LS-1 on the expressions of CEA, c-Myc and Smad proteins in SNU-C5/5-FU. (**A**) Modulation of CEA, c-Myc and Smad protein levels by LS-1 was examined by Western blot; (**B**) Modulation of the p-Smad-3 level by LS-1 (7.1 μM, 24 h) was examined by immunofluorescent stain of p-Smad-3; (**C**) Modulation of Smad-4 by LS-1 (7.1 μM, 24 h) was examined by the immunofluorescent stain of Smad-4. The fluorescence was identified via confocal microscopy (FV500, OLYMPUS, New York, NY, USA).

Recent studies reported that CEA could inhibit TGF-β signaling through CEA direct interaction with TGF-β receptor I (TGFβRI) [10]. We thus examined whether LS-1 could affect direct interaction between TGFβRI and CEA in SNU-C5/5-FU. We observed that TGFβRI could directly interact with the CEA using immunoprecipitation (Figure 7A; control). Furthermore, the amount of CEA combined with TGFβRI was decreased by treatment with LS-1 in a time-dependent manner (Figure 7). The result indicates that LS-1 could inhibit the interaction of CEA and TGFβRI in SNU-C5/5-FU. Consequently, LS-1 seems to effectively activate TGF-β signaling by inhibiting the interaction of CEA and TGFβRI.

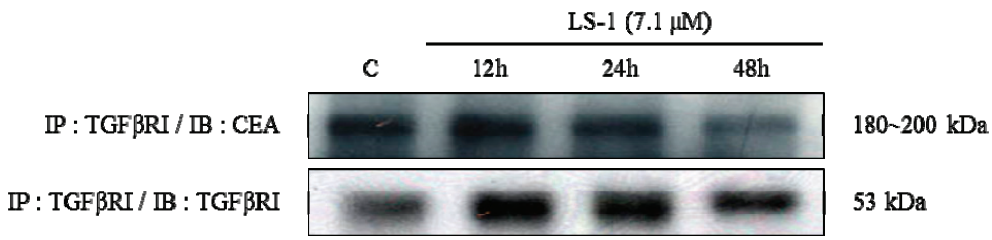

(**A**)

Figure 7. *Cont.*

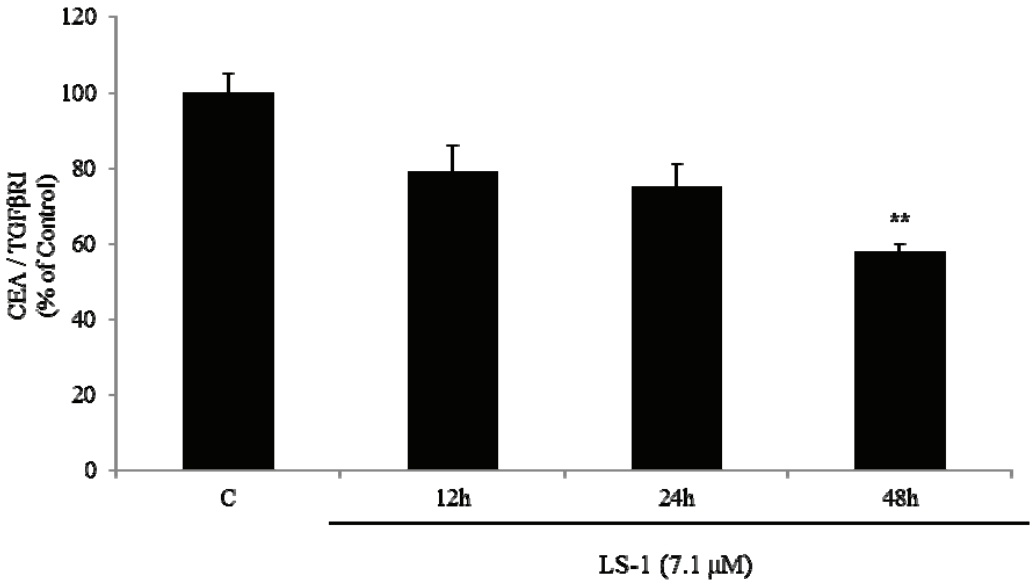

(**B**)

Figure 7. The effect of LS-1 on the interaction between TGFβRI and CEA in SNU-C5/5-FU. (**A**) SNU-C5/5-FU were treated with 7.1 μM of LS-1 for 12, 24 and 48 h. The interaction between TGFβRI and CEA was examined by immunoprecipitation with anti-TGFβRI antibody and with immunoblotting with anti-TGFβRI antibody and anti-CEA antibody; (**B**) Data represent the percentage of CEA expression in SNU-C5/5-FU. The data are presented as the mean value ± SD from three independent trials. * $p < 0.05$ and ** $p < 0.01$ compared with the control.

2.1.4. LS-1 Induced Apoptosis of SNU-C5/5-FU via Activation of TGF-β Signaling

LS-1 induced apoptosis in SNU-C5/5-FU (Figure 4) and activated TGF-β signaling (Figure 6). In order to examine whether LS-1 may induce apoptosis via activation of TGF-β signaling, we treated with LS-1 and/or SB525334 (TGF-βRI kinase inhibitor). As a result, the blocking of the TGF-β signal by SB525334 inhibited the apoptosis-induction effect of LS-1 in SNU-C5/5-FU (Figure 8). When SNU-C5/5-FU was treated with LS-1 and/or SB525334, SB525334 inhibited the LS-1-induced increase of PARP cleavage and procaspase-9 cleavage, and LS-1-induced downregulation of Bcl-2, while LS-1-induced the increase of Bax, which was not affected by SB525334 (Figure 8A). These results indicated that LS-1 could induce apoptosis via the activation of the TGF-β signaling pathway. Taken together, LS-1 seems to induce apoptosis of SNU-C5/5-FU, which has downregulated the TGF-β pathway with overexpressed CEA, compared to wild-type cells, via the activation of TGF-β signaling with downregulation of CEA.

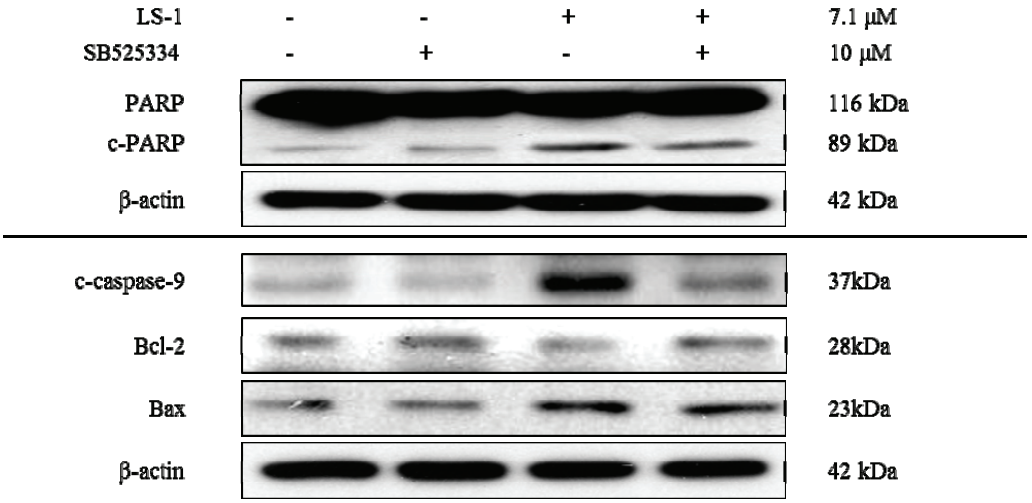

(**A**)

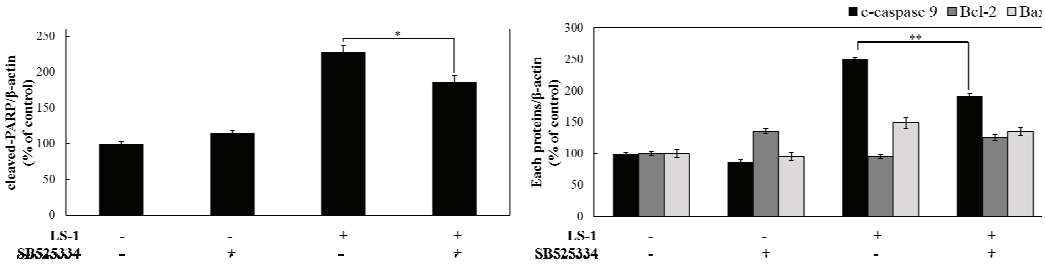

(**B**)

Figure 8. The effect of the TGF-β signaling pathway on the apoptosis-induction effect of LS-1 in SNU-C5/5-FU. (**A**) SNU-C5/5-FU were pre-treated with 10 μM of SB525334 (TGF-βRI kinase inhibitor) and then treated with 7.1 μM of LS-1. The expressions of apoptosis-related proteins were examined by Western blot; (**B**) Data represent the percentage of c-PARP, c-caspase-9, Bcl-2 and Bax expression in SNU-C5/5-FU. The data are presented as the mean value ± SD from three independent trials. * $p < 0.05$ and ** $p < 0.01$ compared with the control.

2.2. Discussion

In the study, we examined whether LS-1 could inhibit the proliferation of SNU-C5/5-FU, fluorouracil-resistant human colon cancer cells. To the best of our knowledge, this study is the first to demonstrate that LS-1 could induce the apoptosis of SNU-C5/5-FU via the activation of TGF-β signaling with downregulation of CEA.

LS-1, a marine cembrenolide diterpene, from *Lobophytum sp.* (Figure 1) is reported to have an anticancer effect in HT-29 human colorectal cancer cells [17,18]. Many studies have reported that various marine cembrenolide diterpenes from soft corals, such as *Sinularia gibberosa, Nephthea*

brassica, *Lobophytum Crassum*, *Lobophytum* sp., *Sarcophyton glaucum* and *Sarcophyton shrenbergi*, exert cytotoxic effects against several human cancer cells, including HepG2 and MCF-7 cancer cells [24–29]. To examine if LS-1 can also inhibit the proliferation of anticancer drug-resistant cancer cells, we used SNU-C5/5-FU cells, which showed a much higher survival rate compared with SNU-C5/WT on 5-FU (Figure 2). Indeed, our results show that LS-1 effectively inhibited the proliferation of SNU-C5/5-FU cells in a dose-dependent manner with an IC_{50} value of 7.1 μM. In addition, LS-1 induced cell death in SNU-C5/WT at lower concentrations than SNU-C5/5-FU (Figure 3). Contrastively, LS-1 barely inhibited the growth of HEL-299, which is a normal cell line, with an IC_{50} value of 43.07 μM (Figure 3). The results show that LS-1 can induce the death of several cancer cells, including SNU-C5/5-FU, fluorouracil-resistant human colon cancer cells.

We know that apoptosis or programmed cell death is the outcome of a complex interplay of pro- and anti-apoptotic molecules. High levels of Bcl-2 expression have been found in several human tumors, and the levels of Bcl-2 expression have been correlated with the aggressiveness of the tumors [30]. Since Bcl-2 functions by forming a heterodimer with its pro-apoptotic partner, such as Bax, the Bcl-2:Bax ratio is proportional to the relative sensitivity or resistance of the cells to various apoptotic stimuli [30]. Apoptotic cell death is induced through two key molecular signaling pathways, the extrinsic and intrinsic pathways. The intrinsic apoptotic pathway is characterized by mitochondrial membrane permeabilization, the release of cytochrome *c* and the formation of apoptosomes. The extrinsic apoptotic pathway is activated in response to ligand binding to death receptors, such as Fas, TNF and TRAIL, and involves the activation of caspase-8. [31]. Here, we showed that LS-1 reduced the Bcl-2 level, whereas the Bax level was rarely changed. In response to LS-1 treatment, caspase-9 was activated, leading to the activation of caspase-3, one of the key executioners of apoptosis. In addition, to clarify the induction of the intrinsic pathway, which works via the activation of caspase-9 by LS-1, we investigated whether LS-1 could affect the release of cytochrome *c* from mitochondria. Treatment of LS-1 increased the cytochrome *c* level in the cytoplasm. When SNU-C5/5-FU cells were treated with LS-1, the activation of caspase-3 was demonstrated by the cleavage of PARP, a nuclear enzyme that is involved in DNA repair in response to various stresses.

TGF-β signaling has important roles in many cellular processes, including apoptosis, cell cycle regulation, cell migration and immune modulation. The TGF-β signaling pathway is initiated by the binding of one of the TGF-β isoforms, which include TGF-β1, TGF-β2 and TGF-β3, on the TGF-β receptor type II (TGF-βRII). The TGF-βRII dimer recruits TGF-βRI and forms the hetero-tetrameric complex. Then, TGF-βRII activates the TGF-βRI via phosphorylation. It induces the recruitment and phosphorylation of receptor-regulated Smad (R-Smad), like Smad-2 and Smad-3. These are substrates for TGF-βRI and act like modulators of the TGF-β signal. Phosphorylated R-Smad could bind with common mediated Smad (Co-Smad) protein, such as Smad-4, followed by complex formation. The phosphorylated R-Smad/Co-Smad complexes translocate into the nucleus, bind transcription promoters and cause the transcription of target gene [23]. Some of the targets of the TGF-β signaling pathway are cell cycle check-point genes, like p15, p21 and p27. Thus, the series of processes evokes G1 arrest in the cell cycle. In cancer, the TGF-β

signaling pathway has been known to act as a double-edged sword. By constraining epithelial cell growth, TGF-β performs as a potent tumor suppressor. However, TGF-β also acts as a key player in the induction of EMT, thereby enhancing invasiveness and metastasis. Furthermore, TGF-β signaling has recently been reported to correlate with resistance to anticancer agents [10,32]. Many colorectal cancers escape the tumor-suppressor effects of TGF-β signaling and are resistant to TGF-β-induced growth inhibition [33]. On the other hand, as a tumor marker for colorectal cancers, CEA expression also correlates well with resistance to cytotoxic chemotherapy [34]. TGF-β signaling also contributes to the stimulation of CEA transcription and secretion in colorectal cancer cells [21,22]. Aberrant upregulation of CEA and the alteration of TGF-β signaling are common features of colorectal cancers [23]. CEA has been reported to inhibit apoptosis and the TGF-β signaling pathway through direct interaction with TGFβRI [10]. In the study, we found the downregulation of the TGF-β signaling pathway along with overexpression of CEA in SNU-C5/5-FU compared with SNU-C5/WT (Figure 5). These expression patterns of SNU-C5/5-FU were similar to those of LOVO, another human colon cancer cell line (Figure 5). These results suggest that SNU-C5/5-FU cells might avoid apoptosis by downregulation of the TGF-β signaling pathway along with overexpression of CEA.

The TGF-β signaling pathway modulates the apoptotic pathway, including the death receptor and intracellular signaling pathway [35]. We thus investigated if LS-1 can affect the expression of CEA and the TGF-β signaling pathway in SNU-C5/5-FU. LS-1 treatment decreased the CEA level, while the TGF-β signaling pathway was activated at the concentration inducing apoptosis in SNU-C5/5-FU (Figure 6). Moreover, LS-1 could inhibit the direct interaction between CEA and TGFβRI (Figure 7). These results indicated that LS-1 can activate TGF-β signaling via inhibition of the interactions of CEA and TGFβRI. In sequence, we examined if the effect of LS-1 on the apoptosis induction of SNU-C5/5-FU results from the activation of the TGF-β signaling pathway. When co-treated with LS-1 and SB525334, a selective inhibitor of TGFβRI, we could observe that SB525334 inhibits the apoptosis-induction effect of LS-1 (Figure 8).

Taken together, the results suggest that LS-1 can restore the activity of the TGF-β signaling pathway and induce apoptosis in SNU-C5/5-FU cells. Our studies provide a rationale for the development of LS-1 as a therapeutic agent against human colon cancers, including chemotherapy-resistant colon cancers, especially with the decrease of TGF-β function. On the other hand, TGF-β has been reported to increase intracellular ROS in various cell types [36,37]. ROS induces cell cycle arrest and apoptosis through activating their transcription factors, such as Sp1 [38,39]. In addition, several studies have documented the significant generation of ROS in a variety of cells, which is usually the consequence of mitochondrial respiration and NADPH oxidase (NOX) activity [40,41]. Our previous findings revealed that the anticancer efficacy of LS-1 could be mediated by the induction of apoptosis via ROS generation in human colon cancer cells [18]. In a further study, we will investigate whether LS-1 can generate ROS and induce apoptosis via the activation of TGF-β signaling in SNU-C5/5-FU and the action mechanism of LS-1 on the relationship between the ROS production and the activation of TGF-β signaling.

3. Experimental Section

3.1. Materials

5-FU, MTT, Hoechst 33342 and propidium iodide (PI) were purchased from Sigma Chemical Co. (St. Louis, MO, USA). Mouse monoclonal anti-c-Myc and anti-smad-4, rabbit polyclonal anti-Bax and anti-TGFβRI and goat polyclonal anti-Smad-2/3 antibodies were purchased from Santa Cruz Biotechnology (Santa Cruz, CA, USA); rabbit monoclonal anti-Bcl-2, anti-p-Smad-3 and anti-cleaved caspase-3, rabbit polyclonal anti-cleaved caspase-9 and anti-PARP and mouse monoclonal anti-CEA antibodies were purchased from Cell Signaling Technology (Beverly, MA, USA); mouse monoclonal β-actin and the selective inhibitor of TGFβRI (SB525334) were purchased from Sigma; Dynabeads® Protein G was purchased from NOVEX® (Invitrogen, Oslo, Norway); aprotinin, leupeptin and Nonidet P-40 were obtained from Roche Applied Science (Indianapolis, IN, USA); the Western blotting reagent, West-zol enhanced chemilumin, was obtained from iNtROn Biotechnology (Gyeonggi, Korea).

3.2. Cell Culture

LOVO, HT-29, HCT-116 and SNU-C5/WT, human colon cancer cell lines, were obtained from the Korean Cell Line Bank (KCLB, Seoul, Korea). SNU-C5/5-FU, a human resistant colon cancer cell line, was obtained from the Research Center for Resistant Cells in South Korea. LOVO, HT-29, HCT-116, SNU-C5/WT and SNU-C5/5-FU cells were cultured in RPMI 1640 (Hyclone, UT, USA) medium supplemented with 10% heat-inactivated fetal bovine serum (Hyclone, Logan, UT, USA), 100 U/mL penicillin and 100 mg/mL streptomycin (GIBCO Inc., Grand Island, NY, USA) at 37 °C in a humidified atmosphere with 5% CO_2. After 2 days, for SNU-C5/5-FU cells, the medium with 140 μM of 5-FU was changed.

3.3. Cell Viability Assay

The effect of 5-FU or LS-1 on the growth of SNU-C5/WT, SNU-C5/5-FU and HEL-299 cells was evaluated using the MTT assay [42]. The cells (2×10^5 cells/mL) were seeded on 96-well microplates for 24 h. The cells were treated with 5-FU (1, 10, 50, 100 and 200 μM) or LS-1 (0.1, 1, 10, 20 and 50 μM) for 72 h. After incubation, the cells were treated with 50 μL (5 mg/mL) MTT dye and incubated at 37 °C for 4 h. The medium was aspirated, and 150 μL/well of dimethyl sulfoxide were added to dissolve the formazan precipitate. Cell viabilities were determined by measuring the absorbance at 540 nm using a microplate enzyme-linked immunosorbent assay (ELISA) reader (BioTek Instruments Inc., Winooski, VT, USA). Each experiment was repeated at least three times. Concentration (X-axis)-response (% control optical density; Y-axis) curves were obtained. We determined the IC_{50} values (compound concentration resulting in 50% inhibition of growth).

3.4. Morphological Analysis of Apoptosis by Hoechst 33342 Staining

SNU-C5/5-FU cells were seeded at 2×10^5 cells/mL in 1 mL on 24-well microplates. After 24 h of incubation, cells were treated with LS-1 (7.1 μM) for 24 h. The cells were incubated in Hoechst 33342 (Invitrogen, Carlsbad, CA, USA, 10 μg/mL medium at final) at 37 °C for 30 min. SNU-C5/5-FU cells were observed with an inverted fluorescent microscope equipped with an IX-71 Olympus camera (Olympus, New York, NY, USA) and photographed (magnification: ×20).

3.5. Flow Cytometric Analysis of Apoptosis

The effect of LS-1 on cell cycle distribution was analyzed by flow cytometry after staining the cells with PI [43]. SNU-C5/5-FU cells (2×10^5 cells/mL) were treated with 7.1 μM of LS-1 for 24 h. The treated cells were detached with trypsin, washed twice with phosphate-buffered saline (PBS) and fixed with 70% ethanol for 30 min at −20 °C. The fixed cells were washed twice with cold PBS, incubated with 50 μg/mL RNase A at 37 °C for 30 min and stained with 50 μg/mL PI at 37 °C for 30 min in the dark. The stained cells were analyzed using fluorescence-activated cell sorter (FACS) caliber flow cytometry (Becton Dickinson, San Jose, CA, USA). Histograms were analyzed with Cell Quest software (Becton-Dickinson). The proportion of cells in the G0/G1, S and G2/M phases was represented as DNA histograms. Apoptotic cells with hypodiploid DNA were measured by quantifying the sub-G1 peak in the cell cycle pattern. For each experiment, 10,000 events per sample were analyzed, and experiments were repeated three times.

3.6. Western Blot Analysis

LOVO, HT-29, HCT-116, SNU-C5/WT and SNU-C5/5-FU cells were seeded at 2×10^5 cells/mL. After 24 h, cells were lysed with lysis buffer (50 mM Tris-HCl (pH 7.5), 150 mM NaCl, 2 mM EDTA, 1 mM EGTA, 1 mM $NaVO_3$, 10 mM NaF, 1 mM phenylmethylsulfonyl fluoride, 25 μg/mL aprotinin, 25 μg/mL leupeptin, 1 mM Dithiothreitol, 1% Nonidet P-40) for 30 min at 4 °C. To examine the effect of LS-1 in the SNU-C5/5-FU cells, the cells were seeded 2×10^5 cells/mL for 24 h and treated with LS-1 (7.1 μM) for 12, 24 and 48 h. After treatment, SNU-C5/5-FU cells were lysed with lysis buffer for 30 min at 4 °C. The lysates were centrifuged at 15,000 rpm, 4 °C, for 15 min. Protein content was determined according to the method of the Bradford assay [44]. The cell lysates were separated by 6%~15% SDS-PAGE gels and then transferred to polyvinylidene fluoride membrane (BIO-RAD, Hercules, CA, USA) by glycine transfer buffer (192 mM glycine, 25 mM Tris-HCl (pH 8.8) and 20% MeOH (v/v)) at 200 mA for 2 h. After blocking with 5% skim milk solution, the membrane was incubated with primary antibody against PARP (1:2000), cleaved caspase-3 (1:1000), cleaved caspase-9 (1:1000), Bcl-2 (1:1000), Bax (1:1000), CEA (1:1000), Smad-2/3 (1:1000), p-Smad-3 (1:1000), TGFβRI (1:1000), c-Myc (1:1000), cytochrome *c* (1:2000) and β-actin (1:5000) antibodies at 4 °C, overnight, and incubated with a secondary HRP antibody (1:5000; Vector Laboratories, Burlingame, VT, USA) at room temperature for 1 h. Protein bands were detected using a WEST-ZOL® plus Western Blot Detection System (iNtRON, Gyeonggi, Korea) with subsequent exposure to X-ray films (AGFA, Krotich, Belgium).

3.7. Co-Immunoprecipitation Assay

SNU-C5/5-FU cells were seeded 2 × 10^5 cells/mL for 24 h and treated with LS-1 (7.1 μM) for 12, 24 and 48 h. After treatment, SNU-C5/5-FU cells were lysed with lysis buffer for 30 min at 4 °C. The lysates were centrifuged at 15,000 rpm, 4 °C, for 15 min. Dynabeads® Protein G was added directly to mouse monoclonal anti-TGFβRI antibody in 200 μL PBS with 0.02% Tween-20 and incubated with rotation for 10 min at room temperature. The supernatant was then removed. The beads-antibody complex was washed using 200 μL PBS with 0.02% Tween-20. The beads-antibody complex was added directly to the cell lysates and incubated with rotation for 10 min at room temperature. The supernatant was removed, and the beads-antibody-Ag complex was washed using 200 μL PBS with 0.02% Tween-20 3 times. The beads-antibody-Ag complex was mixed with 20 μL of elution buffer (50 mM glycine (pH 2.8)) and 10 μL of NuPAGE lithium dodecyl sulfate (LDS) sample buffer (Invitrogen, Carlsbad, CA, USA) and then heated for 10 min at 70 °C. The supernatant was separated from the beads using a magnet and loaded onto an SDS-PAGE gel.

3.8. Confocal Microscopy

SNU-C5/5-FU cells were fixed in 3.5% formaldehyde for 30 min. The fixed cells were permeabilized with 0.1% triton X-100. The cells were blocked in 3% BSA for 1 h at room temperature. The cells were treated with primary mouse monoclonal anti-smad-4 and rabbit monoclonal anti-p-Smad-3 antibodies (1:100) overnight at 4 °C. The immunofluorescence staining of the primary antibodies was performed with Alexa Fluor 488 goat anti-rabbit IgG and Alexa Fluor 594 goat anti-mouse IgG secondary antibody. The fluorescence was identified using confocal microscopy (FV500, OLYMPUS), and the images were acquired at constant photomultiplier tube (PMT), gain, offset, magnification (40 × oil immersion objectives with a zoom factor of 4) and resolution.

3.9. Statistical Analyses

Results are shown as means ± standard deviation (SD) from three independent experiments. Student's *t*-test was used to determine the data with the following significance levels: * $p < 0.05$; ** $p < 0.01$. All assays were performed with at least three independent experiments.

4. Conclusions

We previously reported that LS-1 induced apoptosis in HT-29 human colon cancer cells [18]. In conjunction with the report, in this study, our results indicated that LS-1 could induce SNU-C5/5-FU, 5-FU-resistant colon cancer cells, via the activation of the TGF-β pathway with downregulation of CEA. Taken together, our reports suggest that LS-1 may have the potential for use in the treatment of colon cancer, including chemotherapy-resistant colon cancer.

Acknowledgments

This study was supported by a grant from the National R&D Program for Cancer Control, Ministry for Health and Welfare, Republic of Korea (1120340).

Author Contributions

Eun-ji Kim and Hee-Kyoung Kang conceived the experiments, analyzed the data and wrote the manuscript. Eun-ji Kim, Jung-Il Kang, Jeon-Won Kwak, and Chan-Hee Jeon performed the experiments. Cheol-Hee Choi provided 5-fluorouracil-resistant cancer cell line. Nguyen-Huu Tung and Young-Ho Kim provided (1*S*,2*S*,3*E*,7*E*,11*E*)-3,7,11,15-Cembratetraen-17,2-olide (LS-1). Jin-Won Hyun, Young-Sang Koh, and Eun-Sook Yoo analyzed western blot data and revised the manuscript.

Conflicts of Interest

The authors declare no conflict of interest.

References

1. Jemal, A.; Siegel, R.; Ward, E.; Hao, Y.; Xu, J.; Murray, T.; Thun, M.J. Cancer Statistics, 2008. *CA Cancer J. Clin*. **2008**, *58*, 71–96.
2. Masi, G.; Allegrini, G.; Cupini, S.; Marcucci, L.; Cerri, E.; Brunetti, I.; Fontana, E.; Ricci, S.; Andreuccetti, M.; Falcone, A. First-Line Treatment of Metastatic Colorectal Cancer with Irinotecan, Oxaliplatin and 5-Fluorouracil/Leucovorin (FOLFOXIRI): Results of a Phase II Study with a Simplified Biweekly Schedule. *Ann. Oncol*. **2004**, *15*, 1766–1772.
3. Grivicich, I.; Mans, D.R.; Peters, G.J.; Schwartsmann, G. Irinotecan and Oxaliplatin: An Overview of the Novel Chemotherapeutic Options for the Treatment of Advanced Colorectal Cancer. *Braz. J. Med. Biol. Res*. **2001**, *34*, 1087–1103.
4. Jette, L.; Bissoon-Haqqani, S.; le Francois, B.; Maroun, J.A.; Birnboim, H.C. Resistance of Colorectal Cancer Cells to 5-FUdR and 5-FU Caused by Mycoplasma Infection. *Anticancer Res*. **2008**, *28*, 2175–2180.
5. Lee, H.C.; Ling, Q.D.; Yu, W.C.; Hung, C.M.; Kao, T.C.; Huang, Y.W.; Higuchi, A. Drug-Resistant Colon Cancer Cells Produce High Carcinoembryonic Antigen and might Not be Cancer-Initiating Cells. *Drug Des. Dev. Ther*. **2013**, *7*, 491–502.
6. Correale, P.; Aquino, A.; Giuliani, A.; Pellegrini, M.; Micheli, L.; Cusi, M.G.; Nencini, C.; Petrioli, R.; Prete, S.P.; de Vecchis, L.; *et al.* Treatment of Colon and Breast Carcinoma Cells with 5-Fluorouracil Enhances Expression of Carcinoembryonic Antigen and Susceptibility to HLA-A(*)02.01 Restricted, CEA-Peptide-Specific Cytotoxic T Cells *in Vitro*. *Int. J. Cancer* **2003**, *104*, 437–445.

7. Aquino, A.; Prete, S.P.; Guadagni, F.; Greiner, J.W.; Giuliani, A.; Orlando, L.; Masci, G.; de Santis, S.; Bonmassar, E.; Graziani, G. Effect of 5-Fluorouracil on Carcinoembryonic Antigen Expression and Shedding at Clonal Level in Colon Cancer Cells. *Anticancer Res*. **2000**, *20*, 3475–3484.
8. Samara, R.N.; Laguinge, L.M.; Jessup, J.M. Carcinoembryonic Antigen Inhibits Anoikis in Colorectal Carcinoma Cells by Interfering with TRAIL-R2 (DR5) Signaling. *Cancer Res*. **2007**, *67*, 4774–4782.
9. Camacho-Leal, P.; Stanners, C.P. The Human Carcinoembryonic Antigen (CEA) GPI Anchor Mediates Anoikis Inhibition by Inactivation of the Intrinsic Death Pathway. *Oncogene* **2008**, *27*, 1545–1553.
10. Li, Y.; Cao, H.; Jiao, Z.; Pakala, S.B.; Sirigiri, D.N.; Li, W.; Kumar, R.; Mishra, L. Carcinoembryonic Antigen Interacts with TGF-{Beta} Receptor and Inhibits TGF-{Beta} Signaling in Colorectal Cancers. *Cancer Res*. **2010**, *70*, 8159–8168.
11. Nicklas, D.; Saiz, L. Characterization of Negative Feedback Network Motifs in the TGF-Beta Signaling Pathway. *PLoS One* **2013**, *8*, e83531.
12. Sheen, Y.Y.; Kim, M.J.; Park, S.A.; Park, S.Y.; Nam, J.S. Targeting the Transforming Growth Factor-Beta Signaling in Cancer Therapy. *Biomol. Ther. (Seoul)* **2013**, *21*, 323–331.
13. Thuault, S.; Valcourt, U.; Petersen, M.; Manfioletti, G.; Heldin, C.H.; Moustakas, A. Transforming Growth Factor-Beta Employs HMGA2 to Elicit Epithelial-Mesenchymal Transition. *J. Cell Biol*. **2006**, *174*, 175–183.
14. Portella, G.; Cumming, S.A.; Liddell, J.; Cui, W.; Ireland, H.; Akhurst, R.J.; Balmain, A. Transforming Growth Factor Beta is Essential for Spindle Cell Conversion of Mouse Skin Carcinoma *in Vivo*: Implications for Tumor Invasion. *Cell Growth Differ*. **1998**, *9*, 393–404.
15. Sun, L.; Wu, G.; Willson, J.K.; Zborowska, E.; Yang, J.; Rajkarunanayake, I.; Wang, J.; Gentry, L.E.; Wang, X.F.; Brattain, M.G. Expression of Transforming Growth Factor Beta Type II Receptor Leads to Reduced Malignancy in Human Breast Cancer MCF-7 Cells. *J. Biol. Chem*. **1994**, *269*, 26449–26455.
16. Kim, S.J.; Im, Y.H.; Markowitz, S.D.; Bang, Y.J. Molecular Mechanisms of Inactivation of TGF-Beta Receptors during Carcinogenesis. *Cytokine Growth Factor Rev*. **2000**, *11*, 159–168.
17. Nguyen, H.T.; Chau, V.M.; Phan, V.K.; Hoang, T.H.; Nguyen, H.N.; Nguyen, X.C.; Tran, H.Q.; Nguyen, X.N.; Hyun, J.H.; Kang, H.K.; *et al.* Chemical Components from the Vietnamese Soft Coral *Lobophytum* sp. *Arch. Pharm. Res*. **2010**, *33*, 503–508.
18. Hong, J.Y.; Boo, H.J.; Kang, J.I.; Kim, M.K.; Yoo, E.S.; Hyun, J.W.; Koh, Y.S.; Kim, G.Y.; Maeng, Y.H.; Hyun, C.L.; *et al.* (1*S*,2*S*,3*E*,7*E*,11*E*)-3,7,11,15-Cembratetraen-17,2-Olide, a Cembrenolide Diterpene from Soft Coral *Lobophytum* sp., Inhibits Growth and Induces Apoptosis in Human Colon Cancer Cells through Reactive Oxygen Species Generation. *Biol. Pharm. Bull*. **2012**, *35*, 1054–1063.
19. Galluzzi, L.; Kepp, O.; Trojel-Hansen, C.; Kroemer, G. Mitochondrial Control of Cellular Life, Stress, and Death. *Circ. Res*. **2012**, *111*, 1198–1207.

20. Seal, S.; Chatterjee, P.; Bhattacharya, S.; Pal, D.; Dasgupta, S.; Kundu, R.; Mukherjee, S.; Bhattacharya, S.; Bhuyan, M.; Bhattacharyya, P.R.; *et al.* Vapor of Volatile Oils from Litsea Cubeba Seed Induces Apoptosis and Causes Cell Cycle Arrest in Lung Cancer Cells. *PLoS One* **2012**, *7*, e47014.
21. Han, S.U.; Kwak, T.H.; Her, K.H.; Cho, Y.H.; Choi, C.; Lee, H.J.; Hong, S.; Park, Y.S.; Kim, Y.S.; Kim, T.A.; *et al.* CEACAM5 and CEACAM6 are Major Target Genes for Smad3-Mediated TGF-Beta Signaling. *Oncogene* **2008**, *27*, 675–683.
22. Chakrabarty, S.; Tobon, A.; Varani, J.; Brattain, M.G. Induction of Carcinoembryonic Antigen Secretion and Modulation of Protein Secretion/Expression and Fibronectin/Laminin Expression in Human Colon Carcinoma Cells by Transforming Growth Factor-Beta. *Cancer Res*. **1988**, *48*, 4059–4064.
23. Fabregat, I.; Fernando, J.; Mainez, J.; Sancho, P. TGF-Beta Signaling in Cancer Treatment. *Curr. Pharm. Des*. **2014**, *20*, 2934–2947.
24. Hou, R.S.; Duh, C.Y.; Chiang, M.Y.; Lin, C.N. Sinugibberol, a new cytotoxic cembranoid diterpene from the soft coral *Sinularia gibberosa*. *J. Nat. Prod*. **1995**, *58*, 1126–1130.
25. Duh, C.Y.; Wang, S.K.; Weng, Y.L.; Chiang, M.Y.; Dai, C.F. Cytotoxic terpenoids from the Formosan soft coral *Nephthea brassica*. *J. Nat. Prod*. **1999**, *62*, 1518–1521.
26. Duh, C.Y.; Wang, S.K.; Huang, B.T.; Dai, C.F. Cytotoxic Cembrenolide Diterpenes from the Formosan Soft Coral *Lobophytum Crassum*. *J. Nat. Prod*. **2000**, *63*, 884–885.
27. Zhao, M.; Yin, J.; Jiang, W.; Ma, M.; Lei, X.; Xiang, Z.; Dong, J.; Huang, K.; Yan, P. Cytotoxic and Antibacterial Cembranoids from a South China Sea Soft Coral, *Lobophytum* sp. *Mar. Drugs* **2013**, *11*, 1162–1172.
28. Al-Lihaibi, S.S.; Alarif, W.M.; Abdel-Lateff, A.; Ayyad, S.E.; Abdel-Naim, A.B.; El-Senduny, F.F.; Badria, F.A. Three new cembranoid-type diterpenes from Red Sea soft coral *Sarcophyton glaucum*: Isolation and antiproliferative activity against HepG2 cells. *Eur. J. Med. Chem*. **2014**, *81*, 314–322.
29. Elkhateeb, A.; El-Beih, A.A.; Gamal-Eldeen, A.M.; Alhammady, M.A.; Ohta, S.; Pare, P.W.; Hegazy, M.E. New terpenes from the Egyptian soft coral *Sarcophyton shrenbergi*. *Mar. Drugs* **2014**, *12*, 1977–1986.
30. Yip, K.W.; Reed, J.C. Bcl-2 Family Proteins and Cancer. *Oncogene* **2008**, *27*, 6398–6406.
31. Chen, M.; Guerrero, A.D.; Huang, L.; Shabier, Z.; Pan, M.; Tan, T.H.; Wang, J. Caspase-9-induced mitochondrial disruption through cleavage of anti-apoptotic BCL-2 family members. *J. Biol. Chem.* **2007**, *282*, 33888–33895.
32. Bhola, N.E.; Balko, J.M.; Dugger, T.C.; Kuba, M.G.; Sanchez, V.; Sanders, M.; Stanford, J.; Cook, R.S.; Arteaga, C.L. TGF-Beta Inhibition Enhances Chemotherapy Action Against Triple-Negative Breast Cancer. *J. Clin. Investig.* **2013**, *123*, 1348–1358.
33. Hoosein, N.M.; McKnight, M.K.; Levine, A.E.; Mulder, K.M.; Childress, K.E.; Brattain, D.E.; Brattain, M.G. Differential Sensitivity of Subclasses of Human Colon Carcinoma Cell Lines to the Growth Inhibitory Effects of Transforming Growth Factor-Beta 1. *Exp. Cell Res*. **1989**, *181*, 442–453.

34. Soeth, E.; Wirth, T.; List, H.J.; Kumbhani, S.; Petersen, A.; Neumaier, M.; Czubayko, F.; Juhl, H. Controlled Ribozyme Targeting Demonstrates an Antiapoptotic Effect of Carcinoembryonic Antigen in HT29 Colon Cancer Cells. *Clin. Cancer Res*. **2001**, *7*, 2022–2030.
35. Jang, C.W.; Chen, C.H.; Chen, C.C.; Chen, J.Y.; Su, Y.H.; Chen, R.H. TGF-Beta Induces Apoptosis through Smad-Mediated Expression of DAP-Kinase. *Nat. Cell Biol*. **2002**, *4*, 51–58.
36. Rhyu, D.Y.; Park, J.; Sharma, B.R.; Ha, H. Role of reactive oxygen species in transforming growth factor-beta1-induced extracellular matrix accumulation in renal tubular epithelial cells. *PLoS One* **2012**, *44*, 625–628.
37. Yoon, Y.S.; Lee, J.H.; Hwang, S.C.; Choi, K.S.; Yoon, G. TGF beta1 induces prolonged mitochondrial ROS generation through decreased complex IV activity with senescent arrest in Mv1Lu cells. *Oncogene* **2005**, *24*, 1895–1903.
38. Datto, M.B.; Yu, Y.; Wang, X.F. Functional analysis of the transforming growth factor beta responsive elements in the WAF1/Cip1/p21 promoter. *J. Biol. Chem*. **1995**, *270*, 28623–28628.
39. Masgras, I.; Carrera, S.; de Verdier, P.J.; Brennan, P.; Majid, A.; Makhtar, W.; Tulchinsky, E.; Jones, G.D.; Roninson, I.B.; Macip, S. Reactive oxygen species and mitochondrial sensitivity to oxidative stress determine induction of cancer cell death by p21. *J. Biol. Chem*. **2012**, *287*, 9845–9854.
40. Cheng, G.; Cao, Z.; Xu, X.; van Meir, E.G.; Lambeth, J.D. Homologs of gp91phox: Cloning and tissue expression of Nox3, Nox4, and Nox5. *Gene* **2001**, *269*, 131–140.
41. Bedard, K.; Krause, K.H. The NOX family of ROS-generating NADPH oxidases: Physiology and pathophysiology. *Physiol. Rev*. **2007**, *87*, 245–313.
42. Scudiero, D.A.; Shoemaker, R.H.; Paull, K.D.; Monks, A.; Tierney, S.; Nofziger, T.H.; Currens, M.J.; Seniff, D.; Boyd, M.R. Evaluation of a Soluble Tetrazolium/Formazan Assay for Cell Growth and Drug Sensitivity in Culture using Human and Other Tumor Cell Lines. *Cancer Res*. **1988**, *48*, 4827–4833.
43. Fried, J.; Perez, A.G.; Clarkson, B.D. Flow Cytofluorometric Analysis of Cell Cycle Distributions using Propidium Iodide. Properties of the Method and Mathematical Analysis of the Data. *J. Cell Biol*. **1976**, *71*, 172–181.
44. Bradford, M.M. A Rapid and Sensitive Method for the Quantitation of Microgram Quantities of Protein Utilizing the Principle of Protein-Dye Binding. *Anal. Biochem*. **1976**, *72*, 248–254.

Cytotoxic and Antibacterial Angucycline- and Prodigiosin- Analogues from the Deep-Sea Derived *Streptomyces* sp. SCSIO 11594

Yongxiang Song, Guangfu Liu, Jie Li, Hongbo Huang, Xing Zhang, Hua Zhang and Jianhua Ju

Abstract: Two new C-glycoside angucyclines, marangucycline A (**1**) and marangucycline B (**2**), along with three known compounds, dehydroxyaquayamycin (**3**), undecylprodigiosin (**4**) and metacycloprodigiosin (**5**), have been identified as products of the deep-sea sediment strain *Streptomyces* sp. SCSIO 11594. New structures were elucidated on the basis of HRESIMS, 1D and 2D NMR analyses and comparisons to previously reported datasets. Compounds **2** and **4** displayed *in vitro* cytotoxicity against four cancer cell lines A594, CNE2, HepG2, MCF-7 superior to those obtained with cisplatin, the positive control. Notably, compound **2** bearing a keto-sugar displayed significant cytotoxicity against cancer cell lines with IC_{50} values ranging from 0.24 to 0.56 μM; An IC_{50} value of 3.67 μM was found when using non-cancerous hepatic cell line HL7702, demonstrating the cancer cell selectivity of **2**. Compounds **1**–**3** were proved to have weak antibacterial activities against *Enterococcus faecalis* ATCC29212 with an MIC value of 64.0 μg/mL. Moreover, **3** displayed selective antibacterial activity against methicillin-resistant *Staphylococcus epidermidis* shhs-E1 with an MIC value of 16.0 μg/mL.

Reprinted from *Mar. Drugs*. Cite as: Song, Y.; Liu, G.; Li, J.; Huang, H.; Zhang, X.; Zhang, H.; Ju, J. Cytotoxic and Antibacterial Angucycline- and Prodigiosin- Analogues from the Deep-Sea Derived *Streptomyces* sp. SCSIO 11594. *Mar. Drugs* **2015**, *13*, 1340-1359.

1. Introduction

Reports of increasing incidences of various cancers and the rise of multidrug resistant bacteria have inspired and renewed interest in the discovery of new secondary metabolites from marine-derived microorganisms as new drugs or new drug leads [1–3]. Deep-sea derived microorganisms, by virtue of their extreme living environments and selective pressures to which they have adapted, are considered especially exciting as potentially rich sources of new agents for drug discovery [4,5]. Historically speaking, terrestrial actinomycetes have been instrumental in the discovery of important secondary metabolites including antibiotics, antitumor agents, immunosuppressive agents and enzyme inhibitors [6]. This role of "discovery catalyst" is now gradually shifting to marine-derived actinomyces due to diminishing rates of new compound discovery and increasingly frequent "rediscovery" of known agents from terrestrial actinomyces [7–9]. Our continuing studies of cytotoxic and antibacterial compounds from marine-derived actinomyces, especially from the deep-sea derived strains, have led to the discoveries of antibacterial and cytotoxic cyclic peptide marthiapeptide A [10], antimalarial marinacarbolines and indolactam alkaloids [11] from deep-sea derived *Marinactinospora thermotolerans* SCSIO 00652, cytotoxic and antibacterial marfuraquinocins and phenaziterpenes from a deep-sea sediment actinomycete

Streptomyces niveus SCSIO 3406, antibacterial cyclic peptides desotamides and marformycins from the deep-sea sediment actinomycetes *Streptomyces scopuliridis* SCSIO ZJ46 [12] and *Streptomyces drozdowiczii* SCSIO 10141 [13], respectively.

In expanding our efforts to identify cytotoxic and antibacterial secondary metabolites from deep-sea derived actinomycetes, we isolated and identified *Streptomycetes* sp. strain SCSIO 11594 from a South China Sea sediment at a depth of 2403 m. This strain was found to produce cytotoxic and antibacterial substances warranting more detailed evaluation of these bioactivities. Metabolite analyses and subsequent structure elucidation efforts revealed two new C-glycoside angucyclines, marangucyclines A (**1**) and B (**2**), along with three known compounds identified as dehydroxyaquayamycin (**3**), undecylprodigiosin (**4**) and metacycloprodigiosin (**5**), as shown in Figure 1. Herein, we report the isolation, structure elucidation and bioactivity data for **1**–**5** from *Streptomyces* sp. SCSIO 11594.

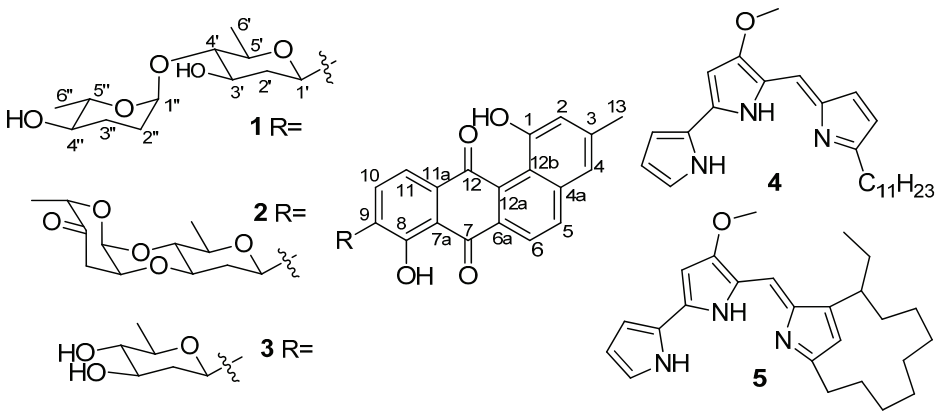

Figure 1. Secondary metabolites **1**–**5** from *Streptomyces* sp. SCSIO 11594.

2. Results and Discussion

2.1. Structure Elucidation

Compound **1**, marangucycline A, was isolated as a brown amorphous powder. The UV spectrum showed maxima at 239, 323 and 437 nm, indicating the presence of a large conjugated moiety. The IR spectrum showed characteristic absorptions at 3418 (hydroxyl), 2928 and 2877 (methyl) and 1632 cm^{-1} (the chelated quinone carbonyl). The compound's molecular formula, $C_{31}H_{32}O_9$, was determined on the basis of the HRESIMS peak at *m/z* 571.1946 $[M + Na]^+$, requiring 16 degrees of unsaturation. Comprehensive analysis of the ^1H and ^{13}C NMR spectroscopic data strongly implied the presence of a typical angucycline of tetrangulol skeleton, with 1,8-dihydroxy-3-methyl-substituted and 9-C-glycosylated [14–17]. Detailed analysis of 1D (^1H and ^{13}C) and 2D (COSY, HMQC, HMBC, NOESY) NMR spectra of **1** (Supplementary Information), allowed the complete assignment of spectra signals (Table 1) and elucidation of the structure (Figures 2 and 3).

Table 1. ^{1}H (500 MHz) and ^{13}C NMR (125 MHz) spectroscopic data of compounds **1** and **2** in $CDCl_3$.

pos.	Marangucycline A (1)		Marangucycline B (2)	
	δ_C	δ_H, mult. (*J* in Hz)	δ_C	δ_H, mult. (*J* in Hz)
1	155.6, C		155.3, C	
2	120.2, CH	7.12, s	120.2, CH	7.15, s
3	142.1, C		142.1, C	
4	121.5, CH	7.23, s	121.3, CH	7.27, s
4a	132.6, C		132.5, C	
5	137.7, CH	8.11, d, *J* = 8.5	137.6, CH	8.14, d, *J* = 8.5
6	122.0, CH	8.29, d, *J* = 8.5	121.8, CH	8.32, d, *J* = 8.5
6a	135.0, C		134.8, C	
7	188.3, C		188.3, C	
7a	114.2, C		114.1, C	
8	158.2, C		157.8, C	
9	138.6, C		137.7, C	
10	133.6, CH	7.90, d, *J* = 8.0	133.6, CH	7.92, d, *J* = 8.0
11	121.3, CH	7.86, d, *J* = 8.0	121.2, CH	7.88, d, *J* = 8.0
11a	133.6, C		133.5, C	
12	189.6, C		189.4, C	
12a	139.3, C		139.2, C	
12b	120.2, C		120.1, C	
13	21.4, CH_3	2.48, s	21.3, CH_3	2.50, s
1-OH		11.43, br s		11.38, br s
8-OH		12.62, br s		12.66, br s
1′	71.3, CH	4.90, d, *J* = 11.2	71.5, CH	5.01, d, *J* = 11.0
2′	38.8, CH_2	2.57, m; 1.46, m	36.6, CH_2	2.48, m; 1.54, m
3′	71.5, CH	3.87, m	77.1, CH	3.84, ddd, *J* = 11.5, 9.0, 4.5
4′	89.2, CH	3.07, t, *J* = 6.5	74.5, CH	3.52, t, *J* = 9.0
5′	74.7, CH	3.57, m	74.6, CH	3.59, m
6′	18.6, CH_3	1.38, d, *J* = 6.0	17.5, CH_3	1.43, d, *J* = 6.0
1″	98.9, CH	4.92, br s	91.4, CH	5.19, d, *J* = 3.0
2″	27.3, CH_2	1.93, m; 1.83, m	71.1, CH	4.35, q, 3.0
3″	30.1, CH_2	1.87, m; 1.25, m	39.9, CH_2	2.65, m
4″	71.8, CH	3.36, td, *J* = 10.0, 4.0	207.7, C	
5″	71.7, CH	3.91, m	77.8, CH	4.75, q, *J* = 6.5
6″	18.0, CH_3	1.33, d, *J* = 6.0	16.2, CH_3	1.39, d, *J* = 6.5

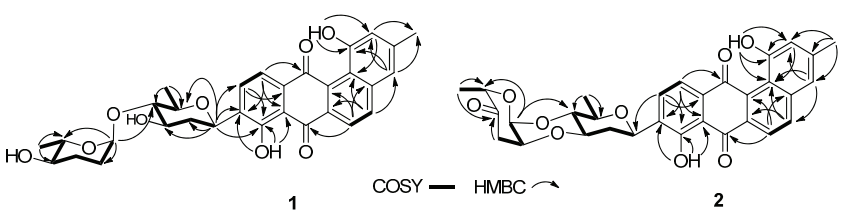

Figure 2. COSY and selected HMBC correlations for compounds **1** and **2**.

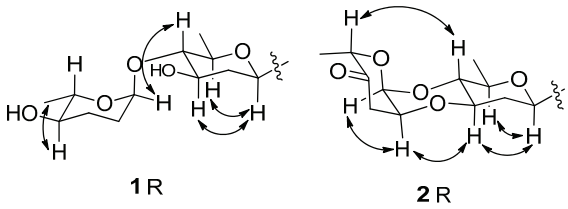

Figure 3. Selected NOESY correlations for the disaccharide moiety (*R*) of compounds **1** and **2**.

^{1}H NMR spectra revealed the presence of two intramolecularly H-bonded hydroxyl groups at δ_H 12.62 and 11.43. Two pairs of *ortho*-coupled aromatic proton signals appeared at δ_H 8.29 (d, J = 8.5 Hz) and δ_H 8.11 (d, J = 8.5 Hz), δ_H 7.90 (d, J = 8.5 Hz) and δ_H 7.86 (d, J = 8.5 Hz), which also were found at C-6 (δ_C 122.0) and C-5 (δ_C 137.7), C-10 (δ_C 133.6) and C-11 (δ_C 121.3) based on HSQC data. Another two singlet proton signals at δ_H 7.23 (s) and δ_H 7.12 (s) were associated with C-4 (δ_C 121.5) and C-2 (δ_C 120.2), respectively. HMBC correlations from δ_H 11.43 to C-1 (δ_C 155.6) and C-2, and from δ_H 12.62 to C-8 (δ_C 158.2), C-7a (δ_C 114.2) and C-9 (δ_C 138.6), enabled assignment of these two hydroxyl groups at C-1 and C-8, respectively. The singlet aromatic methyl (δ_H 2.48, δ_C 21.4) was confirmed at C-3 (δ_C 142.1) by HMBC correlations from δ_H 2.48 to C-3, C-2 and C-4. The tetrangulol skeleton was further elucidated by HBMC correlations of two pairs of *ortho*-coupled protons at C-5, C-6, C-10 and C-11 (Figure 2). Moreover, the ^{1}H NMR spectra displayed seven proton signals between δ_H 4.92 and δ_H 3.07, consistent with seven ^{13}C signals of sp^3 methines between δ_C 98.9 and 71.3. These data support the presence of a disaccharide moiety composed of β-D-olivose and α-L-amicetose on the basis of 2D NMR correlation analyses (Figures 2 and 3), and comparisons with previously reported data [18,19]. COSY correlations of H-1′ (δ_H 4.90)/H-2′b (δ_H 1.46), H-2′a (δ_H 2.57)/H-3′ (δ_H 3.87)/H-4′ (δ_H 3.07)/H-5′ (δ_H 3.57)/H-6' revealed the fragment of C-1′/C-2′/C-3′/C-4′/C-5′/C-6′. The HMBC correlation of H-1′/C-5′ confirmed the existence of an olivose ring. The important HMBC correlations from the anomeric methine proton (CH-1′) to C-8, C-9, and C-10 indicated the C-glycosidic bond (C-9−C-1′) between the aglycone and olivose unit. Similarly, the COSY correlations of H-1″ (δ_H 4.92)/H-2″b (δ_H 1.83)/H-3″a (δ_H 1.87)/H-4″ (δ_H 3.36)/H-5″ (δ_H 3.91)/H-6″ (δ_H 1.33), and the HMBC correlation of H-1″/C-5″ disclosed the presence of a six membered deoxysugar, which was elucidated as amicetose by comparing the ^{1}H and ^{13}C NMR data with those reported [18]. Further HMBC correlations from H-1″ to C-4′ revealed the connection of C-1″-*O*-C-4′ between olivose and amicetose. The relative configurations of two sugar moieties were confirmed by NOESY correlations of H-1′/H-3′, H-1′/H-5′, H-1″/H-4′ and H-4″/CH_3-6″ (Figure 3).

Compound **2**, named marangucycline B, was obtained as a brown amorphous powder. The IR spectrum showed one additional ketone absorption at 1730 cm^{-1} and the characteristic hydroxyl group absorption at ≈3400 cm^{-1} was almost completely absent. The molecular formula $C_{31}H_{28}O_9$ was determined by HR-ESI-MS, which was four mass units less than that of compound **1**, indicating 18 degrees of unsaturation. Therefore, compound **2** was presumed to have one new ketone group and one additional ring relative to compound **1**. The ^{13}C NMR spectrum were similar

with those of **1** (Supplementary Information), except that one carbonyl signal at δ_C 207.7 (C-4″) was observed. Moreover, one of the anomeric carbone (C-1″) signal was changed from δ_C 98.9 in **1** to δ_C 91.4 in **2**. Comparing these characteristic data with the reported [19] revealed the presence of a cinerulose B unit in **2**, which subsequently proved by 2D NMR analyses (Figure 2). COSY spectrum indicated the fragments of C-1″/C-2″/C-3″ and C-5″/C-6″. The HMBC correlations of CH-1″/C-5″, CH_2-3″/C-4″, and CH_3-6″/C-5″ confirmed the structure elucidation of cinerulose B. The HMBC correlation from CH-1″ to C-4′ revealed the C-1″-*O*-C-4′ linkage. Meanwhile, the ^{13}C NMR resonance of C-4′ shifted upfield from δ_C 89.2 in **1** to δ_C 74.5 in **2**, indicating the connection of C-2″-*O*-C-3′. Consequently, the disaccharide in **2** was determined to be a cinerulose B-(1→4, 2→3)-olivosyl unit. The NOESY correlations of H-1′/H-3′, H-1′/H-5′, H-3′/H-2″, H-2″/H-1″ and H-4′/H-5″ confirmed the relative configurations of the two sugars (Figure 3). The ^1H and ^{13}C NMR data for this disaccharide were consistent with these previously reported for compounds with α-cinerulose B-(1→4, 2→3)-β-olivosyl [19]. In a fashion analogous to that applied to compound **1**, the skeleton of **2** was determined by comprehensive analyses of COSY, HMQC and HMBC spectra (Figures 2 and 3).

In addition to compounds **1** and **2**, *Streptomycetes* sp. strain SCSIO 11594 was found to produce known compounds dehydroxyaquayamycin (**3**) [14], undecylprodigiosin (**4**) and metacycloprodigiosin (**5**) [20]. The structures were determined by comparative analyses using previously reported MS, ^1H, and ^{13}C NMR data.

2.2. Cytotoxicities and Antibacterial Activities

The angucyclines are a large group of natural products; members are characterized by an angular tetracyclic (benz[α]anthracene) structure with a hydrolysable sugar moiety. Angucyclines often express a broad range of biological activities. Members of the angucyclines have been noted as potent cytotoxins, antibacterials, antivirals and as inhibitors of assorted enzymes and of platelet aggregation [17,21]. The first reported compounds of this class were tetrangomycin and tetrangulol [17]. To our knowledge, the sugar unit of these species was usually linked at the tetrangomycin C-9 with a C-C bond and at the tetrangulol C-8 with a C-O bond. The antitubercular and cytotoxic compound dehydroxyaquayamycin (**3**), was the first compound shown to have a C-9 linked sugar unit using C-C connectivity with the tetrangulol skeleton. This agent was obtained as a derivative of aquayamycin [15] and later isolated as a natural product from the marine-derived *Streptomyces* sp. BCC45596 [14]. Compounds **1** and **2** were additions to this class of natural products; **1**–**3** were isolated from marine-derived *Streptomyces* sp. SCSIO 11594 as secondary metabolites.

Compounds **1**–**5** were tested for potential *in vitro* cytotoxicity against human lung cancer cell line A549, human nasopharyngeal carcinoma cell line CNE2, human breast adenocarcinoma cell line MCF-7, human hepatocarcinoma cancer cell line HepG2, and the normal hepatic cell line HL7702. The results were shown in Table 2. These data indicate that compound **4** is ≈1–10-fold more cytotoxic than the positive control cisplatin whereas compound **2**, with its keto-sugar moiety, is ≈10–20-fold more potent than cisplatin. Interestingly, **2** and **4** demonstrate significant cytotoxic selectivity, with estimated therapeutic ratio values of 7–5 and 3–45, respectively, as reflected by comparisons of tumor cell-derived IC_{50} values and those obtained using HL7702 cells

(non-cancerous control). Detailed examination of the structure-activity relationship (SAR) of the cytotoxicities of compounds **1**–**3** revealed that (i) the presence of ketone group and C-2″-*O*-C-3′ connection in the disaccharide moiety of compound **2** is critical important for the cytotoxicity; and (ii) the appearance of α-amicetose in the disaccharide chain sharply decreased the cytotoxicity. The SAR study of compounds **4** and **5** revealed that the open form of the aliphatic side chain plays an important role for the cytotoxicity. The anticancer activity of the related natural products has been described in a number of literatures [22–24], and the structure activity relationships of related synthetic natural products have been reported [25–28].

The antibacterial activities of compounds **1**–**5** were evaluated using MRSE shhs-E1, methicillin-resistant *Staphylococcus aureus* (MRSA) shhs-A1, *Staphylococcus aureus* ATCC 29213, *Enterococcus faecalis* ATCC29212, *Escherichia coli* ATCC 25922, *Micrococcus luteus*, and multidrug resistant *Pseudomonas aeruginosa*. These assays revealed that **1**–**3** have weak antibacterial activity against *Enterococcus faecalis* ATCC29212 with a MIC of 64.0 μg/mL in all cases and that **3** is selective against MRSE shhs-E1 demonstrating an MIC of 16.0 μg/mL. Compounds **4** and **5** did not show antibacterial activities against any of the above tested bacteria at a concentration up to 64.0 μg/mL.

Table 2. Summary of *in vitro* cytotoxicities (IC_{50} in μM) for **1**–**5** against four human cancer cell lines and one normal hepatic cell line HL7702 (n = 3) and estimated therapeutic ratio (TR) values.

Agent	A549	CNE2	MCF-7	HepG2	HL7702	TR
1	>50.0	>50.0	>50.0	>50.0	>50.0	-
2	0.45 ± 0.03	0.56 ± 0.02	0.24 ± 0.003	0.43 ± 0.05	3.67 ± 0.07	7–15
3	16.40 ± 0.19	22.27 ± 0.07	23.65 ± 0.09	18.81 ± 0.12	49.34 ± 0.17	2–3
4	0.85 ± 0.01	0.28 ± 0.02	1.11 ± 0.07	4.67 ± 0.09	12.47 ± 0.09	3–45
5	>50.0	>50.0	>50.0	>50.0	>50.0	-
Cisplatin	4.56 ± 0.04	3.75 ± 0.03	5.26 ± 0.07	4.14 ± 0.06	15.34 ± 0.08	3–4

2.3. Identification of Strain SCSIO 11594

Strain SCSIO 11594 (Figure 4a) was isolated from a sediment sample collected from the South China Sea (115°27.751 E, 19°28.581 N) at a depth of 2403 m using HRA medium (histidine 0.1 g, raffinose 1.0 g, Na_2HPO_4 0.3 g, KCl 1.7 g, $MgSO_4 \cdot 7H_2O$ 0.05 g, $FeSO_4 \cdot 7H_2O$ 0.01 g, $CaCO_3$ 0.02 g, agar 12 g, pH7.2, seawater 500 mL, distilled water 500 mL) with incubation at 28 °C for up to 4 weeks. The strain is preserved at the RNAM Center for Marine Microbiology, South China Sea Institute of Oceanology, Chinese Academy of Sciences. Extraction of genomic DNA, PCR amplification, sequencing of the 16S rRNA gene, and phylogenetic analysis were performed as described by You and co-workers [29]. The 16S rRNA gene sequence has been deposited in GenBank with accession no. KP276583. The results of phylogenetic analyses showed that strain SCSIO 11594 should be a member of the genus *Streptomyces*. The 16S rRNA gene sequence of strain SCSIO 11594 demonstrated the highest similarity value to *Streptomyces rubrogriseus* LMG

20318^{T} (99.86%) and was found to cluster with members of the genus *Streptomyces* in the phylogenetic tree (Figure 4b).

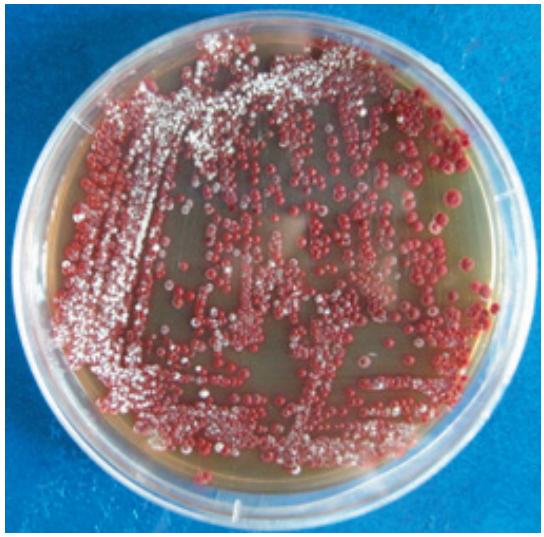

(**a**)

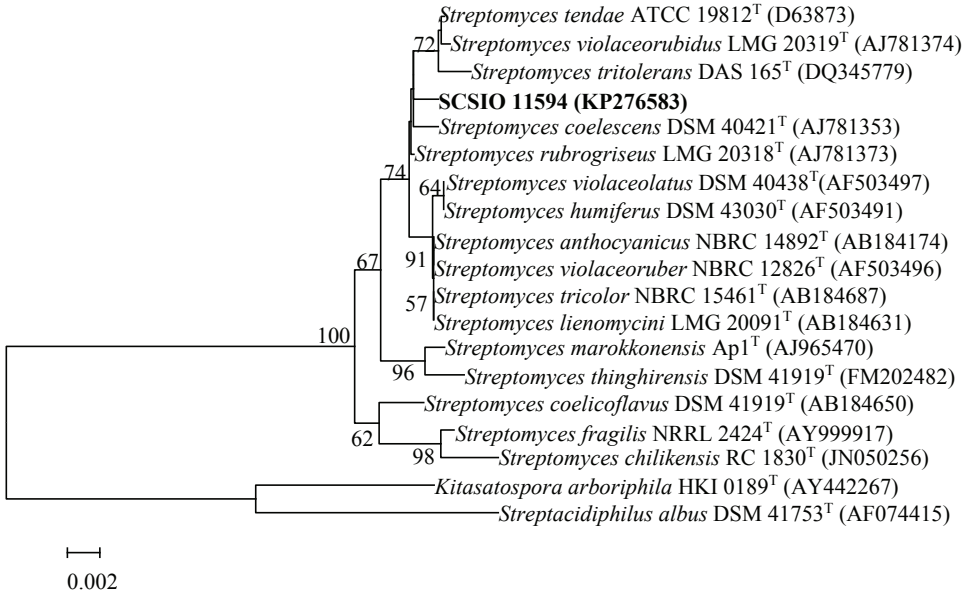

(**b**)

Figure 4. (**a**) Strain SCSIO 11594; (**b**) Neighbor-joining phylogenetic tree based on 16S rRNA gene sequences of strain SCSIO 11594 and members of the family *Streptomycetaceae*. Bootstrap values (expressed as percentages of 1000 replications) exceeding 50% are shown at the branch points.

3. Experimental Section

3.1. General Experimental Procedures

Optical rotations were determined using an MCP-500 polarimeter (Anton Paar, Graz, Austria). UV spectra were obtained with a UV-2600 spectrometer (Shimadzu, Tokyo, Japan). IR spectra were measured using an IRAffinity-1 spectrophotometer (Shimadzu, Tokyo, Japan). NMR spectra were acquired with an Avance 500 spectrometer (Bruker, Fällanden, Switzerland) at 500 MHz for the ^{1}H nucleus and 125 MHz for the ^{13}C nucleus. ESIMS and HRESIMS data were determined using an amaZon SL ion trap mass spectrometer and MaXis quadrupole-time-of-flight mass spectrometer (Bruker, Bremen, Germany), respectively. CC (Column chromatography) was performed on 100–200 mesh silica gel (Yantai Jiangyou Silica Gel Development Co., Ltd., Yantai, China). RP-MPLC (reversed phase-medium pressure preparative liquid chromatography) were carried out using the CHEETAH MP200 (Agela Technologies, Tianjin, China) and Claricep Flash columns filled with ODS (40−63 μm, YMC). RP-HPLC (high performance liquid chromatography) analyses were carried out using a Hitachi HPLC with YMC-Pack ODS-A column (250 × 10 mm, 5 μm).

3.2. Fermentation, Extraction and Isolation of the Compounds

The strain was inoculated to a modified ISP-4 agar plate (soluble starch 1.0%, K_2HPO_4 0.1%, $MgSO_4 \cdot 7H_2O$ 0.1%, $(NH_4)_2SO_4$ 0.2%, $CaCO_3$ 0.2%, sea salt 3.0%, pH 7.2 before sterilization) from a glycerol tube under aseptic conditions and incubated 5 day at 28 °C. The mycelium was then transferred into 250 mL Erlenmeyer flasks each containing 50 mL of modified-AM2ab medium (soluble starch 0.5%, soybean powder 0.5%, yeast exact power 0.2%, bacterial peptone 0.2%, glucose 2.0%, KH_2PO_4 0.05%, $MgSO_4 \cdot 7H_2O$ 0.05%, NaCl 0.40%, sea salt 3.0% $CaCO_3$ 0.2%, pH 7.2 before sterilization) and incubated on rotary shakers with 200 rpm at 28 °C for 36 h. Each culture (seed) was then inoculated into 1 L Erlenmeyer flasks containing 200 mL of modified-AM2ab and fermentation continued under the conditions used to generate the seed cultures. Incubation was carried out under these conditions for 8 day. The 16 L of culture was then harvested and centrifuged at 3214× *g* (3900 rpm) for 10 min to yield the supernatant and mycelial cake, which was extensively extracted by butanone and acetone, respectively. The extracted residues were combined after HPLC analyses to validate extract contents.

The combined residues were subjected to silica gel CC using gradient elution initially using petroleum ether (P)/chloroform (C) (200/0, 100/100, v/v), and then with C/MeOH (M) (150/0, 147/3, 144/6, 141/9, 138/12, 145/15, 130/30, 75/75, v/v), to give ten fractions A1–A10. The fractions A4–A8 were combined and further subjected to ODS column MPLC by eluting with a linear gradient from 70/30/0.1 (MeCN/H_2O/HAc) to 100/0/0.1 over 60 min at 15 mL/min with detection at 323 nm; elution was then continued with 100/0/0.1 for 30 min to ultimately afford fractions B1–B9. The fractions B6 and B7 and B8 and B9 were subjected to CC silica gel with a gradient elution (P/C 10/40, 0/50, C/M 49.5/0.5, 49/1, 48.5/1.5, v/v), respectively, to give fractions C1–17 and D1–17. The fractions C12 and C13 and D9–12 were repeatedly eluted by isocratic SP-HPLC elution with MeCN/H_2O/HAc (95/5/0.1) at 2.5 mL/min and detection at 323 nm,

respectively, to generate compound **1** (30.5 mg) at a retention time of 12.2 min and compound **2** (7.5 mg) with retention time 14.3 min. Similarly, compound **3** (3.7 mg) was isolated from B5 by repeated isocratic RP-HPLC elution with MeCN/H_2O/HAc (85/15/0.1) and a retention time of 8.7 min. Fraction A3 was subjected to silica gel CC with gradient elution (P/C 50/0, 40/10, 30/20, 20/30, 10/40, 0/50, C/M 49.5/0.5, 49/1) to afford fractions E1–E8; E5–E7 were repeatedly subjected to preparative TLC (100% chloroform) to afford **4** (33.2 mg) and **5** (45.3 mg) with R_f values of 0.7 and 0.4, respectively.

Marangucycline A (1): brown amorphous powder; $[\alpha]^{25}_D$ 35.0 (*c* 0.37, $CHCl_3$); UV ($CHCl_3$) λ_{max} (log ε) 239 (4.39), 323 (4.31), 437 (3.87) nm; IR (ATR) ν_{max} 3418, 2928, 2878, 1631, 1269, 1049 cm^{-1}; ^1H and ^{13}C NMR spectroscopic data, Table 1; (−)-ESIMS *m/z* $[M - H]^-$ 547.42, and (+)-HRESIMS *m/z* $[M + Na]^+$ 571.1946, calcd for $C_{31}H_{32}O_9Na$, 571.1939.

Marangucycline B (2): brown amorphous powder; $[\alpha]^{25}_D$ 30.5 (*c* 0.19, $CHCl_3$); UV ($CHCl_3$) λ_{max} (log ε) 239 (4.15), 323 (4.03), 436 (3.58) nm; IR (ATR) ν_{max} 2922, 2852, 1730, 1635, 1254, 1109, 1069 cm^{-1}; ^1H and ^{13}C NMR spectroscopic data, Table 1; (+)-HRESIMS *m/z* $[M + H]^+$ 545.1796, calcd for $C_{31}H_{29}O_9$, 545.1806; $[M + Na]^+$ 567.1620, cacld for $C_{31}H_{28}O_9Na$, 567.1626.

3.3. Cytotoxicity Assays

Compounds **1**–**5** were evaluated for cytotoxic activity using four human cancer cell lines, A549, CNE2, HepG2, MCF-7, one normal hepatic cell line HL7702 and previously reported MTT methodologies [30]. IC_{50} values were calculated using GraphPad Prism 5 software. All data were obtained in triplicate and are presented as means ± SD. Cisplatin was used as a positive control.

3.4. Antibacterial Activities Assay

The antibacterial activities of compounds **1**–**5** were assessed using seven strains of pathogenic bacteria including MRSE shhs-E1, MRSA shhs-A1, *Staphylococcus aureus* ATCC 29213, *Enterococcus faecalis* ATCC29212, *Escherichia coli* ATCC 25922, *Micrococcus luteus*, and multidrug resistant *Pseudomonas aeruginosa*. Dilution antimicrobial susceptibility tests for aerobic bacteria were carried out as previously reported [31,32]. Lowest concentrations of antimicrobial agents that completely inhibit cell growth in microdilution wells were determined by naked eye.

4. Conclusions

Five compounds including two new angucycline antibiotics, marangucycline A (**1**) and marangucycline B (**2**), were isolated from the deep-sea derived *Streptomyces* sp. SCSIO11594. Compounds **2** and **4**, especially the new C-glycoside angucycline compound **2,** displayed *in vitro* cytotoxicities against four cancer cell lines A594, CNE2, HepG2, MCF-7 superior to those noted with cisplatin. Remarkably, compounds **2** and **4** demonstrated significant anti-tumor selectivity. These data enable important correlations of structure to biological function and may be important for future drug lead efforts. Additionally, dehydroxyaquayamycin (**3**) was found to exert selective antibacterial activity against MRSE shhs-E1. This realization may prove important during

the course of structure-activity relationship studies aimed at new antibacterial drug discovery/design studies.

Acknowledgments

This study was supported, in part, by the National Natural Science Foundation of China (41206135, 41476133, and 81425022), Talents Recruitment Grant of "Yangfan Plan" of Guangdong Province, China (YueRenCaiBan (2014) 1), the National High Technology Research and Development Program of China (2012AA092104), and a special financial fund for innovative developments of the Marine Economic Demonstration Project (GD2012-D01-001 and GD2012-D01-002). Additionally, we thank the analytical facility center of the South China Sea Institute of Oceanology, Xiao, and Li for recording NMR data and Sun, and Zhang for acquiring ESIMS and HRESIMS data.

Author Contributions

Y.S. performed the fermentation and isolation of the compounds and wrote the paper. G.L. tested the biological activities. J.L. isolated and identified the strain *Streptomyces* sp. SCSIO11594. H.H. and X.Z. elucidated the compound structures. H.Z. and J.J. designed the study, analyzed results and wrote the paper.

Conflicts of Interest

The authors declare no conflict of interest.

References

1. Xiong, Z.Q.; Wang, J.F.; Hao, Y.Y.; Wang, Y. Recent advances in the discovery and development of marine microbial natural products. *Mar. Drugs* **2013**, *11*, 700–717.
2. Eom, S.H.; Kim, Y.M.; Kim, S.K. Marine bacteria: Potential sources for compounds to overcome antibiotic resistance. *Appl. Microbiol. Biotechnol.* **2013**, *97*, 4763–4773.
3. Cheung, R.C.; Wong, J.H.; Pan, W.L.; Chan, Y.S.; Yin, C.M.; Dan, X.L.; Wang, H.X.; Fang, E.F.; Lam, S.K.; Ngai, P.H.; *et al.* Antifungal and antiviral products of marine organisms. *Appl. Microbiol. Biotechnol.* **2014**, *98*, 3475–3494.
4. Skropeta, D. Deep-sea natural products. *Nat. Prod. Rep.* **2008**, *25*, 1131–1166.
5. Skropeta, D.; Wei, L. Recent advances in deep-sea natural products. *Nat. Prod. Rep.* **2014**, *31*, 999–1025.
6. Berdy, J. Bioactive microbial metabolites. *J. Antibiot.* **2005**, *58*, 1–26.
7. Lam, K.S. Discovery of novel metabolites from marine actinomycetes. *Curr. Opin. Microbiol.* **2006**, *9*, 245–251.
8. Zotchev, S.B. Marine actinomycetes as an emerging resource for the drug development pipelines. *J. Biotechnol.* **2012**, *158*, 168–175.

9. Subramani, R.; Aalbersberg, W. Marine actinomycetes: An ongoing source of novel bioactive metabolites. *Microbiol. Res.* **2012**, *167*, 571–580.
10. Zhou, X.; Huang, H.; Chen, Y.; Tan, J.; Song, Y.; Zou, J.; Tian, X.; Hua, Y.; Ju, J. Marthiapeptide A, an anti-infective and cytotoxic polythiazole cyclopeptide from a 60 L scale fermentation of the deep sea-derived *Marinactinospora thermotolerans* SCSIO 00652. *J. Nat. Prod.* **2012**, *75*, 2251–2255.
11. Huang, H.; Yao, Y.; He, Z.; Yang, T.; Ma, J.; Tian, X.; Li, Y.; Huang, C.; Chen, X.; Li, W.; *et al*. Antimalarial β-carboline and indolactam alkaloids from *Marinactinospora thermotolerans*, a deep sea isolate. *J. Nat. Prod.* **2011**, *74*, 2122–2127.
12. Song, Y.; Li, Q.; Liu, X.; Chen, Y.C.; Zhang, Y.; Sun, A.; Zhang, W.; Zhang, J.; Ju, J. Cyclic hexapeptides from the deep South China Sea-derived *Streptomyces scopuliridis* SCSIO ZJ46 active against pathogenic Gram-positive Bacteria. *J. Nat. Prod.* **2014**, *77*, 1937–1941.
13. Zhou, X.; Huang, H.; Li, J.; Song, Y.; Jiang, R.; Liu, J.; Zhang, S.; Hua, Y.; Ju, J. New anti-infective cycloheptadepsipeptide congeners and absolute stereochemistry from the deep sea-derived *Streptomyces drozdowiczii* SCSIO 10141. *Tetrahedron* **2014**, *70*, 7795–7801.
14. Supong, K.; Thawai, C.; Suwanborirux, K.; Choowong, W.; Supothina, S.; Pittayakhajonwut, P. Antimalarial and antitubercular C-glycosylated benz[α]anthraquinones from the marine-derived *Streptomyces* sp. BCC45596. *Phytochem. Lett.* **2012**, *5*, 651–656.
15. Sezaki, M.; Kondo, S.; Maeda, K.; Umezawa, H.; Ono, M. The structure of aquayamycin. *Tetrahedron* **1970**, *26*, 5171–5190.
16. Kuntsmann, M.P.; Mitscher, L.A. The structural characterization of tetrangomycin and tetrangulol. *J. Org. Chem.* **1966**, *31*, 2920–2925.
17. Rohr, J.; Thiericke, R. Angucycline group antibiotics. *Nat. Prod. Rep.* **1992**, *9*, 103–137.
18. Oki, T.; Kitamura, I.; Matsuzawa, Y.; Shibamoto, N.; Ogasawara, T.; Yoshimoto, A.; Inui, T.; Naganawa, H.; Takeuchi, T.; Umezawa, H. Anti-tumor anthracycline antibiotics, aclacinomycin-A and analogs. 2. structural determination. *J. Antibiot.* **1979**, *32*, 801–819.
19. Huang, H.; Yang, T.; Ren, X.; Liu, J.; Song, Y.; Sun, A.; Ma, J.; Wang, B.; Zhang, Y.; Huang, C.; *et al*. Cytotoxic angucycline class glycosides from the deep sea actinomycete *Streptomyces lusitanus* SCSIO LR32. *J. Nat. Prod.* **2012**, *75*, 202–208.
20. Liu, R.; Cui, C.B.; Duan, L.; Gu, Q.Q.; Zhu, W.M. Potent *in vitro* anticancer activity of metacycloprodigiosin and undecylprodigiosin from a sponge-derived actinomycete *Saccharopolyspora* sp. nov. *Arch. Pharm. Res.* **2005**, *28*, 1341–1344.
21. Abdelfattah, M.S.; Kharel, M.K.; Hitron, J.A.; Baig, I.; Rohr, J. Moromycins A and B, isolation and structure elucidation of C-glycosylangucycline-type antibiotics from *Streptomyces* sp. KY002. *J. Nat. Prod.* **2008**, *71*, 1569–1573.
22. Omura, S.; Tanaka, H.; Oiwa, R.; Awaya, J.; Masuma, R.; Tanaka, K. New antitumor antibiotics, OS-4742 A1, A2, B1 and B2 produced by a strain of *Streptomyces*. *J. Antibiot.* **1977**, *30*, 908–916.
23. Imamura, N.; Kakinuma, K.; Ikekawa, N.; Tanaka, H.; Omura, S. The structure of vineomycin B2. *J. Antibiot.* **1981**, *34*, 1517–1518.

24. Imamura, N.; Kakinuma, K.; Ikekawa, N.; Tanaka, H.; Omura, S. Biosynthesis of vineomycins A1 and B2. *J. Antibiot.* **1982**, *35*, 602–608.
25. Morton, G.E.; Barrett, A.G.M. Iterative benzyne-furan cycloaddition reactions: Studies toward the total synthesis of ent-Sch 47554 and ent-Sch 47555. *Org. Lett.* **2006**, *8*, 2859–2861.
26. Sobti, A.; Kim, K.J.; Sulikowski, G.A. Application of glycosyltetrazoles in oligosaccharide synthesis: Assembly of the C3 trisaccharide component of the antibiotic PI-080. *J. Org. Chem.* **1996**, *61*, 6–7.
27. Yu, X.; O'Doherty, G.A. De novo asymmetric synthesis and biological evaluation of the trisaccharide portion of PI-080 and vineomycin B2. *Org. Lett.* **2008**, *10*, 4529–4532.
28. Yu, X.M.; Li, M.S.; O'doherty, G.A. De novo asymmetric approach to the disaccharide portion of Sch-47554. *Heterocycles* **2011**, *82*, 1577–1584.
29. You, Z.Q.; Li, J.; Qin, S.; Tian, X.P.; Wang, F.Z.; Zhang, S. *Georgenia sediminis* sp. nov. a moderately thermophilic actinobacterium isolated from sediment. *Int. J. Syst. Evol. Microbiol.* **2013**, *63*, 4243–4247.
30. Mosmann, T. Rapid colorimetric assay for cellular growth and survival: Application to proliferation and cytotoxicity assays. *J. Immunol. Methods* **1983**, *65*, 55–63.
31. CLSI. *Methods for Dilution Antimicrobial Susceptibility Tests for Bacteria That Grow Aerobically*, Approved Standard-8th ed.; Clinical and Laboratory Standards Institute: Wayne, PA, USA, 2009; pp. M07–A8.
32. Song, Y.; Huang, H.; Chen, Y.; Ding, J.; Zhang, Y.; Sun, A.; Zhang, W.; Ju, J. Cytotoxic and antibacterial marfuraquinocins from the deep South China Sea-derived *Streptomyces niveus* SCSIO 3406. *J. Nat. Prod.* **2013**, *76*, 2263–2268.

Kalkitoxin Inhibits Angiogenesis, Disrupts Cellular Hypoxic Signaling, and Blocks Mitochondrial Electron Transport in Tumor Cells

J. Brian Morgan, Yang Liu, Veena Coothankandaswamy, Fakhri Mahdi, Mika B. Jekabsons, William H. Gerwick, Frederick A. Valeriote, Yu-Dong Zhou, and Dale G. Nagle

Abstract: The biologically active lipopeptide kalkitoxin was previously isolated from the marine cyanobacterium *Moorea producens* (*Lyngbya majuscula*). Kalkitoxin exhibited *N*-methyl-D-aspartate (NMDA)-mediated neurotoxicity and acted as an inhibitory ligand for voltage-sensitive sodium channels in cultured rat cerebellar granule neurons. Subsequent studies revealed that kalkitoxin generated a delayed form of colon tumor cell cytotoxicity in 7-day clonogenic cell survival assays. Cell line- and exposure time-dependent cytostatic/cytotoxic effects were previously observed with mitochondria-targeted inhibitors of hypoxia-inducible factor-1 (HIF-1). The transcription factor HIF-1 functions as a key regulator of oxygen homeostasis. Therefore, we investigated the ability of kalkitoxin to inhibit hypoxic signaling in human tumor cell lines. Kalkitoxin potently and selectively inhibited hypoxia-induced activation of HIF-1 in T47D breast tumor cells (IC_{50} 5.6 nM). Mechanistic studies revealed that kalkitoxin inhibits HIF-1 activation by suppressing mitochondrial oxygen consumption at electron transport chain (ETC) complex I (NADH-ubiquinone oxidoreductase). Further studies indicate that kalkitoxin targets tumor angiogenesis by blocking the induction of angiogenic factors (*i.e.*, VEGF) in tumor cells.

Reprinted from *Mar. Drugs*. Cite as: Morgan, J.B.; Liu, Y.; Coothankandaswamy, V.; Mahdi, F.; Jekabsons, M.B.; Gerwick, W.H.; Valeriote, F.A.; Zhou, Y.-D.; Nagle, D.G. Kalkitoxin Inhibits Angiogenesis, Disrupts Cellular Hypoxic Signaling, and Blocks Mitochondrial Electron Transport in Tumor Cells. *Mar. Drugs* **2015**, *13*, 1552-1568.

1. Introduction

When environmental factors are conducive, the benthic marine cyanobacterium *Moorea producens* sp. nov. (Oscillatoriaceae), previously classified as *Lyngbya majuscula* Gomont, typically forms localized mini-blooms that may cover sections of a coral reef [1–4]. Marine cyanobacteria produce a wide variety of structurally novel secondary metabolites [5,6]. Most of the more than 300 natural products isolated from *M. producens* can be classified into one of two general biosynthetic classes: (A) non-ribosomally produced linear and cyclic peptides, and cyclic depsipeptides, and (B) lipopeptides of mixed biogenetic origin that combine polyketide or fatty acid derived precursors with peptide-derived structural components [6].

The lipopeptide kalkitoxin (Figure 1A) was first isolated from a Curaçao collection of *M. producens* [7,8] and found to be ichthyotoxic (*Carassius auratus*, LC_{50} 700 nM) and brine shrimp toxic (*Artemia salina*, LC_{50} 170 nM), inhibit cell division (fertilized sea urchin embryo assay, IC_{50} ~50 nM), suppress inflammation, and potently block voltage sensitive-sodium channels in murine neuro-2a cells (EC_{50} 1 nM). Synthetic kalkitoxin analogues were also highly toxic to

A. salina [9]. Kalkitoxin displayed exposure time-dependent potent neurotoxicity towards primary rat cerebellar granular neurons (CGNs) (LC_{50} 3.86 nM) [10]. Mechanistic studies examined the interaction of kalkitoxin with the tetrodotoxin- and voltage-sensitive sodium channel (TTX-VSSC) in CGN cells [11]. Total synthesis and biological evaluation of (+)-kalkitoxin, the naturally occurring form, revealed that kalkitoxin displayed solid tumor-selective cytotoxicity when evaluated in extended duration clonogenic assays (colorectal carcinoma HCT-116 cells: 10% survival at 0.002 μg/mL with 168 h exposure; inactive at 10 μg/mL with 24 h exposure) [12]. However, the molecular mechanism(s) responsible for the potent tumor cell-selective cytotoxicity was unclear.

2. Results and Discussion

2.1. HIF-1 Inhibitory Activity

The transcription factor hypoxia-inducible factor-1 (HIF-1) regulates oxygen homeostasis by activating the expression of genes that increase oxygen availability and those that decrease oxygen consumption, thus mediating cellular adaptation to hypoxia [13]. Preclinical and clinical studies have established that HIF-1 dysregulation directly impacts cancer etiology and progression, while HIF-1 inhibition suppresses tumor growth and enhances the efficacy of both radiation and chemotherapy [14–16]. As part of our ongoing campaign to identify natural product-based inhibitors of HIF-1 activation, a human breast tumor T47D cell-based HIF-1 reporter assay was used to evaluate ~300 purified marine natural products and 15,000 marine invertebrate and algae extracts from the U.S. National Cancer Institute's (NCI's) Open Repository [17–20]. Kalkitoxin (1 μM) completely inhibited HIF-1 activation in the primary screening. Concentration-response studies were performed in T47D cells to determine the effects of kalkitoxin on HIF-1 activation. At low nanomolar concentrations, kalkitoxin selectively blocked hypoxia-induced HIF-1 activation (IC_{50} 5.7 nM, 95% CI: 4.6 to 7.1 nM, Figure 1), relative to its effect on chemical hypoxia (1,10-phenanthroline; 10 μM)-activated HIF-1 (IC_{50} > 1 μM, Figure 1). Parallel viability assay results indicated that kalkitoxin inhibited hypoxic HIF-1 activation without pronounced cytotoxicity, even up to micromolar levels at the 16 h time point (Figure 1).

2.2. Suppression of HIF-1 Target Gene Expression

As a key regulator of oxygen homeostasis, HIF-1 controls the expression of over one hundred genes that modulate critical aspects of cellular physiology [13]. The effects of kalkitoxin on the induction of HIF-1 target genes *VEGF* (vascular endothelial growth factor) and *GLUT-1* (glucose transporter-1) were examined by real time RT-PCR. Hypoxic exposure of T47D cells (1% O_2, 16 h) increased the expression of *VEGF* (Figure 2A) and *GLUT-1* (Figure 2B) at the mRNA level. Kalkitoxin (0.01 and 0.1 μM) inhibited the hypoxic induction of *VEGF* or *GLUT-1* mRNA expression in a concentration-dependent manner (Figure 2). As observed in the T47D cell-based HIF-1 reporter assays (Figure 1B), the inhibitory effects exerted by kalkitoxin were significantly greater for HIF-1 target genes that were induced by hypoxia, compared to those induced by 1,10-phenanthroline (10 μM) (Figure 2).

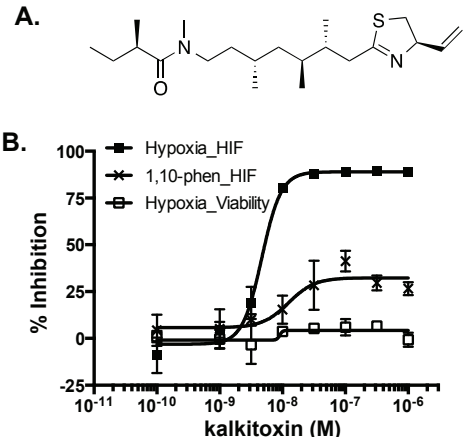

Figure 1. (**A**) Structure of kalkitoxin; (**B**) Kalkitoxin is a potent inhibitor of hypoxia-induced HIF-1 activation. Exponentially grown T47D cells transfected with the pHRE3-TK-luc construct for HIF-1 activity were plated into 96-well plates. Kalkitoxin was added at the specified concentrations and the cells exposed to hypoxia (1% O_2) or 1,10-phenanthroline (10 μM) for 16 h, respectively. Cells were lysed, luciferase activity determined, and the data presented as "% Inhibition" of the induced control. Data shown are average ± standard deviation (n = 3). For the viability study, T47D cells plated into 96-well plates were exposed to kalkitoxin and hypoxia as that described for the reporter assay. Cell viability was determined by the SRB method. Data presentation is the same as that described for the reporter assay.

2.3. Inhibition of Hypoxia-Induced Angiogenesis

Hypoxic regions are commonly found throughout solid tumors. The extent of tumor hypoxia correlates with advanced disease stages and treatment resistance among cancer patients [21–23]. To survive in a low O_2 environment, hypoxic tumor cells stimulate tumor angiogenesis through the HIF-1-dependent induction of the potent angiogenic factor, VEGF [24]. Hypoxic exposure (1% O_2, 16 h) of T47D cells significantly increased the production of secreted VEGF protein, relative to the untreated control (Figure 3A). Kalkitoxin (0.1 μM) suppressed the level of hypoxia-induced secreted VEGF protein by ~50% (Figure 3A). The potential anti-angiogenic activity of kalkitoxin was assessed using a human umbilical vein endothelial cell (HUVEC)-based tube formation assay, a widely employed *in vitro* model for angiogenesis. Under normal culture conditions, HUVEC cells appear scattered (Basal Media, Figure 3B, panel e). When exposed to angiogenic factors, such as recombinant human VEGF protein, HUVEC cells are stimulated to form interconnected tube-like structures (tube formation, VEGF, Figure 3B, panel f) [25]. Tube formation was induced by normoxic T47D cell-conditioned media (Control/Normoxia, Figure 3B, panel a). The angiogenic activity of the T47D cell-conditioned media sample was significantly enhanced by hypoxic exposure (1% O_2, 16 h) (Control/Hypoxia, Figure 3B, panel b), which increases angiogenic factor

(*i.e.*, VEGF) production (Figure 3A). Kalkitoxin (0.1 μM) suppressed the angiogenic activity of the hypoxic T47D cell-conditioned media at a concentration that also inhibited hypoxia-induced HIF-1 activation and VEGF induction (Kalkitoxin/Hypoxia, Figure 3B, panel d). Kalkitoxin did not prevent normoxic T47D cell-conditioned media from inducing angiogenesis (Kalkitoxin/Normoxia, Figure 3B, panel c). Thus, kalkitoxin appears to inhibit tumor angiogenesis by blocking the induction and/or expression of angiogenic factors, not by directly suppressing the tube formation process. These observations are corroborated by quantitative microscopic results (Figure 3C, tube length; Figure 3D, number of branching points).

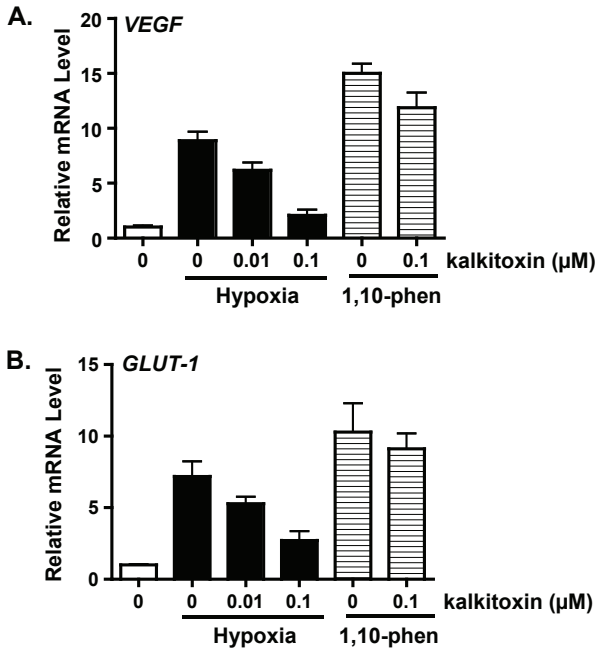

Figure 2. Kalkitoxin blocks hypoxic induction of HIF-1 target genes *VEGF* and *GLUT-1* at the mRNA level. Kalkitoxin was added to exponentially grown T47D cells at the specified concentrations and the incubation continued for another 16 h under hypoxia (1% O_2) or in the presence of 1,10-phenanthroline (1,10-phen, 10 μM), respectively. The cells were lysed and total RNA extracted. The levels of *VEGF* (**A**) and *GLUT-1* mRNAs (**B**) were determined by quantitative real time RT-PCR, normalized to that of an internal control 18S rRNA, and presented as relative values to an untreated control determined by the $\Delta\Delta C_T$ method (mean ± standard deviation, $n = 3$).

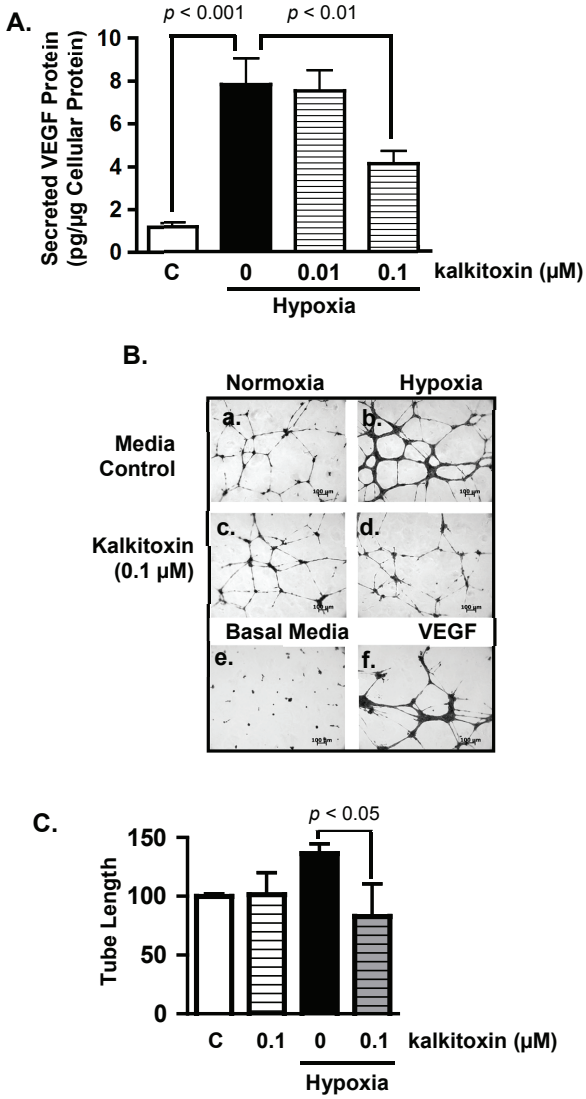

Figure 3. *Cont.*

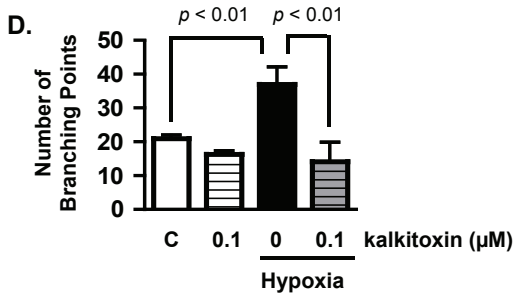

Figure 3. Kalkitoxin inhibits hypoxia-stimulated tumor angiogenesis by blocking the induction of angiogenic factor VEGF. (**A**) T47D cells were exposed to hypoxic conditions (1% O_2, 16 h) in the presence and absence of kalkitoxin at the specified concentrations. The levels of secreted VEGF protein in the conditioned media samples were determined by ELISA and normalized to the amount of total cellular proteins (average + standard deviation, $n = 3$). "C"—media control. The p values of statistically significant differences when compared to the media controls are shown; (**B**) Representative HUVEC tube formation assay results. T47D cell-conditioned media samples were prepared as described in (A). Both negative (Basal Media, **e**) and positive (VEGF, **f**) controls are included at the bottom. A 100 μm scale bar is included in each panel; (**C**) Average + standard deviation of tube length, quantified from three randomly selected fields for each specified condition. The p-values are shown for statistically significant differences; (**D**) Branching points, data determined and presented as described in (C).

2.4. Mechanism of Action Studies

2.4.1. HIF-1α Expression

To discern the mechanism(s) responsible for the inhibition exerted by kalkitoxin on HIF-signaling, its effect on nuclear HIF-1α protein induction was assessed in T47D cells. In general, HIF-1 activity is determined by the concurrent induction and activation of the oxygen-regulated HIF-1α subunit [26]. The nuclear extract from control cells under normoxic conditions did not contain HIF-1α protein (Figure 4). Hypoxic conditions (1% O_2, 4 h) induced nuclear HIF-1α protein accumulation (Figure 4). Kalkitoxin (0.01 and 0.1 μM) blocked the hypoxic induction of HIF-1α protein, without affecting constitutively expressed HIF-1β subunit levels in the nuclear extract samples from hypoxia-exposed cells (Figure 4). In contrast, kalkitoxin did not block the induction of HIF-1α protein by 1,10-phenanthroline under normoxic conditions (10 μM 1,10-phen, 4 h, Figure 4).

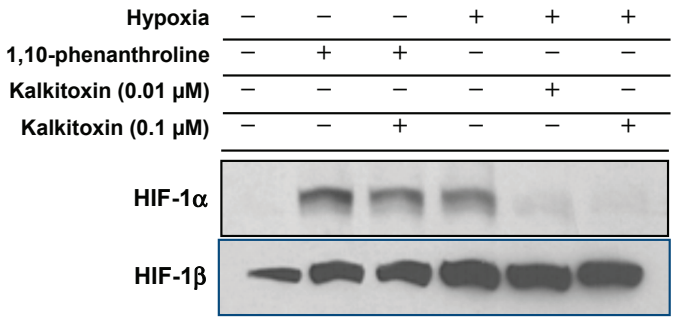

Figure 4. Kalkitoxin selectively inhibited the induction of HIF-1α protein by hypoxia. T47D cells were exposed to kalkitoxin at the specified concentrations, under hypoxic conditions (1% O_2, 4 h) or in the presence of 1,10-phenanthroline (10 μM, 4 h). Nuclear extract samples were prepared from both untreated control and treated cells, and the levels of HIF-1α and HIF-1β proteins determined by Western blot.

2.4.2. Mitochondrial Respiration Studies

Mitochondrial electron transport chain (ETC) inhibitors selectively suppress hypoxia-induced HIF-1 activation [27–30]. The effect of kalkitoxin on mitochondrial function was examined in a T47D cell-based respiration assay [17,25]. The level of respiration correlates with the rate of oxygen consumption by the cell. Kalkitoxin inhibited oxygen consumption within the same range of concentrations that inhibited hypoxia-induced HIF-1 activation (Figure 5A). The potency for kalkitoxin to suppress cellular respiration is comparable to that observed for the ETC complex I inhibitor rotenone (Figure 5B). Mechanistic studies were performed to discern the specific site that kalkitoxin targets within the mitochondrial ETC. Kalkitoxin was first tested to see if it acts as an inhibitor of ETC complex II, III, or IV (Figure 5C). Digitonin-permeabilized T47D cells were treated with a mixture of malate and pyruvate to start respiration by initiating NADH production, thereby providing a source of electrons for complex I (NADH-ubiquinone oxidoreductase). The electrons then pass through a series of ETC electron carriers to oxygen that acts as the end electron acceptor. As anticipated, the standard complex I inhibitor rotenone (1 μM) inhibited oxygen consumption (Figure 5C). The ETC complex II (succinate-ubiquinone oxidoreductase) substrate succinate overcame rotenone-stalled respiration by shuttling electrons to complex III. Because kalkitoxin (30 nM) did not inhibit respiration in the presence of succinate, kalkitoxin did not appear to inhibit complex II, III, or IV (Figure 5C). In contrast, antimycin A (1 μM) [an inhibitor of complex III (ubiquinol-cytochrome c oxidoreductase)] suppressed respiration in the presence of succinate. A mixture of ascorbate and TMPD (*N*,*N*,*N*′,*N*′-tetramethyl-*p*-phenylenediamine) that serves as an electron source for cytochrome c and hence for complex IV (cytochrome c oxidase) resumed respiration that was blocked by antimycin A at complex III. These control experiments indicate that each of the ETC complexes II, III, or IV remain functional and are not affected by kalkitoxin treatment. To confirm that kalkitoxin inhibits mitochondrial respiration by selectively

targeting complex I, kalkitoxin (30 nM) was added to permeabilized T47D cells following respiration initiation by a malate/pyruvate mixture. Kalkitoxin decreased respiration and succinate overcame this inhibition by shuttling electrons directly to complex III, thus circumventing the inhibitory effect of kalkitoxin on complex I (Figure 5D). Taken together, these results indicate that kalkitoxin potently suppresses mitochondrial respiration in tumor cells by selectively inhibiting ETC complex I.

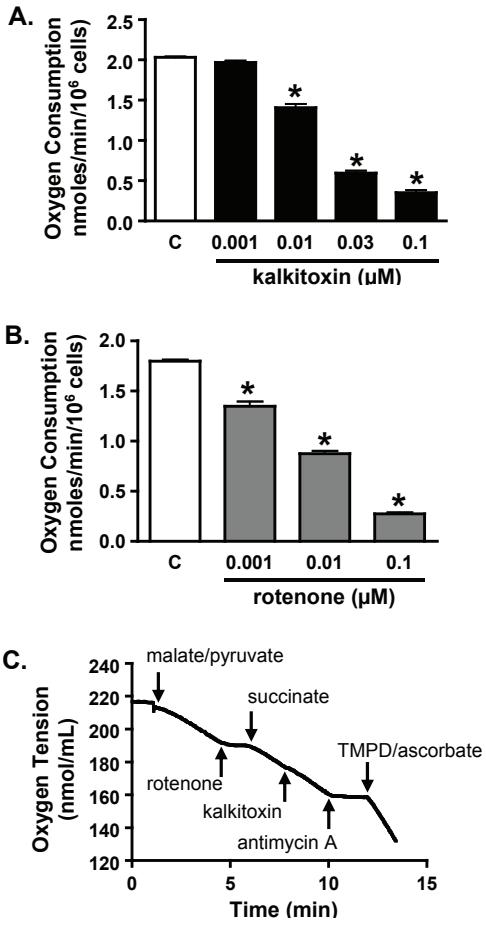

Figure 5. *Cont.*

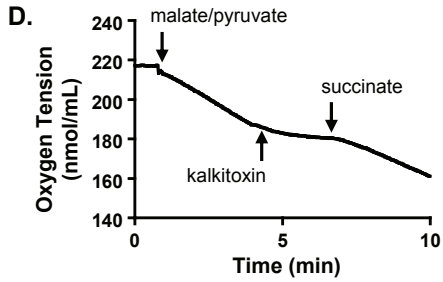

Figure 5. Kalkitoxin inhibits mitochondrial respiration by targeting ETC complex I. (**A**) Kalkitoxin was added to T47D cells at the specified concentrations and the rates of oxygen consumption determined using a Clark-type oxygen electrode. Data shown are average + standard deviation from three independent experiments. An "∗" indicates statistically significant difference when compared to the untreated control ("C"); (**B**) Concentration-response of rotenone on T47D cell respiration. Data presentation in (B) is the same as described in (A); (**C**,**D**) Mitochondrial substrates and inhibitors were added to digitonin-permeabilized T47D cells in the specified sequential order and the rates of oxygen consumption measured.

2.5. Tumor Cell Proliferation/Viability

In general, standard cytostatic/cytotoxic assays of 48 h duration are performed to evaluate the anticancer potential of active leads [31]. Our studies and those of McLaughlin and coworkers' indicate that an extended exposure time (e.g., six days) is required to observe the full impact of mitochondrial ETC inhibitors on tumor cell proliferation and/or viability [28,32]. To determine the effects of kalkitoxin on tumor cell proliferation/viability, concentration-response studies were performed following both standard and extended exposure schedule (48 h and 144 h, respectively). Enhanced inhibition was observed with all three-cell lines (human breast cancer T47D and MDA-MB-231, and neuroblastoma SH-SY5Y) in the extended exposure study (Figure 6A). The most pronounced increase was observed in T47D cells (Figure 6A). Additionally, exponentially grown HCT116 cells were exposed to kalkitoxin at the specified concentrations for five days and the surviving cells monitored using the trypan blue excluding method. Kalkitoxin decreased HCT116 survival with an IC_{50} value of 1 ng/mL (or 2.7 nM, Figure 6B). The impact of kalkitoxin on tumor cell survival was further examined in a clonogenic assay. HCT116 cells were exposed to kalkitoxin for the specified amount of time (2 h, 24 h, and 168 h, respectively), and the ability of treated cells to form colonies determined (Figure 6C). While little if any cell killing occurred for either a 2 or 24 h exposure for concentrations up to 100 μg/mL (270 μM), an extended exposure (168 h) to kalkitoxin was required to significantly suppress tumor cell colony formation, similar to that observed in Figure 6B.

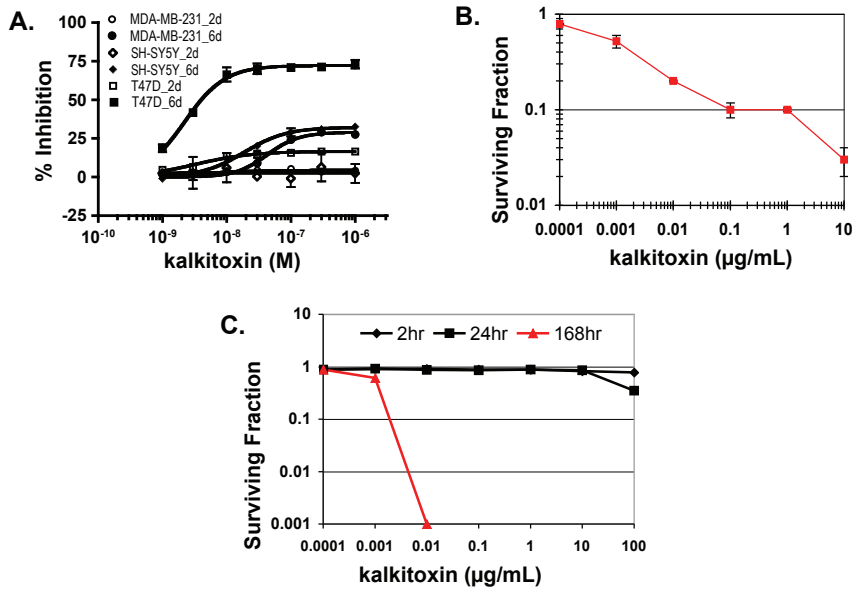

Figure 6. Kalkitoxin suppresses tumor cell proliferation/viability in a cell line- and time-dependent manner. (**A**) Exponentially grown T47D, MDA-MB-231, and SH-SY5Y cells were exposed to kalkitoxin at the specified concentrations for 48 h (2 days) and 144 h (6 days), respectively. Cell viability was determined by the SRB method and presented as "% Inhibition" of the untreated control (average ± standard deviation, $n = 3$); (**B**) HCT116 cells were exposed to kalkitoxin at the specified concentrations for 5 days and the number of surviving cells determined by trypan blue exclusion. Surviving fraction data are presented as the average ± standard deviation ($n = 3$); (**C**) Following kalkitoxin treatment for 2, 24, and 168 h at the specified concentrations, HCT116 cells were detached and plated at low density. Seven days later, the number of colonies was counted and the surviving fraction data presented (average ± standard deviation, $n = 3$).

2.6. Neurotoxicity

Exposure to certain mitochondrial inhibitors is associated with neurotoxicity [33,34]. Kalkitoxin was evaluated for potential neurotoxicity using primary rat cerebellar granule neurons (CGNs) as an in vitro model. Following compound treatment (24 h), CGNs were stained with propidium iodide (PI) for dead cells and Hoechst-33342 for all cells. Because PI does not penetrate intact cell membranes, it stains both late stage apoptotic and necrotic cells (Figure 7A). The cells were counted and grouped, based on morphological characteristics (live *versus* dead, Figure 7B). Relatively high kalkitoxin concentrations (*i.e.*, 100 nM, 24 h) killed most cells, but intermediate concentrations (*i.e.*, 30 nM) induced only moderate cytotoxicity (Figure 7B). The neurotoxicity incurred by kalkitoxin is comparable to that observed with the positive control, mitochondrial ETC

complex I inhibitor, rotenone (Figure 7B). Kalkitoxin was reported to incur CGN toxicity with a LC_{50} value of 3.86 nM [9]. Treatment condition-associated stress (e.g., 22 °C *versus* 37 °C, Locke's buffer *versus* culture media, *etc.*) may have enhanced the neurotoxic effect of kalkitoxin in the previous studies.

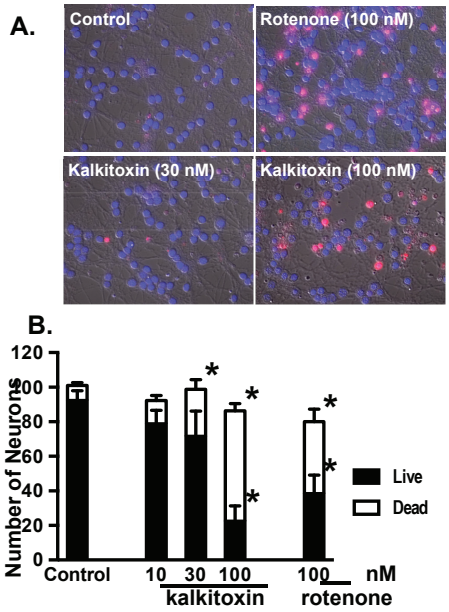

Figure 7. Kalkitoxin induces neurotoxicity *in vitro*. (**A**) Representative images of PI and Hoechst-33342 stained rat CGNs exposed to media (control) and kalkitoxin (30 and 100 nM, respectively) for 24 h; (**B**) The extent of cell death was quantified by counting live and dead (PI positive) neurons in four randomly selected fields for each specified condition. Data shown are mean + standard error (n = 8), pooled from two independent experiments. An "∗" indicates statistically significant difference when compared to the untreated control.

3. Experimental Section

3.1. Tumor Cell Culture, Cell-Based Reporter and Viability Assays

The T47D, MDA-MB-231, SH-SY5Y, and HCT116 cells were from ATCC. Cells were maintained in DMEM/F12 media with L-glutamine (Mediatech, Manassas, VA, USA), supplemented with 10% (v/v) fetal bovine serum (FBS, Hyclone, Logan, UT, USA), 50 units/mL penicillin and 50 µg/mL streptomycin (Gibco, Grand Island, NY, USA). To monitor HIF-1 activity, a T47D cell-based luciferase assay employing the pHRE3-TK-Luc reporter was performed as previously described [17]. Except for the HCT116 studies, the sulfarhodamine B method was used to determine cell viability [25]. For the extended duration six-day exposure study, the conditioned media were replaced after three days by fresh culture medium that contained test compound. The

HCT116 cell-based IC_{50} and clonogenic studies were performed as previously described [35]. Test compounds were prepared as stock solutions in DMSO or isopropanol as appropriate and stored at −20 °C. In general, the final solvent concentration was less than 0.5% (v/v).

3.2. RNA Extraction and Quantitative Real Time RT-PCR

Experimental design, detailed procedures, and data analysis were as previously reported [25].

3.3. ELISA Assay for Human VEGF Protein

T47D cell plating, compound treatments, and ELISA assay for secreted VEGF proteins were as previously reported [17]. Proteins concentrations in the cellular lysate were determined using a micro BCA assay (PIERCE), and the secreted VEGF protein levels were normalized to those of cellular proteins.

3.4. HUVEC-Based Tube Formation Assay

The maintenance of HUVEC cells (Lonza, Walkersville, MD, USA), T47D cell-conditioned media (CM) sample collection, and the HUVEC-based *in vitro* tube formation assays were performed and data quantified as described previously [25].

3.5. Nuclear Extract Preparation and Western Blot Analysis

Preparation of nuclear extract samples from both treated and control T47D cells, and determination of HIF-1α and HIF-1β proteins by Western blot were described previously [25].

3.6. Mitochondria Respiration Assay

The oxygen consumption rates of T47D cells were monitored using an Oxytherm Clarke-type electrode System (Hansatech, Norfolk, UK). The effects of purified compounds on cellular respiration were determined using a non-permeabilized cell-based respiration assay [25]. Mechanistic studies were conducted in digitonin-treated cells with permeabilized plasma membrane to manipulate mitochondrial substrates and inhibitors. Detailed experimental procedures and reagents were as previously described [25].

3.7. Cerebellar Granule Neuron Preparation and Neurotoxicity Assay

Experiments that involved the use of rat-derived materials were approved by the Institutional Animal Care and Use Committee, University of Mississippi (File Number 06-009, approved on 25 October 2005), and were handled in strict accordance with good animal practice as defined by the NIH guidelines. Detailed experimental procedures and reagents were as previously described [28].

3.8. Statistical Analysis

Data were compared using one-way ANOVA followed by Bonfferoni post hoc analyses (GraphPad Prism 4). Differences were considered statistically significant when $p < 0.05$.

4. Conclusions

Sodium channel and mitochondria-associated neurotoxicity may limit the therapeutic potential of kalkitoxin as an antitumor chemotherapeutic agent. Mechanistically, kalkitoxin and other recently reported marine natural product HIF-1 inhibitors (Figure 8) suppress the multi-enzyme mitochondrial NADH-ubiquinone oxidoreductase system (electron transport chain complex I), thus disrupting mitochondria-mediated hypoxic signaling. Examples of mitochondria-targeted HIF-1 inhibitors include an assortment of sponge metabolites (e.g., mycothiazole [28], lehualide B [36], furospongolide [37], and the mycalinitriles [38]), and structurally dissimilar algal natural products [39,40]. Kalkitoxin production by the marine cyanobacterium, *Moorea producens*, is physiologically and ecologically intriguing. The propensity of kalkitoxin to potently and selectively block both voltage-sensitive sodium channels and complex I of the mitochondrial electron transport chain appears to be unnecessarily redundant means of chemical defense. The production of potent sodium channel-targeted toxins would seem to impart a more than adequate defense against herbivorous grazers. However, recent studies indicate that a number of marine invertebrates and fish species have evolved altered sodium channels with reduced sensitivity to TTX-VSSC-targeted toxins (reviewed in [41]). This is not particularly surprising, considering the potential for regular exposure of marine filter feeders and grazers to algae- and bacteria-derived sodium channel inhibitors (e.g., saxitoxin and tetrodotoxin), and adaptive pressure for the presumably defensive physiological accumulation of these neurotoxins in the tissues of invertebrate [e.g., blue-ringed octopus (*Hapalochlaena* spp.)] and vertebrate species [e.g., pufferfish (*Diodon* spp.)]. Thus, by simultaneously acting as both a voltage-gated Na^+ channel blocker and a potent rotenone-like mitochondrial disruptor, kalkitoxin may be able to provide an additional level of grazing defense against a broad range of herbivore species.

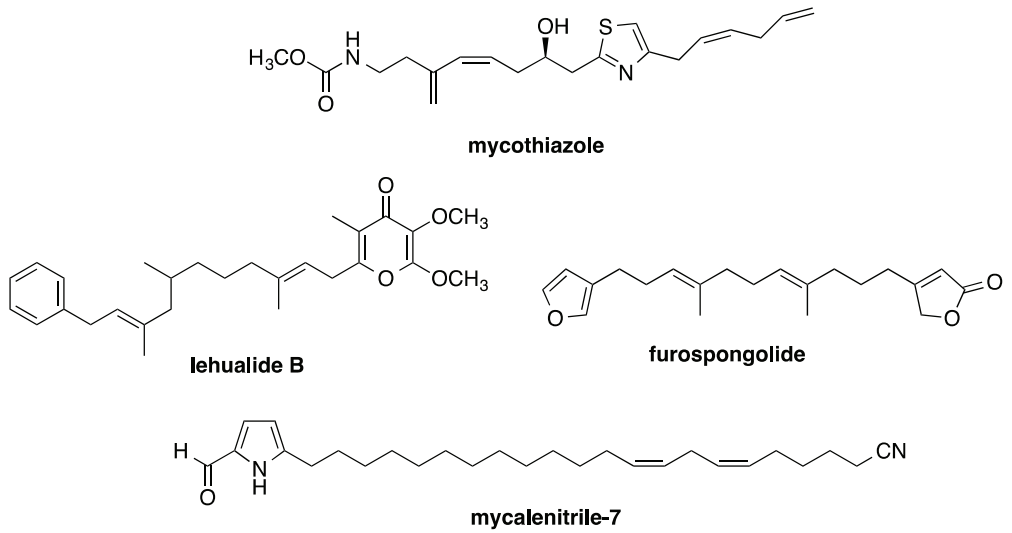

Figure 8. Examples of marine invertebrate metabolites that have recently been found to inhibit mitochondrial electron transport chain complex I and disrupt HIF-mediated hypoxic signaling in tumor cells.

Acknowledgments

The authors thank Steven L. McKnight (University of Texas Southwestern Medical Center at Dallas) for providing the pHRE3-TK-luc construct. This work was supported in part by the U.S. National Institutes of Health (NIH)/National Cancer Institute grant CA98787 (Dale G. Nagle), NIH/NCRR P20RR021929 (J. Brian Morgan, graduate stipend supplement) and in part by NIH CA100851 (Frederick A. Valeriote and William H. Gerwick) and NS053398 (William H. Gerwick). This University of Mississippi portion of this investigation was conducted in a facility constructed with Research Facilities Improvement Grant C06 RR-14503 from the NIH.

Author Contributions

J.B.M., M.B.J., F.A.V., Y.-D.Z., and D.G.N. designed experiments; J.B.M., Y.L., V.C., F.M., and F.A.V. performed experiments; J.B.M., F.A.V., Y.-D.Z., and D.G.N. analyzed the data; W.H.G. contributed reagents; Y.-D.Z. and D.G.N. wrote the manuscript; W.H.G., F.A.V., M.B.J., D.G.N., and Y.-D.Z. edited the manuscript.

Conflicts of Interest

The authors declare no conflict of interest.

References

1. Engene, N.; Rottacker, E.C.; Kastovsky, J.; Byrum, T.; Choi, H.; Ellisman, M.H.; Komarek, J.; Gerwick, W.H. *Moorea producens* gen. nov., sp. nov. and *Moorea bouillonii* comb. nov., tropical marine cyanobacteria rich in bioactive secondary metabolites. *Int. J. Syst. Evol. Microbiol.* **2012**, *62*, 1171–1178.
2. Osborne, N.J.; Shaw, G.R.; Webb, P.M. Health effects of recreational exposure to Moreton Bay, Australia waters during a *Lyngbya majuscula* bloom. *Environ. Int.* **2007**, *33*, 309–314.
3. Albert, S.; O'Neil, J.M.; Udy, J.W.; Ahern, K.S.; O'Sullivan, C.M.; Dennison, W.C. Blooms of the cyanobacterium *Lyngbya majuscula* in coastal Queensland, Australia: Disparate sites, common factors. *Mar. Pollut. Bull.* **2005**, *51*, 428–437.
4. Sharp, K.; Arthur, K.E.; Gu, L.; Ross, C.; Harrison, G.; Gunasekera, S.P.; Meickle, T.; Matthew, S.; Luesch, H.; Thacker, R.W.; *et al.* Phylogenetic and chemical diversity of three chemotypes of bloom-forming *Lyngbya* species (Cyanobacteria: Oscillatoriales) from reefs of southeastern Florida. *Appl. Environ. Microbiol.* **2009**, *75*, 2879–2888.
5. Leao, P.N.; Engene, N.; Antunes, A.; Gerwick, W.H.; Vasconcelos, V. The chemical ecology of cyanobacteria. *Nat. Prod. Rep.* **2012**, *29*, 372–391.
6. Nunnery, J.K.; Mevers, E.; Gerwick, W.H. Biologically active secondary metabolites from marine cyanobacteria. *Curr. Opin. Biotechnol.* **2010**, *21*, 787–793.
7. Wu, M. Novel Bioactive Secondary Metabolites from the Marine Cyanobacterium *Lyngbya majuscula*. Master Thesis, Oregon State University, Corvallis, OR, USA, 1996.
8. Wu, M.; Okino, T.; Nogle, L.M.; Marquez, B.L.; Williamson, R.T.; Sitachitta, N.; Berman, F.W.; Murray, T.F.; McGough, K.; Jacobs, R.; *et al.* Structure, synthesis, and biological properties of kalkitoxin, a novel neurotoxin from the marine cyanobacterium *Lyngbya majuscula*. *J. Am. Chem. Soc.* **2000**, *122*, 12041–12042.
9. Umezawa, T.; Sueda, M.; Kamura, T.; Kawahara, T.; Han, X.; Okino, T.; Matsuda, F. Synthesis and biological activity of kalkitoxin and its analogues. *J. Org. Chem.* **2012**, *77*, 357–370.
10. Berman, F.W.; Gerwick, W.H.; Murray, T.F. Antillatoxin and kalkitoxin, ichthyotoxins from the tropical cyanobacterium *Lyngbya majuscula*, induce distinct temporal patterns of NMDA receptor-mediated neurotoxicity. *Toxicon* **1999**, *37*, 1645–1648.
11. LePage, K.T.; Goeger, D.; Yokokawa, F.; Asano, T.; Shioiri, T.; Gerwick, W.H.; Murray, T.F. The neurotoxic lipopeptide kalkitoxin interacts with voltage-sensitive sodium channels in cerebellar granule neurons. *Toxicol Lett.* **2005**, *158*, 133–139.
12. White, J.D.; Xu, Q.; Lee, C.S.; Valeriote, F.A. Total synthesis and biological evaluation of +-kalkitoxin, a cytotoxic metabolite of the cyanobacterium *Lyngbya majuscula*. *Org. Biomol. Chem.* **2004**, *2*, 2092–2102.
13. Semenza, G.L. Oxygen sensing, hypoxia-inducible factors, and disease pathophysiology. *Annu. Rev. Pathol.* **2014**, *9*, 47–71.

14. Samanta, D.; Gilkes, D.M.; Chaturvedi, P.; Xiang, L.; Semenza, G.L. Hypoxia-inducible factors are required for chemotherapy resistance of breast cancer stem cells. *Proc. Natl. Acad. Sci. USA* **2014**, *111*, E5429–E5438.
15. Meijer, T.W.; Kaanders, J.H.; Span, P.N.; Bussink, J. Targeting hypoxia, HIF-1, and tumor glucose metabolism to improve radiotherapy efficacy. *Clin. Cancer. Res.* **2012**, *18*, 5585–5594.
16. Warfel, N.A.; El-Deiry, W.S. HIF-1 signaling in drug resistance to chemotherapy. *Curr. Med. Chem.* **2014**, *21*, 3021–3028.
17. Hodges, T.W.; Hossain, C.F.; Kim, Y.P.; Zhou, Y.-D.; Nagle, D.G. Molecular-targeted antitumor agents: The *Saururus cernuus* dineolignans manassantin B and 4-*O*-demethylmanassantin B are potent inhibitors of hypoxia-activated HIF-1. *J. Nat. Prod.* **2004**, *67*, 767–771.
18. Du, L.; Mahdi, F.; Datta, S.; Jekabsons, M.B.; Zhou, Y.-D.; Nagle, D.G. Structures and mechanisms of antitumor agents: xestoquinones uncouple cellular respiration and disrupt HIF signaling in human breast tumor cells. *J. Nat. Prod.* **2012**, *75*, 1553–1559.
19. Li, J.; Du, L.; Kelly, M.; Zhou, Y.-D.; Nagle, D.G. Structures and potential antitumor activity of sesterterpenes from the marine sponge *Hyrtios communis*. *J. Nat. Prod.* **2013**, *76*, 1492–1497.
20. Du, L.; Zhou, Y.-D.; Nagle, D.G. Inducers of hypoxic response: marine sesquiterpene quinones activate HIF-1. *J. Nat. Prod.* **2013**, *76*, 1175–1181.
21. Schindl, M.; Schoppmann, S.F.; Samonigg, H.; Hausmaninger, H.; Kwasny, W.; Gnant, M.; Jakesz, R.; Kubista, E.; Birner, P.; Oberhuber, G. Overexpression of hypoxia-inducible factor 1α is associated with an unfavorable prognosis in lymph node-positive breast cancer. Austrian Breast and Colorectal Cancer Study Group. *Clin. Cancer Res.* **2002**, *8*, 1831–1837.
22. Gong, L.; Zhang, W.; Zhou, J.; Lu, J.; Xiong, H.; Shi, X.; Chen, J. Prognostic value of HIFs expression in head and neck cancer: a systematic review. *PLoS One* **2013**, *8*, e75094.
23. Shaida, N.; Chan, P.; Turley, H.; Jones, C.M.; Kanga, S.; Ritchie, R.W.; Malone, P.R.; Harris, A.L.; Fox, S.B. Nuclear localization of factor inhibitor hypoxia-inducible factor in prostate cancer is associated with poor prognosis. *J. Urol.* **2011**, *185*, 1513–1518.
24. Ferrara, N.; Mass, R.D.; Campa, C.; Kim, R. Targeting VEGF-A to treat cancer and age-related macular degeneration. *Annu. Rev. Med.* **2007**, *58*, 491–504.
25. Liu, Y.; Veena, C.K.; Morgan, J.B.; Mohammed, K.A.; Jekabsons, M.B.; Nagle, D.G.; Zhou, Y.-D. Methylalpinumisoflavone inhibits hypoxia-inducible factor-1 (HIF-1) activation by simultaneously targeting multiple pathways. *J. Biol. Chem.* **2009**, *284*, 5859–5868.
26. Wang, G.L.; Jiang, B.H.; Rue, E.A.; Semenza, G.L. Hypoxia-inducible factor 1 is a basic-helix-loop-helix-PAS heterodimer regulated by cellular O_2 tension. *Proc. Natl. Acad. Sci. USA* **1995**, *92*, 5510–5514.
27. Klimova, T.; Chandel, N.S. Mitochondrial complex III regulates hypoxic activation of HIF. *Cell Death Differ.* **2008**, *15*, 660–666.

28. Morgan, J.B.; Mahdi, F.; Liu, Y.; Coothankandaswamy, V.; Jekabsons, M.B.; Johnson, T.A.; Sashidhara, K.V.; Crews, P.; Nagle, D.G.; Zhou, Y.-D. The marine sponge metabolite mycothiazole: A novel prototype mitochondrial complex I inhibitor. *Bioorg. Med. Chem.* **2010**, *18*, 5988–5994.
29. Coothankandaswamy, V.; Liu, Y.; Mao, S.C.; Morgan, J.B.; Mahdi, F.; Jekabsons, M.B.; Nagle, D.G.; Zhou, Y.-D. The alternative medicine pawpaw and its acetogenin constituents suppress tumor angiogenesis via the HIF-1/VEGF pathway. *J. Nat. Prod.* **2010**, *73*, 956–961.
30. Li, J.; Mahdi, F.; Du, L.; Datta, S.; Nagle, D.G.; Zhou, Y.-D. Mitochondrial respiration inhibitors suppress protein translation and hypoxic signaling via the hyperphosphorylation and inactivation of translation initiation factor eIF2α and elongation factor eEF2. *J. Nat. Prod.* **2011**, *74*, 1894–1901.
31. Developmental Therapeutics Program NCI/NIH Screening Services: NCI-60 DTP Human Tumor Cell Line Screen. Available online: http://dtp.nci.nih.gov/branches/btb/ivclsp.html (accessed on 5 January 2015).
32. McLaughlin, J.L. Paw paw and cancer: Annonaceous acetogenins from discovery to commercial products. *J. Nat. Prod.* **2008**, *71*, 1311–1321.
33. Ayala, A.; Venero, J.L.; Cano, J.; Machado, A. Mitochondrial toxins and neurodegenerative diseases. *Front. Biosci.* **2007**, *12*, 986–1007.
34. Hollerhage, M.; Matusch, A.; Champy, P.; Lombes, A.; Ruberg, M.; Oertel, W.H.; Hoglinger, G.U. Natural lipophilic inhibitors of mitochondrial complex I are candidate toxins for sporadic neurodegenerative tau pathologies. *Exp. Neurol.* **2009**, *220*, 133–142.
35. Valeriote, F.A.; Tenney, K.; Medla, J.; Pietraszkiewicz, H.; Edelstein, M.; Johnson, T.A.; Taro Amagata, T.; Crews, P. Discovery and development of anticancer agents from marine sponges: perspectives based on a chemistry-experimental therapeutics collaborative program. *J. Exp. Ther. Oncol.* **2012**, *10*, 119–134.
36. Jeso, V.; Yang, C.; Cameron, M.D.; Cleveland, J.L.; Micalizio, G.C. Synthesis and SAR of lehualide B—A marine-derived natural product with potent anti-multiple myeloma activity. *ACS Chem. Biol.* **2013**, *8*, 1241–1252.
37. Liu, Y.; Liu, R.; Mao, S.-C.; Morgan, J.B.; Jekabsons, M.B.; Zhou, Y.-D.; Nagle, D.G. Molecular-targeted antitumor agents 19: furospongolide from a marine *Lendenfeldia* sp. sponge inhibits hypoxia-inducible factor-1 (HIF-1) activation in breast tumor cells. *J. Nat. Prod.* **2008**, *71*, 1854–1860.
38. Mao, S.-C.; Liu, Y.; Morgan, J.B.; Jekabsons, M.B.; Zhou, Y.-D.; Nagle, D.G. Lipophilic 2,5-disubstituted pyrroles from the marine sponge *Mycale* sp. inhibit mitochondrial respiration and HIF-1 activation. *J. Nat. Prod.* **2009**, *72*, 1927–1936.
39. Liu, Y.; Morgan, J.B.; Coothankandaswamy, V.; Liu, R.; Jekabsons, M.B.; Mahdi, F.; Nagle, D.G.; Zhou, Y.-D. The *Caulerpa* pigment caulerpin inhibits HIF-1 activation and mitochondrial respiration. *J. Nat. Prod.* **2009**, *72*, 2104–2109.

40. Mahdi, F.; Falkenberg, M.; Ioannou, E.; Roussis, V.; Zhou, Y.-D.; Nagle, D.G. Thyrsiferol inhibits mitochondrial respiration and HIF-1 activation. *Phytochem. Lett.* **2011**, *4*, 75–78.
41. Anderson, P.A.V.; Roberts-Misterly, J.; Greenberg, R.M. The evolution of voltage-gated sodium channels: Were algal toxins involved? *Harmful Algae* **2005**, *4*, 95–107.

The Marine Metabolite SZ-685C Induces Apoptosis in Primary Human Nonfunctioning Pituitary Adenoma Cells by Inhibition of the Akt Pathway *in Vitro*

Xin Wang, Ting Tan, Zhi-Gang Mao, Ni Lei, Zong-Ming Wang, Bin Hu, Zhi-Yong Chen, Zhi-Gang She, Yong-Hong Zhu and Hai-Jun Wang

Abstract: Nonfunctioning pituitary adenoma (NFPA) is one of the most common types of pituitary adenoma. The marine anthraquinone derivative SZ-685C has been isolated from the secondary metabolites of the mangrove endophytic fungus *Halorosellinia* sp. (No. 1403) which is found in the South China Sea. Recent research has shown that SZ-685C possesses anticancer and tumor suppressive effects. The tetrazolium-based colorimetric assay (MTT assay) to investigate the different effect of the marine compound SZ-685C on the proliferation of primary human NFPA cells, rat normal pituitary cells (RPCs) and rat prolactinoma MMQ cell lines. Hoechst 33342 dye/propidium iodide (PI) double staining and fluorescein isothiocyanate-conjugated Annexin V/PI (Annexin V-FITC/PI) apoptosis assays detected an enhanced rate of apoptosis in cells treated with SZ-685C. Enhanced expression levels of caspase 3 and phosphate and tensin homolog (PTEN) were determined by Western blotting. Notably, the protein expression levels of Akt were decreased when the primary human NFPA cells were treated with SZ-685C. Here, we show that SZ-685C induces apoptosis of human NFPA cells through inhibition of the Akt pathway *in vitro*. The understanding of apoptosis has provided the basis for novel targeted therapies that can induce death in cancer cells or sensitize them to established cytotoxic agents and radiation therapy.

Reprinted from *Mar. Drugs*. Cite as: Wang, X.; Tan, T.; Mao, Z.-G.; Lei, N.; Wang, Z.-M.; Hu, B.; Chen, Z.-Y.; She, Z.-G.; Zhu, Y.H.; Wang, H.-J. The Marine Metabolite SZ-685C Induces Apoptosis in Primary Human Nonfunctioning Pituitary Adenoma Cells by Inhibition of the Akt Pathway *in Vitro*. *Mar. Drugs* **2015**, *13*, 1569-1580.

1. Introduction

Pituitary adenomas (PAs) are one of the most common intracranial tumors with a prevalence of about 80–90/100,000 people [1–3]. They can be divided into secretory and non-secretory varieties, with nonfunctioning pituitary adenomas (NFPAs) accounting for about 40% of all pituitary adenomas [4]. They can lead to a range of clinical symptoms usually due to local mass effects such as neurological (headache), ophthalmological (visual field defects and visual loss), and endocrine (hypopituitarism and hyperprolactinemia) symptoms [5,6]. At present, no medical treatment is available to control tumor growth in NFPA [7]. The limited effectiveness of surgery and the risks inherent to radiation therapy warrant the search for new therapeutic options.

In recent years, a wide variety of metabolites has been isolated from marine microorganisms and they have demonstrated huge potential for drug development [8]. They are increasingly attracting the attention of pharmaceutical scientists because of their unique structural properties and specific bioactivity profiles [9,10]. Marine-derived fungi have provided more than 1000 new natural

products [11]. *Halorosellinia* sp., a genus of fungi in the family *Xylariaceae*, was first studied for secondary metabolite production by Wyeth [12]. It produce many secondary metabolites, some of them with relevant bioactivity, such as Haloroquinone, a protein kinase B inhibitor [13]. Xia *et al*. [14] isolated the fungus *Halorosellinia* sp., from decayed wood in Hong Kong and a salt lake in the Bahamas, and produced two new anthraquinones.

SZ-685C, a novel marine anthraquinone derivative, was isolated from the secondary metabolites of a mangrove endophytic fungus, *Halorosellinia sp.* (No. 1403) from *Kandelia candel* (L.) druce, which is found in the South China Sea (Figure 1). Recent studies have found that this compound can inhibit the growth of a variety of tumor cells, including human glioma, hepatoma, prostate cancer, breast cancer, and nasopharyngeal carcinoma cells [15–17].

Apoptosis is the process of programmed cell death, regulated by a complex network of proliferation and survival genes. Akt is a central node in several essential cellular functions and also contributes to tumorigenesis and tumor metastasis [18]. Therefore, drugs that inhibit the Akt pathway may be effective against many human cancers. This study was carried out to evaluate the effectiveness of SZ-685C in the treatment of NFPA. Our results showed that SZ-685C suppressed the Akt pathway and induced apoptosis in primary NFPA cells.

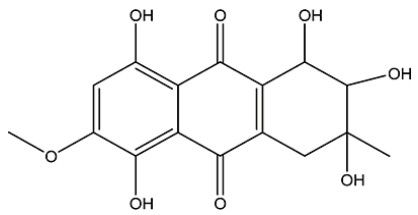

Figure 1. Chemical structure of SZ-685C.

Our current study investigated whether SZ-685C can override chemoresistance by inhibiting Akt signaling in primary human nonfunctioning pituitary adenomas cells.

2. Results and Discussion

2.1. Identification of Nonfunctioning Pituitary Adenoma (NFPA) Cells Using Electron Microscopy and Immunostaining

We evaluated the ultrastructural and morphometric characteristics of NFPAs by using transmission electron microscopy. We found that an intact cell membrane, large nucleus, abundant euchromatin, and the nucleolus are obvious. In the cytoplasm, the abundance of mitochondria and the small number of secretory granules, allowed us to identify the cultured cells as NFPAs (Figure 2).

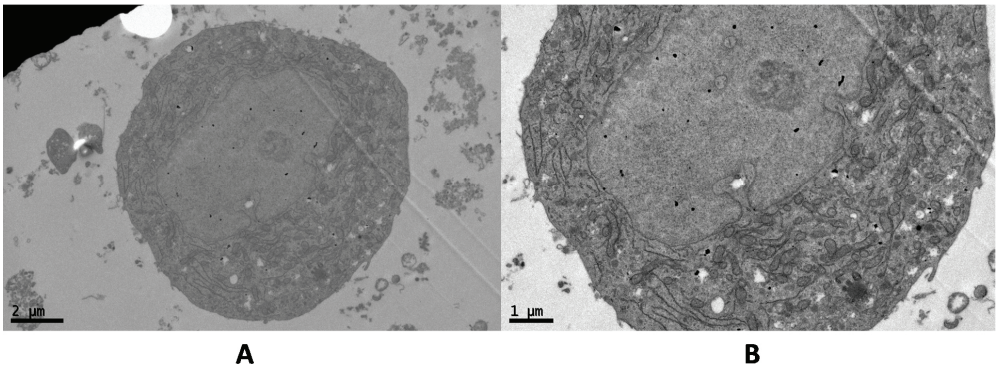

Figure 2. Ultrastructure of an nonfunctioning pituitary adenoma (NFPA) cell. At the ultrastructural level, the large cells possess numerous mitochondria and a few secretory granules, but an otherwise simple cytoplasm. (**A**) Magnification: ×5800, scale bar: 2 μm. (**B**) Magnification: ×9700, scale bar: 1 μm.

Cytokeratins (CKs) are typically expressed in epithelial cells, whereas vimentin can be found in cells of mesenchymal origin. Co-expression of vimentin and CKs is believed to be the hallmark of epithelial-to-mesenchymal or mesenchymal-to-epithelial transformations of developing tissues. In this study, we analyzed the expression and co-expression of simple epithelial CK8 and vimentin in NFPA cells. The cells' nuclei were stained with Hoechst 33342 dye, which emits a blue fluorescence, and CK8 and vimentin, which emit a green fluorescence (Figure 3).

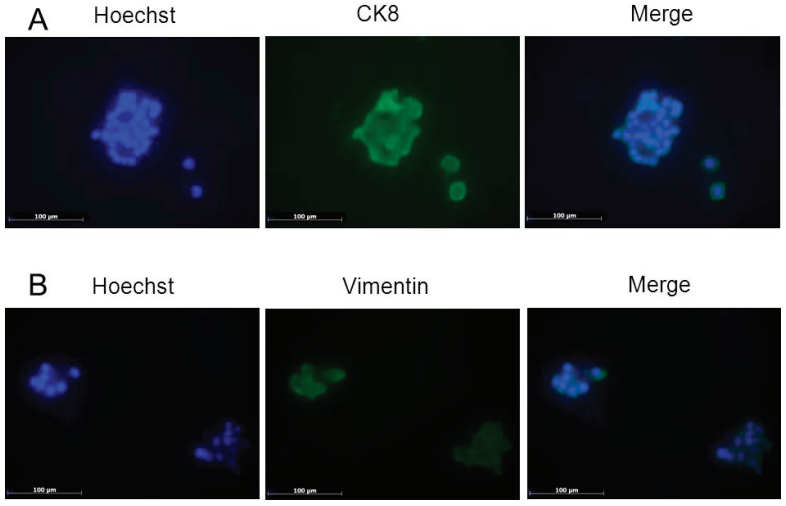

Figure 3. (**A**) CK8 and Hoechst immunofluorescent staining; (**B**) Vimentin and Hoechst immunofluorescent staining. Magnification: × 400, scale bar: 100 μm.

2.2. Growth Inhibition of Primary Human Nonfunctioning Pituitary Adenoma Cells Induced by SZ-685C

We used a 3-(4,5-dimethylthiazol-2-yl)-2,5-diphenyltetrazolium bromide (MTT) assay to investigate the effect of the marine compound SZ-685C on the proliferation of human NFPA. Upon treatment of the cells with different concentrations of SZ-685C for 24 h, an obvious inhibitory effect of SZ-685C on cellular proliferation was observed in both the rat normal pituitary cells (RPCs) and rat pituitary adenoma MMQ cell lines. Primary cultures of human nonfunctioning pituitary adenomas cells also exhibited significantly inhibited growth in a dose-dependent manner. We calculated the half maximal inhibitory concentrations (IC_{50}) using SPSS 13.0, which revealed that the IC_{50s} of SZ-685C in NFPA, MMQ and RPC cells were 18.76 ± 7.43 μM, 14.51 ± 2.11 μM, and 56.09 ± 5.18 μM, respectively. The difference between the IC_{50s} of the two groups was statistically significant ($p < 0.05$) (Figure 4).

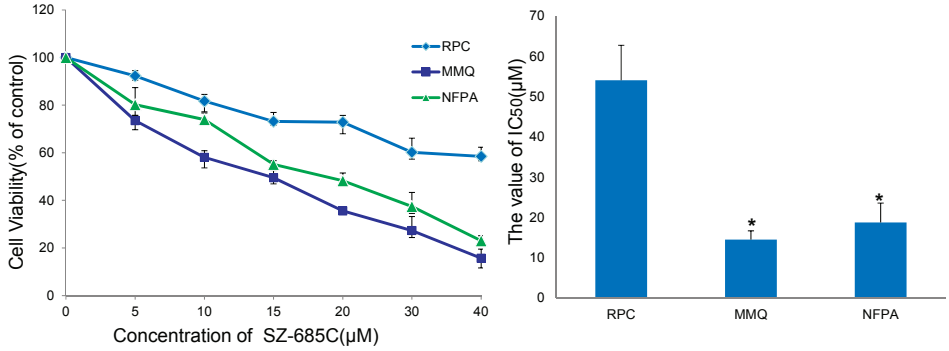

Figure 4. Growth-inhibitory effect of SZ-685C in rat normal pituitary cells (RPCs) and rat prolactinoma MMQ cell lines and primary NFPA cells. All of the cells were treated with the indicated dose of SZ-685C for 24 h and cell viability was determined using an MTT assay.

2.3. SZ-685C Induces Apoptosis in MMQ Pituitary Adenoma Cells

We next investigated whether the inhibition of cell growth induced by SZ-685C in NFPA cells was dependent on the apoptotic pathway. To determine this, we stained MMQ cells with a Hoechst 33342 dye/propidium iodide (PI) double stain after treatment with SZ-685C. The chromatin of cells undergoing apoptosis appears brighter than that of surviving cells due to the red-fluorescence imparted to it by the PI (Figure 5A). A fluorescein isothiocyanate-labeled Annexin V (Annexin V-FITC) and PI apoptosis assay was used to observe programmed cell death by nuclear staining (Figure 5C,D) and flow cytometry (Figure 5B). At the beginning of cellular apoptosis, the membrane phosphatidylserine (PS) flips from the inner face of the plasma membrane to the outer layer, enabling it to bind to Annexin V-FITC. Whereas intact cell membranes exclude PI, dead cells, or those in later stages of apoptosis, are permeable to PI. Flow cytometry showed an

increasing apoptosis rate with increasing concentrations of SZ-685C; the 20 μM group exhibited the highest rate of apoptosis at 58.2%.

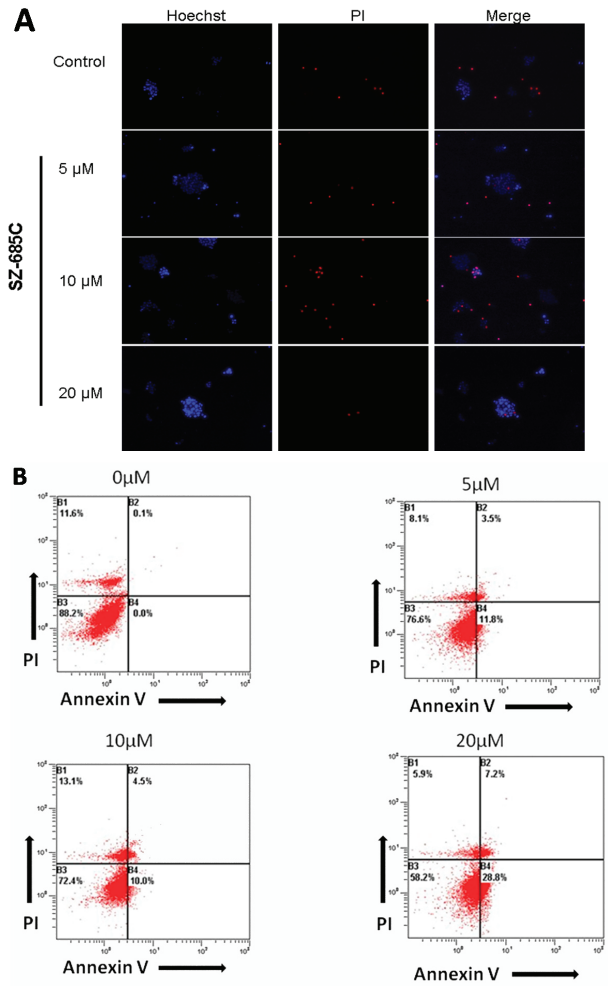

Figure 5. *Cont.*

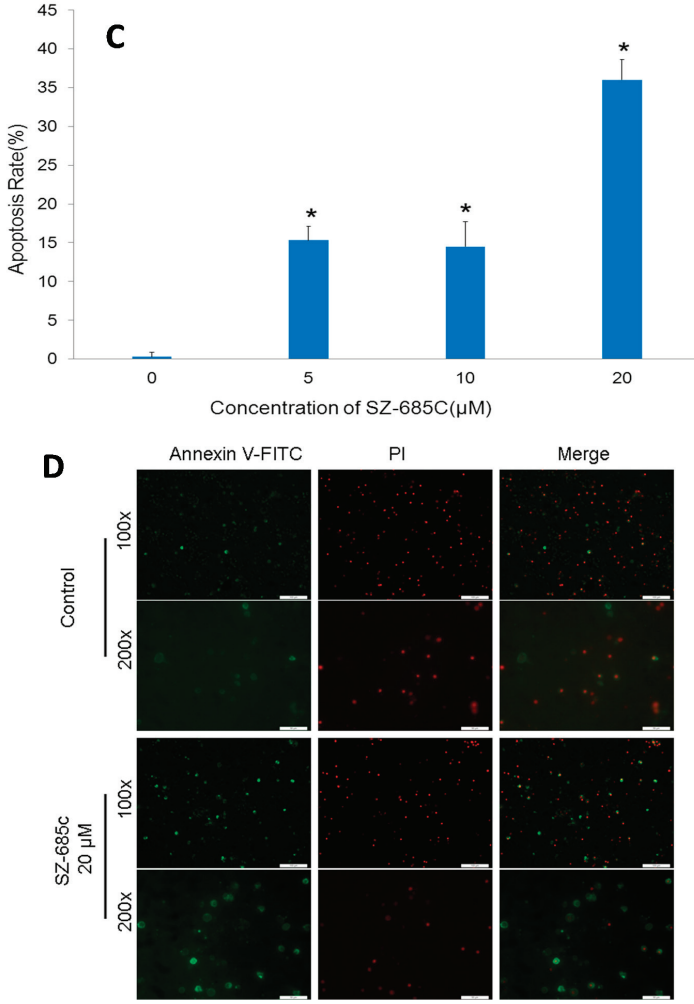

Figure 5. Induction of apoptosis in NFPA cells by SZ-685C. (**A**) Hoechst/propidium iodide (PI) staining and fluorescein isothiocyanate labeled Annexin V (Annexin V-FITC)/PI staining (**D**) of NFPA cells treated with SZ-685C (×100, scale bar: 100 μm; × 200, scale bar: 50 μm); (**B**) Cells were exposed to different concentrations (0, 5, 10, 20 μM) of SZ-685C for 24 h. Cells were then collected and subjected to Annexin V-FITC/PI staining, Hoechst /PI staining and analyzed by flow cytometry (FCM); (**C**) According to the results of FCM (**B**), NFPA cells were treated with SZ-685C for indicated concentration, the apoptosis rate was increased; ***** $p < 0.05$.

Results showed that treatment of NFPA cells with SZ-685C dramatically increased the population of cells stained with both Annexin V and PI ($p = 0.018$, $p = 0.021$), with about 40% of the cells entering apoptosis (Figure 5C). The rates of apoptosis were higher in cells that were treated with SZ-685C than in those which were not. In addition, the expression of both caspase-3 and

phosphate and tensin homolog (PTEN) was up-regulated upon treatment with SZ-685C as demonstrated by Western blotting analysis (Figure 6, $p = 0.004$). Notably, the protein expression levels of Akt were decreased when the NFPA cells were treated with SZ-685C (Figure 6).

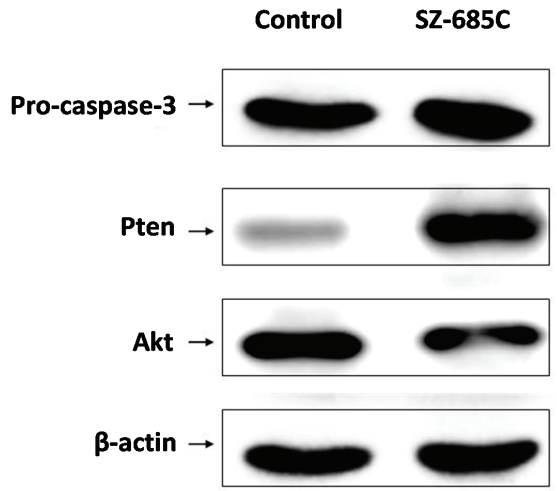

Figure 6. Effects of SZ-685C on apoptosis-related proteins. Western blotting analysis of apoptosis-related proteins incascluding AKT, phosphate and tensin homolog (PTEN), and caspase-3 of the NFPA cells treated with or without 20 μM of SZ-685C. Band intensity was normalized to β-actin expression by densitometry.

3. Discussion

There is currently no medical treatment for NFPA, and surgery and radiotherapy constitute the cornerstone of therapy. The risks associated with surgical complications and the side effects of radiotherapy underscore the need for new treatment modalities. At present, no NFPA cell lines exist that can be cultured *in vitro*; in this study, we cultured primary human nonfunctioning pituitary adenoma cells from pathological specimens obtained during surgery.

Anthracyclines, so far the most effective anti-cancer agents and commonly used in the clinic, such as Doxorubicin (trade name Adriamycin), Daunorubicin (daunomycin or rubidomycin), Zorubicin (Rubidazone), and Carubicin (carminomycin) [19]. They can against various types of cancer, including breast cancer, leukemias, lymphomas and endometrial carcinoma, *etc*. [20]. However, their severe adverse side effects hampered the successful use of these drugs. Cardiac toxicity is the most serious consequence of anthracycline therapy.

In our previous study, we found that the anthraquinone derivative SZ-685C significantly suppressed the proliferation of the MMQ rat pituitary adenoma cell line and induced apoptosis through the downregulation of miR-200c [21]. Caspases play an important role in cell apoptosis. Activation of caspases appears to be directly responsible for many molecular and structural changes involved in apoptosis. The caspase-dependent process of programmed cell death can proceed through two pathways of anticancer drug-induced apoptosis: the extrinsic (death receptor)

pathway and the intrinsic (mitochondrial) pathway. Caspase-3 is one of the downstream effectors of the caspase family, and is thought to be involved in both the mitochondrial apoptotic pathway and the death receptor pathway. In this study, we observed that the SZ-685C induced apoptosis in NFPA cells is accompanied with increased caspase activity. Taken together, our data strongly suggest that SZ-685C-induced cytotoxicity may be mediated through caspase-dependent apoptosis.

The Akt signaling pathway plays a crucial protective role against programmed cell death in cancer cells. Akt is an important oncogenic protein that can regulate various important processes in the cell by influencing the participation of other proteins. We investigated whether inhibition of the Akt signaling pathway had an effect on its downstream targets in SZ-685C-treated NFPA cells. Zhu *et al.* reported that SZ-685C induces apoptosis in adriamycin-resistant human breast cancer cells both *in vitro* and *in vivo*, and that it exerts these antitumor effects through suppressing Akt signaling [17]. Xie *et al.* found that SZ-685C inhibits the growth of six tumor cell lines, including human glioma, hepatoma, prostate cancer, and breast cancer (IC_{50} = 3.0–9.6 μM). They also found that SZ-685C inhibits tumor growth in nude mice by inducing apoptosis via the Akt/FOXO pathway [15]. Wang *et al.* reported that SZ-685C displayed a potent cytocidal effect in both radiosensitive and radioresistant human nasopharyngeal carcinoma (NPC) cells via the miR-205-PTEN-Akt pathway [16].

We have demonstrated that SZ-685C could destroy tumor cells via activating caspase-3-mediated apoptotic mechanisms through suppressing the phosphorylation of Akt. Our study shows that the expression of Akt-related genes is decreased after treatment with SZ-685C.

Our experiments were limited by the scarcity of NFPA samples and their inherently slow growth rate. We need to continue investigating the mechanism of SZ-685C-induced apoptosis and collecting more biological tissue samples from the clinic. Understanding the mechanism of apoptosis could provide the basis for novel targeted therapies that can induce death in cancer cells or sensitize them to established cytotoxic agents and radiation therapy [22].

4. Experimental Section

4.1. Preparation of SZ-685C

SZ-685C was prepared and purified from mangrove endophytic fungus (No. 1403), as previously reported [15]. The compound was dissolved in dimethyl sulfoxide (DMSO, 2.5‰ of final concentration) to a concentration of 1 mM as a stock solution and diluted as indicated, according to experimental requirements.

4.2. Cell Culture

RPC cells (ScienCell, Logan, UT, USA, NO: R1200), an adherent cell line, were cultured in RPMI 1640 medium (Hyclone, Logan, UT, USA) supplemented with 10% fetal bovine serum (Gibco, New York, NY, USA), 100 $mg \cdot mL^{-1}$ streptomycin and 100 $units \cdot mL^{-1}$ penicillin (Invitrogen, Grand Island, NY, USA). The rat pituitary adenoma cell lines, MMQ and GH3, were purchased from Xie-he Bank (Beijing, China). They were cultured in DMEM/F-12 medium (Hyclone, USA)

supplemented with 15% horse serum (Gibco, USA) and 2.5% FBS (Gibco, USA). All of the cell lines were cultured at 37 °C in a humidified atmosphere of 5% CO_2 [23].

4.3. Pituitary Adenoma Samples

All of the pituitary adenoma samples were obtained from the Department of Neurosurgery and Pituitary Tumor Center of the First Affiliated Hospital, Sun Yat-sen University (Guangzhou, China). The local ethical committee approved the patients' treatment, and all of the participants provided informed written consent.

4.4. Cell Viability Assay

MTT assays were used to assess cell viability. NFPA cells and MMQ cells were seeded in 96-well plates (Corning, New York, NY, USA) at a density of 5×10^4 cells per well and cultured in serum-free DMEM/F-12 medium for 24 h. Then, each well was stimulated with the indicated concentration of SZ-685C (0–40 μM) for 24 h. The adherent cell line, RPC, was seeded and stimulated by the drug as described in the NFPA cell protocol. Subsequently, 10 μL MTT (dissolved in phosphate-buffered saline (PBS) at a pH of 7.4 (5 $mg \cdot mL^{-1}$; Sigma, St. Louis, MO, USA) was added to each well and incubated for 4 h at 37 °C in a humidified atmosphere of 5% CO_2. Next, 100 μL acidified isopropyl alcohol was added. Then, the optical density (OD) was measured by a Sunrise microplate reader (TECAN, Männedorf, Switzerland) at 570 nm with a reference wavelength of 630 nm. The IC_{50} was analyzed by SPSS 13.0 (SPSS, Chicago, IL, USA). The cell viability rate was calculated as follows: Cell viability rate = ((OD of treated cells − OD of blank)/(OD of control cells − OD of blank)) × 100%.

4.5. Hoechst 33342/PI Dye Assay

Apoptotic cells were detected by a Hoechst 33342/PI dye assay. The cultured primary NFPA cells were harvested and seeded in 6-well plates (4×10^5/well) and incubated with the indicated concentrations of SZ-685C for 24 h. Then, the cells were collected and washed three times with PBS, and stained using 10 μL Hoechst 33342 (5 μg/mL; Keygen Biotech, Nanjing, China) and 5 μL PI (2.5 μg/mL; Keygen Biotech, Nanjing, China) in PBS. Finally, the apoptotic cells were observed under the fluorescence microscope (Axio Observer Z1, Peabody, MA, USA).

4.6. Annexin V-FITC/PI Staining

The apoptosis rate of MMQ cells was determined using Annexin V-FITC and PI staining (eBioscience, San Diego, CA, USA). NFPA cells were treated with SZ-685C at the indicated concentration for 24 h in 6-well plates (2×10^5 cells/mL). Then, cells were collected and washed with PBS three times and resuspended in 500 μL binding buffer. Next, 5 μL Annexin V-FITC and 10 μL PI were added to each sample, and the samples were incubated in the dark for 10 min. Cell fluorescence was analyzed immediately after staining with the fluorescence microscope and flow cytometer (Epics XL-MCL, Beckman Coulter, Indianapolis, IN, USA). The FITC signal detector

(FL1) and PI staining signal detector (FL3) were used to detect the cells with the flow cytometer (Ex = 488 nm; Em = 530 nm).

4.7. Western Blotting

Total protein was extracted from NFPA cells after treatment at different concentrations of SZ-685C for 24 h using a lysis buffer (Applygen, Beijing, China). The protein concentrations were measured using a Bio-Rad protein assay kit (Bio-Rad Laboratories Inc., Hercules, CA, USA), and 30 μg of total protein was subjected to SDS-PAGE immunoblotting analysis. Polyvinylidene fluoride (PVDF) membranes (Bio-Rad Laboratories Inc., USA) were blocked with 5% non-fat milk in TBST (Tris-buffered saline containing 0.1% Tween 20; Sigma, USA) for 1 h at room temperature. After washing twice with TBST (5 min each), the membrane was incubated with caspase-3 (1:1000; ABclonal, Cambridge, MA, USA), Akt (1:1000; ABclonal, USA), PTEN (1:1000; Cell Signaling Technology, Danvers, MA, USA), and β-actin primary antibodies (1:2000; Santa Cruz, Dallas, TX, USA) at 4 °C overnight. The next day, the membrane was incubated with a horseradish peroxidase-conjugated secondary antibody (ProteinTech, Chicago, IL, USA) for 1 h at room temperature, and signal detection was performed using the ultrasensitive ECL Plus Detection Reagent (Applygen Technologies Inc, Beijing, China).

5. Conclusions

Our data suggest that SZ-685C may be a potentially promising Akt inhibitor and anti-cancer agent for the treatment of NFPA (Nonfunctioning pituitary adenoma).

Acknowledgments

This research was supported in part by two grants from the Guangdong Provincial National Natural Science Foundation of China (No.2011B090400219, S2012010009194) and two Guangzhou Civic Science and Technology Plan (No.2013J4100055).

Author Contributions

Yong-Hong Zhu, Hai-Jun Wang conceived and designed the experiments; Xin Wang, Ting Tan, Ni Lei, Bin Hu, Zong-Ming Wang performed the experiments; Zhi-Gang She contributed materials. Xin Wang, Ting Tan and Zhi-Gang Mao analyzed the data and composed the manuscript.

Conflicts of Interest

The authors declare no conflict of interest.

References

1. Daly, A.F.; Rixhon, M.; Adam, C.; Dempegioti, A.; Tichomirowa, M.A.; Beckers, A. High prevalence of pituitary adenomas: A cross-sectional study in the province of Liege, Belgium. *J. Clin. Endocrinol. Metab*. **2006**, *91*, 4769–4775.

2. Fernandez, A.; Karavitaki, N.; Wass, J.A. Prevalence of pituitary adenomas: A community-based, cross-sectional study in Banbury (Oxfordshire, UK). *Clin. Endocrinol. (Oxf.)* **2010**, *72*, 377–382.
3. Asa, S.L.; Ezzat, S. The pathogenesis of pituitary tumours. *Nat. Rev. Cancer* **2002**, *2*, 836–849.
4. Shao, S.; Li, X. Clinical features and analysis in 1385 Chinese patients with pituitary adenomas. *J. Neurosurg. Sci*. **2013**, *57*, 267–275.
5. Giustina, A. Keep an eye on nonfunctioning pituitary adenomas. *Clin. Endocrinol. (Oxf.)* **2012**, *77*, 656–657.
6. Comtois, R.; Beauregard, H.; Somma, M.; Serri, O.; Aris-Jilwan, N.; Hardy, J. The clinical and endocrine outcome to trans-sphenoidal microsurgery of nonsecreting pituitary adenomas. *Cancer* **1991**, *68*, 860–866.
7. Rubinfeld, H.; Shimon, I. PI3K/Akt/mTOR and Raf/MEK/ERK signaling pathways perturbations in non-functioning pituitary adenomas. *Endocrine*. **2012**, *42*, 285–291.
8. Montaser, R.; Luesch, H. Marine natural products: A new wave of drugs? *Future Med. Chem*. **2011**, *3*, 1475–1489.
9. Vinothkumar, S.; Parameswaran, P.S. Recent advances in marine drug research. *Biotechnol. Adv*. **2013**, *31*, 1826–1845.
10. Wang, X.; Mao, Z.G.; Song, B.B.; Chen, C.H.; Xiao, W.W.; Hu, B.; Wang, J.W.; Jiang, X.B.; Zhu, Y.H.; Wang, H.J. Advances in the study of the structures and bioactivities of metabolites isolated from mangrove-derived fungi in the South China Sea. *Mar. Drugs* **2013**, *11*, 3601–3616.
11. Rateb, M.E.; Ebel, R. Secondary metabolites of fungi from marine habitats. *Nat. Prod. Rep*. **2011**, *28*, 290–344.
12. Abbanat, D.; Leighton, M.; Maiese, W.; Jones, E.B.; Pearce, C.; Greenstein, M. Cell wall active antifungal compounds produced by the marine fungus hypoxylon oceanicum LL-15G256. I. Taxonomy and fermentation. *J. Antibiot. (Tokyo)* **1998**, *51*, 296–302.
13. Blunt, J.W.; Copp, B.R.; Keyzers, R.A.; Munro, M.H.; Prinsep, M.R. Marine natural products. *Nat. Prod. Rep*. **2014**, *31*, 160–258.
14. Xia, X.K.; Huang, H.R.; She, Z.G.; Shao, C.L.; Liu, F.; Cai, X.L.; Vrijmoed, L.L.; Lin, Y.C. ^{1}H and ^{13}C NMR assignments for five anthraquinones from the mangrove endophytic fungus *Halorosellinia* sp. (No. 1403). *Magn. Reson. Chem*. **2007**, *45*, 1006–1009.
15. Xie, G.; Zhu, X.; Li, Q.; Gu, M.; He, Z.; Wu, J.; Li, J.; Lin, Y.; Li, M.; She, Z.; Yuan, J. SZ-685C, a marine anthraquinone, is a potent inducer of apoptosis with anticancer activity by suppression of the Akt/FOXO pathway. *Br. J. Pharmacol*. **2010**, *159*, 689–697.
16. Wang, D.; Wang, S.; Liu, Q.; Wang, M.; Wang, C.; Yang, H. SZ-685C exhibits potent anticancer activity in both radiosensitive and radioresistant NPC cells through the miR-205-PTEN-Akt pathway. *Oncol. Rep*. **2013**, *29*, 2341–2347.
17. Zhu, X.; He, Z.; Wu, J.; Yuan, J.; Wen, W.; Hu, Y.; Jiang, Y.; Lin, C.; Zhang, Q.; Lin, M.; *et al.* A marine anthraquinone SZ-685C overrides adriamycin-resistance in breast cancer cells through suppressing Akt signaling. *Mar. Drugs* **2012**, *10*, 694–711.

18. Manning, B.D.; Cantley, L.C. Akt/PKB signaling: Navigating downstream. *Cell* **2007**, *129*, 1261–1274.
19. Young, R.C.; Ozols, R.F.; Myers, C.E. The anthracycline antineoplastic drugs. *N. Engl. J. Med.* **1981**, *305*, 139–153.
20. Colloca, G.; Venturino, A. Anthracycline-based chemotherapy in metastatic endometrial carcinoma: An update. *Asia Pac. J. Clin. Oncol*. **2014**, *10*, e75–e85.
21. Chen, C.H.; Xiao, W.W.; Jiang, X.B.; Wang, J.W.; Mao, Z.G.; Lei, N.; Fan, X.; Song, B.B.; Liao, C.X.; Wang, H.J.; *et al.* A novel marine drug, SZ-685C, induces apoptosis of MMQ pituitary tumor cells by downregulating miR-200c. *Curr. Med. Chem*. **2013**, *20*, 2145–2154.
22. Ghobrial, I.M.; Witzig, T.E.; Adjei, A.A. Targeting apoptosis pathways in cancer therapy. *CA Cancer J. Clin*. **2005**, *55*, 178–194.
23. Mao, Z.G.; Zhou, J.; Wang, H.; He, D.S.; Xiao, W.W.; Liao, G.Z.; Qiu, L.B.; Zhu, Y.H.; Wang, H.J. Artesunate inhibits cell proliferation and decreases growth hormone synthesis and secretion in GH3 cells. *Mol. Biol. Rep*. **2012**, *39*, 6227–6234.

First Evidence that *Ecklonia cava*-Derived Dieckol Attenuates MCF-7 Human Breast Carcinoma Cell Migration

Eun-Kyung Kim, Yujiao Tang, Yon-Suk Kim, Jin-Woo Hwang, Eun-Ju Choi, Ji-Hyeok Lee, Seung-Hong Lee, You-Jin Jeon and Pyo-Jam Park

Abstract: We investigated the effect of *Ecklonia cava (E. cava)*-derived dieckol on movement behavior and the expression of migration-related genes in MCF-7 human breast cancer cell. Phlorotannins (e.g., dieckol, 6,6′-biecko, and 2,7″-phloroglucinol-6,6′-bieckol) were purified from *E. cava* by using centrifugal partition chromatography. Among the phlorotannins, we found that dieckol inhibited breast cancer cell the most and was selected for further study. Radius™-well was used to assess cell migration, and dieckol (1–100 μM) was found to suppress breast cancer cell movement. Metastasis-related gene expressions were evaluated by RT-PCR and Western blot analysis. In addition, dieckol inhibited the expression of migration-related genes such as matrix metalloproteinase (MMP)-9 and vascular endothelial growth factor (VEGF). On the other hand, it stimulated the expression of tissue inhibitor of metalloproteinase (TIMP)-1 and TIMP-2. These results suggest that dieckol exerts anti-breast cancer activity via the regulation of the expressions of metastasis-related genes, and this is the first report on the anti-breast cancer effect of dieckol.

Reprinted from *Mar. Drugs*. Cite as: Kim, E.-K.; Tang, Y.; Kim, Y.-S.; Hwang, J.-W.; Choi, E.-J.; Lee, J.-H.; Lee, S.-H.; Jeon, Y.-J.; Park, P.-J. First Evidence that *Ecklonia cava*-Derived Dieckol Attenuates MCF-7 Human Breast Carcinoma Cell Migration. *Mar. Drugs* **2015**, *13*, 1785-1797.

1. Introduction

Brown algae, *E. cava* have been reported to possess various pharmaceutical and biological properties, including anti-cancer, anti-oxidant, anti-allergic, and anti-neurodegenerative effects [1–4]. Phlorotannins (e.g., dieckol, 6,6′-bieckol, and 2,7″-phloroglucinol-6,6′-bieckol) are the main bioactive components of *E. cava* [5]. Their chemical structures are shown in Figure 1. In particular, dieckol is reported to possess inhibitory activity against ovarian and hepatocellular cancers [6,7]. However, the anti-breast cancer effect of dieckol has not been investigated.

Breast cancer mortality rates have gradually decreased over the last two decades due to newly developed treatment strategies [8]; however, the disease incidence in the United States is still the highest among all cancers in women [9]. It is also the most frequent cause of cancer-related deaths in women [10]. Moreover, breast cancer incidence is rising more rapidly in Asia than in high-risk countries [11]. Therefore, more effective strategies for breast cancer prevention are needed.

Tumor metastasis is a multi-process phenomenon involving the participation of various metastasis-related genes, and almost all cancer deaths are caused by metastasis [12]. Metastasis is the process by which a cancer cell leaves its original location or organ, moves to another site that is not directly connected to the primary site via the circulatory system, and produces a secondary cancer [13]. Matrix metallopeptidases (MMPs) promote tumor progression and metastasis in invasive cancers by cleaving the extracellular matrix (ECM) surrounding the tumor tissue. The

degradation of ECM not only assists the migration of metastatic cancerous cells, but also allows for enhanced tumor growth by providing the necessary space [14]. Therefore, MMPs are key targets for many oncogenes [15]. Further, it is noteworthy that the ratio of active to latent forms of MMP-9 increases with tumor progression in invasive cancers. MMP-9 and its family members also promote angiogenesis, a critical process required for tumor cell survival, by degrading the vascular basement membrane interstitium and by releasing sequestered vascular endothelial growth factor (VEGF), a well know angiogenic molecule [16,17]. MMP activity is regulated by endogenous inhibitors, the tissue inhibitors of MMP (TIMPs), which closely bind to MMPs with 1:1 stoichiometry, and MMP activity is correlated with the physiological and pathological processes that coordinate the degradation and accumulation of the ECM [18]. Therefore, blocking the progress of these processes is also a valuable approach to cancer therapy.

Therefore, in the present study, we investigated the effects of dieckol obtained from *E. cava* on the migration behavior and the expression of metastasis-related genes *in vitro* using MCF-7 human breast cancer cell.

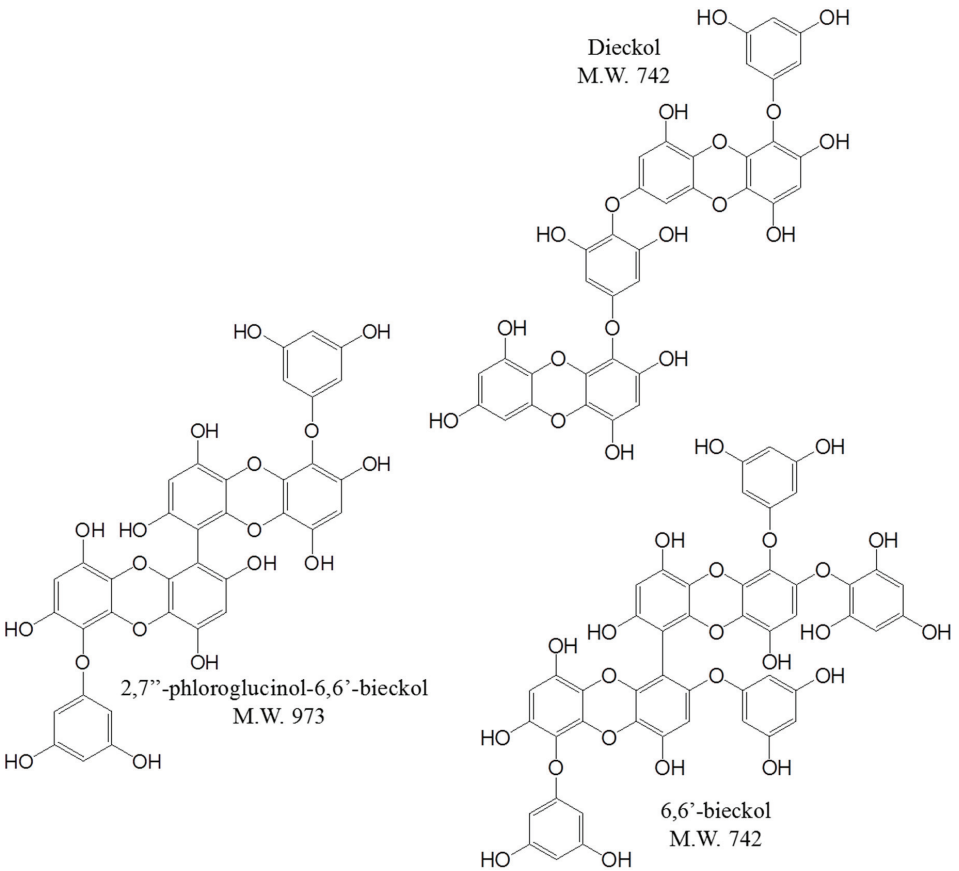

Figure 1. Chemical structures of phlorotannins from *E. cava*.

2. Results and Discussion

2.1. Selection of One of the Biological Components in E. cava

Dieckol showed the greatest inhibitory activity at 2–128 μM, with inhibition percentages ranges of 17.50%–57.69% (Figure 2). Generally, dieckol has been shown to possess inhibitory activity against cancers as well as some enzymes including α-glucosidase and α-amylase *in vitro*, and to alleviate postprandial hyperglycemia in streptozotocin-induced diabetic mice [6,7,19]. In addition, 6,6′-bieckol and 2,7″-phloroglucinol-6,6-bieckol from *E. cava* have been reported to exhibit antioxidant properties [20,21]. However, little information exists concerning which component is effective in breast cancer prevention or therapy. We conducted a cell cytotoxicity assay to determine which molecule most effectively inhibits breast cancer cell viability. MCF-7 cells were treated with three components at the indicated concentrations for 48 h. As a result, dieckol was selected for the anti-breast cancer study.

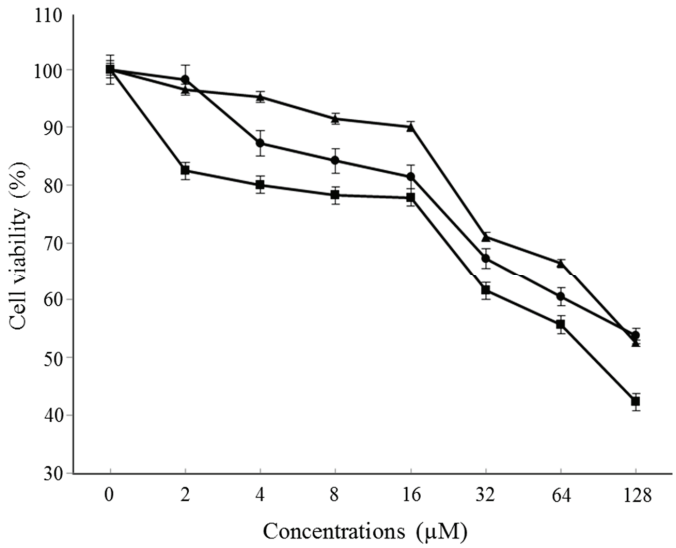

Figure 2. Effect of dieckol on the viability of MCF-7 cells. Cells were treated with various concentrations of dieckol for 48 h followed by MTT assay, and then the absorbance was measured. Cell viability was calculated as the relative absorbance compared to DMSO vehicle control absorbance. —■—, dieckol; —▲—, 6,6′-bieckol; —●—, 2,7″-phloroglucinol-6,6-bieckol.

2.2. The Effect of Dieckol on Migration in Human Breast Cancer Cells

To examine the effect of dieckol on breast cancer cell migration, we carried out gap-closure assay using Radius™ wells. To stimulate cell migration, estradiol (E2) was treated on the cell before dieckol treatment. To compare the differences in migratory gap, images were captured at the same size, and the gap-closure was determined after the indicated times (0, 8, 12, and 24 h) and

compared between each group. After 24 h, the gap closed by approximately 74.7% in the E2 alone-treated group. As shown in Figure 3, dieckol resulted in significantly lower cell motility in a dose-dependent fashion, compared to that in the E2 alone-treated group. Most cancer deaths are caused by the dissemination of tumors from their primary site. Cancer cells migrate in a highly orchestrated manner that depends on both internal and external signals [22], such as integrins [23], adhesion receptors [24], and chemical signals sensed by chemokine and growth factor receptors [25]. The gap-closure zone assay was recently created to assess cell migration. In this assay, cells are grown on a well bottom around something (e.g., a stopper placed in the middle of the well) that prevents them from growing in one particular region [26]. The experiment begins when the stopper is removed, and the migration of the cells to fill the void in the monolayer is studied. The advantage of the gap-closure assay is that the cell movements can be studied continuously in real time without possible complications of wound-related factors. Due to this advantage, time-series pictures were captured (Figure 3A).

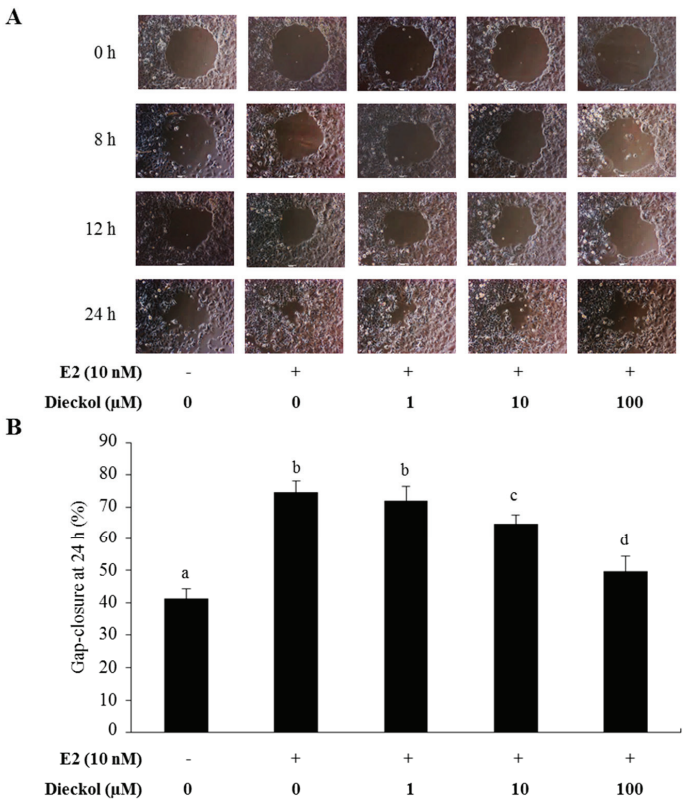

Figure 3. Migration rates of dieckol-treated MCF-7 cells. (**A**) Cell migration time course. Images were captured at the same size after the indicated times (0, 8, 12, and 24 h); (**B**) The gap closure was determined after 24 h using CellProfiler™ software. Values not sharing a common letter are significantly different at $p < 0.05$ by Dunnett's multiple range test.

2.3. The Effect of Dieckol on the Expression of Migration-Related Genes in Human Breast Cancer Cell

As shown in Figure 4A–D, dieckol didn't significantly affect the mRNA expression. On the contrary, dieckol significantly affected the protein expression (Figure 4E–H). Briefly, the protein expression of MMP-9 was significantly inhibited (Figure 4E,F). On the other hand, the protein expressions of TIMP-1 and TIMP-2 were significantly increased in dieckol-treated human breast cancer cell (Figure 4E,G,H). Meanwhile, the protein expression of MMP-9 was in a dose-independent manner, while TIMPs were in a dose-dependent manner. The effect of the concentrations on the genes should be further investigated. Cancers exhibit two modes of motility: adhesion receptor-mediated basal movement and a faster motility in response to soluble growth factors [27]. Growth factor receptor-mediated movement is an essential driver of cancer cell dissemination via metastasis [28,29]. Thus, understanding the key molecular controls of this behavior should provide novel targets to limit initial or secondary dissemination. From this result, it was clearly seen that dieckol stimulated the protein expression of TIMPs. TIMPs are glycoproteins that are natural inhibitors of MMPs as well as a group of peptidases, and are involved in ECM degradation. Therefore, these data suggest that dieckol suppresses cell migration by up-regulating TIMP-1 and TIMP-2 levels in MCF-7 human breast cancer cell.

2.4. The Effect of Dieckol on the Expression of the Angiogenesis-Related Gene VEGF in Human Breast Cancer Cell

Dieckol significantly inhibited the mRNA (Figure 5A,B) and protein (Figure 5C,D) expression of VEGF in a dose-dependent manner. The angiogenic response is induced by growth factors such as VEGF, basic fibroblast growth factor (bFGF), platelet-derived growth factor (PDGF), and chemokines [30]. ECM is degraded by several matrix-degrading enzymes [31], such as MMPs, which are produced by stromal cells, endothelial cells, or tumor cells themselves [32]. Therefore, VEGF has been recognized as a key potential target for pharmacological inhibition of tumor angiogenesis, and from Figure 5, we confirmed that dieckol possessed the inhibitory effect of VEGF.

Recently, Kim *et al*., reported the effect of phloroglucinol which is also a phlorotannin component on breast cancer cells. Phloroglucinol effectively inhibited EMT (epithelial-mesenchymal cell transition)-related genes such as, FN1, VIM, *N*-cadherin, SNAIL, *etc*. EMT is also related to cancer metastasis, therefore, the investigation has given us motivation to do further study to investigate the precise cancer inhibitory mechanism of dieckol. All in all, it was proven that brown algae-derived phlorotannins, including dieckol and phloroglucinol, possessed an inhibitory effect on cancer metastasis. However the investigation of the precise mechanism of each component is needed [33].

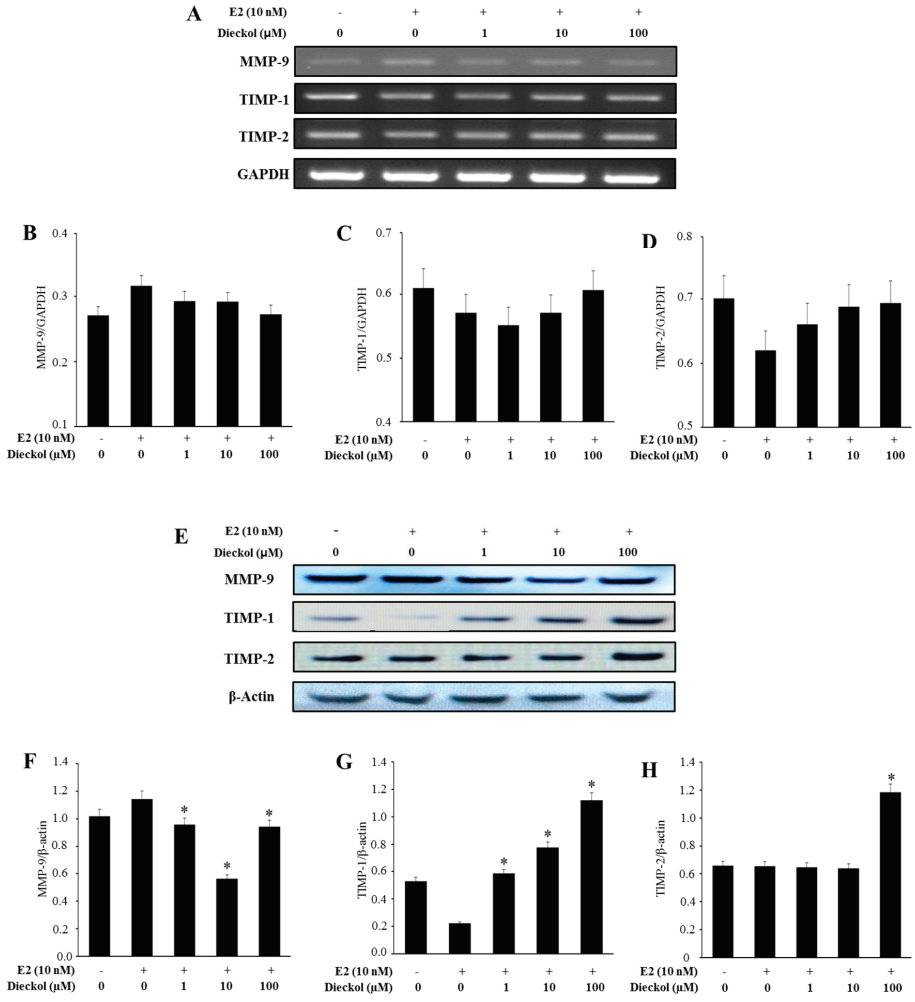

Figure 4. The expression of migration-related genes, based on RT-PCR and Western blot assays. mRNA (**A**–**D**) and protein (**E**–**H**) expression of migration-related genes, quantified by Multi Gauge (Fujifilm, Japan). Cells were treated with various concentrations of dieckol for 48 h with or without E2. The mRNA and protein levels from whole cell lysates were analyzed by RT-PCR or Western blot, respectively. GAPDH and β-actin were used as loading controls. The results were similar in three independent experiments. * Significantly different from the E2 alone group at $p < 0.05$.

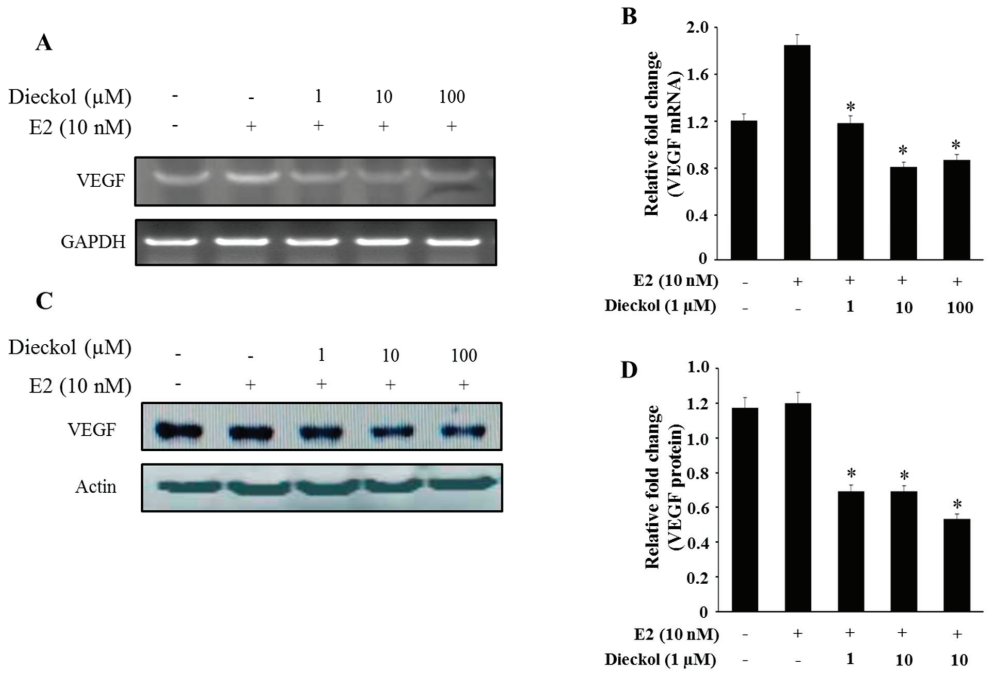

Figure 5. The mRNA and protein expression of VEGF. mRNA (**A**,**B**) and protein (**C**,**D**) expression of VEGF were quantified by Multi Gauge (Fujifilm, Japan). Cells were treated with various concentrations of dieckol for 48 h with or without E2. The mRNA and protein levels from whole cell lysates were analyzed by RT-PCR or Western blot, respectively. GAPDH and β-actin were used as a loading control. The results were similar in three independent experiments. * Significantly different from the E2 alone group at $p < 0.05$.

3. Experimental Section

3.1. Materials

Marine edible brown seaweed, *E. cava*, was collected from Jeju Island off the coast of the Republic of Korea. Fresh *E. cava* was washed three times with water to remove salt, sand, and epiphytes. The cleaned *E. cava* was ground and sifted through a 50 mesh standard testing sieve after drying in a freeze dryer SFDSMO6 (Samwon Freezing Engineering Co., Gyeonggi, Korea). The dried *E. cava* was stored in a refrigerator until use. All solvents used for the preparation of crude samples were of analytical grade (Daejung Chemicals & Metals Co., Seoul, South Korea). HPLC grade solvents were purchased from Burdick & Jackson (MI, USA). MCF-7 human breast cancer cell line was obtained from the Korean Cell Line Bank (Seoul, Korea; KCLB numbers: 30022). RPMI 1640 media for the cells and TRIzol reagent for RNA extraction were from Invitrogen (Carlsbad, CA, USA). E2 was purchased from Sigma (St. Louis, MO, USA). Primary antibodies including MMP-9 (SC-10737), TIMP-1 (Cat. SC-6823), TIMP-2 (Cat. SC-6835), VEGF

(Cat. SC-152), and β-actin (SC-1616) were purchased from Santa Cruz Biotechnology Inc. (Santa Cruz, CA, USA) as well as the peroxidase-conjugated secondary antibodies including anti-gout (SC-2020), and anti-mouse (SC-2005).

3.2. Extraction and Isolation of the Major Components of E. cava

The phlorotannins were isolated according to the previously reported method [34,35]. The dried *E. cava* powder (500 g) was extracted using 5 L of 80% aqueous methanol three times at room temperature. The liquid layer was obtained via filtration, and the filtrate was concentrated using an evaporator under reduced pressure. The extract was suspended in H_2O, and the aqueous layer was partitioned with ethyl acetate (EtOAc). The EtOAc extract was mixed with celite. The mixed celite was then dried and packed into a glass column, and subsequently eluted in the following order: hexane, dichloromethane, diethyl ether, and butanol. The diethyl ether fraction was subjected to Sephadex LH-20 column chromatography using a stepwise gradient with chloroform/methanol (2/1 to 1/1 to 0/1) solvents system. The dieckol, 6,6′-bieckol, and 2,7″-phloroglucinol-6,6′-bieckol were purified by HPLC using a Waters HPLC system equipped with a Waters 996 photodiode array detector and C_{18} column (J'sphere ODS-H80, 150 × 20 mm, 4 μm; YMC Co., Kyoto, Japan) by stepwise elution with a methanol-water gradient. Finally, the purified compounds were identified by comparing the ^{1}H and ^{13}C-NMR spectral data with those in the existing literature [21,34,35]. The chemical structures of the three phlorotannins are indicated in Figure 1.

3.3. Cell Culture

The MCF-7 human breast cancer cell line was cultured in RPMI 1640 media supplemented with 10% FBS and 1% penicillin/streptomycin in a 5% CO_2 atmosphere at 37 °C. The cells were seeded at a density of 5.0×10^5 in a 6-well culture plate. After 24 h, the cells were treated with or without 10 nM of E2 or 1–100 μM of dieckol extracts in media for 48 h and then harvested.

3.4. Cytotoxicity Assay

Cell viability was determined by 3-(4,5-dimethylthiazol-2yl)-2,5-diphenyltetrazolium bromide (MTT) assay in 96-well plates, as previously described [36]. Cells were incubated with various concentrations of dieckol for 48 h followed by MTT for 4 h, and then 100 μL isopropanol (in 0.04 *N*-hydrochloric acid) was added to dissolve the formazan crystals. The absorbance was read at 570 nm using a spectrophotometer (Tecan, Switzerland). Cell viability was calculated as the relative absorbance compared to DMSO vehicle control absorbance [36].

3.5. Gap Closure Migration Assay

We performed the migration assay using the Radius™ 24-well from Cell Biolabs, Inc (San Diego, CA, USA). For the analysis, 500 μL Radius™ gel pretreatment solution was slowly added to each well by carefully pipetting down the wall of the well, and then the plate was covered and incubated at room temperature for 20 min. Radius™ gel pretreatment solution was carefully

aspirated from the wells, and 500 µL Radius™ wash solution was added to each well. The cells were harvested and resuspended in culture medium at 0.2×10^6 cells/mL. Radius™ wash solution was carefully aspirated from the wells, and 500 µL of the cell suspension was added to each well by carefully pipetting down the wall of the well. The plate was transferred to a cell culture incubator for 24 h to allow firm attachment. After 24 h, media was aspirated from each well and washed 3 times with 0.5 mL fresh media. A sufficient amount of 1× Radius™ gel removal solution for all wells was prepared by diluting the stock 1:100 in culture media. The media was aspirated from the wells, and 0.5 mL 1× Radius™ gel removal solution was added to each well and washed 3 times with 0.5 mL fresh media. After the final washing was complete, 1 mL of complete medium with dieckol (1–100 µM) was added to each well, and a photo was taken at 0, 8, 12, and 24 h. To compare differences in the migratory gap, images were captured at the same size, and gap closure was determined after the indicated times (0, 8, 12, and 24 h) using CellProfiler™ software (Broad Institute, Cambridge, MA, USA).

3.6. RNA Isolation and mRNA Expression Analysis

For RT-PCR, total cellular RNA was isolated from cells using TRIzol, according to the manufacturer's protocol. The first-strand complementary DNA (cDNA) was synthesized using Superscript II reverse transcriptase (Invitrogen, Carlsbad, CA, USA). PCR was performed as previously described with primers for MMP-9 (GenBank accession no. AK301446.1; s 5′-CGA CGT CTT CCA GTA CCG AG-3′; as 5′-GTT GGT CCC AGT GGG GAT TT-3′), TIMP-1 (GenBank accession no. AK311937.1; s 5′-CAA GAT GAC CAA GAT GTA TAA AGG-3′; as 5′-AAC AGT GTA GGT CTT GGT GAA G-3′), TIMP-2 (GenBank accession no. AL110197.1; s 5′-CAG CTT TGC TTT ATC CGG GC-3′; as 5′-ATG CTT AGC TGG CGT CAC AT-3′), and VEGF (GenBank accession no. AB209485.1; s 5′-AGG GCA GAA TCA TCA CGA AG-3′; as 5′-TTT CTC CGC TCTGAG CAA GG-3′). GAPDH (GenBank accession no. AB062273.1; s 5′-CCA TGG GGA AGG TGA AGG TC-3′; as 5′-AAA TGA GCC CCA GCC TTC TC-3′) was used as an internal control. The conditions for RT-PCR were similar to ones that have been previously described [37].

3.7. Western Blot Analysis

Cell extracts were prepared by the detergent lysis procedure, as described elsewhere [38]. Samples of protein (40 µg) were used for electrophoresis using Novex 4%–12% Bis-Tris gels (Life Technologies, Carlsbad, CA, USA) and then transferred to nitrocellulose membranes for 7 min in the iBlot dry blotting system (Life Technologies, Carlsbad, CA, USA). The transferred proteins were blocked overnight at 4 °C with clear milk (Thermo Scientific, IL, USA). Blots were subsequently incubated with primary antibodies diluted 1:2000 in 1× TBST for 1 h. Goat anti-rabbit or goat anti-mouse horseradish peroxidase conjugated secondary antibodies (Santa Cruz Biotechnology, Dallas, TX, USA) were used at 1:2000 dilution in 1× TBST. Blots were treated with Western Lightning Western Blot Chemilluminescence Reagent (Advansta, CA, USA) and the proteins were detected by autoradiography. Equal protein loading was ascertained by ponceau S

staining of blotted membranes as well as Western blotting with β-actin bodies. Immunodetection was done using an enhanced chemiluminescence detection kit (Amersham Pharmacia, Piscataway, NJ, USA).

3.8. Data Analysis

The results from the experiments shown are summaries of the data sourced from at least three experiments. All of the data are presented as the mean ± SE. Statistical analyses were performed using SAS statistical software (SAS Institute, Cray, NC, USA). Treatment effects were analyzed using one-way analysis of variance, followed by Dunnett's multiple range test. The results $p < 0.05$ were used to indicate significance.

4. Conclusions

In the present study, we demonstrated for the first time the effects of dieckol derived from *E. cava* ethanol extracts on human MCF-7 breast cancer cell *in vitro*. Cell cytotoxicity was determined using an MTT assay, and migration was detected using a gap closer assay. Further, we evaluated the mRNA and protein expression levels of MMP-9, TIMP-1, TIMP-2, and VEGF using RT-PCR and Western blot, respectively. The results of the present study characterize the signaling cascades that mediate the anti-metastatic activity of dieckol in the human MCF-7 breast cancer cell line. Dieckol was found to significantly suppress the migration of MCF-7 cells and inhibit the expression of MMP-9 and VEGF. On the contrary, TIMP-1 and TIMP-2 were increased in MCF-7 cell by dieckol treatment. These findings demonstrate the biological activity of dieckol in an *in vitro* model of cancer metastasis, and show that dieckol may be a promising new therapeutic in breast cancer therapy.

Acknowledgments

This work was supported by Konkuk University.

Author Contributions

The authors alone are responsible for the content and writing of the paper. Eun-Kyung Kim and Pyo-Jam Park contributed to the design of the study. Yujiao Tang, Yon-Suk Kim, Jin-Woo Hwang, and Eun-Ju Choi were involved in the cell culture, cytotoxicity, and migration assays, RT-PCR, and Western blot. Seung-Hong Lee, Ji-Hyeok Lee, and You-Jin Jeon designed and coordinated the purification and identification of compounds. All authors read and approved the final manuscript.

Conflicts of Interest

The authors declare no conflict of interest.

References

1. Athukorala, Y.; Kim, K.N.; Jeon, Y.J. Antiproliferative and antioxidant properties of an enzymatic hydrolysate from brown alga, *Ecklonia cava*. *Food Chem. Toxicol.* **2006**, *44*, 1065–1074.
2. Kim, K.N.; Heo, S.J.; Song, C.B.; Lee, J.; Heo, M.S.; Yeo, I.K.; Kang, K.A.; Hyun, J.W.; Jeon, Y.J. Protective effect of *Ecklonia cava* enzymatic extracts on hydrogen peroxide-induced cell damage. *Process. Biochem.* **2006**, *41*, 2393–2401.
3. Le, Q.T.; Li, Y.; Qian, Z.J.; Kim, M.M.; Kim, S.K. Inhibitory effects of polyphenols isolated from marine alga *Ecklonia cava* on histamine release. *Process. Biochem.* **2009**, *44*, 168–176.
4. Kang, I.J.; Jeon, Y.E.; Yin, X.F.; Nam, J.S.; You, S.G.; Hong, M.S.; Jang, B.G.; Kim, M.J. Butanol extract of *Ecklonia cava* prevents production and aggregation of beta-amyloid, and reduces beta-amyloid mediated neuronal death. *Food Chem. Toxicol.* **2011**, *49*, 2252–2259.
5. Lee, J.H.; Ko, J.Y.; Oh, J.Y.; Kim, C.Y.; Lee, H.J.; Kim, J.; Jeon, Y.J. Preparative isolation and purification of phlorotannins from *Ecklonia cava* using centrifugal partition chromatography by one-step. *Food Chem.* **2014**, *158*, 433–437.
6. Ahn, J.H.; Yang, Y.I.; Lee, K.T.; Choi, J.H. Dieckol, isolated from the edible brown algae *Ecklonia cava*, induces apoptosis of ovarian cancer cells and inhibits tumor xenograft growth. *J. Cancer Res. Clin. Oncol.* **2015**, *141*, 255–268.
7. Yoon, J.S.; Kasin Yadunandam, A.; Kim, S.J.; Woo, H.C.; Kim, H.R.; Kim, G.D. Dieckol, isolated from *Ecklonia stolonifera*, induces apoptosis in human hepatocellular carcinoma Hep3B cells. *J. Nat. Med.* **2013**, *67*, 519–527.
8. Yue, W.; Yager, J.D.; Wang, J.P.; Jupe, E.R.; Santen, R.J. Estrogen receptor-dependent and independent mechanisms of breast cancer carcinogenesis. *Steroids* **2013**, *78*, 161–170.
9. Siegel, R.; Naishadham, D.; Jemal, A. Cancer Statistics, 2012. *Ca-Cancer J. Clin.* **2012**, *62*, 10–29.
10. DeSantis, C.; Ma, J.; Bryan, L.; Jemal, A. Breast cancer statistics, 2013. *Ca-Cancer J. Clin.* **2014**, *64*, 52–62.
11. Jemal, A.; Siegel, R.; Xu, J.Q.; Ward, E. Cancer statistics, 2010. *Ca-Cancer J. Clin.* **2010**, *60*, 277–300.
12. Susnow, N.; Zeng, L.Y.; Margineantu, D.; Hockenbery, D.M. Bcl-2 family proteins as regulators of oxidative stress. *Semin. Cancer Biol.* **2009**, *19*, 42–49.
13. Tang, Y.; Zhu, J.W.; Chen, L.; Chen, L.Y.; Zhang, S.; Lin, J.Y. Associations of matrix metalloproteinase-9 protein polymorphisms with lymph node metastasis but not invasion of gastric cancer. *Clin. Cancer Res.* **2008**, *14*, 2870–2877.
14. Liabakk, N.B.; Talbot, I.; Smith, R.A.; Wilkinson, K.; Balkwill, F. Matrix metalloprotease 2 (MMP-2) and matrix metalloprotease 9 (MMP-9) type IV collagenases in colorectal cancer. *Cancer Res.* **1996**, *56*, 190–196.
15. Roderfeld, M.; Graf, J.; Giese, B.; Saiguero-Palacios, R.; Tschuschner, A.; Muller-Newen, G.; Roeb, E. Latent MMP-9 is bound to TIMP-1 before secretion. *Biol. Chem.* **2007**, *388*, 1227–1234.

16. Roomi, M.W.; Ivanov, V.; Kalinovsky, T.; Niedzwiecki, A.; Rath, M. *In vivo* antitumor effect of ascorbic acid, lysine, proline and green tea extract on human colon cancer cell HCT 116 xenografts in nude mice: Evaluation of tumor growth and immunohistochemistry. *Oncol. Rep.* **2005**, *13*, 421–425.
17. Manu, K.A.; Shanmugam, M.K.; Ramachandran, L.; Li, F.; Fong, C.W.; Kumar, A.P.; Tan, P.; Sethi, G. First evidence that gamma-tocotrienol inhibits the growth of human gastric cancer and chemosensitizes it to capecitabine in a xenograft mouse model through the modulation of NF-kappa B pathway. *Clin. Cancer Res.* **2012**, *18*, 2220–2229.
18. Verma, S.; Kesh, K.; Ganguly, N.; Jana, S.; Swarnakar, S. Matrix metalloproteinases and gastrointestinal cancers: Impacts of dietary antioxidants. *World J. Biol. Chem.* **2014**, *5*, 355–376.
19. Lee, S.H.; Park, M.H.; Heo, S.J.; Kang, S.M.; Ko, S.C.; Han, J.S.; Jeon, Y.J. Dieckol isolated from *Ecklonia cava* inhibits alpha-glucosidase and alpha-amylase *in vitro* and alleviates postprandial hyperglycemia in streptozotocin-induced diabetic mice. *Food Chem. Toxicol.* **2010**, *48*, 2633–2637.
20. Kang, S.M.; Lee, S.H.; Heo, S.J.; Kim, K.N.; Jeon, Y.J. Evaluation of antioxidant properties of a new compound, pyrogallol-phloroglucinol-6,6′-bieckol isolated from brown algae, *Ecklonia cava*. *Nutr. Res. Pract.* **2011**, *5*, 495–502.
21. Kang, S.M.; Heo, S.J.; Kim, K.N.; Lee, S.H.; Jeon, Y.J. Isolation and identification of new compound, 2,7″-phloroglucinol-6,6′-bieckol from brown algae, *Ecklonia cava* and its antioxidant effect. *J. Funct. Foods* **2012**, *4*, 158–166.
22. Polacheck, W.J.; Zervantonakis, I.K.; Kamm, R.D. Tumor cell migration in complex microenvironments. *Cell Mol. Life Sci.* **2013**, *70*, 1335–1356.
23. Paszek, M.J.; Zahir, N.; Johnson, K.R.; Lakins, J.N.; Rozenberg, G.I.; Gefen, A.; Reinhart-King, C.A.; Margulies, S.S.; Dembo, M.; Boettiger, D.; *et al*. Tensional homeostasis and the malignant phenotype. *Cancer Cell* **2005**, *8*, 241–254.
24. Moore, S.W.; Roca-Cusachs, P.; Sheetz, M.P. Stretchy proteins on stretchy substrates: The important elements of integrin-mediated rigidity sensing. *Dev. Cell* **2010**, *19*, 194–206.
25. Roussos, E.T.; Condeelis, J.S.; Patsialou, A. Chemotaxis in cancer. *Nat. Rev. Cancer* **2011**, *11*, 573–587.
26. Vogt, A. Advances in two-dimensional cell migration assay technologies. *Eur. Pharma. Rev.* **2010**, *5*, 26–29.
27. Wells, A.; Grahovac, J.; Wheeler, S.; Ma, B.; Lauffenburger, D. Targeting tumor cell motility as a strategy against invasion and metastasis. *Trends Pharmacol. Sci.* **2013**, *34*, 283–289.
28. Wells, A. Tumor invasion: Role of growth factor-induced cell motility. *Adv. Cancer Res.* **2000**, *78*, 31–101.
29. Wang, W.G.; Goswami, S.; Sahai, E.; Wyckoff, J.B.; Segall, J.E.; Condeelis, J.S. Tumor cells caught in the act of invading: Their strategy for enhanced cell motility. *Trends Cell Biol.* **2005**, *15*, 138–145.
30. Kalluri, R. Basement membranes: Structure, assembly and role in tumour angiogenesis. *Nat. Rev. Cancer* **2003**, *3*, 422–433.

31. Folkman, J. Angiogenesis in cancer, vascular, rheumatoid and other disease. *Nat. Med.* **1995**, *1*, 27–31.
32. Egeblad, M.; Werb, Z. New functions for the matrix metalloproteinases in cancer progression. *Nat. Rev. Cancer* **2002**, *2*, 161–174.
33. Kim, R.-K.; Suh, Y.J.; Yoo, K.-C.; Cui, Y.-H.; Hwang, E.; Kim, H.-J.; Kang, J.-S.; Kim, M.-J.; Lee, Y.Y.; Lee, S.-J. Phloroglucinol suppresses metastatic ability of breast cancer cells by inhibition of epithelial-mesenchymal cell transition. *Cancer Sci.* **2015**, *106*, 94–101.
34. Ahn, G.N.; Kim, K.N.; Cha, S.H.; Song, C.B.; Lee, J.H.; Heo, M.S.; Yeo, I.K.; Lee, N.H.; Jee, Y.H.; Kim, J.S.; *et al*. Antioxidant activities of phlorotannins purified from *Ecklonia cava* on free radical scavenging using ESR and H_2O_2-mediated DNA damage. *Eur. Food Res. Technol.* **2007**, *226*, 71–79.
35. Lee, S.H.; Li, Y.; Karadeniz, F.; Kim, M.M.; Kim, S.K. α-Glucosidase and α-amylase inhibitory activities of phloroglucinal derivatives from edible marine brown alga, *Ecklonia cava*. *J. Sci. Food Agric.* **2009**, *89*, 1552–1558.
36. Kim, S.H.; Johnson, V.J.; Sharma, R.P. Mercury inhibits nitric oxide production but activates proinflammatory cytokine expression in murine macrophage: differential modulation of NF-kappa B and p38 MAPK signaling pathways. *Nitric Oxide-Biol. Chem.* **2002**, *7*, 67–74.
37. Choi, E.J.; Lee, S.; Chae, J.R.; Lee, H.S.; Jun, C.D.; Kim, S.H. Eupatilin inhibits lipopolysaccharide-induced expression of inflammatory mediators in macrophages. *Life Sci.* **2011**, *88*, 1121–1126.
38. Kim, Y.D.; Choi, S.C.; Oh, T.Y.; Chun, J.S.; Jun, C.D. Eupatilin inhibits T-cell activation by modulation of intracellular calcium flux and NF-kappaB and NF-AT activity. *J. Cell Biochem.* **2009**, *108*, 225–236.

Esters of the Marine-Derived Triterpene Sipholenol A Reverse P-GP-Mediated Drug Resistance

Yongchao Zhang, Yun-Kai Zhang, Yi-Jun Wang, Saurabh G. Vispute, Sandeep Jain, Yangmin Chen, Jessalyn Li, Diaa T. A. Youssef, Khalid A. El Sayed and Zhe-Sheng Chen

Abstract: Our previous studies showed that several sipholane triterpenes, sipholenol A, sipholenone E, sipholenol L and siphonellinol D, have potent reversal effect for multidrug resistance (MDR) in cancer cells that overexpressed P-glycoprotein (P-gp/ABCB1). Through comparison of cytotoxicity towards sensitive and multi-drug resistant cell lines, we identified that the semisynthetic esters sipholenol A-4-*O*-acetate and sipholenol A-4-*O*-isonicotinate potently reversed P-gp-mediated MDR but had no effect on MRP1/ABCC1 and BCRP/ABCG2-mediated MDR. The results from [^{3}H]-paclitaxel accumulation and efflux studies suggested that these two triterpenoids were able to increase the intracellular accumulation of paclitaxel by inhibiting its active efflux. In addition, western blot analysis revealed that these two compounds did not alter the expression levels of P-gp when treated up to 72 h. These sipholenol derivatives also stimulated the ATPase activity of P-gp membranes, which suggested that they might be substrates of P-gp. Moreover, *in silico* molecular docking studies revealed the virtual binding modes of these two compounds into human homology model of P-gp. In conclusion, sipholenol A-4-*O*-acetate and sipholenol A-4-*O*-isonicotinate efficiently inhibit the P-gp and may represent potential reversal agents for the treatment of multidrug resistant cancers.

Reprinted from *Mar. Drugs*. Cite as: Zhang, Y.; Zhang, Y.-K.; Wang, Y.-J.; Vispute, S.G.; Jain, S.; Chen, Y.; Li, J.; Youssef, D.T.A.; El Sayed, K.A.; Chen, Z.-S. Esters of the Marine-Derived Triterpene Sipholenol A Reverse P-GP-Mediated Drug Resistance. *Mar. Drugs* **2015**, *13*, 2267-2286.

1. Introduction

Multi-drug Resistance (MDR) is a major clinical obstacle in the treatment of cancer. The cause of MDR is diversely characterized by multiple alterations in protein expression. The mechanism of drug resistance can occur due to increased drug efflux, reduced drug uptake, activation of detoxifying proteins, activation of DNA repair, and disruption of apoptotic signaling pathways [1–3]. Among these, increased drug extrusion mediated by P-glycoprotein (P-gp/ABCB1) is a major factor [4]. P-gp is a 170-kD transmembrane transporter in the family of ATP-binding cassette (ABC) transporters that are distributed widely across various organs [5,6]. P-gp facilitates the efflux of cytotoxic compounds out of cells with the energy generated by ATP hydrolysis [7]. The transporter also recognizes a large number of therapeutic drugs and is overexpressed in cancer cells [8]. This significantly reduces the therapeutic efficacy of chemotherapeutic agents and disposes the patient to subpar treatments.

Many scientists aim to inhibit the P-gp transporter to reverse MDR and again re-sensitize the cancer cells at clinically effective doses of chemotherapeutic agents. Tsuruo *et al.* in 1981

discovered that verapamil could effectively reverse P-gp-mediated drug resistance *in vitro*, opening the doors to a cascade of compounds to be evaluated for this ability [9]. The first generation agents that can inhibit P-gp-mediated MDR are currently US Food and Drug Administration (FDA) approved therapeutic compounds such as verapamil, quinidine, amiodarone, tamoxifen, progesterone, and cyclosporin A [10]. Although it is attractive to utilize these agents to treat cancer patients with indicated co-morbidities, research has shown that these compounds are effective as MDR reversal agents either at much higher doses or may relate to various undesirable side effects. For example, tamoxifen exhibited 50% of P-gp mediated drug accumulation at 60 μM [11], and cyclosporin A treatment may be associated with potentially serious adverse drug reactions. Thus, second-generation agents with higher affinity for the P-gp transporter were developed with an aim to improve MDR inhibition. Second-generation inhibitors such as PSC-833 (a non-immunosuppressive analogue of cyclosporin A) also failed in clinical trials due to unwarranted pharmacokinetic interactions [2,12]. To minimize these drug interactions, third generation of MDR inhibitors are currently being designed to modulate P-gp activity at nanomolar concentrations, to increase the potency and decrease adverse drug reactions [13].

Although, exploring the marine environment for new therapeutic compounds is not a recent strategy, the amount of unknown correlates to the potential it holds in the ecosystem. Marine environment houses a plethora of bioactive compounds that express diverse therapeutic effects, such as being anti-inflammatory, antiretroviral, analgesic, antitumor, and immunomodulator [14]. In the past, extensive screening of marine sponge compounds has led to the discovery of many potential MDR-reversal agents [15,16]. A group of compounds, the sipholane triterpenoids from the Red Sea sponge *Siphonochalina siphonella*, potently reversed P-gp-mediated MDR in cancer cells. Previous research showed that sodwanones from the Indian Ocean sponge *Axinella weltneri* demonstrated anticancer properties [17,18]. Due to the structural similarity of sodwanes to polyepoxysqualene-derived triterpenoids, it was hypothesized that sipholane triterpenoids could also exhibit potential anticancer effects.

Sipholane triterpenes were extracted from *Callyspongia siphonella*, a Red Sea marine sponge. Several semisynthetic analogs of sipholenol A were synthesized and showed potent breast cancer migration inhibitory activities [19,20]. These sipholenol analogs have close structural and pharmacophoric similarities to the previously described compounds that showed drug-resistance reversal properties. They were first tested for cytotoxicity on cancer cells and then for reversal of P-gp mediated MDR. Among these compounds, sipholenol A-4-*O*-acetate (SSJ26) and sipholenol A-4-*O*-isonicotinate (SSJ32) demonstrated P-gp inhibition comparable to that of verapamil. In this study, these two compounds were further analyzed to elucidate their mechanism of action and strengthen their value as potential P-gp-mediated drug resistance reversal agents.

2. Materials and Methods

2.1. Materials

[^{3}H]-paclitaxel was purchased from Moravek Biochemicals, Inc. (Brea, CA, USA). Monoclonal antibody C-219 (against P-gp) and loading control antibody BA3R (against β-actin) were

purchased from Thermo Fisher Scientific (Rockford, IL, USA). Sipholane analogs were previously synthesized and the structures are shown in Figure 1A and Supplementary Information Figure S1. Fumitremorgin C (FTC) was synthesized by Thomas McCloud Developmental Therapeutics Program, Natural Products Extraction Laboratory, NCI, NIH (Bethesda, MD, USA) and it was a gift from Susan E Bates and Robert W. Robey. The Gentest ATPase kit was purchased from BD Biosciences (San Jose, CA, USA). Doxorubicin, paclitaxel, vincristine, verapamil, 3-(4,5-dimethylthiazol-2-yl)-2,5-diphenyltetrazolium bromide (MTT) and other chemicals were purchased from Sigma Chemical Co. (St. Louis, MO, USA). PAK-104P was a gift of Shin-Ichi Akiyama (Kagoshima University, Kagoshima, Japan) from Nissan Chemical Ind. Co., Ltd. (Chiba, Japan).

2.2. Cell lines and Cell Culture

HEK293/pcDNA3.1, HEK/ABCB1, HEK/ABCG2 and HEK/ABCC1 cells were generated by transfecting the HEK293 cells with either empty pcDNA3.1 vector, *ABCB1* expression vector, *ABCG2* expression vector or *ABCC1* expression vector respectively [21]. HEK/ABCC1 was generated in the laboratory of Suresh V. Ambudkar (NCI, NIH, Bethesda, MD, USA). The human colon cancer cell line SW620 and doxorubicin-selected P-gp overexpressing SW620/Ad300 cell line were used for the reversal study. SW620, SW620/Ad300 and HEK/ABCG2 cells were also kindly provided by Susan Bates and Robert Robey (NCI, NIH, Bethesda, MD, USA). All the cell lines were grown as adherent monolayers in flasks with DMEM culture medium (GE Healthcare Life Sciences, Logan, UT, USA) supplemented with 10% bovine serum in a humidified incubator containing of 5% CO_2 at 37 °C.

2.3. Cell Cytotoxicity by MTT Assay

The MTT colorimetric assay was used to detect the sensitivity of cells to anticancer drugs. Cells were harvested with trypsin treatment. After washing with PBS, cells were resuspended in the culture media. Cells with a final concentration of 5×10^3 cells/well were seeded evenly into 96-well plates with 160 μL media. For the reversal experiments, SSJ compounds, verapamil, FTC or PAK104P (20 μL/well) was added followed by different concentrations of chemotherapeutic drugs (20 μL/well) into designated wells. After 72 h of incubation, 20 μL of MTT solution (5 mg/mL) was added to each well, and the plate was further incubated for 4 h, allowing viable cells to convert the yellow colored MTT into dark-blue formazan crystals. Subsequently, the medium was discarded, and 100 μL of dimethylsulfoxide (DMSO) was added into each well to dissolve the formazan crystals. The absorbance was determined at 570 nm by an OPSYS Microplate Reader from DYNEX Technologies Inc. (Chantilly, VA, USA) followed previously described protocol [22]. The fold of resistance was calculated by dividing the IC_{50} (concentrations required to inhibit growth by 50%) of the MDR cells by that of the parental sensitive cells.

2.4. Preparation of Total Cell Lysates

SW620/Ad300 cells were incubated with SSJ26 and SSJ32 at 5 μM for different time periods (0, 24, 48, and 72 h). Total cell lysates were prepared by harvesting the cells and rinsing twice with

ice cold PBS, then by incubating cells for 30 min on ice with radioimmunoprecipitation assay (RIPA) buffer (1 × PBS, 0.1% SDS, 1% Nonidet P-40, 0.5% sodium deoxycholate, 10 mg/mL leupeptin, 100 mg/mL p-aminophenylmethylsulfonyl fluoride and 10 mg/mL aprotinin) followed by centrifugation at 12,000× *g* at 4 °C for 15 min. The supernatant containing total cell lysates was stored at −80 °C until needed for experiments. The protein concentration was determined by bicinchoninic acid (BCA™)-based protein assay (Thermo Scientific, Rockford, IL, USA).

2.5. Western Blot Analysis

Equal amounts of total cell lysates (50 μg protein) were resolved by sodium dodecyl sulfate polycrylamide gel electrophoresis (SDS-PAGE) and electrophoretically transferred onto polyvinylidene fluoride (PVDF) membranes. After incubation in a blocking solution in TBST buffer (10 mM Tris-HCl, pH 8.0, 150 mM NaCl, and 0.1% Tween 20) for 1 h at room temperature, the membranes were immunoblotted overnight with primary monoclonal antibody against P-gp and against β-actin at 4 °C, and were then incubated for 4 h at room temperature with horseradish peroxide (HRP)-conjugated secondary antibody (1:2000 dilution) modified from our previous protocols [23]. The protein-antibody complex was detected by enhanced chemiluminescence detection system (Amersham, NJ, USA).

2.6. [^{3}H]-Paclitaxel Accumulation and Efflux Assays

The effect of SSJ compounds on the intracellular accumulation of paclitaxel in SW620 and SW620/Ad300 cells was determined by measuring the intracellular accumulation of [^{3}H]-paclitaxel in these cells. Cells were seeded in triplicate at 3×10^5 cells/well into 6-well plates. The next day, the cells were pre-incubated with or without the reversal compound for 2 h at 37 °C. Intracellular drug accumulation was measured by incubating cells with 0.01 μM [^{3}H]-paclitaxel for 2 h in the presence or absence of the inhibitor at 37 °C. The cells were washed three times with ice-cold PBS, trypsinized and lysed in 10 mM lysis buffer (pH 7.4, containing 1% Triton X-100 and 0.2% SDS). An aliquot of cells was used to analyze cell number, and the remaining cells were pelleted at 4°C and washed three more times with ice-cold PBS. Each sample was placed in scintillation fluid and radioactivity was measured by a liquid scintillation counter following our previous protocol [24].

In the efflux study, cells were incubated with 0.1 μM [^{3}H]-paclitaxel as the same in the accumulation study. After washing three times with cold PBS, the cells were incubated at 37 °C in fresh medium in the presence or absence of 5 μM SSJ26, or 5 μM SSJ32. After 0, 30, 60, and 120 min, the cells were washed three times with ice-cold PBS, trypsinized and lysed in 10 mM lysis buffer (pH 7.4, containing 1% Triton X-100 and 0.2% SDS). The cells were then processed for measurement of radioactivity by Packard TRI-CARB 1900CA liquid scintillation analyzer as previously described [25].

2.7. ATPase Assay of SSJ26 and SSJ32

The P-gp associated ATPase activity was measured by BD Gentest ATPase kit. The assay was carried out in white opaque 96-well multiplates in triplicate. Recombinant human P-gp membrane

(5 mg/mL) was quickly thawed and diluted to 1 mg/mL with assay buffer. Sodium orthovanadate (Na_3VO_4) was used as an ATPase inhibitor. Various concentrations of SSJ26 and SSJ32 were incubated in 20 μg (20 μL) diluted recombinant human P-gp membrane at 37 °C for 5 min. The reaction is initiated by adding 20 mL of 15 mM Mg^{2+} ATP to all wells. At this point, each P-gp reaction contains 5 mM ATP. The plate was incubated at 37 °C for 40 min with brief mixing using a plate shaker. Luminescence initiated by ATP detection buffer. After incubation at 37 °C for 20 min to allow luminescent signal to develop, the untreated white opaque 96-well multiplate was read on luminometer (SpectraMax M5, molecular devices, Sunnyvale, CA, USA). The changes of relative light units (DRLU) were determined by comparing Na_3VO_4-treated samples with SSJ26 and SSJ32 combination-treated groups [26].

2.8. Molecular Docking Analysis

SSJ26 and SSJ32 were built and prepared as ligands by our previous molecular modeling protocols [27]. The output files containing at most 100 unique conformers of SSJ26 or SSJ32 were used as input for docking simulations into human homology P-gp.

Human P-gp homology model based on mouse Abcb1 was kindly provided by S. Aller and was used to generate grid for docking [28]. Schrödinger Suite 2014-4 Protein Preparation Wizard (Epik version 3.0; Impact version 6.5, Schrödinger, LLC, New York, NY, USA, 2014) protocol was followed for protein preparation and refinement. Conserved residues previously identified as interacting with cyclic peptides and drugs were selected as centroid for generating docking grid. Docking grid was refined as an enclosing box with length of 20 Å by Glide version 6.4 (Schrödinger, LLC, New York, NY, USA, 2014).

Docking of SSJ26 or SSJ32 into human P-gp was performed using the "Extra Precision" (XP) mode of Glide version 6.4 (Schrödinger, LLC, New York, NY, USA, 2014). The value of Glide Emodel was ranked to determine the best-docked pose for SSJ26 or SSJ32 [29]. The two selected docked poses were used for graphic analysis. XP Glidescores calculated by Glide version 6.4 (Schrödinger, LLC, New York, NY, USA, 2014) were used to rank these two poses. All computations were carried out on a Dell Precision 490n dual processor with Linux OS (Ubuntu 12.04 LTS, Canonical Group Limited, London, UK).

2.9. Statistical Analysis

All experiments were performed as triplicates and the differences were determined by using the Student's *t*-test. The statistical significance was determined at $p < 0.05$ and $p < 0.01$.

3. Results

3.1. Screening for Potential Inhibitors of P-GP Transporter in Comparison with Verapamil

Sipholane analogs (14 compounds) were first tested for cytotoxicity using MTT assay on colon cancer cells SW620 (drug-sensitive) and SW620/Ad300 (drug-resistant). The IC_{50} values of all compounds were above 30 μM (Supplementary Information Table S1). Because these compounds

were used at a concentration of 5 μM, which is the non-toxic concentration for all of them, they were considered to have no direct cytotoxic effect on cells.

Sipholane analogs were then screened for P-gp inhibitory effects in comparison to verapamil. Fold-of-resistance (FR) was calculated to determine which compounds could effectively increase the sensitivity of drug-resistant cells to chemotherapeutic agent. Cell viability was recorded using MTT assay after the following treatments were applied to the same cell lines. Doxorubicin, a known substrate of P-gp transporter, was used as baseline factor. Verapamil was used as positive control inhibitor of P-gp. SSJ26 and SSJ32 were found to be comparable to verapamil in reversing P-gp-mediated drug resistance as shown in Table 1; therefore, these two compounds were selected for further tests.

Table 1. Effect of 14 sipholane analogs on inhibition of P-gp mediated resistance to doxorubicin in SW620 and SW620/Ad300.

Treatment	SW620		SW620/Ad300	
	IC_{50} ± SD [a] (μM)	FR [b]	IC_{50} ± SD [a] (μM)	FR [b]
Doxorubicin	0.0196 ± 0.0022	1.00	4.1082 ± 0.4112	209.60
+Verapamil (5 μM)	0.0167 ± 0.0027	0.85	0.0876 ± 0.0015	4.47 **
+SSJ20 (5 μM)	0.0189 ± 0.0019	0.96	4.2660 ± 0.4016	217.65
+SSJ25 (5 μM)	0.0194 ± 0.0018	0.99	4.0939 ± 0.0083	208.87
+SSJ26 (5 μM)	0.0176 ± 0.0017	0.90	0.0941 ± 0.5238	4.80 **
+SSJ27 (5 μM)	0.0169 ± 0.0019	0.86	3.4125 ± 0.3317	174.11 *
+SSJ28 (5 μM)	0.0202 ± 0.0012	1.03	4.2550 ± 0.3567	217.09
+SSJ29 (5 μM)	0.0195 ± 0.0018	1.00	3.1563 ± 0.4173	161.04 *
+SSJ30 (5 μM)	0.0190 ± 0.0021	0.97	4.2027 ± 0.3513	214.42
+SSJ31 (5 μM)	0.0186 ± 0.0016	0.95	4.2814 ± 0.5122	218.44
+SSJ32 (5 μM)	0.0188 ± 0.0019	0.96	0.1312 ± 0.0101	6.69 **
+SSJ33 (5 μM)	0.0195 ± 0.0020	0.99	2.9758 ± 0.2593	151.83 *
+SSJ34 (5 μM)	0.0218 ± 0.0019	1.11	4.2762 ± 0.4135	218.17
+SSJ35 (5 μM)	0.0231 ± 0.0023	1.18	4.3574 ± 0.5143	222.32
+SSJ36 (5 μM)	0.0169 ± 0.0018	0.86	3.4676 ± 0.4491	176.92
+SSJ37 (5 μM)	0.0167 ± 0.0015	0.85	3.9948 ± 0.4798	203.82

[a] Cell survival was determined by MTT assay as described in Section 2. Data are represented as mean ± SD of at least three independent experiments performed in triplicate; [b] Fold-of-resistance (FR) was determined by dividing the IC_{50} value for doxorubicin of SW620/Ad300 with or without reversal agent, or of SW620 in the presence of reversal agent by the IC_{50} value for doxorubicin of SW620 in the absence of reversal agent; Unpaired Student's t-test was employed to analyze the differences between FR values. * $p < 0.05$; ** $p < 0.01$.

3.2. Effect of SSJ26 and SSJ32 in P-GP Overexpressing Cancer and ABCB1-Transfected Cells

Based on the previous experiment, SSJ26 and SSJ32 were chosen and studied further with three different concentrations. Doxorubicin was applied to SW620 and SW620/Ad300 alone and in combination with various concentrations of the potential P-gp modulators: SSJ26 and SSJ32. As shown in Table 2, the complete reversal of P-gp-mediated resistance is defined as FR = 1.00. When

the SW620/Ad300 (drug-resistant) cells were treated with doxorubicin, it required 209-times the amount of drug needed to achieve the same IC_{50} as that in SW620 (drug-sensitive) cells. This resistance could be significantly reduced by the addition of 5 μM of verapamil, decreasing the fold-of-resistance (FR) from 209 to 4.47. Out of the fourteen compounds, SSJ26 and SSJ32 achieved the similar effect with FR reduced to 4.80 and 6.69, respectively. The fold-of-resistance decreased as concentrations of SSJ26 and SSJ32 increased, demonstrating that the reversal occurs in a concentration-dependent manner. Another chemotherapeutic drug and P-gp substrate, paclitaxel, was also used to test the reversal effect of these compounds. Similar to doxorubicin, SSJ26 and SSJ32 improved paclitaxel sensitivity in P-gp overexpressing SW620/Ad300 cells. Finally, cisplatin, a chemotherapeutic agent that is not a P-gp substrate, was applied with the 5 μM of verapamil, SSJ26, or SSJ32. Since cisplatin is not susceptible to resistance by P-gp [7], the resistant fold of SW620/Ad300 as a ratio to the IC_{50} of SW620 remained at around 1.00 as predicted. Similarly, FR values did not differ significantly with the treatment of verapamil, SSJ26 or SSJ32. This strengthens the hypothesis that SSJ26 and SSJ32 reverse P-gp-mediated resistance in a concentration-dependent manner.

Table 2. SSJ26 and SSJ32 reverse the P-gp-mediated drug resistance to doxorubicin and paclitaxel.

Treatment	SW620		SW620/Ad300	
	IC_{50} ± SD [a] (μM)	FR [b]	IC_{50} ± SD [a] (μM)	FR [b]
Doxorubicin	0.0201 ± 0.0023	(1.00)	4.3221 ± 0.4513	(215.16)
+SSJ26 (1.25 μM)	0.0199 ± 0.0018	(0.99)	0.5314 ± 0.05134	(26.44) *
+SSJ26 (2.5 μM)	0.0185 ± 0.0017	(0.92)	0.3212 ± 0.09021	(15.98) *
+SSJ26 (5 μM)	0.0181 ± 0.0021	(0.90)	0.1017 ± 0.01022	(5.06) **
+SSJ32 (1.25 μM)	0.0210 ± 0.0025	(1.05)	0.6354 ± 0.0724	(31.61) *
+SSJ32 (2.5 μM)	0.0199 ± 0.0021	(0.99)	0.3317 ± 0.0413	(16.50) *
+SSJ32 (5 μM)	0.0189 ± 0.0017	(0.94)	0.1528 ± 0.0132	(7.60) **
+Verapamil (5 μM)	0.0179 ± 0.0015	(0.89)	0.0923 ± 0.0058	(4.59) **
Paclitaxel	0.0072 ± 0.0010	(1.00)	2.7402 ± 0.2813	(380.58)
+SSJ26 (1.25 μM)	0.0063 ± 0.0008	(0.88)	0.2046 ± 0.0194	(28.42) *
+SSJ26 (2.5 μM)	0.0063 ± 0.0009	(0.92)	0.1081 ± 0.0098	(15.01) *
+SSJ26 (5 μM)	0.0057 ± 0.0006	(0.79) *	0.0737 ± 0.0084	(10.23) **
+SSJ32 (1.25 μM)	0.0068 ± 0.0005	(0.94)	0.2977 ± 0.0313	(41.35) *
+SSJ32 (2.5 μM)	0.0064 ± 0.0006	(0.89)	0.1110 ± 0.0092	(15.41) *
+SSJ32 (5 μM)	0.0061 ± 0.0005	(0.85)	0.0872 ± 0.0095	(12.12) **
+Verapamil (5 μM)	0.0062 ± 0.0007	(0.86)	0.0658 ± 0.0068	(9.14) **
Cisplatin	1.8203 ± 0.1744	(1.00)	2.3217 ± 0.3353	(1.28)
+SSJ26 (5 μM)	1.8556 ± 0.2919	(1.02)	2.1842 ± 0.3148	(1.20)
+SSJ32 (5 μM)	1.7453 ± 0.2434	(0.96)	2.1772 ± 0.0210	(1.19)
+Verapamil (5 μM)	1.8012 ± 0.2017	(0.99)	2.0313 ± 0.0251	(1.12)

[a] IC_{50} values are represented as mean ± SD of at least three independent experiments performed in triplicate; [b] Values represent the fold-of-resistance (FR) obtained by dividing IC_{50} value of antineoplastic drug in SW620 and SW620/Ad300 cells with or without reversal agent divided by the IC_{50} value of respective antineoplastic drug in SW620 cells without reversal agent. Cell survival assay was determined by the MTT assay as described in Section 2. Verapamil was used as a positive control of P-gp inhibitor; * $p < 0.05$; ** $p < 0.01$ *versus* the control group without reversal agent.

Drug selected SW620/Ad300 cells may have multiple drug resistant mechanisms besides P-gp-mediated action. Therefore, the effect of sipholane analogs on P-gp was studied in HEK293 cells transfected with the *ABCB1* gene expression vector or empty pcDNA3.1 vector. The transfected HEK/ABCB1 cell was developed to solely exhibit P-gp-mediated resistance. In this cell line, the resistant folds were more significantly reduced by verapamil, SSJ26, and SSJ32 as shown in Table 3. These findings further support the hypothesis that SSJ26 and SSJ32 mainly affect P-gp.

Table 3. SSJ26 and SSJ32 reverse the P-gp-mediated drug resistance to paclitaxel in HEK293/pcDNA3.1 and HEK/ABCB1 cells.

Treatment	HEK293/pcDNA3.1		HEK/ABCB1	
	IC_{50} ± SD [a] (μM)	FR [b]	IC_{50} ± SD [a] (μM)	FR [b]
Paclitaxel	0.0224 ± 0.0030	(1.00)	0.9912 ± 0.1504	(44.25)
+SSJ26 (1.25 μM)	0.0279 ± 0.0047	(1.25)	0.1980 ± 0.0586	(8.84) **
+SSJ26 (5 μM)	0.0242 ± 0.0019	(1.08)	0.0389 ± 0.0040	(1.74) **
+SSJ32 (1.25 μM)	0.0254 ± 0.0025	(1.13)	0.2824 ± 0.016	(12.61) *
+SSJ32 (5 μM)	0.0162 ± 0.026	(0.73)	0.0582 ± 0.051	(2.59) **
+Verapamil (5 μM)	0.0179 ± 0.0043	(0.80)	0.0415 ± 0.0055	(1.85) **

[a] IC_{50} values are represented as mean ± SD of at least three independent experiments performed in triplicate; [b] Values represent fold-of-resistance (FR) obtained by dividing IC_{50} value of antineoplastic drug in HEK293/pcDNA3.1 and HEK/ABCB1 cells with or without reversal agent divided by the IC_{50} value of respective antineoplastic drug in HEK293/pcDNA3.1 cells without reversal agent. Cell survival assay was determined by the MTT assay as described in Section 2. Verapamil was used as a positive control of P-gp inhibitor; * $p < 0.05$; ** $p < 0.01$ *versus* the control group without reversal agent.

Drug selected SW620/Ad300 cells may have multiple drug resistant mechanisms besides P-gp-mediated action. Therefore, the effect of sipholane analogs on P-gp was studied in HEK293 cells transfected with the *ABCB1* gene expression vector or empty pcDNA3.1 vector. The transfected HEK/ABCB1 cell was developed to solely exhibit P-gp-mediated resistance. In this cell line, the resistant folds were more significantly reduced by verapamil, SSJ26, and SSJ32 as shown in Table 3. These findings further support the hypothesis that SSJ26 and SSJ32 mainly affect P-gp.

Similarly, cell survival curves were made by plotting the survival fraction of aforementioned cell lines at various paclitaxel concentrations. As shown in Figure 1B, in the first curve, the application of SSJ26 did not affect potency of paclitaxel, therefore SW620 (drug-sensitive) alone and SW620 with SSJ26 are visualized as almost identical curves. In contrast, SW620/Ad300 (drug-resistant) cells are more viable in the absence of SSJ26 but once they are treated with SSJ26, the kill curve shifts to the left and closer to that of parental SW620 cells. This demonstrates the proportional reversal trend of SSJ26 in inhibiting P-gp-mediated resistance with differing concentrations of paclitaxel. Similar reversal trends were seen with SSJ32 (Figure 1C) and with verapamil (Figure 1D).

In HEK293 cells transfected with the empty vector pcDNA3.1, no change in cell viability was seen when treated with differing paclitaxel concentrations alone or in combination with SSJ26, SSJ32, or verapamil (Figure 1E). In contrast, when HEK293 cells transfected with ABCB1were treated with SSJ26, SSJ32 or verapamil, the curves shifted to the left (Figure 1F). This

demonstrated that P-gp overexpressing HEK/ABCB1 cells were re-sensitized to paclitaxel by SSJ26 and SSJ32 treatment

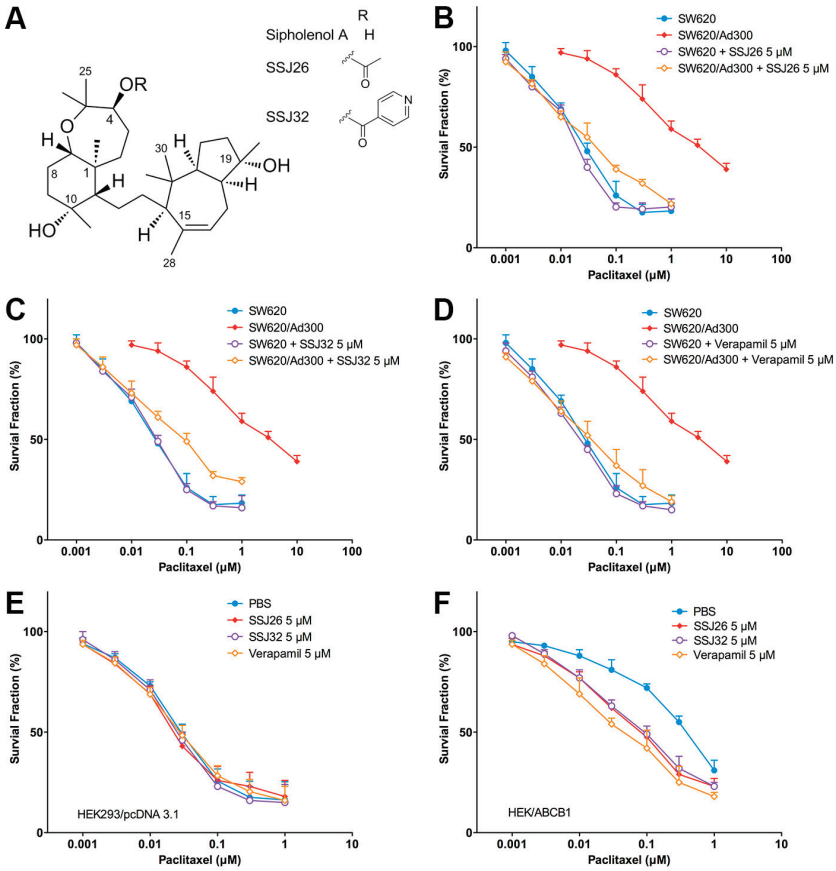

Figure 1. Reversal effect of SSJ26 and SSJ32 against P-gp-mediated MDR in representative cell survival curves. (**A**) Chemical structures of sipholenol A, SSJ26 and SSJ32; (**B**) Concentration-survival curves of SW620 and SW620/Ad300 cell lines treated with combination of SSJ26 and paclitaxel; (**C**) Concentration-survival curves of SW620 and SW620/Ad300 cell lines treated with combination of SSJ32 and paclitaxel; (**D**) Concentration-survival curves of SW620 and SW620/Ad300 cell lines treated with combination of verapamil and paclitaxel; (**E**) Concentration-survival curves of HEK293/pcDNA3.1 cell lines treated with SSJ26, SSJ32 or verapamil in combination of paclitaxel; (**F**) Concentration-survival curves of HEK/ABCB1 cell lines treated with SSJ26, SSJ32 or verapamil in combination of paclitaxel. Cell survival rate was determined by the MTT assay as described in Section 2. Data points with error bars represent the mean ± SD. Each above figure is a representative of three independent experiments, each done in triplicate.

3.3. Effect of SSJ26 and SSJ32 on Transfected HEK/ABCC1 and HEK/ABCG2 Cells

HEK293 cells transfected with ABC transporter genes *ABCC1* and *ABCG2* were used for the experiments to evaluate if the SSJ-26 and SSJ-32 is only specifically affected to P-gp. Vincristine is a substrate of the MRP1/ABCC1. As shown in Table 4, application of SSJ26 or SSJ32 with vincristine did not result in a change in resistant fold for the HEK293/*ABCC1* cells. Similarly, the effect of SSJ26 and SSJ32 in ABCG2-transfected HEK293 cells was also tested with mitoxantrone, a known substrate of BCRP/ABCG2. Our results indicated that SSJ26 and SSJ32 did not show reversal effect on *ABCG2*-mediated MDR. It can be concluded, thus far, that SSJ26 and SSJ32 are potent reversal agents of P-gp-mediated MDR but not of MRP1/ABCC1 or BCRP/ABCG2.

Table 4. Effects of SSJ26 and SSJ32 on the MRP1/ABCC1- and BCRP/ABCG2-mediated multidrug resistance.

Treatment	HEK293/pcDNA3.1		HEK293/ABCC1	
	IC_{50} ± SD [a] (μM)	FR [b]	IC_{50} ± SD [a] (μM)	FR [b]
Vincristine	0.0208 ± 0.0021	(1.00)	0.4731 ± 0.0282	(22.75)
+SSJ26 (5 μM)	0.0193 ± 0.0019	(0.93)	0.4693 ± 0.0184	(22.56)
+SSJ32 (5 μM)	0.0235 ± 0.0027	(1.13)	0.4897 ± 0.0639	(23.54)
+PAK-104P [c] (5 μM)	0.0189 ± 0.0023	(0.91)	0.0778 ± 0.0092	(3.74) **
Treatment	**HEK293/pcDNA3.1**		**HEK293/ABCG2**	
	IC_{50} ± SD [a] (μM)	FR [b]	IC_{50} ± SD [a] (μM)	FR [b]
Mitoxantrone	0.0309 ± 0.0023	(1.0)	0.4259 ± 0.0203	(13.8)
+SSJ26 (5 μM)	0.0294 ± 0.0019	(0.95)	0.3729 ± 0.0553	(12.0)
+SSJ32 (5 μM)	0.0333 ± 0.0028	(1.08)	0.3654 ± 0.0675	(11.8)
+FTC [d] (5 μM)	0.0273 ± 0.0032	(0.88)	0.0381 ± 0.0435	(1.2) **

[a] IC_{50} values are represented as mean ± SD of at least three independent experiments performed in triplicate; [b] Values represent the fold-of-resistance (FR) obtained by dividing IC_{50} value of antineoplastic drug in HEK293/pcDNA3.1, HEK/ABCC1 and HEK/ABCG2 cells with or without reversal agent divided by the IC_{50} value of respective antineoplastic drug in HEK293/pcDNA3.1 cells without reversal agent. Cell survival assay was determined by the MTT assay as described in Section 2. PAK-104P was used as a positive control of ABCC1 inhibitor. FTC was used as a positive inhibitor of ABCG2; [c] PAK-104P: a pyridine analogue, 2-(4-(diphenylmethyl)-1-piperazinyl)ethyl-5-(trans-4,6-dimethyl-1,3,2-dioxaphosphorinan-2-yl)-2,6-dimethyl-4-(3-nitrophenyl)-3-pyridinecarboxylate P-oxide. Positive control of ABCC1 reversal agent; [d] FTC: The fungal toxin fumitremorgin C. Positive control of ABCG2 reversal agent; * $p < 0.05$; ** $p < 0.01$ *versus* the control group without reversal agent.

3.4. SSJ26 and SSJ32 Increased Intracellular Accumulation of [^{3}H]-Paclitaxel by Inhibiting Its Efflux

To further elucidate the mechanism of drug resistance reversal, a drug accumulation study was performed. The results shown in Figure 2 demonstrated that intracellular paclitaxel concentration in SW620 treated with SSJ26, SSJ32, or verapamil did not differ significantly. However, the level of intracellular paclitaxel was much lower in SW620/Ad300 cells as compared with that in parental SW620 cells. When SSJ26, SSJ32, or verapamil was added, the intracellular levels of paclitaxel in

SW620/Ad300 increased to almost comparable to that of SW620 cells. This demonstrates that the increased potency of paclitaxel is a result from increased intracellular accumulation when combined with SSJ26, SSJ32 or verapamil.

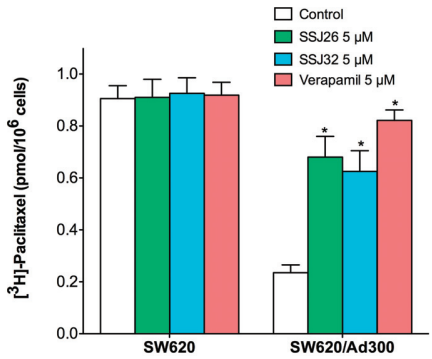

Figure 2. Effects of SSJ26 and SSJ32 on intracellular accumulation of [^3H]-paclitaxel. The accumulation of [^3H]-paclitaxel was measured after the cells were pre-incubated with or without SSJ26, SSJ32 or verapamil for 2 h at 37 °C and then incubated with 0.01 μM [^3H]-paclitaxel for another 2 h at 37 °C. Columns are the mean of triplicate determinations; error bars represent SD. ***** Indicates $p < 0.05$ *versus* the control group.

Then, we conducted efflux assay to further explore the mechanism of intracellular [^3H]-paclitaxel accumulation. In this experiment, intracellular [^3H]-paclitaxel levels were measured at various time points after removal of extracellular [^3H]-paclitaxel. At different time points, cells were harvested and the radioactivity was measured. As shown in Figure 3A, while the paclitaxel level significantly decreased in SW620/Ad300 drug-resistant cells, the levels of paclitaxel remained stable in parental SW620 cells. After treatment with SSJ26, the intracellular remaining [^3H]-paclitaxel was significantly increased at all time-points. The treatment of SSJ26 did not alter the [^3H]-paclitaxel levels in SW620 cells. Similarly, SSJ32 treatment also inhibited the efflux of [^3H]-paclitaxel in SW620/Ad300 (Figure 3B). However, SSJ32 is not as potent as SSJ26 in inhibiting efflux of [^3H]-paclitaxel.

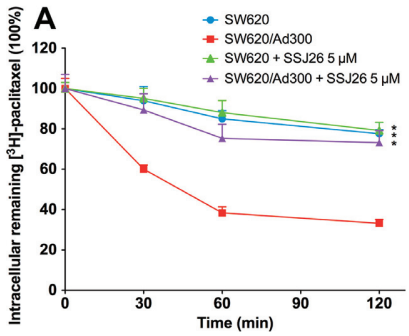

Figure 3. *Cont.*

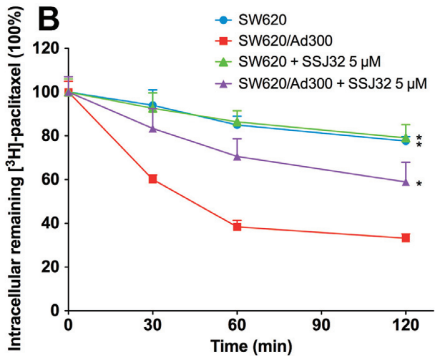

Figure 3. Effects of SSJ26 and SSJ32 on efflux of [^3H]-paclitaxel. (**A**) The effect of SSJ26 on the efflux of [^3H]-paclitaxel from SW620 and SW620/Ad300 cells; (**B**) The effect of SSJ32 on the efflux of [^3H]-paclitaxel from SW620 and SW620/Ad300 cells. A time course *versus* percentage of intracellular [^3H]-paclitaxel remaining (%) was plotted (0, 30, 60, 120 min). Lines are the mean of triplicate determinations; error bars represent SD. ***** Indicates $p < 0.05$ *versus* the control group.

3.5. SSJ26 and SSJ32 Stimulated ATPase Activities but Did not Alter the Expression Level of P-GP

In order to determine whether the sipholenol analogs reverse drug resistance by affecting the P-gp expression, Western blot analysis was performed. As shown in Figure 4A, P-gp expression remains comparable both in presence and absence of treatment with SSJ26 and SSJ32 at 5 μM up to 72 h. Since these compounds do not alter protein expression, the reversal effect is probably due to inhibition of P-gp transporter function. P-gp/ABCB1 transporter utilizes energy derived from the hydrolysis of ATP to efflux its substrates across the membrane against a concentration gradient, thus ATP consumption reflects its ATPase activity. To assess whether SSJ26 and SSJ32 have any effect on the ATPase activity of P-gp/ABCB1, we measured P-gp/ABCB1-mediated ATP hydrolysis in the presence of SSJ26 or SSJ32 at various concentrations from 0 to 10 μM. Interestingly, SSJ26 stimulated the ATPase activity of P-gp/ABCB1 in a concentration-dependent manner, with a maximal stimulation of 2.15-fold of the basal activity. In contrast, the maximal stimulation of SSJ32 was 2.03-fold of the basal activity. The Figure 4B demonstrates that the concentration of SSJ26 required to obtain 50% stimulation is 0.26 μM. The Figure 4B also demonstrates that the concentration of SSJ32 required to obtain 50% stimulation is 0.60 μM.

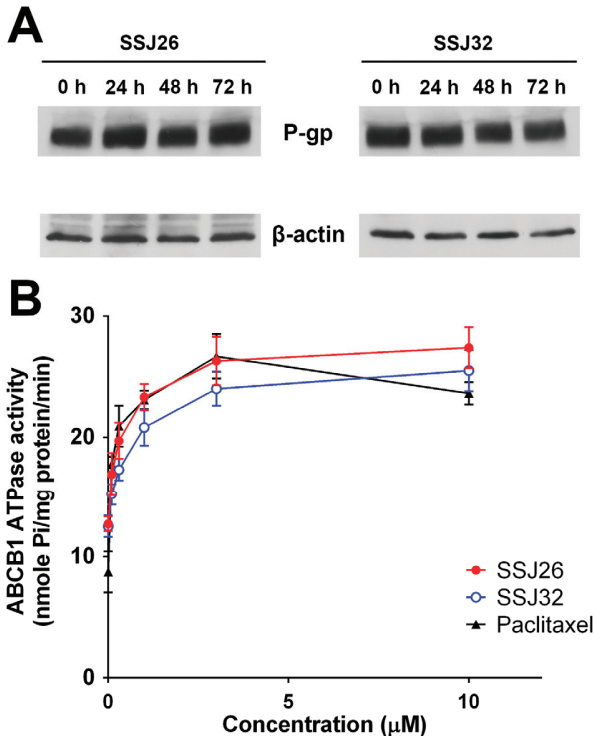

Figure 4. Effects of SSJ26 and SSJ32 on ATPase activity and expression level of P-gp. (**A**) Effect of SSJ26 at 5 μM and SSJ32 at 5 μM on expression level of P-gp in SW620/Ad300 cells for 0, 24, 48 and 72 h; (**B**) The effect of increasing concentration (0 to 10 μM) of SSJ26 and SSJ32 on the Vi-sensitive P-gp ATPase activity.

3.6. Binding Mode of SSJ26 and SSJ32 with Homology Model of P-GP

In the absence of the crystal structure of human P-gp, we developed a homology model, based on the refined crystal structure of mice P-gp. To understand the molecular interactions of SSJ26 (Sipholenol A-4-*O*-acetate) and SSJ32 (Sipholenol A-4-*O*-isonicotinate) with human P-gp, docking simulations were performed at pre-generated grid (Section 2). The docking scores were found to be −7.894 kcal/mol for SSJ26 and −6.956 kcal/mol for SSJ32, respectively.

The docked poses of SSJ26 and SSJ32 into the large drug-binding cavity of human P-gp were shown in Figure 5A. The docked poses of the two ligands were found to be overlapped, however in different molecular orientations. The docked pose of SSJ26 is shown in Figure 5B. The sipholenol A core structure was mainly stabilized into a large hydrophobic pocket formed by several hydrophobic and aromatic residues, such as Leu65, Met69, Phe303, Ile306, Tyr307, Tyr310, Phe336, Leu339, Ile340, Phe343, Gln725, Phe728, Tyr953, Phe 983, Met986, Ala987, and Gln990. The C-4-*O*-acetate substituent on the hexahydro-oxepine ring was involved in hydrogen bonding interaction with Try925 (-CO···HO-Tyr953, 2.10 Å), suggesting the importance of the ester

substituent. Also, the C_{19}-hydroxyl group of the hexahydroazulen ring interacted with Try310 through hydrogen bonding contact (-OH···HO-Tyr310, 2.22 Å).

The docked pose of SSJ32 was found to be rotated as a result of the replacement of the acetate of SSJ26 with a heteroaromatic ester isonicotinate in this compound as shown in Figure 5C. The pyridine ring may be stabilized by nearby aromatic residues Phe336, Phe732 and Phe983. SSJ32 may form two hydrogen bonding interaction with Gln347 (OH···HO-Gln347, 2.19 Å) and Gln725 (CO···H_2N-Gln725, 2.25 Å). However, the change of substituent in SSJ32 seems to bring less tight interactions (255 good contacts counts as compared to 386 in SSJ26) and may lead to imperfect fit with the hydrophobic pocket. This may explain its relatively poorer reversal activity as well as Glide docking score.

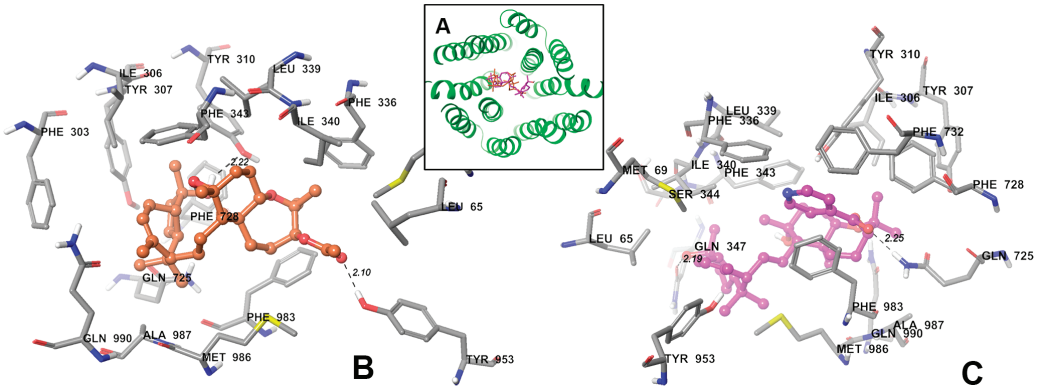

Figure 5. XP-Glide predicted binding mode of SSJ26 and SSJ32 with homology modeled P-gp. (**A**) Docked poses of SSJ26 and SSJ32 into drug binding sites of human P-gp. Backbone of human P-gp is depicted as gray ribbons viewed from the intracellular side of the protein looking into the internal chamber. SSJ26 and SSJ32 are represented as tube models with the same color scheme below; (**B**) Binding mode of SSJ26 within human P-gp. Important residues are depicted as tubes with the atoms colored as carbon—gray, hydrogen—white, nitrogen—blue, oxygen—red, sulfur—yellow, whereas SSJ26 is shown as ball and stick model with the same color scheme as above except carbon atoms are represented in orange. Dotted black lines indicate hydrogen bonds; (**C**) Binding mode of SSJ32 within the human P-gp. The color scheme is same except carbon atoms are represented in purple.

4. Discussion

As cancer continuously evolves, there are powerful antineoplastic therapy regimens that are being developed exponentially. The compounds investigated in this study could contribute to these treatments as significant novel chemotherapy enhancement. P-gp is considered as a strong therapeutic target for MDR reversal agents. A number of natural compounds extracted from marine sponges and their semisynthetic derivatives have previously demonstrated effectiveness against multi-drug resistance in cancer cells [16]. In this study, esters of the marine natural triterpene

sipholenol A, SSJ26 and SSJ32, have shown practical abilities to reverse P-gp-mediated drug resistance and their reversal mechanisms were elucidated. SSJ26 and SSJ32 can re-sensitize cells that have developed drug-resistance to chemotherapeutic agents that are substrates of P-gp such as doxorubicin and paclitaxel. They stabilized the level of intracellular [^{3}H]-paclitaxel accumulated in the cells by inhibiting P-gp mediated drug efflux in a competitive manner. The expression of P-gp protein was not compromised in presence or absence of these reversal agents.

In this study, MTT assay was used to determine the IC_{50} values to quantify the sensitivity of cells to the experimental sipholenol analogs. These compounds were first tested on human colonic adenocarcinoma cells SW620 to visualize their effects on the cancer cells. All the tested compounds have no direct cytotoxic effect on the cells, indicating that they might act through enhancing chemotherapeutic activity of anti-neoplastic agents. These sipholenol analogs went through a further screening and the compounds that have the most potent MDR reversal effect were identified to be SSJ26 and SSJ32.

Various concentrations of SSJ26 and SSJ32 were tested in combination with two chemotherapy agents, doxorubicin and paclitaxel, which are known substrates of P-gp. At increasing concentrations of 1.25, 2.5, and 5 μM of each of the compounds, the FR proportionally decreased, suggesting concentration dependent P-gp inhibition. The FR values at 5 μM were similar to those of verapamil. Cisplatin was used as a negative control drug, since it does not submit to the multi-drug resistance effect of P-gp. Theoretically then the IC_{50} values of cisplatin on SW620 and SW620/Ad300 should remain the same. As predicted, the IC_{50} values of cisplatin were similar in both parental and drug resistant cells, and the application of SSJ26, SSJ32, or verapamil did not significantly alter the resistance fold as well. To further clarify their specificity, these compounds were tested in *ABCB1*-transfected HEK293 cell lines. The transfected cells exhibit resistance of a single mechanism, while the drug-selected cells previously mentioned have resistance induced by doxorubicin and a variety of diverse unidentified mechanisms may be present. At the same concentration of 5 μM, the decrease in drug resistance was significantly greater in HEK/ABCB1 than in SW620/Ad300, indicating the sipholanes may specifically target *ABCB1* mediated MDR. Their sole effect on *ABCB1*-mediated resistance was bolstered by treating HEK293 cells transfected with other known MDR transporter expression vectors, specifically *ABCC1* and *ABCG2*. Vincristine is a known substrate of transporter proteins coded by *ABCC1*, and mitoxantrone, of *ABCG2*. Overexpression of ABCC1 or ABCG2 confers resistance to the aforementioned antineoplastics, which can be significantly reversed by PAK104P or FTC, respectively. When compared to these MDR inhibitors, SSJ26 and SSJ32 negligibly decreased the resistance of *ABCC1*- and *ABCG2*-transfected cells. This evidently indicated how precise the affinity of these compounds is to *ABCB1*-expressing P-gp.

The mechanism of reversal effect of sipholenol triterpenoids is mainly by the inhibition of the P-gp efflux activity. This can be supported by the [^{3}*H*]-paclitaxel intracellular accumulation and the efflux study. Our results show that while the amount of intracellular paclitaxel was significantly lower in the drug resistant SW620/Ad300 cells, the accumulation of paclitaxel increases with the addition of SSJ26, SSJ32, or verapamil. As time increases, drug efflux transporter P-gp removes an

increasing amount of drug from SW620/Ad300 cells. This efflux rate decreases significantly in response to SSJ26 and SSJ32 when treated in combination with paclitaxel.

Immunoblotting experiment showed that SSJ26 and SSJ32 did not change the level of P-gp expression in cells, insinuating that these compounds impact on the function of P-gp protein. Interestingly, SSJ26 stimulated the ATPase activity of P-gp in a concentration-dependent manner, with a maximal stimulation of 2.15-fold of the basal activity. On the other hand, the maximal stimulation of SSJ32 is 2.03-fold of the basal activity. The concentration of SSJ26 and SSJ32 required to obtain 50% stimulation is 0.26 μM and 0.60 μM, respectively. It can be concluded that SSJ26 had a more potent effect on the ATPase activity of P-gp than SSJ32, which was consistent with other results. Furthermore, as shown in Figure 4B, SSJ26 and SSJ32 interacted with P-gp transporter in a similar manner to paclitaxel, indicating that these two compounds might be the substrates of P-gp transporter. Therefore, SSJ26 and SSJ32 may be actively transported out by P-gp, competitively inhibit P-gp mediated efflux of other substrates. Abraham *et al.* reported that Vi-sensitive P-gp ATPase activity was stimulated by sipholenone E, sipholenol L, and siphonellinol D in a concentration-dependent manner with maximum stimulation of over 2.1-, 1.7- or 1.5-fold, respectively. The apparent Km values for sipholenone E, sipholenol L or siphonellinol D were ~14 μM, 5 μM and 4 μM, respectively [30]. Interestingly, the Km values for SSJ26 and SSJ32 were 0.023 μM and 0.07 μM, respectively. Therefore, SSJ26 and SSJ32 had a more potent effect on the ATPase activity of P-gp than sipholenone E, sipholneol L or siphonellinol D. This statement can be further visualized by molecular modeling studies. *In silico* molecular orientations of SSJ26 and SSJ32 at the P-gp homology model suggest varying binding affinities and justify their difference in potency as MDR-reversal agents. The Glide docking score estimates the ligand binding's free energy between the substrate and its binding site [31]. In cell-based assays, SSJ26 showed stronger potency than SSJ32 in modulating P-gp-mediated MDR. The binding energy scores expressed in kcal/mol for the sipholenol A acetate SSJ26 against human P-gp was found to be −7.894. Relatively lower binding energy score was noticed for the isonictoninate ester SSJ32 against ABCB1 (−6.956), thus strengthening the applicability and relevance of human P-gp homology model for virtual studies of binding modes. SSJ32, based on its reversal effect, is a weaker inhibitor of P-gp than SSJ26, which could partially explain its poor binding energy score [32]. Though docking is a useful tool to understand ligand-protein interactions, the present study involves P-gp, which are particularly challenging because it possesses a large drug-binding cavity. Currently, no high-resolution crystal structure of human P-gp is available and this prompted the use of homology model. Without co-crystal complexes with P-gp, docking using P-gp homology model can be used for preliminary assessment of binding modes and affinities of large number of unknown hits.

5. Conclusions

In conclusion, this study demonstrated the potential of the marine natural triterpene sipholenol A-4-*O*-esters as P-gp mediated MDR reversal agents. Their strong affinity and specificity to *ABCB1* expressing efflux proteins would decrease the possibility of other pharmacokinetic interactions with pharmacological agents. Future research will propel these invaluable compounds to be paired with chemotherapeutic drugs in order to deliver advancement in cancer patient care.

Acknowledgments

We thank Susan E. Bates and Robert W. Robey (NCI, NIH, Bethesda, MD, USA) for providing FTC, SW620, SW620/Ad300 and HEK/ABCG2 cell lines, Suresh V. Ambudkar (NCI, NIH, Bethesda, MD, USA) for HEK293/ABCC1 and HEK293/ABCB1, Stephen Aller (The University of Alabama at Birmingham, Birmingham, UK) for providing human ABCB1 homology model. We also thank Shin-Ichi Akiyama (Kagoshima University, Japan) for the Cepharanthine and PAK104P. This work was partially funded by grants from the Key Scientific and Technological Project of Henan Province in China (No.132102310061) and the NIH (1R15CA143701).

Author Contributions

Conceived and designed the experiments: Yongchao Zhang, Diaa T. A. Youssef, Khalid A. El Sayed, and Zhe-Sheng Chen. Performed the experiments: Yongchao Zhang, Yun-Kai Zhang, Yi-Jun Wang, Saurabh G. Vispute, Jessalyn Li, Sandeep Jain. Analyzed the data: Yongchao Zhang, Yun-Kai Zhang, Yangmin Chen, Zhe-Sheng Chen. Wrote the paper: Yongchao Zhang, Yangmin Chen, Yun-Kai Zhang, Diaa T. A. Youssef, Khalid A. El Sayed and Zhe-Sheng Chen.

Conflicts of Interest

The authors declare no conflict of interest.

References

1. Gottesman, M.M.; Fojo, T.; Bates, S.E. Multidrug resistance in cancer: Role of ATP-dependent transporters. *Nat. Rev. Cancer* **2002**, *2*, 48–58.
2. Krishna, R.; Mayer, L.D. Multidrug resistance (MDR) in cancer. Mechanisms, reversal using modulators of MDR and the role of MDR modulators in influencing the pharmacokinetics of anticancer drugs. *Eur. J. Pharm. Sci.* **2000**, *11*, 265–283.
3. Kathawala, R.J.; Gupta, P.; Ashby, C.R., Jr.; Chen, Z.S. The modulation of ABC transporter-mediated multidrug resistance in cancer: A review of the past decade. *Drug Resist. Updat.: Rev. Comment. Antimicrob. Anticancer Chemother.* **2014**, *18*, 1–17.
4. Anreddy, N.; Gupta, P.; Kathawala, R.J.; Patel, A.; Wurpel, J.N.; Chen, Z.S. Tyrosine kinase inhibitors as reversal agents for ABC transporter mediated drug resistance. *Molecules* **2014**, *19*, 13848–13877.
5. Aller, S.G.; Yu, J.; Ward, A.; Weng, Y.; Chittaboina, S.; Zhuo, R.; Harrell, P.M.; Trinh, Y.T.; Zhang, Q.; Urbatsch, I.L.; Chang, G. Structure of P-glycoprotein reveals a molecular basis for poly-specific drug binding. *Science* **2009**, *323*, 1718–1722.
6. Thomas, H.; Coley, H.M. Overcoming multidrug resistance in cancer: An update on the clinical strategy of inhibiting p-glycoprotein. *Cancer Control* **2003**, *10*, 159–165.
7. Tiwari, A.K.; Sodani, K.; Dai, C.L.; Ashby, C.R., Jr.; Chen, Z.S. Revisiting the ABCs of multidrug resistance in cancer chemotherapy. *Curr. Pharm. Biotechnol.* **2011**, *12*, 570–594.

8. Wang, Y.J.; Zhang, Y.K.; Kathawala, R.J.; Chen, Z.S. Repositioning of Tyrosine Kinase Inhibitors as Antagonists of ATP-Binding Cassette Transporters in Anticancer Drug Resistance. *Cancers* **2014**, *6*, 1925–1952.
9. Tsuruo, T.; Iida, H.; Tsukagoshi, S.; Sakurai, Y. Overcoming of vincristine resistance in P388 leukemia *in vivo* and *in vitro* through enhanced cytotoxicity of vincristine and vinblastine by verapamil. *Cancer Res.* **1981**, *41*, 1967–1972.
10. Twentyman, P.R.; Fox, N.E.; White, D.J. Cyclosporin A and its analogues as modifiers of adriamycin and vincristine resistance in a multi-drug resistant human lung cancer cell line. *Br. J. Cancer* **1987**, *56*, 55–57.
11. Callaghan, R.; Higgins, C.F. Interaction of tamoxifen with the multidrug resistance P-glycoprotein. *Br. J. Cancer* **1995**, *71*, 294–299.
12. Baer, M.R.; George, S.L.; Dodge, R.K.; O'Loughlin, K.L.; Minderman, H.; Caligiuri, M.A.; Anastasi, J.; Powell, B.L.; Kolitz, J.E.; Schiffer, C.A.; *et al*. Phase 3 study of the multidrug resistance modulator PSC-833 in previously untreated patients 60 years of age and older with acute myeloid leukemia: Cancer and Leukemia Group B Study 9720. *Blood* **2002**, *100*, 1224–1232.
13. Benet, L.Z.; Cummins, C.L.; Wu, C.Y. Unmasking the dynamic interplay between efflux transporters and metabolic enzymes. *Int. J. Pharm.* **2004**, *277*, 3–9.
14. Newman, D.J.; Cragg, G.M. Marine natural products and related compounds in clinical and advanced preclinical trials. *J. Nat. Products* **2004**, *67*, 1216–1238.
15. Huang, X.C.; Xiao, X.; Zhang, Y.K.; Talele, T.T.; Salim, A.A.; Chen, Z.S.; Capon, R.J. Lamellarin O, a pyrrole alkaloid from an Australian marine sponge, *Ianthella* sp., reverses BCRP mediated drug resistance in cancer cells. *Mar. Drugs* **2014**, *12*, 3818–3837.
16. Abraham, I.; El Sayed, K.; Chen, Z.S.; Guo, H. Current status on marine products with reversal effect on cancer multidrug resistance. *Mar. Drugs* **2012**, *10*, 2312–2321.
17. Funel-Le Bon, C.; Berrue, F.; Thomas, O.P.; Reyes, F.; Amade, P. Sodwanone S, a triterpene from the marine sponge *Axinella weltneri*. *J. Nat. Products* **2005**, *68*, 1284–1287.
18. Rudi, A.; Aknin, M.; Gaydou, E.M.; Kashman, Y. Sodwanones K, L, and M; new triterpenes from the marine sponge *Axinella weltneri*. *J. Nat. Products* **1997**, *60*, 700–703.
19. Foudah, A.I.; Jain, S.; Busnena, B.A.; El Sayed, K.A. Optimization of marine triterpene sipholenols as inhibitors of breast cancer migration and invasion. *ChemMedChem* **2013**, *8*, 497–510.
20. Foudah, A.I.; Sallam, A.A.; Akl, M.R.; El Sayed, K.A. Optimization, pharmacophore modeling and 3D-QSAR studies of sipholanes as breast cancer migration and proliferation inhibitors. *Eur. J. Med. Chem.* **2014**, *73*, 310–324.
21. Patel, A.; Tiwari, A.K.; Chufan, E.E.; Sodani, K.; Anreddy, N.; Singh, S.; Ambudkar, S.V.; Stephani, R.; Chen, Z.S. PD173074, a selective FGFR inhibitor, reverses ABCB1-mediated drug resistance in cancer cells. *Cancer Chemother. Pharmacol.* **2013**, *72*, 189–199.
22. Zhang, H.; Wang, Y.J.; Zhang, Y.K.; Wang, D.S.; Kathawala, R.J.; Patel, A.; Talele, T.T.; Chen, Z.S.; Fu, L.W. AST1306, a potent EGFR inhibitor, antagonizes ATP-binding cassette subfamily G member 2-mediated multidrug resistance. *Cancer Lett.* **2014**, *350*, 61–68.

23. Guo, H.Q.; Zhang, G.N.; Wang, Y.J.; Zhang, Y.K.; Sodani, K.; Talele, T.T.; Ashby, C.R., Jr.; Chen, Z.S. β-Elemene, a compound derived from Rhizoma zedoariae, reverses multidrug resistance mediated by the ABCB1 transporter. *Oncol. Rep.* **2014**, *31*, 858–866.
24. Zhang, H.; Zhang, Y.K.; Wang, Y.J.; Kathawala, R.J.; Patel, A.; Zhu, H.; Sodani, K.; Talele, T.T.; Ambudkar, S.V.; Chen, Z.S.; *et al*. WHI-P154 enhances the chemotherapeutic effect of anticancer agents in ABCG2-overexpressing cells. *Cancer Sci.* **2014**, *105*, 1071–1078.
25. Sodani, K.; Patel, A.; Anreddy, N.; Singh, S.; Yang, D.H.; Kathawala, R.J.; Kumar, P.; Talele, T.T.; Chen, Z.S. Telatinib reverses chemotherapeutic multidrug resistance mediated by ABCG2 efflux transporter *in vitro* and *in vivo*. *Biochem. Pharmacol.* **2014**, *89*, 52–61.
26. Guo, M.; Wang, R.; Wang, J.; Hua, K.; Wang, Y.; Liu, X.; Yao, S. ALT1, a Snf2 family chromatin remodeling ATPase, negatively regulates alkaline tolerance through enhanced defense against oxidative stress in rice. *PLoS ONE* **2014**, *9*, e112515.
27. Wang, Y.J.; Kathawala, R.J.; Zhang, Y.K.; Patel, A.; Kumar, P.; Shukla, S.; Fung, K.L.; Ambudkar, S.V.; Talele, T.T.; Chen, Z.S. Motesanib (AMG706), a potent multikinase inhibitor, antagonizes multidrug resistance by inhibiting the efflux activity of the ABCB1. *Biochem. Pharmacol.* **2014**, *90*, 367–378.
28. Li, J.; Jaimes, K.; Aller, S. Refined structures of mouse P-Glycoprotein. *Protein Sci.* **2014**, *23*, 34–46.
29. Friesner, R.A.; Murphy, R.B.; Repasky, M.P.; Frye, L.L.; Greenwood, J.R.; Halgren, T.A.; Sanschagrin, P.C.; Mainz, D.T. Extra precision glide: Docking and scoring incorporating a model of hydrophobic enclosure for protein-ligand complexes. *J. Med. Chem.* **2006**, *49*, 6177–6196.
30. Abraham, I.; Jain, S.; Wu, C.P.; Khanfar, M.A.; Kuang, Y.; Dai, C.L.; Shi, Z.; Chen, X.; Fu, L.; Ambudkar, S.V.; *et al*. Marine sponge-derived sipholane triterpenoids reverse P-glycoprotein (ABCB1)-mediated multidrug resistance in cancer cells. *Biochem. Pharmacol.* **2010**, *80*, 1497–1506.
31. Sastry, G.M.; Adzhigirey, M.; Day, T.; Annabhimoju, R.; Sherman, W. Protein and ligand preparation: Parameters, protocols, and influence on virtual screening enrichments. *J. Comput.-Aided Mol. Des.* **2013**, 27, 221–234.
32. Sodani, K.; Tiwari, A.K.; Singh, S.; Patel, A.; Xiao, Z.J.; Chen, J.J.; Sun, Y.L.; Talele, T.T.; Chen, Z.S. GW583340 and GW2974, human EGFR and HER-2 inhibitors, reverse ABCG2- and ABCB1-mediated drug resistance. *Biochem. Pharmacol.* **2012**, *83*, 1613–1622.

Xyloketal B Suppresses Glioblastoma Cell Proliferation and Migration *in Vitro* through Inhibiting TRPM7-Regulated PI3K/Akt and MEK/ERK Signaling Pathways

Wen-Liang Chen, Ekaterina Turlova, Christopher L. F. Sun, Ji-Sun Kim, Sammen Huang, Xiao Zhong, Yong-Yuan Guan, Guan-Lei Wang, James T. Rutka, Zhong-Ping Feng and Hong-Shuo Sun

Abstract: Glioblastoma, the most common and aggressive type of brain tumors, has devastatingly proliferative and invasive characteristics. The need for finding a novel and specific drug target is urgent as the current approaches have limited therapeutic effects in treating glioblastoma. Xyloketal B is a marine compound obtained from mangrove fungus *Xylaria* sp. (No. 2508) from the South China Sea, and has displayed antioxidant activity and protective effects on endothelial and neuronal oxidative injuries. In this study, we used a glioblastoma U251 cell line to (1) explore the effects of xyloketal B on cell viability, proliferation, and migration; and (2) investigate the underlying molecular mechanisms and signaling pathways. MTT assay, colony formation, wound healing, western blot, and patch clamp techniques were employed. We found that xyloketal B reduced cell viability, proliferation, and migration of U251 cells. In addition, xyloketal B decreased p-Akt and p-ERK1/2 protein expressions. Furthermore, xyloketal B blocked TRPM7 currents in HEK-293 cells overexpressing TRPM7. These effects were confirmed by using a TRPM7 inhibitor, carvacrol, in a parallel experiment. Our findings indicate that TRPM7-regulated PI3K/Akt and MEK/ERK signaling is involved in anti-proliferation and migration effects of xyloketal B on U251 cells, providing *in vitro* evidence for the marine compound xyloketal B to be a potential drug for treating glioblastoma.

Reprinted from *Mar. Drugs*. Cite as: Chen, W.-L.; Turlova, E.; Sun, C.L.F.; Kim, J.-S.; Huang, S.; Zhong, X.; Guan, Y.-Y.; Wang, G.-L.; Rutka, J.T.; Feng, Z.-P.; *et al*. Xyloketal B Suppresses Glioblastoma Cell Proliferation and Migration *in Vitro* through Inhibiting TRPM7-Regulated PI3K/Akt and MEK/ERK Signaling Pathways. *Mar. Drugs* **2015**, *13*, 2505-2525.

1. Introduction

Glioblastoma Multiforme (GBM) is the highest grade glioma (grade IV) tumor and the most malignant form of astrocytoma. Despite the wide range of treatments, including surgery, radiotherapy, and chemotherapy, a majority of the therapies for GBM have a limited improvement on patients' survival, largely due to the highly proliferative, invasive, and often drug-resistant nature of the tumor. GBM's median survival time is approximately 14.6 months [1]. Because of the ineffective outcomes with conventional therapies, finding novel and specific drug targets for GBM is still a challenge.

Proliferation, survival, and motility of glioblastoma cells are regulated by different intracellular signaling pathways. Among these, the Ras/MAP kinase-ERK kinase (MEK)/extracellular-signal-regulated kinase (ERK) pathway and PI3K/Akt pathway have long been established. A large number of genetic abnormalities were uncovered in human glioblastoma samples, and the most prominent one is deregulation of signal transduction pathways [2]. It happens in glioblastoma through upregulation or a gain-of-function mutation of receptor tyrosine kinases (RTKs), such as epidermal growth factor receptor (EGFR), platelet-derived growth factor receptor (PDGFR), and fibroblast growth factor receptor (FGFR) [3,4]. These abnormalities cause constitutive activation of Ras/MEK/ERK, PI3K/Akt, and other signal transduction pathways [5]. Novel treatments targeting RTKs, PI3K/Akt, and MEK/ERK signaling pathway are currently under evaluation in clinical trials [6]. However, the majority of glioblastoma patients fail to respond to treatments with either PI3K/Akt or MEK/ERK signaling inhibitors [7], suggesting that a single suppression of one signaling pathway may be insufficient for effectively treating this tumor. Therefore, strategies that combine blockage of these two signaling pathways may be essential for the successful glioblastoma treatment. Further study is required to find the novel target in the upstream of these two signaling pathways.

Accumulating studies raise the notion that ion channels play critical roles in the malignant behavior of glioblastoma cells. Thus it would be possible to regulate certain ion channels in glioblastoma cells in order to suppress tumor cell proliferation, migration, and invasion. Several ion channels are involved in regulating the behavior of glioblastoma cells, such as ClC-3, K_{ATP}, and TRPM7 channels [8–11]. TRPM7 channel, a calcium-conducting divalent cation channel, is a member 7 of the Melastatin subfamily of the Transient Receptor Potential ion channel superfamily, and is ubiquitously expressed in almost all tissues. TRPM7 plays a vital role in embryonic development, anoxia/ischemia, cardiovascular disease, and cancer [12–14]. TRPM7 overexpression was found in tissues of several cancer types [15,16]. Recent reports have shown that TRPM7 controls proliferation, migration, and invasion of glioblastoma cells and glioma stem cells [3,10], suggesting that TRPM7 could potentially serve as a clinical biomarker and therapeutic target for glioblastoma [17].

Drug discovery from marine organisms began 60 years ago. There are some successful examples of discovering, developing, and introducing clinical agents derived from marine sources, including the analgesic ziconotide and the anti-cancer compound trabectedin [18,19]. Xyloketal B (chemical structure of xyloketal B shown in Figure 1A) is a novel marine compound isolated from mangrove fungus *Xylaria* sp. (No. 2508) from the South China Sea [20]. Xyloketal B has displayed several bioactive effects, such as protective effects against oxidative endothelial injury, alleviating oxygen glucose deprivation (OGD)-induced mitochondria dysfunction and injury in PC12 cells, protecting against MPP+-induced neurotoxicity in *C. elegans* and PC12 cells, antioxidant activity in endothelial cell and zebrafish through regulating HO-1, and reducing hypoxia-ischemia-induced brain injury of neonatal mice [21–25]. Our preliminary study indicated that xyloketal B reduced cell viability of glioblastoma U251 cells in a dose-dependent manner. This study further reveals the effects of xyloketal B on cell proliferation and migration of U251 cells and its underlying signaling pathway.

2. Results and Discussion

2.1. Xyloketal B Reduces U251 Cell Viability

Firstly, the effects of xyloketal B on cell viability were assessed using MTT assay [21]. As shown in Figure 1B, various concentrations of xyloketal B (from 31.25 to 1000 μM) treatment for 24 h reduced U251 cell viability in a concentration-dependent manner. The cell viability significantly decreased to 85.4% ± 2.9%, 61.4% ± 4.3%, 12.2% ± 2.6% and 1.3% ± 0.1% of control in 125 μM, 250 μM, 500 μM, and 1000 μM xyloketal B, respectively (* $p < 0.05$, $n = 8$). Nonlinear curve fit was carried out to evaluate the dose-response of xyloketal B, and the IC_{50} of xyloketal B was equal to 287.1 ± 1.0 μM (Figure 1C). The concentrations of xyloketal B used in the following experiments were chosen according to this IC_{50} value.

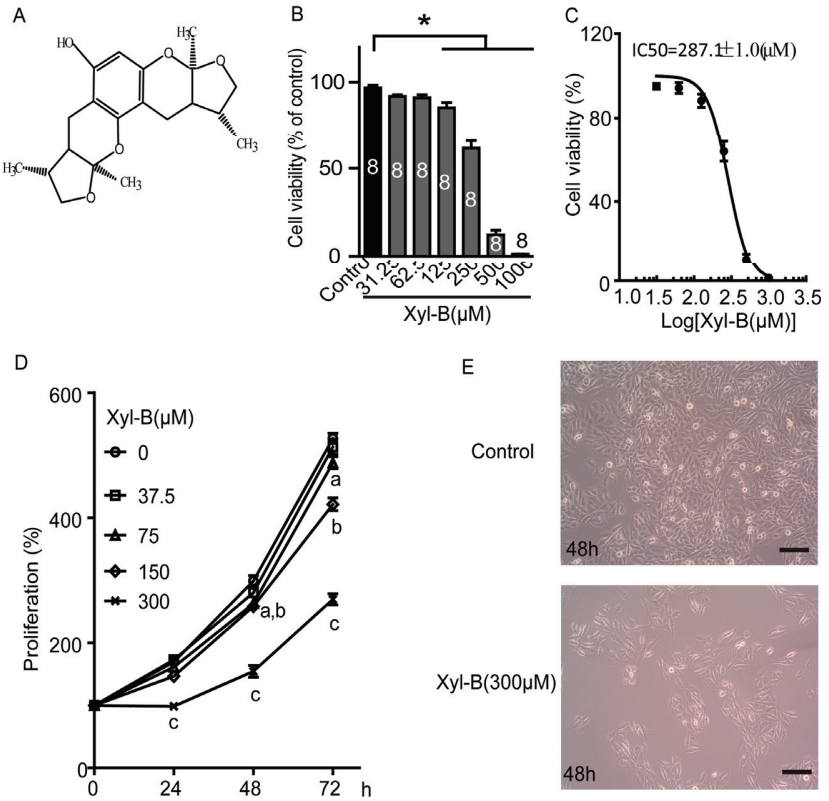

Figure 1. *Cont.*

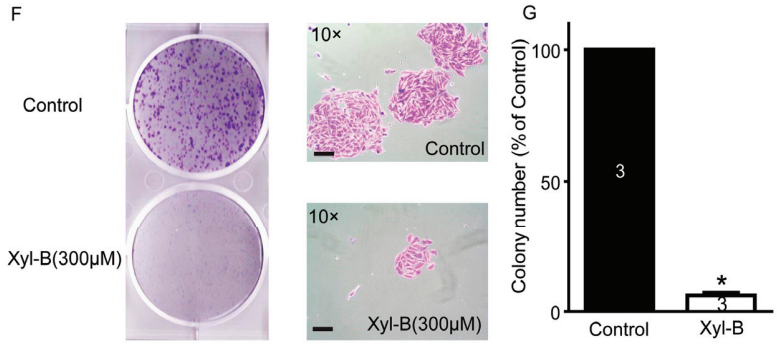

Figure 1. Effects of xyloketal B (Xyl-B) on cell viability and proliferation of U251 cells. (**A**) Chemical structure of xyloketal B; (**B**) Xyloketal B concentration-dependently reduced the cell viability of U251 cell line. U251 cells were incubated with xyloketal B (31.25–1000 μM) for 24 h, following MTT assay. * $p < 0.05$, $n = 8$ independent experiments; (**C**) Nonlinear curve fit for dose-response of xyloketal B treatment in U251 cells for 24 h. IC_{50} = 287.1 ± 1.0 μM; (**D**) Xyloketal B inhibited proliferation of U251 cell line. U251 cells were treated with xyloketal B for 24, 48, and 72 h, and then cell proliferation was detected by MTT assay; a, b, and c represent 75, 150, and 300 μm xyloketal B *versus* the control group, respectively, $p < 0.05$, $n = 6$ independent experiments; (**E**) Representative images of U251 cells with or without xyloketal B treatment for 48 h showed reduction of cell numbers in xyloketal B treatment group. Cell images were obtained with a digital camera connected to a phase-contrast Olympus microscope (CKX41, ×10 objectives). $n = 3$; (**F**) Xyloketal B inhibited colony formation of U251 cells. Cells were plated in six-well culture plates and treated with xyloketal B (300 μM) for 24 h. The culture medium was changed at regular time intervals. Colony formation of U251 cells was detected by crystal violet staining at seven days after xyloketal B treatment. Images were taken using a scanner (CanoScan LiDE 700F, left panel) and a digital camera connected to a phase-contrast Olympus microscope (CKX41, ×10 objectives, right panel). Colony numbers were calculated using Image-Pro Plus software. Representative images were shown. $n = 3$; (**G**) Statistic analysis of colony formation results. Xyloketal B significantly reduced the colony formation of the U251 cells. * $p < 0.05$, $n = 3$. All scale bars = 150 μm.

2.2. Xyloketal B Inhibits U251 Cell Proliferation

Next, cell proliferation was detected using MTT assay [21]. The number of living cells is proportional to the OD value of MTT assay. U251 cells were incubated with 37.5–300 μM xyloketal B for 24, 48, and 72 h before MTT assay was carried out. The OD values of MTT assay were detected once U251 cells were treated with various concentration of xyloketal B and set as a baseline of cell proliferation (100%). As shown in Figure 1D, xyloketal B treatment for 24 h inhibited U251 cell proliferation at 300 μM, showing 98.5% ± 5.9% of baseline in xyloketal B

(300 μM) and 169.4% ± 1.9% of baseline in control group ($p < 0.05$, $n = 6$). When U251 cells were incubated with xyloketal B for 48 and 72 h, cell proliferation was significantly inhibited by xyloketal B at lower concentrations up to 75 μM ($p < 0.05$, $n = 6$). These data indicate that the inhibitive effects of xyloketal B on cell proliferation are time- and concentration-dependent. In addition, xyloketal B (<300 μM) mainly displayed inhibition of cell proliferation, rather than producing cytotoxic effects on the U251 cells. Cell images were also taken at 48 h after treatment with xyloketal B (300 μM), and showed no significant cell damage, but displayed a decreasing cell density compared to the control group, which had a higher cell density in the visual field (Figure 1E, $n = 3$). *In vitro* colony formation assay, which is a cell survival assay, evaluates the ability of a single cell to grow into a colony and also is used to assess the long-term effects on cell proliferation [26]. As shown in Figure 1F,G, a large number of U251 cell colonies was seen in the control group after seeding in six-well plates for seven days with crystal violet staining. The colony formation of U251 cells was significantly decreased after the xyloketal B (300 μM) treatment to 6.1% ± 1.1% of the control (* $p < 0.05$, $n = 3$). The results of colony formation assay further demonstrated the inhibitive effects of xyloketal B on U251 cell proliferation.

2.3. Xyloketal B Inhibits U251 Cell Migration

Wound healing assay was used to evaluate the cell migration [27]. As shown in Figure 2, xyloketal B (300 μM) treatment significantly inhibited U251 cell migration (* $p < 0.05$, $n = 3$). The gap closures in xyloketal B (300 μM) group were 41.1% ± 2.6% and 55.1% ± 3.4%, compared to 52.1% ± 2.7% and 78.4% ± 3.4% in the control group at 24 and 48 h, respectively.

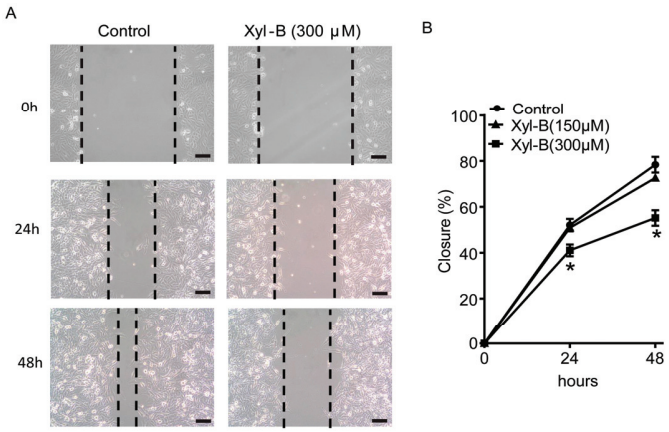

Figure 2. Effects of xyloketal B on the migration of U251 cells. (**A**) Xyloketal B inhibited U251 cell migration. The representative images of wound healing assay were displayed. After being scratched with a 200-μL pipette tip, U251 cells were treated with xyloketal B (300 μM) or vehicle (0.1% DMSO), then images were taken at 0, 24, and 48 h, and gap closure was analyzed; (**B**) Statistical analysis of migration results. Xyloketal B significantly inhibited the cell migration of the U251 cells in both timelines tested. * $p < 0.05$, $n = 3$. Scale bars = 150 μM.

2.4. Xyloketal B Suppresses the PI3K/Akt and MEK/ERK Signaling Pathways

PI3K/Akt and MEK/ERK signaling pathways are involved in the regulation of proliferation and migration of glioblastoma cells [28]. At present, therapeutic agents targeting both signaling pathways have been developed for treating recurrent malignant glioma patients, and are currently in clinical trials [29]. In order to evaluate the underlying mechanisms of xyloketal B regulating U251 cell proliferation and migration, western blotting was carried out to detect alterations in p-Akt/t-Akt and p-ERK1/2/t-ERK1/2, which are key signaling proteins of PI3K/Akt and MEK/ERK signaling pathways. As shown in Figure 3A, the representative images of western blotting showed that both p-Akt and p-ERK1/2 protein expressions in U251 cells were significantly reduced by xyloketal B (300 μM) treatment for 24 h. Densitometry analysis indicated that p-Akt protein expression, normalized to β-actin, decreased in the xyloketal B (300 μM) treatment group (Figure 3B, 71.5% ± 8.0% of control, * $p < 0.05$, $n = 5$), while the total Akt (t-Akt) protein expression did not change significantly (Figure 3C, 108.4% ± 3.4% of control, $p > 0.05$, $n = 5$). The ratio of p-Akt/t-Akt decreased in the xyloketal B (300 μM) group (Figure 3D, 65.9% ± 6.8% of control, * $p < 0.05$, $n = 5$). In addition, xyloketal B (300 μM) treatment for 24 h reduced p-ERK1/2 protein expression and p-ERK1/2-t-ERK1/2 ratio in U251 cells (Figure 3E,G, p-ERK1/2/β-actin: 72.6% ± 9.9% of control; p-ERK1/2/t-ERK1/2: 60.0 ± 4.7% of control, respectively; * $p < 0.05$, $n = 5$). The total ERK1/2 protein expression did not change significantly (Figure 3F, $p > 0.05$, $n = 5$).

2.5. Xyloketal B Blocks the TRPM7 Current

The above results show that the PI3K/Akt and MEK/ERK signaling pathways are regulated by xyloketal B. We further explored the upstream signaling protein for both signaling pathways. Recently, Leng *et al.* reported that the suppression of TRPM7 reduced the proliferation, migration, and invasion of A172 cells, a human glioma cell line [10]. In hepatic stellate cells, TRPM7 regulates its proliferation via the PI3K and ERK pathways [30]. Therefore, we next explored whether xyloketal B could regulate TRPM7 and thus the PI3K/Akt and MEK/ERK signaling pathways. First, we carried out western blotting experiments to detect the TRPM7 protein expression in U251 cells and the effects of xyloketal B on TRPM7 expression. As shown in Figure 4A, TRPM7 protein was found to be expressed in U251 cells. Xyloketal B (150 and 300 μM) did not significantly regulate TRPM7 protein expression ($p > 0.05$, $n = 4$). Next, we performed whole-cell patch-clamp experiments to test the effects of xyloketal B on the TRPM7 current in HEK-293 cells overexpressing TRPM7. As shown in Figure 4B–D, xyloketal B (300 μM) perfusion blocked the TRPM7 current; its inhibitory effect was eliminated by washout of a bath solution, suggesting it was specific and reversible. The inhibitory efficiency of xyloketal B at 300 μM was approximately 33.4% (Figure 4D, * $p < 0.05$, $n = 3$).

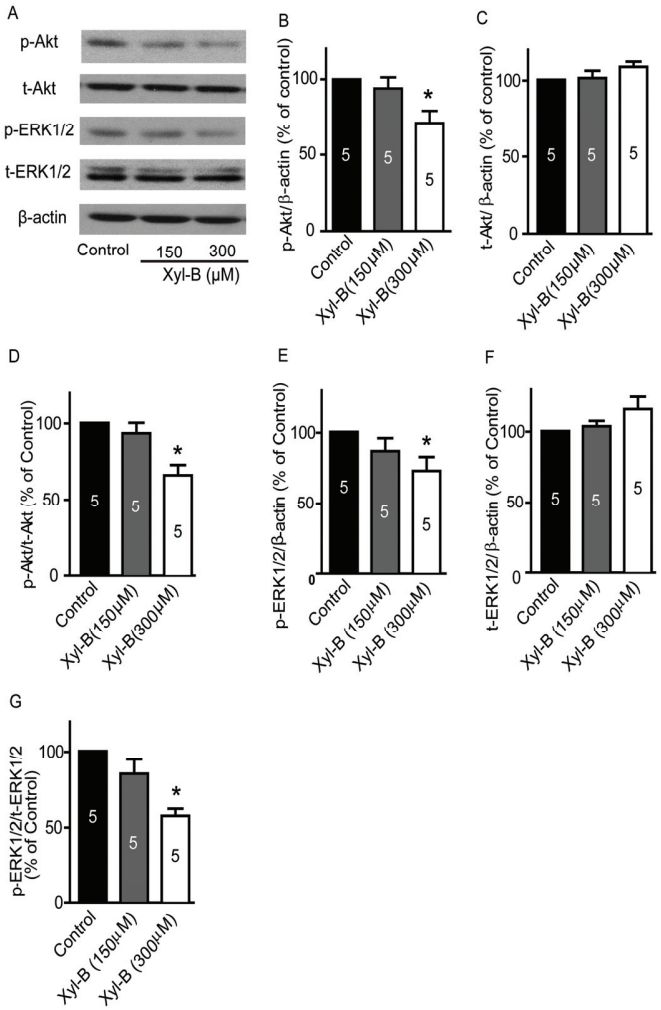

Figure 3. Effects of xyloketal B on p-ERK, t-ERK, p-Akt, and t-Akt protein expressions. U251 cells were treated with xyloketal B (150 and 300 μM) for 24 h, and then the protein expression profile was detected by western blots. (**A**) Representative images of western blotting results; (**B**) Xyloketal B (300 μM) treatment significantly reduced p-Akt protein expression. * $p < 0.05$, $n = 5$; (**C**) Xyloketal B did not significantly alter the t-Akt protein expression; (**D**) Ratio of p-Akt/t-Akt decreased in the xyloketal B (300 μM) treatment group. * $p < 0.05$, $n = 5$; (**E**) Xyloketal B (300 μM) treatment significantly reduced p-ERK1/2 protein expression. * $p < 0.05$, $n = 5$; (**F**) Xyloketal B did not significantly alter t-ERK1/2 protein expression; (**G**) Ratio of p-ERK1/2/t-ERK1/2 decreased in xyloketal B (300 μM) treatment group. * $p < 0.05$, $n = 5$.

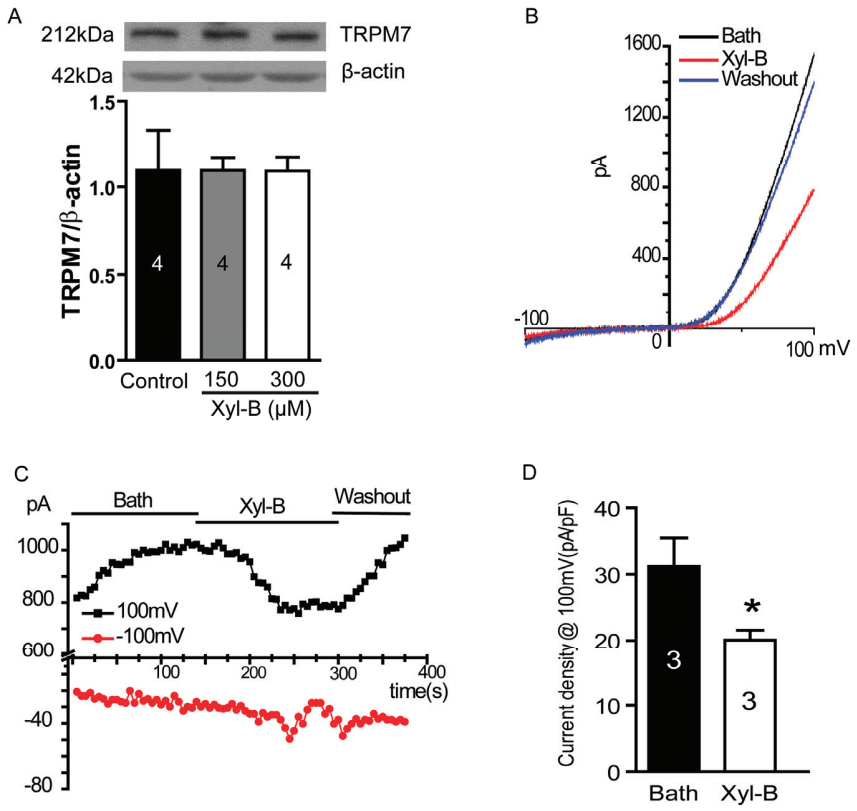

Figure 4. Effects of xyloketal B on TRPM7 currents in HEK-293 cell over-expressing TRPM7. (**A**) Xyloketal B did not significantly regulate TRPM7 protein expressions in U251 cells. U251 cells were treated with xyloketal B (150 and 300 μM) for 24 h followed by detection with western blotting. $n = 4$; (**B**) Xyloketal B (300 μM) blocked TRPM7 currents. TRPM7 protein overexpression in HEK-293 cells was induced by treatment with tetracycline (Tet, 1 μg/mL) for 24 h. Then, TRPM7 currents were recorded using the whole-cell patch-clamp technology with ramp from −100 mV to 100 mV. Representative I–V traces were shown. $n = 3$; (**C**) Representative time course of the inward and outward current of TRPM7 at −100 and 100 mV. $n = 3$; (**D**) Statistical analysis of patch-clamp experiments. Xyloketal B (300 μM) perfusion significantly reduced the outward current of TRPM7. * $p < 0.05$, $n = 3$.

2.6. TRPM7 Inhibitor Carvacrol Reduces U251 Cell Viability, Proliferation, and Migration

Carvacrol, a naturally synthesized, bioactive monoterpenoid phenol, was reported to block TRPM7 currents in HEK cells heterologously expressing mammalian TRPM7 and ectopically expressed in a primary culture of CA3-CA1 hippocampal brain neurons [31]. In our previous study, we have also confirmed blocking of TRPM7 currents in HEK-293 cells overexpressing TRPM7 (data not shown). Hence, we further applied carvacrol as a TRPM7 inhibitor to study the role of

TRPM7 in U251 cell functions and underlying signaling pathways, to support the results of xyloketal B. As shown in Figure 5A, we found that 24 h treatment of carvacrol decreased U251 cell viability in a dose-dependent manner, while its IC_{50} was 348.4 ± 54.1 μM. Carvacrol at 150 and 250 μM inhibited U251 cell proliferation (Figure 5B). Carvacrol (150 and 250 μM) treatment for 72 h decreased cell proliferation by 206.6% ± 13.4% of baseline and 287.7% ± 6.0% of baseline, respectively, compared to 315.2% ± 5.3% of baseline in the control group (Figure 5B, * # $p < 0.05$, *versus* control group, $n = 8$). In addition, carvacrol (500 μM) incubation significantly reduced colony formation of U251 cells (Figure 5C,D, 28.9% ± 1.0% of control, * $p < 0.05$, $n = 6$). We also detected the effects of carvacrol on cell migration in the wound-healing assay. As shown in Figure 5E,F, we found that carvacrol (500 μM) significantly reduced U251 cell migration to approximately 30% of control (* $p < 0.05$, $n = 4$).

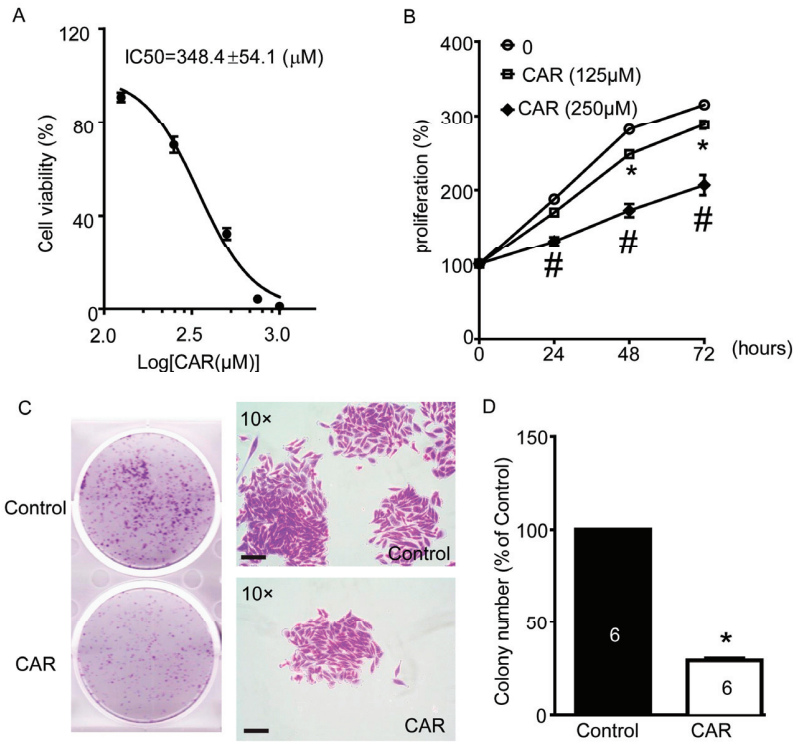

Figure 5. *Cont.*

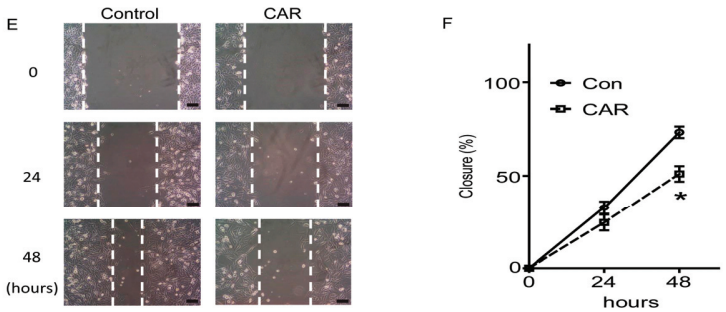

Figure 5. Effects of TRPM7 inhibitor carvacrol (CAR) on viability, proliferation, and migration of U251 cells. (**A**) Carvacrol reduced the viability of U251 cells. U251 cells were treated with various concentrations of carvacrol for 24 h following detection with MTT assay. Nonlinear curve fitting for dose-response of carvacrol treatment was displayed and IC_{50} was calculated as 348.4 ± 54.1 μM. n = 8 independent experiments; (**B**) Carvacrol inhibited the proliferation of U251 cells. U251 cells were treated with carvacrol (125 and 250 μM) or vehicle control (0.1% DMSO) for 24, 48, or 72 h. Cell proliferation was measured using MTT assay. * $p < 0.05$, carvacrol (125 μM) group *versus* control group; # $p < 0.05$, cavarcrol (250 μM) group *versus* control group, n = 8 independent experiments; (**C**) Carvacrol inhibited colony formation of U251 cells. Cells were plated in six-well culture plates and treated with carvacrol (500 μM) for 24 h. Colony formation of U251 cells was detected by crystal violet staining at seven days after carvacrol treatment. Images were taken using a scanner (CanoScan LiDE 700F, left panel) and a digital camera connected to a phase-contrast Olympus microscope (CKX41, ×10 objectives, right panel). Colony numbers were calculated using Image-Pro Plus software. Representative images were shown. n = 6; (**D**) Statistic analysis of colony formation results. Carvacrol B significantly reduced the colony formation of the U251 cells. * $p < 0.05$, n = 6; (**E**) Carvacrol inhibited U251 cell migration. The representative images of wound healing were displayed. After being scratched with 200-μL pipette tip, U251 cells were treated with carvacrol (500 μM) or vehicle (0.1% DMSO), then images were taken at 0, 24, and 48 h and gap closure was analyzed; (**F**) Statistical analysis of migration results. Carvacrol significantly inhibited the cell migration of the U251 cells at 48 h timeline. * $p < 0.05$, n = 4. All scale bars = 150 μM.

2.7. TRPM7 Inhibitor Carvacrol Suppresses the PI3K/Akt and MEK/ERK Signaling Pathways

Next, we measured whether TRPM7 blocked by carvacrol could regulate both PI3K/Akt and MEK/ERK signaling pathways. As shown in Figure 6A, the representative images of western blotting results indicate weaker p-Akt and p-ERK1/2 bands in carvacrol treatment groups. Densitometry analysis showed that carvacrol (250 and 500 μM) significantly reduced p-Akt protein expression (Figure 6B, carvacrol (250 μM): 84.3% ± 3.1% of control; carvacrol (500 μM): 56.6% ± 4.3% of control, * $p < 0.05$, n = 6) and p-ERK1/2 protein expression (Figure 6E, carvacrol (250 μM): 48.9% ± 6.6% of control; carvacrol (500 μM): 65.9% ± 11.6% of control, * $p < 0.05$,

n = 6). The total Akt and ERK1/2 levels were not significantly different between the control and carvacrol treatment groups (Figure 6C,F, $p > 0.05$, n = 6). Thus, both ratios of p-Akt/t-Akt and p-ERK1/2/t-ERK1/2 decreased in the carvacrol (250 and 500 μM) treatment groups (Figure 6D,G, * $p < 0.05$, n = 6).

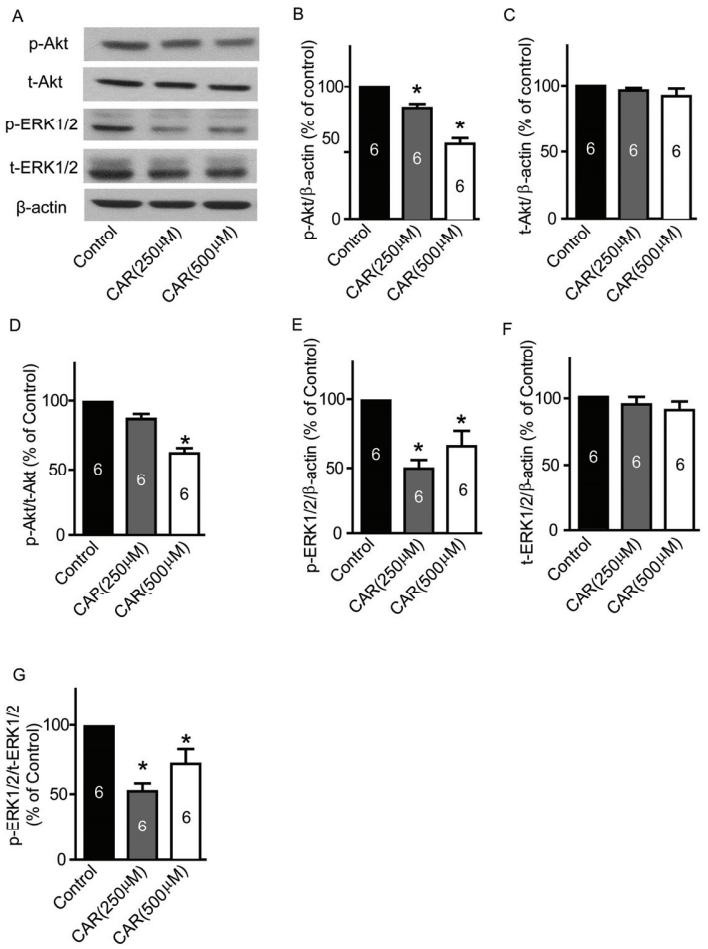

Figure 6. Effects of carvacrol (CAR) on p-ERK, t-ERK, p-Akt, and t-Akt protein expressions. U251 cells were treated with carvacrol (250 and 500 μM) for 24 h, and then protein expressions were detected by western blotting. (**A**) Representative images of western blotting results; (**B**) Carvacrol (500 μM) treatment significantly reduced p-Akt protein expression. * $p < 0.05$, n = 6; (**C**) Carvacrol did not significantly alter t-Akt protein expression; (**D**) Ratio of p-Akt/t-Akt decreased in carvacrol (500 μM) treatment group. * $p < 0.05$, n = 6; (**E**) Carvacrol (250 and 500 μM) treatment significantly reduced p-ERK1/2 protein expression. * $p < 0.05$, n = 6; (**F**) Carvacrol did not significantly alter t-ERK1/2 protein expression; (**G**) Ratio of p-ERK1/2/t-ERK1/2 decreased in carvacrol (250 and 500 μM) treatment group. * $p < 0.05$, n = 6.

2.8. Discussion

In this study, we demonstrate that: (1) xyloketal B reduces cell viability, proliferation, and migration of glioblastoma U251 cell lines; (2) xyloketal B downregulates the PI3K/Akt and MEK/ERK signaling pathways; and (3) xyloketal B blocks the TRPM7 current without altering the TRPM7 protein expression in U251 cells. Furthermore, we report that the TRPM7 inhibitor carvacrol can induce effects similar to those of xyloketal B on U251 cells by inhibiting the PI3K/Akt and MER/ERK signaling pathways. We report here, for the first time, the anti-glioblastoma bioactive effects of the marine compound xyloketal B and the underlying signaling pathways, as well as its ability to block the TRPM7 current.

Xyloketal B, obtained from mangrove fungus *Xylaria* sp. (No. 2508), has a novel chemical structure [20], which appealed to other researchers' interest and was synthesized [32]. Our previous studies reported several bioactive functions of xyloketal B, including protection against endothelial oxidative injury, neuroprotective effects, antioxidant activity, and reducing neonatal hypoxic-ischemic brain injury [21–25,33–35]. Further, it has been suggested that xyloketal B could exert multiple pharmacological properties and may be a candidate compound in the treatment of cardiovascular and nervous system diseases. This study explored the effects of xyloketal B on U251 cells, a human glioblastoma cell line. We found that xyloketal B reduced the viability of U251 cells in a dose-dependent manner, at least partly through its inhibitory effects on the proliferation of U251 cells. Furthermore, xyloketal B also inhibited the migration of U251 cells. The intrinsic nature of GBM tumor cells is that they are highly proliferative, migratory, and invasive. Current therapeutic approaches for glioblastoma include surgery, chemotherapy (temozolomide (TMZ), a DNA alkylating agent), and radiation therapy [36]. However, glioblastoma cells have a high resistance to death-inducing stimuli such as radiotherapy and chemotherapy. Thus, it is critical to continuously search for new therapeutic targets and drugs for glioblastoma. The chemical structure of marine compound xyloketal B is distinct from the existing drugs in clinical therapy, hinting that xyloketal B may serve as a novel candidate compound for the treatment of glioblastoma.

Tyrosine kinase expression and subsequent signaling pathway have long been implicated in the pathogenesis of GBM [37]. Amplification of RTKs in GBM leads to an overactivation of the PI3K/Akt signaling pathway and appears in approximately 45% of GBM cases [38]. Preclinical experiments showed that suppression of PI3K/Akt signaling inhibited the growth of glioblastoma [39]. Selective inhibitors of PI3K/Akt signaling pathway have been undergoing clinical trials [40]. Akt, a downstream serine/threonine kinase in the RTKs/PI3K signaling pathway and an appealing target for potential therapy in treating glioblastoma, is up-regulated in phosphor-Akt levels in the majority of GBM tumor samples and cell lines, and causes an enhanced cell proliferation, migration, and invasion [41]. This study demonstrated that xyloketal B decreased p-Akt level in U251 cells, suggesting that downregulation of the PI3K/Akt signaling pathway is involved in anti-proliferation and migration effects of xyloketal B. In terms of the MEK/ERK signaling pathway, it is also constitutively activated by RTKs. RTKs, through a series of adaptor proteins and exchange factors, stimulate Ras activation, which recruits Raf to the plasma membrane, and then phosphorylates and activates MEK, subsequently phosphorylating and activating ERK1/2 [42]. Activation of ERK1/2

regulates both cytosolic proteins and transcription factors involved in cell proliferation, migration, and invasion [42]. Selective inhibitors of the MEK/ERK signaling pathway are currently under clinical trial in GBM therapies [43]. Moreover, there is a crosstalk between the PI3K/Akt and MEK/ERK signaling pathways in maintaining the self-renewal and tumorigenicity of glioblastoma-like stem cells [44], which may contribute to the unsuccessful therapeutic effects of inhibitors in targeting a single signaling pathway [45]. This suggests that a combined blockage of both PI3K/Akt and MEK/ERK pathways would be a rational and effective approach in treating glioblastoma [44]. Besides reducing p-Akt levels, xyloketal B decreased p-ERK1/2 protein expression in U251 cells. These results indicate that xyloketal B downregulates both the PI3K/Akt and MEK/ERK1/2 pathways, contributing to anti-proliferation and migration effects.

Recently, Liu *et al.* reported that knockdown of TRPM7 inhibited proliferation, migration, and invasion of glioma stem cells and revealed that the JAK2/STAT3 and/or Notch signaling pathways were involved in these effects [11]. The function of TRPM7 on glioma stem cell was further confirmed in glioblastoma A172 cells [10]. Thus, TRPM7 is likely a promising target for therapeutic intervention in glioblastoma. There are several lines of evidences suggesting that TRPM7 regulates the PI3K/Akt and MEK/ERK pathways. Silencing TRPM7 decreased the level of p-Akt in OVCA cells and human lung fibroblasts, and also decreased the level of p-ERK1/2 in breast cancer cells [46–48]. However, silencing TRPM7 in endothelial cells enhanced cell proliferation, migration, and p-ERK1/2 expression [49,50], suggesting that TRPM7 exerts its function in relation to specific cell types. In this study, we found that xyloketal B blocked TRPM7 currents in HEK-293 cells overexpressing TRPM7. Moreover, we detected TRPM7 protein expression in U251 cells, while xyloketal B did not regulate its protein expression. These data indicate that xyloketal B reduces levels of p-Akt and p-ERK1/2 in U251 cells via blockage of the TRPM7 current. Carvacrol was reported to be an inhibitor of TRPM7 [31], which was also confirmed in our study (data not shown). In this study, similar to xyloketal B, carvacrol was found to reduce cell viability, proliferation, migration, and expression levels of p-Akt and p-ERK1/2 in U251 cells in the parallel experiments. Hence, these results provide evidence that blocking TRPM7 with xyloketal B is a critical step in regulating the PI3K/Akt and MEK/ERK pathways, which are involved in the suppression of cell proliferation and migration of U251 cells. Our study is consistent the previous findings in cancer cells [46–48].

The mechanism by which TRPM7 regulates the PI3K/Akt and MEK/ERK pathways remains unclear. Ca^{2+} is a critical second messenger for signal transduction in regulating gene expression, cell proliferation, cell migration, and cell survival, among other activities [51]. In RTK's signaling pathway, Ca^{2+} interacting with phosphoinositide-specific phospholipase C (PLC), regulates downstream signaling, including PI3K/Akt and MEK/ERK signaling [52]. TRPM7 not only has a very high permeability for both Ca^{2+} and Mg^{2+}, but also an α-type serine/threonine protein kinase domain, which has been shown to form a dimer that can autophosphorylate as well as phosphorylate protein substrates [53]. Studies have shown that the C2 domain of several phospholipase C (PLC) isozymes interacts with TRPM7α-type serine/threonine protein kinase domain [54,55]. In our previous study, xyloketal B was shown to regulate calcium entry in endothelial cells and primary cortical neurons [21,25]. Hence, we could speculate that TRPM7

regulates PI3K/Akt and MEK/ERK1/2 signaling through Ca^{2+} entry and interaction with PLC, and thus is involved in the effects of xyloketal B on U251 cells.

In summary, our findings indicate that the effects of marine compound xyloketal B in anti-proliferation and migration of U251 cells are mediated by inhibition of TRPM7 and regulation of the PI3K/Akt and MEK/ERK signaling pathways. Thus, marine compound xyloketal B may be a potential target for drug development for treatment of glioblastoma.

3. Experimental Section

3.1. Reagents

Anti-TRPM7 (cat #ab85016) was purchased from Abcam (Cambridge, MA, USA). Phosphor-Akt (ser 473,) antibody (p-Akt, cat #9271), Akt antibody (t-Akt, cat #9272), and phospho-p44/42 MAPK antibody (p-ERK1/2, cat #5726) were purchased from Cell Signaling Technology (Danvers, MA, USA). Anti-MAP Kinase ERK1/ERK2 Rabbit pAb (t-ERK1/2, cat #442704) was purchased from Millipore (Billerica, MA, USA). Anti-β-actin was purchased from Sigma-Aldrich (St. Louis, MO, USA). Pierce™ BCA Protein Assay Kit was a product of Pierce Biotechnology (Rockford, IL, USA). All cell culture materials were obtained from Gibco Life Technologies Corporation (Burlington, ON, USA). All other reagents used were purchased from Sigma-Aldrich (St. Louis, MO, USA) unless mentioned otherwise.

3.2. Cell Culture

The permanent, well-characterized human glioblastoma cell line U251 was received from the American Type Culture Collection (Manassas, VA, USA) and maintained in Dulbecco's modified eagle's medium (DMEM) supplemented with 10% heat-inactivated fetal bovine serum (FBS), 100 U/mL penicillin, and streptomycin in a 37 °C, 5% CO_2 humidified chamber. HEK-293 cells with stable expression of Flag-murine TRPM7/pCDNA4 were maintained in MEM supplemented with 10% FBS, blasticidin (5 μg/mL), glutamax-1 (2 mM), and zeocin (0.4 mg/mL). HEK-293-Flag-TRPM7 cells were incubated with 1 μg/mL tetracycline to induce TRPM7 overexpression.

3.3. Cell Viability and Proliferation

MTT assay was employed to assess cell viability and cell proliferation, as previously described [21]. U251 cells, seeded in 96-well culture plates at a density of 2×10^4 cells/mL, were treated with various concentrations of xyloketal B (31.25–1000 μM) or carvacrol (from 125 μM to 1000 μM) for the described time points (24, 48, or 72 h). MTT reagent (0.5 mg/mL MTT) in completed medium (100 μL) was added to each well and incubated in a CO_2 incubator for 3 h. Then, the medium was aspirated from each well and 200 μL DMSO was added. The quantity of formazan product of MTT, as measured by absorbance, is directly proportional to the number of living cells. The absorbance was measured in a microplate reader (Syngery H1, Biotek, Winooski, VT, USA) at 490 nm. Cell viability was expressed as a percentage of the control value (0.1% DMSO).

3.4. Colony Formation

Glioblastoma U251 cells (300 cells/well) were seeded in six-well plates overnight and subsequently treated with xyloketal B (300 μM) or carvacrol (500 μM) for 24 h. The culture medium was changed at regular time intervals. After seven days of culture, the cells were washed twice with PBS, and fixed with 4% paraformaldehyde for 30 min at room temperature. The colonies were stained with 0.1% crystal violet for 10 min, then washed with water and air-dried. Cell colonies in plate were scanned using CanoScan LiDE 700F and images were captured using a digital camera connected to a phase-contrast Olympus microscope (CKX41, ×10 objectives). The number of colonies containing >50 cells was counted using Image-Pro Plus software (version 1.47V). Data were presented as a percentage of control.

3.5. Cell Migration

Wound healing assay was employed to assess cell migration, as described elsewhere [56]. In brief, U251 cells were seeded in six-well culture plates at a density of 5×10^4 cells/mL and grown overnight. Wound gap of the monolayer of cells was created using a 200 μL pipette tip. Then, the cells were treated with xyloketal B (300 μM), carvacrol (500 μM) and vehicle control (0.1% DMSO) at various time points. Cell images of each time point were taken with a digital camera connected to a phase-contrast Olympus microscope (CKX41, ×10 objective). The same visual field was marked and used throughout the experiment. The area of wound gap was measured by Image-Pro Plus software with the wound healing tool. Wound closure (%) = [Gap area ($T - T_0$)/Gap area T_0] × 100% (where T is the treatment time and T_0 is the time that the wound was induced).

3.6. Western Blotting

Western blotting experiments were carried out as previously described [21,57]. Total cell lysates were prepared by scraping cells in RIPA buffer plus proteinase inhibitor cocktails (50 mM Tris, 150 mM NaCl, 1 mM EDTA, 1% Triton X-100, 0.1% SDS, 1% Sodium deoxycholate, 1 mM PMSF, 1 mM Na_3VO_4, 1 mM NaF, 1 μg/mL aprotinin, 1 μg/mL leupeptin, 1 μg/mL pepstatin) and centrifuged at 13,000 rpm to pellet the insoluble material. The protein concentrations of cell lysates were determined using was determined with the bicinchoninic acid (BCA) assay method. Equivalent amounts of protein were separated in SDS-PAGE gel and transferred to nitrocellulose membrane (Millipore, Billerica, MA, USA) using a semi-dry transfer method (200 mA per gel, 60 min). The membrane was then blocked with 5% milk in TBS with 0.1% Tween-20 at room temperature for 1 h, and immunoblotted with primary antibodies overnight at 4 °C as follows: anti-TRPM7 (1:1000), anti-p-Akt (1:1000), anti-Akt (1:1000), anti-p-ERK1/2 (1:1000), anti-ERK1/2 (1:1000), and anti-β-actin (1:1000) antibodies, followed by incubation with the corresponding HRP-labeled secondary antibody (Cell Signaling Technology, Danvers, MA, USA, 1:8000) for 1 h at room temperature in conjunction with a chemiluminescence reagent system (PerkinElmer Life Sciences Inc., Boston, MA, USA). Densitometry was carried out using Image-Pro Plus software.

3.7. Patch-Clamp Recording

Whole-cell patch-clamp recording was used to analyze TRPM7 currents using an Axopatch 700B (Axon Instruments, Inc., Sunnyvale, CA, USA), as previously described [58]. Briefly, holding membrane potential was held to 0 mV. Voltage ramp (from −100 to +100 mV for 400 ms) protocol was using to recorded TRPM7 currents with an interval of 5 s at 2 kHz and digitized at 5 kHz. Data were acquired using pClamp 9.2 software and analyzed using Clampfit 9.2. All experiments were performed at room temperature. The patch pipette (3–5 megaohms) was made from hematocrit glass using a micropipette puller (Model P-97, Shutter Instrument, Novato, CA, USA). The pipette solution contained (in mM) 145 cesium methanesulfonate, 8 NaCl, 10 EGTA, and 10 HEPES (pH adjusted to 7.2 with CsOH). The bath solution contained (in mM) 140 NaCl, 5 KCl, 2 $CaCl_2$, 20 HEPES, and 10 glucose (pH was adjusted to 7.4 with NaOH). The cell was perfused with bath solution before perfusing with xyloketal B (300 μM). When the effects of xyloketal B reached the maximum platform, the cell was reperfused with bath solution to wash out xyloketal B.

3.8. Statistical Analysis

Data are presented as the mean ± SEM. One-way ANOVA with subsequent Newman–Keuls test was used to determine the statistical significance for multiple comparisons. Comparison between two groups was analyzed using Student's *t*-test. All reported *p*-values were two-sided and were considered to be statistically significant at $p < 0.05$.

4. Conclusions

Marine compound xyloketal B reduces cell viability, proliferation, and migration through inhibition of TRPM7 and modulation of the PI3K/Akt and MEK/ERK signaling pathways. Thus, marine compound xyloketal B may be a potential target for drug development. Further research, especially *in vivo* study, is essential to explore its value as a potential therapeutic agent for treatment of glioblastoma.

Acknowledgments

This work was supported by the following grants: Natural Sciences and Engineering Research Council of Canada (NSERC) Discovery Grants to ZPF (RGPIN 249962) and to HSS (RGPIN 402733); Canadian Institutes of Health Research (CIHR) China–Canada Joint Health Research Initiative to HSS (CIHR, FRN #132571), Ontario Graduate Scholarships to ET. WC, a lecturer for Department of Pharmacology, School of Pharmaceutical Sciences, Guangzhou Medical University, China, is currently a Postdoctoral Fellow at the University of Toronto.

Author Contributions

WC performed experiments; WC and HSS wrote the manuscript; WC, ET, CLFS, JSK, SH, and ZPF contributed substantially to the manuscript preparation; all authors discussed the results,

analyzed data, and commented on the manuscript; HSS and ZPF designed the project; WC, HSS, and ZPF developed the study.

Conflicts of Interest

The authors declare no conflict of interest.

References

1. Stupp, R.; Hegi, M.E.; Mason, W.P.; van den Bent, M.J.; Taphoorn, M.J.; Janzer, R.C.; Ludwin, S.K.; Allgeier, A.; Fisher, B.; Belanger, K.; *et al*. Effects of radiotherapy with concomitant and adjuvant temozolomide *versus* radiotherapy alone on survival in glioblastoma in a randomised phase iii study: 5-Year analysis of the eortc-ncic trial. *Lancet Oncol.* **2009**, *10*, 459–466.
2. Soni, D.; King, J.A.; Kaye, A.H.; Hovens, C.M. Genetics of glioblastoma multiforme: Mitogenic signaling and cell cycle pathways converge. *J. Clin. Neurosci.* **2005**, *12*, 1–5.
3. Leon, S.P.; Zhu, J.; Black, P.M. Genetic aberrations in human brain tumors. *Neurosurgery* **1994**, *34*, 708–722.
4. Fleming, T.P.; Saxena, A.; Clark, W.C.; Robertson, J.T.; Oldfield, E.H.; Aaronson, S.A.; Ali, I.U. Amplification and/or overexpression of platelet-derived growth factor receptors and epidermal growth factor receptor in human glial tumors. *Cancer Res.* **1992**, *52*, 4550–4553.
5. Pelloski, C.E.; Lin, E.; Zhang, L.; Yung, W.K.; Colman, H.; Liu, J.L.; Woo, S.Y.; Heimberger, A.B.; Suki, D.; Prados, M.; *et al*. Prognostic associations of activated mitogen-activated protein kinase and akt pathways in glioblastoma. *Clin. Cancer Res.* **2006**, *12*, 3935–3941.
6. Furnari, F.B.; Fenton, T.; Bachoo, R.M.; Mukasa, A.; Stommel, J.M.; Stegh, A.; Hahn, W.C.; Ligon, K.L.; Louis, D.N.; Brennan, C.; *et al*. Malignant astrocytic glioma: Genetics, biology, and paths to treatment. *Genes Dev.* **2007**, *21*, 2683–2710.
7. Sathornsumetee, S.; Rich, J.N. Designer therapies for glioblastoma multiforme. *Ann. N. Y. Acad. Sci.* **2008**, *1142*, 108–132.
8. Cuddapah, V.A.; Sontheimer, H. Molecular interaction and functional regulation of clc-3 by Ca^{2+}/calmodulin-dependent protein kinase ii (camkii) in human malignant glioma. *J. Biol. Chem.* **2010**, *285*, 11188–11196.
9. Huang, L.; Li, B.; Li, W.; Guo, H.; Zou, F. Atp-sensitive potassium channels control glioma cells proliferation by regulating erk activity. *Carcinogenesis* **2009**, *30*, 737–744.
10. Leng, T.D.; Li, M.H.; Shen, J.F.; Liu, M.L.; Li, X.B.; Sun, H.W.; Branigan, D.; Zeng, Z.; Si, H.F.; Li, J.; *et al*. Suppression of trpm7 inhibits proliferation, migration, and invasion of malignant human glioma cells. *CNS Neurosci. Ther.* **2015**, *21*, 252–261.
11. Liu, M.; Inoue, K.; Leng, T.; Guo, S.; Xiong, Z.G. Trpm7 channels regulate glioma stem cell through stat3 and notch signaling pathways. *Cell. Signal.* **2014**, *26*, 2773–2781.
12. Sun, H.S.; Jackson, M.F.; Martin, L.J.; Jansen, K.; Teves, L.; Cui, H.; Kiyonaka, S.; Mori, Y.; Jones, M.; Forder, J.P.; *et al*. Suppression of hippocampal trpm7 protein prevents delayed neuronal death in brain ischemia. *Nat. Neurosci.* **2009**, *12*, 1300–1307.

13. Jin, J.; Desai, B.N.; Navarro, B.; Donovan, A.; Andrews, N.C.; Clapham, D.E. Deletion of trpm7 disrupts embryonic development and thymopoiesis without altering Mg^{2+} homeostasis. *Science* **2008**, *322*, 756–760.
14. Lehen'kyi, V.; Shapovalov, G.; Skryma, R.; Prevarskaya, N. Ion channnels and transporters in cancer. 5. Ion channels in control of cancer and cell apoptosis. *Am. J. Physiol. Cell Physiol.* **2011**, *301*, C1281–C1289.
15. Wang, J.; Xiao, L.; Luo, C.H.; Zhou, H.; Hu, J.; Tang, Y.X.; Fang, K.N.; Zhang, Y. Overexpression of trpm7 is associated with poor prognosis in human ovarian carcinoma. *Asian Pac. J. Cancer Prev. APJCP* **2014**, *15*, 3955–3958.
16. Rybarczyk, P.; Gautier, M.; Hague, F.; Dhennin-Duthille, I.; Chatelain, D.; Kerr-Conte, J.; Pattou, F.; Regimbeau, J.M.; Sevestre, H.; Ouadid-Ahidouch, H.; *et al*. Transient receptor potential melastatin-related 7 channel is overexpressed in human pancreatic ductal adenocarcinomas and regulates human pancreatic cancer cell migration. *Int. J. Cancer* **2012**, *131*, E851–E861.
17. Yee, N.S.; Kazi, A.A.; Yee, R.K. Cellular and developmental biology of trpm7 channel-kinase: Implicated roles in cancer. *Cells* **2014**, *3*, 751–777.
18. Lopez-Guerrero, J.A.; Romero, I.; Poveda, A. Trabectedin therapy as an emerging treatment strategy for recurrent platinum-sensitive ovarian cancer. *Chin. J. Cancer* **2015**, *34*, 41–49.
19. Alicino, I.; Giglio, M.; Manca, F.; Bruno, F.; Puntillo, F. Intrathecal combination of ziconotide and morphine for refractory cancer pain: A rapidly acting and effective choice. *Pain* **2012**, *153*, 245–249.
20. Lin, Y.; Wu, X.; Feng, S.; Jiang, G.; Luo, J.; Zhou, S.; Vrijmoed, L.L.; Jones, E.B.; Krohn, K.; Steingrover, K.; *et al*. Five unique compounds: Xyloketals from mangrove fungus *Xylaria* sp. From the south China sea coast. *J. Org. Chem.* **2001**, *66*, 6252–6256.
21. Chen, W.L.; Qian, Y.; Meng, W.F.; Pang, J.Y.; Lin, Y.C.; Guan, Y.Y.; Chen, S.P.; Liu, J.; Pei, Z.; Wang, G.L.; *et al*. A novel marine compound xyloketal b protects against oxidized ldl-induced cell injury *in vitro*. *Biochem. Pharmacol.* **2009**, *78*, 941–950.
22. Zhao, J.; Li, L.; Ling, C.; Li, J.; Pang, J.Y.; Lin, Y.C.; Liu, J.; Huang, R.; Wang, G.L.; Pei, Z.; *et al*. Marine compound xyloketal B protects pc12 cells against ogd-induced cell damage. *Brain Res.* **2009**, *1302*, 240–247.
23. Lu, X.L.; Yao, X.L.; Liu, Z.; Zhang, H.; Li, W.; Li, Z.; Wang, G.L.; Pang, J.; Lin, Y.; Xu, Z.; *et al*. Protective effects of xyloketal B against mpp+-induced neurotoxicity in caenorhabditis elegans and pc12 cells. *Brain Res.* **2010**, *1332*, 110–119.
24. Li, Z.X.; Chen, J.W.; Yuan, F.; Huang, Y.Y.; Zhao, L.Y.; Li, J.; Su, H.X.; Liu, J.; Pang, J.Y.; Lin, Y.C.; *et al*. Xyloketal B exhibits its antioxidant activity through induction of ho-1 in vascular endothelial cells and zebrafish. *Mar. Drugs* **2013**, *11*, 504–522.
25. Xiao, A.J.; Chen, W.; Xu, B.; Liu, R.; Turlova, E.; Barszczyk, A.; Sun, C.L.; Liu, L.; Deurloo, M.; Wang, G.L.; *et al*. Marine compound xyloketal b reduces neonatal hypoxic-ischemic brain injury. *Mar. Drugs* **2014**, *13*, 29–47.
26. Franken, N.A.; Rodermond, H.M.; Stap, J.; Haveman, J.; van Bree, C. Clonogenic assay of cells *in vitro*. *Nat. Protoc.* **2006**, *1*, 2315–2319.

27. Liang, C.C.; Park, A.Y.; Guan, J.L. *In vitro* scratch assay: A convenient and inexpensive method for analysis of cell migration *in vitro*. *Nat. Protoc.* **2007**, *2*, 329–333.
28. Yajima, I.; Kumasaka, M.Y.; Thang, N.D.; Goto, Y.; Takeda, K.; Yamanoshita, O.; Iida, M.; Ohgami, N.; Tamura, H.; Kawamoto, Y.; *et al*. Ras/raf/mek/erk and pi3k/pten/akt signaling in malignant melanoma progression and therapy. *Dermatol. Res. Pract.* **2012**, *2012*, 354191, doi:10.1155/2012/354191.
29. Rich, J.N.; Bigner, D.D. Development of novel targeted therapies in the treatment of malignant glioma. *Nat. Rev. Drug Discov.* **2004**, *3*, 430–446.
30. Fang, L.; Zhan, S.; Huang, C.; Cheng, X.; Lv, X.; Si, H.; Li, J. Trpm7 channel regulates pdgf-bb-induced proliferation of hepatic stellate cells via pi3k and erk pathways. *Toxicol. Appl. Pharmacol.* **2013**, *272*, 713–725.
31. Parnas, M.; Peters, M.; Dadon, D.; Lev, S.; Vertkin, I.; Slutsky, I.; Minke, B. Carvacrol is a novel inhibitor of drosophila trpl and mammalian trpm7 channels. *Cell Calcium* **2009**, *45*, 300–309.
32. Pettigrew, J.D.; Wilson, P.D. Synthesis of xyloketal a, b, c, d, and g analogues. *J. Org. Chem.* **2006**, *71*, 1620–1625.
33. Su, J.; Chang, C.; Xiang, Q.; Zhou, Z.W.; Luo, R.; Yang, L.; He, Z.X.; Yang, H.; Li, J.; Bei, Y.; *et al*. Xyloketal B, a marine compound, acts on a network of molecular proteins and regulates the activity and expression of rat cytochrome p450 3a: A bioinformatic and animal study. *Drug Des. Dev. Ther.* **2014**, *8*, 2555–2602.
34. Li, S.; Shen, C.; Guo, W.; Zhang, X.; Liu, S.; Liang, F.; Xu, Z.; Pei, Z.; Song, H.; Qiu, L.; *et al*. Synthesis and neuroprotective action of xyloketal derivatives in parkinson's disease models. *Mar. Drugs* **2013**, *11*, 5159–5189.
35. Xu, Z.; Li, Y.; Xiang, Q.; Pei, Z.; Liu, X.; Lu, B.; Chen, L.; Wang, G.; Pang, J.; Lin, Y.; *et al*. Design and synthesis of novel xyloketal derivatives and their vasorelaxing activities in rat thoracic aorta and angiogenic activities in zebrafish angiogenesis screen. *J. Med. Chem.* **2010**, *53*, 4642–4653.
36. Cheng, Y.; Zhao, J.; Qiao, W.; Chen, K. Recent advances in diagnosis and treatment of gliomas using chlorotoxin-based bioconjugates. *Am. J. Nucl. Med. Mol. Imaging* **2014**, *4*, 385–405.
37. Wong, A.J.; Ruppert, J.M.; Bigner, S.H.; Grzeschik, C.H.; Humphrey, P.A.; Bigner, D.S.; Vogelstein, B. Structural alterations of the epidermal growth factor receptor gene in human gliomas. *Proc. Natl. Acad. Sci. USA* **1992**, *89*, 2965–2969.
38. Mellinghoff, I.K.; Wang, M.Y.; Vivanco, I.; Haas-Kogan, D.A.; Zhu, S.; Dia, E.Q.; Lu, K.V.; Yoshimoto, K.; Huang, J.H.; Chute, D.J.; *et al*. Molecular determinants of the response of glioblastomas to egfr kinase inhibitors. *N. Engl. J. Med.* **2005**, *353*, 2012–2024.
39. Klingler-Hoffmann, M.; Bukczynska, P.; Tiganis, T. Inhibition of phosphatidylinositol 3-kinase signaling negates the growth advantage imparted by a mutant epidermal growth factor receptor on human glioblastoma cells. *Int. J. Cancer* **2003**, *105*, 331–339.
40. Wen, P.Y.; Lee, E.Q.; Reardon, D.A.; Ligon, K.L.; Alfred Yung, W.K. Current clinical development of pi3k pathway inhibitors in glioblastoma. *Neuro-Oncology* **2012**, *14*, 819–829.

41. McDowell, K.A.; Riggins, G.J.; Gallia, G.L. Targeting the akt pathway in glioblastoma. *Curr. Pharm. Des.* **2011**, *17*, 2411–2420.
42. De Luca, A.; Maiello, M.R.; D'Alessio, A.; Pergameno, M.; Normanno, N. The ras/raf/mek/erk and the pi3k/akt signalling pathways: Role in cancer pathogenesis and implications for therapeutic approaches. *Expert Opin. Ther. Targets* **2012**, *16* (Suppl. 2), S17–S27.
43. Sathornsumetee, S.; Reardon, D.A.; Desjardins, A.; Quinn, J.A.; Vredenburgh, J.J.; Rich, J.N. Molecularly targeted therapy for malignant glioma. *Cancer* **2007**, *110*, 13–24.
44. Sunayama, J.; Matsuda, K.; Sato, A.; Tachibana, K.; Suzuki, K.; Narita, Y.; Shibui, S.; Sakurada, K.; Kayama, T.; Tomiyama, A.; *et al*. Crosstalk between the pi3k/mtor and mek/erk pathways involved in the maintenance of self-renewal and tumorigenicity of glioblastoma stem-like cells. *Stem Cells* **2010**, *28*, 1930–1939.
45. Hottinger, A.F.; Stupp, R.; Homicsko, K. Standards of care and novel approaches in the management of glioblastoma multiforme. *Chin. J. Cancer* **2014**, *33*, 32–39.
46. Wang, J.; Liao, Q.J.; Zhang, Y.; Zhou, H.; Luo, C.H.; Tang, J.; Wang, Y.; Tang, Y.; Zhao, M.; Zhao, X.H.; *et al*. Trpm7 is required for ovarian cancer cell growth, migration and invasion. *Biochem. Biophys. Res. Commun.* **2014**, *454*, 547–553.
47. Yu, M.; Huang, C.; Huang, Y.; Wu, X.; Li, X.; Li, J. Inhibition of trpm7 channels prevents proliferation and differentiation of human lung fibroblasts. *Inflamm. Res.* **2013**, *62*, 961–970.
48. Meng, X.; Cai, C.; Wu, J.; Cai, S.; Ye, C.; Chen, H.; Yang, Z.; Zeng, H.; Shen, Q.; Zou, F.; *et al*. Trpm7 mediates breast cancer cell migration and invasion through the mapk pathway. *Cancer Lett.* **2013**, *333*, 96–102.
49. Inoue, K.; Xiong, Z.G. Silencing trpm7 promotes growth/proliferation and nitric oxide production of vascular endothelial cells via the erk pathway. *Cardiovasc. Res.* **2009**, *83*, 547–557.
50. Zeng, Z.; Inoue, K.; Sun, H.; Leng, T.; Feng, X.; Zhu, L.; Xiong, Z.G. Trpm7 regulates vascular endothelial cell adhesion and tube formation. *Am. J. Physiol. Cell Physiol.* **2015**, *308*, C308–C318.
51. Berridge, M.J.; Bootman, M.D.; Roderick, H.L. Calcium signalling: Dynamics, homeostasis and remodelling. *Nat. Rev. Mol. Cell Biol.* **2003**, *4*, 517–529.
52. Yang, Y.R.; Follo, M.Y.; Cocco, L.; Suh, P.G. The physiological roles of primary phospholipase c. *Adv. Biol. Regul.* **2013**, *53*, 232–241.
53. Clark, K.; Middelbeek, J.; Lasonder, E.; Dulyaninova, N.G.; Morrice, N.A.; Ryazanov, A.G.; Bresnick, A.R.; Figdor, C.G.; van Leeuwen, F.N. Trpm7 regulates myosin iia filament stability and protein localization by heavy chain phosphorylation. *J. Mol. Biol.* **2008**, *378*, 790–803.
54. Deason-Towne, F.; Perraud, A.L.; Schmitz, C. Identification of ser/thr phosphorylation sites in the c2-domain of phospholipase c gamma2 (plcgamma2) using trpm7-kinase. *Cell. Signal.* **2012**, *24*, 2070–2075.
55. Langeslag, M.; Clark, K.; Moolenaar, W.H.; van Leeuwen, F.N.; Jalink, K. Activation of trpm7 channels by phospholipase c-coupled receptor agonists. *J. Biol. Chem.* **2007**, *282*, 232–239.

56. Goldberg, L.; Kloog, Y. A ras inhibitor tilts the balance between rac and rho and blocks phosphatidylinositol 3-kinase-dependent glioblastoma cell migration. *Cancer Res.* **2006**, *66*, 11709–11717.
57. Chen, W.L.; Huang, X.Q.; Zhao, L.Y.; Li, J.; Chen, J.W.; Xiao, Y.; Huang, Y.Y.; Liu, J.; Wang, G.L.; Guan, Y.Y.; *et al*. Involvement of kv1.5 protein in oxidative vascular endothelial cell injury. *PLoS ONE* **2012**, *7*, e49758.
58. Aarts, M.; Iihara, K.; Wei, W.L.; Xiong, Z.G.; Arundine, M.; Cerwinski, W.; MacDonald, J.F.; Tymianski, M. A key role for trpm7 channels in anoxic neuronal death. *Cell* **2003**, *115*, 863–877.

Functional and Structural Characterization of FAU Gene/Protein from Marine Sponge *Suberites domuncula*

Dragutin Perina, Marina Korolija, Marijana Popović Hadžija, Ivana Grbeša, Robert Belužić, Mirna Imešek, Christine Morrow, Melanija Posavec Marjanović, Tatjana Bakran-Petricioli, Andreja Mikoč and Helena Ćetković

Abstract: Finkel-Biskis-Reilly murine sarcoma virus (FBR-MuSV) ubiquitously expressed (*FAU*) gene is down-regulated in human prostate, breast and ovarian cancers. Moreover, its dysregulation is associated with poor prognosis in breast cancer. Sponges (Porifera) are animals without tissues which branched off first from the common ancestor of all metazoans. A large majority of genes implicated in human cancers have their homologues in the sponge genome. Our study suggests that *FAU* gene from the sponge *Suberites domuncula* reflects characteristics of the *FAU* gene from the metazoan ancestor, which have changed only slightly during the course of animal evolution. We found pro-apoptotic activity of sponge FAU protein. The same as its human homologue, sponge FAU increases apoptosis in human HEK293T cells. This indicates that the biological functions of FAU, usually associated with "higher" metazoans, particularly in cancer etiology, possess a biochemical background established early in metazoan evolution. The ancestor of all animals possibly possessed FAU protein with the structure and function similar to evolutionarily more recent versions of the protein, even before the appearance of true tissues and the origin of tumors and metastasis. It provides an opportunity to use pre-bilaterian animals as a simpler model for studying complex interactions in human cancerogenesis.

Reprinted from *Mar. Drugs*. Cite as: Perina, D.; Korolija, M.; Hadžija, M.P.; Grbeša, I.; Belužić, R.; Imešek, M.; Morrow, C.; Marjanović, M.P.; Bakran-Petricioli, T.; Mikoč, A.; *et al*. Functional and Structural Characterization of FAU Gene/Protein from Marine Sponge *Suberites domuncula*. *Mar. Drugs* **2015**, *13*, 4179-4196.

1. Introduction

The evolution of cancer is still not fully understood. However, it is known that the genes of cellular cooperation that evolved along with multicellularity, when malfunctioned, contribute to cancer development [1]. The majority of these genes are involved not only in cell division and cell growth, but also in cell adhesion, apoptosis, developmental signaling pathways, recognition of self and non-self and differentiation of various cell types. All living animals descended from the 600 million year old common ancestor, including sponges and humans [2]. Sponges are the simplest animals, but despite the absence of tissues, their genomes contain a large majority of genes that have been implicated in human cancer [2]. However, the functions of these genes and biochemical characteristics of their products within the sponge cells remained largely unknown [3,4]. Tumors have not yet been identified in sponges, although computational studies have predicted that most metazoans might be prone to develop tumors [5]. Moreover, naturally occurring tumors have recently been described in two cnidarian species [6]. These findings suggest

that understanding of cancer associated genes in simpler animals without tissues and blood vessels could help in understanding the more complex interactions of their homologues in higher Metazoa.

Ribosome assembly is a complex process requiring coordinated activation of more than 200 non-ribosomal factors, including numerous small nucleolar RNAs (snoRNAs). Their role in modification of ribosomal RNAs (rRNAs) was shown to be essential for the correct assembly of the ribosome [7,8]. Three major classes of snoRNAs include: C/D box snoRNAs (primarily guide the 2′-*O*-methylation of target rRNAs), H/ACA box snoRNAs (typically guide pseudouridylation of target rRNAs) and small Cajal-body-specific RNAs (scaRNAs) (typically target snoRNAs). snoRNAs are believed to be the most ancient non-coding RNAs (ncRNAs) [9]. Many examples of ncRNAs displaying both snoRNA and microRNA (miRNA) characteristics suggest a possible evolution from one type to the other [10]. snoRNAs are nonautonomous transposable elements that can gain additional genomic copies, usually by a copy-and-paste mechanism involving an RNA intermediate. These snoRNA retroposons (snoRTs), like Alu element, use the LINE L1 machinery for their mobilization, and probably play an important role in evolution of mammalian genome [11].

Ribosomal proteins (RPs) are an evolutionarily conserved component of ribosome in every cell of every organism. Analysis of 66 complete genomes revealed that 34 RPs are common to all living organisms [12]. Many RPs possess additional extraribosomal functions in cells. They are involved in many processes within the ribosome system, surveillance of ribosome synthesis, but also in replication and regulation of cell growth, apoptosis and cancer [13]. Human *FAU* gene (Finkel-Biskis-Reilly murine sarcoma virus (FBR-MuSV) ubiquitously expressed) encodes the ribosomal protein S30 (RPS30) fused with an ubiquitin-like protein FUBI [14]. Retrovirus FBR-MuSV, which contains genes *v-fos* and *fox*, can induce osteosarcomas in susceptible mice [15]. *Fox* is an antisense sequence to the cellular gene *FAU*, which indicates a putative tumor suppressor role for FAU. Moreover, the *FAU* gene is down-regulated in human breast, prostate and ovarian tumors and its down-regulation is strongly associated with poor prognosis in breast cancer [16–18]. Pro-apoptotic regulatory role for FAU has recently been described [19]. Since the failure of apoptosis is fundamental to the development of many cancers, regulation of apoptosis may serve as the functional background for the extraribosomal function of this RP.

Our study suggests that *FAU* gene from the sponge *Suberites domuncula* probably reflects the characteristics of the *FAU* gene from metazoan ancestor that changed only slightly during animal evolution. FAU protein from sponge possesses pro-apoptotic activity and increases apoptosis in human HEK293T cells, same as its human homologue. This suggests that biological functions of FAU, usually associated with the origin of cancer in “higher” metazoans, possess biochemical background established early in metazoan evolution. Our results implicate that the ancestor of all animals possessed FAU protein with the structure and the function similar to its evolutionarily recent versions, even before the appearance of true tissues and the origin of tumors and metastasis.

2. Results and Discussion

2.1. Structure and Evolution of Metazoan FAU Gene

FAU gene encodes an ubiquitin-like protein (FUBI) fused to the ribosomal protein S30 (RPS30). This type of gene organization seems to be conserved throughout metazoan evolution (Figure 1A). Sponge FAU protein has 61% amino acid sequence identity (78% sequence similarity) with human FAU and is more similar to its homologues from human or rat, than to those from invertebrates *Caenorhabditis elegans* (47% sequence identity, 62% similarity) and *Drosophila melanogaster* (50% sequence identity, 68% similarity). Both invertebrate model organisms underwent recent accelerated evolution [20]. Since sponge FAU changed only slightly during metazoan evolution, it seems to be a promising candidate to effectively reflect FAU protein structure of the ancestral metazoan ribosome. It is also noteworthy that FUBI domain is much less conserved than RPS30. However, G–G dipeptide motif, which participates in bond formation between ubiquitin and lysine residues of target proteins, is conserved in all analyzed metazoans (Figure 1A). As already observed in human FAU, none of the lysine residues which serve as sites for polyubiquitin chain formation, are present in any of the analyzed FAU homologues (Figure 1A). This indicates that FUBI is unlikely to have an analogous role to ubiquitin in protein degradation and that this diverse role was probably established early in metazoan evolution.

Synchronized expression of ribosomal protein genes (RPGs), driven by the promoters of similar strength, ascertains equimolecular amount of ribosomal proteins in the cell, which is prerequisite for the ribosome assembly [21,22]. Human over-represented motifs in RPG promoters are identified as targets for YY1, NRF1, c-Myc and SP1 transcription factors [21]. The 5′-terminal oligopyrimidine (TOP) tract in human RP transcripts is also known to be essential for the control of gene expression, at both the transcriptional and the translational levels [23,24]. To test which elements are present in the *FAU* promoter, we compared over-represented motifs in RPG promoters of the sponge *Amphimedon queenslandica* with *FAU* sequence. In the majority of analyzed human RPG promoters, YY1 motifs were found downstream of the transcription start site (TSS) [25]. This motif is also present downstream in the sponge *FAU* ($p = 3.00 \times 10^{-7}$) (Figure 1B). Two SP1 and one NRF1 binding sites were found upstream of the TSS ($p = 4.08 \times 10^{-7}$, $p = 1.39 \times 10^{-7}$, $p = 7.10 \times 10^{-7}$, respectively), while E-box palindromic core CACGTG was also identified in *FAU* promoter ($p = 3.12 \times 10^{-6}$). Among many transcription factors that recognize the E-box, oncoprotein c-Myc (MYC) is known to bind to it [26]. c-Myc enhances ribosomal biogenesis by up-regulating transcription mediated by all three RNA polymerases [27]. This implies possible participation of the FAU protein in the analogous c-Myc-enhanced ribosomal biogenesis established early in metazoan evolution. The TSS was identified in TOP (Figure 1B). The TOP motif has a dual regulatory function in vertebrates. It is a part of a *cis*-regulatory element in transcriptional regulation and has a role at the translational level [23,24]. In certain physiological conditions, it inhibits binding of the translational regulatory proteins or the translational machinery to the mRNA [28]. The presence of TOP and all other elements in sponge *FAU* promoter indicates that the foundations of the human *FAU cis*-regulation were established early in metazoan evolution.

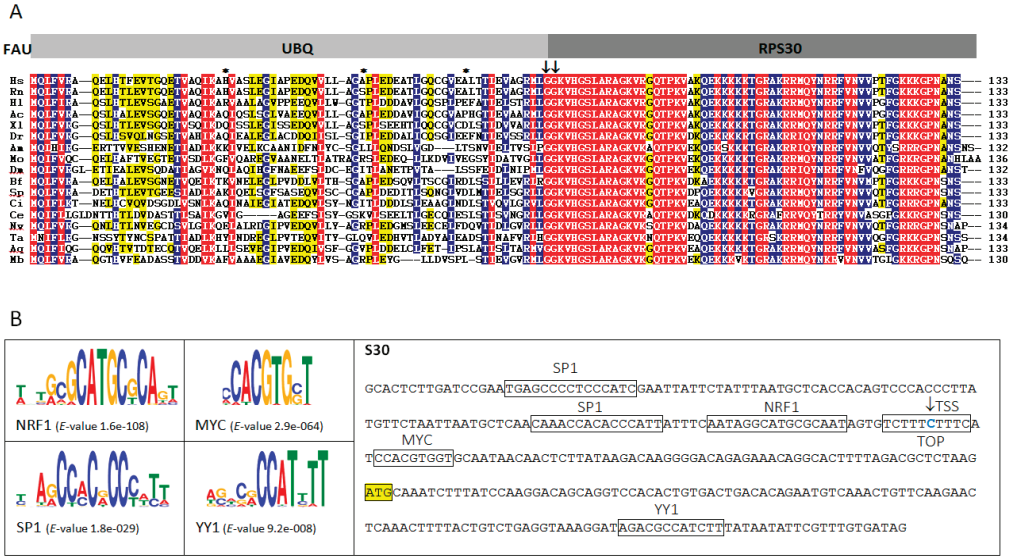

Figure 1. (**A**) Multiple sequence alignment of FAU proteins from representative species (*Homo sapiens* (Hs), *Rattus norvegicus* (Rn), *Haliaeetus leucocephalus* (Hl), *Anolis carolinensis* (Ac), *Xenopus laevis* (Xl), *Danio rerio* (Dr), *Apis mellifera* (Am), *Metaseiulus occidentalis* (Mo), *Drosophila melanogaster* (Dm), *Branchiostoma floridae* (Bf), *Strongylocentrotus purpuratus* (Sp), *Ciona intestinalis* (Ci), *Caenorhabditis elegans* (Ce), *Nematostella vectensis* (Nv), *Trichoplax adhaerens* (Ta), *Amphimedon queenslandica* (Aq), *Monosiga brevicollis* (Mb)). G–G dipeptide motif and missing lysine residues which serve as sites for polyubiquitin chain formation are marked with arrows and asterisks, respectively; red = 100%, blue = 80% and yellow = 60% identity; (**B**) Over-represented motifs in sponge ribosomal protein gene (RPG) promoters and promoter sequence of sponge *FAU* with indicated translational start site (marked with yellow rectangle), transcription start site (TSS, marked with arrow) and transcription factor binding sites and terminal 5′-terminal oligopyrimidine (TOP) tract (marked with rectangles).

Multiple sequence alignment of *FAU* gene orthologues was used to characterize intron dynamics by comparing the intron positions (Figure 2). Most of the positions, phases, and the number of introns in *FAU* genes were not significantly changed from sponge to human (Figure 2). The most conserved intron position separates the UBQ from RPS30 domain in *FAU* and varies from 25 to 3339 bp. The average value of sponge RPG intron length is 164 bp [29], while human RPGs have significantly longer introns, with the average length of 760 bp [30]. Transposable element insertions play an important role in the evolution of intron size [31]. Therefore, we searched for over-represented elements in *FAU* introns.

2.2. Identification of snoRNAs in FAU Introns of Sponges

The accumulating genomic data strongly confirm the tendency of snoRNAs to colonize RPGs and ribosome related genes in eukaryotes [32]. The total set of 16 introns in *FAU* gene from eight sponges produced four candidate H/ACA snoRNAs. After a more detailed analysis, we were able to identify three snoRNAs that match a sequence motif of known snoRNAs available on Rfam, the snOPY database and the snoRNA-LBME database. This snoRNA is the sponge orthologue of the human SNORA62 (E2) (Figure 3A). SNORA62 is predicted to guide the pseudouridylation of uridine residues at the position 3830 and 3832 in human 28S rRNA [33]. This target sequence of 28S rRNA is highly conserved between human and analyzed sponges (Figure 3B). The sponge SNORA62 pseudouridylation guide sequence, as well as the H- and ACA-boxes, are also well conserved (Figure 3A). Its expression was verified experimentally (Figure 3C). Phylogenetic analysis of SNORA62/SNORA6 is presented in Figure 3D. The SNORA62 and SNORA6 share the same host gene in vertebrates and SNORA6 probably arose by *cis*-duplication of SNORA62. The SNORA62 homologues from sponges clearly group together and reflect the characteristics of snoRNA ancestral to this snoRNA family, before the duplications and diversifications within the metazoan lineage. snoRNAs are mobile genetic elements, often transferred through retrotransposition, and can therefore participate in diversification and enrichment of transcriptomes through various mechanisms such as intron/exon gain/loss [34]. It is known that snoRNAs can change their genomic location within relatively short vertebrate evolutionary time scales [35]. Since all of examined RPG intron positions were conserved in three *Suberites* species, it was presumed that on this shorter evolutionary time scale, mobility of snoRNAs is not a significant factor that determines intron dynamics [29]. However, we found that within the same genus (*Suberites*), SNORA62 can change its genomic location. In *S. pagurorum*, *S. domuncula* and *S. ficus* this snoRNA is present in the same intron, but apparently is missing in the same conserved intron in *S. massa* (Figure 2). Our results indicate that RPG introns are more dynamic than previously documented and that mobility of snoRNAs plays an important role in RPG (and *FAU*) evolution even on shorter evolutionary time scales.

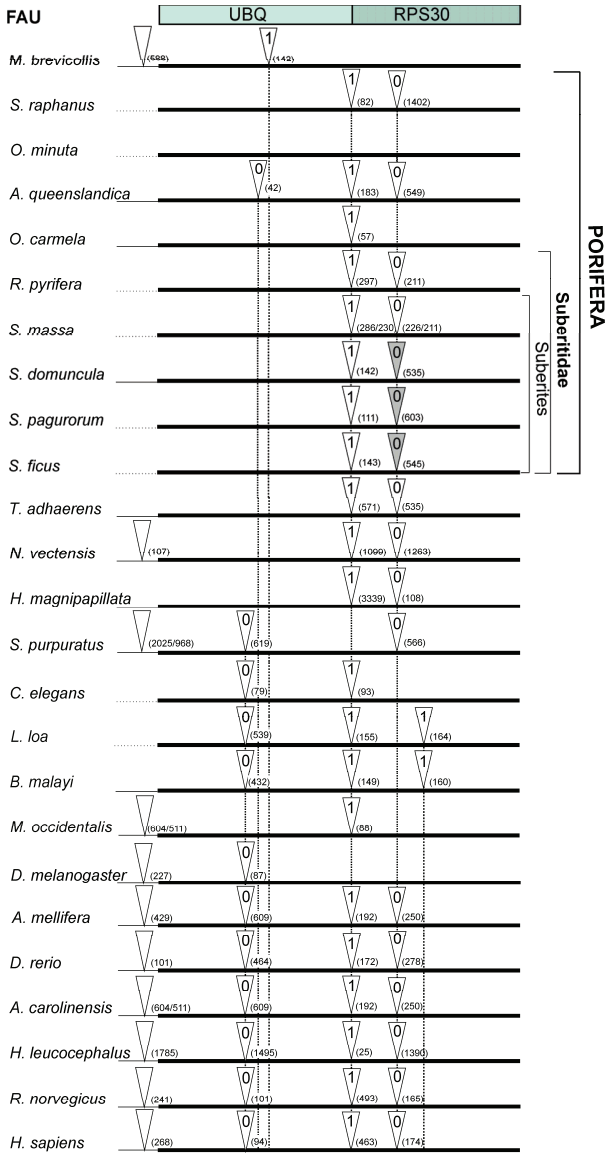

Figure 2. Intron-mapping of *FAU* genes from representative species. White triangles indicate positions of the introns and gray triangles indicate presence of SNORA62. The number within triangle denotes the intron phase and the number in brackets intron length. The thin line indicates the 5′ UTR region.

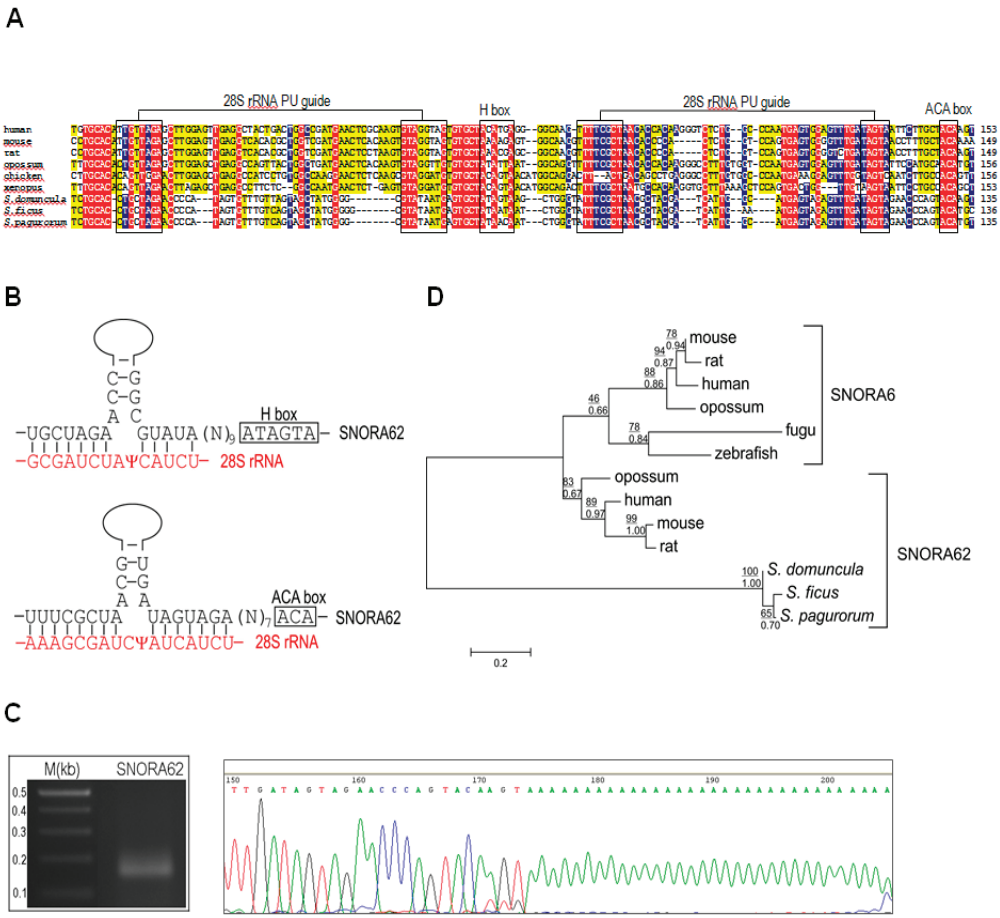

Figure 3. (**A**) SNORA62 conserved in the last introns of the *FAU* gene in *S. domuncula*, *S. ficus* and *S. pagurorum*. All essential snoRNA elements are conserved and a putative pseudouridylation (PU) guide site is designated; red = 100%, blue = 80% and yellow = 60% identity; (**B**) Target sites of SNORA62 are conserved in sponges and marked with psi; (**C**) Experimental verification of transcription of sponge SNORA62. Polyadenylated snoRNAs were amplified, cloned and sequenced; (**D**) Maximum likelihood (ML) phylogenetic tree of snoRNAs from representative species. Bootstrap values for ML are given above and MCMC below the line. The scale bar indicates the genetic distance of the branch lengths.

The other snoRNA shows stable secondary structure with conserved snoRNA parts (Figure S1). In the first intron of FAU gene of the sponge *Rhizaxinella pyrifera*, a single snoRNA with a potential target rRNA was found (Figure S1). This target is not conserved in humans nor has it yet been described as a pseudouridylation site, so we can only speculate about the possible function of this snoRNA.

2.3. Subcellular Localization of Sponge FAU

RPs are mainly cytoplasmic, being incorporated into translating ribosomes, but they can be found, at least transiently, in the nucleus [36]. As mentioned before, RPs have non-ribosomal functions when they are off-ribosomal subunits. We transiently transfected HEK293T and HeLa cells with GFP-FAU from *S. domuncula* and DsRed-FAU from human and analyzed the cells 48 hours post transfection using confocal laser scanning microscopy. Proteins show the same localization pattern in both cell types. Both human and sponge proteins exhibit the same subcellular localization (Figure 4A). Proteins are dispersed throughout the cytoplasm rather than being associated with a specific cytoplasmic organelle (Figure 4B,C). Although the signals are present mainly in the cytoplasm, portions can also be clearly observed in the nuclei (Figure 4A). This result matches the finding of the previous study, where subcellular localization of *Drosophila* RPS30 was analyzed [36]. It has been observed that a fraction of RPS30 is localized in the nucleus and is associated with transcription sites. We presume that, according to cellular localization, extraribosomal functions of FAU at transcription sites were already present in ancestor of all metazoans and remained conserved throughout the evolution.

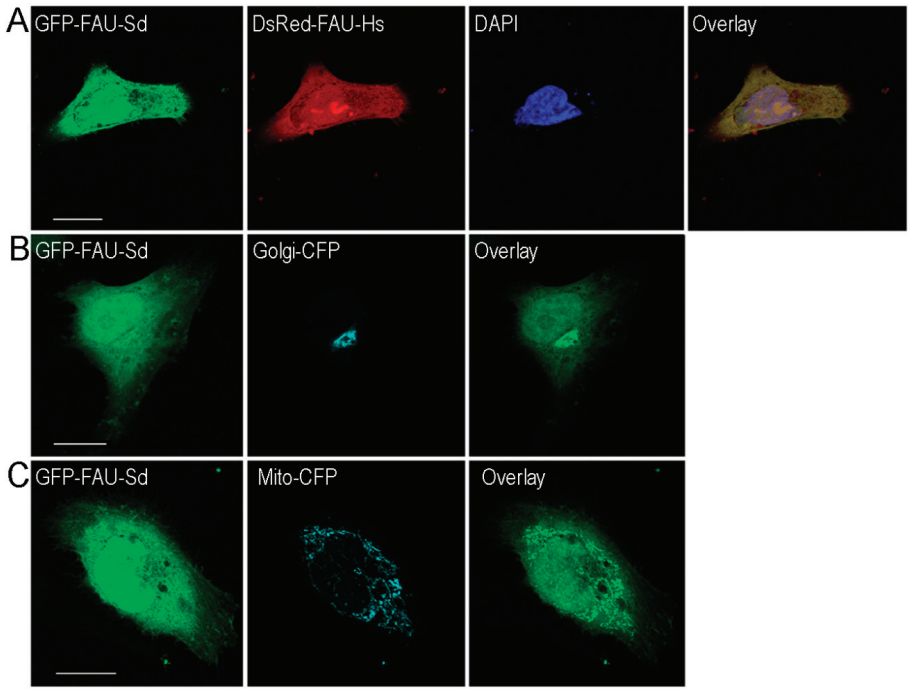

Figure 4. (**A**) Subcellular localization of sponge and human FAU. HeLa cells transiently transfected with sponge (Sd) pEGFP-FAU (green fluorescence), human (Hs) pDsRed-FAU (red fluorescence); (**B**) pECFP-Golgi (cyan) and (**C**) pECFP-mitochondria (cyan). The overlay (yellow) shows colocalization of the human and sponge homologs in panel **A**. Scale bar = 10 μm.

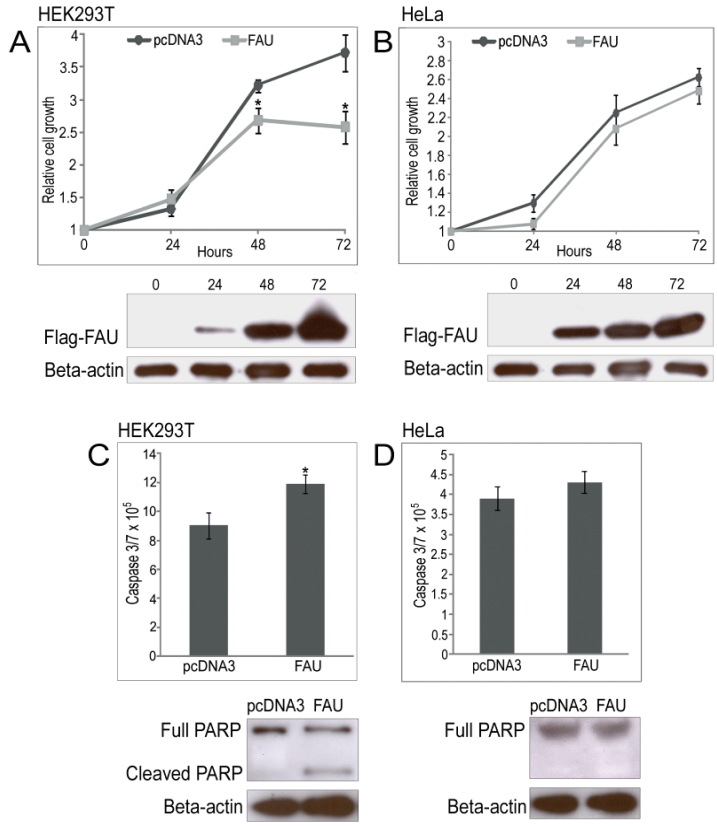

Figure 5. Protein blot validation of sponge Flag-FAU expression and the relative growth rates assessed by CellTiter-Glo assay of HEK293T (**A**) and HeLa cells (**B**); Activities of caspase were measured by a Caspase-Glo 3/7 assay kit and by cleavage of caspase substrate PARP in HEK293T (**C**) and HeLa cells (**D**) transfected with pcDNA3-FAU or empty vector pcDNA3. Data are representative of three independent experiments (***** $p < 0.05$).

2.4. Overexpression of Sponge FAU in Human Cell Lines

Transient transfection with human pcDNA3-FAU increased apoptosis and decreased short-term cell viability in HEK293T, Jurkat and CEM cell lines [19]. To test whether these functions of FAU protein were established early in metazoan evolution, we transfected HEK293T and HeLa cell lines with sponge pcDNA3-FAU. The growth rate of cells was evaluated at different time points after transfection, to determine whether overexpression of sponge FAU affects cell proliferation. Transfection markedly increased Flag-FAU levels (Figure 5A,B). Empty vector pcDNA3 was used as control. Subsequently, the proliferation of pcDNA3-FAU-transfected HEK293T cells was decreased 1.44-fold ($p = 0.008$) when compared to cells with pcDNA3 control (Figure 5A). Cell viability decreased by 30.1% 72 h post-transfection compared to cells possessing the control

vector. Interestingly, these effects were not observed in HeLa cancer cell line (Figure 5A). To further investigate the mechanism underlying the observed, we measured caspase-3 and -7 activities in transfected cell lines. pcDNA3-FAU-transfected HEK293T cells show 1.31-fold (p = 0.014) increased caspase activity as compared to pcDNA3 transfected cells (Figure 5C). However, apoptotic cells were not elevated in HeLa cell line, and neither the cleavage of PARP, caspase-3 substrate, was observed (Figure 5D). Interestingly, similar results were obtained when human Flag-FAU was overexpressed in HeLa cells (Figure S2). Our results indicate that pro-apoptotic activity of FAU was established early in metazoan evolution, but appears to be cell type specific as its expression leads to efficient apoptosis in HEK293T but not in HeLa cell line. Since both human and sponge FAU do not activate caspases in HeLa cells significantly, but both activate caspases in HEK293T cells, we believe that the mechanism underlying this effect was already present in metazoan ancestor. It was proposed that Bcl-G plays an essential down-stream role in mediating the pro-apoptotic activity of FAU [19]. The molecular mechanisms of apoptosis regulation by FAU remain to be elucidated, but possibly include FUBI-mediated targeting of Bcl-G and/or modulation of the interaction of Bcl-G with other constituents of the cellular apoptotic machinery (caspases for example) [19]. Although down-regulation of Bcl-G inhibits apoptosis induced by FAU, basal apoptosis rates are higher in certain cellular contexts [19]. However, this effect has not been observed in human breast cancer and prostate cell lines [16,17]. This indicates that in certain cell lines, Bcl-G can have anti-apoptotic effects, in addition to the pro-apoptotic activity. Moreover, mouse Bcl-G is expressed in a range of epithelial, as well as in dendritic cells and its loss does not appear to affect any of these cell types [37]. This intriguing contrast in the effects of FAU/Bcl-G on cell fate in different cellular contexts presents attractive possibilities for the development of novel therapies for cancers and could be used for targeted elimination of cancer cells.

From all presented data we can conclude that the structure and the functions of the recent *FAU* gene were established early in metazoan lineage. Tumor suppressor gene function of FAU probably arose before tumor appearance. As sponges do not possess tissues and organs, formation of tumors within them is unlikely. It seems that tumors evolved in parallel with the development of true tissues and organs, yet the extraribosomal functions of RPs were probably established in the metazoan ancestor well before the Cambrian explosion, *i.e.*, before the appearance of diverse groups of multicellular animals. Other highly sophisticated extraribosomal functions of RPs, involved in the origin of cancer and metastasis, evolved together with the appearance of different cell types, tissues and organs. Whereas synchronized *cis*-regulation of RPGs needs to be conserved for equimolecular presence of RPs in the metazoan cell, the evolution of RPGs together with the extraribosomal functions of RPs on shorter evolutionary time scale is probably driven by snoRNAs. snoRNAs can promote, but also suppress tumor development [38]. Numerous studies already provided evidence for the functional importance of snoRNAs in cancerogenesis [39,40]. Our results show that SNORA62 is found in *FAU* gene in the subset of sponges from the genus *Suberites*, which suggests its dynamic and fast evolving nature. This snoRNA is located in the human ribosomal protein gene *SA* (*RPSA*). Both host RPGs possess an extraribosomal function involved in the maintenance of cellular viability through the caspase-dependent regulation of

apoptosis [19,41]. Interestingly, *SNORA62* is the most upregulated gene in diallyl sulfide (DAS)-induced apoptosis in HeLa cells, as a part of p53, mitochondria- and caspase- pathways [42]. It would be interesting to test whether this snoRNA can act as an oncogene like SNORA42 [43], or tumor suppressor like U50 snoRNA [44] and if these functions interfere and modulate similar functions of its host genes. The number of ncRNA is exceedingly lower in basal metazoans than in "higher" animals, which may indicate that metazoan complexity correlates with an increasing number of ncRNAs [45]. If SNORA62 can modulate apoptotic effect of its host genes, it will provide new strategies for targeting FAU. In the longer term, the development of techniques for the manipulation of snoRNAs may also be productively directed towards the manipulation of genes involved in cancerogenesis for cancer therapy. Analyses of sponge FAU gene presented in our paper provides the opportunity to determine direction for further investigation of FAU and evaluate its potential for cancer treatment. Undoubtedly, sponges could be used as an informative model in cancer research, not only in terms of targeting genes involved in cancerogenesis by snoRNAs, but also in targeting snoRNAs themselves. In order to evaluate their potential for cancer treatment, further investigation of highly conserved and mobile snoRNAs found in the metazoan common ancestor is needed.

3. Experimental Section

3.1. Materials

Live specimens of the sponge *Suberites domuncula* (Porifera, Demospongiae, Tetractinomorpha, Hadromerida, Suberitidae) and *Sycon raphanus* (Porifera, Calcarea, Calcaronea, Leucosolenida, Sycettidae) were collected in the Northern Adriatic Sea near Rovinj, Croatia, and stored at −80 °C. Specimens of *Oopsacas minuta* (Porifera, Hexactinellida, Hexasterophora, Lyssacinosida, Leucopsacidae) were collected in the cold water pit in the Middle Adriatic and specimens of *Rhizaxinella pyrifera* (Porifera, Demospongiae, Tetractinomorpha, Hadromerida, Suberitidae) were collected in the Middle Adriatic Pit, around 200 m depth and stored in 96% EtOH. *Suberites ficus* and *Suberites pagurorum* were collected in Ireland, while *Suberites massa* in the English Channel.

3.2. Sequence Analyses

Homology searches and sequence retrievals were done using BLAST (NCBI, NIH, Bethesda, MD, USA: http://www.ncbi.nlm.nih.gov). Sequences were analyzed using Lasergene (DNAStar, Madison, WI, USA). Multiple sequence alignments (MSA) were performed with CLUSTALX [46]. The exact position and the phase of each intron were verified by manual inspection and statistical data were extracted from GeneDoc (http://www.psc.edu/biomed/genedoc).

Over-represented motifs were searched using MEME [47], as described earlier [22]. Statistical significance of the motif (*E*-value) and *p*-value (statistical significance of predicted sites in *FAU*) were extracted from MEME. The location of transcription factor binding sites relative to the transcription start site was also extracted from MEME results for *FAU* sequence within a set of

sequences with the same identified motif. Obtained motifs were then compared using TOMTOM [48] against the TRANSFAC database of known motifs [49].

3.3. Isolation of Genomic DNA and Sequencing of FAU Gene

For genomic DNA preparation, sponge specimens were cut into pieces, frozen in liquid nitrogen and grounded to fine powder from which total DNA was isolated using the Genomic DNA Purification kit (QIAGEN, Redwood City, CA, USA). Sponge *FAU* gene was amplified by PCR, using LA Taq DNA polymerase (Takara, Japan) and primers specific for ends of the coding sequence of: Demospongiae (5′-GCAAGTTTTCGTACAAGGAGGGGC-3′ and 5′-GGTGCATTTGAGTTTGGTCCAC-3′), Hexactinellida (5′-ATGCAAGTGTTTGCACAAAC-3′ and 5′-CTAACTAGCTGAGTTTGAG-3′) and Calcarea (5′-CAGATTTTCATTCAGGCCCAGGC-3′ and 5′-GCGTTAGAGTTGGGTC-3′). The amplified fragments were separated on a 0.8% agarose gel, purified and cloned into the pGEM-T vector (Promega, Madison, WI, USA). Positive clones were sequenced using T7/pUC primers.

3.4. Isolation and Characterization of Small RNAs

snoSeeker was used to identify snoRNAs in introns of *FAU* genes [50]. Rfam [51], snOPY (http://snoopy.med.miyazaki-u.ac.jp/) and the snoRNA-LBME databases [52] were used to check whether snoRNAs match to any of the known snoRNAs' motifs. The secondary structure of snoRNA was computed using the RNAfold program of the Vienna RNA Package [53]. Isolation of small RNAs from sponge was described previously [29]. In brief, fresh specimens of *S. domuncula* were cut into pieces, frozen in liquid nitrogen and grounded to a fine powder. mirPremier microRNA Isolation Kit (Sigma, St. Louis, MO, USA) was used, according to the manufacturer's protocol for plant tissue. Polyadenylation was performed by incubation with *E. coli* Poly(A) Polymerase (BioLabs). Poly(A) tailing reaction mixture was then reverse transcribed using the SuperScript II Reverse Transcriptase (Invitrogen, Waltham, MA, USA) and a modified poly-d(T) primer (5′-GCGTAAGTGACTAGCGTGTTTTTTTTTTTTVN-3′). The resulting cDNA was used for PCR with a reverse primer (5′-GCGTAAGTGACTAGCGTG-3′) and forward primer specific for predicted SNORA62 (5′-CCCCATAGTGTTTGTTAGTAGC-3′). The product was cloned into the pGEM-T vector (Promega). Positive clones were sequenced using the ABI PRISM BigDye Terminator v3.1 Ready Reaction Cycle Sequencing Kit and T7/pUC primers.

For phylogenetic analyses, multiple alignments were performed with CLUSTALW Ver. 1.6 [54]. Aligned sequences were imported into MEGA version 6 [55], and analyzed by Maximum Likelihood (ML), while the Bayesian MCMC analysis was conducted in MrBayes v. 3.1.2. [56]. Bootstrap tests were performed with 1000 replicates. The model for ML analysis was selected using Modeltest 3.7 and the Akaike Information Criterion (AIC) [57], which indicated Hasegawa-Kishino-Yano model (I + G) [58].

3.5. Cell Culture

Human HeLa cell line (ATCC) and HEK293T cell line were cultured in L-glutamine DMEM (Invitrogene) supplemented with 10% fetal bovine serum (FBS, Invitrogene) and GA-1000 (30 mg/mL Gentamicin and 15 µg/mL Amphotericin) (Lonza, Basel, Switzerland) at a 1:1000 ratio in humidified chamber with 5% CO_2 at 37 °C.

3.6. Plasmid Constructions

Eukaryotic expression vector pcDNA3 (Invitrogen) was digested with BamHI and EcoRI. The insert containing the FLAG sequence and sponge FAU was cloned using these sets of primers: 5′-GTCTAGGGATCCACGAGATGGACTACAAGGACGACGACGATAAGATGCAAGTTTTCGTA-3′ and 5′-CTAGACGAATTCTCATCACTGAGGTGCATTTG-3′, and human FAU using: 5′-GTCTAGGGATCCACGAGATGGACTACAAGGACGACGACGATAAGATGCAGCTCTTTGTC-3′ and 5′-CTAGACGAATTCTTATTAAGAGTTGGCATTGG-3′ For localization assay, sponge FAU was cloned in fusion with GFP using pEGFP-C1 (XhoI/BamHI restriction sites) with the following set of primers: 5′-CCACTCGAGCTATGCAAGTTTTCGTACAAGG-3′ and 5′-GACGGATCCTCATCACTGAGGTGCATTTG-3′, and human using pDsRed-C1 with 5′-CCACTCGAGCTATGCAGCTCTTTGTCCGCGC-3′ and 5′-ACAGGATCCTTAAGAGTTGGCATTGGGGCCC-3′ set of primers.

3.7. Transient Transfections and Laser Scanning Confocal Microscopy

Lipofectamine 3000 reagent (Invitrogen) was used for HeLa cells transfections, according to the manufacturer's instructions. Twenty four hours before transfection 5×10^4 cells were seeded onto 24-well culture slides containing DMEM supplemented with 10% FBS to obtain 80% confluence. Cells were transfected with 500 ng of plasmid DNA. Forty eight hours post transfection, the cells were washed with PBS pH 7.5, fixed in 4% formaldehyde, and mounted in SlowFade Diamond Antifade Mountant with or without DAPI (Molecular Probes, Waltham, MA, USA).

Fluorescent images were obtained by Leica SP8 X FLIM laser scanning confocal microscopy equipped with HC PL APO CS2 63×/1.40 OIL objective. GFP was excited by 488 nm laser line, CFP using 433 nm, DAPI using 405 nm and DsRed at 560 nm laser lines.

3.8. Immunoblotting

The cell lysates were loaded on SDS-PAGE and electrotransferred to a PVDF Hybond-P membrane (Amersham Biosciences, Piscataway, NJ, USA). The membranes were incubated with anti-FLAG M2 antibody (1:5000) (Sigma) for detection of FLAG-FAU or anti-PARP antibody (1:5000) (ab137653). Protein bands were visualized using chemiluminescence detection (Amersham ECL Plus, GE Healthcare, Parramatta, Australia).

3.9. Cell Viability Assay

HeLa cells were transfected as described above, trypsinized 24 h post-transfection and 10^3 viable cells suspended in 100 µL 10% FBS DMEM were added to each well of 96-well plates. HEK293T cells were transfected using standard calcium phosphate method [59]. Cell proliferation was measured using CellTiter-Glo Luminescent Cell Viability Assay (Promega) according to the manufacturer's instructions with luminometer Infinite 200 (TECAN). Concentration of ATP was measured in triplicate.

3.10. Apoptosis Assay

Cells were transfected as described above, trypsinized 24 h post-transfection and 5×10^3 viable cells suspended in 100 µL 10% FBS DMEM were seeded in 96-well culture plates. Caspase-3/7 activity was measured using the Caspase-Glo 3/7 Assay Kit (Promega) according to the manufacturer's instructions with luminometer Infinite 200 (TECAN).

3.11. Statistical Analyses

Statistical analysis was performed using Student's *t*-test. Probabilities of less than 0.05 were considered statistically significant.

Acknowledgment

This work was supported by the Unity through Knowledge Fund (grant number UKF 1B 2/13) (Andreja Mikoč), Croatian Ministry of Science, Education and Sports grant 098-0982913-2478 (Helena Ćetković) and FP7-REGPOT-2012-2013-1, Grant Agreement Number 316289-InnoMol.

Tatjana Bakran-Petricioli is grateful to Marco Taviani, National Research Council Research Director at ISMAR Institute of Marine Sciences, Bologna, Italy for providing her opportunity to participate in the ARCO (AdRiatic COrals) cruise (13–22 December 2008; in the scope of HERMES Hotspot Ecosystem Research on the Margins of the European Seas project) aboard Research Vessel Urania, for which he was the scientific leader.

Author Contributions

Live specimens of the sponges were obtained by Christine Morrow and Tatjana Bakran-Petricioli. Andreja Mikoč, Helena Ćetković and Dragutin Perina carried out the molecular genetic studies and the sequence analyses. Andreja Mikoč, Marina Korolija, Christine Morrow, Mirna Imešek, Melanija Posavec Marjanović and Dragutin Perina participated in genomic DNA preparation, sequencing and cloning of FAU. Marina Korolija, Marijana Popović Hadžija, Ivana Grbeša, Robert Belužić and Dragutin Perina carried out colocalization, proliferation, caspase assays. Andreja Mikoč, Helena Ćetković and Dragutin Perina conceived and oversaw the project. Marina Korolija, Andreja Mikoč, Helena Ćetković and Dragutin Perina wrote the manuscript. All authors read and approved the final manuscript.

Conflicts of Interest

The authors declare no conflict of interest.

References

1. Davies, P.C.; Lineweaver, C.H. Cancer tumors as Metazoa 1.0: Tapping genes of ancient ancestors. *Phys. Biol.* **2011**, *8*, 015001.
2. Srivastava, M.; Simakov, O.; Chapman, J.; Fahey, B.; Gauthier, M.E.; Mitros, T.; Richards, G.S.; Conaco, C.; Dacre, M.; Hellsten, U.; *et al*. The *Amphimedon queenslandica* genome and the evolution of animal complexity. *Nature* **2010**, *466*, 720–726.
3. Perina, D.; Bosnar, M.H.; Bago, R.; Mikoc, A.; Harcet, M.; Dezeljin, M.; Cetkovic, H. Sponge non-metastatic Group I NME gene/protein-structure and function is conserved from sponges to humans. *BMC Evol. Biol.* **2011**, *11*, 87.
4. Perina, D.; Bosnar, M.H.; Mikoc, A.; Muller, W.E.; Cetkovic, H. Characterization of NME6-like gene/protein from marine sponge Suberites domuncula. *Naunyn Schmiedeberg Arch. Pharmacol.* **2011**, *384*, 451–460.
5. Domazet-Loso, T.; Tautz, D. Phylostratigraphic tracking of cancer genes suggests a link to the emergence of multicellularity in metazoa. *BMC Biol.* **2010**, *8*, 66.
6. Domazet-Loso, T.; Klimovich, A.; Anokhin, B.; Anton-Erxleben, F.; Hamm, M.J.; Lange, C.; Bosch, T.C. Naturally occurring tumours in the basal metazoan Hydra. *Nat. Commun.* **2014**, *5*, 4222.
7. Perry, R.P. Balanced production of ribosomal proteins. *Gene* **2007**, *401*, 1–3.
8. Kressler, D.; Hurt, E.; Bassler, J. Driving ribosome assembly. *Biochim. Biophys. Acta* **2010**, *1803*, 673–683.
9. Gardner, P.P.; Bateman, A.; Poole, A.M. SnoPatrol: How many snoRNA genes are there? *J. Biol.* **2010**, *9*, 4.
10. Scott, M.S.; Ono, M. From snoRNA to miRNA: Dual function regulatory non-coding RNAs. *Biochimie* **2011**, *93*, 1987–1992.
11. Weber, M.J. Mammalian small nucleolar RNAs are mobile genetic elements. *PLoS Genet.* **2006**, *2*, e205.
12. Lecompte, O.; Ripp, R.; Thierry, J.C.; Moras, D.; Poch, O. Comparative analysis of ribosomal proteins in complete genomes: An example of reductive evolution at the domain scale. *Nucleic Acids Res.* **2002**, *30*, 5382–5390.
13. Warner, J.R.; McIntosh, K.B. How common are extraribosomal functions of ribosomal proteins? *Mol. Cell* **2009**, *34*, 3–11.
14. Kas, K.; Michiels, L.; Merregaert, J. Genomic structure and expression of the human *FAU* gene: Encoding the ribosomal protein S30 fused to a ubiquitin-like protein. *Biochem. Biophys. Res. Commun.* **1992**, *187*, 927–933.
15. Michiels, L.; van der Rauwelaert, E.; van Hasselt, F.; Kas, K.; Merregaert, J. FAU cDNA encodes a ubiquitin-like-S30 fusion protein and is expressed as an antisense sequence in the Finkel-Biskis-Reilly murine sarcoma virus. *Oncogene* **1993**, *8*, 2537–2546.

16. Pickard, M.R.; Green, A.R.; Ellis, I.O.; Caldas, C.; Hedge, V.L.; Mourtada-Maarabouni, M.; Williams, G.T. Dysregulated expression of FAU and MELK is associated with poor prognosis in breast cancer. *Breast Cancer Res.* **2009**, 11, R60.
17. Pickard, M.R.; Edwards, S.E.; Cooper, C.S.; Williams, G.T. Apoptosis regulators FAU and Bcl-G are down-regulated in prostate cancer. *Prostate* **2010**, *70*, 1513–1523.
18. Moss, E.L.; Mourtada-Maarabouni, M.; Pickard, M.R.; Redman, C.W.; Williams, G.T. FAU regulates carboplatin resistance in ovarian cancer. *Genes Chromosomes Cancer* **2010**, *49*, 70–77.
19. Pickard, M.R.; Mourtada-Maarabouni, M.; Williams, G.T. Candidate tumour suppressor FAU regulates apoptosis in human cells: An essential role for Bcl-G. *Biochim. Biophys. Acta* **2011**, *1812*, 1146–1153.
20. Alba, M.M.; Castresana, J. Inverse relationship between evolutionary rate and age of mammalian genes. *Mol. Biol. Evol.* **2005**, *22*, 598–606.
21. Roepcke, S.; Zhi, D.; Vingron, M.; Arndt, P.F. Identification of highly specific localized sequence motifs in human ribosomal protein gene promoters. *Gene* **2006**, *365*, 48–56.
22. Perina, D.; Korolija, M.; Roller, M.; Harcet, M.; Jelicic, B.; Mikoc, A.; Cetkovic, H. Over-represented localized sequence motifs in ribosomal protein gene promoters of basal metazoans. *Genomics* **2011**, *98*, 56–63.
23. Meyuhas, O. Synthesis of the translational apparatus is regulated at the translational level. *Eur. J. Biochem.* **2000**, *267*, 6321–6330.
24. Shibui-Nihei, A.; Ohmori, Y.; Yoshida, K.; Imai, J.; Oosuga, I.; Iidaka, M.; Suzuki, Y.; Mizushima-Sugano, J.; Yoshitomo-Nakagawa, K.; Sugano, S. The 5′ terminal oligopyrimidine tract of human elongation factor *1A-1* gene functions as a transcriptional initiator and produces a variable number of US at the transcriptional level. *Gene* **2003**, *311*, 137–145.
25. Perry, R.P. The architecture of mammalian ribosomal protein promoters. *BMC Evol. Biol.* **2005**, *5*, 15.
26. Van Riggelen, J.; Yetil, A.; Felsher, D.W. MYC as a regulator of ribosome biogenesis and protein synthesis. *Nat. Rev. Cancer* **2010**, *10*, 301–309.
27. Oskarsson, T.; Trumpp, A. The Myc trilogy: Lord of RNA polymerases. *Nat. Cell Biol.* **2005**, *7*, 215–217.
28. Yamashita, R.; Suzuki, Y.; Takeuchi, N.; Wakaguri, H.; Ueda, T.; Sugano, S.; Nakai, K. Comprehensive detection of human terminal oligo-pyrimidine (*TOP*) genes and analysis of their characteristics. *Nucleic Acids Res.* **2008**, *36*, 3707–3715.
29. Perina, D.; Korolija, M.; Mikoc, A.; Roller, M.; Plese, B.; Imesek, M.; Morrow, C.; Batel, R.; Cetkovic, H. Structural and functional characterization of ribosomal protein gene introns in sponges. *PLoS ONE* **2012**, *7*, e42523.
30. Yoshihama, M.; Uechi, T.; Asakawa, S.; Kawasaki, K.; Kato, S.; Higa, S.; Maeda, N.; Minoshima, S.; Tanaka, T.; Shimizu, N.; *et al*. The human ribosomal protein genes: Sequencing and comparative analysis of 73 genes. *Genome Res.* **2002**, *12*, 379–390.
31. Sela, N.; Kim, E.; Ast, G. The role of transposable elements in the evolution of non-mammalian vertebrates and invertebrates. *Genome Biol.* **2010**, *11*, R59.

32. Dieci, G.; Preti, M.; Montanini, B. Eukaryotic snoRNAs: A paradigm for gene expression flexibility. *Genomics* **2009**, *94*, 83–88.
33. Ganot, P.; Caizergues-Ferrer, M.; Kiss, T. The family of box ACA small nucleolar RNAs is defined by an evolutionarily conserved secondary structure and ubiquitous sequence elements essential for RNA accumulation. *Genes Dev.* **1997**, *11*, 941–956.
34. Luo, Y.; Li, S. Genome-wide analyses of retrogenes derived from the human box H/ACA snoRNAs. *Nucleic Acids Res.* **2007**, *35*, 559–571.
35. Bompfunewerer, A.F.; Flamm, C.; Fried, C.; Fritzsch, G.; Hofacker, I.L.; Lehmann, J.; Missal, K.; Mosig, A.; Muller, B.; Prohaska, S.J.; *et al*. Evolutionary patterns of non-coding RNAs. *Theory Biosci.* **2005**, *123*, 301–369.
36. Brogna, S.; Sato, T.A.; Rosbash, M. Ribosome components are associated with sites of transcription. *Mol. Cell* **2002**, *10*, 93–104.
37. Giam, M.; Okamoto, T.; Mintern, J.D.; Strasser, A.; Bouillet, P. Bcl-2 family member Bcl-G is not a proapoptotic protein. *Cell Death Dis.* **2012**, *3*, e404.
38. Williams, G.T.; Farzaneh, F. Are snoRNAs and snoRNA host genes new players in cancer? *Nat. Rev. Cancer* **2012**, *12*, 84–88.
39. Mannoor, K.; Liao, J.; Jiang, F. Small nucleolar RNAs in cancer. *Biochim. Biophys. Acta* **2012**, *1826*, 121–128.
40. Esteller, M. Non-coding RNAs in human disease. *Nat. Rev. Genet.* **2011**, *12*, 861–874.
41. Moodley, K.; Weiss, S.F. Down-regulation of the non-integrin laminin receptor reduces cellular viability by inducing apoptosis in lung and cervical cancer cells. *PLoS ONE* **2013**, *8*, e57409.
42. Wu, P.P.; Chung, H.W.; Liu, K.C.; Wu, R.S.; Yang, J.S.; Tang, N.Y.; Lo, C.; Hsia, T.C.; Yu, C.C.; Chueh, F.S.; *et al.* Diallyl sulfide induces cell cycle arrest and apoptosis in HeLa human cervical cancer cells through the p53, caspase- and mitochondria-dependent pathways. *Int. J. Oncol.* **2011**, *38*, 1605–1613.
43. Mei, Y.P.; Liao, J.P.; Shen, J.; Yu, L.; Liu, B.L.; Liu, L.; Li, R.Y.; Ji, L.; Dorsey, S.G.; Jiang, Z.R.; *et al*. Small nucleolar RNA 42 acts as an oncogene in lung tumorigenesis. *Oncogene* **2012**, *31*, 2794–2804.
44. Dong, X.Y.; Rodriguez, C.; Guo, P.; Sun, X.; Talbot, J.T.; Zhou, W.; Petros, J.; Li, Q.; Vessella, R.L.; Kibel, A.S.; *et al.* SnoRNA U50 is a candidate tumor-suppressor gene at 6q14.3 with a mutation associated with clinically significant prostate cancer. *Hum. Mol. Genet.* **2008**, *17*, 1031–1042.
45. Grimson, A.; Srivastava, M.; Fahey, B.; Woodcroft, B.J.; Chiang, H.R.; King, N.; Degnan, B.M.; Rokhsar, D.S.; Bartel, D.P. Early origins and evolution of microRNAs and Piwi-interacting RNAs in animals. *Nature* **2008**, *455*, 1193–1197.
46. Thompson, J.D.; Gibson, T.J.; Plewniak, F.; Jeanmougin, F.; Higgins, D.G. The CLUSTAL_X windows interface: Flexible strategies for multiple sequence alignment aided by quality analysis tools. *Nucleic Acids Res.* **1997**, *25*, 4876–4882.
47. Bailey, T.L.; Elkan, C. Fitting a mixture model by expectation maximization to discover motifs in biopolymers. *Proc. Int. Conf. Intell. Syst. Mol. Biol.* **1994**, *2*, 28–36.

48. Gupta, S.; Stamatoyannopoulos, J.A.; Bailey, T.L.; Noble, W.S. Quantifying similarity between motifs. *Genome Biol.* **2007**, *8*, R24.
49. Matys, V.; Fricke, E.; Geffers, R.; Gossling, E.; Haubrock, M.; Hehl, R.; Hornischer, K.; Karas, D.; Kel, A.E.; Kel-Margoulis, O.V.; *et al*. TRANSFAC: Transcriptional regulation, from patterns to profiles. *Nucleic Acids Res.* **2003**, *31*, 374–378.
50. Yang, J.H.; Zhang, X.C.; Huang, Z.P.; Zhou, H.; Huang, M.B.; Zhang, S.; Chen, Y.Q.; Qu, L.H. snoSeeker: An advanced computational package for screening of guide and orphan snoRNA genes in the human genome. *Nucleic Acids Res.* **2006**, *34*, 5112–5123.
51. Gardner, P.P.; Daub, J.; Tate, J.G.; Nawrocki, E.P.; Kolbe, D.L.; Lindgreen, S.; Wilkinson, A.C.; Finn, R.D.; Griffiths-Jones, S.; Eddy, S.R.; *et al*. Rfam: Updates to the RNA families database. *Nucleic Acids Res.* **2009**, *37*, D136–D140.
52. Lestrade, L.; Weber, M.J. snoRNA-LBME-db, a comprehensive database of human H/ACA and C/D box snoRNAs. *Nucleic Acids Res.* **2006**, *34*, D158–D162.
53. Hofacker, I.L.; Fontana, W.; Stadler, P.F.; Bonhoeffer, L.S.; Tacker, M.; Schuster, P. Fast folding and comparison of RNA secondary structures. *Monatsh. Chem.* **1994**, *125*, 167–188.
54. Thompson, J.D.; Higgins, D.G.; Gibson, T.J. CLUSTAL W: Improving the sensitivity of progressive multiple sequence alignment through sequence weighting, position-specific gap penalties and weight matrix choice. *Nucleic Acids Res.* **1994**, *22*, 4673–4680.
55. Tamura, K.; Stecher, G.; Peterson, D.; Filipski, A.; Kumar, S. MEGA6: Molecular evolutionary genetics analysis version 6.0. *Mol. Biol. Evol.* **2013**, *30*, 2725–2729.
56. Ronquist, F.; Huelsenbeck, J.P. MrBayes 3: Bayesian phylogenetic inference under mixed models. *Bioinformatics* **2003**, *19*, 1572–1574.
57. Posada, D.; Crandall, K.A. MODELTEST: Testing the model of DNA substitution. *Bioinformatics* **1998**, *14*, 817–818.
58. Hasegawa, M.; Kishino, H.; Yano, T. Dating of the human-Ape splitting by a molecular clock of mitochondrial DNA. *J. Mol. Evol.* **1985**, *22*, 160–174.
59. Graham, F.L.; van der Eb, A.J. A new technique for the assay of infectivity of human adenovirus 5 DNA. *Virology* **1973**, *52*, 456–467.

MDPI AG
Klybeckstrasse 64
4057 Basel, Switzerland
Tel. +41 61 683 77 34
Fax +41 61 302 89 18
http://www.mdpi.com/

Marine Drugs Editorial Office
E-mail: marinedrugs@mdpi.com
http://www.mdpi.com/journal/marinedrugs

MDPI • Basel • Beijing • Wuhan
ISBN 978-3-03842-131-3
www.mdpi.com